



TECHNISCHE
UNIVERSITÄT
WIEN

Vienna University of Technology

DISSERTATION

Pentacene- and Chalcogenophene-Based Conjugated Compounds as Functional Organic Materials

ausgeführt zum Zwecke der Erlangung des akademischen Grades eines
Doktors der technischen Wissenschaften
unter der Leitung von

Univ. Prof. Dipl.-Ing. Dr.techn. Johannes **Fröhlich** und
Ass. Prof. Dipl.-Ing. Dr.techn. Christian **Hametner**

163 - Institut für Angewandte Synthesechemie

eingereicht an der **Technischen Universität Wien**
Fakultät für Technische Chemie

von

Dipl.-Ing. Brigitte **Holzer**

0425995

Dempschergasse 8/6, A-1180 Wien

Wien, am 10.10.2015

Table of Contents

Danksagung	1
Abstract	3
Kurzfassung	5
Aims and Structure of the Thesis	7
Collaborations	8
1. Organic Field-Effect Transistors – Introduction	9
1.1. Introduction	11
1.2. Organic Field-Effect Transistors	11
1.3. Semiconducting Materials for OFET Application	14
1.4. Influence of the Organic Semiconductor on Device Performance	16
1.5. Conclusion	21
2. Organic Field-Effect Transistors – Results and Discussion	25
2.1. Overview of Contributions	27
2.2. Context of Contributions	29
2.3. Original Works	35
Manuscript # 1	37
Manuscript # 2	57
Manuscript # 3	75
Manuscript # 4	81
Manuscript # 5	95
Manuscript # 6	121
3. Nonlinear Optics – Introduction	135
3.1. Introduction	137
3.2. Concept of Nonlinear Optical Phenomena	137
3.3. Second Harmonic Generation	139
3.4. Two-Photon Absorption	140
3.5. Conclusion	146
4. Nonlinear Optics – Results and Discussion	149
4.1. Overview of Contributions	151
4.2. Context of Contributions	153
4.3. Original Works	157
Manuscript # 7	159
Manuscript # 8	175
Manuscript # 9	189
Manuscript # 10	205
5. Summary and Outlook	227
6. Statement of Contribution	233

7. Appendix	237
Supporting Information - Manuscript # 1	239
Supporting Information - Manuscript # 2	267
Supporting Information - Manuscript # 4	283
Supporting Information - Manuscript # 5	305
Supporting Information - Manuscript # 6	379
Supporting Information - Manuscript # 7	403
Supporting Information - Manuscript # 8	433
Supporting Information - Manuscript # 9	449
Supporting Information - Manuscript # 10	463
8. Curriculum Vitae	487

Danksagung

Univ.Prof. Dipl.-Ing. Dr. Johannes Fröhlich danke ich für die Unterstützung in den letzten Jahren sowie den zugestandenen Freiraum für meine Forschungsaktivitäten, die es mir ermöglicht haben viele eigene Ideen einzubringen und wertvolle Erfahrungen zu sammeln. Dr. Christian Hametner möchte ich besonders für die vielen NMR Messungen, Ratschläge und Korrekturen sowie seine Unterstützung und Betreuung während und vor allem in der Endphase meiner Arbeit danken. Dr. Berthold Stöger vom Institut für Chemische Technologien und Analytik sowie Univ.Prof. Mag. Dr. Georg Reider vom Institut für Photonik danke ich für die konstruktive Zusammenarbeit und die Möglichkeit meine Arbeit unterstützt durch diese Kooperationen durchführen zu können. Allen weiteren, namentlich nicht genannten Co-Autoren möchte ich selbstverständlich ebenfalls für die hervorragende Zusammenarbeit danken!

Ganz besonders danke ich allen, die einen entscheidenden Beitrag zu dieser Arbeit geleistet haben: Alexander Aster, Dorian Bader, Jacqueline Bitai, Daniel Bomze, Barbara Dellago, Rene Klaffenböck, Daniel Koch, Markus Lunzer, Marlene Mathuber, Thomas Schwartz und Anna Maria Wagner. Vielen Dank für euer Engagement und die tolle gemeinsame Zeit!

DI Johannes Bintinger, DI Christoph Denk, Dr. Philipp Fruhmann, DI Florian Glöcklhofer, Dr. Ernst Horkel, Thomas Kader, DI Paul Kautny, Stefan Kronister, DI Stefan Lexmüller, Dr. Daniel Lumpi, Dr. Hannes Mikula, DI Markus Schwarz, DI Philipp Skrinjar, DI Barbara Sohr, DI Dennis Svatoněk and DI Julia Weber danke ich für die gemeinsame Zeit im Labor und abseits, sowie für die vielen interessanten, wissenschaftlichen Diskussionen! Der gesamten FG HF möchte ich für die letzten sechs Jahre danken!

Bei allgemeinen Mitarbeitern des IAS und der TU Wien möchte ich mich aufrichtig bedanken. Insbesondere bei Sabine Stiedry, Tanja Halbarth, Emiliya Hillebrand, Johannes Van der Winden, Daniel Stankic, Gerhard und Thomas Seebauer und Florian Untersteiner ohne die ein Laborbetrieb in dieser Form nicht möglich wäre.

Bei meinen Eltern möchte ich mich herzlich für die konstante Unterstützung während meines Studiums bedanken. Meinem Freund Maximilian Wohlgemuth möchte ich von ganzem Herzen für das entgegengebrachte Verständnis und die stetige Unterstützung vor allem während des Verfassens der Dissertation danken.

Abstract

Compounds based on conjugated π -electron systems have attracted much attention due to their potential application in organic electronics such as organic light-emitting diodes (OLEDs), field effect transistors (OFETs), and photovoltaics (OPV) but also as functional organic compounds capable of two-photon absorption and applicable as nonlinear optic chromophores. The unique electronic properties of organic materials are strongly associated with their π -electron topology. Alteration of the molecular design of conjugated organic compounds and their functional groups crucially influences electrochemical and photophysical properties (like HOMO/LUMO levels, band gap, quantum yields etc.).

The main goals of this thesis were on the one hand the synthesis of potential novel semiconductors for OFET application, aiming for materials with high charge carrier mobilities, improved molecular oxidation stability, solubility and film-forming behavior. On the other hand reliable synthetic strategies toward materials capable of second harmonic generation and compounds suitable for two-photon absorption are presented, intending to improve molecular properties like second harmonic efficiency and two-photon absorption cross-section.

The first part of this thesis focused on synthetic pathways toward acene derivatives bearing electron-deficient substituents (e.g. triazoles and isoxazoles), which were introduced by copper-catalyzed cycloaddition reactions. This study demonstrates that the attachment of *N*-hexyltriazole moieties to pentacene leads to a significant improvement in both photostability and solubility, which makes these compounds attractive for OFET application. Also, the introduction of bromo(trialkylsilyl)thienyl scaffolds was sought by addition of an appropriate lithium species to pentacene-6,13-dione and subsequent reductive aromatization aiming for improved charge carrier mobilities. For this novel substance class hole transport mobilities up to $3 \times 10^{-4} \text{ cm}^2 \text{ V}^{-1} \text{ s}^{-1}$ could be determined.

Further strategies to improve the conductivity by enhancing intermolecular interaction focused on the introduction of benzo[*b*]selenophenes in conjugated π -electron scaffolds based on symmetric fused heteroaromatic compounds. First, an efficient one-pot procedure toward substituted benzo[*b*]selenophenes had to be established. The obtained benzo[*b*]selenophene derivatives were used as starting materials for the preparation of symmetric chalcogenopheno[1]benzochalcogenophene building blocks based on a Fiesselmann reaction. The incorporation of selenophenes proved to be an efficient method to decrease the bandgaps and induce strong intermolecular interactions (proven by crystal packing arrangements) of these target molecules compared to their thiophene-based analogs.

Another strategy toward efficient semiconductors for OFET application was pursued by preparing star-shaped triphenylamine-substituted tris(2-thienyl)benzene cores aiming for improved

film morphology. This approach yielded a compound with a charge carrier mobility of nearly $10^{-3} \text{ cm}^2 \text{ V}^{-1} \text{ s}^{-1}$.

The second part of this thesis evaluated compounds applicable as materials for nonlinear optics. Synthetic pathways toward ene-yne compounds based on a selenophene ring fragmentation were pursued. Functionalization by copper-catalyzed cycloaddition yielded phenyltriazole and -isoxazole based compounds exhibiting attractive nonlinear optical (NLO) properties. The obtained materials showing non-centrosymmetric crystallization behavior revealed efficient second harmonic generation. Thus, the developed molecular design combining phenyltriazoles or -isoxazoles as acceptors (A) and *Z*-(methylseleno)alkenyl groups as donors (D) represents an interesting type of novel NLO chromophore.

Furthermore, a series of thiophene-based cap-linker-cap systems were evaluated as materials capable of two-photon absorption. The combination of thiophenes with substituted triphenylamines bearing electron-donating or -withdrawing substituents was realized by either Suzuki cross-coupling or nucleophilic aromatic substitution giving rise to two basic structural families of D- π -D and A- π -D- π -A chromophores. Although these novel materials exhibit high quantum yields and only low two-photon cross-sections, the potential photoinitiators were successfully tested in the generation of microstructures by two-photon induced polymerization processes of acrylate resins. A further aim of this thesis was to apply synthetic strategies toward quadrupolar cap-linker-cap type molecules offering increased two-photon cross-section and thus efficiency of two-photon absorption. Alteration of the initial cap-linker-cap design was pursued by planarization of the triphenylamine cap, elongation and planarization of the π -linker, as well as enhancing the electron density of the linker using more electron donating scaffolds. To overcome the shortcoming of low solubility of the original cap-linker-cap photoinitiators in the respective monomer formulations, all target compounds were designed bearing hexyl substituents on the triarylamine building blocks. The obtained materials exhibit increased cross-sections and selected materials proved to be efficient two-photon initiators in structuring tests.

In summary, several synthetic methods and protocols were evaluated towards novel materials in order to gain insight into structure-property relationships. Triazole moieties proved to be efficient scaffolds for improving the photostability of pentacene and as acceptors in nonlinear optics chromophores. Additionally, the introduction of selenophene-based moieties yielded materials with strong intermolecular interactions and also nonlinear behavior. All these methods and substances represent valuable results, which can be used for further research in the fields of organic functional materials.

Kurzfassung

In den letzten Jahrzehnten haben auf konjugierten π -Elektronensystemen basierende Verbindungen aufgrund ihrer potentielle Anwendungen in elektronischen Bauteilen an kommerziellem und wissenschaftlichem Interesse gewonnen. Möglichen Einsatz finden solche Materialien in organischen lichtemittierenden Dioden (OLEDs), Feldeffekttransistoren (OFETs) und in der Photovoltaik (OPV), aber auch als funktionelle organische Verbindungen, welche sich zur Zwei-Photonen-Absorption oder als Chromophore für nichtlineare Optik eignen. Die einzigartigen Eigenschaften von organischen Materialien sind eng mit ihrer π -Elektronen-Topologie verknüpft. So kann durch Änderung des molekularen Designs dieser Verbindungen und deren funktionellen Gruppen entscheidend Einfluss auf die elektrochemischen sowie photophysikalischen Eigenschaften (wie etwa auf HOMO/LUMO Energielevels, Bandlücke, Quantenausbeuten etc.) genommen werden.

Ziel dieser Arbeit war es einerseits potentiell neue Halbleiter für OFET-Applikationen zu synthetisieren, welche hohe Ladungsträgermobilitäten, verbesserte Oxidationsstabilität, Löslichkeit sowie filmbildende Eigenschaften aufweisen. Andererseits sollten zuverlässige synthetische Strategien zu Materialien entwickelt werden, welche sich aufgrund ihrer Zwei-Photonen-Querschnitte sowie Effizienz der Frequenzverdopplung für nichtlineare Optik eignen.

Im ersten Teil dieser Arbeit wurden synthetische Strategien zur Derivatisierung von Acenen mittels elektronenziehenden heteroaromatischen Systemen (z.B. Triazolen und Isoxazolen) verfolgt, welche durch kupferkatalysierte Cycloadditionen mit der Acen-basierten Grundstruktur realisiert wurden. Die Verknüpfung von *N*-Hexyltriazolen und Pentacen führte zu entscheidenden Verbesserungen von sowohl Photostabilität als auch Löslichkeit der Zielsubstanzen, was für die Anwendung dieser Materialien als OFETs essentiell ist. Weiters wurde der Einsatz von Brom(trialkylsilyl)thienyl-Substituenten an Pentacenen getestet, um deren Einfluss auf die Ladungsträgermobilität zu bestimmen. Hierfür wurde durch Addition der entsprechenden Lithiumspezies an Pentacen-6,13-dion und anschließende reduktive Aromatisierung die gewünschte Verbindungsklasse hergestellt, welche Mobilitäten bis zu $3 \times 10^{-4} \text{ cm}^2 \text{ V}^{-1} \text{ s}^{-1}$ zeigte.

Die Leifähigkeit organischer Verbindungen kann durch intermolekulare Wechselwirkung erhöht werden. Diese Strategie wurde durch Einbringen von Selen mit guter Polarisierbarkeit in π -konjugierten Materialien basierend auf kondensierten heteroaromatischen Strukturen verfolgt. Hierfür wurden zuerst synthetische Methoden zur effizienten Darstellung von Benzo[*b*]selenophenen mittels One-pot Synthese entwickelt. Die erhaltenen Benzo[*b*]selenophen-Derivate wurden im Anschluss als Ausgangsmaterialien zur Synthese von symmetrischen Chalcogenopheno[1]benzochalcogenophen-Bausteinen mittels Fiesselmann-Reaktion verwendet. Das Einbringen von Selenophen-Einheiten in die Zielverbindungen stellte sich als effizient heraus, da gezeigt werden konnte, dass Bandlücken verringert sowie starke intermolekulare Wechselwirkungen induziert werden konnten.

Eine weitere Strategie um effiziente Halbleiter für OFET-Anwendungen zu erhalten, wurde durch Verknüpfung von substituierten Triphenylaminen mit Tris(2-thienyl)benzol zu sternförmigen Materialien mit guten Filmbildungseigenschaften verfolgt, welche Ladungsträgermobilitäten von nahezu $10^{-3} \text{ cm}^2 \text{ V}^{-1} \text{ s}^{-1}$ aufweisen.

Der zweite Teil dieser Arbeit widmete sich der Synthese von neuen Materialien, welche sich für nichtlineare Optik (NLO) eignen. Hierfür wurde mittels Selenophen-Ringfragmentierung ein Zugang zu π -konjugierten En-In-Verbindungen geschaffen, welche durch Funktionalisierung mittels kupferkatalysierter Cycloaddition zu Phenyltriazol und -isoxazol basierten Verbindungen mit attraktiven nichtlinearen Eigenschaften umgesetzt werden konnten. Die erhaltenen Materialien, welche nicht-zentrosymmetrische Kristallisationseigenschaften zeigen, weisen effiziente Frequenzverdopplung auf. Folglich repräsentiert dieses molekulare Design, welches Phenyltriazol und -isoxazol als Akzeptoren (A) und Z-(Methylseleno)alkenyl-Gruppen als Donor (D) verbindet, einen neuen Typus von NLO-Chromophoren.

Weiters wurde eine neue Substanzklasse von Thiophen-basierten Cap-Linker-Cap Systemen als Materialien für Zwei-Photonen-Absorption evaluiert. Die Verknüpfung von Thiophenen mit Triphenylaminen mit elektronenspendenden oder -ziehenden Substituenten wurde entweder durch Suzuki-Kreuzkupplung oder nukleophile aromatische Substitution hergestellt. Diese neuen Verbindungen der Typen D- π -D sowie A- π -D- π -A erwiesen sich trotz ihrer hohen Quantenausbeuten sowie niedrigen Zwei-Photonen-Querschnitten als geeignete Zwei-Photonen-Absorptionsinitiatoren, welche in Acrylat-Formulierungen zur Fabrikation von Mikrostrukturen eingesetzt wurden. Weitere Synthesestrategien wurden auf das molekulare Design von Verbindungen mit hohen Zwei-Photonen-Querschnitten und folglich hoher Effizienz der Zwei-Photonen-Absorption gerichtet. Die Variationen der ursprünglichen Materialien wurden mittels Planarisierung der Triphenylamin-Caps, Erweiterung und Planarisierung der π -Linker sowie Erhöhung der Elektrondichte der Linker durch elektronenspendende Derivate verfolgt. Aufgrund der geringen Löslichkeit der ursprünglichen Verbindungsklasse in den entsprechenden Monomerlösungen wurden an die Triphenylamin-Einheiten Hexylketten angebracht. Ausgewählte Zielstrukturen wurden in Zwei-Photonen-Absorption-induzierten Polymerisationen eingesetzt und erwiesen sich als effiziente Photoinitiatoren.

Zusammenfassend konnten verschiedene synthetische Methoden und Protokolle zu neuen Materialien evaluiert werden und neue Einsichten in die Struktur-Eigenschaftsbeziehung gewonnen werden. Triazol-basierte Verbindungen erwiesen sich als effiziente Materialien um einerseits die Photostabilität von Pentacenen zu erhöhen, und andererseits um als Akzeptoren in Verbindungen für nichtlineare Optik zu agieren. Weiters führte die Verwendung von polarisierbaren Selenverbindungen zu Materialien mit starken intermolekularen Wechselwirkungen und nichtlinearem Verhalten. Die erzielten Erkenntnisse und funktionellen organischen Verbindungen repräsentieren interessante Resultate für die aktive Forschung.

Aims and Structure of the Thesis

The main objectives of this doctoral research were on the one hand the development of reliable strategies and methods for the synthesis of pentacenes, fused selenophene-based and star-shaped materials as potential novel semiconductors for OFET application, aiming for materials with high charge carrier mobilities, improved molecular oxidation stability, solubility and morphology. On the other hand straightforward synthetic approaches toward materials capable of second harmonic generation and compounds suitable for two-photon absorption are presented intending to improve molecular properties like two-photon absorption cross-section and second harmonic efficiency. Several methods for the preparation of reasonable amounts of functional organic materials were developed and electrochemical as well as spectroscopic techniques were applied for structure-property studies.

This thesis is written as a cumulative work and consists of two parts: (1) brief introductions to the overall topics and (2) the main parts including the *Results and Discussion* sections for materials applicable as organic field effect transistors and for nonlinear optics. Original works (manuscripts #1 to #10, already published, submitted or in preparation) are included in the second part. Supporting Information of these manuscripts can be found in the Appendix of the thesis and contains most of the experimental details and data. The applicant (B. Holzer) is first author of 7 (including two co-first authorships) and corresponding author of 4 (including two co-corresponding authorships) of these publications. Seven manuscripts were written and composed predominantly by B. Holzer. Contributions of the applicant to the other manuscripts were manifold and essential for successful completion of the respective research projects.

The thesis is thematically divided into two main topics: (I) *Synthesis of Materials as Potential Organic Field Effect Transistors* and (II) *Materials Suitable for Nonlinear Optics*. Within topic I, pentacenes, fused heterocycle-based and star-shaped materials as potential novel semiconductors for OFET were prepared following the development of reliable synthetic strategies and procedures. All compounds were characterized with respect to their electrochemical as well as photophysical properties. The chemistry and structures of the novel materials exhibiting nonlinear behavior as well as their photophysical properties were investigated within topic II.

Collaborations

The following collaborations were essential for a successful completion and the scientific outcome of this PhD thesis:

- Univ.Prof. Dr. Bertram Batlogg, Laboratory of Solid State Physics, Swiss Federal Institute of Technology Zurich, Otto-Stern-Weg 1, 8093 Zurich, Switzerland
- Univ.Ass. DI Dr. Berthold Stöger, Institute of Chemical Technologies and Analytics, Technische Universität Wien, Karlsplatz 13, 1040 Wien, Vienna, Austria
- Ao.Univ.Prof. Mag. Dr.rer.nat. Georg Reider, Photonics Institute, Technische Universität Wien, Gußhausstr. 25-29, 1040 Vienna, Austria
- Univ.Ass. DI Dr. Arnulf Rosspeintner, Department of Physical Chemistry – Sciences II, University of Geneva, 30, Quai Ernest Ansermet, 1211 Geneva 4, Switzerland

1 – Organic Field-Effect Transistors – Introduction

1.1. Introduction

Field-effect transistors (FETs) are electronic devices that amplify and switch electrical signals. The development of metal oxide semiconductor field-effect transistors (MOSFETs) and integrated circuits (like microprocessors) has changed our everyday lives since their inventions more than 50 years ago.¹ Today, we are facing a new technological evolution that could possibly have a similar impact: the emergence of flexible and printed electronics. Among these organic or plastic electronics, organic field-effect transistors (OFETs) have attracted particular attention due to their potential advantages of flexibility, large-area fabrication and low weight.² Accordingly, OFETs are being considered for applications in electronic paper,³ organic light emitting displays, and sensor devices,⁴ such as electronic noses (e-nose),⁵ electronic skin (e-skin),⁶ medical diagnostics,⁷ environmental monitoring⁸ but also in everyday technology like radio frequency identification tags (RFIDs)⁹ (*Figure 1*).



Figure 1: Organic electronic products based on OFETs from left to right: e-paper,¹⁰ flexible display,¹¹ e-skin,¹² smart contact lens monitoring glucose level.¹³

Since the first OFETs emerged, many efforts have been devoted to improving their performance by adopting new organic semiconductors (OSC) or optimizing the device configuration. Despite the broad field of promising applications of organic semiconductors, there is still a need for further research to obtain a stable and soluble material bearing high charge carrier mobility for fast electrical switching, low operating voltages, and large on/off ratios.

1.2. Organic Field-Effect Transistors

1.2.1. Working Principle and Device Structure

In field-effect transistors the electrical conductivity in the semiconducting material originates from the drift of mobile charge carriers induced by an electric field perpendicular to its surface generated by an applied voltage. In general OFET devices consist of three different components: an isolator, a thin semiconducting layer and three electrodes. The so-called source and drain electrodes are in direct contact with the organic semiconductor, whereas the gate electrode is isolated from the semiconductor by an isolator with high permittivity and modulates the current flow across the source-drain electrodes.¹⁴ Because of the fragility of most organic semiconducting materials, many devices are fabricated by deposition of the thin semiconducting layer on the dielectric (*Figure 2*).¹⁵ Usually all elements are made of films with a thickness largely lower than one micrometer, consequently the device is constructed on a thicker, insulating substrate that does not play any role in the operation of the device.¹⁶ Possible OFET device architectures, bottom-gate top-contact (BGTC), bottom-gate bottom-contact (BGBC) and top-gate bottom-contacts are shown in *Figure 2*.

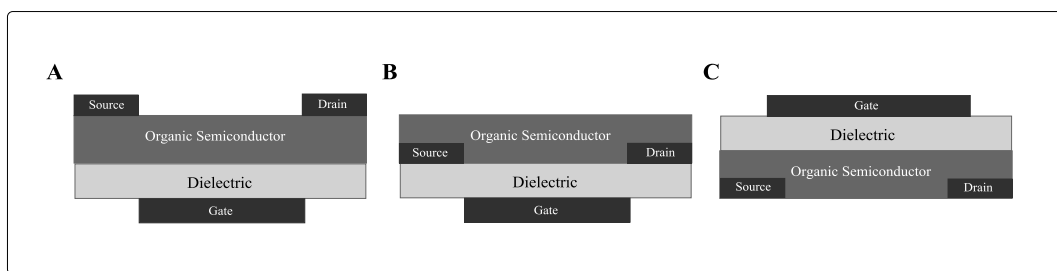


Figure 2: Schematic view of organic field-effect transistor configurations: (A) Bottom-gate, top-contacts (BGTC); (B) Bottom-gate bottom-contact (BGBC); (C) Top-gate bottom-contacts (TGBC) configuration.

The device can be viewed as a plane capacitor (*Figure 3, A*) where one of the plates constitutes one electrode, the gate, while the semiconductor element composes the second plate. The role of the source and drain electrodes is to inject and retrieve charge carriers to and from the semiconductor. If no voltage is applied between gate and source electrode, hardly any current flows between the source and the drain electrode and the transistor is switched off. However, if a potential is applied, the transistor basically operates like a capacitor (loading of the dielectric layer) and charge is induced in the semiconducting layer and a conducting channel is formed. The conductance of the semiconductor increases due to the rising number of charge carriers in the channel and the transistor is switched on.

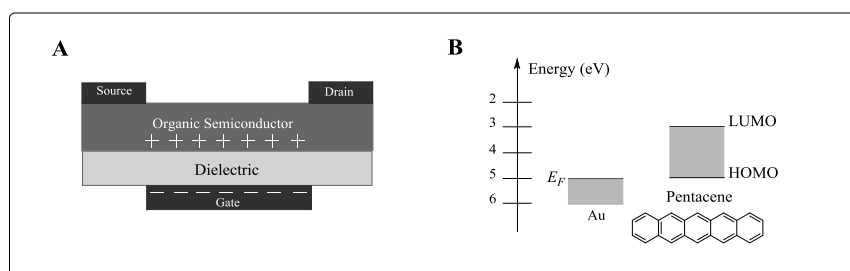


Figure 3: Charge injection in p-type transistors: (A) Charge transport; (B) Energy scheme of the gold electrode matching the HOMO of pentacene.

Based on the charge carriers formed in the conducting channel, organic semiconductors are classified into two types, namely p-type (hole-conducting) and n-type (electron-conducting). Thus, in devices where the semiconducting layer is p-type, the transistors are turned on using negative gate voltages, while for n-types, positive gate voltages are required switch the device on. In some organic semiconductors both holes and electrons are formed in the channel depending on the sign of the gate bias. These materials are classified as ambipolar materials.¹⁷ In order to ensure efficient charge carrier injection, the work function of the applied electrodes have to match the frontier orbital of the organic semiconductor.¹⁸ Most organic transistors are based on p-channel organic semiconductors (e.g. pentacene), therefore, the applied electrodes are made of high work function metals (most usually Au, but also Pd, Pt and Ni).¹⁶ The energy scheme in *Figure 3, B* indicates the respective positions of the Fermi energy level of the applied gold electrode and the highest occupied molecular orbital (HOMO) of pentacene.¹⁷

Characteristic device parameters such as charge carrier mobility (μ), on/off current ratio, and threshold voltage (V_T) essentially determine the applicability of the OSC in OFETs and can be estimated using the standard saturation regime current-voltage characteristics with the drain-source current (I_{DS}) given by

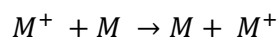
$$I_{DS} = \frac{WC_i}{2L} \mu (V_G - V_T)^2$$

where C_i is the capacitance per unit area of the dielectric, W and L are OFET channel width and length, and V_G is the gate voltage. It is clear that C_i must be high in order to obtain high I_{DS} at low V_G . The dielectric capacitance is given by $C = \kappa \epsilon_0 A/d$, where κ is the dielectric constant, ϵ_0 is the permittivity of free space, A is the area of the capacitor, and d is the dielectric thickness.¹⁹

The key parameters included in these equations are relevant for the device performance in the following terms: (I) the mobility, which is defined as the drift velocity of a charge carrier (cm s^{-1}) per unit applied field (V cm^{-1}), determines the possible bit speed of the organic integrated circuits. High speed commercial applications in organic digital circuits require mobilities in the magnitude of $1 \text{ cm}^2 \text{ V}^{-1} \text{ s}^{-1}$, whereas for other possible applications, such as chemical sensors, lower mobilities of $0.01 - 0.1 \text{ cm}^2 \text{ V}^{-1} \text{ s}^{-1}$ are sufficient.²⁰ (II) Additionally, a large on/off current ratio of 10^5 is essential for the OCS's practical applications in high speed, low power, high reliability circuits.²¹ Improvement of the on/off ratio can be achieved by increasing the on current by chemical doping, enhancing the charge injection at the electrodes or using high- k dielectrics. Another possibility to increase the on/off ratio is the reduction of the off current by controlling the doping level to minimize the conductivity of the active layer, optimization of the material purity or post processing, such as annealing.²⁰ (III) The last key parameter that determines the performance of an OSC is the threshold voltage, i.e. the voltage at which a conductive channel begins to form, which should be zero or slightly negative.

1.2.2. Charge Transport in Organic Semiconductors

Organic semiconductors are generally easily oxidized to radical cations (M^+ , p-type) or reduced to radical anions (n-type) to yield stable species with charge delocalized over a conjugated system. The hole transport in p-type materials (M) can be described as a self-exchange reaction:



The rate at which the formed charges migrate through an organic semiconductor depends on the π -bonding orbitals and quantum mechanical wave function (frontier orbital) overlap between neighboring molecules in the semiconductor layer. In order to achieve high field-effect charge carrier mobilities of both thin film and single crystal devices the semiconducting molecules should preferentially exhibit good π - π stacking in the direction of the current flow. Both intrinsic factors like molecular structure and crystal packing and extrinsic factors such as crystallinity and device configuration contribute to the charge carrier mobility. Carrier transport in amorphous organic solids is often modeled as thermally activated hopping. The Marcus theory gives intrinsic hopping mobility as:

$$k_{ET} = \frac{4\pi^2}{h} \frac{1}{\sqrt{4\pi\lambda k_B T}} t^2 e^{-\frac{\lambda}{4k_B T}}$$

where k_B is the Boltzmann constant, T the temperature, and h the Planck constant. At a microscopic level one of the key parameters for transport is the interchain transfer integral t , that expresses the ease of transfer of a charge between two interacting chains and is strongly related to the energetic splitting of the HOMO and lowest unoccupied molecular orbital (LUMO) level.²² The reorganization energy λ describes the strength of hole(electron)-vibration coupling energy of a charge localized on a single molecule, which needs to be small in order to ensure efficient charge transport.²³ Therefore, high charge carrier mobility, which means rapid exchange of carrier between molecules, can be realized by small reorganization energy and large intermolecular orbital coupling.²⁴

1.3. Semiconducting Materials for OFET Application

In general, for the realization of OFETs two distinct classes of materials exist: conjugated polymers and small molecules. Polymers exhibit the advantage that the deposition of the organic semiconductor on a substrate can usually be realized via solution processed spin-coating, drop-casting, coating and printing techniques.²⁵ However, polymers tend to have a large polydispersity, which impedes efficient packing and leads to defects in the resulting films and crystals.²⁶ Small molecules may be superior to polymers due to their consistent size and shape, which enables an improved control of defects and film quality.²⁷ Currently, both conducting materials, polymers and small conjugated molecules, are subjects of intense research promoting this technology to an industrial stage in many application fields. In this chapter the focus will be set on the principles behind the development of soluble and air stable conjugated small molecules as semiconducting materials applicable in p-type OFET devices.

1.3.1. Acene-based Semiconductors

Acenes exhibit ideal transistor behaviors when employed in OFETs due to their expanded π -framework enabling strong intermolecular overlap, which allows the charge carrier transport in the solid state. Their strong tendency to crystallize in a herringbone packing is suitable to construct two-dimensional electronic structure when fabricated in thin-film-based devices.²⁸ The π -conjugated system of acenes is similar to that of single layers of graphene, which comprises the highest mobility for organic compounds and for which its discoverers were recently awarded the 2010 Noble Prize in physics.²⁸

In the series of acenes with each additional benzene ring the HOMO level increases and the HOMO-LUMO gap diminishes.²⁹ The frontier orbitals of the homologous set of acenes from naphthalene to pentacene are depicted in *Figure 4*. Although important electronic properties such as increased charge carrier mobility, decreased reorganization energy and band gaps beneficially scale with the size of acenes, the elongation of the π -electron system also brings along some disadvantages.²¹ Unfortunately, the instability of higher acene-based OFETs can be attributed to the high-lying HOMO level and narrow HOMO-LUMO gap, which cause their propensity toward air-oxidation in ambient conditions and photo-degradation.³⁰

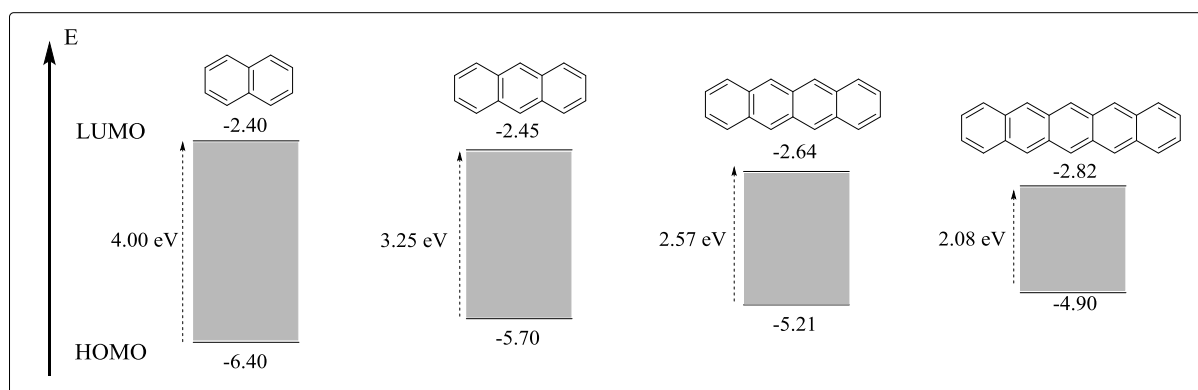


Figure 4: Frontier orbitals of acenes.³¹

Among small molecule semiconductors pentacene-based materials - exhibiting charge carrier mobility up to $5.5 \text{ cm}^2 \text{ V}^{-1} \text{ s}^{-1}$ in thin films (vacuum deposition of the OSC)³² - have been the most widely studied class of organic compounds mainly due to their ability to form highly ordered

crystalline films.³³ Pentacene packs in a herringbone pattern with edge to face interactions (*Figure 8, A*).³⁴ However, pentacene exhibits poor solubility in common organic solvents,^{21,35} which limits processing procedures primarily to vacuum deposition^{36,37} and therefore prevents low-cost high-throughput printing techniques suitable for organic electronics technology. Another critical limitation is pentacene's propensity to degrade *via* cycloaddition reactions with dienophiles like singlet oxygen ($^1\text{O}_2$). According to literature, there are two primary mechanisms by which polyaromatic hydrocarbons such as pentacene degrade with oxygen in the presence of light. Early investigators into the mechanism of photooxidation proposed a singlet oxygen sensitization mechanism: once the organic molecule is excited by light singlet oxygen formation is stimulated, and degradation occurs via further reactions of singlet oxygen and the organic compound (*Figure 5, A*).³⁸ In the second mechanism, the excited pentacene serves as an electron donor and transfers an electron to oxygen to generate a superoxide radical anion and the corresponding pentacene radical cation, which is prone to further degradative steps. The photoreactivity of acenes is especially predominant in solution through photo-induced endoperoxide formation, however, "butterfly" dimerization (*Figure 5, B*) also poses a problem in the solid state.³⁹

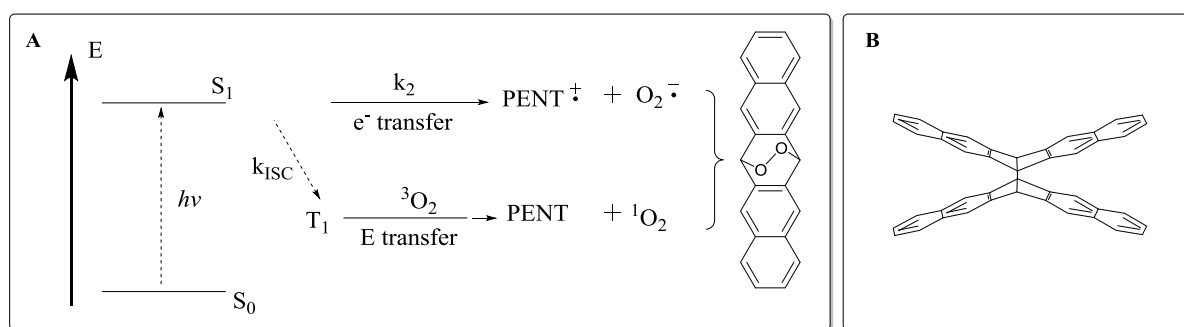


Figure 5: (A) Two suggested mechanistic pathways of the photooxidation of pentacene derivatives: electron transfer and energy transfer and (B) "butterfly" dimerization product of pentacene.

Although numerous groups have prepared pentacene derivatives bearing either solubilizing or stabilizing substituents (refer to Chapter 4.2) the outstanding challenge to develop soluble organic semiconductors that are highly stable towards photodegradation remains.

1.3.2. Thiophene-based Heterocyclic Semiconductors

Thiophene-based fused oligomers and polymers have attracted growing interest owing to their desirable characteristics for fabricating electronic devices.²⁰ In particular, heteroacene-based materials proved to be environmentally stable and robust in nature. One of the first sulfur-based materials used in organic field-effect transistors was polythiophene (*Figure 6, A*) exhibiting low charge carrier mobility of $10^{-5} \text{ cm}^2 \text{ V}^{-1} \text{ s}^{-1}$.⁴⁰ Since then, polymers,⁴¹ oligomers,⁴² and fused ring aromatic materials⁴¹ containing thiophene units have been thoroughly examined. This rapid development of chalcogen-containing heterocyclic semiconductors can be attributed to their advantages over acene derivatives, which in turn can be ascribed to their unique structural features. Although the thiophene moiety with six π electrons ($4n + 2$) is electronically similar to the benzene ring predominant in acenes, fused thiophene compounds exhibit a much higher stability due to the absence of a Diels-Alder cyclization active center.²⁷ Furthermore all the sulfur atoms are positioned at the molecular periphery, facilitating multiple short intermolecular S-S contacts which increase the effective dimensionality of the electronic structure, which may result in enhanced transport properties.²⁰

Many of the highest-performing small molecules are based on fused heteroacene materials

such as 2,7-dioctyl[1]benzothieno[3,2-*b*][1]benzothiophene (C₈-BTBT, *Figure 6, B*), exhibiting the highest recorded carrier mobility of 31.3 cm² V⁻¹ s⁻¹ to date for organic thin-film transistors.⁴⁴ Another efficient material is dianthra[2,3-*b*:2',3'-*f*]thieno[3,2-*b*]thiophene (DATT, *Figure 6, C*), for which charge carrier mobilities of 16.0 cm² V⁻¹ s⁻¹ have been observed.

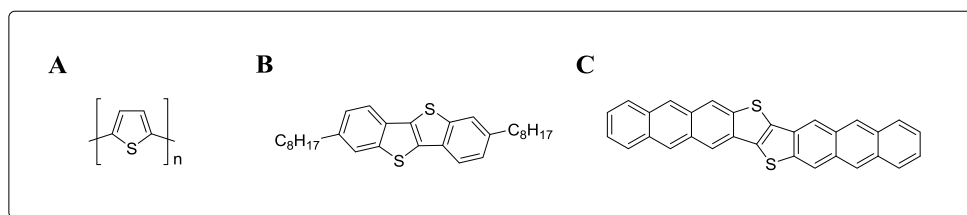


Figure 6: Thiophene-based materials applicable for organic field-effect transistors. (A) polythiophene, (B) 2,7-dioctyl[1]benzothieno[3,2-*b*][1]benzothiophene (C₈-BTBT) and (C) dianthra[2,3-*b*:2',3'-*f*]thieno[3,2-*b*]thiophene (DATT).

Structural variation of thiophene-based materials allows fine tuning of the electronic properties.⁴⁵ Similar to acenes, the extension of the π -electron system of heteroacenes increases the conjugated length of the molecule, which decreases band gap and increases charge carrier mobility.⁴⁶ Contrary to acenes and linear linked thiophenes, ring-fused or annulated thiophenes have more rigid structures possessing an extended π -conjugation, which could be employed for adjusting the band gap⁴⁷ of organic materials and increasing intermolecular interactions in the solid state.⁴⁵ Furthermore, the high polarizability of sulfur atoms in thiophene rings leads to a stabilization of the conjugated systems with excellent charge transport properties, which are one of the most crucial assets for applications in organic and molecular electronics.

Thiophene-based semiconductors constitute stable materials further research in this area focusses on attaining optimized charge carrier mobilities. The enhancement of intermolecular interaction by incorporating heavier chalcogene heteroatoms (Se and Te) with large atomic radii may contribute to the effective π -electron overlap in the solid state.

1.4. Influence of the Organic Semiconductor on Device Performance

1.4.1. Molecular Factors

Both the molecular arrangement and film morphology in organic semiconducting layers play significant roles in the performance of OFETs.²¹ Regarding semiconducting π -conjugated systems incorporated in OFETs, one of the most important factors determining the ultimate performance of a device is high charge carrier mobility. In order to achieve an efficient charge transport, the organic molecules ideally should pack perpendicular to the direction of current flow,²⁸ which is illustrated schematically in *Figure 7* (π -stacking is indicated by parallel sheets; charge transport is indicated by the black arrow across the long axis of the molecule). The strongest form of intermolecular coupling arises from interactions between the π -electron clouds of aromatic molecules, which are maximized when molecules adopt a face-to-face orientation.

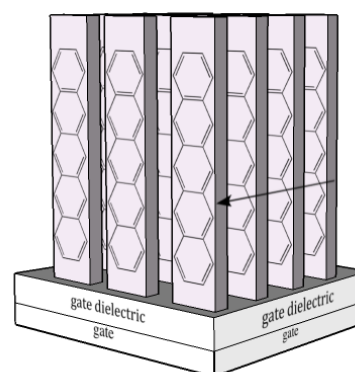


Figure 7: Illustration of an idealized molecular arrangement of the OSC on the dielectric.

1.4.1.1. Molecular Arrangement

Unsubstituted acenes tend to crystallize in a herringbone-packing motif, in which the molecules form 2D layers interacting face-to-edge through C-H- π interactions minimizing the electrostatic π -orbital repulsion (Figure 8, A).⁴⁸ Substitution of the acene backbone leads to modification of the packing motif and therefore, an alteration of the transfer integral π -overlap between neighboring molecules. A remarkable strategy, yielding both high performance (as a result of improved stacking) and better stability (due to electronic and steric effects), was followed by Anthony et al. by introducing sterically demanding (triisopropylsilyl)ethynyl substituents to the acene backbone (TIPS-pentacene) forming slipped stacks (brickwork arrays, Figure 8, B).^{38,49,50}

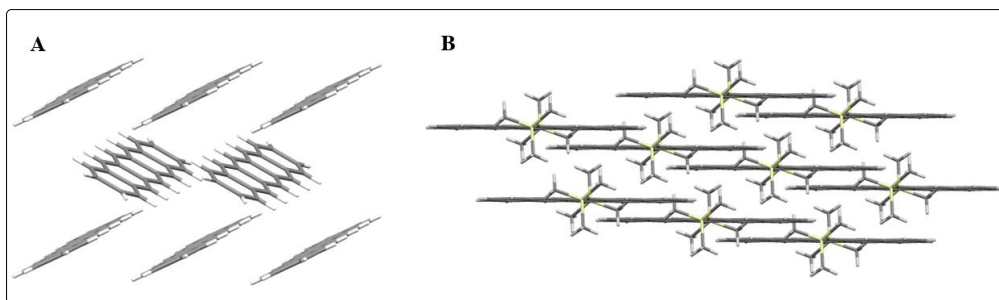


Figure 8: Molecular packing motifs of (A) pentacene (herringbone packing (face-to-edge) without π - π overlap (face-to-face) between adjacent molecules); (B) TIPS-pentacene (lamellar motif, 2-D π -stacking).

Besides substituting the acene system a common approach to enhance OFET performance is the incorporation of heteroatoms in these π -conjugated organic compounds. Fused thiophene moieties can improve the extent of intermolecular π - π overlap in the solid state, a feature that is closely related to the charge carrier mobility.⁵¹ Therefore, thiophene-based materials proved to be highly efficient yielding mobilities up to $16.0 \text{ cm}^2 \text{ V}^{-1} \text{ s}^{-1}$ as reported for dianthra[2,3-*b*:2',3'-*f*]thieno[3,2-*b*]thiophene (DATT, Figure 6, C).⁵² Furthermore, sulfur-induced intermolecular interactions like S-S, S-H, and S- π facilitate charge transport, but also positively influence the packing motifs of the organic semiconductors, for example, from face-to-edge (present in pentacene,⁵³ Figure 8, A) to face-to-face stacking or slipped π -stacking (pentathienoacene,⁵³ Figure 9, A).²⁸ Consequently, sulfur-based materials have become essential frameworks for the design of efficient semiconductors in OFET devices.

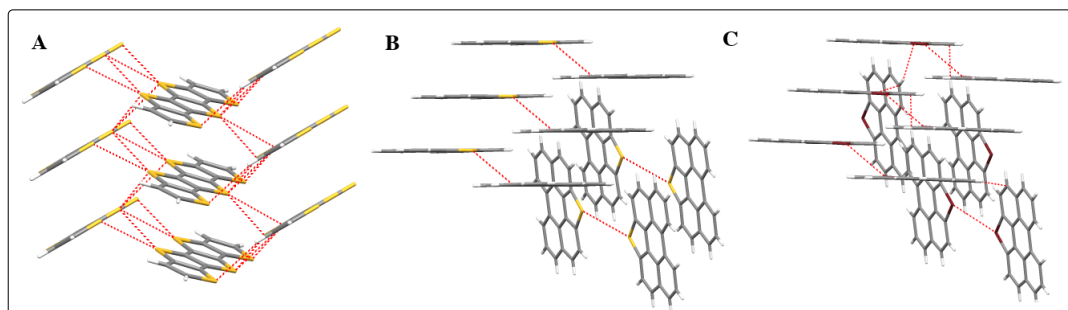


Figure 9: Strategies to increase π - π stacking: (A) pentathienoacene (PTA), slipped π -stacking caused by high C-H ratios (diminished C-H- π interactions) and chalcogen-chalcogen interactions (red dashed lines).⁵⁴ Slipped π -stacking is caused by chalcogen-chalcogen interactions (red dashed lines) in (B) perylo[1,12-*b,c,d*]thiophene (PET),⁵⁴ and in (C) perylo[1,12-*b,c,d*]selenophene (PESE).⁵⁵

An important synthetic concept for organic chemists is the variation of heteroatoms in

conjugated molecules: for instance, frequently used thiophene moieties can be replaced by selenophene frameworks.³⁰ The larger atomic radius and higher polarizability⁵⁶ of selenium compared to sulfur atoms enhances intermolecular heteroatomic interactions in organic compounds. Therefore, the substitution of sulfur atoms by selenium is a reasonable strategy to enhance device performances by improvement of intermolecular overlap and thus charge carrier mobility, thus making selenophene-fused aromatics attractive candidates for electronic applications. Further studies have also revealed clear evidence that replacement of sulfur by selenium can induce stronger intermolecular charge transfer in the solid state.⁵⁶

This effect has been clearly demonstrated by replacing sulfur in perylo[1,12-*b,c,d*]thiophene (PET, *Figure 9, B*) with selenium. Perylo[1,12-*b,c,d*]selenophene (PESE, *Figure 9, C*) exhibits shorter Se-Se contacts of 3.49 Å compared to the S-S distance of 3.51 Å in PET molecules, indicating a more compressed molecular packing structure.³⁰ This arrangement based on π - π and Se-Se contacts exhibiting mobilities of up to $2.66 \text{ cm}^2 \text{ V}^{-1} \text{ s}^{-1}$ makes PESE an attractive candidate for OFET devices. In contrast, its sulfur analog PET exhibits only p-channel behavior with mobilities up to $0.8 \text{ cm}^2 \text{ V}^{-1} \text{ s}^{-1}$. The efficiency of incorporating selenium instead of sulfur in π -conjugated materials has also been successfully demonstrated for 2,6-diphenylbenzo[1,2-*b*:4,5-*b'*]dichalcogenophenes (*Figure 10*). This sulfur/selenium exchange proved to significantly enhance charge carrier mobility from $4.6 \times 10^{-3} \text{ cm}^2 \text{ V}^{-1} \text{ s}^{-1}$ in DPh-BDT to $0.2 \text{ cm}^2 \text{ V}^{-1} \text{ s}^{-1}$ in the selenium analog DPh-BDSe.⁵⁷

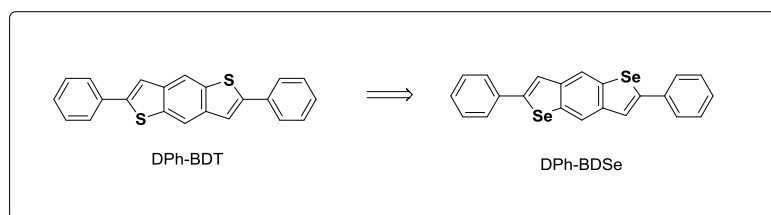


Figure 10: 2,6-Diphenylbenzo[1,2-*b*:4,5-*b'*]dichalcogenophenes.

1.4.1.2. Film Morphology

Although the application of single crystals in OFETs is of significant importance for the investigation of the intrinsic properties of the semiconducting material and evaluation of the upper limit of device performance, they are not practical with regard to high volume manufacturing. Solution-processable small-molecule organic semiconductors have attracted scientific and technological interest because of their excellent film-forming properties and field-effect mobilities. The charge carrier mobility is strongly influenced by the film morphology. Since grain boundaries impede transport, much effort has been devoted to producing small-molecule well-ordered films resulting in devices with desirable electronic properties.

The major emphasis of OFET material development has been set on linear-structured organic semiconductors (see chapter 3). However, it has been shown that star-shaped tritopic molecules possess better solubility and improved film-forming properties as active material in OFETs compared to their linear counterparts. Amorphous phases of such molecules have a very low tendency to crystallize and show an excellent long-term stability under ambient conditions.⁵⁸ The glass transitions of these compounds occur at sufficiently high temperatures to allow their application in electronic devices.⁵⁹

Among suitable materials of this type for OFET application are on the one hand triarylamine

polymers, on the other hand small star-shaped molecules with triphenylamine cores and carbazole or fluorene side arms (*Figure 11, A*).⁵⁹ Furthermore, star-shaped oligothiophenes gave a mobility of $2 \times 10^{-4} \text{ cm}^2 \text{ V}^{-1} \text{ s}^{-1}$ with an on/off ratio of 10^2 (*Figure 11, B*).⁶⁰ Materials consisting of a triphenylamine core and π -conjugated terthieryl branches have been synthesized displaying a hole mobility of $0.011 \text{ cm}^2 \text{ V}^{-1} \text{ s}^{-1}$ (*Figure 11, C*).⁶¹

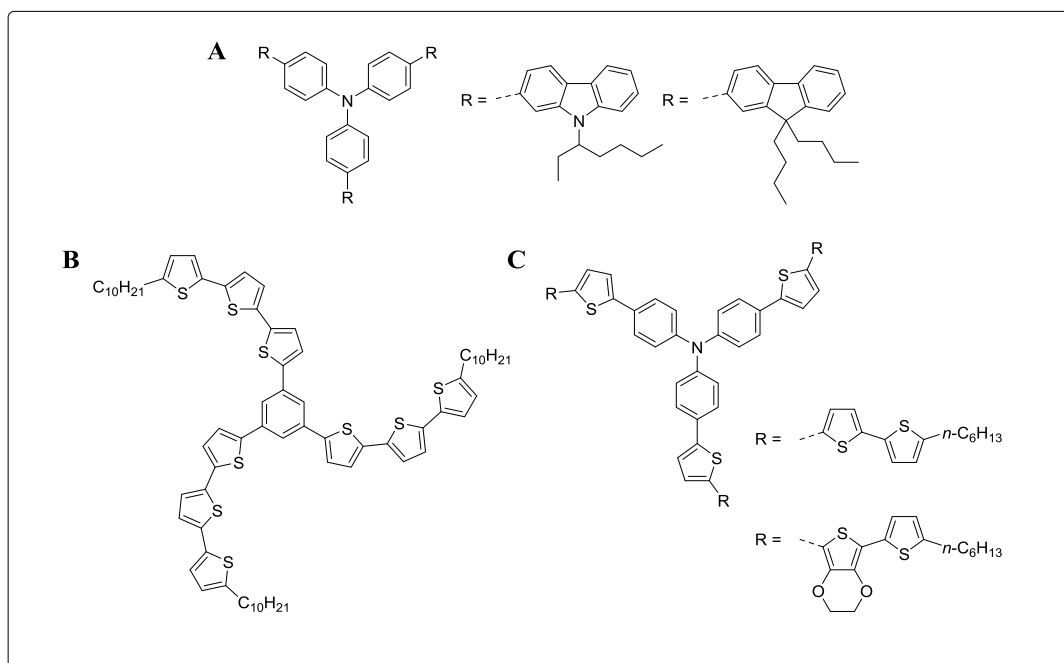


Figure 11: Star-shaped OFET materials.

1.4.2. Stability Considerations

Although pentacene exhibits hole mobilities up to $5.5 \text{ cm}^2 \text{ V}^{-1} \text{ s}^{-1}$ in thin-film devices,²¹ its drawback is its chemical instability towards oxygen^{62,63} owing to the relatively high HOMO energy level of -5.0 eV ,⁶⁴ which originates from its highly π -electron-conjugated nature. Consequently, the instability of pentacene-based OFETs can be partially attributed to the high-lying HOMO level and narrow band gap (Chapter 3.1). Approaches to improve the stability and to enhance electronic properties at the same time have been suggested.⁶⁵⁻⁶⁷ Molecular engineering based on modification of the core of π -conjugated small molecules by substituents Z (*Figure 12, A*, Z = electron-donating or -withdrawing), side chains R (e.g. applying solubilizing alkyl or silyl groups, *Figure 12, B*) and heteroatoms (*Figure 12, C*) beneficially influences acene properties.¹

Electron-withdrawing groups Z (*Figure 12, A*), such as -F, -Cl, -Br, and -CN, are capable of depriving the π -conjugated system of electron density either through a resonance or inductive effect^{68,69} and decrease the HOMO and LUMO energy levels of acenes. Therefore substitution of π -conjugated molecules with electron-withdrawing groups generally leads to an increase in stability toward oxidation, but also to a potential transition from p-type materials to ambipolar or n-type materials, and a change in molecular packing.¹ For instance the introduction of electron accepting $-\text{C}_6\text{F}_5$ group in the 6,13-positions of the pentacene core represents an efficient strategy in order to achieve improved stability against photooxidation.⁷⁰

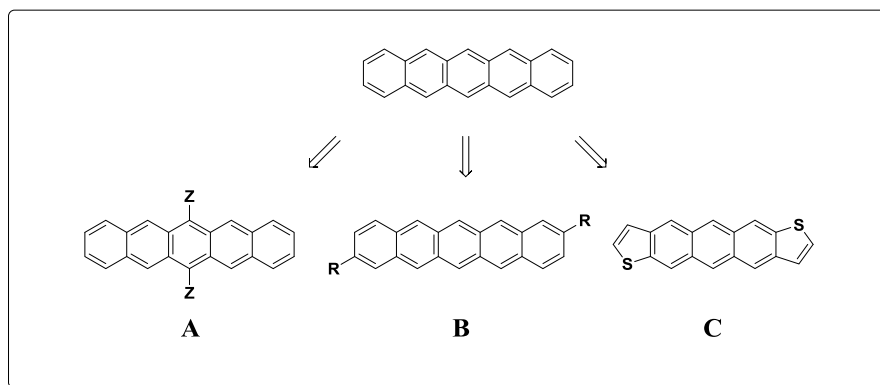


Figure 12: Modification approaches starting from pentacene. (A) Introduction of electron-donating or -withdrawing groups; (B) Addition of side chains (e.g. alkyl or silyl groups); (C) Incorporation of thiophenes in pentacene toward isoelectronic anthra[2,3-*b*:6,7-*b'*]dithiophene.

Furthermore, substitution of the core also affects electronic properties, solubility, and molecular arrangements through modifying the dipole, changing the C-H ratio, or chalcogen-chalcogen interactions. Replacement of benzene rings with heteroaromatic groups increases the molecular oxidation stability. It has been shown that the introduction of thiophenes reduces the aromatic π -delocalization, enhances the benzenoid character of the π -framework and thus lowers the HOMO levels and increases the band gaps.⁷¹ Application of this strategy to pentacene by replacement of two terminal benzene rings leads to isoelectronic anthra[2,3-*b*:6,7-*b'*]dithiophene (ADT, *Figure 12*, C), which has a higher barrier against oxidation (HOMO -5.1 eV compared to -4.9 eV for pentacene).

The outlined strategy to improve the stability of π -conjugated small molecules by the introduction of heteroatoms has recently been also demonstrated for the picene moiety (*Figure 13*), which incorporates the same number of benzene rings as pentacene.⁷² Although picene is highly conductive,^{72,73} it is very sensitive to atmospheric conditions and therefore not appropriate for practical semiconductor devices.⁷⁴ Enhanced stability is achieved by alteration of the conjugated core, which determines most of the electronic properties (e.g., energy level and bandgap, inter/intramolecular interaction, and solubility) and influences molecular packing.

These structural modifications have been reported by Mitsui⁷⁴ based on dinaphtho[1,2-*b*:2',1'-*d*]chalcogenophenes, which include the chalcogen atoms $Z = O, S,$ or Se at the C-13 and C-14 position of the picene core (*Figure 13*). The ionization potentials (IP) of vacuum-deposited thin films of these materials (*Figure 13*, IP = 5.85 eV for $Z = O$, 5.87 eV for $Z = S$, and 5.81 eV for $Z = Se$)⁷⁴ indicate higher stability than picene (IP = 5.5 eV).⁷⁵

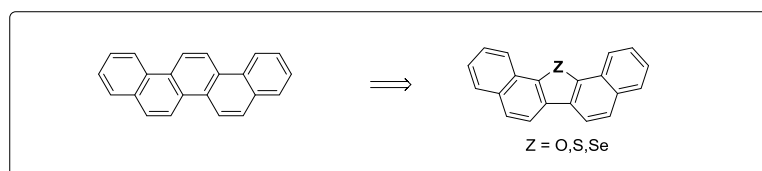


Figure 13: Substitution approach from picene.

The incorporation of heteroatoms also leads to substances with large orbital coefficients on the chalcogen atoms, excellent molecular packing structures, and high hole mobilities up to $2.0 \text{ cm}^2 \text{ V}^{-1} \text{ s}^{-1}$. Hence, heteroatom replacement is an effective way to tune electronic properties of the organic

compound and thus solubility, molecular packing, and - most importantly - stability by lowering the HOMO level.^{1,66,76} Therefore, the introduction of sulfur in π -conjugated compounds gives rise to stable semiconductors.

1.5. Conclusion

Although acenes exhibiting high charge carrier mobilities have been developed, there is still a need to overcome their disadvantages like low solubility and propensity to degradation. Contrary, most thiophene-based materials demonstrate good stability, however, only low charge carrier mobilities are observed. Therefore, the development of conductive and stable novel semiconductors suitable for OFET applications remains in the focus of scientific interest. The methods described in this chapter have given insight in altering physicochemical properties by molecular engineering. The aim of this thesis is the development and evaluation of novel stable acene- and chalcogenophene-based compounds suitable as semiconductors bearing high charge carrier mobilities.

REFERENCES

- (1) Mei, J.; Diao, Y.; Appleton, A. L.; Fang, L.; Bao, Z. *J. Am. Chem. Soc.* **2013**, *135* (18), 6724.
- (2) Meng, Q.; Dong, H.; Hu, W.; Zhu, D. *J. Mater. Chem.* **2011**, *21* (32), 11708.
- (3) Heikenfeld, J.; Drzaic, P.; Yeo, J.-S.; Koch, T. *J. Soc. Inf. Disp.* **2011**, *19* (2), 129.
- (4) Sokolov, A. N.; Roberts, M. E.; Bao, Z. *Mater. Today* **2009**, *12* (9), 12.
- (5) Li, L.; Gao, P.; Baumgarten, M.; Müllen, K.; Lu, N.; Fuchs, H.; Chi, L. *Adv. Mater.* **2013**, *25* (25), 3419.
- (6) Hammock, M. L.; Chortos, A.; Tee, B. C.-K.; Tok, J. B.-H.; Bao, Z. *Adv. Mater.* **2013**, *25* (42), 5997.
- (7) Rivnay, J.; Owens, R. M.; Malliaras, G. G. *Chem. Mater.* **2014**, *26* (1), 679.
- (8) Knopfmacher, O.; Hammock, M. L.; Appleton, A. L.; Schwartz, G.; Mei, J.; Lei, T.; Pei, J.; Bao, Z. *Nat. Commun.* **2014**, *5*.
- (9) Tinivella, R.; Camarchia, V.; Pirola, M.; Shen, S.; Ghione, G. *Org. Electron.* **2011**, *12* (8), 1328.
- (10) <http://www.tomshardware.com/news/LG-Display-E-Paper-Skiff-Flexible,9443.html>.
- (11) <http://thecreatorsproject.vice.com/blog/electronic-skin-future>.
- (12) <http://www.daisygroupplc.com/2013/11/samsung-planning-foldable-smartphones-and-4k-capabilities-for-2015/>.
- (13) <http://googleblog.blogspot.co.at/2014/01/introducing-our-smart-contact-lens.html>.
- (14) Briseno, A. L.; Mannsfeld, S. C. B.; Jenekhe, S. A.; Bao, Z.; Xia, Y. *Mater. Today* **2008**, *11* (4), 38.
- (15) Forrest, S. R. *Nature* **2004**, *428* (6986), 911.
- (16) Braga, D.; Horowitz, G. *Adv. Mater.* **2009**, *21* (14-15), 1473.
- (17) Klauk, H. *Organic Electronics: Materials, Manufacturing, and Applications*; John Wiley & Sons, **2006**.
- (18) Khim, D.; Baeg, K.-J.; Kim, J.; Yeo, J.-S.; Kang, M.; Amegadzea, P. S. K.; Kim, M.-G.; Cho, J.; Lee, J. H.; Kim, D.-Y.; Noh, Y.-Y. *J. Mater. Chem.* **2012**, *22* (33), 16979.
- (19) *Nanotechnology 2014: electronics, manufacturing, environment, energy & water*; Nanotech Conference and Expo, Nano-Science and Technology Institute, Laudon, M., Romanowicz, B., Eds.; Technical proceedings of the 2014 NSTI Nanotechnology Conference and Expo, Nano Science and Technology Institute: Danville, Calif., **2014**.
- (20) Wu, W.; Liu, Y.; Zhu, D. *Chem. Soc. Rev.* **2010**, *39* (5), 1489.
- (21) Anthony, J. E. *Angew. Chem. Int. Ed.* **2008**, *47* (3), 452.
- (22) Bredas, J. L.; Calbert, J. P.; da Silva Filho, D. A.; Cornil, J. *Proc. Natl. Acad. Sci.* **2002**, *99* (9), 5804.
- (23) Park, Y.-H.; Kim, Y.-H.; Kwon, S.-K.; Koo, I.-S.; Yang, K.-Y. *Bull. Korean Chem. Soc.* **2010**, *31* (6), 1649.
- (24) Takimiya, K.; Shinamura, S.; Osaka, I.; Miyazaki, E. *Heterocycles* **2011**, *83* (6), 1187.
- (25) Carr, O.; Gozzi, G.; Santos, L. F.; Faria, R. M.; Chinaglia, D. L. *Transl. Mater. Res.* **2015**, *2* (1), 015002.
- (26) DeLongchamp, D. M.; Kline, R. J.; Fischer, D. A.; Richter, L. J.; Toney, M. F. *Adv. Mater.* **2011**, *23* (3), 319.
- (27) Qu, L.; Dai, L. in *Introduction to organic electronic and optoelectronic materials and devices*; Sun, S.-S., Dalton, L. R., Eds.; Optical science and engineering; CRC Press: Boca Raton, 2008.
- (28) Wang, C.; Dong, H.; Hu, W.; Liu, Y.; Zhu, D. *Chem. Rev.* **2012**, *112* (4), 2208.
- (29) Takimiya, K.; Yamamoto, T.; Ebata, H.; Izawa, T. *Sci. Technol. Adv. Mater.* **2007**, *8* (4), 273.
- (30) Tan, L.; Jiang, W.; Jiang, L.; Jiang, S.; Wang, Z.; Yan, S.; Hu, W. *Appl. Phys. Lett.* **2009**, *94* (15), 153306.
- (31) Djurovich, P. I.; Mayo, E. I.; Forrest, S. R.; Thompson, M. E. *Org. Electron.* **2009**, *10* (3), 515.
- (32) Lee, S.; Koo, B.; Shin, J.; Lee, E.; Park, H.; Kim, H. *Appl. Phys. Lett.* **2006**, *88* (16), 162109.
- (33) Witte, G.; Wöll, C. *Phys. Status Solidi A* **2008**, *205* (3), 497.
- (34) Campbell, R. B.; Robertson, J. M.; Trotter, J. *Acta Crystallogr.* **1962**, *15* (3), 289.
- (35) Kaur, I.; Jia, W.; Kopreski, R. P.; Selvarasah, S.; Dokmeci, M. R.; Pramanik, C.; McGruer, N. E.; Miller, G. P. *J. Am. Chem. Soc.* **2008**, *130* (48), 16274.
- (36) Natsume, Y. *Phys. Status Solidi A* **2008**, *205* (12), 2958.
- (37) Chen, K.-Y.; Hsieh, H.-H.; Wu, C.-C.; Hwang, J.-J.; Chow, T. J. *Chem Commun* **2007**, No. 10, 1065.
- (38) Maliakal, A.; Raghavachari, K.; Katz, H.; Chandross, E.; Siegrist, T. *Chem. Mater.* **2004**, *16* (24), 4980.
- (39) Northrop, B. H.; Houk, K. N.; Maliakal, A. *Photochem. Photobiol. Sci.* **2008**, *7* (12), 1463.
- (40) Koezuka, H.; Tsumura, A.; Ando, T. *Synth. Met.* **1987**, *18* (1-3), 699.
- (41) Park, S.; Lim, B. T.; Kim, B.; Son, H. J.; Chung, D. S. *Sci. Rep.* **2014**, *4*.
- (42) Back, J. Y.; Kim, Y.; An, T. K.; Kang, M. S.; Kwon, S.-K.; Park, C. E.; Kim, Y.-H. *Dyes Pigm.* **2015**, *112*, 220.
- (43) Niimi, K.; Shinamura, S.; Osaka, I.; Miyazaki, E.; Takimiya, K. *J. Am. Chem. Soc.* **2011**, *133* (22), 8732.

- (44) Minemawari, H.; Yamada, T.; Matsui, H.; Tsutsumi, J.; Haas, S.; Chiba, R.; Kumai, R.; Hasegawa, T. *Nature* **2011**, *475* (7356), 364.
- (45) Mishra, A.; Ma, C.-Q.; Bäuerle, P. *Chem. Rev.* **2009**, *109* (3), 1141.
- (46) Cinar, M. E.; Ozturk, T. *Chem. Rev.* **2015**, *115* (9), 3036.
- (47) Aragó, J.; Viruela, P. M.; Gierschner, J.; Ortí, E.; Milián-Medina, B. *Phys Chem Chem Phys* **2011**, *13* (4), 1457.
- (48) Mas-Torrent, M.; Rovira, C. *Chem. Rev.* **2011**, *111* (8), 4833.
- (49) Anthony, J. E.; Eaton, D. L.; Parkin, S. R. *Org. Lett.* **2002**, *4* (1), 15.
- (50) Anthony, J. E.; Brooks, J. S.; Eaton, D. L.; Parkin, S. R. *J. Am. Chem. Soc.* **2001**, *123* (38), 9482.
- (51) Galbrecht, F.; Bünnagel, T. W.; Bilge, A.; Scherf, U.; Farrell, T. in *Functional organic materials: syntheses, strategies and applications*; Müller, T. J. J., Bunz, U. H. F., Eds.; Wiley-VCH: Weinheim, **2007**.
- (52) Sokolov, A. N.; Atahan-Evrenk, S.; Mondal, R.; Akkerman, H. B.; Sánchez-Carrera, R. S.; Granados-Focil, S.; Schrier, J.; Mannsfeld, S. C. B.; Zoombelt, A. P.; Bao, Z.; Aspuru-Guzik, A. *Nat. Commun.* **2011**, *2*, 437.
- (53) Xiao, K.; Liu, Y.; Qi, T.; Zhang, W.; Wang, F.; Gao, J.; Qiu, W.; Ma, Y.; Cui, G.; Chen, S.; Zhan, X.; Yu, G.; Qin, J.; Hu, W.; Zhu, D. *J. Am. Chem. Soc.* **2005**, *127* (38), 13281.
- (54) Zhang, X.; Côté, A. P.; Matzger, A. J. *J. Am. Chem. Soc.* **2005**, *127* (30), 10502.
- (55) Sun, Y.; Tan, L.; Jiang, S.; Qian, H.; Wang, Z.; Yan, D.; Di, C.; Wang, Y.; Wu, W.; Yu, G.; Yan, S.; Wang, C.; Hu, W.; Liu, Y.; Zhu, D. *J. Am. Chem. Soc.* **2007**, *129* (7), 1882.
- (56) Chung, D. S.; Kang, I.; Kim, Y.-H.; Kwon, S.-K. *Phys. Chem. Chem. Phys.* **2013**, *15* (35), 14777.
- (57) Takimiya, K.; Kunugi, Y.; Konda, Y.; Niihara, N.; Otsubo, T. *J. Am. Chem. Soc.* **2004**, *126* (16), 5084.
- (58) Bao, Z.; Locklin, J. J. *Organic field-effect transistors*; CRC Press: Boca Raton, **2007**.
- (59) Sonntag, M.; Kreger, K.; Hanft, D.; Strohrriegl, P.; Setayesh, S.; de Leeuw, D. *Chem. Mater.* **2005**, *17* (11), 3031.
- (60) Ponomarenko, S. A.; Kirchmeyer, S.; Elschner, A.; Huisman, B.-H.; Karch, A.; Drechsler, D. *Adv. Funct. Mater.* **2003**, *13* (8), 591.
- (61) Cravino, A.; Roquet, S.; Alévêque, O.; Leriche, P.; Frère, P.; Roncali, J. *Chem. Mater.* **2006**, *18* (10), 2584.
- (62) Northrop, B. H.; Houk, K. N.; Maliakal, A. *Photochem. Photobiol. Sci.* **2008**, *7* (12), 1463.
- (63) Reddy, A. R.; Bendikov, M. *Chem. Commun.* **2006**, No. 11, 1179.
- (64) Klauk, H.; Zschieschang, U.; Weitz, R. T.; Meng, H.; Sun, F.; Nunes, G.; Keys, D. E.; Fincher, C. R.; Xiang, Z. *Adv. Mater.* **2007**, *19* (22), 3882.
- (65) Huang, J.; Luo, H.; Wang, L.; Guo, Y.; Zhang, W.; Chen, H.; Zhu, M.; Liu, Y.; Yu, G. *Org. Lett.* **2012**, *14* (13), 3300.
- (66) Chen, L.; Baumgarten, M.; Guo, X.; Li, M.; Marszalek, T.; Alsewailam, F. D.; Pisula, W.; Müllen, K. *J. Mater. Chem. C* **2014**, *2* (18), 3625.
- (67) Qiu, L.; Yu, C.; Zhao, N.; Chen, W.; Guo, Y.; Wan, X.; Yang, R.; Liu, Y. *Chem. Commun.* **2012**, *48* (100), 12225.
- (68) Swartz, C. R.; Parkin, S. R.; Bullock, J. E.; Anthony, J. E.; Mayer, A. C.; Malliaras, G. G. *Org. Lett.* **2005**, *7* (15), 3163.
- (69) Okamoto, T.; Senatore, M. L.; Ling, M.-M.; Mallik, A. B.; Tang, M. L.; Bao, Z. *Adv. Mater.* **2007**, *19* (20), 3381.
- (70) Ono, K.; Totani, H.; Hiei, T.; Yoshino, A.; Saito, K.; Eguchi, K.; Tomura, M.; Nishida, J.; Yamashita, Y. *Tetrahedron* **2007**, *63* (39), 9699.
- (71) Yamada, K.; Okamoto, T.; Kudoh, K.; Wakamiya, A.; Yamaguchi, S.; Takeya, J. *Appl. Phys. Lett.* **2007**, *90* (7), 072102.
- (72) Mitsuhashi, R.; Suzuki, Y.; Yamanari, Y.; Mitamura, H.; Kambe, T.; Ikeda, N.; Okamoto, H.; Fujiwara, A.; Yamaji, M.; Kawasaki, N.; Maniwa, Y.; Kubozono, Y. *Nature* **2010**, *464* (7285), 76.
- (73) Kosugi, T.; Miyake, T.; Ishibashi, S.; Arita, R.; Aoki, H. *J. Phys. Soc. Jpn.* **2009**, *78* (11), 113704.
- (74) Mitsui, C.; Okamoto, T.; Matsui, H.; Yamagishi, M.; Matsushita, T.; Soeda, J.; Miwa, K.; Sato, H.; Yamano, A.; Uemura, T.; Takeya, J. *Chem. Mater.* **2013**, *25* (20), 3952.
- (75) Okamoto, H.; Kawasaki, N.; Kaji, Y.; Kubozono, Y.; Fujiwara, A.; Yamaji, M. *J. Am. Chem. Soc.* **2008**, *130* (32), 10470.
- (76) Gao, P.; Beckmann, D.; Tsao, H. N.; Feng, X.; Enkelmann, V.; Baumgarten, M.; Pisula, W.; Müllen, K. *Adv. Mater.* **2009**, *21* (2), 213.
- (77) Takimiya, K.; Shinamura, S.; Osaka, I.; Miyazaki, E. *Adv. Mater.* **2011**, *23* (38), 4347.

2 – Organic Field-Effect Transistors – Results and Discussion

2.1 Overview of Contributions

Part I – Materials for Organic Field-Effect Transistors

* corresponding author, # equal contribution

- # 1 **B. Holzer**, R. Klaffenböck, A. Aster, D. Lumpi*, E. Horkel, and J. Fröhlich, Heteroaryl Substituted Anthracenes and Pentacenes as Potential Materials for Organic Field-Effect Transistors, *manuscript draft*.

- #2 **B. Holzer**^{#*}, D. Lumpi^{#*}, T. Mathis, E. Horkel, C. Hametner, B. Batlogg and J. Fröhlich. Novel Thiophene-Substituted Pentacenes as Soluble Materials for Organic Field-Effect Transistors, *manuscript draft*.

- # 3 T. Mathis*, Y. Liu, L. Ai, Z. Ge*, D. Lumpi*, E. Horkel, **B. Holzer**, J. Froehlich, and B. Batlogg. Stable organic field-effect-transistors with high mobilities unaffected by supporting dielectric based on phenylene-bridged thienobenzothiophene, *J. Appl. Phys.*, **2014**, 115, 043707-1 - 043707-4.

- # 4 **B. Holzer***, C. Hametner, and J. Fröhlich. Facile Synthesis of Benzo[*b*]selenophene Building Blocks, *manuscript draft*.

- # 5 **B. Holzer***, B. Dellago, C. Hametner, B. Stöger, D. Lumpi*, E. Horkel, and J. Fröhlich. Symmetric Mixed Sulfur-Selenium Fused Ring Systems as Potential Materials for Organic Field-Effect Transistors, *manuscript draft*.

- # 6 D. Lumpi[#], **B. Holzer**[#], J. Bintinger, E. Horkel,* S. Waid, H. D. Wanzenböck, M. Marchetti-Deschmann, C. Hametner, E. Bertagnolli, I. Kymissis, and J. Fröhlich. Substituted triphenylamines as building blocks for star shaped organic electronic materials, *New J. Chem.*, **2015**, 39, 1840 - 1851.

2.2 Context of Contributions

In this chapter the context of the subsequently introduced manuscripts or paper drafts will be outlined. This chapter can be categorized into three main sections, namely the synthesis and characterization of:

1. Pentacene Derivatives
2. Benzo[*b*]chalcogenophene-based Materials
3. Star shaped Compounds

The first part is focusing on the development of strategies to enhance the stability and solubility of pentacene derivatives by side chain engineering. The second part outlines reliable synthetic methods toward selenium-based building blocks, which are applied in the synthesis of stable chalcogenophene-based semiconducting materials. The last section will focus on the evaluation of thiophene-based star shaped molecules as functional organic materials. All target compounds were characterized by electrochemical and photophysical means in order to evaluate their properties toward application as organic field-effect transistors.

The next paragraphs will briefly explain the focus of research in the individual topics, refer to theoretical fundamentals and reveal how these contribute to the main topic of this thesis. For detailed background information and respective references see Chapter 2.3.

Pentacene Derivatives

Pentacene is known to be prone to photooxidation by cycloaddition of molecular oxygen in positions 6 and 13 to form endo-peroxides. The incorporation of electron-withdrawing substituents in these positions constitutes an accepted strategy to improve molecular stability. This part deals with the efficient introduction of stabilizing (Manuscript #1) and solubilizing substituents (Manuscript #2) in acene backbones by side chain engineering. Since post-synthetic modification of pentacene frameworks is known to be difficult because of the low photostability of higher acenes, a general mild synthetic protocol was sought. The resulting synthetic approach was first evaluated for model anthracene derivatives and subsequently applied to target pentacene.

The attachment of electron-withdrawing 1,2,3-triazole and isoxazole heterocyclic moieties was pursued to improve photostability of the pentacene backbone (Manuscript #1). The synthetic modification of alkyne-substituted dihydro-acene diols was either realized by Copper-catalyzed Azide–Alkyne Huisgen Cycloaddition (CuAAC) toward triazoles or copper catalyzed cycloaddition of in situ generated nitrile oxides, followed by reductive aromatization, which readily gave rise to triazole- or isoxazole-substituted acenes. The synthetic methodology was first probed toward anthracene model compounds and subsequently applied in the preparation of pentacene derivatives (*Figure 1*).

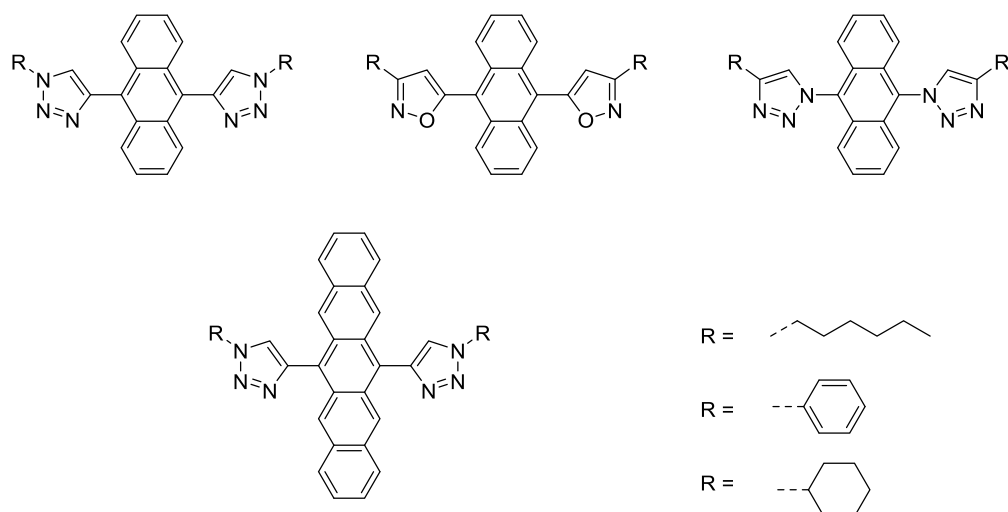


Figure 1: Triazole- and isoxazole-substituted target acenes.

All anthracene and pentacene compounds were characterized by optical and electrochemical means. The obtained pentacene derivatives show good solubility in organic solvents compared to unsubstituted pentacene. Furthermore a clear reduction of the bandgaps and decreased HOMO levels are evident, indicating higher stability. Photokinetic studies also reveal higher photostability compared to pentacene, which can be attributed to the 1,2,3-triazole moiety.

Manuscript #2 deals with the introduction of solubilizing and stabilizing thiophene moieties. The combination of (trialkylsilyl)thienyl moieties and pentacene joins the unique properties (high charge carrier mobilities, stability and solubility) of the two materials. Experimental data are supported by DFT calculations. Again, synthetic strategies focusing on mild procedures were primarily developed toward anthracene derivatives and subsequently applied to pentacene target compounds (*Figure 2*).

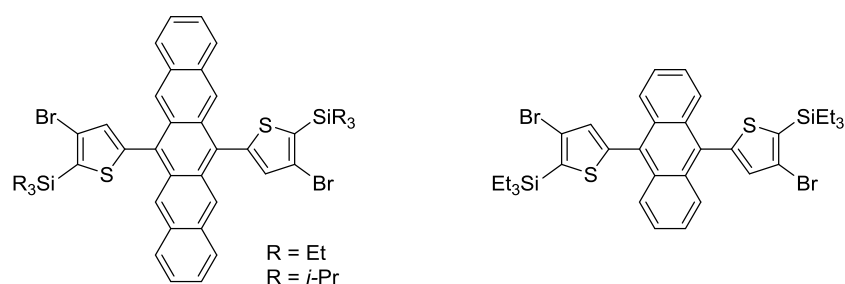


Figure 2: Thiophene-substituted pentacene derivatives.

In close cooperation with colleagues at the Laboratory of Solid State Physics, ETH Zurich the obtained materials were characterized with respect to their electrochemical and photophysical properties as well as their semiconducting behavior (charge carrier mobility in an OFET configuration). Charge carrier mobilities of $3 \times 10^{-4} \text{ cm}^2 \text{ V}^{-1} \text{ s}^{-1}$ were observed.

Benzo[*b*]chalcogenophene-based Materials

This section deals with the synthesis and characterization of benzo[*b*]chalcogenophene-derived compounds. A series of benzo[*b*]thiophene-based materials was probed toward their applicability as semiconductors (Manuscript #3). The evaluation of the electrochemical and physicochemical properties led to the conclusion that these materials are particularly stable and suitable for OFET application. Based on these results a series of symmetrical selenium-based materials was designed (Manuscript #5). In order to realize these materials a reliable synthetic approach was developed giving rise to benzo[*b*]selenophene building blocks (Manuscript #4).

In close cooperation with colleagues at the Laboratory of Solid State Physics, ETH Zurich a new class of thieno[2,3-*b*][1]benzothiophene building blocks, directly connected or joined by different π -bridge spacers (ethylene, phenylene, and tetrafluorophenylene) (Figure 3) was investigated toward their applicability in organic field-effect transistors (Manuscript #3). Highest occupied molecular orbital (HOMO), lowest unoccupied molecular orbital (LUMO) energies, and bandgaps were determined by cyclic voltammetric and UV-Vis absorption measurements.

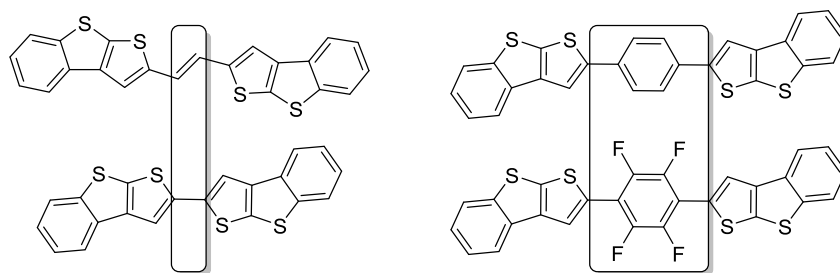


Figure 3: Thieno[2,3-*b*][1]benzothiophene building blocks connected directly or by different bridging spacers.

Given the observed long-term stability of these materials, the charge carrier mobility of over $1 \text{ cm}^2 \text{ V}^{-1} \text{ s}^{-1}$ and the beneficial position of HOMO levels, this substance class was chosen for further synthetic variations. The integration of electron-donating and polarizable selenium in π -conjugated molecules is known to strongly influence intermolecular interactions and therefore may strongly affect charge carrier mobility. Hence, a systematic strategy was pursued to incorporate selenium atoms in these compounds in order to obtain stable and highly conducting materials.

However, although benzo[*b*]selenophenes constitute important synthetic starting materials, the lack of a low-cost, high-yielding and convenient synthesis is evident considering the few commercial suppliers available and the high costs of these scaffolds. Therefore, a convenient one-pot synthesis toward benzo[*b*]selenophene-2-carboxylates starting from commercially available *o*-chlorobenzaldehyde or *o*-chloroacetophenone was evaluated (Manuscript #4) based on a Fiessemann-type reaction (Figure 4). The synthetic sequence was first probed by a stepwise approach (route 2) and developed into a one-pot procedure (route 1) without the need of isolating intermediates, giving rise to the desired product in good yields. Further derivatization of the obtained compounds with strong emphasis on functionalization possibilities in 2- and 3-position provided access to a broad spectrum of substituted benzo[*b*]selenophenes suitable as building blocks for various scientific disciplines.

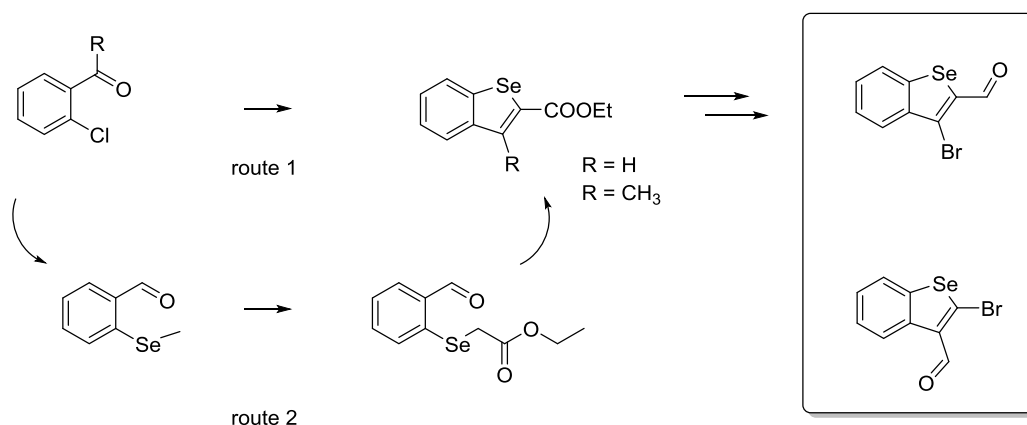


Figure 4: One-pot procedure (route 1) and stepwise procedure toward benzo[*b*]selenophene-2-carboxylates and regioisomers of bromobenzo[*b*]selenophene carbaldehydes.

The benzo[*b*]selenophene building blocks obtained in Manuscript #4 were further utilized for the synthesis of symmetrical semiconductors based on chalcogenopheno[1]benzochalcogenophenes (CBCs) in Manuscript #5. Substituted benzo[*b*]selenophenes and benzo[*b*]thiophenes constituted suitable starting materials for the step by step introduction of selenium giving rise to novel regioisomeric functionalized π -conjugated building blocks based on an optimized Fiesselmann-type reaction (Figure 5).

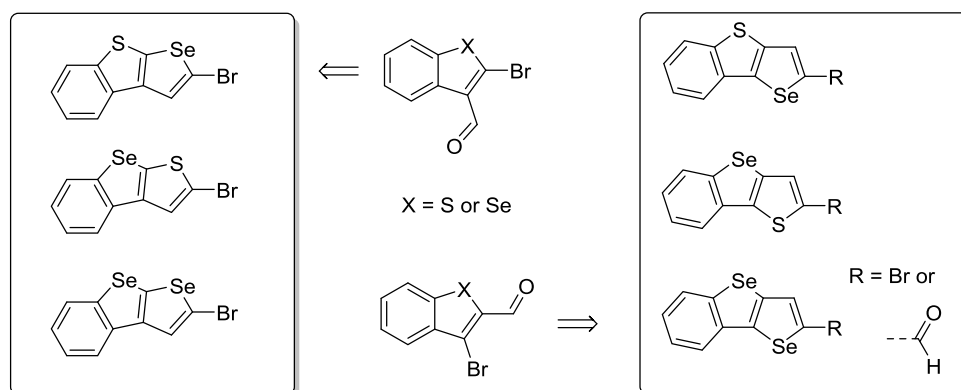


Figure 5: Functionalized building blocks based on chalcogenopheno[1]benzochalcogenophenes.

The obtained functionalized CBCs were further applied in either Stille coupling or McMurry reaction yielding stereoselectively *E*-isomers of symmetrical selenium-based target compounds depicted in Figure 6. In order to prove the applicability of the chalcogenopheno[1]benzochalcogenophenes in further coupling reactions, also yne-bridged symmetrical target compounds were synthesized (Figure 7).

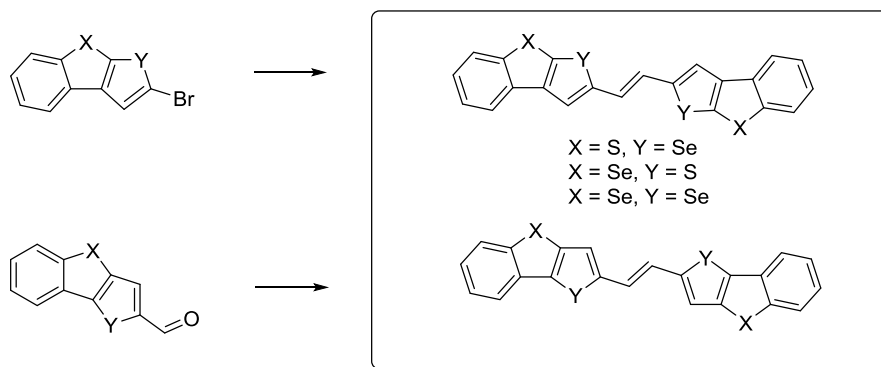


Figure 6: Ene-bridged symmetrical selenium-based target compounds.

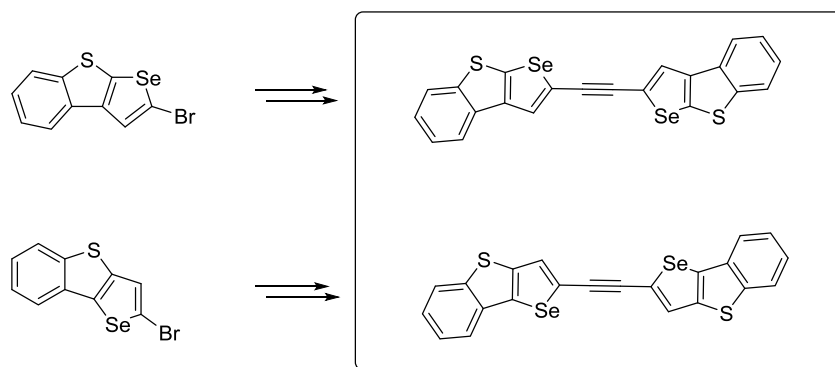


Figure 7: Yne-bridged symmetrical selenium-based target compounds.

The target ene and yne bridged potential semiconductors were purified by sublimation and characterized by ^1H , ^{13}C , and ^{77}Se NMR. X-ray analysis revealed the strong intermolecular interactions of these compounds. HOMO, LUMO, and bandgaps were determined by cyclic voltammetric and UV-Vis absorption measurements. The obtained data give strong indications that these materials should be applicable for OFET device fabrication.

Star shaped Compounds

In the last part a combination of substituted triphenylamines (TPA) and tris(2-thienyl)benzene structures in C₃ symmetric configurations evaluated. These materials offer tunable electronic and luminescent properties depending on the applied substituents and the benefit of solution processability (Manuscript #6).

This contribution outlines an optimized synthetic pathway toward a broad spectrum of p-substituted triphenylamines, suitable as building blocks for organic semiconducting materials. Key steps during synthesis were either realized by Ullman condensations or nucleophilic aromatic substitutions giving rise to triphenylamines bearing either electron-donating or withdrawing substituents. The synthesis of substituted triphenylamines, which were applied for the development of star shaped target compounds (Figure 8), was predominantly performed during the applicant's diploma thesis. Suzuki reaction yielded a set of three star shaped luminescent materials bearing substituents with different electronic nature (Figure 8), which were characterized with regard to their photophysical, electrochemical and thermal properties.

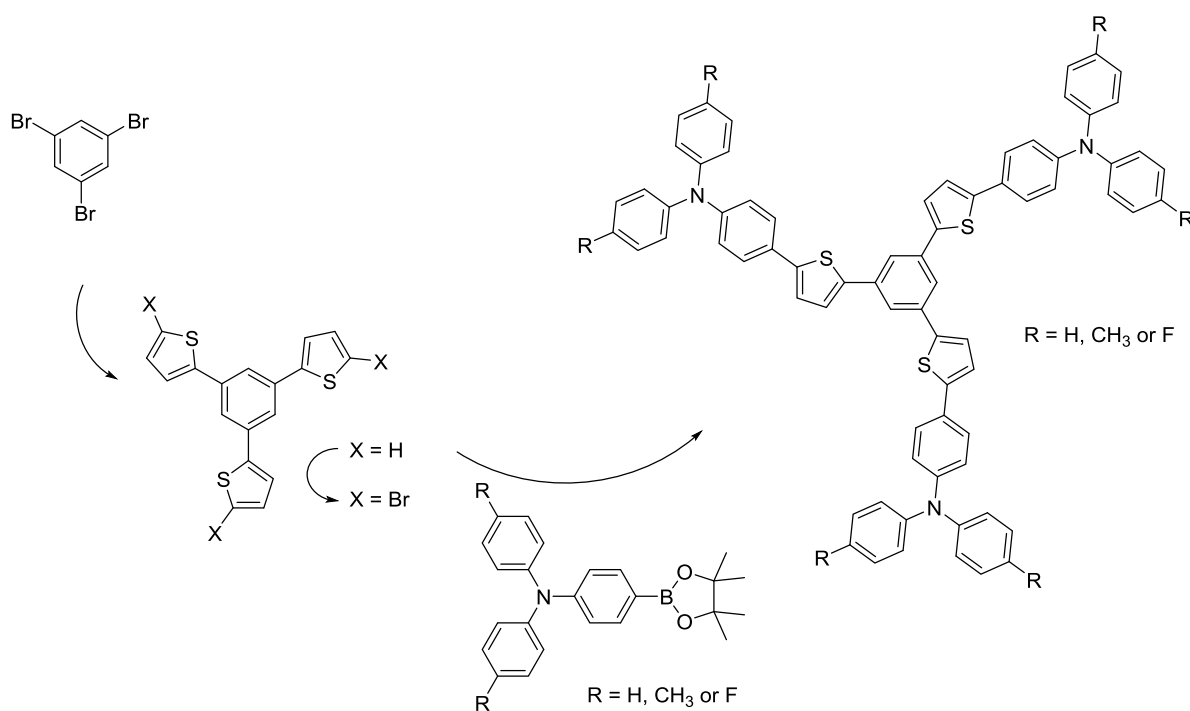


Figure 8: Star shaped target compounds.

Measurements of electrochemical and optical properties (e.g. fluorescence spectra and quantum yields) of the star shaped compounds reveal the strong influence of the substituents' nature moiety on the above-mentioned properties. Spin coating experiments were performed in order to investigate the morphology of the resulting thin films. These experiments showed that the substituent on the triphenylamine subunit strongly influences the film-forming behavior. The novel materials were tested as semiconductors in organic field-effect transistor devices.

2.3. Original works

Manuscript # 1

Brigitte Holzer, Rene Klaffenböck, Alexander Aster, Daniel Lumpi*, Ernst Horkel, and
Johannes Fröhlich

Heteroaryl Substituted Anthracenes and Pentacenes as Potential Materials for Organic Field-
Effect Transistors

Manuscript draft

Heteroaryl Substituted Anthracenes and Pentacenes as Potential Materials for Organic Field-Effect Transistors

Brigitte Holzer,^a Rene Klaffenböck,^a Alexander Aster,^a Daniel Lumpi,^{a} Ernst Horkel,^a and
Johannes Fröhlich^a*

^aInstitute of Applied Synthetic Chemistry, Vienna University of Technology,

Getreidemarkt 9/163OC, A-1060 Vienna, Austria

* daniel.lumpi@tuwien.ac.at

A series of acenes substituted with electron deficient heteroaryl scaffolds was synthesized. A reliable synthetic protocol toward 1,2,3-triazole- and isoxazole-functionalized anthracenes and pentacenes was developed based on copper-catalyzed cycloaddition of the appropriately substituted acene diols with azides or *in situ* generated nitrile oxides. The heteroaromatic scaffolds exhibiting electron withdrawing properties offer access to soluble and stabilized acenes after reductive aromatization. All novel anthracene and pentacene derivatives were characterized by NMR, cyclic voltammetry and UV-Vis spectroscopy. Photokinetic studies of 6,13-di-(1,2,3-triazole)-substituted pentacenes revealed improved air stability and high solubility compared to unsubstituted pentacene.

INTRODUCTION

Organo-electronics gained considerable scientific as well as commercial interest in recent years.^{1,2} Conductive organic π -conjugated molecules constitute essential components of device configurations. In particular the semiconducting material pentacene proved to be a reliable and highly efficient material in the area of organic field-effect transistors (OFETs).^{3,4} However, its application suffers from poor solubility and facile photo-degradation involving photooxidation⁵ and to a lesser extent photodimerization.⁶ Hence, numerous groups have put tremendous efforts in the design of novel stable and soluble pentacene-based materials by introducing appropriate substituents.⁷⁻⁹ A remarkable strategy, yielding both high performance (as a result of improved stacking) and better stability (due to electronic and steric effects), was developed by Anthony et al. by attaching sterically demanding triisopropylsilylethynyl substituents to the acene backbone.¹⁰⁻¹² The application of electron-accepting moieties in the 6,13-positions of the pentacene core represents another reliable strategy to achieve improved stability against photooxidation.^{7,9} Electron-withdrawing groups (e.g. $-\text{C}_6\text{F}_5$) are capable of depriving the π -conjugated system of electron density either through a resonance or inductive effect^{13,14} and decrease the HOMO and LUMO energy levels of acenes triggering an increase in stability. Hence, substitution of a conjugated core by electron-withdrawing groups generally leads to enhanced stability toward oxidation, a potential transition from p-type materials to ambipolar or n-type materials, and a change in molecular packing.¹⁵ In literature 1,2,3-triazole moieties are frequently presented as electron-withdrawing scaffolds exhibiting poor electron conduct or as photoluminescence quencher.¹⁶ Since the 1,2,3-triazole moiety provides adequate acceptor performance,^{17,18} the aim of this project is the incorporation of 1,2,3-triazoles and electronically similar isoxazoles as electron acceptor substituents in acene-based structures to improve both stability and OFET performance.

Due to the low photostability of higher acenes functionalization of 6,13-disubstituted pentacenes ought to be carried out applying mild reaction conditions and purification procedures. Herein we report reliable syntheses toward 1,2,3-triazole- and isoxazole-substituted acenes bearing different connectivities of the heteroaryl moiety to the acene backbone (Figure 1). The synthetic methodologies were designed for model compound anthracenes, but are sought to be also applicable for pentacene derivatives. The key step toward modified anthracenes was realized via Copper-catalyzed Azide-Alkyne Huisgen Cycloaddition (CuAAC, known as click chemistry¹⁹⁻²¹) of azides or cycloaddition of *in situ* generated nitrile oxides with alkyne-substituted dihydroanthracene diols, followed by reductive aromatization. A sequence of CuAAC and reductive aromatization was also applied toward pentacene derivatives (Figure 1).

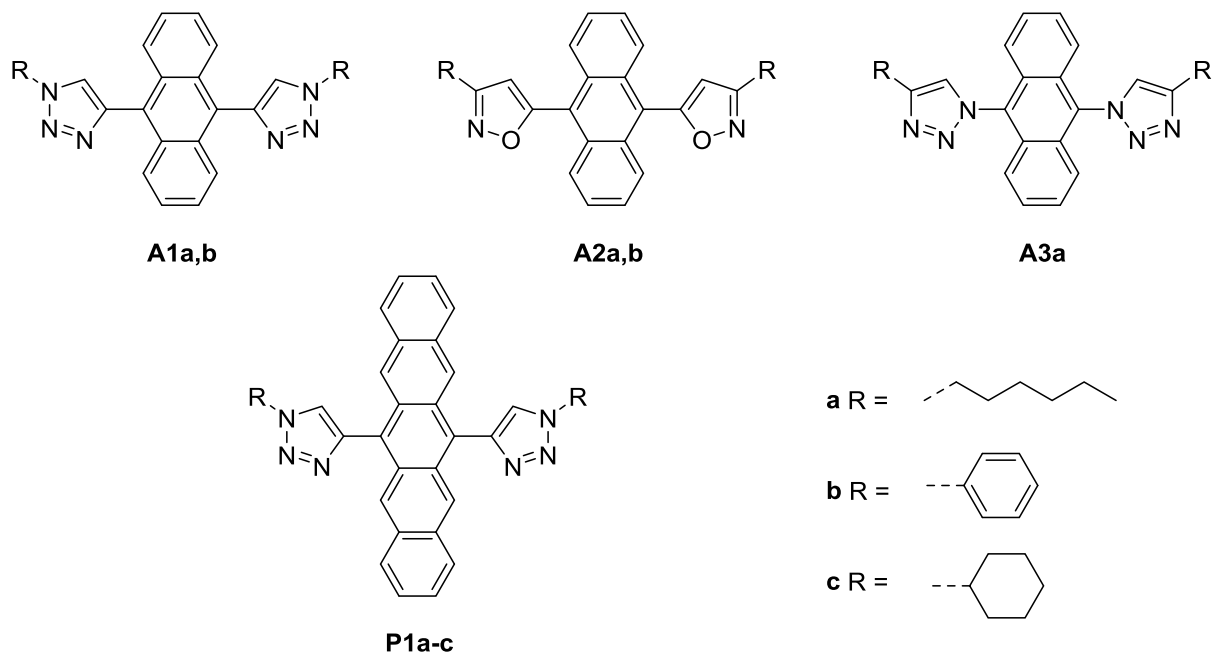


Figure 1: Synthetic target compounds based on anthracene and pentacene moieties.

All anthracene and pentacene compounds were characterized by optical and electrochemical means. Measurements of optical properties (absorption) and photodegradation kinetics of pentacene derivatives revealed the strong influence of the heterocycle's nature on the solubility and photostability.

EXPERIMENTAL SECTION

Substances purchased from commercial sources were used as received. Anhydrous acetonitrile (ACN), ethynyltrimethylsilane, 1-octyne, n-butyllithium solution (2.5 M in hexanes) and anthracene-9,10-dione were purchased from Aldrich Chemical Co. Pentacene-6,13-dione (CAS 3029-32-1),²² 2,2'-(9,10-anthracenediyl)bis[4,4,5,5-tetramethyl-1,3,2-dioxaborolane] (CAS 863992-56-7),²³ all azides,^{24,25} and oxime chlorides²⁶ were synthesized according to literature. Anhydrous tetrahydrofuran (THF), dichloromethane (DCM), diethyl ether, methanol (MeOH), and toluene were prepared immediately prior to use by a *PURESOLV*-plant (*it-innovative technology inc.*). Technical grade solvents were distilled prior to use. Analytical TLC was performed on Merck silica gel 60 F254 plates. Chromatographic separations at preparative scale were carried out on silica gel (Merck silica gel 60, 40 - 63 μm). Nuclear magnetic resonance (NMR) spectra were obtained using a Bruker Avance III HD 600 MHz with cryo probe, Avance III HD 400 MHz, Avance DRX-400 or DPX-200 fourier transform spectrometer operating at the following frequencies: Avance III HD 600 MHz: 600.2 MHz (^1H) and 150.9 MHz (^{13}C); Avance III HD 400 MHz and DRX-400: 400.1 MHz (^1H) and 100.6 MHz (^{13}C); DPX-200: 200.1 MHz (^1H) and 50.3 MHz (^{13}C). The chemical shifts are reported in δ units, parts per million (ppm) downfield from tetramethylsilane using residual solvent signals for calibration. Coupling constants are reported in Hertz; multiplicity of signals is indicated by using following abbreviations: s=singlet, d=doublet, t=triplet, q=quartet, quin=quintet. The multiplicity of

^{13}C signals was obtained by measuring JMOD spectra. UV-Vis absorption spectra were recorded in ACN or DCM solutions (5 μM) with a Perkin Elmer Lambda 750 spectrometer. Cyclic voltammetry was performed using a three electrode configuration consisting of a Pt working electrode, a Pt counter electrode and an Ag/AgCl reference electrode and a PGSTAT128N, ADC164, DAC164, External, DI048 potentiostat provided by Metrohm Autolab B. V. Measurements were carried out in a 0.5 mM solution in anhydrous DCM or 0.1 mM solution in anhydrous ACN with Bu_4NBF_4 (0.1 M) as the supporting electrolyte. The solutions were purged with argon for 15 minutes prior to measurement. HOMO and LUMO energy levels were calculated from the onset of oxidation and reduction, respectively. The onset potential was determined by the intersection of two tangents drawn at the background and the rising of oxidation. Ferrocene served as an external standard for calibrating the potential and calculating the HOMO levels (-4.8 eV). High-resolution mass spectra (HRMS) were acquired using a Thermo Scientific LTQ Orbitrap XL hybrid FTMS (Fourier Transform Mass Spectrometer) equipped with Thermo Fischer Exactive Plus Orbitrap (LC-ESI+) and a Shimadzu IT-TOF Mass Spectrometer.

The thermal behavior of substances **A1a,b**, **A2a,b** and **A3a** was studied with differential scanning calorimetry (DSC) and thermogravimetric analysis (TGA) using a Netzsch simultaneous thermal analyzer (STA 449 F1 Jupiter). Powder samples with a mass of approx. 10 mg were slightly pressed into the bottom of open aluminum pans and heated at 10 $^\circ\text{C}/\text{min}$ from 25 $^\circ\text{C}$ to 500 $^\circ\text{C}$ under N_2 gas at a flow rate of 40 mL/min. The STA 449 Type-K thermocouples were calibrated using indium, tin, bismuth and zinc metals.

trans-9,10-Dihydro-9,10-bis(trimethylsilylethynyl)anthracene-9,10-diol (**2**). Ethynyltrimethylsilane (2.94 g, 30 mmol, 3 eq.) was dissolved in 100 mL anhydrous THF and cooled to -60 $^\circ\text{C}$ under argon atmosphere. Subsequently n-BuLi (12.00 mL, 30 mmol, 3 eq.) was added slowly. The solution was stirred at room temperature for 45 min, cooled to -78 $^\circ\text{C}$ and anthracene-9,10-dione **1** (2.08 g, 10.0 mmol, 1 eq.) was added and stirred overnight. The reaction mixture was quenched with a saturated solution of NH_4Cl and the product was extracted with ethyl acetate. The product was purified by column chromatography (90 g silica gel, light petroleum / ethyl acetate 5:1) yielding **2** in 98% (3.96 g). ^1H NMR (200 MHz, CDCl_3): δ = 8.09 - 8.04 (m, 4 H), 7.50 - 7.45 (m, 4 H), 3.12 (s, 2 H), 0.18 (s, 18 H) ppm. ^{13}C NMR (50 MHz, CDCl_3): δ = 138.1 (s), 129.0 (d), 126.5 (d), 107.1 (s), 92.5 (s), 68.6 (s), -0.4 (q) ppm.

trans-6,13-Dihydro-6,13-bis(trimethylsilylethynyl)pentacene-6,13-diol (**8**). n-BuLi (2.5 M, 18 mL, 45 mmol, 3 eq.) was added dropwise to a solution of ethynyltrimethylsilane (4.42 g, 45 mmol, 3 eq.) in 75 ml abs. THF at -50 $^\circ\text{C}$. After the solution was stirred for 1.5 hours at constant temperature, pentacene-6,13-dione **7** (4.62 g, 15 mmol, 1 eq.) was added. The reaction mixture was slowly warmed to room temperature, stirred overnight and poured into a saturated solution of ammonium

chloride. After addition of chloroform, the organic layer was separated and the aqueous layer was extracted with chloroform. The combined organic solutions were washed with water and dried over anhydrous Na_2SO_4 . Afterwards the solvent was removed and the residue purified by column chromatography (light petroleum / ethyl acetate 5:1) to afford **8** (5.31 g, 70 %). $R_f = 0.73$ (DCM). ^1H NMR (CDCl_3 , 200 MHz): $\delta = 8.61$ (s, 4 H), 7.99 - 7.89 (m, 4 H), 7.59 - 7.50 (m, 4 H), 3.64 (s, 2 H), 0.22 (s, 18 H) ppm. ^{13}C NMR (50 MHz, CDCl_3): $\delta = 136.1$ (s), 133.1 (s), 128.2 (d), 126.9 (d), 125.7 (d), 106.8 (s), 93.6 (s), 69.7 (s), -0.3 (q) ppm.

Synthesis of 9,10-diazidoanthracene (**6**). 2,2'-(9,10-Anthracenediyl)bis[4,4,5,5-tetramethyl-1,3,2-dioxaborolane] **5** (714 mg, 1.66 mmol, 1 eq.), $\text{Cu}(\text{OAc})_2 \cdot \text{H}_2\text{O}$ (663 mg, 0.33 mmol, 0.2 eq.) and sodium azide (324 mg, 4.98 mmol, 3.0 eq.) were dissolved in 50 mL methanol. The solution was stirred under argon for 8 h at 55 °C. The reaction mixture was quenched by addition of water and extracted with Et_2O . The combined organic solutions were washed with water, dried over Na_2SO_4 and concentrated in vacuo. **6** (266 mg) was obtained as yellow solid in 61% yield after purification by column chromatography (90 g silica gel, light petroleum / ethyl acetate 10 \rightarrow 30%). ^1H NMR (600 MHz, CDCl_3): $\delta = 8.40 - 8.37$ (m, 4 H), 7.64 - 7.61 (m, 4 H) ppm. ^{13}C NMR (150 MHz, CDCl_3): $\delta = 129.7$ (s), 126.7 (d), 125.7 (s), 123.1 (d) ppm. HR-ESI-FTMS $[\text{M}+\text{Na}]^+$ m/z calcd. 283.0703 for $\text{C}_{14}\text{H}_8\text{N}_6\text{Na}^+$, found 283.0733.

General procedure for copper catalyzed azide-alkyne cycloaddition (CuAAC). Diol (1 eq.), potassium fluoride (2.4 eq.), $\text{CuSO}_4 \cdot 5\text{H}_2\text{O}$ (0.3 eq.), sodium ascorbate (0.6 eq.) and the appropriate azide or oxime chloride derivative (2.4 eq.) were dispersed in a mixture of water and tert-butyl alcohol (t-BuOH : H_2O , 1:1, ~0.1 M in regard to the diol). The dispersion was stirred under argon overnight at room temperature and afterwards poured onto chloroform. After the organic layer was separated, the aqueous layer was extracted with chloroform. The combined organic solutions were washed with water, dried over anhydrous Na_2SO_4 and concentrated in vacuo.

trans-9,10-Bis(1-hexyl-1*H*-1,2,3-triazol-4-yl)-9,10-dihydroanthracene-9,10-diol (**3a**). According to the general procedure KF (557 mg, 9.6 mmol), sodium ascorbate (476 mg, 2.4 mmol), $\text{CuSO}_4 \cdot 5\text{H}_2\text{O}$ (300 mg, 1.2 mmol), **2** (1.61 g, 4.0 mmol) and 1-azidohexane (1.22 g, 9.6 mmol) were suspended in 30 mL t-BuOH : H_2O (1:1). The suspension was stirred overnight and work-up proceeded according to the general procedure. **3a** was obtained in 79% yield (1.62 g). $R_f = 0.66$ (DCM : MeOH 9:1). ^1H NMR (400 MHz, CDCl_3): $\delta = 7.93$ (s, 2 H), 7.36 - 7.32 (m, 4 H), 7.22 - 7.19 (m, 4 H), 5.25 (s, 2 H), 4.34 (t, $J = 7.4$ Hz, 4 H), 1.97 - 1.89 (m, 4 H), 1.37 - 1.26 (m, 12 H), 0.89 (t, $J = 6.9$ Hz, 6 H) ppm. ^{13}C NMR (50 MHz, CDCl_3): $\delta = 154.1$ (s), 140.5 (s), 128.4 (d), 126.7 (d), 121.2 (s), 71.5 (s), 50.6 (t), 31.2 (t), 30.2 (t), 26.2 (t), 22.4 (t), 13.9 (q) ppm. HR-ESI-FTMS $[\text{M}+\text{H}]^+$ m/z calcd. 515.3129 for $\text{C}_{30}\text{H}_{39}\text{N}_6\text{O}_2^+$, found 515.3114.

trans-9,10-Dihydro-9,10-bis(1-phenyl-*1H*-1,2,3-triazol-4-yl)anthracene-9,10-diol (**3b**). According to the general procedure KF (418 mg, 7.2 mmol), sodium ascorbate (357 mg, 1.8 mmol), CuSO₄·5H₂O (225 mg, 0.9 mmol), **2** (1.21 g, 3.0 mmol) and azidobenzene (858 mg, 7.2 mmol) were suspended in 30 mL t-BuOH : H₂O (1:1). The suspension was stirred overnight and work-up proceeded according to the general procedure. **3b** was obtained in 49% yield (734 mg) as colorless solid. R_f = 0.80 (DCM : MeOH 9:1). ¹H NMR (200 MHz, DMSO-d₆): δ = 9.01 (s, 2 H), 8.03 - 8.01 (m, 4 H), 7.64 - 7.60 (m, 4 H), 7.53 - 7.49 (m, 2 H), 7.46 - 7.44 (m, 4 H), 7.33 - 7.31 (m, 4 H), 7.01 (s, 2 H) ppm. ¹³C NMR (100 MHz, DMSO-d₆): δ = 155.4 (s), 140.7 (s), 136.6 (s), 129.8 (d), 128.6 (d), 127.8 (d), 127.2 (d), 120.7 (d), 120.0 (d), 70.5 (s) ppm. HR-ESI-FTMS [M+H]⁺ m/z calcd. 499.1877 for C₃₀H₂₃N₆O₂⁺, found 499.1863.

trans-9,10-Bis(3-hexylisoxazol-5-yl)-9,10-dihydroanthracene-9,10-diol (**4a**). According to the general procedure KF (417 mg, 7.2 mmol), sodium ascorbate (357 mg, 1.8 mmol), CuSO₄·5H₂O (225 mg, 0.9 mmol), **2** (1.21 g, 3.0 mmol), and *N*-hydroxyheptanimidoyl chloride (1.17 g, 7.2 mmol) were suspended in 30 mL t-BuOH : H₂O (1:1). The suspension was stirred overnight and work-up proceeded according to the general procedure. Purification of the product was achieved by column chromatography (light petroleum / ethyl acetate 15 -> 30%). **4a** was obtained in 22% yield (336 mg). R_f = 0.52 (DCM : MeOH 9:1). ¹H NMR (200 MHz, CDCl₃): δ = 7.51 - 7.45 (m, 4 H), 7.40 - 7.34 (m, 4 H), 6.47 (s, 2 H), 3.26 (bs, 2 H), 2.68 - 2.60 (m, 4 H), 1.71 - 1.59 (m, 4 H), 1.40 - 1.26 (m, 12 H), 0.89 (t, J = 6.6 Hz, 6 H) ppm. ¹³C NMR (50 MHz, CDCl₃): δ = 174.9 (s), 164.1 (s), 137.1 (s), 129.5 (d), 127.5 (d), 101.8 (d), 71.5 (s), 31.4 (t), 28.9 (t), 28.1 (t), 26.1 (t), 22.5 (t), 14.0 (q) ppm. HR-ESI-FTMS [M+H]⁺ m/z calcd. 515.2904 for C₃₂H₃₉N₂O₄⁺, found 515.2897.

trans-9,10-Dihydro-9,10-bis(3-phenylisoxazol-5-yl)anthracene-9,10-diol (**4b**). According to the general procedure KF (417 g, 7.20 mmol), sodium ascorbate (357 mg, 1.80 mmol), CuSO₄·5H₂O (225 mg, 0.90 mmol), **2** (1.21 g, 3.00 mmol, 1.00 eq.), and *N*-hydroxybenzenecarboximidoyl chloride (1.12 g, 7.20 mmol) were suspended in 30 mL t-BuOH : H₂O (1:1). The suspension was stirred overnight and work-up proceeded according to the general procedure. Product **4b** was obtained in 43% yield (651 mg). R_f = 0.48 (DCM : MeOH 9:1). F_p = 134.8 -135.5 °C. ¹H NMR (200 MHz, DMSO-d₆): δ = 8.09 - 8.06 (m, 4 H), 7.62 - 7.59 (m, 4 H), 7.32 - 7.16 (m, 12 H), 5.76 (s, 2 H) ppm. ¹³C NMR (50 MHz, DMSO-d₆): δ = 174.5 (s), 160.8 (s), 138.0 (s), 129.7 (d), 128.5 (d), 128.2 (d), 127.9 (s), 126.2 (d), 126.2 (d), 100.7 (s), 68.6 (s) ppm. HR-ESI-FTMS [M+H]⁺ m/z calcd. 499.1652 for C₃₂H₂₃N₂O₄⁺, found 499.1644.

trans-6,13-Bis(1-hexyl-*1H*-1,2,3-triazol-4-yl)-6,13-dihydropentacene-6,13-diol (**9a**). The synthesis of **9a** was carried out according to the general reaction procedure. Starting from **8** (1.01 g, 2 mmol), potassium fluoride (279 mg, 4.8 mmol), CuSO₄·5H₂O (149 mg, 0.6 mmol), sodium ascorbate (238 mg, 1.2 mmol) and hexyl azide (601 mg, 4.8 mmol) **9a** (826 mg) was obtained in 68% yield after

recrystallization from acetonitrile. $R_f = 0.52$ (DCM : MeOH 9:1). $^1\text{H NMR}$ (200 MHz, CD_2Cl_2): $\delta = 8.07$ (s, 2 H), 7.92 (s, 4 H), 7.72 - 7.67 (m, 4 H), 7.41 - 7.35 (m, 4 H), 5.70 (bs, 2 H), 4.37 (t, $J = 7.4$ Hz, 2 H), 1.96 (quin, $J = 7.4$ Hz, 4 H), 1.41 - 1.26 (m, 12 H), 0.90 (t, $J = 6.6$ Hz, 6 H) ppm. $^{13}\text{C NMR}$ (50 MHz, CDCl_3): $\delta = 154.7$ (s), 138.8 (s), 133.3 (s), 127.9 (d), 126.5 (d), 126.2 (d), 121.4 (d), 72.3 (s), 50.6 (t), 31.1 (t), 30.2 (t), 26.2 (t), 22.4 (t), 13.9 (q) ppm. HR-ESI-FTMS $[\text{M}+\text{H}]^+$ m/z calcd. 615.3442 for $\text{C}_{38}\text{H}_{43}\text{N}_6\text{O}_2^+$, found 615.3482.

trans-6,13-Dihydro-6,13-bis(1-phenyl-1*H*-1,2,3-triazol-4-yl)pentacene-6,13-diol (**9b**). The synthesis of **9b** was carried out according to the general reaction procedure. Starting from **8** (1.01 g, 2 mmol), potassium fluoride (279 mg, 4.8 mmol), $\text{CuSO}_4 \cdot 5\text{H}_2\text{O}$ (149 mg, 0.6 mmol), sodium ascorbate (238 mg, 1.2 mmol) and phenyl azide (572 mg, 4.8 mmol) **9b** (870 mg, 72 %) was obtained after column chromatography (90g SiO_2 , light petroleum : ethyl acetate 25% \rightarrow 50%). $R_f = 0.80$ (DCM : MeOH 9:1). $^1\text{H NMR}$ (600 MHz, CD_2Cl_2): $\delta = 8.65$ (s, 2 H), 8.08 (s, 4 H), 7.89-7.87 (m, 4 H), 7.82 - 7.80 (m, 4 H), 7.61 - 7.58 (m, 4 H), 7.51 - 7.48 (m, 2 H), 7.47 - 7.44 (m, 4 H), 5.59 (s, 2 H) ppm. $^{13}\text{C NMR}$ (150 MHz, CD_2Cl_2): $\delta = 156.0$ (s), 139.3 (s), 137.8 (s), 133.8 (s), 130.4 (d), 129.4 (d), 128.4 (d), 127.3 (d), 127.2 (d), 121.0 (d), 120.5 (d), 72.8 (s) ppm. HR-ESI-FTMS $[\text{M}+\text{Na}]^+$ m/z calcd. 621.2009 for $\text{C}_{38}\text{H}_{26}\text{N}_6\text{O}_2\text{Na}^+$, found 621.2023.

trans-6,13-Bis(1-cyclohexyl-1*H*-1,2,3-triazol-4-yl)-6,13-dihydropentacene-6,13-diol (**9c**). The synthesis of **9c** was carried out according to the general reaction procedure. Starting from **8** (1.01 g, 2 mmol), KF (279 mg, 4.8 mmol), sodium ascorbate (238 mg, 1.2 mmol), $\text{CuSO}_4 \cdot 5\text{H}_2\text{O}$ (149 mg, 0.6 mmol) and cyclohexyl azide (611 mg, 4.8 mmol) **9c** (826 mg, 68 %) was obtained after recrystallization from acetonitrile. $R_f = 0.56$ (DCM : MeOH 9:1). $^1\text{H NMR}$ (400 MHz, CDCl_3): $\delta = 8.12$ (s, 2 H), 7.92 (s, 4 H), 7.74 - 7.72 (m, 4 H), 7.40 - 7.38 (m, 4 H), 4.55 - 4.47 (m, 2 H), 2.34 - 1.25 (m, 20 H) ppm. $^{13}\text{C NMR}$ (100 MHz, CDCl_3): $\delta = 154.1$ (s), 139.0 (s), 133.1 (s), 128.0 (d), 126.5 (d), 126.2 (d), 119.2 (d), 72.4 (s), 60.3 (d), 33.6 (t), 25.2 (t), 25.2 (t) ppm. HR-ESI-FTMS $[\text{M}+\text{H}]^+$ m/z calcd. 611.3129 for $\text{C}_{38}\text{H}_{39}\text{N}_6\text{O}_2^+$, found 611.3117.

1,1'-(9,10-Anthracenediyl)-bis[4-hexyl-1*H*-1,2,3-triazole] (**A3a**). The synthesis of **A3a** was carried out according to the general reaction procedure. Starting from **6** (270 mg, 1.04 mmol), potassium fluoride (145 mg, 2.49 mmol), $\text{CuSO}_4 \cdot 5\text{H}_2\text{O}$ (78 mg, 0.31 mmol), sodium ascorbate (123 mg, 0.62 mmol) and 1-octyne (274 mg, 2.49 mmol) **A3a** (292 mg) was obtained in 59% yield after purification by column chromatography (90 g silica gel, light petroleum : ethyl acetate 2 \rightarrow 10%). $R_f = 0.63$ (light petroleum : ethyl acetate 2:1). $^1\text{H NMR}$ (200 MHz, CDCl_3): $\delta = 7.77$ (s, 2 H), 7.57 - 7.54 (m, 4 H), 7.38 - 7.35 (m, 4 H), 2.99 (t, $J = 7.6$ Hz, 4 H), 1.89 (t, $J = 7.6$ Hz, 4 H), 1.63 - 1.48 (m, 4 H), 1.42 - 1.35 (m, 8 H), 0.93 (t, $J = 6.7$ Hz, 6H) ppm. $^{13}\text{C NMR}$ (100 MHz, CDCl_3): $\delta = 148.8$ (s), 131.2 (s), 128.4 (d), 128.3 (s), 125.3 (d), 122.5 (d), 31.6 (t), 29.4 (t), 29.0 (t), 25.7 (t), 22.6 (t), 14.0 (q) ppm. HR-ESI-FTMS $[\text{M}+\text{H}]^+$ m/z calcd. 481.3074 for $\text{C}_{30}\text{H}_{37}\text{N}_6^+$, found 481.3059.

General procedure for reduction of the functionalized anthracene and pentacene diols. SnCl₂ (4 eq.) was added to a dispersion of diol **3a,b**, **4a,b**, **9a** or **9c** (1 eq.) in acetonitrile (~0.05 M) and the mixture was stirred under argon atmosphere overnight at room temperature. The synthesis of pentacene derivatives had to be carried under exclusion of ambient light and oxygen. Furthermore all solvents were purged with argon before use. The work-up for both pentacene and anthracene derivatives was achieved by filtration of the precipitate. Anthracenes were washed with DCM, whereas pentacene derivatives were washed with methanol, water and acetonitrile. The obtained solids were dried in vacuo.

4,4'-(9,10-Anthracenediyl)bis[1-hexyl-*IH*-1,2,3-triazole] (**A1a**). According to the general procedure **A1a** was obtained by reduction of **3a** (1.33 g, 2.6 mmol) with SnCl₂ (1.90 g, 10.0 mmol). Product **A1a** was obtained in 91% (1.13 g) yield. R_f = 0.49 (DCM : MeOH 9:1). ¹H NMR (400 MHz, CDCl₃): δ = 7.82 - 7.80 (m, 4 H), 7.79 (s, 2 H), 7.39 - 7.37 (m, 4 H), 4.57 (t, J = 7.1 Hz, 4 H), 2.11 (quin, J = 7.1 Hz, 4 H), 1.49 - 1.36 (m, 12 H), 0.93 (t, J = 6.8 Hz, 6 H) ppm. ¹³C NMR (100 MHz, CDCl₃): δ = 143.9 (s), 131.0 (s), 126.6 (s), 126.2 (d), 125.8 (d), 124.7 (d), 50.6 (t), 31.2 (t), 30.4 (t), 26.2 (t), 22.4 (t), 13.9 (q) ppm. HR-ESI-FTMS [M+H]⁺ m/z calcd. 481.3074 for C₃₀H₃₇N₆⁺, found 481.3066.

4,4'-(9,10-Anthracenediyl)bis[1-phenyl-*IH*-1,2,3-triazole] (**A1b**). According to the general procedure **A1b** was obtained by reduction of **3b** (499 mg, 1.0 mmol) with SnCl₂ (758 mg, 4.0 mmol). Product **A1b** was obtained in 93% (430 mg) yield. R_f = 0.42 (light petroleum : ethyl acetate 2:1). ¹H NMR (600 MHz, CDCl₃): δ = 8.31 (s, 2 H), 7.98 - 7.94 (m, 8 H), 7.65 - 7.62 (m, 4 H), 7.54 - 7.51 (m, 2 H), 7.48 - 7.45 (m, 4 H) ppm. ¹³C NMR (150 MHz, CDCl₃): δ = 144.7 (s), 137.1 (s), 131.1 (s), 129.9 (d), 128.9 (d), 126.3 (d), 126.2 (s), 126.2(d), 122.9 (d), 120.5 (d) ppm. HR-ESI-FTMS [M+H]⁺ m/z calcd. 465.1822 for C₃₀H₂₁N₆⁺, found 465.1813.

5,5'-(9,10-Anthracenediyl)bis[3-hexylisoxazole] (**A2a**). According to the general procedure **A2a** was obtained by reduction of **4a** (134 mg, 0.26 mmol) with SnCl₂ (197 mg, 1.04 mmol). Product **A2a** was obtained as yellow solid in 50% (62 mg) yield. R_f = 0.67 (DCM). ¹H NMR (400 MHz, CDCl₃): δ = 7.85 - 7.82 (m, 4 H), 7.52 - 7.49 (m, 4 H), 6.51 (s, 2 H), 2.91 (t, J = 7.6 Hz, 4 H), 1.86 (quin, J = 7.6 Hz, 4 H), 1.55 - 1.48 (m, 4 H), 1.42 - 1.36 (m, 8 H), 0.94 (t, J = 7.4 Hz 6 H) ppm. ¹³C NMR (100 MHz, CDCl₃): δ = 167.3 (s), 164.4 (s), 130.5 (s), 126.8 (d), 125.8 (d), 125.4 (s), 107.0 (d), 31.6 (t), 29.0 (t), 28.5 (t), 26.3 (t), 22.6 (t), 14.0 (q) ppm. HR-ESI-FTMS [M+H]⁺ m/z calcd. 481.2850 for C₃₂H₃₇N₂O₂⁺, found 481.2873.

5,5'-(9,10-Anthracenediyl)bis[3-phenylisoxazole] (**A2b**). According to the general procedure **A2b** was obtained by reduction of **4b** (299 mg, 0.6 mmol) with SnCl₂ (455 mg, 2.4 mmol). Product **A2b** was obtained as yellow solid in 45% (125 mg) yield. R_f = 0.69 (DCM). ¹H NMR (600 MHz, CDCl₃): δ = 8.03 - 8.01 (m, 4 H), 7.97 - 7.94 (m, 4 H), 7.58 - 7.52 (m, 10 H), 7.02 (s, 2 H) ppm. ¹³C NMR

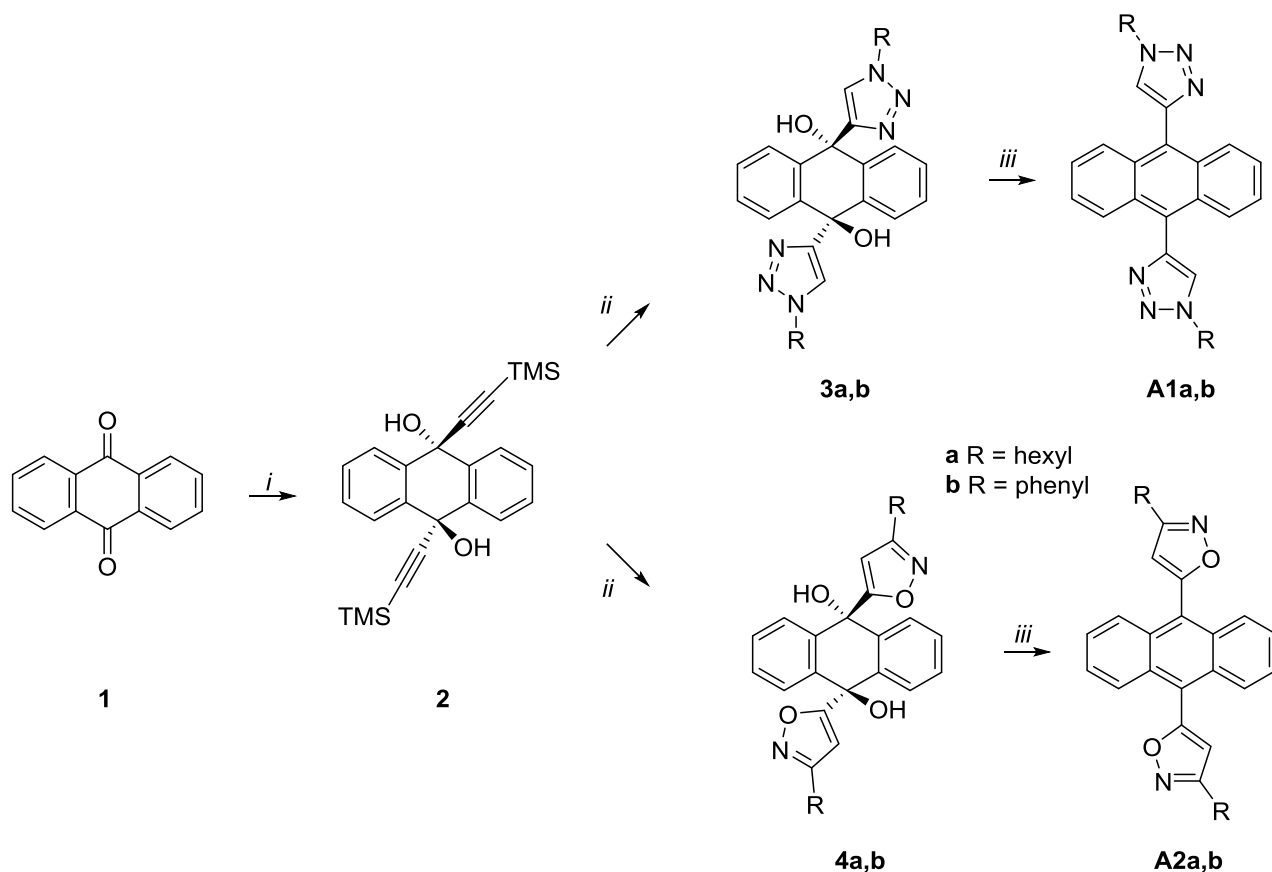
(150 MHz, CDCl₃): δ = 168.3 (s), 162.7 (s), 130.5 (s), 130.3 (d), 129.1 (d), 128.9 (s), 127.1 (d), 127.0 (d), 125.8 (d), 125.1 (s), 105.4 (d) ppm. HR-ESI-FTMS [M+H]⁺ m/z calcd. 465.1598 for C₃₂H₂₁N₂O₂⁺, found 465.1595.

4,4'-(6,13-Pentacenediyl)bis[1-hexyl-*IH*-1,2,3-triazole] (**P1a**). The synthesis of **P1a** was carried out according to the general reaction procedure. Starting from **9a** (824 mg, 1.34 mmol) and SnCl₂ (1.02 g, 5.36 mmol), **P1a** was obtained as dark blue solid, after column chromatography (90 g silica gel, DCM / degassed anhydrous MeOH 5 → 10%) in 94% yield (546 mg). ¹H NMR (400 MHz, CD₂Cl₂): δ = 8.48 (s, 4 H), 8.02 (s, 2 H), 7.79 - 7.74 (m, 4 H) ppm, 7.29 - 7.24 (m, 4 H), 4.65 (t, J = 7.1 Hz, 4 H), 2.18 - 2.11 (m, 4 H), 1.46 - 1.37 (m, 8 H), 1.28 - 1.20 (m, 4 H), 0.97 (t, J = 7.0 Hz, 6 H) ppm. ¹³C NMR (100 MHz, CD₂Cl₂): δ = 144.7 (s), 132.1 (s), 130.1 (s), 128.9 (d), 127.3 (s), 126.2 (d), 126.0 (d), 125.5 (d), 51.3 (t), 31.9 (t), 31.0 (t), 27.0 (t), 23.2 (t), 14.4 (q) ppm; HR-ESI-FTMS [M+H]⁺ m/z calcd. 581.3387 for C₃₈H₄₁N₆⁺, found 581.3378.

4,4'-(6,13-Pentacenediyl)bis[1-cyclohexyl-*IH*-1,2,3-triazole] (**P1c**). The synthesis of **P1c** was carried out according to the general reaction procedure. Starting from **9c** (776 mg, 1.27 mmol) and SnCl₂ (960 mg, 5.06 mmol), **P1c** was obtained as dark blue solid after purification by column chromatography (90 g silica gel, DCM / degassed anhydrous MeOH 5 → 10%) in 95% yield (578 mg). ¹H NMR (400 MHz, CD₂Cl₂): δ = 8.50 (s, 4 H), 8.03 (s, 2 H), 7.83 - 7.79 (m, 4 H), 7.33 - 7.29 (m, 4 H), 4.82 - 4.65 (m, 2 H), 2.57 - 2.52 (m, 4 H), 2.10 - 2.00 (m, 8 H), 1.90 - 1.83 (m, 2 H), 1.70 - 1.59 (m, 4 H), 1.48 - 1.38 (m, 2 H) ppm. ¹³C NMR (100 MHz, CD₂Cl₂): δ = 144.3 (s), 132.0 (s), 130.1 (s), 129.0 (d), 127.4 (s), 126.2 (d), 125.6 (d), 124.0 (d), 61.2 (d), 34.4 (t), 25.9 (t), 25.9 (t) ppm; HR-ESI-FTMS [M+H]⁺ m/z calcd. 611.3129 C₃₈H₃₉N₆O₂⁺, found 611.3123.

RESULTS AND DISCUSSION

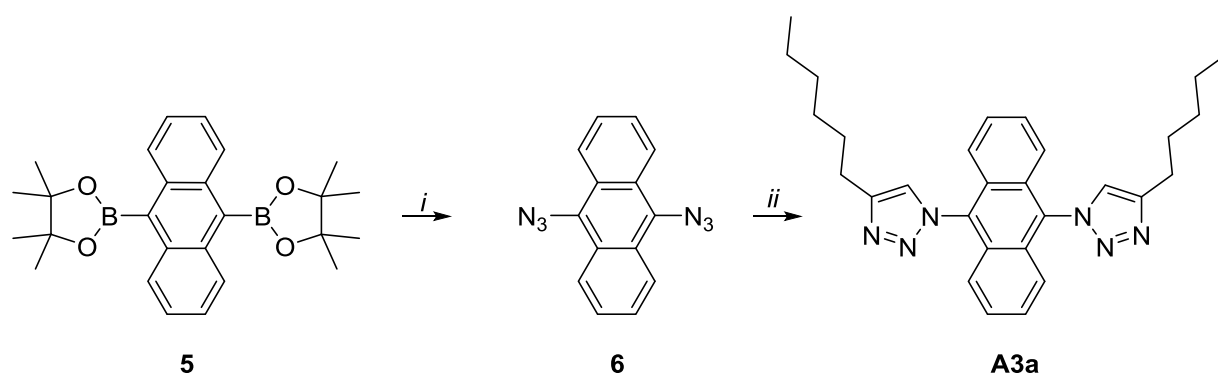
Since post-synthetic modification of pentacene frameworks is known to be difficult because of the low photostability of the acene backbone, a general mild synthetic protocol was sought suitable for both model anthracene derivatives **A1a,b**, **A2a,b** and **A3a** as well as pentacenes **P1a-c**. Target compounds were planned combining 9,10-disubstituted anthracene or 6,13-disubstituted pentacene cores with electron-withdrawing structural scaffolds like 1,2,3-triazoles or isoxazoles.



Scheme 1: Synthetic pathways toward 9,10-triazole- and isoxazole-substituted anthracenes; *i*: ethynyltrimethylsilane, *n*-BuLi, THF; *ii*: alkyl/aryl azide or imidoyl chloride, CuSO₄·5H₂O, Na-ascorbate, KF, *t*-BuOH/H₂O, 50 °C, *iii*: SnCl₂, ACN, rt.

Synthetic pathways were initially probed toward anthracene derivatives **A1a,b**, **A2a,b** and **A3a**. Nucleophilic addition of *in situ* generated lithium (trimethylsilyl)acetylide to commercially available anthracene-9,10-dione following a procedure by Taylor et al.²⁷ resulted in a mixture of diol isomers in 66% total yield (*trans*-isomer 46%; *cis*-isomer 20%). After optimization of the reaction conditions by applying tetrahydrofuran as solvent at -78 °C *trans*-isomer **2** was obtained selectively in 98%. The introduction of 1,2,3-triazoles or isoxazoles was achieved by *in situ* deprotection of the terminal alkyne groups applying potassium fluoride and subsequent copper catalyzed cycloaddition as the key step toward electron-accepting moieties. All cycloadditions could be accomplished in good to excellent yields. Reductive aromatization of diols **3a,b** and **4a,b** applying anhydrous SnCl₂ afforded anthracenes **A1a,b** and **A2a,b** (Scheme 1)

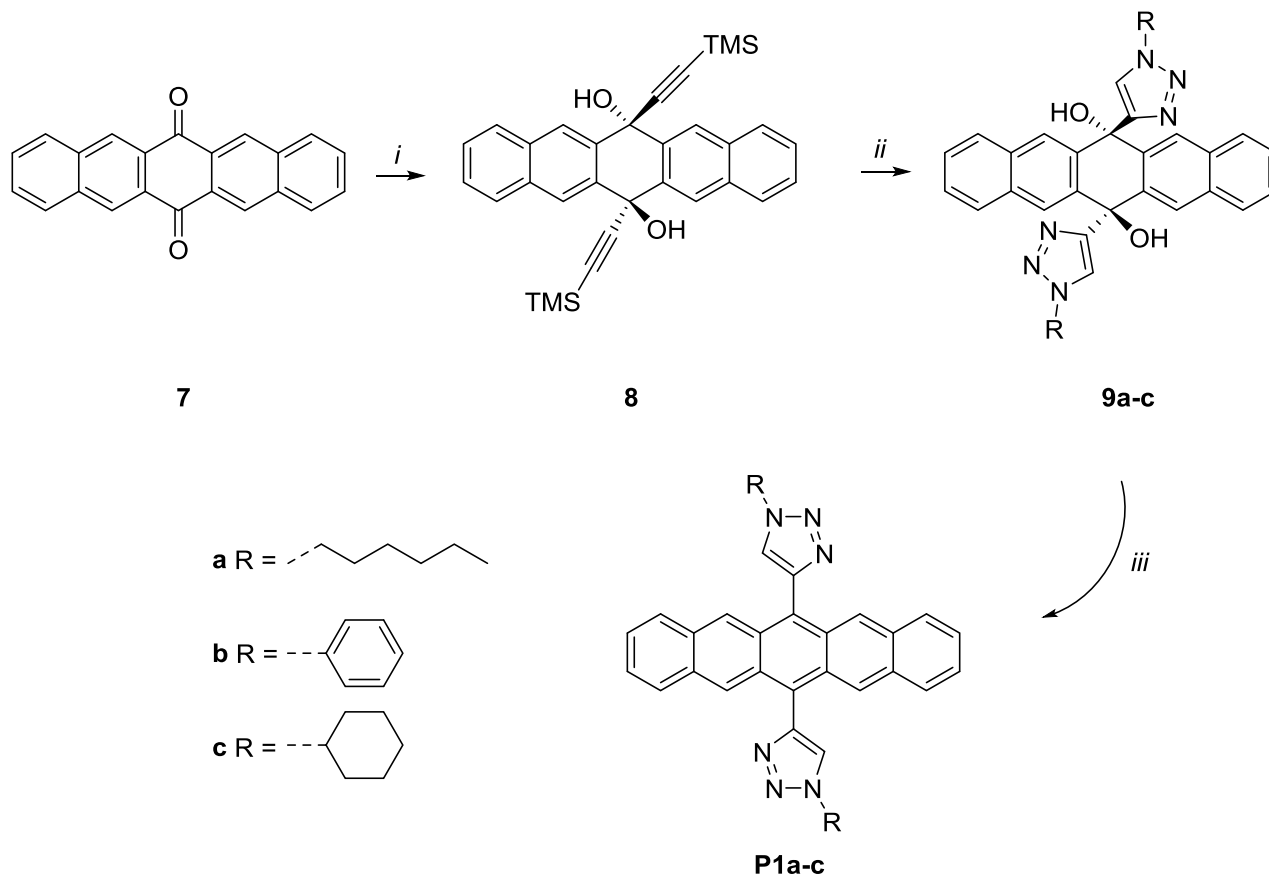
The synthetic key step toward regioisomer **A3a** was realized by copper catalyzed Huisgen cycloaddition of 1-octyne and 9,10-diazidoanthracene **6**, which was synthesized applying a copper catalyzed procedure starting from diboronate **5** according to Grimes et al.²⁸ (Scheme 2).



Scheme 2: Synthetic pathway toward compound **A3a**: *i*: NaN_3 , $\text{Cu}(\text{OAc})_2 \cdot \text{H}_2\text{O}$, *ii*: 1-octyne, $\text{CuSO}_4 \cdot 5\text{H}_2\text{O}$, Na-ascorbate, KF, t-BuOH/ H_2O , 50 °C.

The synthetic protocol was further applied toward pentacene (Scheme 3): nucleophilic addition of *in situ* generated lithium (trimethylsilyl)acetylide to pentacene-6,13-dione readily provided *trans*-diol **8** in 70% yield. The relative stereochemistry of **8** could be deduced from an X-ray measurement of the successive compound **9b** (given in the supporting information).

The introduction of 1,2,3-triazoles was again achieved by *in situ* deprotection of the terminal alkyne groups of **8** applying potassium fluoride and subsequent copper catalyzed cycloaddition yielding triazole-substituted **9** (Scheme 3). Applying the same synthetic protocol toward isoxazole-substituted pentacene derivatives, however, proved to be more troublesome, since the obtained diols were highly unstable and therefore, further synthetic efforts were focused on triazole-based compounds only. Pentacene precursors **9** were subjected to reductive aromatization using an excess of SnCl_2 in degassed acetonitrile under strict exclusion of ambient light. The resulting mixture turned deep blue, and reaction progress monitored by TLC showed complete conversion after approx. 4 - 6 h. The resulting pentacenes could be isolated by filtration and subsequent washing with water, methanol and acetone. However, phenyl-substituted **P1b** proved to be insoluble in organic solvents and therefore was not subjected to further purification and characterization. Instead, **P1c** bearing a cyclohexyl substituent attached to the triazole moiety was synthesized via **9c** to achieve better solubility. Pure products **P1a** and **P1c** were obtained in high yields by column chromatography under exclusion of ambient light applying degassed solvents. Both pentacene derivatives are soluble in common organic solvents such as CH_2Cl_2 , CHCl_3 , THF, and toluene and appear dark blue in color. The characterization of **P1a** and **P1c** was performed by ^1H / ^{13}C NMR spectroscopy and HR-MS analysis. The data are consistent with the proposed structural formulations.



Scheme 3: Synthetic pathway toward **P1a-c**. Reaction conditions: *i*: ethynyltrimethylsilane, *n*-BuLi, THF, *ii*: alkyl/aryl azide, $\text{CuSO}_4 \cdot 5\text{H}_2\text{O}$, Na-ascorbate, KF, *t*-BuOH/ H_2O , 50 °C, *iii*: SnCl_2 , ACN, rt.

In order to evaluate general physical properties and to determine electrochemical characteristics of both anthracene **A1a,b**, **A2a,b** and **A3a** as well as pentacene derivatives **P1a** and **P1c**, UV-Vis spectroscopy and cyclic voltammetric methods were applied (Table 1).

Electronic absorption characteristics of molecules **A1a,b**, **A2a,b** and **A3a** were recorded in degassed 5 μM ACN solutions, and representative spectra are presented in Figure 3 (left). Both 1,2,3-triazole- and isoxazole-containing anthracenes show characteristic absorptions in the lower energy region: a series of four absorption maxima at approximately 394, 374, 356 and 338 nm is evident. Interestingly, little changes in the absorption maxima values (± 1 nm) are observed by varying either the heterocyclic moieties or the substituent on the heterocycle (**A1a,b** and **A2a,b**), whereas **A3a** shows a hypsochromic shift of about 4 nm.

The electronic absorption characteristics of pentacenes **P1a** and **P1c** were examined in degassed 5 μM CH_2Cl_2 solutions and representative spectra are presented in Figure 3 (right). Both triazole containing pentacenes showed characteristic absorption maxima at approximately 601, 556 and 517 nm (Figure 3, Table 1) with little change of position upon variation of the substituent (hexyl or cyclohexyl) on the 1,2,3-triazole. A clear bathochromic shift of about 24 nm is evident for triazole-

substituted pentacenes **P1a** and **P1c** compared to pentacene, which also manifests in the reduced bandgap (Table 1).

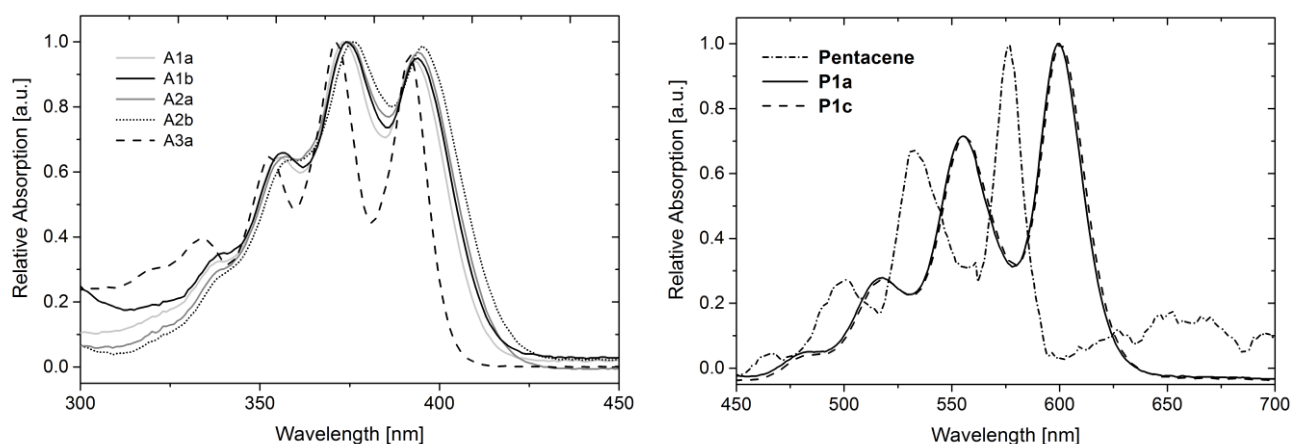


Figure 3: Absorption spectra of anthracene (left) in ACN and pentacene (right) derivatives in DCM solution.

Electrochemical properties of both anthracenes **A1a,b**, **A2a,b** and **A3a** as well as pentacene derivatives **P1a** and **P1c** (see supporting information) were determined by cyclic voltammetric methods. The first oxidation potentials were used to determine the HOMO energy levels. The obtained data outlined in Table 1 clearly show that the HOMOs of triazole-substituted anthracenes **A1a** and **A1b** are slightly higher in energy compared to unsubstituted anthracene, whereas the HOMOs of isoxazole-substituted anthracenes **A2a** and **A2b** are about 0.3 eV lower. The HOMO of triazole-substituted **A3a** is the lowest in energy at -6.01 eV, probably due to the direct linkage of the acene backbone to the heteroatom of the heterocycle. The LUMO levels were determined from optical bandgap and the HOMO energy level and range from -2.65 to -2.96 eV. The pertinent data are depicted in Table 1. The photo-physical and electrochemical properties obtained for the anthracene derivatives reveal a clear trend: a distinct reduction of the bandgap is evident, while the HOMO level is slightly decreased or nearly the same as for unsubstituted anthracene. Therefore, in terms of enhancing the stability of acenes and at the same time reducing the bandgap the introduction of heterocycles appears to be a suitable methodology.

The electrochemical characteristics of pentacene derivatives **P1a** and **P1c** (determined as 0.5 mM argon purged solutions in DCM) also reveal only small variations of HOMO levels (-5.02 eV to -5.03 eV). However, the HOMO level is clearly about 0.1 eV lower in energy compared to unsubstituted pentacene contributing to higher stability of **P1a** and **P1c**. The LUMO levels were determined from optical bandgap and the HOMO energy level (Table 1).

Table 1: Experimental data and physical characterization of target compounds.

Comp.	F _p ^a (°C)	T _d ^b (°C)	λ _{max} ^c (nm)	Bandgap ^d (nm, eV)	HOMO/LUMO ^e (eV)	HOMO/LUMO ^f (eV) calc	Bandgap ^g (eV) calc
Anthracene			376, 357, 340, 324	383, 3.24	-5.68/-2.44	-5.55/-2.00	3.56
A1a	204	355	393, 373, 355, 337	412, 3.01	-5.62/-2.61	-5.39/-2.01	3.39
A1b	-	348	394, 374, 356, 338	414, 2.99	-5.67/-2.68	-5.54/-2.14	3.39
A2a	-	322	394, 374, 357, 338	416, 2.98	-5.91/-2.93	-5.84/-2.48	3.36
A2b	293	351	395, 376, 357, 338	418, 2.97	-5.91/-2.94	-5.91/-2.56	3.35
A3a	182	307	392, 371, 353, 333	403, 3.08	-6.01/-2.93	-6.16/-2.74	3.42
Pentacene			577, 532, 499	592, 2.10	-4.90 ²⁹ /-3.00	-4.92/-2.73	2.19
P1a	-		601, 556, 517	626, 1.98	-5.03/-3.05	-4.81/-2.69	2.12
P1c	-	305	601, 556, 517	626, 1.98	-5.02/-3.04	-4.76/-2.65	2.11

^a Obtained from DSC measurements. ^b Thermal decomposition temperature determined from 5% mass loss. ^c Anthracenes measured in acetonitrile and pentacenes in DCM solution. ^d Optical bandgaps determined from the onset of lowest energy visible band. ^e HOMO-levels determined from solutions measured in ACN for anthracene and in DCM for pentacene derivatives. All E_{ox} data are reported relative to ferrocene (Fc/Fc⁺, E_{ox} = 354 mV in ACN; Fc/Fc⁺, E_{ox} = 453 mV in DCM). The concentration of the compounds used in these experiments was 0.1 mM for anthracene derivatives in ACN and 0.5 mM for pentacene derivatives in DCM; the scan rate was 50 mV s⁻¹. LUMO levels were determined from the optical bandgap and the HOMO energy level according to the following equation: E_{LUMO} = E_{HOMO} + E_g. ^f Calculated HOMO/LUMO levels (B3LYP / 6-311+G(d)). ^g Calculated bandgaps (B3LYP / 6-311+G(d)).

These experiments are supported by quantum chemical calculations of target compounds **A1a,b**, **A2a,b**, **A3a**, **P1a** and **P1c**. Values for the HOMO and LUMO orbital energy levels, calculated at the B3LYP/6-11+G(d) level, are listed in Table 1, along with the experimental optical gap. Comparison of theoretical calculations for the HOMO-LUMO gap and the experimentally measured gaps from UV-Vis data indicates good agreement between theory and experiment.

Thermal properties of both anthracene and pentacene derivatives were investigated by DSC and TGA measurements. Glass-forming properties and thermal stability of the compounds were examined by simultaneous thermal analysis (STA). The melting points (F_p) were estimated from DSC curves for **A1a**, **A2b**, and **A3a** (see supporting information) and range from 182 to 293 °C. The phenyl-substituted derivative **A2b** shows the highest melting point, while **A1b** and **A2a** do not melt before decomposition. All materials exhibit high thermal stability as evidenced by decomposition temperatures corresponding to 5% mass loss between 307 and 355 °C (Table 1). Pentacene derivative **P1c** shows no melting point and no glass transition points, but a decomposition temperature corresponding to 5% mass loss at 305 °C (Table 1).

In order to evaluate the stability of **P1a** and **P1c** kinetic analyses of the photooxidation were conducted by separately dissolving purified pentacenes in degassed CH_2Cl_2 to give 10^{-4} M stock solutions followed by exposure to ambient light and air at 22 °C for prolonged periods. UV-Vis spectra were recorded of solutions (diluted to 10^{-5} M) at regular intervals enabling a quantitative determination of absorbance-time profiles for both the starting pentacenes **P1a** and **P1c** (Figure 4, D). The solutions gradually became colorless by exposure to ambient conditions. Oxidation products were characterized by ^1H NMR spectroscopy (given in the supporting information). A distinct high field shift of 0.52 ppm for the singlet of the pentacene backbone (H5, H7, H12, H14) can be observed which corresponds to the shift typically observed in literature for pentacene endo-peroxide formation.^{30,31}

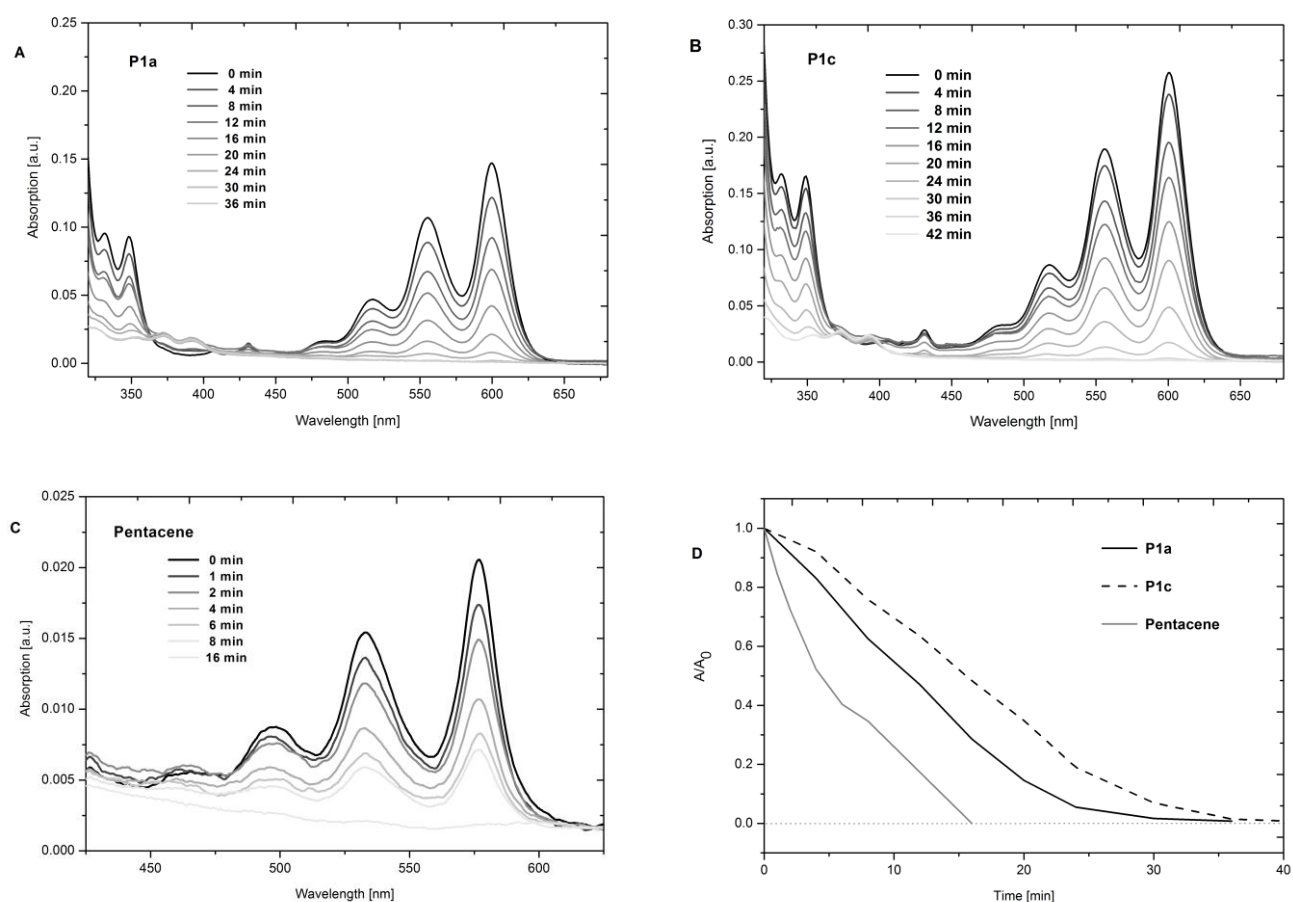


Figure 4: UV-Vis spectra associated with the photooxidation of **P1a** (A), **P1c** (B) and pentacene (C) measured in DCM solutions; Absorbance-time profiles for pentacene derivatives **P1a** and **P1c** and pentacene.

In the UV-Vis spectra the long wavelength bands of 601, 556 and 517 nm and the short wavelength bands of 332 and 348 nm were all observed to diminish with reaction progress while a new set of bands at 392, 372 and 352 nm corresponding to oxidation products were observed to emerge (Figure 4, A and B).

The decrease in intensity of the longest wavelength absorption peak as a function of time was used to monitor the degradation of each compound as a function of time (Figure 4, D). To compare the data, the half-lives of both pentacene derivatives **P1a** and **P1c** were determined under these

conditions and qualitatively compared to the decaying behavior of a saturated solution of pentacene in CH₂Cl₂ (Figure 4, C; approx. 0.1 μM). The half-life of pentacene obtained by this methodology (7.5 min) corresponds to the value observed by Kaur et al.⁹ As can be clearly seen in Figure 4, D both pentacene derivatives show similar decaying behavior, yielding half-life values of 14 min for **P1a** and 16 min for **P1c**. Therefore, **P1a** and **P1c** prove to be approximately twice as stable as unsubstituted pentacene under similar condition due to the influence of the heteroaryl substituent.

CONCLUSION

This work offers a reliable synthetic protocol toward heteroaryl-substituted acene frameworks based on copper-catalysed cycloaddition reactions. Various alkyl and aryl azides have been successfully applied in CuAAC reactions. Additionally, in situ generated nitrile oxides have been used for attachment of isoxazoles to the anthracene backbone. The obtained heteroaryl-substituted anthracenes have been subjected to UV-Vis spectroscopy and cyclic voltammetric measurements indicating, that the nature of the heteroaryl system and the position of the linkage of acene backbone to the heteroaryl moiety show little influence on the absorption spectra. However, a clear reduction of the bandgaps and decreased HOMO levels are evident, indicating higher stability. Based on these findings 6,13-symmetrically disubstituted pentacene derivatives have been synthesized bearing alkyl 1,2,3-triazole moieties as electron-withdrawing groups. The isolated pentacenes show good solubility in organic solvents compared to unsubstituted pentacene. UV-Vis spectroscopy reveals bathochromically shifted absorption maxima correlating with a decreased bandgap compared to the unsubstituted acene backbone. Photokinetic studies also reveal higher photoresistance compared to pentacene, which can be attributed to the 1,2,3-triazole moiety.

ACKNOWLEDGMENT

The authors thank Dr. Karin Föttinger for supporting the photo-physical characterization, Daniel Koch, Anna-Maria Wagner, Thomas Schwartz and Thomas Raab for contributing to the synthetic experiments.

ELECTRONIC SUPPLEMENTARY INFORMATION

¹H and ¹³C NMR spectra of compounds **2**, **3a,b**, **4a,b**, **8**, **9a-c**, **A1a,b**, **A2a,b**, **A3a**, **P1a** and **P1c**, cyclic voltammetry measurements as well as DFT-calculation of **A1a,b**, **A2a,b**, **A3a**, **P1a** and **P1c** and molecular structure of **9b**.

REFERENCES

- (1) De Mello, J.; Anthony, J.; Lee, S. *Chem. Phys. Chem.* **2015**, *16* (6), 1099.
- (2) Wang, Z.; Zhao, J.; Dong, H.; Qiu, G.; Zhang, Q.; Hu, W. *Phys. Chem. Chem. Phys.* **2015**.
- (3) Anthony, J. E. *Angew. Chem. Int. Ed.* **2008**, *47* (3), 452.
- (4) Galbrecht, F.; Bünnagel, T. W.; Bilge, A.; Scherf, U.; Farrell, T. in *Functional organic materials: syntheses, strategies and applications*; Müller, T. J. J., Bunz, U. H. F., Eds.; Wiley-VCH: Weinheim, **2007**.
- (5) Reddy, A. R.; Bendikov, M. *Chem. Commun.* **2006**, No. 11, 1179.
- (6) Berg, O.; Chronister, E. L.; Yamashita, T.; Scott, G. W.; Sweet, R. M.; Calabrese, J. *J. Phys. Chem. A* **1999**, *103* (14), 2451.
- (7) Ono, K.; Totani, H.; Hiei, T.; Yoshino, A.; Saito, K.; Eguchi, K.; Tomura, M.; Nishida, J.; Yamashita, Y. *Tetrahedron* **2007**, *63* (39), 9699.
- (8) Lehnerr, D.; Gao, J.; Hegmann, F. A.; Tykwinski, R. R. *Org. Lett.* **2008**, *10* (21), 4779.
- (9) Kaur, I.; Jia, W.; Kopreski, R. P.; Selvarasah, S.; Dokmeci, M. R.; Pramanik, C.; McGruer, N. E.; Miller, G. P. *J. Am. Chem. Soc.* **2008**, *130* (48), 16274.
- (10) Anthony, J. E.; Eaton, D. L.; Parkin, S. R. *Org. Lett.* **2002**, *4* (1), 15.
- (11) Anthony, J. E.; Brooks, J. S.; Eaton, D. L.; Parkin, S. R. *J. Am. Chem. Soc.* **2001**, *123* (38), 9482.
- (12) Maliakal, A.; Raghavachari, K.; Katz, H.; Chandross, E.; Siegrist, T. *Chem. Mater.* **2004**, *16* (24), 4980.
- (13) Swartz, C. R.; Parkin, S. R.; Bullock, J. E.; Anthony, J. E.; Mayer, A. C.; Malliaras, G. G. *Org. Lett.* **2005**, *7* (15), 3163.
- (14) Okamoto, T.; Senatore, M. L.; Ling, M.-M.; Mallik, A. B.; Tang, M. L.; Bao, Z. *Adv. Mater.* **2007**, *19* (20), 3381.
- (15) Mei, J.; Diao, Y.; Appleton, A. L.; Fang, L.; Bao, Z. *J. Am. Chem. Soc.* **2013**, *135* (18), 6724.
- (16) Baron, A.; Herrero, C.; Quaranta, A.; Charlot, M.-F.; Leibl, W.; Vauzeilles, B.; Aukauloo, A. *Chem. Commun.* **2011**, *47* (39), 11011.
- (17) Parent, M.; Mongin, O.; Kamada, K.; Katan, C.; Blanchard-Desce, M. *Chem. Commun.* **2005**, No. 15, 2029.
- (18) Lumpi, D.; Stöger, B.; Hametner, C.; Kubel, F.; Reider, G.; Hagemann, H.; Karpfen, A.; Fröhlich, J. *Cryst. Eng. Comm.* **2011**, *13* (24), 7194.
- (19) Hein, J. E.; Fokin, V. V. *Chem. Soc. Rev.* **2010**, *39* (4), 1302.
- (20) Kolb, H. C.; Finn, M. G.; Sharpless, K. B. *Angew. Chem. Int. Ed.* **2001**, *40* (11), 2004.
- (21) Rostovtsev, V. V.; Green, L. G.; Fokin, V. V.; Sharpless, K. B. *Angew. Chem. Int. Ed.* **2002**, *41* (14), 2596.
- (22) Vogel, D. E.; Vogel, K. V. 6,13-Bis(thienyl)pentacene compounds. US 2007/0023748A1, January 2, 2007.
- (23) Oh, J.-J.; Pu, Y.-J.; Sasabe, H.; Nakayama, K.; Kido, J. *Chem. Lett.* **2011**, *40* (10), 1092.
- (24) Kwok, S. W.; Fotsing, J. R.; Fraser, R. J.; Rodionov, V. O.; Fokin, V. V. *Org. Lett.* **2010**, *12* (19), 4217.
- (25) Ngai, M. H.; Yang, P.-Y.; Liu, K.; Shen, Y.; Wenk, M. R.; Yao, S. Q.; Lear, M. J. *Chem. Commun.* **2010**, *46* (44), 8335.
- (26) Lam, P. Y. S.; Adams, J. J.; Clark, C. G.; Calhoun, W. J.; Luetzgen, J. M.; Knabb, R. M.; Wexler, R. R. *Bioorg. Med. Chem. Lett.* **2003**, *13* (10), 1795.
- (27) Taylor, M. S.; Swager, T. M. *Org. Lett.* **2007**, *9* (18), 3695.
- (28) Grimes, K.; Gupte, A.; Aldrich, C. *Synthesis* **2010**, *2010* (09), 1441.
- (29) Dediu, V. A.; Hueso, L. E.; Bergenti, I.; Taliani, C. *Nat. Mater.* **2009**, *8* (9), 707.
- (30) Fudickar, W.; Linker, T. *J. Am. Chem. Soc.* **2012**, *134* (36), 15071.
- (31) Yamada, H.; Yamashita, Y.; Kikuchi, M.; Watanabe, H.; Okujima, T.; Uno, H.; Ogawa, T.; Ohara, K.; Ono, N. *Chem. - Eur. J.* **2005**, *11* (21), 6212.

Manuscript # 2

Brigitte Holzer^{#*}, Daniel Lumpi^{#*}, Thomas Mathis, Ernst Horkel, Christian Hametner,
Bertram Batlogg, and Johannes Fröhlich

Novel Thiophene-substituted Pentacenes as Soluble Materials for Organic Field-Effect
Transistors

Manuscript draft

[#] contributed equally to this article

Novel Thiophene-Substituted Pentacenes as Soluble Materials for Organic Field-Effect Transistors

Brigitte Holzer,^{a,#} Daniel Lumpi,^{a,b,#}* Thomas Mathis,^b Ernst Horkel,^a Christian Hametner,^a Bertram Batlogg^b and Johannes Fröhlich^a*

^aInstitute of Applied Synthetic Chemistry, Vienna University of Technology,
Getreidemarkt 9/163OC, 1060 Vienna, Austria

^bLaboratory for Solid State Physics, ETH Zurich,
Otto-Stern-Weg 1, 8093 Zurich, Switzerland

[#]authors contributed equally

* brigitte.holzer@tuwien.ac.at

* daniel.lumpi@tuwien.ac.at

A series of (trialkylsilyl)thienyl-substituted pentacenes was designed, synthesized and characterized. Based on the results of DFT calculations, revealing the influence of thienyl substituents on the stability and electronic properties of acenes, compounds bearing both bulky trialkylsilyl- and electron-withdrawing bromo substituents (to counteract the electron-donating effects of the trialkylsilyl group) on the thienyl moiety were selected for further investigations. Mild reliable synthetic reaction conditions were evaluated toward disubstituted acene derivatives. All novel acene compounds were characterized by NMR, cyclic voltammetry and UV-Vis spectroscopy, which reveal a significant reduction of the HOMO energy level and the bandgap induced by the bromo(trialkylsilyl)thienyl scaffolds, indicating improved stability compared to the unsubstituted acene backbone. The applicability of these materials in organic electronic devices was demonstrated in an organic field-effect transistor configuration yielding a hole mobility of $3 \times 10^{-4} \text{ cm}^2 \text{ V}^{-1} \text{ s}^{-1}$.

INTRODUCTION

Pentacene **1a** represents a highly attractive compound for the preparation of organic thin film transistors (OTFTs) exhibiting excellent p-type semiconducting properties with charge carrier mobilities up to $5.5 \text{ cm}^2 \text{ V}^{-1} \text{ s}^{-1}$.¹ Owing to its outstanding properties, such as high mobility, low cost, and ordered crystal structure, pentacene has been intensively investigated for the applications in OTFT-based sensors.² However, it also exhibits some disadvantages like low solubility and stability in solution,^{3,4} which limits processing techniques primarily to vacuum deposition.^{5,6} In order to overcome these disadvantages structural variations of the pentacene backbone have been performed,^{7,8} supported by a study by Glen et al. revealing that the photooxidative resistance of substituted 6,13-difunctionalized pentacenes is strongly impacted by both steric as well as electronic factors.⁴ Anthony et al. successfully showed that the introduction of (triisopropylsilyl)ethynyl groups in these positions (TIPS-pentacene, **1b**, Figure 1) leads to a modification of molecular π -stacking, resulting in high-performance semiconducting properties as well as improved solubility and stability of the pentacene derivative.⁹⁻¹¹ Further strategies to improve the stability of pentacene compounds also suitable as n-type semiconductors are based on the incorporation of electron-withdrawing groups in 6- and 13-position like nitrile⁸ or chloro¹² substituents. Among p-type materials aryl substitution (e.g. with phenyl,¹³ 3,4-dichlorophenyl¹⁴ or pentafluorophenyl¹⁵) proved to be an efficient method to increase stability against oxidation. Also heterocyclic substituents based on oligothieryl groups,¹⁶ benzo[*b*]thiophenes¹⁷ and thiophenes have been successfully applied. Advantageously (6,13-pentacenediyl)bisthiophene **1c** exhibits good solubility and hole mobilities up to $0.10 \text{ cm}^2 \text{ V}^{-1} \text{ s}^{-1}$.¹³

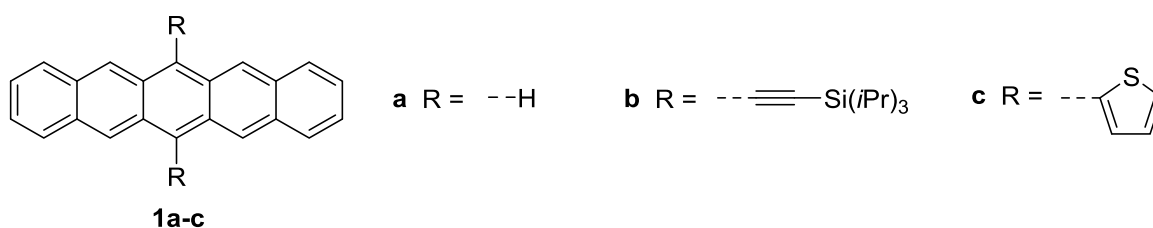


Figure 1: Structures of pentacene derivatives.

The objective of this work is to increase device performance (charge carrier mobility) of molecular acene motives by optimizing the solid-state ordering. We propose to adapt the strategy of Anthony et al.¹⁸ by introducing bulky silyl groups to the (6,13-pentacenediyl)bisthiophene scaffold in order to enhance the π -stacking of the acene subunit. The selection of final target structures was guided by theoretical calculations particularly taking stability considerations into account. Positive effects of bromine substituents on the oxidation potential of the pentacene backbone have been demonstrated previously for p-type materials^{14,19,20} as well as for core substitution of various n-type materials²¹⁻²³ aiming for good transistor performance and stability. Schmidt et al. showed that

among halogen substituents the attachment of bromine to perylene bisimide backbones leads to the most efficient lowering of the molecular energy levels, although bromine possesses the smallest electronegativity.²⁴ To the best of our knowledge, the approach of applying bromine substituents, exhibiting a sufficiently strong $-I$ effect to counteract the $+I$ effect of the silyl groups, is unique for the design of silyl-based p-type organic semiconducting materials.

EXPERIMENTAL SECTION

Computations were performed using the Gaussian 09 package, revision A.02.²⁵ The ground state (S0) geometries were optimized in gas phase using the Becke three parameters hybrid functional with Lee–Yang–Perdew correlation (B3LYP)^{26,27} in combination with Pople basis set 6-311+G(d).²⁸ Substances purchased from commercial sources were used as received. Anhydrous acetonitrile (ACN), n-butyllithium solution (2.5 M in hexanes) and anthracene-9,10-dione were purchased from Aldrich Chemical Co. Pentacene-6,13-dione (CAS 3029-32-1),²⁹ 3-bromo-2-iodothiophene³⁰ (CAS 60404-24-2), and 3-bromo-5-iodo-2-[tris(1-methylethyl)silyl]thiophene³¹ were synthesized according to literature. Anhydrous tetrahydrofuran (THF), dichloromethane (DCM), methanol (MeOH), and toluene were prepared immediately prior to use by a *PURESOLV*-plant (*it-innovative technology inc.*). Technical grade solvents were distilled prior to use. Analytical TLC was performed on Merck silica gel 60 F254 plates. Chromatographic separations at preparative scale were carried out on silica gel (Merck silica gel 60, 40 – 63 μm). Nuclear magnetic resonance (NMR) spectra were obtained using a Bruker Avance III HD 600 MHz with cryo probe, Avance III HD 400 MHz, Avance DRX-400 or DPX-200 fourier transform spectrometer operating at the following frequencies: Avance III HD 600 MHz: 600.2 MHz (^1H) and 150.9 MHz (^{13}C); Avance III HD 400 MHz and DRX-400: 400.1 MHz (^1H) and 100.6 MHz (^{13}C); DPX-200: 200.1 MHz (^1H) and 50.3 MHz (^{13}C). The chemical shifts are reported in δ units, parts per million (ppm) downfield from tetramethylsilane using residual solvent signals for calibration. Coupling constants are reported in Hertz; multiplicity of signals is indicated by using following abbreviations: s=singlet, d=doublet, t=triplet, q=quartet, quin=quintet. The multiplicity of ^{13}C signals was obtained by measuring JMOD spectra. A Thermo Scientific LTQ Orbitrap XL hybrid FTMS (Fourier Transform Mass Spectrometer) equipped with Thermo Scientific MALDI Interface or Thermo Fischer Exactive Plus Orbitrap (LC-ESI+) and a Shimadzu IT-TOF Mass Spectrometer were used for high-resolution mass spectrometry. α -Cyano-4-hydroxycinnamic acid was used as matrix for MALDI measurements. UV-Vis absorption spectra were recorded in ACN or DCM solutions (5 μM) with a Perkin Elmer Lambda 750 spectrometer. Cyclic voltammetry was performed using a three electrode configuration consisting of a Pt working electrode, a Pt counter electrode and an Ag/AgCl reference electrode and a PGSTAT128N, ADC164, DAC164, External, DI048 potentiostat provided by Metrohm Autolab B. V. Measurements were carried out in 0.5 mM solution in anhydrous DCM with Bu_4NBF_4 (0.1 M) as

the supporting electrolyte. The solutions were purged with argon for 15 min prior to measurement. HOMO energy levels were calculated from the onset of absorption. The onset potential was determined by the intersection of two tangents drawn at the background and the rising of oxidation. Ferrocene served as an external standard for calibrating the potential and calculating the HOMO levels (-4.8 eV).

3-Bromo-5-iodo-2-(triethylsilyl)thiophene (**3a**). To a solution of diisopropylamine (5.08 g, 50.2 mmol, 1.35 eq.) in 250 mL anhydrous THF under argon n-BuLi (17.7 mL, 44.3 mmol, 2.5 M in hexanes, 1.19 eq) was slowly added at -40 °C. After 40 min 3-bromo-2-iodothiophene (10.75 g, 37.2 mmol, 1.0 eq.) was added in 60 mL anhydrous THF at -75 °C and the reaction stirred for 2 h. Subsequently triethylsilylchloride (6.68 g, 44.3 mmol, 1.2 eq.) was added and the mixture stirred at rt overnight. The reaction was poured on water, extracted with Et₂O, the organic phases were dried over anhydrous Na₂SO₄ and concentrated under reduced pressure to give the crude product. Bulb-to-bulb distillation yielded **3a** (13.67 g, 91%) as a yellow oil. ¹H NMR (200 MHz, CDCl₃): δ = 7.20 (s, 1H), 1.07 - 0.85 (m, 15 H) ppm. ¹³C NMR (50 MHz, CDCl₃): δ = 140.8 (d), 140.1 (s), 117.3 (s), 78.1 (s), 7.3 (q), 3.6 (t) ppm.

General Procedure: addition of substituted thiophenes to anthracene-9,10-dione and pentacene-6,13-dione. n-BuLi (2.5 M, 4.2 eq.) was added dropwise to a solution of the appropriate thiophene derivative (4 eq.) in anhydrous THF (~0.05 M) at -78 °C under argon atmosphere. The solution was stirred for 2 hours at constant temperature, then dione (1 eq.) was added and the mixture was slowly warmed to room temperature. After the reaction mixture was stirred at room temperature overnight, it was poured in a saturated ammonium chloride solution and extracted with diethyl ether. The combined organic layers were washed with saturated sodium chloride solution, dried over Na₂SO₄ and concentrated in vacuo.

9,10-Bis[4-bromo-5-(triethylsilyl)-2-thienyl]-9,10-dihydroanthracene-9,10-diol (**5**). **3a** (11.29 g, 28 mmol) was dissolved in 160 mL anhydrous THF, n-BuLi (11.8 mL, 29.4 mmol) was added dropwise. Anthracene-9,10-dione (1.47 g, 7 mmol) was added. After work-up according to the general procedure the crude product was purified by column chromatography (180 g silica gel, light petroleum : ethyl acetate 9:1) and **5** was isolated as colorless solid in 77% yield (4.10 g). R_f = 0.56 (light petroleum : ethyl acetate = 9:1). ¹H NMR (200 MHz, CDCl₃): δ = 7.62 - 7.56 (m, 4 H), 7.43 - 7.37 (m, 4 H), 6.70 (s, 2 H), 2.77 (bs, 2 H), 1.04 - 0.82 (m, 30 H) ppm. ¹³C NMR (50 MHz, CDCl₃): δ = 157.3 (s), 139.6 (s), 131.7 (s), 131.0 (d), 129.1 (d), 127.6 (d), 116.5 (s), 73.3 (s), 7.4 (q), 3.7 (t) ppm.

6,13-Bis[4-bromo-5-(triethylsilyl)-2-thienyl]-6,13-dihydropentacene-6,13-diol (**8a**). According to the general procedure **8a** was synthesized starting from **3a** (3.23 g, 8 mmol), n-BuLi (3.4 mL, 8.4 mmol) and pentacene-6,13-dione (616 mg, 2 mmol). After work-up the crude product was purified by column chromatography (90 g silica gel, light petroleum : DCM 1:1) and **8a** was isolated as

colorless solid in 75% yield (1.29 g). $R_f = 0.52$ (light petroleum : ethyl acetate 5:1). $^1\text{H NMR}$ (200 MHz, CDCl_3): $\delta = 8.17$ (s, 4H), 7.91 - 7.86 (m, 4 H), 7.57 - 7.52 (m, 4 H), 6.79 (s, 2 H), 2.86 (bs, 2 H), 1.00 - 0.82 (m, 30 H) ppm. $^{13}\text{C NMR}$ (50 MHz, CDCl_3): $\delta = 156.5$ (s), 138.2 (s), 137.8 (s), 133.0 (s), 132.2 (d), 128.3 (d), 127.0 (d), 126.7 (d), 116.7 (s), 74.4 (s), 7.4 (q), 3.6 (t) ppm. HR-ESI-FTMS $[\text{M}+\text{H}]^+$ m/z calcd. 861.0917 for $\text{C}_{42}\text{H}_{47}\text{Br}_2\text{O}_2\text{S}_2\text{Si}_2^+$, found 861.0740.

6,13-Bis[4-bromo-5-[tris(1-methylethyl)silyl]-2-thienyl]-6,13-dihydropentacene-6,13-diol (**8b**). According to the general procedure **8b** was synthesized starting from 3-bromo-5-iodo-2-[tris(1-methylethyl)silyl]thiophene **3b** (1.78 g, 4 mmol), $n\text{-BuLi}$ (1.68 mL, 4.2 mmol) and pentacene-6,13-dione (310 mg, 1 mmol). After work-up the crude product was purified by column chromatography (90 g silica gel, light petroleum : ethyl acetate 20:1) and **8b** was isolated as yellow solid in 56% yield (536 mg). $R_f = 0.68$ (light petroleum : ethyl acetate 5:1). $^1\text{H NMR}$ (400 MHz, CDCl_3): $\delta = 8.18$ (s, 4 H), 7.89 - 7.86 (m, 4 H), 7.56 - 7.52 (m, 4 H), 6.83 (s, 2 H), 2.86 (bs, 2 H), 1.53 (sept, $J = 7.7$ Hz, 6 H), 1.13 (d, $J = 7.7$ Hz, 36 H) ppm. $^{13}\text{C NMR}$ (100 MHz, CDCl_3): $\delta = 156.5$ (s), 138.4 (s), 133.0 (s), 132.8 (d), 131.7 (s), 128.2 (d), 127.0 (d), 126.8 (d), 117.0 (s), 74.3 (s), 18.8 (q), 12.3 (d) ppm. HR-ESI-FTMS $[\text{M}+\text{H}]^+$ m/z calcd. 945.1856 for $\text{C}_{48}\text{H}_{59}\text{Br}_2\text{O}_2\text{S}_2\text{Si}_2^+$, found 945.2054.

General procedure for reduction of the functionalized 9,10-dihydroanthracene-9,10-diol and 6,13-dihydropentacene-6,13-diols. SnCl_2 (4 eq.) was added to a dispersion of the substituted diol **5**, **8a**, or **8b** (1 eq.) in acetonitrile (~ 0.05 M) and the mixture was stirred under argon atmosphere overnight at room temperature. The reaction mixture of the anthracene derivative was quenched with water, extracted with chloroform, dried over Na_2SO_4 and concentrated in vacuo. The synthesis of the pentacene derivatives had to be carried under exclusion of ambient light and oxygen. Furthermore all solvents were purged with argon before use. The work-up for pentacene derivatives was achieved by filtration of the precipitate and washing with methanol, water and acetonitrile. The obtained solids were dried in vacuo.

2,2'-(9,10-Anthracenediyl)bis[4-bromo-5-(triethylsilyl)thiophene] (**6**). According to the general procedure **6** was synthesized starting from **5** (3.1 g, 4 mmol) and SnCl_2 (3.04 g, 16 mmol) in 50 mL anhydrous acetonitrile. After work-up the crude product was purified by column chromatography (90 g silica gel, light petroleum) and isolated as yellow solid in 88% yield (2.57 g). $F_p = 197.4 - 199.2$ °C. $R_f = 0.62$ (light petroleum : ethyl acetate 10:1). $^1\text{H NMR}$ (200 MHz, CDCl_3): $\delta = 7.96 - 7.91$ (m, 4 H), 7.53 - 7.47 (m, 4 H), 7.30 (s, 2 H), 1.24 - 1.03 (m, 30 H) ppm. $^{13}\text{C NMR}$ (50 MHz, CDCl_3): $\delta = 144.8$ (s), 134.5 (d), 133.9 (s), 131.0 (s), 129.4 (s), 126.4 (d), 126.0 (s), 116.9 (s), 7.5 (q), 3.8 (t) ppm.

2,2'-(6,13-Pentacenediyl)bis[4-bromo-5-(triethylsilyl)thiophene] (**1h**). According to the general procedure **1h** was synthesized starting from **8a** (997 mg, 1.15 mmol) and SnCl_2 (874 mg, 4.6 mmol) in 15 mL anhydrous acetonitrile. After work-up **1h** was isolated as a dark blue solid in 90% yield (860 mg). Further purification was realized by column chromatography (9 g silica gel, anhydrous

DCM : anhydrous methanol 5%→10%). ¹H NMR (400 MHz, CD₂Cl₂): δ = 8.48 (s, 4 H), 7.85 - 7.83 (m, 4 H), 7.43 (s, 2 H), 7.34 - 7.32 (m, 4 H), 1.19 - 1.07 (m, 30 H) ppm. ¹³C NMR (100 MHz, CD₂Cl₂): δ = 145.8 (s), 135.5 (d), 135.0 (s), 132.0 (s), 130.1 (s), 129.8 (s), 129.0 (d), 126.4 (d), 125.6 (d), 117.6 (s), 7.8 (q), 4.3 (t) ppm. HR-ESI-FTMS [M+H]⁺ m/z calcd. 827.0863 for C₄₂H₄₅Br₂S₂Si₂⁺, found 827.0818.

2,2'-(6,13-Pentacenediyl)bis[4-bromo-5-[tris(1-methylethyl)silyl]thiophene] (**1i**). According to the general procedure **1i** was synthesized starting from **8b** (423 mg, 0.45 mmol) and SnCl₂ (337 mg, 1.78 mmol) in 10 mL anhydrous acetonitrile. After work-up **1i** was isolated as a dark blue solid in 91% yield (370 mg). Further purification was realized by column chromatography (9 g silica gel, anhydrous DCM : anhydrous methanol 5%→10%). ¹H NMR (600 MHz, CD₂Cl₂) : δ = 8.51 (s, 4 H), 7.84 - 7.82 (m, 4 H), 7.46 (s, 2 H), 7.34 - 7.33 (m, 4 H), 1.74 (sept, J = 7.1 Hz, 6 H), 1.31 (d, J = 7.1 Hz, 36 H) ppm. ¹³C NMR (150 MHz, CD₂Cl₂): δ = 145.9 (s), 136.1 (d), 133.7 (s), 132.0 (s), 130.0 (s), 129.7 (s), 129.0 (d), 126.4 (d), 125.7 (d), 118.0 (s), 19.2 (q), 13.1 (d) ppm. HR-ESI-FTMS [M+H]⁺ m/z calcd. 911.1802 for C₄₈H₅₇Br₂S₂Si₂⁺, found 911.1767.

RESULTS AND DISCUSSION

It has been shown that **1c** (Figure 2) crystallizes in a “sandwich herringbone” molecular arrangement featuring a slight slip in the π-stacking motive (off-set along the short axis of pentacene by approx. 0.7 Å).¹³ The aforementioned goal of this study is the introduction of bulky silyl groups in order to improve the solid-state ordering toward a 2-D stacking arrangement along the long axis of pentacene, similar to “running bond” bricklayers,⁹ and to reduce the off-set along the short axis of pentacene. Studies of Anthony et al. disclosed that the substituent diameter of the spherical silyl group relative to the short axis length of the acene plays a crucial role for the molecular arrangement^{9,18} and, thus, for the performance as semiconductive material.³ Therefore triethylsilyl (TES) and triisopropylsilyl (TIPS) groups, which induce 1-D and 2-D slip stacking, respectively, in bis(silylethynyl)pentacenes, were chosen for the synthesis of target compounds.³

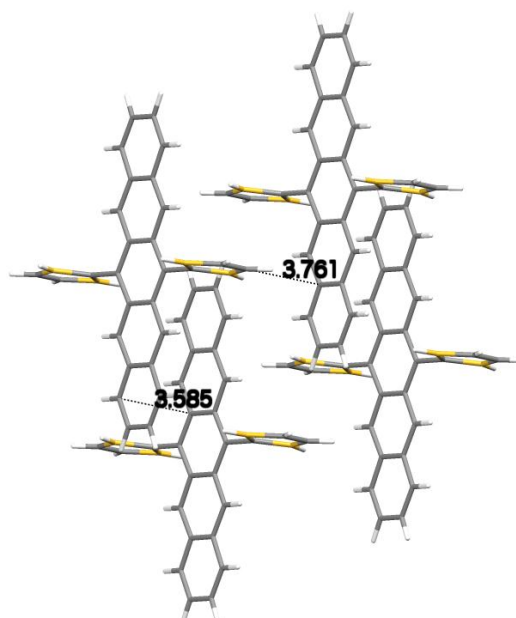
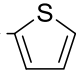
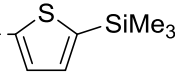
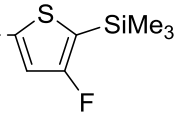
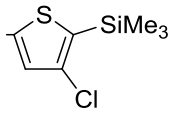
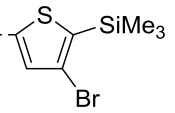
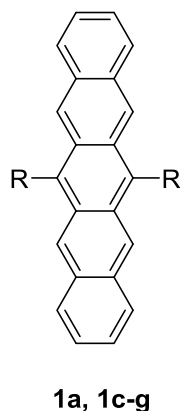


Figure 2: Packing motif of **1c** arranging in a slipped stack along the short axis of pentacene. Close contacts between the acene faces (~ 3.6 Å) and neighboring columns (~ 3.8 Å) are depicted.

To evaluate the impact of introducing silyl groups on electronic properties and, thus, the effects on material characteristics (e.g. stability, charge carrier injection, etc.) an initial DFT study for model compounds **1a** and **1c-g** has been conducted (see Table 1).

Table 1: HOMO and LUMO energy levels and bandgaps of the investigated molecules. *Calculated bandgaps and HOMO/LUMO levels (B3LYP / 6-311+G(d)).

	R	Bandgap* (eV)	HOMO/LUMO* (eV)
1a	--H	2.19	-4.92/-2.73
1c	-- 	2.12	-4.96/-2.84
1d	-- 	2.12	-4.91/-2.79
1e	-- 	2.11	-5.08/-2.96
1f	-- 	2.11	-5.08/-2.97
1g	-- 	2.11	-5.08/-2.97



Many studies showed that the introduction of electron-withdrawing substituents leads to a decrease of the HOMO level and an increase in stability.^{4,32-34} DFT calculations reveal that

thiophene substitution of the pentacene core results in a lowered HOMO level (**1c**, -4.96 eV) by 0.04 eV compared to pentacene **1a**, which indicates a slightly improved oxidative stability. However, the introduction of silyl groups raises the HOMO level (TMS (trimethylsilyl) – model **1d**, -4.91 eV) even above the value of pentacene (4.92 eV) indicating a destabilization of **1d** as a consequence of the +I effect.

To counteract the electron-donating effect of the trialkylsilyl group a suitably strong –I substituent in the 4-position of the 5-(trialkylsilyl)-2-thienyl moiety (ortho position to the silyl group) was introduced. For spatial reasons only halogen atoms (F, Cl, and Br) were taken into account in this study (iodine was omitted due to its size and limited synthetic accessibility). For all halogen substituted derivatives **1e-g** the same HOMO level (-5.08 eV) was calculated, which is significantly decreased compared to pentacene **1a** (by 0.16 eV) indicating an increase in stability. These results show that the electron-withdrawing effect of all halogens is sufficiently strong to counter the electronic effects induced by the silyl group in this substitution pattern. Since the 4-bromo-5-silyl-2-thienyl pattern can be easily achieved via the halogen dance^{31,35–37} approach, the bromine moiety was chosen for the synthesis of target compounds bearing TES (**1h**) and TIPS (**1i**) as silyl groups (DFT calculations: Table 2, contour plots: Figures 3 and 4).

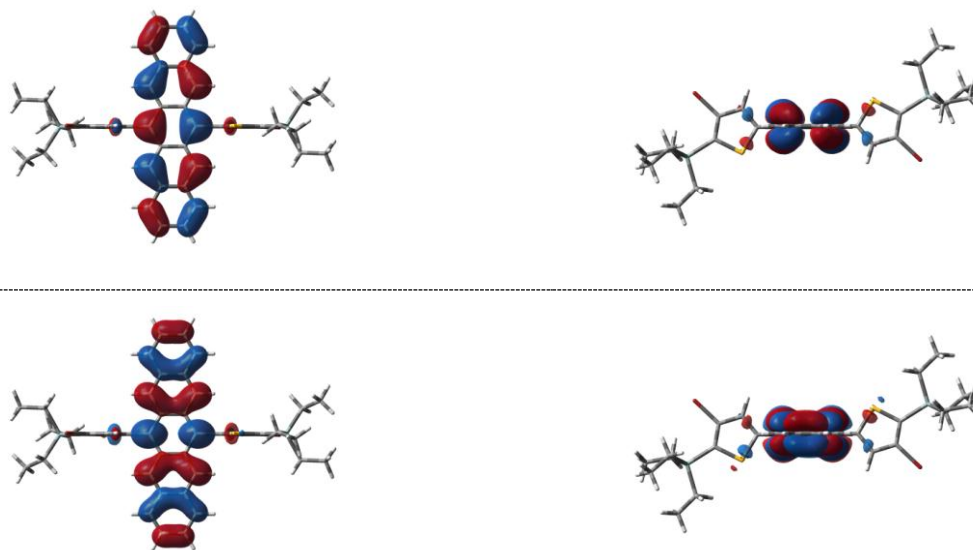


Figure 3: HOMO (bottom) and LUMO (top) of **1h**.

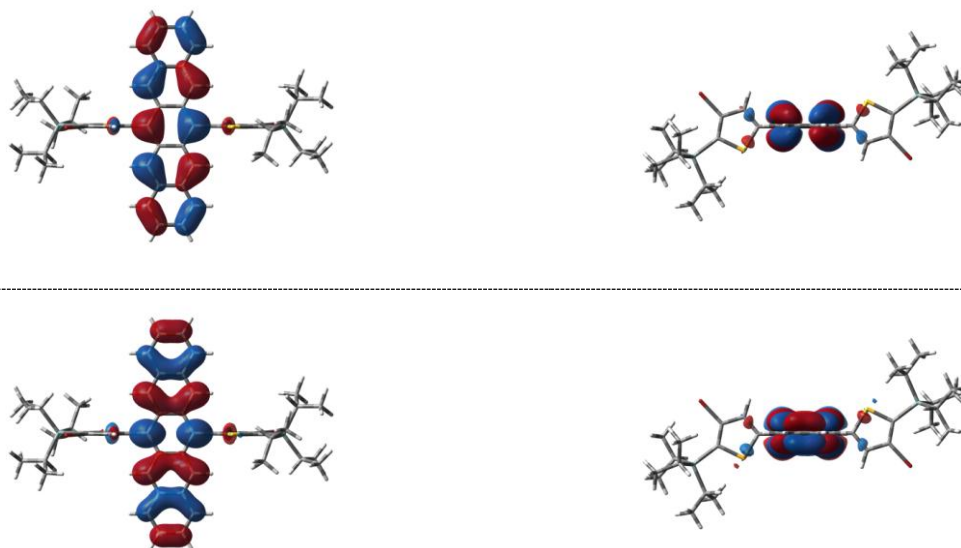
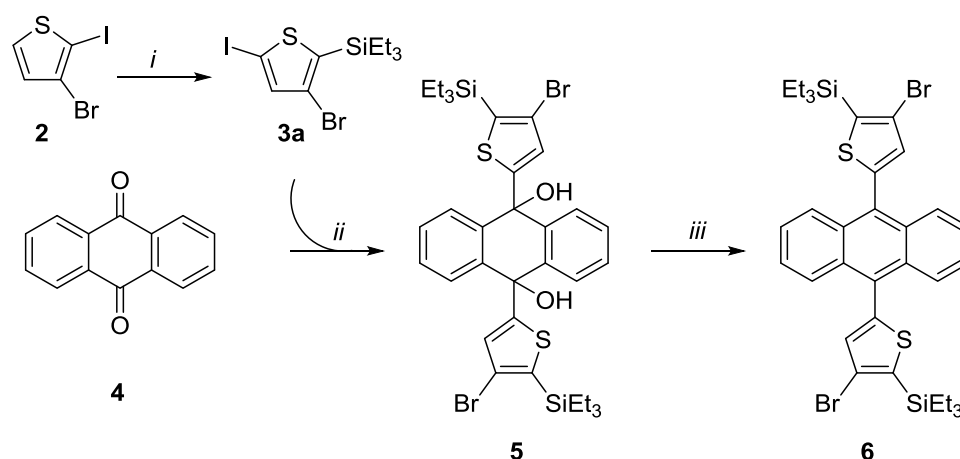


Figure 4: HOMO (bottom) and LUMO (top) of **1i**.

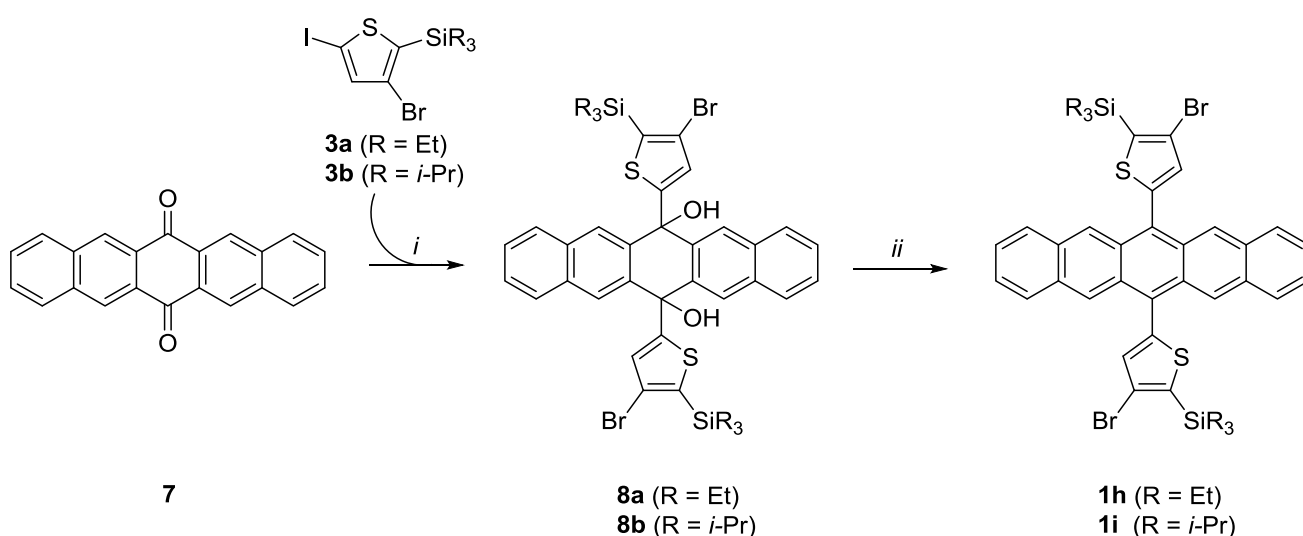
Since post-synthetic modification of pentacene frameworks is known to be difficult because of the low photostability of the acene backbone, a general mild synthetic protocol was sought suitable for model anthracenes derivative as well as pentacenes. Synthetic pathways were initially probed toward anthracene derivative **6** (Scheme 1): iodothiophene **3a** was obtained in a halogen dance reaction starting from dihalogenide **2** in 91% yield. Nucleophilic addition of [4-bromo-5-(triethylsilyl)-2-thienyl]lithium, *in situ* generated by lithium–halogen exchange of **3a** by treatment with *n*-BuLi, to anthracene-9,10-dione **4** gave diol **5** as a single isomer. Subsequently, a mild reductive aromatization method using an excess of SnCl₂ in degassed acetonitrile, which was shown to be also suitable for pentacene derivatives by Li et al.,³⁸ was applied to compound **5** and provided **6** in 88% yield.



Scheme 1: Synthetic pathway toward anthracene compound **6**; *i*: *n*-BuLi, DIPA, triethylsilylchloride, THF, -78 °C; *ii*: *n*-BuLi, THF, -78 °C; *iii*: SnCl₂, ACN, rt.

The developed synthetic protocol was further successfully applied toward pentacenes **1h** and **1i** (Scheme 2): nucleophilic addition of *in situ* generated [4-bromo-5-(trialkylsilyl)-2-thienyl]lithium to

pentacene-6,13-dione **7** readily provided diols **8a** and **8b** in 75% and 56% yield, respectively. These pentacene precursors were subjected to reductive aromatization under strict exclusion of ambient light. The resulting mixture turned deep blue, and monitoring by TLC showed that the reactions were complete after approximately 4 – 6 h. The resulting pentacenes could be isolated by filtration and subsequently washing with water, methanol and acetone. Filtration yielded analytically pure compounds (Table 2), small samples were further purified by column chromatography applying degassed solvents and under exclusion of ambient light for further OFET device characterization. Pentacene derivatives **1h** and **1i** are soluble in common organic solvents such as DCM, CHCl₃, and toluene and appear dark blue in color. The characterization of **1h** and **1i** was performed by ¹H / ¹³C NMR spectroscopy and HR-MS analysis, and the data are consistent with the proposed structural formulations.



Scheme 2: Synthetic pathway toward target pentacenes. *i*: n-BuLi, THF, -78 °C; *ii*: SnCl₂, ACN, rt.

The electronic absorption characteristics of anthracene **6** and pentacene derivatives **1h** and **1i** were examined by UV-vis spectrometry in degassed DCM solutions. The respective spectra are depicted in Figure 5 in comparison to anthracene and pentacene.

Compound **6** shows a series of four absorption maxima (343 – 401 nm) characteristic for acene moieties. Similar absorption characteristics were detected for pentacene derivatives **1h** and **1i** at higher wavelength (486 – 608 nm). A bathochromic shift of the absorption maxima of **1h** and **1i** by approximately 30 nm compared to non-substituted pentacene **1a** ($\lambda_{\text{max}} = 577$ nm), which also corresponds to the observations for **6** compared to anthracene (23 nm), can be attributed to an extended π -conjugation partially incorporating the thiophene subunits¹⁵ (also see contour plots in Figure 3 and 4).

For anthracene derivative **6** a reduced bandgap by approximately 0.2 eV compared to anthracene could be observed (determined from the onset of the lowest energy absorption band). Both pentacene derivatives exhibit **1h** and **1i** the same optical bandgap (1.96 eV), which corresponds to a decrease in

optical bandgap by 0.15 eV compared to pentacene.

Table 2: Experimental data and physical characterization of compounds **1h**, **1i**, and **6**.

Comp.	Yield (%)	Bandgap ^a (nm, eV)	λ_{\max} ^b (nm)	HOMO/LUMO ^c (eV)	HOMO/LUMO ^d (eV)
Anthracene	-	386, 3.21	378, 359, 341, 325	-5.70/-1.70 ^g	-5.55/-2.00
6	88	422, 2.93	401, 381, 361, 343	-5.64/-2.71	-5.73/-2.35
Pentacene	-	592, 2.10	577, 532, 499, 465	-4.90/-3.20 ^f	-4.92/-2.73
1h	90	633, 1.96	608, 562, 523, 486	-5.10/-3.17	-5.06/-2.95
1i	91	634, 1.96	608, 562, 522, 486	-5.13/-3.14	-5.08/-2.97

^a Optical bandgaps determined from the onset of lowest energy visible band. ^b Absorption maxima determined from DCM solutions. ^c HOMO levels determined from solutions measured in DCM. All E_{ox} data are reported relative to ferrocene (Fc/Fc^+ , $E_{\text{ox}} = 463$ mV). The concentration of the compounds used in these experiments was 0.5 mM; the scan rate was 50 mV s⁻¹. LUMO levels were determined from the optical bandgap and the HOMO energy level according to the following equation: $E_{\text{LUMO}} = E_{\text{HOMO}} + E_g$. ^d Calculated bandgaps and HOMO/LUMO levels (B3LYP / 6-311+G(d)). ^f HOMO and LUMO levels according to Dediu et al.³⁹ ^g HOMO and LUMO levels according to Djurovich et al.⁴⁰

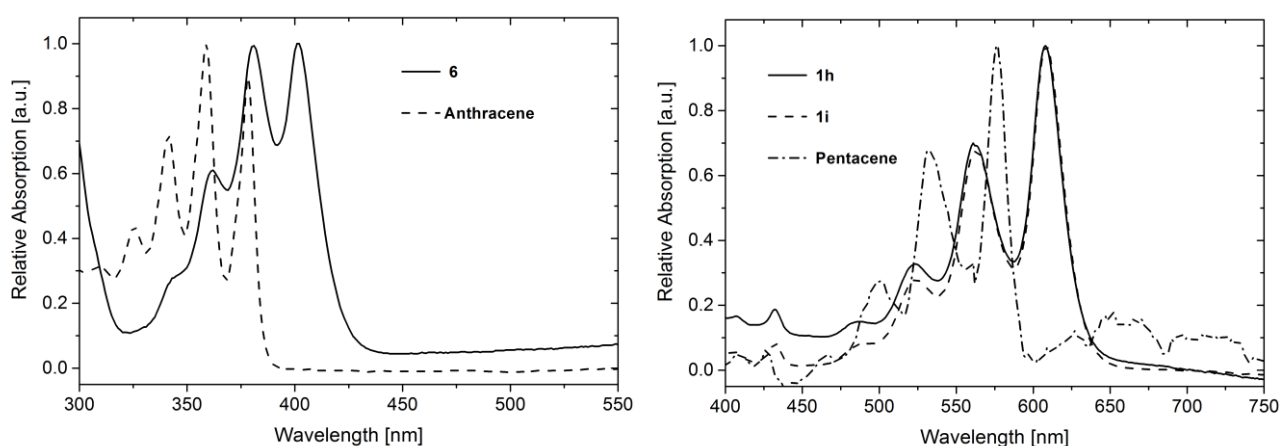


Figure 5: Absorption spectra of **6** (left), **1h** and **1i** (right) in DCM solution.

The cyclic voltammetric (CV) measurements of anthracene **6** and pentacene derivatives **1h** and **1i** were performed in degassed DCM and are depicted in Figure 6. The first oxidation potentials were used to determine the HOMO energy levels (Table 2). The HOMO energy level of **6** of -5.64 eV suggests limitations for charge carrier (hole) injection for the anthracene derivative. Only small

variations of the detected HOMO levels of pentacene derivatives **1h** (-5.09 eV) and **1i** (-5.13 eV) were observed, indicating good charge carrier injection behavior and reasonable stabilities although being low-bandgap (< 2.0 eV) materials suitable for OFET applications. The LUMO levels were acquired from the optical bandgap (UV-Vis) and the HOMO energy levels obtained from CV measurements.

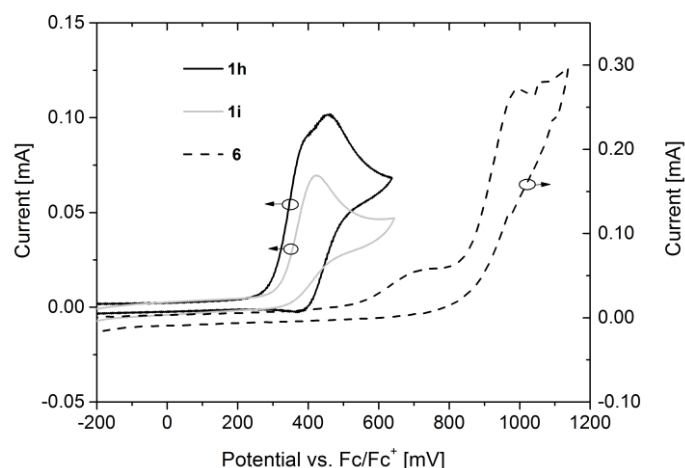


Figure 6: Cyclic voltammograms of **1h**, **1i** and **6** measured in DCM solution.

The semiconducting properties of the materials **1h** and **1i** were tested in a top-contact OFET configuration by 4-point measurements. Hydrophobic Cytop fluoropolymer (approx. 30 nm) spin-coated on SiO₂ (263 nm) / Si (n-doped) was applied as gate dielectric. Transfer curve (Figure 7, left) and corresponding output characteristics (Figure 7, right) of **1h** and **1i** could be obtained.

For pentacene **1h** hole mobilities up to $3 \times 10^{-4} \text{ cm}^2 \text{ V}^{-1} \text{ s}^{-1}$, an on/off ratio of 10^4 and an average threshold voltage of approximately 12 V could be acquired. These rather low mobility values point out that the intended 2-D slip stack arrangement could not be realized by the introducing the TES groups. However, stable and reproducible OFET devices could be engineered from target materials. In addition, stability trials based on repeated device fabrication and characterization proved that **1h** is stable at room temperature for > 1 year. The hole mobilities for **1i**, being one order of magnitude lower, support the assumption that the intended solid-state ordering is not achieved in the designed materials; it is concluded that the TIPS group further reduces the π -overlap due to the enlarged diameter (TES = 6.6 Å vs. TIPS = 7.5 Å).⁹

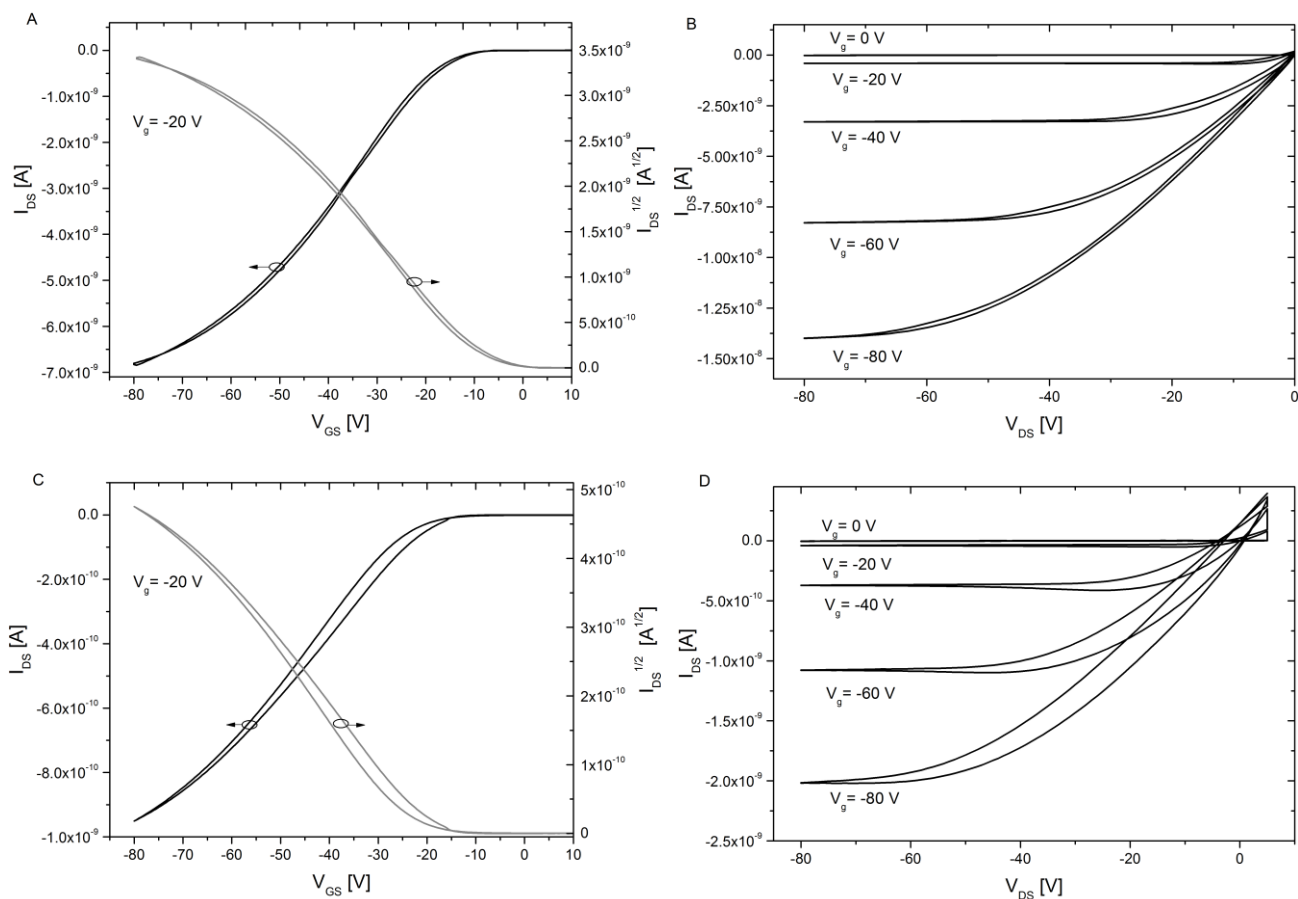


Figure 7: Transfer and corresponding output characteristics of **1h** (A, B) and **1i** (C, D).

CONCLUSION

This contribution outlines the applicability of (trialkylsilyl)thienyl substituents in acene frameworks guided by DFT calculations. Novel pentacene derivatives bearing bulky (trialkylsilyl)-2-thienyl groups and an additional bromo substituent (to counteract the electron-donating effects of the trialkylsilyl group) on the thienyl moiety were synthesized and characterized regarding their photophysical and electrochemical properties. Absorption spectra reveal a red shift of the absorption maxima of pentacene derivatives, indicating a decreased bandgap. The reduced HOMO levels compared to pentacene demonstrate the efficiency of the introduction of these bromo(trialkylsilyl)thienyl side groups. Both pentacene derivatives were tested as semiconductors in organic field-effect transistor devices, however, only low charge carrier mobilities of almost $3 \times 10^{-4} \text{ cm}^2 \text{ V}^{-1} \text{ s}^{-1}$ for **1h** could be observed. The introduction of silyl groups on the thiophene moiety obviously impedes efficient charge transfer, which may be caused by inefficient π -stacking due to steric hindrance.

ACKNOWLEDGMENT

The authors thank Thomas Schwartz, Alexander Aster, Rene Klaffenböck and Günes Kavala for contributing to the synthetic experiments. Tobias Morf, Tino Zimmerling and Roger Häusermann are acknowledged for supporting the device characterization.

ELECTRONIC SUPPLEMENTARY INFORMATION

¹H and ¹³C NMR spectra of compounds **1h**, **1i**, **3a**, **5**, **6**, **8a**, and **8b**. DFT-Calculations of **1a-g** and **6**. Cyclic voltammetric measurements and absorption spectra of **1h**, **1i**, and **6**.

REFERENCES

- (1) Lee, S.; Koo, B.; Shin, J.; Lee, E.; Park, H.; Kim, H. *Appl. Phys. Lett.* **2006**, *88* (16), 162109.
- (2) Liao, C.; Yan, F. *Polym. Rev.* **2013**, *53* (3), 352.
- (3) Anthony, J. E. *Angew. Chem. Int. Ed.* **2008**, *47* (3), 452.
- (4) Kaur, I.; Jia, W.; Kopreski, R. P.; Selvarasah, S.; Dokmeci, M. R.; Pramanik, C.; McGruer, N. E.; Miller, G. P. *J. Am. Chem. Soc.* **2008**, *130* (48), 16274.
- (5) Natsume, Y. *Phys. Status Solidi A* **2008**, *205* (12), 2958.
- (6) Chen, K.-Y.; Hsieh, H.-H.; Wu, C.-C.; Hwang, J.-J.; Chow, T. J. *Chem. Comm.* **2007**, *10*, 1065.
- (7) Waterloo, A. R.; Sale, A.-C.; Lehnerr, D.; Hampel, F.; Tykwinski, R. R. *Beilstein J. Org. Chem.* **2014**, *10*, 1692.
- (8) Katsuta, S.; Miyagi, D.; Yamada, H.; Okujima, T.; Mori, S.; Nakayama, K.; Uno, H. *Org. Lett.* **2011**, *13* (6), 1454.
- (9) Anthony, J. E.; Eaton, D. L.; Parkin, S. R. *Org. Lett.* **2002**, *4* (1), 15.
- (10) Maliakal, A.; Raghavachari, K.; Katz, H.; Chandross, E.; Siegrist, T. *Chem. Mater.* **2004**, *16* (24), 4980.
- (11) Anthony, J. E. *Nat. Mater.* **2014**, *13* (8), 773.
- (12) Li, J.; Wang, M.; Ren, S.; Gao, X.; Hong, W.; Li, H.; Zhu, D. *J. Mater. Chem.* **2012**, *22* (21), 10496.
- (13) Miao, Q.; Chi, X.; Xiao, S.; Zeis, R.; Lefenfeld, M.; Siegrist, T.; Steigerwald, M. L.; Nuckolls, C. *J. Am. Chem. Soc.* **2006**, *128* (4), 1340.
- (14) Kim, D.-S.; Jung, J. E.; Baek, N. S.; Kim, T.-D. *Org. Electron.* **2015**, *17*, 319.
- (15) Ono, K.; Totani, H.; Hiei, T.; Yoshino, A.; Saito, K.; Eguchi, K.; Tomura, M.; Nishida, J.; Yamashita, Y. *Tetrahedron* **2007**, *63* (39), 9699.
- (16) Wang, J.; Liu, K.; Liu, Y.-Y.; Song, C.-L.; Shi, Z.-F.; Peng, J.-B.; Zhang, H.-L.; Cao, X.-P. *Org. Lett.* **2009**, *11* (12), 2563.
- (17) Vets, N.; Smet, M.; Dehaen, W. *Synlett* **2005**, *2*, 217.
- (18) Anthony, J. E.; Brooks, J. S.; Eaton, D. L.; Parkin, S. R. *J. Am. Chem. Soc.* **2001**, *123* (38), 9482.
- (19) Okamoto, T.; Reese, C.; Senatore, M. L.; Tang, M. L.; Jiang, Y.; Parkin, S. R.; Bao, Z. *Synth. Met.* **2010**, *160* (23-24), 2447.
- (20) Chien, C.-T.; Watanabe, M.; Chow, T. J. *Tetrahedron* **2015**, *71* (11), 1668.
- (21) Geib, S.; Zschieschang, U.; Gsänger, M.; Stolte, M.; Würthner, F.; Wadepohl, H.; Klauk, H.; Gade, L. H. *Adv. Funct. Mater.* **2013**, *23* (31), 3866.
- (22) Geib, S.; Martens, S. C.; Zschieschang, U.; Lombeck, F.; Wadepohl, H.; Klauk, H.; Gade, L. H. *J. Org. Chem.* **2012**, *77* (14), 6107.
- (23) Usta, H.; Kim, C.; Wang, Z.; Lu, S.; Huang, H.; Facchetti, A.; Marks, T. J. *J. Mater. Chem.* **2012**, *22* (10), 4459.
- (24) Schmidt, R.; Oh, J. H.; Sun, Y.-S.; Deppisch, M.; Krause, A.-M.; Radacki, K.; Braunschweig, H.; Könemann, M.; Erk, P.; Bao, Z.; Würthner, F. *J. Am. Chem. Soc.* **2009**, *131* (17), 6215.
- (25) Frisch, M. J.; Trucks, G. W.; Schlegel, H. B.; Scuseria, G. E.; Robb, M. A.; Cheeseman, J. R.; Scalmani, G.; Barone, V.; Mennucci, B.; Petersson, G. A.; Nakatsuji, H.; Caricato, M.; Li, X.; Hratchian, H. P.; Izmaylov, A. F.; Bloino, J.; Zheng, G.; Sonnenberg, J. L.; Hada, M.; Ehara, M.; Toyota, K.; Fukuda, R.; Hasegawa, J.; Ishida, M.; Nakajima, T.; Honda, Y.; Kitao, O.; Nakai, H.; Vreven, T.; Montgomery Jr., J. A.; Peralta, J. E.; Ogliaro, F.; Bearpark, M. J.; Heyd, J.; Brothers, E. N.; Kudin, K. N.; Staroverov, V. N.; Kobayashi, R.; Normand, J.; Raghavachari, K.; Rendell, A. P.; Burant, J. C.; Iyengar, S. S.; Tomasi, J.; Cossi, M.; Rega, N.; Millam, N. J.; Klene, M.; Knox, J. E.; Cross, J. B.; Bakken, V.; Adamo, C.; Jaramillo, J.; Gomperts, R.; Stratmann, R. E.; Yazyev, O.; Austin, A. J.; Cammi, R.; Pomelli, C.; Ochterski, J. W.; Martin, R. L.; Morokuma, K.; Zakrzewski, V. G.; Voth, G. A.; Salvador, P.; Dannenberg, J. J.; Dapprich, S.; Daniels, A. D.; Farkas, Ö.; Foresman, J. B.; Ortiz, J. V.; Cioslowski, J.; Fox, D. J. *Gaussian 09*; Gaussian, Inc.: Wallingford, CT, USA, 2009.
- (26) Lee, C.; Yang, W.; Parr, R. G. *Phys. Rev. B* **1988**, *37* (2), 785.
- (27) Becke, A. D. *J. Chem. Phys.* **1993**, *98* (7), 5648.
- (28) Krishnan, R.; Binkley, J. S.; Seeger, R.; Pople, J. A. *J. Chem. Phys.* **1980**, *72* (1), 650.
- (29) Vogel, D. E.; Vogel, K. V. 6,13-Bis(thienyl)pentacene compounds. US 2007/0023748A1, January 2, 2007.
- (30) Gronowitz, S.; Holm, B. *Acta Chem. Scand. B* **1976**, *B30*, 423.
- (31) Lumpi, D. Ene-Yne Compounds as Functional Organic Materials, University of Technology Vienna: Vienna, 2013.
- (32) Takimiya, K.; Shinamura, S.; Osaka, I.; Miyazaki, E. *Adv. Mater.* **2011**, *23* (38), 4347.
- (33) Beatrup, D.; Wade, J.; Biniek, L.; Bronstein, H.; Hurhangee, M.; Kim, J.-S.; McCulloch, I.; Durrant, J. R. *Chem Commun* **2014**, *50* (92), 14425.
- (34) McCulloch, I.; Bailey, C.; Giles, M.; Heeney, M.; Love, I.; Shkunov, M.; Sparrowe, D.; Tierney, S. *Chem. Mater.* **2005**, *17* (6), 1381.
- (35) Vinicius Nora de Souza, M. *Curr. Org. Chem.* **2007**, *11* (7), 637.
- (36) Froehlich, J. *Bull. Soc. Chim. Belg.* **1996**, *105* (10-11), 615.
- (37) Froehlich, J. *Prog. Heterocycl. Chem.* **1994**, *6*, 1.
- (38) Li, S.; Zhou, L.; Nakajima, K.; Kanno, K.; Takahashi, T. *Chem. - Asian J.* **2010**, *5* (7), 1620.
- (39) Dediu, V. A.; Hueso, L. E.; Bergenti, I.; Taliani, C. *Nat. Mater.* **2009**, *8* (9), 707.
- (40) Djurovich, P. I.; Mayo, E. I.; Forrest, S. R.; Thompson, M. E. *Org. Electron.* **2009**, *10* (3), 515.

Manuscript # 3

T. Mathis*, Y. Liu, L. Ai, Z. Ge*, D. Lumpi*, E. Horkel, **B. Holzer**, J. Froehlich, and B.
Batlogg

Stable organic field-effect-transistors with high mobilities unaffected by supporting dielectric
based on phenylene-bridged thienobenzothiophene

J. Appl. Phys., **2014**, 115, 043707-1 - 043707-4

Reproduced with permission from *Journal of Applied Physics*. Copyright 2014, AIP Publishing LLC.

<http://dx.doi.org/10.1063/1.4863209>

Stable organic field-effect-transistors with high mobilities unaffected by supporting dielectric based on phenylene-bridged thienobenzothiophene

T. Mathis,^{1,a)} Y. Liu,² L. Ai,² Z. Ge,^{2,b)} D. Lumpi,^{3,c)} E. Horkel,³ B. Holzer,³ J. Froehlich,³ and B. Batlogg¹

¹Laboratory for Solid State Physics, ETH Zurich, 8093 Zurich, Switzerland

²Ningbo Institute of Material Technology and Engineering, Chinese Academy of Science, 315201 Ningbo, China

³Institute of Applied Synthetic Chemistry, Vienna University of Technology, 1060 Vienna, Austria

(Received 9 October 2013; accepted 13 January 2014; published online 24 January 2014)

We report on the electrical properties of organic field-effect transistors (OFET) based on a new class of organic semiconductors. The molecules consist of the same thieno[2,3-*b*][1]benzothiophene building blocks, connected by different π -bridge spacers (ethylene, phenylene, and fluorophenylene). Molecular orbitals and highest occupied molecular orbital/lowest unoccupied molecular orbital energies were calculated and compared with results from cyclic voltammetric and UV-vis absorption measurements. In order to study the influence of the bridge groups on the molecular arrangement and surface interaction, the transistor performance on a wide range of dielectrics has been investigated in detail. These include as grown SiO₂ and Al₂O₃ and also treated with octadecyltrichlorosilane and octadecylphosphonic acid, as well as Cytop and Parylene C. An extended study of the multitude of combinations of these materials revealed mobilities up to $\sim 1 \text{ cm}^2/\text{Vs}$, measured for devices made of the phenylene-bridged compound. Surprisingly, the mobility was quite independent of the supporting gate dielectric. Stability over time has been observed with no degradation after 5 months. By eliminating the hysteresis using Cytop, we were able to show that some of the molecules form films without long-term charge carrier trapping. These are interesting features for practical industrial processing of organic electronics. © 2014 AIP Publishing LLC. [<http://dx.doi.org/10.1063/1.4863209>]

INTRODUCTION

In the ongoing search for organic semiconductor materials that would enable easily producible electronics and with long lifetime, the focus is on charge carrier mobility, long-term stability, and easy but high yield fabrication. In addition, particular electronic performance characteristics, such as turn-on voltage, sub-threshold swing, and electric hysteresis are also optimized. These factors are taken into account in this extensive study when we explore four new molecules for their application potential in organic electronics. The compounds have common TBT (thieno[2,3-*b*][1]benzothiophene) building blocks, connected by distinctly different bridging units. They are deposited as thin films by thermal evaporation on several substrates with nine different gate dielectric stacks, to form organic field-effect-transistors (OFET). By evaluating more than 80 such devices, we find clear trends in the device performance for the various material combinations. Hole mobility up to $\sim 1 \text{ cm}^2/\text{Vs}$ is observed as well as vanishing electronic hysteresis and excellent long-term stability.

THE MOLECULES

Here, we study a new substance class based on two TBT building blocks linked by different π -bridge spacers (Figure 1).

The TBT building block and bridge concept was introduced by Chen *et al.*¹ The TBT structure is expected to provide good redox and thus environmental stability. Furthermore, the extended π -conjugation system in the fused TBT molecules provides efficient orbital overlap and the molecular packaging in sulfur rich TBT in the combination with intermolecular multiple sulfur-sulfur, sulfur-carbon, and carbon-hydrogen π -interactions could lead to high charge mobilities.¹ The introduction of thieno[2,3-*b*]benzothiophene, a regioisomer of Chen's TBT building block, linked to various π -spacer leads to a novel substance class. Here, we focus on four TBT based molecules with the following bridge spacers: a single bond (BTT), 1,2-ethendiyl (ENE), 2,3,5,6-tetrafluoro-1,4-phenylene (4F), and finally 1,4-phenylene (PHEN) completed the substance ensemble shown in Figure 1.

To explore similarities and differences between these molecules, density functional calculations have been performed.^{2,3} The structural configuration was optimized in the ground state, and the local minima in the potential energy surface were verified by a frequency analysis (Gaussian Version 09, Rev.A.02, B3LYP/6-311+G(d)).⁴⁻⁸ These calculations reveal that in the BTT molecule the TBT building blocks are twisted with respect to each other by 32.3°, a potential impediment to defect free stacking in thin film growth. This could lead to less than ideal charge carrier propagation inside the solid. ENE on the other hand shows a fully planar molecular structure, while the π -bridges at the center, in both the 4F and PHEN, are slightly rotated (approx. 14° and 31°, respectively). While these properties

^{a)}Electronic address: mathis@phys.ethz.ch

^{b)}Electronic address: geziyi@nimte.ac.cn

^{c)}Electronic address: dlumpi@ioc.tuwien.ac.at

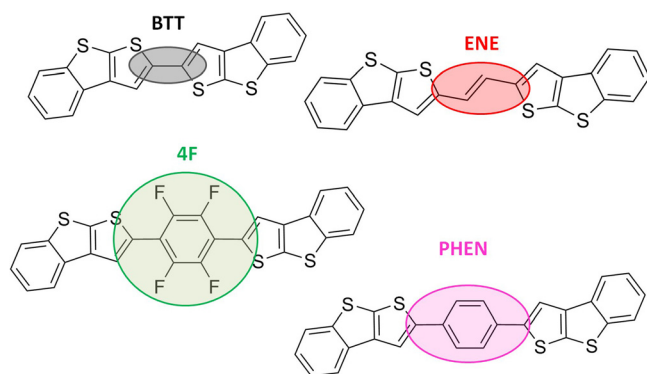


FIG. 1. Molecular structure of the TBT building blocks connected by four different π -bridge spacers: direct linkage of TBT units (black, BTT), an ethene double bond (red, ENE), a fluorinated phenyl ring (green, 4F), and a phenyl ring (pink, PHEN).

might be relevant for the structural packing, also the electronic energies are of importance for the device performance (Figure 2). The highest occupied molecular orbital (HOMO) level for each molecule was determined by cyclic voltammetry. The optical band gap was obtained from the onset of the UV-vis absorption. These experimental results are compared to the data from density functional theory calculations in Table I. The energy of the lowest unoccupied molecular orbital (LUMO) is between -1.6 and -2.4 eV, and those of the HOMO between -5.1 and -5.8 eV. As expected, the levels for the fluorine containing compounds are the lowest due to the high electronegativity of the fluorine. Also shown in Figure 2 is the value for the gold work function ranging in value from -5.2 to -4.8 eV, depending on the quality of the gold film and the surface contamination.^{9,10} Accordingly, we can expect gold contacts to be suitable for hole injection in p-type devices. This is indeed born out in the results.

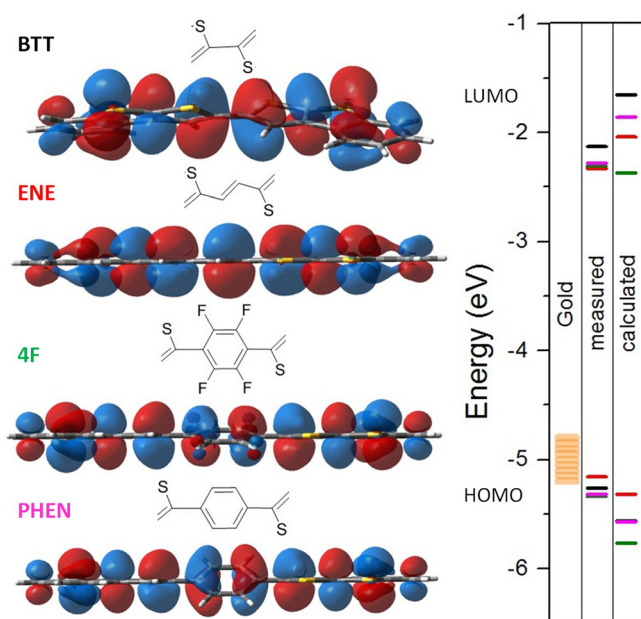


FIG. 2. Graphical illustration of the HOMO and structural configuration of the four TBT based molecules calculated with DFT. On the right side: measured and calculated energies of the HOMO and LUMO levels and the wide range of realistic values of the gold work function.

TABLE I. Energy levels (HOMO and LUMO) of the investigated molecules comparing experimental values obtained using cyclic voltammetry for the HOMO value and the optical band gap (Gap_{opt}) from UV-vis absorption, and calculated values from density functional theory calculations. LUMO was determined from the HOMO and optical band gap.

Bridge	λ_{ABSmax} (eV)	Gap_{opt} (eV)	HOMO/LUMO	
			Meas. (eV)	Calc. (eV)
BTT	356	3.13	$-5.26/-2.13$	$-5.56/-1.65$
ENE	386	2.78	$-5.16/-2.38$	$-5.32/-2.04$
4F	371	3.03	$-5.34/-2.31$	$-5.77/-2.37$
PHEN	365	3.04	$-5.32/-2.28$	$-5.57/-1.86$

DEVICE FABRICATION AND STRUCTURE

To evaluate the potential of the four molecules in organic semiconductor applications, they have been combined, in the form of evaporated thin films, with various dielectrics. For almost all devices, standard highly doped silicon wafer was used as substrate. As gate dielectric, the following materials were used: SiO_2 (260 nm) as purchased and also modified with a self assembled monolayer (SAM) of octadecyltrichlorosilane (OTS)¹¹ or a thin layer of Cytop (30 nm).^{12,13} Al_2O_3 (100 nm) was also used as purchased and also modified with SAMs of OTS or octadecylphosphonic acid (ODPA).¹⁴ The SiO_2 surface was used as substrate to thermally evaporate a 2 nm adhesion layer of chromium and a gold gate electrode with a dielectric layer of spin coated Cytop^{12,13,15-17} or evaporated Parylene C.¹⁸ Cytop is a fluoropolymer with a highly hydrophobic surface and forms trap free interfaces to organic semiconductors as shown by Kalb *et al.*^{15,16} Parylene C is an organic dielectric, also with a highly hydrophobic surface, and is deposited from vapor. Considering the list of dielectrics used, we have covered most major fabrication techniques: thermal evaporation, sputtering, self assembly, spin coating, and deposition from vapor phase. Additionally, we employ high-k (Al_2O_3 , $\epsilon \sim 10$) and low-k (Cytop, $\epsilon \sim 2$) materials.

The organic semiconductors were thermally evaporated through a shadow mask. The thickness of the films was in average around 24 nm. The ~ 25 nm gold source/drain electrodes were evaporated onto the semiconductor resulting in a bottom gate top electrode device structure. The semiconductors were deposited, in general, with the substrate at room-temperature. For particular material combinations, the temperature of the substrate was raised during evaporation to optimize the film growth conditions: PHEN on Al_2O_3 (60°C), PHEN on Al_2O_3 with OTS (120°C for the first 10 nm, final 20 nm at RT), and PHEN on SiO_2 with OTS (same as Al_2O_3 with OTS). The mobility from the optimal conditions is used for analysis and discussions of this study.

OFET PERFORMANCE

An Agilent 4155A semiconductor analyzer was used to measure the transfer and output characteristics of the FETs, with the samples kept in helium atmosphere.¹⁹ From the many trends observed in these measurements, we focus on the hole mobility, drain current, and hysteresis in the transfer

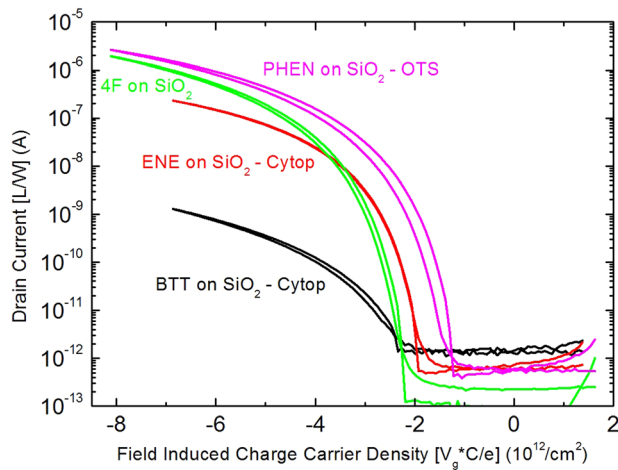


FIG. 3. Transfer characteristics for transistors made with the four semiconductors: BTT (black) and ENE (red) on SiO_2 and thin Cytop, 4F (green) on bare SiO_2 and PHEN (pink) on OTS treated SiO_2 . The source-drain current, normalized by the channel dimensions, is plotted against the field induced charge carrier density to account for the different capacitance of the dielectrics.

curve. Four transfer curves representing the four semiconductors are shown in Figure 3. They are chosen to show an optimal combination of narrow hysteresis, low off-current, and high mobility on comparable gate dielectric. The slightly different values of their capacitances have been taken into account by plotting the field induced charge carrier density instead of the applied gate voltage. All materials yield transistors with good characteristics, including high on-off ratios. Noteworthy are the low saturation currents for BTT, despite the otherwise comparable parameters. We surmise this to be not an intrinsic property of the semiconductor, but the result of a poorly crystalline thin film, e.g., only sparsely connected semiconducting islands embedded in an otherwise insulating surrounding.

HOLE MOBILITY SYSTEMATICS

The hole mobility, as a key quantity, has been evaluated from the saturation regime of the transfer curve, according to the following equation:

$$\mu = \frac{2L}{WC} \left(\frac{\partial \sqrt{I_D}}{\partial V_G} \right)^2. \quad (1)$$

More than 80 devices were measured to study the various material combinations and their mobilities are shown in Figure 4. The results, grouped by the dielectric, show the clustering for each molecule/dielectric combination and reveal the “best” and “worst” choices. PHEN shows the highest mobility and BTT by far the lowest, and the two others (ENE and 4F) are in between. Particularly noteworthy is the fact that PHEN tends to perform similarly well on the different dielectrics. This result suggests the formation of high quality films on all dielectrics, quite independent on the particular surface property. Apparently, the inter-molecular forces are sufficiently strong to overcome interactions with the surface. On the other hand, one might speculate the twisting of the BTT molecule (Figure 2) to be the origin of the low mobility, as the resulting non-optimal microscopic packing of the molecules induces disorder in the orbital overlap and charge localization. Also worth noting is the distinctly non-uniform performance of 4F: the apparent mobility is very low when deposited on the highly hydrophobic surfaces of Cytop or Parylene C, yet it forms a good semiconductor on most other dielectrics. One might ascribe this inferior performance to an adverse interaction between the fluorine of the 4F molecule and the substrates.

LONG TERM STUDY

We refer here to the device performance in terms of mobility only. A full stability study would address the influences of a very wide range of external parameters, including room temperature annealing of structural defects, chemical modification by, e.g., oxygen or humid air, illumination with UV light, etc. In the present study, we have chosen to keep and measure the devices in a controlled He environment (O_2 0.1 ppm, H_2O 0.1 ppm) for up to 5 months. During this time, all samples have been moved into ambient air and UV light five times for 1 day and returned for measurements. No significant variations in the mobility were observed for PHEN on three different dielectrics (Figure 5).

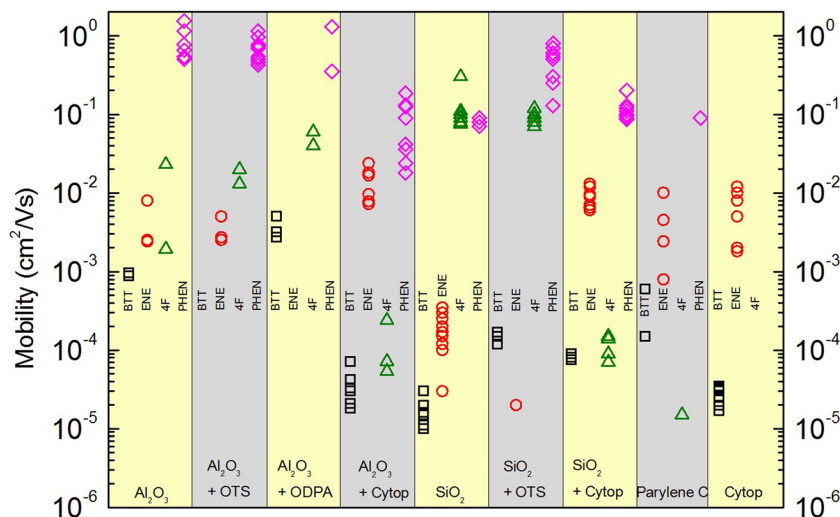


FIG. 4. Summary of the hole mobility for OFETs produced by evaporating the four semiconducting materials on nine different gate dielectric stacks. Values as high as $\sim 1 \text{ cm}^2/\text{Vs}$ and above are recorded for PHEN, and systematic trends are revealed for the other semiconductors.

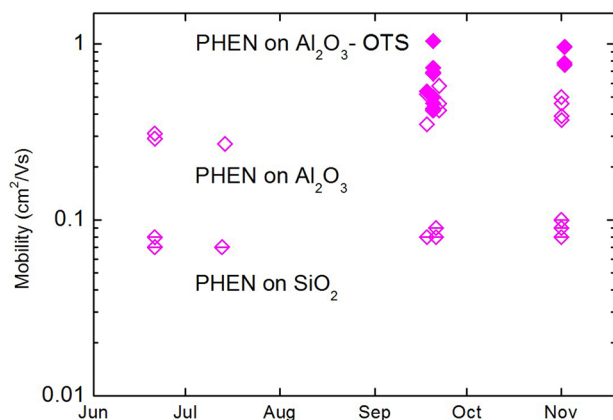


FIG. 5. Long term mobility study of PHEN thin film FETs on SiO_2 and Al_2O_3 . The mobility is stable over more than 5 months.

ELIMINATION OF HYSTERESIS

Long-term charge trapping (hold and release time of trap state exceeds measurement time, typically in the range of minutes) and hysteresis in the transfer curve can originate from trapping of charge carriers in the semiconductor and/or the dielectric. To distinguish between the two situations, we employ a powerful tool: Cytop has been shown to be free of long-term trapping and to form trap free interfaces.^{13,15} When, for example, ENE is deposited on bare SiO_2 or Al_2O_3 , a distinct hysteresis is measured (Figure 6). However, when these dielectrics are coated with an additional thin film of Cytop (30 nm), the hysteresis completely vanishes and, in addition, the mobility improves. Thus, no long-term charge trapping occurs in these TBT based semiconductors. From this, we conclude that the molecular alignment of the semiconductor thin film is improved on Cytop and no long term charge trapping occurs.

SUMMARY

In this study, we have explored new organic semiconductor materials based on TBT building blocks with four different π -bridge spacers (BTT, ENE, 4F, and PHEN) and have

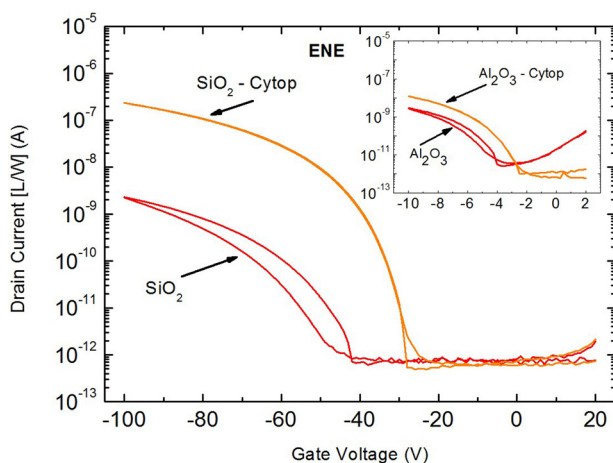


FIG. 6. ENE films deposited on 30 nm Cytop on SiO_2 yield hysteresis-free transfer characteristics, while deposition on bare SiO_2 forms an OFET with a clearly visible hysteresis. The inset shows an equivalent behavior for another dielectric, Al_2O_3 .

combined them with various gate dielectrics. Clear trends in the OFET performance have been established. The ENE π -bridge material showed no long-term charge trapping in the semiconductor, indicating optimal growth and molecular stacking for charge transport, with no hysteresis to speak of in the transfer curve. In PHEN π -bridge devices, the mobility exceeds $1 \text{ cm}^2/\text{Vs}$ and was stable over time. The overall superior mobility of PHEN might originate in a microscopically more advantageous geometric arrangement of the adjacent molecules: the slightly twisted (31°) phenylene bridge will favor lateral “lock-in” of the molecules, preventing the sliding along the long axis, and thus optimizing orbital overlap. This is reminiscent of the role of the side-groups in rubrene. Moreover, the supporting gate dielectric upon which the semiconductor films are evaporated has a limited effect on the high mobility. Apparently, the interaction among the molecules within the films dominates over the interaction with the dielectric substrate, a very interesting result for practical industrial processing of organic electronic applications.

ACKNOWLEDGMENTS

We gratefully acknowledge Kurt Mattenberger for his excellent experimental support and the Sino-Swiss Science and Technology Cooperation (SSSTC) grant for financial support.

- ¹H. Chen, Q. Cui, Y. Guo, J. Huang, M. Zhu, X. Guo, and Y. Liu, *J. Phys. Chem. C* **115**, 23984–23991 (2011).
- ²P. Hohenberg and W. Kohn, *Phys. Rev.* **136**, B864–871 (1964).
- ³K. Burke, *J. Chem. Phys.* **136**, 150901 (2012).
- ⁴M. J. Frisch, G. W. Trucks, H. B. Schlegel, G. E. Scuseria, M. A. Robb, J. R. Cheeseman, G. Scalmani, V. Barone, B. Mennucci, G. A. Petersson, H. Nakatsuji, M. Caricato, X. Li, H. P. Hratchian, A. F. Izmaylov, J. Bloino, G. Zheng, J. L. Sonnenberg, M. Hada, M. Ehara, K. Toyota, R. Fukuda, J. Hasegawa, M. Ishida, T. Nakajima, Y. Honda, O. Kitao, H. Nakai, T. Vreven, J. A. Montgomery, Jr., J. E. Peralta, F. Ogliaro, M. Bearpark, J. J. Heyd, E. Brothers, K. N. Kudin, V. N. Staroverov, R. Kobayashi, J. Normand, K. Raghavachari, A. Rendell, J. C. Burant, S. S. Iyengar, J. Tomasi, M. Cossi, N. Rega, J. M. Millam, M. Klene, J. E. Knox, J. B. Cross, V. Bakken, C. Adamo, J. Jaramillo, R. Gomperts, R. E. Stratmann, O. Yazyev, A. J. Austin, R. Cammi, C. Pomelli, J. W. Ochterski, R. L. Martin, K. Morokuma, V. G. Zakrzewski, G. A. Voth, P. Salvador, J. J. Dannenberg, S. Dapprich, A. D. Daniels, O. Farkas, J. B. Foresman, J. V. Ortiz, J. Cioslowski, and D. J. Fox, *Gaussian 09 Revision A. 02*, (Gaussian, Inc., Wallingford, CT, 2009).
- ⁵A. D. Becke, *J. Chem. Phys.* **98**, 5648 (1993).
- ⁶A. D. McLean and G. S. Chandler, *J. Chem. Phys.* **72**, 5639 (1980).
- ⁷M. J. Frisch, J. A. Pople, and J. S. Binkley, *J. Chem. Phys.* **80**, 3265 (1984).
- ⁸C. Lee, W. Yang, and R. G. Parr, *Phys. Rev. B* **37**, 785–789 (1988).
- ⁹N. D. Lang and W. Kohn, *Phys. Rev. B* **3**, 1215–1223 (1971).
- ¹⁰S. Trasatti, *J. Electroanal. Chem. Interfacial Electrochem.* **54**, 19–24 (1974).
- ¹¹K. P. Pernstich, C. Goldmann, C. Krellner, D. Oberhoff, D. J. Gundlach, and B. Batlogg, *Synth. Met.* **146**, 325 (2004).
- ¹²M. P. Walser, W. L. Kalb, T. Mathis, and B. Batlogg, *Appl. Phys. Lett.* **95**, 233301 (2009).
- ¹³R. Haeusermann and B. Batlogg, *Appl. Phys. Lett.* **99**, 083303 (2011).
- ¹⁴Y. Zhou, V. A. L. Roy, Z. X. Xu, H. Y. Kwong, H. B. Wang, and C. S. Lee, *Appl. Phys. Lett.* **98**, 092904 (2011).
- ¹⁵W. Kalb, T. Mathis, S. Haas, A. Strassen, and B. Batlogg, *Appl. Phys. Lett.* **90**, 092104 (2007).
- ¹⁶K. P. Pernstich, B. Roessner, and B. Batlogg, *Nature Mater.* **7**, 321–325 (2008).
- ¹⁷K. Willa, R. Haeusermann, T. Mathis, A. Facchetti, Z. Chen, and B. Batlogg, *J. Appl. Phys.* **113**, 133707 (2013).
- ¹⁸N. Kawasaki, W. L. Kalb, T. Mathis, Y. Kaji, R. Mitsuhashi, H. Okamoto, Y. Sugawara, A. Fujiwara, Y. Kubozono, and B. Batlogg, *Appl. Phys. Lett.* **96**, 113305 (2010).
- ¹⁹K. P. Pernstich, *J. Res. Natl. Inst. Stand. Technol.* **117**, 176–184 (2012).

Manuscript # 4

Brigitte Holzer*, Christian Hametner, and Johannes Fröhlich

Facile Synthesis of Benzo[*b*]selenophene Building Blocks

Manuscript draft

Facile Synthesis of Benzo[*b*]selenophene Building Blocks

*Brigitte Holzer, * Christian Hametner, and Johannes Fröhlich*

Institute of Applied Synthetic Chemistry, Vienna University of Technology,

Getreidemarkt 9/163OC, A-1060 Vienna, Austria

* brigitte.holzer@tuwien.ac.at

A novel one-pot synthesis toward benzo[*b*]selenophene carboxylic acid esters starting from commercially available *o*-chlorobenzaldehyde or *o*-chloroacetophenone applying lithium alkylselenides and a Fiesselmann type reaction is presented. Further derivatization of the obtained products gives rise to a broad spectrum of benzo[*b*]selenophene building blocks valuable for various scientific disciplines.

INTRODUCTION

The synthesis of benzo[*b*]selenophene derivatives is of considerable scientific interest owing to their potential applications in diverse scientific disciplines like medicinal chemistry,^{1,2} crystallography,³ and materials chemistry.^{4,5} While the benzo[*b*]selenophene heterocyclic moiety itself has not been found in natural compounds, it is considered to be a bioisostere of naphthalene, benzofuran, benzothiophene, and indole,² which especially makes the selenium analog of tryptophan a potentially interesting building block in medicinal and biochemistry. Substitution at 2- and 3-position of benzo[*b*]chalcogenophenes gives rise to important building blocks for the preparation of potential drugs.⁶ Recently, benzo[*b*]selenophene analogues of raloxifene (Figure 1, A) and milfasartan have been evaluated toward their applications as antiproliferative agents in treatment of breast cancer⁷ or as AT₁ receptor antagonists.⁸ Replacement of indole by benzo[*b*]selenophene toward the selenotryptophan (Figure 1, B) derivatives may reduce phase problems in X-ray crystallographic protein studies,³ since the heavy selenium atoms are easily distinguishable from atoms typically present in biological samples because of their larger electron densities.⁹ In addition, benzo[*b*]selenophene moieties proved to be very useful synthetic intermediates in materials chemistry and can function as suitable building blocks to synthesize narrow bandgap bulk heterojunction solar cell devices¹⁰ or high-performance field-effect transistors (e.g. DPh-BSBS, Figure 1, C).^{4,5,11}

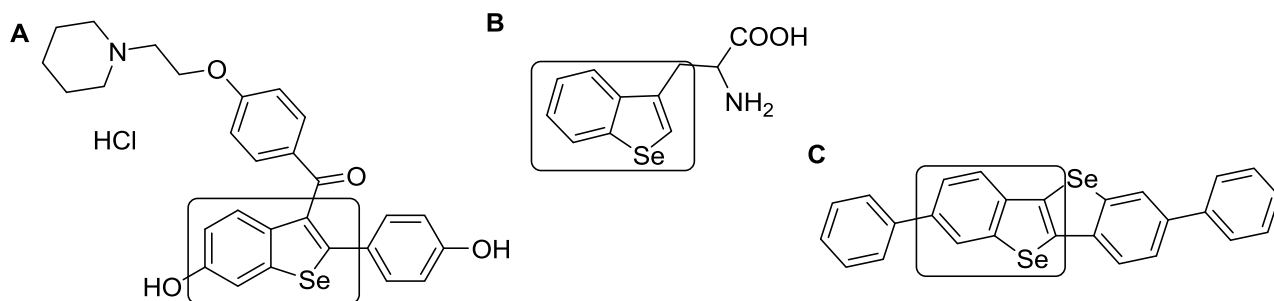


Figure 1: Benzo[*b*]selenophene derivatives: (A) raloxifene analog, (B) selenotryptophan, and (C) 2,7-diphenyl[1]benzoselenopheno[3,2-*b*][1]benzoselenophene (DPh-BSBS).

Although benzo[*b*]selenophenes constitute important synthetic starting materials, the lack of a low-cost, high-yielding and convenient synthesis is evident considering the few commercial suppliers available and the high costs of these scaffolds. Various syntheses have been proposed based on tandem free-radical addition/substitution sequences starting from rather explosive diazonium salts,⁸ intramolecular cyclization of costly ethynylbenzenes using sodium chalcogenides,¹² and radical cyclisation of 2-(benzylseleno)-1-(2-iodophenyl)ethanols,¹³ which in turn are prepared in a multistep synthesis, to name a few.

Herein we report a convenient one-pot synthesis toward benzo[*b*]selenophene-2-carboxylates starting from commercially available *o*-chlorobenzaldehyde or *o*-chloroacetophenone. Further derivatization of the obtained compounds with strong emphasis on functionalization possibilities in 2- and 3-position gives rise to a broad spectrum of substituted benzo[*b*]selenophenes suitable as building blocks for various scientific disciplines.

EXPERIMENTAL SECTION

Substances purchased from commercial sources were used as received. Anhydrous *N,N*-dimethylformamide (DMF), methyllithium (1.6 M in diethyl ether), *n*-butyllithium solution (2.5 M in hexanes), *o*-chlorobenzaldehyde and *o*-chloroacetophenone were purchased from Aldrich Chemical Co. Anhydrous tetrahydrofuran (THF) and 1,4-dioxane were prepared immediately prior to use by a *PURESOLV*-plant (*it-innovative technology inc.*). Technical grade solvents were distilled prior to use. Analytical TLC was performed on Merck silica gel 60 F254 plates. Chromatographic separations at preparative scale were carried out on silica gel (Merck silica gel 60, 40 - 63 μm). Nuclear magnetic resonance (NMR) spectra were obtained using a Bruker Avance III HD 600 MHz with cryo probe or Avance III HD 400 MHz fourier transform spectrometer operating at the following frequencies: Avance III HD 600 MHz: 600.2 MHz (^1H), 150.9 MHz (^{13}C) and 114.5 MHz (^{77}Se); Avance III HD 400 MHz: 400.1 MHz (^1H), 100.6 MHz (^{13}C) and 76.5 MHz (^{77}Se). The chemical shifts are reported in δ units, parts per million (ppm) downfield from tetramethylsilane using solvent residual signals for calibration. ^{77}Se chemical shifts are given in ppm relative to dimethylselenide, using selenophene (δ 605 ppm)¹⁴ as an external secondary standard. Coupling constants are reported in Hertz; multiplicity of signals is indicated by using following abbreviations: s=singlet, d=doublet, t=triplet, q=quartet, quin=quintet. The multiplicity of ^{13}C signals was obtained by measuring JMOD spectra. High-resolution mass spectra (HRMS) were acquired using a Thermo Scientific LTQ Orbitrap XL hybrid FTMS (Fourier Transform Mass Spectrometer) equipped with Thermo Fischer Exactive Plus Orbitrap (LC-ESI+) and a Shimadzu IT-TOF Mass Spectrometer.

2-(Methylseleno)benzaldehyde (**2**). Grey selenium (1.58 g, 20 mmol, 1 eq.) was suspended in 40 mL anhydrous degassed THF under argon atmosphere. The suspension was cooled to 0 °C and MeLi (1.45 mL, 22 mmol, 1.1 eq.) was added dropwise. The resulting white suspension was stirred for 40 minutes. *o*-Chlorobenzaldehyde **1a** (2.80 g, 20 mmol, 1 eq.) was added dropwise giving a clear orange solution, which was stirred overnight at room temperature, quenched with water and extracted repeatedly with ethyl acetate. The organic layer was washed with brine, dried over anhydrous Na_2SO_4 and the solution was concentrated in vacuo. **2** was purified by column chromatography (40 g silica gel, light petroleum : ethyl acetate 20:1) and isolated in 42% yield as a yellow oil (1.70 g). TLC (silica gel, light petroleum : ethyl acetate 7:1): R_f = 0.45. ^1H NMR (600 MHz, CDCl_3): δ = 10.15 (s, 1 H), 7.81 (dd, J = 7.6, 1.5 Hz, 1 H), 7.51 - 7.49 (m, 1 H), 7.46 - 7.45

(m, 1 H), 7.35 (td, $J = 7.3, 1.1$ Hz, 1 H), 2.30 (s, 3 H) ppm. ^{13}C NMR (150 MHz, CDCl_3): $\delta = 192.4$ (d), 138.7 (s), 135.5 (d), 134.2 (s), 133.8 (d), 127.8 (d), 124.8 (d), 5.77 (q) ppm. ^{77}Se NMR (114 MHz, CDCl_3): $\delta = 248$ ppm. HR-ESI-FTMS $[\text{M}+\text{H}]^+$ m/z calcd. 200.9813 for $\text{C}_8\text{H}_9\text{OSe}^+$, found 200.9811.

Ethyl 2-[(2-formylphenyl)seleno]acetate (**3**). **2** (1.70 g, 8.5 mmol, 1 eq.) and ethyl bromoacetate (1.40 g, 8.5 mmol, 1 eq.) were heated to reflux. Conversion was monitored by TLC. After 12 hours the resulting red liquid was dissolved in dichloromethane and directly concentrated on 6 g silica gel and purified by column chromatography (40 g silica gel, light petroleum : ethyl acetate 10:1). **3** was isolated in 73% yield (1.68 g) as a yellow solid. TLC (silica gel, light petroleum : ethyl acetate 7:1): $R_f = 0.52$. $F_p = 34.2 - 36.0$ °C. ^1H NMR (600 MHz, CDCl_3): $\delta = 10.15$ (s, 1 H), 7.85 (dd, $J = 7.6, 1.5$ Hz, 1 H), 7.76 (m, 1 H), 7.53 (m, 1 H), 7.40 (m, 1 H), 4.17 (q, $J = 7.2$ Hz, 2 H), 3.58 (s, 2 H), 1.24 (t, $J = 7.2$ Hz, 3 H) ppm. ^{13}C NMR (150 MHz, CDCl_3): $\delta = 192.6$ (d), 170.9 (s), 136.9 (s), 135.2 (d), 134.5 (s), 134.1 (d), 129.3 (d), 125.8 (d), 61.4 (t), 25.3 (t), 14.1 (q) ppm. ^{77}Se NMR (114 MHz, CDCl_3): $\delta = 367$ ppm. HR-ESI-FTMS $[\text{M}+\text{H}]^+$ m/z calcd. 273.0024 for $\text{C}_{11}\text{H}_{13}\text{O}_3\text{Se}^+$, found 273.0058.

Ethyl benzo[*b*]selenophene-2-carboxylate (**4a**). **3** (1.68 g, 6.2 mmol, 1 eq.) was dissolved in 20 mL anhydrous DMF, K_2CO_3 (1.71 g, 12.4 mmol, 2 eq.) was added and the reaction mixture was heated to 120 °C for two hours. The solution was quenched with water and extracted repeatedly with ethyl acetate. The organic layer was washed with brine, dried over anhydrous Na_2SO_4 and concentrated in vacuo. **4a** was purified by column chromatography (40 g silica gel, light petroleum : ethyl acetate 20:1) and isolated in 96% yield as a yellow oil (1.50 g). TLC (silica gel, light petroleum : ethyl acetate 9:1): $R_f = 0.59$. ^1H NMR (400 MHz, CDCl_3): $\delta = 8.29$ (s, 1 H), 7.94 - 7.87 (m, 2 H), 7.43 - 7.36 (m, 2 H), 4.39 (q, $J = 7.3$ Hz, 2 H), 1.41 (t, $J = 7.3$ Hz, 3 H) ppm. The obtained NMR data are in accordance with literature.⁸ HR-ESI-FTMS $[\text{M}+\text{H}]^+$ m/z calcd. 254.9919 for $\text{C}_{11}\text{H}_{11}\text{O}_2\text{Se}^+$, found 254.9916.

General Procedure for the one-pot synthesis of **4a** and **4b**: Grey selenium (1 eq.) was suspended in anhydrous degassed THF under argon atmosphere. The suspension was cooled to 0 °C and *n*-BuLi (1.1 eq.) was added dropwise. The resulting white suspension was stirred for 40 minutes. **1a** or **1b** (1 eq.) dissolved in 20 mL anhydrous DMF was added dropwise giving a clear orange solution. The resulting solution was stirred overnight at room temperature. Full conversion of starting material was confirmed by GC-MS analysis. THF and hexanes were distilled off under reduced pressure and 100 mL anhydrous DMF was added. Ethyl bromoacetate (2 eq.) was added and the resulting solution was refluxed overnight. Potassium carbonate (2 eq.) was added and the reaction mixture was refluxed for four hours. The reaction mixture was cooled to room temperature, 100 mL 2N NaOH was added and the product was extracted repeatedly with ethyl acetate. The organic layer was washed with brine, dried over anhydrous Na_2SO_4 and concentrated in vacuo.

Ethyl benzo[*b*]selenophene-2-carboxylate (**4a**). Starting from *n*-BuLi (44 mL, 110 mmol) in 160 mL THF, freshly distilled *o*-chlorobenzaldehyde (14.06 g, 100 mmol), ethyl bromoacetate (33.6 g, 200 mmol) and potassium carbonate (27.6 g, 200 mmol) **4a** was synthesized according to the general procedure. **4a** was purified by distillation (0.15 mbar, 120 °C) and isolated in 74% yield (18.81 g) as a yellow oil. The obtained NMR and HRMS data were consistent with those acquired from the multistep procedure.

Ethyl 3-methylbenzo[*b*]selenophene-2-carboxylate (**4b**). Starting from *n*-BuLi (26.4 mL, 66 mmol) in 100 mL THF, *o*-chloroacetophenone (9.30 g, 60 mmol), ethyl bromoacetate (20.04 g, 120 mmol) and potassium carbonate (16.58 g, 120 mmol) **4b** was synthesized according to the general procedure. **4b** was purified by column chromatography (light petroleum: ethyl acetate 9:1) and isolated in 57% yield (9.10 g) as a yellow solid. TLC (180 g silica gel, light petroleum : ethyl acetate 7:1): $R_f = 0.61$. $F_p = 42.3 - 43.1$ °C. ^1H NMR (400 MHz, CDCl_3): $\delta = 7.89 - 7.81$ (m, 2 H), 7.45 - 7.38 (m, 2 H), 4.38 (q, $J = 7.3$ Hz, 2 H), 2.73 (s, 3 H), 1.41 (t, $J = 7.3$ Hz, 3 H) ppm. ^{13}C NMR (100 MHz, CDCl_3): $\delta = 164.5$ (s), 143.9 (s), 142.7 (s), 141.7 (s), 129.1 (s), 127.0 (d), 125.6 (d), 125.5 (d), 124.6 (d), 61.1 (t), 14.3 (q), 14.4 (q) ppm. ^{77}Se NMR (76 MHz, CDCl_3): $\delta = 521$ ppm. HR-ESI-FTMS $[\text{M}+\text{H}]^+$ m/z calcd. 269.0075 for $\text{C}_{12}\text{H}_{13}\text{O}_2\text{Se}^+$, found 269.0075.

3-Methylbenzo[*b*]selenophene-2-carboxylic acid (**5**). **4b** (5.44 g, 20 mmol, 1 eq.) and sodium hydroxide (1.60 g, 40 mmol, 2 eq.) were refluxed in 60 mL solvent (methanol : H_2O 2:3) for four hours. Conversion was monitored by TLC (dichloromethane : methanol 9:1). The reaction mixture was cooled to room temperature and 2 N HCl was added. The precipitate was filtrated and dried in vacuo. **5** was isolated in 91% yield (4.34 g) as a colourless solid. TLC (silica gel, dichloromethane : methanol 9:1): $R_f = 0.38$. $F_p = 189.2 - 191.4$ °C. ^1H NMR (600 MHz, DMSO-d_6): $\delta = 13.32$ (bs, 1 H), 8.08 - 8.07 (m, 1 H), 7.94 - 7.92 (m, 1 H), 7.50 - 7.45 (m, 2 H), 2.66 (s, 3 H) ppm. ^{13}C NMR (150 MHz, DMSO-d_6): $\delta = 165.5$ (s), 142.6 (s), 142.6 (s), 140.9 (s), 130.6 (s), 127.3 (d), 126.1 (d), 125.8 (d), 125.0 (d), 14.1 (q) ppm. ^{77}Se NMR (114 MHz, DMSO-d_6): $\delta = 516$ ppm.

3-Methylbenzo[*b*]selenophene (**6**). **5** (4.07 g, 17 mmol, 1 eq.) and copper (486 mg, 7.7 mmol, 0.45 eq.) were refluxed in 40 mL quinoline for three hours. The reaction mixture was cooled to room temperature and 2 N HCl was added. The aqueous layer was extracted repeatedly with diethyl ether. The organic layer was washed with brine, dried over anhydrous Na_2SO_4 and concentrated in vacuo. **6** was purified by column chromatography (90 g silica gel, light petroleum) and isolated in 94% yield (3.12 g) as a yellow liquid. TLC (silica gel, light petroleum): $R_f = 0.63$. ^1H NMR (400 MHz, CDCl_3): $\delta = 8.12 - 8.10$ (m, 1 H), 7.90 - 7.88 (m, 1 H), 7.71 (d, $J = 1.3$ Hz, 1 H), 7.61 (ddd, $J = 8.1, 7.0, 1.1$ Hz, 1 H), 7.50 (ddd, $J = 8.3, 7.0, 1.2$ Hz, 1 H), 2.57 (d, $J = 1.3$ Hz, 3 H) ppm. ^{13}C NMR (100 MHz, CDCl_3): $\delta = 141.8$ (s), 141.4 (s), 134.9 (s), 125.8 (d), 124.1 (d), 124.1 (d), 123.4 (d), 123.2 (d), 15.8 (q) ppm. ^{77}Se NMR (76 MHz, CDCl_3): $\delta = 479$ ppm. HR-ESI-FTMS $[\text{M}+\text{H}]^+$ m/z calcd. 196.9864 for $\text{C}_9\text{H}_9\text{Se}^+$, found 196.9882.

Benzo[*b*]selenophene-3-carbaldehyde (**7**). **6** (1.07 g, 5.5 mmol, 1 eq.) and SeO₂ (732 mg, 6.6 mmol, 1.2 eq.) were refluxed in 10 mL anhydrous 1,4-dioxane for six hours. The reaction mixture was cooled to room temperature, grey selenium was filtered over celite and the obtained solution was concentrated in vacuo. The crude product was purified by column chromatography (90 g silica gel, light petroleum : ethyl acetate 8:1) and isolated in 90% yield (1.04 g) as a colourless solid. TLC (silica gel, light petroleum : ethyl acetate 9:1): R_f = 0.42. F_p = 87.8 - 88.2 °C. ¹H NMR (600 MHz, CDCl₃): δ = 10.08 (s, 1 H), 9.00 (s, 1 H), 8.78 - 8.77 (m, 1 H), 7.93 - 7.91 (m, 1 H), 7.52 - 7.49 (m, 1 H), 7.42 - 7.40 (m, 1 H) ppm. ¹³C NMR (150 MHz, CDCl₃): δ = 186.1 (d), 149.3 (d), 142.4 (s), 140.0 (s), 137.0 (s), 126.6 (d), 126.3 (d), 126.0 (d), 125.3 (d) ppm. ⁷⁷Se NMR (114 MHz, CDCl₃): δ = 537 ppm. HR-ESI-FTMS [M+H]⁺ m/z calcd. 210.9657 for C₉H₇OSe⁺, found 210.9659.

Benzo[*b*]selenophene-2-methanol (**8a**). **4a** (10.13 g, 40 mmol, 1 eq.) was dissolved in 100 mL anhydrous THF. The solution was cooled to 0 °C and LiAlH₄ (1.52 g, 40 mmol, 1 eq.) was added in portions. The reaction mixture was stirred at room temperature for one hour and hydrolysed with 2 N NaOH. The aqueous layer was extracted repeatedly with diethyl ether. The organic layer was washed with brine, dried over anhydrous Na₂SO₄ and concentrated in vacuo. **8a** was isolated in 97% yield (8.20 g) as a colourless solid. TLC (silica gel, light petroleum : ethyl acetate 3:1): R_f = 0.49. F_p = 107.7 - 108.5 °C. ¹H NMR (400 MHz, CDCl₃): δ = 7.88 - 7.86 (m, 1 H), 7.73 - 7.71 (m, 1 H), 7.37 - 7.33 (m, 2 H), 7.27 - 7.23 (m, 1 H), 4.95 (d, J = 1.2 Hz, 2 H) ppm. ¹³C NMR (100 MHz, CDCl₃): δ = 149.2 (s), 141.9 (s), 141.3 (s), 125.6 (d), 125.2 (d), 124.6 (d), 124.4 (d), 124.4 (d), 62.9 (t) ppm. ⁷⁷Se NMR (76 MHz, CDCl₃): δ = 513 ppm.

Benzo[*b*]selenophene-3-methanol (**8b**). **7** (1.34 g, 6.4 mmol, 1 eq.) was dissolved in 20 mL anhydrous ethanol. The solution was cooled to 0 °C and NaBH₄ (242 mg, 6.4 mmol, 1 eq.) was added in portions. The reaction mixture was stirred at room temperature for three hours and hydrolysed with water. The aqueous layer was extracted repeatedly with diethyl ether. The organic layer was washed with brine, dried over anhydrous Na₂SO₄ and concentrated in vacuo. **8b** was isolated in 92% yield (1.24 g) as a yellow oil. TLC (silica gel, light petroleum : ethyl acetate 3:1): R_f = 0.46. ¹H NMR (600 MHz, CDCl₃): δ = 7.93 - 7.92 (m, 1 H), 7.91 (s, 1 H), 7.86 - 7.84 (m, 1 H), 7.41 (ddd, J = 8.1, 7.1, 1.1 Hz, 1 H), 7.33 (ddd, J = 8.5, 6.9, 1.2 Hz, 1 H), 4.87 (d, J = 0.9 Hz, 2 H) ppm. ¹³C NMR (150 MHz, CDCl₃): δ = 142.1 (s), 139.8 (s), 139.0 (s), 126.1 (d), 126.0 (d), 124.8 (d), 124.5 (d), 123.7 (d), 61.3 (t) ppm. ⁷⁷Se NMR (114 MHz, CDCl₃): δ = 491 ppm.

3-Bromobenzo[*b*]selenophene-2-methanol (**9a**). **8a** (7.39 g, 35 mmol, 1 eq.) was dissolved in 150 mL chloroform. The solution was cooled to 0 °C and *N*-bromosuccinimide (6.22 g, 35 mmol, 1 eq.) was added in portions. The reaction mixture was stirred at room temperature for one hour and hydrolysed with 50 mL 2 N NaOH. The aqueous layer was extracted repeatedly with chloroform. The organic layer was dried over anhydrous Na₂SO₄ and **9a** was isolated in 86% yield (8.68 g). TLC (silica gel, light petroleum : ethyl acetate 3:1): R_f = 0.62. F_p = 103.2 - 104.9 °C. ¹H NMR (600 MHz,

CDCl₃): δ = 7.91 (dd, J = 8.3, 0.8 Hz, 1 H), 7.78 (dd, J = 8.2, 0.9 Hz, 1 H), 7.39 (ddd, J = 8.3, 7.0, 1.3 Hz, 1 H), 7.31 (ddd, J = 8.2, 6.8, 1.3 Hz, 1 H), 4.87 (s, 2 H) ppm. ¹³C NMR (150 MHz, CDCl₃): δ = 141.7 (s), 139.8 (s), 137.7 (s), 125.3 (d), 125.2 (d), 125.1 (d), 124.0 (d), 116.4 (s), 58.7 (t) ppm. ⁷⁷Se NMR (114 MHz, CDCl₃): δ = 581 ppm. HR-ESI-FTMS [M+H]⁺ m/z calcd. 290.8918 for C₉H₈BrOSe⁺, found 290.8915.

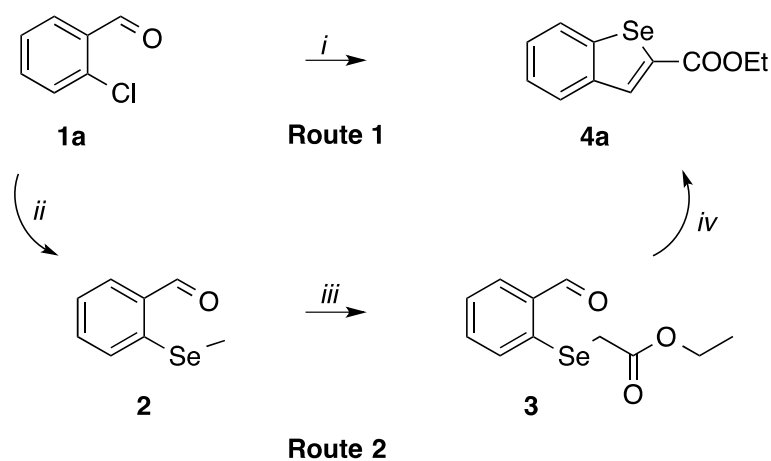
2-Bromobenzo[*b*]selenophene-3-methanol (**9b**). **8b** (2.01 g, 9.5 mmol, 1 eq.) was dissolved in 10 mL anhydrous chloroform. The solution was cooled to 0 °C and *N*-bromosuccinimide (1.69 g, 9.5 mmol, 1 eq.) was added in portions. The reaction mixture was stirred at room temperature for one hour and hydrolysed with 50 mL 2 N NaOH. The aqueous layer was extracted repeatedly with diethyl ether. The organic layer was dried over anhydrous Na₂SO₄, the crude product was purified by column chromatography (50 g silica gel, light petroleum : ethyl acetate 9:1). **9b** was isolated as yellow oil in 45% yield (1.23 g). TLC (silica gel, light petroleum : ethyl acetate 3:1): R_f = 0.60. F_p = 139.6 - 142.1 °C. ¹H NMR (600 MHz, CDCl₃): δ = 7.91 - 7.90 (m, 1 H), 7.79 - 7.77 (m, 1 H), 7.39 (ddd, J = 8.2, 6.9, 1.3 Hz, 1 H), 7.31 (ddd, J = 8.2, 6.9, 1.3 Hz, 1 H), 4.87 (s, 2 H) ppm. ¹³C NMR (150 MHz, CDCl₃): δ = 141.7 (s), 139.9 (s), 137.7 (s), 125.3 (d), 125.2 (d), 125.1 (d), 124.0 (d), 116.5 (s), 58.8 (t) ppm. ⁷⁷Se NMR (114 MHz, CDCl₃): δ = 581 ppm. HR-ESI-FTMS [M+H]⁺ m/z calcd. 290.8918 for C₉H₈BrOSe⁺, found 290.8913.

3-Bromobenzo[*b*]selenophene-2-carbaldehyde (**10a**). **9a** (8.70 g, 30 mmol, 1 eq.) was dissolved in 150 mL ethyl acetate. MnO₂ (15.65 g, 180 mmol, 6 eq.) was added and the reaction mixture was stirred at room temperature overnight. The reaction mixture was filtered over celite, concentrated, dissolved in dichloromethane and stirred with active charcoal for one hour. The charcoal was filtered over celite and **10a** was isolated in 75% yield (6.50 g) as a colourless solid. TLC (silica gel, light petroleum : ethyl acetate 15:1): R_f = 0.54. F_p = 99.7 - 102.1 °C. ¹H NMR (600 MHz, CDCl₃): δ = 10.20 (s, 1 H), 8.12 - 8.10 (m, 1 H), 7.93 - 7.92 (m, 1 H), 7.54 - 7.49 (m, 2 H) ppm. ¹³C NMR (150 MHz, CDCl₃): δ = 186.2 (d), 141.2 (s), 140.1 (s), 139.5 (s), 129.2 (d), 127.2 (d), 126.3 (d), 126.1 (d), 120.4 (s) ppm. ⁷⁷Se NMR (114 MHz, CDCl₃): δ = 536 ppm. HR-ESI-FTMS [M+H]⁺ m/z calcd. 288.8762 for C₉H₆BrOSe⁺, found 288.8758.

2-Bromobenzo[*b*]selenophene-3-carbaldehyde (**10b**). **9b** (1.62 g, 5.6 mmol, 1 eq.) was dissolved in 150 mL ethyl acetate. MnO₂ (2.92 g, 33.6 mmol, 6 eq.) was added and the reaction mixture refluxed for 30 hours. The reaction mixture was filtered over celite, concentrated and **10b** was isolated in 98% yield (1.58 g) as a colourless solid. TLC (silica gel, light petroleum : ethyl acetate 7:1): R_f = 0.60. F_p = 140.8 - 143.6 °C. ¹H NMR (400 MHz, CDCl₃): δ = 10.21 (s, 1 H), 8.79 (dd, J = 8.1, 1.4 Hz, 1 H), 7.76 (dd, J = 8.1, 1.0 Hz, 1 H), 7.46 - 7.36 (m, 2 H) ppm. ¹³C NMR (100 MHz, CDCl₃): δ = 186.3 (d), 140.7 (s), 137.4 (s), 137.1 (s), 134.5 (s), 126.4 (d), 126.3 (d), 125.6 (d), 124.3 (d) ppm. ⁷⁷Se NMR (76 MHz, CDCl₃): δ = 618 ppm. HR-ESI-FTMS [M+H]⁺ m/z calcd. 288.8762 for C₉H₆BrOSe⁺, found 288.8756.

RESULTS AND DISCUSSION

The synthetic pathway toward benzo[*b*]selenophene carboxylic acid esters is based on a Fiesselmann type reaction (Scheme 1) and was planned to give target compounds in a one-pot procedure (route 1) without the need of isolating intermediate products. The synthetic sequence was first probed by a stepwise approach yielding **4a** (route 2). Introduction of selenium in commercially available **1a** was achieved by nucleophilic aromatic substitution applying *in situ* generated lithium methyl selenide giving rise to methyl selenide **2** in 42% yield. The applied method inspired by Tiecco et al.¹⁶ introduces selenium as organo-selenide, while earlier reports on the synthesis toward phenyl selenides are based on lithiation of the phenyl ring and subsequent conversion with elemental selenium requiring protective groups for carbonyl substituents.¹⁵ Thus the need for derivatization of the carbonyl functionality and the tedious preparation of unstable Na₂Se or NaHSe frequently used to prepare phenyl selenides are avoided by the applied synthetic protocol.^{17,18} Further conversion toward **3** was realized by refluxing **2** with ethyl bromoacetate following a similar procedure reported by Renson et al.¹⁹ This step was proposed to proceed by the addition of ethyl bromoacetate to the aryl methyl selenide forming an intermediate selenonium bromide.²⁰ Thermal decomposition of this salt gave rise to arylselenoacetic ester **3** in 73% yield. Finally ring closure toward benzo[*b*]selenophene carboxylate **4a** was achieved by applying a base-induced condensation reaction in 96% yield.

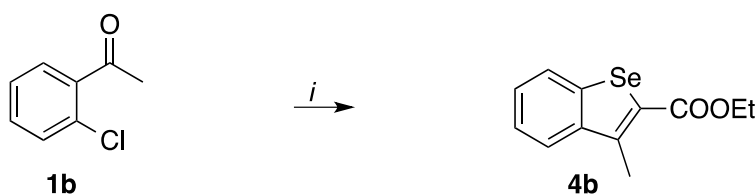


Scheme 1: One-pot (route 1): *i*: grey selenium, n-BuLi, THF, r.t. 40 min / DMF, ethyl bromoacetate, reflux / K₂CO₃, 120 °C; and stepwise synthesis procedure (route 2): *ii*: grey selenium, MeLi THF, r.t. 40 min; *iii*: ethyl bromoacetate, reflux; *iv*: DMF, K₂CO₃, 120 °C.

Based on the obtained results a one-pot approach toward **4a** avoiding the necessity of isolating **2** and **3** was pursued. Since the decomposition of the *in situ* generated triorgano-selenonium bromide generates toxic bromomethane as side product, the first step of the synthetic pathway was altered: instead of lithium methyl selenide its butyl analog, generated *in situ* from elementary selenium and n-butyllithium, was applied. The reaction progress was monitored by GC-MS analysis and clean

conversion toward the respective aryl butyl selenide could be observed. Subsequently the solvent was distilled off under vacuum and replaced by DMF in order to achieve the high reaction temperatures necessary for the decomposition of the selenonium salt. Ethyl bromoacetate was added, the reaction mixture was refluxed and after an appropriate reaction time base was added. The desired compound **4a** was obtained in 74% yield, however GC-MS analysis revealed butyl benzo[*b*]selenophene-2-carboxylate as side product. The formation of the latter can be attributed to trans-esterification of **4a** with butanol, which originates from the hydrolysis of butyl bromide generated during the decomposition of the selenonium bromide.

The developed procedure was also applied to *o*-chloroacetophenone (Scheme 2) giving rise to **4b** in 57% yield.

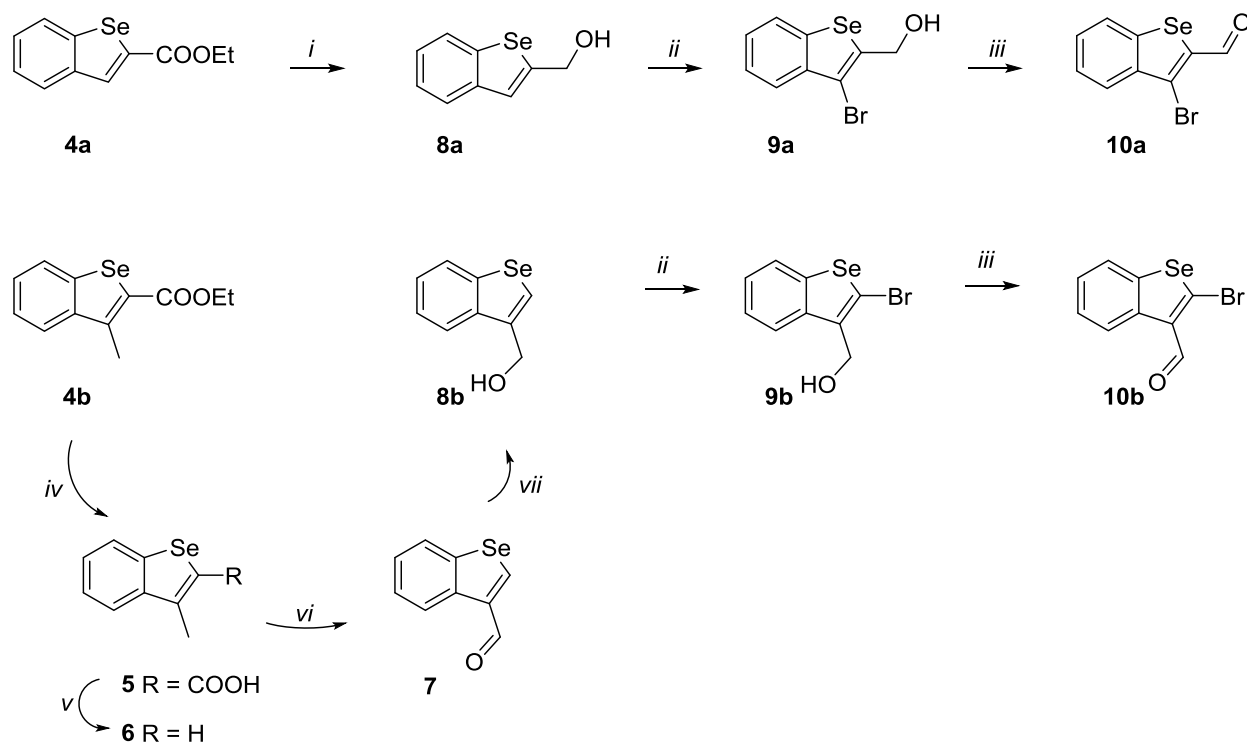


Scheme 2: Synthesis of **4b**. Reaction conditions: *i*: grey selenium, *n*-BuLi, THF, r.t., 40 min / DMF, ethyl bromoacetate, reflux / K₂CO₃, 120 °C.

Since benzo[*b*]selenophenes substituted in the 2- and 3-position bearing both a carbonyl group and a properly substituted reaction site for successive cross-coupling (e.g., a halogenide) constitute essential building blocks for various disciplines (Figure 1), an efficient and reliable synthetic methodology was probed toward both isomers **10a** and **10b**. Both functional groups provide valuable strategic linking points for further transformation. Furthermore, the planned strategy should be high-yielding and based on the application of low-cost reagents suitable for materials science and medicinal chemistry without the need of complex purification.

The reaction toward **10a** (Scheme 3) was achieved by reducing the obtained ester **4a** applying LiAlH₄ in 97% yield. Subsequent bromination of alcohol **8a** gave **9a** in 86% yield, further oxidation with MnO₂ led to aldehyde **10a** in 75% yield.

The synthetic pathway toward isomer **10b** (Scheme 3) was planned to proceed *via* alcohol **8b** including two additional steps to remove the carboxylate functionality. Saponification of **4b** in 91% yield, decarboxylation of the obtained acid **5** in 94% yield, and oxidation of **6** using SeO₂ gave aldehyde **7** (90% yield). Further reduction applying NaBH₄ led to alcohol **8b** in 92% yield. Bromination of **8b** with *N*-bromosuccinimide led to **9b** in 45% yield, which gave rise to **10b** in 98% yield after oxidation.



Scheme 3: Synthesis of substituted benzo[*b*]selenophenes. Reaction conditions: *i*: LiAlH₄, THF; *ii*: NBS, CHCl₃ or THF; *iii*: MnO₂, CHCl₃ or ethyl acetate; *iv*: NaOH, H₂O / MeOH, reflux; *v*: Cu, quinoline, 160 °C; *vi*: SeO₂, 1,4-dioxane, reflux; *vii*: NaBH₄, EtOH.

CONCLUSION

In conclusion, a synthetic methodology toward benzo[*b*]selenophene carboxylic acid esters could be devised and developed into a one-pot procedure, which supersedes the isolation of intermediate compounds and is superior in yield over a stepwise approach. The synthetic protocol is applicable for commercially available low-cost starting materials giving rise to valuable substitution patterns. The benzo[*b*]selenophene carboxylic acid esters could easily be converted to bromo-substituted benzo[*b*]selenophene carbaldehydes, which constitute attractive building blocks for different disciplines.

ACKNOWLEDGMENT

ELECTRONIC SUPPLEMENTARY INFORMATION

¹H, ¹³C, and ⁷⁷Se NMR spectra of compounds **2**, **3**, **4a-b**, **5-7**, **8a-b**, **9a-b**, and **10a-b**.

REFERENCES

- (1) Erben, F.; Kleeblatt, D.; Sonneck, M.; Hein, M.; Feist, H.; Fahrenwaldt, T.; Fischer, C.; Matin, A.; Iqbal, J.; Plötz, M.; Eberle, J.; Langer, P. *Org. Biomol. Chem.* **2013**, *11* (24), 3963.
- (2) Paegle, E.; Belyakov, S.; Arsenyan, P. *Eur. J. Org. Chem.* **2014**, *2014* (18), 3831.
- (3) Goswami, K.; Chakraborty, A.; Sinha, S. *Eur. J. Org. Chem.* **2013**, *2013* (18), 3645.
- (4) Takimiya, K.; Shinamura, S.; Osaka, I.; Miyazaki, E. *Heterocycles* **2011**, *83* (6), 1187.
- (5) Takimiya, K.; Kunugi, Y.; Konda, Y.; Ebata, H.; Toyoshima, Y.; Otsubo, T. *J. Am. Chem. Soc.* **2006**, *128* (9), 3044.
- (6) Racharlawar, S. S.; Shankar, D.; Karkhelikar, M. V.; Sridhar, B.; Likhar, P. R. *J. Organomet. Chem.* **2014**, *757*, 14.
- (7) Arsenyan, P.; Paegle, E.; Domracheva, I.; Gulbe, A.; Kanepe-Lapsa, I.; Shestakova, I. *Eur. J. Med. Chem.* **2014**, *87*, 471.
- (8) Staples, M. K.; Grange, R. L.; Angus, J. A.; Ziogas, J.; Tan, N. P. H.; Taylor, M. K.; Schiesser, C. H. *Org. Biomol. Chem.* **2011**, *9* (2), 473.
- (9) Welch, M.; Phillips, R. S. *Bioorg. Med. Chem. Lett.* **1999**, *9* (5), 637.
- (10) Park, Y. S.; Kale, T. S.; Nam, C.-Y.; Choi, D.; Grubbs, R. B. *Chem. Commun.* **2014**, *50* (59), 7964.
- (11) Takimiya, K.; Kunugi, Y.; Konda, Y.; Niihara, N.; Otsubo, T. *J. Am. Chem. Soc.* **2004**, *126* (16), 5084.
- (12) Kashiki, T.; Shinamura, S.; Kohara, M.; Miyazaki, E.; Takimiya, K.; Ikeda, M.; Kuwabara, H. *Org. Lett.* **2009**, *11* (11), 2473.
- (13) Lyons, J. E.; Schiesser, C. H.; Sutej, K. *J. Org. Chem.* **1993**, *58* (21), 5632.
- (14) Christiaens, L.; Piette, J.-L.; Laitem, L.; Baiwir, M.; Denoel, J.; Llabres, G. *Org. Magn. Reson.* **1976**, *8* (7), 354.
- (15) Comasseto, J. V.; Omori, A. T.; Porto, A. L. M.; Andrade, L. H. *Tetrahedron Lett.* **2004**, *45* (3), 473.
- (16) Tiecco, M.; Testaferri, L.; Tingoli, M.; Chianelli, D.; Montanucci, M. *J. Org. Chem.* **1983**, *48* (23), 4289.
- (17) Potapov, A. S.; Chernova, N. P.; Ogorodnikov, V. D.; Petrenko, T. V.; Khlebnikov, A. I. *Sci. World J.* **2014**, *2014*, 1.
- (18) Mughesh, G.; Singh, H. B. *Chem. Soc. Rev.* **2000**, *29* (5), 347.
- (19) J. Renson, M.; Andreas Jakobs, E.; E. Christiaens, L. *Heterocycles* **1992**, *34* (6), 1119.
- (20) Paulmier, C. *Selenium reagents and intermediates in organic synthesis*, 1st ed.; Organic chemistry series; Pergamon: Oxford [Oxfordshire]; New York, 1986.

Manuscript # 5

Brigitte Holzer*, Barbara Dellago, Christian Hametner, Berthold Stöger, Daniel Lumpi*,
Ernst Horkel, and Johannes Fröhlich

Symmetric Mixed Sulfur-Selenium Fused Ring Systems as Potential Materials for Organic
Field Effect Transistors

Manuscript draft

Symmetric Mixed Sulfur-Selenium Fused Ring Systems as Potential Materials for Organic Field-Effect Transistors

Brigitte Holzer,^{a} Barbara Dellago,^a Christian Hametner,^a Berthold Stöger,^b Daniel Lumpi,^{a*} Ernst Horkel,^a and Johannes Fröhlich^a*

^a Institute of Applied Synthetic Chemistry, Vienna University of Technology,

Getreidemarkt 9/163OC, A-1060 Vienna, Austria

^b Institute of Chemical Technologies and Analytics, Vienna University of Technology,

Getreidemarkt 9/164, A-1060 Vienna, Austria

[*brigitte.holzer@tuwien.ac.at](mailto:brigitte.holzer@tuwien.ac.at)

[*daniel.lumpi@tuwien.ac.at](mailto:daniel.lumpi@tuwien.ac.at)

A reliable synthetic protocol toward a series of fused chalcogenopheno[1]benzochalcogenophene (CBC) building blocks was developed based on a Fiesselmann reaction. The obtained CBC units were applied in McMurry, Sonogashira and Stille coupling reactions toward symmetric ene- and yne-linked dimers. These potentially semiconducting compounds were characterized regarding their photophysical, electrochemical and thermal properties and proved to be thermally stable materials with reduced bandgaps and low HOMO energy levels. Single-crystal X-ray diffraction experiments revealed strong intermolecular selenium-selenium and selenium-carbon interactions.

INTRODUCTION

Organic electronic field-effect transistors (OFETs) have attracted attention due to their potential advantages of flexibility, large-area fabrication, and low weight.¹ Accordingly, OFETs are being considered for applications in electronic paper,² organic light emitting displays, and sensor devices,³ such as electronic noses (e-nose),⁴ electronic skin (e-skin),⁵ medical diagnostics,⁶ environmental monitoring⁷ but also in everyday technology like radio frequency identification tags (RFIDs).⁸

Since the first OFETs emerged,⁹ many efforts have been dedicated to improving their performance by adopting new organic semiconductors (OSC) or optimizing the device configuration.¹⁰ Despite the broad fields of promising applications of organic semiconductors, there is still a need for further research to obtain stable materials bearing high charge carrier mobility for fast electrical switching, low operating voltages, and large on/off ratios.¹¹

In order to achieve good OFET performance both the film morphology and the molecular arrangement in organic semiconducting layers play significant roles.¹² The molecular packing and consequently charge carrier mobility are essentially determined by intermolecular coupling between the π -electron clouds of aromatic molecules, which is maximized when molecules adopt a face-to-face orientation.^{10,13,14} Intermolecular $\pi\cdots\pi$ and C-H $\cdots\pi$ interactions are predominant in acenes and their thiophene analogues. The incorporation of sulfur in acenes may induce an effective overlap between the HOMOs of neighbouring molecules in the solid state due to the large electron densities on the heteroatoms.¹⁵ Consequently, the molecular packing in sulfur-rich thienoacenes is strongly influenced by the combination of intermolecular multiple S \cdots S, S \cdots C, and CH $\cdots\pi$ interactions, which in turn can be correlated to high charge carrier mobility.^{16,17} Another benefit of replacing benzene rings with heteroaromatic groups is the increase of the molecular oxidation stability.¹

Recently, we have published on the electrical properties of OFET materials based on thieno[2,3-*b*][1]benzothiophene building blocks connected by different π -spacers (e.g. ethylene spacer, **BTTE**; Figure 1, left) exhibiting both high stability and charge carrier mobility.¹⁸ Also **DTBTE** materials (Figure 1, right) were reported revealing strong intermolecular S \cdots S, S \cdots C, and CH $\cdots\pi$ interactions, which can be correlated with high charge carrier mobility.¹⁹

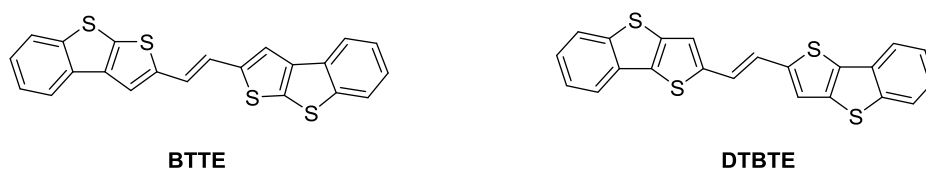


Figure 1: Thieno[1]benzothiophene-based organic field-effect transistors **BTTE** (left) and **DTBTE** (right) exhibiting mobilities up to $3.3 \times 10^{-3} \text{ cm}^2 \text{ V}^{-1} \text{ s}^{-1}$ and $0.5 \text{ cm}^2 \text{ V}^{-1} \text{ s}^{-1}$, respectively.

Further enhancement of intermolecular overlap may be achieved by molecular modification of thienoacenes: the substitution of sulfur with selenium atoms may increase interactions in organic

compounds due to the larger atomic radius and therefore higher polarizability of selenium atoms,²⁰ possibly enhancing device performance by improvement of intermolecular overlap in the solid state and thus charge carrier mobility. Thus, selenophene-fused aromatics constitute attractive candidates for electronic applications. However, due to a lack of available starting materials up to now development of reliable synthetic pathways toward selenium-based materials is matter of ongoing research.²¹

Herein, we report on the design and synthesis of regioisomeric chalcogenopheno[1]benzo-chalcogenophene (CBC) building blocks. These selenium-based moieties were applied in a series of symmetrical ene- and yne-linked potential organic semiconductors (Schemes 1 and 3), which were characterized by NMR, UV-Vis absorption spectroscopy, cyclic voltammetry, and X-ray diffraction (XRD). In particular, the effect of the selenium position and the annelation side of the CBC subunits on the electronic and optical properties of these materials was matter of interest.

EXPERIMENTAL SECTION

Substances purchased from commercial sources were used as received. *trans*-1,2-Bis(tri-*n*-butylstannyl)ethylene and titanium tetrachloride were purchased from ACROS Co, *N*-bromosuccinimide from Apollo Scientific Ltd. and grey selenium from Aldrich Chemical Co. 3-Bromobenzo[*b*]thiophene-2-carboxaldehyde (CAS 10135-00-9),²² 2-bromobenzo[*b*]thiophene-3-carboxaldehyde (CAS 39856-98-9),²³ 3-bromobenzo[*b*]selenophene-2-carboxaldehyde (CAS 26581-53-3)²⁴ and 2-bromobenzo[*b*]selenophene-3-carboxaldehyde (CAS 26526-30-7)²⁴ were synthesized according to literature. Anhydrous tetrahydrofuran (THF), diethyl ether, toluene and dichloromethane (DCM) were prepared immediately prior to use by a *PURESOLV*-plant (*it-innovative technology inc.*). Technical grade solvents were distilled prior to use. Analytical TLC was performed on Merck silica gel 60 F254 plates. Chromatographic separations at preparative scale were carried out on silica gel (Merck silica gel 60, 40 - 63 μm). Nuclear magnetic resonance (NMR) spectra were obtained using a Bruker Avance III HD 600 MHz with cryo probe or Avance III HD 400 MHz fourier transform spectrometer operating at the following frequencies: Avance III HD 600 MHz: 600.2 MHz (¹H), 150.9 MHz (¹³C) and 114.5 MHz (⁷⁷Se); Avance III HD 400 MHz: 400.1 MHz (¹H), 100.6 MHz (¹³C) and 76.5 MHz (⁷⁷Se). The ¹H and ¹³C chemical shifts are reported in δ units, parts per million (ppm) downfield from tetramethylsilane using residual solvent signals for calibration. ⁷⁷Se chemical shifts are given in ppm relative to dimethylselenide, using selenophene ($\delta = 605$ ppm)²⁵ as an external secondary standard. Coupling constants are reported in Hertz; multiplicity of signals is indicated by using following abbreviations: s=singlet, d=doublet, t=triplet, q=quartet, quin=quintet. The multiplicity of ¹³C signals was obtained by measuring JMOD spectra. High-resolution mass spectra (HRMS) were acquired using a Thermo Scientific LTQ Orbitrap XL

hybrid FTMS (Fourier Transform Mass Spectrometer) equipped with Thermo Fischer Exactive Plus Orbitrap (LC-ESI+) and a Shimadzu IT-TOF Mass Spectrometer.

UV-Vis absorption spectra were recorded in DCM solutions (5 μM) with a Perkin Elmer Lambda 750 spectrometer. Cyclic voltammetry was performed using a three electrode configuration consisting of a Pt working electrode, a Pt counter electrode and an Ag/AgCl reference electrode and a PGSTAT128N, ADC164, DAC164, External, DI048 potentiostat provided by Metrohm Autolab B. V. Measurements were carried out in a 0.5 mM solution in anhydrous DCM (oxidation scan) with Bu_4NBF_4 (0.1 M) as the supporting electrolyte. The solutions were purged with nitrogen for 15 minutes prior to measurement. HOMO energy levels were calculated from the onset of oxidation. The onset potential was determined by the intersection of two tangents drawn at the background and the rising of oxidation peaks. The thermal behavior of substances **7a-c** was studied with differential scanning calorimetry (DSC) and thermogravimetric analysis (TGA) using a Netzsch simultaneous thermal analyzer (STA 449 F1 Jupiter). Powder samples with a mass of approx. 10 mg were slightly pressed into the bottom of open aluminum pans and heated at 10 $^\circ\text{C}/\text{min}$ from 25 $^\circ\text{C}$ to 500 $^\circ\text{C}$ under N_2 gas at a flow rate of 40 mL/min. The STA 449 Type-K thermocouples were calibrated using indium, tin, bismuth and zinc metals.

All DFT computations were performed using the Gaussian 09 package, revision A.02.²⁶ For the calculation of HOMO/LUMO levels of compounds **7a-c**, **11a-c**, **17** and **20** ground state (S_0) geometries were optimized in gas phase within C3 symmetry using the Becke three parameters hybrid functional with Lee–Yang–Perdew correlation (B3LYP)^{27,28} in combination with Pople basis set 6-311+G*.²⁹

General procedure toward **3a**, **3c**, **4a** and **4c**. Grey selenium (1.1 eq.) was suspended in anhydrous ethanol under argon atmosphere and cooled to 0 $^\circ\text{C}$. Sodium borohydride (1.43 eq.) was added in portions and stirred for 40 minutes. Sodium hydride was added as dispersion (60%, 0.98 eq.). After 30 minutes a solution of **1a,b** or **2a,b** (1 eq.) in anhydrous THF was added and the obtained solution was stirred for two hours at room temperature. Subsequently, ethyl bromoacetate (2.16 eq.) was added dropwise resulting in a suspension. After one hour sodium ethanolate (2 eq.) was added and the reaction mixture was stirred for further 12 hours at room temperature. The reaction mixture was quenched with water, the aqueous phase was extracted repeatedly with ethyl acetate, the obtained organic layers were washed with water and 10% NH_4Cl solution, dried over anhydrous sodium sulfate and concentrated under reduced pressure. The obtained crude product was purified by column chromatography.

Ethyl selenolo[3,2-*b*][1]benzothiophene-2-carboxylate (**3a**). According to the general procedure **3a** was synthesized applying grey selenium (533 mg, 6.7 mmol) suspended in 30 mL anhydrous ethanol, sodium borohydride (332 mg, 8.8 mmol), sodium hydride (240 mg, 6 mmol), a solution of **1a** (1.48 g, 6.1 mmol) in 40 mL anhydrous THF, ethyl bromoacetate (2.38 g, 13.3 mmol) and sodium

ethanolate (12.2 mmol). After work-up the crude product was purified by column chromatography (light petrol / ethyl acetate 5%, 90 g silica gel) and **3a** was obtained as yellow solid in 72% yield (1.37 g). $R_f = 0.74$ (light petrol / ethyl acetate 6:1). $F_p = 108.3 - 109.2$ °C. ^1H NMR (600 MHz, CDCl_3): $\delta = 8.27$ (s, 1 H), 7.89 - 7.81 (m, 2 H), 7.45 - 7.42 (m, 2 H), 4.40 (q, $J = 7.2$ Hz, 2 H), 1.41 (t, $J = 7.2$ Hz, 3 H) ppm. ^{13}C NMR (150 MHz, CDCl_3): $\delta = 163.3$ (s), 143.0 (s), 141.2 (s), 139.4 (s), 138.4 (s), 134.8 (s), 129.0 (d), 125.9 (d), 125.0 (d), 123.8 (d), 122.5 (d), 61.6 (t), 14.3 (q) ppm. ^{77}Se NMR (114 MHz, CDCl_3): $\delta = 542.2$ ppm. HR-ESI-FTMS $[\text{M}+\text{H}]^+$ m/z calcd. 310.9639 for $\text{C}_{13}\text{H}_{11}\text{O}_2\text{SSe}^+$, found 310.9634.

Ethyl selenolo[3,2-*b*][1]benzoselenophene-2-carboxylate (**3c**). According to the general procedure **3c** was synthesized applying selenium (869 mg, 11 mmol) suspended in 50 mL anhydrous ethanol, sodium borohydride (541 mg, 14.3 mmol), sodium hydride (376 mg, 9.8 mmol), a solution of **1b** (2.88 g, 10 mmol) in 20 mL anhydrous THF, ethyl bromoacetate (3.89 g, 21.6 mmol) and sodium ethanolate (20 mmol). After work-up the crude product was purified by column chromatography (light petrol / ethyl acetate 5%, 90 g silica gel) and **3c** was obtained as yellow solid in 95% yield (3.38 g). $R_f = 0.69$ (light petrol / ethyl acetate 6:1). $F_p = 90.1 - 90.9$ °C. ^1H NMR (CDCl_3 , 400 MHz): $\delta = 8.27$ (s, 1 H), 7.93 - 7.92 (m, 1 H), 7.85 (dd, $J = 7.7, 1.0$ Hz, 1 H), 7.44 (ddd, $J = 8.1, 7.1, 1.2$ Hz, 1 H), 7.35 (ddd, $J = 8.2, 7.1, 1.2$ Hz, 1 H), 4.39 (q, $J = 7.2$ Hz, 2 H), 1.41 (t, $J = 7.2$ Hz, 3 H) ppm. ^{13}C NMR (100 MHz, CDCl_3): $\delta = 163.2$ (s), 144.4 (s), 143.2 (s), 138.8 (s), 137.0 (s), 135.7 (s), 131.8 (d), 126.9 (d), 126.0 (d), 125.5 (d), 124.1 (d), 61.6 (t), 14.4 (q) ppm. ^{77}Se NMR (76 MHz, CDCl_3): $\delta = 569.7, 494.0$ ppm. HR-ESI-FTMS $[\text{M}+\text{H}]^+$ m/z calcd. 358.9084 for $\text{C}_{13}\text{H}_{11}\text{O}_2\text{Se}_2^+$, found 358.9081.

Ethyl selenolo[2,3-*b*][1]benzothiophene-2-carboxylate (**4a**). According to the general procedure **4a** was synthesized applying grey selenium (1.30 g, 16.5 mmol) suspended in 30 mL anhydrous ethanol, sodium borohydride (811 mg, 21.45 mmol), sodium hydride (546 mg, 14.7 mmol), a solution of **2a** (3.62 g, 15 mmol) in 20 mL THF, ethyl bromoacetate (5.83 g, 32.4 mmol) and sodium ethanolate (30 mmol). After work-up the crude product was purified by column chromatography (light petrol / DCM 40%, 90 g silica gel) and **4a** was obtained as yellow solid in 91% yield (4.24 g). $R_f = 0.68$ (light petrol / ethyl acetate 6:1). $F_p = 89.7 - 92.2$ °C. ^1H NMR (CDCl_3 , 600 MHz): $\delta = 8.47$ (s, 1 H), 7.95 - 7.93 (m, 1 H), 7.83 - 7.82 (m, 1 H), 7.43 (ddd, $J = 8.7, 6.8, 1.1$ Hz, 1 H), 7.35 (ddd, $J = 8.9, 6.6, 1.1$ Hz, 1 H), 4.40 (q, $J = 7.2$ Hz, 2 H), 1.42 (t, $J = 7.2$ Hz, 3 H) ppm. ^{13}C NMR (150 MHz, CDCl_3): $\delta = 163.2$ (s), 144.8 (s), 144.1 (s), 143.0 (s), 139.3 (s), 133.9 (s), 127.7 (d), 124.9 (d), 124.6 (d), 122.8 (d), 121.6 (d), 61.5 (t), 14.4 (q) ppm. ^{77}Se NMR (114 MHz, CDCl_3): $\delta = 571.1$ ppm. HR-ESI-FTMS $[\text{M}+\text{H}]^+$ m/z calcd. 310.9695 for $\text{C}_{13}\text{H}_{11}\text{O}_2\text{SSe}^+$, found 310.9633.

Ethyl selenolo[2,3-*b*][1]benzoselenophene-2-carboxylate (**4c**). According to the general procedure **4c** was synthesized applying grey selenium (304 mg, 3.85 mmol) suspended in 10 mL anhydrous ethanol, sodium borohydride (189 mg, 5 mmol), sodium hydride (82 mg, 3.4 mmol), a solution of **2b**

(1.01 g, 3.5 mmol) in 3 mL THF, ethyl bromoacetate (1.36 g, 7.6 mmol) and sodium ethanolate (7 mmol). After work-up the crude product was purified by column chromatography (light petrol / ethyl acetate 5%, 90 g silica gel) and **4c** was obtained as colorless solid in 68% yield (851 mg). $R_f = 0.66$ (light petrol / ethyl acetate 6:1). $F_p = 100.4 - 102.5$ °C. $^1\text{H NMR}$ (CDCl_3 , 600 MHz): $\delta = 8.47$ (s, 1 H), 7.95 (dd, $J = 8.0, 1.0$ Hz, 1 H), 7.86 - 7.85 (m, 1 H), 7.42 (ddd, $J = 8.2, 6.6, 1.1$ Hz, 1 H), 7.30 (ddd, $J = 8.3, 6.6, 1.3$ Hz, 1H), 4.40 (q, $J = 7.1$ Hz, 2 H), 1.42 (t, $J = 7.1$ Hz, 3 H) ppm. $^{13}\text{C NMR}$ (150 MHz, CDCl_3): $\delta = 163.1$ (s), 145.9 (s), 144.4 (s), 142.6 (s), 140.6 (s), 136.1 (s), 128.9 (d), 125.9 (d), 125.3 (d), 124.9 (d), 123.1 (d), 61.5 (t), 14.4 (q) ppm. $^{77}\text{Se NMR}$ (114 MHz, CDCl_3): $\delta = 601.5, 512.0$ ppm.

General procedure toward **3b** and **4b**. The properly substituted aldehyde **1b** or **2b** (1 eq.), ethyl mercaptoacetate (1.17 eq.) and K_2CO_3 (2 eq.) were suspended in anhydrous DMF and stirred at room temperature for 48 hours. The reaction mixture was quenched with water and the aqueous phase was extracted repeatedly with DCM. The obtained organic phases were washed with a saturated NH_4Cl solution, dried over anhydrous sodium sulfate and concentrated under reduced pressure. The obtained crude product was purified by column chromatography.

Ethyl [1]benzoselenopheno[3,2-*b*]thiophene-2-carboxylate (**3b**). **1b** (500 mg, 1.7 mmol), ethyl mercaptoacetate (240 mg, 2 mmol) and K_2CO_3 (484 mg, 3.5 mmol) were suspended in 3.5 mL DMF. After work-up the crude product was purified by column chromatography (light petrol / ethyl acetate 5%, 90 g silica gel) and **3b** was isolated as yellow solid in 48% yield (253 mg). $R_f = 0.68$ (light petrol / ethyl acetate 6:1). $F_p = 94.4 - 95.3$ °C. $^1\text{H NMR}$ (600 MHz, CDCl_3): $\delta = 8.03$ (s, 1 H), 7.91 - 7.88 (m, 2 H), 7.44 (ddd, $J = 8.3, 6.7, 1.1$ Hz, 1 H), 7.35 (ddd, $J = 8.3, 6.7, 1.1$ Hz, 1 H), 4.41 (q, $J = 7.1$ Hz, 2 H), 1.41 (t, $J = 7.1$ Hz, 3 H) ppm. $^{13}\text{C NMR}$ (150 MHz, CDCl_3): $\delta = 162.1$ (s), 143.7 (s), 142.8 (s), 134.8 (s), 134.4 (s), 134.2 (s), 129.3 (d), 127.0 (d), 126.1 (d), 125.5 (d), 123.2 (d), 61.5 (t), 14.4 (q) ppm. $^{77}\text{Se NMR}$ (114 MHz, CDCl_3): $\delta = 462.3$ ppm. HR-ESI-FTMS $[\text{M}+\text{H}]^+$ m/z calcd. 310.9695 for $\text{C}_{13}\text{H}_{11}\text{O}_2\text{SSe}^+$, found 310.9637.

Ethyl [1]benzoselenopheno[2,3-*b*]thiophene-2-carboxylate (**4b**). **2b** (1.01 g, 3.5 mmol), ethyl mercaptoacetate (492 mg, 4.1 mmol) and K_2CO_3 (967 mg, 7 mmol) were suspended in 7 mL DMF. After work-up the crude product was purified by column chromatography (light petrol / ethyl acetate 5%, 90 g silica gel) and **4b** was isolated as yellow solid in 92% yield (995 mg). $R_f = 0.67$ (light petrol / ethyl acetate 6:1). $F_p = 94.3 - 95.6$ °C. $^1\text{H NMR}$ (600 MHz, CDCl_3): $\delta = 8.21$ (s, 1 H), 7.94 (dd, $J = 7.9, 1.0$ Hz, 1 H), 7.85 (m, 1 H), 7.44 (ddd, $J = 8.3, 6.7, 1.2$ Hz, 1 H), 7.32 (ddd, $J = 8.2, 6.7, 1.2$ Hz, 1 H), 4.41 (q, $J = 7.2$ Hz, 2 H), 1.42 (t, $J = 7.2$ Hz, 3 H) ppm. $^{13}\text{C NMR}$ (150 MHz, CDCl_3): $\delta = 161.9$ (s), 144.4 (s), 143.6 (s), 141.2 (s), 137.1 (s), 134.7 (s), 126.2 (d), 126.2 (d), 125.4 (d), 125.4 (d), 123.1 (d), 61.4 (t), 14.4 (q) ppm. $^{77}\text{Se NMR}$ (114 MHz, CDCl_3): $\delta = 484.8$ ppm. HR-ESI-FTMS $[\text{M}+\text{H}]^+$ m/z calcd. 310.9640 for $\text{C}_{13}\text{H}_{11}\text{O}_2\text{SSe}^+$, found 310.9637.

General procedure toward **5a-c**. LiAlH₄ (1 eq.) was suspended in anhydrous THF and cooled to 0 °C. The appropriate ester **3a-c** (1 eq.) was added as a THF solution. The reaction mixture was stirred at room temperature and conversion was monitored by TLC (light petrol / ethyl acetate 7:1). The reaction mixture was quenched drop wise with 2 N NaOH and the aqueous phase was extracted with DCM. The organic layer was washed with water, dried over anhydrous sodium sulfate and concentrated under reduced pressure.

Selenolo[3,2-*b*][1]benzothiophene-2-methanol (**5a**). According to the general procedure **3a** (1.24 g, 4.00 mmol) was dissolved in 10 mL anhydrous THF and added to a suspension of LiAlH₄ (152 mg, 4.00 mmol) in 20 mL anhydrous THF. After work-up the crude product was purified by column chromatography (light petrol / ethyl acetate 10%, 90 g silica gel) and **5a** was isolated as yellow solid in 80% yield (858 mg). R_f = 0.23 (light petrol / ethyl acetate 4:1). F_p = 130.3 - 132.3 °C. ¹H NMR (400 MHz, CDCl₃): δ = 7.87 - 7.85 (m, 1 H), 7.78 - 7.76 (m, 1 H), 7.43 - 7.32 (m, 3 H), 4.97 (d, J = 5.3 Hz, 2 H), 2.06 (t, J = 5.3 Hz, 1 H) ppm. ¹³C NMR (100 MHz, CDCl₃): δ = 153.1 (s), 141.5 (s), 138.1 (s), 135.5 (s), 135.0 (s), 124.7 (d), 124.4 (d), 123.7 (d), 121.6 (d), 120.0 (d), 62.9 (t) ppm. ⁷⁷Se NMR (76 MHz, CDCl₃): δ = 521.2 ppm. HR-ESI-FTMS [M+H]⁺ m/z calcd. 268.9534 for C₁₁H₉OSSe⁺, found 268.9531.

[1]Benzoselenopheno[3,2-*b*]thiophene-2-methanol (**5b**). According to the general procedure **3b** (2.78 g, 9.00 mmol) was dissolved in 10 mL anhydrous THF and added to a suspension of LiAlH₄ (342 mg, 9.00 mmol) in 30 mL anhydrous THF. After work-up the crude product was purified by column chromatography (light petrol / ethyl acetate 10%, 90 g silica gel) and **5b** was isolated as yellow solid in 67% yield (1.61 g). R_f = 0.24 (light petrol / ethyl acetate 4:1). F_p = 128.2 - 130.0 °C. ¹H NMR (600 MHz, CD₂Cl₂): δ = 7.88 - 7.87 (m, 1 H), 7.79 - 7.78 (m, 1 H), 7.43 - 7.34 (m, 3 H), 4.95 (d, J = 5.4 Hz, 2 H), 2.24 (t, J = 5.4 Hz, 1 H) ppm. ¹³C NMR (150 MHz, CD₂Cl₂): δ = 154.5 (s), 142.0 (s), 138.7 (s), 136.0 (s), 135.2 (s), 125.3 (d), 124.9 (d), 124.2 (d), 122.0 (d), 120.2 (d), 63.2 (t) ppm. ⁷⁷Se NMR (114 MHz, CD₂Cl₂): δ = 517.4 ppm. HR-ESI-FTMS [M+H]⁺ m/z calcd. 268.9534 for C₁₁H₉OSSe⁺, found 268.9533.

Selenolo[3,2-*b*][1]benzoselenophene-2-methanol (**5c**). According to the general procedure **3c** (3.21 g, 9.00 mmol) was dissolved in 10 mL anhydrous THF and added to a suspension of LiAlH₄ (342 mg, 9.00 mmol) in 10 mL anhydrous THF. After work-up the crude product was purified by column chromatography (light petrol / ethyl acetate 10%, 90 g silica gel) and **5c** was isolated as yellow solid in 66% yield (1.85 g). R_f = 0.23 (light petrol / ethyl acetate 4:1). F_p = 104.4 - 105.8 °C. ¹H NMR (600 MHz, CD₂Cl₂): δ = 7.93 - 7.91 (m, 1 H), 7.77 - 7.76 (m, 1 H), 7.43 - 7.40 (m, 2 H), 7.28 (ddd, J = 8.3, 6.6, 1.2 Hz, 1 H), 4.95 (dd, J = 6.1, 1.1 Hz, 2H), 2.19 (t, J = 6.1 Hz, 1 H) ppm. ¹³C NMR (100 MHz, CD₂Cl₂): δ = 153.8 (s), 142.2 (s), 138.1 (s), 138.0 (s), 136.0 (s), 127.3 (d), 125.8 (d), 125.1 (d), 123.6 (d), 123.0 (d), 63.1 (t) ppm. ⁷⁷Se NMR (114 MHz, CD₂Cl₂): δ = 541.3, 483.6 ppm. HR-ESI-FTMS [M+H]⁺ m/z calcd. 316.8978 for C₁₁H₉OSe₂⁺, found 316.8912.

General procedure toward **6a-c**. The appropriate alcohol **5a-c** (1 eq.) and MnO₂ (6 eq.) were stirred in ethyl acetate for 12 hours. The reaction progress was monitored by TLC (light petrol / ethyl acetate 5:1). The reaction mixture was filtrated over celite and the obtained solution was concentrated under reduced pressure.

Selenolo[3,2-*b*][1]benzothiophene-2-carbaldehyde (**6a**). To a solution of **5a** (3.47 g, 13 mmol) in 50 mL ethyl acetate MnO₂ (6.64 g, 76 mmol) was added. After work-up according to the general procedure the crude product was purified by column chromatography (light petrol / ethyl acetate 50%, 90 g silica gel) and **6a** was isolated as yellow solid in 75% yield (2.60 g). R_f = 0.50 (light petrol / ethyl acetate 4:1). F_p = 88.9 - 100.5 °C. ¹H NMR (400 MHz, CDCl₃): δ = 9.86 (s, 1 H), 8.20 (s, 1 H), 7.91 - 7.88 (m, 2 H), 7.48 - 7.43 (m, 2 H) ppm. ¹³C NMR (100 MHz, CDCl₃): δ = 184.1 (d), 150.1 (s), 143.8 (s), 143.0 (s), 138.8 (s), 134.6 (s), 132.7 (d), 126.6 (d), 125.3 (d), 123.8 (d), 123.2 (d) ppm. ⁷⁷Se NMR (76 MHz, CDCl₃): δ = 519.0 ppm. HR-ESI-FTMS [M+H]⁺ m/z calcd. 266.9377 for C₁₁H₇OSSe⁺, found 266.9374.

[1]Benzoselenopheno[3,2-*b*]thiophene-2-carbaldehyde (**6b**). To a solution of **5b** (1.34 g, 5 mmol) in 25 mL ethyl acetate MnO₂ (2.61 g, 30 mmol) was added. After work-up according to the general procedure the crude product was purified by column chromatography (light petrol / ethyl acetate 50%, 90 g silica gel) and **6b** was isolated as yellow solid in 87% yield (1.15 g). R_f = 0.49 (light petrol / ethyl acetate 4:1). F_p = 112.1 - 115.6 °C. ¹H NMR (600 MHz, CDCl₃): δ = 9.87 (s, 1 H), 8.22 (s, 1 H), 7.92 - 7.89 (m, 2 H), 7.48 - 7.45 (m, 2 H) ppm. ¹³C NMR (150 MHz, CDCl₃): δ = 184.2 (d), 150.1 (s), 143.8 (s), 143.0 (s), 138.8 (s), 134.6 (s), 132.7 (d), 126.7 (d), 125.3 (d), 123.9 (d), 123.2 (d) ppm. ⁷⁷Se NMR (114 MHz, CDCl₃): δ = 517.0 ppm. HR-ESI-FTMS [M+H]⁺ m/z calcd. 266.9377 for C₁₁H₇OSSe⁺, found 266.9377.

Selenolo[3,2-*b*][1]benzoselenophene-2-carbaldehyde (**6c**). To a solution of **5c** (1.57 g, 5 mmol) in 25 mL ethyl acetate MnO₂ (2.61 g, 30 mmol) was added. After work-up according to the general procedure the crude product was purified by column chromatography (light petrol / ethyl acetate 50%, 90 g silica gel) and **6c** was isolated as yellow solid in 86% yield (1.34 g). R_f = 0.49 (light petrol / ethyl acetate 4:1). F_p = 110.3 - 112.1 °C. ¹H NMR (600 MHz, CDCl₃): δ = 9.85 (s, 1 H), 8.20 (s, 1 H), 7.93 - 7.92 (m, 1 H), 7.89 (dd, J = 7.8, 0.9 Hz, 1 H), 7.45 (ddd, J = 8.4, 6.6, 0.9 Hz, 1 H), 7.38 (ddd, J = 8.6, 6.6, 1.2 Hz, 1 H) ppm. ¹³C NMR (CDCl₃, 150 MHz): δ = 184.0 (d), 149.4 (s), 146.3 (s), 143.9 (s), 136.7 (s), 136.0 (s), 135.6 (d), 126.9 (d), 126.7 (d), 125.7 (d), 124.7 (d) ppm. ⁷⁷Se NMR (114 MHz, CDCl₃): δ = 542.2, 494.2 ppm. HR-ESI-FTMS [M+H]⁺ m/z calcd. 314.8822 for C₁₁H₇OSe₂⁺, found 314.8820.

General procedure toward **8a-c** and **12a-c**. The obtained esters **3a-c** or **4a-c** and (1 eq.) and sodium hydroxide (2 eq.) were refluxed in a mixture of methanol and water (2:3). The conversion was monitored by TLC (DCM / MeOH 10:1). The reaction mixture was cooled to room temperature and

the respective acid was precipitated by addition a sufficient amount of 2 N HCl. The precipitate was filtered, washed with water and dried in vacuo.

Selenolo[2,3-*b*][1]benzothiophene-2-carboxylic acid (**8a**). A mixture of **4a** (760 mg, 2.5 mmol) and sodium hydroxide (200 mg, 5 mmol) was refluxed in 15 mL solvent for 6 hours. After work-up according to the general procedure **8a** was isolated as yellow solid in 90% yield (623 mg). $R_f = 0.24$ (DCM / MeOH 10:1). $F_p = 240.5 - 243.6$ °C. $^1\text{H NMR}$ (600 MHz, DMSO- d_6): $\delta = 13.18$ (bs, 1 H), 8.66 (s, 1 H), 8.23 - 8.22 (m, 1 H), 8.04 - 8.03 (m, 1 H), 7.46 - 7.37 (m, 2 H) ppm. $^{13}\text{C NMR}$ (150 MHz, DMSO- d_6): $\delta = 164.4$ (s), 145.0 (s), 143.7 (s), 142.4 (s), 140.9 (s), 133.8 (s), 128.1 (d), 124.9 (d), 124.6 (d), 123.1 (d), 121.9 (d) ppm. $^{77}\text{Se NMR}$ (114 MHz, DMSO- d_6): $\delta = 582.0$ ppm.

[1]Benzoselenopheno[2,3-*b*]thiophene-2-carboxylic acid (**8b**). A mixture of **4b** (989 mg, 3.2 mmol) and sodium hydroxide (255 mg, 6.4 mmol) was refluxed in 15 mL solvent for 6 hours. After work-up according to the general procedure **8b** was isolated as yellow solid in 74% yield (663 mg). $R_f = 0.21$ (DCM / MeOH 10:1). $F_p = 234.0 - 237.6$ °C. $^1\text{H NMR}$ (600 MHz, DMSO- d_6): $\delta = 13.19$ (bs, 1 H), 8.41 (s, 1 H), 8.19 - 8.18 (m, 1 H), 8.11 - 8.09 (m, 1 H), 7.44 - 7.43 (m, 1 H), 7.35 - 7.33 (m, 1 H) ppm. $^{13}\text{C NMR}$ (150 MHz, DMSO- d_6): $\delta = 162.9$ (s), 143.9 (s), 143.7 (s), 142.3 (s), 137.8 (s), 134.6 (s), 126.7 (d), 126.6 (d), 125.2 (d), 125.1 (d), 123.3 (d) ppm. $^{77}\text{Se NMR}$ (114 MHz, DMSO- d_6): $\delta = 498.7$ ppm.

Selenolo[2,3-*b*][1]benzoselenophene-2-carboxylic acid (**8c**). A mixture of **4c** (854 mg, 2.4 mmol) and sodium hydroxide (192 mg, 4.8 mmol) was refluxed in 15 mL solvent for 6 hours. After work-up according to the general procedure **8c** was isolated as yellow solid in 81% yield (640 mg). $R_f = 0.20$ (DCM / MeOH 10:1). $F_p = 233.5 - 235.3$ °C. $^1\text{H NMR}$ (600 MHz, DMSO- d_6): $\delta = 13.09$ (bs, 1 H), 8.62 (s, 1 H), 8.19 - 8.18 (m, 1 H), 8.09 - 8.08 (m, 1 H), 7.43 - 7.40 (m, 1 H), 7.32 - 7.29 (m, 1 H) ppm. $^{13}\text{C NMR}$ (150 MHz, DMSO- d_6): $\delta = 164.4$ (s), 144.8 (s), 144.6 (s), 144.4 (s), 141.8 (s), 136.3 (s), 129.7 (d), 126.8 (d), 125.5 (d), 125.1 (d), 123.6 (d) ppm. $^{77}\text{Se NMR}$ (114 MHz, DMSO- d_6): $\delta = 611.0, 526.1$ ppm.

Selenolo[3,2-*b*][1]benzothiophene-2-carboxylic acid (**12a**). A mixture of **3a** (1.37 g, 4.4 mmol) and sodium hydroxide (350 mg, 8.8 mmol) was refluxed in 15 mL solvent for 6 hours. After work-up according to the general procedure **12a** was isolated as colorless solid in 92% yield (1.15 g). $R_f = 0.24$ (DCM / MeOH 10:1). $F_p = 242.7 - 246.5$ °C. $^1\text{H NMR}$ (600 MHz, DMSO- d_6): $\delta = 8.41$ (bs, 1 H), 8.15 - 8.08 (m, 2 H), 7.50 - 7.47 (m, 2 H) ppm. $^{13}\text{C NMR}$ (150 MHz, DMSO- d_6): $\delta = 164.2$ (s), 142.2 (s), 141.9 (s), 139.7 (s), 138.5 (s), 134.5 (s), 129.1 (d), 126.0 (d), 125.2 (d), 124.1 (d), 122.9 (d) ppm. $^{77}\text{Se NMR}$ (114 MHz, DMSO- d_6): $\delta = 541.5$ ppm.

[1]Benzoselenopheno[3,2-*b*]thiophene-2-carboxylic acid (**12b**). A mixture of **3b** (248 mg, 0.8 mmol) and sodium hydroxide (60 mg, 1.6 mmol) was refluxed in 9 mL solvent for 2 hours. After work-up according to the general procedure **12b** was isolated as colorless solid in 81% yield (184 mg). $R_f = 0.21$ (DCM / MeOH 10:1). $^1\text{H NMR}$ (400 MHz, DMSO- d_6): $\delta = 13.41$ (bs, 1 H), 8.20 (s, 1

H), 8.17 (d, $J = 7.9$ Hz, 1 H), 8.03 (d, $J = 7.9$ Hz, 1 H), 7.48 (t, $J = 6.8$ Hz, 1 H), 7.40 (t, $J = 6.8$ Hz, 1 H) ppm. ^{13}C NMR (100 MHz, DMSO-d_6): $\delta = 162.9$ (s), 143.6 (s), 141.2 (s), 135.6 (s), 135.4 (s), 133.6 (s), 130.3 (d), 127.5 (d), 126.1 (d), 125.5 (d), 123.1 (d) ppm. ^{77}Se NMR (76 MHz, DMSO-d_6): $\delta = 471.6$ ppm.

Selenolo[3,2-*b*][1]benzoselenophene-2-carboxylic acid (**12c**). A mixture of **3c** (3.56 g, 10 mmol) and sodium hydroxide (800 mg, 20 mmol) was refluxed in 60 mL solvent for 2 hours. After work-up according to the general procedure **12c** was isolated as colorless solid in 76% yield (2.48 g). $R_f = 0.19$ (DCM / MeOH 10:1). ^1H NMR (600 MHz, DMSO-d_6): $\delta = 13.33$ (bs, 1 H), 8.43 (s, 1 H), 8.17 (d, $J = 7.9$ Hz, 1 H), 8.08 (d, $J = 7.7$ Hz, 1 H), 7.48 - 7.45 (m, 1 H), 7.41 - 7.38 (m, 1 H) ppm. ^{13}C NMR (150 MHz, DMSO-d_6): $\delta = 164.1$ (s), 143.1 (s), 142.9 (s), 139.9 (s), 136.9 (s), 136.6 (s), 132.7 (d), 127.3 (d), 126.0 (d), 125.6 (d), 124.2 (d) ppm. ^{77}Se NMR (114 MHz, DMSO-d_6): $\delta = 564.3$, 498.2 ppm.

General procedure toward **9a-c** and **13a-c**. Decarboxylation of carboxylic acids was achieved by refluxing **8a-c** or **12a-c** and copper (0.45 eq.) in quinoline. The conversion was monitored by TLC (DCM / MeOH 10:1). The reaction mixture was cooled to room temperature and repeatedly extracted with chloroform after addition of 2 N HCl. The obtained organic phases were washed with water, dried over anhydrous sodium sulfate and concentrated under reduced pressure. The obtained crude product was purified by column chromatography (light petrol, 90 g silica gel).

Selenolo[2,3-*b*][1]benzothiophene (**9a**). **8a** (815 mg, 2.9 mmol) and copper (83 mg, 1.3 mmol) were refluxed in 40 mL quinoline for four hours. After work-up according to the general procedure **9a** was isolated as yellow solid in 58% yield (403 mg). $R_f = 0.45$ (light petrol). $F_p = 81.6 - 82.4$ °C. ^1H NMR (CDCl_3 , 600 MHz): $\delta = 8.01$ (d, $J = 5.5$ Hz, 1 H), 7.95 - 7.94 (m, 1 H), 7.85 - 7.83 (m, 1 H), 7.80 (d, $J = 5.5$ Hz, 1 H), 7.42 - 7.40 (m, 1 H), 7.34 - 7.31 (m, 1 H) ppm. ^{13}C NMR (150 MHz, CDCl_3): $\delta = 144.8$ (s), 143.6 (s), 138.0 (s), 134.0 (s), 131.2 (d), 124.4 (d), 123.8 (d), 122.9 (d), 121.8 (d), 121.5 (d) ppm. ^{77}Se NMR (114 MHz, CDCl_3): $\delta = 551.7$ ppm.

[1]Benzoselenopheno[2,3-*b*]thiophene (**9b**). **8b** (647 mg, 2.3 mmol) and copper (66 mg, 1 mmol) were refluxed in 40 mL quinoline for four hours. After work-up according to the general procedure **9b** was isolated as yellow solid in 43% yield (237 mg). $R_f = 0.37$ (light petrol). $F_p = 50.7 - 51.6$ °C. ^1H NMR (CDCl_3 , 600 MHz): $\delta = 7.93 - 7.92$ (m, 1 H), 7.86 - 7.85 (m, 1 H), 7.57 (d, $J = 5.2$ Hz, 1 H), 7.50 (d, $J = 5.2$ Hz, 1 H), 7.43 - 7.41 (m, 1 H), 7.29 - 7.28 (m, 1 H) ppm. ^{13}C NMR (150 MHz, CDCl_3): $\delta = 144.5$ (s), 144.1 (s), 135.1 (s), 133.7 (s), 128.9 (d), 126.3 (d), 125.0 (d), 124.6 (d), 123.0 (d), 120.5 (d) ppm. ^{77}Se NMR (114 MHz, CDCl_3): $\delta = 471.3$ ppm.

Selenolo[2,3-*b*][1]benzoselenophene (**9c**). **8c** (623 mg, 1.9 mmol) and copper (54 mg, 0.86 mmol) were refluxed in 40 mL quinoline for four hours. After work-up according to the general procedure **9c** was isolated as yellow solid in 77% yield (413 mg). $R_f = 0.42$ (light petrol). $F_p = 61.9 - 62.3$ °C.

^1H NMR (CDCl_3 , 600 MHz): δ = 8.10 (d, J = 5.6 Hz, 1 H), 7.95 - 7.93 (m, 1 H), 7.88 - 7.87 (m, 1 H), 7.81 (d, J = 5.6 Hz, 1 H), 7.41 (ddd, J = 8.2, 6.9, 1.1 Hz, 1 H), 7.27 (ddd, J = 8.2, 6.9, 1.1 Hz, 1 H) ppm. ^{13}C NMR (150 MHz, CDCl_3): δ = 146.2 (s), 144.9 (s), 136.3 (s), 134.6 (s), 132.5 (d), 126.1 (d), 124.9 (d), 124.2 (d), 123.2 (d), 123.1 (d) ppm. ^{77}Se NMR (114 MHz, CDCl_3): δ = 580.4, 496.4 ppm.

Selenolo[3,2-*b*][1]benzothiophene (**13a**). **12a** (3.66 g, 13 mmol) and copper (371 mg, 5.85 mmol) were refluxed in 10 mL quinoline for four hours. After work-up according to the general procedure **13a** was isolated as colorless solid in 90% yield (2.78 g). R_f = 0.45 (light petrol). F_p = 108.9 - 109.4 °C. ^1H NMR (600 MHz, CDCl_3): δ = 8.11 (d, J = 5.6 Hz, 1 H), 7.88 - 7.87 (m, 1 H), 7.82 - 7.81 (m, 1 H), 7.57 (d, J = 5.6 Hz, 1 H), 7.42 (ddd, J = 7.9, 7.1, 0.9 Hz, 1 H), 7.36 (ddd, J = 8.2, 7.3, 1.2 Hz, 1 H) ppm. ^{13}C NMR (150 MHz, CDCl_3): δ = 142.0 (s), 139.2 (s), 135.4 (s), 135.2 (s), 131.6 (d), 124.7 (d), 124.4 (d), 123.7 (d), 122.9 (d), 121.7 (d) ppm. ^{77}Se NMR (114 MHz, CDCl_3): δ = 522.2 ppm.

[1]Benzoselenopheno[3,2-*b*]thiophene (**13b**). **12b** (184 mg, 0.7 mmol) and copper (19 mg, 0.3 mmol) were refluxed in 2 mL quinoline for four hours. After work-up according to the general procedure **13b** was isolated as yellow solid in 77% yield (120 mg). R_f = 0.32 (light petrol). F_p = 64.6 - 65.4 °C. ^1H NMR (600 MHz, CDCl_3): δ = 7.91 - 7.89 (m, 1 H), 7.86 - 7.84 (m, 1 H), 7.47 (d, J = 5.1 Hz, 1 H), 7.42 (ddd, J = 8.2, 7.0, 0.9 Hz, 1 H), 7.35 (d, J = 5.1 Hz, 1 H), 7.28 (ddd, J = 8.1, 7.1, 1.3 Hz, 1 H) ppm. ^{13}C NMR (150 MHz, CDCl_3): δ = 142.5 (s), 137.3 (s), 134.9 (s), 134.8 (s), 127.1 (d), 126.9 (d), 125.1 (d), 124.6 (d), 123.2 (d), 122.4 (d) ppm. ^{77}Se NMR (114 MHz, CDCl_3): δ = 457.1 ppm.

Selenolo[3,2-*b*][1]benzoselenophene (**13c**). **12c** (2.29 g, 7 mmol) and copper (200 mg, 3.2 mmol) were refluxed in 50 mL quinoline for four hours. After work-up according to the general procedure **13c** was isolated as yellow solid in 77% yield (1.53 g). R_f = 0.29 (light petrol). F_p = 103.8 - 104.5 °C. ^1H NMR (600 MHz, CD_2Cl_2): δ = 8.11 (d, J = 5.6 Hz, 1 H), 7.94 - 7.93 (m, 1 H), 7.82 - 7.81 (m, 1 H), 7.60 (d, J = 5.6 Hz, 1 H), 7.43 (ddd, J = 8.3, 7.1, 1.0 Hz, 1 H), 7.30 (ddd, J = 8.4, 7.0, 1.3 Hz, 1 H) ppm. ^{13}C NMR (150 MHz, CD_2Cl_2): δ = 142.6 (s), 138.7 (s), 137.9 (s), 137.0 (s), 131.8 (d), 127.4 (d), 126.3 (d), 125.8 (d), 125.2 (d), 123.8 (d) ppm. ^{77}Se NMR (114 MHz, CD_2Cl_2): δ = 545.8, 482.0 ppm.

General procedure toward **10a-c** and **14a-c**. Bromination of **9a-c** and **13a-c** was achieved by addition of NBS (1.0 eq.) to a cooled solution of **9a-c** and **13a-c** in THF. The reaction progress was monitored by TLC (light petrol). After full conversion the reaction mixture was quenched with 2 N sodium hydroxide solution and repeatedly extracted with chloroform. The obtained organic phase was washed with water, dried over anhydrous sodium sulfate and concentrated under reduced pressure. The obtained crude product was purified by column chromatography (light petrol, 90 g silica gel).

2-Bromoselenolo[2,3-*b*][1]benzothiophene (**10a**). **9a** (403 mg, 1.7 mmol) was dissolved in 20 mL THF and cooled to 0 °C. NBS (302 mg, 1.7 mmol) was added in portions. After work-up according to the general procedure **10a** was isolated as yellow solid in 98% yield (528 mg). $R_f = 0.58$ (light petrol). $F_p = 95.8 - 98.0$ °C. $^1\text{H NMR}$ (CDCl_3 , 600 MHz): $\delta = 7.86 - 7.85$ (m, 1 H), 7.83 - 7.82 (m, 1 H), 7.77 (s, 1 H), 7.41 (ddd, $J = 8.3, 6.8, 1.1$ Hz, 1 H), 7.33 (ddd, $J = 8.0, 6.8, 1.1$ Hz, 1 H) ppm. $^{13}\text{C NMR}$ (150 MHz, CDCl_3): $\delta = 143.4$ (s), 141.9 (s), 137.9 (s), 133.3 (s), 125.3 (d), 124.7 (d), 124.1 (d), 122.8 (d), 121.4 (d), 114.4 (s) ppm. $^{77}\text{Se NMR}$ (114 MHz, CDCl_3): $\delta = 625.9$ ppm.

2-Bromo[1]benzoselenopheno[2,3-*b*]thiophene (**10b**). **9b** (237 mg, 1 mmol) was dissolved in 20 mL THF and cooled to 0 °C. NBS (178 mg, 1 mmol) was added in portions. After work-up according to the general procedure **10b** was isolated as yellow solid in 67% yield (212 mg). $R_f = 0.50$ (light petrol). $F_p = 95.8 - 100.3$ °C. $^1\text{H NMR}$ (CDCl_3 , 600 MHz): $\delta = 7.85 - 7.84$ (m, 2 H), 7.54 (s, 1 H), 7.42 (ddd, $J = 8.1, 6.9, 1.1$ Hz, 1 H), 7.29 (ddd, $J = 8.1, 6.9, 1.1$ Hz, 1 H) ppm. $^{13}\text{C NMR}$ (150 MHz, CDCl_3): $\delta = 143.6$ (s), 143.1 (s), 134.5 (s), 132.9 (s), 126.2 (d), 125.2 (d), 124.8 (d), 123.6 (d), 122.9 (d), 113.1 (s) ppm. $^{77}\text{Se NMR}$ (114 MHz, CDCl_3): $\delta = 491.7$ ppm.

2-Bromoselenolo[2,3-*b*][1]benzoselenophene (**10c**). **9c** (398 mg, 1.4 mmol) was dissolved in 20 mL THF and cooled to 0 °C. NBS (249 mg, 1.4 mmol) was added in portions. After work-up according to the general procedure **10c** was isolated as yellow solid in 95% yield (484 mg). $R_f = 0.51$ (light petrol). $F_p = 93.7 - 96.1$ °C. $^1\text{H NMR}$ (CDCl_3 , 600 MHz): $\delta = 7.87 - 7.84$ (m, 2 H), 7.76 (s, 1 H), 7.42 - 7.39 (m, 1 H), 7.29 - 7.26 (m, 1 H) ppm. $^{13}\text{C NMR}$ (150 MHz, CDCl_3): $\delta = 144.7$ (s), 143.9 (s), 135.7 (s), 134.7 (s), 126.7 (d), 126.0 (d), 125.1 (d), 124.5 (d), 123.1 (d), 115.1 (s) ppm. $^{77}\text{Se NMR}$ (114 MHz, CDCl_3): $\delta = 652.6, 512.4$ ppm.

2-Bromoselenolo[3,2-*b*][1]benzothiophene (**14a**). **13a** (2.4 mmol, 560 mg) was dissolved in 15 mL THF and cooled to 0 °C. NBS (426 mg, 2.4 mmol) was added in portions. After work-up according to the general procedure **14a** was isolated as yellow solid in 97% yield (722 mg). $R_f = 0.49$ (light petrol). $F_p = 76.8 - 77.6$ °C. $^1\text{H NMR}$ (CDCl_3 , 600 MHz): $\delta = 7.86 - 7.84$ (m, 1 H), 7.71 - 7.70 (m, 1 H), 7.52 (s, 1 H), 7.40 (ddd, $J = 8.3, 6.9, 1.3$ Hz, 1 H), 7.36 (ddd, $J = 8.1, 6.8, 1.4$ Hz, 1 H) ppm. $^{13}\text{C NMR}$ (150 MHz, CDCl_3): $\delta = 140.9$ (s), 137.4 (s), 136.0 (s), 134.9 (s), 126.0 (d), 124.9 (d), 124.6 (d), 123.6 (d), 121.5 (d), 115.8 (s) ppm. $^{77}\text{Se NMR}$ (114 MHz, CDCl_3): $\delta = 606.9$ ppm.

2-Bromo[1]benzoselenopheno[3,2-*b*]thiophene (**14b**). **13b** (419 mg, 1.8 mmol) was dissolved in 60 mL THF and cooled to 0 °C. NBS (327 mg, 1.8 mmol) was added in portions. After work-up according to the general procedure **14b** was isolated as colorless solid in 90% yield (501 mg). $R_f = 0.45$ (light petrol). $F_p = 65.4 - 69.0$ °C. $^1\text{H NMR}$ (CDCl_3 , 400 MHz): $\delta = 7.89 - 7.86$ (m, 1 H), 7.76 - 7.74 (m, 1 H), 7.41 (ddd, $J = 8.3, 7.0, 1.0$ Hz, 1 H), 7.32 (s, 1 H), 7.28 (ddd, $J = 8.3, 6.8, 1.1$ Hz, 1 H) ppm. $^{13}\text{C NMR}$ (100 MHz, CDCl_3): $\delta = 141.6$ (s), 137.6 (s), 134.4 (s), 133.8 (s), 126.8 (d), 125.9 (d), 125.3 (d), 124.8 (d), 122.3 (d), 113.3 (s) ppm. $^{77}\text{Se NMR}$ (76 MHz, CDCl_3): $\delta = 477.8$ ppm.

2-Bromoselenolo[3,2-*b*][1]benzoselenophene (**14c**). **13c** (1.42 g, 5 mmol) was dissolved in 30 mL THF and cooled to 0 °C. NBS (890 mg, 5 mmol) was added in portions. After work-up according to the general procedure **14c** was isolated as colorless solid in 96% yield (1.74 g). $R_f = 0.41$ (light petrol). $F_p = 105.0 - 109.1$ °C. $^1\text{H NMR}$ (600 MHz, CD_2Cl_2): $\delta = 7.92 - 7.91$ (m, 1 H), 7.72 - 7.70 (m, 1 H), 7.55 (s, 1 H), 7.43 - 7.40 (m, 1 H), 7.31 - 7.29 (m, 1 H) ppm. $^{13}\text{C NMR}$ (150 MHz, CD_2Cl_2): $\delta = 141.8$ (s), 139.6 (s), 137.6 (s), 135.4 (s), 129.4 (d), 127.2 (d), 126.0 (d), 125.4 (d), 123.6 (d), 115.7 (s) ppm. $^{77}\text{Se NMR}$ (114 MHz, CD_2Cl_2): $\delta = 628.7, 502.9$ ppm.

General procedure toward **7a-c**. To a suspension of zinc powder (10 eq.) in THF was slowly added titanium tetrachloride (5 eq.) at 0 °C, and then the mixture was refluxed for 3 h under an argon atmosphere. A solution of compound **6a-c** (1 eq.) and pyridine (11 eq.) in 30 mL THF was slowly added to the mixture, and then the mixture was refluxed for another 6 h. After cooling to room temperature, the mixture was diluted with 50 mL saturated sodium bicarbonate and stirred for 30 min. The solid was filtered and washed with diluted hydrochloric acid, water, and acetone and then dried in vacuo.

(*E*)-2,2'-(1,2-Ethenediyl)bis[selenolo[3,2-*b*][1]benzothiophene] (**7a**). The synthesis of **7a** was carried out according to the general procedure starting from **6a** (1.59 g, 6 mmol), zinc powder (3.92 g, 60 mmol) and titanium tetrachloride (5.69 g, 30 mmol). The crude product was sublimated twice to give a bright yellow solid (1.02 g, 68%). $R_f = 0.30$ (light petrol : DCM 4:1). $^1\text{H NMR}$ (600 MHz, CD_2Cl_2): $\delta = 7.89 - 7.87$ (m, 2 H), 7.80 - 7.79 (m, 2 H), 7.49 (s, 2 H), 7.43 (ddd, $J = 8.0, 6.9, 1.0$ Hz, 2 H), 7.37 (ddd, $J = 8.0, 6.9, 1.0$ Hz, 2 H), 7.17 (s, 2 H) ppm. $^{13}\text{C NMR}$ (150 MHz, CD_2Cl_2): $\delta = 149.7, 142.5, 140.0, 135.7, 133.9, 126.0, 125.5, 125.3, 124.2, 122.9, 122.2$ ppm. $^{77}\text{Se NMR}$ (114 MHz, CD_2Cl_2): $\delta = 495.6$ ppm.

(*E*)-2,2'-(1,2-Ethenediyl)bis[[1]benzoselenopheno[3,2-*b*]thiophene] (**7b**). The synthesis of **7b** was carried out according to the general procedure starting from **6b** (1.06 g, 4 mmol), zinc powder (2.62 g, 40 mmol) and titanium tetrachloride (3.79 g, 20 mmol). The crude product was sublimated twice to give a bright yellow solid (548 mg, 55%). $R_f = 0.27$ (light petrol : DCM 4:1). $^1\text{H NMR}$ (400 MHz, CD_2Cl_2): $\delta = 7.92 - 7.90$ (m, 2 H), 7.83 - 7.81 (m, 2 H), 7.44 (ddd, $J = 8.0, 6.9, 1.0$ Hz, 2 H), 7.36 (s, 2 H), 7.29 (ddd, $J = 8.0, 6.9, 1.0$ Hz, 2 H), 7.24 (s, 2 H) ppm. $^{13}\text{C NMR}$ (150 MHz, CDCl_3): $\delta = 144.2$ (s), 142.6 (s), 136.0 (s), 135.4 (s), 134.8 (s), 126.9 (d), 125.3 (d), 124.8 (d), 122.5 (d), 122.4 (d), 122.1 (d) ppm. $^{77}\text{Se NMR}$ (114 MHz, CD_2Cl_2): $\delta = 457.5$ ppm.

(*E*)-2,2'-(1,2-Ethenediyl)bis[selenolo[3,2-*b*][1]benzoselenophene] (**7c**). The synthesis of **7c** was carried out according to the general procedure starting from **6c** (1.87 g, 6 mmol), zinc powder (3.92 g, 60 mmol) and titanium tetrachloride (5.69 g, 30 mmol). The crude product was purified by column chromatography (90 g activated basic aluminum oxide, Brockmann 1, light petrol / DCM 0 \rightarrow 100%) to give a bright yellow solid (1.12 g, 63%). $R_f = 0.24$ (light petrol : DCM 4:1). $^1\text{H NMR}$

(600 MHz, CD₂Cl₂): δ = 7.93 - 7.92 (m, 2 H), 7.79 - 7.77 (m, 2 H), 7.50 (s, 2 H), 7.43 (ddd, J = 8.3, 6.8, 0.9 Hz, 2 H), 7.30 (ddd, J = 8.3, 6.9, 1.2 Hz, 2 H), 7.16 (s, 2 H) ppm. ¹³C NMR (150 MHz, CD₂Cl₂): δ = 149.2 (s), 142.8 (s), 137.9 (s), 137.4 (s), 136.8 (s), 127.3 (d), 126.0 (d), 125.9 (d), 125.9 (d), 125.4 (d), 123.8 (d) ppm. ⁷⁷Se NMR (114 MHz, CD₂Cl₂): δ = 518.5, 486.1 ppm.

General procedure toward **11a-c**. Bromide **10a-c** (2.5 eq.) and (*E*)-1,2-bis(tri-*n*-butylstannyl)ethylene (1 eq.) were dissolved in anhydrous toluene. The mixture was bubbled with argon for 30 min. Pd(PPh₃)₄ (0.03 eq.) was added and the mixture was heated to 90 °C for 48 hours under an argon atmosphere. The reaction mixture was cooled to room temperature, the obtained precipitate filtered, washed with methanol as well as acetone and dried in vacuo.

(*E*)-2,2'-(1,2-Ethenediyl)bis[selenolo[2,3-*b*][1]benzothiophene] (**11a**). **11a** was synthesized according to the general procedure starting from **10a** (506 mg, 1.6 mmol), (*E*)-1,2-bis(tri-*n*-butylstannyl)ethylene (388 mg, 0.64 mmol) and Pd(PPh₃)₄ (22 mg, 0.02 mmol). The crude product was sublimated twice to give a bright yellow solid (73 mg, 23%). R_f = 0.34 (light petrol : DCM 4:1). ¹H NMR (600 MHz, CD₂Cl₂): δ = 7.94 - 7.93 (m, 2 H), 7.87 - 7.86 (m, 2 H), 7.69 (s, 2 H), 7.44 (ddd, J = 8.1, 7.0, 1.2 Hz, 2 H), 7.35 (ddd, J = 8.0, 7.0, 1.2 Hz, 2 H), 7.10 (s, 2 H) ppm.

(*E*)-2,2'-(1,2-Ethenediyl)bis[[1]benzoselenopheno[2,3-*b*]thiophene] (**11b**). **11b** was synthesized according to the general procedure starting from **10b** (190 mg, 0.6 mmol), (*E*)-1,2-bis(tri-*n*-butylstannyl)ethylene (120 mg, 0.2 mmol) and Pd(PPh₃)₄ (2 mg, 0.002 mmol). The crude product was sublimated twice to give a bright yellow solid (36 mg, 30%). R_f = 0.31 (light petrol : DCM 4:1). ¹H NMR (600 MHz, CD₂Cl₂): δ = 7.96 - 7.91 (m, 2 H), 7.91 - 7.86 (m, 2 H), 7.53 (s, 2 H), 7.47 - 7.43 (m, 2 H), 7.33 - 7.29 (m, 2 H), 7.18 (s, 2 H) ppm. ¹³C NMR (150 MHz, CD₂Cl₂): δ = 146.7 (s), 145.4 (s), 144.2 (s), 135.5 (s), 134.2 (s), 126.8 (d), 125.8 (d), 125.3 (d), 123.5 (d), 122.1 (d), 119.9 (d) ppm.

(*E*)-2,2'-(1,2-Ethenediyl)bis[selenolo[2,3-*b*][1]benzoselenophene] (**11c**). **11c** was synthesized according to the general procedure starting from **10c** (474 mg, 1.5 mmol), (*E*)-1,2-bis(tri-*n*-butylstannyl)ethylene (303 mg, 0.5 mmol) and Pd(PPh₃)₄ (17 mg, 0.02 mmol). The crude product was purified by column chromatography (90 g activated basic aluminum oxide, Brockmann 1, light petrol / DCM 0 → 100%) as brownish solid (83 mg, 28%). R_f = 0.29 (light petrol / DCM 4:1). ¹H NMR (600 MHz, CD₂Cl₂): δ = 7.95 - 7.86 (m, 4 H), 7.69 (s, 2 H), 7.47 - 7.40 (m, 2 H), 7.33 - 7.26 (m, 2 H), 7.10 (s, 2 H) ppm. ¹³C NMR (150 MHz, CD₂Cl₂): δ = 150.8 (s), 146.7 (s), 145.0 (s), 136.8 (s), 125.7 (d), 125.4 (d), 125.0 (d), 123.6 (d), 122.7 (d) ppm.

2-[(Trimethylsilyl)ethynyl]selenolo[3,2-*b*][1]benzothiophene (**15**). **14a** (632 mg, 2 mmol, 1 eq.), ethynyltrimethylsilane (294 mg, 3 mmol, 1.5 eq.), Pd(PPh₃)₄ (46 mg, 0.04 mmol, 0.02 eq.), CuI (15 mg, 0.08 mmol, 0.04 eq.) and 5 mL Et₃N were stirred at 98 °C under argon atmosphere for one hour. Triethylamine was evaporated and the residue filtrated over 10 g silica gel using light petrol as

eluent. **15** was isolated as brownish oil in 85% yield (566 mg). $R_f = 0.23$ (light petrol). ^1H NMR (400 MHz, CDCl_3): $\delta = 7.86 - 7.85$ (m, 1 H), $7.78 - 7.76$ (m, 1 H), 7.62 (s, 1 H), $7.42 - 7.36$ (m, 2 H), 0.28 (s, 9 H) ppm. ^{13}C NMR (100 MHz, CDCl_3): $\delta = 142.6$ (s), 138.0 (s), 136.7 (s), 135.0 (s), 128.0 (d), 128.0 (s), 125.0 (d), 124.9 (d), 123.7 (d), 121.8 (d), 102.6 (s), 99.5 (s), -0.2 (q) ppm. ^{77}Se NMR (76 MHz, CDCl_3): $\delta = 609.6$ ppm.

2-Ethynylselenolo[3,2-*b*][1]benzothiophene (**16**). **15** (566 mg, 1.7 mmol, 1 eq.), and K_2CO_3 (704 mg, 5.1 mmol, 3 eq.) were dissolved in 5 mL methanol and stirred for one hour at room temperature. The reaction mixture was quenched with water and extracted with diethyl ether. The organic layer was dried over Na_2SO_4 and the solvent was evaporated. The product was purified by column chromatography (10 g silica gel, light petrol / ethyl acetate 9 : 1) and obtained as brownish oil in 52% yield (230 mg). $R_f = 0.24$ (light petrol). ^1H NMR (400 MHz, CDCl_3): $\delta = 7.88 - 7.85$ (m, 1 H), $7.79 - 7.76$ (m, 1 H), 7.68 (s, 1 H), $7.43 - 7.35$ (m, 2 H), 3.66 (s, 1 H) ppm. ^{13}C NMR (100 MHz, CDCl_3): $\delta = 142.7$ (s), 138.0 (s), 137.0 (s), 135.0 (s), 128.6 (d), 126.8 (s), 125.1 (d), 125.0 (d), 123.8 (d), 121.9 (d), 84.6 (s), 79.2 (d) ppm. ^{77}Se NMR (76 MHz, CDCl_3): $\delta = 608.1$ ppm.

2,2'-(1,2-Ethynediyl)bis[selenolo[3,2-*b*][1]benzothiophene] (**17**). **16** (230 mg, 0.9 mmol, 1 eq.), **14a** (306 mg, 0.97 mmol, 1.1 eq.), CuI (6.7 mg, 0.04 mmol, 0.04 eq.), $\text{Pd}(\text{PPh}_3)_4$ (20.4 mg, 0.02 mmol, 0.02 eq.) and 2 mL triethylamine were stirred at 98 °C under argon atmosphere overnight. Triethylamine was evaporated and the residue filtrated over 10 g silica gel using light petrol as eluent. **17** was isolated as yellow solid in 55% yield (245 mg). $R_f = 0.23$ (light petrol). ^1H NMR (600 MHz, CD_2Cl_2): $\delta = 7.92 - 7.90$ (m, 2 H), $7.84 - 7.82$ (m, 2 H), 7.74 (s, 2 H), 7.45 (ddd, $J = 8.0, 6.9, 1.2$ Hz, 2 H), 7.41 (ddd, $J = 8.0, 6.9, 1.2$ Hz, 2 H) ppm. ^{13}C NMR (150 MHz, CD_2Cl_2): $\delta = 143.1$ (s), 139.2 (s), 138.0 (s), 135.5 (s), 128.2 (d), 127.6 (s), 125.8 (d), 125.6 (d), 124.3 (d), 122.4 (d), 92.4 (s) ppm. ^{77}Se NMR (114 MHz, CD_2Cl_2): $\delta = 601.3$ ppm.

2-[(Trimethylsilyl)ethynyl]selenolo[2,3-*b*][1]benzothiophene (**18**). **10a** (430 mg, 1.36 mmol, 1 eq.), ethynyltrimethylsilane (200 mg, 2 mmol, 1.5 eq.), $\text{Pd}(\text{PPh}_3)_4$ (31 mg, 0.03 mmol, 0.02 eq.), CuI (10 mg, 0.05 mmol, 0.04 eq.) and 4 mL Et_3N were stirred at 98 °C under argon atmosphere overnight. Triethylamine was evaporated and the residue filtrated over 10 g silica gel using light petrol as eluent. **18** was isolated as brownish oil in 43% yield (195 mg). $R_f = 0.23$ (light petrol). ^1H NMR (600 MHz, CDCl_3): $\delta = 7.92 - 7.86$ (m, 2 H), $7.85 - 7.80$ (m, 1 H), 7.41 (ddd, $J = 8.2, 7.0, 1.2$ Hz, 1 H), 7.33 (ddd, $J = 8.2, 7.0, 1.2$ Hz, 1 H), 0.28 (s, 9 H) ppm. ^{13}C NMR (150 MHz, CDCl_3): $\delta = 144.3$ (s), 142.2 (s), 139.6 (s), 133.7 (s), 127.9 (s), 126.9 (d), 124.7 (d), 124.2 (d), 122.9 (d), 121.6 (d), 101.5 (s), 99.5 (s), -0.2 (q) ppm. ^{77}Se NMR (114 MHz, CDCl_3): $\delta = 628.5$ ppm.

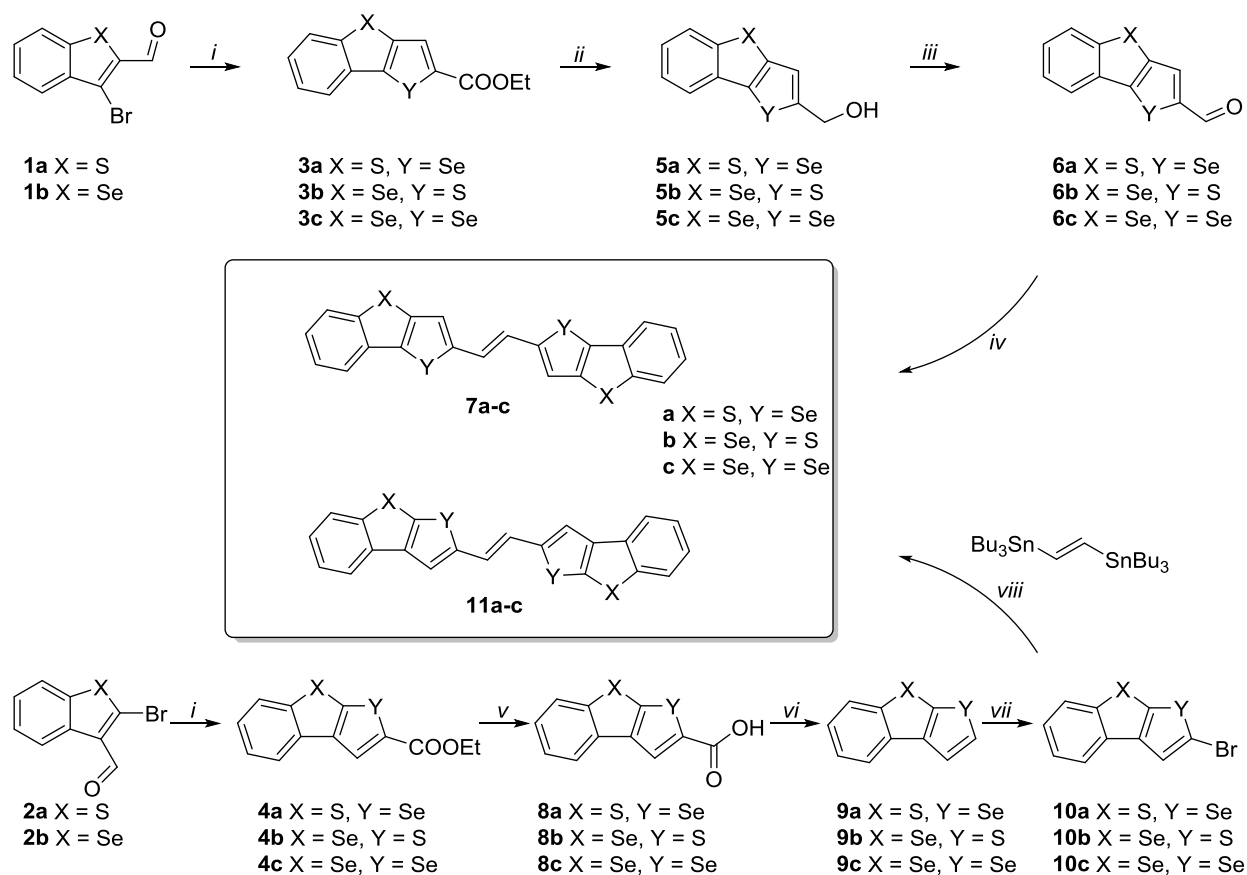
2-Ethynylselenolo[2,3-*b*][1]benzothiophene (**19**). **18** (184 mg, 0.55 mmol, 1 eq.), and K₂CO₃ (229 mg, 1.66 mmol, 3 eq.) were dissolved in 2 mL methanol and stirred for one hour at room temperature. The reaction mixture was quenched with water and extracted with diethyl ether. The organic layer was dried over Na₂SO₄ and the solvent was evaporated. The product was purified by column chromatography (10 g silica gel, light petrol / ethyl acetate 9:1) and obtained as brownish oil in 95% yield (137 mg). R_f = 0.23 (light petrol). ¹H NMR (600 MHz, CDCl₃): δ = 7.92 (s, 1 H), 7.91 - 7.86 (m, 1 H), 7.86 - 7.80 (m, 1 H), 7.42 (ddd, J = 8.1, 7.0, 1.2 Hz, 1 H), 7.34 (ddd, J = 8.1, 7.0, 1.2 Hz, 1 H), 3.61 (s, 1 H) ppm. ¹³C NMR (150 MHz, CDCl₃): δ = 144.5 (s), 142.1 (s), 139.8 (s), 133.7 (s), 127.5 (d), 126.7 (s), 124.8 (d), 124.3 (d), 122.9 (d), 121.6 (d), 83.7 (d), 79.1 (s) ppm. ⁷⁷Se NMR (114 MHz, CDCl₃): δ = 629.2 ppm.

2,2'-(1,2-Ethynediyl)bis[selenolo[2,3-*b*][1]benzothiophene] (**20**). **19** (129 mg, 0.5 mmol, 1 eq.), **10a** (173 mg, 0.55 mmol, 1.1 eq.), CuI (3.8 mg, 0.02 mmol, 0.04 eq.), Pd(PPh₃)₄ (11.4 mg, 0.009 mmol, 0.02 eq.) and 2 mL triethylamine were stirred at 98 °C under argon atmosphere overnight. Triethylamine was evaporated and the residue filtrated over 10 g silica gel using light petrol as eluent. **20** was isolated as yellow solid in 22% yield (54 mg). R_f = 0.22 (light petrol). ¹H NMR (600 MHz, CDCl₃): δ = 7.96 - 7.91 (m, 4 H), 7.88 - 7.84 (m, 2 H), 7.45 - 7.42 (m, 2 H), 7.37 - 7.34 (m, 2 H) ppm.

RESULTS AND DISCUSSION

Synthesis. The synthesis toward ene- and yne-bridging target molecules was planned by linkage of chalcogenopheno[1]benzochalcogenophene (CBC) building blocks. Starting from properly substituted benzo[*b*]thiophenes **1a** and **2a** and benzo[*b*]selenophenes **1b** and **2b** reported earlier,²⁴ the key step toward fused CBC moieties **3a-c** as well as **4a-c** is based on an optimized one-pot Fiesselmann reaction adapted from Machara et al.³⁰ Nucleophilic aromatic substitutions of aldehydes with *in situ* generated sodium hydroselenide and subsequent addition of ethyl bromoacetate or applying ethyl thioglycolate in triethylamine gave access to annelated ring systems **3a-c** as well as **4a-c** in good to excellent yield (Scheme 1).

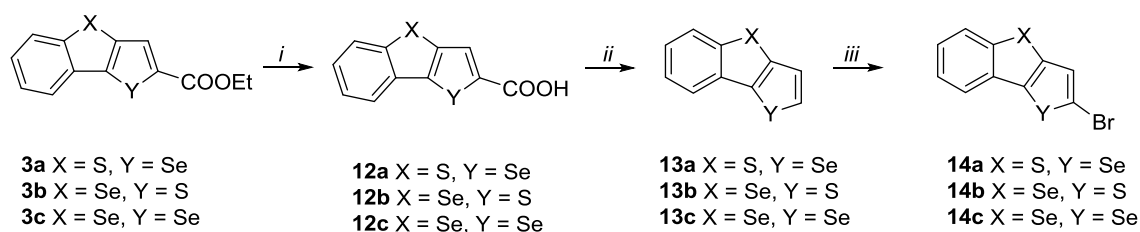
Based on previously reported approaches toward ene-bridged substrates^{19,31} derivatization of the obtained CBCs for McMurry reactions was the basis of further synthetic efforts. Functionalization of CBCs as aldehydes was realized by reduction of **3a-c** applying LiAlH₄ and subsequent re-oxidation of the obtained alcohols **5a-c** to yield aldehydes **6a-c**. Finally, regioisomers **7a-c** (Scheme 1, Table 1) were selectively accessible as *E*-isomers in good yields applying reductive McMurry reaction conditions according to procedures toward DTBTE systems (X, Y = S) applied in literature.¹⁹



Scheme 1: Synthetic strategy toward target molecules **7** and **11**: *i*: NaHSe, ethyl bromoacetate or triethylamine, ethyl thioglycolate, base; *ii*: LiAlH₄, THF; *iii*: MnO₂; *iv*: Zn, TiCl₄, pyridine, THF; *v*: NaOH, H₂O / MeOH; *vi*: Cu, quinoline, 160 °C; *vii*: NBS, THF; *viii*: Pd(PPh₃)₄, toluene, reflux.

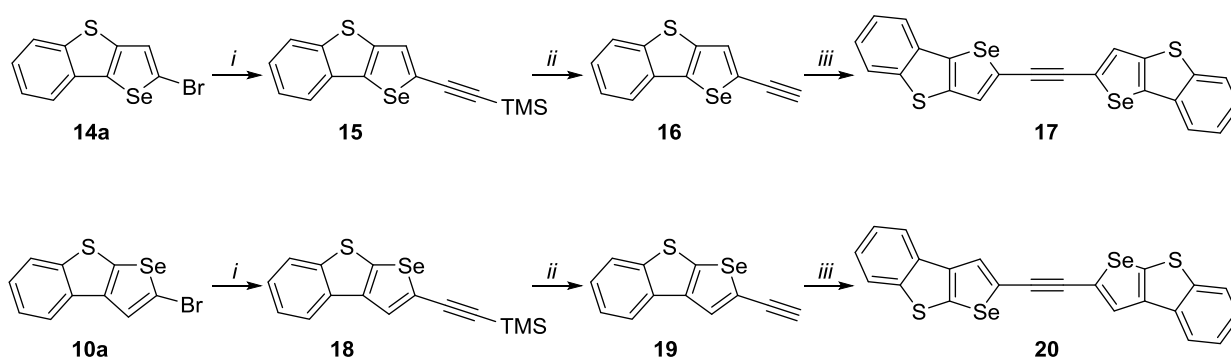
For regioisomers **11a-c** an alternative synthetic pathway was chosen since the reduction of **4a-c** yielded the respective alcohols only in low yield. Therefore, hydrolysis of CBC esters **4a-c** and subsequent decarboxylation of the acquired acids **8a-c** led to CBC cores **9a-c** (Scheme 1). Further bromination of the latter applying NBS gave the respective CBC bromides **10a-c** in good to excellent yields. The synthesis toward **11a-c** was realized applying brominated CBC cores **10a-c** in a Stille coupling reaction with *trans*-1,2-bis(tri-*n*-butylstannyl)ethylene according to literature.³¹

For the purpose of proving the applicability of the developed methods for all regioisomers, functionalization procedures were also applied toward CBC derivatives **14a-c**. Saponification of **3a-c** and subsequent decarboxylation of the acquired acids **12a-c** led to **13a-c** in good to excellent yields. Bromination applying NBS gave the respective CBC bromides **14a-c** in high yields (Scheme 2).



Scheme 2: Synthetic strategy toward **14a-c**: *i*: NaOH, H₂O/MeOH, *ii*: Cu, quinoline, 160 °C, *iii*: NBS, THF.

In order to investigate the influence of more rigid yne linkers on material properties, bromides **10a** and **14a** were applied in a stepwise Sonogashira coupling sequence (Scheme 3) for both regioisomers **17** and **20** proving the applicability of CBCs in further cross coupling reactions.



Scheme 3: Synthetic strategy toward target molecules **17** and **20**: *i*: ethynyltrimethylsilane, Pd(PPh₃)₄, CuI, *ii*: K₂CO₃, MeOH, *iii*: Pd(PPh₃)₄, CuI.

The obtained solid materials **7a-c**, **11a-c**, **17** and **20** appear yellow to orange in color and are slightly soluble in chlorinated organic solvents. The characterization of all compounds was

performed by $^1\text{H} / ^{13}\text{C} / ^{77}\text{Se}$ NMR spectroscopy, HR-MS analysis, and single-crystal XRD. The data are consistent with the proposed structural formulations.

Optical and Electrochemical Properties. Photophysical properties of **7a-c**, **11a-c**, **17** and **20** were determined in 5 μM CH_2Cl_2 by UV-Vis spectroscopy (Figure 3, Table 1 and supporting information) and compared to the sulfur-based compounds **BTTE** and **DTBTE**. According to the data, it is clear that the UV-Vis absorption spectra of the compounds are strongly affected by the heteroatoms incorporated. Three absorption maxima were observed for each substance: the maxima for all selenium containing compounds are shifted to higher wavelengths, which can be attributed to the higher electron density induced by the selenium heteroatom. Obviously, the heterocycle next to the ene-bridge of **7a-c** plays an important role and strongly correlates with the position of the absorption maximum: while for the thiophene ene-conjugated moieties **7b** and **11b** bathochromic shifts can be observed, its selenophene analogues **7c** and **11c** exhibit red shifts compared to **DTBTE** and **BTTE**, respectively.

Table 1: Experimental data, physical characterization and computational data of compounds **7a-c**, **11a-c**, **17** and **20**.

Comp.	Yield (%)	T_m^a (°C)	T_d^b (°C)	λ_{max}^c (nm)	Bandgap ^d (nm, eV)	HOMO ^e (eV)	LUMO ^f (eV)	Bandgap ^g (eV)	HOMO ^g (eV)	LUMO ^g (eV)
DTBTE	-	-	-	433, 409, 388	452, 2.74	-5.31	-2.57	2.99	-5.39	-2.40
7a	68	304	353	447, 420, 398	467, 2.65	-5.23	-2.58	2.91	-5.37	-2.40
7b	55	250	396	438, 412, 392	456, 2.72	-5.26	-2.54	2.97	-5.39	-2.48
7c	63	294	350	451, 424, 400	470, 2.64	-5.28	-2.64	2.89	-5.37	-2.48
BTTE	-	-	-	402, 385	446, 2.78	-5.16	-2.38	3.28	-5.32	-2.04
11a	23	-	-	417, 397	441, 2.81	-5.30	-2.49	3.18	-5.32	-2.14
11b	30	-	-	405, 387	434, 2.86	-5.30	-2.44	3.26	-5.29	-2.03
11c	28	-	-	419, 398	450, 2.76	-5.27	-2.51	3.16	-5.29	-2.13
17	55	-	-	421, 392, 350	435, 2.85	-5.61	-2.76	3.09	-5.53	-2.44
20	22	-	-	395, 371	420, 2.95	-5.50	-2.55	3.39	-5.46	-2.07

^a Obtained from DSC measurements. ^b Thermal decomposition temperature determined from 5% mass loss. ^c Absorption maxima measured in DCM solutions. ^d Bandgaps were determined from the onsets of the absorption in DCM solutions. ^e HOMO levels determined by cyclic voltammetric measurements. All E_{ox} data are reported relative to ferrocene (Fc/Fc^+ , $E_{\text{ox}} = 446$ mV). The concentration of the compounds used in this experiment was 5 μM in DCM; the scan rate was 50 mV s^{-1} . ^f LUMO levels were determined from the optical bandgap and the HOMO energy level according to the following equation: $E_{\text{LUMO}} = E_{\text{HOMO}} + E_{\text{bandgap}}$. ^g Calculated bandgaps and HOMO/LUMO levels (B3LYP / 6-311+G(d)).

The optical bandgaps were obtained from the onset of the UV-Vis absorption (Table 1). The bandgaps of selenium-based materials **7a-c** are reduced compared to sulfur based compound **DTBTE**, therefore charge carrier mobilities are expected to be enhanced. For **7c** a reduction of the bandgap of 0.1 eV could be observed. In general the bandgaps of regioisomers **11a-c** are higher than for **7a-c**. The regioisomers **11a,b** show increased bandgaps compared to the sulfur-based **BTTE**,

whereas the bandgap of **11c** is slightly decreased. The introduction of an yne spacer leads to an increase in bandgap, which may not be beneficial for charge carrier transport.

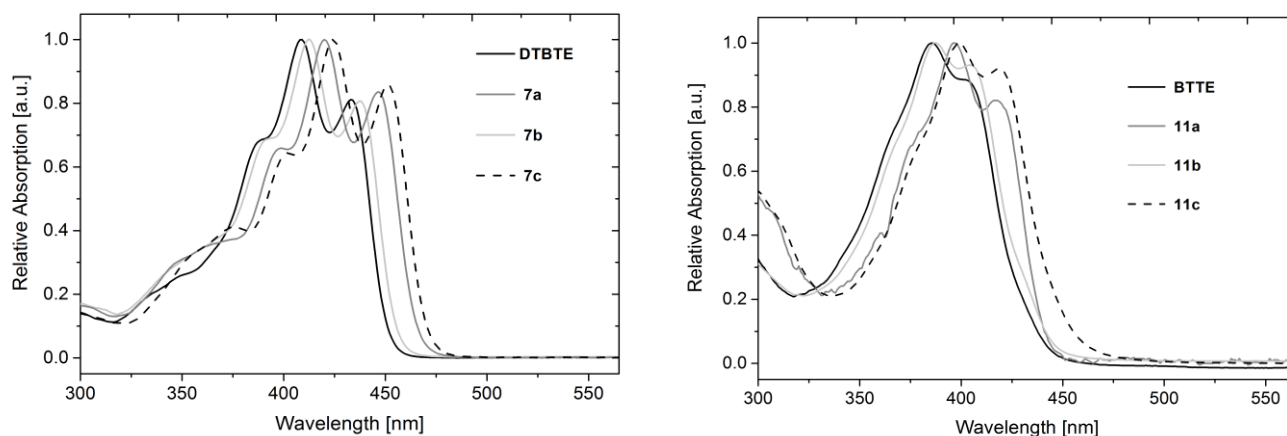


Figure 3: Absorption spectra of **7a-c** as well as **DTBTE** (left) and **11a-c** as well as **BTTE** (right).

Electrochemical characteristics of compounds **7a-c** and **11a-c** were investigated by cyclic voltammetric (CV) methods and compared to those of **DTBTE** and **BTTE**, respectively (Figure 4). The first oxidation potentials were used to determine the HOMO energy levels. All compounds **7a-c** undergo reversible oxidation indicating the formation of stable cation radicals. The HOMO levels of selenium-based compounds are slightly increased (ranging from -5.28 eV to -5.23 eV) compared to **DTBTE** (-5.31 eV). When comparing the regioisomer **11a-c** with **BTTE**, however, a significant reduction of the HOMO level can be observed, which may indicate good stability. The LUMO energy levels were determined from the optical bandgaps and the HOMO levels obtained from CV data and vary in the range from -2.58 to -2.64 eV. These findings are supported by quantum chemical calculations (Table 1). Calculated HOMO/LUMO levels are in good accordance with the experimental data for compounds **7a-c** (the pertinent data are listed in Table 1).

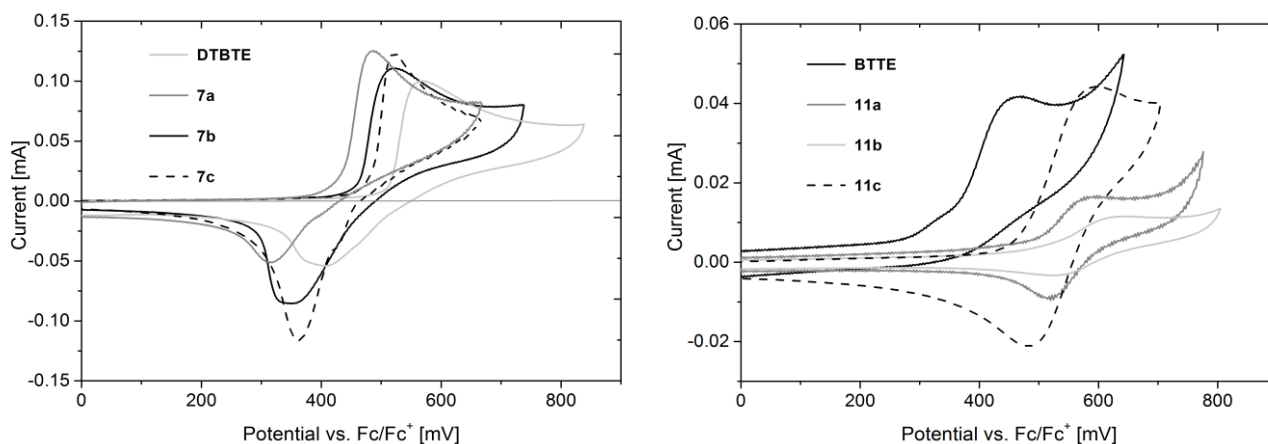


Figure 4: Cyclic voltammograms of **7a-c** as well as **DTBTE** (left) and **11a-c** as well as **BTTE** (right) in DCM solution.

Thermal properties. Glass-forming properties and thermal stability of the compounds were examined by simultaneous thermal analysis (STA). Compounds **7a-c** exhibit melting points in the range of 250 °C to 304 °C and good thermal stability was evidenced by decomposition temperatures corresponding to 5% mass loss between 350 °C and 396 °C (Table 1, see also supporting information). The thermal stability may allow for fabrication of homogeneous and stable amorphous thin films by vacuum deposition.

Single crystal structures. The effect of molecular conformation and packing properties in single crystals on charge carrier transport is a fundamental issue for organic semiconducting materials. Single crystals of **7a-c**, **17** and **20** were obtained by slow evaporation of solutions of the respective substrate in dichloromethane. All CBC subunits have almost planar forms and adopt an anti-conformation of the two fused chalcogenophenes, which may be favorable for charge carrier transport.³²

Similarly to **DTBTE**, the molecular structures of **7a** and **7b** show a nearly coplanar confirmation with a condensed herringbone arrangement, comparable with that of pentacene as depicted in Figure 5.³³ In contrast to **7a,b** the crystal structure of **7c** is arranging considerably different in a sandwich-herringbone arrangement.

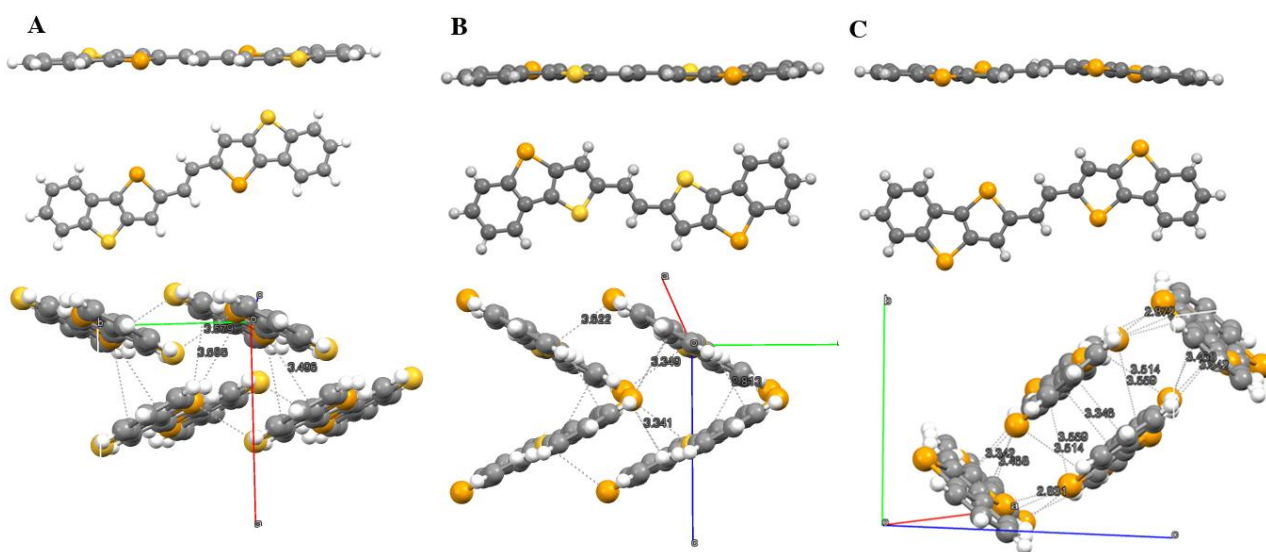


Figure 5: Front view and side views of the molecular structures and neighboring interactions of **7a** (A), **7b** (B) and **7c** (C).

The observed intermolecular distances are listed in Table 2. Strong short Se \cdots C interactions are dominant in the packing motives of **7a-c**. Whereas additional Se \cdots S as well as S \cdots C interactions can be observed in **7a**, **7c** also exhibits Se \cdots Se short contacts of up to 3.959 Å, which is close to the sum of the van der Waals radii of Se (3.80 Å).³⁴ All these short interactions form an effective three-dimensional structure, which may be beneficial to obtaining a high charge transport performance.

connected by yne linkers give rise to an increase in bandgap. The incorporation of yne linkers leads to less intermolecular interactions, therefore, lower charge carrier mobilities are expected. Further research will focus on the evaluation of the obtained materials as active semiconductors in organic thin film transistor devices.

ACKNOWLEDGMENT

The authors thank A. Aster and J. Bitai for contributing to the synthetic experiments. O. Liske is acknowledged for STA measurements.

ELECTRONIC SUPPLEMENTARY INFORMATION

¹H, ¹³C and ⁷⁷Se NMR spectra of compounds **3a-c**, **4a-c**, **5a-c**, **6a-c**, **7a-c**, **8a-c**, **9a-c**, **10a-c**, **11b,c**, **12a-c**, **13a-c**, **14a-c**, **15**, **16**, **17**, **18**, **19** and ¹H NMR of **11a** and **20**. Absorption spectra and cyclic voltammetric measurements of **17** and **20**. Thermal analysis of **7a-c**.

REFERENCES

- (1) Meng, Q.; Dong, H.; Hu, W.; Zhu, D. *J. Mater. Chem.* **2011**, *21* (32), 11708.
- (2) Heikenfeld, J.; Drzaic, P.; Yeo, J.-S.; Koch, T. *J. Soc. Inf. Disp.* **2011**, *19* (2), 129.
- (3) Sokolov, A. N.; Roberts, M. E.; Bao, Z. *Mater. Today* **2009**, *12* (9), 12.
- (4) Li, L.; Gao, P.; Baumgarten, M.; Müllen, K.; Lu, N.; Fuchs, H.; Chi, L. *Adv. Mater.* **2013**, *25* (25), 3419.
- (5) Hammock, M. L.; Chortos, A.; Tee, B. C.-K.; Tok, J. B.-H.; Bao, Z. *Adv. Mater.* **2013**, *25* (42), 5997.
- (6) Rivnay, J.; Owens, R. M.; Malliaras, G. G. *Chem. Mater.* **2014**, *26* (1), 679.
- (7) Knopfmacher, O.; Hammock, M. L.; Appleton, A. L.; Schwartz, G.; Mei, J.; Lei, T.; Pei, J.; Bao, Z. *Nat. Commun.* **2014**, *5*.
- (8) Tinivella, R.; Camarchia, V.; Pirola, M.; Shen, S.; Ghione, G. *Org. Electron.* **2011**, *12* (8), 1328.
- (9) Koezuka, H.; Tsumura, A.; Ando, T. *Synth. Met.* **1987**, *18* (1-3), 699.
- (10) Mas-Torrent, M.; Rovira, C. *Chem. Rev.* **2011**, *111* (8), 4833.
- (11) Zhao, Y.; Guo, Y.; Liu, Y. *Adv. Mater.* **2013**, *25* (38), 5372.
- (12) Anthony, J. E. *Angew. Chem. Int. Ed.* **2008**, *47* (3), 452.
- (13) Wang, C.; Dong, H.; Li, H.; Zhao, H.; Meng, Q.; Hu, W. *Cryst. Growth Des.* **2010**, *10* (9), 4155.
- (14) Wang, C.; Dong, H.; Hu, W.; Liu, Y.; Zhu, D. *Chem. Rev.* **2012**, *112* (4), 2208.
- (15) Takimiya, K.; Shinamura, S.; Osaka, I.; Miyazaki, E. *Heterocycles* **2011**, *83* (6), 1187.
- (16) Wu, W.; Liu, Y.; Zhu, D. *Chem. Soc. Rev.* **2010**, *39* (5), 1489.
- (17) Shi, J.; Xu, L.; Li, Y.; Jia, M.; Kan, Y.; Wang, H. *Org. Electron.* **2013**, *14* (3), 934.
- (18) Mathis, T.; Liu, Y.; Ai, L.; Ge, Z.; Lumpi, D.; Horkel, E.; Holzer, B.; Fröhlich, J.; Batlogg, B. *J. Appl. Phys.* **2014**, *115* (4), 043707.
- (19) Chen, H.; Cui, Q.; Yu, G.; Guo, Y.; Huang, J.; Zhu, M.; Guo, X.; Liu, Y. *J. Phys. Chem. C* **2011**, *115* (48), 23984.
- (20) Heeney, M.; Zhang, W.; Crouch, D. J.; Chabynyc, M. L.; Gordeyev, S.; Hamilton, R.; Higgins, S. J.; McCulloch, I.; Skabara, P. J.; Sparrowe, D.; Tierney, S. *Chem. Commun.* **2007**, *47*, 5061.
- (21) Izawa, T.; Miyazaki, E.; Takimiya, K. *Chem. Mater.* **2009**, *21* (5), 903.
- (22) Björk, M.; Grivas, S. *J. Heterocycl. Chem.* **2006**, *43* (1), 101.
- (23) Pedras, M. S. C.; Suchy, M. *Bioorg. Med. Chem.* **2006**, *14* (3), 714.
- (24) Holzer, B.; Hametner, C.; Fröhlich, J. manuscript in preparation.
- (25) Christiaens, L.; Piette, J.-L.; Laitem, L.; Baiwir, M.; Denoel, J.; Llabres, G. *Org. Magn. Reson.* **1976**, *8* (7), 354.
- (26) Frisch, J.; Trucks, G. W.; Schlegel, H. B.; Scuseria, G. E.; Robb, M. A.; Cheeseman, J. R.; Scalmani, G.; Barone, V.; Mennucci, B.; Petersson, G. A.; Nakatsuji, H.; Caricato, M.; Li, X.; Hratchian, H. P.; Izmaylov, A. F.; Bloino, J.; Zheng, G.; Sonnenberg, J. L.; Hada, M.; Ehara, M.; Toyota, K.; Fukuda, R.; Hasegawa, J.; Ishida, M.; Nakajima, T.; Honda, Y. *Gaussian 09, Revision A.02*; Gaussian, Inc., Wallingford CT, 2009.
- (27) Lee, C.; Yang, W.; Parr, R. G. *Phys. Rev. B* **1988**, *37* (2), 785.
- (28) Becke, A. D. *J. Chem. Phys.* **1993**, *98*, 5648.
- (29) Krishnan, R.; Binkley, J. S.; Seeger, R.; Pople, J. A. *J. Chem. Phys.* **1980**, *72* (1), 650.
- (30) Machara, A.; Kozmik, V.; Pojarová, M.; Dvořáková, H.; Svoboda, J. *Collect. Czechoslov. Chem. Commun.* **2009**, *74*, 1.
- (31) Liu, Y.; Liu, Z.; Luo, H.; Xie, X.; Ai, L.; Ge, Z.; Yu, G.; Liu, Y. *J. Mater. Chem. C* **2014**, *2* (41), 8804.
- (32) Drolet, N.; Morin, J.-F.; Leclerc, N.; Wakim, S.; Tao, Y.; Leclerc, M. *Adv. Funct. Mater.* **2005**, *15* (10), 1671.
- (33) Campbell, R. B.; Robertson, J. M.; Trotter, J. *Acta Crystallogr.* **1962**, *15* (3), 289.
- (34) Bondi, A. *J. Phys. Chem.* **1964**, *68* (3), 441.

Manuscript # 6

Daniel Lumpi[#], **Brigitte Holzer**[#], Johannes Bintinger, Ernst Horkel,* Simon Waid, Heinz D. Wanzenböck, Martina Marchetti-Deschmann, Christian Hametner, Emmerich Bertagnolli, Ioannis Kymissis, and Johannes Fröhlich

Substituted triphenylamines as building blocks for star shaped organic electronic materials

New J. Chem., **2015**, 39, 1840 - 1851

[#] contributed equally to this article

Reproduced by permission of The Royal Society of Chemistry (RSC) on behalf of the Centre National de la Recherche Scientifique (CNRS) and the RSC.


 CrossMark
click for updates

 Cite this: *New J. Chem.*, 2015,
39, 1840

Substituted triphenylamines as building blocks for star shaped organic electronic materials†

 Daniel Lumpi,[‡] Brigitte Holzer,[‡] Johannes Binting,^{ab} Ernst Horkel,^{*a}
Simon Waid,^c Heinz D. Wanzenböck,^c Martina Marchetti-Deschmann,^d
Christian Hametner,^a Emmerich Bertagnolli,^c Ioannis Kymissis^b and
Johannes Fröhlich^a

A versatile synthetic protocol toward a series of various substituted triphenylamine derivatives serving as building blocks for organic electronic materials was developed. Key steps during synthesis were either Ullmann condensations or nucleophilic aromatic substitutions giving rise to structural modification of triphenylamines and their electronic nature. In turn, these scaffolds were exemplarily attached to a dendritic tris(2-thienyl)benzene core affording star shaped organic semiconducting materials which were characterized regarding their photo-physical, electro-chemical and thermal properties. A strong influence of the substituent's nature on both photo-physical and morphological thin film characteristic of star shaped target compounds was observed. The applicability of these materials in organic electronic devices was demonstrated in an organic field effect transistor configuration yielding a hole mobility of nearly $10^{-3} \text{ cm}^2 \text{ V}^{-1} \text{ s}^{-1}$. The performance of the materials can be correlated to the substituents applied.

 Received (in Montpellier, France)
30th September 2014,
Accepted 15th December 2014

DOI: 10.1039/c4nj01695e

www.rsc.org/njc

Introduction

Organic electronic (OE) thin film devices have gained raising interest from academia and industry due to the variety of possible applications with enormous commercial potential.¹ This field covers the application of conducting and semi-conducting organic materials within electronic devices such as organic field effect transistors (OFETs),² organic light emitting devices (OLEDs)³ and organic photovoltaics (OPVs).^{4,5} The application of these materials in the field of organic electronics allows for solution processability, thus rendering OE-technology compatible with established high-throughput printing techniques and with the potential to realize thin, flexible and light-weight devices with low manufacturing costs.⁶

In general, a high charge carrier mobility is mandatory for the performance of different devices and strongly depends both

on the molecular structure and the morphology of the semiconducting material.^{2,7} Therefore, a broadly applicable material with high charge carrier mobility independent of processing techniques is desirable.^{8,9} The quest for novel compounds is an ongoing process in material science.

Poly- and oligothiophene based compounds have a long history in the field of OE.¹⁰ While high hole mobilities (up to $1.3 \text{ cm}^2 \text{ V}^{-1} \text{ s}^{-1}$) have been observed for thin films of poly-(3-hexylthiophene) (P3HT),¹¹ the material cannot be used in the light emitting layers of an OLED due to fluorescent self-quenching caused by strong π - π stacking.¹² Another useful class of OE materials are modified triphenylamine (TPA) structures, which have excellent electron donor and hole transport properties.¹³⁻¹⁷ The combination of these structural scaffolds results in a material class incorporating good charge carrier transport as a result of the oligothiophene unit and enhanced luminescent properties by circumventing self-quenching (*e.g.* **BMA-1T**, Fig. 1).¹⁸ Moreover, star-shaped compounds are found to exhibit better solubility and film-forming properties than their linear counterparts.^{8,19,20}

Combining TPA and thiophenes in C_3 symmetric configurations leads to enhanced electronic and luminescent properties with the benefit of solution processability.²¹ To realize C_3 symmetry, one can think of two possible molecular designs. One possibility is to use the TPA moiety as a central node with thiophene moieties as dendrons.^{19,22,23} Alternatively, a core (*e.g.* tris(2-thienyl)benzene) can be used to ensure C_3 symmetry bearing TPA units as side arms.²⁴ Based on these two possible

^a Institute of Applied Synthetic Chemistry, Vienna University of Technology, Getreidemarkt 9/163OC, A-1060 Vienna, Austria.

E-mail: ernst.horkel@tuwien.ac.at

^b Department of Electrical Engineering, Columbia University, 520W 120th street, Suite 1300, 10027 New York, NY, USA

^c Institute of Solid State Electronics, Vienna University of Technology, Floragasse 7, A-1040 Vienna, Austria

^d Institute of Chemical Technologies and Analytics, Vienna University of Technology, Getreidemarkt 9/164IAC, A-1060 Vienna, Austria

† Electronic supplementary information (ESI) available: ¹H and ¹³C NMR spectra of compounds **6c**, **6e-1**, **8c**, **8e-g**, **2**, **S2-3**, absorption and emission spectra of compounds **S1-3** and HOMO-LUMO plots of **S1-3**. See DOI: 10.1039/c4nj01695e

‡ Daniel Lumpi and Brigitte Holzer contributed equally to this article.

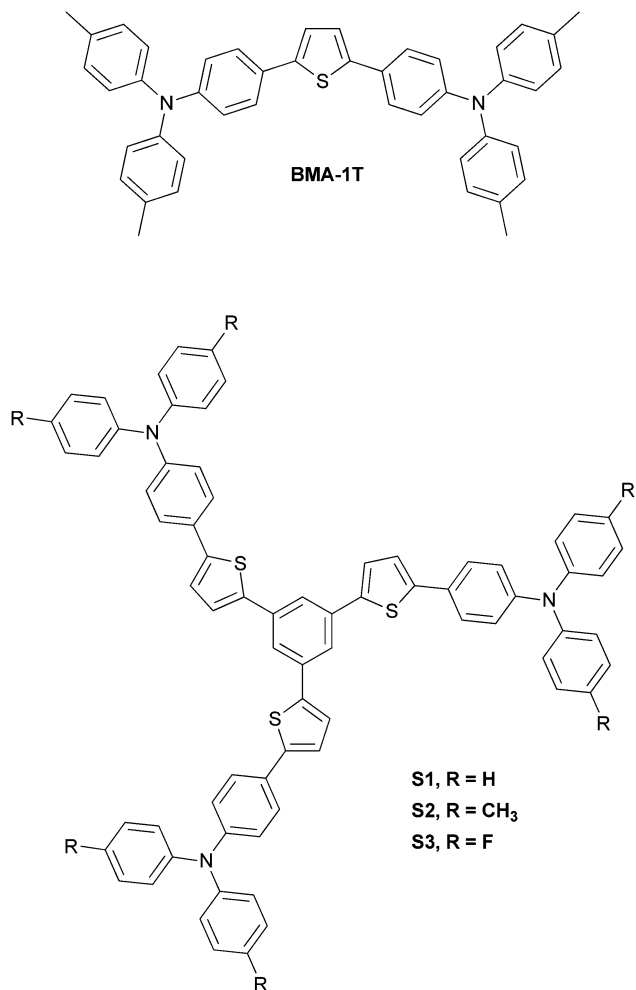


Fig. 1 Linear motifs (top) presented by Noda,¹⁸ star shaped molecules described in this work (bottom).

structural connectivities, this paper focuses on the latter possibility, since substituent alteration on the three TPA moieties constituting the outer sphere of the molecule strongly influences glass- and film-forming behaviour⁸ of the resulting materials, in turn affecting device performance.

Due to the widespread application of TPA-based compounds as building blocks in the field of organic electronics,²⁵ the synthetic protocol presented in this work is of considerable interest for the molecular design and potential modifications (e.g. in terms of photo-physical properties) toward a broad range of novel materials. Fine tuning of material properties can be realized by applying structurally and electronically diverse TPA motifs. However, due to the broad spectrum of substituents (electron donating or withdrawing) attached to the TPA, no general synthetic protocol is available. Access to TPAs bearing electron donating substituents is often described in literature, mainly applying Ullmann condensation.²⁶ On the other hand, this synthetic technique often fails when applied towards the synthesis of electron withdrawing groups. As a result of our investigations to overcome this drawback, we present a general protocol using nucleophilic aromatic substitution in order to

gain access to TPAs bearing electron withdrawing substituents. Reaction conditions for the consecutive transformation to the above-mentioned boronic acid esters also depend on the substituents' nature. While lithiation protocols can be applied for most TPAs under investigation, Miyaura borylation is required for TPAs bearing $-M$ substituents (Scheme 2).

With these TPA boronic acid esters in hand, a set of three star shaped compounds **S1–3** was realized using a Suzuki reaction. This nontoxic procedure proved superior in yield to a previously reported procedure incorporating a Stille reaction for the same compound **S1**.²⁴

Measurements of electro-chemical and optical properties (e.g. fluorescence spectra and quantum yields) of the star shaped compounds **S1–3** reveal the strong influence of the substituents' nature on the TPA moiety on the above-mentioned properties. The materials were characterized with respect to thermal stability, film-forming upon spin coating and semiconducting behaviour (charge carrier mobility in OFET configuration) to probe device applicability. Mobilities of almost $10^{-3} \text{ cm}^2 \text{ V}^{-1} \text{ s}^{-1}$ and low threshold voltages of approx. 0 V were recorded using methyl-TPA substituted derivative **S2**.

Experimental section

Synthesis and characterization

Substances purchased from commercial sources were used as received. Anhydrous *N,N*-dimethylformamide (DMF), *n*-butyllithium solution (2.5 M in hexanes) and 1,3,5-tribromobenzene were purchased from Aldrich Chemical Co. Isopropyl pinacol borate²⁷ (CAS 61676-62-8), (IPr)Pd(allyl)Cl²⁸ (CAS 478980-03-9) were synthesized according to literature. Anhydrous tetrahydrofuran (THF), diethyl ether, toluene were prepared immediately prior to use by a *PURESOLV*-plant (*it-innovative technology inc.*). Technical grade solvents were distilled prior to use. Analytical TLC was performed on Merck silica gel 60 F254 plates. Chromatographic separations at preparative scale were carried out on silica gel (Merck silica gel 60, 40–63 μm), alox or RP-gel. Nuclear magnetic resonance (NMR) spectra were obtained using a Bruker DPX-200 or Avance DRX-400 Fourier transform spectrometer operating at the following frequencies: DPX-200: 200.1 MHz (^1H) and 50.3 MHz (^{13}C); DRX-400: 400.1 MHz (^1H) and 100.6 MHz (^{13}C). The chemical shifts are reported in delta (δ) units, parts per million (ppm) downfield from tetramethylsilane using solvent residual signals for calibration. Coupling constants are reported in Hertz; multiplicity of signals is indicated by using following abbreviations: s = singlet, d = doublet, t = triplet, q = quartet. The multiplicity of ^{13}C signals were obtained by measuring JMOD spectra. UV/VIS absorption and fluorescence emission spectra were recorded in THF solutions ($1 \mu\text{g mL}^{-1}$) with a Perkin Elmer Lambda 750 spectrometer and an Edinburgh FLS920, respectively. Cyclic voltammetry was performed using a three electrode configuration consisting of a Pt working electrode, a Pt counter electrode and an Ag/AgCl reference electrode and a PGSTAT128N, ADC164, DAC164, external, DI048 potentiostat provided by Metrohm Autolab B. V. Measurements were carried

out in a 0.5 mM solution in anhydrous DCM (oxidation scan) with Bu_4NBF_4 (0.1 M) as the supporting electrolyte. The solutions were purged with nitrogen for 15 minutes prior to measurement. HOMO energy levels were calculated from the onset of oxidation. The onset potential was determined by the intersection of two tangents drawn at the background and the rising of oxidation peaks. High-resolution mass spectra (HRMS) were acquired as radical cations using a SYNAPT HDMS instrument (Waters, Manchester, UK) equipped with a matrix-assisted laser desorption/ionization (MALDI) source (MALDI-HRMS). Samples were applied at 1 mg mL^{-1} in THF on stainless steel using nitroanthracene (3 mg mL^{-1} in THF) as MALDI matrix. All MS spectra were recorded as accurate mass data with Angiotensin II (m/z 1046.542) as internal lock mass achieving a mass accuracy of 15–40 ppm (*i.e.* $\Delta m/z$ 0.01–0.04 amu). GC-MS measurements were conducted on a GC-MS hyphenation from Thermo Finnigan: focus GC with a BGB5 column ($l = 30 \text{ m}$, $\varnothing = 0.25 \text{ mm}$, $0.25 \text{ }\mu\text{m}$ film); DSQ II Quadrupole (EI^+ mode). The thermal behavior of substances **S1–3** was studied with differential scanning calorimetry (DSC) and thermogravimetric analysis (TGA) using a Netzsch simultaneous thermal analyzer (STA 449 F1 Jupiter). Powder samples with a mass of approx. 10 mg were lightly pressed into the bottom of open aluminum pans and heated at $10 \text{ }^\circ\text{C min}^{-1}$ from $25 \text{ }^\circ\text{C}$ to $500 \text{ }^\circ\text{C}$ under N_2 gas at a flow rate of 40 mL min^{-1} . The STA 449 type-K thermocouples were calibrated using indium, tin, bismuth and zinc metals.

Bottom-gate, top-contact OFETs were fabricated on ITO substrates with a 250 nm layer of vacuum deposited parylene-C which serves as a common gate electrode/gate dielectric structure. The substrates were ultrasonically cleaned with water, acetone and isopropanol followed by a 20 min treatment of UV/ozone. Compounds **S1–3** (25 nm) were vacuum deposited through a shadow mask ($p = 10^{-7}$ Torr, rate 0.1 \AA s^{-1}). The devices were completed by evaporation of gold source and drain electrodes (50 nm) on top. All characterizations were performed in ambient air. Current–voltage characteristics of the fabricated devices were recorded using a Keithley model 4200 semiconductor characterization system. Output and transfer characterization were recorded for at least four samples of the same channel width ($W = 2000 \text{ }\mu\text{m}$) and channel length ($L = 100 \text{ }\mu\text{m}$).

The spin-coated samples were prepared by the following procedure: the ITO substrates were ultrasonically cleaned with water, acetone and isopropanol followed by blow-drying with N_2 . 400 μL of a solution of the organic substance in chloroform (20 mg mL^{-1}) was prepared and filtered through a syringe filter (Teflon \varnothing 25 mm, $0.20 \text{ }\mu\text{m}$). Consecutively 300 μL of the prepared organic solution was spin-coated (2000 rpm s^{-1} ; 30 s) directly on ITO.

The typical layer thickness was in the range of 30–50 nm as revealed from atomic force microscopy (AFM)-measurements. For AFM studies, a Multimode V scanner in conjunction with a Nanoscope V controller (Veeco Instruments) was used. Image processing and data analysis was performed using Gwyddion software version 2.40. Samples were measured in tapping mode using PPP-NCHR probes obtained from Nanoandmore in air.

Several scans were performed from different parts of the samples to check the uniformity of the surface. Final images were measured from a scanning area of $10 \times 10 \text{ }\mu\text{m}^2$ with a tip velocity in the range from 16 to $18 \text{ }\mu\text{m s}^{-1}$. No image processing except flattening was done. Roughness values were calculated as root-mean-square (rms) values.

All computations were performed using the Gaussian 09 package, revision A.02.²⁹ For the calculation of HOMO/LUMO levels of compounds **S1–3**, ground state (S_0) geometries were optimized in gas phase within C_3 symmetry using the Becke three parameters hybrid functional with Lee–Yang–Perdew correlation (B3LYP)^{30,31} in combination with Pople basis set 6-311+G*.³² To obtain vertical absorption and emission of model compounds **S_m1–3**, ground state S_0 and first excited singlet state S_1 were optimized applying DFT and time-dependent (TD) DFT level of theory using M06-2X^{33,34} functional in combination with the polarized double zeta SVP basis set.³⁵ This parameterization was shown to be superior in terms of accuracy for the calculation of vertical transitions.³⁶ Geometry optimizations were performed without symmetry constraints and solvent effects were included through the polarizable continuum model (PCM)³⁷ in its linear response (LR-PCM)³⁸ and state specific (SS-PCM)³⁹ formulations, always considering the equilibrium time regime (eq.) for the excited state.

General procedure for the synthesis of 6a–f

Synthesis was performed according to Goodbrand.²⁶ 4-Bromoaniline **4a** (1.0 eq.), substituted iodobenzene **5a–f** (2.2 eq.), KOH (7.8 eq.), CuCl (0.04 eq) and 1,10-phenanthroline monohydrate (0.04 eq.) were suspended in anhydrous toluene. After purging the apparatus with argon, the reaction mixture was refluxed on a Dean Stark trap for an appropriate time maintaining the argon atmosphere. Reaction progress was monitored by GC/MS. The reaction mixture was cooled to room temperature and water was added to solve the potassium hydroxide. Phases were separated and the hydrous phase was extracted with toluene three times. The combined organic layer was washed with brine, dried over anhydrous sodium sulfate and evaporated to dryness under reduced pressure. The obtained crude product was purified by Kugelrohr distillation and subsequent recrystallisation from methanol or acetonitrile.

4-Bromo-*N,N*-bis(4-fluorophenyl)benzeneamine (6c). According to the general procedure; **4a** (7.04 g, 41 mmol), **5c** (20.0 g, 90 mmol), KOH (17.94 g, 320 mmol), CuCl (162 mg, 1.6 mmol) and phenanthroline monohydrate (325 mg, 1.6 mmol) were refluxed for 16 h using 250 mL anhydrous toluene. Kugelrohr distillation ($130 \text{ }^\circ\text{C}$, 3.8×10^{-1} mbar) and recrystallization from methanol gave colourless crystals of **6c** (10.33 g, 70% of theory). TLC (silica gel, hexanes): $r_f = 0.36$. $F_p = 56\text{--}58 \text{ }^\circ\text{C}$. $^1\text{H NMR}$ (200 MHz, CD_2Cl_2): $\delta = 7.38\text{--}7.25$ (m, 2H), 7.11–6.91 (m, 4H), 6.89–6.72 (m, 8H), 6.91–6.80 (m, 2H) ppm. $^{13}\text{C NMR}$ (50 MHz, CD_2Cl_2): $\delta = 159.7$ (s, $J_{\text{CF}} = 242.6$ Hz), 147.8 (s), 144.0 (s, $J_{\text{CF}} = 2.8$ Hz), 132.7 (d), 126.9 (d, $J_{\text{CF}} = 8.1$ Hz), 124.3 (d), 116.7 (d, $J_{\text{CF}} = 22.6$ Hz), 114.7 (s) ppm. MS (EI): m/z 359 (M^+ , 100%), 279 (22), 184 (14).

4-Bromo-*N,N*-bis[4-(trimethylsilyl)phenyl]benzeneamine (6e). According to the general procedure; **4a** (7.82 g, 45.5 mmol), **5e** (27.62 g, 100 mmol), KOH (19.89 g, 355 mmol), CuCl (180 mg, 1.8 mmol) and phenanthroline monohydrate (360 mg, 1.8 mmol) were refluxed for 24 h using 250 mL anhydrous toluene. Kugelrohr distillation (130 °C, 6.5×10^{-2} mbar) and recrystallization from acetonitrile gave colourless crystals of **6e** (12.9 g, 60% of theory). TLC (silica gel, hexanes): $r_f = 0.39$. $F_p = 143\text{--}145$ °C. $^1\text{H NMR}$ (200 MHz, CDCl_3): $\delta = 7.42\text{--}7.27$ (m, 6H), 7.08–6.90 (m, 6H), 0.24 (s, 18H) ppm. $^{13}\text{C NMR}$ (100 MHz, CDCl_3): $\delta = 147.9$ (s), 146.9 (s), 134.64 (s), 134.61 (d), 132.4 (d), 126.1 (d), 123.5 (d), 115.5 (s), 112.4 (s), –0.8 (q) ppm. MS (EI): m/z 469 (M^+ , 100%), 454 (61), 452 (58), 220 (65).

4-Bromo-*N,N*-bis[4-(1,1-dimethylethyl)phenyl]benzeneamine (6f). According to the general procedure; **4a** (3.7 g, 21.5 mmol), **5f** (12.3 g, 47.3 mmol), KOH (9.4 g, 168 mmol), CuCl (85 mg, 0.86 mmol) and phenanthroline monohydrate (170 mg, 0.86 mmol) were refluxed for 36 h using 130 mL anhydrous toluene. Kugelrohr distillation (160 °C, 2.2×10^{-1} mbar) and recrystallization from acetonitrile gave colourless crystals of **6f** (5.8 g, 61% of theory). TLC (silica gel, hexanes): $r_f = 0.33$. $F_p = 165\text{--}168$ °C. $^1\text{H NMR}$ (200 MHz, CD_2Cl_2): $\delta = 7.36\text{--}7.22$ (m, 6H), 7.07–6.95 (m, 4H), 6.95–6.82 (m, 2H), 1.32 (s, 18H) ppm. $^{13}\text{C NMR}$ (50 MHz, CD_2Cl_2): $\delta = 148.1$ (s), 146.9 (s), 145.3 (s), 132.4 (d), 126.8 (d), 124.8 (d), 124.5 (d), 114.0 (s), 34.8 (s), 31.8 (q) ppm. MS (EI): m/z 435 (M^+ , 73%), 422 (96), 420 (100), 204 (35), 176 (47).

General procedure for the synthesis of **6g–6l** (nucleophilic substitution)

Synthesis was performed according to Davey⁴⁰ and Gorvin.^{40,41} Under an argon atmosphere, 4-haloaniline **4a,b** (1 eq.), fluoro-benzene **8a–c** (2.2 eq.) and base (CsF or KO^tBu , 2.0–2.2 eq.) were stirred in DMSO (stored over molecular sieve, 3 Å) at 120 °C overnight. The solvent was removed under reduced pressure and the remaining crude product dissolved in chloroform. After washing with water, the organic layer was dried over anhydrous sodium sulfate and evaporated to dryness under reduced pressure. Further purification was achieved by column chromatography or recrystallization.

4-Bromo-*N,N*-bis(4-nitrophenyl)benzeneamine (6g). Under an argon atmosphere, 4-bromoaniline (6.88 g, 40 mmol) and CsF (12.15 g, 80 mmol) were suspended in 100 mL of dry DMSO. To the stirred suspension **7a** (12.42 g, 88 mmol) was added drop wise and the reaction was heated to 110 °C for 40 h. After cooling to r.t., the reaction mixture was poured on 800 mL of water. The formed brown precipitate was filtered over a glass sinter funnel and crystallized from pyridine to give **6g** (9.00 g, 54% of theory) as yellow crystals. TLC (silica gel, hexanes/ethyl acetate = 9/1): $r_f = 0.76$. $F_p = 312\text{--}315$ °C. $^1\text{H NMR}$ (400 MHz, CDCl_3): $\delta = 8.19\text{--}8.10$ (m, 4H), 7.57–7.49 (m, 2H), 7.17–7.09 (m, 4H), 7.07–7.00 (m, 2H) ppm. $^{13}\text{C NMR}$ (100 MHz, CDCl_3): $\delta = 151.7$ (s), 144.2 (s), 143.3 (s), 133.9 (d), 128.7 (d), 125.9 (d), 122.8 (d), 120.5 (s) ppm. MS (EI): m/z 413 (M^+ , 100%), 323 (20), 321 (20), 241 (96).

4-Bromo-*N,N*-bis[4-(methylsulfonyl)phenyl]benzeneamine (6h). Under an argon atmosphere, 4-bromoaniline (86 mg, 0.5 mmol),

7b (192 mg, 1.1 mmol) and KO^tBu (118 mg, 1.05 eq.) were stirred in 2 mL of dry DMSO at 120 °C for 12 h. After cooling to r.t., the solvent was removed under reduced pressure. The residue was taken up with chloroform and filtered over a pad of celite. The solvent was removed under reduced pressure and the crude product purified by column chromatography (40 g silica gel, hexanes/ethyl acetate gradient 20 → 50%) to give **6h** as light brown powder (184 mg, 77% of theory). TLC (silica gel, hexanes/ethyl acetate = 1/1): $r_f = 0.20$. $F_p = 240$ °C. $^1\text{H NMR}$ (200 MHz, CDCl_3): $\delta = 7.86\text{--}7.73$ (m, 4H), 7.55–7.44 (m, 2H), 7.22–7.11 (m, 4H), 7.06–6.96 (m, 2H), 3.05 (s, 6H) ppm. $^{13}\text{C NMR}$ (50 MHz, CDCl_3): $\delta = 151.0$ (s), 144.5 (s), 134.8 (s), 133.6 (d), 129.4 (d), 128.4 (d), 123.2 (d), 119.7 (s), 44.8 (q) ppm.

4,4'-[[4-Bromophenyl]imino]bisbenzotrile (6i). Under an argon atmosphere, 4-bromoaniline (8.1 g, 47 mmol) and CsF (14.3 g, 94 mmol) were suspended in 120 mL of dry DMSO. A solution of **7c** (12.5 g, 103 mmol) in 50 mL of dry DMSO was added drop wise and the reaction mixture was heated to 110 °C for 50 h. After cooling to r.t., the reaction mixture was poured on 800 mL of water and extracted three times with 200 mL chloroform. The combined organic layer was washed with brine, dried over anhydrous sodium sulfate and the solvent was removed under reduced pressure. The crude product was crystallized from ethanol to give **6i** (4.05 g, 23% of theory) as light brown solid. TLC (silica gel, hexanes/ethyl acetate = 4/1): $r_f = 0.41$. $F_p = 261\text{--}262$ °C. $^1\text{H NMR}$ (200 MHz, CDCl_3): $\delta = 7.58\text{--}7.42$ (m, 6H), 7.14–7.03 (m, 4H), 7.03–6.93 (m, 2H) ppm. $^{13}\text{C NMR}$ (50 MHz, CDCl_3): $\delta = 149.9$ (s), 144.3 (s), 133.8 (d), 133.6 (d), 128.3 (d), 123.3 (d), 119.7 (s), 118.9 (s), 106.5 (s) ppm. MS (EI): m/z 373 (M^+ , 100%), 293 (29), 192 (38), 147 (80).

4-Iodo-*N,N*-bis(4-nitrophenyl)benzeneamine (6j). Under an argon atmosphere, 4-iodoaniline (5.6 g, 26 mmol) and KO^tBu (6.1 g, 54 mmol) were suspended in 150 mL of dry DMSO. To the stirred suspension **7a** (8.00 g, 57 mmol) was added drop wise and the reaction was heated to 120 °C for 40 h. After cooling to r.t., the solvent was removed under reduced pressure. The residue was taken up with chloroform and filtered over a pad of celite. The solvent was removed under reduced pressure and the crude product crystallized from pyridine to give **6j** (6.96 g, 58% of theory) as orange solid. TLC (silica gel, hexanes/ethyl acetate = 9/1): $r_f = 0.26$. $F_p = 295\text{--}297$ °C. $^1\text{H NMR}$ (400 MHz, CDCl_3): $\delta = 8.19\text{--}8.10$ (m, 4H), 7.76–7.68 (m, 2H), 7.17–7.09 (m, 4H), 6.94–6.87 (m, 2H) ppm. $^{13}\text{C NMR}$ (100 MHz, CDCl_3): $\delta = 151.6$ (s), 144.9 (s), 143.4 (s), 139.8 (d), 128.8 (d), 125.9 (d), 122.9 (d), 91.4 (s) ppm. MS (EI): m/z 461 (M^+ , 100%), 369 (11), 241 (83).

4-Iodo-*N,N*-bis[4-(methylsulfonyl)phenyl]benzeneamine (6k). Under an argon atmosphere, 4-iodoaniline (4.38 g, 20 mmol), **7b** (7.6 g, 44 mmol) and KO^tBu (4.94 g, 44 mmol) were stirred in 150 mL of dry DMSO at 120 °C for 18 h. After cooling to r.t., the solvent was removed under reduced pressure. The residue was taken up with 100 mL of chloroform and washed with 50 mL of water. After drying over anhydrous sodium sulfate, the solvent was removed under reduced pressure and the crude product was purified by recrystallization from acetic acid/water ($v/v = 15/1$) to give **6k** as a brown solid (6.74 g, 64% of theory).

TLC (silica gel, hexanes/ethyl acetate = 1/1): r_f = 0.19. F_p = 232–235 °C. ^1H NMR (200 MHz, CDCl_3): δ = 7.83–7.73 (m, 4H), 7.70–7.62 (m, 2H), 7.23–7.11 (m, 4H), 6.92–6.83 (m, 2H), 3.04 (s, 6H) ppm. ^{13}C NMR (50 MHz, CDCl_3): δ = 151.0 (s), 145.2 (s), 139.5 (d), 134.8 (s), 129.4 (d), 128.5 (d), 123.3 (d), 90.5 (s), 44.8 (q) ppm.

4,4'-[(4-Iodophenyl)imino]bisbenzotrile (6l). Under an argon atmosphere, 4-iodoaniline (4.48 g, 20.5 mmol) and CsF (6.52 g, 43 mmol) were suspended in 40 mL of dry DMSO. A solution of **7c** (5.45 g, 45 mmol) in 20 mL of dry DMSO was added drop wise and the reaction mixture was heated to 140 °C for 18 h. After cooling to r.t., the solvent was removed under reduced pressure. The residue was taken up with chloroform and filtered over a pad of celite. The solvent was removed under reduced pressure and the crude product purified by column chromatography (90 g silica gel, dry loading on 10 g silica, hexanes/ethyl acetate gradient 5 → 20%) to give **6l** (2.10 g, 24% of theory) as light yellow solid. TLC (silica gel, hexanes/ethyl acetate = 4/1): r_f = 0.42. F_p = 228–230 °C. ^1H NMR (200 MHz, CDCl_3): δ = 7.73–7.61 (m, 2H), 7.59–7.45 (m, 4H), 7.15–7.02 (m, 4H), 6.92–6.81 (m, 2H) ppm. ^{13}C NMR (50 MHz, CDCl_3): δ = 149.9 (s), 145.0 (s), 139.5 (d), 133.8 (d), 128.5 (d), 123.4 (d), 118.9 (s), 106.5 (s), 90.5 (s) ppm. MS (EI): m/z 421 (M^+ , 100%), 294 (12), 192 (12).

General procedure for the synthesis of 8a–f

Synthesis was performed according to Anemian:⁴² all operations were performed under argon atmosphere. Triphenylamine (**6a–f**) (1.0 eq.) was dissolved in anhydrous THF. The solution was cooled to –80 °C and a solution of *n*-butyllithium (2.5 M in hexanes) (1.2 eq.) was added *via* a syringe, keeping the temperature below –75 °C. The reaction mixture was stirred at –80 °C for appropriate time before isopropyl pinacol borate (1.2 eq.) was added drop-wise at the same temperature. After slowly warming to room temperature (approx. 2 h), stirring was continued overnight. The solvent was distilled off under reduced pressure and the residue was distributed between water and chloroform. The phases were separated and the aqueous phase was extracted twice with chloroform. The combined organic layer was washed with brine and dried over sodium sulfate. The solvent was removed under reduced pressure to give the crude product, which was further purified by recrystallization or Kugelrohr distillation.

***N,N*-Bis(4-fluorophenyl)-4-(4,4,5,5-tetramethyl-1,3,2-dioxaborolan-2-yl)benzeneamine (8c).** According to the general procedure; **6c** (4.8 g, 13.3 mmol) was lithiated with *n*-BuLi (6.4 mL, 16 mmol) in 50 mL anhydrous THF for 2 h before isopropyl pinacol borate (3.0 g, 16 mmol) was added. After general workup the crude product was purified by Kugelrohr distillation (130 °C, 8.0×10^{-2} mbar) to give **8c** as white crystalline powder (4.9 g, 91% of theory). TLC (silica gel, hexanes/ethyl acetate = 8/1): r_f = 0.67. F_p = 92–95 °C. ^1H NMR (200 MHz, CD_2Cl_2): δ = 7.65–7.53 (m, 2H), 7.16–6.84 (m, 10H), 1.31 (s, 12H) ppm. ^{13}C NMR (50 MHz, CD_2Cl_2): δ = 159.8 (s, J_{CF} = 242.8 Hz), 151.2 (s), 143.9 (s, J_{CF} = 3.2 Hz), 136.3 (d), 127.5 (d, J_{CF} = 8.2 Hz), 120.7 (d), 116.7 (d, J_{CF} = 22.6 Hz), 84.1 (s), 25.2 (q) ppm (C–B not detected). MS (EI): m/z 407 (M^+ , 100%), 349 (10), 307 (18).

***N,N*-Bis[4-(trimethylsilyl)phenyl]-4-(4,4,5,5-tetramethyl-1,3,2-dioxaborolan-2-yl)benzeneamine (8e).** According to the general

procedure; **6e** (7.03 g, 15 mmol) was lithiated with *n*-BuLi (7.2 mL, 18 mmol) in 75 mL of anhydrous THF for 2 h before isopropyl pinacol borate (3.35 g, 18 mmol) was added. After general workup the crude product was purified by recrystallization from acetonitrile to give **8e** as white crystalline powder (6.60 g, 85% of theory). TLC (silica gel, hexanes/ethyl acetate = 8/1): r_f = 0.72. F_p = 206–209 °C. ^1H NMR (200 MHz, CDCl_3): δ = 7.73–7.64 (m, 2H), 7.44–7.34 (m, 4H), 7.13–7.02 (m, 6H), 1.34 (s, 12H), 0.26 (s, 18H) ppm. ^{13}C NMR (50 MHz, CDCl_3): δ = 150.4 (s), 147.9 (s), 136.1 (d), 134.7 (s), 134.5 (d), 124.0 (d), 122.8 (d), 83.8 (s), 25.1 (q), –0.8 (q) ppm (C–B not detected). MS (EI): m/z 515 (M^+ , 100%), 500 (22), 400 (11), 243 (11).

***N,N*-Bis[4-(1,1-dimethylethyl)phenyl]-4-(4,4,5,5-tetramethyl-1,3,2-dioxaborolan-2-yl)benzeneamine (8f).** According to the general procedure; **6f** (10.91 g, 25 mmol) was lithiated with *n*-BuLi (12 mL, 30 mmol) in 150 mL of anhydrous THF for 2 h before isopropyl pinacol borate (5.58 g, 30 mmol) was added. After general workup the crude product was triturated with methanol to give **8f** as white crystalline powder (9.05 g, 79% of theory). TLC (silica gel, hexanes/ethyl acetate = 8/1): r_f = 0.71. F_p = 212–214 °C. ^1H NMR (200 MHz, CDCl_3): δ = 7.64–7.53 (m, 2H), 7.37–7.26 (m, 4H), 7.10–7.00 (m, 4H), 7.00–6.91 (m, 2H), 1.37–1.29 (m, 30H) ppm. ^{13}C NMR (50 MHz, CDCl_3): δ = 151.5 (s), 147.2 (s), 145.2 (s), 136.2 (d), 126.8 (d), 125.4 (d), 120.9 (d), 84.0 (s), 34.8 (s), 31.8 (q), 25.3 (q) ppm (C–B not detected). MS (EI): m/z 483 (M^+ , 16%), 468 (18), 368 (12), 168 (11), 57 (100).

***N,N*-Bis(4-nitrophenyl)-4-(4,4,5,5-tetramethyl-1,3,2-dioxaborolan-2-yl)benzeneamine (8g).** Synthesis was performed according to Murata.⁴³ In a 100 mL round-bottom flask, **6j** (2.08 g, 4.5 mmol, 1.0 eq.) and $\text{PdCl}_2(\text{dppf})$ (98.8 mg, 0.135 mmol, 0.03 eq.) were suspended in 20 mL of dry dioxane. After flushing the apparatus with argon, triethylamine (1.37 g, 13.5 mmol, 3.0 eq.) and pinacolborane (749 mg, 5.85 mmol, 1.3 eq.) were added drop wise. After stirring for 15 h at room temperature the solvent was removed under reduced pressure. The crude product was purified by column chromatography (100 g basic alumina, dry loading on 6 g neutral alumina, hexanes/DCM gradient 25 → 100%) to give **8g** as orange powder (390 mg, 19% of theory). TLC (silica gel, hexanes/ethyl acetate = 8/1): r_f = 0.52. F_p = 175–178 °C. ^1H NMR (200 MHz, CDCl_3): δ = 8.18–8.06 (m, 4H), 7.89–7.77 (m, 2H), 7.20–7.07 (m, 6H), 1.33 (s, 12H) ppm. ^{13}C NMR (50 MHz, CDCl_3): δ = 151.9 (s), 147.6 (s), 143.2 (s), 137.1 (d), 126.0 (d), 125.7 (d), 123.0 (d), 84.3 (s), 25.1 (q) ppm (C–B not detected). MS (EI): m/z 461 (M^+ , 100%), 361 (21), 268 (17).

General procedure for the Suzuki coupling towards 2, S1–3

The synthesis was performed according to Marion.⁴⁴ Under an argon atmosphere, (hetero)aromatic halide (1.0 eq.), boronic ester (3.0–4.5 eq.) and KO^tBu (3.0–4.5 eq.) were suspended in a sufficient amount of solvent (IPA/ H_2O = 3/1; degassed by bubbling with argon). A solution of (IPr)Pd(allyl)Cl (0.02–0.05 eq.) in degassed IPA was added and the reaction mixture was refluxed for an appropriate time, monitoring the conversion by TLC. After completion, the reaction mixture was distributed between water and chloroform; the phases were separated and the aqueous

layer was extracted with chloroform three times. The combined organic layer was dried over anhydrous sodium sulfate and the solvent removed under reduced pressure to give the crude product. Purification was achieved by column chromatography.

2,2',2''-(1,3,5-Benzenetriyl)tristhiophene (2). According to the general procedure; 1,3,5-tribromobenzene (0.787 g, 2.5 mmol), 2-thiopheneboronic acid pinacol ester (2.364 g, 11.25 mmol) and KO^tBu (1.262 g, 11.25 mmol) were suspended in 50 mL solvent. (IPr)Pd(allyl)Cl (71.4 mg, 125 μmol; dissolved in 1 mL IPA) was added before refluxing for 1 h. After general workup the crude product was purified by column chromatography (90 g silica gel, hexanes/DCM 0 → 3%) to give **2** as white powder (0.697 g, 86% of theory). TLC (silica gel, hexanes/ethyl acetate = 20/1): r_f = 0.35. ¹H NMR (200 MHz, CDCl₃): δ = 7.74 (s, 3H), 7.40 (dd, J = 1.1, 3.6 Hz, 3H), 7.33 (dd, J = 1.1, 5.1 Hz, 3H), 7.11 (dd, J = 3.6, 5.1 Hz, 3H) ppm. ¹³C-NMR (50 MHz, CDCl₃): δ = 143.7 (s), 135.9 (s), 128.3 (d), 125.6 (d), 124.1 (d), 122.9 (d) ppm.

4,4',4''-(1,3,5-Benzenetriyltri-5,2-thiophenediyl)tris[*N,N*-diphenylbenzenamine] (S1). According to the general Suzuki procedure; compound **3** (280.1 mg, 0.5 mmol), boronic acid pinacol ester **6a** (835.0 mg, 2.25 mmol) and KO^tBu (252.5 mg, 2.25 mmol) were suspended in 12 mL solvent. (IPr)Pd(allyl)Cl (14.3 mg, 25 μmol; dissolved in 1 mL IPA) was added before refluxing for 2 h. After general workup the crude product was purified by column chromatography (90 g silica gel, hexanes/DCM = 6/1); after removing the solvent under reduced pressure, the residue was dissolved in 40 mL of boiling 2-butanone. The product was precipitated by adding 50 mL of 2-propanol to give **S1** as yellow powder (512.8 mg, 97% of theory). TLC (silica gel, cyclohexane/DCM = 3/1): r_f = 0.30. ¹H NMR and ¹³C NMR data according to literature.²¹ MS (MALDI-TOF): calcd for C₇₂H₅₁N₃S₃: 1053.3245; found: 1053.3020.

4,4',4''-(1,3,5-Benzenetriyltri-5,2-thiophenediyl)tris[*N,N*-bis-(4-methylphenyl)benzenamine] (S2). According to the general Suzuki procedure; compound **3** (280.1 mg, 0.5 mmol), boronic acid pinacol ester **6b** (898.5 mg, 2.25 mmol) and KO^tBu (252.5 mg, 2.25 mmol) were suspended in 12 mL solvent. (IPr)Pd(allyl)Cl (14.3 mg, 25 μmol; dissolved in 1 mL IPA) was added before refluxing for 2 h. After general workup the crude product was purified by column chromatography (90 g silica gel, hexanes/DCM 25 → 27%) to give **S2** as yellow powder (473.3 mg, 83% of theory). TLC (silica gel, cyclohexane/DCM = 3/1): r_f = 0.30. ¹H NMR (200 MHz, CD₂Cl₂): δ = 7.74 (s, 3H), 7.53–7.44 (m, 6H), 7.40 (d, J = 3.78 Hz, 3H), 7.23 (d, J = 3.80 Hz, 3H), 7.15–7.05 (m, 12H), 7.05–6.94 (m, 18H), 2.32 (s, 18H) ppm. ¹³C NMR (50 MHz, CD₂Cl₂): δ = 148.5 (s), 145.5 (s), 144.9 (s), 141.8 (s), 136.2 (s), 133.7 (s), 130.50 (d), 127.5 (s), 126.8 (d), 125.45 (d), 125.39 (d), 123.4 (d), 122.6 (d), 121.7 (d), 20.1 (s) ppm. MS (MALDI-TOF): calcd for C₇₈H₆₃N₃S₃: 1137.4184; found: 1137.4006.

4,4',4''-(1,3,5-Benzenetriyltri-5,2-thiophenediyl)tris[*N,N*-bis-(4-fluorophenyl)benzenamine] (S3). According to the general procedure; compound **3** (280.6 mg, 0.5 mmol), boronic acid pinacol ester **6c** (916.3 mg, 2.25 mmol) and KO^tBu (252.5 mg, 2.25 mmol) were suspended in 12 mL solvent. (IPr)Pd(allyl)Cl (14.3 mg, 25 μmol; dissolved in 1 mL IPA) was added before refluxing for 2 h. After general workup the crude product was

purified by column chromatography (90 g silica gel, hexanes/DCM 25 → 30%) to give **S3** as yellow powder (323.3 mg, 56% of theory). TLC (silica gel, hexanes/DCM = 5/1): r_f = 0.32. ¹H NMR (200 MHz, CD₂Cl₂): δ = 7.72 (s, 3H), 7.56–7.45 (m, 6H), 7.39 (d, J = 3.76 Hz, 3H), 7.24 (d, J = 3.78 Hz, 3H), 7.14–6.92 (m, 30H) ppm. ¹³C NMR (50 MHz, CD₂Cl₂): δ = 159.7 (s, J_{CF} = 242.5 Hz), 148.2 (s), 144.6 (s), 144.1 (s, J_{CF} = 3.0 Hz), 142.1 (s), 136.1 (s), 128.2 (s), 126.98 (d), 126.97 (d, J_{CF} = 8.1 Hz), 125.4 (d), 123.7 (d), 122.8 (d), 121.8 (d), 116.7 (d, J_{CF} = 22.7 Hz) ppm. MS (MALDI-TOF): calcd for C₇₂H₄₅F₆N₃S₃: 1161.2680; found: 1161.3152.

Results and discussion

Synthesis

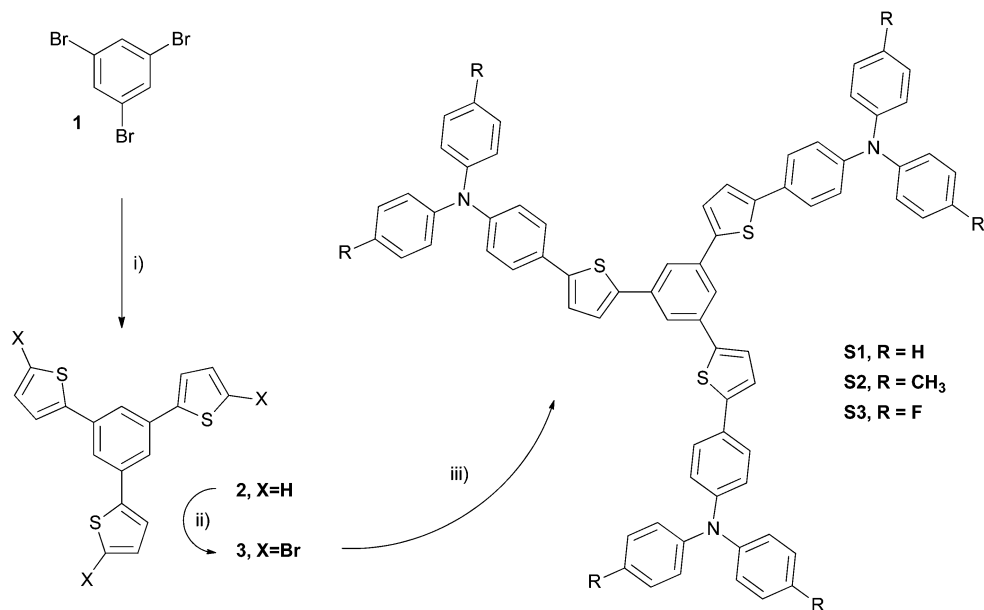
The synthetic linkage of TPA structures **8** bearing either electron withdrawing (–I, –M-effect) or donating (+I, +M) substituents with **3** is realized *via* Suzuki cross-coupling reactions.^{45,46} Therefore, a general cross-coupling procedure was developed tolerating a broad spectrum of functionalized TPA boronic acid esters (Scheme 1).

Stille cross-coupling reactions are commonly applied in literature,⁴⁷ however they require toxic stannyl intermediates. In order to avoid these undesirable precursors, highly stable pinacol boronic acid esters are used in Suzuki cross-coupling reactions ensuring high conversion, selectivity, and tolerance of functional groups representing a more convenient synthetic approach.⁴⁸ Herein we report the synthetic pathway towards diversely substituted triphenylamine structures (R = –H, –Me, –OMe, –TMS, –*t*Bu, –F, –NO₂, –CN, –SO₂Me), functionalization towards boronic acid esters and subsequent cross-coupling with brominated tris(2-thienyl)benzene **3** *via* Suzuki reaction.

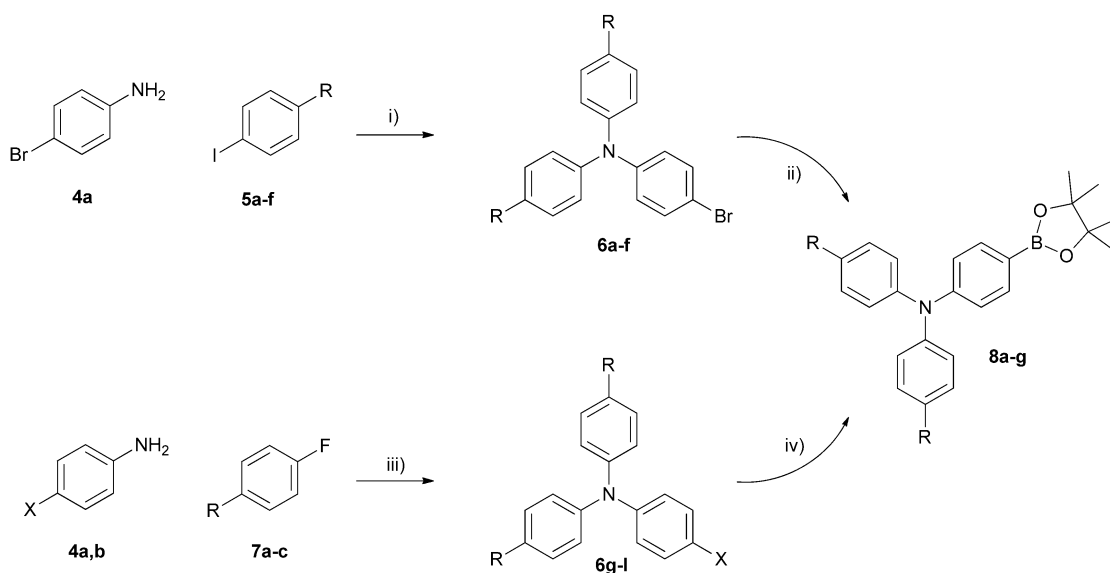
In order to synthesize the desired TPA building blocks two synthetic pathways towards halide species **6a–l** were developed depending on the nature of substituent R (Scheme 2).

The conversion of suitably substituted iodobenzenes **5a–f** and 4-bromoaniline **4a** to the corresponding bromo substituted triphenylamines **6a–f** was realized in good to excellent yields *via* Ullmann condensation applying copper(i)chloride and 1,10-phenanthroline as catalytic system.²⁶ When applying the same strategy on substrates bearing –M substituents relatively low conversions have been observed. Consequently, nucleophilic aromatic substitution of properly substituted fluorobenzenes **7a–c** with anilines **4a,b** was chosen as an alternative synthetic approach leading to bromo (**6g–i**) and iodo (**6j–l**) substituted triphenylamine derivatives in good yields (Table 1).

The synthesis of the boronic acid pinacolates **8a–f** was achieved *via* metal halogen exchange using *n*-butyllithium and further conversion with isopropyl pinacol borate in good yields (Table 1). Again, substrates bearing –M substituent turned out to be troublesome, since neither bromo **6g–i** nor iodo derivatives **6k,l** showed proper conversion. Nevertheless, starting from iodo derivative **6j** the synthesis of boronic acid esters **8g** could be achieved (despite the rather low yields of 18%) when switching to the palladium catalyzed Miyaura borylation using pinacol borane as boron source (Scheme 2).



Scheme 1 Synthetic pathway towards **S1–3**. Reaction conditions: (i) thiophene-2-boronic acid pinacol ester, KO^tBu , $(\text{IPr})\text{Pd}(\text{allyl})\text{Cl}$, isopropanol/water, reflux; (ii) NBS, chloroform/glacial acetic acid, r.t.; (iii) **8a–c**, KO^tBu , $(\text{IPr})\text{Pd}(\text{allyl})\text{Cl}$, isopropanol/water, reflux.



Scheme 2 Synthesis of intermediates **6** and boronic acid esters **8**. Reaction conditions: (i) KOH , CuCl , phenanthroline in toluene, reflux; (ii) $n\text{-BuLi}$, $-78\text{ }^\circ\text{C}$ in THF, then isopropyl pinacol borate; (iii) CsF or KO^tBu in DMSO, ΔT ; (iv) pinacolborane, triethylamine, $\text{PdCl}_2(\text{dppf})$ in dioxane, r.t. For a definition of R and X please refer to Table 1.

Table 1 Experimental data for compounds **6a–l** and boronic acid esters **8a–f**

Ullmann condensation		Nucleophilic aromatic substitution		Synthesis of boronic esters					
R	Yield (%)	X	R	Yield (%)	R	Yield (%)			
6a	H	74	6g	Br	NO_2	54	8a	H	77
6b	Me	89	6h	Br	SO_2Me	77	8b	Me	74
6c	F	70	6i	Br	CN	23	8c	F	91
6d	OMe	86	6j	I	NO_2	58	8d	OMe	76
6e	TMS	60	6k	I	SO_2Me	64	8e	TMS	85
6f	<i>t</i> Bu	61	6l	I	CN	24	8f	<i>t</i> Bu	79

For the consecutive Suzuki cross-coupling reaction, palladium NHC-complex $(\text{IPr})\text{Pd}(\text{allyl})\text{Cl}$ showed superior efficiency over tetrakis(triphenyl)palladium(0) in terms of reactivity and selectivity. Additionally, high conversion and high tolerance of TPA boronic acid esters **8a–f** bearing either electron donating (e.g. $-\text{Me}$) or electron withdrawing substituents (e.g. $-\text{F}$) were observed using isopropanol–water as solvent and K^tOBu as base.

Applying these reaction conditions, compounds **2** and **S1–3** were obtained. The synthesis of **2** was achieved in good yield of 86% *via* cross-coupling of thiophene-2-boronic acid pinacol

Table 2 Photophysical characterization of compounds **S1–3** and computational data for compounds **S_m1–3**

Comp.	λ_{\max} (ϵ_{\max}) ^a (nm)	λ_{\max} ^b (nm)	λ_{em} (ϕ_f) ^c (nm)	λ_{em} ^d (nm)	λ_{em} ^e (nm)	Comp.	λ_{\max} ^f (nm)	λ_{em} ^g (nm)	λ_{em} ^h (nm)
S1	302 (61.2), 387 (112.9)	474	461 (62)	471	486	S_m1	344	450	445
S2	304 (61.7), 394 (104.2)	482	474 (71)	477	498	S_m2	349	454	459
S3	297 (51.0), 384 (104.7)	472	459 (62)	466	482	S_m3	343	449	445

^a Measured in THF solution, $\epsilon_{\max} \times 10^{-3}$ in $\text{M}^{-1} \text{cm}^{-1}$ in parentheses. ^b Absorption of solid samples. ^c Measured in a THF solution; ϕ_f fluorescence quantum yield. ^d Film samples. ^e Solid samples. ^f Calculated absorption of model compounds **S_m1–3**. ^g Calculated emission (LR-PCM) of model compounds **S_m1–3**. ^h Calculated emission (SS-PCM) of model compounds **S_m1–3**.

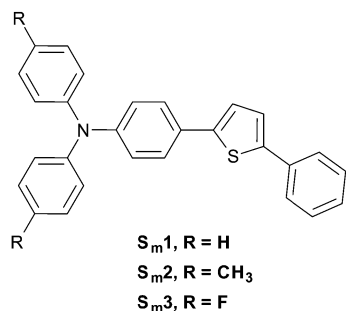
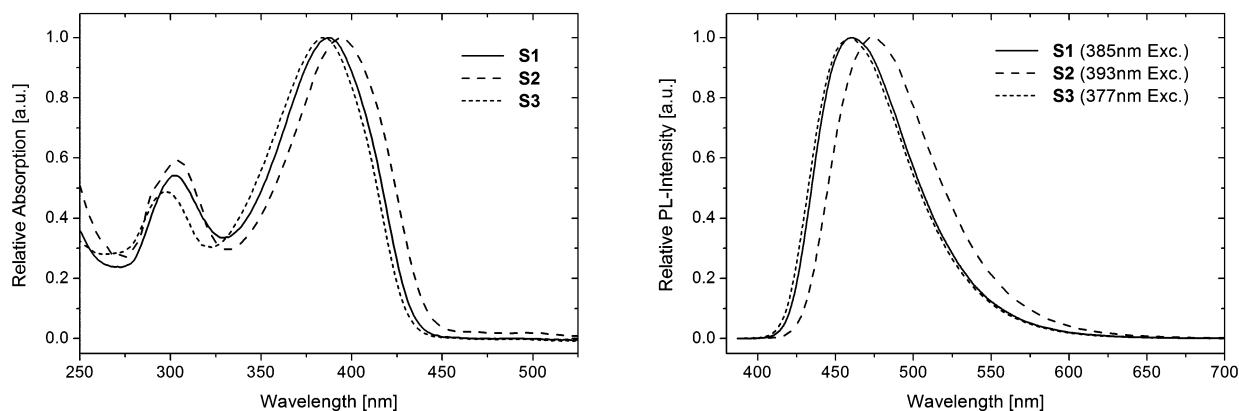
ester and 1,3,5-tribromobenzene **1** according to the above protocol. Consecutive bromination with NBS in chloroform/glacial acetic acid gave the tribromo derivative **3**, the precursor for the final Suzuki coupling with boronic acid esters **8a–c**. Star-shaped compounds **S1–3** bearing either electron donating or withdrawing substituents were obtained in satisfactory to excellent yields (Table 3). These solid materials appear yellow in color and are soluble in common organic solvents. The characterization of **S1–3** was performed by $^1\text{H}/^{13}\text{C}$ -NMR spectroscopy and HR-MS analysis. The data are consistent with the proposed structural formulations.

Photo-physical properties of **S1–3** were determined by UV-VIS and fluorescence spectrometry in THF solution, for amorphous films and in the solid state (Table 2 and Fig. 3). Two absorption maxima were located in relatively narrow ranges of 297–304 and 384–394 nm for substances **S1–3** when measured in THF solution. While the former is assigned to the

$n-\pi^*$ transition of the triphenylamine moiety, the longer wavelength absorption originates from the $\pi-\pi^*$ transitions of the electron-donating triphenylamine moiety to the electron-accepting thiophene moiety.⁴⁹ A clear trend can be observed, as the electron withdrawing fluoro derivative **S3** shows the absorption maximum with the highest energy, whereas the electron donating methyl derivative **S2** has the absorption maximum at the longest wavelength; the absorption maximum of the electron neutral **S1** lies in between.

These findings are supported by quantum chemical calculations of model substances **S_m1–3** (Fig. 2). In order to mimic C_3 symmetric substances **S1–3**, suitable model substances were chosen, comprising one dendritic arm and the benzene core. This approach ensures a realistic representation of **S1–3** while keeping the computational costs at a reasonable level. Absorption and emission wavelengths in THF of **S_m1–3** were estimated by applying density functional (DFT) and time dependent density functional (TDDFT) level of theory according to a protocol presented recently.³⁶ The calculated absorption and emission wavelengths of **S_m1–3** are in agreement with experimental data of **S1–3** showing the lowest shift in emission for fluoro-substituted **S3/S_m3** and highest emission shifts for methyl-substituted compounds **S2/S_m2** (Table 2).

Again this behavior can be correlated to the increased electron density on the aromatic ring (Fig. 3) in the case of **S2** ($\lambda_{\text{em}} = 474 \text{ nm}$) causing a significant bathochromic shift and a decreased electron density in the case of **S3** ($\lambda_{\text{em}} = 459 \text{ nm}$) causing a hypsochromic shift in reference to **S1** ($\lambda_{\text{em}} = 461 \text{ nm}$) (Table 2). Stokes shifts for all compounds **S1–3** are comparable and range from 0.51–0.53 eV. Quantum yields in solution are

Fig. 2 Model substances **S_m1–3**.Fig. 3 Absorption (left) and emission (right) spectra of **S1–3** in THF solution.

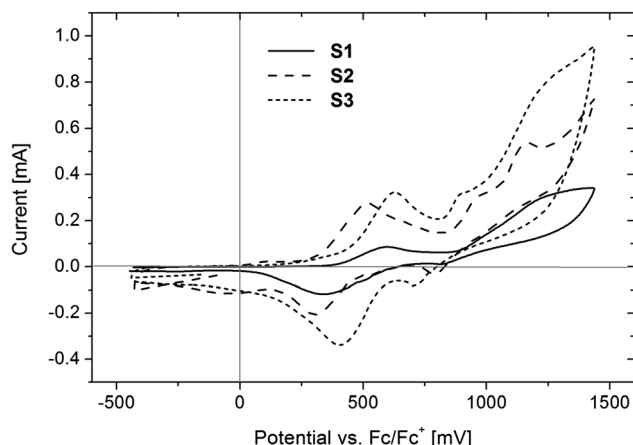


Fig. 4 Cyclic voltammograms of **S1–3** in DCM.

shifted to higher values correlating with enhanced electron density (Table 2). The values of **S1** and **S3** are identical ($\phi_f = 0.62$), whereas

Table 3 Experimental data, physical characterization and computational data of compounds **S1–3**

Comp.	Yield (%)	T_g^a (°C)	T_d^b (°C)	Band gap ^c (nm, eV)	HOMO/LUMO ^d (eV)	HOMO/LUMO ^e (eV)
S1	97	128	541	387, 3.20	−5.19/−1.99	−5.17/−1.76
S2	83	135	528	394, 3.14	−5.24/−2.10	−5.01/−1.66
S3	50	121	538	384, 3.23	−5.21/−1.98	−5.36/−1.91

^a Obtained from DSC measurements. ^b Thermal decomposition temperature determined from 5% mass loss. ^c Bandgaps were determined from the onsets of the absorption in THF solution. ^d HOMO-levels determined from solutions measured in DCM. All E_{ox} data are reported relative to ferrocene (Fc/Fc^+ , $E_{ox} = 446$ mV). The concentration of the compounds used in this experiment was $1 \text{ mg } \mu\text{L}^{-1}$ and the scan rate was 50 mV s^{-1} . LUMO levels were determined from the optical band gap and the HOMO energy level according to the following equation: $E_{LUMO} = E_{HOMO} + E_{bandgap}$. ^e Calculated HOMO/LUMO levels (B3LYP/6-311+G(d)).

the quantum yield is considerably higher ($\phi_f = 0.71$) for the methyl substituted derivative **S2**.

Emission spectra of solid samples **S1–3** are in the narrow range of 482–498 nm, whereas spin coated samples are in the range of 466–477 nm (for spectra please refer to the ESI†).

Electro-chemical characteristics of the star-shaped molecules **S1–3** were investigated by cyclic voltammetric methods (Fig. 4). The first oxidation potentials were used to determine the HOMO energy levels. Ferrocene served as an external standard for calibrating the potential and calculating the HOMO levels (−4.8 eV). All compounds **S1–3** undergo reversible oxidation indicating the formation of stable cation radicals. Only small variations of HOMO levels (−5.19 eV to −5.24 eV) were observed. The LUMO levels were determined from the optical bandgap and the HOMO energy level obtained from CV measurements and vary in the range from −1.98 to −2.10 eV. Calculated HOMO/LUMO levels are in good accordance with the experimental data for compounds **S1** and **S3**, whereas the deviation is somewhat higher for substance **S2**. The pertinent data are listed in Table 3.

Thermal properties were investigated by DSC and TGA measurements. Glass-forming properties and thermal stability of the compounds were examined by simultaneous thermal analysis (STA). The glass transition temperature (T_g) was estimated from DSC curves (Fig. 5). The determined T_g values are in the range from 121 to 135 °C, the methyl substituted **S2** showing the highest value while fluoro substituted **S3** exhibits the lowest T_g . All materials exhibit high thermal stability as evidenced by decomposition temperatures corresponding to 5% mass loss between 528 and 541 °C (Table 3 and Fig. 5). This high thermal stability allows for fabrication of homogeneous and stable amorphous thin films by vacuum deposition.

The semiconducting properties of the materials under investigation were tested by using a top-contact OFET architecture as shown in Fig. 6. A hole mobility up to $7.7 \times 10^{-4} \text{ cm}^2 \text{ V}^{-1} \text{ s}^{-1}$

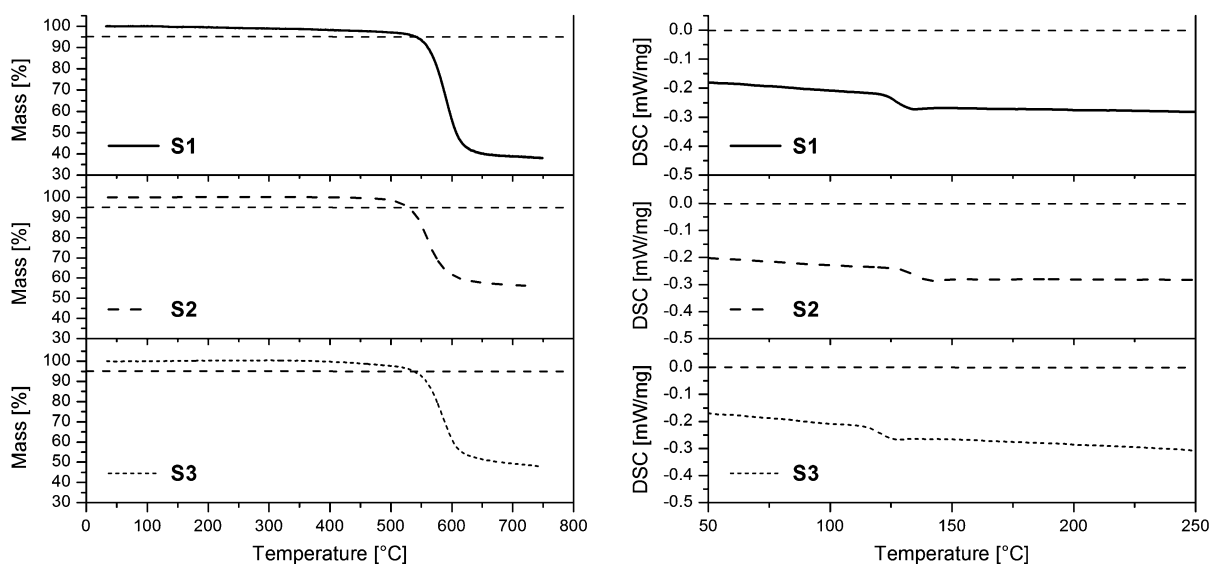


Fig. 5 TGA (left) and DSC (right) measurements of **S1–3**.

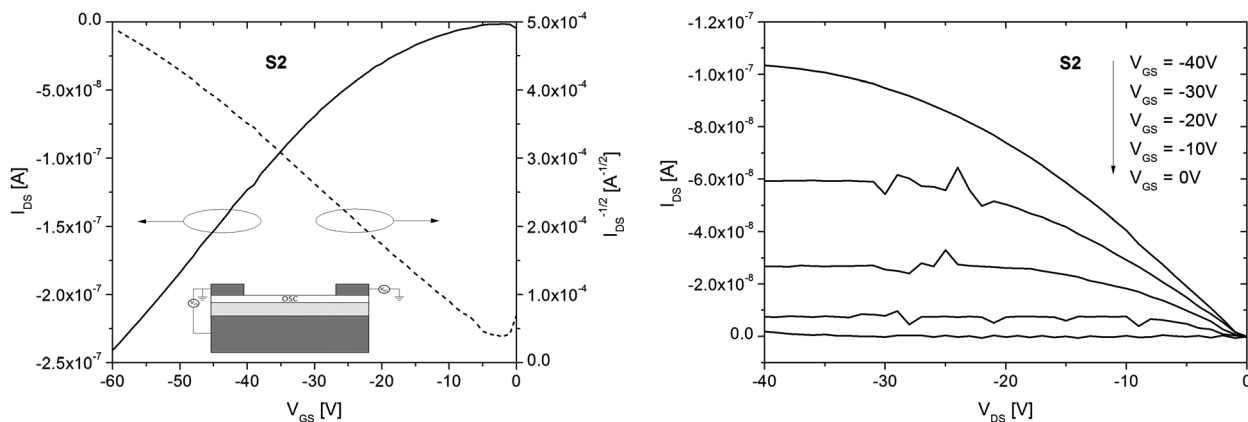


Fig. 6 Output characteristics (left) and corresponding transfer curve (right) of **S2**.

and average threshold voltages of approx. 0 V which can be attributed to a low background charge density in the material were recorded using **S2** as semiconducting layer (Fig. 6), while no working OFET device could be fabricated using **S1** or **S3**. As the performance of an OFET highly depends on the quality of the interface between dielectric and organic semiconductor, these results might be correlated to the tendency of **S2** to form nearly defect free films, which was observed in spin coating experiments.

All compounds **S1–3** readily form stable glasses. Spin coated thin films of **S1–3** were produced on ITO substrates using chloroform as solvent. Their surface morphology and thickness were further investigated by atomic force microscopy (AFM, Fig. 7). In principle, all films showed very little average

thickness (30–50 nm) and low roughness of the surface (root mean square = 0.63, 0.32 and 0.34 nm for **S1**, **S2** and **S3** respectively). However, when examining the surface of **S1** sub- μm sized pinholes were observed. Potential reasons for pinholes are trapped air, solvent gas-bubble formation or contaminations on the substrate or in the organic solution. Since numerous spin coating samples were prepared applying the same procedure yielding reproducible results, the origin of these defects is unlikely to come from the fabrication process. Therefore, the formation of these pinholes is probably substance specific and might be attributed to higher propensity to crystallization of **S1** compared to **S2** and **S3**. Thus, in contrast to **S1**, solution-processed films of **S2** and **S3** can readily be prepared.

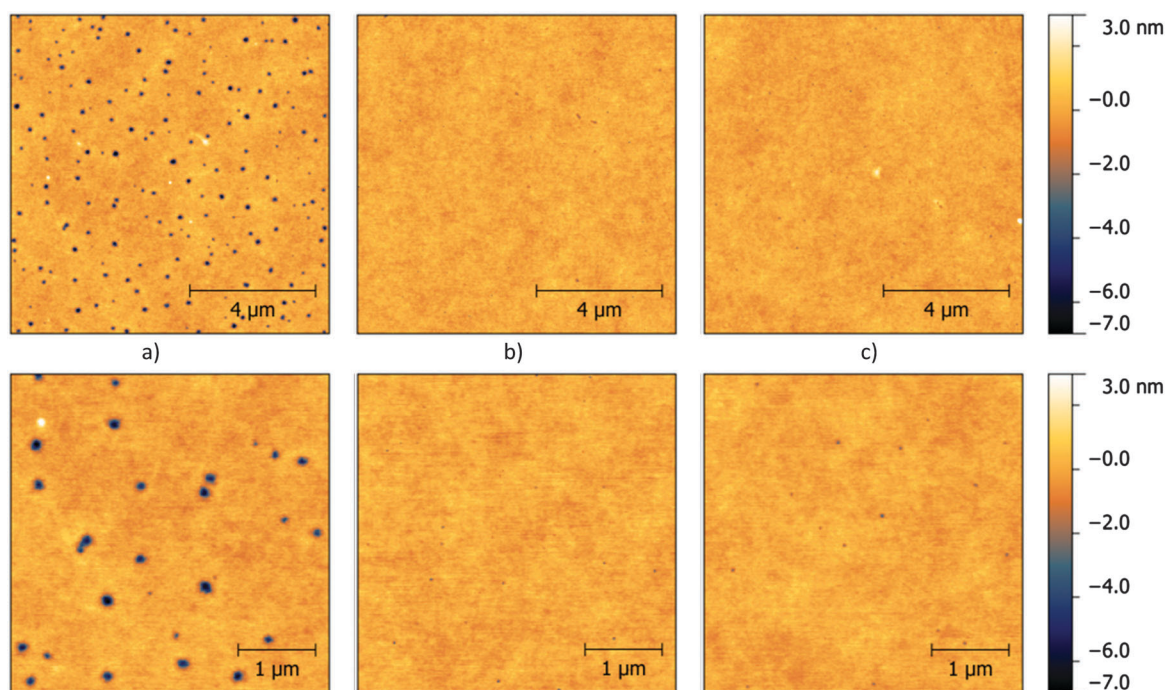


Fig. 7 Topography AFM images of **S1–3** (a–c).

Conclusion

This contribution outlines an optimized synthetic pathway towards a broad spectrum of *p*-substituted triphenylamines, suitable as building blocks for organic semiconducting materials.

We employed these triphenylamine moieties in C_3 symmetric dendritic tris(2-thienyl)benzene structures and elucidated the influence of the molecular design on photo-physical properties. The electronic characteristics of the substituents show a strong influence on the fluorescence spectra thus enabling color tuning. These star shaped materials exhibit good solubility and thermal stability allowing for both solution processing and physical vapor deposition, respectively. The novel materials were tested as semiconductors in organic field effect transistor devices, exhibiting hole mobilities of almost $10^{-3} \text{ cm}^2 \text{ V}^{-1} \text{ s}^{-1}$.

Spin coating experiments showed a strong correlation between the nature of the substituents and the morphology of the resulting thin film; similar results were observed for transistor performance. The structural versatility and capability of our molecular design will contribute to the further development of functional organic materials.

Acknowledgements

J. Binting gratefully acknowledges funding from the Marshall Plan Foundation. The authors thank Dr K. Föttinger for supporting the photophysical characterization, D. Bomze, A. Aster, M. Lunzer and K. Kandra for contributing to the synthetic experiments. M. Eberl is acknowledged for assisting in cyclic voltammetric measurements and K. Fohringer and P. Kautny for STA measurements.

References

- 1 S. R. Forrest, *Nature*, 2004, **428**, 911.
- 2 J. Mei, Y. Diao, A. L. Appleton, L. Fang and Z. Bao, *J. Am. Chem. Soc.*, 2013, **135**, 6724.
- 3 Y.-S. Tyan, *J. Photonics Energy*, 2011, **1**, 011009.
- 4 M. C. Scharber and N. S. Sariciftci, *Prog. Polym. Sci.*, 2013, **38**, 1929.
- 5 B. Kippelen and J.-L. Brédas, *Energy Environ. Sci.*, 2009, **2**, 251.
- 6 H. Klauk, *Organic electronics II: more materials and applications*, Wiley-VCH, Weinheim, 2012.
- 7 Y. Yamashita, *Sci. Technol. Adv. Mater.*, 2009, **10**, 024313.
- 8 Y. Shirota and H. Kageyama, *Chem. Rev.*, 2007, **107**, 953.
- 9 J. Kwon, M. K. Kim, J.-P. Hong, W. Lee, S. Lee and J.-I. Hong, *Bull. Korean Chem. Soc.*, 2013, **34**, 1355.
- 10 F. Geiger, M. Stoldt, H. Schweizer, P. Bäuerle and E. Umbach, *Adv. Mater.*, 1993, **5**, 922.
- 11 S. H. Kim, K. Hong, K. H. Lee and C. D. Frisbie, *ACS Appl. Mater. Interfaces*, 2013, **5**, 6580.
- 12 Y. Shirota, *J. Mater. Chem.*, 2000, **10**, 1.
- 13 N. Metri, X. Sallenave, C. Plesse, L. Beouch, P.-H. Aubert, F. Goubard, C. Chevrot and G. Sini, *J. Phys. Chem. C*, 2012, **116**, 3765.
- 14 J. Zhang, D. Deng, C. He, Y. He, M. Zhang, Z.-G. Zhang, Z. Zhang and Y. Li, *Chem. Mater.*, 2011, **23**, 817.
- 15 Z. Ning and H. Tian, *Chem. Commun.*, 2009, 5483.
- 16 A. Iwan, D. Sek, D. Pocięcha, A. Sikora, M. Palewicz and H. Janeczczek, *J. Mol. Struct.*, 2010, **981**, 120.
- 17 A. Iwan and D. Sek, *Prog. Polym. Sci.*, 2011, **36**, 1277.
- 18 T. Noda, H. Ogawa, N. Noma and Y. Shirota, *Adv. Mater.*, 1997, **9**, 720.
- 19 J. Roncali, P. Leriche and A. Cravino, *Adv. Mater.*, 2007, **19**, 2045.
- 20 C. He, Q. He, Y. Yi, G. Wu, F. Bai, Z. Shuai and Y. Li, *J. Mater. Chem.*, 2008, **18**, 4085.
- 21 A. Cravino, S. Roquet, P. Leriche, O. Alévêque, P. Frère and J. Roncali, *Chem. Commun.*, 2006, 1416.
- 22 T.-T. Bui, L. Beouch, X. Sallenave and F. Goubard, *Tetrahedron Lett.*, 2013, **54**, 4277.
- 23 N. Metri, X. Sallenave, L. Beouch, C. Plesse, F. Goubard and C. Chevrot, *Tetrahedron Lett.*, 2010, **51**, 6673.
- 24 K. R. Justin Thomas, J. T. Lin, Y.-T. Tao and C.-W. Ko, *Chem. Mater.*, 2002, **14**, 1354.
- 25 A. Iwan, H. Janeczczek, B. Kaczmarczyk, B. Jarzabek, M. Sobota and P. Rannou, *Spectrochim. Acta, Part A*, 2010, **75**, 891.
- 26 H. B. Goodbrand and N.-X. Hu, *J. Org. Chem.*, 1999, **64**, 670.
- 27 M. W. Andersen, B. Hildebrandt, G. Köster and R. W. Hoffmann, *Chem. Ber.*, 1989, **122**, 1777.
- 28 O. Navarro and S. P. Nolan, *Synthesis*, 2006, 366.
- 29 J. Frisch, G. W. Trucks, H. B. Schlegel, G. E. Scuseria, M. A. Robb, J. R. Cheeseman, G. Scalmani, V. Barone, B. Mennucci, G. A. Petersson, H. Nakatsuji, M. Caricato, X. Li, H. P. Hratchian, A. F. Izmaylov, J. Bloino, G. Zheng, J. L. Sonnenberg, M. Hada, M. Ehara, K. Toyota, R. Fukuda, J. Hasegawa, M. Ishida, T. Nakajima and Y. Honda, *Gaussian 09, Revision A.02*, Gaussian, Inc., Wallingford, CT, 2009.
- 30 C. Lee, W. Yang and R. G. Parr, *Phys. Rev. B: Condens. Matter Mater. Phys.*, 1988, **37**, 785.
- 31 A. D. Becke, *J. Chem. Phys.*, 1993, **98**, 5648.
- 32 R. Krishnan, J. S. Binkley, R. Seeger and J. A. Pople, *J. Chem. Phys.*, 1980, **72**, 650.
- 33 Y. Zhao and D. G. Truhlar, *Theor. Chem. Acc.*, 2007, **120**, 215.
- 34 Y. Zhao and D. G. Truhlar, *Theor. Chem. Acc.*, 2008, **119**, 525.
- 35 A. Schäfer, H. Horn and R. Ahlrichs, *J. Chem. Phys.*, 1992, **97**, 2571.
- 36 D. Lumpi, E. Horkel, F. Plasser, H. Lischka and J. Fröhlich, *ChemPhysChem*, 2013, **14**, 1016.
- 37 M. Cossi, V. Barone, R. Cammi and J. Tomasi, *Chem. Phys. Lett.*, 1996, **255**, 327.
- 38 M. Cossi and V. Barone, *J. Chem. Phys.*, 2001, **115**, 4708.
- 39 R. Improta, G. Scalmani, M. J. Frisch and V. Barone, *J. Chem. Phys.*, 2007, **127**, 074504.
- 40 M. H. Davey, V. Y. Lee, L.-M. Wu, C. R. Moylan, W. Volksen, A. Knoesen, R. D. Miller and T. J. Marks, *Chem. Mater.*, 2000, **12**, 1679.
- 41 J. H. Gorvin, *J. Chem. Soc., Perkin Trans. 1*, 1988, 1331.

- 42 R. Anemian, D. C. Cupertino, P. R. Mackie and S. G. Yeates, *Tetrahedron Lett.*, 2005, **46**, 6717.
- 43 M. Murata, T. Oyama, S. Watanabe and Y. Masuda, *J. Org. Chem.*, 2000, **65**, 164.
- 44 N. Marion, O. Navarro, J. Mei, E. D. Stevens, N. M. Scott and S. P. Nolan, *J. Am. Chem. Soc.*, 2006, **128**, 4101.
- 45 A. Leliège, J. Grolleau, M. Allain, P. Blanchard, D. Demeter, T. Rousseau and J. Roncali, *Chem. – Eur. J.*, 2013, **19**, 9948.
- 46 J. K. Choi, K. Cho and T.-H. Yoon, *Synth. Met.*, 2010, **160**, 1938.
- 47 R. A. Rossi, *J. Organomet. Chem.*, 2014, **751**, 201.
- 48 R. Martin and S. L. Buchwald, *Acc. Chem. Res.*, 2008, **41**, 1461.
- 49 Z. Ge, T. Hayakawa, S. Ando, M. Ueda, T. Akiike, H. Miyamoto, T. Kajita and M. Kakimoto, *Adv. Funct. Mater.*, 2008, **18**, 584.

3 – Nonlinear Optics –

Introduction

3.1. Introduction

The first discovery of nonlinear optic (NLO) behavior can be dated back to 1875 when J. Kerr discovered a change in the refractive index of CS₂ when subjected to an electric field (a process now known as the Kerr-effect).¹ But it was not until the early 1960s with the invention of the laser, that the scope of NLO properties could be further evaluated and the search for materials with nonlinear optical applications was initialized. Since then a number of optical frequency mixing phenomena, collectively known as the nonlinear optical processes, have been observed in a variety of dielectric media.²

Such NLO phenomena include a broad range of interactions of light (electromagnetic radiation) with materials ranging from sum- and difference-frequency generation, the electro-optic effect, self-focusing and defocusing effects to multi-photon absorption processes. On the one hand these material properties may be used to control the phase, polarization state and frequency of light beams, suitable for a variety of applications in telecommunications and other photonic technologies. On the other hand the application of these processes involves the formation of excited states (and, therefore, their associated physical and chemical properties) with a high degree of three-dimensional confinement allowing excellent spatial control within the focal volume of the laser beams, which may be employed in 3D fluorescence imaging, photodynamic therapy, nonlinear optical transmission and 3D microfabrication.

In emerging photonic technologies for use in areas such as telecommunications, sensors and information technology, light is used as the carrier of information. Optical waveguides including optical fibers are used to modulate and transport this light.³ The majority of modern commercial optoelectronic devices (such as LEDs, solar cells, and nonlinear-optics) are built on the basis of traditional inorganic semiconductors.⁴ Over the last couple of decades, however, a lot of scientific efforts has been made in producing devices based on organic electronic materials, which for many applications may become less expensive alternatives to their inorganic counterparts⁵ and feature the advantage of broad versatility due to the possibility of tuning optical properties by changing their chemical structure.⁶ Various organic compounds based on small molecules, conjugated polymers, or carbon nanotubes have been shown to be suitable for nonlinear applications. However, drawbacks of organic materials are on the one hand low efficiency of frequency mixing processes and on the other hand reduced photochemical stability in comparison to inorganic counterparts. Therefore, there is still a need for further research to overcome these shortcomings.

3.2. Concept of Nonlinear Optical Phenomena

Nonlinear optical properties are associated with the ability of a material to undergo nonlinear polarization under the influence of electric fields (either static fields or the oscillating fields associated with electromagnetic radiation). Application of an electric field to a system of charges will result in charge separation (i.e. a dipole moment is induced) within the more polarizable π -system of a conjugated organic molecule.³ Nonlinear optics give rise to a multitude of higher order optical phenomena. Among 2nd order optical nonlinear effects are second harmonic generation (SHG), sum-frequency generation (SFG), difference-frequency generation (DFG), optical parametric amplification (OPA) and optical parametric oscillation (OPO). Optical Kerr effect, third harmonic generation (THG), two photon absorption or stimulated Raman scattering (SRS) constitute 3rd order optical nonlinear effects. In the following the discussion will be limited to frequency mixing processes of second harmonic generation and two-photon absorption, since the materials synthesized in this work may be suitable for generating these physical phenomena.

The size of the induced dipole moment (P) depends both on the magnitude of the applied electric field (E) and on the ease, with which the molecule can be distorted. Mathematically, the optical response of the medium can be described on a molecular scale by expressing the induced polarization $P(t)$ as a power series of the optical field strength $E(t)$ of the incident light:

$$P(t) = \chi^{(1)} E(t) + \chi^{(2)} E^2(t) + \chi^{(3)} E^3(t) + \dots$$

where the constant $\chi^{(n)}$ is the n^{th} -order susceptibility of the material, $\chi^{(1)}$, $\chi^{(2)}$, and $\chi^{(3)}$ corresponding to optical effects such as absorption or reflection, second harmonic and third harmonic generation, respectively.⁷ Thus, a second-order phenomenon results in frequency doubling, while a third-order process leads to frequency tripling. Second harmonic generation is a second-order nonlinear optical process in which two photons of the frequency ω interact with a non-centrosymmetrical medium (i.e., material lacking a generalized mirror symmetry) and combine to form a new photon with half the wavelength, i.e., twice the frequency (2ω) and therefore twice the energy of the initial photons (*Figure 1, A*). Such phenomena are ‘nonlinear’ since the observed effect depends quadratically on the strength of the optical field.

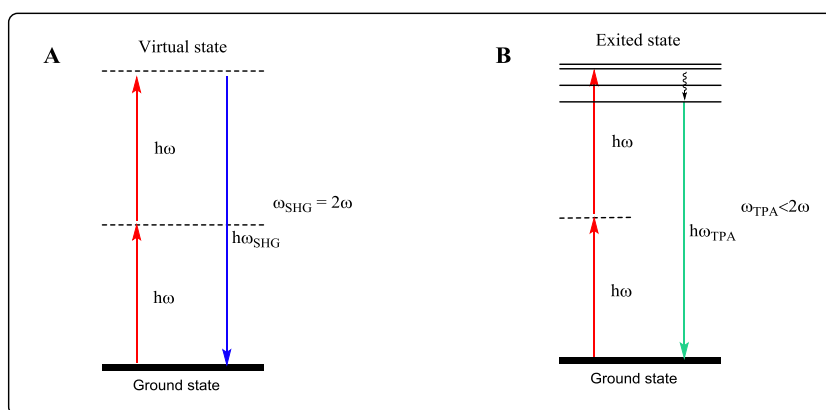


Figure 1: Jablonski energy-level diagram (A) and absorption/fluorescence diagram (B) describing SHG and two-photon excited fluorescence, respectively.

In contrast two-photon absorption involves the uptake of two photons with frequency ω (*Figure 1, B*), resulting in various relaxation processes, e.g. in emitting light at approximately the frequency 2ω (twice the original frequency, with half the wavelength). While SHG involves only virtual energy transition, two-photon excited absorption involves real energy states based on transitions of electrons. Consequently, when using ultrafast femtosecond pulsed lasers, the response time of SHG is at the femtosecond level, about several orders of magnitude faster than the nanosecond response time of fluorescence as an excitation source, allowing very fast and sensitive detection.⁷

3.3. Second Harmonic Generation

The design and preparation of new materials exhibiting SHG is attractive due to fast responses and high-speed applications, large nonresonant nonlinearities, and potentially low costs. Consequently, in recent years these nonlinear optical phenomena have been subject of scientific research owing to their potential employment in ultrafast signal processing, optical computing, optical telecommunications, optical limiting, optical data storage devices, and harmonic generation.

Potentially, any material lacking a center of symmetry may generate a second harmonic, however, some requirements have to be fulfilled, e.g. high nonlinear susceptibility, delocalized electrons as well as adequate thermal and mechanical stability.⁸ The first applications exploiting the nonlinear optical properties of materials relied almost exclusively on ferroelectric inorganic crystals such as potassium dihydrogen phosphate (KH₂PO₄, KDP), lithium niobate (LiNbO₃), potassium niobate (KNbO₃), or β -barium borate (BaB₂O₄, BBO), despite shortcomings such as difficulties in materials processing.⁶ The search for novel materials led to organic single crystals possessing unique optoelectronic properties which are based on their delocalized electrons in conjugated electron systems, causing various photo-responses such as photoconductive, photovoltaic and photocatalytic behavior.⁹ Moreover, there is a sheer unlimited versatility of design possibilities for tailoring the NLO properties of organic molecules, suitable oligomers and polymers. Organic crystals exhibit large nonlinear susceptibilities in comparison to inorganic NLO crystals, although reduced thermal and photochemical stability is a drawback of organic materials.¹⁰

The enhancement of the nonlinear process efficiency by the appropriate choice of NLO materials exhibiting high first hyperpolarizability (β) based on push-pull molecules represents a central scientific interest. In approximation β can be described as follows:

$$\beta \propto \frac{\mu_{ge}^2 (\Delta\mu_{ge})}{\omega_{ge}^2}$$

where μ_{ge} is the transition dipole moment linking ground (g) and excited state (e), $\Delta\mu_{ge}$ is the change in static dipole moment between ground and excited state and ω_{ge} is the frequency corresponding to the excited-state energy. Consequently, for second-order NLO properties structures are required that will provide (i) large change in dipole moment on excitation, (ii) large transition dipole moment, and (iii) small energy difference between the excited and ground states.¹¹ Based on this model, the design of chromophores with ideal nonlinear response was primarily based on molecules with donor and acceptor moieties separated by a π -conjugated bridge (*Figure 2, A*). As a first approximation, the SHG behavior of organic materials in the bulk may be estimated by the determination of the nonlinear response at the molecular level characterized by the hyperpolarizability β .

Effective strategies to increase the hyperpolarizability of donor–acceptor-based materials have been demonstrated by elongating of the conjugated spacer (e.g., proceeding from $n = 1$ to 3 in *Figure 2, B*).¹² Also, the incorporation of heterocycles like thiophene, furan or thiazole into the conjugation pathway in the center of the bridge leads to greater nonlinearities exhibiting a larger β , which can be attributed to the reduced aromaticity of the heterocycle compared to phenylene species (*Figure 2, C*).^{13,14} Recently, a second-order nonlinear optical material combining a *Z*-(alkylthio)alkenyl donor and a triazole acceptor bearing high stability and optical quality exhibiting an SHG efficiency of twice the value of KDP was reported (*Figure 2, D*).¹⁵ Another possible method enhancing the nonlinearities is the incorporation of heavier heteroatoms in the heterocyclic ring. Kamada et al. report increases in optical nonlinearities in neat heterocycles with increasing atomic number of the heteroatom (O \rightarrow S \rightarrow

Se), which was ascribed to the effect of the localized electrons of the heteroatom.¹⁶

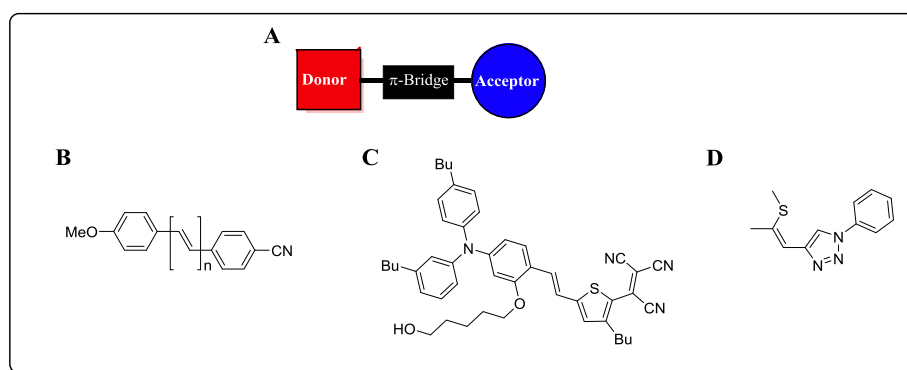


Figure 2: (A) Chromophore design. (B-D) Compounds exhibiting SHG.

Despite these design strategies, there is only limited insight into molecular structure–property relations, since the SHG signal strongly depends on the acentric nature of the crystal packing, e.g. non-centrosymmetric molecules without any permanent dipole (molecules with D_2 , D_{3h} , C_{3h} , T_d symmetry).¹⁷ However, many compounds with large β values also possess rather high dipole moments, consequently, these molecules tend to align antiparallel with one another leading to zero $\chi^{(2)}$ due to dipole-dipole interactions.¹⁸ So the most effective and facile way to improve the macroscopic nonlinearity values of these materials is the optimization of the push–pull chromophores.

3.4. Two-Photon Absorption

Interestingly for many years two-photon absorption (2PA) has been regarded as an adverse effect by the nonlinear optics community. This is especially true in the case of optical switching, where 2PA can lead to attenuation of signals and sample damage through severe heating. Consequently, there was no pursuit for high 2PA materials, indeed, efforts were made to prevent or minimize its presence. However, the applicability of 2PA in other scientific fields led to increasing interest in optimized 2PA properties.

3.4.1. Physics of Two-Photon Absorption

In general, molecules can be excited to an elevated state (e) from the ground state (g) with an energy equal to the difference between e and g by absorption of one photon (1PA) (*Figure 3, A, left*). Another possible process to generate excited states is based on two-photon absorption (2PA), which refers to the “simultaneous” absorption of two photons. This physical process occurs within the lifetime of a metastable intermediate excited state (virtual state, formed by the first photon) by absorption of the second photon (*Figure 3, A, right*). 2PA can be observed in molecules without an inversion center, is inherently weak at normal light intensities and requires the use of high intensities of light provided by focused pulsed laser beams. While the absorption of two photons of different energy is called non-degenerate 2PA (*Figure 3, B*), absorbing two photons of the same energy is referred to as degenerate 2PA (*Figure 3, C*). The energy of the excited state formed is equal to the sum of the energies of the two photons absorbed and in case of the latter corresponds to twice the wavelength normally required to reach an excited state.

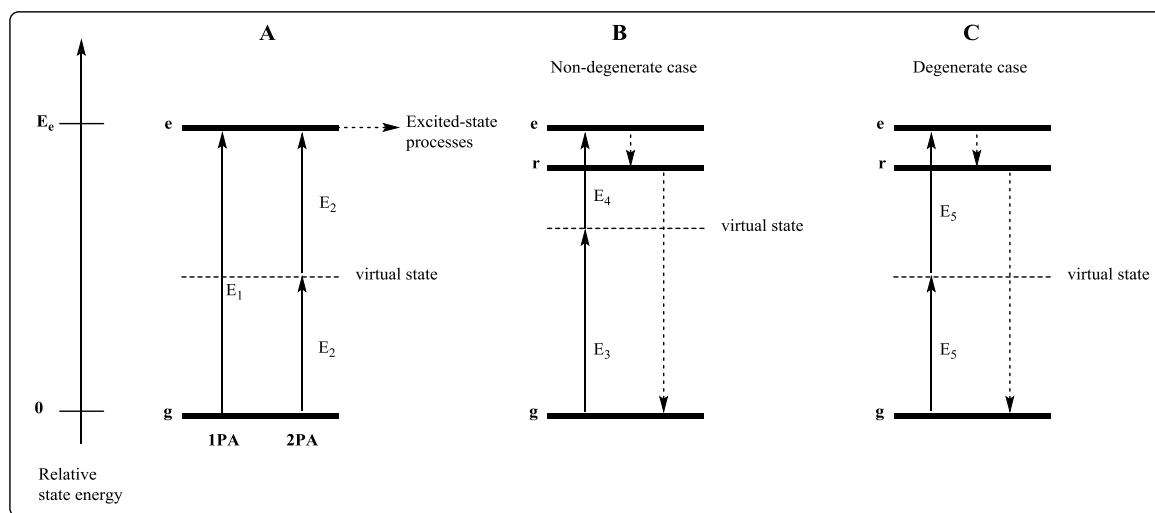


Figure 3: Schematic energy level diagrams illustrating the process of (A) one-photon absorption (1PA) and two-photon absorption (2PA), (B) excitation of a molecule from the ground state g to the excited state e for photons with differing energies (non-degenerated case) and (C) the same energies (degenerated case). After excitation to state e the system relaxates quickly to state r , the lowest vibronic level of the lowest-energy excited state, by internal conversion (IC) or vibrational relaxation, from which further physical or chemical processes continue (e.g. relaxation to ground state g via fluorescence). The length of each arrow is proportional to the photon energy. The dotted arrows represent possible relaxation pathways.

Because of the conservation of momentum, 1PA is only possible between states of different parity. The existence of an electronic state of the appropriate energy, e.g. $E_1 + E_2$, is in principle not sufficient to lead to the absorption of two photons, since symmetry selection rules also have to be fulfilled to allow 2PA processes. The selection rules for 2PA differ from those for 1PA: for systems having an inversion center transitions are two-photon allowed only if they connect states with the same symmetry with respect to the inversion operation. The lowest electronic state accessible through 2PA usually lies at higher energy than the 1PA-allowed state. Thus optical transitions that are not visible by 1PA may be intense in the 2PA spectrum. In contrast these selection rules are not applicable for non-centrosymmetric molecules, where the same state can be reached by 1PA and 2PA transitions.

3.4.2. Advantages of Two-Photon Absorption

In recent years materials exhibiting high two-photon absorption have attracted growing interest due to their potential applications in materials and biomedical science,^{19,20} including three-dimensional optical data storage,^{21,22} lithographic microfabrication,^{23,24} optical power limiting,²⁵ two-photon fluorescence imaging,^{26,27} and photodynamic therapy.^{28,29} 2PA induced photopolymerization (2PIP) allows for stereolithography and rapid prototyping of structures with resolutions in the sub-micrometer range. Numerous potential applications of 2PIP have been reported, including 3D microfabrication of electronic and optical microdevices,³⁰ photonic crystals,³¹ microfluidics channels,³² optical data storage,³³ as well as polymer-based optical waveguides on integrated circuit boards³⁴ and biological applications such as the fabrication of scaffolds for cell culturing and tissue engineering.^{35,36}

Although 2PA is several orders of magnitude weaker than linear absorption, these applications take advantage of the following key features of 2PA: on the one hand excited states can be created with photons of half the nominal excitation energy allowing the application of excitation sources near the IR regime. The use of longer wavelengths provides much better penetration depth in absorbing or scattering media compared to 1PA, since biological media, for example, are considerably less absorbing in the near-infrared than in the visible/ultraviolet range. On the other hand another major advantage over 1PA is the possibility of exciting molecules with precise three-dimensional spatial confinement. Since the 2PA excitation rate depends on the square of the light intensity, the excitation

of chromophores can be achieved with a high degree of spatial selectivity in three dimensions by using a tightly focused laser beam. The intensity of a laser beam decreases approximately with the square of the distance from the focal plane along the propagation direction, thus 2PA diminishes with the fourth power of distance from the focus, consequently 2PA above and below the focal plane is negligible.

These advantages led to various concepts to exploit 2PA. Especially, this nonlinear process is important for application in biological media, since less photodamage is caused in the surrounding living tissues and less photobleaching of the fluorophore occurs.³⁷ In the following 2PA induced photopolymerization will be considered in detail.

3.4.3. 2PA Induced Photopolymerization

The two-photon absorption process itself is rather inefficient and only occurs to a significant extent in the presence of intense laser pulses. Therefore, in many applications 2PA is followed by a second step, giving rise to further physical transitions. For example, in the case if 2PA is followed by internal conversion to an emissive singlet excited state, radiative decay from the excited state back to the ground state can be observed (i.e., light emission), which can be exploited for biomedical imaging. The excitation of a 2PA initiator corresponds to a transition from the ground state to an excited singlet state by absorbing combined two-photon energy followed by intersystem crossing (ISC) to a triplet state T_1 , which is described in a Jablonski diagram (*Figure 4, A*). T_1 either deactivates to S_0 by phosphorescence emission or by ISC. These photophysical processes are in competition with photochemical processes, which encompass isomerization, coupling, or cleavage reactions.³⁸ One of these triplet deactivation pathways proceeds by photogeneration of free radicals, which may be generated by at least two different methods.³⁹ On the one hand the direct photocleavage of the initiator yields initiating radicals. On the other hand molecules with excitation energies below the fragmentation energies may generate radicals by reaction with another constituent of the polymerization mixture, namely by abstraction of hydrogen from a co-initiator (e.g., amines).³⁸

2PA induced photopolymerization is applied for fabrication of microstructures by using a focused laser beam in a resin composed of a cross-linkable monomer resin and a 2PA chromophore. Cross-linking of acrylates to form insoluble solid structures occurs along and close to the path traced by the beam. Unreacted monomer may be removed with solvent, leaving the insoluble cross-linked structure. An example of a cross-linked acrylate structure obtained in this way is shown in *Figure 4, B*.

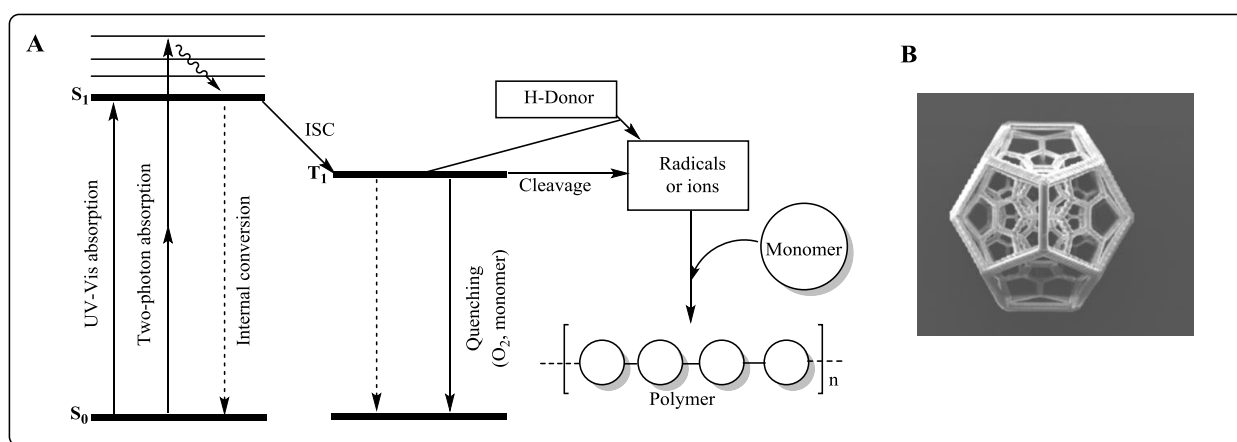


Figure 4: (A) Various activation and deactivation pathways of photoinitiators according to Nguyen et al.³⁹ and (B) SEM image of a complex object obtained by 2PIP.

Although there are some uncertainties about the initiation mechanism, in the simplest case of radical polymerization for molecules with the general structural motif D- π -D being sufficiently electron-rich, the initiation step is currently accepted as the following: a non-radiative transfer process from a higher energetic state excited by two-photons to S_1 induces intra- and intermolecular charge transfer interactions between the two-photon excited initiator and monomer forming radicals to initiate polymerization.^{40,41} The kinetic equilibrium of the electron transfer through the formation of an intramolecular exciplex is shown in *Figure 5*. The rate constants of the electron transfers are given as $k_{\text{inter-et}}$ and $k'_{\text{inter-bet}}$.

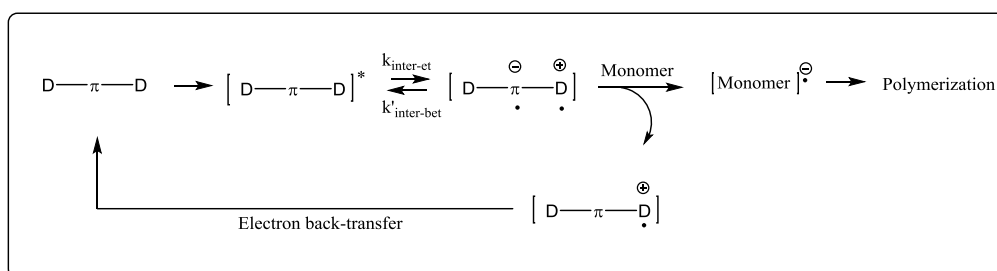


Figure 5: Photoinitiating mechanism of two-photon absorption active initiators.

Compounds with both large 2PA cross-section and high initiating efficiency are required to achieve highly sensitive 2PIP initiators. So far, the structure–property relations governing 2PA have been studied and many strategies were proposed to provide guidance in the development of materials with large 2PA cross-section.⁴² However, no specific rationale for the design of efficient 2PA initiators has yet been found. Moreover, there are other factors that influence the polymerization rate constitute the intensity of the light source, the concentration of the PI, the presence of oxygen and additives, the quantum yield for the generation of radicals, as well as the initiation efficiency of the formed radicals.

3.4.4. Chromophore Design

The strength of 2PA is described in terms of 2PA cross-sections, σ_{2PA} , which are often given in GM units (1 GM = 10^{-50} s cm⁴ photon⁻¹ molecule⁻¹). Typical chromophores have cross-section values σ_{2PA} ranging from ~ 1 to 100 GM and require photon flux varying from 10^{10} to 10^{12} W/cm for excitation comparable in efficiency to 1PA excitation typical to linear spectroscopy. Such high intensities can be readily attained with the help of femtosecond lasers.

The structure–property relations strongly influencing 2PA behavior have been studied extensively both experimentally and theoretically. Many molecular design strategies were proposed to provide guidelines for the development of materials exhibiting large 2PA cross-sections. The application of electron-donating and -accepting groups in 2PA initiators can cause a redistribution of the π -electronic density leading to an increase of electron delocalization in the first excited state, which results in a substantial enlargement in the transition dipole moment, which is a major factor in increasing σ_{2PA} .⁴³ In the last decades the synthetic work was focused on organic molecules with large change of dipole moment $\Delta\mu$ based on electron-rich donor (D) and electron-deficient acceptor (A) motifs connected by a π -system with growing complexity: the variety of dyes can be classified in dipolar (D- π -A), quadrupolar (D- π -A- π -D, A- π -D- π -A,...), and octupolar (A₃-D, D₃-A,...) types (*Figure 6*).⁴⁴

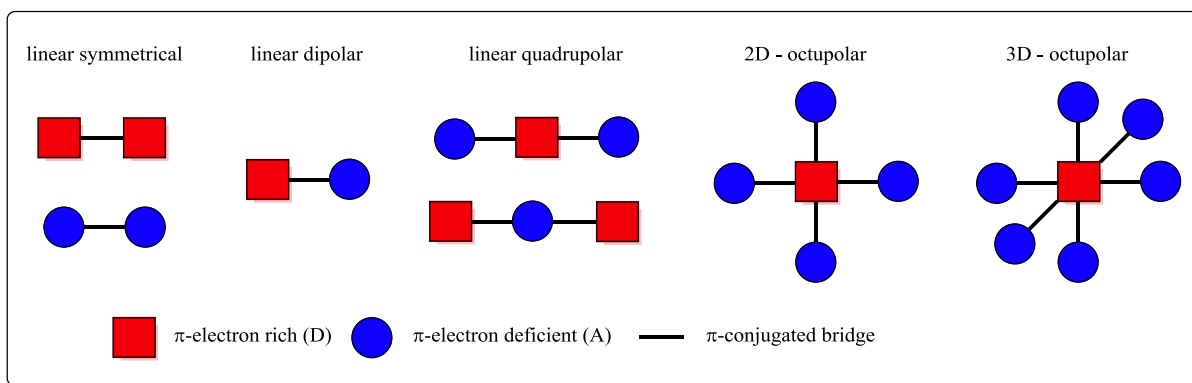


Figure 6: Structural motifs for molecular systems applicable for 2PA design.

These chromophores function on the basis of symmetric charge transfer, from the ends of a conjugated system to the middle or vice versa. From the viewpoint of electronic structures and photophysical processes, there is a strong correlation between intramolecular charge-transfer processes and two-photon absorptivity. Thus, it follows that the permanent ground-state dipole moment as well as the transition dipole connected to either the ground state or the excited state are theoretically considered to be key factors in 2PA processes. From the standpoint of designing an ideal molecular structure for a highly active 2PA chromophore, a number of key features have been identified. Theoretical investigations predict and experimental findings confirm that 2PA cross-sections can be enhanced by increasing the conjugation length, as it leads to states with extended charge separation.³⁰ Strongly linked with the enhancement of 2PA cross-section is the strategy to introduce coplanarity, which will increase the dimension of π -electron delocalization and therefore intramolecular charge transfer.⁴⁵ Increasing the number of conjugation paths or connecting several linear paths to form a two- or three-dimensional configuration has led to a remarkable increase in the 2PA cross-section.⁴⁶

3.4.5. High Efficiency Two-Photon Materials

The first 2PA photopolymerization processes have been conducted with commercial radical chromophores, which were originally designed for 1PA photopolymerization in the UV-Vis range and had rather low efficiency for absorbing two photons, i.e. low 2PA cross-sections.⁴⁷ Accordingly, 2PA did not really have a technological impact (except for its use in detailed spectroscopic studies) until the late 1980s and early 1990s,⁴⁸ when it became easier to investigate as sub-picosecond pulsed lasers were more readily available in the 1990s (particularly the Ti:sapphire laser). In response to the low σ_{2PA} of commercially available photoinitiators, efforts have been made to prepare novel photoactive materials possessing higher 2PA cross-sections, with the expectation that larger σ_{2PA} values allow for lower laser powers and shorter irradiation time, resulting in minimal optical damage to materials.

Though larger donor-acceptor strength is important for higher 2PA cross-section, the nature and length of the π -linker do play a decisive role in increasing the 2PA cross-section and nonlinear optical properties. It has been shown in dipolar chromophores that richer π -electron systems improve the intramolecular charge-transfer character and thereby enhance the NLO properties.⁴⁹ Among electron-rich π -linkers, alkene π -bridging is considered to be highly efficient (*Figure 7, A*). *trans*-Stilbene-based compounds exhibit high 2PA cross-sections and proved to be efficient for two-photon induced polymerization. Modification of the central bridge, by increasing its donating or accepting ability, is a widely explored approach for tuning 2PA properties. The attachment of electron-withdrawing nitrile groups to the central core proved to be useful increasing the σ_{2PA} value by a factor of three in going from unsubstituted to nitrile-substituted *trans*-stilbene derivative (*Figure 7, A*).^{43,50}

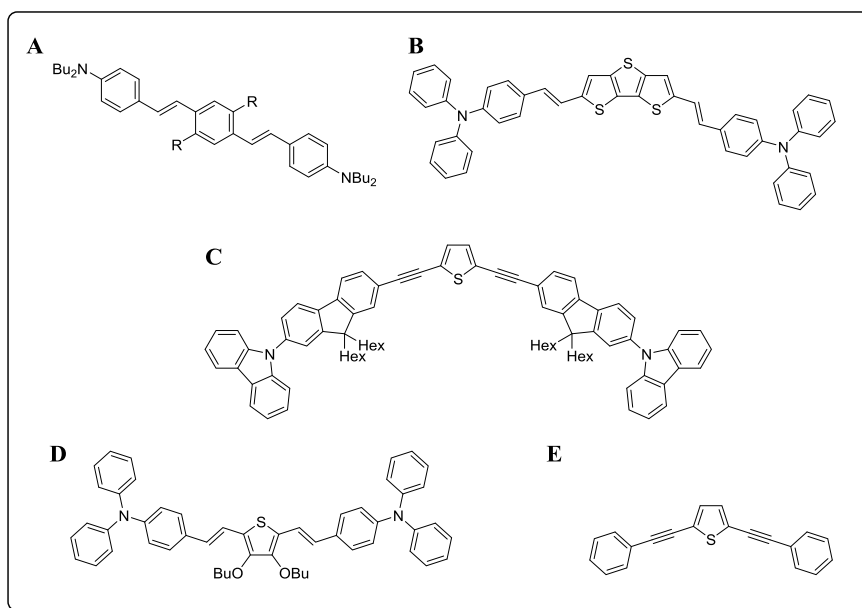


Figure 7: Efficient 2PA initiators.

Several π -bridge linkers, like *trans*-stilbene,³⁰ fluorene,⁵¹ and butadiyne⁵² (Figure 7, A and C), have been reported as efficient chromophores.⁵³ The incorporation of electron-rich sulfur-based heterocycles, like thiophene or dithienothiophene (Figure 7, B, D and E),^{55,56} is known to enhance 2PA cross-sections compared to benzenoid counterparts because of enhanced $\chi^{(3)}$ effects,⁵⁴ which are associated with the polarizability of sulfur.⁵⁵ The incorporation of selenium in 2PA materials was suggested to manifold fast intersystem crossing from excited singlet to triplet state due to the heavy-atom effect with subsequent triplet state absorption.⁵⁷

Also strong donors like triphenylamines⁴⁴ and carbazole⁵⁸ derivatives (Figure 7, B, D and C) have been efficiently applied in 2PA initiators. In the case of the latter the superior initiator properties can be attributed to its rigid plane and conjugation length. Push-pull triphenylamine-based structures with phenyl bridges, strong electron-donating (triarylamine) and electron-accepting (trifluoromethyl) groups showed large changes in the transition and permanent dipole moments varying with electron-withdrawing strength.⁵⁹ Although a variety of 2PA initiators has been synthesized, the insight into conclusive structure-property relationship is not comprehensive.

3.5. Conclusion

Both materials exhibiting SHG properties as well as substances capable of two-photon absorption constitute attractive compounds with potential commercial application. While the former may be designed as optical switches processing signals of specific wavelength, the latter are useful for fluorescent microscopy or the generation of 3D microstructures. However, there are some limitations since organic compounds have low thermal and photochemical stability, which constitutes a disadvantage of these materials for the application as optical switches. Therefore, increasing stability and enhancement of the efficiency of the nonlinear process by the appropriate choice of NLO material represents a central scientific concern. Materials applicable in two-photon absorption processes like 2PA induced polymerization are on the verge of commercialization. Nevertheless conclusive structure-property relationship elucidations, which may give further insight into the mechanism involved in two-photon absorption induced polymerization, are missing. Identifying simple structure-property relationships is crucial, although the factors influencing two-photon absorption are strongly interdependent.

REFERENCES

- (1) Bredas, J. L.; Adant, C.; Tackx, P.; Persoons, A.; Pierce, B. M. *Chem. Rev.* **1994**, *94* (1), 243.
- (2) Karna, S. P.; Yeates, A. T. In *Nonlinear Optical Materials*; Karna, S. P., Yeates, A. T., Eds.; American Chemical Society: Washington, DC, 1996; Vol. 628, pp 1–22.
- (3) Barlow, S.; Marder, S. R. in *Functional organic materials: syntheses, strategies and applications*; Müller, T. J. J., Bunz, U. H. F., Eds.; Wiley-VCH: Weinheim, **2007**.
- (4) Agranovich, V. M.; La Rocca, G. C. *J. Lumin.* **2015**, in press, DOI: 10.1016/j.jlumin.2014.12.054i.
- (5) Agranovich, V. M.; Gartstein, Y. N.; Litinskaya, M. *Chem. Rev.* **2011**, *111* (9), 5179.
- (6) Tykwinski, R. R.; Gubler, U.; Martin, R. E.; Diederich, F.; Bosshard, C.; Günter, P. *J. Phys. Chem. B* **1998**, *102* (23), 4451.
- (7) Pantazis, P.; Maloney, J.; Wu, D.; Fraser, S. E. *Proc. Natl. Acad. Sci.* **2010**, *107* (33), 14535.
- (8) Nagapandiselvi, P.; Baby, C.; Gopalakrishnan, R. *Opt. Mater.* **2015**, *47*, 398.
- (9) Meenatchi, V.; Meenakshisundaram, S. *RSC Adv* **2015**, *5* (79), 64180.
- (10) Jazbinsek, M.; Mutter, L.; Gunter, P. *IEEE J. Sel. Top. Quantum Electron.* **2008**, *14* (5), 1298.
- (11) Nielsen, M. B. *Organic synthesis and molecular engineering*; Wiley: Hoboken, New Jersey, **2014**.
- (12) Cheng, L. T.; Tam, W.; Marder, S. R.; Stiegman, A. E.; Rikken, G.; Spangler, C. W. *J. Phys. Chem.* **1991**, *95* (26), 10643.
- (13) Shu, C.; Wang, Y. *J. Mater. Chem.* **1998**, *8* (4), 833.
- (14) Varanasi, P. R.; Jen, A. K.-Y.; Chandrasekhar, J.; Namboothiri, I. N. N.; Rathna, A. *J. Am. Chem. Soc.* **1996**, *118* (49), 12443.
- (15) Lumpi, D.; Stöger, B.; Hametner, C.; Kubel, F.; Reider, G.; Hagemann, H.; Karpfen, A.; Fröhlich, J. *Cryst. Eng. Comm.* **2011**, *13* (24), 7194.
- (16) Van Keuren, E.; Wakebe, T.; Andreaus, R.; Möhwald, H.; Schrof, W.; Belov, V.; Matsuda, H.; Rangel-Rojo, R. *Appl. Phys. Lett.* **1999**, *75* (21), 3312.
- (17) Ray, P. C. *Chem. Rev.* **2010**, *110* (9), 5332.
- (18) Wang, C.; Zhang, T.; Lin, W. *Chem. Rev.* **2012**, *112* (2), 1084.
- (19) Kufelt, O.; El-Tamer, A.; Sehring, C.; Schlie-Wolter, S.; Chichkov, B. N. *Biomacromolecules* **2014**, *15* (2), 650.
- (20) Zeng, H.; Martella, D.; Wasylczyk, P.; Cerretti, G.; Lavocat, J.-C. G.; Ho, C.-H.; Parmeggiani, C.; Wiersma, D. S. *Adv. Mater.* **2014**, *26* (15), 2319.
- (21) Lott, J.; Ryan, C.; Valle, B.; Johnson, J. R.; Schiraldi, D. A.; Shan, J.; Singer, K. D.; Weder, C. *Adv. Mater.* **2011**, *23* (21), 2425.
- (22) Li, L.; Wang, P.; Hu, Y.; Lin, G.; Wu, Y.; Huang, W.; Zhao, Q. *Spectrochim. Acta. A. Mol. Biomol. Spectrosc.* **2015**, *139*, 243.
- (23) Ushiba, S.; Shoji, S.; Kuray, P.; Masui, K.; Kono, J.; Kawata, *Proc. SPIE* 8613, **2013**, 86130Y.
- (24) Malval, J.-P.; Achelle, S.; Bodiou, L.; Spangenberg, A.; Gomez, L. C.; Soppera, O.; Guen, F. R. *J. Mater. Chem. C* **2014**, *2* (37), 7869.
- (25) Qian, Y.; Meng, K.; Lu, C.-G.; Lin, B.; Huang, W.; Cui, Y.-P. *Dyes Pigm.* **2009**, *80* (1), 174.
- (26) Polavarapu, L.; Manna, M.; Xu, Q.-H. *Nanoscale* **2011**, *3* (2), 429.
- (27) Drobizhev, M.; Makarov, N. S.; Tillo, S. E.; Hughes, T. E.; Rebane, A. *Nat. Methods* **2011**, *8* (5), 393.
- (28) Idris, N. M.; Gnanasammandhan, M. K.; Zhang, J.; Ho, P. C.; Mahendran, R.; Zhang, Y. *Nat. Med.* **2012**, *18* (10), 1580.
- (29) Gary-Bobo, M.; Mir, Y.; Rouxel, C.; Brevet, D.; Basile, I.; Maynadier, M.; Vaillant, O.; Mongin, O.; Blanchard-Desce, M.; Morère, A.; Garcia, M.; Durand, J.-O.; Raehm, L. *Angew. Chem.* **2011**, *123* (48), 11627.
- (30) Cumpston, B. H.; Sundaravel, A. P.; Barlow, S.; Dyer, D. L.; Ehrlich, J. E.; Erskine, L. L.; Heikal, A. A.; Kuebler, S. M.; Lee, S. I.-Y.; McCord-Maughon, D.; Qin, J.; Röckel, H.; Rumi, M.; Wu, X.-L.; Marder, S. R.; Perry, J. W. *Nature* **1999**, *398*, 51.
- (31) Sun, H.-B.; Matsuo, S.; Misawa, H. *Appl. Phys. Lett.* **1999**, *74* (6), 786.
- (32) Liu, Y.-J.; Yang, J.-Y.; Nie, Y.-M.; Lu, C.-H.; Huang, E. D.; Shin, C.-S.; Baldeck, P.; Lin, C.-L. *Microfluid. Nanofluidics* **2015**, *18* (3), 427.
- (33) Lott, J.; Ryan, C.; Valle, B.; Johnson, J. R.; Schiraldi, D. A.; Shan, J.; Singer, K. D.; Weder, C. *Adv. Mater.* **2011**, *23* (21), 2425.
- (34) Woods, R.; Feldbacher, S.; Zidar, D.; Langer, G.; Satzinger, V.; Schmid, G.; Leeb, W.; Kern, W. *Appl. Opt.* **2013**, *52* (3), 388.
- (35) Kim, D.; So, P. T. C. in *Proc. SPIE 7569, Multiphoton Microscopy in the Biomedical Sciences X*, Eds. So, P. T. C.; Periasamy, A.; König, K. **2010**; 75691V.
- (36) Ciuciu, A. I.; Cywiński, P. *J. RSC Adv* **2014**, *4* (85), 45504.

- (37) Benninger, R. K. P.; Piston, D. W. In *Current Protocols in Cell Biology*; Bonifacino, J. S., Dasso, M., Harford, J. B., Lippincott-Schwartz, J., Yamada, K. M., Eds.; John Wiley & Sons, Inc.: Hoboken, NJ, USA, **2013**.
- (38) Chatani, S.; Kloxin, C. J.; Bowman, C. N. *Polym Chem* **2014**, *5* (7), 2187.
- (39) Nguyen, L. H.; Straub, M.; Gu, M. *Adv. Funct. Mater.* **2005**, *15* (2), 209.
- (40) Lu, Y.; Hasegawa, F.; Kawazu, Y.; Totani, K.; Yamashita, T.; Toshiyuki, W. *FIBER* **2004**, *60* (6), 165.
- (41) Qin, X.-H.; Ovsianikov, A.; Stampfl, J.; Liska, R. *BioNanoMaterials* **2014**, *15* (3-4), 49.
- (42) Xing, J.-F.; Zheng, M.-L.; Chen, W.-Q.; Dong, X.-Z.; Takeyasu, N.; Tanaka, T.; Zhao, Z.-S.; Duan, X.-M.; Kawata, S. *Phys. Chem. Chem. Phys.* **2012**, *14* (45), 15785.
- (43) Albota, M. *Science* **1998**, *281* (5383), 1653.
- (44) Namboodiri, C. K. R.; Bongu, S. R.; Bisht, P. B.; Mukkamala, R.; Chandra, B.; Aidhen, I. S.; Kelly, T. J.; Costello, J. T. *J. Photochem. Photobiol. Chem.* **2016**, *314*, 60.
- (45) Cheng, J.-Z.; Lin, C.-C.; Chou, P.-T.; Chaskar, A.; Wong, K.-T. *Tetrahedron* **2011**, *67* (4), 734.
- (46) Collini, E. *Phys. Chem. Chem. Phys.* **2012**, *14* (11), 3725.
- (47) Schafer, K. J.; Hales, J. M.; Balu, M.; Belfield, K. D.; Van Stryland, E. W.; Hagan, D. J. *J. Photochem. Photobiol. Chem.* **2004**, *162* (2-3), 497.
- (48) Marder, S. R. *Chem Commun* **2006**, No. 2, 131.
- (49) Bhaskar, A.; Ramakrishna, G.; Lu, Z.; Twieg, R.; Hales, J. M.; Hagan, D. J.; Van Stryland, E.; Goodson, T. *J. Am. Chem. Soc.* **2006**, *128* (36), 11840.
- (50) Pond, S. J. K.; Rumi, M.; Levin, M. D.; Parker, T. C.; Beljonne, D.; Day, M. W.; Brédas, J.-L.; Marder, S. R.; Perry, J. W. *J. Phys. Chem. A* **2002**, *106* (47), 11470.
- (51) Sui, N.; Zou, L.; Song, Y.; Zhong, Q.; Wang, Y.; Wei, X.; Wang, Z.; Ma, Y.; Yang, Y.; Zhang, H. *Chin. J. Chem. Phys.* **2014**, *27* (3), 315.
- (52) Kamada, K.; Ohta, K.; Iwase, Y.; Kondo, K. *Chem. Phys. Lett.* **2003**, *372* (3-4), 386.
- (53) Ogawa, K. *Appl. Sci.* **2014**, *4* (1), 1.
- (54) Warther, D.; Gug, S.; Specht, A.; Bolze, F.; Nicoud, J.-F.; Mourrot, A.; Goeldner, M. *Bioorg. Med. Chem.* **2010**, *18* (22), 7753.
- (55) Kim, O.-K.; Lee, K.-S.; Woo, H. Y.; Kim, K.-S.; He, G. S.; Swiatkiewicz, J.; Prasad, P. N. *Chem. Mater.* **2000**, *12* (2), 284.
- (56) Vegiraju, S.; Liu, Y.-Y.; Prabakaran, K.; Ni, J.-S.; Ezhumalai, Y.; Yu, H.-C.; Yau, S. L.; Lin, J. T.; Chen, M.-C.; Lin, T.-C. *RSC Adv* **2015**, *5* (67), 54003.
- (57) Lind, P.; Carlsson, M.; Eliasson, B.; Glimsdal, E.; Lindgren, M.; Lopes, C.; Boman, L.; Norman, P. *Mol. Phys.* **2009**, *107* (7), 629.
- (58) Zhou, H.; Zhou, F.; Tang, S.; Wu, P.; Chen, Y.; Tu, Y.; Wu, J.; Tian, Y. *Dyes Pigm.* **2012**, *92* (1), 633.
- (59) Vivas, M. G.; Silva, D. L.; Malinge, J.; Boujtita, M.; Zalesny, R.; Bartkowiak, W.; Ågren, H.; Canuto, S.; De Boni, L.; Ishow, E.; Mendonca, C. R. *Sci. Rep.* **2014**, *4*.

4 – Nonlinear Optics – Results and Discussion

4.1 Overview of Contributions

Part II – Materials Suitable for Nonlinear Optics

* corresponding author, # equal contribution

- # 7 D. Lumpi*, F. Glöcklhofer, **B. Holzer**, B. Stöger, C. Hametner, G. A. Reider, and J. Fröhlich. Systematic Investigations on 1,2,3-Triazole-Based Compounds Capable of Second Harmonic Generation. *Cryst. Growth Des.*, **2014**, 14, 1018 – 1031.

- #8 **B. Holzer**, B. Stöger, D. Lumpi*, G. A. Reider, C. Hametner, and J. Fröhlich. Isoxazole-Based Ene-Yne Compounds as Potential Materials Exhibiting Nonlinear Optical Properties, *manuscript draft*.

- # 9 **B. Holzer***, M. Tromayer, M. Lunzer, D. Lumpi, E. Horkel, C. Hametner, A. Rosspointner, E. Vauthey, R. Liska and J. Fröhlich. Initiators for Two-Photon Induced Polymerization Based on a Novel Cap-Linker-Cap System, *manuscript draft*.

- # 10 M. Lunzer, **B. Holzer***, A. Rosspointner, M. Tromayer, D. Lumpi, E. Horkel, C. Hametner, E. Vauthey, R. Liska, and J. Fröhlich. Synthesis and Characterization of Triphenylamine-based Two-Photon Initiators, *manuscript draft*.

4.2 Context of Contributions

In this chapter the context of the subsequently introduced manuscripts or paper drafts will be outlined. This chapter can be categorized into two main sections, namely the synthesis and characterization of:

1. Materials Capable of Second Harmonic Generation
2. Compounds Applicable for Two-Photon Absorption

The first part focusses on the design of non-centrosymmetric donor-acceptor-based compounds suitable for nonlinear optics. Synthetic strategies for enhancing the donor strength by introducing selenium as electron-donating moiety and triazole or isoxazole as acceptors are presented. The second part outlines reliable synthetic methods toward chalcogenophene-based materials applicable for two-photon absorption. All target compounds were characterized by photophysical means in order to evaluate their properties with regard to second harmonic generation or application as two-photon initiators, respectively.

The next paragraphs will briefly explain the focus of research in the individual topics, refer to theoretical fundamentals and reveal how these contribute to the main topic of this thesis. For detailed background information and respective references see Chapter 4.3.

Materials Capable of Second Harmonic Generation

In order to design efficient compounds exhibiting nonlinear behavior, hyperpolarization based on strong donor and acceptor moieties is essential. The replacement of sulfur in such organic compounds by heavier atoms represents a possible strategy to enhance these nonlinearities. 1,2,3-Triazole-functionalized ene-yne compounds (*Figure 1, left*) synthesized by thiophene ring fragmentation and subsequent azide-alkyne cycloaddition have shown efficient second harmonic generation (SHG) exhibiting more than twice the value of potassium dihydrogen phosphate (KDP), as described in an earlier study. Based on these findings the introduction of selenium as stronger donor was sought (*Figure 1, right*) taking advantage of its high polarizability compared to sulfur (Manuscript #7).

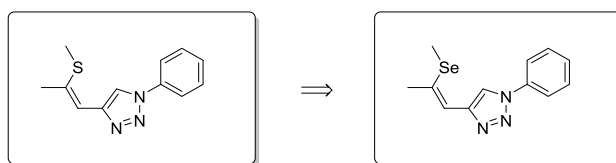


Figure 1: Sulfur-selenium exchange: a possible strategy to enhance the donor strength.

Starting from 2,3,5-tribromoselenophene a sequence of metal halogen exchange reaction (M-H ex.) and subsequent quenching with electrophiles afforded a selenophene derivative suitable for ring fragmentation (SRF), which selectively gave rise to the *Z*-isomer of an ene-yne precursor (*Figure 2*). The introduction of the acceptor in this material was realized by Copper-catalyzed Azide-Alkyne Huisgen Cycloaddition (CuAAC).

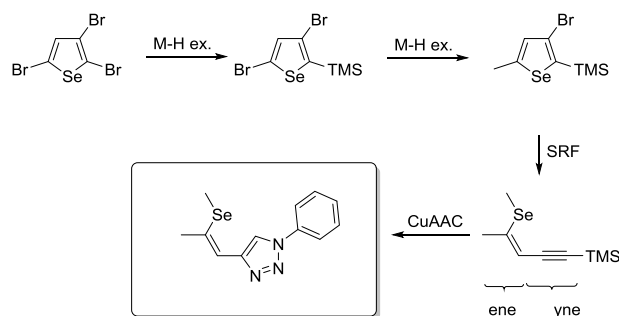


Figure 2: Reaction sequence toward novel materials exhibiting SHG.

The target compound crystallizes in a non-centrosymmetric space group ($P2_12_12_1$), a prerequisite of NLO activity. In cooperation with Prof. Reider from the Photonics Institute at the Technische Universität Wien (TUW) the obtained material was investigated regarding its optical characteristics. A significant enhancement in SH efficiency by a factor of more than 20 for the selenium-based compound compared to its sulfur analogue was obtained, which can be attributed to an increased electron density of the π -electron system.

In order to further evaluate the influence of the acceptor strength, phenylisoxazole-based materials were designed bearing either electron-neutral, donating or withdrawing substituents (*Figure 3*, Manuscript #8). The syntheses of these compounds were pursued by a modification of the ene-yne moiety *via* copper(I)-catalyzed nitrile oxide-alkyne cycloaddition.

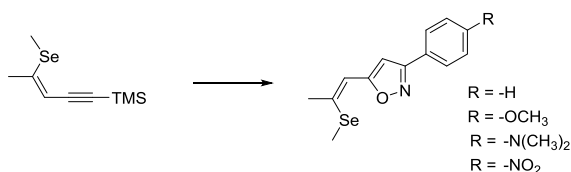


Figure 3: Materials based on phenylisoxazoles potentially exhibiting SHG.

Again, the obtained materials were evaluated toward their application for nonlinear optics. Only electron-neutral phenylisoxazole (R = H) exhibits enantiomorphic crystallization, albeit being a non-chiral flexible molecule it displays second-order nonlinear optical properties with an estimated efficiency of approximately 30 times the value of KDP.

Compounds Applicable for Two-Photon Absorption

The molecular design strategies aiming for efficient two-photon absorption include materials with large change of dipole moment, e.g. donor and acceptor moieties connected by elongated π -electron systems. Continuing earlier studies conducted in the diploma thesis of the applicant a series of cap-linker-cap systems combining thiophene and substituted triphenylamines bearing electron-donating or -withdrawing substituents were synthesized by either Suzuki cross-coupling or nucleophilic aromatic substitution giving rise to two basic structural families of chromophores: D- π -D and A- π -D- π -A (*Figure 4*, Manuscript #9).

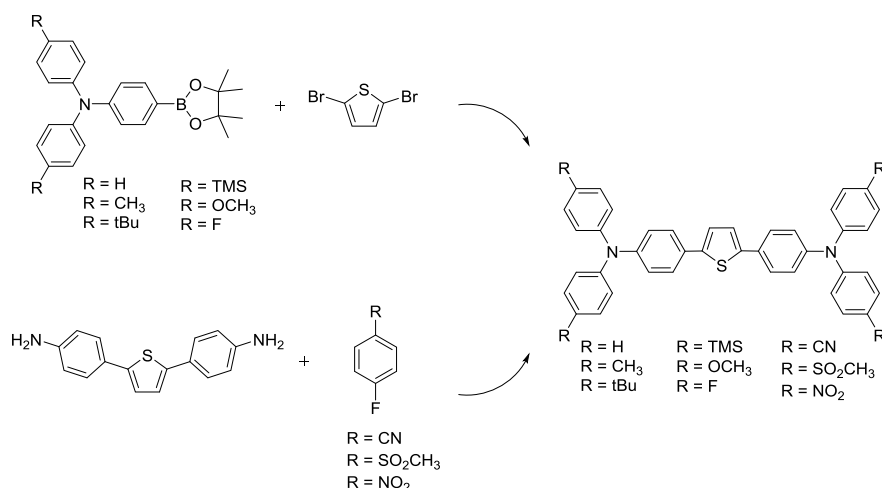


Figure 4: Synthetic strategies toward triphenylamine-substituted thiophenes.

The obtained materials were characterized regarding their photochemical behavior revealing strong structure-property relationships. All compounds were tested toward their applicability as two-photon absorption initiators by fabrication of defined 3D test structures *via* photopolymerization of an acrylate resin applying various laser intensities and writing speeds. Although these substances exhibit only moderate two-photon cross-sections and high quantum yields, which is generally believed to be not beneficial for the two-photon absorption, the initiators showed broad processing windows.

The enlargement of two-photon absorption cross-sections can be realized by structural variation of the organic dye introducing coplanarity, enhancing the donor strength or incorporation of selenium in materials suitable for two-photon absorption. In close cooperation with Markus Lunzer from the Institute of Applied Synthetic Chemistry at the TUW the following strategies (*Figure 5*) altering the molecular design of the initial cap-linker-cap system (*Figure 4*, Manuscript #9) are applied in Manuscript #10: (i) planarization of the triphenylamine (TPA) cap by introduction of indolocarbazole (ICz) and phenylcarbazole (PCz) moieties, (ii) elongation and planarization of the π -linker by applying bithiophene (BT), benzo[1,2-*b*:4,5-*b'*]dichalcogenophenes (BDT, BDS) or dithieno[3,2-*b*:2',3'-*d*]thiophene (DTT), as well as (iii) enhancing the electron density of the linker using more electron-donating selenophene (S) and 2,3-dihydrothieno[3,4-*b*]-1,4-dioxine (EDOT). Due to the shortcoming of low solubility of the original cap-linker-cap photoinitiators in the respective monomer formulation all target compounds were designed bearing hexyl substituents on the triarylamine building blocks. The synthetic linkage of TPA, indolocarbazole as well as phenylcarbazole scaffolds and chalcogenophene-based linkers toward symmetrical α,ω -

bis(triarylamines) was intended by cross-coupling reactions based on Suzuki or Stille coupling or CH activation.

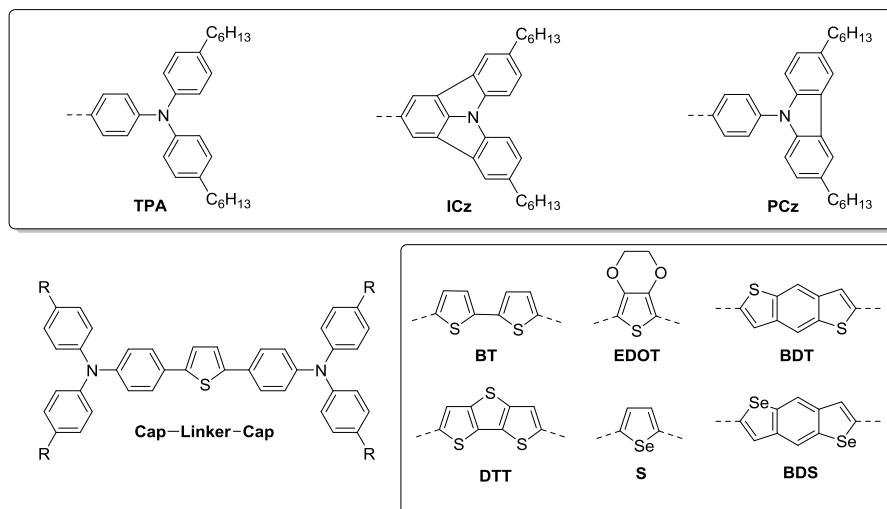


Figure 5: Cap-linker-cap systems based on triphenylamine substituted thiophene (left, bottom) and structural motives applied in target compounds.

This manuscript elucidates the molecular structure / effective two-photon absorption relationship by systematic variation of substituents of the dye compound applying UV-Vis, fluorescence and two-photon excited fluorescence spectroscopy. Although these materials are highly fluorescent, two-photon absorption cross-sections up to 5200 GM have been determined. Structuring tests of the target compounds in monomer formulations reveal the efficiency of these materials as two-photon absorption initiators.

4.3. Original works

Manuscript # 7

Daniel Lumpi*, Florian Glöcklhofer, **Brigitte Holzer**, Berthold Stöger, Christian Hametner,
Georg A. Reider, and Johannes Fröhlich

Systematic Investigations on 1,2,3-Triazole-Based Compounds Capable of Second Harmonic
Generation

Cryst. Growth Des., **2014**, 14, 1018 – 1031

Reproduced with permission from “Crystal Growth and Design”, © 2014 American Chemical Society.

Systematic Investigations on 1,2,3-Triazole-Based Compounds Capable of Second Harmonic Generation

Daniel Lumpi,^{*,†} Florian Glöckhofer,[†] Brigitte Holzer,[†] Berthold Stöger,[‡] Christian Hametner,[†] Georg A. Reider,[§] and Johannes Fröhlich[†]

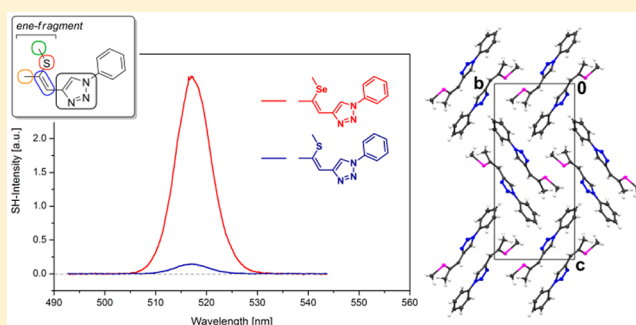
[†]Institute of Applied Synthetic Chemistry, Vienna University of Technology, Getreidemarkt 9/163, A-1060 Vienna, Austria

[‡]Institute of Chemical Technologies and Analytics, Vienna University of Technology, Getreidemarkt 9/164, A-1060 Vienna, Austria

[§]Photonics Institute, Vienna University of Technology, Gußhausstraße 27-29, A-1040 Vienna, Austria

Supporting Information

ABSTRACT: 1,2,3-Triazole-functionalized ene-yne compounds, synthesized by thiophene (selenophene) ring fragmentation followed by azide-alkyne cycloaddition, were investigated as a basis for nonlinear optical (NLO) materials capable of second harmonic generation (SHG). The structure-property relationship was mapped by systematic variation of the molecular scaffold, viz., elongation of the alkyl groups, isomerizations of both the double bond as well as the triazole moiety, sulfur oxidations, and a sulfur-selenium exchange. Nine novel molecular compounds were synthesized, of which eight are solids at room temperature. The latter were characterized by single-crystal X-ray diffraction (XRD). Five crystal structures lacked of inversion symmetry, a prerequisite for NLO activity. The corresponding materials were examined regarding SHG, UV-vis absorption, and powder XRD. By substituting S for Se, we were able to increase the SH intensity by a factor of 20. On the basis of the results, we propose a strategy to further improve the SHG efficiency of this class of materials.



Five crystal structures lacked of inversion symmetry, a prerequisite for NLO activity. The corresponding materials were examined regarding SHG, UV-vis absorption, and powder XRD. By substituting S for Se, we were able to increase the SH intensity by a factor of 20. On the basis of the results, we propose a strategy to further improve the SHG efficiency of this class of materials.

INTRODUCTION

Quadric nonlinear optical (NLO) materials are of critical importance for applications in quantum electronics and telecommunication technology.¹ There are several manifestations of this nonlinearity such as the electro-optic effect, optical three wave mixing, second harmonic generation (SHG), parametric amplification, and downconversion. The common material property responsible for this phenomenologically disparate effect is the second-order susceptibility, which, on a microscopic level, relates to the first-order hyperpolarizability. It should be noted that for symmetry reasons quadric nonlinear optical materials are also potentially piezoelectric, rendering them useful for integrated sensor applications as well. A necessary (but not sufficient) condition for SHG to appear in a crystal is that it belongs to one of the noncentrosymmetric crystal classes, with the exception of 432.²

Organic NLO crystals are particularly attractive for these applications.³⁻⁷ Their NLO figures of merit can be orders of magnitude higher compared to inorganics, and their long-term stability is orders of magnitude better than that of electrooptic polymers. The reason for the fast response of nonlinear organic compounds is that their hyperpolarizability is due to (delocalized) electrons in contrast to inorganic materials where polar optical lattice vibrations may play a large role. Thus, organic molecules capable of second-order NLO

applications generally rely on a donor-(π -linker)-acceptor design to impart the electronic bias.⁸

Just recently, we reported on a novel class of NLO materials capable of second harmonic generation yielding an estimated SH efficiency of more than twice the value of potassium dihydrogen phosphate (KDP).^{9,10} The introduced NLO chromophore **4ba** (Figure 1) relies on the application of a 1,2,3-triazole as the electron acceptor subunit, which was demonstrated to be conveniently accessible within the concept of “click” chemistry.¹¹⁻¹³ As an electron donor part of the molecule the *Z*-(methylthio)propenyl group derived from thiophene ring-opening¹⁴⁻¹⁶ reactions is applied. The donor-acceptor interactions on the one hand lead to promising SHG efficiencies but on the other hand also feature desirable optical properties (wide transparency window).

In addition, the particular configuration of the molecule, namely, a phenyl/triazole pair extended by a *Z*-(methylthio)-propenyl subunit, was revealed to promote enantiomorphic crystallization as a consequence of alkyl-alkyl group interactions (supported by torsion angle dependent potential calculations (DFT)).¹⁰ The chiral crystallization, although the molecule is nonchiral and flexible, is a relatively rare

Received: October 4, 2013

Revised: January 24, 2014

Published: January 31, 2014

phenomenon¹⁷ and combines the advantages of a convenient and straightforward synthesis (of nonchiral compounds) with the capability of characteristics such as, e.g., SHG.

Hence, the molecular structure of this class of compounds is of great interest as it comprises both an attractive donor–acceptor scaffold and a subunit facilitating noncentrosymmetric crystallization. This paper presents a systematic study on the structure–function relationship of these promising materials. The investigations focus on the effects induced by variations of both steric as well as electronic constitution on quadric NLO properties. As a result of the aforementioned applications of noncentrosymmetric (chiral) materials, clearly outlining the broad scope of potential applications of these structural building blocks, the findings are of relevance for diverse fields of material chemistry.

EXPERIMENTAL SECTION

The syntheses of 2-bromo-5-methylthiophene (**1b**),¹⁸ 2-bromo-5-ethylthiophene (**1c**),¹⁹ 3-bromo-2-(trimethylsilyl)thiophene (**2a**),²⁰ 3-bromo-5-methyl-2-(trimethylsilyl)thiophene (**2b**),²¹ trimethyl[(3Z)-4-(methylthio)-3-buten-1-yn-1-yl]-silane (**3aa**),²² trimethyl[(3Z)-4-(methylthio)-3-penten-1-yn-1-yl]silane (**3ba**),¹⁰ trimethyl[(3Z)-4-(butylthio)-3-penten-1-yn-1-yl]silane (**3bd**),²³ 4-[(1Z)-2-(methylthio)-ethenyl]-1-phenyl-1H-1,2,3-triazole (**4aa**),²² 4-[(1Z)-2-(methylthio)-1-propen-1-yl]-1-phenyl-1H-1,2,3-triazole (**4ba**),¹⁰ and azidobenzene²⁴ were performed in analogy to published protocols; full characterization of the compounds is also given in the indicated references.

Single crystals for compounds **4aa**, **4ba**, **4bb**, **4ca**, **5ba**, **7ba**, and **16** were obtained by slow evaporation of *n*-hexane at rt. **4bd** was isolated as an oil which slowly crystallized upon standing at ~5 °C. Crystals of the sulfone **9ba** and **12ba** were grown by slow evaporation of CD₂Cl₂ in NMR tubes at ~5 °C. Similar to **4ba** (see literature for details)¹⁰ noncentrosymmetric compounds **4bb**, **4ca**, and **7ba** tend to crystallize in thin needles, which are still suitable for a general screening of NLO properties via the powder method; prior to technological application, however, further optimization of the crystallization process will be necessary. In contrast, oxidized species **12ba** readily crystallize in blocks of >1 × 1 × 1 mm. The seleno derivative **16** crystallizes as rods with a significantly larger crystal size compared to **4ba**, **4bb**, etc., making the latter two particularly interesting for applications in optics.

Crystals of the title compounds suitable for X-ray diffraction were selected under a polarizing microscope, embedded in perfluorinated oil and mounted on a Bruker APEX II diffractometer with κ -geometry equipped with a CCD detector. Intensity data were recorded at 100 K in a dry stream of nitrogen with Mo K α radiation ($\lambda = 0.71073$ Å). Full reciprocal spheres were collected in ω - and φ -scan modes with 0.5° rotation width.

Frames were integrated using SAINT PLUS,²⁵ and an absorption correction was applied using a multiscan approach with SADABS.²⁵ The crystal structures were solved using charge-flipping implemented in SUPERFLIP.²⁶ All non-H atoms were directly located in the resulting electron density maps. The structures were refined with JANA2006.²⁷ The protons were located in subsequent difference Fourier maps. In general, protons were freely refined. In **4bb** and **4ca**, the terminal H atoms of the thioalkyl group, and in **4bd** all H atoms were placed at calculated positions and refined as riding on the parent C atoms. The H atoms in the heavy atom structure **16** were likewise constrained. In the final refinement cycles, all non-H atoms were refined anisotropically.

Powder diffractograms were recorded on a Philips X'Pert Pro diffractometer system [Cu K α _{1,2} radiation ($\lambda = 1.54060$, 1.54439 Å), X'Celerator multichannel detector, Bragg–Brentano geometry, silicon single-crystal sample holder, 5–70° 2 θ , 2.546° scan length (2 θ)]. The scans were converted into 0.02° step-size bins.

For SHG measurements the powder samples were produced by grinding with a mortar; the maximum particle size was below <1 μ m. Because of the inhomogeneous particle size, our experiments could

not clarify whether phase matching was possible or not for a particular material. Nonetheless, a relative measurement of the nonlinear optical coefficients is possible since the SH efficiency scales quadratically with the nonlinear coefficient in this particle size regime.²⁸

The quadric nonlinear properties of our samples were probed by second harmonic (SH) generation from powder samples. The output of an ultrafast (pulse duration 70 fs) Yb:KGW-Laser (Light Conversion) with 600 mW output power at a repetition rate of 75 MHz and a wavelength of 1034 nm was directed, with a 100 mm focusing lens, onto powder samples between thin sheets of glass. The diffusely reflected SH radiation was collected with a NA = 0.1 lens, separated from fundamental radiation with a color filter, and spectrally analyzed with a 0.25 m grating monochromator and a photomultiplier tube. The sample plane was positioned somewhat out of the focal plane (toward the lens) to prevent any damage to the sample. After each measurement, the samples were carefully checked for the absence of any damage or thermal modification.

Halogen Dance (HD) Procedure toward 3-Bromo-5-ethyl-2-(trimethylsilyl)thiophene 2c. To a solution of diisopropylamine (DIPA, 6.83 g, 67.5 mmol, 1.5 equiv) in dry THF (180 mL) under argon was added *n*-BuLi (21.6 mL, 54.0 mmol, 2.5 M in hexanes, 1.2 equiv) slowly at –30 °C. After 20 min **1c** (8.55 g, 45.0 mmol, 1.0 equiv) was added in dry THF at –70 °C and the reaction stirred for 1.5 h at a temperature of –70 to –40 °C. Subsequently TMS–Cl (6.12 g, 56.3 mmol, 1.25 equiv) was added as a solution in dry THF and the mixture stirred at rt overnight. The reaction was poured on water (200 mL) and repeatedly extracted with Et₂O, and the organic phases were dried over anhydrous Na₂SO₄ and concentrated under reduced pressure. Purification by vacuum distillation yielded **2c** (9.50 g, 80%) as slightly yellow oil. BP: 108–110 °C (12 mbar). ¹H NMR (200 MHz, CDCl₃): $\delta = 6.82$ (m, 1H), 2.83 (m, 2H), 1.31 (t, $J = 7.5$ Hz, 3H), 0.39 (s, 9H) ppm. ¹³C NMR (50 MHz, CDCl₃): $\delta = 152.7$ (s), 131.4 (s), 129.1 (d), 116.4 (s), 23.3 (t), 15.5 (q), –0.7 (q) ppm. Anal. Calcd for C₉H₁₃BrSSi: m/z 261.98 [M]⁺. Found: MS (EI) m/z 261.96 [M]⁺.

General Procedure for the Thiophene Ring-Fragmentation (TRF) reaction. To a solution of **2b,c** (1.0 equiv) in dry Et₂O (~0.2–0.3 M)/dry THF (~0.15 M) under an argon atmosphere at –60 to –80 °C was injected *n*-BuLi (1.1 equiv)/ethylthium (1.1 equiv) dropwise. After the addition the reaction was immediately warmed to rt, stirred for 30 min, and again cooled to –40 °C. The appropriate alkyl iodide (1.5 equiv) was added and the temperature subsequently raised to rt. After a reaction time of 30 min the mixture was poured on water and extracted with Et₂O, and the combined organic layers were dried over anhydrous Na₂SO₄ and concentrated in vacuo. Purification was performed by column chromatography (light petroleum).

Trimethyl[(3Z)-4-(ethylthio)-3-penten-1-yn-1-yl]silane 3bb. Starting from **2b** (498 mg, 2.0 mmol) in dry THF (13 mL), ethyllithium (4.4 mL, 2.2 mmol, 0.5 M in benzene:cyclohexane), and iodoethane (468 mg, 3.0 mmol), the pure *Z*-isomer **3bb** (201 mg, 51%) was isolated as a colorless liquid. ¹H NMR (200 MHz, CDCl₃): $\delta = 5.43$ (m, 1H), 2.89 (q, $J = 7.4$ Hz, 2H), 2.07 (m, 3H), 1.29 (t, $J = 7.4$ Hz, 3H), 0.19 (s, 9H) ppm. ¹³C NMR (50 MHz, CDCl₃): $\delta = 148.6$ (s), 103.7 (d), 101.8 (s), 100.9 (s), 24.8 (t), 22.8 (q), 15.0 (q), –0.0 (q) ppm. Anal. Calcd for C₁₀H₁₈SSi: m/z 199.0971 [M + H]⁺. Found: MS (APCI) m/z 199.0981 [M + H]⁺.

Trimethyl[(3Z)-4-(propylthio)-3-penten-1-yn-1-yl]silane 3bc. Starting from **2b** (2.49 g, 10.0 mmol) in dry Et₂O (33 mL), *n*-BuLi (4.4 mL, 11.0 mmol, 2.5 M in hexanes), and 1-iodopropane (2.55 g, 15.0 mmol), **3bc** (221 mg, 10%) was obtained as a mixture with **3bd** (27.5 mol % **3bd** content; determined by ¹H NMR spectroscopy). The low yield can be explained by the fact that only the best product fraction (in terms of **3bd** content) was considered for the yield calculation and subjected to further conversion. ¹H NMR (200 MHz, CDCl₃): 5.45–5.43 (m, 1H), 2.85 (t, $J = 7.4$ Hz, 2H), 2.07 (m, 3H), 1.65 (sext, $J = 7.4$ Hz, 2H), 1.02 (t, $J = 7.3$ Hz, 3H), 0.20 (s, 9H) ppm. ¹³C NMR (50 MHz, CDCl₃): $\delta = 148.7$ (s), 103.9 (d), 102.0 (s), 100.9 (s), 32.7 (t), 23.4 (t), 23.0 (q), 13.4 (q), 0.0 (q) ppm. Anal. Calcd for C₁₁H₂₀SSi: m/z 213.1128 [M + H]⁺. Found: MS (APCI) m/z 213.1125 [M + H]⁺. The NMR code is obtained from calculated

difference spectra (subtraction of **3bd**) of the mixture (original spectrum of the product mixture is illustrated in the Supporting Information).

Trimethyl[(3Z)-4-(methylthio)-3-hexen-1-yn-1-yl]silane 3ca. Starting from **2c** (2.63 g, 10.0 mmol) in dry Et₂O (50 mL), *n*-BuLi (4.4 mL, 11.0 mmol, 2.5 M in hexanes), and iodomethane (3.12 g, 22.0 mmol, 2.2 equiv, *minor alteration from the general procedure*), pure *Z*-isomer **3ca** (1.55 g, 78%) was isolated as a slightly yellow liquid. ¹H NMR (200 MHz, CDCl₃): δ = 5.47 (m, 1H), 2.37–2.26 (m, 5H), 1.11 (t, *J* = 7.4 Hz, 3H), 0.19 (s, 9H) ppm. ¹³C NMR (50 MHz, CDCl₃): δ = 154.7 (s), 102.2 (d), 101.9 (s), 101.4 (s), 28.8 (t), 14.0 (q), 13.3 (q), –0.0 (q) ppm. Anal. Calcd for C₁₀H₁₈SSi: *m/z* 199.0971 [M + H]⁺. Found: MS (APCI) *m/z* 199.0964 [M + H]⁺.

Isomerization Procedure toward Trimethyl[(3E)-4-(methylthio)-3-penten-1-yn-1-yl]silane 10ba. **3ba** (200 mg, 1.08 mmol, 1.0 equiv) was dissolved in CHCl₃ (~8 mL) and one drop (~5 μL) of HCl in dioxane (saturated solution) added at rt. The mixture was stirred overnight (~18 h), and an aqueous saturated NaHCO₃ solution was added and extracted with CH₂Cl₂. The combined organic layers were dried over anhydrous Na₂SO₄, and the solvent was removed under reduced pressure. Column chromatography afforded **10ba** (74 mg, 37%) as slightly yellow oil. ¹H NMR (400 MHz, CDCl₃): δ = 5.12 (m, 1H), 2.25 (s, 3H), 2.14 (m, 3H), 0.19 (s, 9H) ppm. ¹³C NMR (100 MHz, CDCl₃): δ = 150.9 (s), 102.5 (s), 99.0 (d), 97.7 (s), 20.6 (q), 14.7 (q), 0.1 (q) ppm. Anal. Calcd for C₉H₁₆SSi: *m/z* 185.0815 [M + H]⁺. Found: MS (APCI) *m/z* 185.0810 [M + H]⁺.

General Oxidation Protocol Using *m*-CPBA (3-Chloroperbenzoic Acid).²⁹ To a stirred solution of ene-yne species (**3ba/10ba**, 1.0 equiv) in CHCl₃ was added *m*-CPBA (4.0 equiv) (a slight heat generation was observed). After 30–45 min an aqueous solution of KOH (10 wt %) was added and the mixture extracted with CHCl₃, and the organic phases were washed with brine and dried over anhydrous Na₂SO₄. The solvent was removed under reduced pressure. Column chromatography yielded the desired sulfones (**8ba/11ba**).

Trimethyl[(3Z)-4-(methylsulfonyl)-3-penten-1-yn-1-yl]silane 8ba.³⁰ **3ba** (461 mg, 2.5 mmol), *m*-CPBA (1.73 g, 10.0 mmol), and column chromatography (light petroleum/EE (20%)) resulted in **8ba** (440 mg, 81%) as a slightly yellow highly viscous oil which slowly crystallizes at ~0 °C. ¹H NMR (400 MHz, CDCl₃): δ = 6.12 (m, 1H), 3.16 (s, 3H), 2.16 (m, 3H), 0.22 (s, 9H) ppm. ¹³C NMR (100 MHz, CDCl₃): δ = 149.7 (s), 116.6 (d), 109.1 (s), 98.5 (s), 41.5 (q), 18.7 (q), –0.7 (q) ppm. Anal. Calcd for C₉H₁₆O₂SSi: *m/z* 217.0713 [M + H]⁺, 239.0532 [M + Na]⁺. Found: MS (ESI) *m/z* 217.0722 [M + H]⁺, 239.0531 [M + Na]⁺.

Trimethyl[(3E)-4-(methylsulfonyl)-3-penten-1-yn-1-yl]silane 11ba. **10ba** (129 mg, 0.7 mmol), *m*-CPBA (483 mg, 2.8 mmol), and column chromatography (light petroleum/Et₂O (30%)) resulted in **11ba** (92 mg, 61%) as slightly yellow solid. ¹H NMR (200 MHz, CDCl₃): δ = 6.60 (m, 1H), 2.90 (s, 3H), 2.24 (m, 3H), 0.23 (s, 9H) ppm. ¹³C NMR (50 MHz, CDCl₃): δ = 148.1 (s), 119.8 (d), 109.9 (s), 98.1 (s), 40.4 (q), 14.5 (q), –0.4 (q) ppm. Anal. Calcd for C₉H₁₆O₂SSi: *m/z* 217.0713 [M + H]⁺, 239.0532 [M + Na]⁺. Found: MS (APCI/ESI) *m/z* 217.0707 [M + H]⁺, 239.0531 [M + Na]⁺.

Deprotection Procedure toward 4-(Methylthio)-(3Z)-3-penten-1-yne 6ba.³¹ **3ba** (701 mg, 3.8 mmol, 1.0 equiv) was added to a solution of tetra-*n*-butylammonium fluoride (4.6 mL, 4.6 mmol, 1.2 equiv, 1.0 M in THF) and stirred for 1 h at rt. The reaction was poured on water and repeatedly extracted with Et₂O, and the combined organic layers were dried over anhydrous Na₂SO₄ and concentrated in vacuo. Purification by column chromatography (light petroleum/Et₂O (2%)) yielded **6ba** (324 mg, 76%) as slightly yellow liquid. ¹H NMR (400 MHz, CDCl₃): δ = 5.40 (m, 1H), 3.33 (m, 1H), 2.37 (s, 3H), 2.09 (m, 3H) ppm. ¹³C NMR (100 MHz, CDCl₃): δ = 149.6, 102.0, 83.4, 80.4, 22.2, 13.8 ppm. Anal. Calcd for C₆H₈S: *m/z* 113.0419 [M + H]⁺. Found: MS (APCI) *m/z* 113.0429 [M + H]⁺.

General CuAAC (1,4-Click) Procedure. To a *t*-BuOH/H₂O (1:1, ~0.4 M) suspension of ene-yne species **3** (1.0 equiv), azidobenzene (1.25 equiv), CuSO₄·5H₂O (20 mol %), and sodium ascorbate (40 mol %) in a reaction vessel was added potassium fluoride (1.20 equiv)

at room temperature. Subsequently the vessel was sealed and heated to 50 °C for 15–20 h. The reaction mixture was diluted with water and extracted repeatedly with Et₂O. The combined organic layers were washed with brine and dried over anhydrous Na₂SO₄. Evaporation of the solvent and following column chromatography afforded target compounds **4**.

4-[(1Z)-2-(Ethylthio)-1-propen-1-yl]-1-phenyl-1H-1,2,3-triazole 4bb. **3bb** (377 mg, 1.9 mmol), azidobenzene (283 mg, 2.4 mmol), CuSO₄·5H₂O (95 mg, 0.4 mmol), sodium ascorbate (151 mg, 0.8 mmol), potassium fluoride (132 mg, 2.3 mmol), and column chromatography (light petroleum/Et₂O (25%)) resulted in **4bb** (286 mg, 61%) as a slightly yellow solid. MP: 86–87 °C. ¹H NMR (400 MHz, CD₂Cl₂): δ = 8.48 (s, 1H), 7.78 (d, *J* = 7.8 Hz, 2H), 7.54 (m, 2H), 7.44 (t, *J* = 7.3 Hz, 1H), 6.67 (s, 1H), 2.91 (q, *J* = 7.4 Hz, 2H), 2.27 (s, 3H), 1.30 (t, *J* = 7.4 Hz, 3H) ppm. ¹³C NMR (100 MHz, CD₂Cl₂): δ = 145.8 (s), 137.7 (s), 135.5 (s), 130.2 (d), 128.9 (d), 120.9 (d), 120.6 (d), 116.7 (d), 25.8 (t), 24.1 (q), 15.6 (q) ppm. Anal. Calcd for C₁₃H₁₅N₃S: *m/z* 246.1059 [M + H]⁺. Found: MS (ESI) *m/z* 246.1054 [M + H]⁺.

4-[(1Z)-2-(Propylthio)-1-propen-1-yl]-1-phenyl-1H-1,2,3-triazole 4bc. A mixture of **3bc** and **3bd** (27.5 mol % **3bd** content; determined by ¹H NMR spectroscopy) was obtained from the TRF reaction (see procedure for details). The mixture (215 mg, 1.0 mmol), azidobenzene (149 mg, 1.3 mmol), CuSO₄·5H₂O (50 mg, 0.2 mmol), sodium ascorbate (79 mg, 0.4 mmol), potassium fluoride (70 mg, 1.2 mmol), and column chromatography (light petroleum/Et₂O (25%)) resulted in **4bc** (125 mg, 68% corrected yield in relation to **3bc** content) as a colorless liquid. ¹H NMR (400 MHz, CD₂Cl₂): δ = 8.49 (s, 1H), 7.78 (d, *J* = 8.0 Hz, 2H), 7.55 (m, 2H), 7.45 (t, *J* = 7.4 Hz, 1H), 6.66 (s, 3H), 2.87 (t, *J* = 7.3 Hz, 2H), 2.27 (s, 3H), 1.65 (sext, *J* = 7.3 Hz, 2H), 1.02 (t, *J* = 7.3 Hz, 3H) ppm. ¹³C NMR (100 MHz, CD₂Cl₂): δ = 145.9 (s), 137.8 (s), 135.6 (s), 130.2 (d), 129.0 (d), 121.0 (d), 120.7 (d), 116.8 (d), 33.6 (t), 24.3 (q), 24.2 (t), 13.7 (q) ppm. Anal. Calcd for C₁₄H₁₇N₃S: *m/z* 260.1216 [M + H]⁺. Found: MS (ESI) *m/z* 260.1213 [M + H]⁺.

4-[(1Z)-2-(Butylthio)-1-propen-1-yl]-1-phenyl-1H-1,2,3-triazole 4bd. Compound **4bd** was isolated as a byproduct. A mixture of **3bb** and **3bd** (19 mol % **3bd** content determined by ¹H NMR spectroscopy) was obtained from an earlier TRF reaction (*n*-BuLi used instead of EtLi). The mixture (264 mg, 1.8 mmol), azidobenzene (268 mg, 2.2 mmol), CuSO₄·5H₂O (90 mg, 0.4 mmol), sodium ascorbate (143 mg, 0.7 mmol), potassium fluoride (125 mg, 2.2 mmol), and column chromatography (light petroleum/Et₂O (25 → 30%)) resulted in **4bd** (57 mg, 62% corrected yield in relation to **3bd** content) as colorless oil, which slowly crystallized to form single crystals upon standing at ~5 °C. ¹H NMR (400 MHz, CD₂Cl₂): δ = 8.49 (s, 1H), 7.78 (d, *J* = 7.8 Hz, 2H), 7.54 (m, 2H), 7.44 (t, *J* = 7.4 Hz, 1H), 6.67 (s, 1H), 2.89 (t, *J* = 7.5 Hz, 2H), 2.27 (s, 3H), 1.62 (quint, *J* = 7.5 Hz, 2H), 1.45 (sext, *J* = 7.4 Hz, 2H), 0.93 (t, *J* = 7.4 Hz, 3H) ppm. ¹³C NMR (100 MHz, CD₂Cl₂): δ = 145.9 (s), 137.7 (s), 135.7 (s), 130.2 (d), 129.0 (d), 120.9 (d), 120.6 (d), 116.7 (d), 32.9 (t), 31.3 (t), 24.2 (q), 22.5 (t), 14.0 (q) ppm. Anal. Calcd for C₁₅H₁₉N₃S: *m/z* 274.1372 [M + H]⁺. Found: MS (ESI) *m/z* 274.1362 [M + H]⁺.

4-[(1Z)-2-(Methylthio)-1-buten-1-yl]-1-phenyl-1H-1,2,3-triazole 4ca. **3ca** (397 mg, 2.0 mmol), azidobenzene (298 mg, 2.5 mmol), CuSO₄·5H₂O (100 mg, 0.4 mmol), sodium ascorbate (158 mg, 0.8 mmol), potassium fluoride (139 mg, 2.4 mmol), and column chromatography (light petroleum/Et₂O (20%)) resulted in **4ca** (339 mg, 69%) as beige solid. MP: 44–45 °C. ¹H NMR (400 MHz, CD₂Cl₂): δ = 8.47 (s, 1H), 7.78 (d, *J* = 8.2 Hz, 2H), 7.54 (m, 2H), 7.45 (t, *J* = 7.4 Hz, 1H), 6.68 (s, 1H), 2.54 (q, *J* = 7.4 Hz, 2H), 2.38 (s, 3H), 1.25 (t, *J* = 7.4 Hz, 3H) ppm. ¹³C NMR (100 MHz, CD₂Cl₂): δ = 145.8 (s), 142.1 (s), 137.8 (s), 130.2 (d), 129.0 (d), 121.0 (d), 120.7 (d), 114.7 (d), 29.9 (t), 14.4 (q), 14.2 (q) ppm. Anal. Calcd for C₁₃H₁₅N₃S: *m/z* 246.1059 [M + H]⁺. Found: MS (ESI) *m/z* 246.1059 [M + H]⁺.

4-[(1Z)-2-(Methylsulfonyl)-1-propen-1-yl]-1-phenyl-1H-1,2,3-triazole 9ba. **8ba** (222 mg, 1.0 mmol), azidobenzene (153 mg, 1.3 mmol), CuSO₄·5H₂O (51 mg, 0.2 mmol), sodium ascorbate (81 mg, 0.4 mmol), potassium fluoride (72 mg, 1.2 mmol), and column

chromatography (light petroleum/Et₂O (80%)) resulted in **9ba** (190 mg, 70%) as a yellowish solid. ¹H NMR (400 MHz, CD₂Cl₂): δ = 8.84 (s, 1H), 7.77 (d, *J* = 7.9 Hz, 2H), 7.59–7.54 (m, 2H), 7.48 (t, *J* = 7.4 Hz, 1H), 7.25 (q, *J* = 1.5 Hz, 1H), 2.97 (s, 3H), 2.32 (d, *J* = 1.5 Hz, 3H) ppm. ¹³C NMR (100 MHz, CD₂Cl₂): δ = 142.0 (s), 137.3 (s), 137.0 (s), 130.3 (d), 129.6 (d), 128.4 (d), 124.7 (d), 121.3 (d), 41.4 (q), 21.7 (q) ppm. Anal. Calcd for C₁₂H₁₃N₃O₂S: *m/z* 264.0807 [M + H]⁺, 286.0621 [M + Na]⁺. Found: MS (ESI) *m/z* 264.0805 [M + H]⁺, 286.0618 [M + Na]⁺.

4-[(1E)-2-(Methylsulfonyl)-1-propen-1-yl]-1-phenyl-1H-1,2,3-triazole 12ba. **11ba** (173 mg, 0.8 mmol), azidobenzene (119 mg, 1.0 mmol), CuSO₄·5H₂O (40 mg, 0.2 mmol), sodium ascorbate (63 mg, 0.3 mmol), potassium fluoride (56 mg, 1.0 mmol), and column chromatography (light petroleum/Et₂O (80%)) resulted in **12ba** (120 mg, 57%) as a yellowish solid. MP: 128–130 °C. ¹H NMR (400 MHz, CD₂Cl₂): δ = 8.22 (s, 1H), 7.77 (d, *J* = 7.9 Hz, 2H), 7.59–7.55 (m, 3H), 7.50 (m, *J* = 7.3 Hz, 1H), 2.97 (s, 3H), 2.58 (d, *J* = 1.4 Hz, 3H) ppm. ¹³C NMR (100 MHz, CD₂Cl₂): δ = 143.2 (s), 138.7 (s), 137.1 (s), 130.4 (d), 129.7 (d), 125.7 (d), 123.9 (d), 121.2 (d), 40.9 (q), 14.6 (q) ppm. Anal. Calcd for C₁₂H₁₃N₃O₂S: *m/z* 264.0807 [M + H]⁺, 286.0621 [M + Na]⁺. Found: MS (ESI) *m/z* 264.0795 [M + H]⁺, 286.0618 [M + Na]⁺.

RuAAC (1,5-Click) toward 5-[(1Z)-2-(Methylthio)-1-propen-1-yl]-1-phenyl-1H-1,2,3-triazole 7ba. **6ba** (37 mg, 0.33 mmol, 1.00 equiv), azidobenzene (48 mg, 0.40 mmol, 1.20 equiv), and DMF (2 mL) were added to [Cp*⁺RuCl]₄ (4.5 mg, 0.017 mmol, 5 mol %) in a sealed vial under oxygen-free conditions. The solution was heated to 110 °C in a microwave reactor for 1 h. After evaporation of the solvent under reduced pressure, addition of saturated aqueous NH₄Cl solution, and repeated extraction with Et₂O, the combined organic layers were dried over anhydrous Na₂SO₄. Evaporation of the solvent in vacuo and purification by column chromatography (light petroleum/Et₂O (50%)) afforded **7ba** (30 mg, 39%) as a white solid. MP: 76–77 °C. ¹H NMR (400 MHz, CD₂Cl₂): δ = 8.14 (s, 1H), 7.59–7.53 (m, 3H), 7.48–7.45 (m, 2H), 6.07 (m, 1H), 2.43 (s, 3H), 2.19 (d, *J* = 1.3 Hz, 3H) ppm. ¹³C NMR (100 MHz, CD₂Cl₂): δ = 141.9 (s), 137.0 (s), 134.5 (s), 133.6 (d), 130.0 (d), 129.9 (d), 126.3 (d), 108.2 (d), 24.2 (q), 14.7 (q) ppm. Anal. Calcd for C₁₂H₁₃N₃S: *m/z* 232.0903 [M + H]⁺. Found: MS (ESI) *m/z* 232.0909 [M + H]⁺.

Isomerization Reaction toward 4-[(1E)-2-(methylthio)-1-propen-1-yl]-1-phenyl-1H-1,2,3-triazole 5ba. **4ba** (102 mg, 0.44 mmol, 1.0 equiv) was dissolved in CDCl₃ (4.0 mL, chloride content of ~280 ppm) in an NMR glass tube and kept at rt for 12 h. Reference experiments revealed that isomerization can also be achieved by applying catalytic amounts of HCl (in dioxane). Evaporation of the solvent and column chromatography (light petroleum) yielded compound **5ba** (43 mg, 42%) as white solid. ¹H NMR (400 MHz, CD₂Cl₂): δ = 7.89 (s, 1H), 7.75 (d, *J* = 8.0 Hz, 2H), 7.55 (m, 2H), 7.45 (t, *J* = 7.4 Hz, 1H), 6.18 (s, 1H), 2.40 (s, 3H), 2.28 (s, 3H) ppm. ¹³C NMR (100 MHz, CD₂Cl₂): δ = 146.5 (s), 139.2 (s), 137.7 (s), 130.3 (d), 129.1 (d), 120.9 (d), 118.9 (d), 108.7 (d), 21.1 (q), 15.5 (q) ppm. Anal. Calcd for C₁₂H₁₃N₃S: *m/z* 232.0903 [M + H]⁺. Found: MS (ESI) *m/z* 232.0913 [M + H]⁺.

Isomerization Experiments toward 5bb, 5bd, 5ca. To prove the identity of *E*-isomers **5** obtained during isomerization experiments (Figure 6), performed at a concentration of ~80 μmol/mL, the respective mixtures were quantitatively separated by preparative TLC and the pure *E*-isomers **5** subjected to ¹H and ¹³C NMR spectroscopy and high-resolution mass spectrometry.

4-[(1E)-2-(Ethylthio)-1-propen-1-yl]-1-phenyl-1H-1,2,3-triazole 5bb. ¹H NMR (400 MHz, CD₂Cl₂): δ = 7.89 (s, 1H), 7.75 (d, *J* = 8.0 Hz, 2H), 7.54 (m, 2H), 7.45 (t, *J* = 7.4 Hz, 1H), 6.31 (s, 1H), 2.88 (q, *J* = 7.4 Hz, 2H), 2.28 (s, 3H), 1.35 (t, *J* = 7.4 Hz, 3H) ppm. ¹³C NMR (100 MHz, CD₂Cl₂): δ = 146.4 (s), 137.9 (s), 137.6 (s), 130.3 (d), 129.1 (d), 120.9 (d), 119.1 (d), 110.6 (d), 26.1 (t), 21.1 (q), 13.8 (q) ppm. Anal. Calcd for C₁₃H₁₅N₃S: *m/z* 246.1059 [M + H]⁺. Found: MS (ESI) *m/z* 246.1061 [M + H]⁺.

4-[(1E)-2-(Butylthio)-1-propen-1-yl]-1-phenyl-1H-1,2,3-triazole 5bd. ¹H NMR (400 MHz, CD₂Cl₂): δ = 7.88 (s, 1H), 7.75 (d, *J* = 7.9 Hz, 2H), 7.55 (m, 2H), 7.46 (t, *J* = 7.4 Hz, 1H), 6.31 (s, 1H),

2.87 (t, *J* = 7.4 Hz, 2H), 2.28 (s, 3H), 1.68 (quint, *J* = 7.4 Hz, 2H), 1.48 (sext, *J* = 7.5 Hz, 2H), 0.96 (t, *J* = 7.3 Hz, 3H) ppm. ¹³C NMR (100 MHz, CD₂Cl₂): δ = 146.5 (s), 138.2 (s), 137.7 (s), 130.3 (d), 129.1 (d), 120.9 (d), 119.0 (d), 110.5 (d), 31.8 (t), 31.0 (t), 22.8 (t), 21.2 (q), 14.0 (q) ppm. Anal. Calcd for C₁₅H₁₉N₃S: *m/z* 274.1372 [M + H]⁺. Found: MS (ESI) *m/z* 274.1377 [M + H]⁺.

4-[(1E)-2-(Methylthio)-1-buten-1-yl]-1-phenyl-1H-1,2,3-triazole 5ca. ¹H NMR (400 MHz, CD₂Cl₂): δ = 7.86 (s, 1H), 7.75 (d, *J* = 8.0 Hz, 2H), 7.55 (m, 2H), 7.46 (t, *J* = 7.4 Hz, 1H), 6.08 (s, 1H), 2.69 (q, *J* = 7.5 Hz, 2H), 2.38 (s, 3H), 1.25 (t, *J* = 7.5 Hz, 3H) ppm. ¹³C NMR (100 MHz, CD₂Cl₂): δ = 146.4, 146.0, 137.7, 130.3, 129.1, 121.0, 118.7, 107.5, 27.9, 15.3, 13.7 ppm. Anal. Calcd for C₁₃H₁₅N₃S: *m/z* 246.1059 [M + H]⁺. Found: MS (ESI) *m/z* 246.1059 [M + H]⁺.

3,5-Dibromo-2-(trimethylsilyl)selenophene 13. 2,3,5-Tribromoselenophene³³ was obtained by bromination of commercially available selenophene according to the literature³⁴ in 92% yield (¹H NMR (200 MHz, CDCl₃): δ = 7.11 (s, 1H) ppm. ¹³C NMR (50 MHz, CDCl₃): δ = 134.9 (d), 115.4 (s), 114.6 (s), 112.9 (s) ppm. Spectral data (NMR) are given in the Supporting Information. Anal. Calcd for C₄HBr₂Se: *m/z* 365.68 [M]⁺. Found: MS (EI) 365.71 *m/z* [M]⁺. To a solution of 2,3,5-tribromoselenophene (5.0 g, 13.6 mmol, 1.0 equiv) in anhydrous Et₂O (50 mL) was added *n*-BuLi (5.4 mL, 13.6 mmol, 2.5 M in hexanes, 1.0 equiv) dropwise at –78 °C. The reaction was stirred for 30 min; subsequently chlorotrimethylsilane (1.8 g, 16.3 mmol, 1.2 equiv) was added, and the solution was allowed to warm to rt and stirred overnight. The mixture was poured on water and the aqueous phase extracted with Et₂O. The organic layers were washed with brine, dried over anhydrous Na₂SO₄, and concentrated under reduced pressure. **13** (3.9 g, 79%) was isolated by distillation in vacuo. BP: 62 °C (1.6 × 10^{–1} mbar). ¹H NMR (200 MHz, CD₂Cl₂): δ = 7.30 (s, 1H), 0.40 (s, 9H) ppm. ¹³C NMR (50 MHz, CD₂Cl₂): δ = 144.9 (s), 138.5 (d), 119.5 (s), 117.0 (s), –0.1 (q) ppm. Anal. Calcd for C₇H₁₀Br₂SeSi: *m/z* 359.81 [M]⁺. Found: MS (EI) *m/z* 359.87 [M]⁺.

3-Bromo-5-methyl-2-(trimethylsilyl)selenophene 14. To a solution of **13** (3.9 g, 10.8 mmol, 1.0 equiv) in anhydrous Et₂O (50 mL) was added *n*-BuLi (4.3 mL, 10.8 mmol, 2.5 M in hexanes, 1.0 equiv) dropwise at –78 °C. The solution was stirred for 30 min; subsequently, dimethyl sulfate (1.6 g, 13.0 mmol, 1.2 equiv) was added, and the reaction was allowed to warm to rt and stirred overnight. The mixture was poured on water and the aqueous phase extracted with Et₂O. The organic layers were washed with brine, dried over anhydrous Na₂SO₄, and concentrated in vacuo. Distillation (under reduced pressure) yielded **14** (2.2 g, 69%). BP: 70 °C (3.3 × 10^{–1} mbar). ¹H NMR (200 MHz, CDCl₃): δ = 6.98 (d, *J* = 1.1 Hz, 1H), 2.55 (d, *J* = 1.1 Hz, 3H), 0.37 (s, 9H) ppm. ¹³C NMR (50 MHz, CDCl₃): δ = 151.1 (s), 138.1 (s), 133.6 (d), 116.3 (s), 17.8 (q), –0.3 (q) ppm. Anal. Calcd for C₈H₁₃BrSeSi: *m/z* 295.91 [M]⁺. Found: MS (EI) *m/z* 295.86 [M]⁺.

Trimethyl[(3Z)-4-(methylseleno)-3-penten-1-yn-1-yl]silane 15. A solution of **14** (1.47 g, 5.0 mmol, 1.0 equiv) in anhydrous Et₂O (50 mL) was cooled to –78 °C. At this temperature *t*-BuLi (6.4 mL, 11.0 mmol, 1.7 M in pentane, 2.2 equiv) was added dropwise. The solution was allowed to warm to –20 °C, kept at this temperature for 30 min, and again cooled to –78 °C. Na₂SO₃ (1.50 g, 12.0 mmol, 2.4 equiv) and subsequently iodomethane (1.69 g, 12.0 mmol, 2.4 equiv) were added, and the mixture was allowed to warm to rt and stirred overnight. The reaction was poured on water and the aqueous phase extracted with Et₂O. The organic layers were washed with brine, dried over anhydrous Na₂SO₄, and concentrated under reduced pressure. Purification by column chromatography (light petroleum/EE (1%)) gave **15** (0.75 g, 65%). ¹H NMR (200 MHz, CDCl₃): δ = 5.70 (m, 1H), 2.19 (s, 3H), 2.14 (m, 3H), 0.20 (s, 9H) ppm. ¹³C NMR (50 MHz, CDCl₃): δ = 146.7 (s), 106.3 (d), 102.4 (s), 100.6 (s), 23.8 (q), 4.3 (q), –0.05 (q) ppm. Anal. Calcd for C₉H₁₆BrSeSi: *m/z* 232.0255 [M + H]⁺. Found: MS (APCI) *m/z* 233.0255 [M + H]⁺.

4-[(1Z)-2-(Methylseleno)-1-propen-1-yl]-1-phenyl-1H-1,2,3-triazole 16. To a *t*-BuOH/H₂O (1:1, 2 mL, ~0.5 M) suspension of **14** (213 mg, 0.92 mmol, 1.0 equiv), azidobenzene (137 mg, 1.15 mmol, 1.25 equiv), CuSO₄·5H₂O (46 mg, 0.18 mmol, 20 mol %), and sodium ascorbate (73 mg, 0.37 mmol, 40 mol %) was added potassium

fluoride (64 mg, 1.10 mmol, 1.2 equiv) in a sealed vial under oxygen-free conditions. The solution was heated to 150 °C in a microwave reactor for 30 min. The reaction mixture was diluted with water and extracted repeatedly with CHCl₃. The combined organic layers were washed with brine and dried over anhydrous Na₂SO₄. Suction filtration and evaporation of the solvent followed by column chromatography (light petroleum/Et₂O (25% → 30%)) afforded **16** (77 mg, 30%) as colorless needles. MP: 83–85 °C. ¹H NMR (400 MHz, CD₂Cl₂): δ = 8.23 (s, 1H), 7.76 (d, *J* = 8.1 Hz, 2H), 7.56–7.53 (m, 2H), 7.45 (d, *J* = 7.4 Hz, 1H), 6.83 (s, 1H), 2.36 (s, 3H), 2.26 (s, 3H) ppm. ¹³C NMR (100 MHz, CD₂Cl₂): δ = 146.4 (s), 137.7 (s), 133.7 (s), 130.3 (d), 129.1 (d), 121.0 (d), 120.0 (d), 116.8 (d), 25.9 (q), 5.4 (q) ppm. Anal. Calcd for C₁₂H₁₃N₃Se: *m/z* 280.0348 [M + H]⁺. Found: MS (ESI) *m/z* 280.0344 [M + H]⁺.

RESULTS AND DISCUSSION

Overview. To acquire a more detailed understanding of the structure–property relationship of the previously developed novel family of NLO active materials,¹⁰ the initial compound **4ba** was subjected to systematic investigations regarding the influence of structural and electronic modifications on quadric NLO properties (Figure 1).

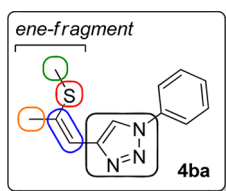


Figure 1. Intended structural and electronic modifications of the initial compound **4ba**.

Besides the technological application, we were also interested in the crystallization behavior: does the particular configuration of the molecules under investigation indeed promote chiral or noncentrosymmetric crystallization?

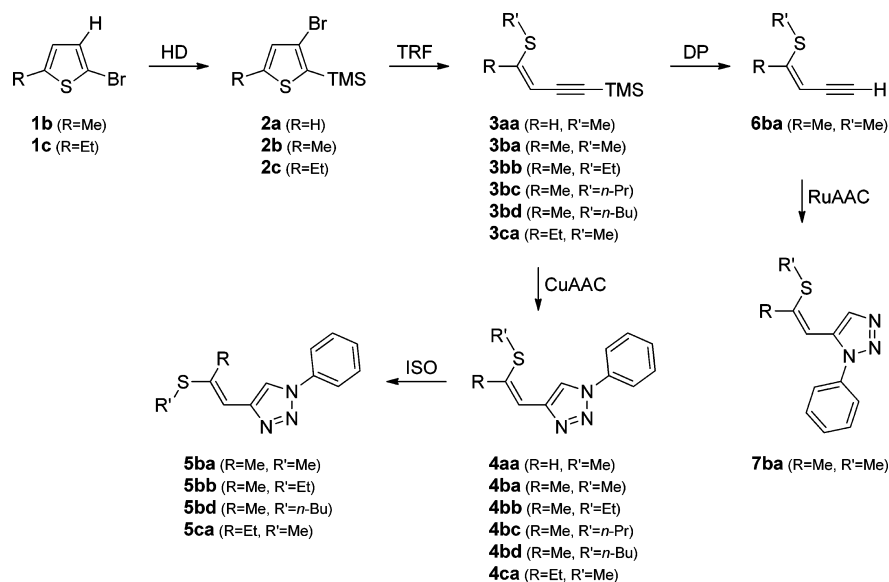
The variations and modifications include alkyl group variations at the sulfur (green) as well as at the double bond (orange), selective sulfur oxidation (red), sulfur–selenium exchange (red), and isomerization at the double bond (blue; stereoisomers) or the 1,2,3-triazole motive (black; regioisomers). The phenyl group was held constant throughout the study.

After two subchapters on general synthetic methods and structural features common to all molecules, each class of applied molecular variations will be discussed in a separate subchapter. The subchapters will be divided into parts detailing synthesis, crystal chemistry, and NLO properties. A comprehensive collection of the relevant crystallographic parameters is given in the Supporting Information.

Synthesis. The synthetic approach (Scheme 1) primarily relies on two types of reactions: (1) the base-induced thiophene ring-fragmentation (TRF) reaction^{10,14–16,23,35,36} and (2) the copper(I)-catalyzed azide–alkyne cycloaddition (CuAAC),^{37,38} typically referred to as one of the most reliable reactions within the “click”-chemistry concept.^{11–13} Remarkably, both the TRF as well as the CuAAC reactions yield the desired compounds selectively as stereo- (*Z*-isomers **3**) or regioisomers (1,4-isomers **4**), respectively.

The *Z*-selectivity is given by the cyclic structure of the thiophene precursor, which can be readily obtained from a halogen dance (HD)^{39–42} reaction. The specific substitution pattern is essential for an efficient ring opening yielding the desired ene–yne compounds **3**.^{14–16} During the cycloaddition of alkynes **3** and azidobenzene, the formation of the different species is prevented by copper catalysis yielding pure 1,4-regioisomers of 1,2,3-triazoles **4**.^{37,38} Further, a selective synthesis of the 1,5-regioisomer **7ba** is accomplished from the terminal alkyne species **6ba** (F[−]-induced TMS cleavage) by ruthenium catalysis (RuAAC).^{32,43} Microwave-assisted synthesis^{10,44–46} was pointed out to significantly accelerate these metal-assisted cycloadditions for this substance class.^{10,32,44} The

Scheme 1. General Synthetic Approach Towards Target Materials **4**, **5**, and **7a**^a



^aHD: halogen dance reaction. TRF: thiophene ring fragmentation. CuAAC: copper(I)-catalyzed azide–alkyne cycloaddition. ISO: isomerization (acid-induced). DP: deprotection (F[−]-induced). RuAAC: ruthenium-catalyzed azide–alkyne cycloaddition.

Table 1. Crystal Class and Characteristic Angles in the Crystal Structures under Investigation: Tilt Angles of the Least Squares (LS) Planes of the Aromatic Rings, Torsion Angles between the S-Alkyl Group and the Ene Fragment, and Tilt Angles of the LS Planes of the Triazole and the Ene Fragment

compound	crystal class	benzene/triazole tilt angle [deg]	C=CH–S–C torsion angle [deg]	triazole/ene fragment tilt angle [deg]
4aa	2/m, centrosymmetric	36.87(8)	168.38(15)	-
4ba	222, enantiomorph	8.87(8)	153.96(15)	7.38(18)
4bb	222, enantiomorph	15.74(7)	161.17(10)	9.39(14)
4bd	2/m, centrosymmetric	16.88(9)	167.71(14)	1.56(18)
4ca, polymorph 1	m, noncentrosymmetric	12.28(4)	177.52(5)	3.21(8)
4ca, polymorph 2	2/m, centrosymmetric	24.54(6)	163.80(11)	2.16(14)
5ba	$\bar{1}$, centrosymmetric	31.49(6)	2.09(11)	21.76(13)
7ba	222, enantiomorph	39.48(6)	171.55(10)	24.82(13)
9ba	2/m, centrosymmetric	24.06(5)	72.04(10)	4.07(12)
12ba	mm2, noncentrosymmetric	24.83(5)	99.86(8)	9.08(12)
16	222, enantiomorph	6.83(11)	173.32(17)	8.3(2)

conversion of the *Z*- to the *E*-isomer (**5**) is accomplished by acid-induced isomerization.

Crystallography. In solution all molecules described in this manuscript are flexible and achiral, allowing for a straightforward synthetic access. Indeed, the average symmetry of the molecules can be considered *m*, with the mirror plane coinciding with the main molecular plane defined by the conjugated aromatic system (phenyl/triazole/ene-fragment). However, the molecules possess rotational barriers preventing *m* symmetry in the solid state, namely, the twist angle between the phenyl and the triazole rings, the C=CH–S–C torsion angle, and the twist angle between the triazole ring and the ene fragment. All of these are mainly attributed to steric interactions: The tilt of benzene and triazole is caused by the steric repulsion of the H atoms of the aromatic systems and has been intensely discussed for the case of biphenyl.⁴⁷ The out-of-plane conformation is a consequence of alkyl–alkyl group interactions between the S-alkyl and the alkyl moieties of the ene fragment as previously energetically quantified by theoretical calculations.¹⁰ Finally, the tilting of the triazole and the ene fragment can be explained by steric repulsion of the S atom and the H atom of the triazole.

Indeed, in all crystal structures under investigation, at least the benzene/triazole tilt angle is distinctly nonzero (Table 1), and the molecules are therefore located on general positions. Thus, in the solid state the presented molecules behave as chiral molecules. We observed three crystallization behaviors: “chiral resolution” toward enantiomorphous crystals, polar “racemates” without center of symmetry (enantiomorphs, which are related by glides only), and centrosymmetric “racemates” (Table 1). Only the former two are capable of quadric NLO activity. All structures under investigation were crystallographically simple, containing only one crystallographically unique molecule (*Z'* = 1) located on a general position.

The fact that all the molecules contained sulfur or selenium atoms (*Z* ≥ 16) and that complete spheres of the reciprocal space were collected enabled us to analyze the chirality/polarity of the investigated crystals. In general we were able to unambiguously determine the absolute structure;⁴⁸ i.e., the crystals under investigation were not twinned by inversion. Thus, we demonstrated the possibility to grow macroscopic single-domain crystals, which are of crucial importance for the application as NLO materials. We attribute this to the tight packing of the molecules and the lack of higher local symmetry which makes it impossible for the structure to “flip” to the opposite chirality/polarity. A notable exception is the crystal

structure of **4aa**, in which the benzene rings are arranged in layers with higher symmetry leading to OD twinning.²²

Alkyl Variations (R'–S, R–C=C). Although the variations of the alkyl groups on both the sulfur atom and the double bond are not expected to significantly affect the π -electron system and thus the second-order hyperpolarizability, the impact of molecular packing and the associated structural anisotropy on NLO properties are matters of interest.

Synthesis. The synthesis of the TRF precursor **2b** and **2c** relies on the application of a halogen dance (HD) reaction. It is worth mentioning that during our research on NLO materials the HD reaction has emerged as an efficient method to obtain the desired 3-bromothiophene derivatives, suitable as TRF precursors (yields of 83% (**2b**)⁴⁹ and 80% (**2c**)).

Substances **2a** and **3aa** were obtained via a metal halogen exchange reaction from 2,3-dibromothiophene utilizing *n*-BuLi and a standard TRF procedure, respectively, as recently published by our group.²²

For alkyl variations at the sulfur group, the substituent R (at the double bond) was limited to methyl (R = Me). Thus, all ring-opening reactions toward **3b(a–d)** were performed using thiophene species **2b**. A protocol for an efficient synthesis of **3ba** and **4ba** was recently described in detail in the literature by our group.¹⁰ The pathway toward ene–yne compounds **3bb** and **3bc** was accomplished by a similar TRF protocol applying iodoethane and 1-iodopropane, respectively. For the reaction toward **3bb** (51% isolated yield) also the organo-lithium species was replaced by commercially available EtLi (ethylolithium) to avoid the *n*-butyl-substituted byproduct **3bd** as a result of the formation of 1-bromobutane during the metal halogen exchange using *n*-BuLi. The use of alkyl bromides was found to be less efficient and selective. Functionalization of **3bb** toward target material **4bb** (61% yield) was accomplished by the standard CuAAC procedure. In contrast, **3bc** was isolated as a mixture of **3bc** and **3bd** (27.5 mol % content of **3bd**) due to the application of *n*-BuLi. The separation of these substance was not possible for ene–yne species **3bc** and **3bd**; however, pure target compound **4bc** (68% corrected yield, see Experimental Section for details) was afforded by column chromatography after the cycloaddition step. Compounds **3bd** and **4bd** (62% corrected yield) were isolated as byproducts of the reactions mentioned before. Due to the centrosymmetric crystallization of **4bd** (see crystallographic discussion below), no further reaction optimization was performed; however the synthesis of **3bd**, which can be readily converted into **4bd**, has been described in the literature.²³ The introduction of

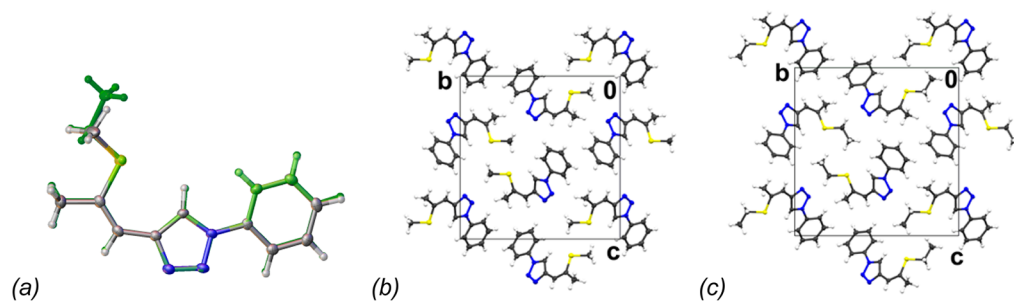


Figure 2. Graphical overlay (a) of the molecular structures of **4bb** and **4ba** (green) and crystal structures of **4ba** (b) and **4bb** (c) viewed down [100]. C, H, N, and S atoms are gray, white, blue, and yellow, respectively.

hydrogen ($R' = H$), as performed for the substituents at the double bond, was not intended as a result of instability of the formed ene–yne species, which was isolated as thioenol ether.⁵⁰

The syntheses of **3ca** and **4ca** were performed in analogy to the just described **3b** and **4b** series. Similarly good yields of 78% for **3ca** and 69% for **4ca** were obtained.

Due to a significantly decreased tendency of crystallization (melting points of 82 °C (**4ba**) vs 44–45 °C (**4ca**)) and the lack of NLO activity of **4bd** and **4ca** (see discussion below), no further effort was put into the synthesis of further alkyl-chain elongated structures (R at the double bond) or a possible diethylated compound (R = Et, $R' = Et$).

Crystallography. Compound **4aa**²² crystallizes in the centrosymmetric space group $P2_1/c$ and therefore does not fulfill the basic requirement for quadric NLO properties. However, an interesting OD-twinning was observed and discussed in detail in another paper.²²

The crystal structure of **4bb**⁵¹ is isostructural⁵² to the initial compound **4ba**.¹⁰ Moreover, highly similar crystal morphology was observed for both materials. As shown in Figure 2(a), the conformation of both molecules in the solid state is virtually identical. Thus, **4bb** represents a potential candidate for SHG.

The extra space needed by the elongation of the thiomethyl to a thioethyl group is provided by an enlarging of the lattice parameters b (15.4009(6) to 15.968(6) Å) and c (15.6421(5) to 16.294(6) Å). Indeed, the thioalkyl groups extend nearly parallel to the (100) plane (Figure 2(b,c)). The additional space in the (100) plane allows for a denser packing in the [100] direction: the a parameter decreases slightly (4.8314(2) to 4.7643(15) Å). In total, and as expected, the unit cell volume of the thioethyl compound is distinctly larger (1163.90(8) vs 1239.6(8) Å³). The geometries of the molecules differ slightly, probably due to packing effects; most notably the tilt angle of the aromatic rings increases from 8.87(8)° to 15.74(7)°, due to the less dense packing (Table 1).

4bc was isolated as colorless oil which did not crystallize; however, single crystals of **4bd**⁵³ could be prepared. The crystal structure of **4bd** is centrosymmetric (space group $P2_1/c$) and unrelated to the structures of **4ba** and **4bb**. Indeed, as has been noted by Kálmán,⁵² isotypic structures can only be expected for replacement of a H atom by a single methyl group, but not with longer alkyl chains. As opposed to the three-dimensional network of **4ba**, a distinct separation into layers composed of the alkyl side chains and the aromatic systems was observed for **4bd** (Figure 3). We expect this effect to become even more pronounced for further thioalkyl group elongation.

4ca⁵⁴ (Figure 4) is dimorphic: Polymorph 1 (Cc) is noncentrosymmetric, whereas the symmetry of polymorph 2 ($P2_1/c$) includes inversion symmetry. Crystals of both

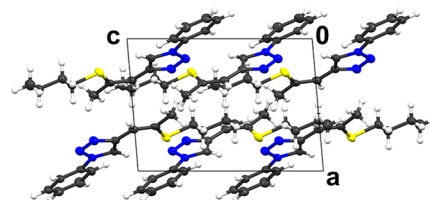


Figure 3. Crystal structure of **4bd** viewed down [010] showing separation into aliphatic and aromatic layers; color codes as in Figure 2.

polymorphs were extracted from the same crystallization experiment. Whereas the overall geometries of the molecules in both polymorphs are similar, they feature distinctly different tilt angles (Table 1), demonstrating the importance of packing effects. Notably, the benzene/triazole tilt angle is twice as large in polymorph 2 (24.54(6)° vs 12.28(4)°). Uniquely among the *Z*-isomers, the polymorph 1 of **4ca** features an in-plane conformation of the *S*-Me group ($C=C-S-C$ torsion angle of 177.52(5)°).

NLO Properties. The SHG signal detected for **4bb** was virtually identical to reference **4ba** ($4ba/4bb = 1/\sim 0.95$), which exhibits an SHG efficiency of somewhat higher than twice the value of KDP. This is expected, given the similar unit cell volumes (1163.90(8) vs 1239.6(8) Å³) and the virtually identical π -electron architectures.

XRD of the bulk powdered **4ca** sample revealed that the centrosymmetric polymorph 2 is the major component. No significant peaks attributed to the potentially NLO-active polymorph 1 were observed. Indeed, no SH signal was observed for the **4ca** sample (detection limit of the SH setup was about 1% of the KDP signal). So far the formation conditions of both polymorphs as well as the thermodynamic stability ranges are not understood. It has to be noted, though, that **4ca** is not a candidate for optical applications due to its low melting point (44–45 °C).

Double Bond Isomerization. As a second step, the influence of the *Z*-geometry of the double bond was examined, to give insight into structure–function relationships of compounds of identical molecular constitution.

Synthesis. The first evidence of isomerization was observed during NMR experiments on **4ba** using $CDCl_3$. Ion chromatography showed a chloride content of ~ 280 ppm, which was attributed to the decomposition of $CDCl_3$ resulting in the formation of DCl .⁵⁵ Hence, the synthesis of *E*-isomer **5ba** was performed by acid-induced isomerization on the experimental scale (isolated yield **5ba**: 42%).

Crystallography. The *E*-isomer **5ba**⁵⁶ crystallizes in the centrosymmetric space group $P\bar{1}$ (Figure 5(a)); therefore, no

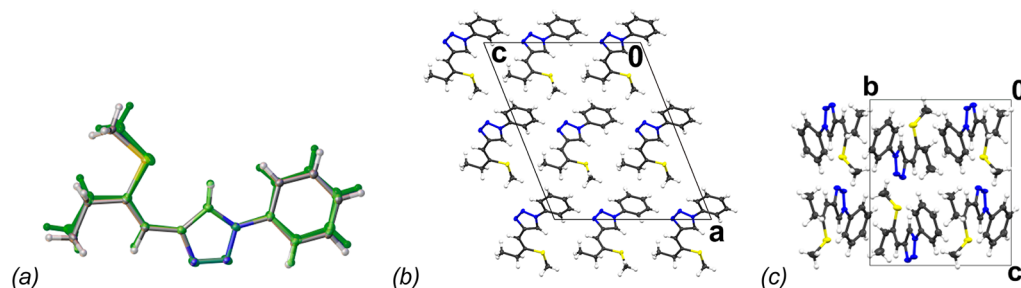


Figure 4. Graphical overlay (a) of the molecular structures of polymorphs 1 and 2 (green) of **4cb** and crystal structures of polymorph 1 viewed down [010] (b) and polymorph 2 viewed down [100] (c); color codes as in Figure 2.

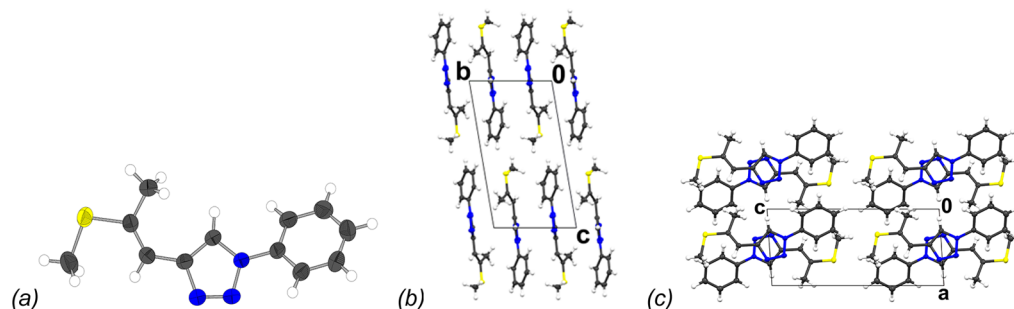


Figure 5. Molecular (a) and crystal structure (b,c) of **5ba**, viewed down [100] and [010], respectively, showing the coplanar arrangement of the triazole rings; color codes as in Figure 2, and ellipsoids are drawn at 90% probability level.

SHG experiments were performed. The most striking difference to the *Z*-isomer **4ba** is the lack of intramolecular thiomethyl to ene-methyl interactions. Indeed, in **5ba** the thiomethyl group is practically in-plane with the ene fragment ($C=C-S-C$ torsion angle of $2.09(11)^\circ$ vs $153.96^\circ = 180 - 26.04(15)^\circ$ for **4ba**). In return, the LS (least-squares) planes of the propenyl group and the triazole are distinctly more tilted ($21.76(13)^\circ$) than in the *Z*-isomers, probably due to steric repulsion of the ene-methyl group and the proton of the triazole.

The **5ba** molecules are arranged in rods running along [010], whereby two adjacent molecules are related by inversion. The planes of the triazole rings are nearly coplanar with a centroid to centroid distance of 3.422 Å. The rods in turn are arranged to layers parallel to (001) which connect via the phenyl rings and the thiomethyl groups (Figure 5(b,c)).

Isomerization Experiments. To further investigate the phenomenon of acid-induced isomerization, effects of the aforementioned variations of the alkyl groups (**4a–c**) on isomerization rates and equilibrium states of this process were evaluated. The reactions, monitored by NMR spectroscopy, were carried out in standard NMR tubes utilizing the same batch of $CDCl_3$ (chloride content of ~ 280 ppm) for all experiments.

The results illustrated in Figure 6 reveal relatively similar reaction rates for all compounds but a significant difference in the equilibrium states for **4ba** ($R = Me, R' = Me$) compared to **4bb** ($R = Me, R' = Et$), **4bd** ($R = Me, R' = n-Bu$), and **4ca** ($R = Et, R' = Me$). The equilibrium states follow the order of **4ba** < **4bd** \leq **4bb** = **4ca** (relative *Z*-amounts for **4ba**: 43%, **4db**: 55%, and **4bb**, **4ca**: 56%). In fact, identical *E/Z*-ratios starting from both the pure *Z*- (**4ba**) and *E*-isomer (**5ba**) indicate that complete equilibration is reached during the experiments. Surprisingly, for compound **4aa** ($R = H, R' = Me$) no isomerization progress could be observed. Analytic samples of *E*-isomers **5bb**, **5bd**, and **5ca** were isolated by preparative TLC

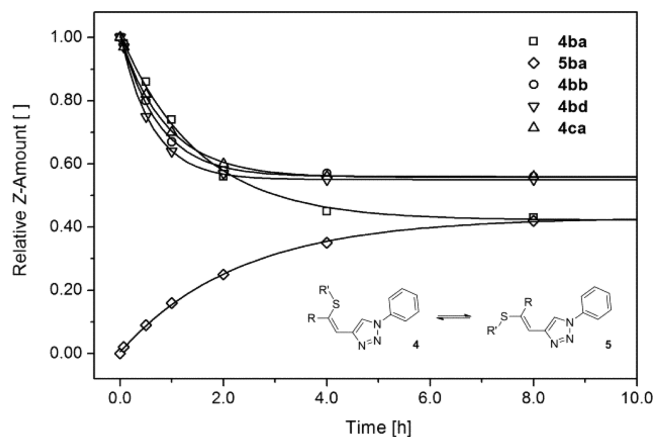


Figure 6. Acid-induced isomerization experiments (concentration: ~ 80 mM).

(quantitative separations) and characterized by NMR and MS to ensure identity.

Triazole Modification. In this subchapter the effect of regioisomerization, directly influencing electronic properties of the 1,2,3-triazole, is examined. Retaining the principal substitution pattern (identical sum formula), the characteristics of the 1,5-regioisomer **7ba** in relation to the 1,4-compound **4ba** are determined.

Synthesis. The synthesis is based on microwave-assisted Ru-catalyzed cycloaddition of terminal alkyne **6ba** and azidobenzene affording 39% of 1,5-species **7ab**.³² The rather low yield is attributed to a limited stability of **6ba** under RuAAC conditions. More sophisticated reaction optimization, which is beyond the scope of this study, may be achieved by applying, e.g., recently developed transition-metal-free methods.⁵⁷ Compound **6ba** was obtained by F^- -induced silyl cleavage utilizing TBAF in 76% yield.

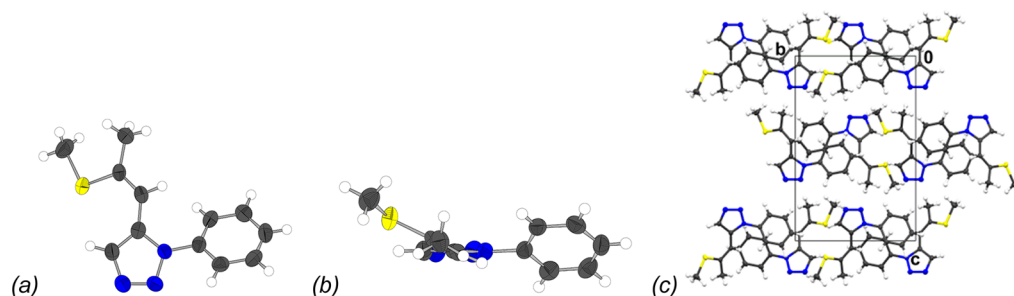


Figure 7. Molecular structure (a,b) showing the configuration and the out-of-plane conformation of the ene fragment and crystal structure (c) of **7ba** viewed down [100] showing the layered arrangement; color codes as in Figure 2, and ellipsoids are drawn at the 90% probability level.

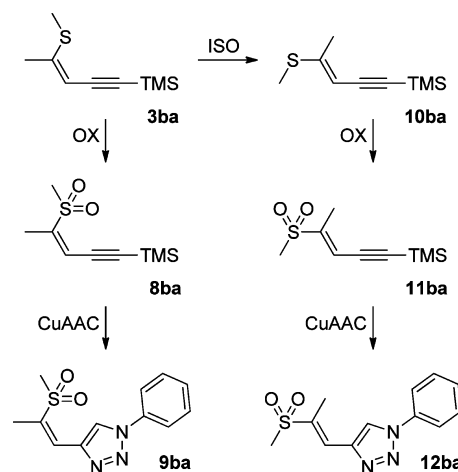
Crystallography. The crystal structure of **7ba**⁵⁸ is enantiomorphic (space group $P2_12_12_1$). The unique feature of **7ba** compared to the 1,4-isomers is the steric repulsion of the protons of the ene fragment and the phenyl ring (Figure 7(a,b)). In consequence, **7ba** features an even more intense tilting of the ene fragment to the triazole ($24.82(13)^\circ$) than **5ba** and additionally an unusually large tilting of the phenyl and triazole rings ($39.48(6)^\circ$). The thiomethyl group is located slightly out-of-plane like in most other *Z*-isomers (with the exception of **4ca**). Molecules of **7ba** are arranged in distinct layers parallel to (001), as opposed to the three-dimensional network of the original **4ba** (Figure 7(c)).

NLO Properties. The SHG signal detected for **7ba** was ~ 1.25 times higher than the value of **4ba**, corresponding to a 10% enhancement of the nonlinear susceptibility. It is hard to tell whether this rather small improvement is due to changes in the molecular hyperpolarizability or to the aforementioned structural modifications. Moreover, the limited synthetic yield, which is currently subject to optimization in our group, is a drawback of the 1,5-isomer for this specific class of compounds.

Sulfur Oxidations. The oxidation of the methylthio group (+M-effect) toward the sulfone moiety (−M-effect) represents a crucial alteration in terms of electronic and crystallo-chemical properties and also crystallization behavior due to the introduction of hydrogen bond acceptors. The previous concept of the ene fragment displaying the donor part and the triazole unit being the acceptor part of the NLO chromophore is no longer valid for this class of materials. The *Z*-isomer showed centrosymmetric crystallization (structures discussed in detail below), which ruled out the existence of quadric NLO properties. Due to the sustained interest in the oxidized scaffold as NLO materials, the *E*-isomer was prepared, which revealed the desired noncentrosymmetric crystallization.

Synthesis. The approach toward target structures **9ba** and **12ba** is based on an oxidation procedure of the ene fragment utilizing *m*-CPBA (Scheme 2). Due to the formation of benzoic acid as byproduct and the aforementioned tendency of isomerization of the target materials, it was not possible to directly convert triazole-based compounds **4ba** and **5ba** into structures **9ba** and **12ba**. Therefore, the oxidation was performed at the stage of the ene–yne species **3ba** and **10ba**, which were found to be less prone to isomerization. In accordance to previously described protocols²⁹ **3ba** and **10ba** were reacted with *m*-CPBA to isolate **8ba**³⁰ and **11ba** in yields of 81% and 61%, respectively. The reaction of **3ba** toward **10ba** was also performed by acid-induced isomerization affording the *E*-species in yields of 37%. Finally, the CuAAC resulted in target compounds **9ba** (70%) and **12ba** (57%) in good yields.

Scheme 2. Synthetic Pathway Towards Sulfone Species **9ba** and **12ba**^a



^aOX: oxidation (*m*-CPBA), ISO: acid-induced isomerization, CuAAC: copper(I)-catalyzed azide–alkyne cycloaddition.

Crystallography. As mentioned before, the *Z*-isomer **9ba**⁵⁹ crystallizes in the centrosymmetric space group $P2_1/n$, whereas the *E*-isomer **12ba**⁶⁰ crystallizes in the noncentrosymmetric space group $Pna2_1$ (Figure 8). Both crystal structures feature similar tilting angles between the propenyl group and the triazole core ($4.07(12)^\circ$ and $9.08(12)^\circ$) as well as between the phenyl and triazole moieties ($24.06(5)^\circ$ and $24.83(5)^\circ$ for **9ba**

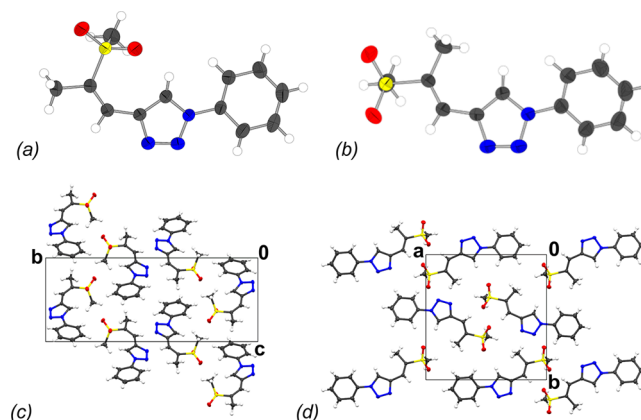


Figure 8. Molecular (a,b) and crystal (c,d) structures of **9ba** (a,c) and **12ba** (b,d); crystal structures are viewed down [100] (**9ba**) and [001] (**12ba**), respectively; color codes as in Figure 2, and ellipsoids are drawn at 90% probability level.

Table 2. Hydrogen Bond Geometries in 9ba Involving the Sulfonyl Group

C–H...O	symmetry code of acceptor	C–H [Å]	H...O [Å]	C...O [Å]	C–H...O [deg]
C7–H7...O1	intramolecular	0.909(16)	2.317(15)	2.9187(14)	123.5(11)
C2–H2...O2	$x - 1/2, -y + 1/2, z - 1/2$	0.954(17)	2.599(17)	3.5301(15)	165.2(14)
C11–H112...O1	$x + 1, y, z$	1.032(17)	2.353(17)	3.3606(14)	164.9(13)

Table 3. Hydrogen Bond Geometries in 12ba Involving the Sulfonyl Group

C–H...O	symmetry code of acceptor	C–H [Å]	H...O [Å]	C...O [Å]	C–H...O [deg]
C9–H9...O1	intramolecular	0.951(13)	2.396(13)	2.8482(10)	108.8(9)
C2–H2...O2	$y - 1/2, -y + 1/2, z$	0.967(12)	2.405(12)	3.3073(11)	155.0(11)
C7–H7...O2	$y - 1/2, -y + 1/2, z$	0.917(13)	2.480(13)	3.3632(10)	161.9(11)
C2–H3...O1	$x - 1, y, z$	0.915(15)	2.593(14)	3.2647(11)	130.7(11)
C12–H121...O1	$-x + 2, -y, z - 1/2$	0.979(15)	2.501(15)	3.4735(13)	172.3(11)

and 12ba, respectively (Table 1)). The most striking difference compared to the nonoxidized molecules though is the extreme out-of-plane conformation of the sulfonyl methyl groups (C=C–S–C torsion angles of 72.04(10) and 99.86(8)°). For 9ba this can be adequately explained by an intramolecular nonclassical hydrogen bond from the triazole–H to the sulfonyl group (Table 2) which stabilizes the conformation. 12ba likewise features a possible intramolecular hydrogen bond, in this case of the ene–H atom (Table 3). It has to be noted that the C–H...O angle of 108.8(9)° is close to 100°, which is generally accepted as the lower limit of relevant H bonding.

The packings are determined by nonclassical hydrogen bonding: In 9ba, every molecule connects via two H atoms belonging to the phenyl and the triazole ring, respectively, to two further molecules forming layers parallel to (010). The hydrogen bonding network in 12ba is more complex. Each molecule connects to three further molecules forming a three-dimensional network: via two H atoms of the phenyl and the triazole to the first molecule, via a phenyl H to the second, and via a sulfonylmethyl H to the third.

NLO Properties. The SH response from the noncentrosymmetric (but nonchiral) crystals of 12ba was approximately 45% of the value of the initial compound 4ba. The electron acceptor–donor design of the scaffold, imparting the electronic bias, is still a prerequisite for an SH efficiency in this order of magnitude.⁸ In comparison to the previously developed scaffold 4ba the ene fragment changes from an electron-donating to an electron-accepting moiety. The acceptor moiety of the initial structure is represented by the 1,2,3-triazole structure, where the electron-withdrawing properties are primarily assigned to the triazole nitrogens N2 and N3. For 12ab it is not obvious at first sight which structural unit of the novel NLO chromophore represents the electron donor. The electron-donating properties potentially derive from the N1 nitrogen and/or the phenyl substituent itself, implying an ambipolarity of the triazole-phenyl unit.

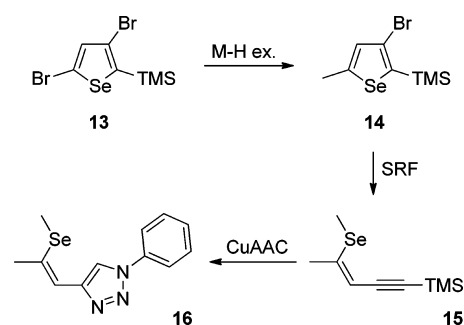
One reason for the reduced SH efficiency may also be found in the blue shift of the absorption feature of 12ba of ~30 nm compared to 4ba (Figure 12); resonances in the linear response (absorption peaks) are known to boost the nonlinear response if either the fundamental or the two-photon frequency is in the vicinity of the resonance. While this enhancement declines with increasing spectral separation, the impact of a resonance particularly on the real part of the hyperpolarizability may extend far beyond the absorption band.⁶¹ The increased spectral separation of the absorption line from the experimental

photon energy therefore may be responsible for the reduction of the observed NLO response.

Still, compound 12ba with a SH efficiency in the range of KDP remains an attractive NLO material, given its thermal properties, such as a higher melting point of 128 °C (12ba) vs 82 °C (4ca) as well as an improved stability up to ~230 °C (compared to ~180 °C of the thiomethyl-based compounds; determined by TGA measurements). Moreover, crystals of the size of roughly 2 × 2 × 1 mm could be grown from solution.

Sulfur–Selenium Exchange. In a final synthetic step, sulfur was replaced by selenium, in the intuitive expectation that the electronic configuration of Se would lead to an increased density of delocalized electrons and consequently to an enhanced hyperpolarizability.

Synthesis. Starting from 2,3,5-tribromoselenophene^{33,34} a metal halogen exchange reaction using *n*-BuLi and subsequent quenching with chlorotrimethylsilane afforded 13 in 80% yield. Another lithiation step using dimethyl sulfate as an electrophile resulted in ene–yne precursor 14 (69% yield). This sequential lithiation approach was shown to be more efficient (55% overall yield) in comparison to the HD approach (40% overall yield) as applied for the sulfur analogues. In contrast to the TRF reaction, the selenophene ring fragmentation (SRF) was performed utilizing *t*-BuLi leading to ene–yne species 15 in 65% yield. The use of *t*-BuLi arises as a consequence of the formation of Se-butyl byproduct when applying *n*-BuLi (enhanced nucleophilicity of Se⁶²). Functionalization of 15 toward target material 16 (30% yield) was accomplished by the standard CuAAC procedure (Scheme 3).

Scheme 3. Synthesis of Selenium-Based Compound 16^a

^aM–H ex: metal halogen exchange; SRF, selenophene ring fragmentation; CuAAC: copper(I)-catalyzed azide–alkyne cycloaddition.

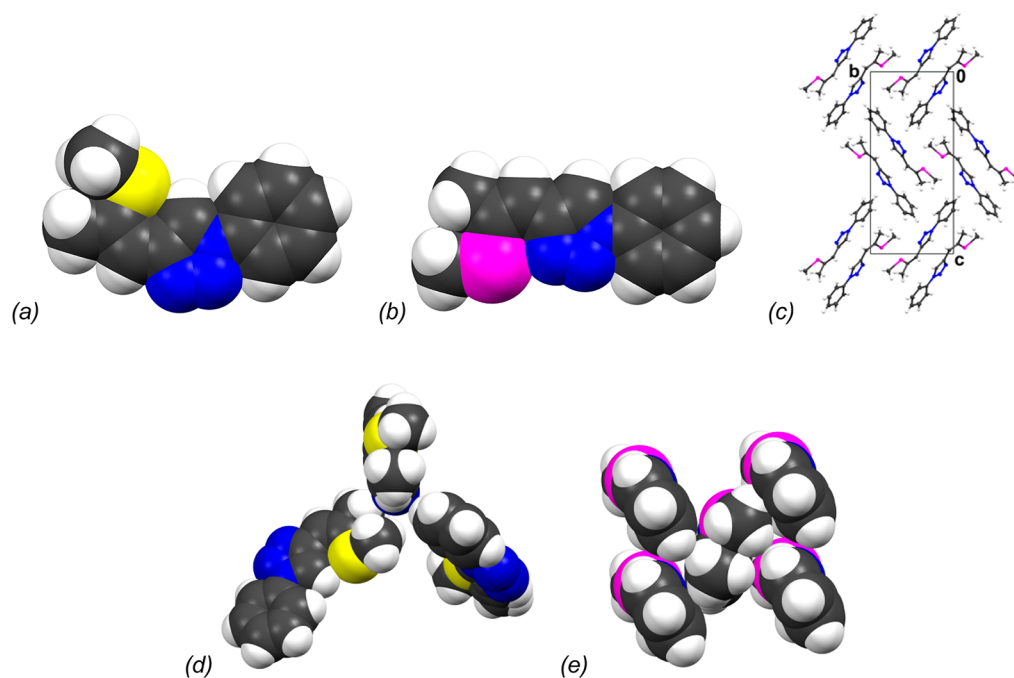


Figure 9. Space filling models of the molecular structures of **4ba** (a) and **16** (b), of intermolecular contacts in **4ba** (d) and **16** (e) viewed down the main axis of a molecule, and the crystal structure of **16** (c) viewed down $[100]$; color codes as in Figure 2, and Se atoms are colored pink.

Crystallography. The crystal structure of **16**⁶³ is enantiomorphic and isopointal (same space group $P2_12_12_1$ and same Wyckoff positions) but otherwise crystallographically unrelated to **4ba** and **4bb**. The most outstanding difference is the opposite conformation of the single bond connecting the triazole to the propenyl group: Whereas in the S-containing Z-isomers the thiomethyl group is located on the side of the C–H fragment of the triazole, the selenomethyl group is located on the opposite side near a N atom (Figure 9(a,b)). We attribute this to an increased ionic radius of Se compared to S (1.98 vs 1.84 Å)⁶⁴ and consequently more repulsion between Se and the triazole–H atom, which has also been observed for structurally related compounds crystallizing in similar modifications. The triazole/phenyl tilt angle in **16** is the smallest of any of the compounds under investigation, and likewise the out-of-plane conformation of the selenomethyl group (C=C–Se–C torsion angle of $173.32(17)^\circ$) is not pronounced. The triazole/propylene tilt angle is distinctly nonzero, possibly due to steric repulsion of the Se and N atoms.

The different molecular geometries of **4ba** and **16** lead to different packing: the packing of **4ba** is defined by C–H \cdots N contacts, resulting in an arrangement where the main axes of the connecting molecules are highly inclined to each other (Figure 9(d)). In **16**, on the other hand, the N atoms of the triazole ring are sterically “shielded” by the large Se atom. The intermolecular contacts are therefore of the C–H \cdots C kind, whereby the C–H bond is strongly inclined to the aromatic system of the adjacent molecule. Thus, the molecules are arranged in layers parallel to (001) in which the main axes of all molecules are parallel (Figures 9(c,e)). The overall arrangement of the molecules can be described as a herringbone pattern (Figure 9(c)).

NLO Properties. The examination of quadric NLO properties of **16** revealed a more than 20-fold increase of the SH efficiency over reference material **4ba** (Figure 10) or more than 40 times the value of KDP. The significantly improved

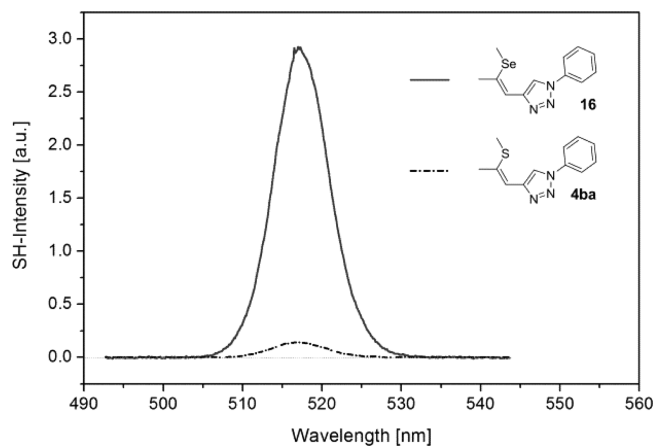


Figure 10. SHG spectra of **16** (full) and **4ba** (dash-dot); the large line width (~ 8 nm) results from the broad spectrum of the ultrashort (70 fs) driving laser pulses.

nonlinear performance of this novel NLO chromophore is attributed to the increased electron density due to the introduction of Se and an altered molecular packing, which clearly impacts the crystal anisotropy.

In summary, it could be shown that the synthetic approach allows a broad diversity of potential modifications of the initial molecular structure (**4ba**). Thus, alkyl group variations, isomerizations, oxidations, and a sulfur–selenium exchange were successfully demonstrated. As a result, four novel NLO materials have been obtained and characterized.

The results for the acquired SH efficiencies are illustrated in Figure 11. In particular, the selenium-based compound **16** reveals a significant enhancement of the SH efficiency. Compounds **4bb** and **7ba** showed similar SH values; however, an improvement of $\sim 25\%$ in performance for **7ba** also promotes the interest in 1,5-triazole isomers. Thus, experiments to improve the synthesis of 1,5-isomers are currently

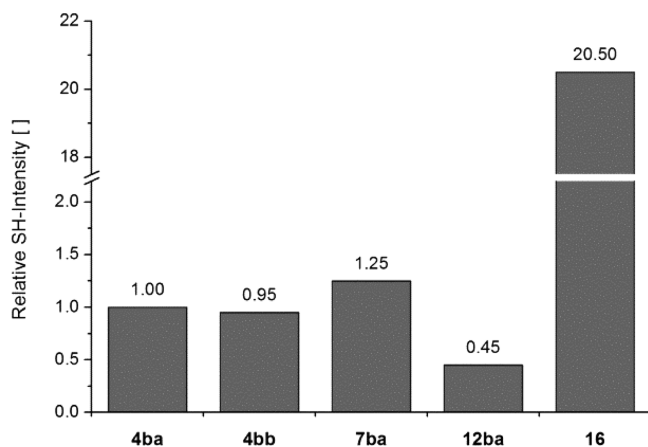


Figure 11. Relative SH intensities plotted for target materials capable of SHG.

performed. Although the sulfone species **12ba** shows a decreased SH value of $\sim 50\%$, attractive photophysical (see below) and thermal properties (stability) have been demonstrated.

As demonstrated by the dimorphic **4ca**, an important factor for NLO materials represents the phase purity. Thus, all obtained crystalline compounds capable of SHG were examined by powder diffraction experiments. Phase purity was proven for structures **4ba**, **4bb**, **7ba**, and **16**; **12ba** was obtained as a large single crystal.

It should be noted that while powder SHG measurements are useful in screening for potential frequency doubling crystals, they do not tell the whole story about the performance of a single crystal as a frequency doubler. Useful nonlinear materials must combine a host of properties such as inertness under environmental (atmospheric) conditions, sufficient optical damage threshold, and of course, the potential for phase matching. Even if phase matching can be achieved (which can be tested by the Kurtz method), it may still happen that the dominating SH coefficients do not couple efficiently to the wave propagation directions prescribed by the phase matching condition.

On the other hand, nonphase matchable compounds could still be quasi-phase matchable.⁶⁵ The successful growth of macroscopic single crystals is therefore a prerequisite not only for practical applications of nonlinear materials but also for their characterization. Systematic crystal growth and a complete optical characterization of the compounds under study are beyond the scope of the present study, however.

Another property of crucial importance is the laser-induced damage threshold (LIDT) of a nonlinear material since the efficiency of the nonlinear process increases with the intensity of the incoming laser field. In our study, which employs a low power femtosecond laser for compound screening, we have not undertaken any systematic laser-induced damage threshold studies.

However, to ensure wide transparency windows, absorption spectra (in THF) of new NLO materials were recorded. The results are depicted in Figure 12 and show similar absorption onsets for all compounds (340–350 nm) except of the sulfone species **12ba** which is blue-shifted by ~ 30 nm. Hence, good optical transparencies are guaranteed for all performed modifications.

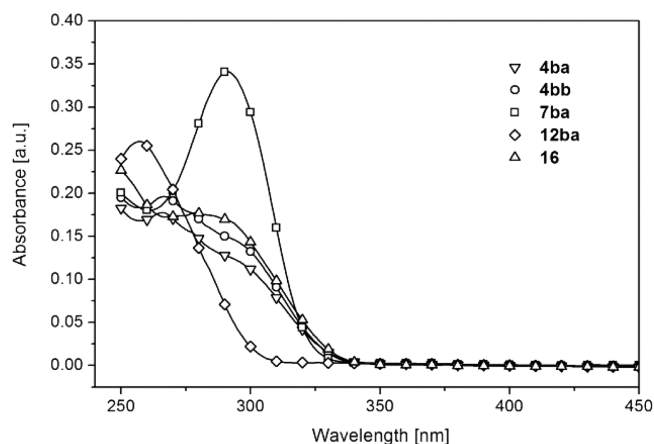


Figure 12. Absorption spectra of target NLO compounds.

Due to the general applicability of the developed strategies, efforts to improve the synthetic accessibility of ene-yne compounds are currently performed in our group.

Of the 10 investigated molecules with an alkyl(thio/sulfonyl/seleno)-alkenyl-phenyl-triazole backbone, six (60%) crystallize in a noncentrosymmetric space group and four (40%) in an enantiomorphic space group (Table 1), one showing dimorphism (the mainly observed polymorph is centrosymmetric). The dimorphism of **4ca** demonstrates the importance of polymorph control for potential applications.⁶⁶ Yet, in a recent statistical study on crystal structures of flexible achiral organic molecules with $Z' = 1$ crystallizing in one of the six most common space groups,¹⁷ only 11% of the molecules crystallized in an enantiomorphic space group (all noncentrosymmetric space groups of the six most common are enantiomorphic). Thus, the chosen backbone of our structural investigations indeed seems to promote polar crystallization. More synthetic and theoretical work will be needed to confirm the trend.

CONCLUSION

In conclusion, four novel NLO materials capable of SHG have been designed, synthesized, and characterized regarding optical properties. As expected, the acquired SH efficiencies strongly depend on both the electronic constitution and the anisotropy in the crystal structure. Hence, the principal strategies to further improve physical characteristics of this class of NLO materials are proposed.

First, a significant improvement in stability combined with reasonable SHG values is obtained for the sulfone (oxidized species **12ba**), which relies on the formation of an entirely new NLO chromophore. Second, a drastic enhancement in SH efficiency (by a factor of more than 20 for the selenium-based compound **16** compared to the initial compound **4ba**) is obtained by an increased electron density of the π -electron system. Therefore, we postulate that the introduction of electron-donating motives at the triazole N1 position further improves the performance, yielding chromophores in a donor-acceptor-donor type fashion.

Moreover, it is suggested that the Z-alkyl(thio/sulfonyl/seleno)-alkenyl-phenyl-triazole motive facilitates the noncentrosymmetric crystallization behavior of this class of nonchiral compounds. This fact is emphasized by three novel ene-yne-based scaffolds showing enantiomorphic crystallization and two more obtained in noncentrosymmetric space groups. Thus, the general applicability of the CuAAC reaction

makes ene-yne compounds attractive molecular building blocks, e.g., for the design of further NLO chromophores. In fact, the demand of noncentrosymmetric materials in diverse fields of material science, as outlined in the Introduction, significantly broadens the scope of potential application.

■ ASSOCIATED CONTENT

📄 Supporting Information

General synthetic methods, spectroscopic (NMR) and crystallographic (X-ray) data, as well as information regarding the SHG experiments. This material is available free of charge via the Internet at <http://pubs.acs.org>.

■ AUTHOR INFORMATION

Corresponding Author

*Phone: 0043 650 5008277/0041 78 8799874. Fax: 0043 1 58801 16399. E-mail: daniel.lumpi@tuwien.ac.at.

Notes

The authors declare no competing financial interest.

■ ACKNOWLEDGMENTS

The authors acknowledge H. Schmidtbauer, A. Hammerl, and M. Möller for supporting the synthetic experiments, P. Kautny for performing the TGA analysis, as well as K. Föttinger for assisting the photophysical analysis. F. Kubel and E. Horkel are acknowledged for fruitful discussion, E. Rosenberg for performing the high resolution mass spectrometry, and N. Jankowski for conducting the ion chromatography. The authors also thank T. Balciunas and A. Pugzlys (Photonics Institute TU Wien) for their great support with the SHG measurements. The X-ray center of the Vienna University of Technology is acknowledged for providing access to the single-crystal diffractometer.

■ REFERENCES

- (1) Yariv, A.; Yeh, P. *Photonics: Optical Electronics in Modern Communications*; Oxford University Press: New York, 2007.
- (2) Klapper, H.; Hahn, T. In *International Tables for Crystallography*; Hahn, T., Ed.; Springer: Dordrecht, 2005; p 804.
- (3) Barlow, S.; Marder, S. R. In *Functional Organic Materials Syntheses, Strategies and Applications*; Mueller, T. J. J., Bunz, U. H. F., Eds.; Wiley-VCH Verlag: Weinheim, 2007; Vol. 1, p 393.
- (4) Zyss, J. *Molecular Nonlinear Optics: Materials, Physics and Devices*; Academic Press: New York, 1994.
- (5) Chemla, D. S.; Zyss, J. *Nonlinear Optical Properties of Organic Molecules and Crystals*; Academic Press: Orlando, 1987.
- (6) Cho, M. J.; Choi, D. H.; Sullivan, P. A.; Akelaitis, A. J. P.; Dalton, L. R. *Prog. Polym. Sci.* **2008**, *33*, 1013.
- (7) Dalton, L. In *Polymers for Photonics Applications I*; Lee, K. S., Ed.; Springer: Berlin: Heidelberg, 2002; Vol. 158, p 1.
- (8) Marder, S. R. *Chem. Commun.* **2006**, 131.
- (9) Lumpi, D.; Horkel, E.; Stoeger, B.; Hametner, C.; Kubel, F.; Reider, G. A.; Froehlich, J. *Proc. SPIE* **2011**, *8306*, 830615/1.
- (10) Lumpi, D.; Stoeger, B.; Hametner, C.; Kubel, F.; Reider, G.; Hagemann, H.; Karpfen, A.; Froehlich, J. *CrystEngComm* **2011**, *13*, 7194.
- (11) Kolb, H. C.; Finn, M. G.; Sharpless, K. B. *Angew. Chem., Int. Ed.* **2001**, *40*, 2004.
- (12) Moses, J. E.; Moorhouse, A. D. *Chem. Soc. Rev.* **2007**, *36*, 1249.
- (13) Hein, J. E.; Fokin, V. V. *Chem. Soc. Rev.* **2010**, *39*, 1302.
- (14) Gronowitz, S.; Frejd, T. *Chem. Heterocycl. Compd.* **1978**, *14*, 353.
- (15) Iddon, B. *Heterocycles* **1983**, *20*, 1127.
- (16) Gilchrist, T. L. *Adv. Heterocycl. Chem.* **1987**, *41*, 41.
- (17) Pidcock, E. *Chem. Commun.* **2005**, 3457.
- (18) Nakayama, J.; Konishi, T.; Murabayashi, S.; Hoshino, M. *Heterocycles* **1987**, *26*, 1793.
- (19) In analogy to the literature¹⁸ (isolated yield: 69%).
- (20) Froehlich, H.; Kalt, W. *J. Org. Chem.* **1990**, *55*, 2993.
- (21) Froehlich, J.; Hametner, C.; Kalt, W. *Monatsh. Chem.* **1996**, *127*, 325.
- (22) Stoeger, B.; Lumpi, D.; Froehlich, J. *Acta Crystallogr., Sect. C: Cryst. Struct. Commun.* **2011**, *C67*, o464.
- (23) Gronowitz, S.; Frejd, T.; Karlsson, O.; Lawitz, K.; Pedaja, P.; Pettersson, K. *Chem. Scr.* **1981**, *18*, 192.
- (24) Cwiklicki, A.; Rehse, K. *Arch. Pharm.* **2004**, *337*, 156.
- (25) SAINT and SADABS; Bruker Analytical X-ray Instruments, Inc.: Madison, WI, USA, 2008.
- (26) Palatinus, L.; Chapuis, G. *J. Appl. Crystallogr.* **2007**, *40*, 786.
- (27) Petříček, V.; Dušek, M.; Palatinus, L. *Jana2006: The crystallographic computing system*; Institute of Physics: Praha, Czech Republic, 2006.
- (28) Kurtz, S. K.; Perry, T. T. *J. Appl. Phys.* **1968**, *39*, 3798.
- (29) Skranc, W. *PhD Thesis*, Vienna University of Technology, 1999.
- (30) Kryukova, T. B.; Stadnichuk, M. D.; Timofeeva, T. N. *Zh. Obshch. Khim.* **1974**, *44*, 789.
- (31) Bohlmann, F.; v, K. W.; Rybak, C.; Repplinger, J. *Chem. Ber.* **1965**, *98*, 1736.
- (32) Rasmussen, L. K.; Boren, B. C.; Fokin, V. V. *Org. Lett.* **2007**, *9*, 5337.
- (33) Suginome, H.; Umezawa, S. *Bull. Chem. Soc. Jpn.* **1936**, *11*, 157.
- (34) Purushothaman, B. *PhD Thesis*, University of Kentucky, 2011.
- (35) Gronowitz, S.; Frejd, T. *Acta Chem. Scand.* **1970**, *24*, 2656.
- (36) Jakobsen, H. J. *Acta Chem. Scand.* **1970**, *24*, 2663.
- (37) Rostovtsev, V. V.; Green, L. G.; Fokin, V. V.; Sharpless, K. B. *Angew. Chem., Int. Ed.* **2002**, *41*, 2596.
- (38) Tornøe, C. W.; Christensen, C.; Meldal, M. *J. Org. Chem.* **2002**, *67*, 3057.
- (39) Schnuerch, M.; Spina, M.; Khan, A. F.; Mihovilovic, M. D.; Stanetty, P. *Chem. Soc. Rev.* **2007**, *36*, 1046.
- (40) Nora, d. S. M. V. *Curr. Org. Chem.* **2007**, *11*, 637.
- (41) Froehlich, J. *Bull. Soc. Chim. Belg.* **1996**, *105*, 615.
- (42) Froehlich, J. *Prog. Heterocycl. Chem.* **1994**, *6*, 1.
- (43) Zhang, L.; Chen, X.; Xue, P.; Sun, H. H. Y.; Williams, I. D.; Sharpless, K. B.; Fokin, V. V.; Jia, G. *J. Am. Chem. Soc.* **2005**, *127*, 15998.
- (44) Appukkuttan, P.; Dehaen, W.; Fokin, V. V.; Van, d. E. E. *Org. Lett.* **2004**, *6*, 4223.
- (45) de la Hoz, A.; Diaz-Ortiz, A.; Moreno, A. *Chem. Soc. Rev.* **2005**, *34*, 164.
- (46) Loupy, A. *Microwaves in Organic Synthesis*, 2nd ed.; Wiley-VCH: Weinheim, 2006.
- (47) Cailleau, H.; Baudour, J. L.; Zeyen, C. M. E. *Acta Crystallogr., Sect. B* **1979**, *B35*, 426.
- (48) Flack, H. D.; Bernardinelli, G. *Acta Crystallogr., Sect. A: Found. Crystallogr.* **1999**, *A55*, 908.
- (49) Pucher, N. *Diploma Thesis*, Vienna University of Technology, 2006.
- (50) Skranc, W. *Diploma Thesis*, Vienna University of Technology, 1996.
- (51) (**4bb**): C₁₃H₁₅N₃S, M_r = 245.3, orthorhombic, P2₁2₁1, a = 4.7643(15) Å, b = 15.968(6) Å, c = 16.294(6) Å, V = 1239.6(8) Å³, Z = 4, μ = 0.242 mm⁻¹, T = 100 K, 25 530 measured, 3514 independent and 3076 observed [I > 3σ(I)] reflections, 203 parameters, wR (all data) = 0.062, R [I > 3σ(I)] = 0.029; CCDC reference number 927487.
- (52) Kalman, A.; Parkanyi, L.; Argay, G. *Acta Crystallogr., Sect. B: Struct. Sci.* **1993**, *B49*, 1039.
- (53) (**4bd**): C₁₅H₁₉N₃S, M_r = 273.4, monoclinic, P2₁/c, a = 7.9302(11) Å, b = 17.223(2) Å, c = 10.8814(14) Å, β = 94.771(7)°, V = 1481.1(3) Å³, Z = 4, μ = 0.209 mm⁻¹, T = 100 K, 26 938 measured, 4157 independent and 2248 observed [I > 3σ(I)] reflections, 172 parameters, wR (all data) = 0.049, R [I > 3σ(I)] = 0.045; CCDC reference number 927488.
- (54) (**4ca**, polymorph 1): C₁₃H₁₅N₃S, M_r = 245.3, monoclinic, Cc, a = 17.6465(9) Å, b = 5.0684(3) Å, c = 14.7768(8) Å, β = 112.225(2)°,

$V = 1223.44(12) \text{ \AA}^3$, $Z = 4$, $\mu = 0.245 \text{ mm}^{-1}$, $T = 100 \text{ K}$, 13 776 measured, 6313 independent, and 6081 observed [$I > 3\sigma(I)$] reflections, 201 parameters, wR (all data) = 0.030, R [$I > 3\sigma(I)$] = 0.023; CCDC reference number 927489. (4ca, polymorph 2): $\text{C}_{13}\text{H}_{15}\text{N}_3\text{S}$, $M_r = 245.3$, monoclinic, $P2_1/c$, $a = 10.0699(6) \text{ \AA}$, $b = 10.4586(6) \text{ \AA}$, $c = 12.3674(7) \text{ \AA}$, $\beta = 98.777(2)^\circ$, $V = 1287.25(13) \text{ \AA}^3$, $Z = 4$, $\mu = 0.233 \text{ mm}^{-1}$, $T = 100 \text{ K}$, 23 292 measured, 3783 independent and 3017 observed [$I > 3\sigma(I)$] reflections, 214 parameters, wR (all data) = 0.048, R [$I > 3\sigma(I)$] = 0.038; CCDC reference number 955415.

(55) Hill, D. G. *J. Am. Chem. Soc.* **1932**, *54*, 32.

(56) (5ba): $\text{C}_{12}\text{H}_{13}\text{N}_3\text{S}$, $M_r = 231.3$, triclinic, $P\bar{1}$, $a = 5.9338(2) \text{ \AA}$, $b = 7.3798(2) \text{ \AA}$, $c = 13.2891(4) \text{ \AA}$, $\alpha = 99.4247(11)^\circ$, $\beta = 93.1907(12)^\circ$, $\gamma = 92.2136(12)^\circ$, $V = 572.51(3) \text{ \AA}^3$, $Z = 2$, $\mu = 0.257 \text{ mm}^{-1}$, $T = 100 \text{ K}$, 11 475 measured, 4115 independent and 3365 observed [$I > 3\sigma(I)$] reflections, 197 parameters, wR (all data) = 0.043, R [$I > 3\sigma(I)$] = 0.033; CCDC reference number 927490.

(57) Kwok, S. W.; Fotsing, J. R.; Fraser, R. J.; Rodionov, V. O.; Fokin, V. V. *Org. Lett.* **2010**, *12*, 4217.

(58) (7ba): $\text{C}_{12}\text{H}_{13}\text{N}_3\text{S}$, $M_r = 231.3$, orthorhombic, $P2_12_12_1$, $a = 7.1809(3) \text{ \AA}$, $b = 10.2986(5) \text{ \AA}$, $c = 15.7680(8) \text{ \AA}$, $V = 1166.09(10) \text{ \AA}^3$, $Z = 4$, $\mu = 0.253 \text{ mm}^{-1}$, $T = 100 \text{ K}$, 27 604 measured, 3333 independent and 2884 observed [$I > 3\sigma(I)$] reflections, 198 parameters, wR (all data) = 0.035, R [$I > 3\sigma(I)$] = 0.027; CCDC reference number 927491.

(59) (9ba): $\text{C}_{12}\text{H}_{13}\text{N}_3\text{O}_2\text{S}$, $M_r = 263.3$, monoclinic, $P2_1/n$, $a = 5.7944(6) \text{ \AA}$, $b = 23.318(2) \text{ \AA}$, $c = 9.1374(9) \text{ \AA}$, $\beta = 97.601(4)^\circ$, $V = 1223.7(2) \text{ \AA}^3$, $Z = 4$, $\mu = 0.262 \text{ mm}^{-1}$, $T = 100 \text{ K}$, 19 745 measured, 5297 independent and 4624 observed [$I > 3\sigma(I)$] reflections, 215 parameters, wR (all data) = 0.056, R [$I > 3\sigma(I)$] = 0.041; CCDC reference number 927492.

(60) (12ba): $\text{C}_{12}\text{H}_{13}\text{N}_3\text{O}_2\text{S}$, $M_r = 263.3$, orthorhombic, $Pna2_1$, $a = 12.7982(8) \text{ \AA}$, $b = 13.6159(8) \text{ \AA}$, $c = 7.1310(4) \text{ \AA}$, $V = 1242.64(13) \text{ \AA}^3$, $Z = 4$, $\mu = 0.258 \text{ mm}^{-1}$, $T = 100 \text{ K}$, 53 360 measured, 6545 independent and 5940 observed [$I > 3\sigma(I)$] reflections, 215 parameters, wR (all data) = 0.037, R [$I > 3\sigma(I)$] = 0.029; CCDC reference number 927493.

(61) Shen, J. R. *The Principles of Nonlinear Optics*; Wiley-Interscience: New York, 2002.

(62) Mehta, S.; Waldo, J. P.; Larock, R. C. *J. Org. Chem.* **2009**, *74*, 1141.

(63) (16): $\text{C}_{12}\text{H}_{13}\text{N}_3\text{Se}$, $M_r = 278.2$, orthorhombic, $P2_12_12_1$, $a = 5.71930(10) \text{ \AA}$, $b = 9.5627(2) \text{ \AA}$, $c = 20.9579(5) \text{ \AA}$, $V = 1146.23(4) \text{ \AA}^3$, $Z = 4$, $\mu = 3.251 \text{ mm}^{-1}$, $T = 100 \text{ K}$, 25 987 measured, 3289 independent and 3081 observed [$I > 3\sigma(I)$] reflections, 146 parameters, wR (all data) = 0.031, R [$I > 3\sigma(I)$] = 0.024; CCDC reference number 927494.

(64) Shannon, R. D. *Acta Crystallogr., Sect. A* **1976**, *A32*, 751.

(65) Boyd, R. W. *Nonlinear Optics*; 3rd ed.; Elsevier: New York, 2008; p 84.

(66) Llinas, A.; Goodman, J. M. *Drug Discovery Today* **2008**, *13*, 198.

Manuscript # 8

Brigitte Holzer, Berthold Stöger, Daniel Lumpi*, Georg Reider, Christian Hametner, and
Johannes Fröhlich

Isoxazole-Based Ene-Yne Compounds as Potential Materials Exhibiting Nonlinear Optical
Properties

Manuscript draft

Isoxazole-Based Ene-Yne Compounds as Potential Materials Exhibiting Nonlinear Optical Properties

Brigitte Holzer,^a Berthold Stöger,^b Daniel Lumpi,^{a} Georg A. Reider,^c Christian Hametner,^a and Johannes Fröhlich^a*

^a Institute of Applied Synthetic Chemistry, Vienna University of Technology, Getreidemarkt 9/163, A-1060 Vienna, Austria.

^b Institute of Chemical Technologies and Analytics, Vienna University of Technology, Getreidemarkt 9/164, A-1060 Vienna, Austria

^c Photonics Institute, Vienna University of Technology, Gußhausstraße 27- 29, A-1040 Vienna, Austria

*daniel.lumpi@tuwien.ac.at

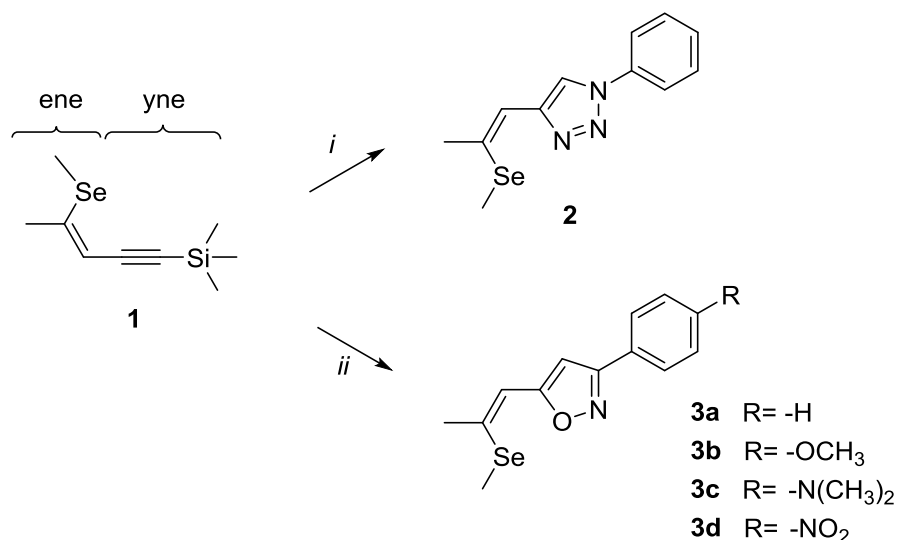
Herein we report the synthesis of Z-(methylseleno)alkenyl-substituted phenylisoxazoles applying a copper-catalyzed cycloaddition. An achiral molecule containing a 3,5-disubstituted isoxazole subunit as acceptor moiety forming untwinned enantiomorphous single crystals in the space group $P2_12_12_1$ could be obtained. This novel compound was characterized with regard to its ability to generate second harmonics and its absorption behavior. The material exhibits nonlinear optical properties approximately 30 times higher than potassium dihydrogen phosphate. Thus, the developed molecular scaffold represents an interesting novel type of NLO chromophore.

INTRODUCTION

Organic electronic materials have become interesting target compounds for optoelectronic applications (such as LEDs, solar cells, and nonlinear optical devices) and may constitute inexpensive alternatives to their traditional inorganic semiconductor counterparts.¹ The optical properties of photochromic materials change under the irradiation of light at a specific wavelength. The crucial advantage of organic compounds is that these materials can be designed toward specific interaction with light in order to process concrete optical signals.² In recent years, a large number of push–pull systems asymmetrically linked to π -conjugated spacers exhibiting first hyperpolarizability β have been synthesized and probed in electronic and optical applications.^{3,4,5} However, a considerable interest to improve the performance of materials capable of second harmonic generation remains. Modifications of structures at a molecular level are sought by crystal engineering taking advantage of structure / property relationships.^{6,7}

Recently, we have published on the synthesis and properties of the selenium-substituted 1-phenyl-1,2,3-triazole **2** (Scheme 1) exhibiting a 40 times increased SH efficiency value compared to potassium dihydrogen phosphate (KDP).⁸ The NLO characteristic relies on the combination of structural motives of a *Z*-(methylseleno)alkenyl group (Scheme 1, ene-substructure) as an electron donor directly connected to an electron-withdrawing heteroaromatic moiety providing sufficient acceptor performance. The electron-deficient isoxazole fragment has previously been applied as conjugative π -linker in donor– π -acceptor organic sensitizers and represents an adequate acceptor.⁹ This contribution focuses on the structural variation of the triazole-based acceptor subunit in **2** toward materials **3a-d** bearing isostructural isoxazole cores. The presented materials are examined in detail regarding their crystallization behavior as well as their structural and NLO properties.

The syntheses of compounds **3a-d** are based on a modification of the ene–yne compound **1** via copper(I)-catalyzed nitrile oxide–alkyne cycloaddition,^{10–12} which allows a direct functionalization of the yne-structure (Scheme 1). The cleavage of the trimethylsilyl group in **1** is induced by potassium fluoride giving rise to a terminal alkyne subunit, which reacts with the appropriate nitrile oxides (generated in situ from substituted phenyl imidoyl chlorides) yielding 3,5-disubstituted isoxazoles **3a-d**. Single crystals of **3a-d** were obtained by crystallization from ethanol.



Scheme 1: Synthetic approach toward **2** and **3a-d**; *i*: azidobenzene, CuSO₄·5H₂O, Na ascorbate, KF, t-BuOH/H₂O (1 : 1, 0.4 M), MW 150 °C; *ii*: substituted phenyl imidoyl chlorides, CuSO₄·5H₂O, Na ascorbate, KF, t-BuOH/H₂O (1 : 1, 0.4 M), 50 °C.

EXPERIMENTAL SECTION

All reactions were performed in oven-dried glassware. Reagents were purchased from commercial sources and used without prior purification. Anhydrous tetrahydrofuran (THF), diethyl ether and toluene were prepared immediately prior to use by a PURESOLV-plant (it-innovative technology inc.). Technical grade solvents were distilled prior to use. Analytical TLC was performed on Merck silica gel 60 F254 plates. Chromatographic separations at preparative scale were carried out on silica gel (Merck silica gel 60, 40 – 63 μm). Melting points were recorded on an OptiMelt Automated Melting Point System (Stanford Research Systems) and are corrected. Experiments under microwave irradiation were performed in a Biotage Initiator Sixty microwave reactor. The syntheses of trimethyl[(3*Z*)-4-(methylseleno)-3-penten-1-yn-1-yl]silane **1**,⁸ *N*-hydroxybenzimidoyl chloride **4**,¹³ *N*-hydroxy-4-methoxybenzimidoyl chloride **5**,¹³ 4-(*N,N*-dimethylamino)benzaldehyde oxime,¹³ and *N*-hydroxy-4-nitrobenzimidoyl chloride **7**¹³ were performed according to literature.

Nuclear magnetic resonance (NMR) spectra were obtained using a Bruker Avance III HD 600 MHz with cryo probe fourier transform spectrometer operating at the following frequencies: Avance III HD 600 MHz: 600.2 MHz (¹H), 150.9 MHz (¹³C) and 114.5 MHz (⁷⁷Se). The ¹H and ¹³C chemical shifts are reported in δ units, parts per million (ppm) downfield from tetramethylsilane using residual solvent signals for calibration. ⁷⁷Se chemical shifts are given in ppm relative to dimethylselenide, using selenophene (δ = 605 ppm)³ as an external secondary standard. Coupling constants are reported in Hertz; multiplicity of signals is indicated by using following abbreviations: s=singlet, d=doublet, t=triplet, q=quartet, quin=quintet. The multiplicity of ¹³C signals was obtained by measuring JMOD spectra.

General procedure towards **3a**, **3b** and **3d**. To a tBuOH/H₂O (1:1, 0.4 M) suspension of **1** (1.0 equiv.) substituted *N*-hydroxybenzimidoyl chloride (1.1 equiv.), CuSO₄*5H₂O (0.02 equiv.), sodium ascorbate (0.1 equiv.) and potassium fluoride (1.2 equiv.) were added. Subsequently the reaction mixture was heated to 50 °C for 60 min, diluted with water and extracted with Et₂O. The combined organic layers were washed with brine and dried over anhydrous Na₂SO₄. Suction filtration and evaporation of the solvent followed by column chromatography yielded **3a**, **3b** and **3d**.

5-[(1*Z*)-2-(Methylseleno)-1-propen-1-yl]-3-phenylisoxazole (**3a**). The reaction of **1** (231 mg, 1 mmol), *N*-hydroxybenzimidoyl chloride **4** (171 mg, 1.1 mmol), CuSO₄*5H₂O (5 mg, 0.02 mmol), sodium ascorbate (20 mg, 0.1 mmol), and potassium fluoride (71 mg, 1.2 mmol) following the general procedure afforded **3a** (141 mg, 51%) as a colorless solid after column chromatography (light petroleum / ethyl acetate 7:1). Single crystals were obtained by crystallization from saturated solution in ethanol. F_p = 87.6 - 91.2 °C. R_f = 0.50 (light petroleum : ethyl acetate 5 : 1). ¹H NMR (600 MHz, CD₂Cl₂): δ = 7.83 – 7.81 (m, 2 H), 7.49 - 7.44 (m, 3 H), 6.72 (q, J = 1.3 Hz, 1 H), 6.70 (s, 1 H), 2.37 (d, J = 1.3 Hz, 3 H), 2.32 (s, 3 H) ppm. ¹³C NMR (150 MHz, CD₂Cl₂): δ = 168.5 (s), 162.3 (s), 140.8 (s), 129.9 (d), 129.4 (s), 128.9 (d), 126.8 (d), 112.5 (d), 99.9 (d), 25.7 (q), 5.21 (q) ppm. ⁷⁷Se NMR (114 MHz, CD₂Cl₂): δ = 246 ppm. HR-ESI-FTMS [M+H]⁺ m/z calcd. 280.0235 for C₁₃H₁₄NOSe⁺, found 280.0231.

5-[(1*Z*)-2-(Methylseleno)-1-propen-1-yl]-3-(4-methoxyphenyl)isoxazole (**3b**). The reaction of **1** (231 mg, 1 mmol), *N*-hydroxy-4-methoxybenzimidoyl chloride **5** (204 mg, 1 mmol), CuSO₄*5H₂O (5 mg, 0.02 mmol), sodium ascorbate (20 mg, 0.1 mmol), and potassium fluoride (71 mg, 1.2 mmol) following the general procedure afforded **3b** (147 mg, 48%) as a colorless solid after column chromatography (light petroleum / ethyl acetate 5:1). Single crystals were obtained by crystallization from saturated solution in ethanol. R_f = 0.25 (light petroleum : ethyl acetate 5 : 1). ¹H NMR (600 MHz, CDCl₃): δ = 7.77 (d, J = 8.9 Hz, 2 H), 6.97 (d, J = 8.9 Hz, 2 H), 6.71 (q, J = 1.3 Hz, 1 H), 6.64 (s, 1 H), 3.85 (s, 3 H), 2.36 (d, J = 1.3 Hz, 3 H), 2.30 (s, 3 H) ppm. ¹³C NMR (150 MHz, CDCl₃): δ = 168.1 (s), 162.0 (s), 160.8 (s), 139.6 (s), 128.2 (d), 121.9 (s), 114.2 (d), 113.2 (d), 99.9 (d), 55.3 (q), 25.9 (q), 5.2 (q) ppm. ⁷⁷Se NMR (114 MHz, CDCl₃): δ = 243 ppm. HR-ESI-FTMS [M+H]⁺ m/z calcd. 310.0341 for C₁₄H₁₆NO₂Se⁺, found 310.0330.

5-[(1*Z*)-2-(Methylseleno)-1-propen-1-yl]-3-(4-nitrophenyl)isoxazole (**3d**). The reaction of **1** (173 mg, 0.75 mmol), *N*-hydroxy-4-nitrobenzimidoyl chloride **7** (165 mg, 0.825 mmol), CuSO₄*5H₂O (4 mg, 0.015 mmol), sodium ascorbate (15 mg, 0.075 mmol) and potassium fluoride (52 mg, 0.9 mmol) following the general procedure afforded **3d** (88 mg, 36%) as an orange solid after column chromatography (light petroleum / ethyl acetate 9:1). Single crystals were obtained by crystallization from saturated solution in ethanol. R_f = 0.33 (light petroleum : ethyl acetate 5 : 1). ¹H NMR (600 MHz, CDCl₃): δ = 8.31 (d, J = 8.8 Hz, 2 H), 8.01 (d, J = 8.8 Hz, 2 H), 6.75 (s, 1 H), 6.73

(q, $J = 1.3$ Hz, 1 H), 2.38 (d, $J = 1.3$ Hz, 3 H), 2.32 (s, 3 H) ppm. ^{13}C NMR (150 MHz, CDCl_3): $\delta = 169.6$ (s), 160.6 (s), 148.9 (s), 141.5 (s), 135.5 (s), 127.7 (d), 124.2 (d), 112.7 (d), 99.9 (d), 26.0 (q), 5.4 (q) ppm. ^{77}Se NMR (114 MHz, CDCl_3): $\delta = 247$ ppm. HR-ESI-FTMS $[\text{M}+\text{H}]^+$ m/z calcd. 325.0086 for $\text{C}_{13}\text{H}_{13}\text{N}_2\text{O}_3\text{Se}^+$, found 325.0080.

N,N-Dimethyl-4-[5-[(1*Z*)-2-(methylseleno)-1-propen-1-yl]isoxazol-3-yl]benzenamine (**3c**). 4-(*N,N*-Dimethylamino)benzaldehyde oxime **6** (369 mg, 2.25 mmol, 4.5 equiv.), was dissolved in 5 mL chloroform and cooled to 0 °C. *N*-Chlorosuccinimide (300 mg, 2.25 mmol, 4.5 equiv.) was added in portions. The reaction mixture was allowed to stir at room temperature for one hour and poured onto water. The aqueous phase was extracted repeatedly with dichloromethane. The organic layers were dried over Na_2SO_4 , filtrated and concentrated. 4-(Dimethylamino)-*N*-hydroxybenzimidoyl chloride was used without further purification and added to a solution of **1** (116 mg, 0.5 mmol, 1 equiv.), $\text{CuSO}_4 \cdot 5\text{H}_2\text{O}$ (10 mg, 0.05 mmol, 0.1 equiv.), crown ether (40 mg, 0.15 mmol, 0.3 equiv.), sodium ascorbate (10 mg, 0.05 mmol, 0.1 equiv.) and potassium fluoride (174 mg, 3 mmol, 6 equiv.) in 3 mL THF. The reaction solution was stirred at 50 °C overnight, diluted with water and extracted with Et_2O . The combined organic layers were washed with brine and dried over anhydrous Na_2SO_4 . Suction filtration and evaporation of the solvent followed by column chromatography (8 g silica gel, light petroleum / ethyl acetate 5:1) afforded **3c** (48 mg, 30%) as a yellow solid. Single crystals were obtained by crystallization from saturated solution in ethanol. $R_f = 0.40$ (light petroleum : ethyl acetate 5 : 1). ^1H NMR (600 MHz, CDCl_3): $\delta = 7.71$ (d, $J = 8.7$ Hz, 2 H), 6.76 (d, $J = 8.7$ Hz, 2 H), 6.69 (q, $J = 1.3$ Hz, 1 H), 6.61 (s, 1 H), 3.01 (s, 6 H), 2.35 (d, $J = 1.3$ Hz, 3 H), 2.29 (s, 3H) ppm. ^{13}C NMR (150 MHz, CDCl_3): $\delta = 167.6$ (s), 162.4 (s), 151.3 (s), 139.0 (s), 127.8 (d), 116.9 (s), 113.4 (d), 112.0 (d), 99.8 (d), 40.3 (q), 25.9 (q), 5.2 (q) ppm. ^{77}Se NMR (114 MHz, CDCl_3): $\delta = 241$ ppm. HR-ESI-FTMS $[\text{M}+\text{H}]^+$ m/z calcd. 323.0657 for $\text{C}_{15}\text{H}_{19}\text{N}_2\text{OSe}^+$, found 323.0646.

CRYSTALLOGRAPHY

While **3b-d** crystallize in the centrosymmetric space group $P2_1/c$ (figures of the molecular structures are given in the supplementary information), **3a** crystallizes in the enantiomorphic Sohncke space group $P2_12_12_1$ and is therefore isostructural to **2**. Compound **3a** exhibits non-centrosymmetric crystallization, although being a flexible achiral molecule. The absolute structure and consequently configuration was determined by anomalous dispersion (Flack parameter 0.018(7)). The crystals are generally not twinned, i.e. they are composed of only one enantiomorph.

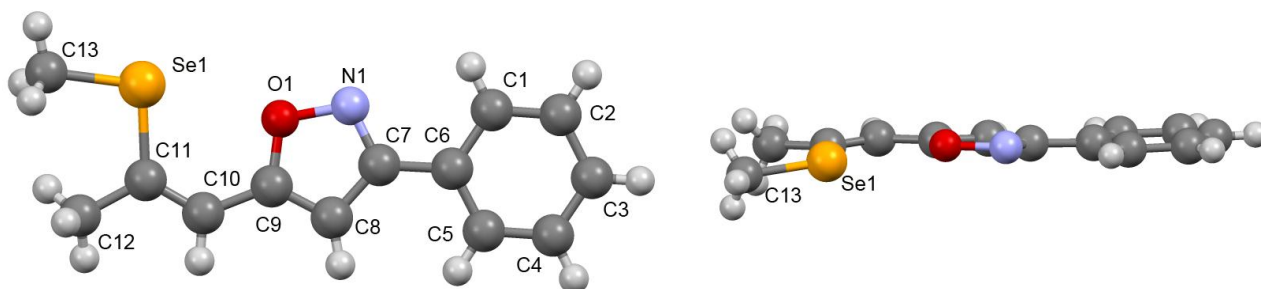


Figure 1: Molecular structure of **3a**; viewed normal (a, top) and parallel (b, bottom) to the molecular plane. C, N, O and Se atoms are represented by grey, blue, red and orange, respectively.

The unit cell contains four crystallographically equivalent molecules located on a general position (Figure 2). Since the symmetry group of the crystal is enantiomorphic, all molecules are congruent. As expected, the phenyl and isoxazole rings are practically planar. Hence, **3a** adopts a planar configuration (Figure 1) with the exception of the Se-methyl group. The propenyl group in compound **3a** is coplanar with the phenyl ring (torsion angle 2.37° , which is slightly larger than in **2** (1.59°)). The Se-methyl group is distinctly located off the main molecular plane with a C11–C12–Se1–C13 torsion angle of 175.58° , which can also be observed for compounds **3b-d** (Table 1). A strong intramolecular interaction in **3a** between the selenium (Se1) and the oxygen atom can be observed (2.867 \AA) comparable to the selenium-nitrogen interaction in the triazole compound **2** (2.935 \AA).

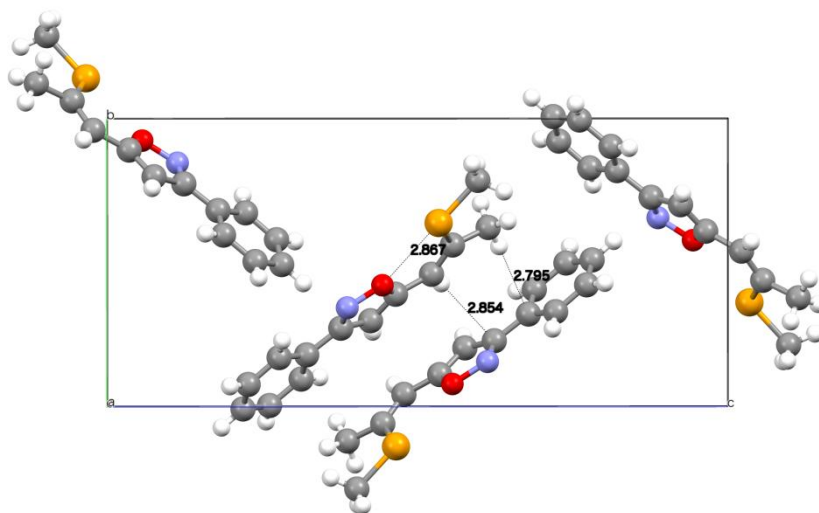


Figure 2: Intra- and intermolecular hydrogen bonds in the crystal structure of **3a**.

The overall arrangement of the molecules can be described as a herringbone pattern. Intramolecular interactions are given in Table 1.

Table 1. Intramolecular interactions and torsion angles of **3a-d**.

Compound	Se1...O1/ Å	C11–C12–Se1–C13 / °	Torsion angle benzene–isoxazole / °
3a	2.867(2)	175.58	4.42
3b	2.921(1)	175.75	6.37
3c	2.848(2)	176.23	16.41
3d	2.864(3)	170.95	6.31

The comparison of the torsion angle between the phenyl ring and the isoxazole moiety reveals that **3a** has the smallest angle of 4.42°, while the introduction of para-substituents on the phenyl ring increases this angle. Consequently, the introduction of both electron-withdrawing and -donating substituents leads to a decrease in π -electron conjugation, which is obviously the most efficient in **3a**.

PHOTOPHYSICAL PROPERTIES

The crystals of **3a** show good optical transparency, exhibiting a wide transmission window above the absorption onset at 398 nm in the visible region (Figure 3). The absorption spectrum of the novel NLO material **3a** in the solid state reveals a red shift of the absorption onset of about 20 nm compared to that of **2**, which may indicate lower acceptor properties of the isoxazole compared to the triazole moiety.

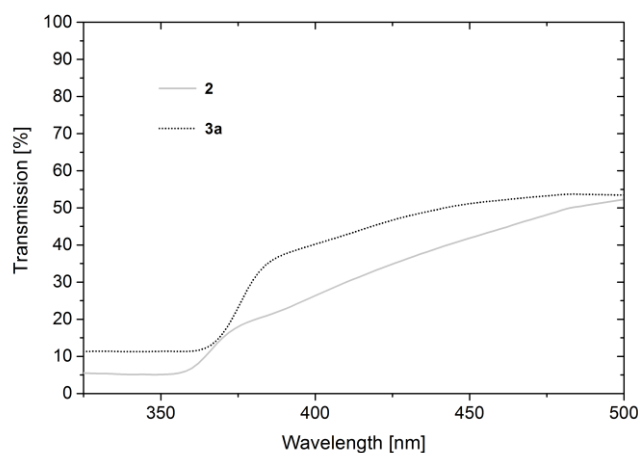


Figure 3: Optical transmission spectra of single crystalline probes of **2** and **3a**.

NLO PROPERTIES

Since **3a** crystallizes in a non-centrosymmetric point group, a prerequisite of NLO activity, the material was investigated regarding these optical characteristics.¹⁴ For a qualitative evaluation of the NLO properties of **3a**, we employed the process of frequency doubling or second harmonic generation (SHG), utilizing the powder technique developed by Kurtz and Perry, and compared the results to those obtained for **2**.¹⁵ The freshly prepared powder samples, sandwiched between microscope slides, were irradiated with the output of an ultrafast Yb:KGW-Laser (light conversion, pulse duration 70 femtoseconds, average power 400 mW, repetition rate 75 MHz, wavelength 1034 nm), moderately focused with a 100 mm focusing lens, impinging onto the sample under an angle of incidence of 50°. The diffusely reflected SH radiation was collected with a NA = 0.1 lens, separated from the fundamental radiation with a color filter, and spectrally analyzed with a 0.25 m grating monochromator and a photomultiplier detector in the range between 450 and 600 nm. The angle between the optical axis of the monochromator and the sample surface normal was 40°, so that no specular reflection from the glass slides was incident on the monochromator input. The resulting SH spectrum was identical to that obtained by inserting a commercial SH crystal into the beam path, displaying the peak at $1034 \text{ nm} / 2 = 517 \text{ nm}$ and an FWHM of 6 nm, which is due to the relatively

broad spectrum of the femtosecond laser source. The sample plane was positioned somewhat out of the focal plane (toward the lens) so as to prevent any damage to the sample. After each measurement, the samples were carefully checked for the absence of damage or thermal modification.

The SH signal of **3a** was compared to that of a similarly prepared powder sample of the isostructural **2**, which also crystalizes in the space group $P2_12_12_1$ and exhibits SHG efficiency 40 times the value of potassium dihydrogen phosphate (KDP). The SH yield of **3a** is about two thirds of this value. Therefore, **3a** represents a highly attractive new nonlinear optical material yielding approx. 27 times the SHG efficiency of KDP. Figure 4 shows spectra of **3a** and **2**.

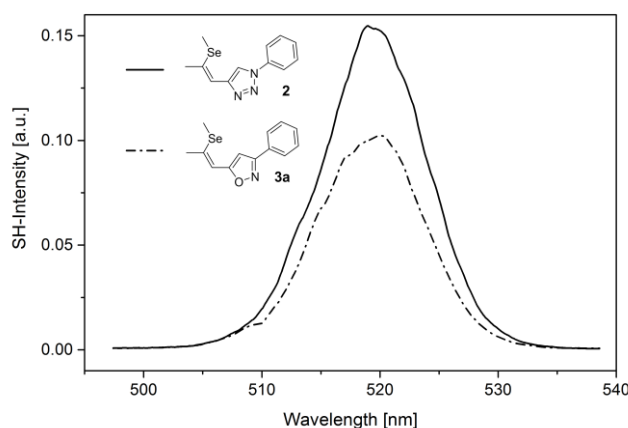


Figure 4: Optical second harmonic spectrum from sub-micron powder samples of **2** (full) and **3a** (dash-dot); the bandwidth of the signal results from the characteristic output spectrum of the femtosecond laser used for SHG; the irregularities of the spectral shape are due to laser power fluctuations during the measurement of the SH spectrum; the error of the SH peak value resulting from these fluctuations is estimated to be $\pm 10\%$. Note that because of the quadratic relation $I^{(2\omega)} \propto (I^{(\omega)}\chi^{(2)})^2$ between the SH signal and nonlinear polarizability $\chi^{(2)}$, the measured SH ratio of $\approx 15/10 = 1.5$ corresponds to a ratio of the nonlinear polarizabilities of the two substances of $\approx \sqrt{1.5} = 1.25$; for the same reason, the estimated error of the polarizability values is about 5%.

CONCLUSION

In conclusion, we report on a novel material exhibiting enantiomorphic crystallization and displaying second-order nonlinear optical properties with an estimated efficiency of approximately 30 times the value of KDP. The combination of phenylisoxazole and *Z*-(methylseleno)alkenyl moieties with extended π -electron conjugation represents an efficient method for designing donor-acceptor-based materials potentially capable of second harmonic generation. Structural variation of these scaffolds may give rise to further SH compounds.

ACKNOWLEDGMENT

We thank Dorian Bader for contributing to the synthetic experiments. We also acknowledge Paul Kautny for recording the transmission spectra. The X-Ray Center of the TU Vienna is acknowledged for providing access to the single crystal and powder diffractometers.

REFERENCES

- (1) Agranovich, V. M.; La Rocca, G. C. *J. Lumin.* **2015**, doi:10.1016/j.jlumin.2014.12.054.
- (2) Zheng, Y.; Ye, Q.; Wang, C.; Wang, J.; Deng, Z.; Mei, J.; Zhou, W.; Zhang, C.; Tian, J. *Opt. Laser Technol.* **2015**, *75*, 132.
- (3) Yang, Y.; Liu, J.; Zhang, M.; Liu, F.; Wang, H.; Bo, S.; Zhen, Z.; Qiu, L.; Liu, X. *J. Mater. Chem. C* **2015**, *3* (16), 3913.
- (4) Praveen Menezes, A.; Jayarama, A.; Weng Ng, S. *J. Cryst. Growth* **2014**, *402*, 130.
- (5) Marder, S. R. *Chem. Commun.* **2006**, *2*, 131.
- (6) Wu, W.; Qin, J.; Li, Z. *Polymer* **2013**, *54* (17), 4351.
- (7) Evans, O. R.; Lin, W. *Acc. Chem. Res.* **2002**, *35* (7), 511.
- (8) Lumpi, D.; Glöcklhofer, F.; Holzer, B.; Stöger, B.; Hametner, C.; Reider, G. A.; Fröhlich, J. *Cryst. Growth Des.* **2014**, *14* (3), 1018.
- (9) Li, Y.-T.; Chen, C.-L.; Hsu, Y.-Y.; Hsu, H.-C.; Chi, Y.; Chen, B.-S.; Liu, W.-H.; Lai, C.-H.; Lin, T.-Y.; Chou, P.-T. *Tetrahedron* **2010**, *66* (23), 4223.
- (10) Tornøe, C. W.; Christensen, C.; Meldal, M. *J. Org. Chem.* **2002**, *67* (9), 3057.
- (11) Rostovtsev, V. V.; Green, L. G.; Fokin, V. V.; Sharpless, K. B. *Angew. Chem. Int. Ed.* **2002**, *41* (14), 2596.
- (12) Moses, J. E.; Moorhouse, A. D. *Chem. Soc. Rev.* **2007**, *36* (8), 1249.
- (13) Lam, P. Y. S.; Adams, J. J.; Clark, C. G.; Calhoun, W. J.; Luetgen, J. M.; Knabb, R. M.; Wexler, R. R. *Bioorg. Med. Chem. Lett.* **2003**, *13* (10), 1795.
- (14) Hahn, T., *Space-group symmetry*, 5. ed., reprinted with corrections.; International Union of Crystallography, International tables for crystallography; Springer: Dordrecht, 2005.
- (15) Kurtz, S. K. *J. Appl. Phys.* **1968**, *39* (8), 3798.

Manuscript # 9

Brigitte Holzer*, Maximilian Tromayer, Markus Lunzer, Daniel Lumpi, Ernst Horkel,
Christian Hametner, Arnulf Rosspointner, Eric Vauthey, Robert Liska and Johannes Fröhlich
Initiators for Two-Photon Induced Polymerization Based on a Novel Cap-Linker-Cap System

Manuscript draft

Initiators for Two-Photon Induced Polymerization Based on a Novel Cap-Linker-Cap System

Brigitte Holzer,^{a,} Maximilian Tromayer,^{a,b} Markus Lunzer,^{a,c} Daniel Lumpi,^a Ernst Horkel,^a
Christian Hametner,^a Arnulf Rosspointner,^c Eric Vauthey,^c Robert Liska^a and Johannes Fröhlich^a*

^aInstitute of Applied Synthetic Chemistry, Vienna University of Technology,

Getreidemarkt 9/163OC, A-1060 Vienna, Austria

^bInstitute of Materials Science and Technology, Vienna University of Technology,

Favoritenstraße 9-11, A-1040 Vienna, Austria

^cPhysical Chemistry Department, University of Geneva,

Quai Ernest Ansermet 30, CH-1211 Geneva, Switzerland

[*brigitte.holzer@tuwien.ac.at](mailto:brigitte.holzer@tuwien.ac.at)

A series of cap-linker-cap systems based on thiophene and triphenylamines bearing electron-donating or -withdrawing substituents was synthesized by either Suzuki cross-coupling or nucleophilic aromatic substitution giving rise to two basic structural families of D- π -D and A- π -D- π -A chromophores. This study elucidates the relationship between molecular structure and effective two-photon absorption by systematic variation of substituents in the structure of the organic dye molecules. Although most substances exhibit high quantum yields, two-photon absorption screening tests revealed the efficiency of these materials as photoinitiators.

INTRODUCTION

In recent years materials exhibiting high two-photon (2PA) absorption have attracted growing interest due to their potential applications in materials and biomedical science,^{1,2} including three-dimensional optical data storage,^{3,4} lithographic microfabrication,^{5,6} optical power limiting,⁷ two-photon fluorescence imaging,⁸ and photodynamic therapy.^{9,10} Since two-photon induced photopolymerization (2PIP) allows excellent spatial control within the focal volume of the laser beams¹¹ and takes advantage of well-defined penetration depth^{12,13} by the use of a long wavelength excitation source (typically ~ 800 nm), this polymerization technique offers high resolution while minimizing unwanted thermal or photochemical degradation processes usually associated with excitation of UV-photoinitiators.^{14,15}

An efficient two-photon absorption induced process requires active two-photon absorption photoinitiators, which ensure high writing speeds and low polymerization threshold, resulting in high-quality structures.¹⁵ In the past decades, the design of efficient 2PA chromophores exhibiting high two-photon cross-sections (σ_{2PA}) remained of high scientific interest.^{16,17} However, since low achievable writing speeds and the lack of highly efficient two-photon initiators still constitute major drawbacks of this technology,¹¹ the need for specifically engineered organic molecules constituting highly efficient two-photon absorption initiators still persists.

General design strategies to ensure materials with large σ_{2PA} are based on the introduction of chromophoric groups with good molecular coplanarity^{18,19} (guaranteed by planar π systems) based on strong donors or acceptors. Incorporation of coplanar heterocyclic rings in the molecular design of chromophores gives rise to extended π -conjugated networks with enhanced optical properties, increasing both the extinction coefficient and the σ_{2PA} values.^{13,20,21} Recent studies show that particularly thiophene as π -electron bridge increases σ_{2PA} for both the π - σ - π and A- π -D- π -A type molecules (where π is a π -conjugated bridge, D is a donor, and A is an acceptor).²² Generally, thiophene comprising 2PA chromophores can be applied in a dipolar form with a D- π -A functionality and a quadrupolar mode with a D- π -D, A- π -A, D- π -A- π -D or A- π -D- π -A motif.¹⁴ Although thiophenes can be used as versatile platforms or building blocks in order to modulate the degree of electronic delocalization within a molecular architecture, their application as two-photon fluorescent probes remains rare.

Recently, we published on triphenylamine (TPA) substituted oligothiophenes constituting a new substance class suitable for organic electronics (Figure 1, left, $n = 1 - 4$).²³ The synthetic linkage of TPAs and thiophenes is known to lead to an extended π -conjugation system which may promote strong optical nonlinearities.²⁴ Although these materials exhibit high photoluminescence, first results also revealed, that TPA-substituted thiophene (Figure 1, left, $n = 1$) exhibited suitable two-photon absorption inducing efficiently photopolymerization probed in speed power screening tests (Figure 1, right).

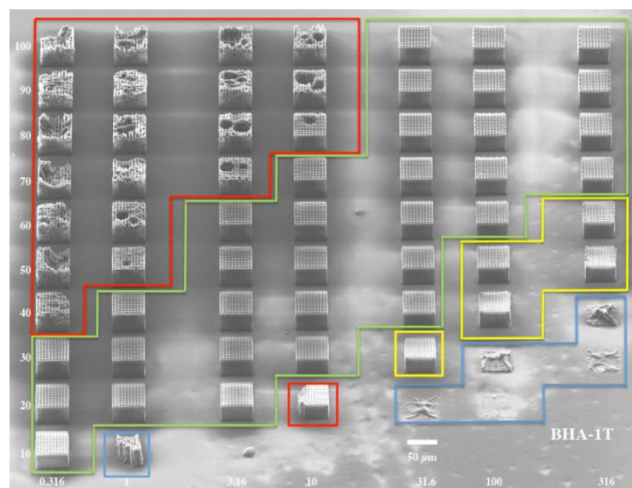
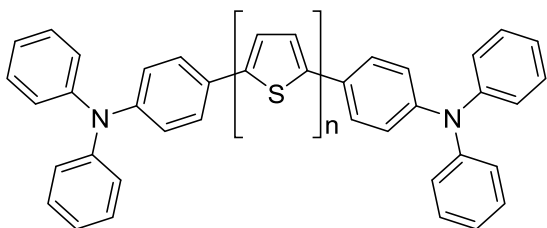


Figure 1: Triphenylamine (TPA) substituted oligothiophenes (left, $n=1$) and SEM-image of woodpile structures obtained from speed power screening tests of TPA substituted thiophene (right). The color classification system according to Li et al.¹⁵ is given in the section results and discussion.

Based on these findings, this article examines the variation of the substituent on the TPA moiety including both electron-withdrawing as well as electron-donating scaffolds (varying from $-OCH_3$, $-TMS$, $-tBu$, $-CH_3$, $-F$, $-CN$, $-SO_2Me$, to $-NO_2$) giving rise to novel two-photon absorption initiators. Due to the electronic nature of the applied TPAs both $D-\pi-D$ and $A-\pi-D-\pi-A$ chromophores are viable. Measurements of optical properties (e.g., absorption, fluorescence spectra, quantum yields and σ_{2PA}) of the obtained materials reveal the strong influence of the substituent's nature on these properties. The obtained materials were characterized with respect to their applicability in 2PIP structuring tests.

EXPERIMENTAL SECTION

Synthesis and Characterization: Substances purchased from commercial sources were used as received without further purification. 4-Fluorobenzonitrile and 1-fluoro-4-nitrobenzene were purchased from ABCR GmbH. Allyl[1,3-bis(2,6-diisopropylphenyl)imidazol-2-ylidene]chloropalladium(II) ((IPr)Pd(allyl)Cl, CAS 478980-03-9),²⁵ 1-fluoro-4-(methylsulfonyl)benzene (CAS 455-15-2),²⁶ 4,4'-(2,5-thiophenediyl)bis(benzenamine) (CAS 70010-49-0)²⁷ and all applied boronic esters²⁸ were synthesized according to literature. Isopropylalcohol (IPA) and dimethylsulfoxide (DMSO) were used in p.a. quality. Technical grade solvents were distilled prior to use. Analytical TLC was performed on Merck silica gel 60 F254 plates. Chromatographic separations at preparative scale were carried out on silica gel (Merck silica gel 60, 40 - 63 μm). Nuclear magnetic resonance (NMR) spectra were obtained using a Bruker DPX-200 or Avance DRX-400 fourier transform spectrometer operating at the following frequencies: DPX-200: 200.1 MHz (1H) and 50.3 MHz (^{13}C); DRX-400: 400.1 MHz (1H) and 100.6 MHz (^{13}C). The

chemical shifts are reported in delta (δ) units, parts per million (ppm) downfield from tetramethylsilane using solvent residual signals for calibration. Coupling constants are reported in Hertz; multiplicity of signals is indicated by using following abbreviations: s=singlet, d=doublet, t=triplet, q=quartet. The multiplicity of ^{13}C signals was obtained by measuring JMOD spectra. UV-Vis absorption spectra and fluorescence emission spectra were recorded in THF solutions (1 $\mu\text{g/mL}$) with a Perkin Elmer Lambda 750 spectrometer and an Edinburgh FLS920, respectively. High-resolution mass spectra (HRMS) were acquired as radical cations using either a SYNAPT HDMS instrument (Waters, Manchester, UK) equipped with a matrix-assisted laser desorption/ionization (MALDI) source or a Thermo Scientific LTQ Orbitrap XL hybrid FTMS (Fourier Transform Mass Spectrometer) equipped with Thermo Fischer Exactive Plus Orbitrap (LC-ESI+) and a Shimadzu IT-TOF Mass Spectrometer. Samples for MALDI-HRMS were applied at 1 mg/mL in THF on stainless steel using nitroanthracene (3 mg/mL in THF) as MALDI matrix. All MS spectra were recorded as accurate mass data with angiotensin II ($m/z = 1046.542$) as internal lock mass achieving a mass accuracy of 15 - 40 ppm (i.e. $\Delta m/z = 0.01 - 0.04$ amu).

General procedure for the synthesis of **3a-f** according to Marion.²⁹ Under an argon atmosphere, 2,5-dibromothiophene **2** (1.0 eq.), boronic ester (3.0 eq.) and KOtBu (3.0 eq.) were suspended in 16 mL solvent (IPA : H₂O, 3 : 1; degassed by bubbling with argon). A solution of (IPr)Pd(allyl)Cl (0.02 eq.) in degassed IPA was added and the reaction mixture was refluxed for 1.5 hours, monitoring the conversion by TLC. After completion, the reaction mixture was distributed between water and chloroform; the phases were separated and the aqueous layer was extracted with chloroform three times. The combined organic layer was dried over anhydrous sodium sulfate and the solvent removed under reduced pressure to give the crude product. Purification was achieved by column chromatography.

4,4'-(2,5-Thiophenediyl)bis[*N,N*-diphenylbenzenamine] (**3a**). According to the general procedure **3a** was synthesized applying 2,5-dibromothiophene **2** (242 mg, 1 mmol), boronic acid pinacol ester **1a** (1114 mg, 3.0 mmol), KOtBu (337 mg, 3.0 mmol) and (IPr)Pd(allyl)Cl (11.4 mg, 20 μmol ; dissolved in 1 mL IPA). After general workup the crude product was purified by column chromatography (90 g silica gel, cyclohexane : DCM, 5 \rightarrow 10 %) and subsequently recrystallized from cyclohexane to give **3a** as yellow powder (525 mg, 92%). ^1H NMR (400 MHz, CD₂Cl₂): $\delta = 7.49$ (d, $J = 8.5$ Hz, 4 H), 7.30 - 7.26 (m, 8 H), 7.21 (s, 2 H), 7.12 - 7.10 (m, 8 H), 7.10 - 7.03 (m, 8 H) ppm. ^{13}C NMR (100 MHz, CD₂Cl₂): $\delta = 148.1$ (s), 147.8 (s), 143.1 (s), 129.9 (d), 128.9 (s), 126.8 (d), 125.1 (d), 124.2 (d), 123.7 (d), 123.7 (d) ppm. $R_f = 0.24$ (light petrol : DCM 10 : 1). $F_P = 192.2 - 193.3$ °C. MS (MALDI-TOF): calcd for C₄₀H₃₀N₂S: 570.2130; found: 570.1812.

4,4'-(2,5-Thiophenediyl)bis[*N,N*-bis(4-methylphenyl)benzenamine] (**3b**). According to the general procedure **3b** was synthesized applying 2,5-dibromothiophene **2** (242 mg, 1 mmol), boronic acid pinacol ester **1b** (1198 mg, 3.0 mmol), KOtBu (337 mg, 3.0 mmol) and (IPr)Pd(allyl)Cl (11.4 mg, 20

μmol ; dissolved in 1 mL IPA). After general workup the crude product was purified by column chromatography (90 g silica gel, cyclohexane : DCM, 7 \rightarrow 14 %) and subsequently recrystallized from cyclohexane to give **3b** as yellow powder (551 mg, 88 %). ^1H NMR (400 MHz, CD_2Cl_2): δ = 7.44 (d, J = 8.7 Hz, 4 H), 7.16 (s, 2 H), 7.10- 7.08 (m, 8 H), 7.00- 6.96 (m, 12 H), 2.32 (s, 12 H) ppm. ^{13}C NMR (100 MHz, CD_2Cl_2): δ = 148.3 (s), 145.6 (s), 143.1 (s), 133.6 (s), 130.5 (d), 128.0 (s), 126.6 (d), 125.3 (d), 123.4 (d), 122.8 (d), 21.1 (q) ppm. R_f = 0.19 (light petrol : DCM 10 : 1). F_p = 206.1 – 210.7 $^\circ\text{C}$. MS (MALDI-TOF): calcd for $\text{C}_{44}\text{H}_{38}\text{N}_2\text{S}$: 626.2756; found: 626.2672.

4,4'-(2,5-Thiophenediyl)bis[*N,N*-bis[4-(1,1-dimethylethyl)phenyl]benzenamine] (**3c**). According to the general procedure **3c** was synthesized applying 2,5-dibromothiophene **2** (242 mg, 1 mmol), boronic acid pinacol ester **1c** (1451 mg, 3.0 mmol), KOtBu (337 mg, 3.0 mmol) and $(\text{IPr})\text{Pd}(\text{allyl})\text{Cl}$ (11.4 mg, 20 μmol ; dissolved in 1 mL IPA). After general workup the crude product was purified by column chromatography (90 g silica gel, cyclohexane : DCM, 9 \rightarrow 17 %) and subsequently recrystallized from cyclohexane to give **3c** as yellow powder (724 mg, 91 %). ^1H NMR (400 MHz, CD_2Cl_2): δ = 7.46 (d, J = 8.6 Hz, 4 H), 7.30 (d, J = 8.6 Hz, 8 H), 7.18 (s, 2 H), 7.04 - 7.00 (m, 12 H), 1.32 (s, 36 H) ppm. ^{13}C NMR (100 MHz, CD_2Cl_2): δ = 148.2 (s), 146.8 (s), 145.4 (s), 143.1 (s), 128.1 (s), 126.7 (d), 126.6 (d), 124.8 (d), 123.4 (d), 123.1 (d), 34.8 (s), 31.7 (q) ppm. R_f = 0.27 (light petrol : DCM 10 : 1). MS (MALDI-TOF): calcd for $\text{C}_{56}\text{H}_{62}\text{N}_2\text{S}$: 794.4634; found: 794.4633.

4,4'-(2,5-Thiophenediyl)bis[*N,N*-bis[4-(trimethylsilyl)phenyl]benzenamine] (**3d**). According to the general procedure **3d** was synthesized applying 2,5-dibromothiophene **2** (242 mg, 1 mmol), boronic acid pinacol ester **1d** (1547 mg, 3.0 mmol), KOtBu (337 mg, 3.0 mmol) and $(\text{IPr})\text{Pd}(\text{allyl})\text{Cl}$ (11.4 mg, 20 μmol ; dissolved in 1 mL IPA). After general workup the crude product was purified by column chromatography (90 g silica gel, cyclohexane : DCM, 9 \rightarrow 17 %) and subsequently recrystallized from cyclohexane to give **3d** as yellow powder (705 mg, 82 %). ^1H NMR (400 MHz, CD_2Cl_2): δ = 7.51 (d, J = 8.4 Hz, 4 H), 7.42 (d, J = 8.2 Hz, 8 H), 7.22 (s, 2 H), 7.09 - 7.07 (m, 12 H), 0.26 (s, 36 H) ppm. ^{13}C NMR (100 MHz, CD_2Cl_2): δ = 148.4 (s), 147.4 (s), 143.2 (s), 135.0 (s), 134.9 (d), 129.3 (s), 126.8 (d), 124.9 (d), 124.0 (d), 123.9 (d), -0.8 (q) ppm. R_f = 0.18 (light petrol : DCM 10 : 1). MS (MALDI-TOF): calcd for $\text{C}_{52}\text{H}_{62}\text{N}_2\text{SSi}_4$: 858.3711; found: 858.3618.

4,4'-(2,5-Thiophenediyl)bis[*N,N*-bis(4-methoxyphenyl)benzenamine] (**3e**). According to the general procedure **3e** was synthesized applying 2,5-dibromothiophene **2** (242 mg, 1 mmol), boronic acid pinacol ester **1e** (1294 mg, 3.0 mmol), KOtBu (337 mg, 3.0 mmol) and $(\text{IPr})\text{Pd}(\text{allyl})\text{Cl}$ (11.4 mg, 20 μmol ; dissolved in 1 mL IPA). After general workup the crude product was purified by column chromatography (90 g silica gel, hexanes : Et_2O 30 \rightarrow 100 %) and subsequently recrystallized from cyclohexane to give **3e** as yellow powder (647 mg, 94 %). ^1H NMR (400 MHz, CD_2Cl_2): δ = 7.42 (d, J = 8.8 Hz, 4 H), 7.13 (s, 2 H), 7.10 - 7.04 (m, 8 H), 6.93 - 6.82 (m, 12 H), 3.79 (s, 12 H) ppm. ^{13}C NMR (100 MHz, CD_2Cl_2): δ = 156.7 (s), 148.7 (s), 142.9 (s), 141.1 (s), 127.3 (d),

127.0 (s), 126.5 (d), 123.1 (d), 120.9 (d), 115.2 (d), 56.0 (q) ppm. $R_f = 0.55$ (DCM : methanol 6 : 1). MS (MALDI-TOF): calcd for $C_{44}H_{38}N_2O_4S$: 690.2552; found: 690.2450.

4,4'-(2,5-Thiophenediyl)bis[*N,N*-bis(4-fluorophenyl)benzenamine] (**3f**). According to the general procedure **3f** was synthesized applying 2,5-dibromothiophene **2** (242 mg, 1 mmol), boronic acid pinacol ester **1f** (1222 mg, 3.0 mmol), KOtBu (337 mg, 3.0 mmol) and (IPr)Pd(allyl)Cl (11.4 mg, 20 μ mol; dissolved in 1 mL IPA). After general workup the crude product was purified by column chromatography (90 g silica gel, cyclohexane : DCM, 15 \rightarrow 20 %) and subsequently recrystallized from cyclohexane to give **3f** as yellow powder (590 mg, 92 %). 1H NMR (400 MHz, CD_2Cl_2): $\delta = 7.48$ (d, $J = 8.8$ Hz, 4 H), 7.18 (s, 2 H), 7.14 - 6.90 (m, 20 H) ppm. ^{13}C NMR (100 MHz, CD_2Cl_2): $\delta = 159.6$ (s, $J_{CF} = 243.2$ Hz), 147.9 (s), 144.1 (s, $J_{CF} = 2.8$ Hz), 143.0 (s), 128.6 (s), 126.9 (d, $J_{CF} = 7.9$ Hz), 126.8 (d), 123.7 (d), 123.0 (d), 116.7 (d, $J_{CF} = 22.6$ Hz) ppm. $R_f = 0.11$ (light petrol : DCM 10 : 1). $F_p = 201.5 - 203.5$ °C. MS (MALDI-TOF): calcd for $C_{40}H_{26}F_4N_2S$: 642.1753; found: 642.1710.

General procedure for the synthesis of **3g-3i** according to Davey³⁰ and Gorvin.²⁶ Under an argon atmosphere 4,4'-(2,5-thiophenediyl)bisbenzenamine **4** (1 eq.), fluorobenzene **5a-c** (4.4 eq.) and KOtBu (4.2 eq.) were stirred in 10 mL DMSO (stored over molecular sieve, 3 Å) at 110 °C for 40 h. Conversion was monitored by TLC. The solvent was removed under reduced pressure and the remaining crude product dissolved in chloroform. After washing with water, the organic layer was dried over anhydrous sodium sulfate and evaporated to dryness under reduced pressure. Further purification was achieved by column chromatography.

4,4',4',4'''-[2,5-Thiophenediylbis(4,1-phenylene)dinitrilo]tetrakis[benzonitrile] (**3g**). According to the general procedure **3g** was synthesized applying **4** (133 mg, 0.5 mmol), KOtBu (236 mg, 2.1 mmol) and **5a** (266 mg, 2.2 mmol). After general workup the crude product was purified by column chromatography (40 g silica gel, light petrol : ethyl acetate, 5 : 1) yielding **3g** (109 mg, 33 %) as brown powder. 1H NMR (400 MHz, $CDCl_3$): $\delta = 7.65$ (d, $J = 8.5$ Hz, 4 H), 7.56 (d, $J = 8.8$ Hz, 8 H), 7.33 (s, 2H), 7.16 (d, $J = 8.6$ Hz, 12 H) ppm. ^{13}C NMR (100 MHz, $CDCl_3$): $\delta = 150.5$ (s), 145.1 (s), 143.3 (s), 134.2 (d), 132.4 (s), 127.7 (d), 127.6 (d), 125.1 (d), 123.8 (d), 119.4 (s), 106.6 (s) ppm. $R_f = 0.45$ (DCM). MS (MALDI-TOF): calcd for $C_{44}H_{26}N_6S$: 670.1940; found: 670.333.

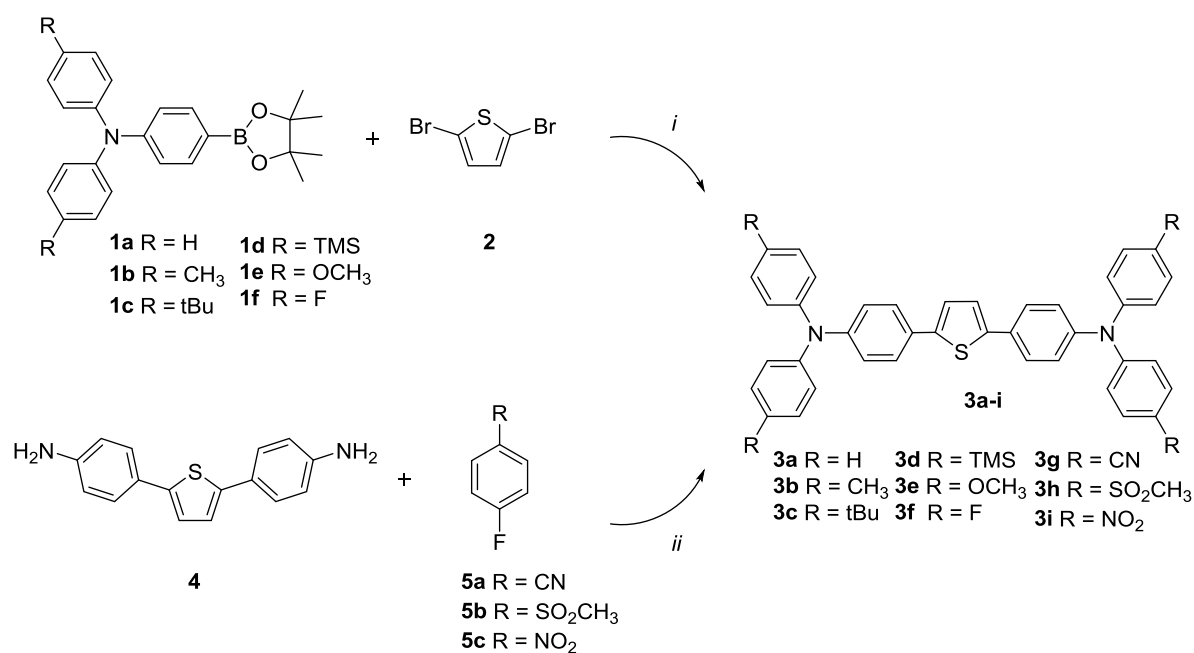
4,4'-(2,5-Thiophenediyl)bis[*N,N*-bis[4-(methylsulfonyl)phenyl]benzenamine] (**3h**). According to the general procedure **3h** was synthesized applying **4** (133 mg, 0.5 mmol), KOtBu (236 mg, 2.1 mmol) and **5b** (383 mg, 2.2 mmol). After general workup the crude product was purified by column chromatography (40 g silica gel, Et_2O : DCM, 1 : 3) yielding **3h** (184 mg, 42 %) as brown powder. 1H NMR (400 MHz, CD_2Cl_2) $\delta = 7.81$ (d, $J = 8.7$ Hz, 8 H), 7.67 (d, $J = 8.7$ Hz, 4 H), 7.34 (s, 2 H), 7.26 (d, $J = 8.7$ Hz, 8 H), 7.20 (d, $J = 8.7$ Hz, 4 H), 3.06 (s, 12 H) ppm. ^{13}C NMR (100 MHz, CD_2Cl_2): $\delta = 151.6$ (s), 145.3 (s), 143.3 (s), 135.2 (s), 132.4 (s), 129.6 (d), 127.6 (d), 127.5 (d), 125.1 (d), 123.8 (d), 45.1 (q) ppm. $R_f = 0.80$ (DCM : methanol 10 : 1). HR-ESI-FTMS $[M+H]^+$ m/z calcd. 883.1305 for $C_{44}H_{39}N_2O_8S_5^+$, found 833.1321.

4,4'-(2,5-Thiophenediyl)bis[*N,N*-bis(4-nitrophenyl)benzenamine] (**3i**). According to the general procedure **3i** was synthesized applying **4** (133 mg, 0.5 mmol), KOtBu (236 mg, 2.1 mmol) and **5c** (310 mg, 2.2 mmol). After general workup the crude product was purified by column chromatography (40 g silica gel, cyclohexane : DCM, 15 → 20 %) yielding **3i** (139 mg, 38 %) as an orange powder. ¹H NMR (600 MHz, CD₂Cl₂): δ = 8.16 (d, J = 9.2 Hz, 8 H), 7.70 (d, J = 8.7 Hz, 4 H), 7.37 (s, 2 H), 7.23 - 7.20 (m, 12 H) ppm. ¹³C NMR (150 MHz, CD₂Cl₂): δ = 152.2 (s), 144.8 (s), 143.5 (s), 143.3 (s), 133.0 (s), 127.9 (d), 127.8 (d), 126.0 (d), 125.3 (d), 123.2 (d) ppm. R_f = 0.83 (DCM). MS (MALDI-TOF): calcd for C₄₀H₂₆N₆O₈S: 750.1533; found: 750.1450.

2PIP Structuring Tests. For the direct laser writing of 3D structures, a Ti:sapphire laser from High Q Lasers providing NIR pulses at 797.5 nm with a pulse duration of 72 fs was used. The system operates at a repetition rate of 73 MHz and a maximum output power of 427 mW. Direct laser writing with this system was carried out at laser powers between 10 – 100 mW (measured after passing the microscope objective). The laser is focused by a 20× microscope objective (NA = 0.8), and the sample is mounted on a high-precision piezoelectric XYZ scanning stage with 200 nm positioning accuracy. For all samples the same fabrication process was implemented: the optical material was drop-cast from a liquid acrylate-based test resin formulation (5 μmol/g of the 2PI in a 1:1 mixture of trimethylolpropane triacrylate (TTA, Genomer 1330) and ethoxylated-(20/3)-trimethylolpropane triacrylate (ETA, Sartomer 415)) onto a methacrylate functionalized glass substrate. However, **3d** proved to be less soluble, therefore a concentrated formulation of the 2PI in the resin was applied. Subsequently, the samples were exposed to the laser beam, and the focus was moved across the photosensitive material, which leads to an embedded 3D structure (lateral dimension: 50 × 50 μm, 5 μm hatch distance, 0.7 μm layer distance, 20 layers) inside the material volume. After laser writing, the unexposed material was removed by development of the structure in ethanol (rinsing). The resulting structures, particularly their dimensions, were studied by means of scanning electron microscopy (SEM).

RESULTS AND DISCUSSION

Synthesis. The synthetic assembly of TPA structures was realized for compounds **3a-f** bearing donating substituents *via* Suzuki cross-coupling reactions and for compounds **3g-i** bearing electron-withdrawing substituents by nucleophilic aromatic substitution. A general Suzuki cross-coupling procedure developed in an earlier study tolerating a broad spectrum of functionalized TPA boronic acid esters²⁸ was applied for the synthesis of **3a-f** from **1a-f** and dibromothiophene **2** (Scheme 1, Table 1). Since the synthesis of triphenylamineboronic acid pinacolates bearing electron-withdrawing substituents proved to be troublesome in earlier studies, nucleophilic aromatic substitution was chosen as an alternative synthetic approach towards **3g-i**. The application of amine **4** and fluorobenzenes **5a-c** using KOtBu as base in DMSO at 120 °C yielded target compounds bearing electron-withdrawing substituents (Table 1).



Scheme 1: Synthetic pathways towards **3a-i**. *i*: KOtBu, (IPr)Pd(allyl)Cl, isopropanol / water, reflux; *ii*: KOtBu, DMSO, 120 °C.

The obtained solid materials appear yellow to brown in color and are soluble in common organic solvents. The characterization of **3a-i** was performed by ¹H / ¹³C-NMR spectroscopy and HR-MS analysis. The data are consistent with the proposed structural formulations.

Photophysics. Photophysical properties of **3a-i** were determined by UV-Vis and fluorescence spectroscopy (Table 1). Two absorption maxima were located in the ranges of 279 - 354 and 381 - 403 nm for substances **3a-i** when measured in THF solution (Figure 2). While the former can be attributed to the n-π* transition of the triphenylamine moiety, the longer wavelength absorption originates from the charge transfer π-π* transitions of the electron-donating triphenylamine moiety to the electron-accepting thiophene moiety.^{32,33} A clear trend can be observed, as the electron-

withdrawing sulfone derivative **3h** shows the absorption maximum with the highest energy, whereas the electron-donating methoxy derivative **3e** has the absorption maximum at the longest wavelength.

Table 1: Experimental data and photophysical characteristics of compounds **3a-i**.

Comp.	Yield (%)	$\lambda_{\text{max}}^{\text{a}}$ (nm)	$\lambda_{\text{em}}^{\text{b}}$ (nm)	$\Delta\nu^{\text{c}}$ (cm^{-1})	$\phi_{\text{f}}^{\text{d}}$ (%)	$\sigma_{2\text{PA}}^{\text{e}}$ (GM)	$\lambda_{\text{max}}^{\text{f}}$ (nm)
3a	92	302, 390	441, 486	2965	18	323	693
3b	88	304, 396	453, 480	3566	44	462	705
3c	91	304, 398	451, 476	3080	48	461	709
3d	84	320, 394	447, 475	3009	50	406	704
3e	94	296, 399	471, 485	3831	56	497	715
3f	92	298, 388	441, 465	3097	26	255	674
3g	33	354, 380	432, 457	3167	48	215	663
3h	38	345, 381	432, 456	3099	45	244	657
3i	42	279, 403	-	-	-	-	-

^a Absorption maxima determined from spectra measured in 1 mg/ μL THF solution. ^b Emission maxima. ^c Stokes shifts. ^d Fluorescence quantum yield. ^e Two-photon cross-sections determined by two-photon excited fluorescence. ^f Maximum of two-photon absorption spectra.

The corresponding emission spectra of **3b-e** exhibit a significant red shift, correlating with higher electron density on the triphenylamine moiety. A hypsochromic shift of the emission maxima of **3f-h** of approximately 10 nm compared to **3a** in solution was observed. The measurement of the fluorescence of **3i** gave no emission of radiation, which may be attributed to triplet-level formation from the original excited singlet states. Therefore, no further photophysical analysis was performed for this compound.

Stokes shifts for all compounds **3a-h** are comparable and range from 2965 - 3831 cm^{-1} . The quantum yields determined in solution are generally high and range from $\phi_{\text{f}} = 0.18$ for the electronically neutral **3a** to $\phi_{\text{f}} = 0.56$ for the methoxy substituted derivative **3e** (Table 2).

Two-photon excited fluorescence (TPEF) spectra are depicted in Figure 2, right: The maxima of 2PA cross-sections range in the moderate area from 215 to 497 GM (Table 1). When increasing the donor strength of the TPA moiety (e.g. from **3a** to **3e**) a significant increase of the 2PA cross-section value can be observed, indicating good applicability for 2PIP. In general target compounds **3g-h** bearing electron-withdrawing substituents 2PA cross-sections tend to be lower compared to materials with electron-donating residues.

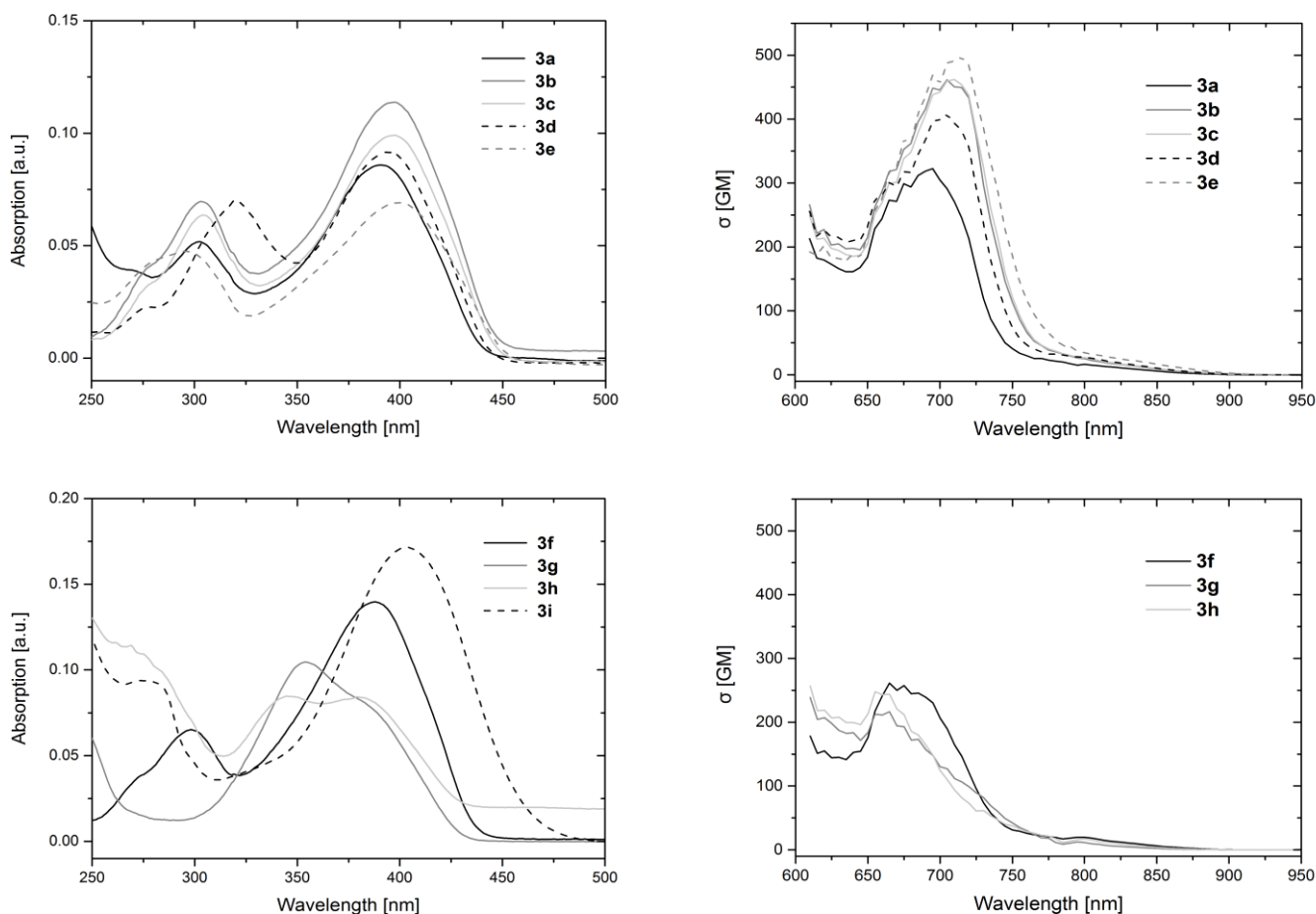


Figure 2: Absorption spectra (left) of **3a-i** and TPEF spectra (right) of **3a-h** in THF solution.

2PIP Structuring Tests. An important parameter determining the applicability of a two-photon photopolymer system is the sensitivity in correlation with low laser power and short exposure times, which are also essential for high throughput in mass production. An efficient method to evaluate the activity of PIs constitutes the fabrication of defined 3D test structures applying various laser intensities and writing speeds for the evaluation. In order to assess the ideal processing window of potential PIs **3a-i**, defined woodpiles (lateral dimension: $50 \times 50 \mu\text{m}$, $5 \mu\text{m}$ hatch distance, $0.7 \mu\text{m}$ layer distance, 20 layers) were structured in an acrylate-based test resin formulation by means of 2PIP. **B3FL** (2,7-bis[[4-(dibutylamino)phenyl]ethynyl]-9H-fluoren-9-one), recently reported by us,³⁴ was used as reference material. The laser intensity and the writing speed were varied in a range of 10 - 100 mW (measured after passing the $100\times$ microscope objective) and 0.316 - 316 mm/s, respectively.

Scanning electron microscopy (SEM) of the obtained 3D woodpile structures was performed (see supplementary information). Evaluation of the quality of these measurements (Figure 3) was achieved using a four color classification reported earlier¹⁵: class A (green) defines excellent structures with fine hatch lines and class B (yellow) good structures with thick hatch lines or slightly

contorted structures. Structures rated as class C (red) have identified shapes but with small mistakes (e.g., holes, burst regions caused by overexposure). Parts structured with laser intensities rated as class D (blue) no longer show acceptable results.

All 2PI compounds **3a-i** gave defined woodpile structures: while compounds **3b-e** bearing electron-donating substituents on the triphenylamine generally show a broad processing window, compounds **3f-i** with electron-withdrawing substituents only gave clear structures at low laser intensities and moderate writing speed. Electronically neutral **3a** exhibits excellent performance at both low and high writing speed and laser intensities. Compared to the reference material **B3FL**, **3a** shows an even broader processing window, especially at higher writing speeds.

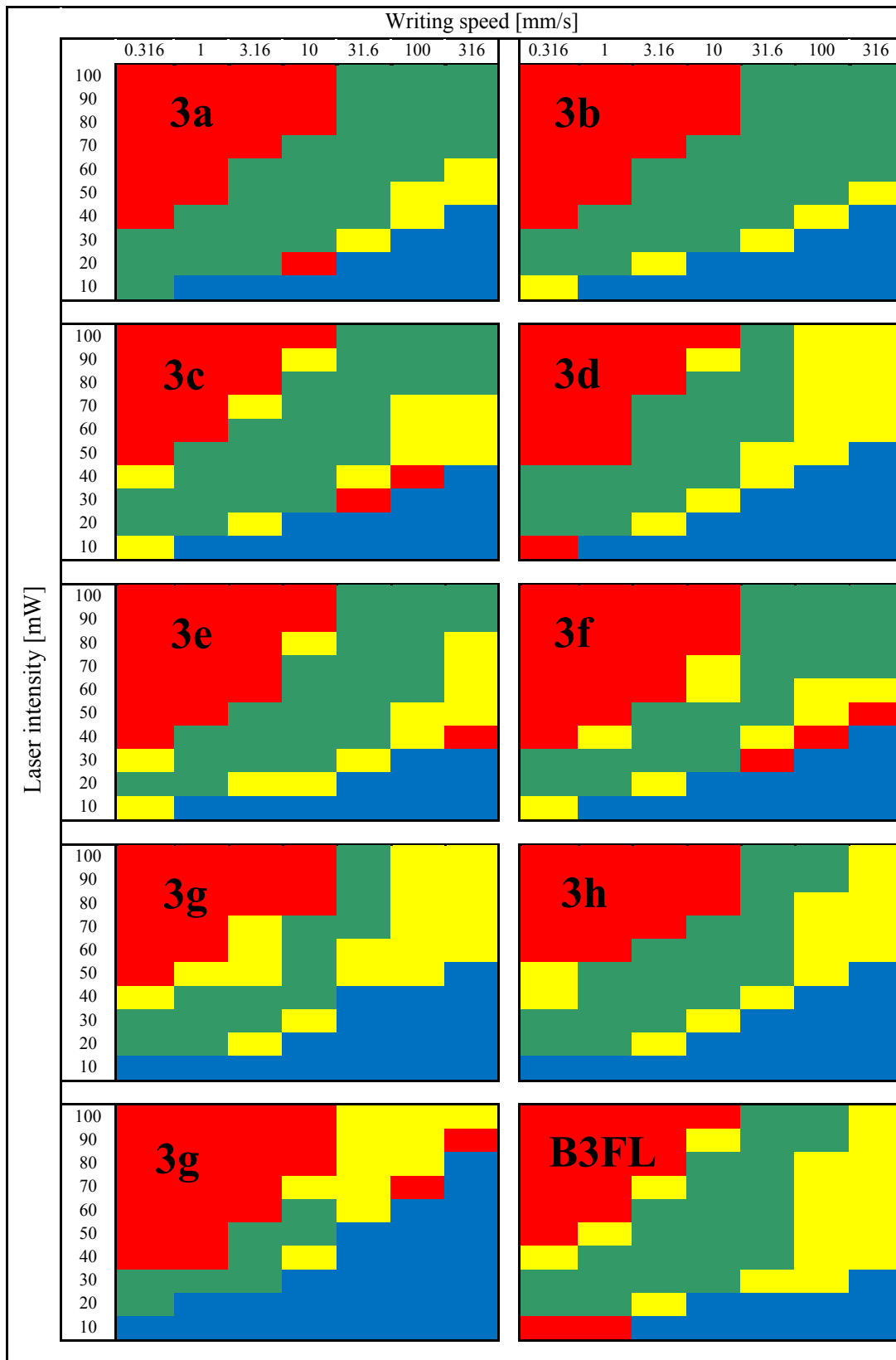


Figure 3: 2PIP screening tests of 3a-i and reference material B3FL.

CONCLUSION

A series of thiophenes bearing *p*-substituted triaryl amines with different substituents has been synthesized via Suzuki cross-coupling or nucleophilic aromatic substitution. The systematic evaluation of structure-property relationships via UV-Vis spectroscopy and two-photon absorption structuring tests confirmed the significant influence of the electronic characteristics of the substituents on the photophysical and photochemical properties. When tested as 2PIs all compounds showed broad processing windows, although most substances exhibit only moderate two-photon cross-sections and high quantum yields, which is generally believed to be not beneficial for the two-photon absorption. Compound **3a** bearing no substituent on the triphenylamine moiety proved to be the most efficient photoinitiator among this series. The straightforward synthetic route combined with high 2PA initiation efficiency of these initiators makes these compounds attractive for two-photon absorption structuring. However, these materials exhibit low solubility in the applied acrylate formulation, which may hamper commercial application. Therefore, future investigations will focus on the development of soluble thiophene-based two-photon initiators. The structural versatility and capability of our molecular design, however, may contribute to the further developments in other areas of functional organic materials.

ACKNOWLEDGMENT

The authors thank Dr. K. Föttinger for supporting the photophysical characterization, M. Mathuber and T. Schwartz for contributing to the synthetic experiments. The authors thank M. Marchetti-Deschmann for MALDI-HRMS measurements.

ELECTRONIC SUPPLEMENTARY INFORMATION

¹H and ¹³C NMR spectra of compounds **3a-i** as well as SEM images of the two-photon absorption structuring tests.

REFERENCES

- (1) Kufelt, O.; El-Tamer, A.; Sehring, C.; Schlie-Wolter, S.; Chichkov, B. N. *Biomacromolecules* **2014**, *15* (2), 650.
- (2) Zeng, H.; Martella, D.; Wasylczyk, P.; Cerretti, G.; Lavocat, J.-C. G.; Ho, C.-H.; Parmeggiani, C.; Wiersma, D. S. *Adv. Mater.* **2014**, *26* (15), 2319.
- (3) Lott, J.; Ryan, C.; Valle, B.; Johnson, J. R.; Schiraldi, D. A.; Shan, J.; Singer, K. D.; Weder, C. *Adv. Mater.* **2011**, *23* (21), 2425.
- (4) Li, L.; Wang, P.; Hu, Y.; Lin, G.; Wu, Y.; Huang, W.; Zhao, Q. *Spectrochim. Acta. A. Mol. Biomol. Spectrosc.* **2015**, *139*, 243.
- (5) Ushiba, S.; Shoji, S.; Kuray, P.; Masui, K.; Kono, J.; Kawata, S. in *Proc. SPIE*; von Freymann, G., Schoenfeld, W. V., Rumpf, R. C., Eds.; **2013**; Conference Volume 86130.
- (6) Malval, J.-P.; Achelle, S.; Bodiou, L.; Spangenberg, A.; Gomez, L. C.; Soppera, O.; Guen, F. R. *J. Mater. Chem. C* **2014**, *2* (37), 7869.
- (7) Qian, Y.; Meng, K.; Lu, C.-G.; Lin, B.; Huang, W.; Cui, Y.-P. *Dyes Pigm.* **2009**, *80* (1), 174.
- (8) Polavarapu, L.; Manna, M.; Xu, Q.-H. *Nanoscale* **2011**, *3* (2), 429.
- (9) Idris, N. M.; Gnanasammandhan, M. K.; Zhang, J.; Ho, P. C.; Mahendran, R.; Zhang, Y. *Nat. Med.* **2012**, *18* (10), 1580.
- (10) Gary-Bobo, M.; Mir, Y.; Rouxel, C.; Brevet, D.; Basile, I.; Maynadier, M.; Vaillant, O.; Mongin, O.; Blanchard-Desce, M.; Morère, A.; Garcia, M.; Durand, J.-O.; Rachm, L. *Angew. Chem.* **2011**, *123* (48), 11627.
- (11) Pawlicki, M.; Collins, H. A.; Denning, R. G.; Anderson, H. L. *Angew. Chem. Int. Ed.* **2009**, *48* (18), 3244.
- (12) Cumpston, B. H.; Ananthavel, S. P.; Barlow, S.; Dyer, D. L.; Ehrlich, J. E.; Erskine, L. L.; Heikal, A. A.; Kuebler, S. M.; Lee, I.-Y. S.; McCord-Maughon, D.; Qin, J.; Rockel, H.; Rumi, M.; Wu, X.-L.; Marder, S. R.; Perry, J. W. *Nature* **1999**, *398* (6722), 51.
- (13) Warther, D.; Gug, S.; Specht, A.; Bolze, F.; Nicoud, J.-F.; Mourot, A.; Goeldner, M. *Bioorg. Med. Chem.* **2010**, *18* (22), 7753.
- (14) Chow, C.-F. *RSC Adv.* **2013**, *3* (41), 18835.
- (15) Li, Z.; Pucher, N.; Cicha, K.; Torgersen, J.; Ligon, S. C.; Ajami, A.; Husinsky, W.; Rosspeintner, A.; Vauthey, E.; Naumov, S.; Scherzer, T.; Stampfl, J.; Liska, R. *Macromolecules* **2013**, *46* (2), 352.
- (16) Gao, Y.; Qu, Y.; Jiang, T.; Zhang, H.; He, N.; Li, B.; Wu, J.; Hua, J. *J. Mater. Chem. C* **2014**, *2* (31), 6353.
- (17) Albota, M. *Science* **1998**, *281* (5383), 1653.
- (18) Huang, P.-H.; Shen, J.-Y.; Pu, S.-C.; Wen, Y.-S.; Lin, J. T.; Chou, P.-T.; Yeh, M.-C. *J. Mater. Chem.* **2006**, *16* (9), 850.
- (19) He, G. S.; Tan, L.-S.; Zheng, Q.; Prasad, P. N. *Chem. Rev.* **2008**, *108* (4), 1245.
- (20) Zheng, S.; Beverina, L.; Barlow, S.; Zojer, E.; Fu, J.; Padilha, L. A.; Fink, C.; Kwon, O.; Yi, Y.; Shuai, Z.; Stryland, E. W. V.; Hagan, D. J.; Brédas, J.-L.; Marder, S. R. *Chem. Commun.* **2007**, *13*, 1372.
- (21) Kim, O.-K.; Lee, K.-S.; Woo, H. Y.; Kim, K.-S.; He, G. S.; Swiatkiewicz, J.; Prasad, P. N. *Chem. Mater.* **2000**, *12* (2), 284.
- (22) Zhou, H.; Zhou, F.; Tang, S.; Wu, P.; Chen, Y.; Tu, Y.; Wu, J.; Tian, Y. *Dyes Pigm.* **2012**, *92* (1), 633.
- (23) Lumpi, D.; Horkel, E.; Plasser, F.; Lischka, H.; Fröhlich, J. *Chem. Phys. Chem.* **2013**, *14* (5), 1016.
- (24) Van Keuren, E.; Wakebe, T.; Andreaus, R.; Möhwald, H.; Schrof, W.; Belov, V.; Matsuda, H.; Rangel-Rojo, R. *Appl. Phys. Lett.* **1999**, *75* (21), 3312.
- (25) Navarro, O.; Nolan, S. P. *Synthesis* **2006**, 366.
- (26) Almansa, C.; Alfón, J.; de Arriba, A. F.; Cavalcanti, F. L.; Escamilla, I.; Gómez, L. A.; Miralles, A.; Soliva, R.; Bartolí, J.; Carceller, E.; Merlos, M.; García-Rafanell, J. *J. Med. Chem.* **2003**, *46* (16), 3463.
- (27) Gonzalez, J. L.; Stephens, C. E.; Wenzler, T.; Brun, R.; Tanius, F. A.; Wilson, W. D.; Barszcz, T.; Werbovetz, K. A.; Boykin, D. W. *Eur. J. Med. Chem.* **2007**, *42* (4), 552.
- (28) Lumpi, D.; Holzer, B.; Binting, J.; Horkel, E.; Waid, S.; Wanzenböck, H. D.; Marchetti-Deschmann, M.; Hametner, C.; Bertagnolli, E.; Kymissis, I.; Fröhlich, J. *New J. Chem.* **2015**, *39* (3), 1840.
- (29) Marion, N.; Navarro, O.; Mei, J.; Stevens, E. D.; Scott, N. M.; Nolan, S. P. *J. Am. Chem. Soc.* **2006**, *128* (12), 4101.
- (30) Davey, M. H.; Lee, V. Y.; Wu, L.-M.; Moylan, C. R.; Volksen, W.; Knoesen, A.; Miller, R. D.; Marks, T. J. *Chem. Mater.* **2000**, *12* (6), 1679.
- (31) Gorvin, J. H. *J. Chem. Soc. Perkin I* **1988**, *6*, 1331.
- (32) Ge, Z.; Hayakawa, T.; Ando, S.; Ueda, M.; Akiike, T.; Miyamoto, H.; Kajita, T.; Kakimoto, M. *Adv. Funct. Mater.* **2008**, *18* (4), 584.
- (33) Kong, M.; Wang, T.; Tian, X.; Wang, F.; Liu, Y.; Zhang, Q.; Wang, H.; Zhou, H.; Wu, J.; Tian, Y. *J. Mater. Chem. C* **2015**, *3* (21), 5580.
- (34) Li, Z.; Siklos, M.; Pucher, N.; Cicha, K.; Ajami, A.; Husinsky, W.; Rosspeintner, A.; Vauthey, E.; Gescheidt, G.; Stampfl, J.; Liska, R. *J. Polym. Sci. Part Polym. Chem.* **2011**, *49* (17), 3688.

Manuscript # 10

Markus Lunzer, **Brigitte Holzer***, Arnulf Rosspeintner, Maximilian Tromayer, Daniel Lumpi, Ernst Horkel, Christian Hametner, Eric Vauthey, Robert Liska, and Johannes Fröhlich

Synthesis and Characterization of Triphenylamine-based Two-Photon Initiators

Manuscript draft

Synthesis and Characterization of Triphenylamine-based Two-Photon Initiators

Markus Lunzer,^{a,c} Brigitte Holzer,^{a,} Arnulf Rosspointner,^c Maximilian Tromayer,^{a,b} Daniel Lumpi,^a Ernst Horkel,^a Christian Hametner,^a Eric Vauthey,^c Robert Liska^a and Johannes Fröhlich^a*

^aInstitute of Applied Synthetic Chemistry, Vienna University of Technology,

Getreidemarkt 9/163OC, A-1060 Vienna, Austria

^bInstitute of Materials Science and Technology, Vienna University of Technology,

Favoritenstraße 9-11, A-1040 Vienna, Austria

^cPhysical Chemistry Department, University of Geneva,

Quai Ernest Ansermet 30, CH-1211 Geneva, Switzerland

*brigitte.holzer@tuwien.ac.at

A series of soluble symmetric chalcogenophenes bearing hexyl-substituted triphenylamines, indolocarbazoles and phenylcarbazoles was designed and synthesized as potential two-photon absorption initiators. The influence of both planarized linkers and caps as well as electron rich linkers was evaluated aiming to increase two-photon absorption and thus the performance of these D- π -D type target molecules. This study elucidates the molecular structure / two-photon absorption efficiency relationship by systematic variation of substituents of the dye molecules applying UV-Vis, fluorescence and two-photon excited fluorescence spectroscopy. Although these materials are highly fluorescent, two-photon absorption cross-sections up to 5200 GM have been determined. Structuring tests of the target compounds in monomer formulations reveal the efficiency of these materials as two-photon absorption initiators.

INTRODUCTION

Two-photon absorption (2PA) is a third-order nonlinear optical (NLO) process involving electronic excitation of a molecule induced by simultaneous absorption of a pair of photons of the same or different energies.¹ Unlike linear one-photon absorption 2PA provides excellent spatial control, therefore 3D writing with very high resolution can be achieved due to the confinement of the photoactivated polymerization within the focal volume of the laser beam. The use of a long wavelength excitation source, typically a Ti:sapphire femtosecond laser (approximately 800 nm), allows deeper penetration into the resin than UV^{2,3} and consequently reduces unwanted thermal or photochemical side reactions.⁴

In the last decades, different types of two-photon absorption initiators have been proposed exhibiting large two-photon cross-sections (σ_{2PA}) based on dipolar (A- π -D), quadrupolar (D- π -D, A- π -A, D- π -A- π -D, A- π -D- π -A) and octupolar (A₃-D, D₃-A) chromophores, where D and A refer to electron-donating and electron-withdrawing groups, respectively, linked through a bridge of π -conjugated bonds.⁵ Extensive research efforts have been made aiming for large 2PA cross-sections: the extension of the effective π -conjugation length, incorporation of π -conjugated bridges in symmetrical and asymmetrical configurations, and variation of substructures with strong electron-donating and/or electron-accepting effects are believed to facilitate the effect of intramolecular charge transfer.^{3,6-8} Although many structures, macrocycles, dendrimers, polymers and multibranching molecules have been developed, there remains some uncertainty in the particulars of design criteria for molecules with large 2PA cross-sections at desired wavelengths.

Recently, we have reported on the synthesis and photophysical properties of a series of cap-linker-cap systems based on substituted thiophenes bearing various triphenylamines with either electron-withdrawing or donating residues (Figure 1). Although these materials exhibit efficient 2PA verified by structuring tests, they lack solubility in monomer formulations, which hampers their application. In this work we adapt strategies to further increase the two-photon absorption and thus the efficiency of two-photon absorption initiators based on quadrupolar cap-linker-cap type molecules. The following strategies are applied altering the design of the initial cap-linker-cap system (Figure 1): (i) planarization of the triphenylamine (TPA) cap by introduction of indolocarbazole (ICz) and phenylcarbazole (PCz) moieties, (ii) elongation and planarization of the π -linker by applying bithiophene (BT), benzo[1,2-*b*:4,5-*b'*]dichalcogenophenes (BDT, BDS) or dithieno[3,2-*b*:2',3'-*d*]thiophene (DTT), as well as (iii) enhancing the electron density of the linker using more electron-donating selenophene (S) and 2,3-dihydrothieno[3,4-*b*]-1,4-dioxine (EDOT). To overcome the shortcoming of low solubility of the original cap-linker-cap PIs in the respective monomer formulation all target compounds were designed bearing hexyl substituents on the triarylamine building blocks.

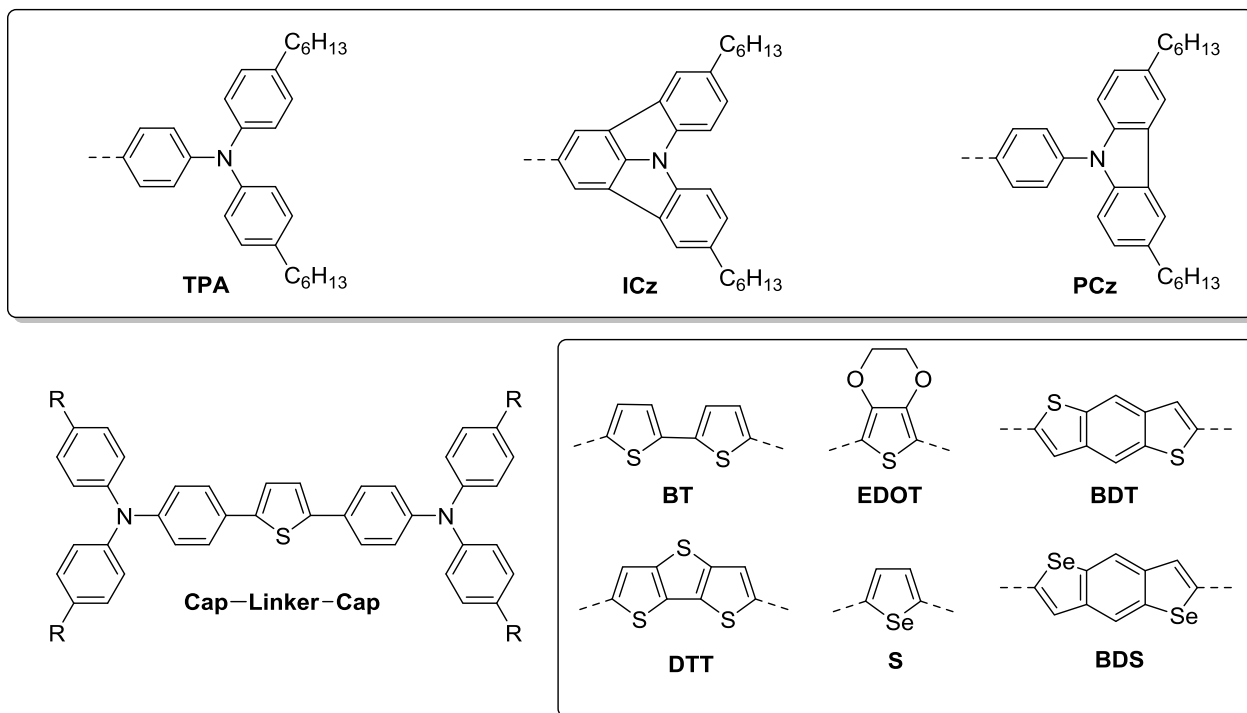


Figure 1: Cap-linker-cap systems based on triphenylamine-substituted thiophene (left, bottom) and structural motives applied in target compounds.

EXPERIMENTAL SECTION

Synthesis and Characterization. 2,3-Dihydrothieno[3,4-*b*]-1,4-dioxine (EDOT), anhydrous *N,N*-dimethylformamide (DMF), anhydrous *N,N*-dimethylacetamide (DMAc), *n*-butyllithium solution (2.5 M in hexanes) and *n*-hexyllithium solution (2.3 M in hexanes) were purchased from Aldrich Chemical Co. All substances purchased from commercial sources were used as received without further purification. Isopropyl pinacol borate (CAS 61676-62-8),⁹ allyl[1,3-bis(2,6-diisopropylphenyl)imidazol-2-ylidene]chloropalladium(II) ((IPr)Pd(allyl)Cl, CAS 478980-03-9),¹⁰ 3,6-dihexyl-9*H*-carbazole (CAS 1131605-21-4),¹¹ 1,1'-benzo[1,2-*b*:4,5-*b'*]dithiophene-2,6-diylbis(1,1,1-trimethylstannane) (CAS 1242077-07-1),¹² 1,1'-benzo[1,2-*b*:4,5-*b'*]diselenophene-2,6-diylbis(1,1,1-trimethylstannane) (CAS 1465181-53-6),¹³ 1,1'-(2,5-selenophenediyl)bis(1,1,1-trimethylstannane) (CAS 220770-41-2),¹⁴ 2,5-dibromothiophene (CAS 3141-27-3),¹⁵ 5,5'-dibromo-2,2'-bithiophene (CAS 4805-22-5)¹⁶ and 2,6-dibromodithieno[3,2-*b*:2',3'-*d*]thiophene (CAS 67061-69-2)¹⁷ were synthesized according to literature. Isopropylalcohol (IPA) and dimethylsulfoxide (DMSO) were used in p.a. quality. Technical grade solvents were distilled prior to use. Analytical TLC was performed on Merck silica gel 60 F254 plates. Chromatographic separations at preparative scale were carried out on silica gel (Merck silica gel 60, 40 - 63 μm). Nuclear magnetic resonance (NMR) spectra were obtained using a Bruker DPX-200 or Avance DRX-400 fourier transform spectrometer operating at the following frequencies: DPX-200: 200.1 MHz (^1H) and 50.3 MHz (^{13}C); DRX-400: 400.1 MHz (^1H) and 100.6 MHz (^{13}C). The chemical shifts are reported in delta (δ) units, parts per million (ppm) downfield from tetramethylsilane using residual solvent signals for calibration. Coupling constants are reported in Hertz; multiplicity of signals is indicated by using

following abbreviations: s=singlet, d=doublet, t=triplet, q=quartet. The multiplicity of ^{13}C signals was obtained by measuring JMOD spectra. High-resolution mass spectra (HRMS) were acquired using a Thermo Scientific LTQ Orbitrap XL hybrid FTMS (Fourier Transform Mass Spectrometer) equipped with Thermo Fischer Exactive Plus Orbitrap (LC-ESI+) and a Shimadzu IT-TOF Mass Spectrometer. UV-Vis absorption spectra and fluorescence emission spectra were recorded in THF solutions (5 μM) with a Perkin Elmer Lambda 750 spectrometer and an Edinburgh FLS920, respectively.

2PIP Structuring Tests. For the direct laser writing of 3D structures, a Ti:sapphire laser from High Q Lasers providing NIR pulses at 797.5 nm with a pulse duration of 72 fs was used. The system operates at a repetition rate of 73 MHz and a maximum output power of 427 mW. Direct laser writing with this system was carried out at laser powers between 10 – 100 mW (measured after passing the microscope objective). The laser is focused by a 20 \times microscope objective (NA = 0.8), and the sample is mounted on a high-precision piezoelectric XYZ scanning stage with 200 nm positioning accuracy. For all samples the same fabrication process was implemented: the optical material was drop-cast from a liquid formulation (8.8 $\mu\text{mol/g}$ two-photon absorption initiator dissolved in a 1:1 mixture of trimethylolpropane triacrylate (TTA, Genomer 1330) and ethoxylated-(20/3)-trimethylolpropane triacrylate (ETA, Sartomer 415)) onto a methacrylate functionalized glass substrate. Subsequently, the samples were exposed to the laser beam, and the focus was moved across the photosensitive material, which leads to an embedded 3D structure (lateral dimension: 50 \times 50 μm , 5 μm hatch distance, 0.7 μm layer distance, 20 layers) inside the material volume. After laser writing, the unexposed material was removed by development of the structure in ethanol (rinsing). The resulting structures, particularly their dimensions, were studied by means of scanning electron microscopy (SEM).

1-Hexyl-4-iodobenzene (2). The synthesis of **2** was adapted from a procedure described by Doszczak.¹⁸ 1,4-Diodobenzene **1** (49.49 g, 150.0 mmol, 1.00 eq) was suspended in 150 mL anhydrous Et_2O under argon atmosphere and cooled below $-78\text{ }^\circ\text{C}$. Subsequently n-HexLi (66 mL, 151.5 mmol, 1.01 eq) was added dropwise over 2 hours to the reaction mixture. After complete addition the suspension was stirred for 15 min below $-78\text{ }^\circ\text{C}$ and then warmed to $-20\text{ }^\circ\text{C}$. Thereafter it was cooled to $-70\text{ }^\circ\text{C}$ and 1-iodohexane (39.76 g, 187.5 mmol, 1.25 eq) was slowly added before the cooling bath was replaced by an ice-bath and the suspension was stirred overnight. The reaction mixture was quenched with 100 mL water and extracted repeatedly with Et_2O . The combined organic layers were dried over Na_2SO_4 , filtered and dried *in vacuo*. Remains of 1-iodohexane were removed on a high-vacuum rotary evaporator before the crude product was fractionated by high-vacuum distillation ($88 - 98\text{ }^\circ\text{C}$, 0.0018 mbar). Compound **2** was obtained in sufficient purity as a pinkish liquid (28.88 g, 100.2 mmol, 67%). ^1H NMR (200 MHz, CDCl_3): $\delta = 7.62 - 7.55$ (m, 2 H), 6.95 - 6.91 (m, 2 H), 2.54 (t, $J = 7.6\text{ Hz}$, 2 H), 1.61 - 1.50 (m, 2 H), 1.42 - 1.18 (m, 6H), 0.88 (t, $J =$

7.7, 3 H) ppm. ^{13}C NMR (50 MHz, CDCl_3): δ = 142.4, 137.2, 130.5, 90.5, 35.4, 31.6, 31.2, 28.8, 22.5, 14.1 ppm.

General procedure for the synthesis of triphenylamines **4** and **7** according to Goodbrand.¹⁹ Substituted aniline (1.0 eq), iodobenzene (2.2 eq), KOH (7.8 eq), Cu(I)Cl (0.04 eq) and 1,10-phenanthroline monohydrate (0.04 eq) were suspended in anhydrous toluene in a round-bottomed flask equipped with a Dean-Stark trap under a reflux condenser and an argon balloon. The reaction mixture was stirred magnetically at reflux until GC-MS analysis showed full conversion. After cooling the reaction mixture to room temperature water was added to the stirred suspension until the solid KOH residue was dissolved. The aqueous phase was extracted with toluene repeatedly. The combined organic layers were washed with brine, dried over Na_2SO_4 and filtered before the toluene was removed by rotary evaporation. Purification was performed as stated in the detailed descriptions.

4-Bromo-*N,N*-bis(4-hexylphenyl)benzenamine (**4**). 4-Bromoaniline **3** (9.77 g, 57 mmol, 1.0 eq), 1-hexyl-4-iodobenzene **2** (36.00 g, 125 mmol, 2.2 eq), KOH (24.87 g, 443 mmol, 7.8 eq), Cu(I)Cl (230 mg, 2.3 mmol, 0.04 eq) and 1,10-phenanthroline monohydrate (450 mg, 2.3 mmol, 0.04 eq) were refluxed in 120 mL of anhydrous toluene until TLC showed full conversion (4 d). The crude product was flashed over a pad of silica. Remaining impurities were distilled off (120 °C, 0.24 mbar) and **4** was obtained as yellow oil (24.17 g, 49 mmol, 86%). R_f = 0.44 (light petroleum). ^1H NMR (200 MHz, CH_2Cl_2): δ = 7.31 - 7.24 (m, 2 H), 7.11 - 7.06 (m, 4 H), 6.98 - 6.94 (m, 4 H), 6.90 - 6.83 (m, 2 H), 2.56 (t, J = 7.9 Hz, 4 H), 1.63 - 1.52 (m, 4 H), 1.42 - 1.31 (m, 12 H), 0.89 (t, J = 6.6 Hz, 6 H) ppm. ^{13}C NMR (50 MHz, CDCl_3): δ = 147.4 (s), 145.0 (s), 138.0 (s), 131.9 (d), 129.2 (d), 124.5 (d), 124.0 (d), 113.6 (s), 35.4 (t), 31.7 (t), 31.5 (t), 29.1 (t), 22.6 (t), 14.1 (q) ppm.

2,6-Dichloro-*N,N*-bis(4-hexylphenyl)benzenamine (**7**). The synthesis of **7** followed the general procedure, 2,6-dichloroaniline **6** (4.86 g, 30 mmol, 1.0 eq), 1-hexyl-4-iodobenzene **2** (17.79 g, 61.7 mmol, 2.06 eq), KOH (13.13 g, 234 mmol, 7.8 eq), Cu(I)Cl (120 mg, 1.2 mmol, 0.04 eq) and 1,10-phenanthroline monohydrate (240 mg, 1.2 mmol, 0.04 eq) were refluxed in 43 mL anhydrous toluene until GC-MS showed full conversion (8 d). After work-up according the crude product (15.94 g) was flashed over silica gel (420 g) applying light petroleum. Impure fractions were further purified by distilling impurities off *via* Kugelrohr-distillation (140 °C, 0.014 mbar) yielding **7** as a yellowish oil (5.09 g, 10.5 mmol, 35%). R_f = 0.47 (light petroleum). ^1H NMR (200 MHz, CDCl_3): δ = 7.44 - 7.39 (m, 2 H), 7.24 - 7.16 (m, 1 H), 7.12 - 6.98 (m, 4 H), 6.98 - 6.84 (m, 4 H), 2.57 (t, J = 7.6 Hz, 4 H), 1.69 - 1.53 (m, 4 H), 1.39 - 1.28 (m, 12 H), 0.91 (t, J = 6.6 Hz, 6 H) ppm. ^{13}C NMR (100 MHz, CDCl_3): δ = 143.1 (s), 140.6 (s), 137.2 (s), 136.4 (s), 129.5 (d), 128.8 (d), 128.1 (d), 120.3 (d), 35.3 (t), 31.7 (t), 31.5 (t), 29.1 (t) 22.6 (t), 14.1 (q) ppm.

9-(4-Bromophenyl)-3,6-dihexyl-9*H*-carbazole (**13**). The synthesis of **13** was realized according to Aizawa.²⁰ **11** (4.64 g, 13.8 mmol, 1.0 eq), 1-bromo-4-iodobenzene **12** (4.30 g, 15.2 mmol, 1.1 eq), Cu(0) powder (2.73 g, 42.9 mmol, 3.1 eq) and K₂CO₃ (5.93 g, 42.9 mmol, 3.1 eq) were refluxed in 30 mL anhydrous DMF under argon atmosphere until TLC (light petroleum) showed full conversion (20 h). After cooling to room temperature the reaction mixture was suspended in DCM and filtered over Celite. The solution was washed with water, dried over Na₂SO₄ and filtered before it was concentrated under high vacuum. **13** was isolated by column chromatography (200 g silica gel, light petroleum) as a white solid (6.08 g, 12.4 mmol, 90%). R_f = 0.51 (light petroleum). ¹H NMR (200 MHz, CDCl₃): δ = 7.91 - 7.81 (m, 2 H), 7.68 - 7.61 (m, 2 H), 7.47 - 7.35 (m, 2 H), 7.24 - 7.14 (m, 4 H), 2.74 (t, J = 7.5 Hz, 4 H), 1.67 (quin, J = 7.5 Hz, 4 H), 1.42 - 1.23 (m, 12 H), 0.85 (t, J = 6.9 Hz, 6 H) ppm. ¹³C NMR (50 MHz, CDCl₃): δ = 139.2 (s), 137.3 (s), 134.8 (s), 133.0 (d), 128.4 (d), 126.6 (d), 123.6 (s), 120.3 (s), 119.6 (d), 109.2 (d), 36.0 (t), 32.3 (t), 31.8 (t), 29.0 (t), 22.7 (t), 14.1 (q) ppm. HR-ESI-FTMS [M+H]⁺ m/z calcd. 490.2104 for C₃₀H₃₇BrN⁺, found 490.2098.

5,11-Dihexylindolo[3,2,1-*jk*]carbazole (**8**). The synthesis of **8** followed an adapted protocol by Campeau.²¹ In order to adjust the water content of the solvent to 1000 ppm deionized water (22 mg) was added to 26 mL anhydrous DMAc. **7** (4.66 g, 9.6 mmol, 1.0 eq) and K₂CO₃ (2.68 g, 19.3 mmol, 2.0 eq) were suspended in 26 mL degassed DMAc before (IPr)Pd(allyl)Cl (276 mg, 0.5 mmol, 5 mol%) was added in a countercurrent flow of argon and the reaction mixture was heated to 130 °C. The reaction progress was monitored by GC-MS analysis. After 3 days of heating no further conversion could be observed and additional catalyst (276 mg, 0.5 mmol, 5 mol%) was added and the temperature was raised to 160 °C. After 4 hours the reaction was complete. The reaction mixture was poured onto water and extracted with DCM. The combined organic layers were dried over Na₂SO₄, filtered and dried under reduced pressure. The crude product (7.52 g) was flashed over a silica pad (60 g silica gel, light petroleum : DCM, 2 : 1) yielding **8** (3.70 g, 9.0 mmol, 94%) as an off-white powder. R_f = 0.52 (light petroleum). ¹H NMR (400 MHz, CDCl₃): δ = 8.02 (d, J = 7.4 Hz, 2 H), 7.97 - 7.91 (m, 2 H), 7.77 (d, J = 8.2 Hz, 2 H), 7.56 (t, J = 8.1 Hz, 1 H), 7.39 - 7.32 (m, 2 H), 2.82 (t, J = 7.6 Hz, 4 H), 1.76 (quin, J = 7.6 Hz, 4 H), 1.45 - 1.35 (m, 12 H), 0.93 (t, J = 7.0 Hz, 6 H) ppm. ¹³C NMR (100 MHz, CDCl₃): δ = 144.3 (s), 137.0 (s), 136.2 (s), 130.0 (s), 127.0 (d), 122.8 (d), 122.4 (d), 119.1 (d), 118.5 (s), 111.5 (d), 36.1 (t), 32.1 (t), 31.8 (t), 29.0 (t), 22.7 (t), 14.1 (q) ppm. HR-ESI-FTMS [M+H]⁺ m/z calcd. 410.2842 for C₃₀H₃₆N⁺, found 410.2836.

2-Bromo-5,11-dihexylindolo[3,2,1-*jk*]carbazole (**9**). The bromination of **8** was performed according to Bintinger.²¹ Dihexylindolocarbazole **8** (3.50 g, 8.5 mmol, 1.0 eq) was suspended in a 1:1 mixture of CHCl₃ and AcOH (42 mL) under argon atmosphere and heated to 55 °C. To this suspension *N*-bromosuccinimide (1.52 g, 8.5 mmol, 1.0 eq) was added in small portions over a period of 2.5 hours. During the addition a white precipitate formed. The mixture was further stirred for 30 min before it was poured onto 300 mL 2 N NaOH solution and extracted with DCM. **9** was

purified by recrystallization from acetonitrile and obtained as fine yellowish needles (3.54 g, 7.2 mmol, 85%). $R_f = 0.58$ (light petroleum). $^1\text{H NMR}$ (400 MHz, CDCl_3): $\delta = 8.06$ (s, 2H), 7.85 - 7.79 (m, 2 H), 7.72 - 7.64 (m, 2 H), 7.38 - 7.30 (m, 2 H), 2.78 (t, $J = 7.8$ Hz, 4 H), 1.73 (quin, $J = 7.1$ Hz, 4 H), 1.42 - 1.33 (m, 12 H), 0.91 (t, $J = 6.7$ Hz, 6 H) ppm. $^{13}\text{C NMR}$ (100 MHz, CDCl_3): $\delta = 142.4$ (s), 137.3 (s), 136.6 (s), 129.1 (s), 127.7 (d), 122.9 (d), 122.0 (d), 119.6 (s), 115.3 (s), 111.7 (d), 36.0 (t), 32.0 (t), 31.8 (t), 29.0 (t), 22.6 (t), 14.1 (q) ppm. HR-ESI-FTMS $[\text{M}+\text{H}]^+$ m/z calcd. 488.1947 for $\text{C}_{30}\text{H}_{35}\text{BrN}^+$, found 488.1946.

General procedure for the synthesis of **5**, **10** and **14** according to Anémian.²² The brominated precursor (1.0 eq) was dissolved in anhydrous THF (~0.2 M) under argon atmosphere and cooled below -78 °C. To the stirred solution $n\text{-BuLi}$ (1.2 eq) was added dropwise and the reaction mixture was stirred below -65 °C for at least 1.5 h before isopropyl pinacol borate (1.2 eq) was added. After warming the solution to room temperature slowly it was stirred overnight. THF was removed *in vacuo* before the residue was partitioned between DCM and water. The aqueous phase was extracted with DCM. The combined organic layers were dried over Na_2SO_4 followed by evaporation of the solvent *in vacuo*.

N,N-Bis(4-hexylphenyl)-4-(4,4,5,5-tetramethyl-1,3,2-dioxaborolan-2-yl)benzenamine (**5**). Starting from bromide **4** (13.21 g, 26.8 mmol, 1.0 eq), $n\text{-BuLi}$ (11.8 mL, 29.4 mmol, 1.1 eq) and isopropyl pinacol borate (5.47 g, 29.4 mmol, 1.1 eq) in 120 mL of anhydrous THF **5** (11.11 g, 20.5 mmol, 77%) was isolated as a pale yellowish oil by column chromatography (350 g silica gel, light petroleum : Et_2O , 2 \rightarrow 3%). $R_f = 0.26$ (light petroleum : DCM, 17 : 3). $^1\text{H NMR}$ (400 MHz, CDCl_3): $\delta = 7.66 - 7.60$ (m, 2 H), 7.10 - 6.93 (m, 10 H), 2.57 (t, $J = 7.8$ Hz, 4 H), 1.68 - 1.54 (m, 4 H), 1.39 - 1.25 (m, 24 H), 0.90 (t, $J = 6.5$ Hz, 6 H) ppm. $^{13}\text{C NMR}$ (100 MHz, CDCl_3): $\delta = 151.0$ (s), 145.0 (s), 138.2 (s), 135.7 (d), 129.2 (d), 125.1 (d), 120.7 (d), 83.4 (s), 35.4 (t), 31.7 (t), 31.4 (t), 29.1 (t), 24.8 (q), 22.6 (t), 14.1 (q) ppm. HR-ESI-FTMS $[\text{M}+\text{H}]^+$ m/z calcd. 540.4007 for $\text{C}_{36}\text{H}_{51}\text{BNO}_2^+$, found 540.4005.

5,11-Dihexyl-2-(4,4,5,5-tetramethyl-1,3,2-dioxaborolan-2-yl)indolo[3,2,1-*jk*]carbazole (**10**). Starting from bromide **9** (3.17 g, 6.5 mmol, 1.0 eq), $n\text{-BuLi}$ (3.1 mL, 7.8 mmol, 1.2 eq) and isopropyl pinacol borate (1.45 g, 7.8 mmol, 1.2 eq) in 110 mL anhydrous THF, **10** was isolated by recrystallization from acetonitrile and subsequent flash chromatography (34 g silica gel, light petroleum : ethyl acetate, 0 \rightarrow 7%) as a grayish solid (2.02 g, 3.8 mmol, 58%). $R_f = 0.53$ (light petroleum : DCM, 7 : 3). $^1\text{H NMR}$ (400 MHz, CD_2Cl_2): $\delta = 8.51$ (s, 2 H), 8.01 - 7.94 (m, 2 H), 7.82 - 7.94 (m, 2 H), 7.42 - 7.34 (m, 2 H), 2.82 (t, $J = 7.8$ Hz, 4 H), 1.74 (quin, $J = 7.6$ Hz, 4 H), 1.44 - 1.34 (m, 24 H), 0.92 (t, $J = 6.8$ Hz, 6 H) ppm. $^{13}\text{C NMR}$ (100 MHz, CD_2Cl_2): $\delta = 146.9$ (s), 137.7 (s), 137.3 (s), 130.4 (s), 127.8 (d), 126.5 (d), 123.4 (d), 118.8 (s), 112.2 (d), 84.4 (s), 36.6 (t), 32.6 (t), 32.4 (t), 29.6 (t), 25.4 (q), 23.3 (t), 14.5 (q) ppm. HR-ESI-FTMS $[\text{M}+\text{H}]^+$ m/z calcd. 536.3694 for $\text{C}_{36}\text{H}_{47}\text{BNO}_2^+$, found 536.3687.

3,6-Dihexyl-9-[4-(4,4,5,5-tetramethyl-1,3,2-dioxaborolan-2-yl)phenyl]-9*H*-carbazole (**14**).

The synthesis of **14** followed the general protocol starting from bromide **13** (2.55 g, 5.2 mmol, 1.0 eq), *n*-BuLi (2.5 mL, 6.2 mmol, 1.2 eq) and isopropyl pinacol borate (1.16 g, 6.2 mmol, 1.2 eq) in 26 mL of anhydrous THF. **14** was isolated as a white solid (2.09 g, 3.9 mmol, 75%) by passing through a pad of silica (15 g silica gel, light petroleum : DCM). $R_f = 0.20$ (light petroleum: DCM, 17 : 3). $^1\text{H NMR}$ (400 MHz, CD_2Cl_2): $\delta = 8.02$ (d, $J = 8.5$ Hz, 2 H), 7.97 - 7.89 (m, 2 H), 7.61 (d, $J = 8.5$ Hz, 2 H), 7.39 (d, $J = 8.5$ Hz, 2 H), 7.25 (dd, $J = 8.5, 1.6$ Hz, 2 H), 2.81 (t, $J = 7.5$ Hz, 4 H), 1.81 - 1.67 (m, 4 H), 1.49 - 1.30 (m, 24 H), 0.93 (t, $J = 6.9$ Hz, 6 H) ppm. $^{13}\text{C NMR}$ (100 MHz, CD_2Cl_2): $\delta = 141.4$ (s), 139.17 (s), 136.8 (d), 135.4 (s), 127.2 (d), 126.2 (d), 124.2 (s), 120.0 (d), 110.1 (d), 84.6 (s), 36.5 (t), 33.0 (t), 32.5 (t), 29.7 (t), 25.3 (q), 23.3 (t), 14.5 (q) ppm. HR-ESI-FTMS $[\text{M}+\text{H}]^+$ m/z calcd. 538.3809 for $\text{C}_{36}\text{H}_{49}\text{BNO}_2^+$, found 538.3847.

General procedure for the synthesis of **16**, **18**, **20**, **21** and **22** according to Marion.²³ To a suspension of the dihalogenide (1 eq), the boronic ester (~ 3 eq) and KOtBu (3 eq) in a mixture of IPA / H_2O (3 : 1) under argon atmosphere (IPr)Pd(allyl)Cl (20 μmol , 2 mol%) was added. The reaction mixture was refluxed until TLC showed full conversion (2 - 4 h). After cooling of the reaction mixture it was poured onto water and repeatedly extracted with DCM. The combined organic layers were dried over Na_2SO_4 and concentrated under reduced pressure.

4,4'-(2,5-Thiophenediyl)bis[*N,N*-bis(4-hexylphenyl)benzenamine] (**16**). To a suspension of boronic ester **5** (1715 mg, 3.2 mmol, 3.2 eq), bromide **15** (242 mg, 1.0 mmol, 1.0 eq) and KOtBu (337 mg, 3.0 mmol, 3.0 eq) in 16 mL of IPA / H_2O mixture under argon atmosphere (IPr)Pd(allyl)Cl (11 mg, 20 μmol , 2 mol%) was added. The reaction mixture was refluxed until TLC showed full conversion (2 h). After standard workup procedure purification of **16** was performed by column chromatography (90 g silica gel, light petroleum : DCM, 9 : 1), recrystallization from *n*-BuOH and column chromatography (90 g silica gel, light petroleum : toluene, 4 : 1). **16** could be obtained as a green sticky mass (518 mg, 0.57 mmol, 57%). $^1\text{H NMR}$ (400 MHz, CD_2Cl_2): $\delta = 7.49 - 7.41$ (m, 4 H), 7.17 (s, 2 H), 7.12 - 7.06 (m, 8 H), 7.04 - 6.95 (m, 12 H), 2.57 (t, $J = 7.9$ Hz, 8 H), 1.65 - 1.57 (m, 8 H), 1.40 - 1.32 (m, 24 H), 0.90 (t, $J = 6.7$ Hz, 12 H) ppm. $^{13}\text{C NMR}$ (100 MHz, CD_2Cl_2): $\delta = 148.2$ (s), 145.7 (s), 143.1 (s), 138.7 (s), 129.8 (d), 128.0 (s), 126.6 (d), 125.2 (d), 123.4 (d), 122.9 (d), 35.9 (t), 32.3 (t), 32.1 (t), 29.6 (t), 23.2 (t), 14.4 (q) ppm. HR-ESI-FTMS $[\text{M}+\text{H}]^+$ m/z calcd. 907.5958 for $\text{C}_{64}\text{H}_{79}\text{N}_2\text{S}^+$, found 907.5931.

4,4'-(2,2'-Bithiophene-5,5'-diyl)bis[*N,N*-bis(4-hexylphenyl)benzenamine] (**18**). To a suspension of boronic ester **5** (1680 mg, 3.1 mmol, 3.1 eq), bithiophene **17** (324 mg, 1.0 mmol, 1.0 eq) and KOtBu (337 mg, 3.0 mmol, 3.0 eq) in 16 mL of IPA / H_2O mixture in argon atmosphere (IPr)Pd(allyl)Cl (11 mg, 20 μmol , 2 mol%) was added. The reaction mixture was refluxed until TLC showed full conversion (1.5 h). After standard workup procedure purification of **18** was performed by column chromatography (90 g silica gel, light petroleum : DCM, 9 : 1) followed by

recrystallization from n-BuOH yielding **18** as a red sticky mass (809 mg, 0.82 mmol, 82%). ¹H NMR (400 MHz, CD₂Cl₂): δ = 7.52 - 7.33 (m, 4 H), 7.19 - 7.06 (m, 12 H), 7.05 - 6.93 (m, 12 H), 2.58 (t, J = 7.7 Hz, 8 H), 1.63 - 1.58 (m, 8 H), 1.41 - 1.34 (m, 24 H), 0.92 - 0.89 (m, 12 H) ppm. ¹³C NMR (100 MHz, CD₂Cl₂): δ = 148.5 (s), 145.6 (s), 143.6 (s), 138.9 (s), 136.2 (s), 129.8 (d), 127.5 (s), 126.7 (d), 125.4 (d), 124.8 (d), 123.2 (d), 122.7 (d), 35.9 (t), 32.2 (t), 32.1 (t), 29.7 (t), 23.2 (t), 14.5 (q) ppm. HR-ESI-FTMS [M+H]⁺ m/z calcd. 989.5836 for C₆₈H₈₁N₂S₂⁺, found 989.5795.

4,4'-(Dithieno[3,2-*b*:2',3'-*d*]thiophene-2,6-diyl)bis[*N,N*-bis(4-hexylphenyl)benzenamine] (**20**). Boronic ester **5** (1619 mg, 3.0 mmol, 3 eq), dithienothiophene **19** (354 mg, 1.0 mmol, 1 eq), KOtBu (337 mg, 3.0 mmol, 3 eq) and (IPr)Pd(allyl)Cl (11 mg, 20 μmol, 2 mol%) were refluxed in 20 mL of IPA / H₂O mixture for 2 h. Purification was performed by column chromatography (90 g silica gel, light petroleum : toluene, 9 → 14%) yielding **20** as a yellow glass (590 mg, 0.58 mmol, 58%). ¹H NMR (400 MHz, CD₂Cl₂): δ = 7.50 - 7.43 (m, 4 H), 7.40 (s, 2 H), 7.15 - 7.08 (m, 8 H), 7.04 - 6.97 (m, 12 H), 2.58 (t, J = 7.7 Hz, 8 H), 1.65 - 1.58 (m, 8 H), 1.40 - 1.30 (m, 24 H), 0.90 (t, J = 6.9 Hz, 12 H) ppm. ¹³C NMR (100 MHz, CD₂Cl₂): δ = 148.7 (s), 145.6 (s), 145.5 (s), 142.1 (s), 139.0 (s), 129.9 (s), 129.8 (d), 127.8 (s), 126.8 (d), 125.4 (d), 122.6 (d), 115.8 (d), 35.9 (t), 32.3 (t), 32.1 (t), 29.6 (t), 23.2 (t), 14.5 (q) ppm. HR-ESI-FTMS [M+H]⁺ m/z calcd. 1019.5400 for C₆₈H₇₉N₂S₃⁺, found 1019.5360.

2,2'-(2,2'-Bithiophene-5,5'-diyl)bis[5,11-dihexylindolo[3,2,1-*jk*]carbazole] (**21**). Boronic ester **10** (1607 mg, 3.0 mmol, 3 eq), bithiophene **17** (324 mg, 1.0 mmol, 1 eq), KOtBu (337 mg, 3.0 mmol, 3 eq) and (IPr)Pd(allyl)Cl (11 mg, 20 μmol, 2 mol%) were refluxed in 20 mL of IPA / H₂O mixture for 4 h. **21** was isolated as an orange solid (642 mg, 0.65 mmol, 65%) after column chromatography (90 g silica gel, light petroleum : DCM, 10% → 100%) and subsequent digesting in acetone. ¹H NMR (400 MHz, CD₂Cl₂): δ = 8.31 (s, 4 H), 8.00 (s, 4 H), 7.80 (d, J = 8.2 Hz, 4 H), 7.44 - 7.41 (m, 6 H), 7.32 (d, J = 3.5 Hz, 2 H), 2.83 (t, J = 7.8 Hz, 8 H), 1.76 (quin, J = 7.7 Hz, 8 H), 1.45 - 1.33 (m, 24 H), 0.92 (t, J = 7.8 Hz, 12 H) ppm. ¹³C NMR (100 MHz, CD₂Cl₂): δ = 145.9 (s), 144.8 (s), 138.1 (s), 137.4 (s), 136.6 (s), 130.2 (s), 130.1 (s), 128.2 (d), 124.9 (d), 123.9 (d), 123.5 (d), 119.3 (s), 118.0 (d), 112.4 (s), 36.6 (t), 32.7 (t), 32.4 (t), 29.6 (t), 23.2 (t), 14.5 (q) ppm. HR-ESI-FTMS [M+H]⁺ m/z calcd. 981.5210 for C₆₈H₇₃N₂S₂⁺, found 981.5216.

9,9'-(2,2'-Bithiophene-5,5'-diyl)di-4,1-phenylene)bis[3,6-dihexyl-9*H*-carbazole] (**22**). Boronic ester **14** (1619 mg, 3.0 mmol, 3 eq), bithiophene **17** (324 mg, 1.0 mmol, 1 eq), KOtBu (337 mg, 3.0 mmol, 3 eq) and (IPr)Pd(allyl)Cl (11 mg, 20 μmol, 2 mol%) were refluxed in 20 mL of IPA / H₂O mixture for 2 h. Purification was performed by column chromatography (90 g silica gel, light petroleum : DCM, 9 : 1) followed by recrystallization from n-heptane yielding **22** as a yellow solid (827 mg, 0.84 mmol, 84%). ¹H NMR (400 MHz, CD₂Cl₂): δ = 7.98 - 7.90 (m, 4 H), 7.88 - 7.79 (m, 4 H), 7.65 - 7.56 (m, 4 H), 7.40 - 7.38 (m, 6 H), 7.29 - 7.24 (m, 6 H), 2.80 (t, J = 7.8 Hz, 8 H), 1.76 - 1.69 (m, 8 H), 1.41 - 1.34 (m, 24 H), 0.91 (t, J = 6.9 Hz, 12 H) ppm. ¹³C NMR (100 MHz, CD₂Cl₂):

δ = 142.9 (s), 139.8 (s), 138.1 (s), 137.4 (s), 135.4 (s), 133.1 (s), 127.6 (d), 127.4 (d), 127.2 (d), 125.4 (d), 124.9 (d), 124.1 (s), 120.1 (d), 110.0 (d), 36.5 (t), 32.9 (t), 32.4 (t), 29.7 (t), 23.3 (t), 14.5 (q) ppm. HR-ESI-FTMS $[M+H]^+$ m/z calcd. 985.5523 for $C_{68}H_{77}N_2S_2^+$, found 985.5490.

General procedure for the synthesis of **24**, **26** and **28** according to Haid.¹⁴ Organodistannane (1.0 eq), bromide (2.1 eq) and $Pd(PPh_3)_4$ (5 mol%) were dissolved in degassed anhydrous DMF under argon atmosphere. The solution was degassed again before it was stirred at 80 °C until TLC showed full conversion. After cooling of the solution it was poured onto water and repeatedly extracted with DCM. The combined organic layers were dried over Na_2SO_4 and concentrated *in vacuo*. Purification was performed as stated in the detailed descriptions.

4,4'-(Benzo[1,2-*b*:4,5-*b'*]dithiophene-2,6-diyl)bis[*N,N*-bis(4-hexylphenyl)benzenamine] (**24**). Bromide **4** (1034 mg, 2.1 mmol, 2.1 eq), organodistannane **23** (516 mg, 1.0 mmol, 1 eq) and $Pd(PPh_3)_4$ (58 mg, 50 μ mol, 5 mol%) were heated to 80 °C in 25 mL anhydrous degassed DMF under argon atmosphere for 44 h. Purification was performed by column chromatography (110 g silica gel, light petroleum : toluene, 9 \rightarrow 22%, 90 g silica gel, light petroleum : DCM, \sim 10%) followed by dissolving the product in light petroleum, filtration and concentration of the obtained solution yielding **24** as an orange glass (405 mg, 0.58 mmol, 40%). 1H NMR (400 MHz, CD_2Cl_2): δ = 8.09 (s, 2 H), 7.58 - 7.50 (m, 4 H), 7.43 (s, 2 H), 7.16 - 7.07 (m, 8 H), 7.06 - 6.96 (m, 12 H), 2.58 (t, J = 7.7 Hz, 8 H), 1.64 - 1.58 (m, 8 H), 1.43 - 1.34 (m, 24 H), 0.91 (t, J = 6.7 Hz, 12 H) ppm. ^{13}C NMR (100 MHz, CD_2Cl_2): δ = 149.2 (s), 145.5 (s), 144.8 (s), 139.2 (s), 139.1 (s), 137.3 (s), 129.9 (d), 127.5 (d), 127.4 (s), 125.6 (d), 122.3 (d), 117.5 (d), 116.5 (d), 35.9 (t), 32.3 (t), 32.1 (t), 29.7 (t), 23.2 (t), 14.5 (q) ppm. HR-ESI-FTMS $[M+H]^+$ m/z calcd. 1013.5836 for $C_{70}H_{81}N_2S_2^+$, found 1013.5796.

4,4'-(2,5-Selenophenediyl)bis[*N,N*-bis(4-hexylphenyl)benzenamine] (**26**). Bromide **4** (940 mg, 1.91 mmol, 2.2 eq), organodistannane **25** (400 mg, 0.88 mmol, 1 eq) and $Pd(PPh_3)_4$ (51 mg, 44 μ mol, 5 mol%) were heated to 80 °C in 20 mL anhydrous degassed DMF under argon atmosphere for 4 h. **26** was obtained as a green glass (460 mg, 0.48 mmol, 55%) after column chromatography (90 g silica gel, light petroleum : DCM, 10%; 90 g silica gel, light petroleum : toluene, 9 \rightarrow 14%). 1H NMR (400 MHz, CD_2Cl_2): δ = 7.43 - 7.35 (m, 4 H), 7.32 (s, 2 H), 7.14 - 7.07 (m, 8 H), 7.04 - 6.99 (m, 8 H), 6.99 - 6.93 (m, 4 H), 2.57 (t, J = 7.8 Hz, 8 H), 1.65 - 1.57 (m, 8 H), 1.40 - 1.28 (m, 24 H), 0.90 (t, J = 7.0 Hz, 12 H) ppm. ^{13}C NMR (100 MHz, CD_2Cl_2): δ = 149.0 (s), 148.4 (s), 145.6 (s), 138.8 (s), 130.0 (s), 129.8 (d), 127.0 (d), 125.5 (d), 125.3 (d), 122.8 (d), 35.9 (t), 32.3 (t), 32.1 (t), 29.6 (t), 23.2 (t), 14.5 (q) ppm. HR-ESI-FTMS $[M+H]^+$ m/z calcd. 955.5403 for $C_{64}H_{79}N_2Se^+$, found 955.5368.

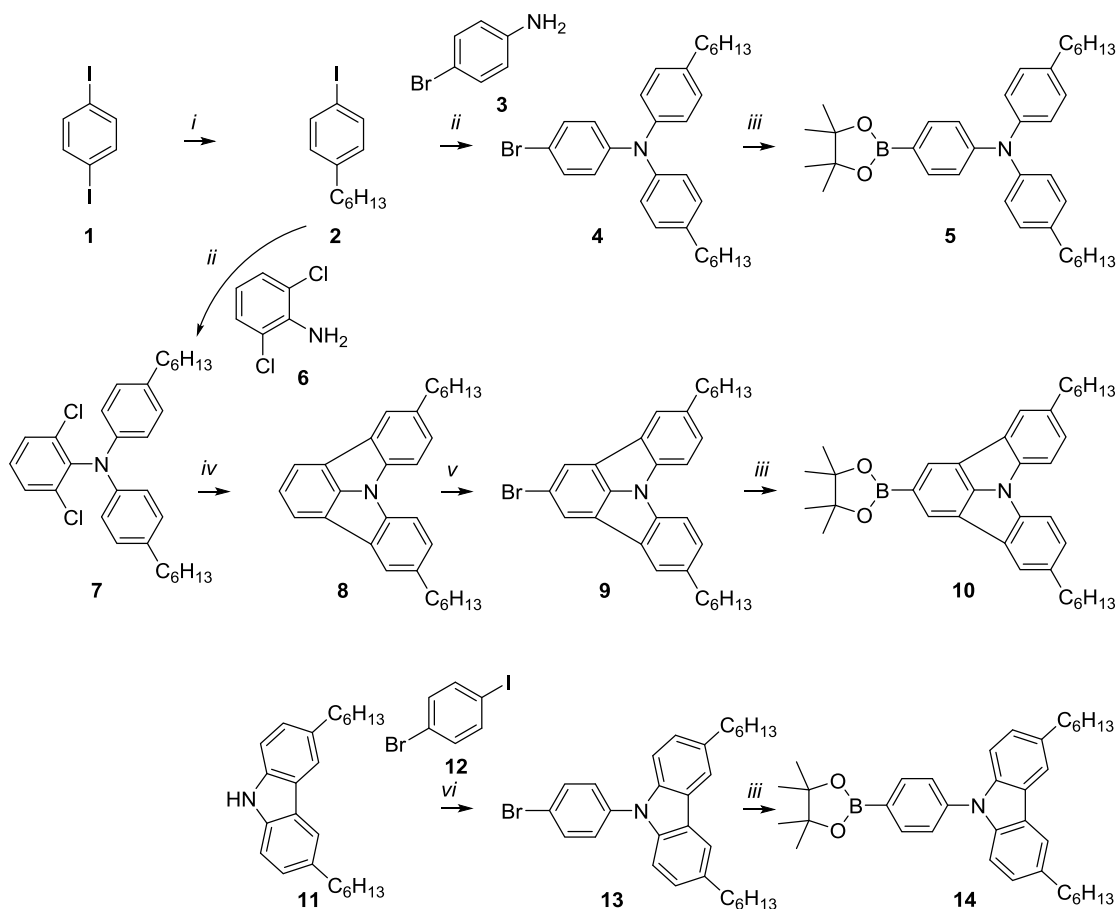
4,4'-(Benzo[1,2-*b*:4,5-*b'*]diselenophene-2,6-diyl)bis[*N,N*-bis(4-hexylphenyl)benzenamine] (**28**). Bromide **4** (1034 mg, 2.1 mmol, 2.1 eq), organodistannane **27** (610 mg, 1.0 mmol, 1 eq) and $Pd(PPh_3)_4$ (58 mg, 50 μ mol, 5 mol%) were heated to 90 °C in 25 mL anhydrous degassed DMF

under argon atmosphere for 54 h. **28** was isolated as a yellow glass (364 mg, 0.33 mmol, 33%) after column chromatography (110 g silica gel, light petroleum : toluene, 7 → 15%). ¹H NMR (400 MHz, CD₂Cl₂): δ = 8.11 (s, 2 H), 7.57 (s, 2 H), 7.49 - 7.40 (m, 4 H), 7.15 - 7.06 (m, 8 H), 7.06 - 6.93 (m, 12 H), 2.59 (t, J = 7.6 Hz, 8 H), 1.64 - 1.59 (m, 8 H), 1.39 - 1.35 (m, 24 H), 0.92 (t, J = 6.9 Hz, 12 H) ppm. ¹³C NMR (100 MHz, CD₂Cl₂): δ = 149.1 (s), 147.7 (s), 145.5 (s), 141.6 (s), 139.1 (s), 137.8 (s), 129.9 (d), 129.3 (s), 127.9 (d), 125.6 (d), 122.3 (d), 121.7 (d), 121.0 (d), 35.9 (t), 32.3 (t), 32.1 (t), 29.7 (t), 23.2 (t), 14.5 (q) ppm. HR-ESI-FTMS [M+H]⁺ m/z calcd. 1109.4725 for C₇₀H₈₁N₂Se₂⁺, found 1109.4704.

4,4'-(2,3-Dihydrothieno[3,4-*b*]-1,4-dioxine-5,7-diyl)bis[*N,N*-bis(4-hexylphenyl)benzenamine] (**30**). **30** was synthesized adapting a procedure from literature.²⁴ To a solution of bromide **4** (1034 mg, 2.1 mmol, 2.1 eq) and Cs₂CO₃ (782 mg, 2.4 mmol, 2.4 eq) in 5 mL anhydrous degassed toluene were added Pd(OAc)₂ (11 mg, 50 μmol, 5 mol%), P(*m*-tol)₃ (30 mg, 0.1 mmol, 0.10 eq) and EDOT **29** (142 mg, 1.0 mmol, 1.0 eq) under argon atmosphere. The reaction mixture was refluxed for 40 h before it was diluted with DCM and washed with water. The organic phase was dried over Na₂CO₃ and concentrated in vacuo. Purification of **30** was performed by column chromatography (90 g silica gel, light petroleum : DCM, 15%), recrystallization from *n*-BuOH and column chromatography (90 g silica gel, light petroleum : toluene, 4 : 1) yielding **30** as green sticky mass (361 mg, 0.37 mmol, 37%). ¹H NMR (400 MHz, CD₂Cl₂): δ = 7.57 (bm, 4 H), 7.10 - 7.08 (bm, 8 H), 7.00 - 6.98 (bm, 12 H), 4.29 (bs, 4 H), 2.58 (t, J = 7.5 Hz, 8 H), 1.65 - 1.58 (m, 8 H), 1.41 - 1.28 (m, 24 H), 0.91 (t, J = 6.4 Hz, 12 H) ppm. ¹³C NMR (400 MHz, CD₂Cl₂): δ = 147.3 (s), 145.8 (s), 138.5 (s), 138.5 (s), 129.8 (d), 127.2 (d), 127.1 (s), 125.1 (d), 123.1 (d), 65.2 (t), 35.9 (t), 32.4 (t), 32.2 (t), 29.7 (t), 23.3 (t), 14.5 (q) ppm. HR-ESI-FTMS [M+H]⁺ m/z calcd. 965.6013 for C₆₆H₈₁N₂O₂S⁺, found 965.6157.

RESULTS AND DISCUSSION

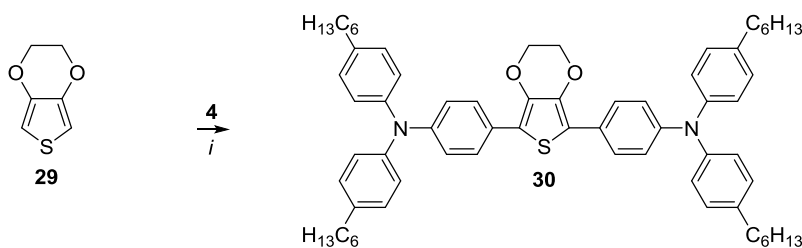
Synthesis. The synthetic linkage of TPA, indolocarbazole (ICz) as well as phenylcarbazole (PCz) scaffolds and chalcogenophene-based linkers toward symmetrical bis(triarylamines) was intended by Suzuki or Stille cross-coupling reactions or CH activation.



Scheme 1: Synthetic pathway towards boronates **5**, **10** and **14**. *i*: Et₂O, -78 °C, n-hexyllithium, 1-iodohexane; *ii*: KOH, CuCl, phenanthroline in toluene, reflux; *iii*: n-BuLi, -78 °C in THF, then isopropyl pinacol borate; *iv*: (IPr)Pd(allyl)Cl, K₂CO₃, DMAc, 130 °C; *v*: NBS, CHCl₃/AcOH, 55 °C; *vi*: Cu(0), K₂CO₃, DMF, reflux.

The synthesis of the required TPA, ICz and PCz building blocks was realized by copper-catalyzed Ullmann condensations of amines and iodides as key steps. Iodide **2** was prepared by lithiation of 1,4-diiodobenzene **1** and subsequent addition of hexyl iodide, and further applied in copper catalyzed Ullmann condensation toward **4**. Substituted indolocarbazole **9** was synthesized by condensation of **2** and aniline **6** followed by intramolecular CH-activation of triphenylamine **7** and subsequent bromination applying *N*-bromosuccinimide. The synthesis of phenylcarbazole **13** was realized using 3,6-dihexyl-9*H*-carbazole **11**, 1-bromo-4-iodobenzene **12** and copper powder adapting a procedure by Aizawa.²⁰ The synthesis of the boronic acid pinacolates **5**, **10** and **14** was achieved by metal halogen exchange of the obtained bromides **4**, **9** and **13** using n-butyllithium and further conversion with isopropyl pinacol borate (Scheme 1).

Joining the obtained TPA, ICz and PCz scaffolds with π -linkers was planned by either CH-activation, Suzuki or Stille cross coupling. A general Suzuki cross-coupling procedure developed in an earlier study²⁵ was used for connecting thiophene, bithiophene and dithieno[3,2-*b*:2',3'-*d*]thiophene (DTT) bromides **15**, **17** and **19** with boronate **5** (Scheme 2). The same protocol was successfully applied for the combination of bromide **17** and boronic esters **10** and **14** toward target compounds **21** and **22**. The syntheses of **24**, **26** and **28** were achieved by Stille cross coupling using distannanes **23**, **25** as well as **27** and bromide **4** (Scheme 2). The introduction of the EDOT linker in **30** was realized by CH activation applying bromide **4** adapting a procedure by Liu et al.²⁴ (Scheme 3).

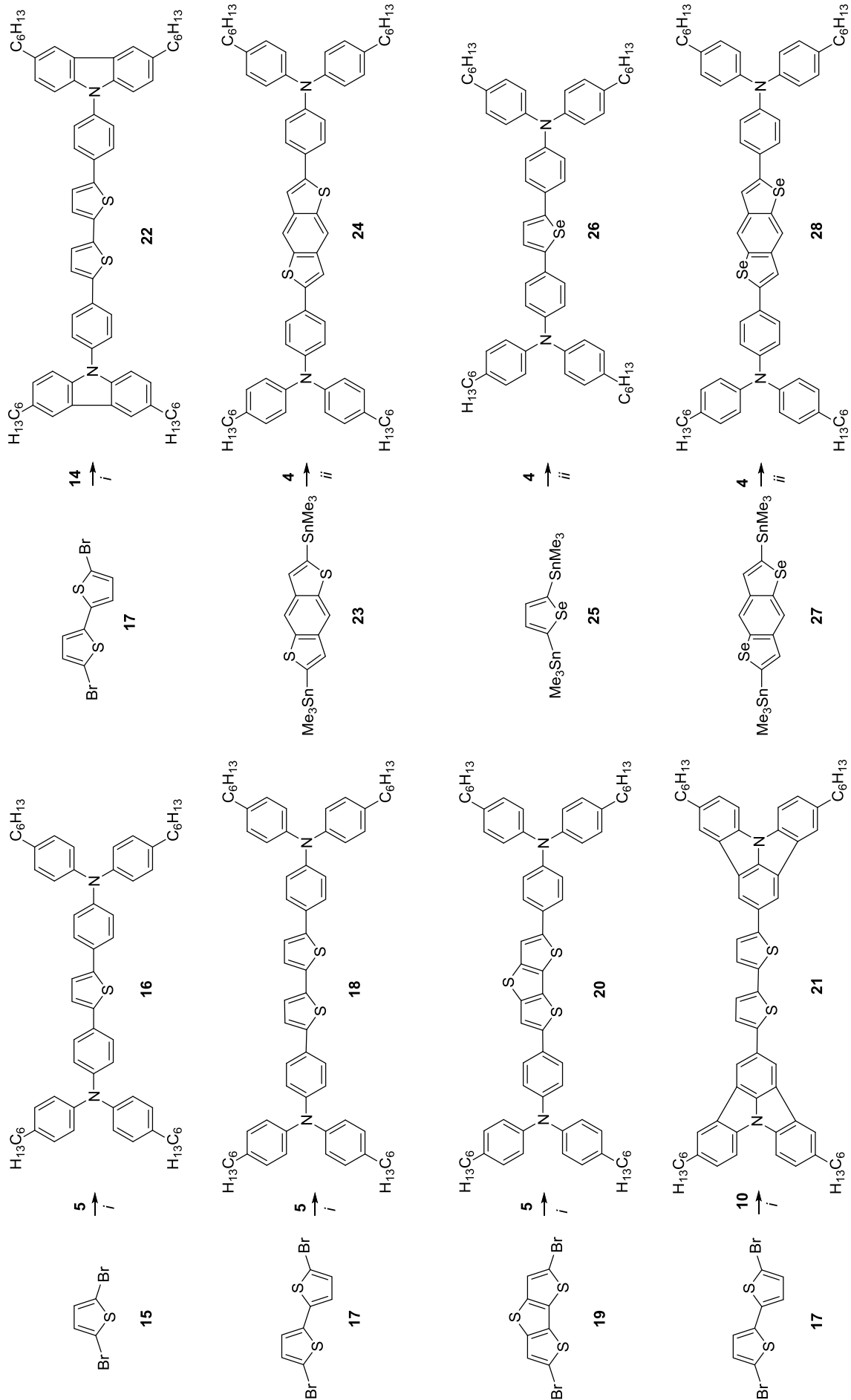


Scheme 3. Synthesis of **30**: *i*: Pd(OAc)₂, P(*m*-tol)₃, Cs₂CO₃, toluene.

The obtained solid to viscous materials appear yellow to red in color and are soluble in common organic solvents. The characterization of all target compounds was performed by ¹H / ¹³C NMR spectroscopy and HR-MS analysis. The data are consistent with the proposed structural formulations.

Photophysics. Photophysical properties of all target compounds were determined by UV-Vis, two-photon excited fluorescence spectroscopy (TPEF) and fluorescence spectroscopy (Table 1). Two absorption maxima were located in the narrow ranges of 298 - 307 and 392 - 422 nm for substances **16**, **18**, **20**, **21**, **22**, **24**, **26**, **28** and **30** when measured in THF solution (Figure 2). While the former can be attributed to the $n-\pi^*$ transition, the longer wavelength absorption originates from the charge transfer $\pi-\pi^*$ transitions of the electron-donating TPA, ICz or PCz moiety to the electron-accepting chalcogenophene moiety.^{26,27}

Compounds **24** and **28** exhibit three absorption maxima at 298/305, 412/422 and 406/427 nm. The highest maximum of selenophene-based compound **28** is shifted to longer wavelengths compared to its sulfur analog **24** and corresponds to charge transfer $\pi-\pi^*$ transition. The elongation of π -linkers from



Scheme 2: Synthetic pathway towards target compounds. *i*: KOtBu, (IPr)Pd(allyl)Cl, isopropanol / water, reflux; *ii*: DMF, Pd(PPh₃)₄, 80 °C.

thiophene to bithiophene in **18** as well as the planarization of the linker applying dithieno[3,2-*b*:2',3'-*d*]thiophene (**20**) only leads to a shift of about 20 nm, incorporating benzo[1,2-*b*:4,5-*b'*]diselenophene as linker (**28**) results in an even higher shift of 30 nm compared to **16**. The introduction of ICz and PCz scaffolds in **21** and **22** leads to a significant blue shift compared to TPA-substituted **18**, indicating increased optical bandgaps as a result of planarization.

Table 1: Experimental data and photophysical characteristics of all target compounds.

Comp.	Yield (%)	λ_{\max}^a (nm)	λ_{em}^b (nm)	$\Delta\nu^c$ (cm ⁻¹)	ϵ_{\max}^d (M ⁻¹ cm ⁻¹)	$\sigma_{2\text{PA}}^e$ (GM)	λ_{\max}^f (nm)
16	57	304, 397	453, 476	3100	79500	701	709
18	82	304, 422	487, 519	3200	64400	1661	733
20	58	305, 418	469, 498	2600	71700	5220	720
21	65	299, 392	459, 487	3300	56100	362	663
22	84	298, 396	456, 485	3300	51400	499	708
24	40	305, 406, 422	454, 475	1700	93600	726	1295
26	55	305, 407	465, 491	3100	58600	924	718
28	15	298, 412, 427	459, 486	1600	86700	1396	730
30	37	307, 401	450, 477	2700	59900	558	709

^a Absorption maxima determined from absorption spectra measured in 5 μM THF solution. ^b Emission maxima measured in 5 μM THF solution. ^c Stokes shifts. ^d Extinction coefficients. ^e Two-photon cross-sections determined by TPEF in THF. ^f Maximum of two-photon absorption spectra.

The corresponding emission spectra (see supporting information) of **16**, **18**, **21**, **22** and **26** reveal that the difference between absorption and emission maxima amounts to about 60 nm, while this value is only about 30 nm for **24** and **28**. Consequently, stokes shifts for the former are nearly doubled compared to the latter. A clear trend can also be observed when introducing more electron rich π -linkers (Figure 2, C): as the electron-donating effect of the chalcogenophene linker increases from thiophene **16** to electron-donating selenophene **26** or EDOT **30** the absorption maxima are shifted to longer wavelengths (10 nm for **26** and 5 nm for **30**).

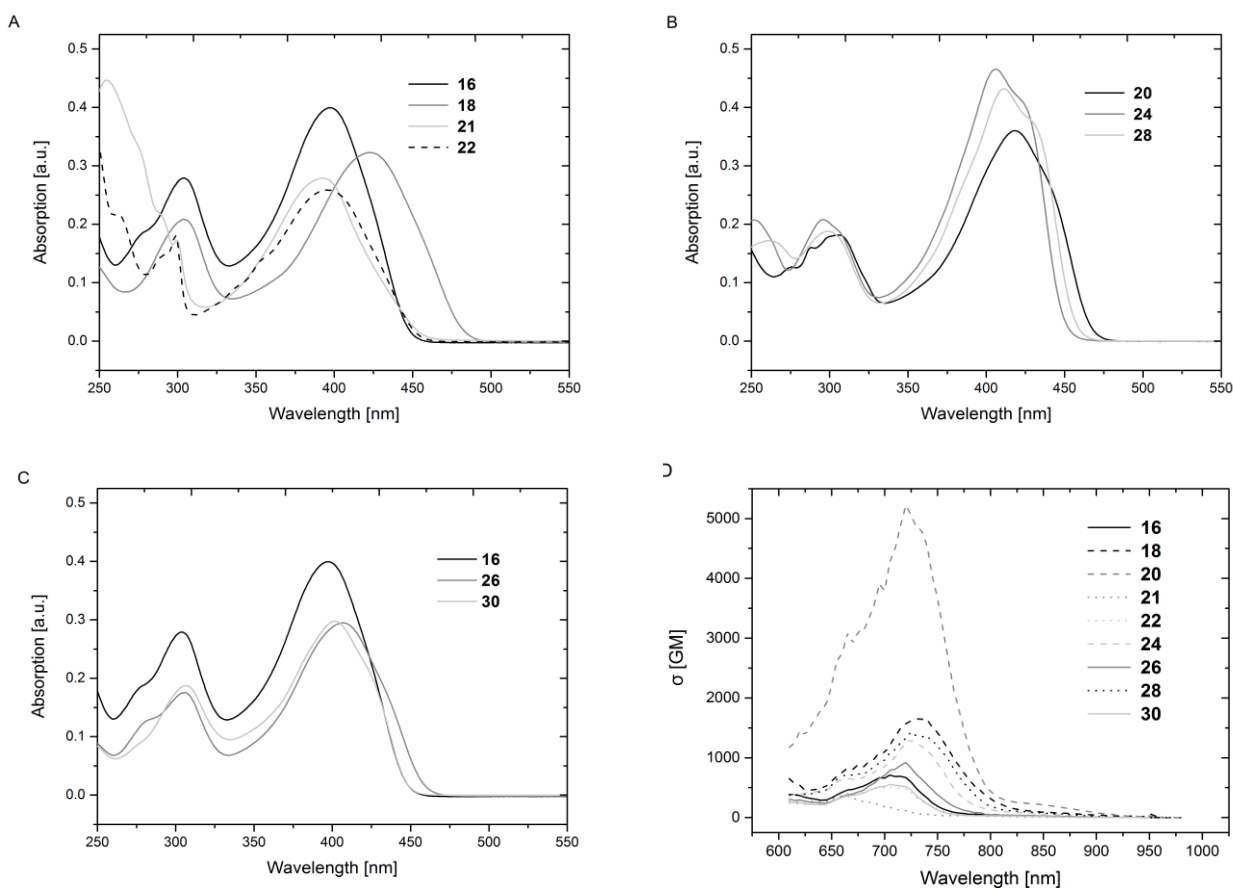


Figure 2: Absorption spectra (A, B and C) and TPEF spectra (D) of all target compounds.

Two-photon excited fluorescence (TPEF) spectra were measured (Figure 2, D) for all target compounds. The maxima of 2PA cross-sections are in the moderate range of 362 to 5220 GM (Table 1). The combination of TPA moieties and dithieno[3,2-*b*:2',3'-*d*]thiophene (**20**) results in an effective increase of 2PA cross-section, which may be attributed to the electronic properties of the DTT moiety such as polarizability brought about by the rigid, planar fused dithienothiophene structure contributing to a great deal to extended π -electron delocalization.²⁸ The planarization of the TPA scaffold from **16** exhibiting moderate 701 GM to ICz (**21**) and PCz (**22**) moieties leads to a significant reduction of 2PA cross-sections of approximately 340 and 200 GM, respectively. An increase of 2PA cross-section was observed when introducing the electron rich selenophene moiety (**26**), whereas EDOT as π -linker in **30** turned out to be not beneficial.

Two-Photon Induced Photopolymerization (2PIP) Tests. An important parameter determining the applicability of a two-photon photopolymer system is the sensitivity in correlation with low laser power and short exposure times, which are also essential for high throughput in mass production. An efficient method to evaluate the activity of PIs constitutes the fabrication of defined 3D test structures applying various laser intensities and writing speeds for the evaluation. In order to assess the ideal processing

window of potential PIs, defined woodpiles were structured in the monomer formulation by means of 2PIP. Selected compounds (**16**, **20**, **26**, and **30**) were tested toward their applicability as 2PIs and compared to the highly efficient reference material **B3FL** (2,7-bis[[4-(dibutylamino)phenyl]ethynyl]-9*H*-fluoren-9-one), recently reported by us,²⁹ and **BMA-1T** (4,4'-(2,5-Thiophenediyl)bis[*N,N*-bis(4-methylphenyl)benzenamine]).³⁰ The laser intensity and the writing speed were varied in a range of 10 - 100 mW (measured after passing the 100× microscope objective) and 0.316 - 316 mm/s, respectively.

Scanning electron microscopy (SEM) of the obtained 3D woodpile structures was performed (see supplementary information). Evaluation of the quality of these microfabrication was achieved by a four color classification (Figure 3) reported earlier⁴: class A (green) defines excellent structures with fine hatch lines and class B (yellow) good structures with thick hatch lines or slightly contorted structures. Structures rated as class C (red) have identified shapes but with small mistakes (e.g., holes, burst regions caused by overexposure). Parts structured with laser intensities rated as class D (blue) no longer show acceptable results.

All characterized compounds showed good 2PA activity, though exhibiting extensive photoluminescence. Although compound **16** is structurally closely related to **BMA-1T** (bearing an hexyl group instead of a methyl group on the TPA moiety), which has recently been published by us as an efficient 2PI, **16** showed inferior results at high energy and low writing speeds related to more lattices being damaged due to overexposure. At lower laser powers, however, **16** proved to be as efficient as reference material **BMA-1T**. TPA-based compound **26** incorporating selenophene as π -linker showed the broadest processing window, yielding excellent structures at both low and high laser intensities. Thus, **26** features the lowest polymerization threshold, even slightly superior to reference material **B3FL**. Although DTT-based compound **20** exhibits an increased 2PA cross-section compared to **26** (Table 1), structuring tests show inferior behavior at low writing speed and high energies.

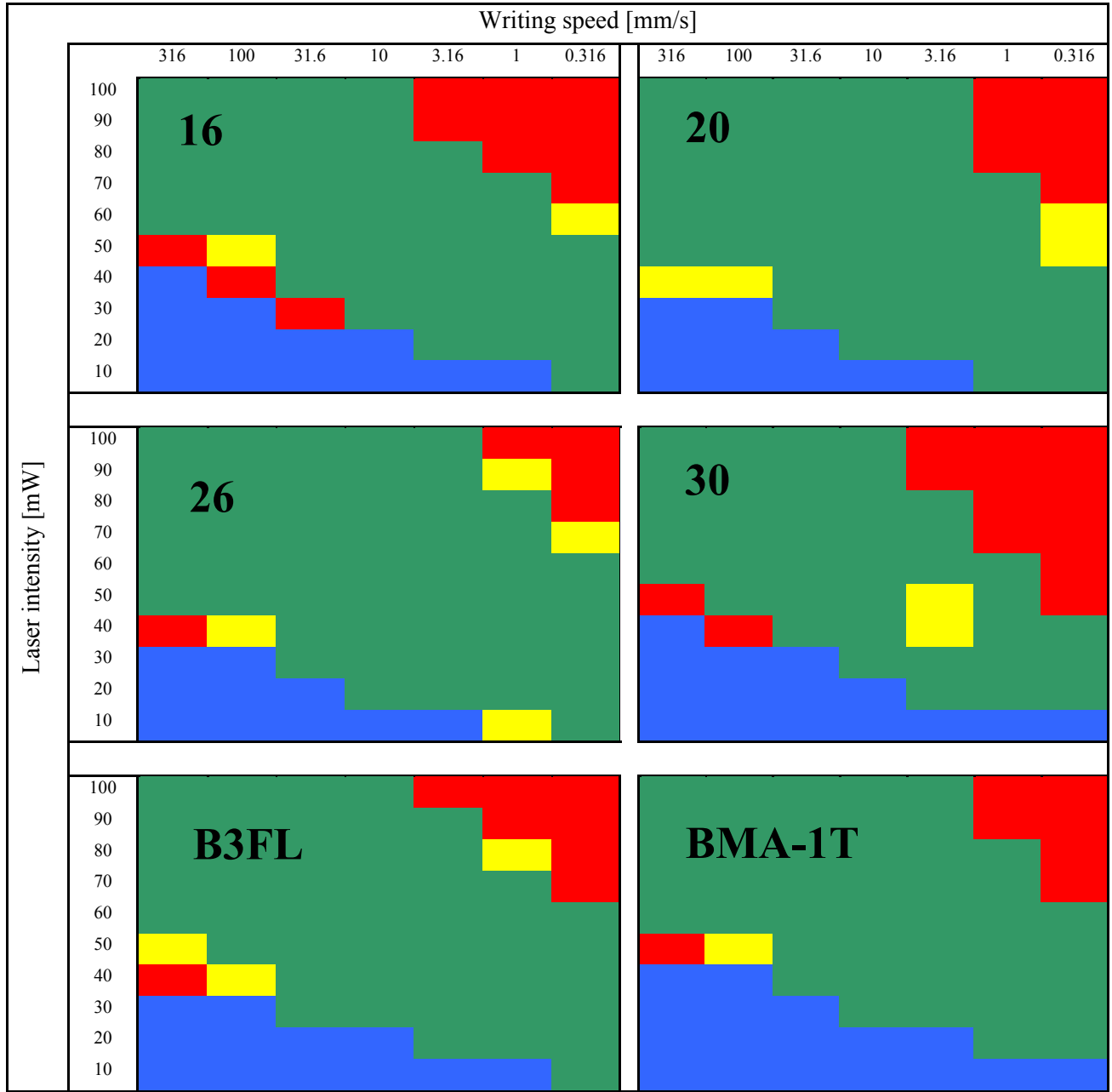


Figure 3: 2PIP screening tests of 16, 20, 26, 30 and reference materials B3FL as well as BMA-1T.

CONCLUSION

A series of soluble symmetric chalcogenophenes bearing hexyl-substituted triphenylamines, indolocarbazoles and phenylcarbazoles was synthesized as potential two-photon absorption initiators. Structural variations of the molecular design based on introduction of both planarized linkers and caps as well as electron rich linkers were evaluated aiming to increase two-photon absorption and thus the efficiency of these D- π -D type target molecules. The systematic comparison of structure-property relationships via UV-Vis, fluorescence and two-photon excited fluorescence spectroscopy and two-photon absorption structuring tests confirmed the significant influence of the substituent's electronic characteristics on the photophysical and photochemical properties. While the planarization of caps (indolocarbazole and phenylcarbazole) led to a decrease in two-photon cross-sections, a significant increase could be observed upon incorporation of planarized or electron rich derivatives as π -linkers. Two-photon excited fluorescence spectroscopy also revealed a two-photon cross-section of 5200 GM for **22**. Selected compounds were tested as two-photon absorption initiators and showed broad processing windows. Selenophene derivative **26** even exhibited superior behavior compared to reference material **B3FL** and surprisingly also to **22**. These novel compounds combine the benefits of straightforward synthesis, high two-photon absorption initiation efficiencies and at the same time high quantum yields, which makes these materials attractive for two-photon absorption structuring. Future investigations will focus on the evaluation of applying laser wavelengths at the two-photon absorption maxima for structuring tests.

ACKNOWLEDGMENT

The authors thank Dr. K. Föttinger for supporting the photophysical characterization, D. Möstl and M. Kury for contributing to the synthetic experiments. The authors thank P. Kautny for assistance in the measurement of emission spectra and M. Schwarz as well as P. Skrinjar for HRMS measurements.

ELECTRONIC SUPPLEMENTARY INFORMATION

¹H and ¹³C NMR spectra of compounds **2**, **4**, **5**, **7-10**, **13**, **14**, **16**, **18**, **20**, **21**, **22**, **24**, **26**, **28** and **30**, SEM-images of the two-photon absorption structuring tests of **16**, **20**, **26** and **30** and emission spectra of target compounds **16**, **18**, **20**, **21**, **22**, **24**, **26**, **28** and **30**.

REFERENCES

- (1) Nayyar, I. H.; Masunov, A. E.; Tretiak, S. *J. Phys. Chem. C* **2013**, *117* (35), 18170.
- (2) Cumpston, B. H.; Ananthavel, S. P.; Barlow, S.; Dyer, D. L.; Ehrlich, J. E.; Erskine, L. L.; Heikal, A. A.; Kuebler, S. M.; Lee, I.-Y. S.; McCord-Maughon, D.; Qin, J.; Rockel, H.; Rumi, M.; Wu, X.-L.; Marder, S. R.; Perry, J. W. *Nature* **1999**, *398* (6722), 51.
- (3) Warther, D.; Gug, S.; Specht, A.; Bolze, F.; Nicoud, J.-F.; Mourot, A.; Goeldner, M. *Bioorg. Med. Chem.* **2010**, *18* (22), 7753.
- (4) Li, Z.; Pucher, N.; Cicha, K.; Torgersen, J.; Ligon, S. C.; Ajami, A.; Husinsky, W.; Rosspeintner, A.; Vauthey, E.; Naumov, S.; Scherzer, T.; Stampfl, J.; Liska, R. *Macromolecules* **2013**, *46* (2), 352.
- (5) Sheng, N.; Liu, D.; Wu, J.; Gu, B.; Wang, Z.; Cui, Y. *Dyes Pigm.* **2015**, *119*, 116.
- (6) Zheng, S.; Beverina, L.; Barlow, S.; Zojer, E.; Fu, J.; Padilha, L. A.; Fink, C.; Kwon, O.; Yi, Y.; Shuai, Z.; Stryland, E. W. V.; Hagan, D. J.; Brédas, J.-L.; Marder, S. R. *Chem. Commun.* **2007**, 13, 1372.
- (7) Kim, O.-K.; Lee, K.-S.; Woo, H. Y.; Kim, K.-S.; He, G. S.; Swiatkiewicz, J.; Prasad, P. N. *Chem. Mater.* **2000**, *12* (2), 284.
- (8) Xu, B.; He, J.; Liu, Y.; Xu, B.; Zhu, Q.; Xie, M.; Zheng, Z.; Chi, Z.; Tian, W.; Jin, C.; Zhao, F.; Zhang, Y.; Xu, J. *J. Mater. Chem. C* **2014**, *2* (17), 3416.
- (9) Andersen, M. W.; Hildebrandt, B.; Köster, G.; Hoffmann, R. W. *Chem. Ber.* **1989**, *122* (9), 1777.
- (10) Navarro, O.; Nolan, S. P. *Synthesis* **2006**, 366.
- (11) Yasuda, T.; Shimizu, T.; Liu, F.; Ungar, G.; Kato, T. *J. Am. Chem. Soc.* **2011**, *133* (34), 13437.
- (12) Søndergaard, R.; Manceau, M.; Jørgensen, M.; Krebs, F. C. *Adv. Energy Mater.* **2012**, *2* (4), 415.
- (13) Leenen, M. A. M.; Vian, F.; Cucinotta, F.; Pisula, W.; Thiem, H.; Anselmann, R.; De Cola, L. *Macromol. Chem. Phys.* **2010**, *211* (21), 2286.
- (14) Haid, S.; Mishra, A.; Weil, M.; Uhrich, C.; Pfeiffer, M.; Bäuerle, P. *Adv. Funct. Mater.* **2012**, *22* (20), 4322.
- (15) Roncali, J.; Giffard, M.; Frère, P.; Jubault, M.; Gorgues, A. *J. Chem. Soc. Chem. Commun.* **1993**, 8, 689.
- (16) Wang, N.-X. *Synth. Commun.* **2003**, *33* (12), 2119.
- (17) Odom, S. A.; Lancaster, K.; Beverina, L.; Lefler, K. M.; Thompson, N. J.; Coropceanu, V.; Brédas, J.-L.; Marder, S. R.; Barlow, S. *Chem. Eur. J.* **2007**, *13* (34), 9637.
- (18) Doszczak, L.; Kraft, P.; Weber, H.-P.; Bertermann, R.; Triller, A.; Hatt, H.; Tacke, R. *Angew. Chem. Int. Ed.* **2007**, *46* (18), 3367.
- (19) Goodbrand, H. B.; Hu, N.-X. *J. Org. Chem.* **1999**, *64* (2), 670.
- (20) Aizawa, N.; Pu, Y.-J.; Sasabe, H.; Kido, J. *Org. Electron.* **2012**, *13* (11), 2235.
- (21) Kautny, P.; Lumpi, D.; Wang, Y.; Tissot, A.; Bintinger, J.; Horkel, E.; Stöger, B.; Hametner, C.; Hagemann, H.; Ma, D.; Fröhlich, J. *J. Mater. Chem. C* **2014**, *2* (11), 2069.
- (22) Anémian, R.; Cupertino, D. C.; Mackie, P. R.; Yeates, S. G. *Tetrahedron Lett.* **2005**, *46* (39), 6717.
- (23) Marion, N.; Navarro, O.; Mei, J.; Stevens, E. D.; Scott, N. M.; Nolan, S. P. *J. Am. Chem. Soc.* **2006**, *128* (12), 4101.
- (24) Liu, C.-Y.; Zhao, H.; Yu, H. *Org. Lett.* **2011**, *13* (15), 4068.
- (25) Lumpi, D.; Holzer, B.; Bintinger, J.; Horkel, E.; Waid, S.; Wanzenböck, H. D.; Marchetti-Deschmann, M.; Hametner, C.; Bertagnolli, E.; Kymissis, I.; Fröhlich, J. *New J. Chem.* **2015**, *39* (3), 1840.
- (26) Ge, Z.; Hayakawa, T.; Ando, S.; Ueda, M.; Akiike, T.; Miyamoto, H.; Kajita, T.; Kakimoto, M. *Adv. Funct. Mater.* **2008**, *18* (4), 584.
- (27) Kong, M.; Wang, T.; Tian, X.; Wang, F.; Liu, Y.; Zhang, Q.; Wang, H.; Zhou, H.; Wu, J.; Tian, Y. *J. Mater. Chem. C* **2015**, *3* (21), 5580.
- (28) Kim, O.-K.; Lee, K.-S.; Woo, H. Y.; Kim, K.-S.; He, G. S.; Swiatkiewicz, J.; Prasad, P. N. *Chem. Mater.* **2000**, *12* (2), 284.
- (29) Li, Z.; Siklos, M.; Pucher, N.; Cicha, K.; Ajami, A.; Husinsky, W.; Rosspeintner, A.; Vauthey, E.; Gescheidt, G.; Stampfl, J.; Liska, R. *J. Polym. Sci. Part Polym. Chem.* **2011**, *49* (17), 3688.
- (30) Holzer, B.; Tromayer, M.; Lunzer, M.; Lumpi, D.; Horkel, E.; Hametner, C.; Rosspeintner, A.; Vauthey, E.; Liska, R.; Fröhlich, J. *Manuscript in preparation*.

5 – Summary and Outlook

5. Summary and Outlook

In summary, different methods and reliable procedures were developed and applied for the synthesis of a variety of organic functional materials. Organic semiconductors for OFET application were realized based on pentacene derivatives and selenium-based fused heterocyclic moieties. Also, potential materials exhibiting nonlinear behavior were obtained.

In the course of this thesis pentacenes bearing electron-deficient heterocyclic substituents 6- and 13-position were prepared and revealed increased stability and solubility compared to unsubstituted pentacene (*Figure 1, left*). This project will be continued with colleagues at the Laboratory of Solid State Physics, ETH Zurich evaluating the obtained materials in an OFET configuration. First results proved high charge carrier mobilities.

Also, thienyl-substituted pentacenes bearing both bulky trialkylsilyl and electron-withdrawing bromo groups (to counteract the electron-donating effects of the trialkylsilyl moiety) on the thiophene ring (*Figure 1, right*) were synthesized yielding materials with charge carrier mobilities up to $3 \times 10^{-4} \text{ cm}^2 \text{ V}^{-1} \text{ s}^{-1}$.

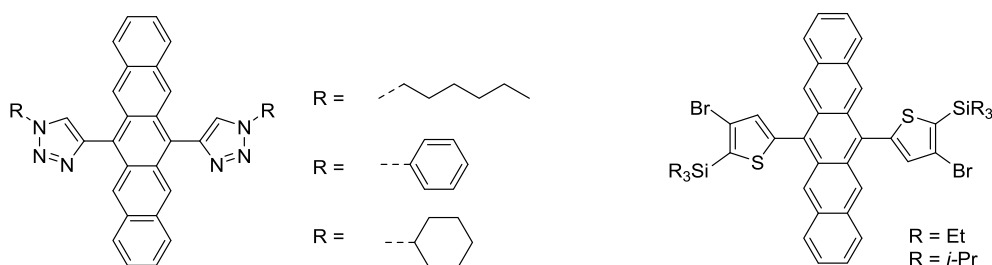


Figure 1: Triazole- and thienyl-substituted target pentacenes.

Furthermore a facile one-pot synthesis toward benzo[*b*]selenophenes was developed, which may be also useful in other scientific disciplines, e.g. medicinal chemistry or crystallography. The obtained benzo[*b*]selenophenes were applied in the synthesis of symmetric selenium-based fused heterocyclic scaffolds (*Figure 2*) revealing strong intermolecular interactions and reduced bandgaps compared to their sulfur analogs. These materials will be tested towards their applicability in OFET devices in cooperation with colleagues at the Laboratory of Solid State Physics, ETH Zurich.

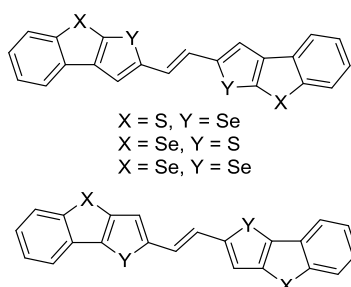


Figure 2: Ene-bridged symmetrical selenium-based target compounds.

A combination of substituted triphenylamines and tris(2-thienyl)benzene in C₃ symmetric configuration (*Figure 3*) was evaluated yielding materials with tunable electronic and luminescent properties. These materials offer good solution processability giving rise to smooth surfaces and high thermal stability, which are beneficial for device fabrication. This approach yielded a compound with a charge carrier mobility of nearly $10^{-3} \text{ cm}^2 \text{ V}^{-1} \text{ s}^{-1}$.

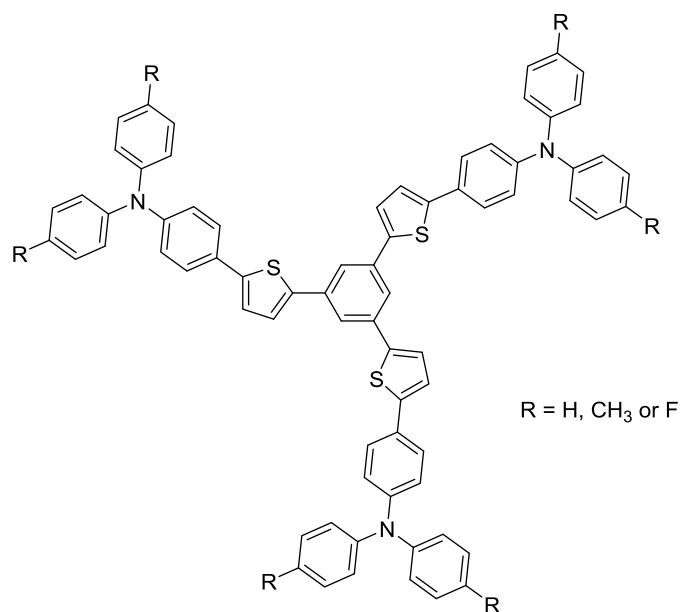


Figure 3: Star shaped target compounds.

The second part of this thesis focused on the development of novel chromophores for nonlinear optics. Firstly, potential compounds capable of second harmonic generation were designed and synthesized combining phenyltriazoles or -isoxazoles as acceptors (A) and Z-(methylseleno)alkenyl groups as donors (D) (Figure 4). The introduction of more polarizable selenium constitutes a valuable approach to increase second harmonic efficiency. This novel chromophore represents an interesting type of NLO material.

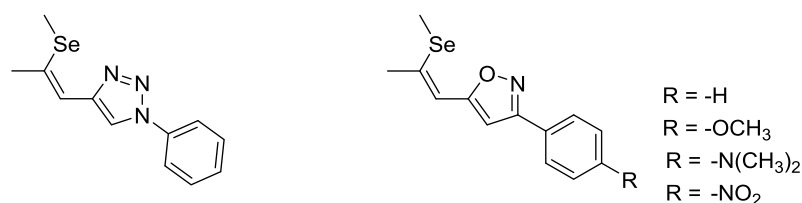


Figure 4: Potential materials exhibiting second harmonic generation.

Secondly, cap-linker-cap systems were prepared by combining thiophene with substituted triphenylamines bearing various electron-withdrawing and -donating effects aiming for highly efficient two-photon absorption initiators (Figure 5), which were successfully applied two-photon absorption induced photopolymerization.

Further investigations were intended to increase the two-photon absorption cross-section by planarization of the applied triphenylamine substituents as well as introduction of planar and electron rich π -electron extended linkers (Figure 5, top and right, bottom). Again, these materials were tested in two-photon absorption induced photopolymerization and proved to be efficient photoinitiators.

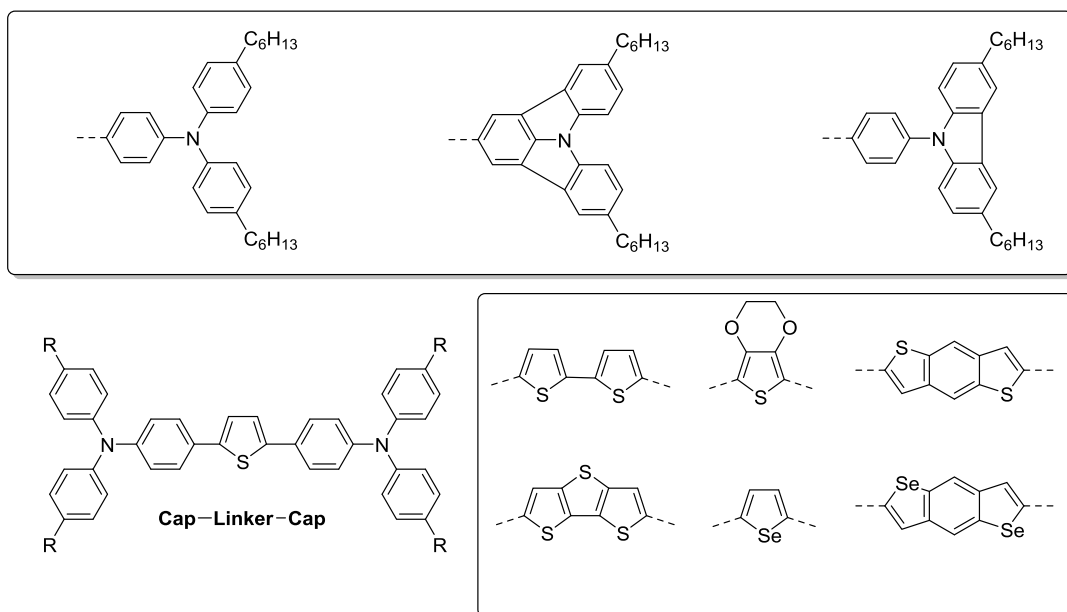


Figure 5: Cap-linker-cap systems based on triphenylamine substituted thiophene (left, bottom) and structural motives applied in target compounds.

Based on these findings the investigation of structure-property relationships will be intensified with regard to the two-photon absorption maxima in cooperation with Arnulf Rosspeintner at the Department of Physical Chemistry at the University of Geneva. Microfabrication of structures will be performed at various wavelengths in cooperation with Markus Lunzer from the Institute of Applied Synthetic Chemistry at the Technische Universität Wien to study the polymerization behavior at the two-photon absorption maximum.

6 – Statement of Contribution

6. Statement of Contribution

Manuscript #1

The synthetic work toward anthracene and pentacene derivatives within Manuscript #1 was either carried out in the course of the PhD thesis of the applicant (B. Holzer) or (co-)supervised (theses of R. Klaffenöck, A. Aster, D. Koch, T. Raab and A. M. Wagner) by the applicant (B. Holzer). The photophysical and electrochemical characterization of the target compounds was performed by the applicant (B. Holzer) supported by A. Aster and D. Lumpi. DFT calculations were carried out by E. Horkel. The manuscript was composed and written by the applicant. C. Hametner and D. Lumpi supported the data assembly and corrected the manuscript.

Manuscript #2

The synthetic work toward anthracene and pentacene derivatives within Manuscript #2 was either carried out in the course of the PhD thesis of the applicant (B. Holzer) or (co-)supervised (theses of R. Klaffenböck and A. Aster) by the applicant. The photophysical and electrochemical characterization of the target compounds was performed by the applicant (B. Holzer) supported by A. Aster and D. Lumpi. DFT calculations were carried out by E. Horkel. OFET characteristics were determined by D. Lumpi and Thomas Mathis supervised by B. Batlogg. The manuscript was composed and written by the applicant (B. Holzer) and D. Lumpi. C. Hametner supported the data assembly and corrected the manuscript.

Manuscript #3

The research subject of Manuscript #3 was initiated by Bertram Batlogg, Z. Ge and D. Lumpi. DFT calculations were carried out by E. Horkel. The photophysical and electrochemical analyses were performed by the applicant (B. Holzer) and D. Lumpi. OFET characteristics were determined by Thomas Mathis supervised by B. Batlogg. The manuscript was written by T. Matthis. All authors contributed to the manuscript discussion and correction.

Manuscript #4

The research subject of Manuscript #4 was initiated and all synthetic work was performed by the applicant (B. Holzer). Correlated NMR spectra were recorded by C. Hametner. The manuscript was composed and written by the applicant (B. Holzer). C. Hametner supported the data assembly and corrected the manuscript.

Manuscript #5

The research subject of the project presented in Manuscript #5, including all relevant experiments and analyses, was independently initiated, performed or (co-)supervised (theses of B. Dellago and J. Bitai) by the applicant (B. Holzer) and D. Lumpi. The syntheses were partly performed in the course of bachelor thesis by B. Dellago and J. Bitai (co-)supervised by B. Holzer. Correlated NMR spectra were recorded by C. Hametner. DFT calculations were carried out by E. Horkel. Investigations of photophysical and electrochemical characteristics (with support of B. Dellago) as well as crystallization (X-ray analysis performed by B. Stöger) and thermal behavior (DSC / TGA measurements supported by O. Liske) were performed by the applicant (B. Holzer). B. Holzer composed and wrote the manuscript draft. C. Hametner supported the data assembly and corrected the manuscript.

Manuscript #6

The synthetic work toward star-shaped compounds within Manuscript #6 was (co-)supervised (theses of D. Bomze) by the applicant (B. Holzer). The photophysical and electrochemical characterization of the target compounds was performed by the applicant (B. Holzer) and D. Lumpi. DFT calculations were carried out by E. Horkel. M. Machetti-Deschmann contributed with HRMS measurements. AFM measurements were performed by S. Waid supervised by H. Wanzenböck and E. Bertagnolli. OFET characteristics were determined by J. Bintinger supervised by I. Kymissis. The manuscript was composed and written by the applicant (B. Holzer), D. Lumpi, J. Bintinger and E. Horkel. All authors contributed to the manuscript discussion and correction.

Manuscript #7

The synthetic part of the research project in Manuscript #7 was independently initiated, performed or (co-)supervised (theses of F. Glöcklhofer, M. Möller and H. Schmidtbauer) by D. Lumpi. The syntheses of selenium-based compounds were performed by the applicant (B. Holzer) in the course of her PhD thesis. Absorption measurements (with support of K. Föttinger) were conducted by D. Lumpi. N. Jankowski conducted the IC measurements. The crystallographic part, including data acquisition, interpretation and discussion was performed by B. Stöger. Optical characteristics (SHG) were acquired by G. Reider. The manuscript was composed and written by D. Lumpi, B. Stöger and G. Reider. The experimental parts as well as the supporting information were composed by B. Holzer, F. Glöcklhofer and D. Lumpi.

Manuscript #8

The synthetic part of the research project in Manuscript #8 was either performed or (co-) supervised (bachelor theses of D. Bader) by B. Holzer. Absorption spectra were acquired by Paul Kautny. The acquisition of crystallographic data was performed by B. Stöger. Optical characteristics (SHG) were acquired by G. Reider. The manuscript was composed and written by B. Holzer. B. Stöger and C. Hametner supported the data assembly and corrected the manuscript.

Manuscript #9

A great part of the synthetic work within Manuscript #9 was carried out in the course of the diploma thesis of the applicant (B. Holzer). During this PhD thesis materials bearing electron withdrawing substituents were synthesized. All materials were characterized with respect to their photophysical properties (e.g. quantum yields, absorption and emission spectra were acquired by the applicant and D. Lumpi, two-photon excited fluorescence spectra were measured by A. Rosspointner with the support of M. Lunzer). Structuring tests were performed by M. Tromayer with the support of the applicant (B. Holzer). B. Holzer composed and wrote the manuscript draft. C. Hametner supported the data assembly and corrected the manuscript.

Manuscript #10

The research subject of manuscript #10 including all experiments was carried out by Markus Lunzer within his diploma thesis (co-)supervised by the applicant (B. Holzer). All materials were characterized with respect to their photophysical properties (e.g. absorption and emission spectra were acquired by M. Lunzer and P. Kautny, two-photon excited fluorescence spectra were measured by A. Rosspointner with the support of M. Lunzer). Structuring tests were performed by M. Tromayer with the support of M. Lunzer. B. Holzer composed and wrote the manuscript draft. The experimental parts were composed by M. Lunzer. C. Hametner supported the data assembly and corrected the manuscript.

7 – Appendix

Manuscript # 1

Supporting Information

Heteroaryl Substituted Anthracenes and Pentacenes as Potential Materials for Organic Field-Effect Transistors

Brigitte Holzer,^a Rene Klaffenböck,^a Alexander Aster,^a Daniel Lumpi,^a Ernst Horkel,^a and Johannes Fröhlich^a

^aInstitute of Applied Synthetic Chemistry, Vienna University of Technology,

Getreidemarkt 9/163OC, A-1060 Vienna, Austria

daniel.lumpi@tuwien.ac.at

Content

A) NMR Spectra

B) Cyclic Voltammetry

C) Molecular Structure of 9b

D) Thermal Analysis

E) DFT Calculations

A) NMR Spectra

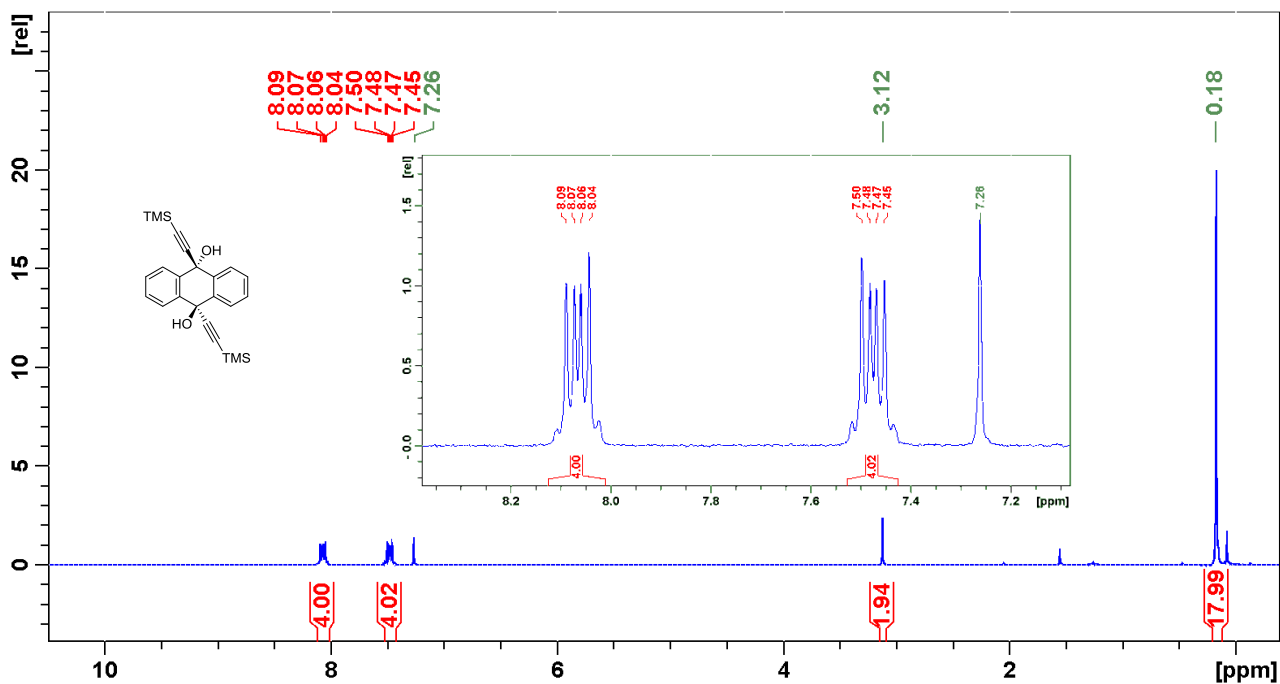


Figure S1. Proton NMR spectrum of compound 2.

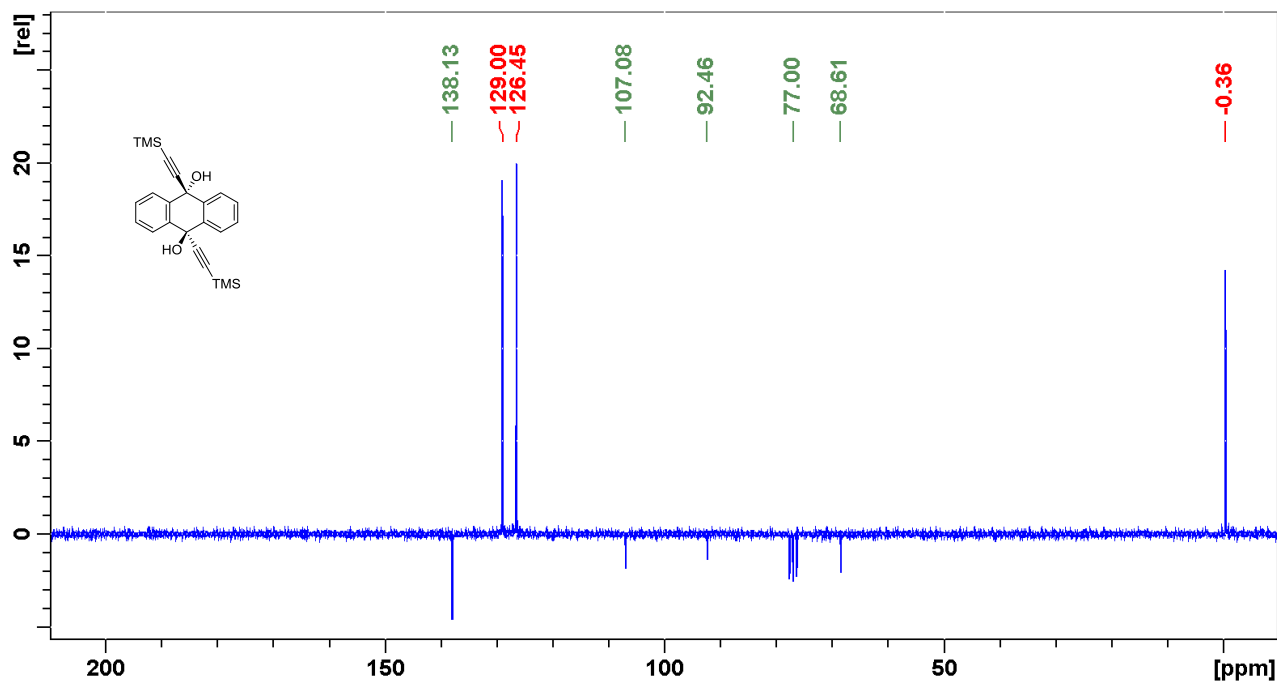


Figure S2. Carbon NMR spectrum of compound 2.

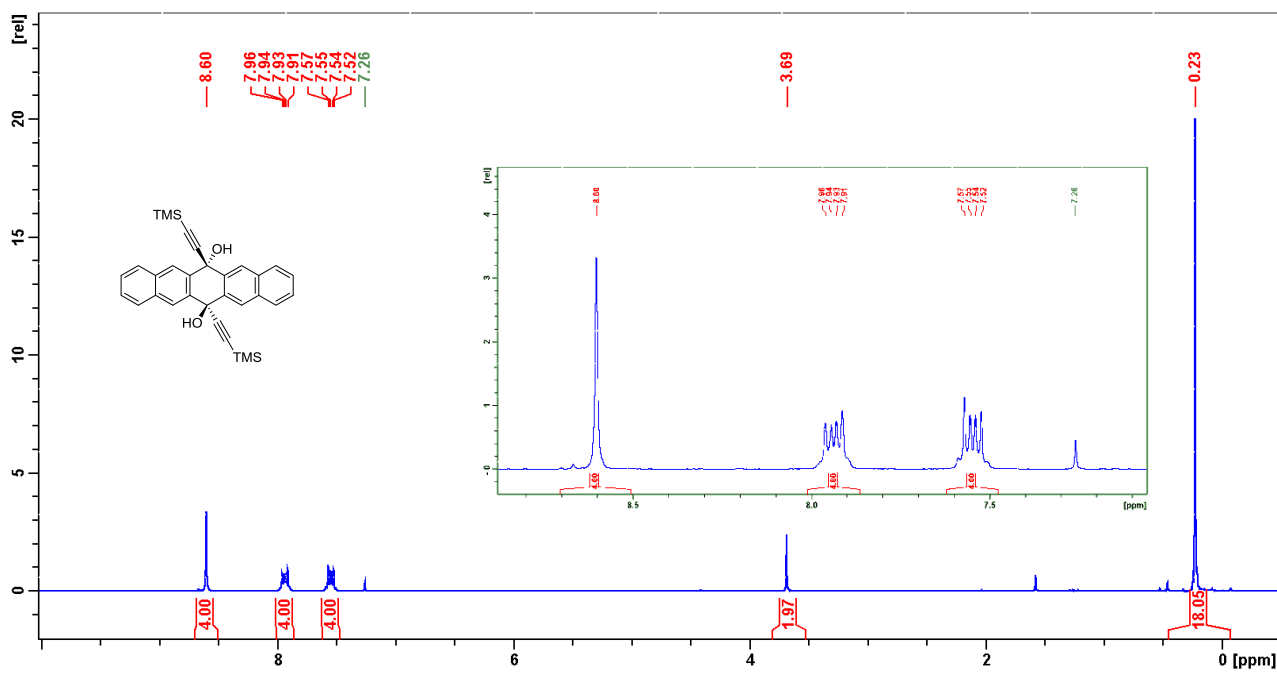


Figure S3. Proton NMR spectrum of compound 8.

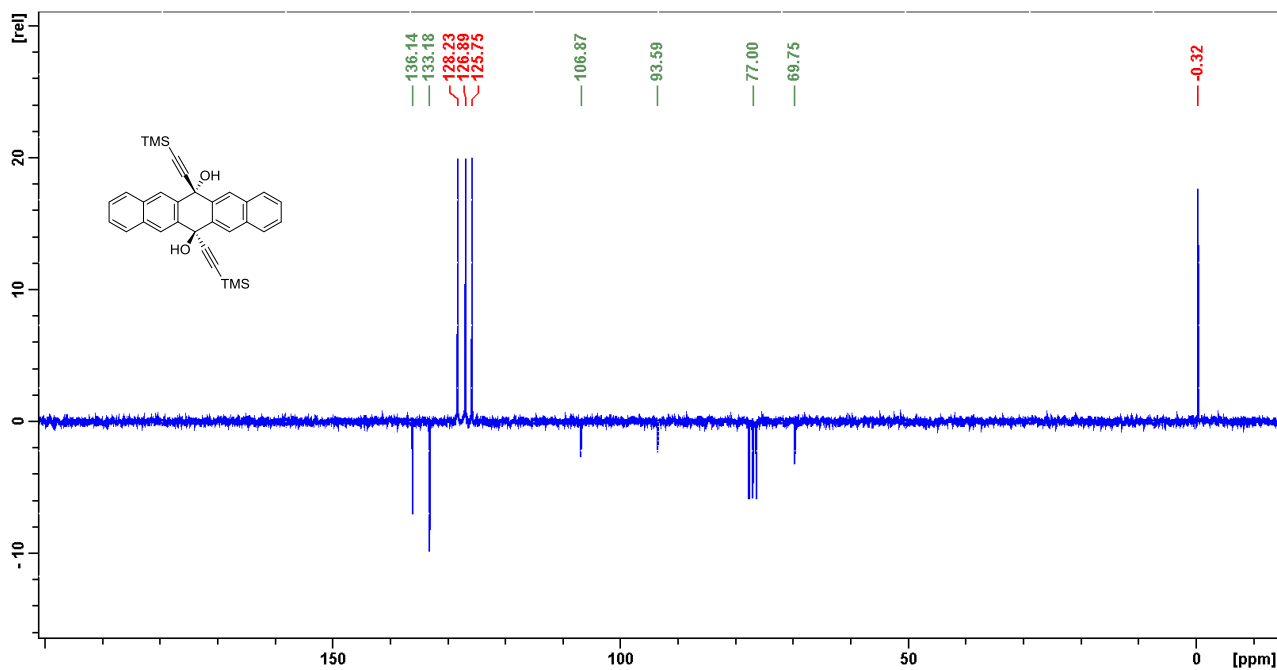


Figure S4. Carbon NMR spectrum of compound 8.

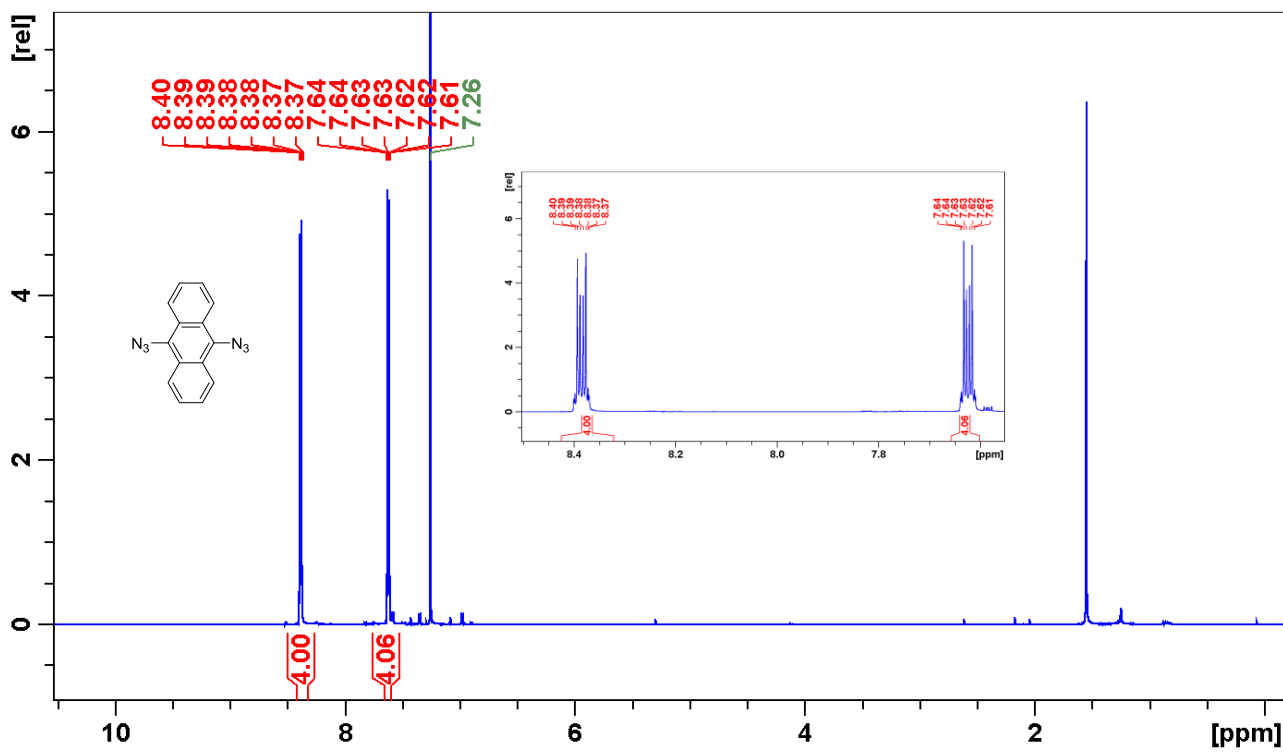


Figure S5. Proton NMR spectrum of compound 6.

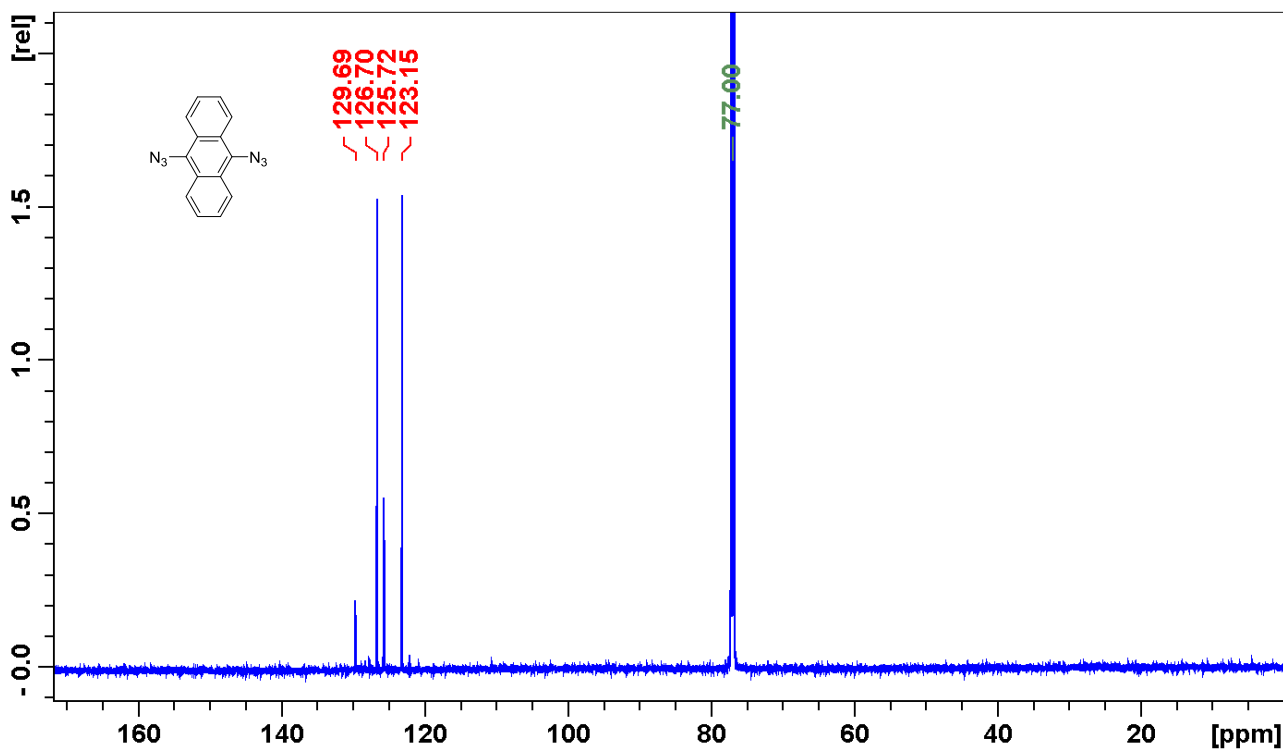


Figure S6. Carbon NMR spectrum of compound 6.

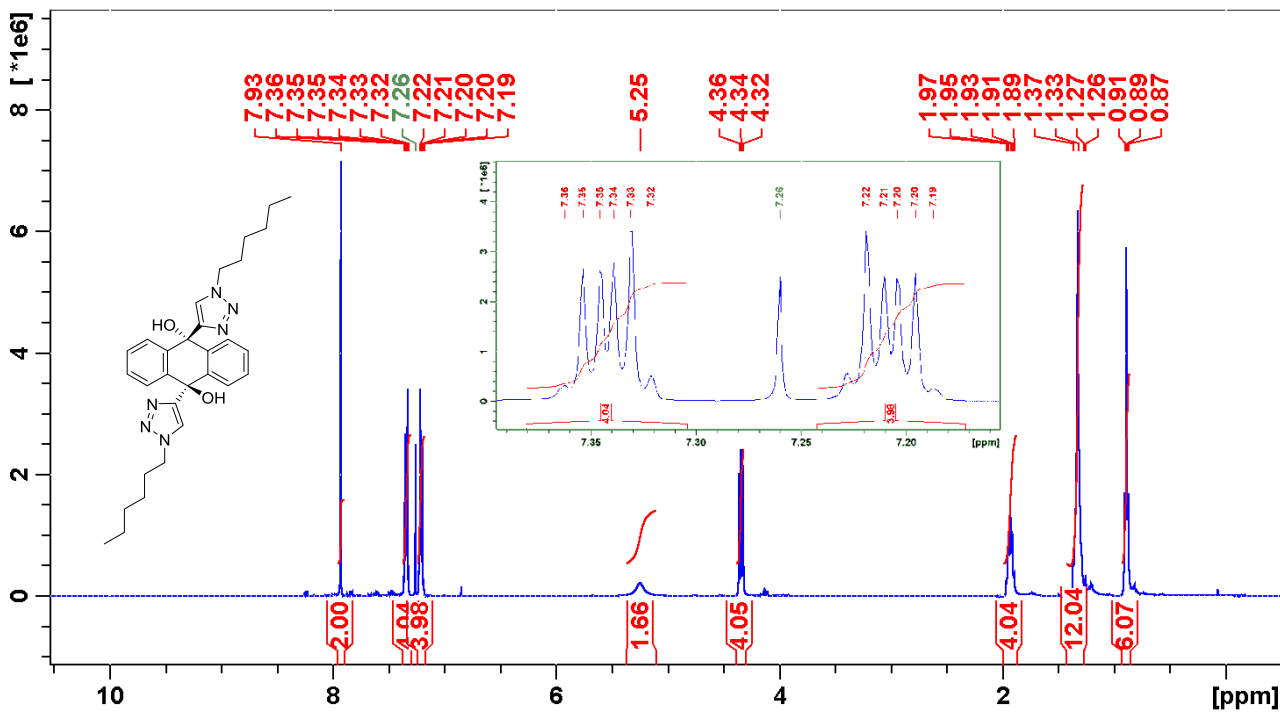


Figure S7. Proton NMR spectrum of compound 3a.

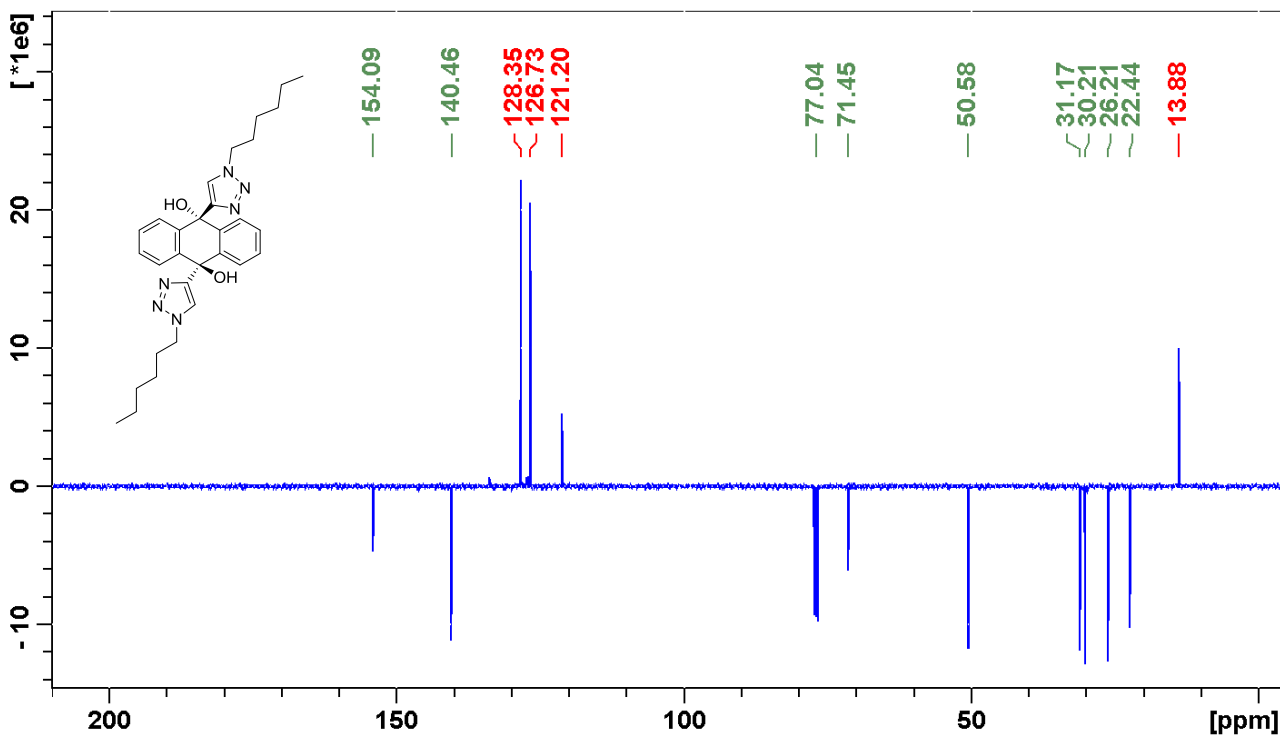


Figure S8. Carbon NMR spectrum of compound 3a.

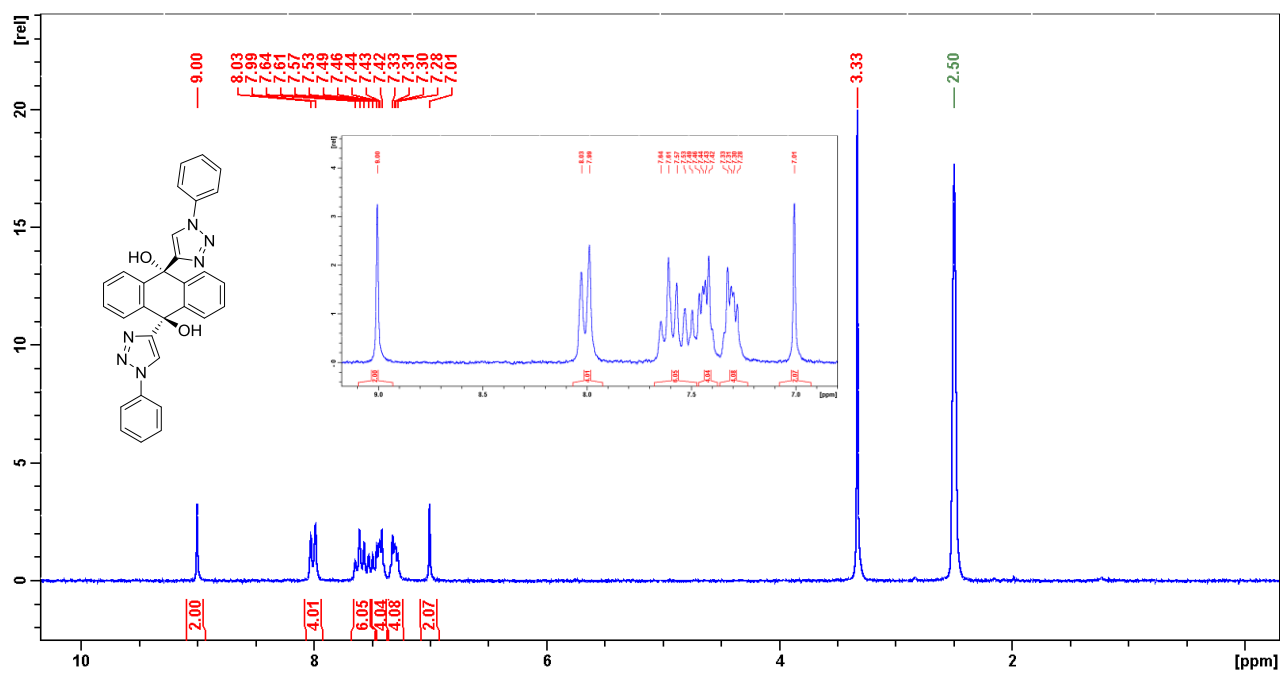


Figure S9. Proton NMR spectrum of compound **3b**.

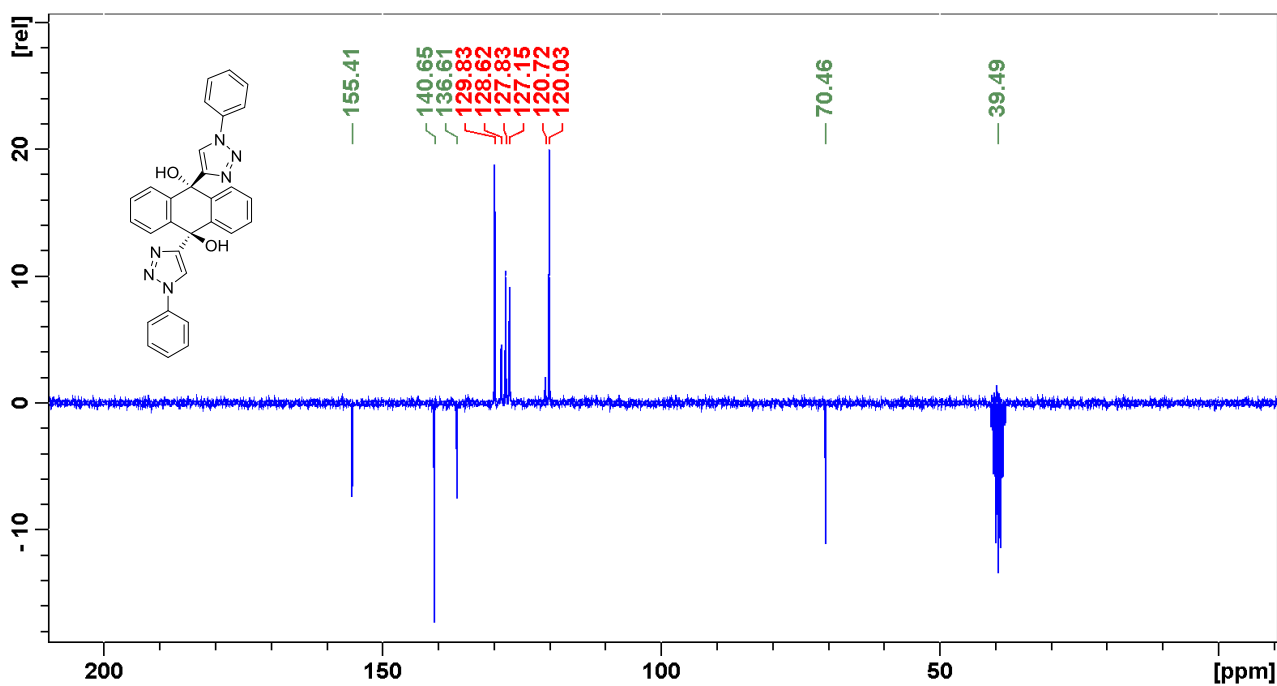


Figure S10. Carbon NMR spectrum of compound **3b**.

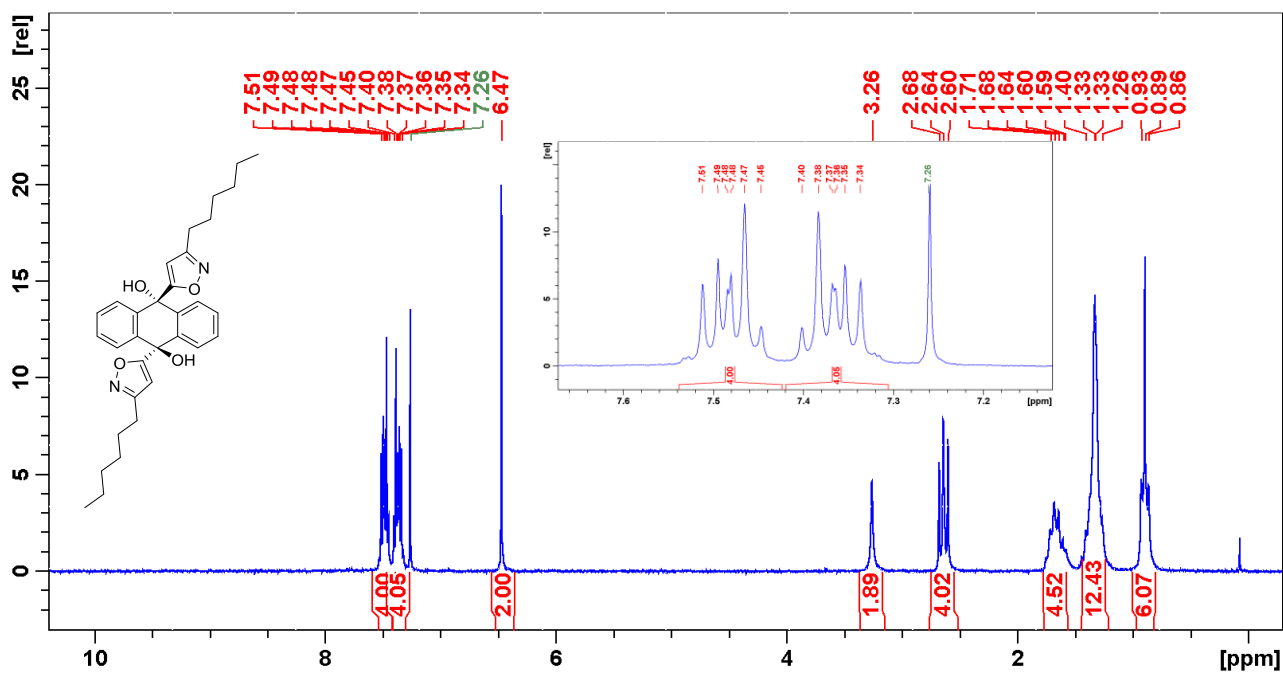


Figure S11. Proton NMR spectrum of compound 4a.

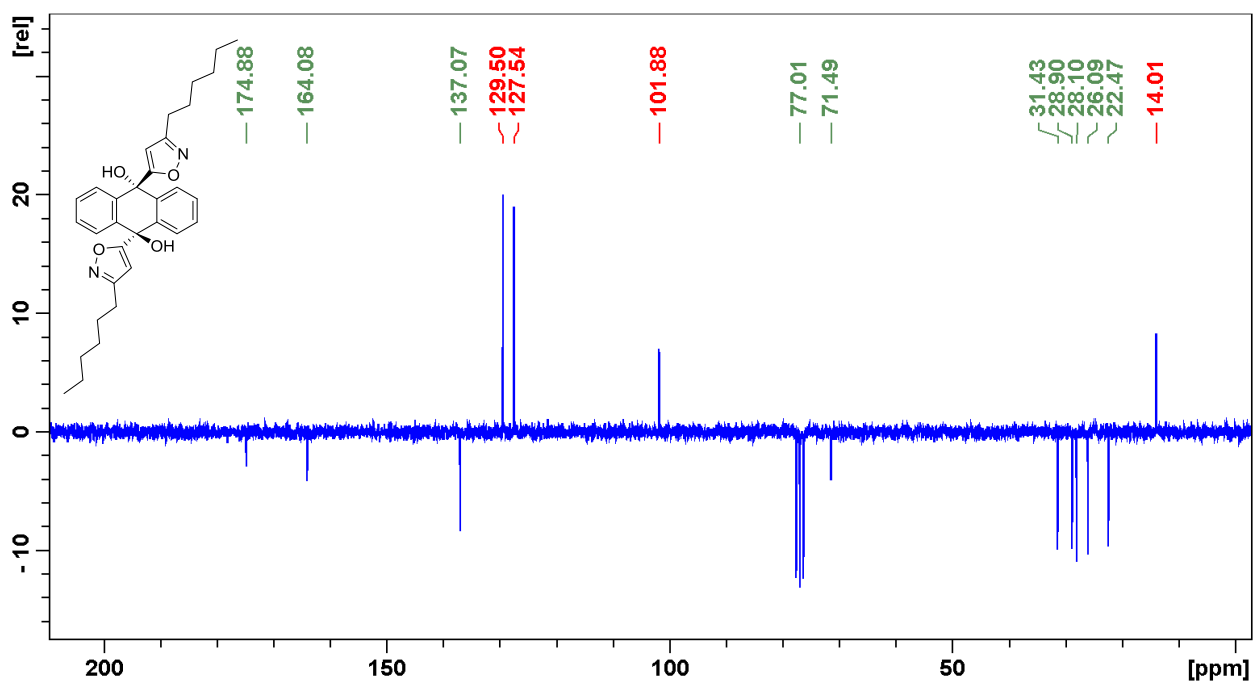


Figure S12. Carbon NMR spectrum of compound 4a.

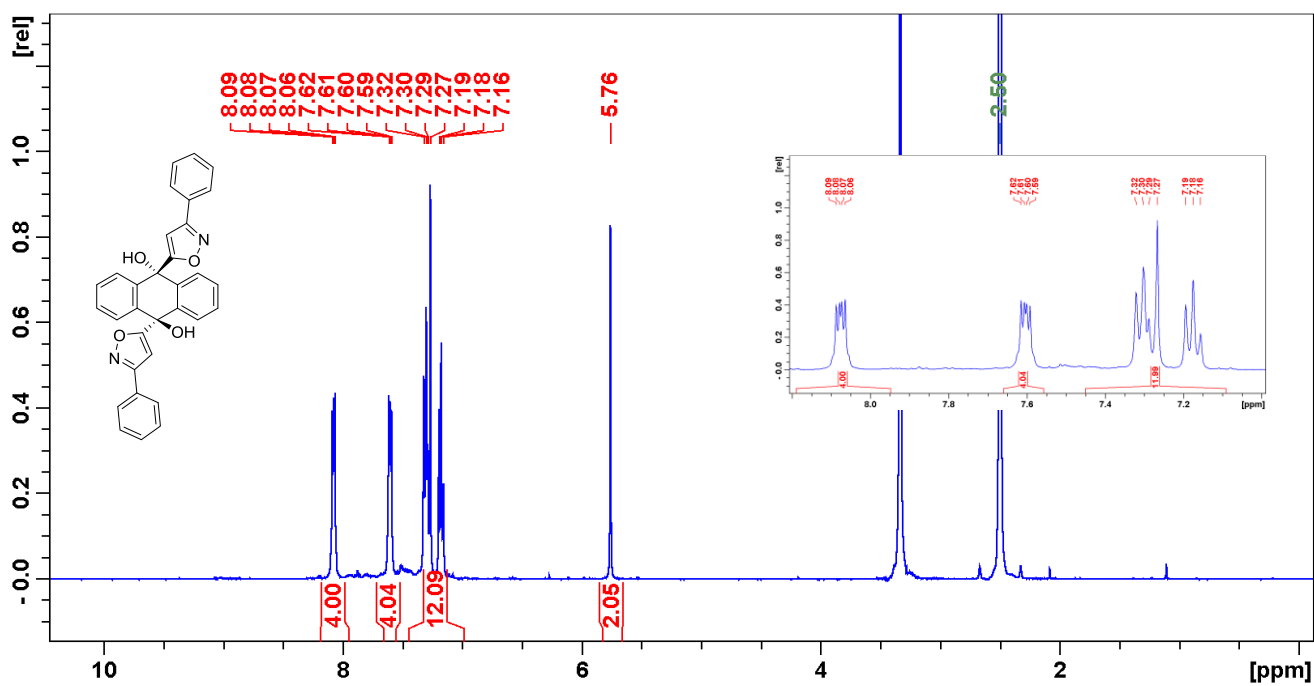


Figure S13. Proton NMR spectrum of compound 4b.

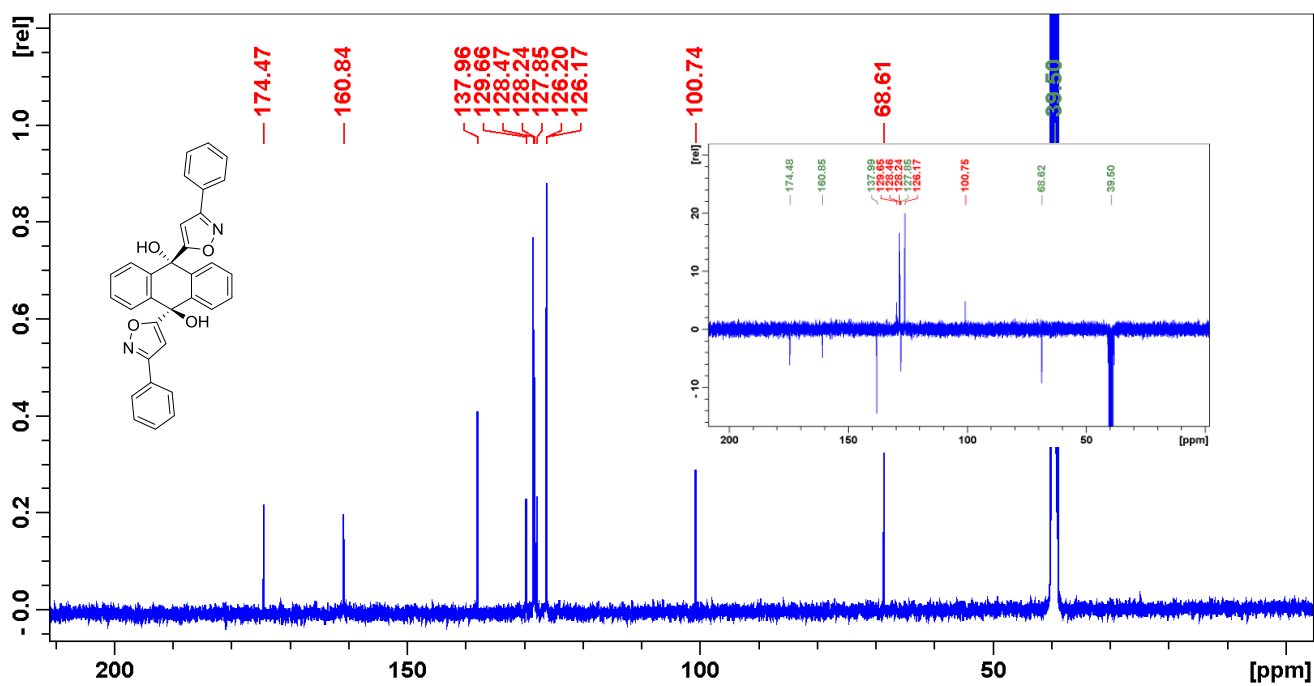


Figure S14. Carbon NMR spectrum of compound 4b.

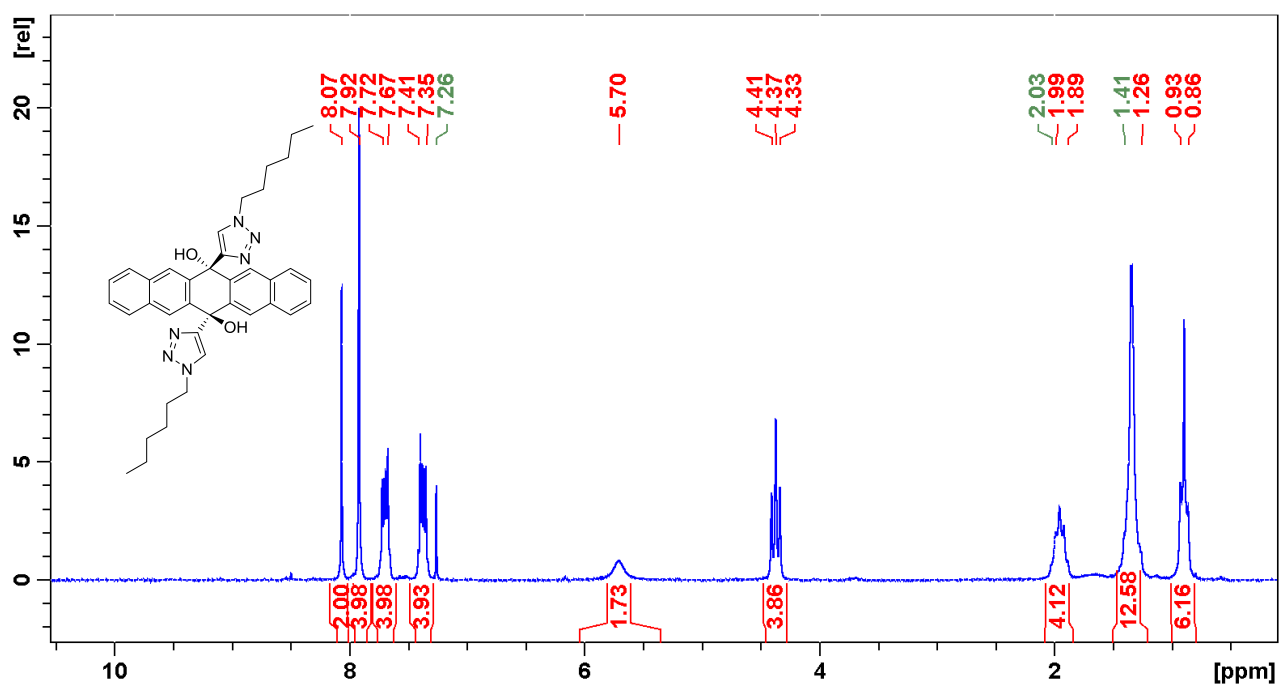


Figure S15. Proton NMR spectrum of compound 9a.

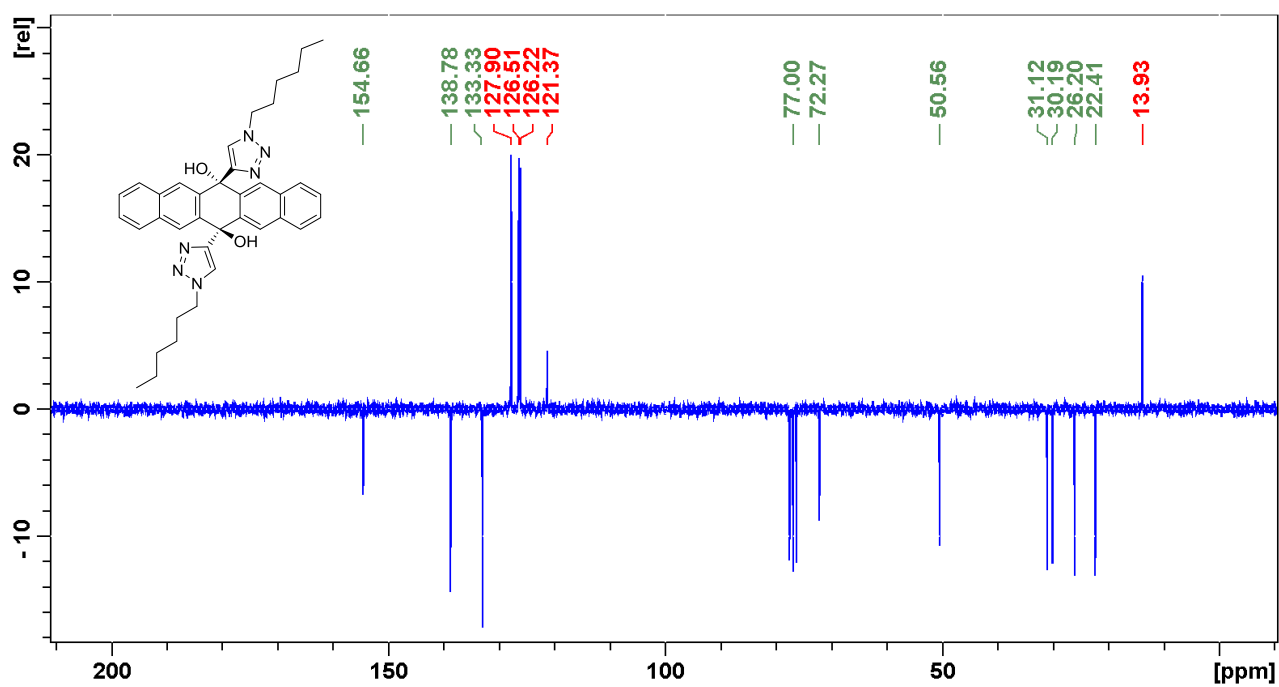


Figure S16. Carbon NMR spectrum of compound 9a.

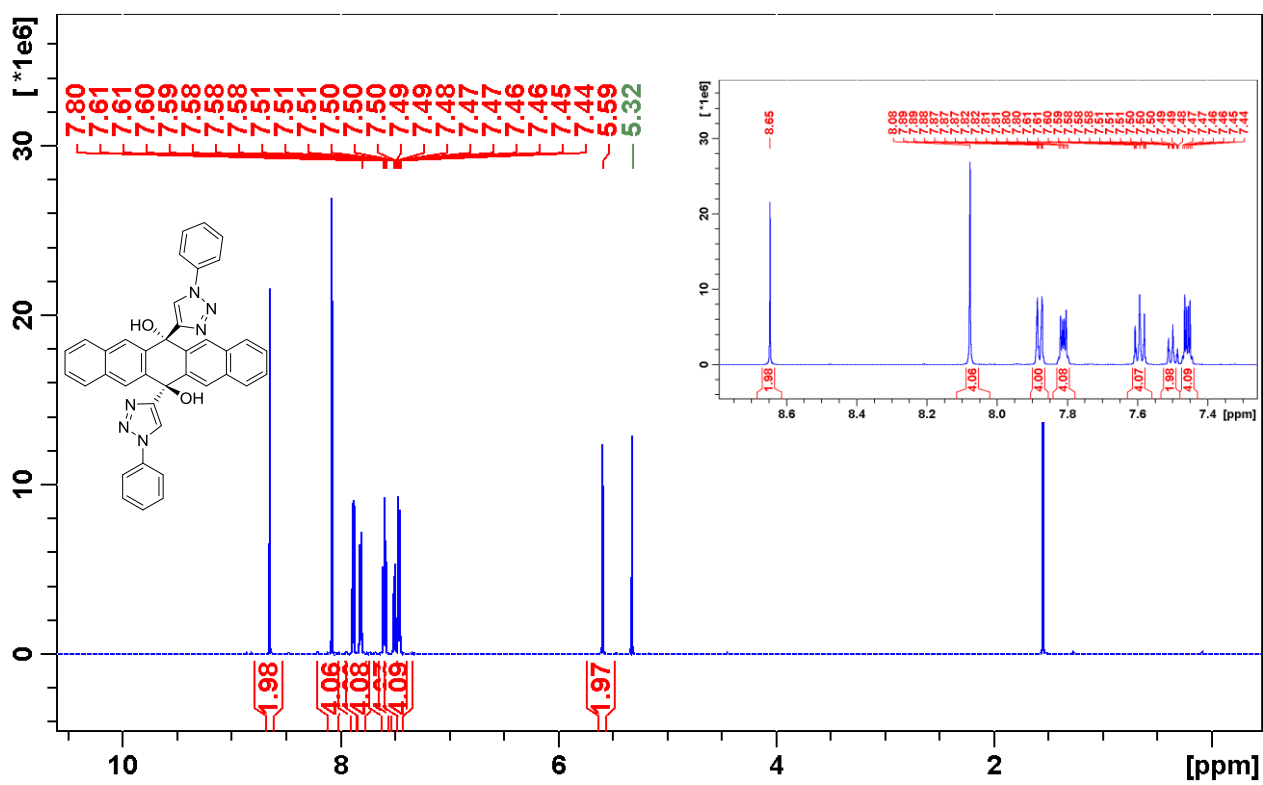


Figure S17. Proton NMR spectrum of compound **9b**.

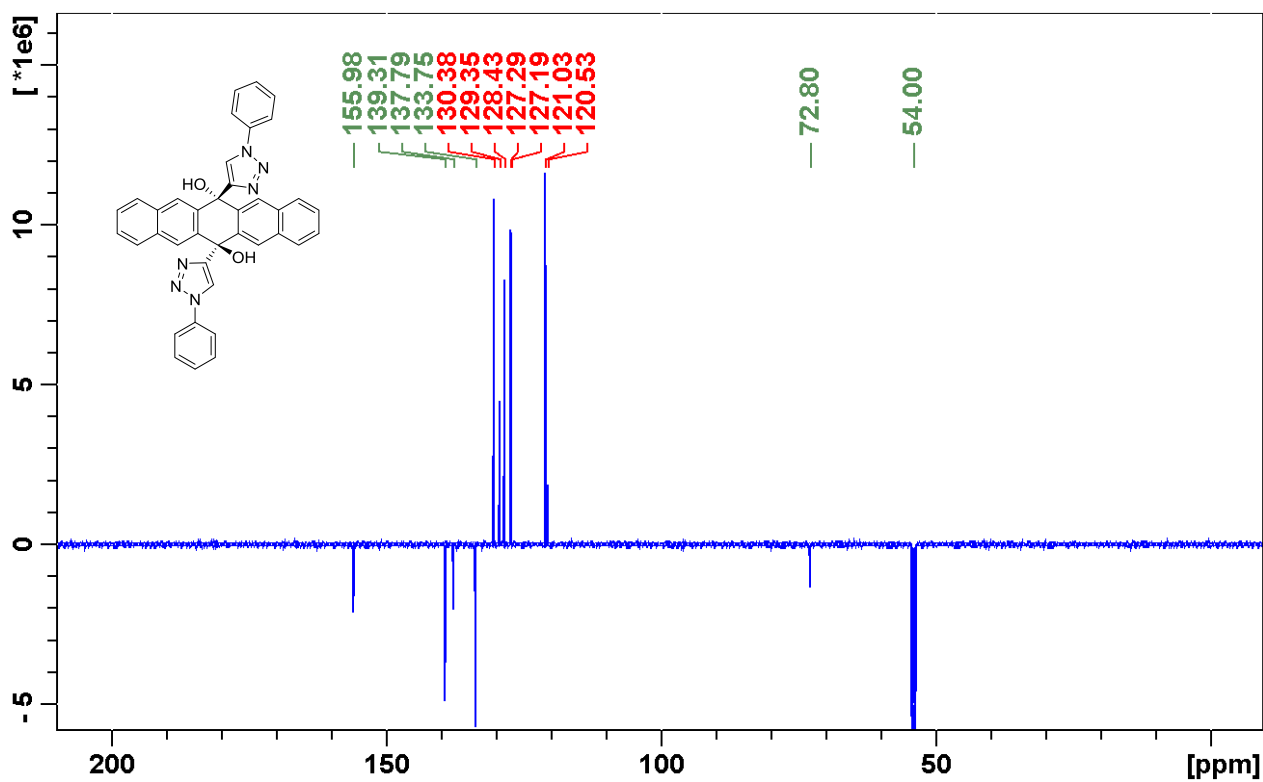


Figure S18. Carbon NMR spectrum of compound **9b**.

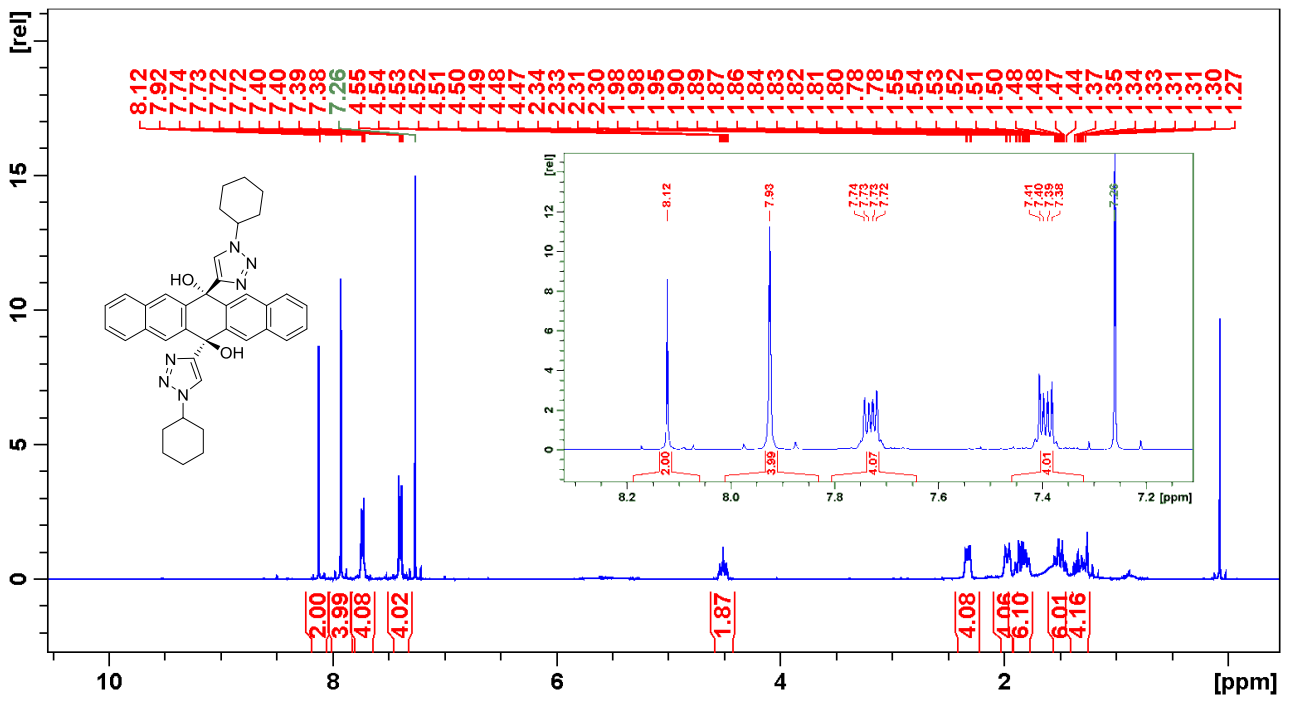


Figure S19. Proton NMR spectrum of compound 9c.

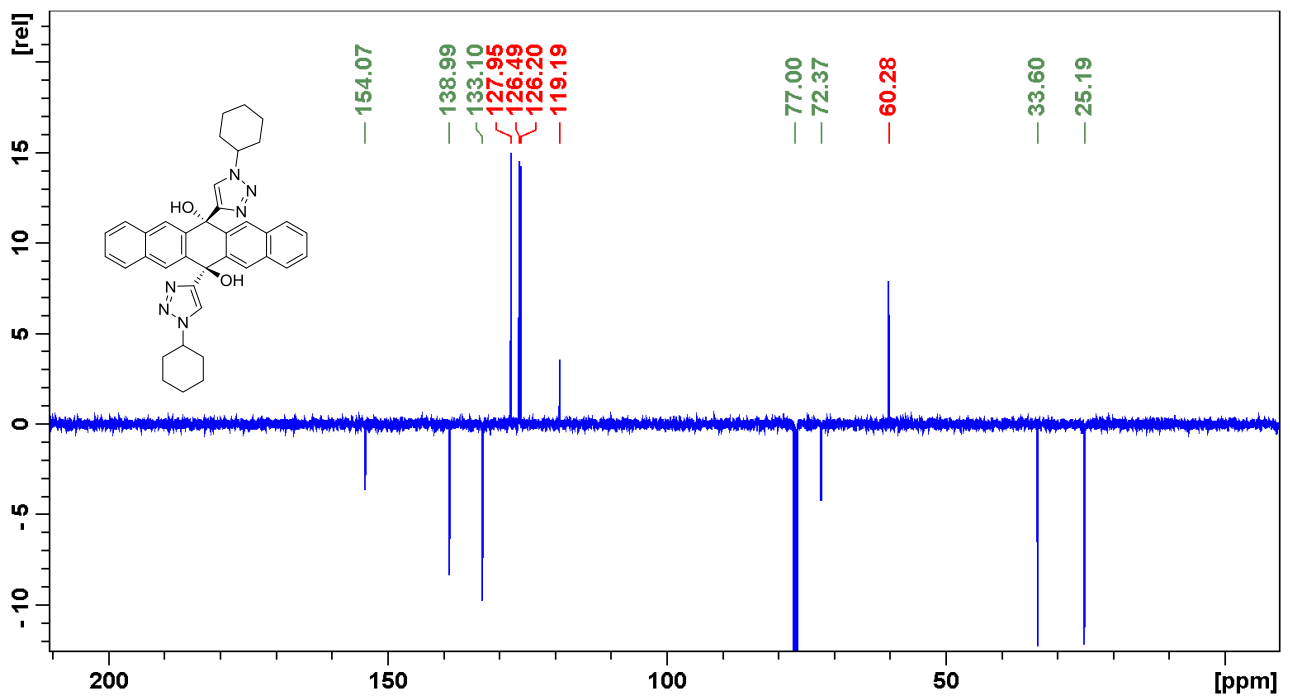


Figure S20. Carbon NMR spectrum of compound 9c.

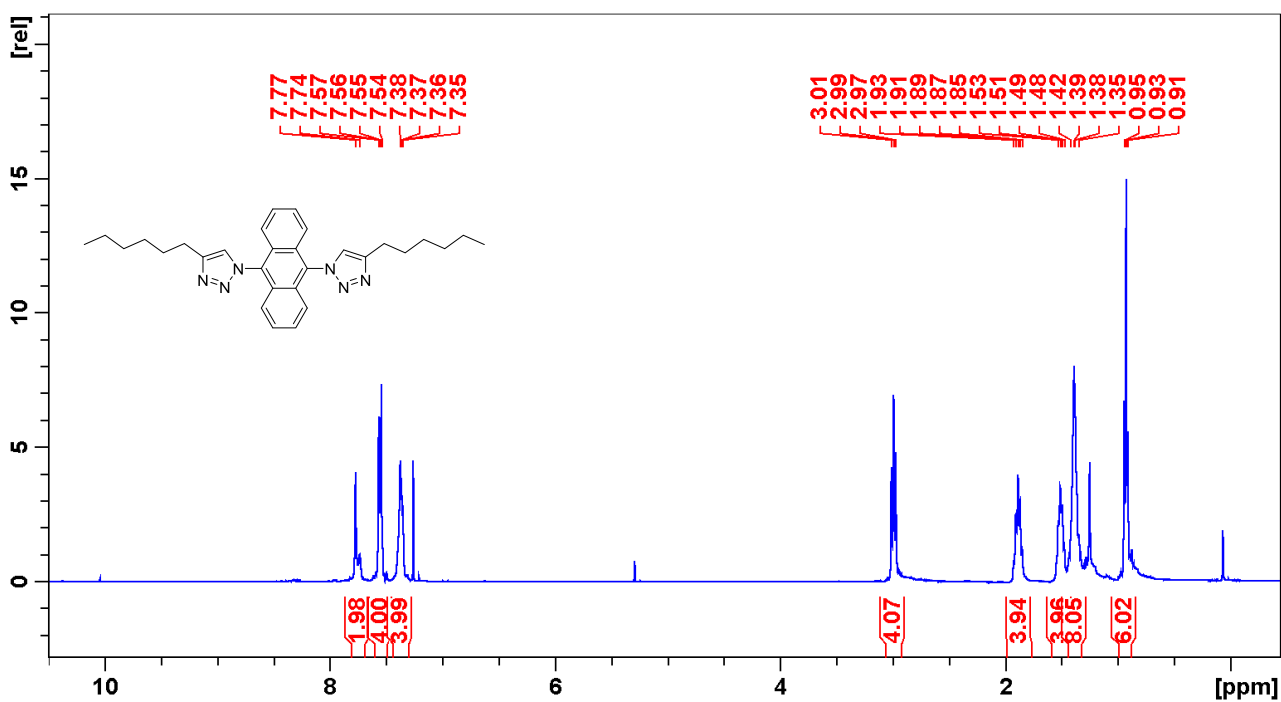


Figure S21. Proton NMR spectrum of compound A3a.

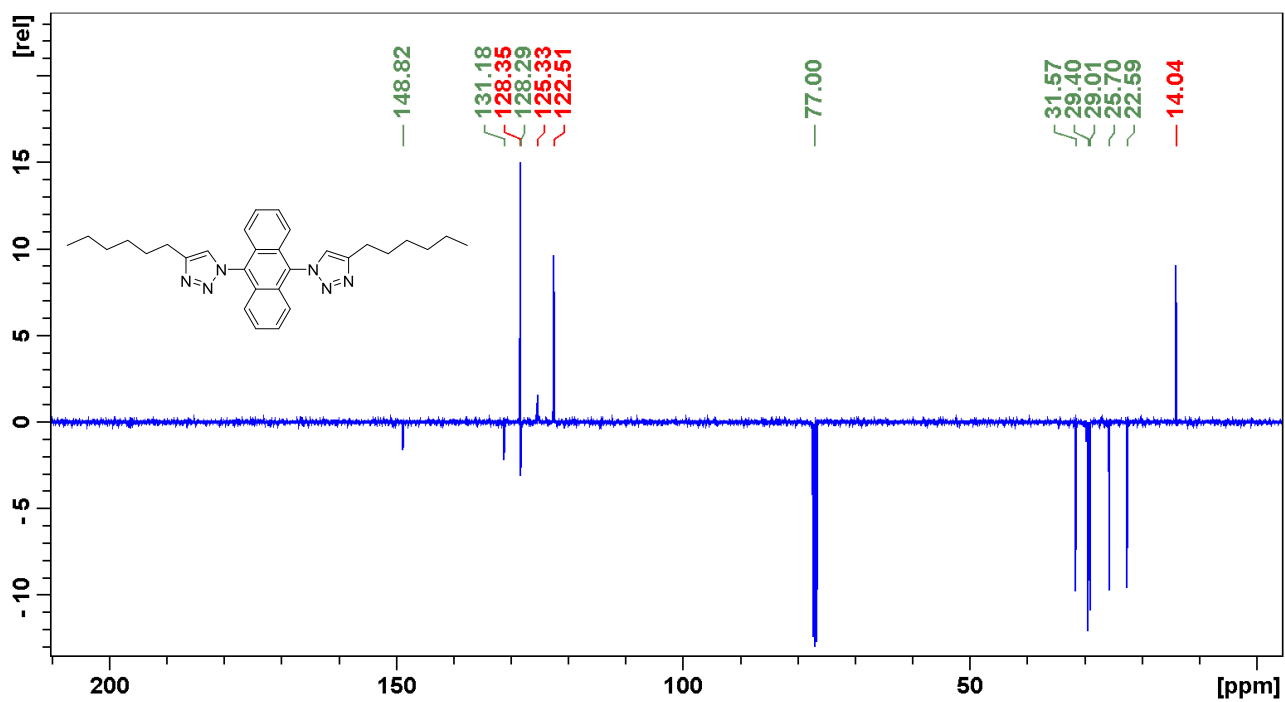


Figure S22. Carbon NMR spectrum of compound A3a.

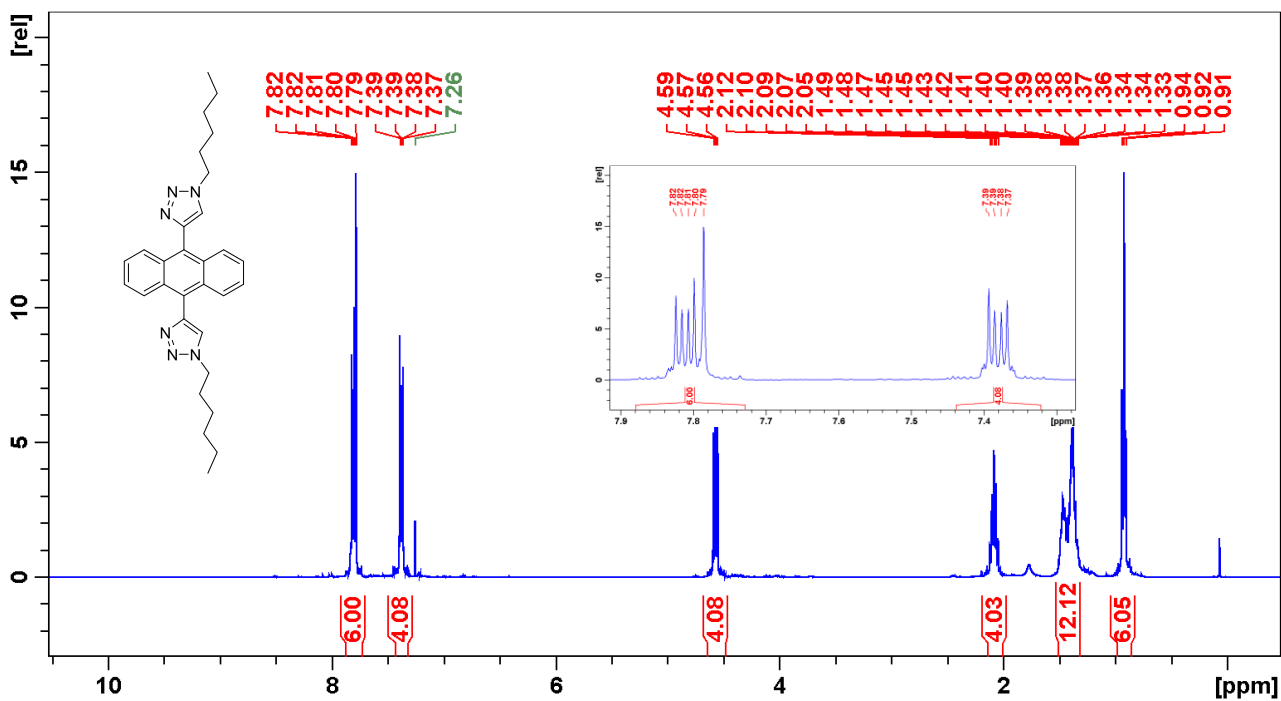


Figure S23. Proton NMR spectrum of compound A1a.

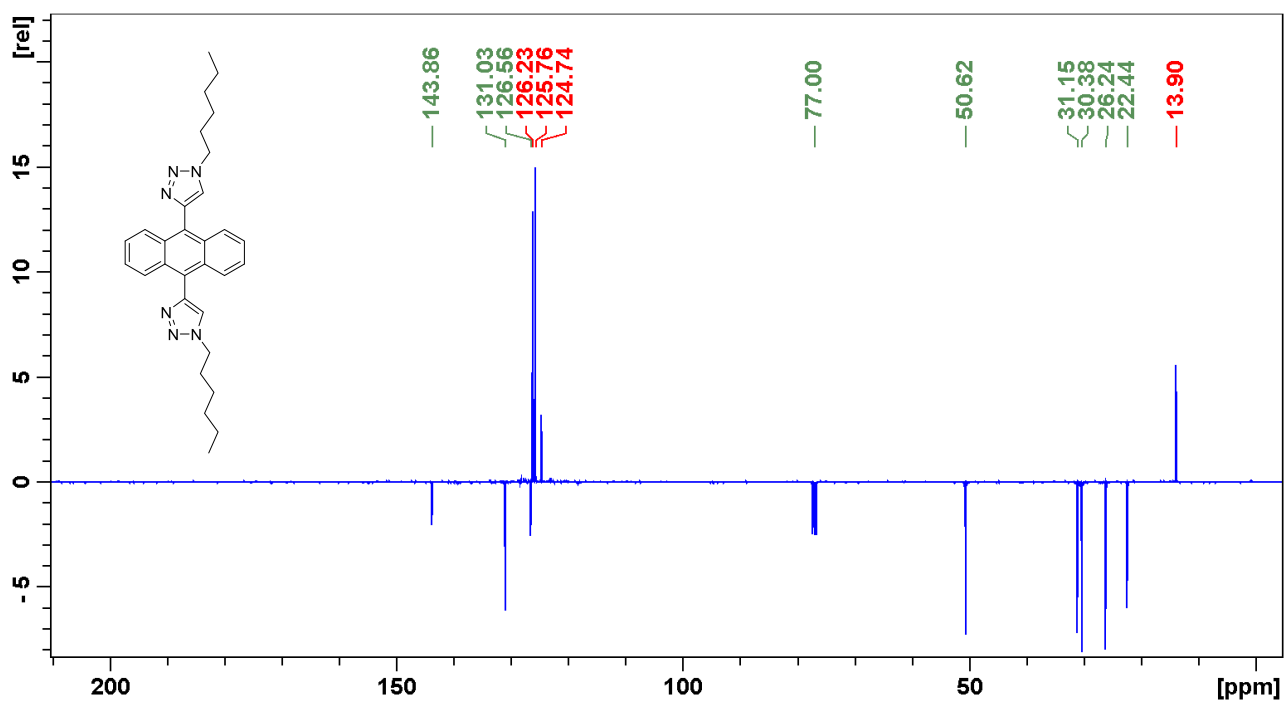


Figure S24. Carbon NMR spectrum of compound A1a.

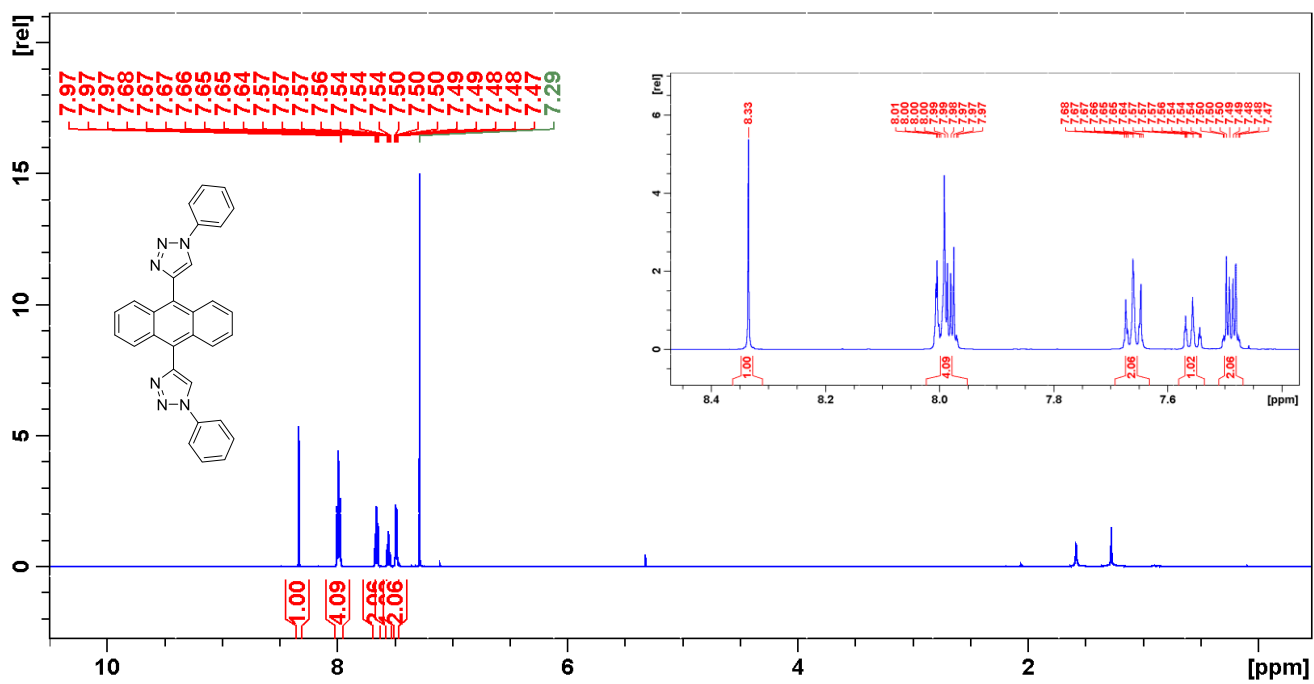


Figure S25. Proton NMR spectrum of compound A1b.

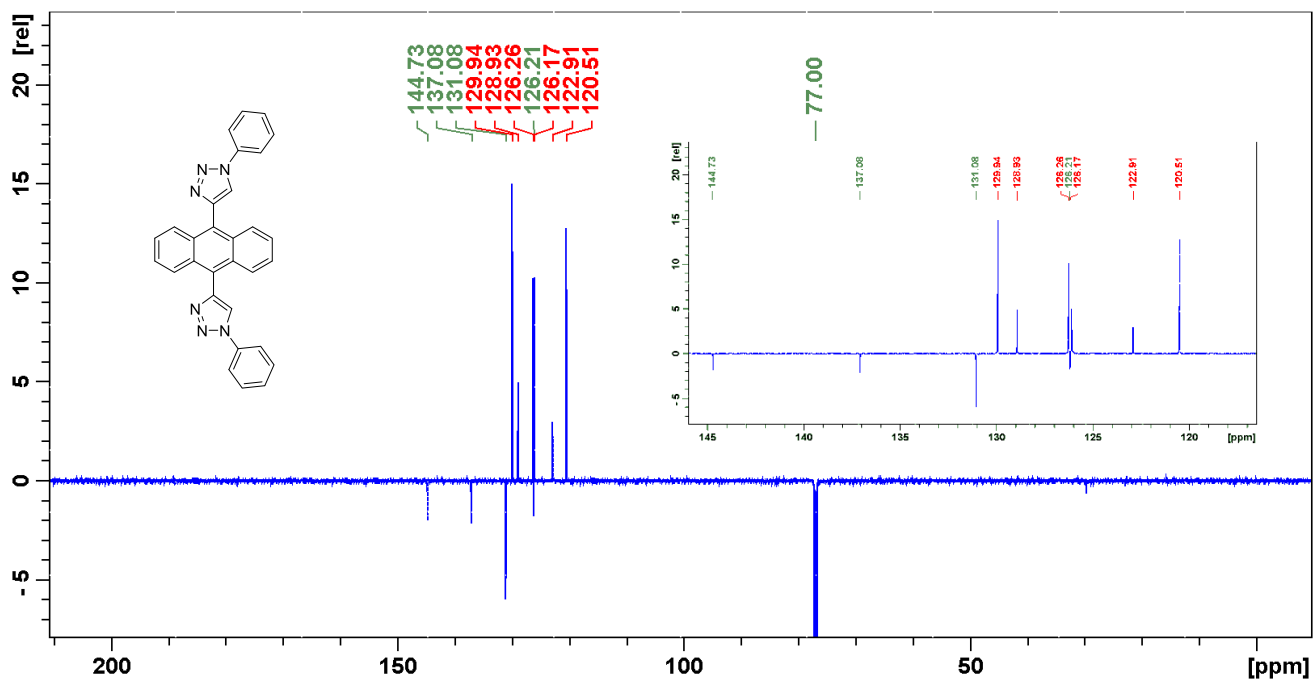


Figure S26. Carbon NMR spectrum of compound A1b.

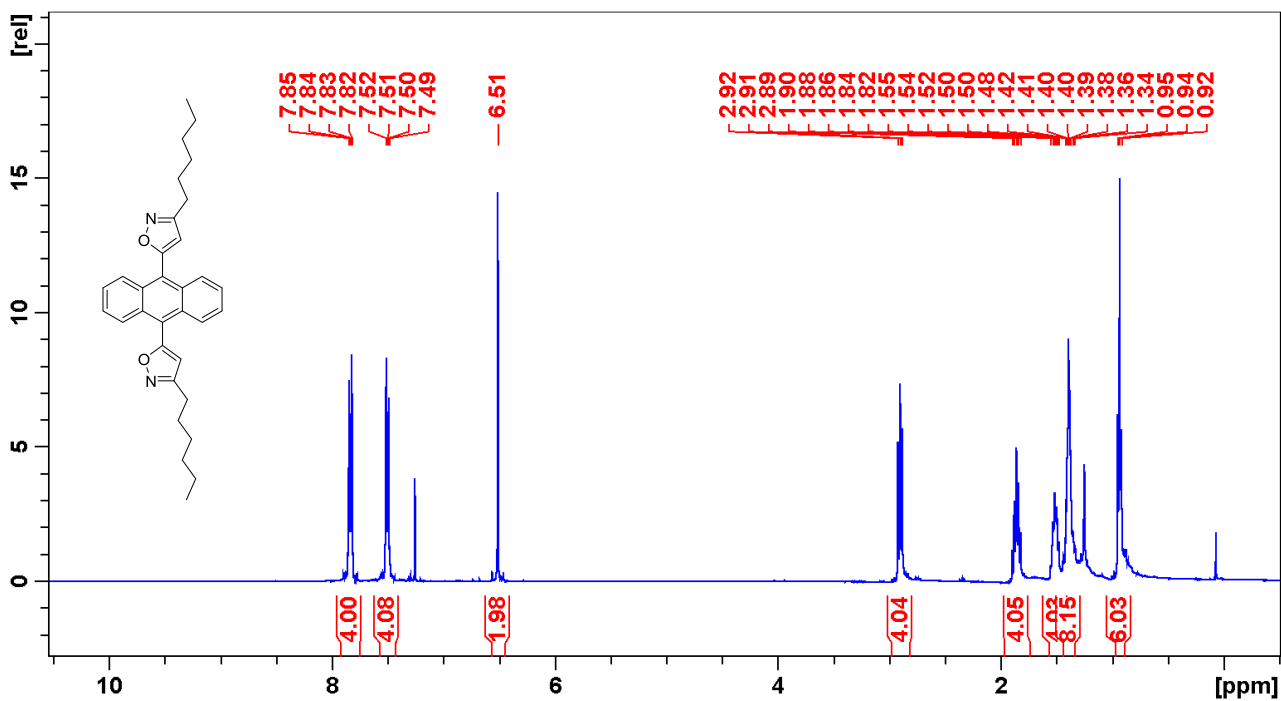


Figure S27. Proton NMR spectrum of compound A2a.

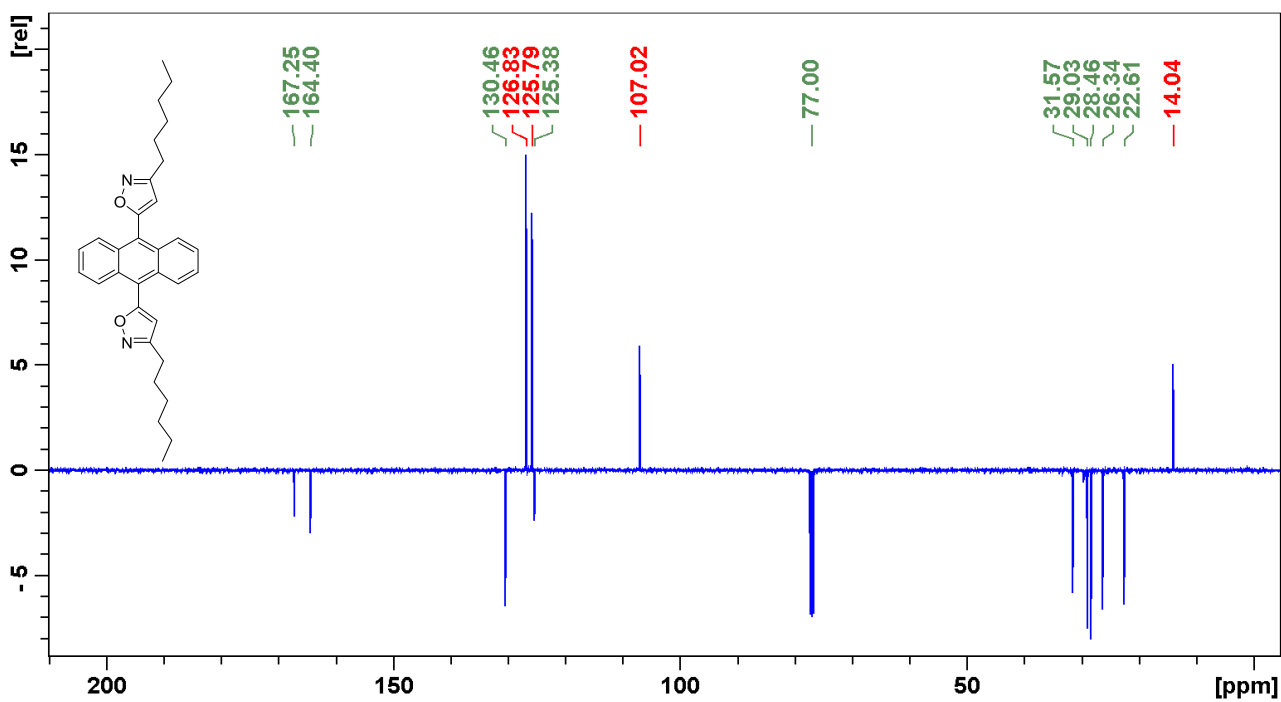


Figure S28. Carbon NMR spectrum of compound A2a.

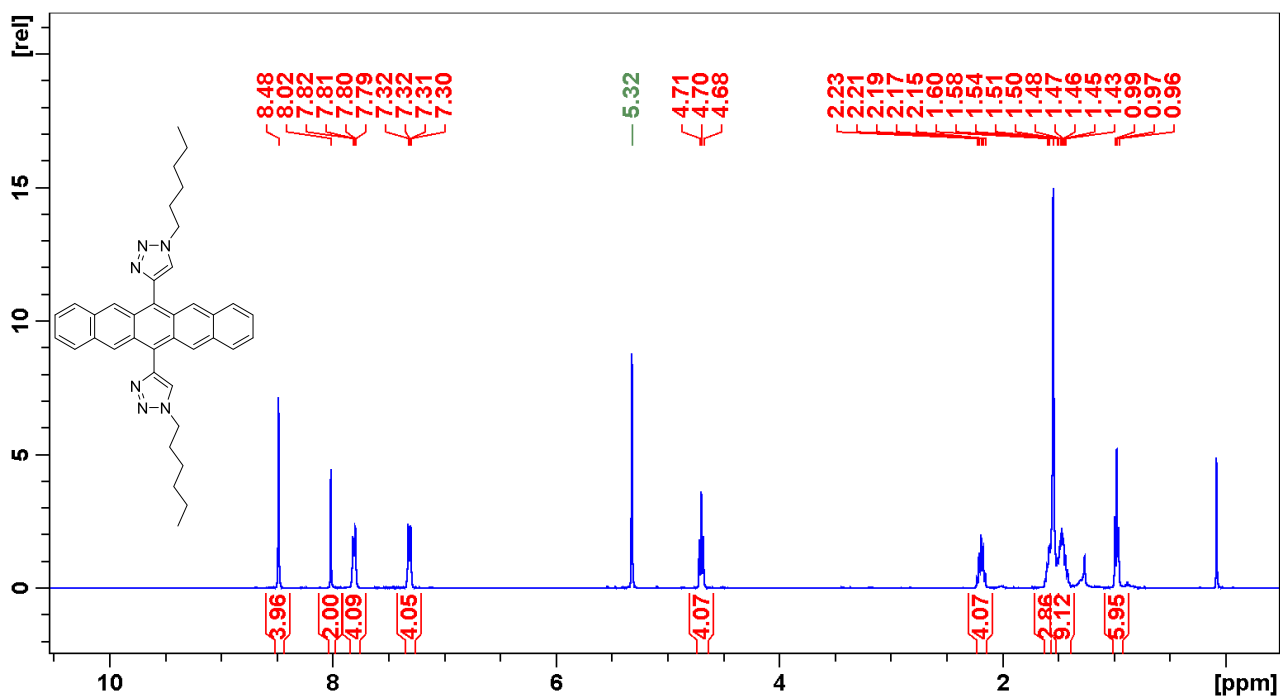


Figure S31. Proton NMR spectrum of compound P1a.

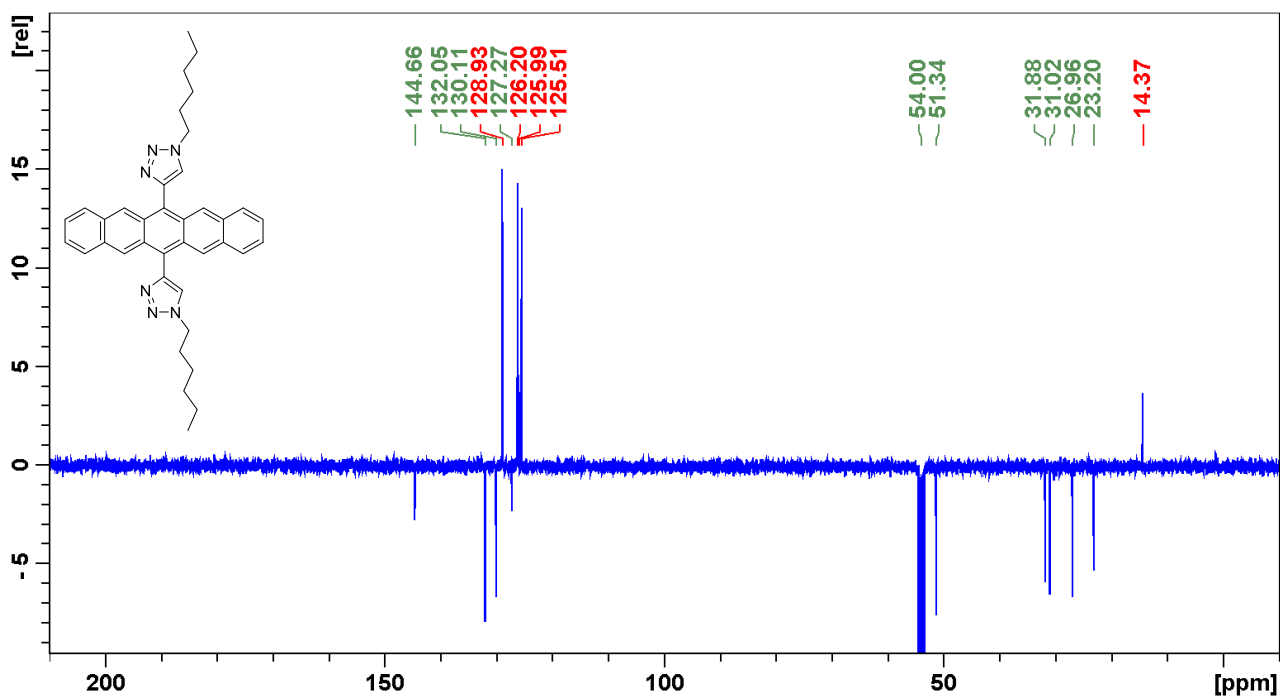


Figure S32. Carbon NMR spectrum of compound P1a.

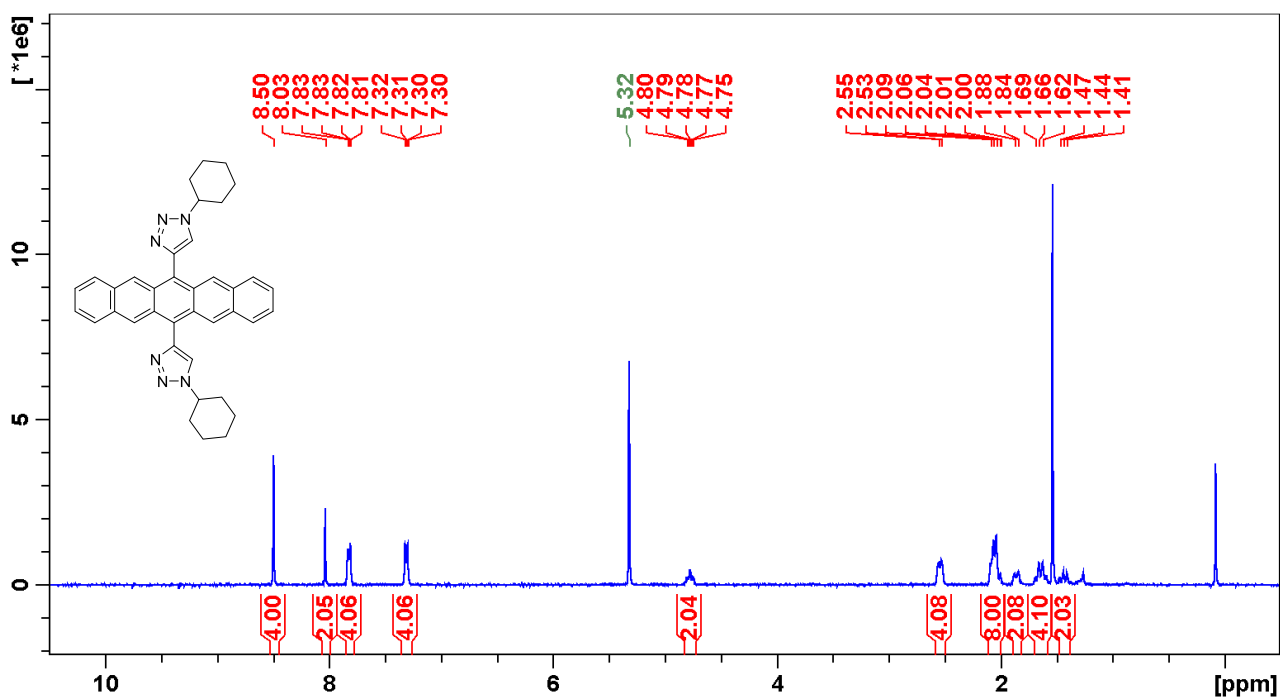


Figure S33. Proton NMR spectrum of compound **P1c**.

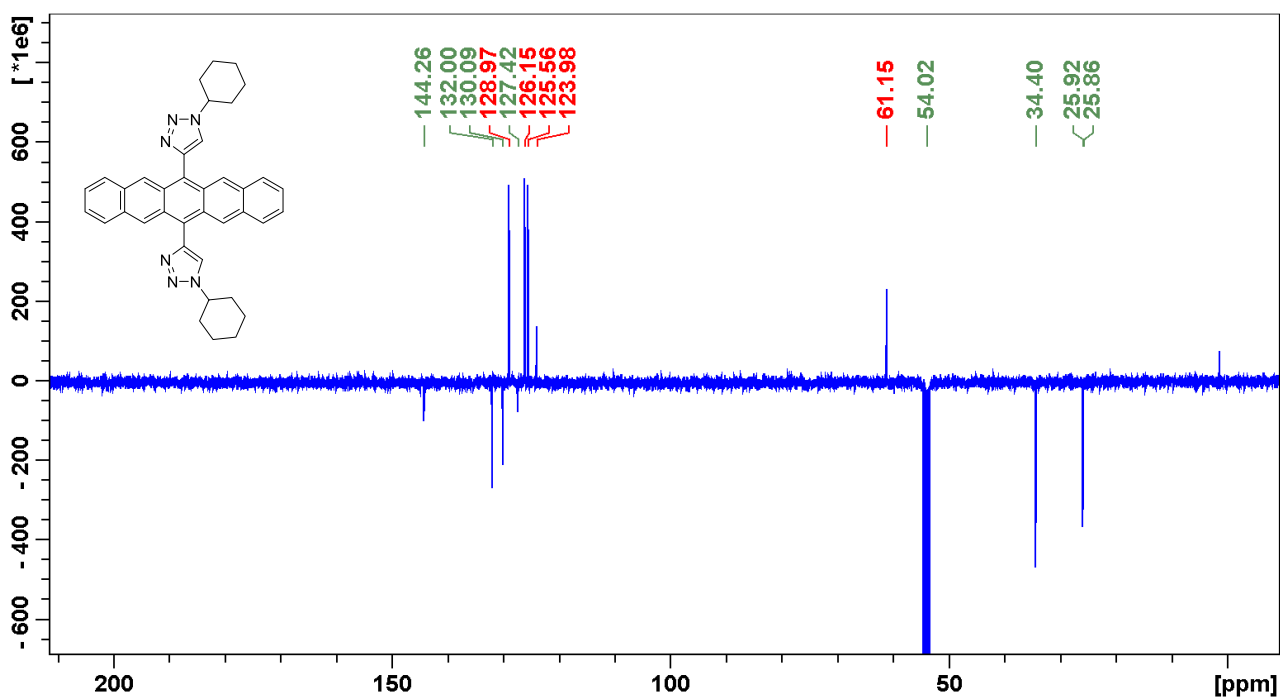


Figure S34. Carbon NMR spectrum of compound **P1c**.

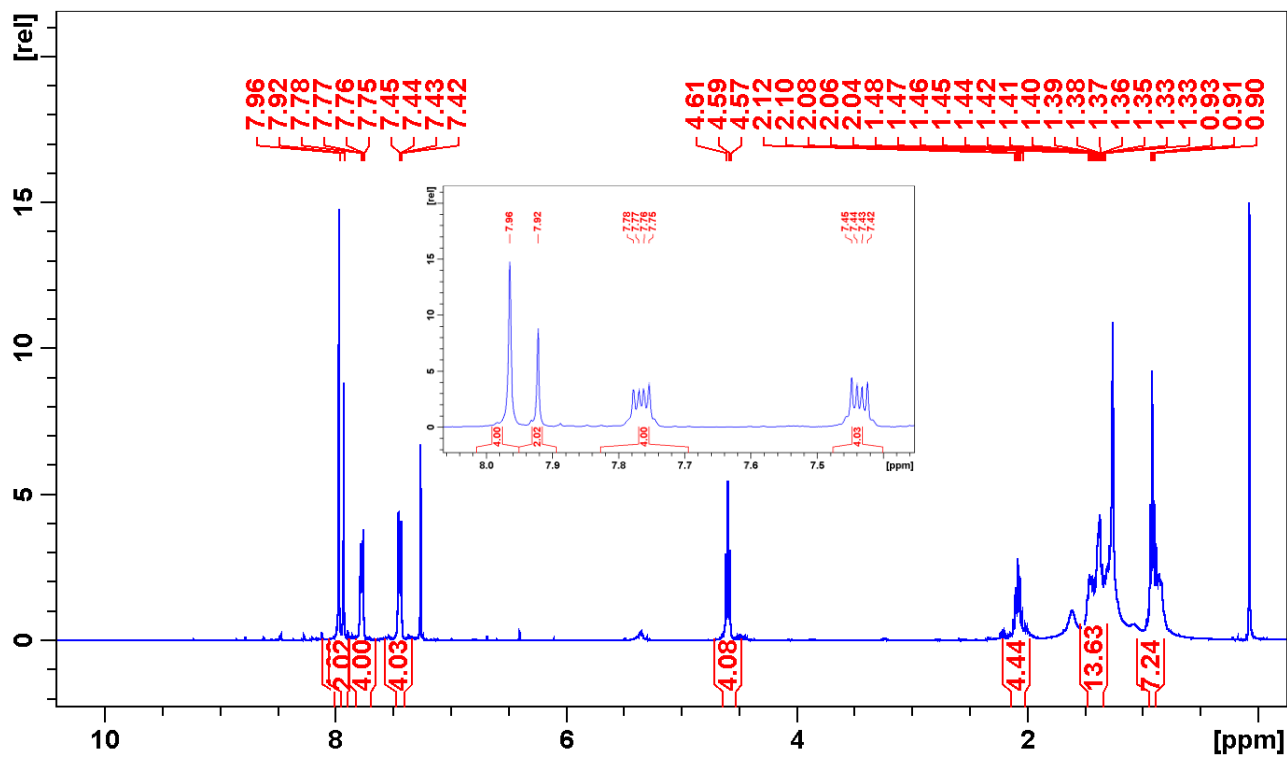


Figure S35. Proton NMR spectrum of the photooxidation product of **P1a**.

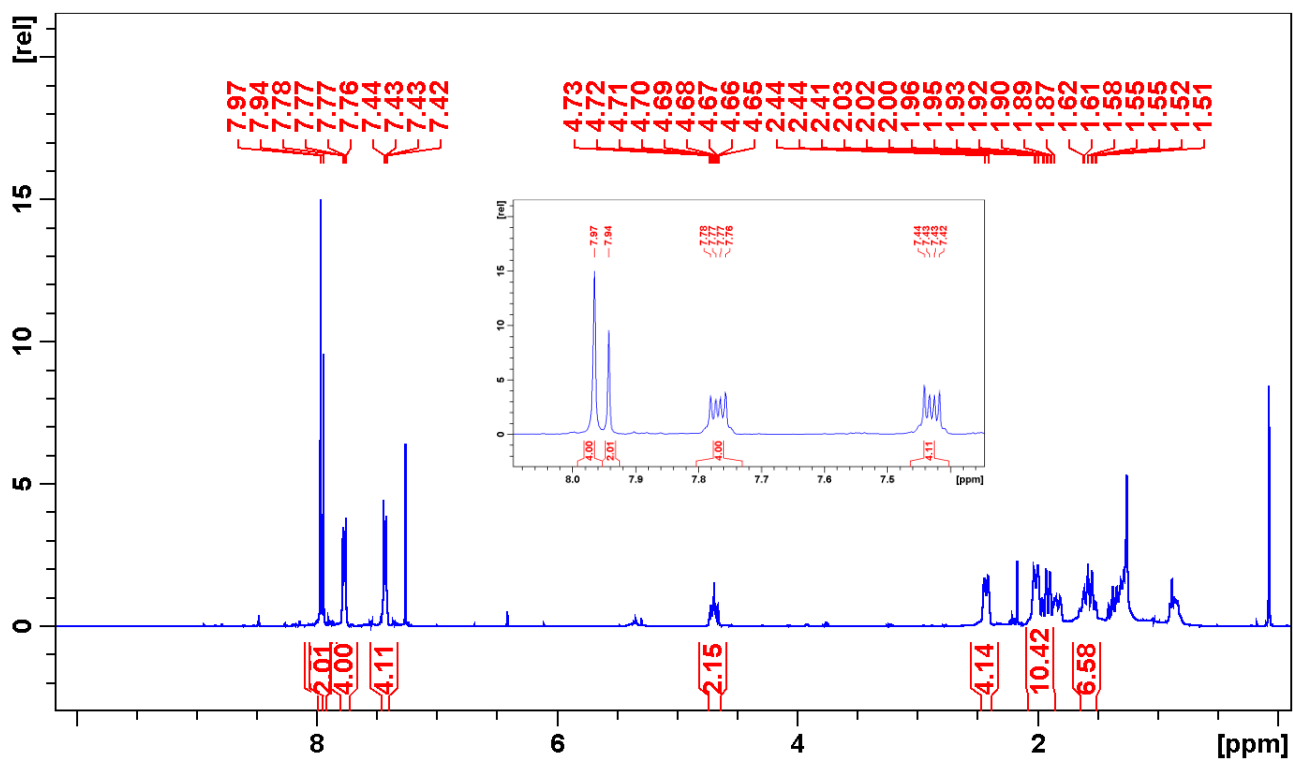


Figure S36. Proton NMR spectrum of the photooxidation product of **P1c**.

B) Cyclic Voltammetry

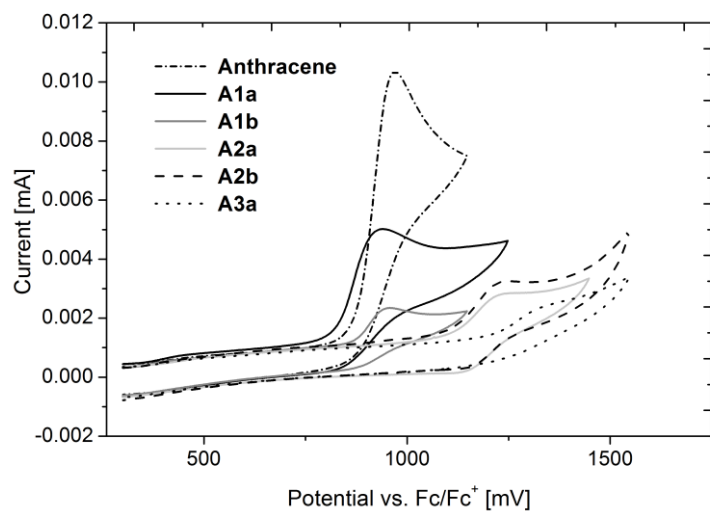


Figure S37: Cyclic voltammograms of **A1a**, **A1b**, **A2a**, **A2b** and **A3a**.

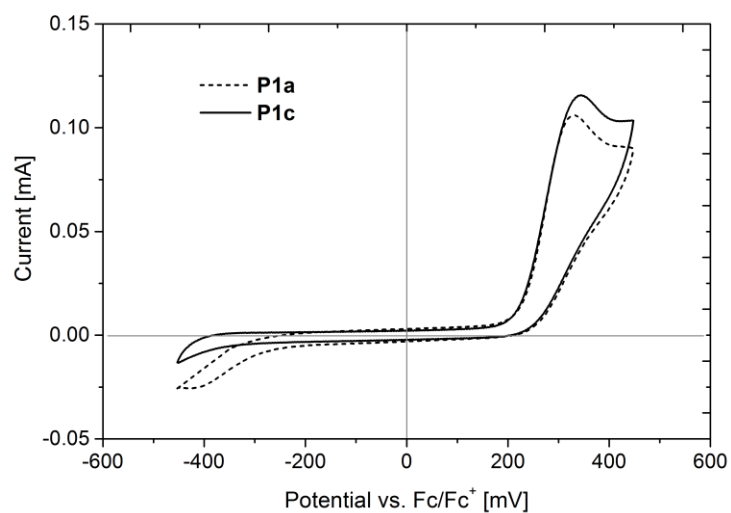


Figure S38: Cyclic voltammograms of **P1a** and **P1c**.

C) Molecular Structure of 9b

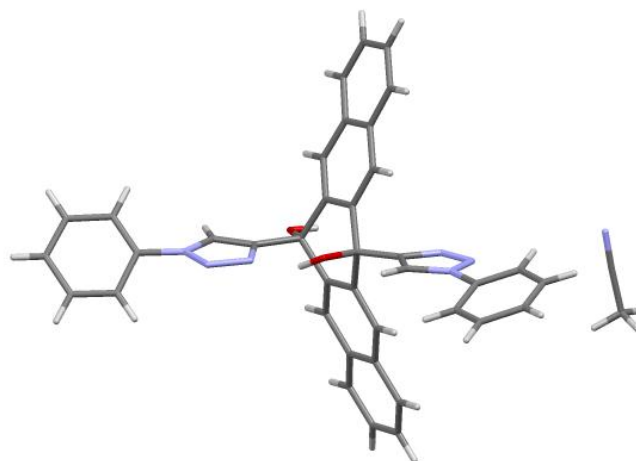


Figure S39: Molecular structure of **9b** as solvate (ACN).

D) Thermal Analysis

a. TGA Measurement

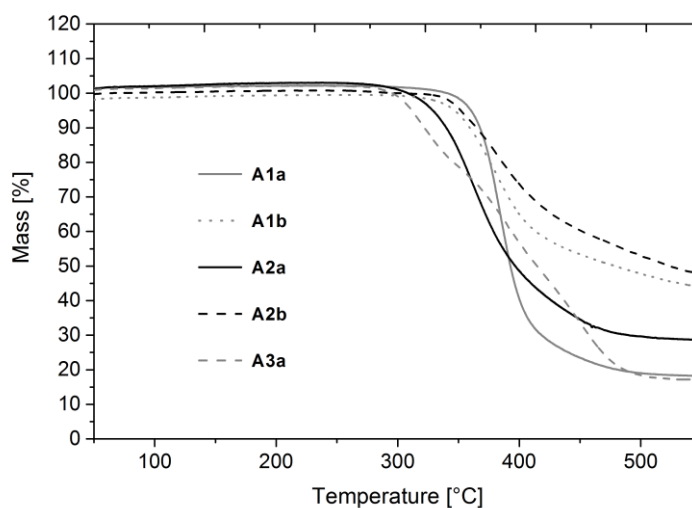


Figure S40: Thermogravimetric analysis of anthracene derivatives **A1a**, **A1b**, **A2a**, **A2b** and **A3a** in the temperature range 50-550°C under a stream of dry nitrogen with a heating rate of 10 K/min.

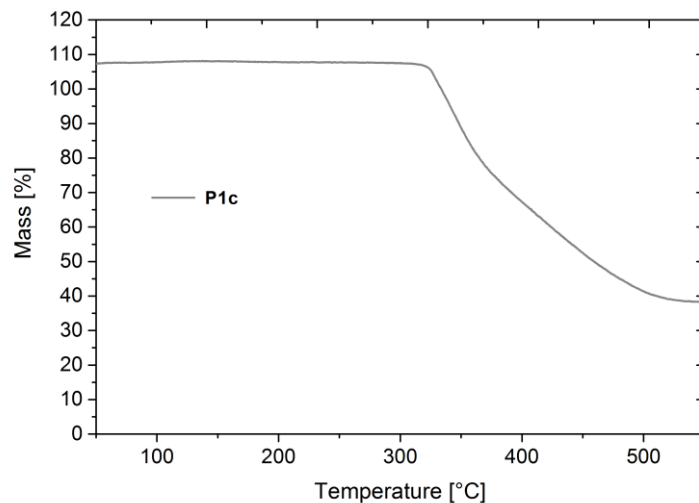


Figure S41: Thermogravimetric analysis of pentacene derivative **P1c** in the temperature range 50-550°C under a stream of dry nitrogen with a heating rate of 10 K/min.

b. DSC Analysis.

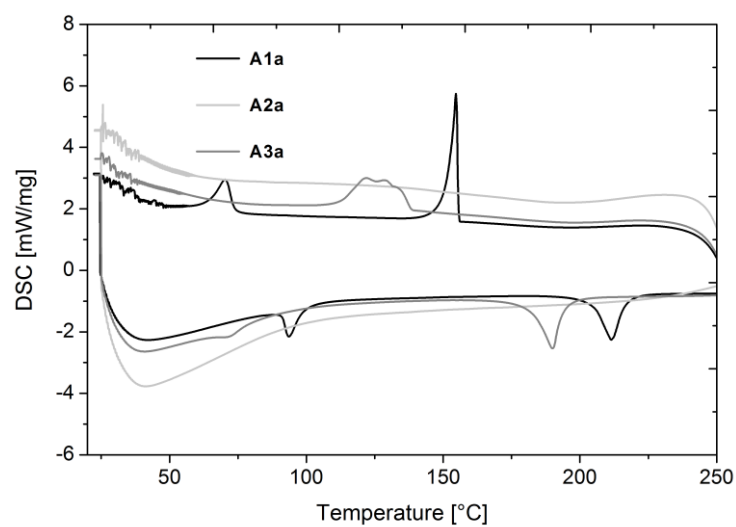


Figure S42: Two DSC heating/cooling cycles of anthracene derivatives **A1a**, **A1b**, **A2a**, **A2b** and **A3a** in the temperature range 22-250°C under a stream of dry nitrogen with a heating/cooling rate of 10 K/min.

E) DFT Calculations

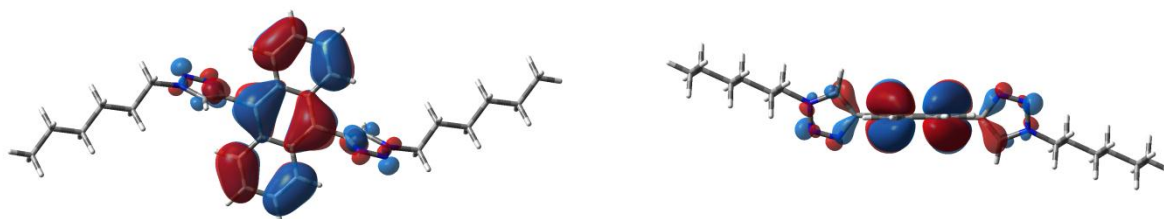
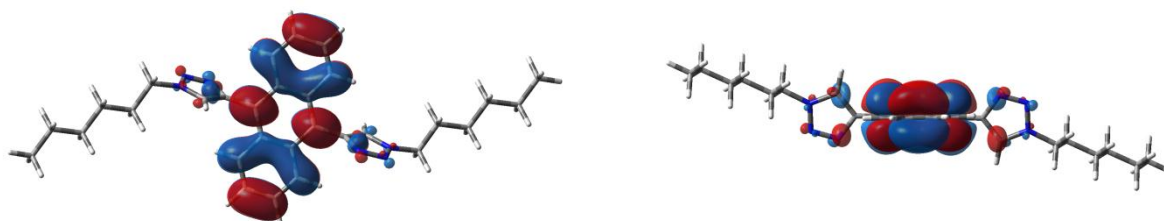


Figure S43: HOMO (bottom) and LUMO (top) of **A1a**.

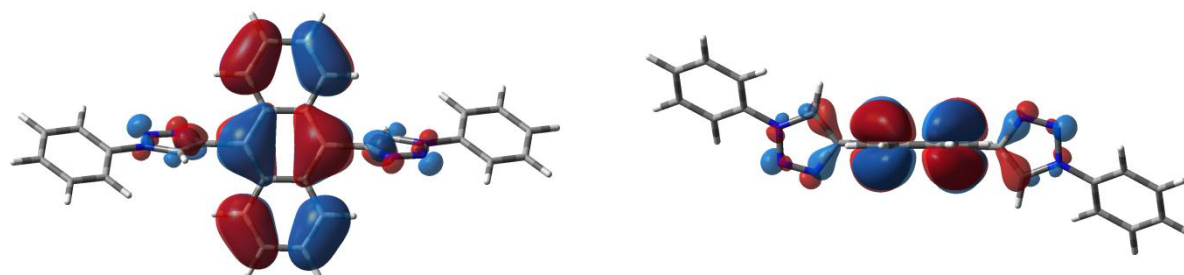
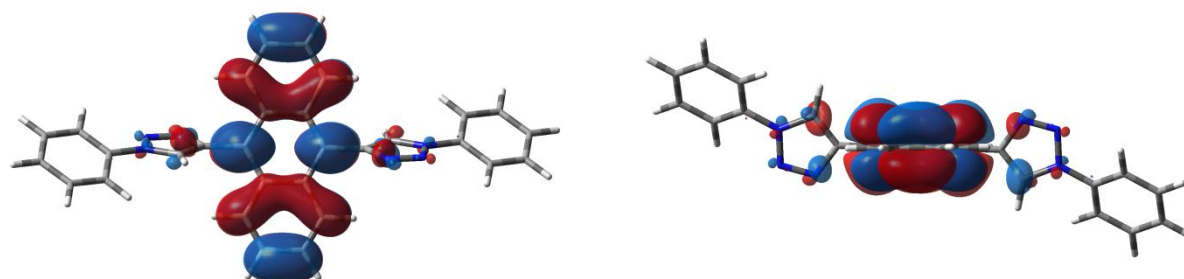


Figure S44: HOMO (bottom) and LUMO (top) of **A1b**.

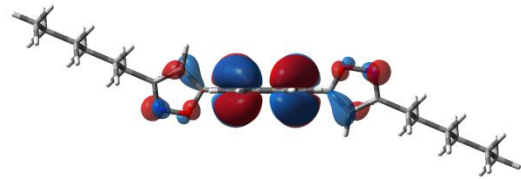
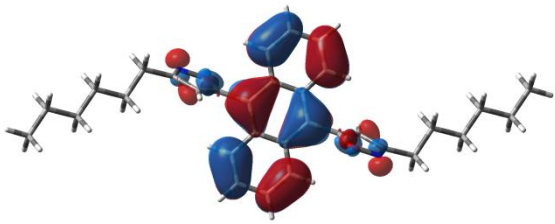
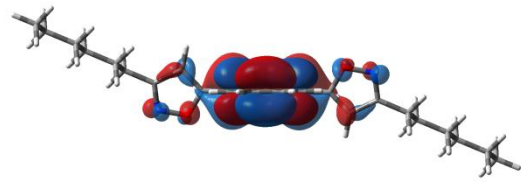
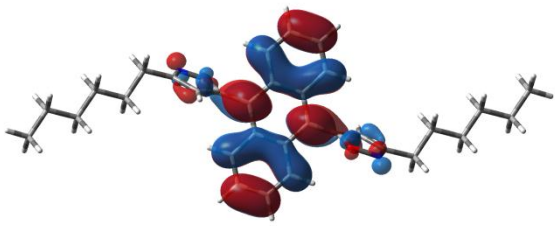


Figure S45: HOMO (bottom) and LUMO (top) of **A2a**.

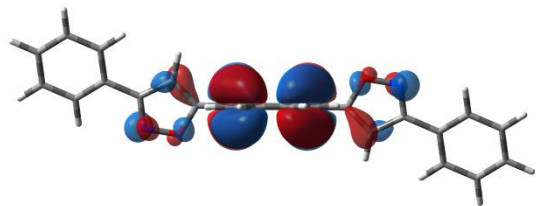
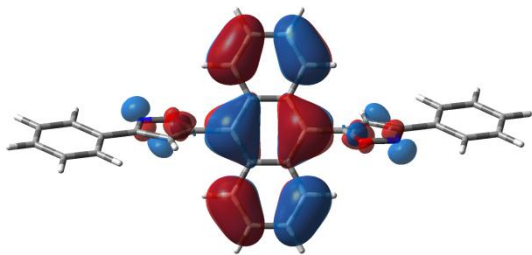
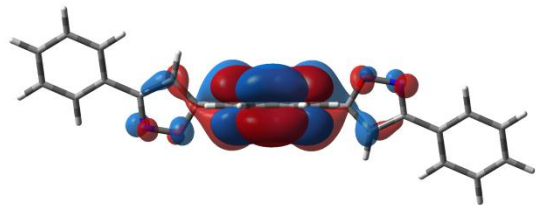
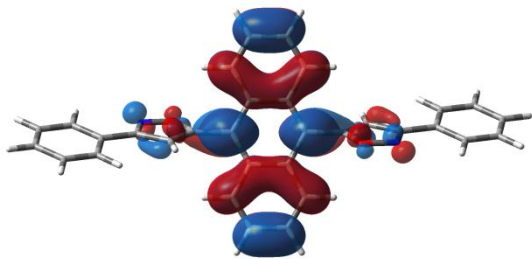


Figure S46: HOMO (bottom) and LUMO (top) of **A2b**.

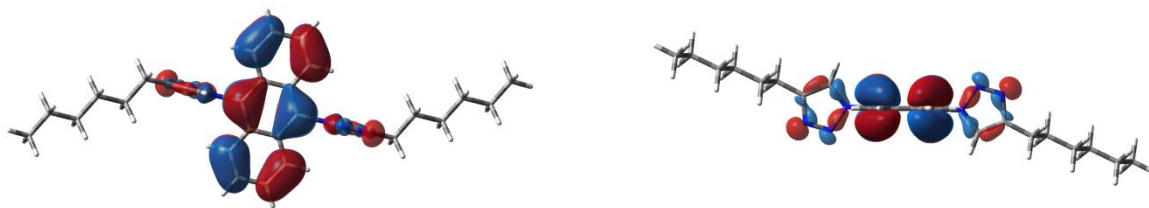
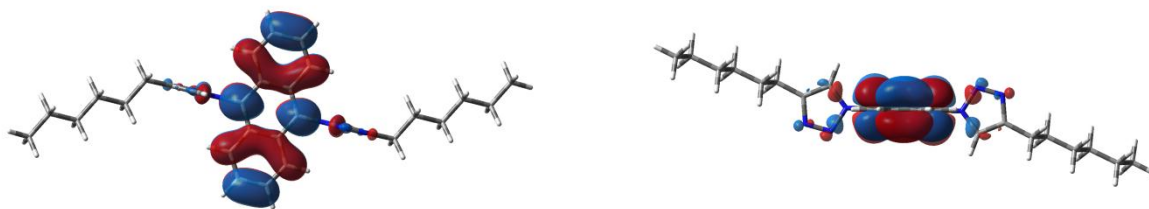


Figure S47: HOMO (bottom) and LUMO (top) of **A3a**.



Figure S48: HOMO (bottom) and LUMO (top) of **P1a**.

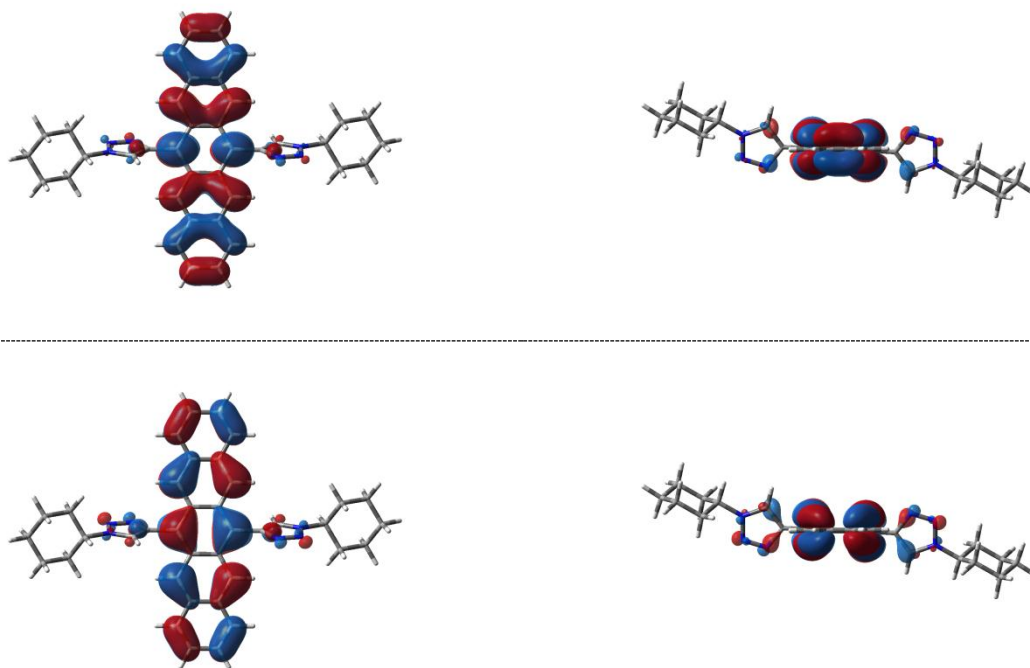


Figure S49: HOMO (bottom) and LUMO (top) of **P1c**.

Manuscript # 2

Supporting Information

Novel Thiophene-Substituted Pentacenes as Soluble Materials for Organic Field-Effect Transistors

Brigitte Holzer,^{a,#} Daniel Lumpi,^{a,b,#,} Thomas Mathis,^b Ernst Horkel,^a Christian Hametner,^a Bertram Batlogg^b and Johannes Fröhlich^a*

^aInstitute of Applied Synthetic Chemistry, Vienna University of Technology,
Getreidemarkt 9/163OC, 1060 Vienna, Austria

^bLaboratory for Solid State Physics, ETH Zurich,
Otto-Stern-Weg 1, 8093 Zurich, Switzerland

[#]authors contributed equally

* brigitte.holzer@tuwien.ac.at

* daniel.lumpi@tuwien.ac.at

Content

A) NMR Spectra

B) DFT Calculations

C) Cyclic Voltammetric Measurements

D) Absorption Spectra

A) NMR Spectra

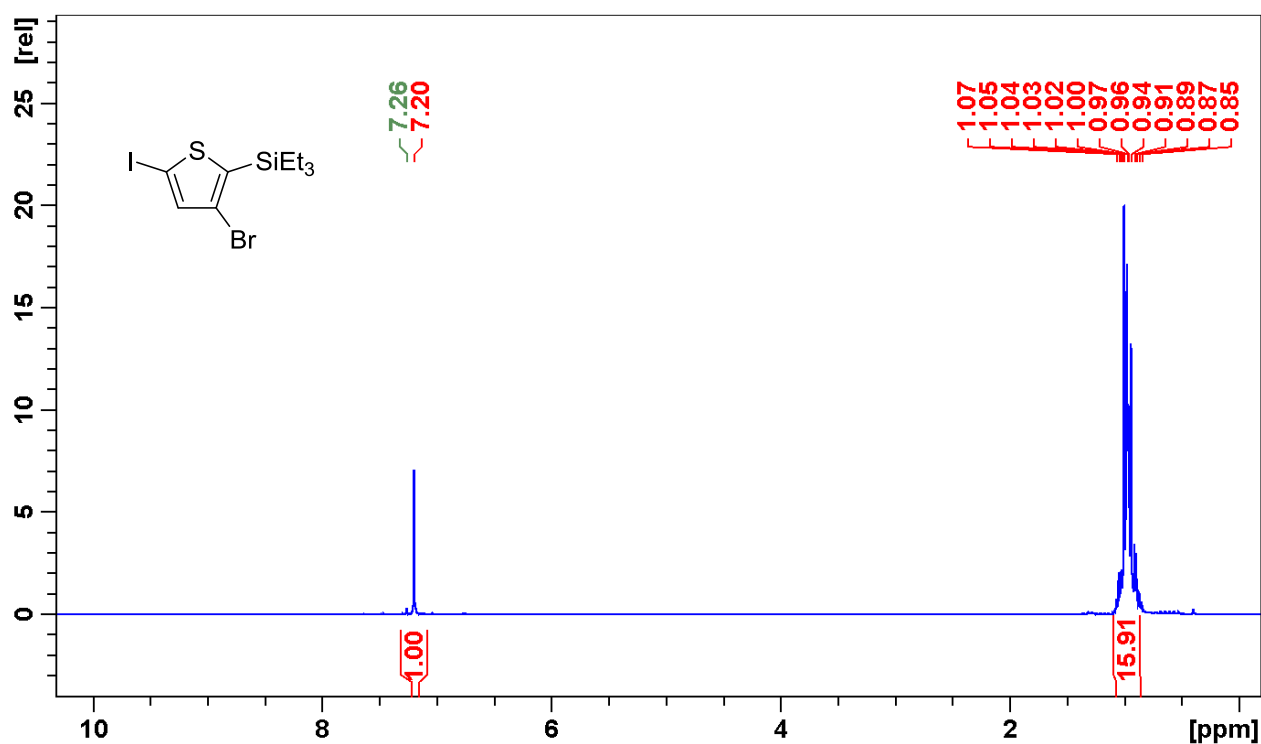


Figure S1. ¹H NMR spectrum of compound 3a.

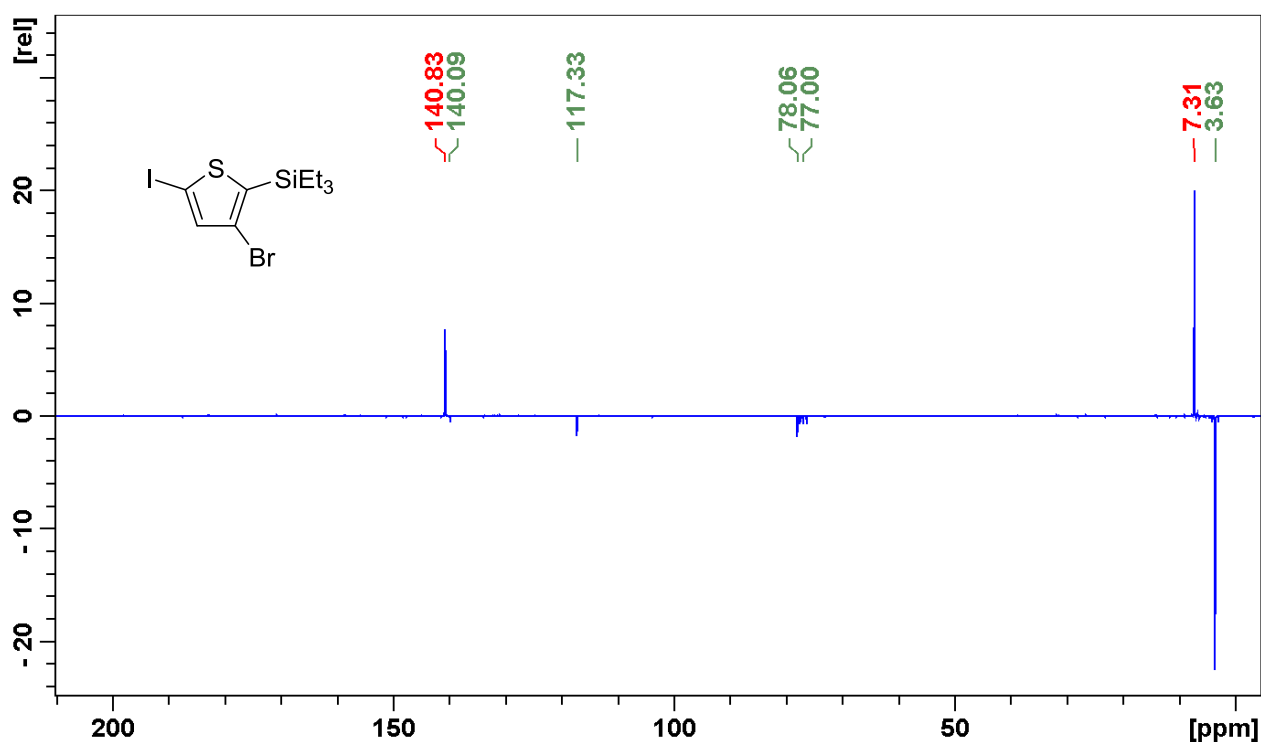


Figure S2. ¹³C NMR spectrum of compound 3a.

^

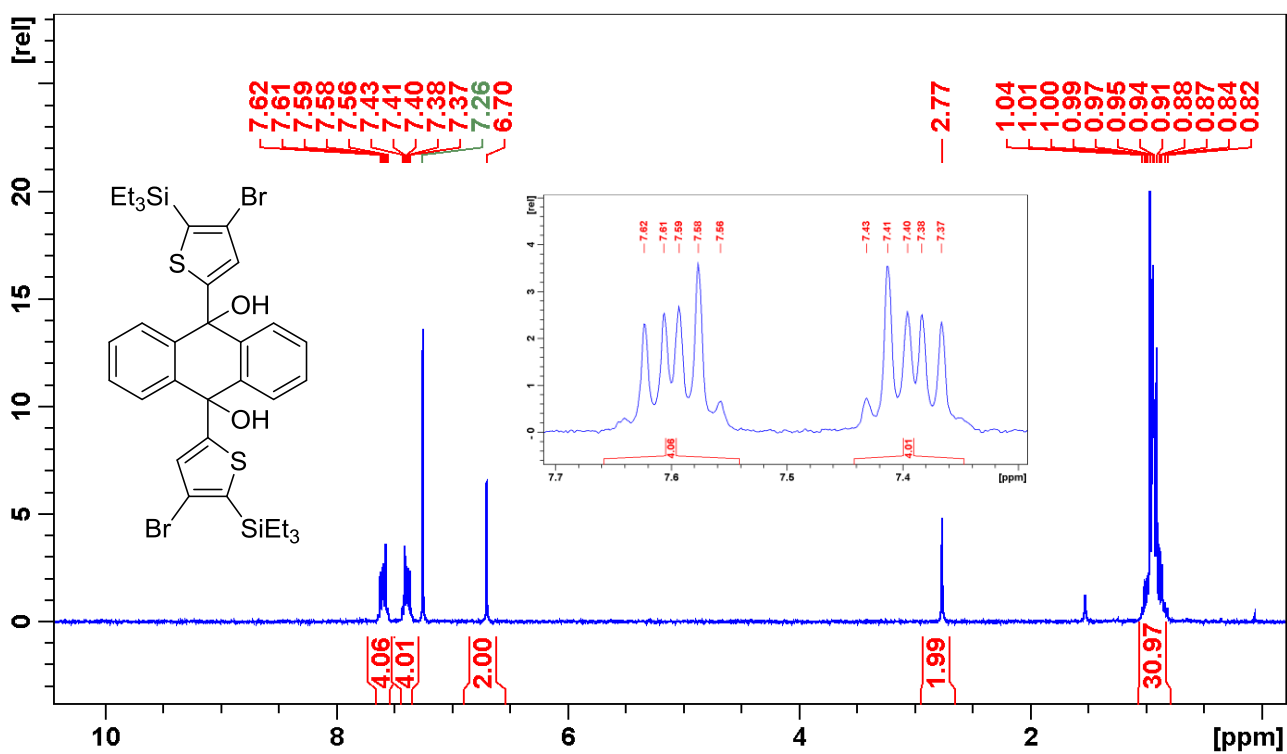


Figure S3. ¹H NMR spectrum of compound 5.

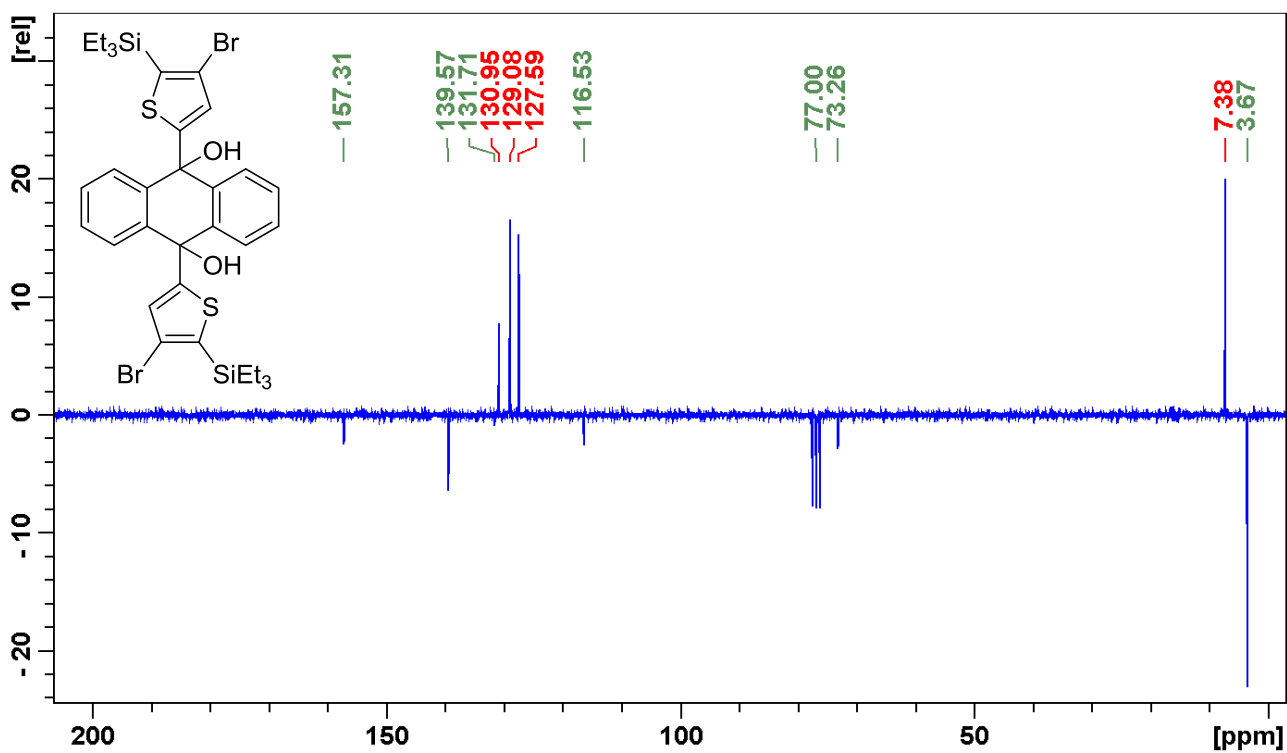


Figure S4. ¹³C NMR spectrum of compound 5.

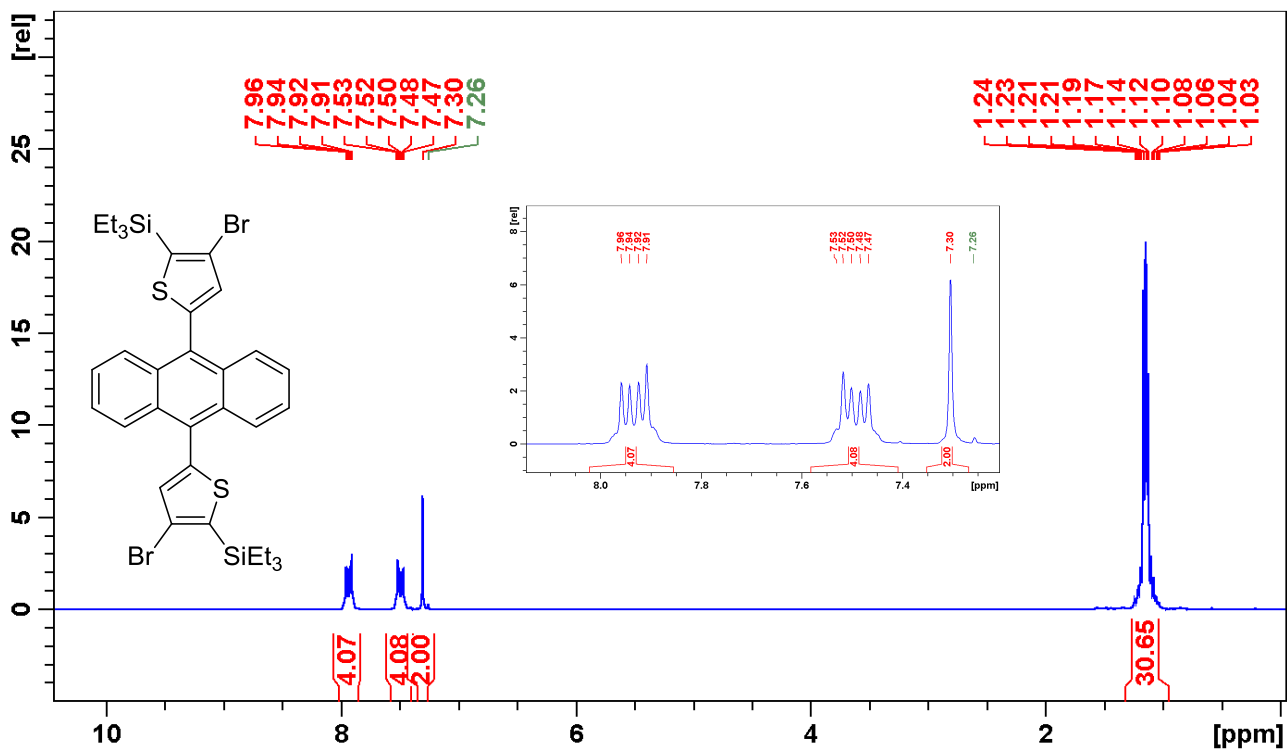


Figure S5. ¹H NMR spectrum of compound 6.

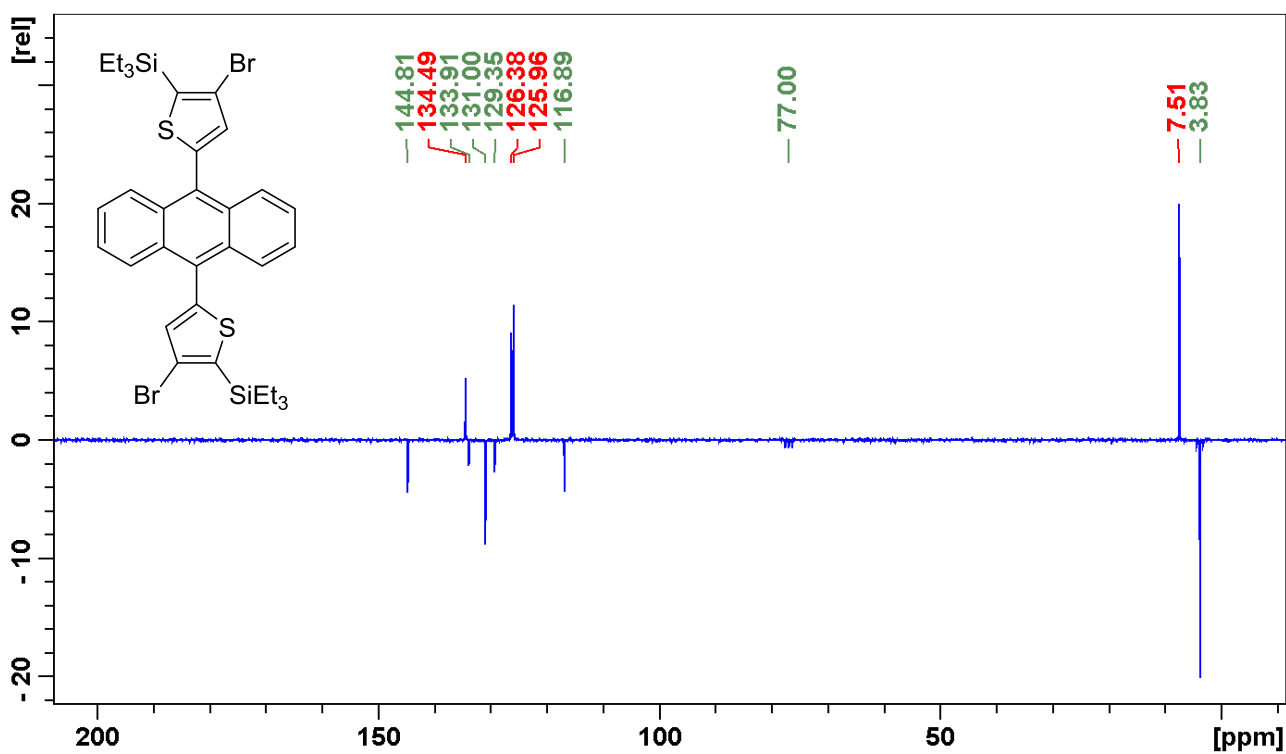


Figure S6. ¹³C NMR spectrum of compound 6.

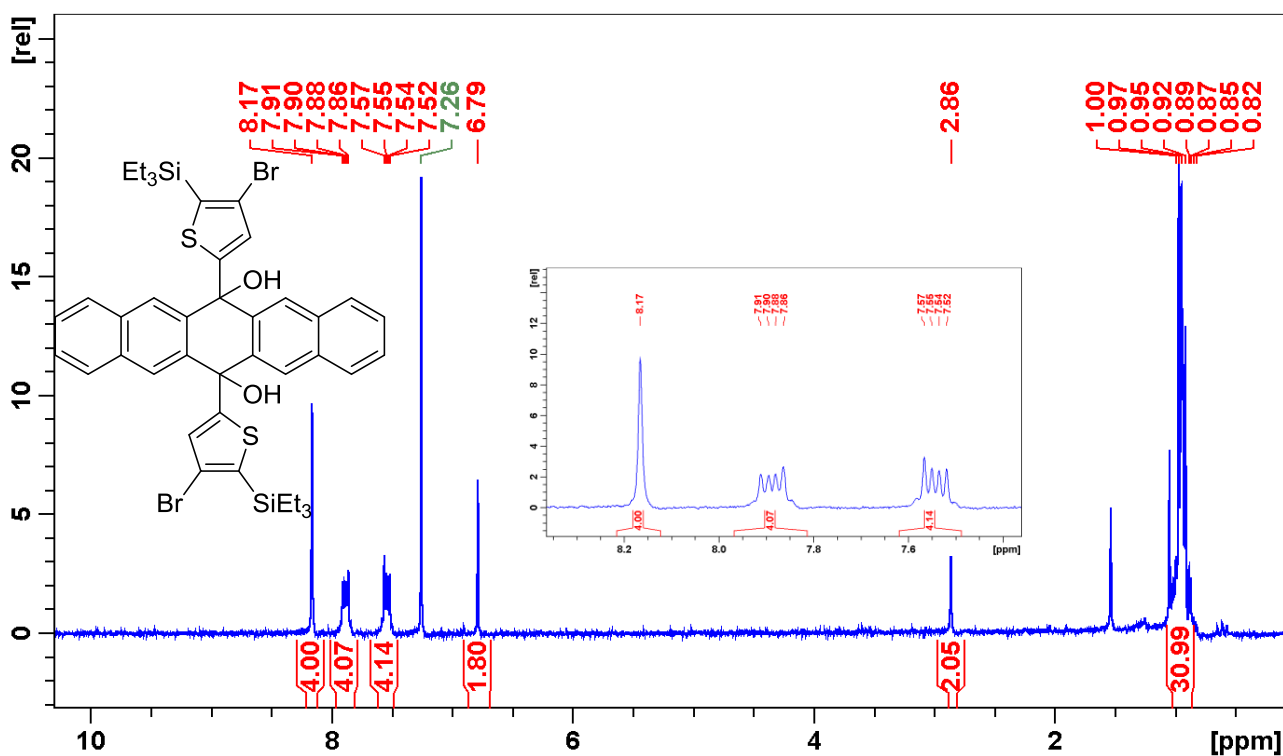


Figure S7. ¹H NMR spectrum of compound **8a**.

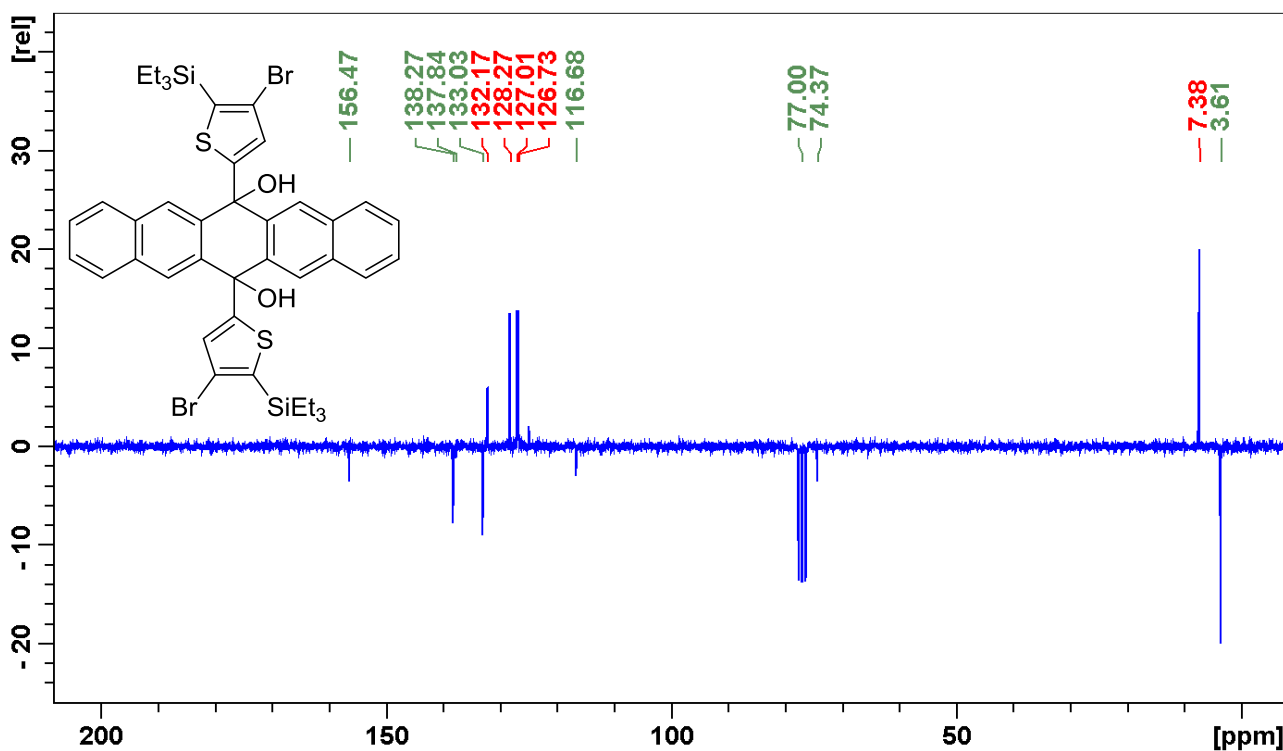


Figure S8. ¹³C NMR spectrum of compound **8a**.

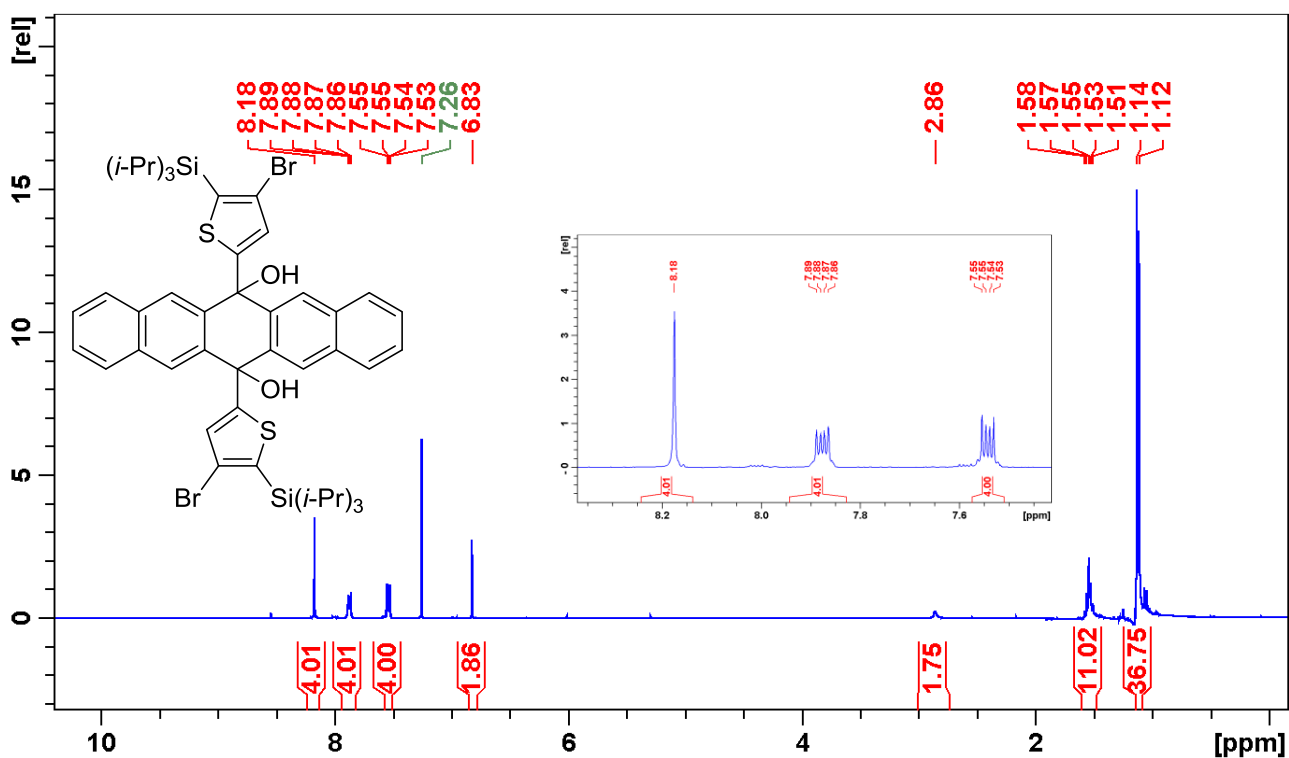


Figure S9. ^1H NMR spectrum of compound **8b**.

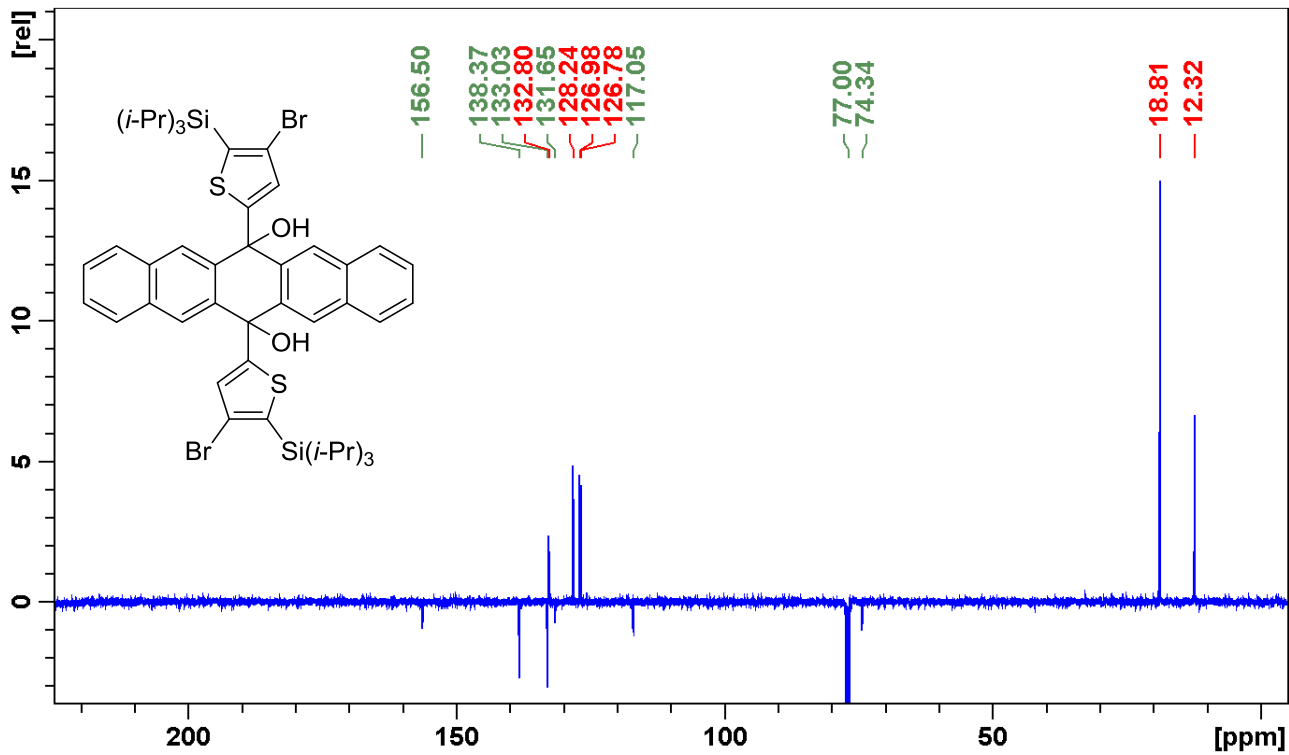


Figure S10. ^{13}C NMR spectrum of compound **8b**.

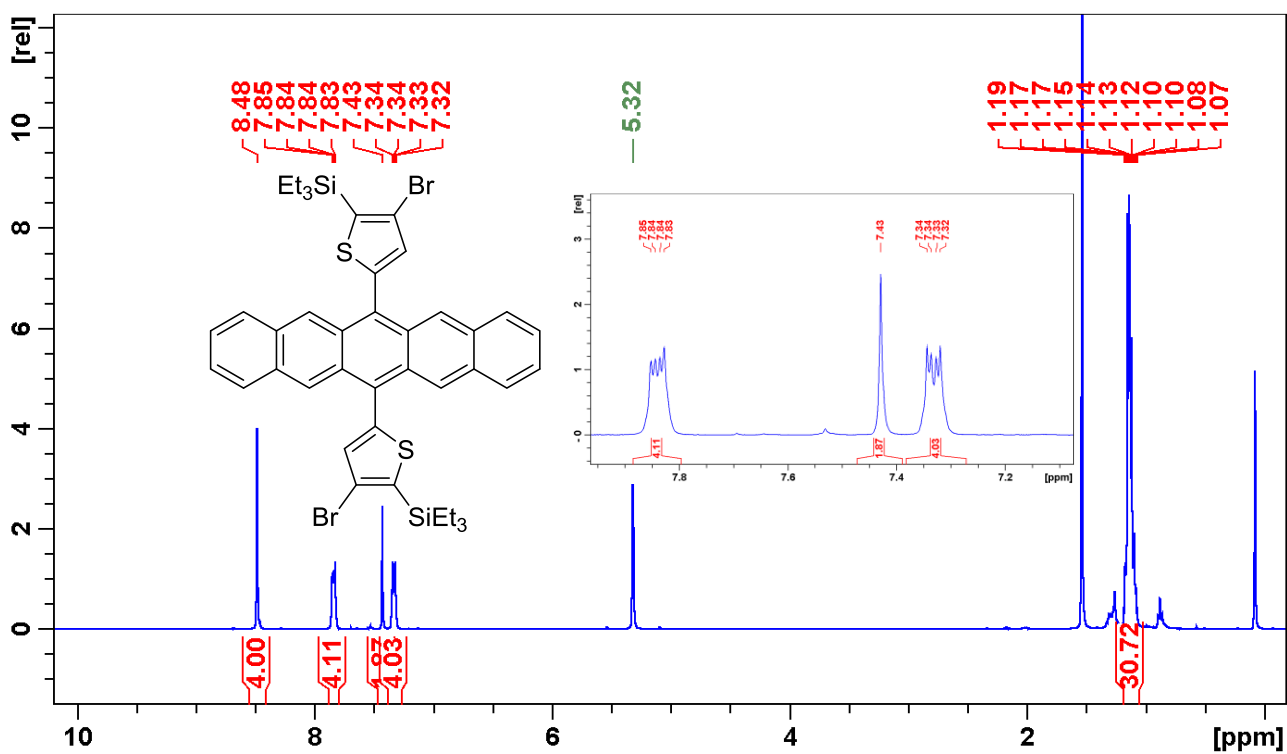


Figure S11. ¹H NMR spectrum of compound **1h**.

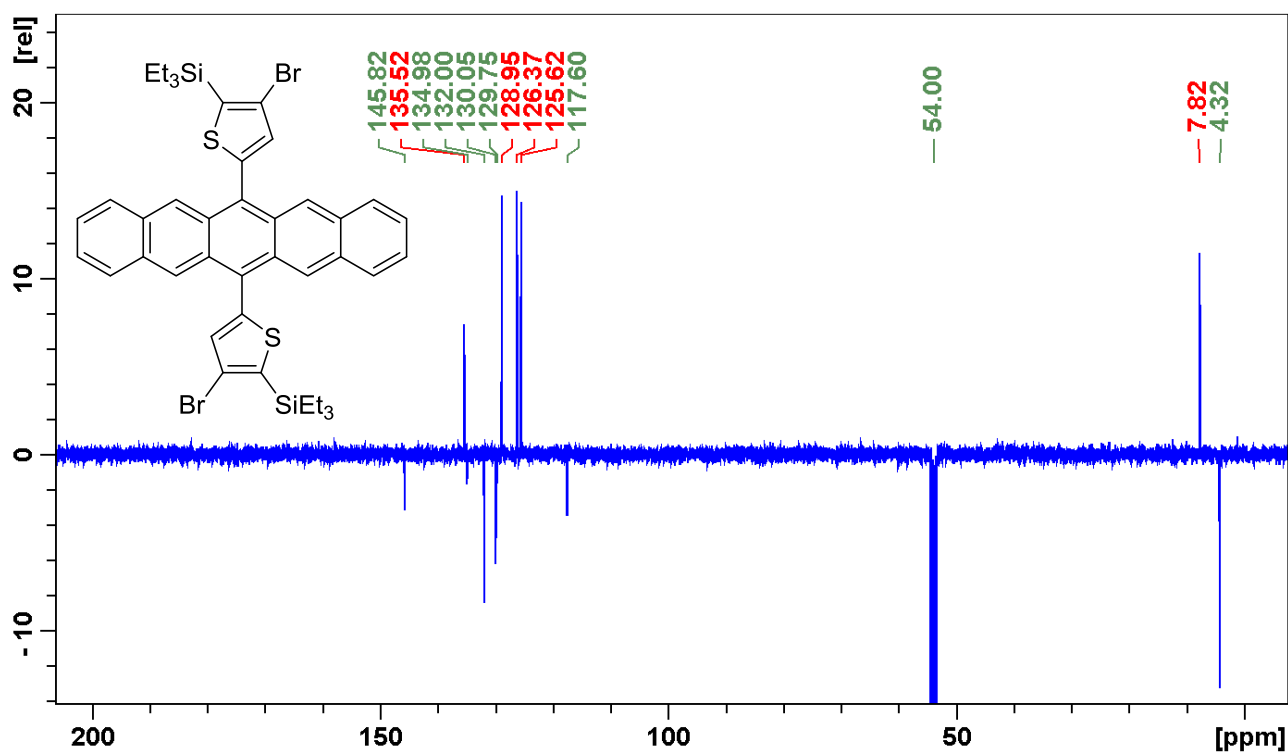


Figure S12. ¹³C NMR spectrum of compound **1h**.

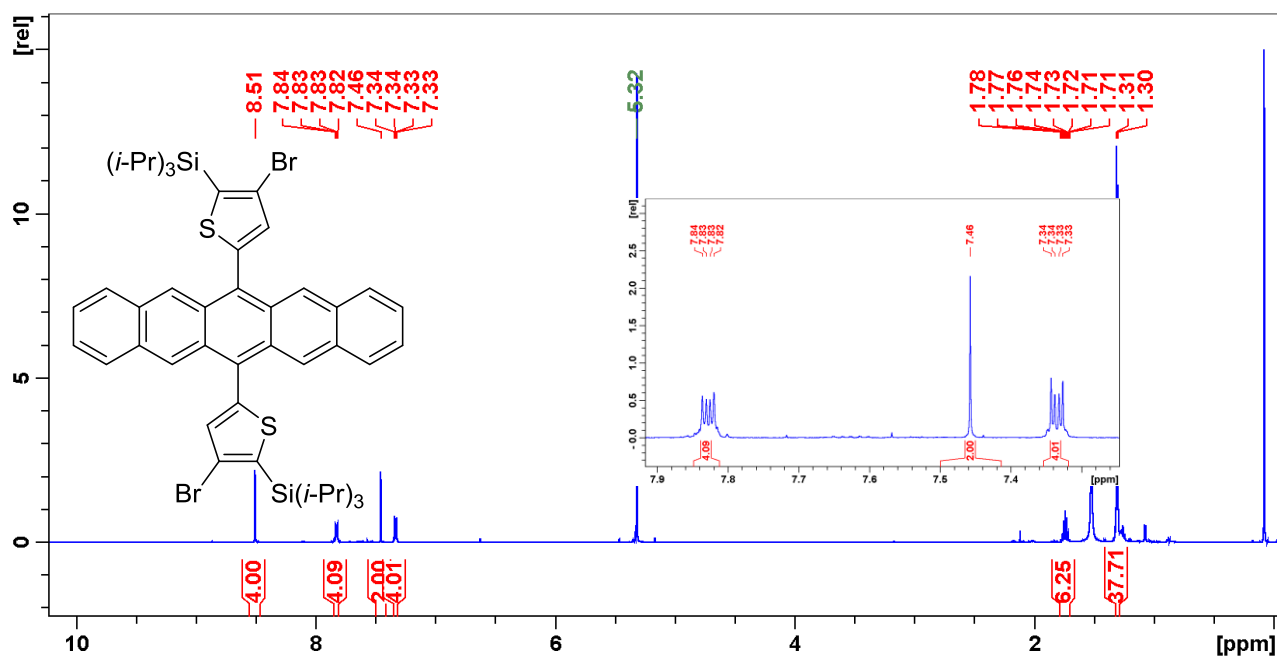


Figure S13. ¹H NMR spectrum of compound **1i**.

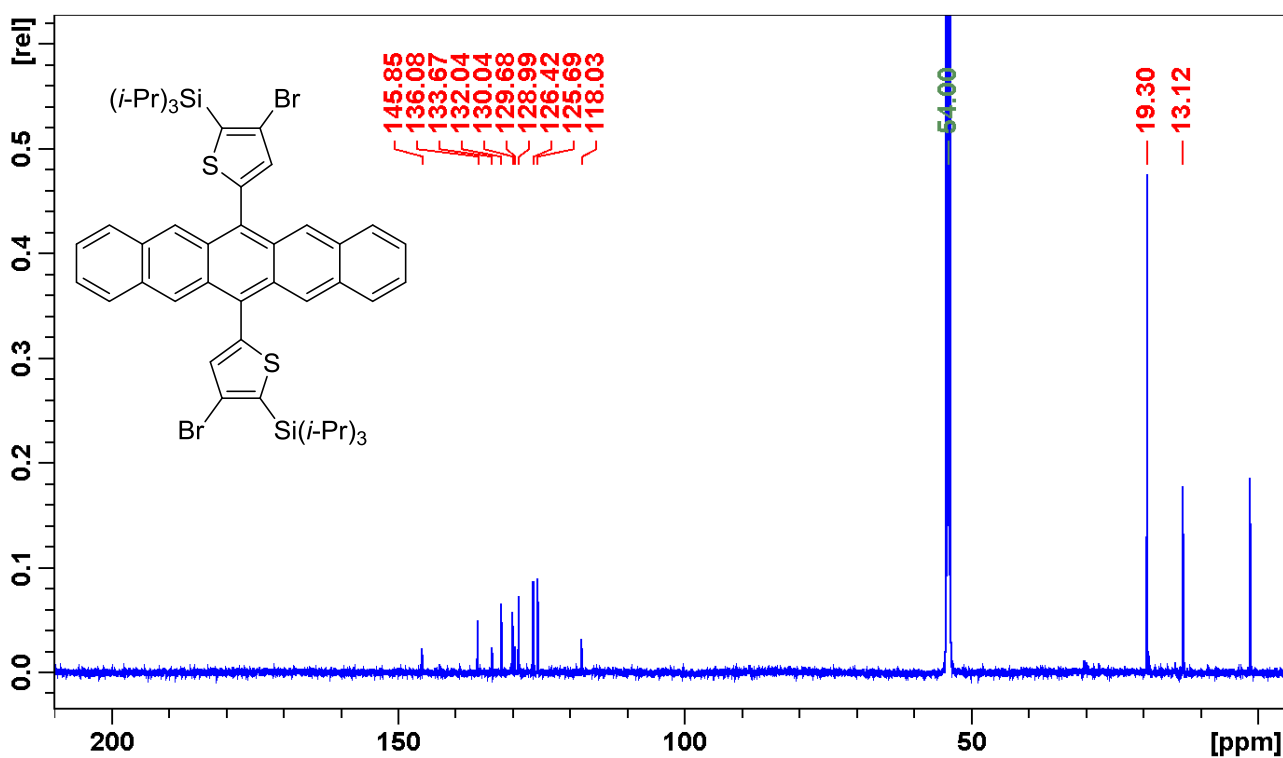


Figure S14. ¹³C NMR spectrum of compound **1i**.

B) DFT Calculations

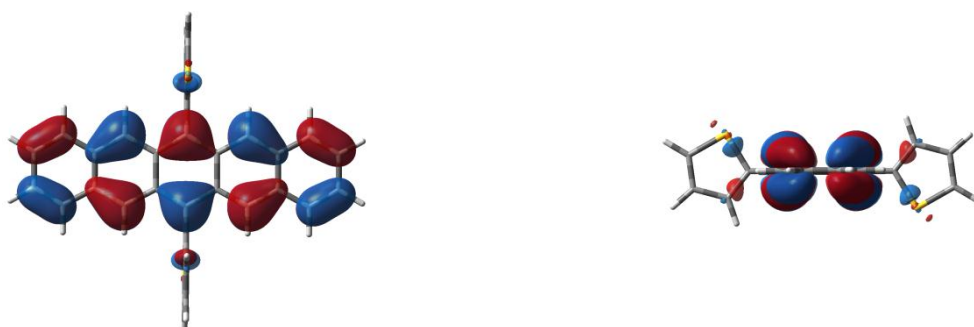


Figure S15: HOMO (bottom) and LUMO (top) of **1c**.

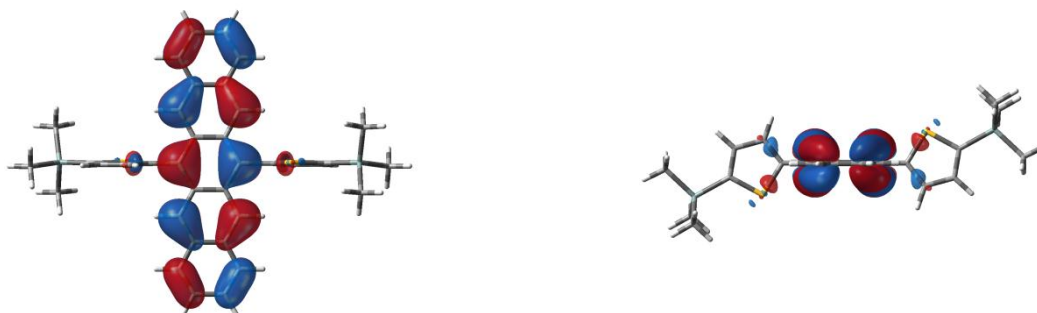
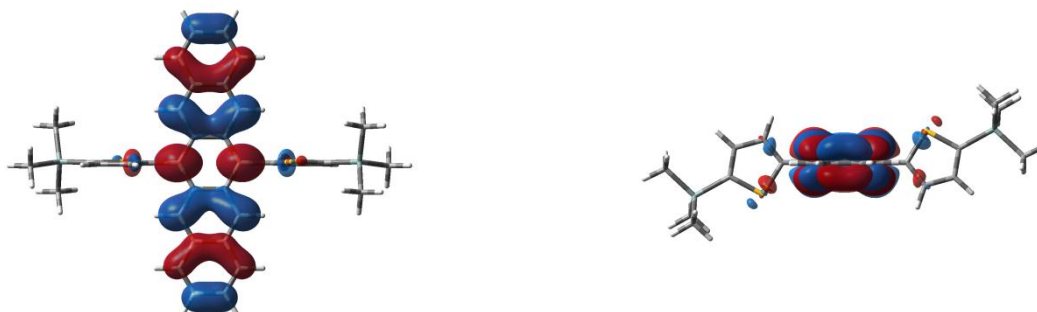


Figure S16: HOMO (bottom) and LUMO (top) of **1d**.

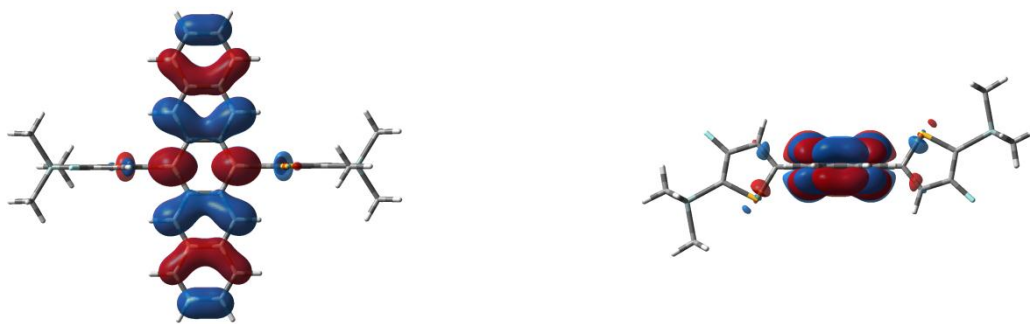


Figure S17: HOMO (bottom) and LUMO (top) of **1e**.

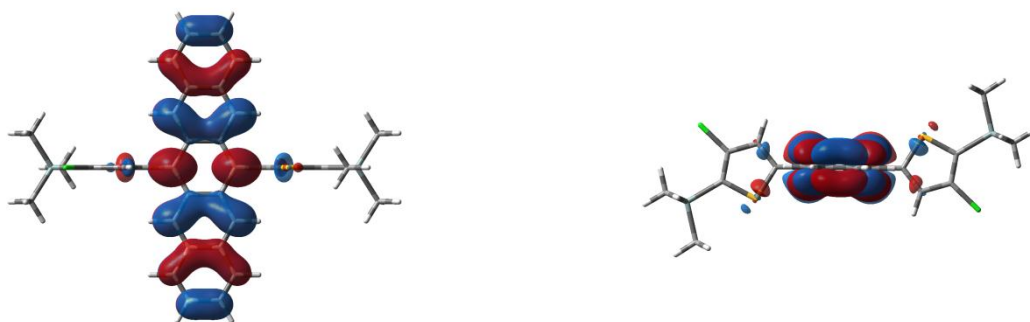


Figure S18: HOMO (bottom) and LUMO (top) of **1f**.

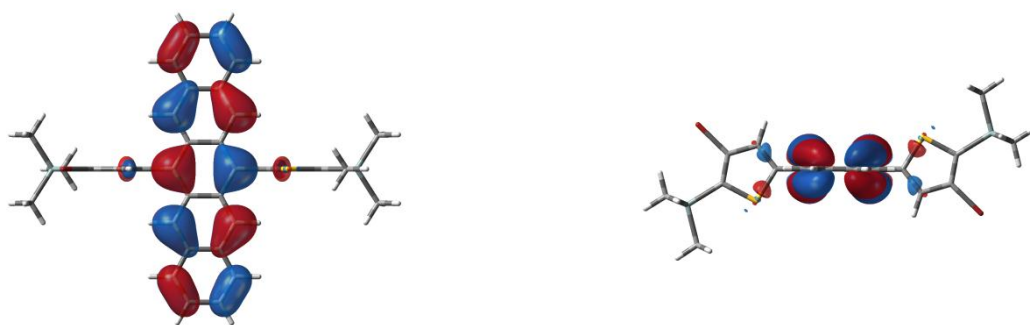
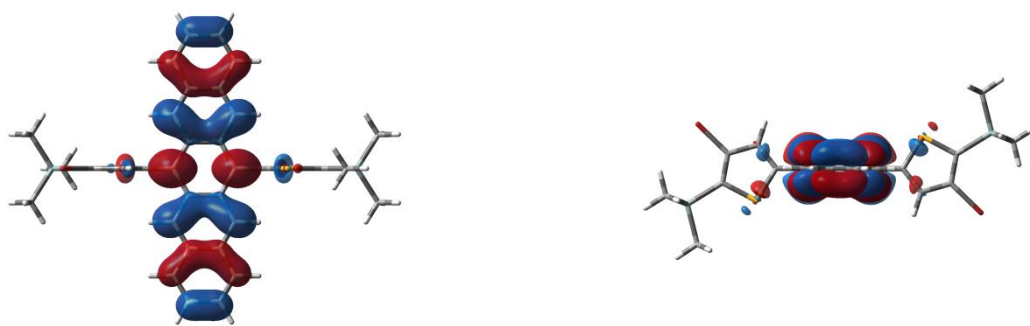


Figure S19: HOMO (bottom) and LUMO (top) of **1g**.

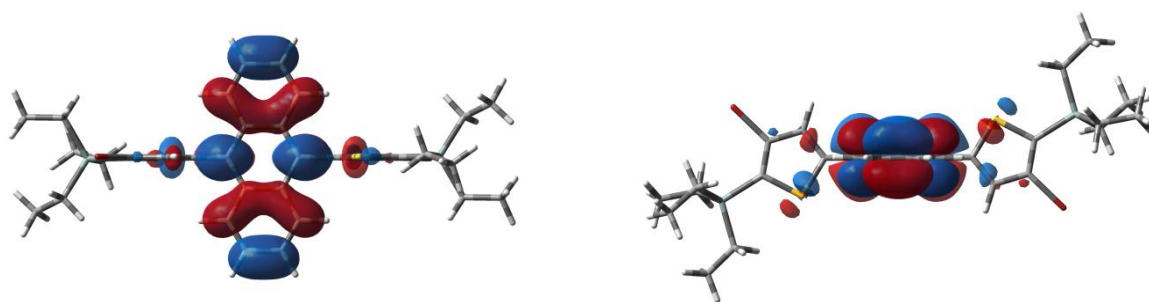
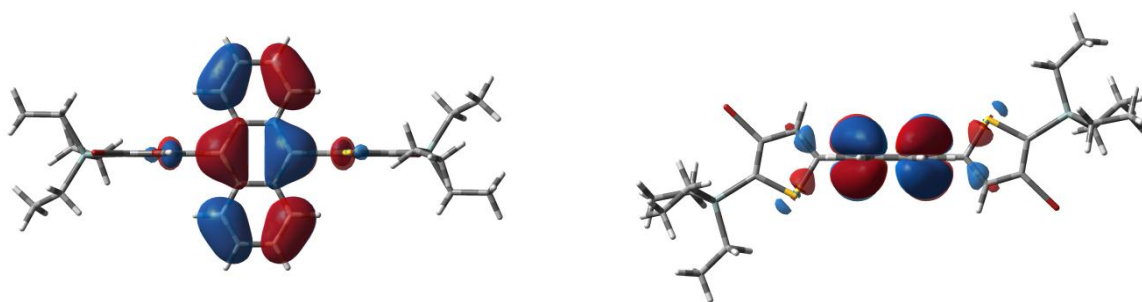


Figure S20: HOMO (bottom) and LUMO (top) of **6**.

C) Cyclic Voltammetric Measurements

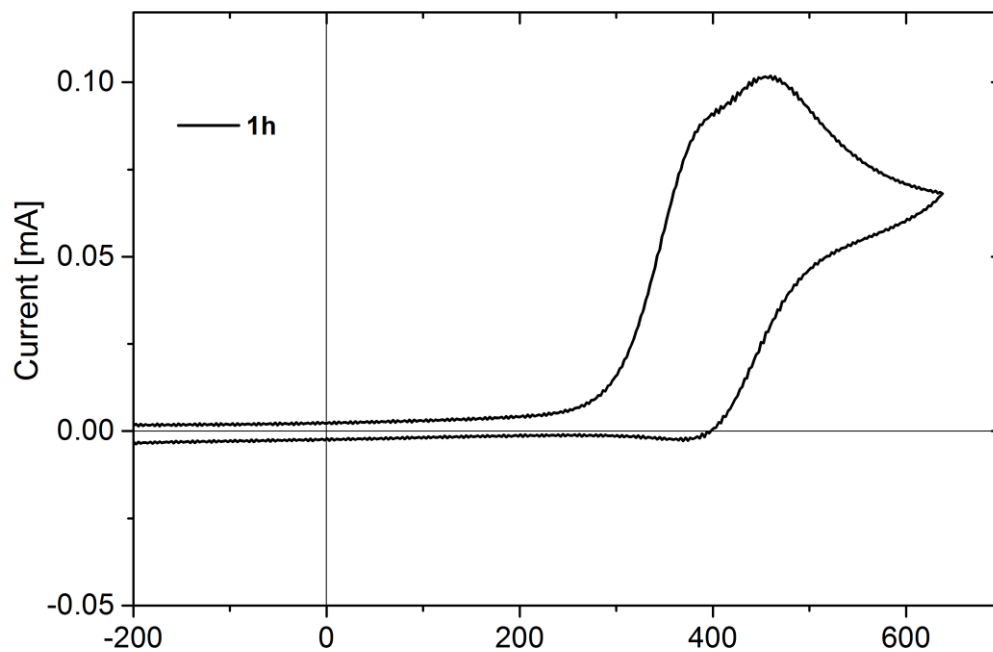


Figure S21: Cyclic voltammograms of **1h** measured in DCM solution.

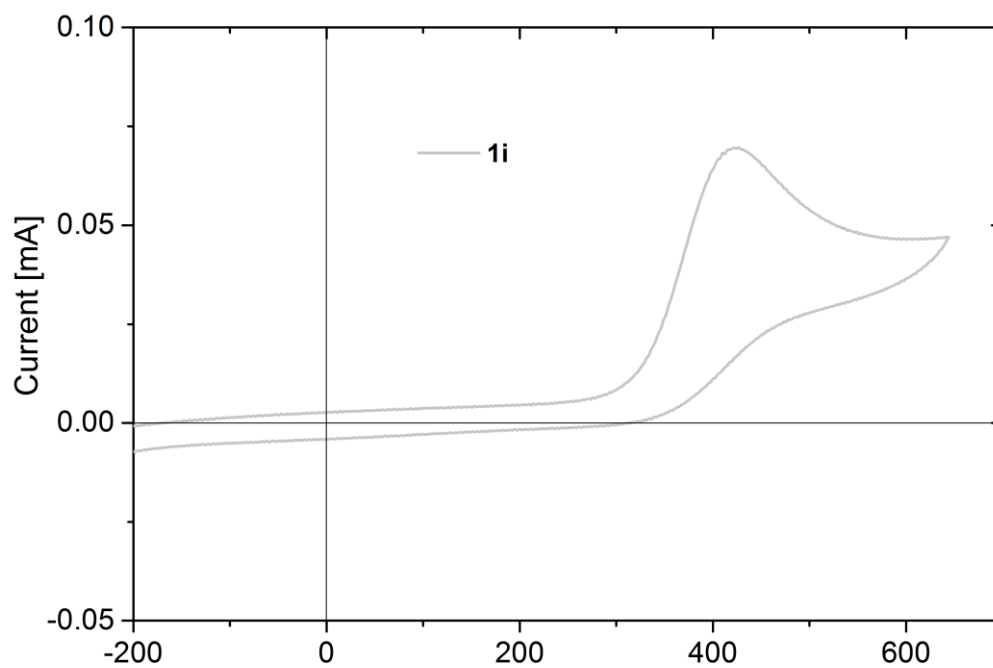


Figure S22: Cyclic voltammograms of **1i** measured in DCM solution.

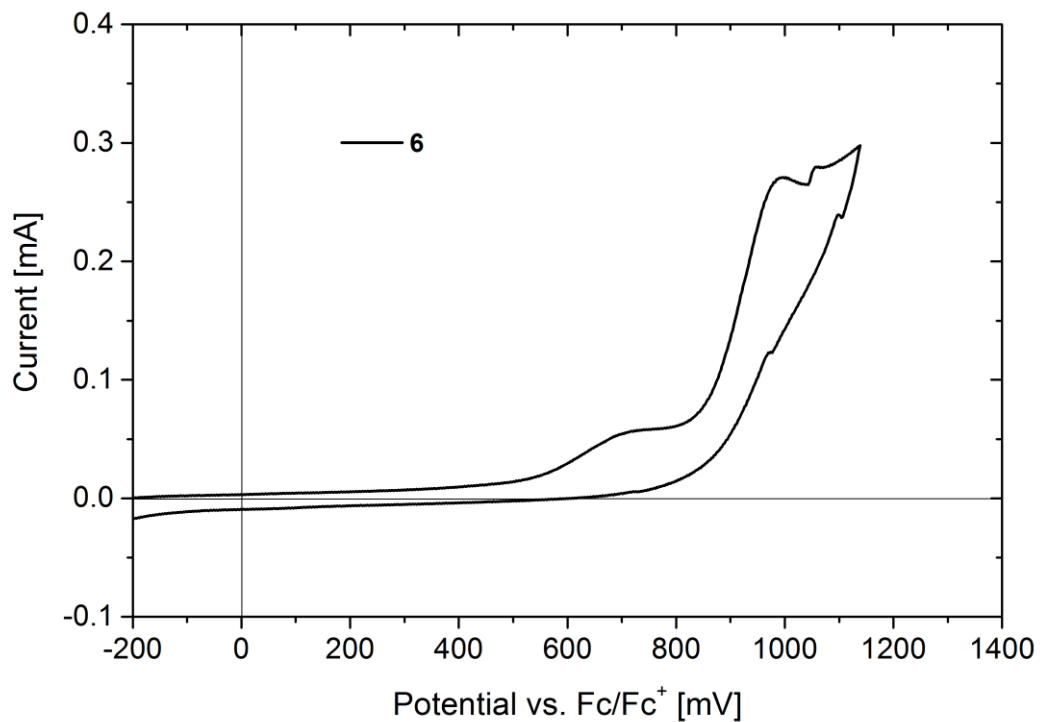


Figure S23: Cyclic voltammograms of **6** measured in DCM solution.

D) Absorption Spectra

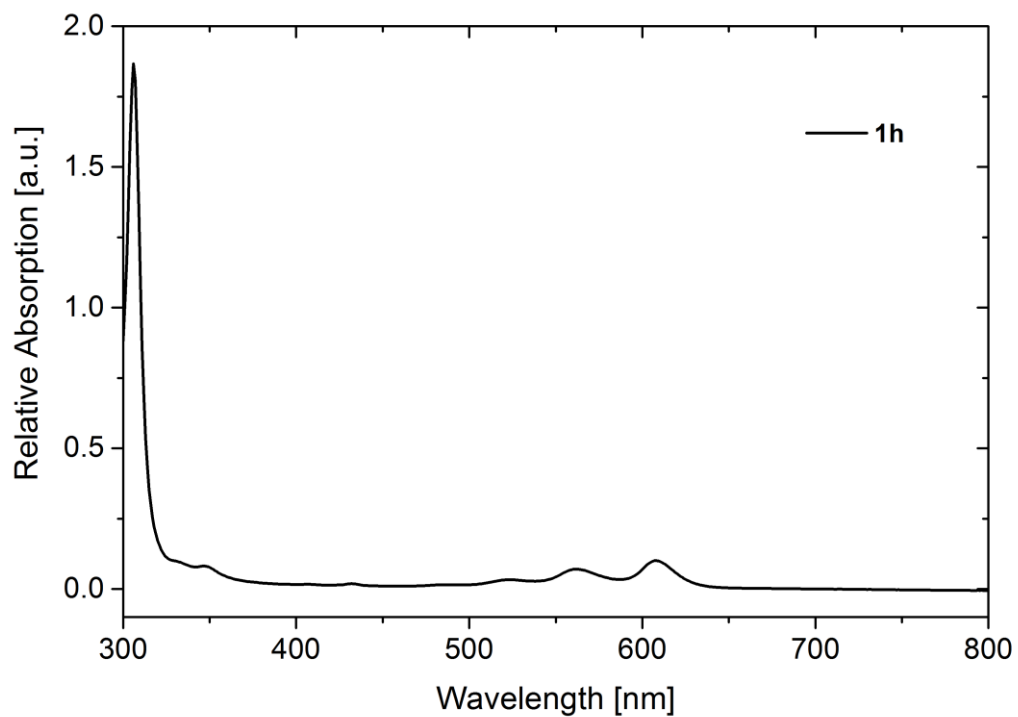


Figure S24: Absorption Spectrum of **1h** measured in DCM solution.

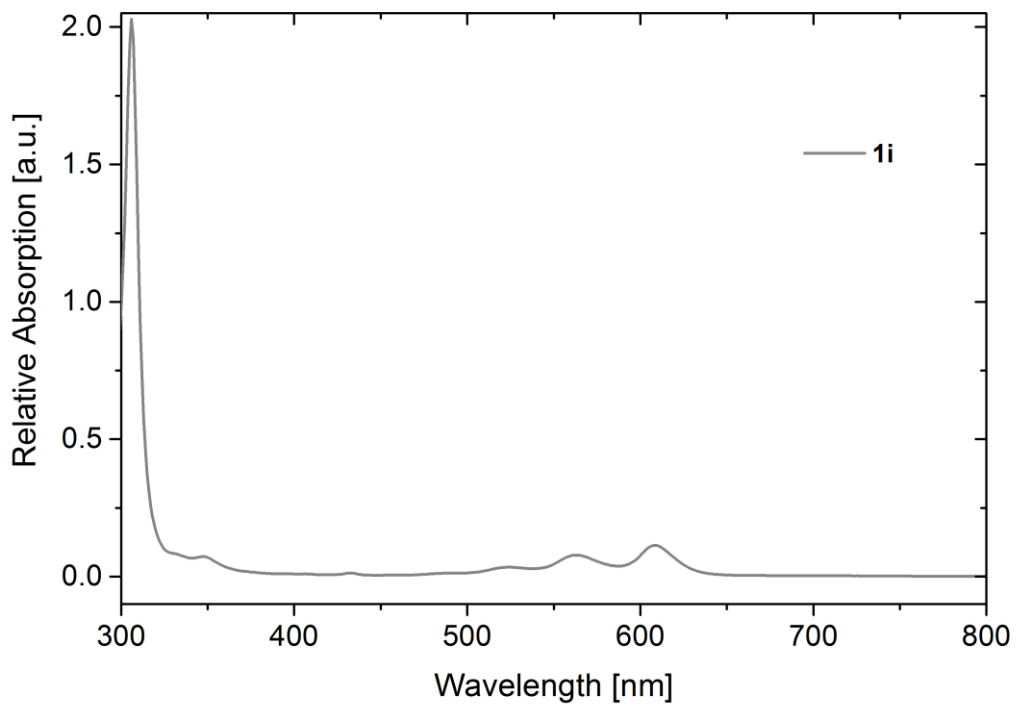


Figure S25: Absorption Spectrum of **6** measured in DCM solution.

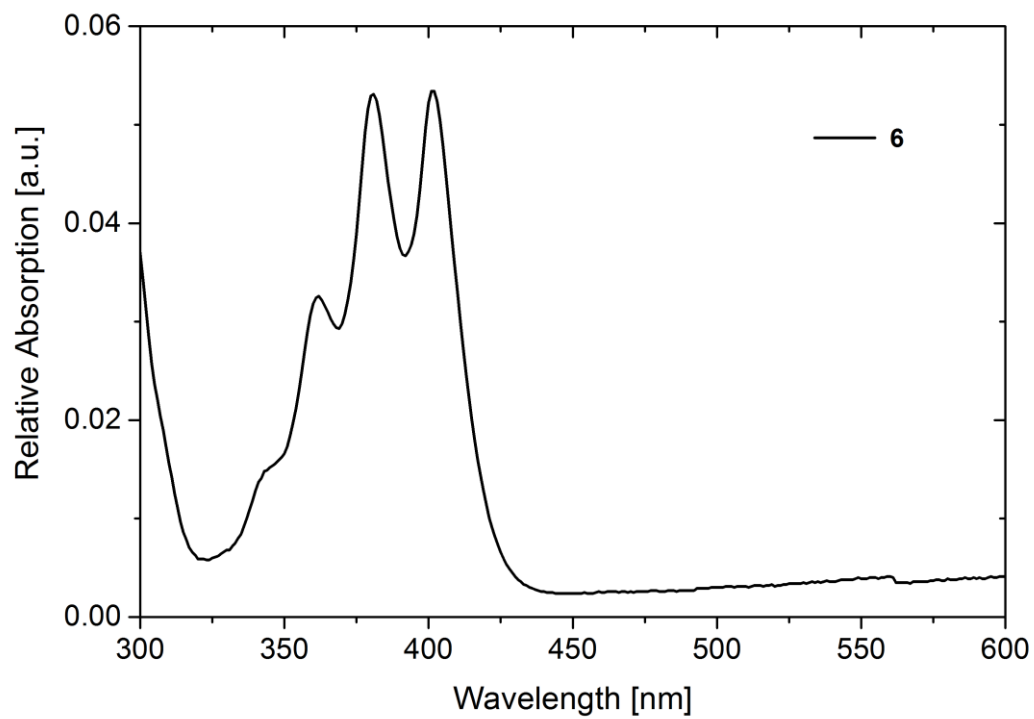


Figure S26: Absorption Spectrum of **1i** measured in DCM solution.

Manuscript # 4

Supporting Information

Facile Synthesis of Benzo[*b*]selenophene Building Blocks

*Brigitte Holzer, * Christian Hametner, and Johannes Fröhlich*

Institute of Applied Synthetic Chemistry, Vienna University of Technology,

Getreidemarkt 9/163OC, A-1060 Vienna, Austria

* brigitte.holzer@tuwien.ac.at

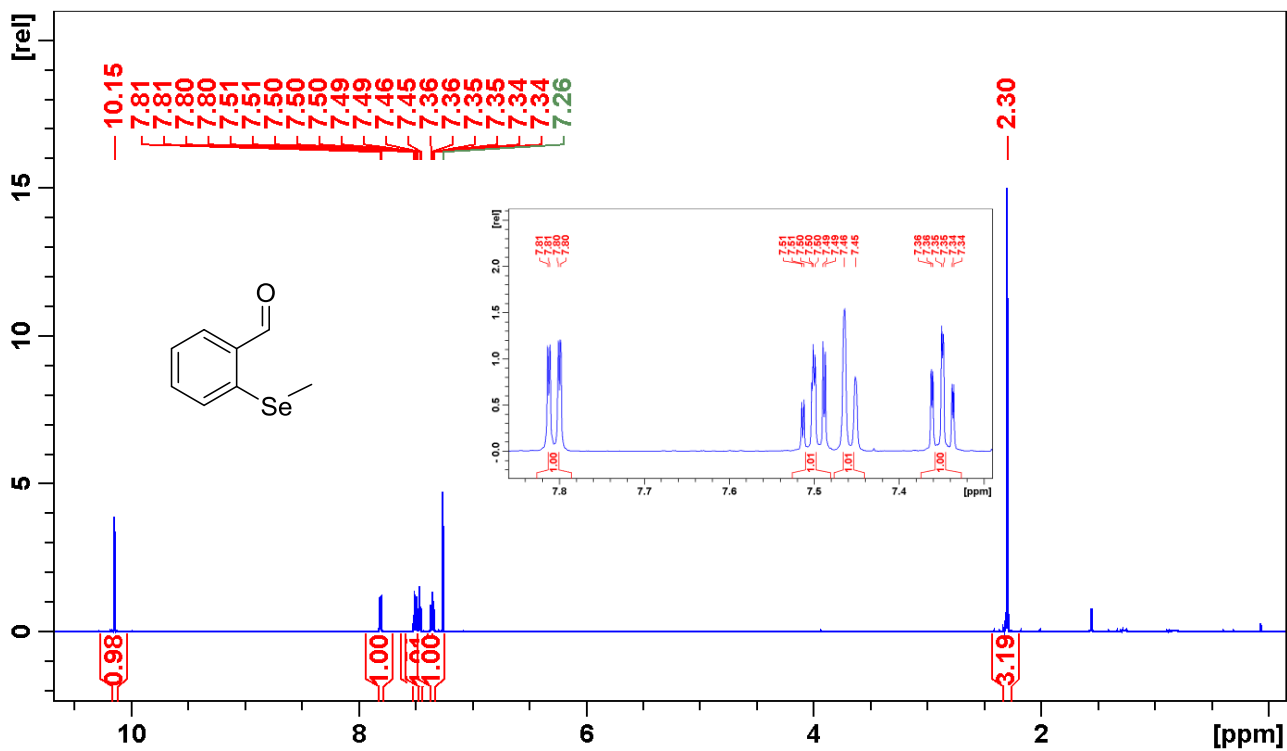


Figure S1. ¹H NMR spectrum of compound 2.

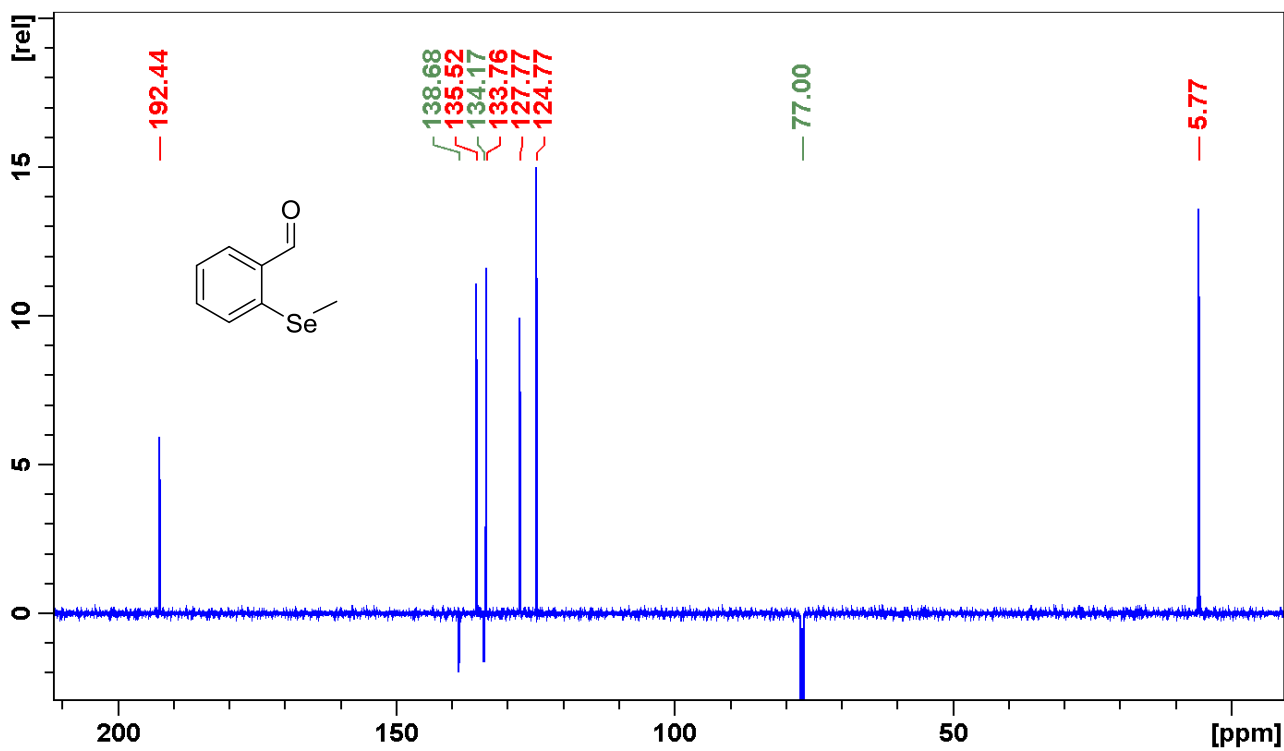


Figure S2. ¹³C NMR spectrum of compound 2.

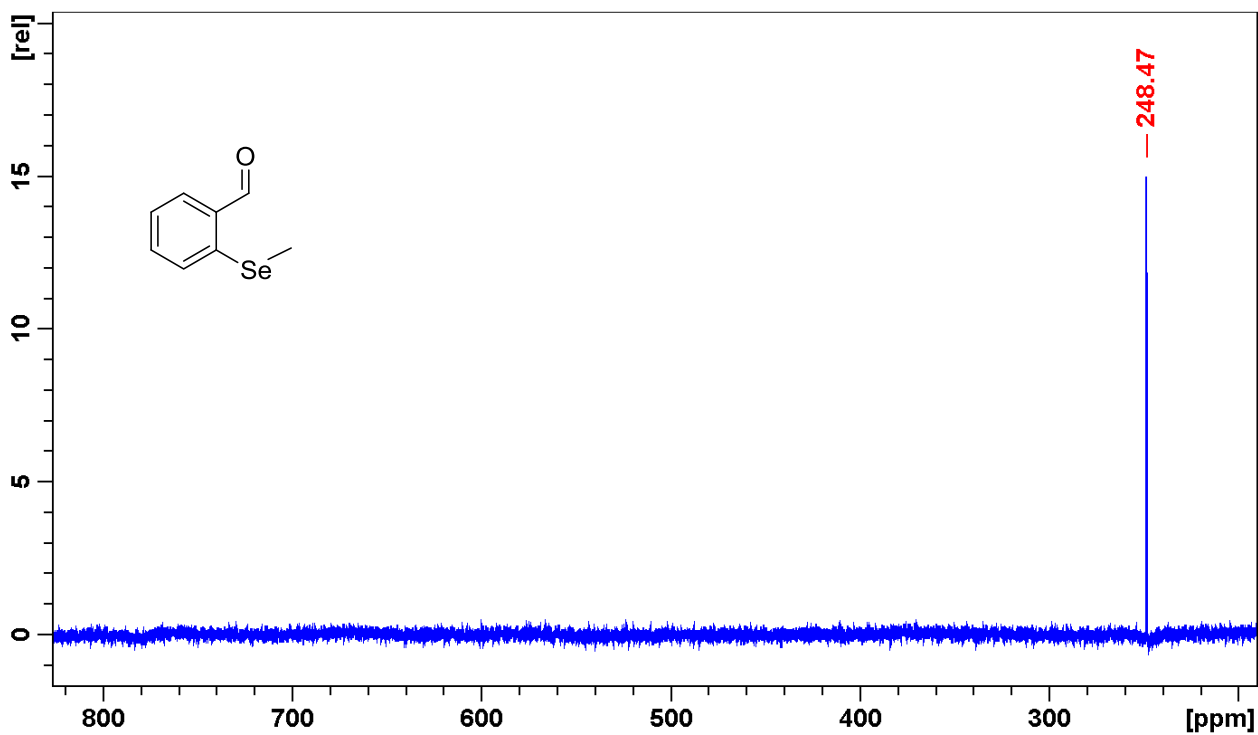


Figure S3. ^{77}Se NMR spectrum of compound 2.

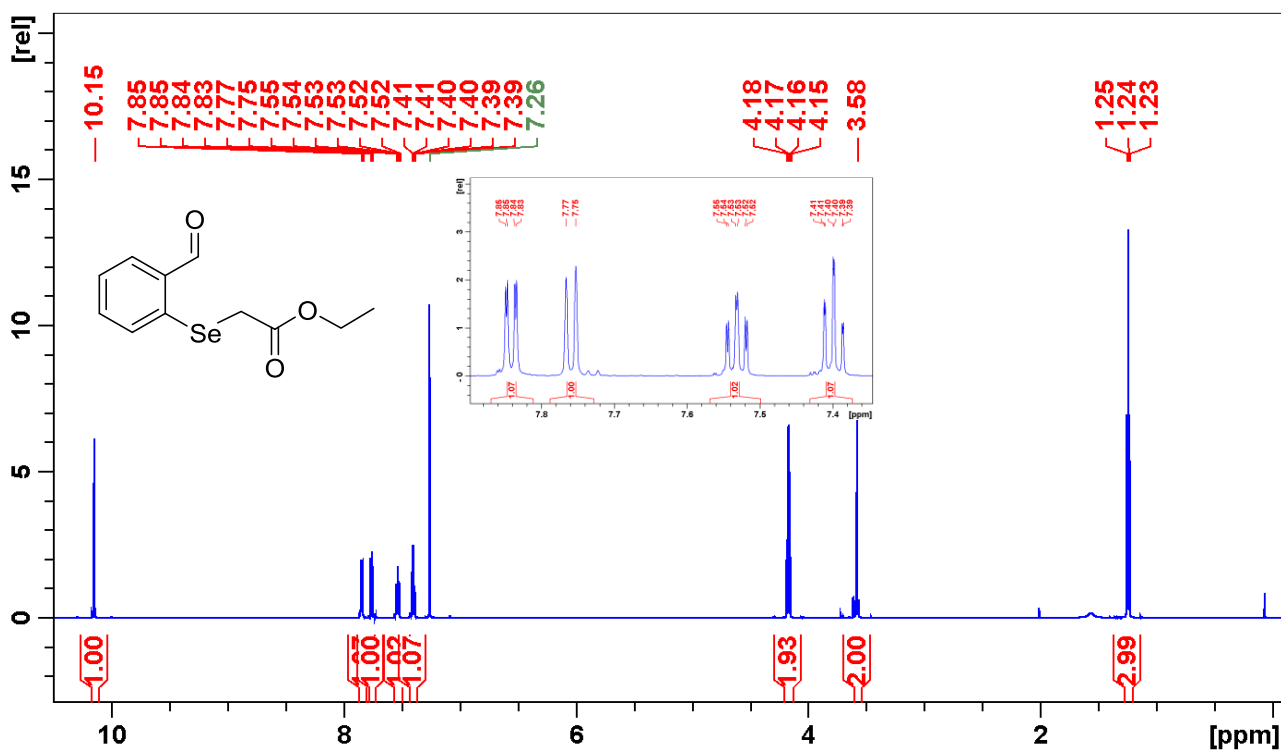


Figure S4. ^1H NMR spectrum of compound 3.

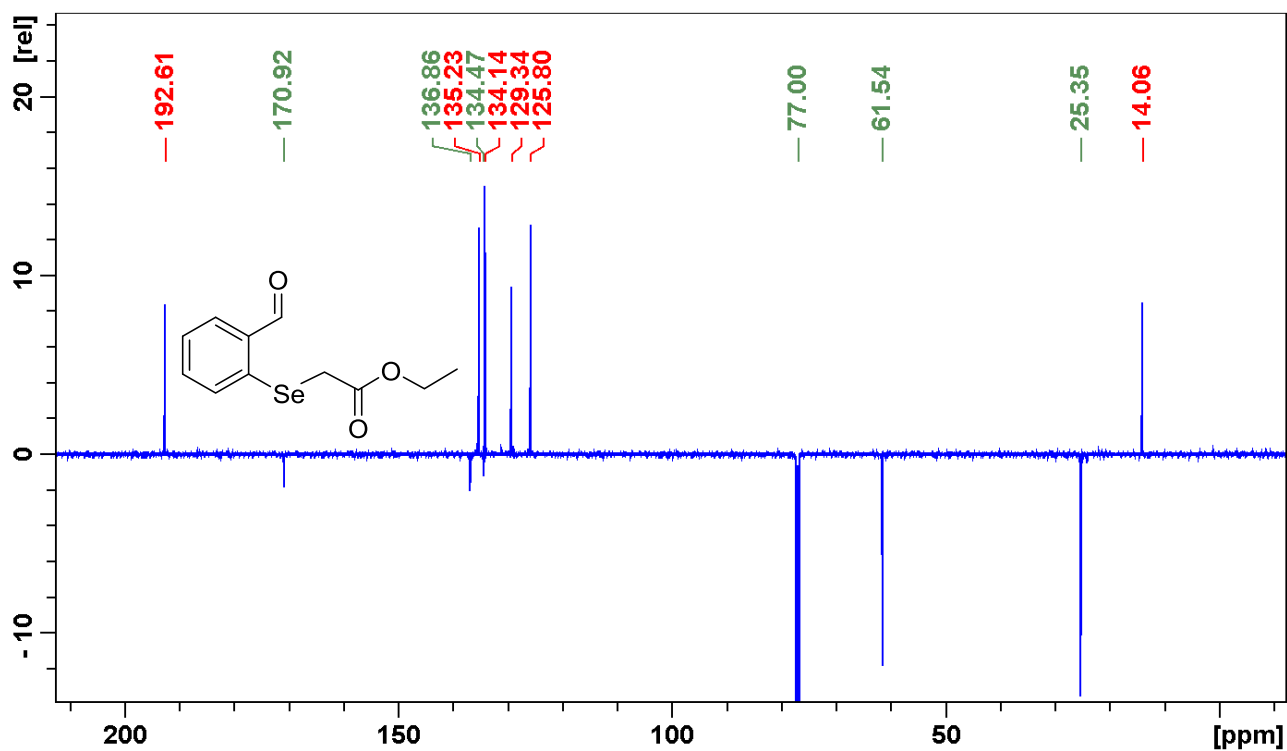


Figure S5. ¹³C NMR spectrum of compound 3.

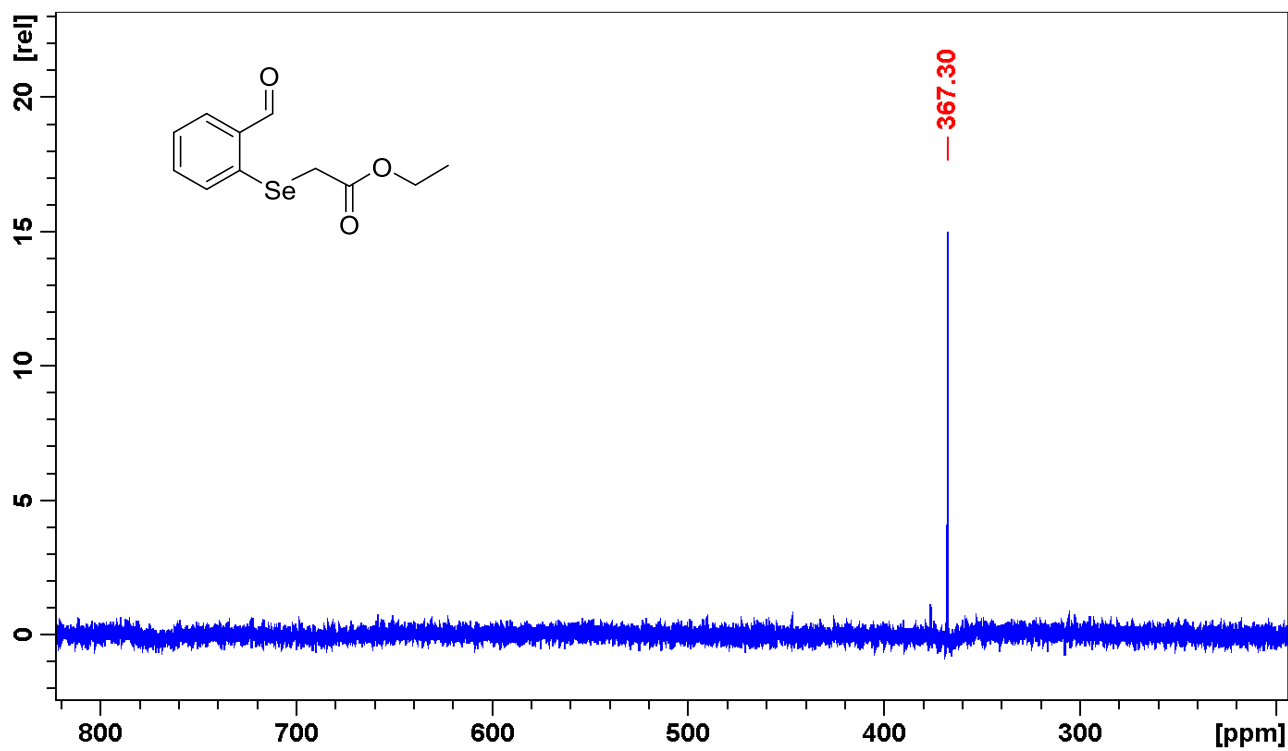


Figure S6. ⁷⁷Se NMR spectrum of compound 3.

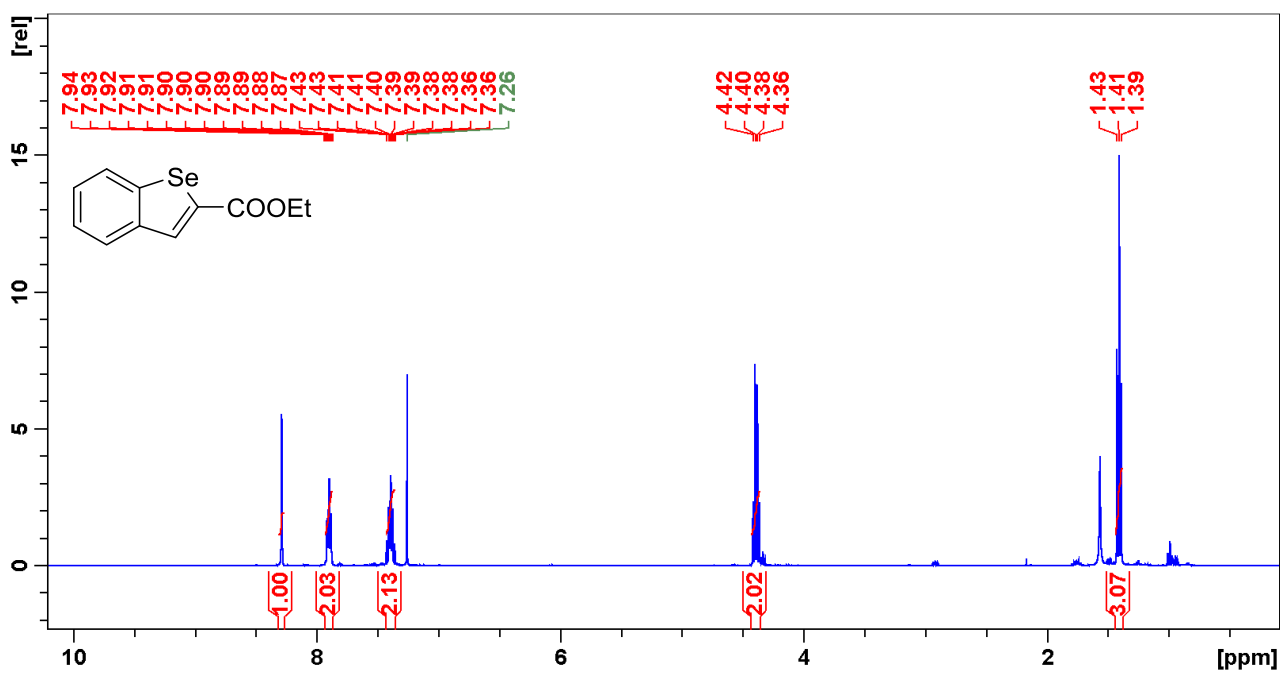


Figure S7. ¹H NMR spectrum of compound 4a.

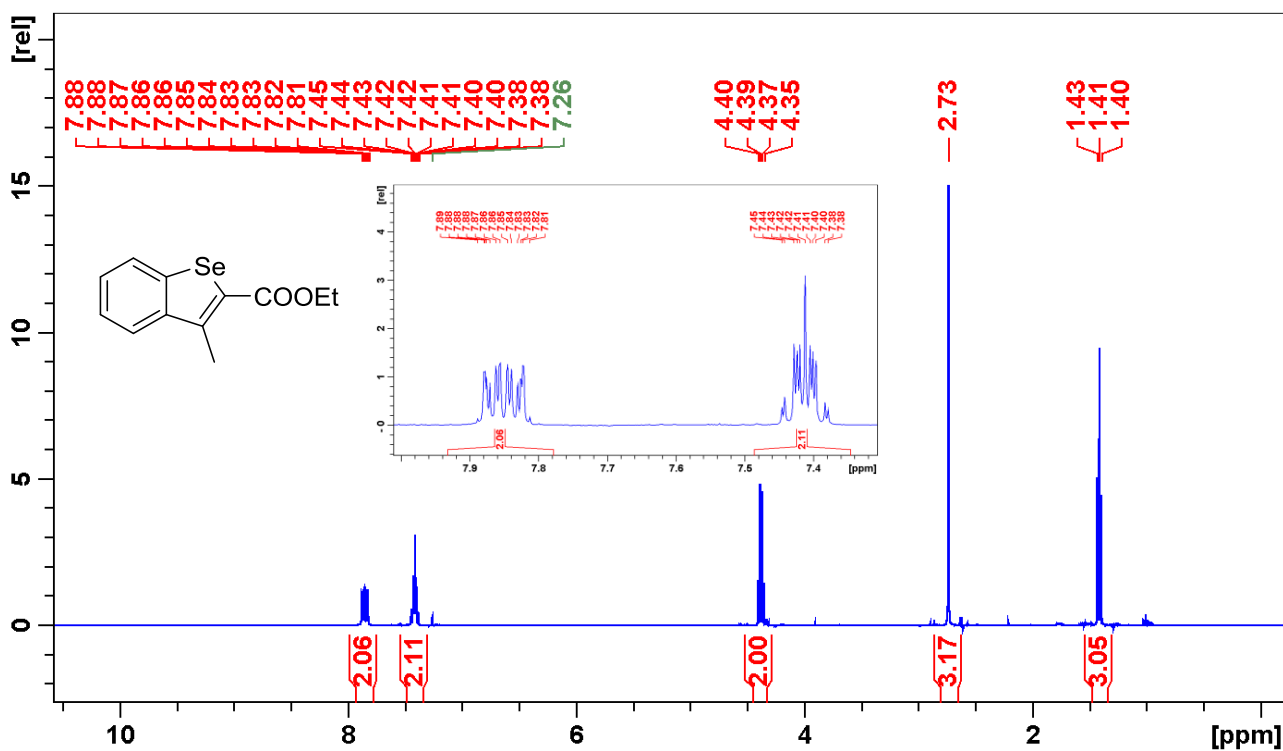


Figure S8. ¹H NMR spectrum of compound 4b.

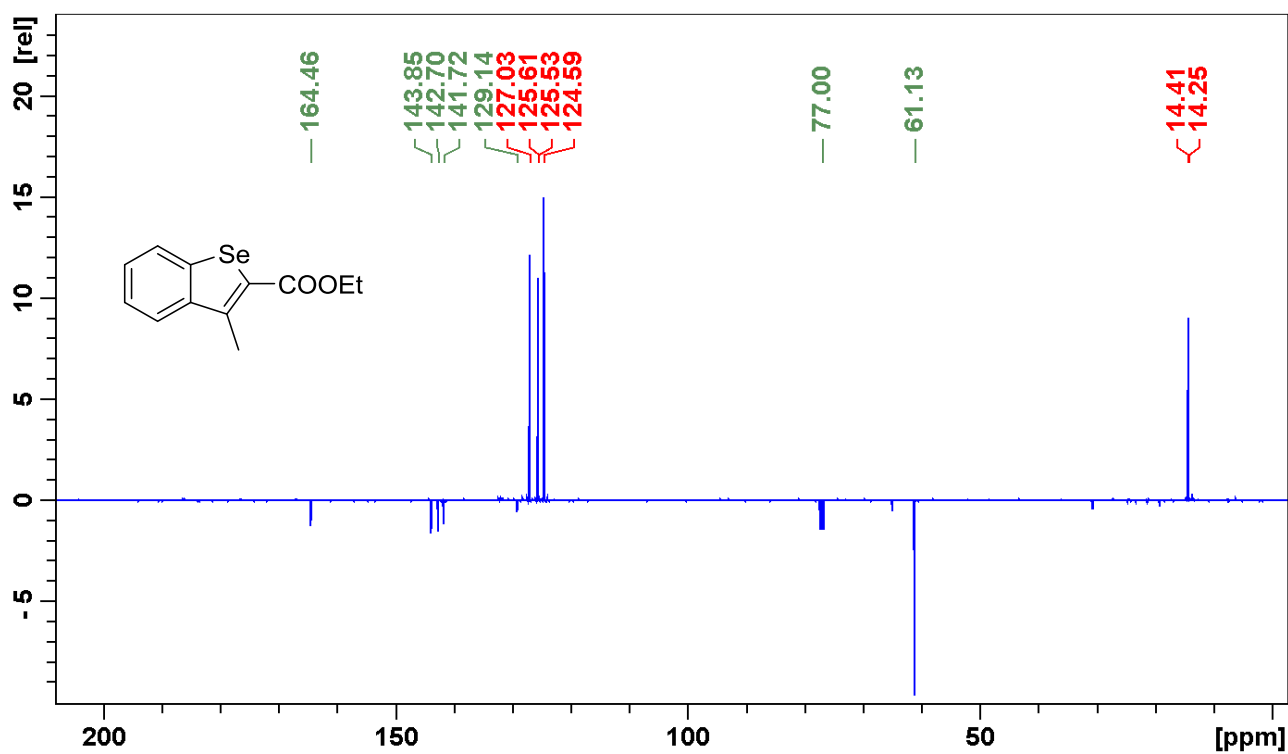


Figure S9. ¹³C NMR spectrum of compound 4b.

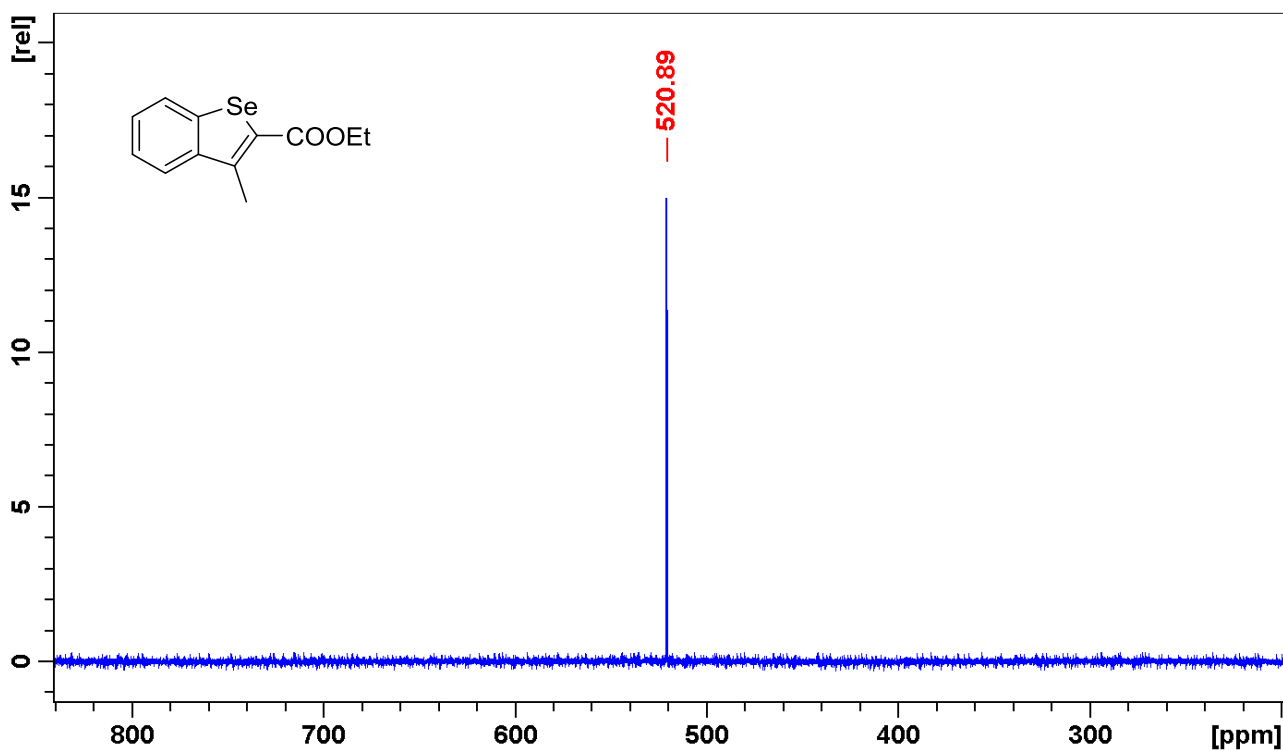


Figure S10. ⁷⁷Se NMR spectrum of compound 4b.

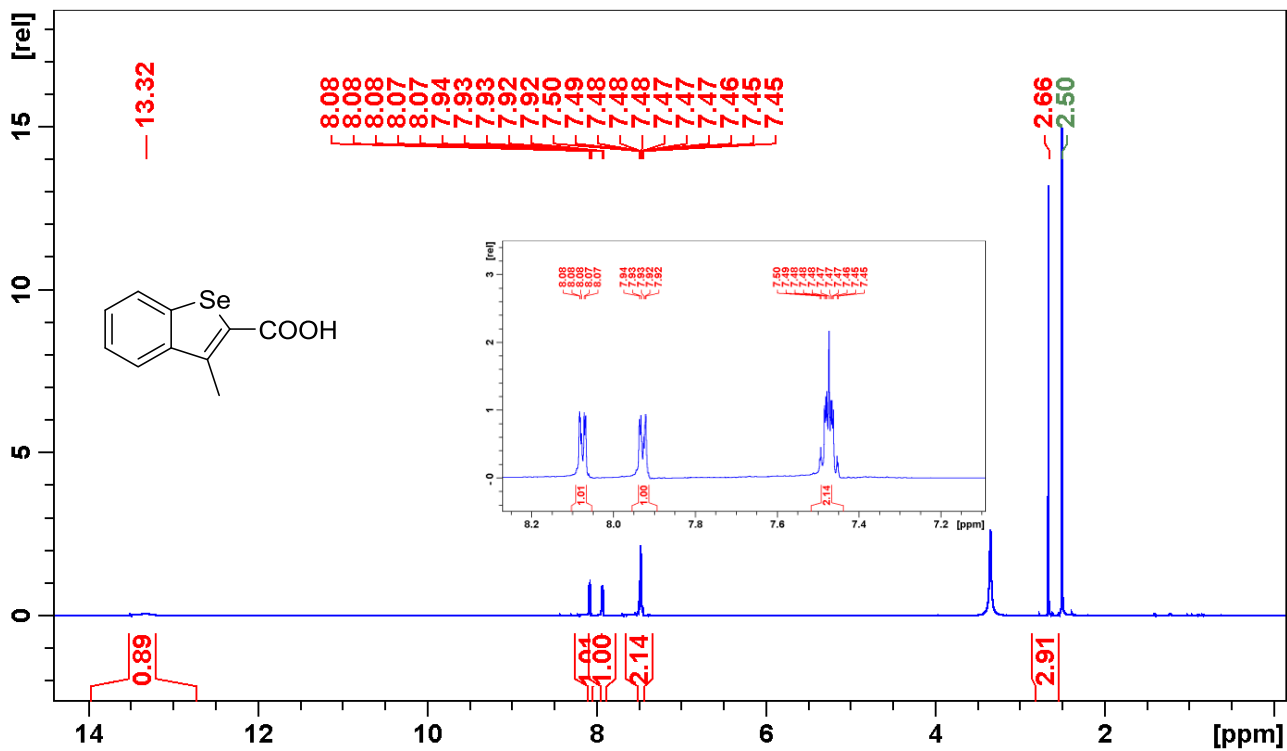


Figure S11. ^1H NMR spectrum of compound 5.

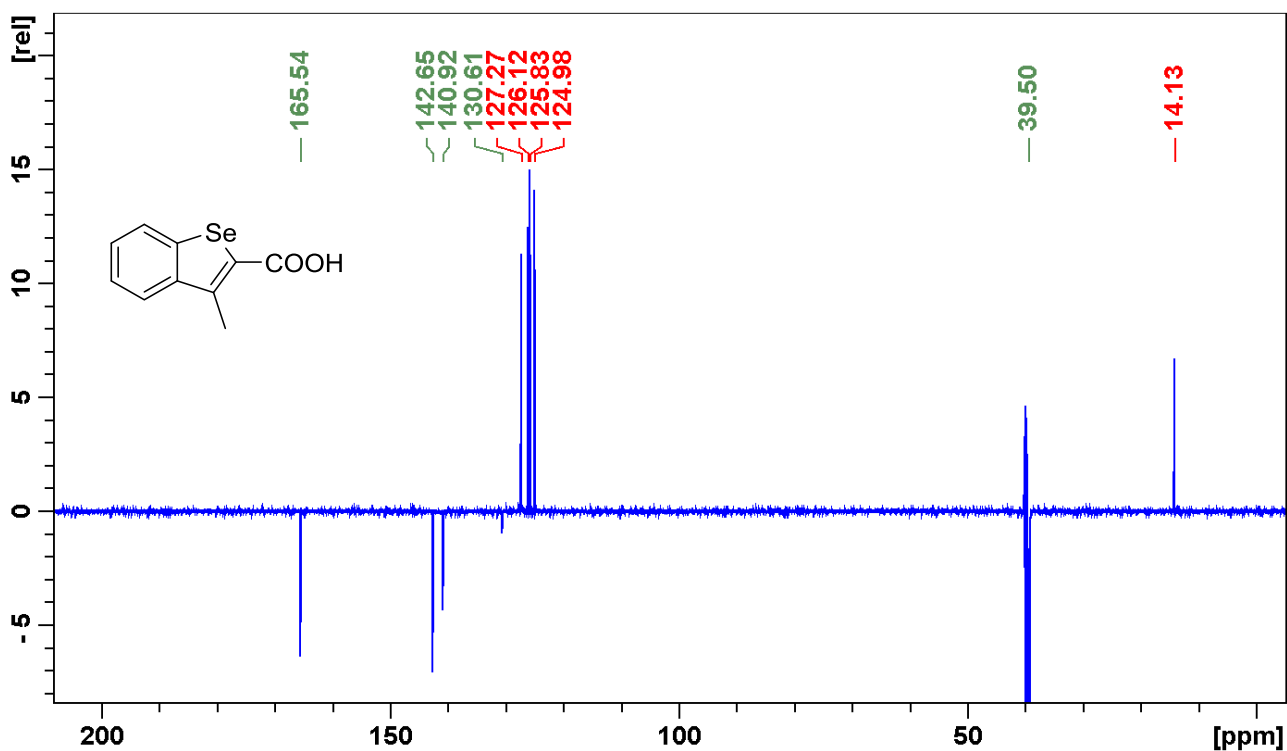


Figure S12. ^{13}C NMR spectrum of compound 5.

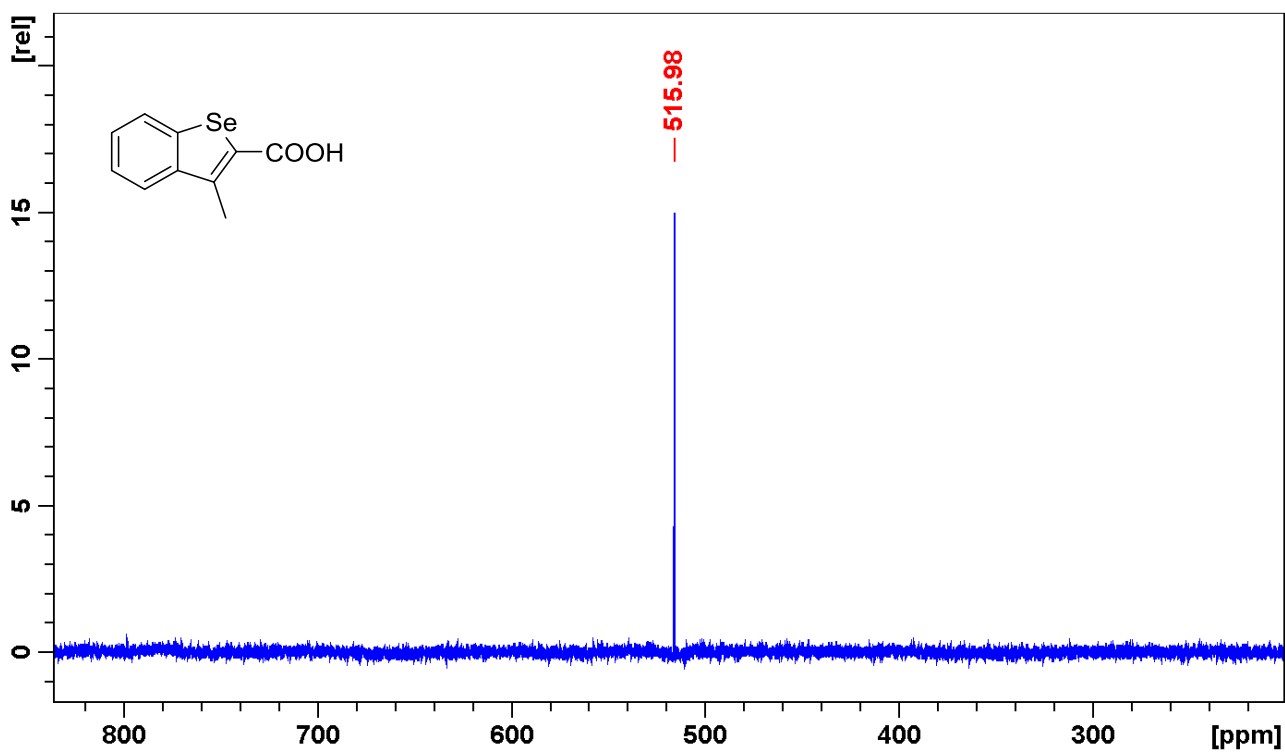


Figure S13. ^{77}Se NMR spectrum of compound 5.

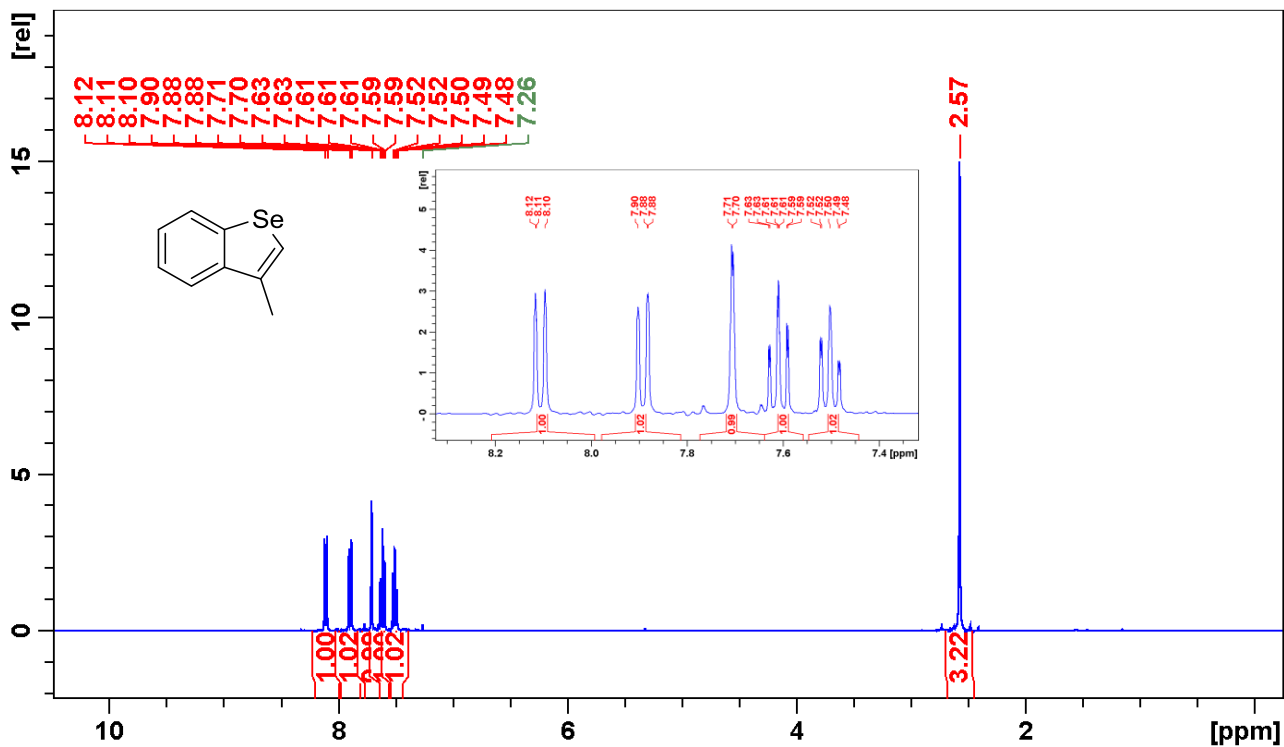


Figure S14. ^1H NMR spectrum of compound 6.

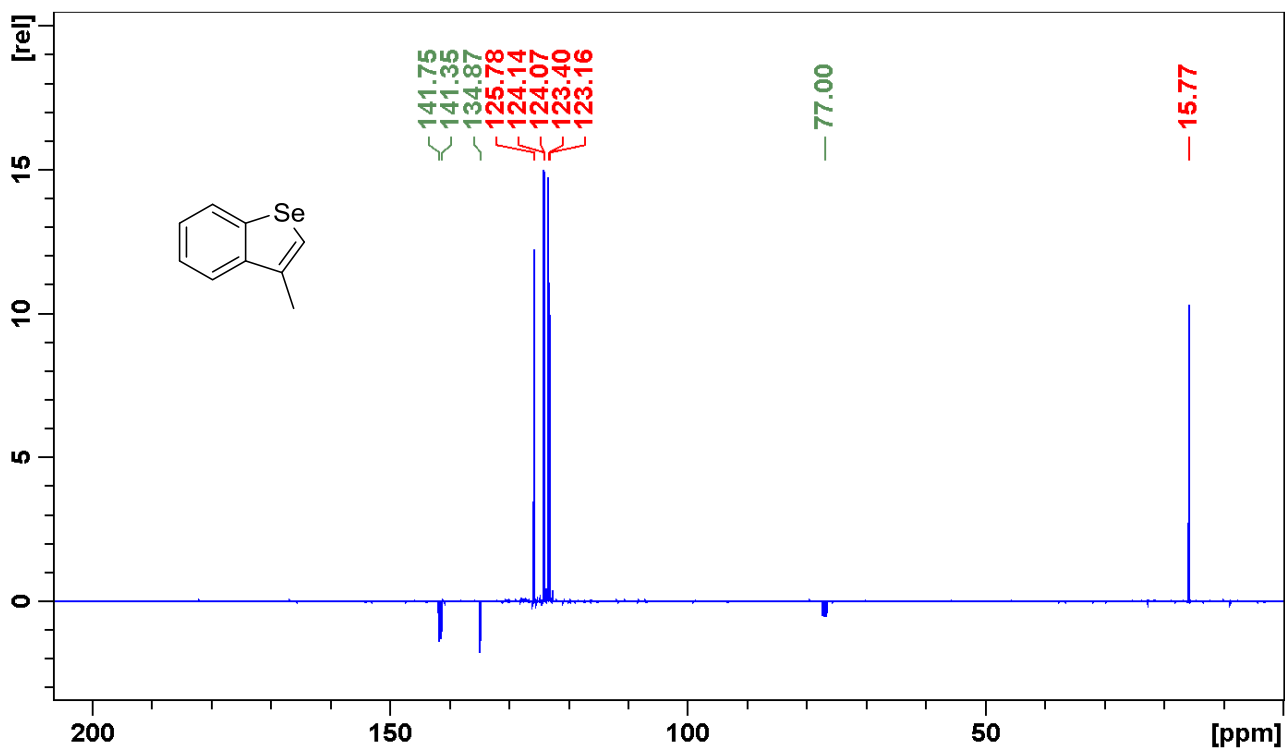


Figure S15. ¹³C NMR spectrum of compound 6.

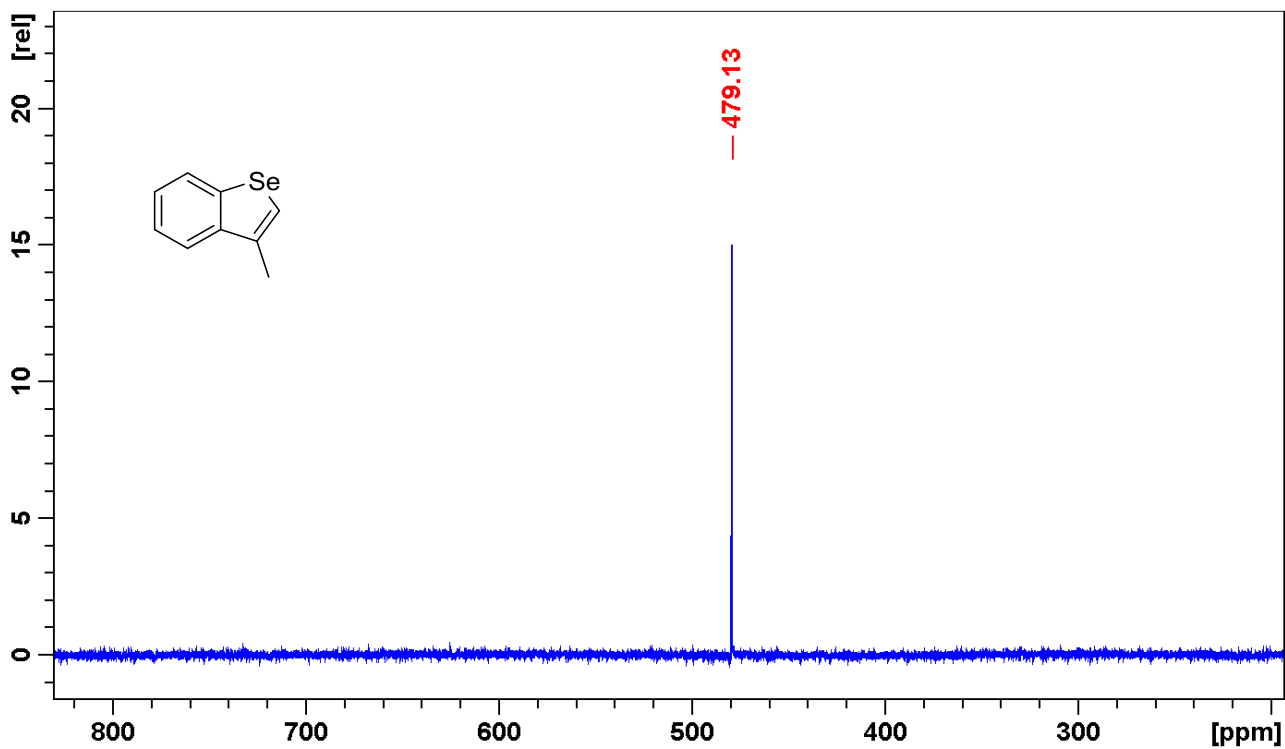


Figure S16. ⁷⁷Se NMR spectrum of compound 6.

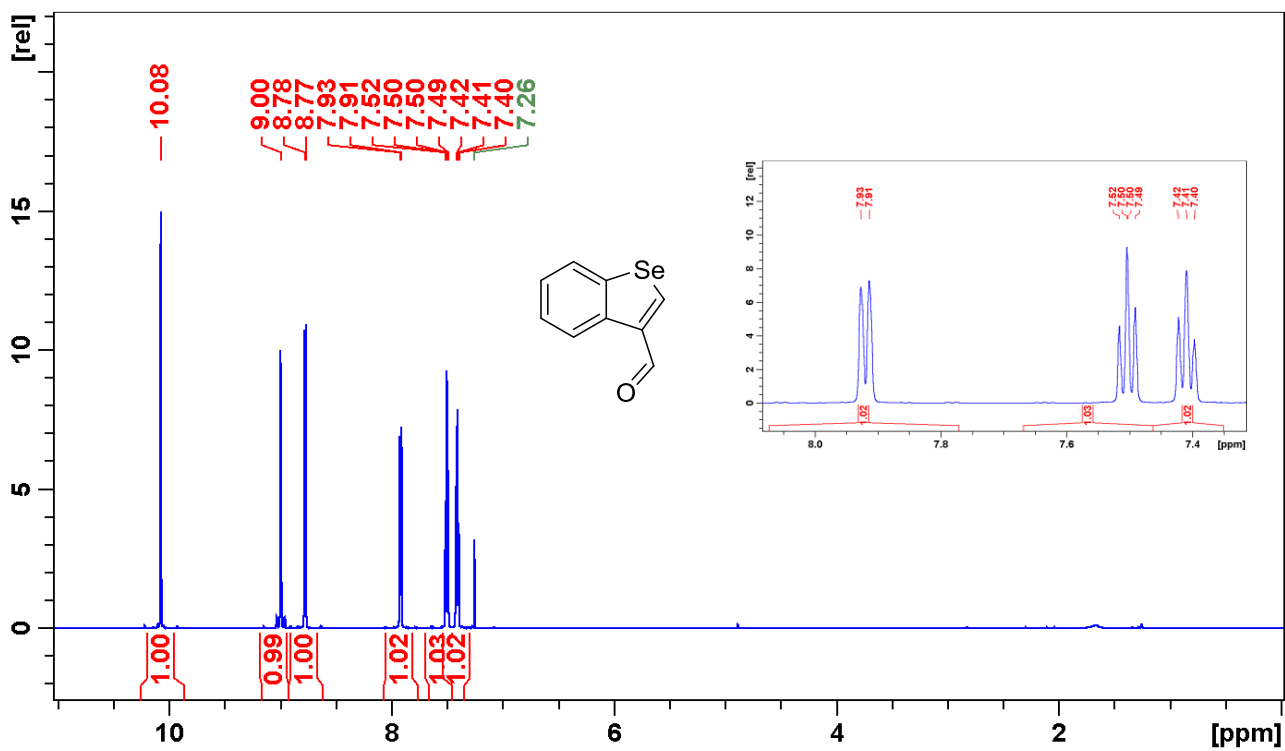


Figure S17. ^1H NMR spectrum of compound 7.

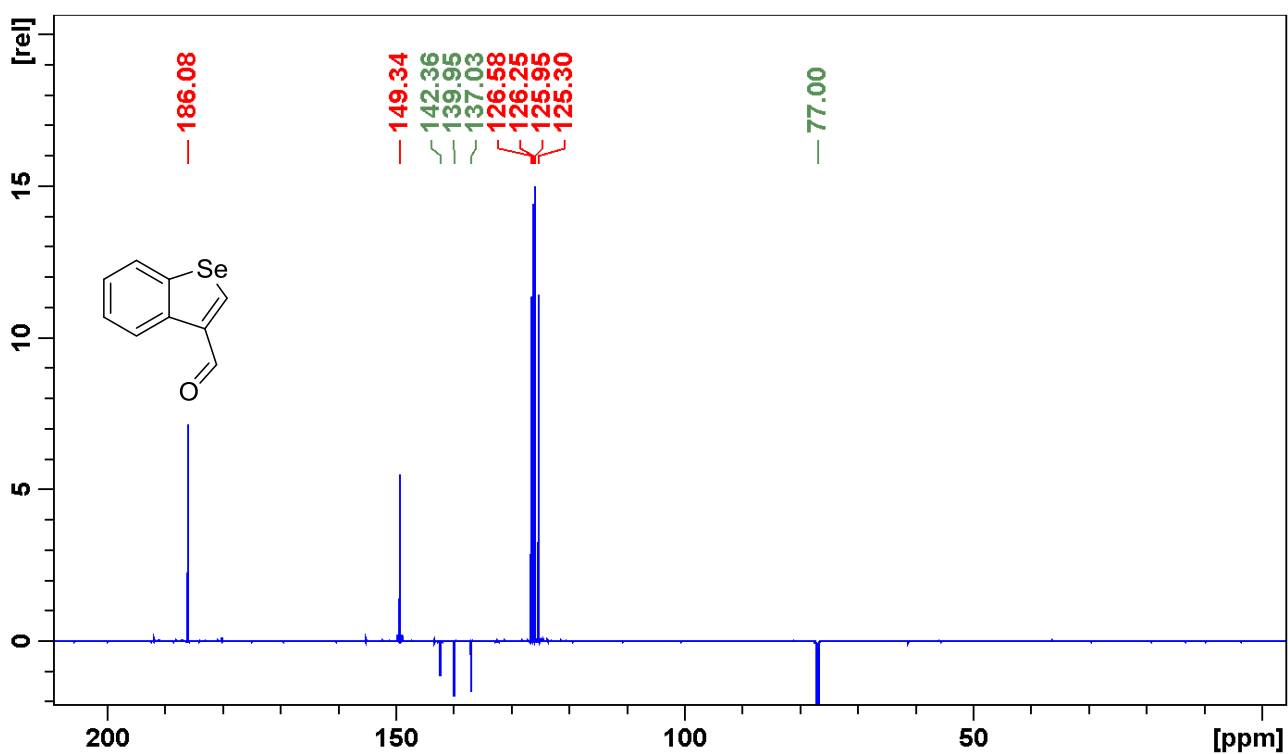


Figure S18. ^{13}C NMR spectrum of compound 7.

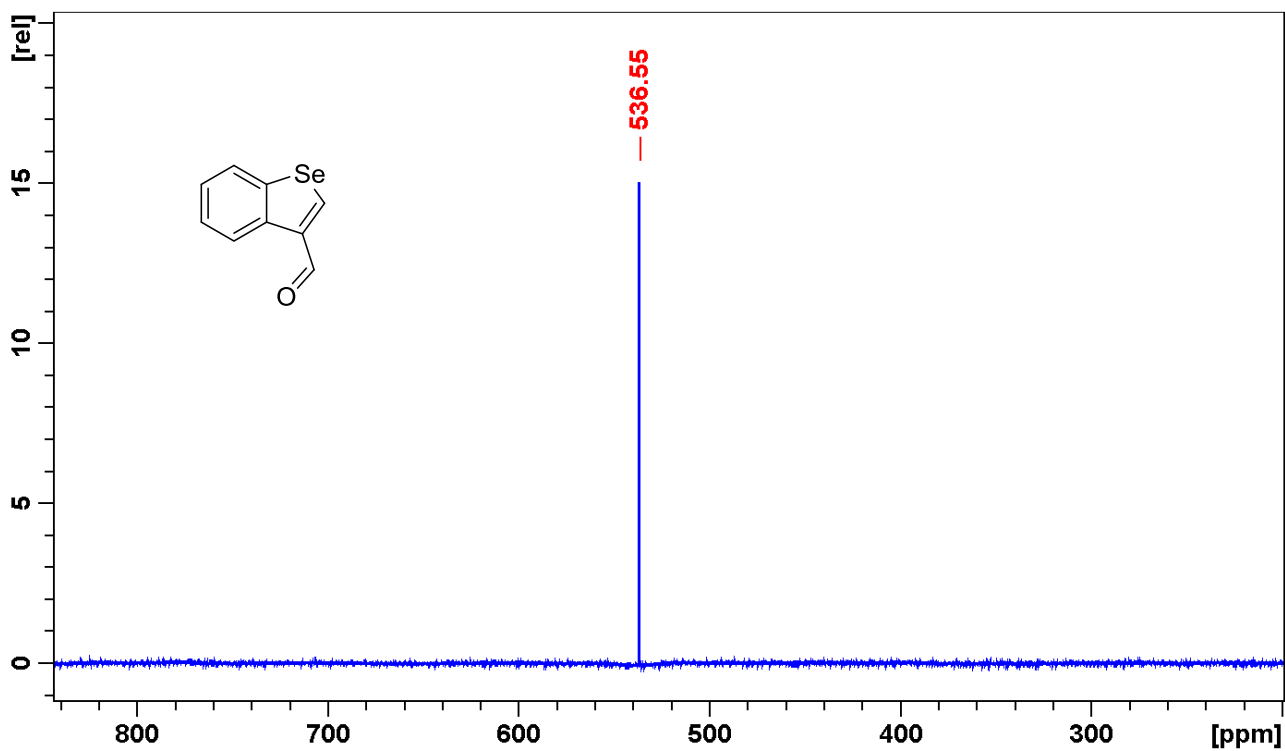


Figure S19. ^{77}Se NMR spectrum of compound 7.

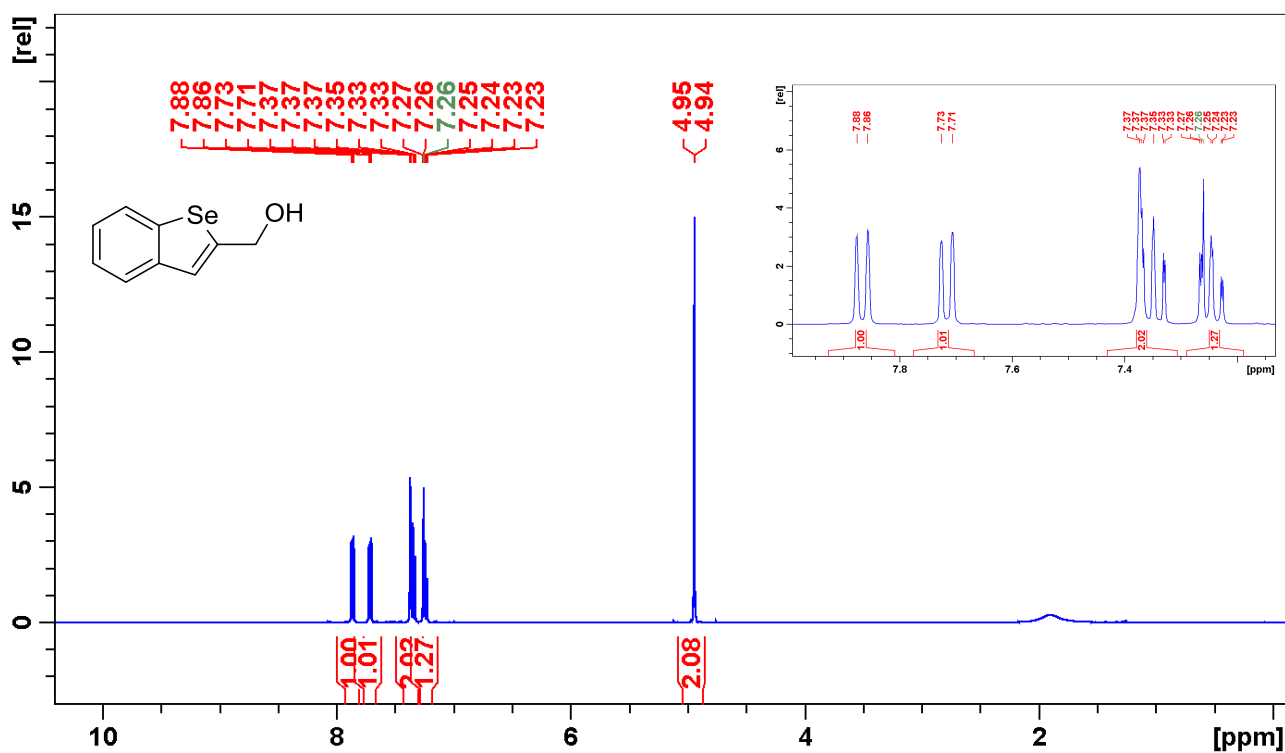


Figure S20. ^1H NMR spectrum of compound 8a.

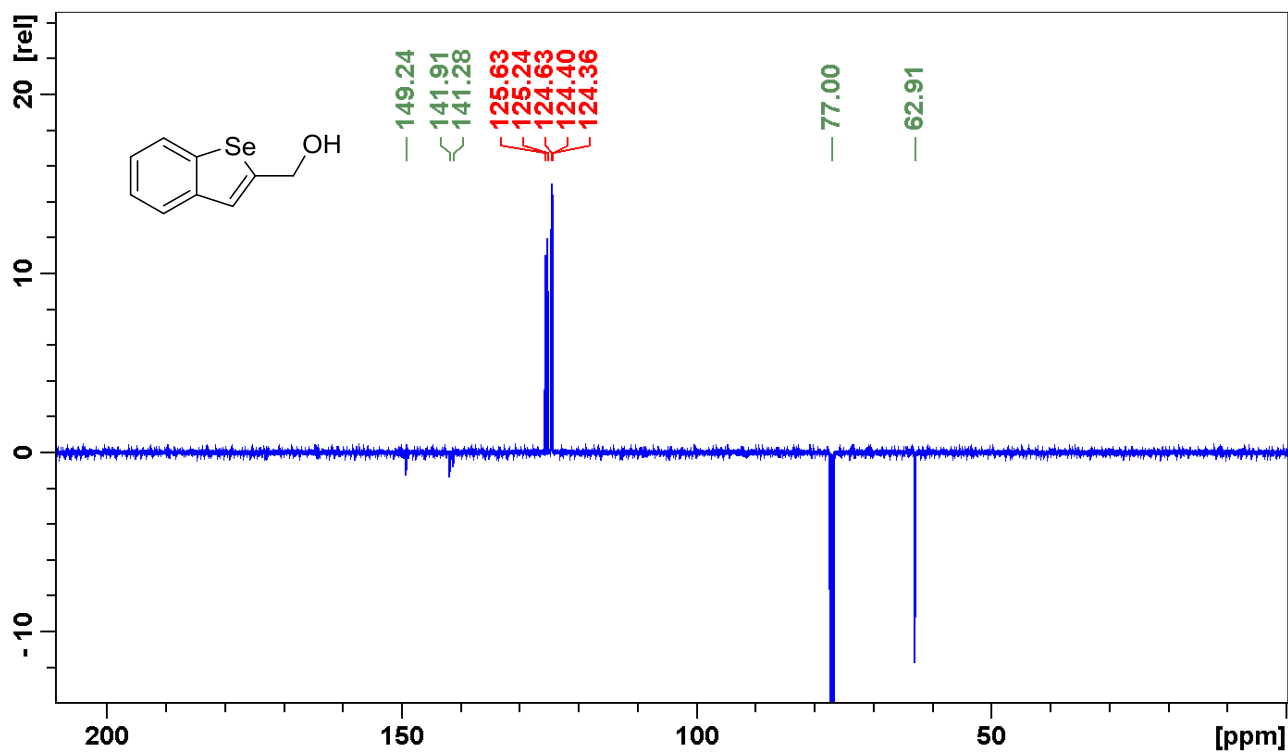


Figure S21. ¹³C NMR spectrum of compound 8a.

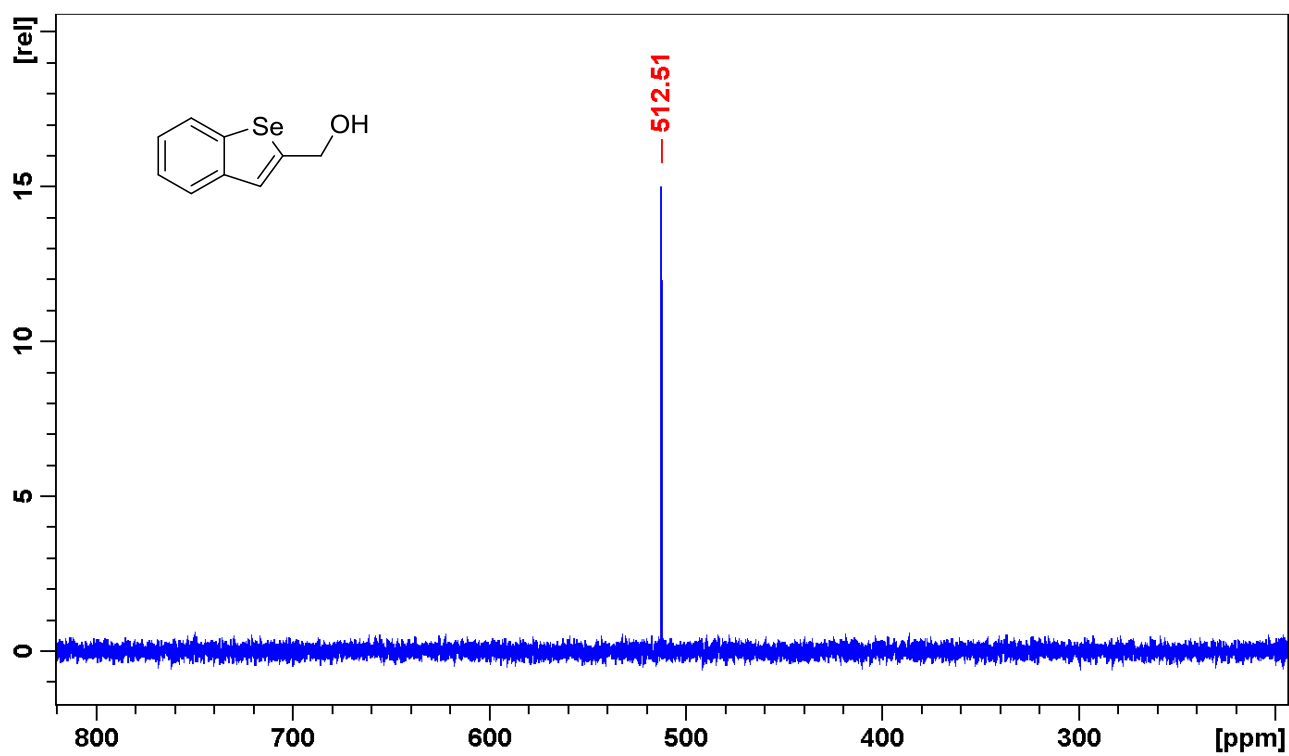


Figure S22. ⁷⁷Se NMR spectrum of compound 8a.

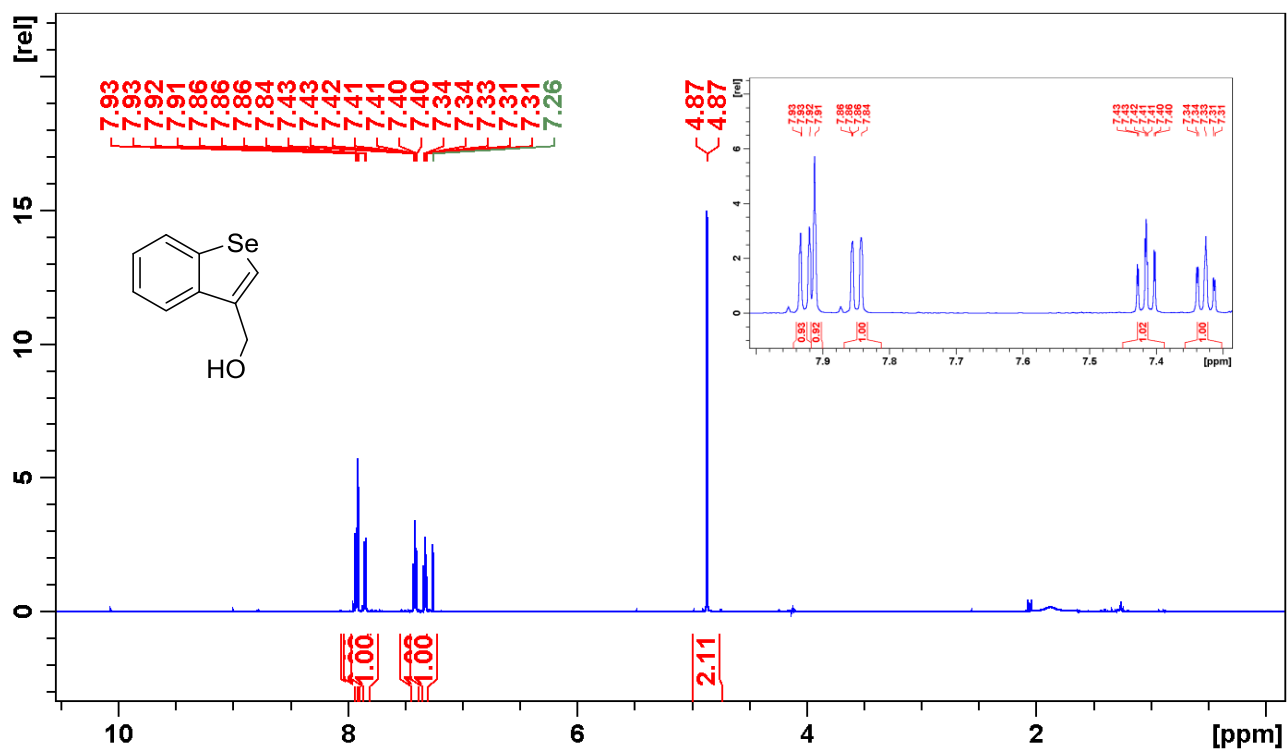


Figure S23. ¹H NMR spectrum of compound **8b**.

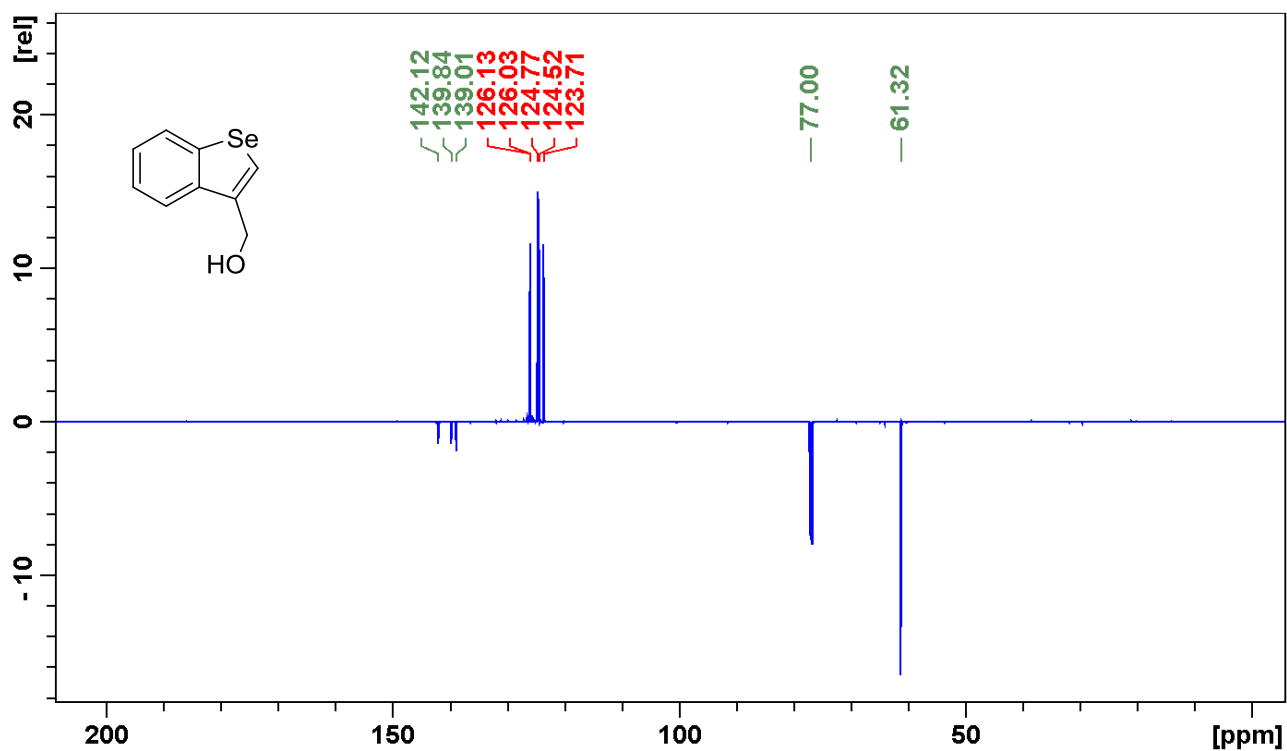


Figure S24. ¹³C NMR spectrum of compound **8b**.

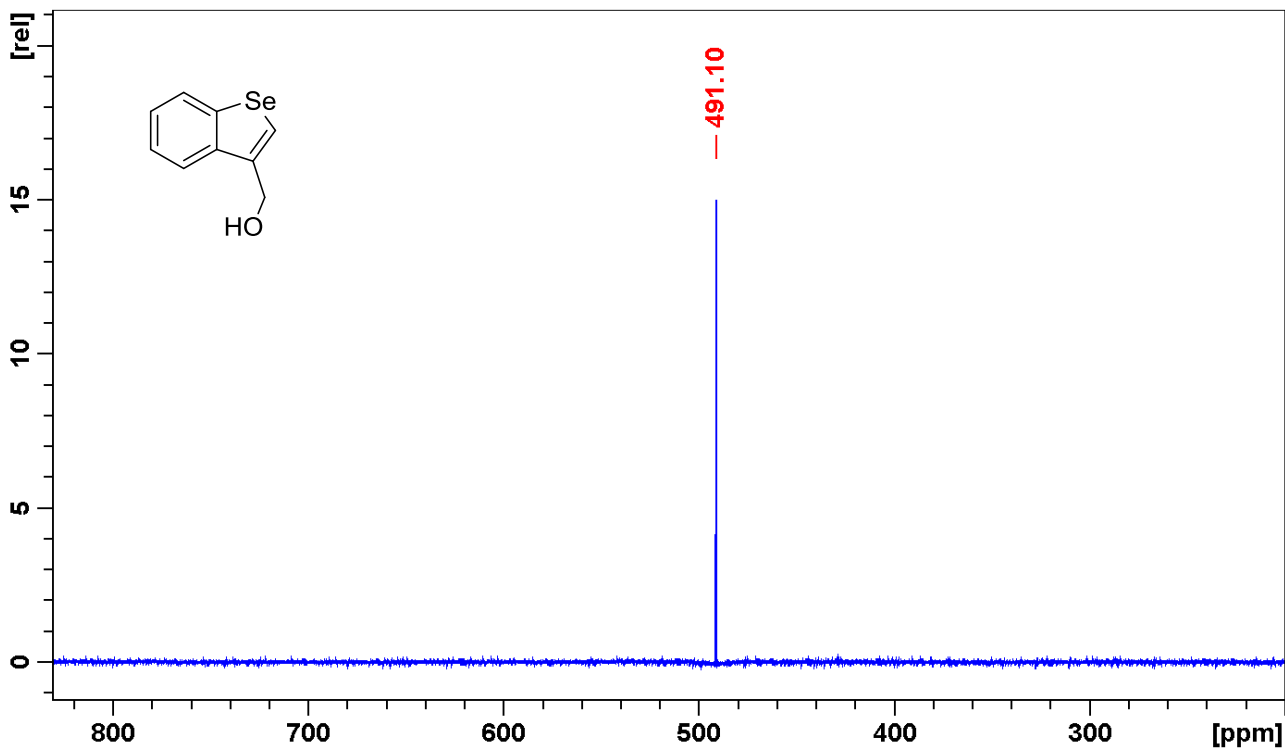


Figure S25. ^{77}Se NMR spectrum of compound **8b**.

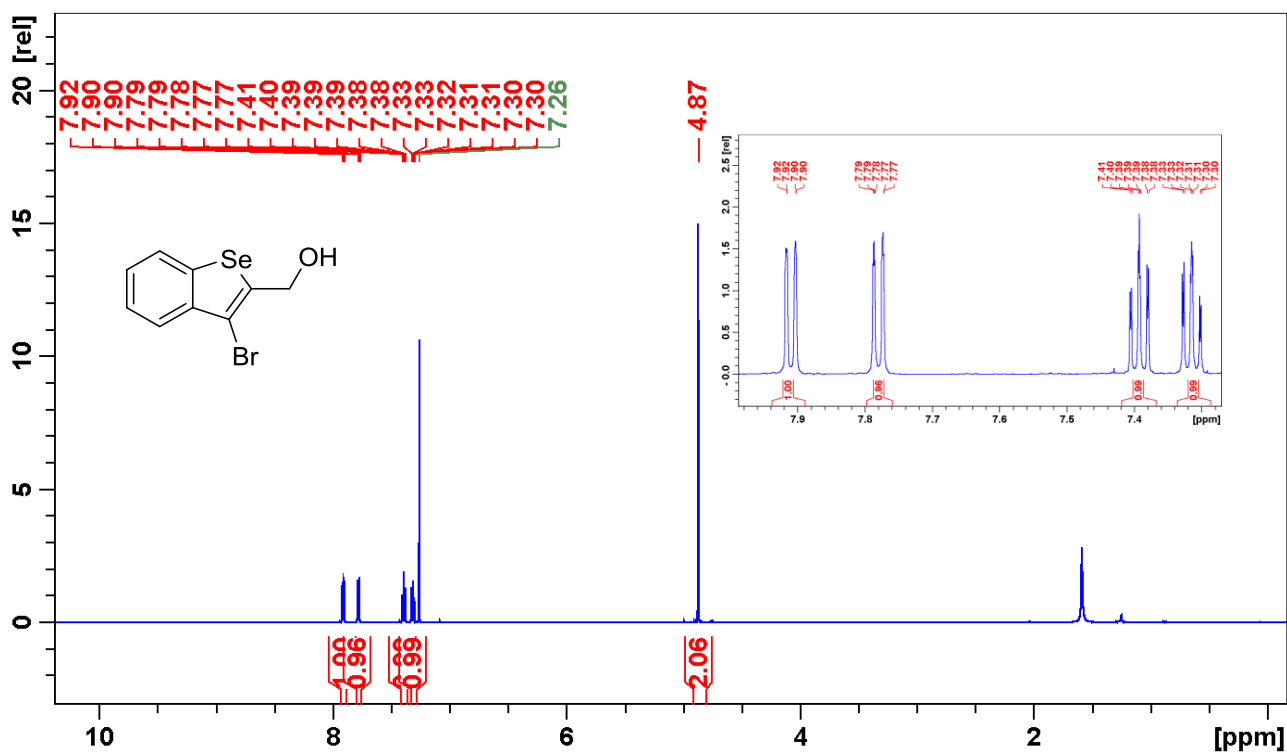


Figure S26. ^1H NMR spectrum of compound **9a**.

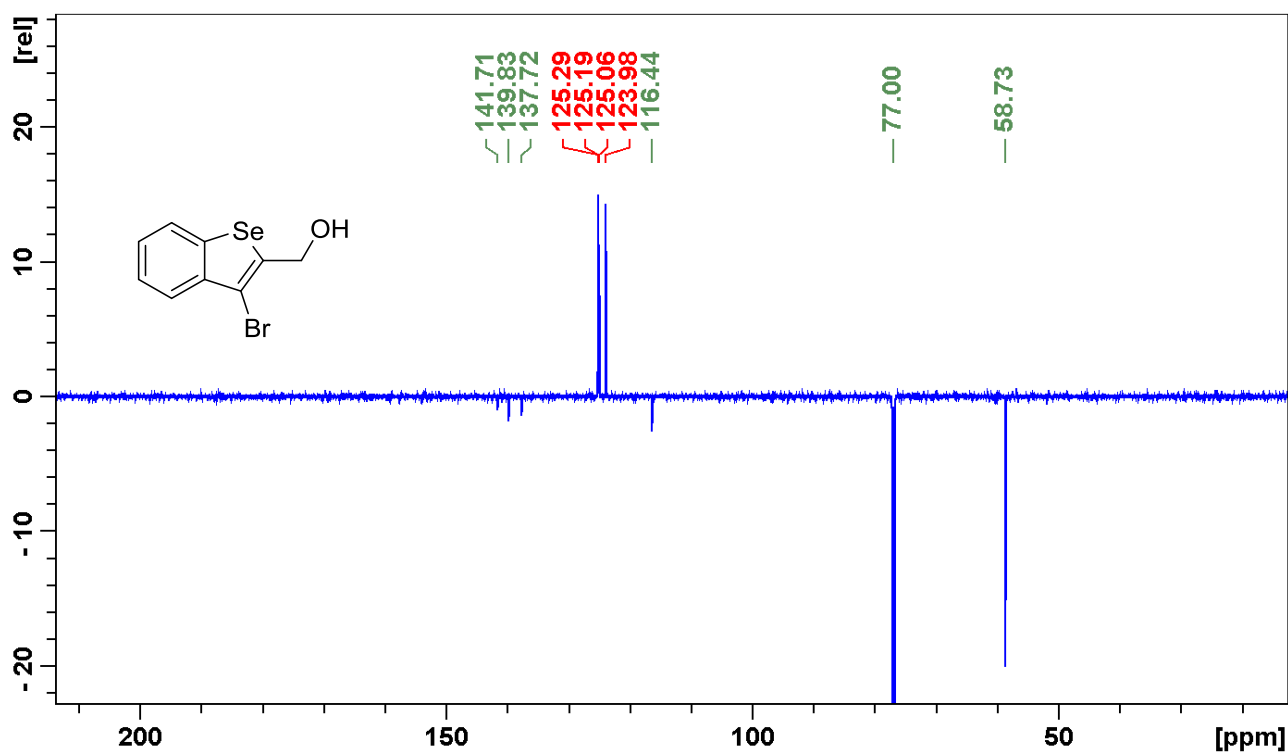


Figure S27. ¹³C NMR spectrum of compound 9a.

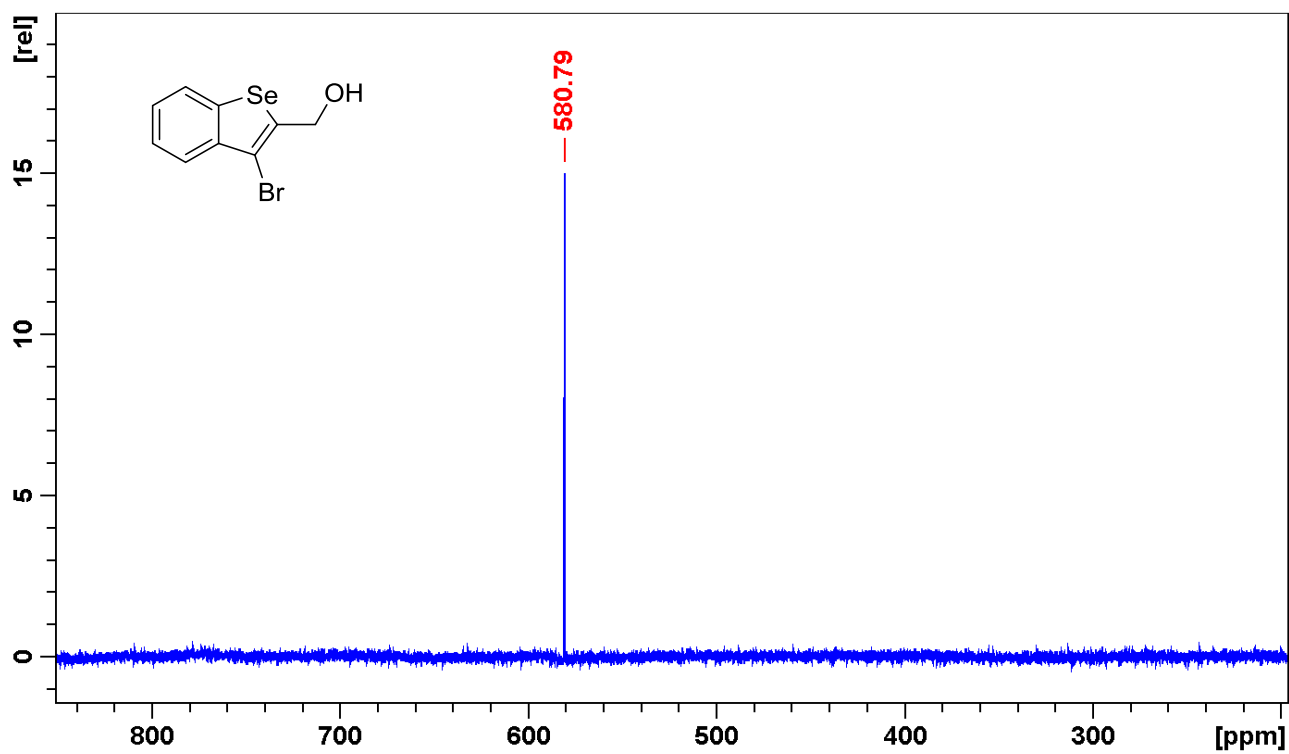


Figure S28. ⁷⁷Se NMR spectrum of compound 9a.

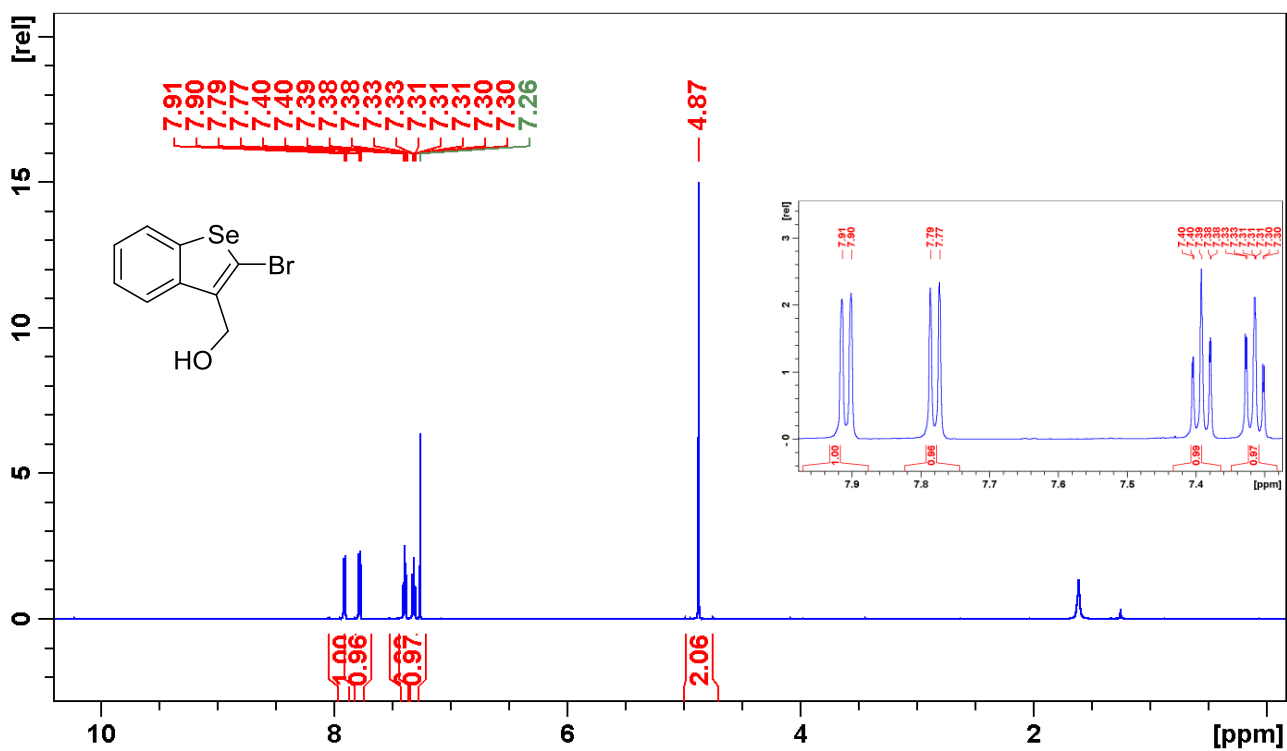


Figure S29. ¹H NMR spectrum of compound **9b**.

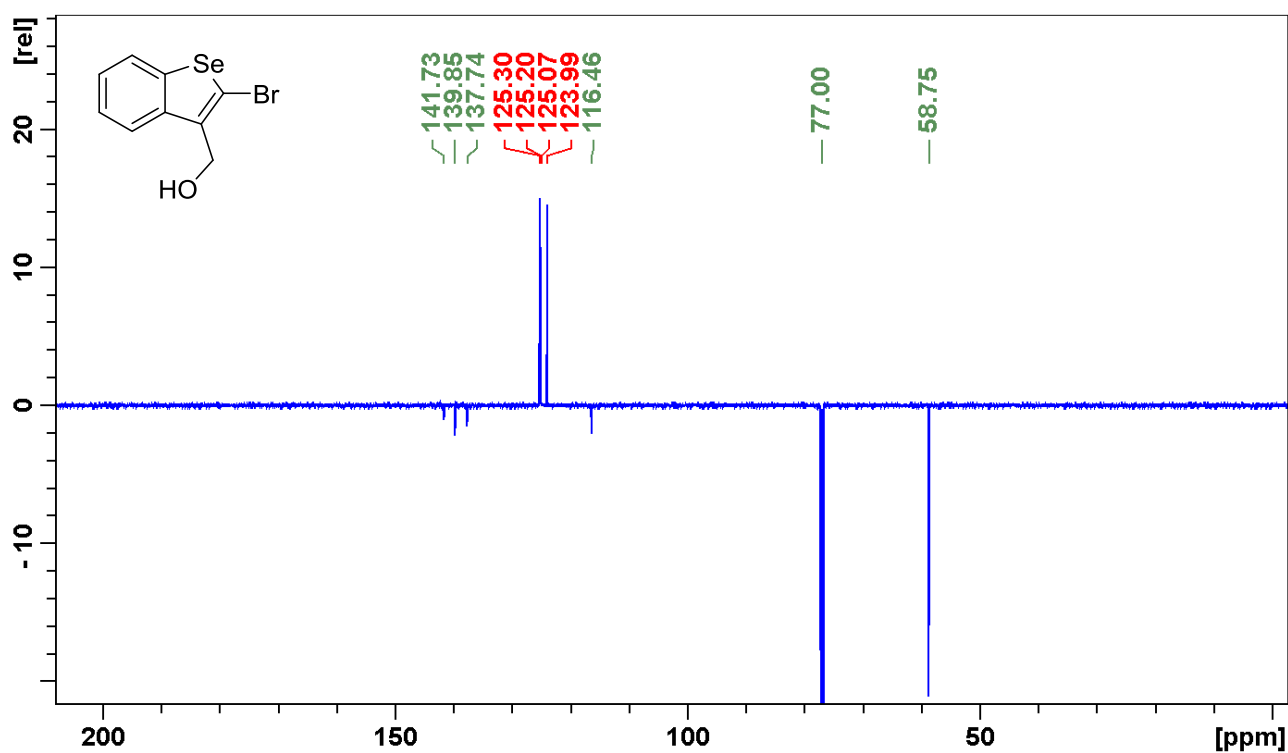


Figure S30. ¹³C NMR spectrum of compound **9b**.

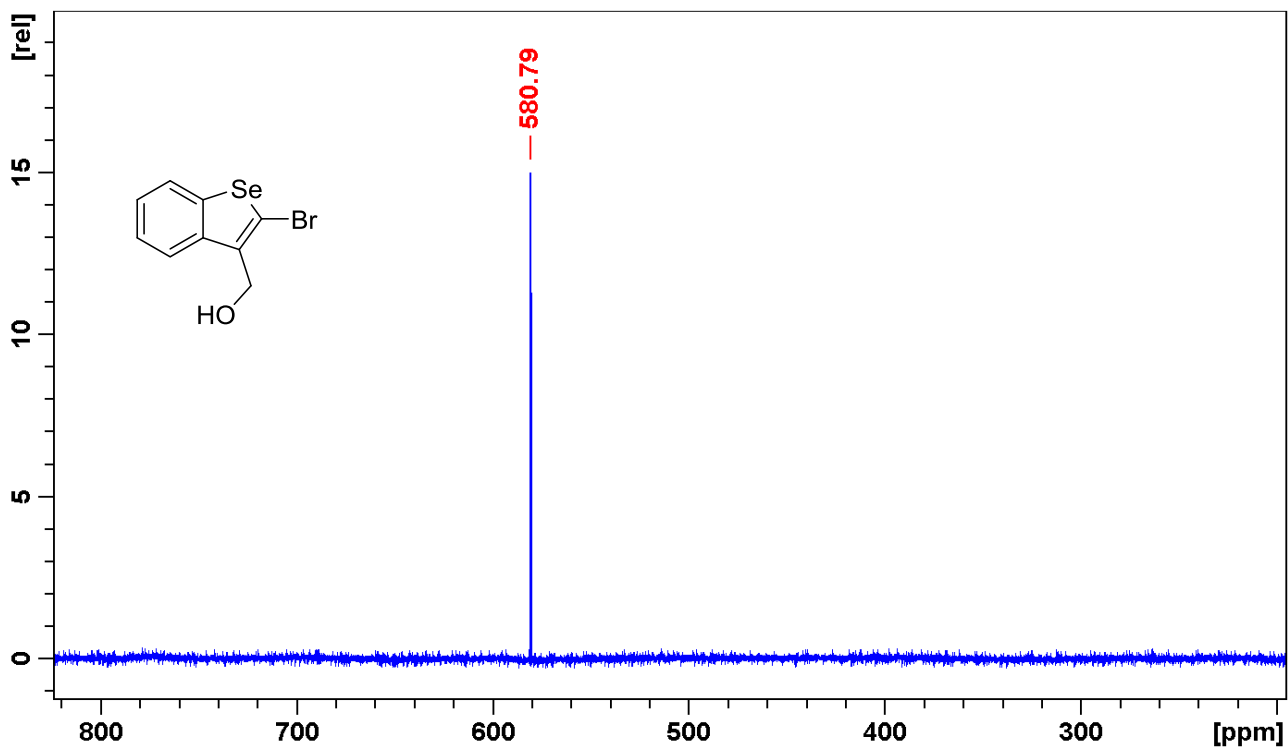


Figure S31. ⁷⁷Se NMR spectrum of compound **9b**.

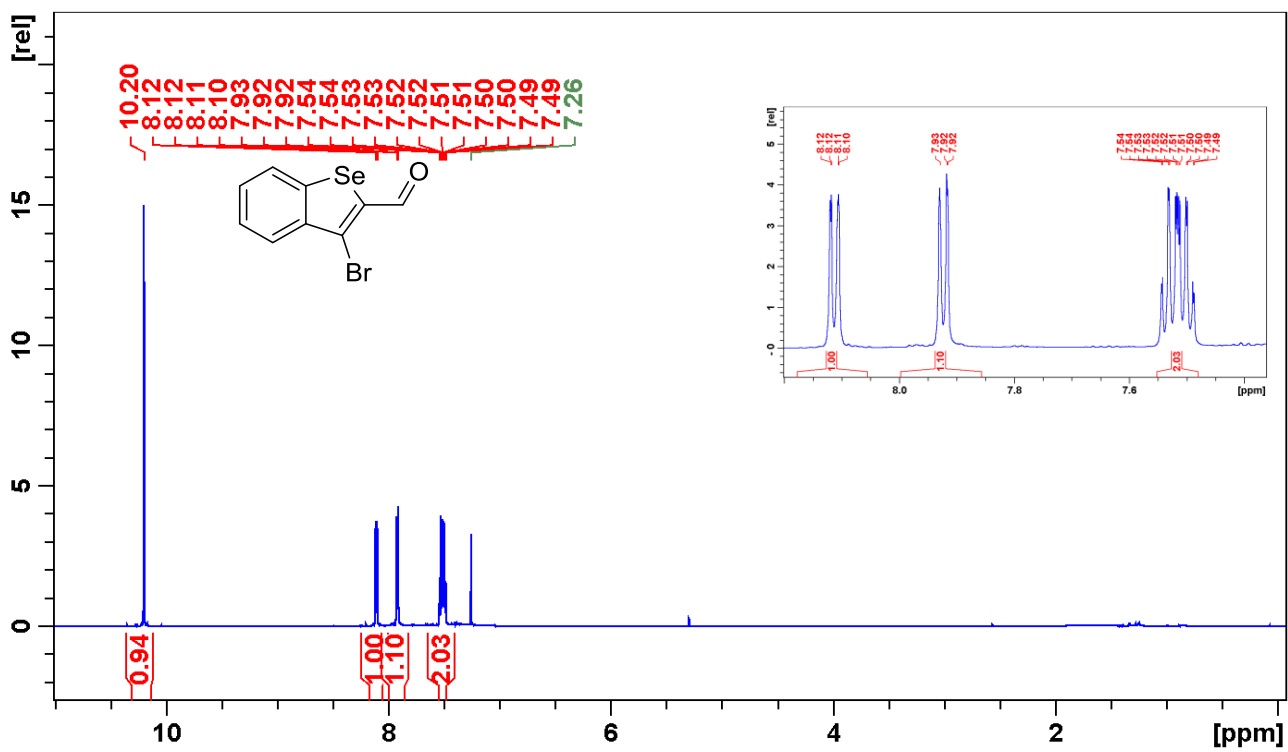


Figure S32. ¹H NMR spectrum of compound **10a**.

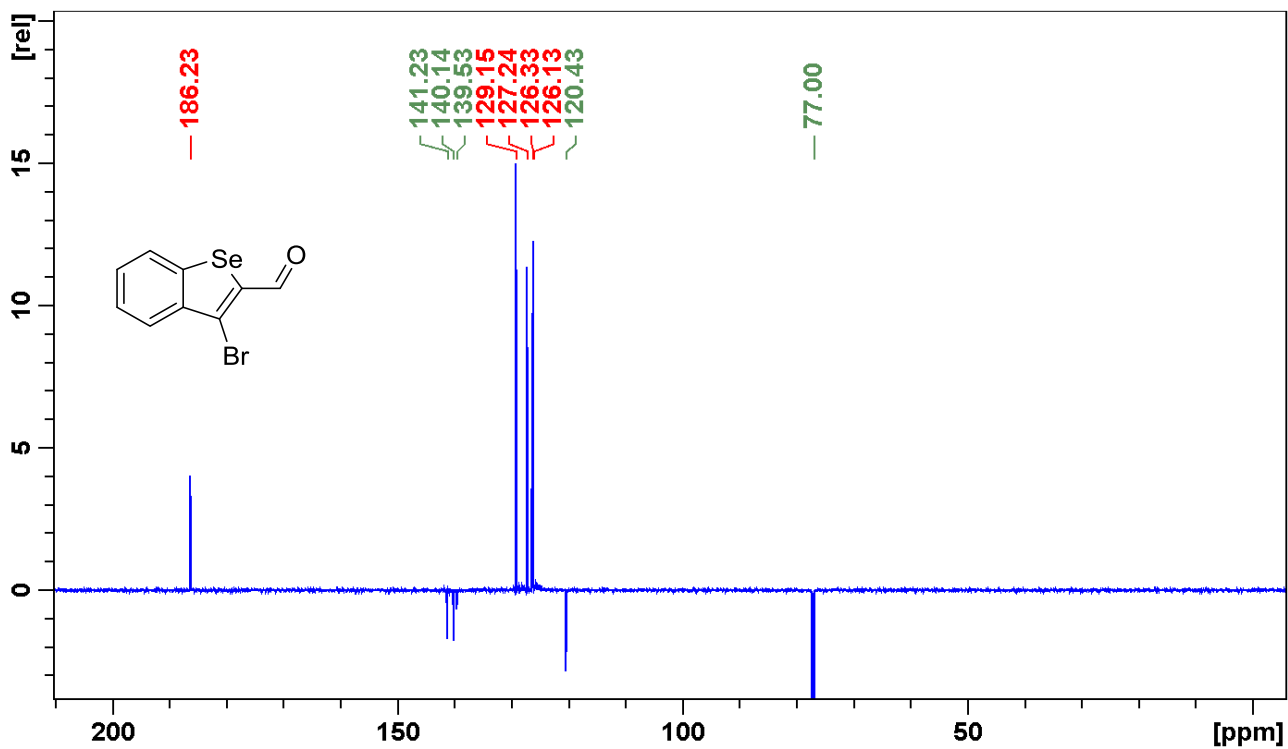


Figure S33. ^{13}C NMR spectrum of compound **10a**.

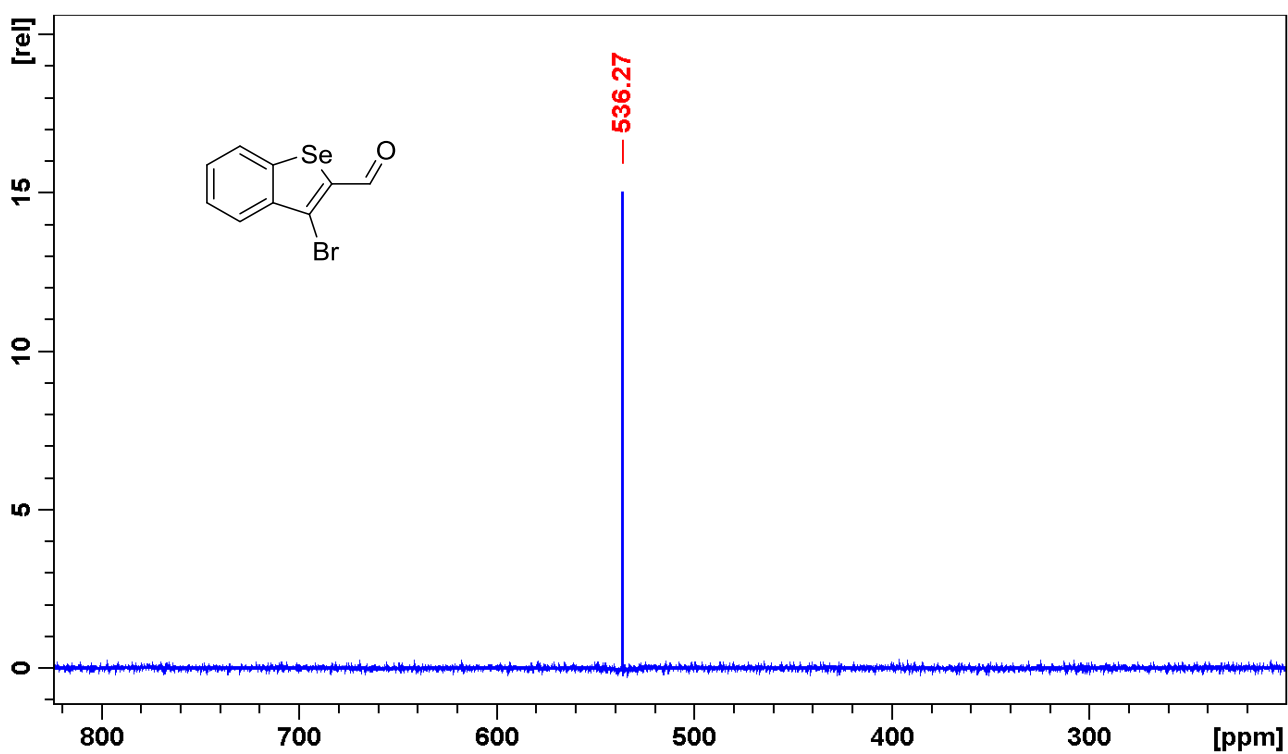


Figure S34. ^{77}Se NMR spectrum of compound **10a**.

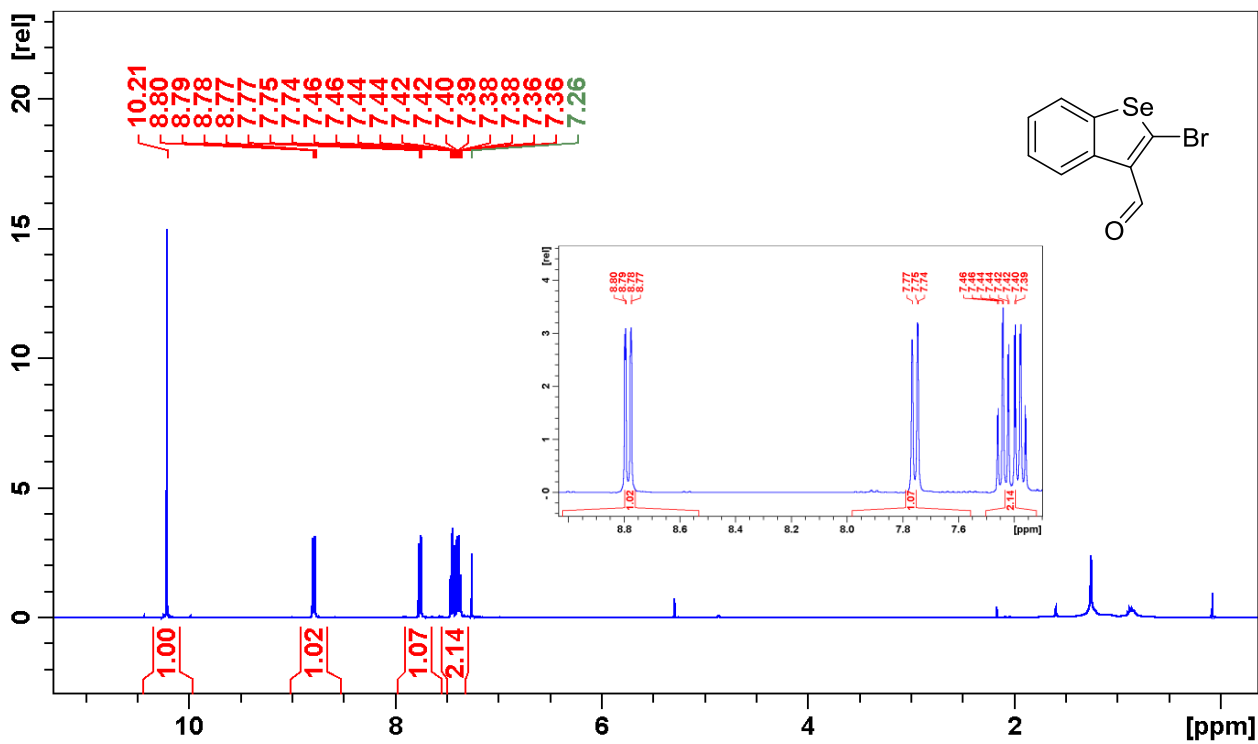


Figure S35. ^1H NMR spectrum of compound 10b.

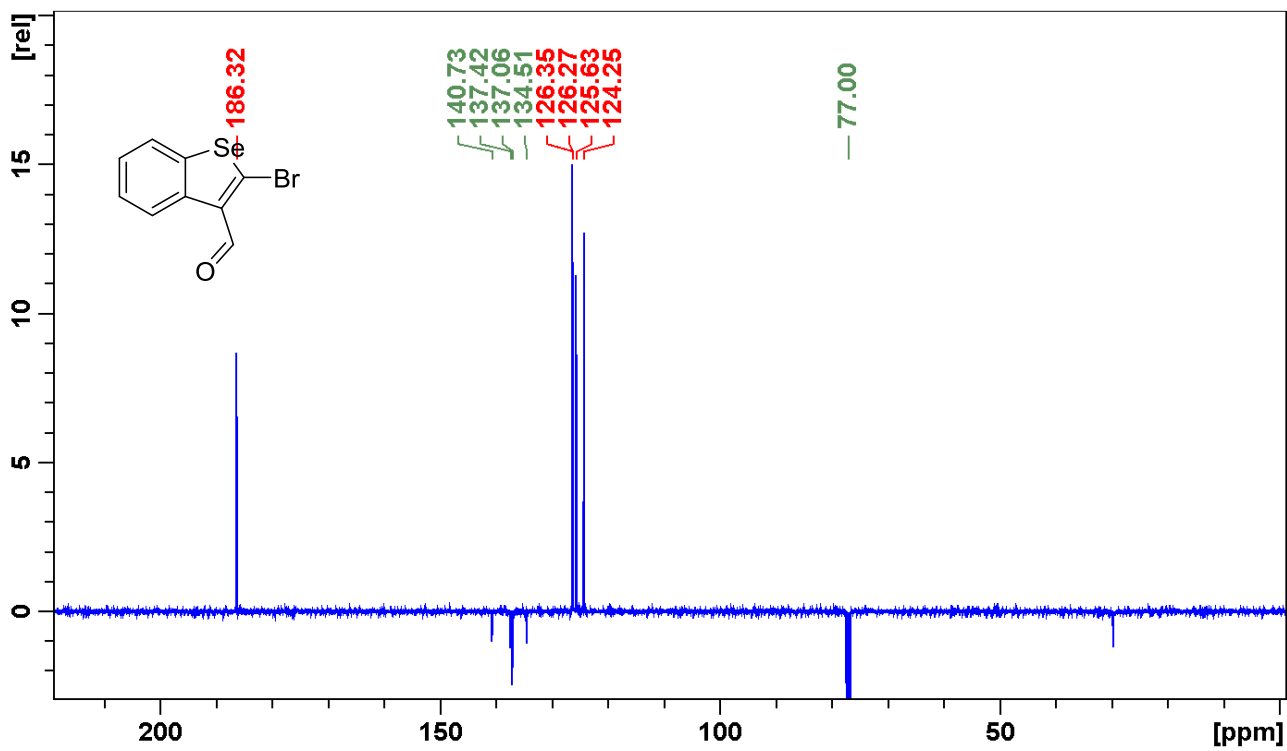


Figure S36. ^{13}C NMR spectrum of compound 10b.

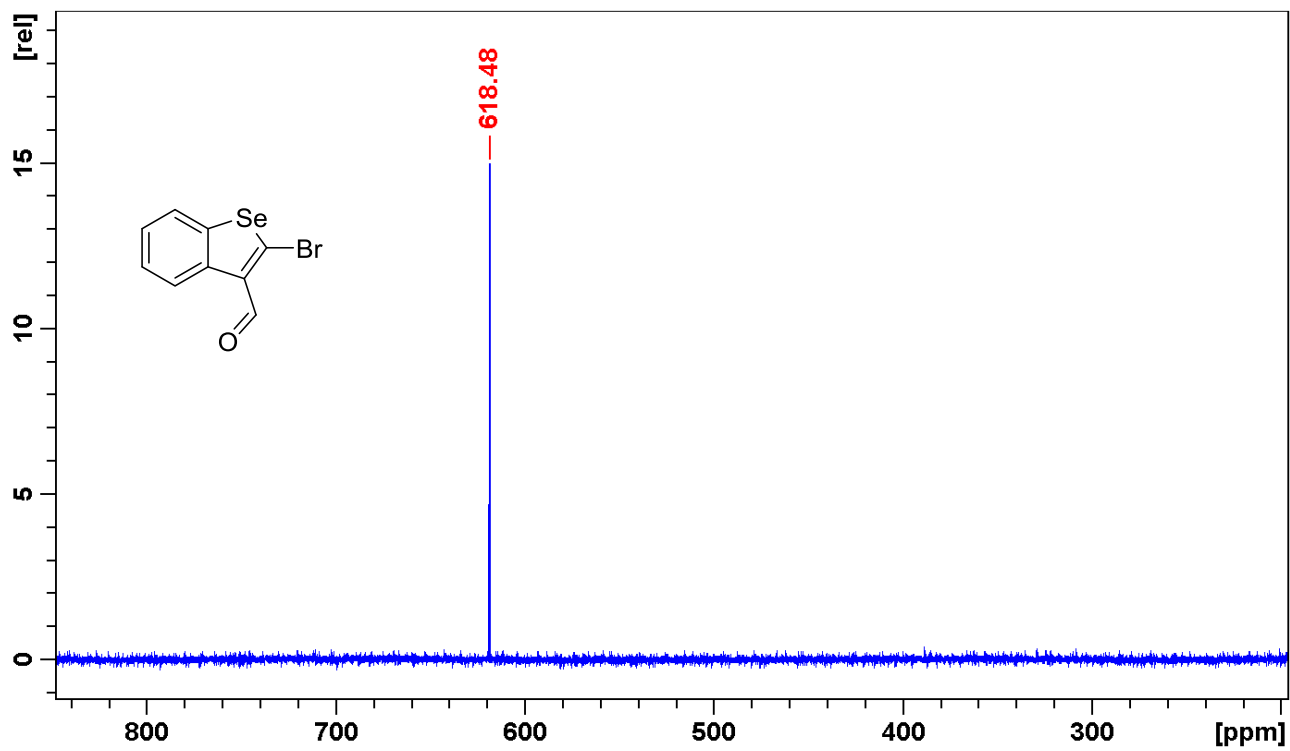


Figure S37. ^{77}Se NMR spectrum of compound **10b**.

Manuscript # 5

Supporting Information

Symmetric sulfur-selenium mixed semiconductors: synthesis, characterization and applications in organic field-effect transistors

Brigitte Holzer,^{a} Barbara Dellago,^a Christian Hametner,^a Berthold Stöger,^b Daniel Lumpi,^{a*}
Ernst Horkel,^a and Johannes Fröhlich^a*

^a Institute of Applied Synthetic Chemistry, Vienna University of Technology,

Getreidemarkt 9/163OC, A-1060 Vienna, Austria

^b Institute of Chemical Technologies and Analytics, Vienna University of Technology,

Getreidemarkt 9/164, A-1060 Vienna, Austria

*brigitte.holzer@tuwien.ac.at

*daniel.lumpi@tuwien.ac.at

Content

A) NMR Spectra

B) Absorption Spectra of 17 and 20

C) Cyclic voltammetric measurements of 17 and 20

D) Thermal Analysis

E) DFT Calculations

A) NMR Spectra

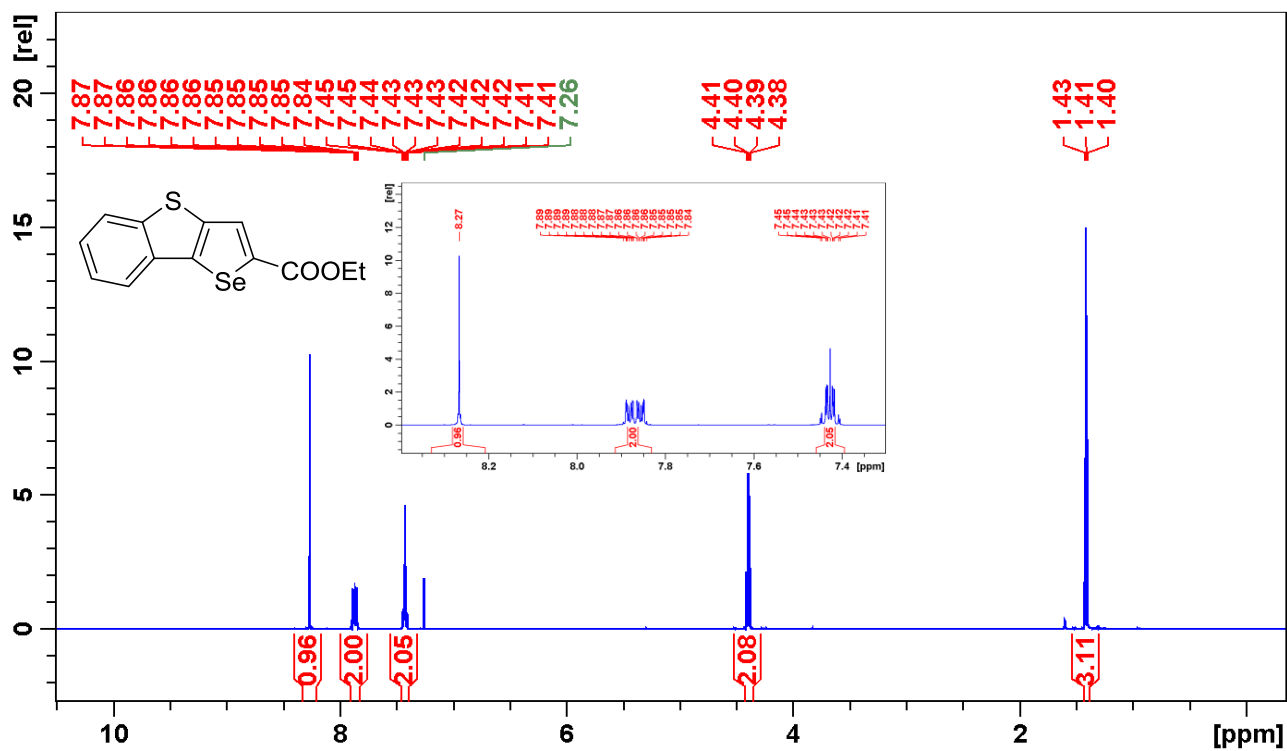


Figure S1. ¹H NMR spectrum of compound 3a.

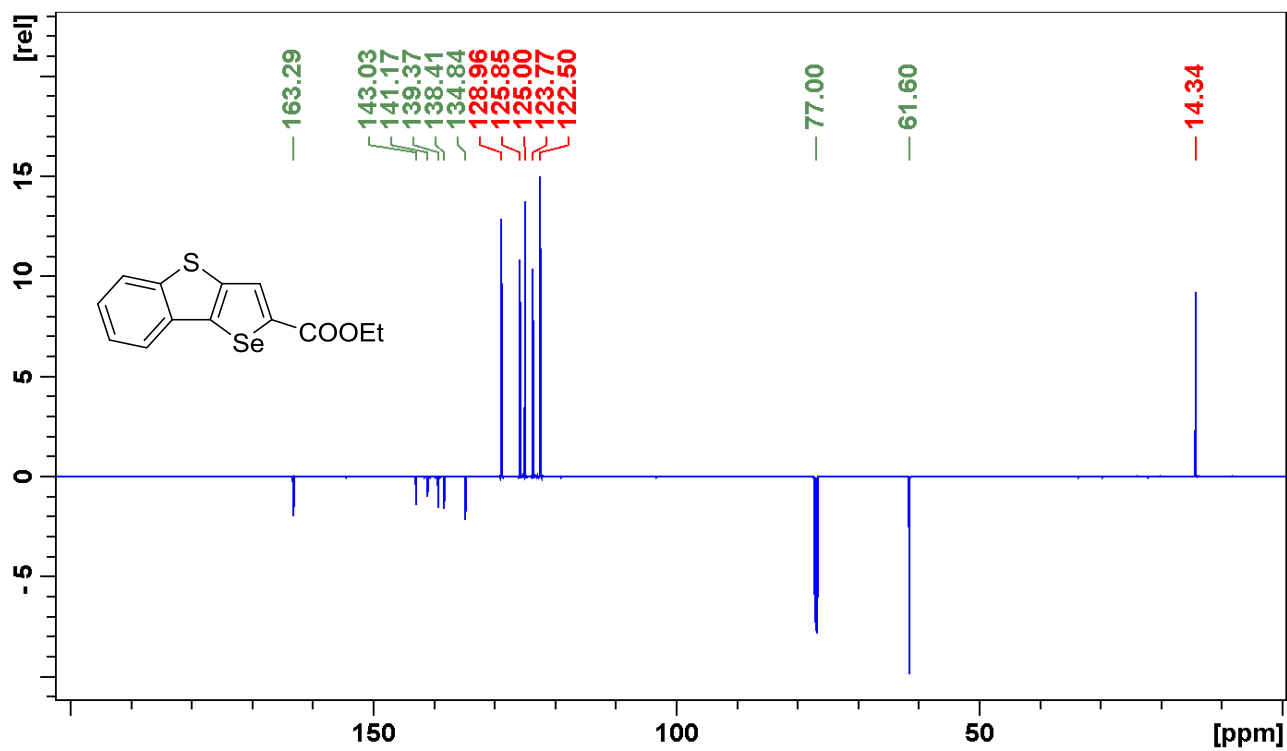


Figure S2. ¹³C NMR spectrum of compound 3a.

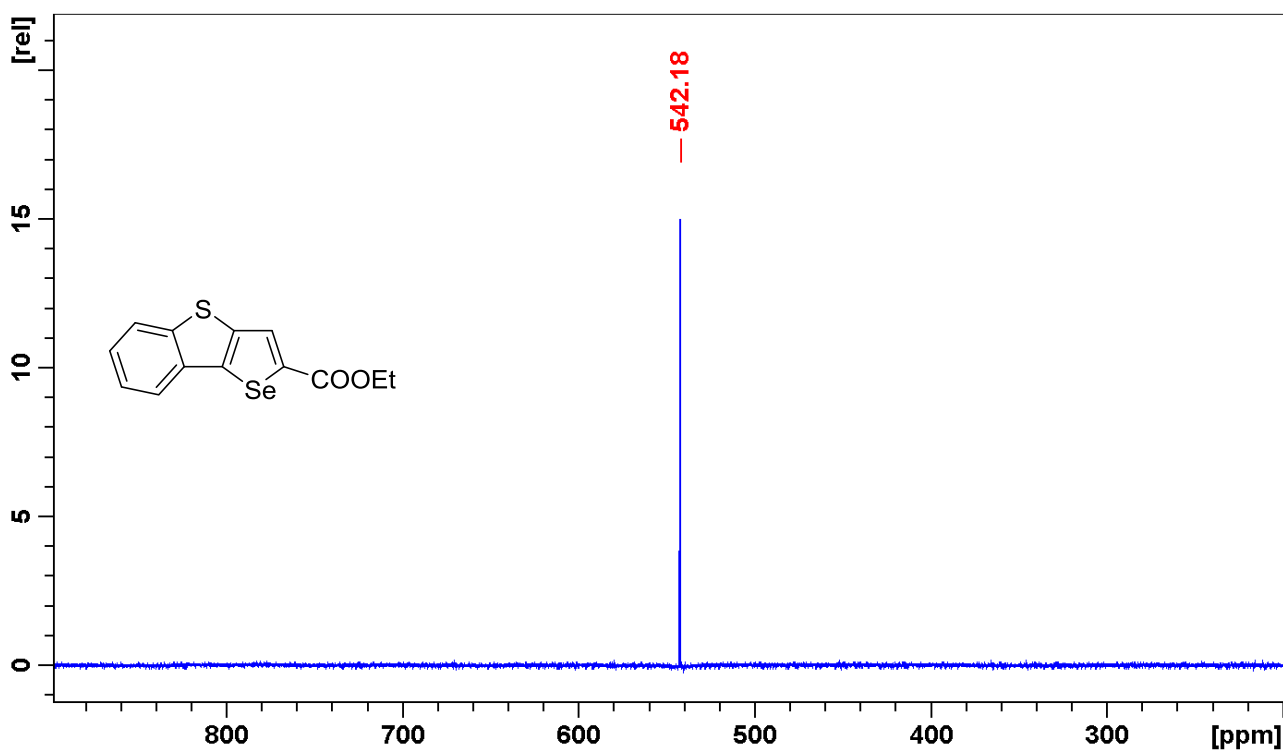


Figure S3. ⁷⁷Se NMR spectrum of compound 3a.

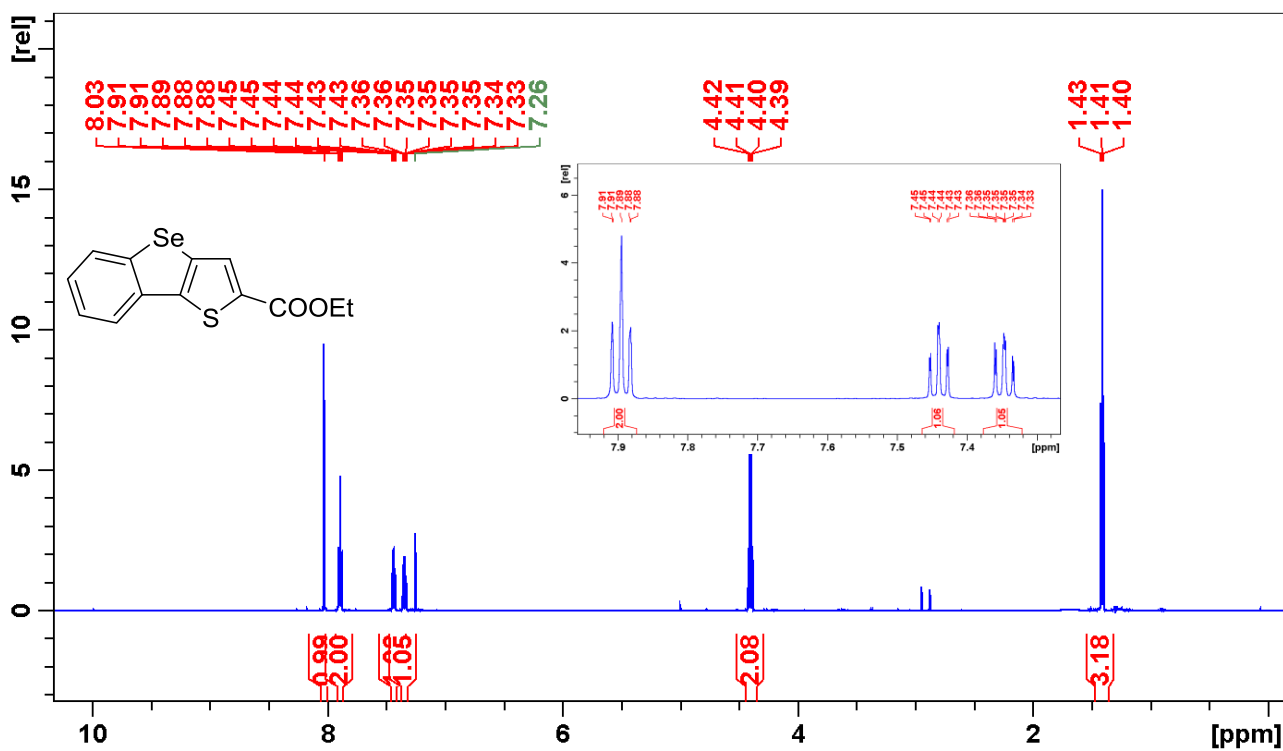


Figure S4. ¹H NMR spectrum of compound 3b.

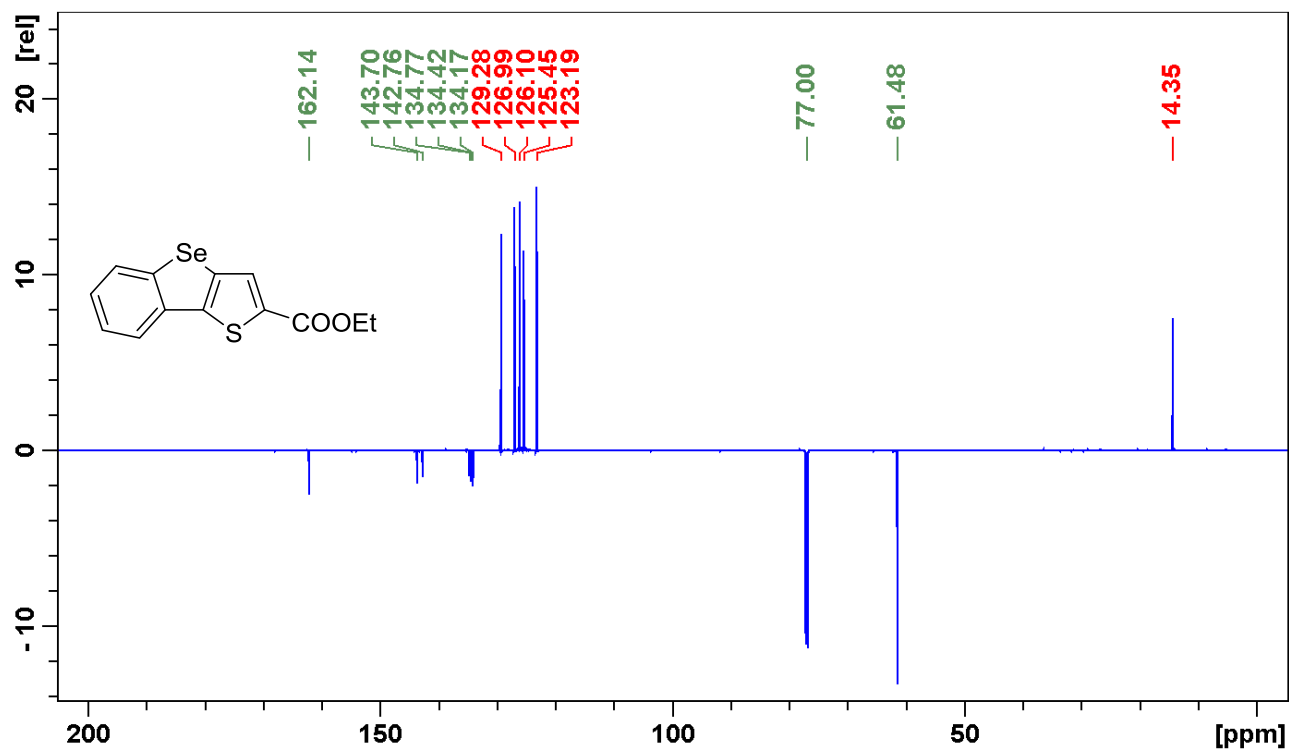


Figure S5. ¹³C NMR spectrum of compound 3b.

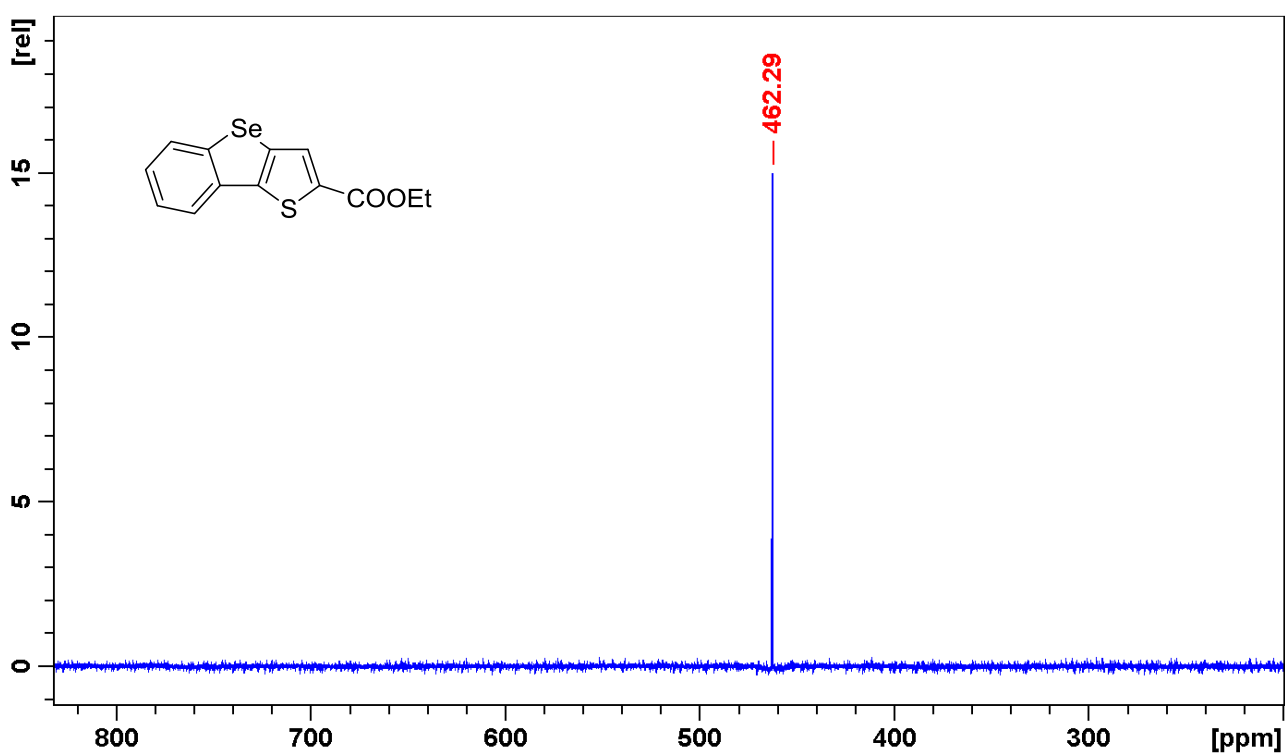


Figure S6. ⁷⁷Se NMR spectrum of compound 3b.

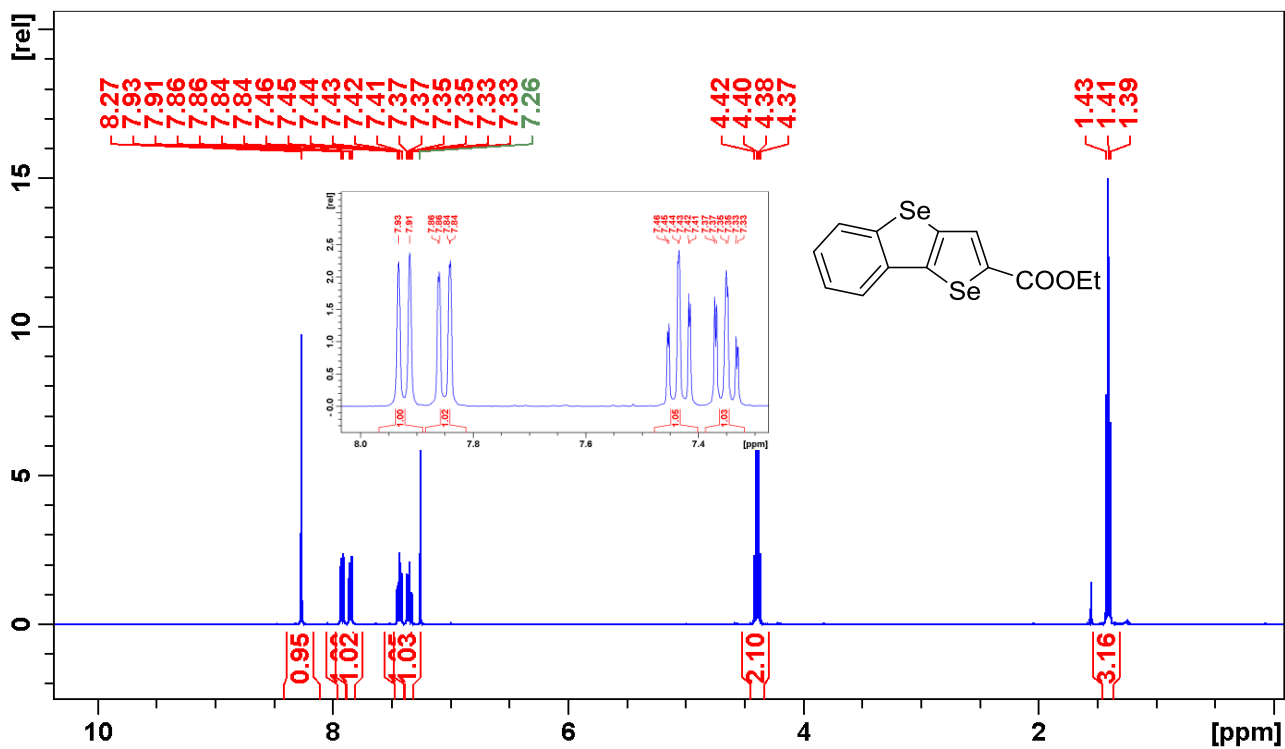


Figure S7. ¹H NMR spectrum of compound 3c.

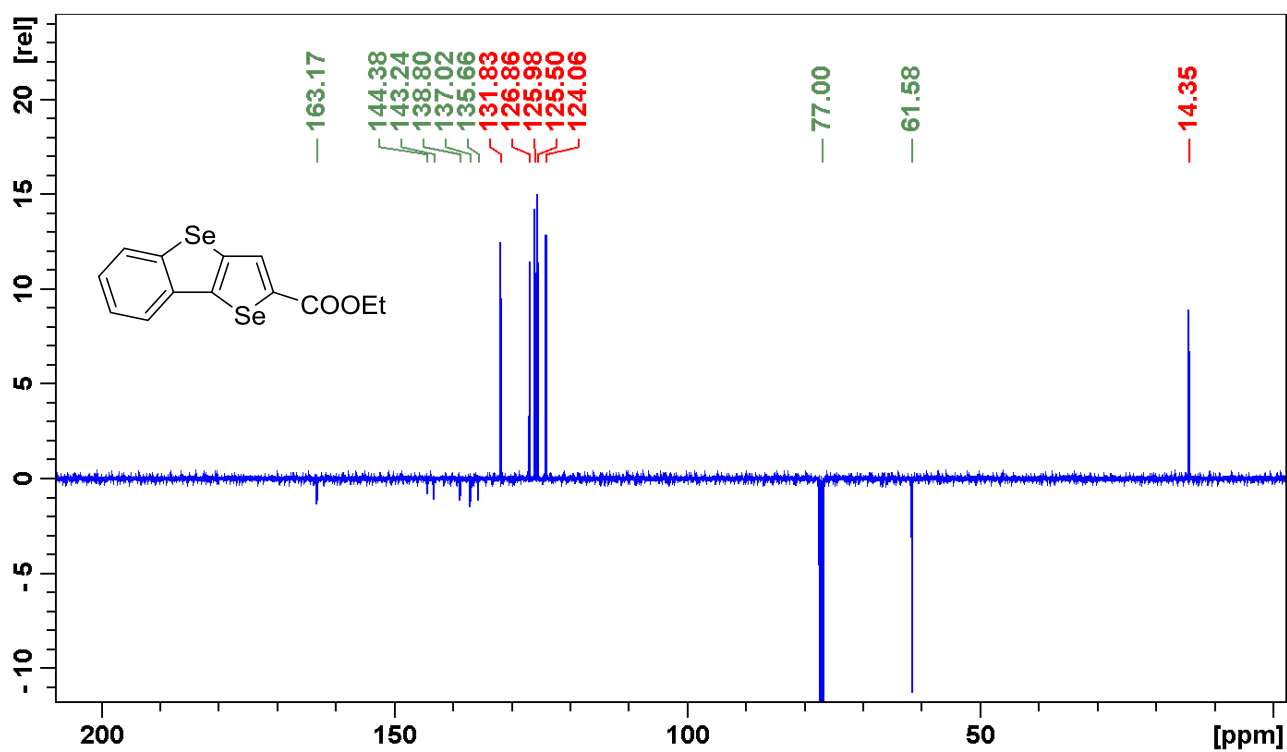


Figure S8. ¹³C NMR spectrum of compound 3c.

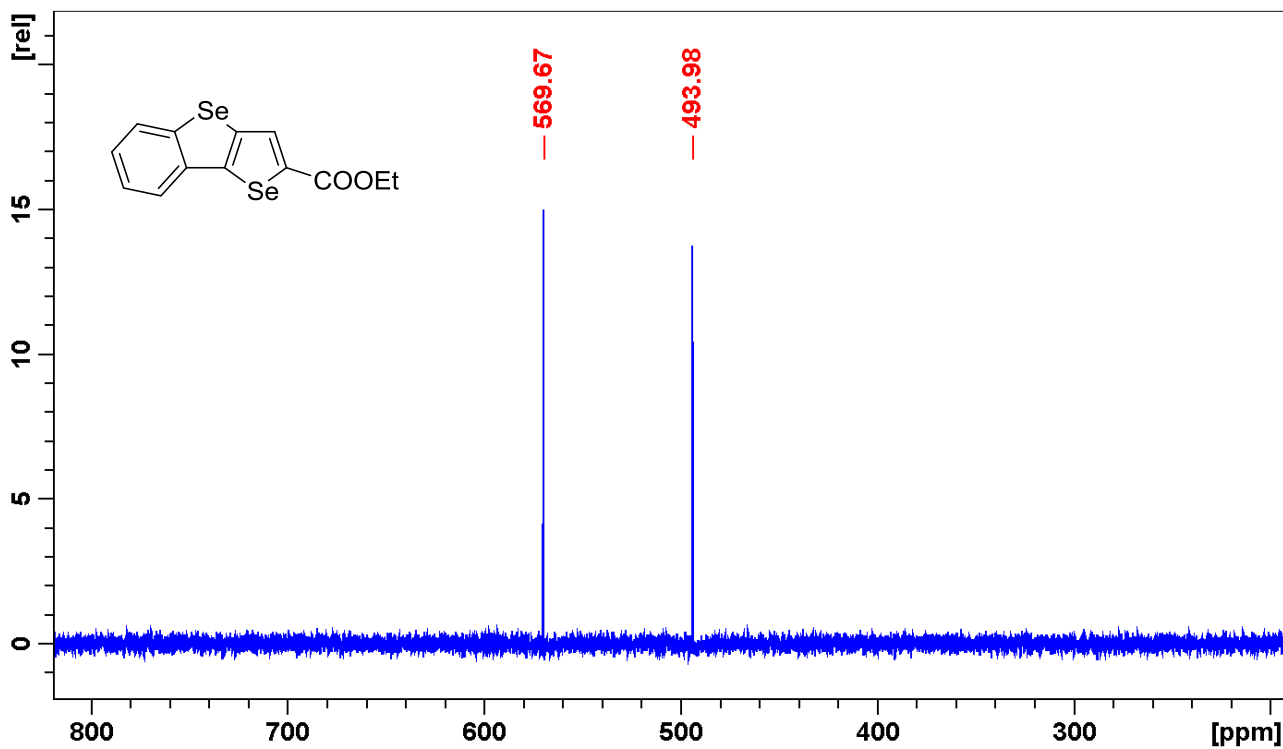


Figure S9. ^{77}Se NMR spectrum of compound **3c**.

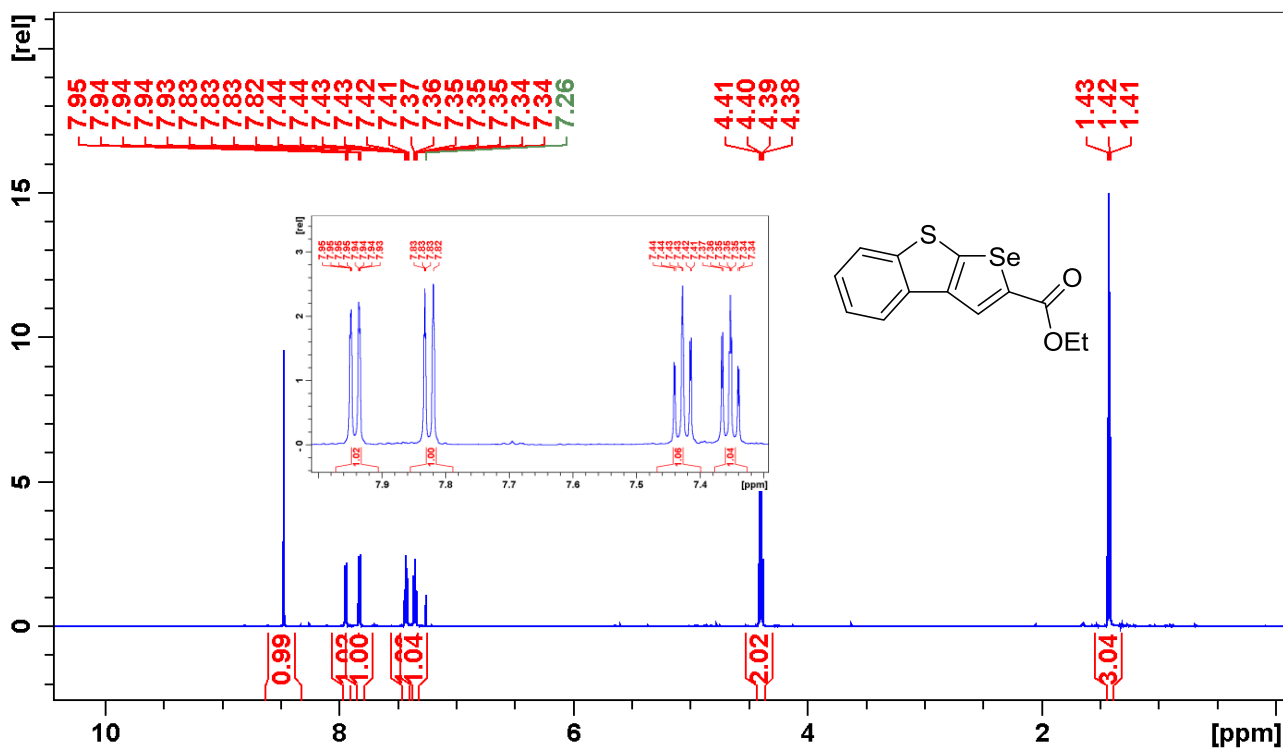


Figure S10. ^1H NMR spectrum of compound **4a**.

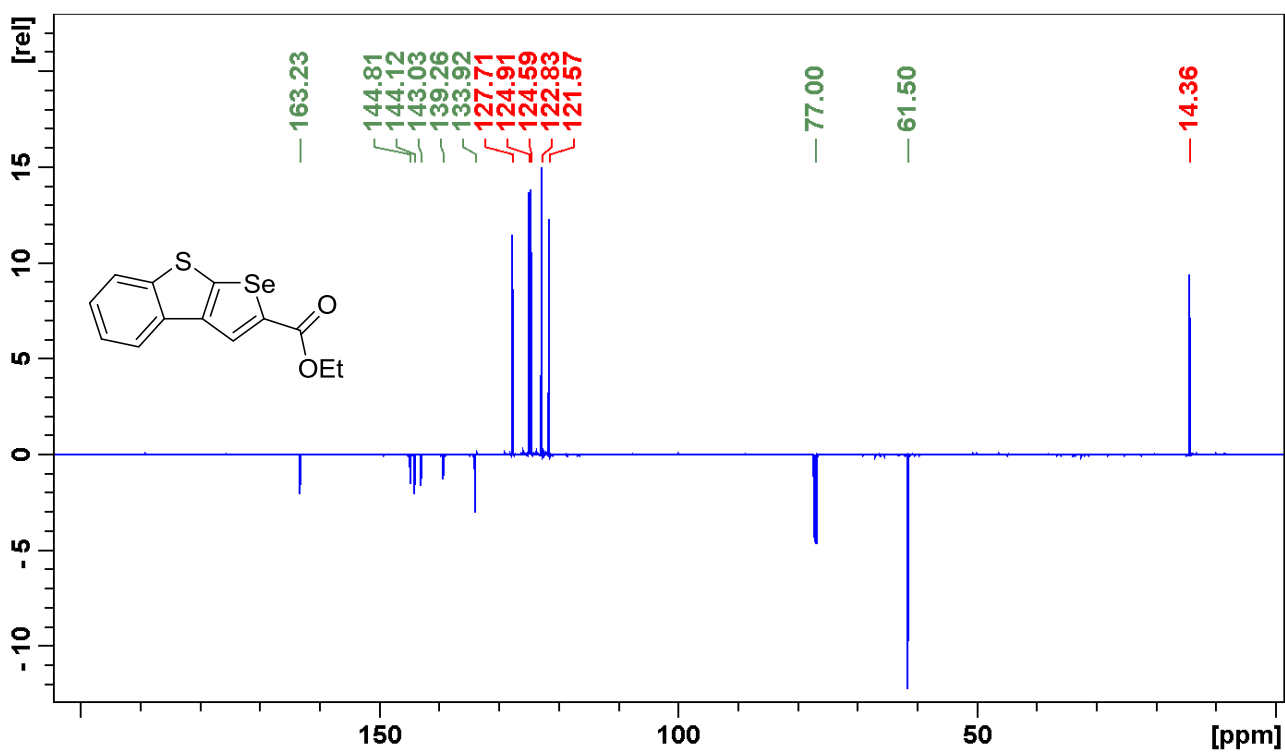


Figure S11. ¹³C NMR spectrum of compound 4a.

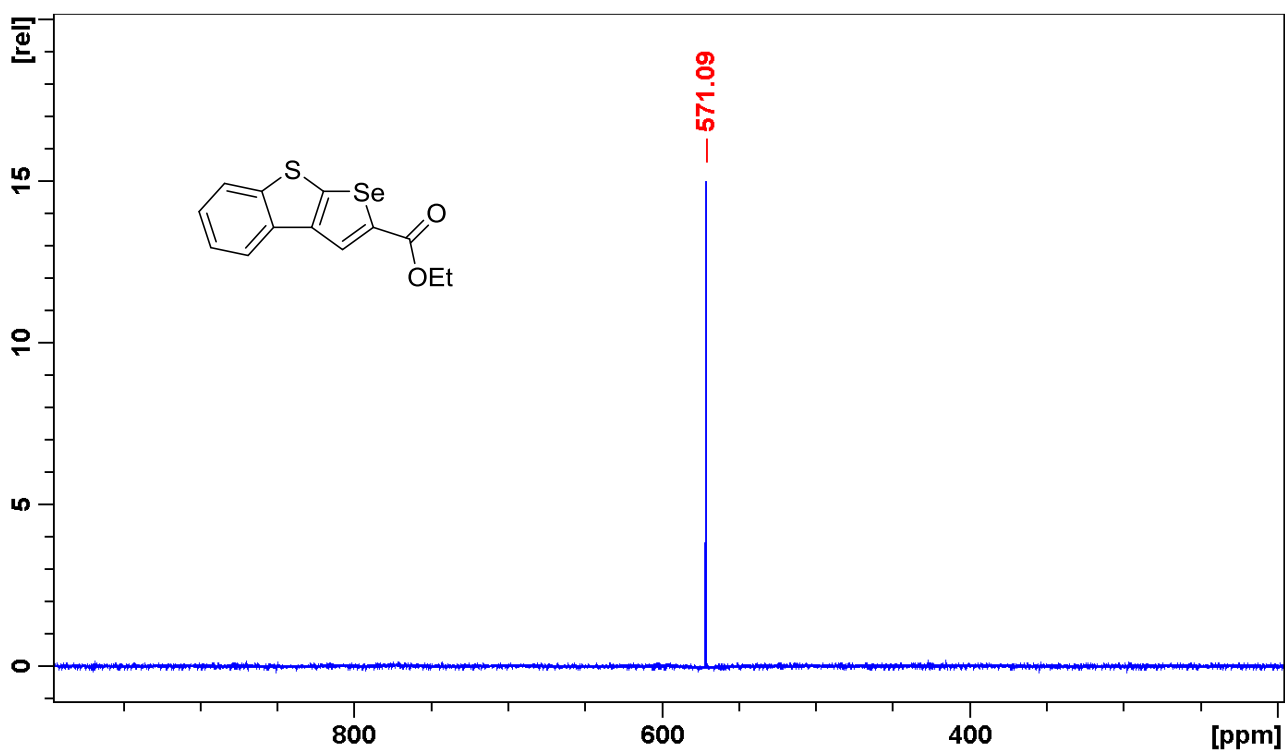


Figure S12. ⁷⁷Se NMR spectrum of compound 4a.

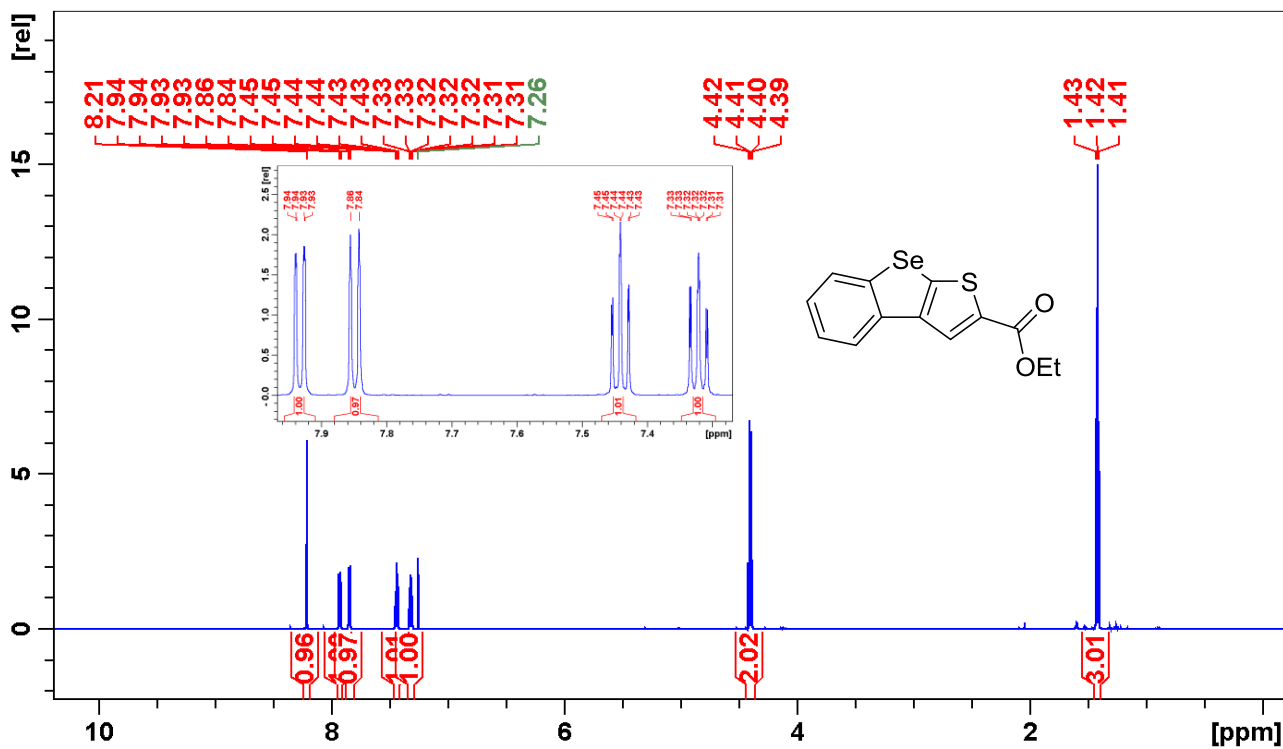


Figure S13. ^1H NMR spectrum of compound **4b**.

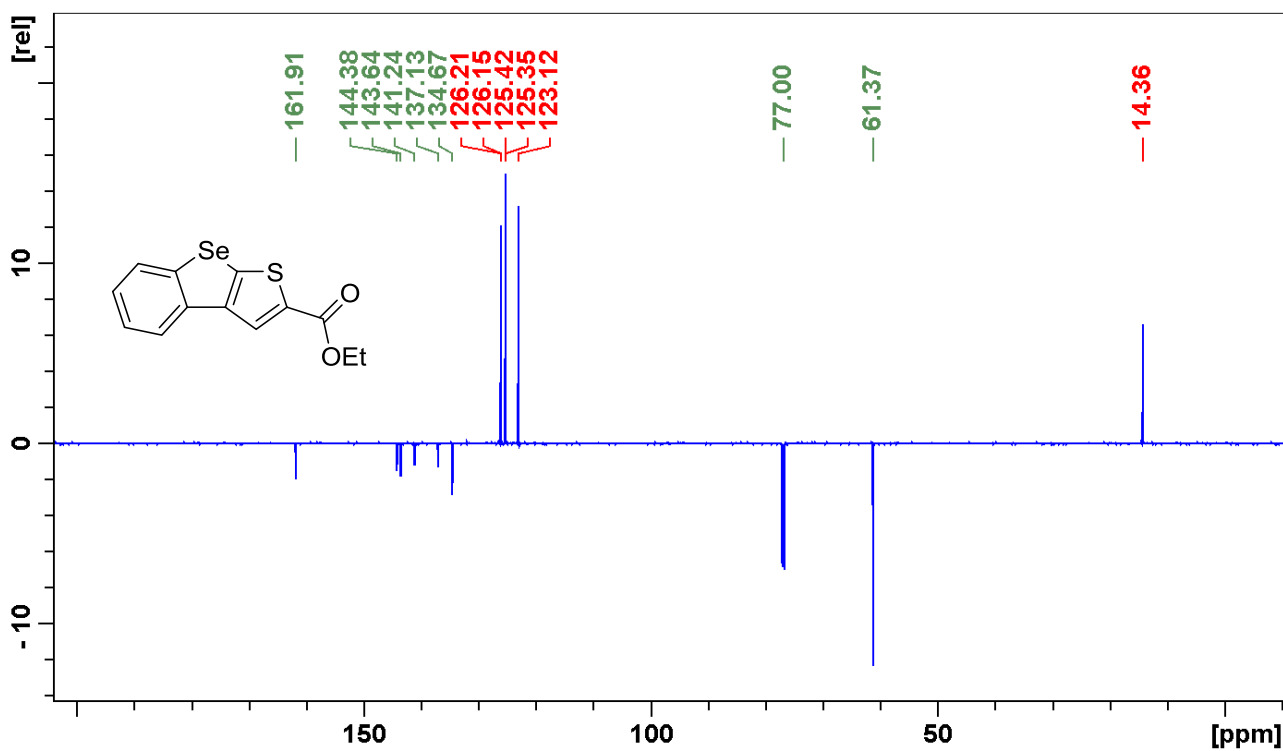


Figure S14. ^{13}C NMR spectrum of compound **4b**.

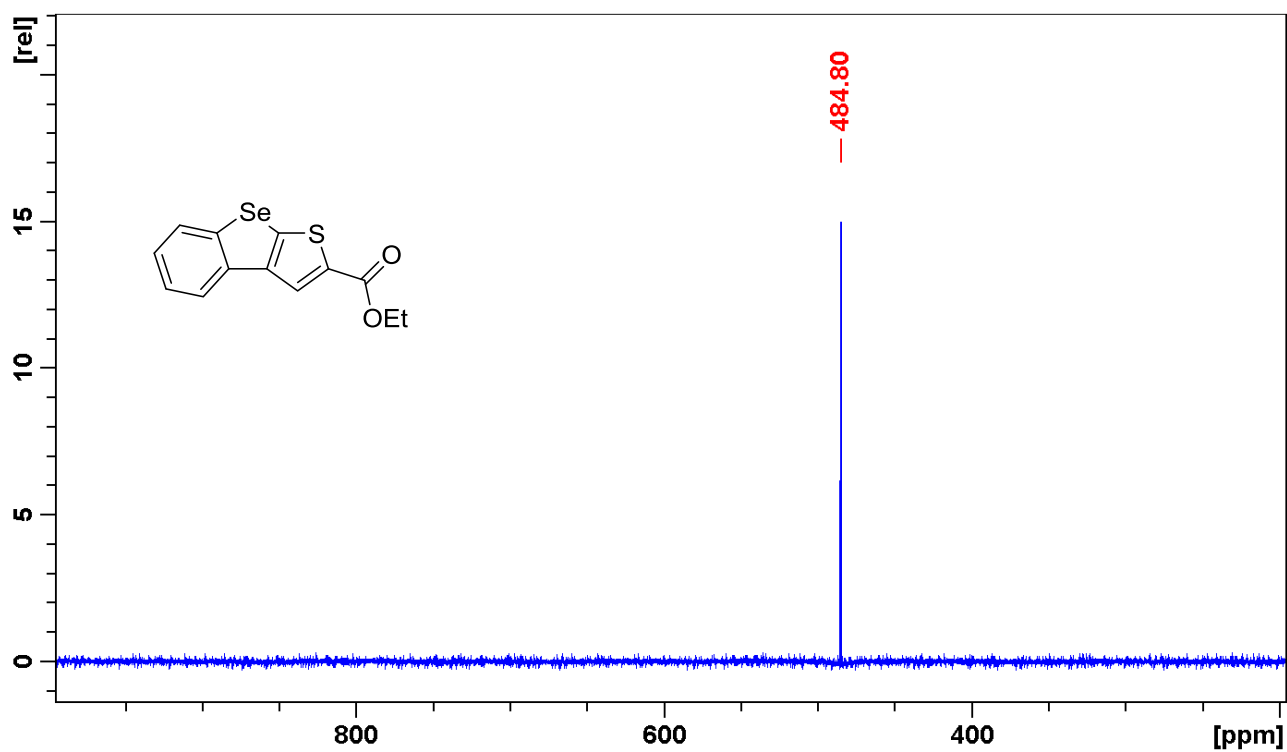


Figure S15. ^{77}Se NMR spectrum of compound 4b.

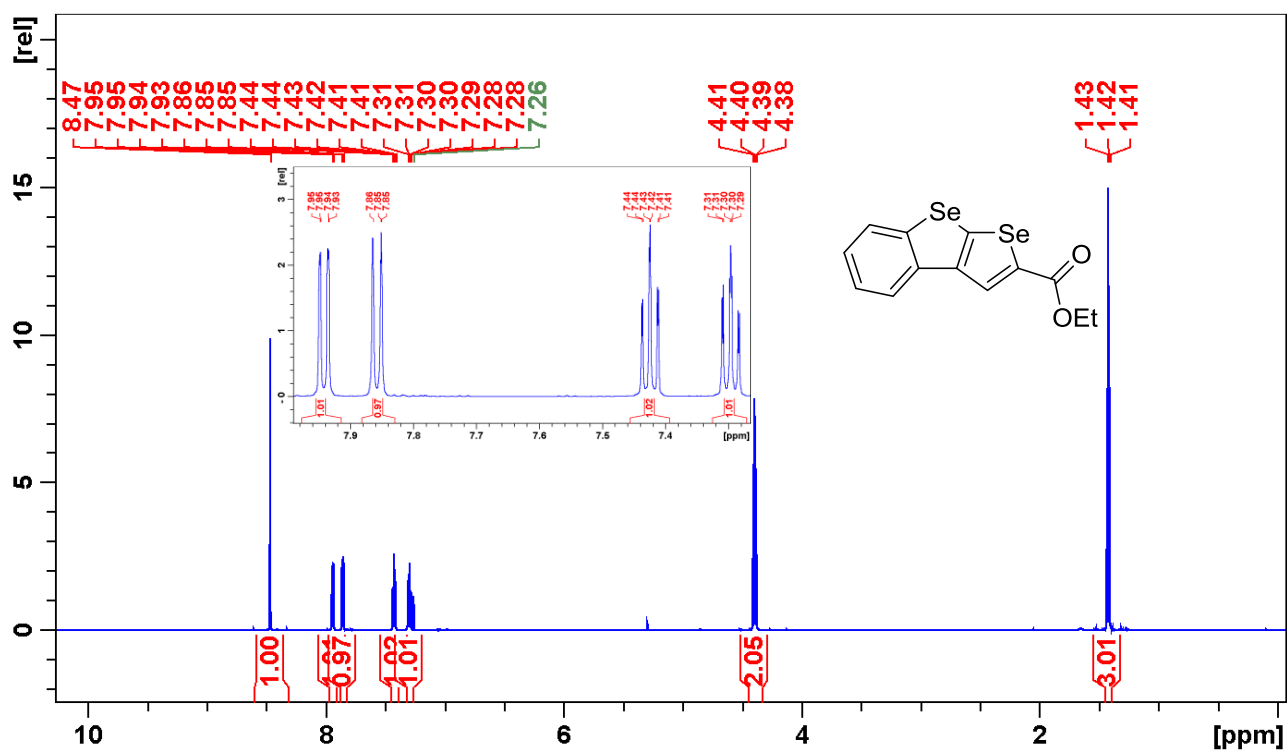


Figure S16. ^1H NMR spectrum of compound 4c.

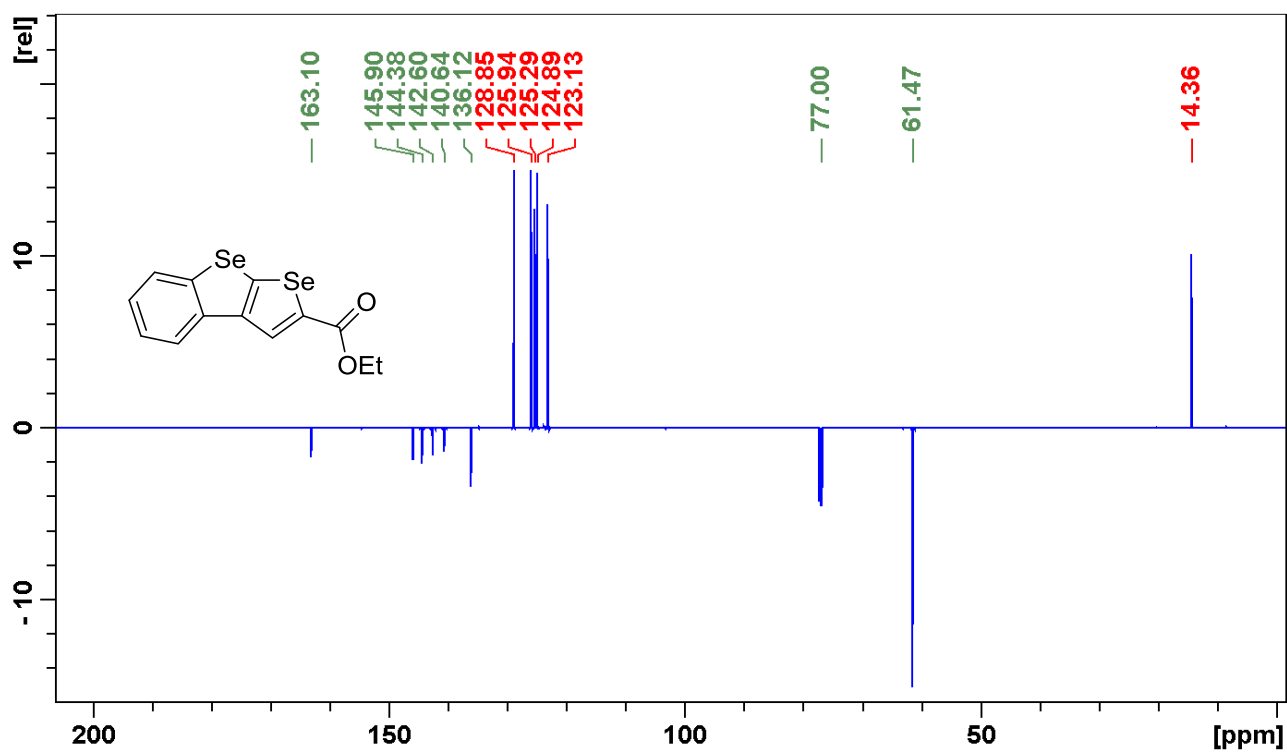


Figure S17. ^{13}C NMR spectrum of compound 4c.

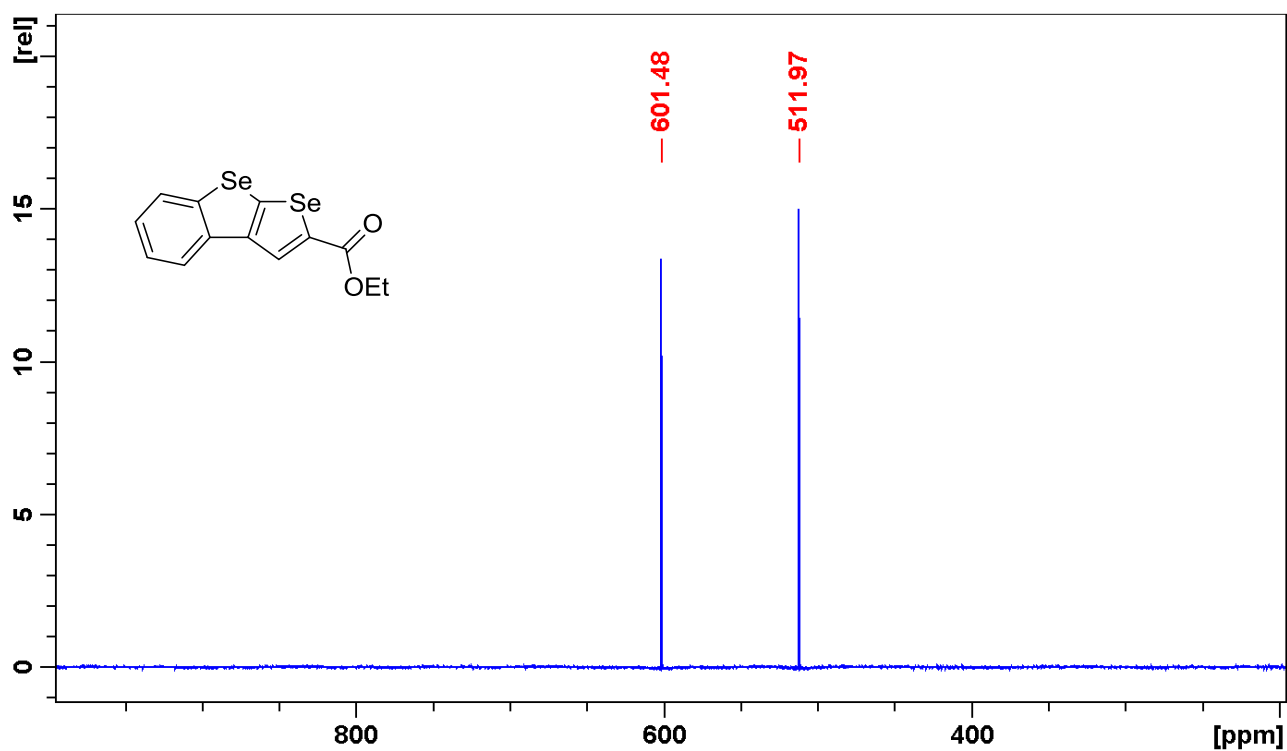


Figure S18. ^{77}Se NMR spectrum of compound 4c.

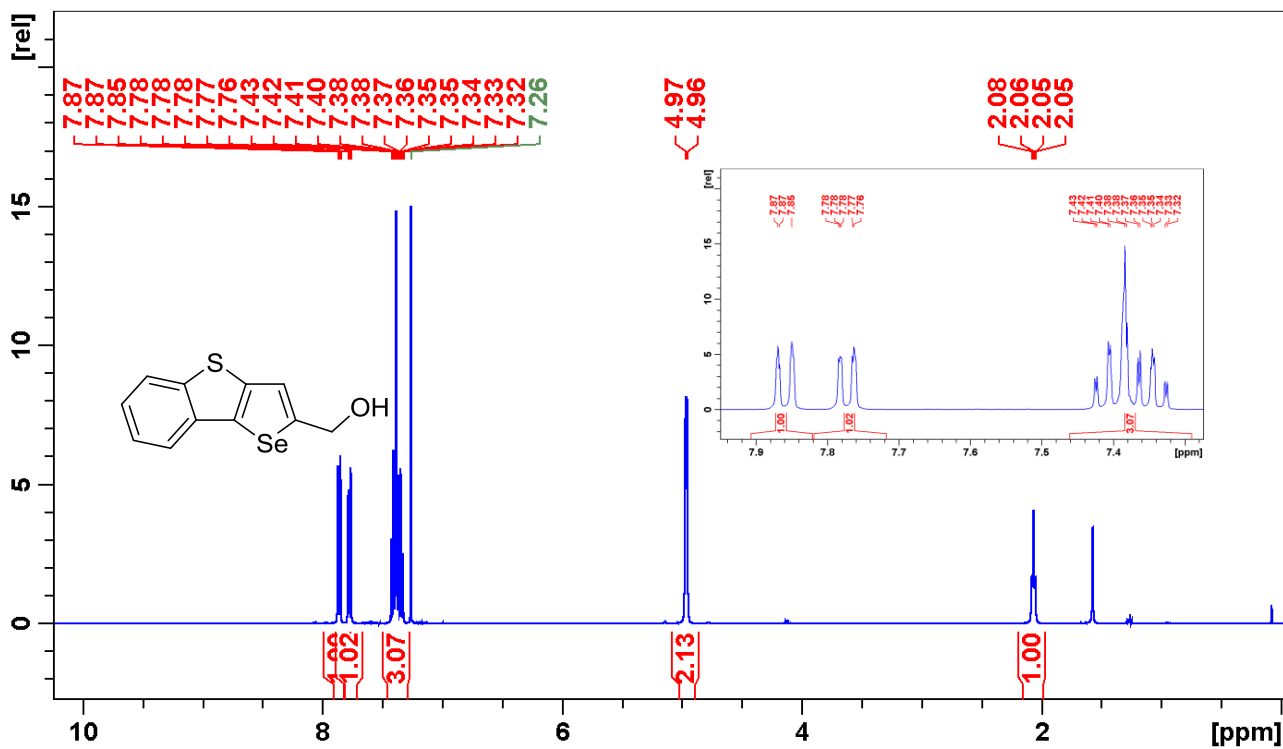


Figure S19. ¹H NMR spectrum of compound 5a.

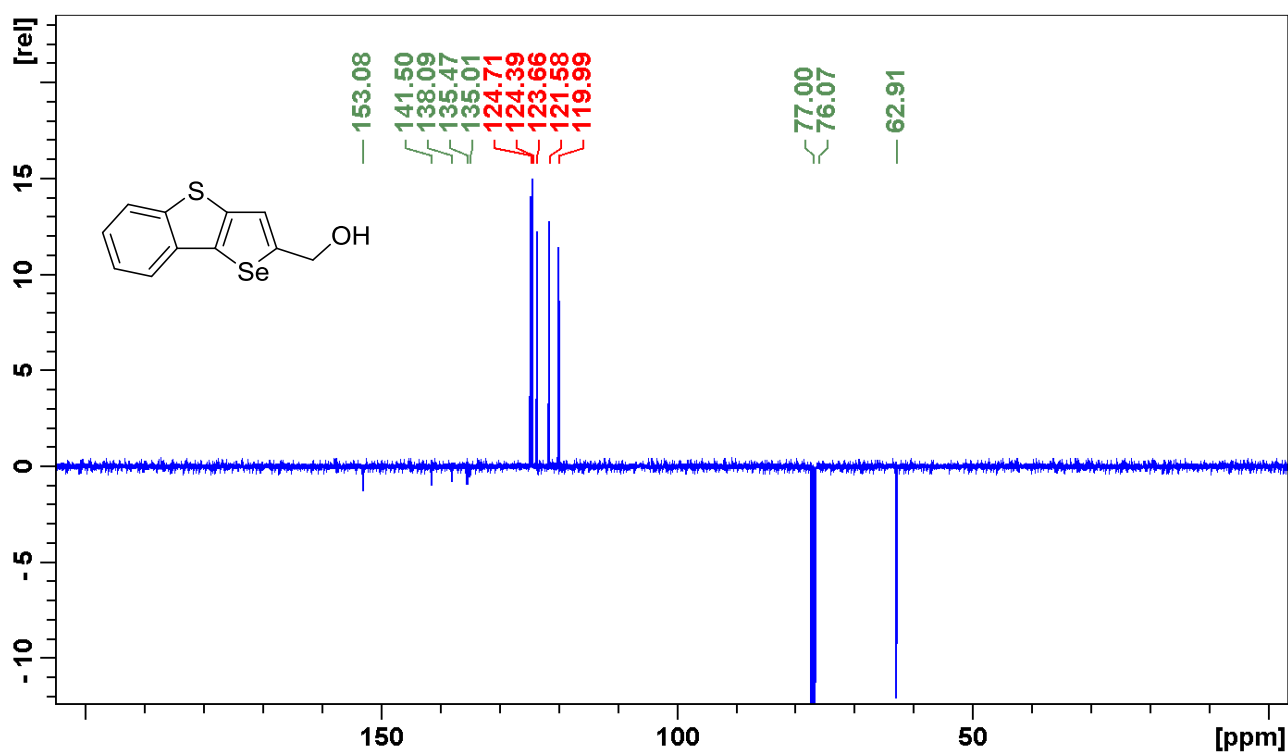


Figure S20. ¹³C NMR spectrum of compound 5a.

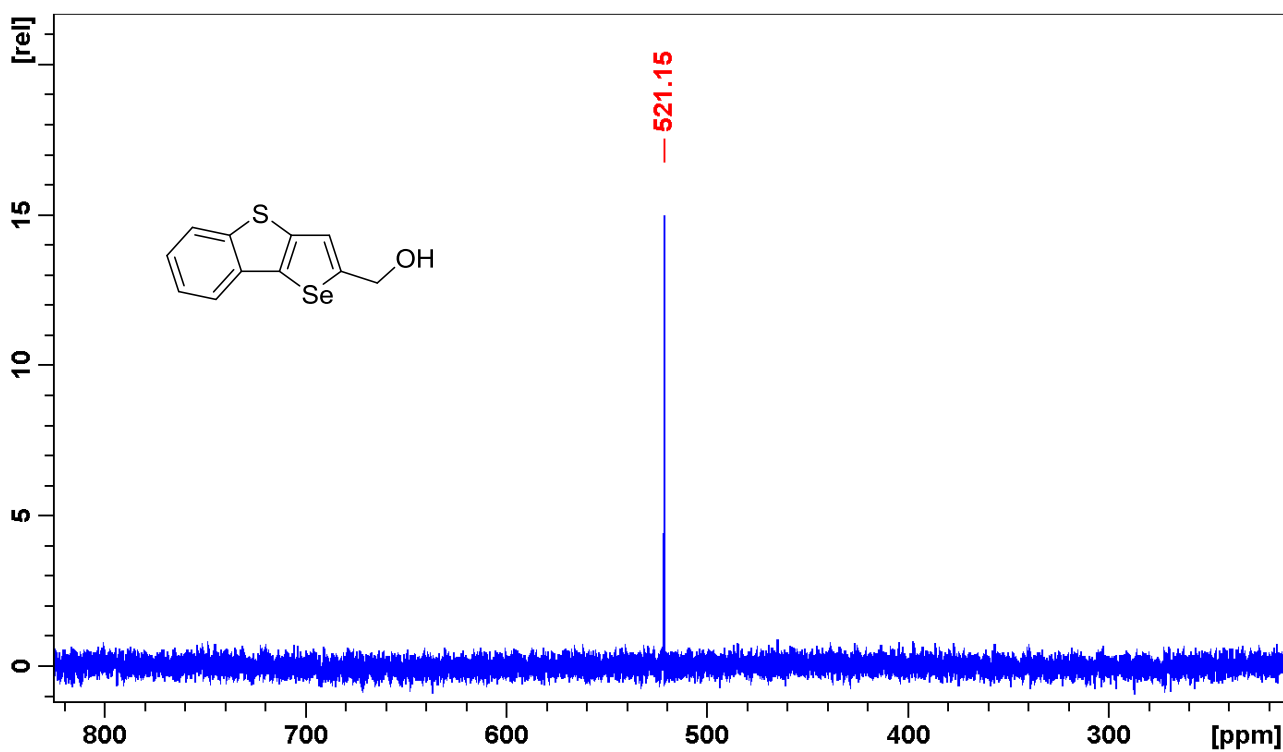


Figure S21. ^{77}Se NMR spectrum of compound 5a.

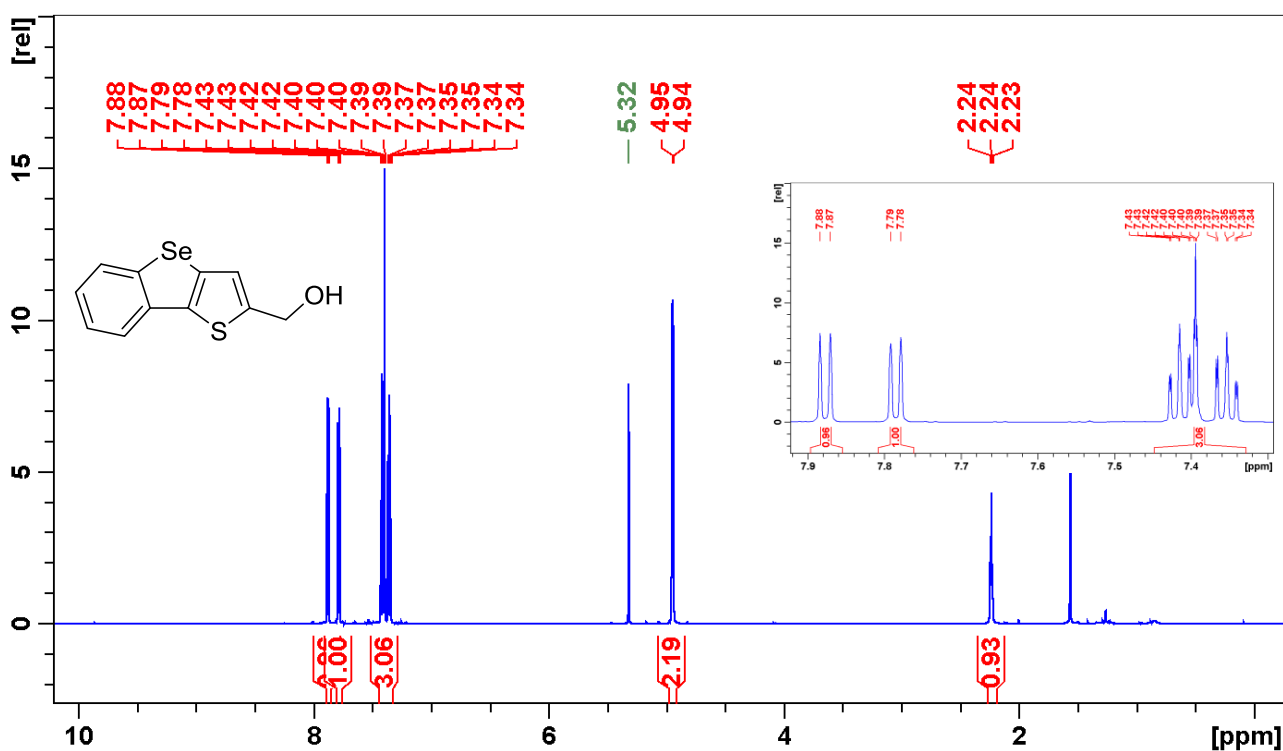


Figure S22. ^1H NMR spectrum of compound 5b.

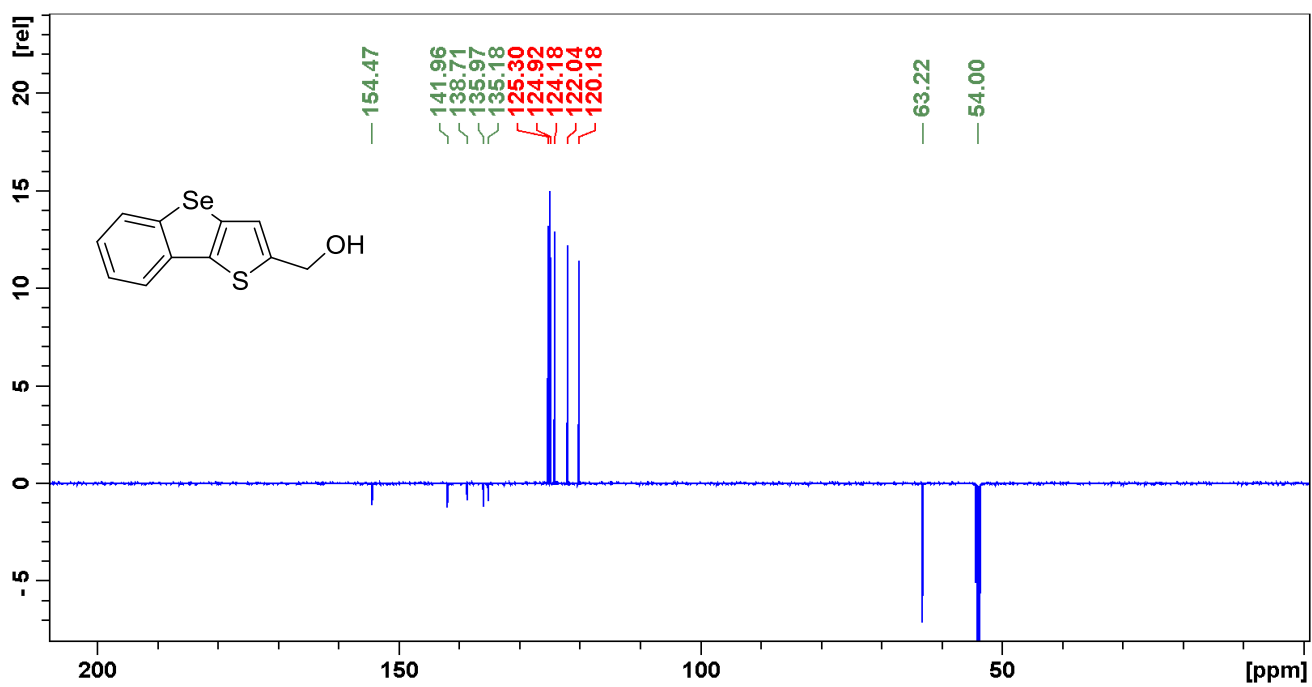


Figure S23. ¹³C NMR spectrum of compound **5b**.

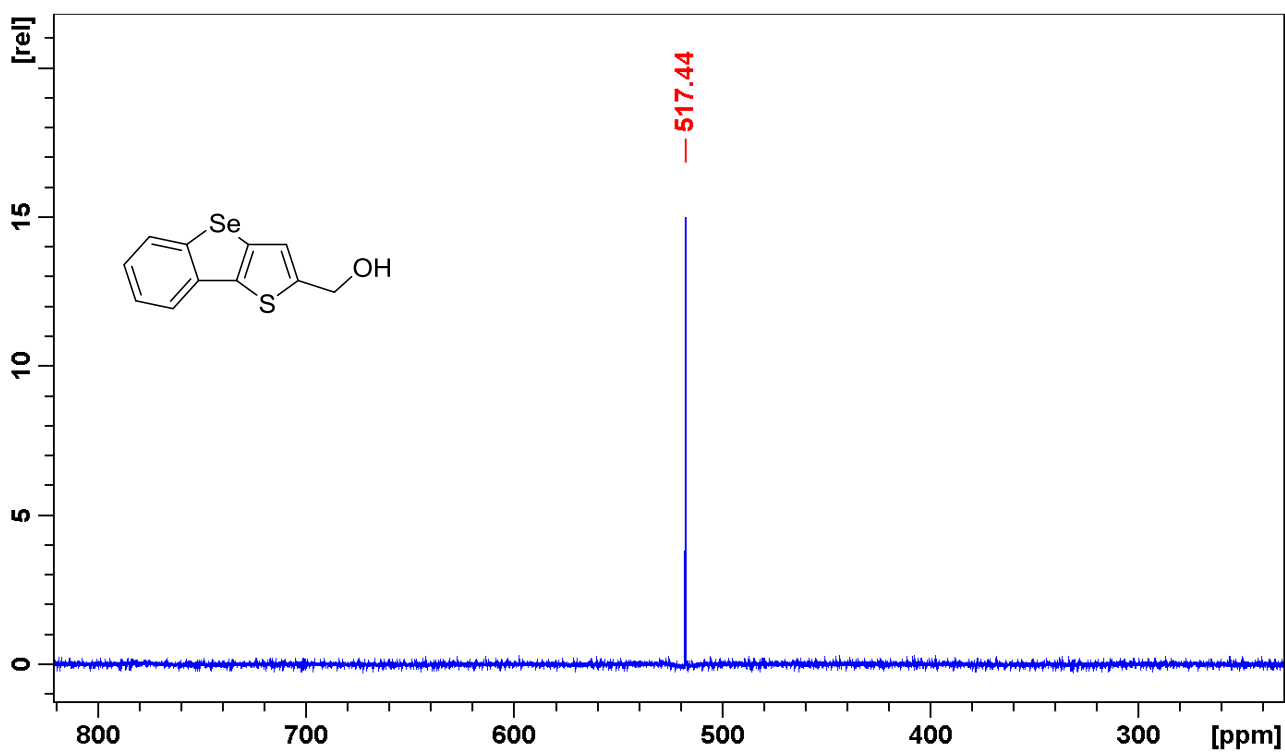


Figure S24. ⁷⁷Se NMR spectrum of compound **5b**.

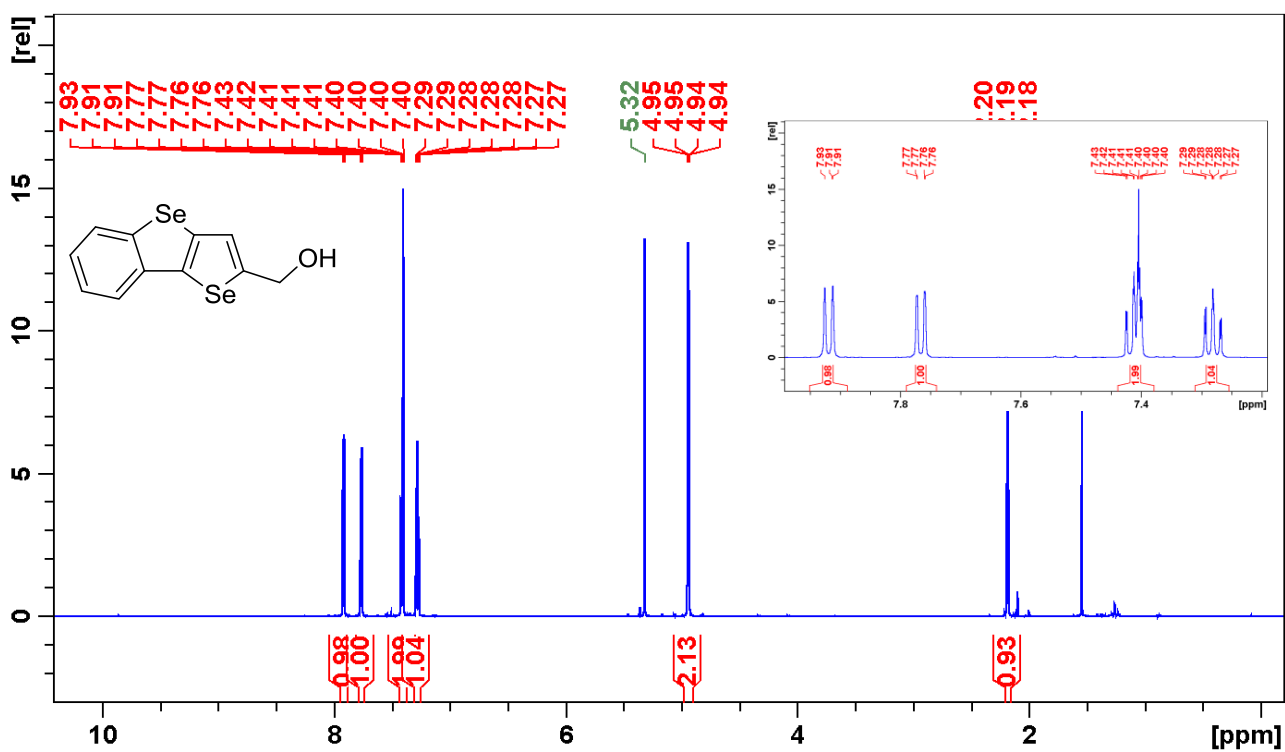


Figure S25. ¹H NMR spectrum of compound 5c.

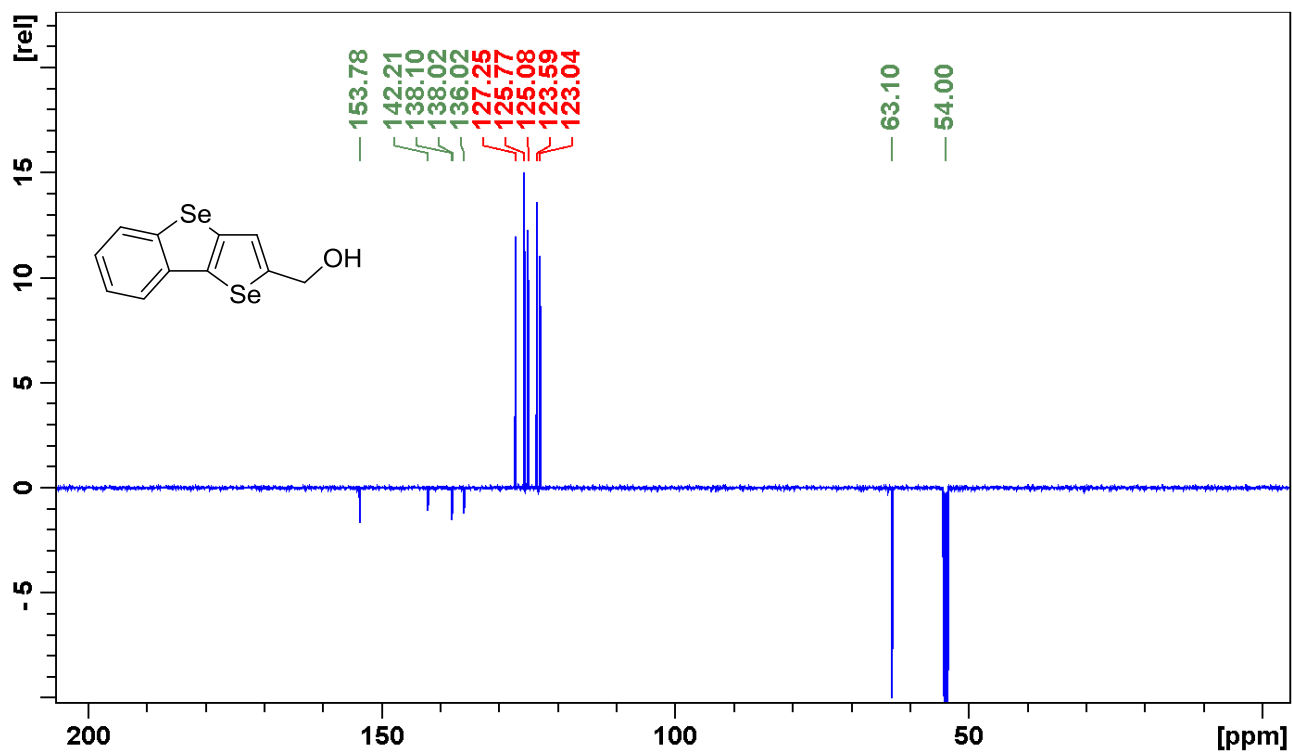


Figure S26. ¹³C NMR spectrum of compound 5c.

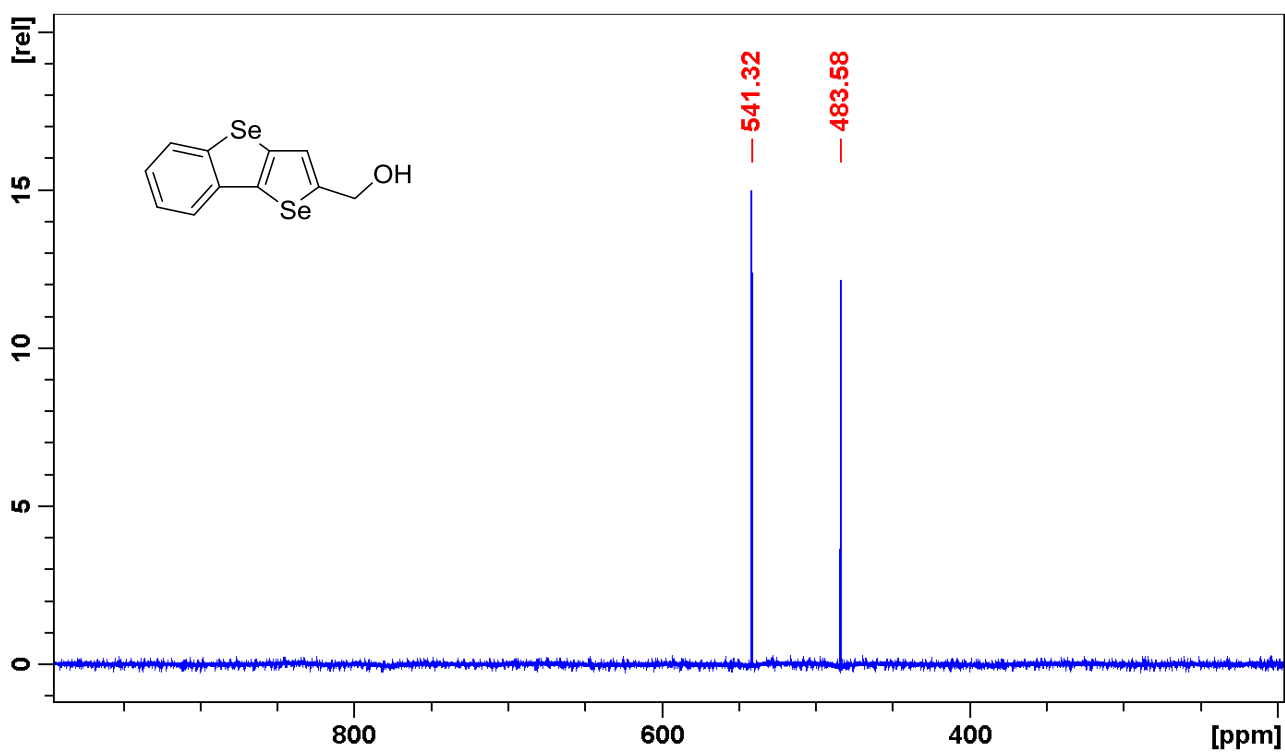


Figure S27. ^{77}Se NMR spectrum of compound **5c**.

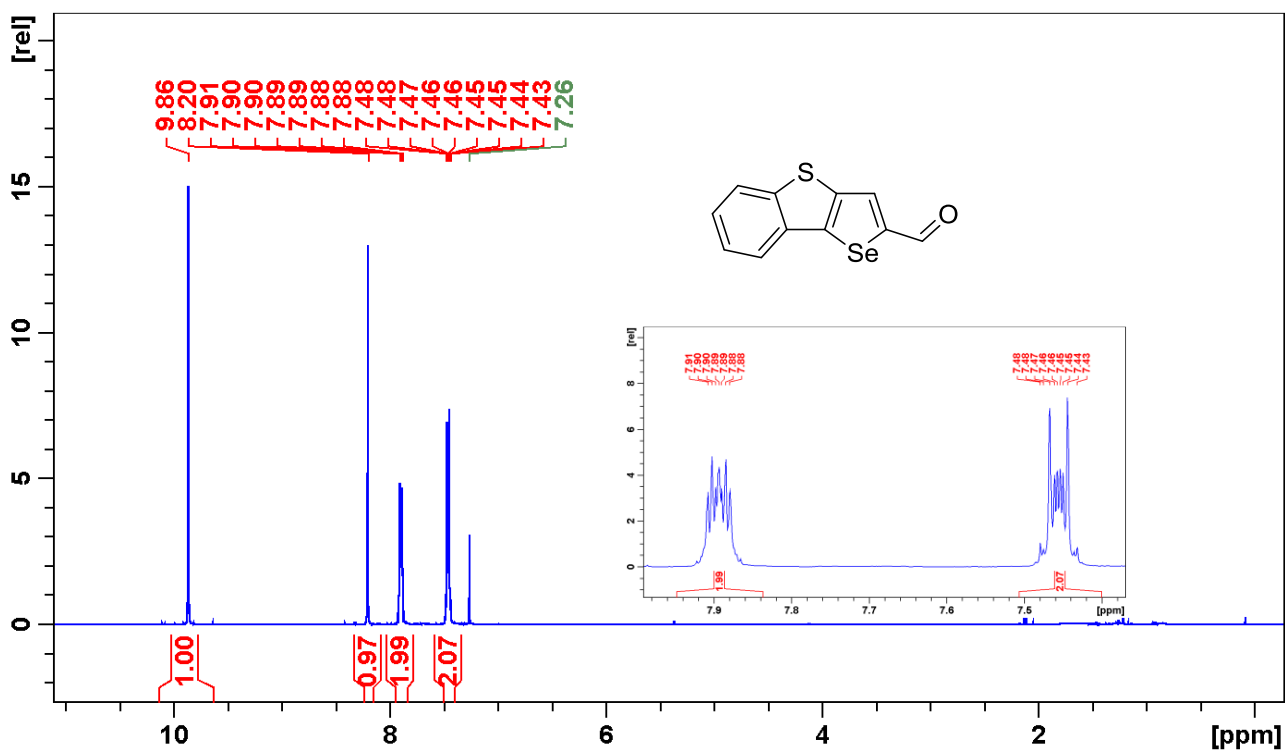


Figure S28. ^1H NMR spectrum of compound **6a**.

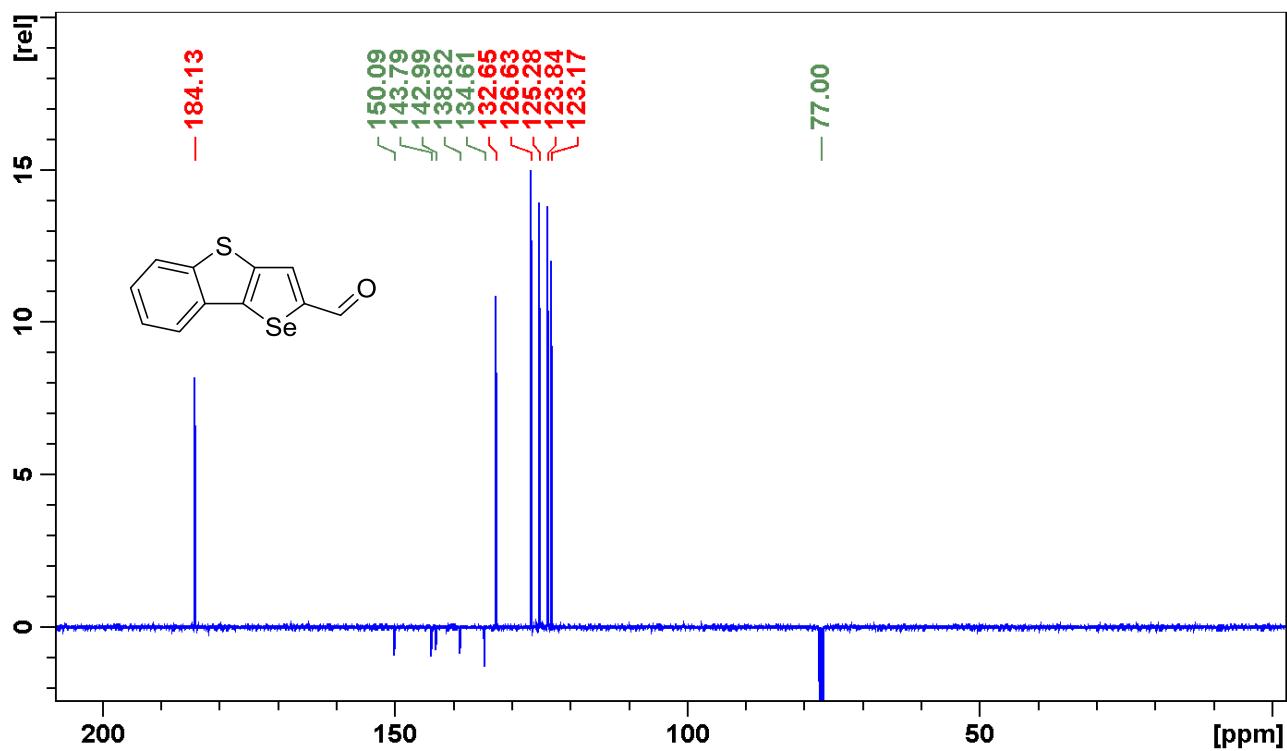


Figure S29. ^{13}C NMR spectrum of compound **6a**.

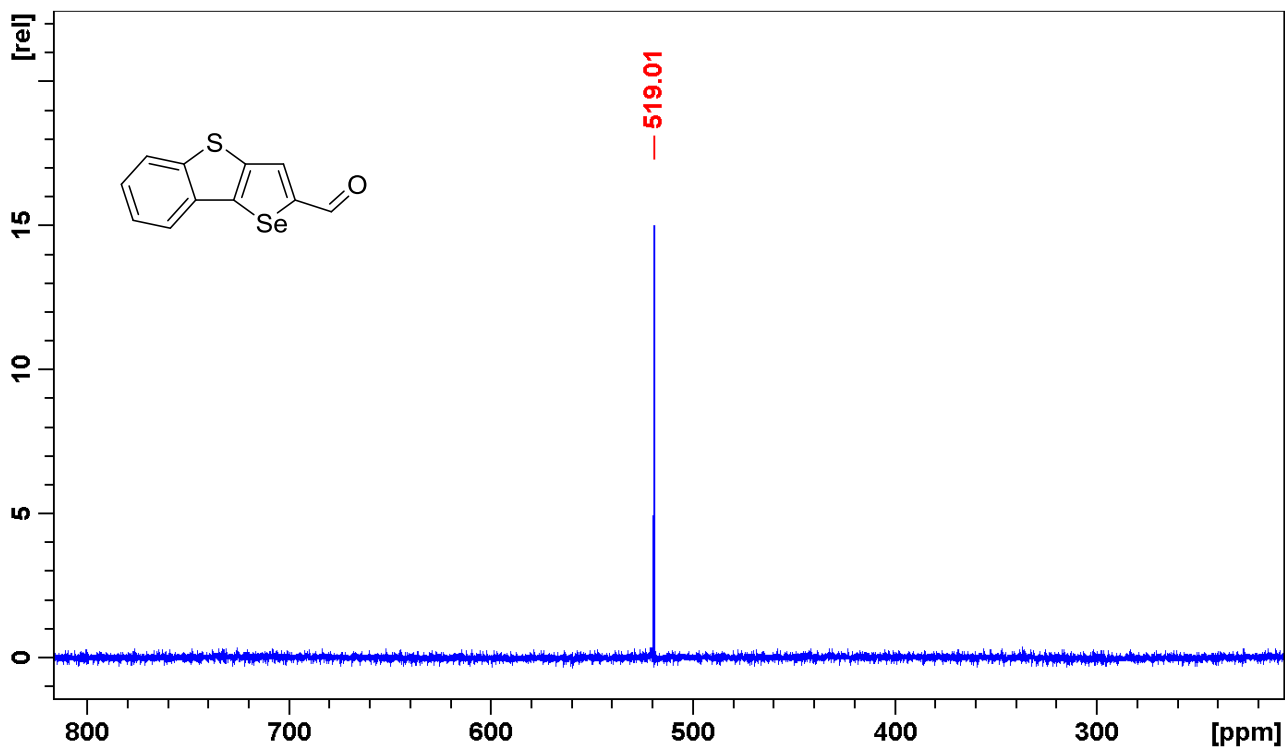


Figure S30. ^{77}Se NMR spectrum of compound **6a**.

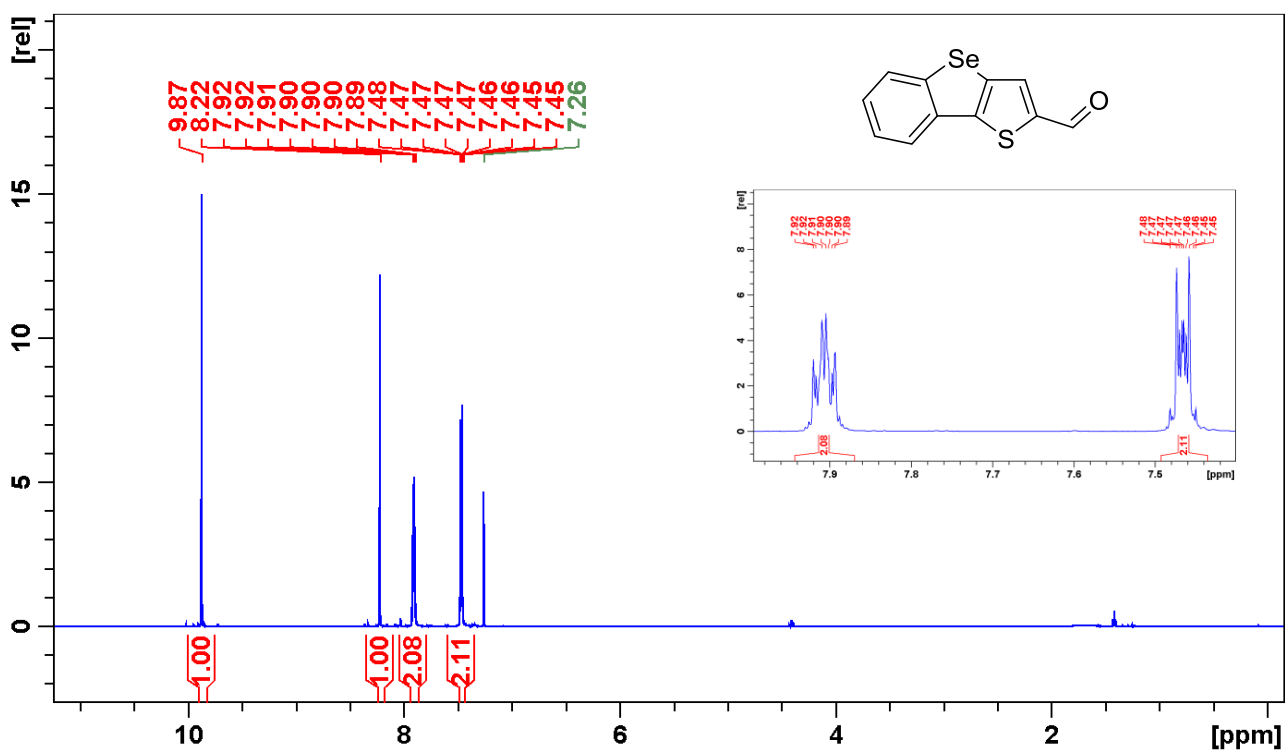


Figure S31. ¹H NMR spectrum of compound **6b**.

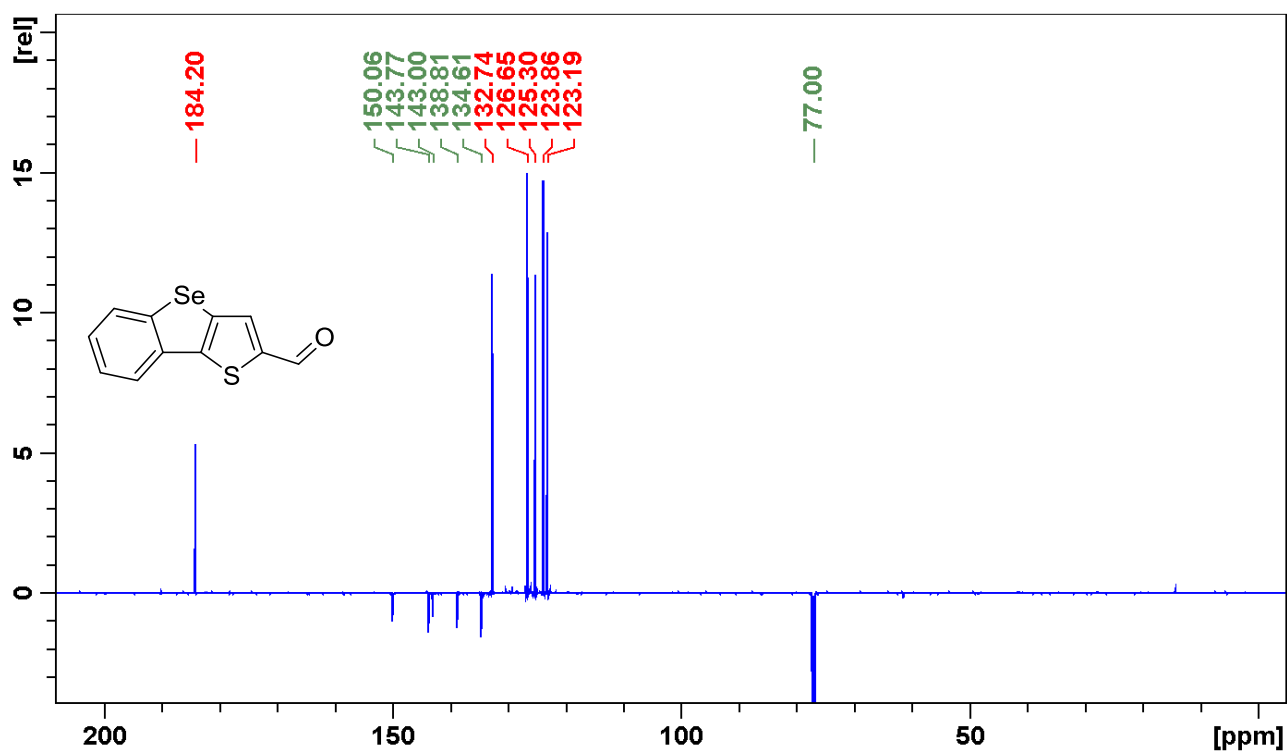


Figure S32. ¹³C NMR spectrum of compound **6b**.

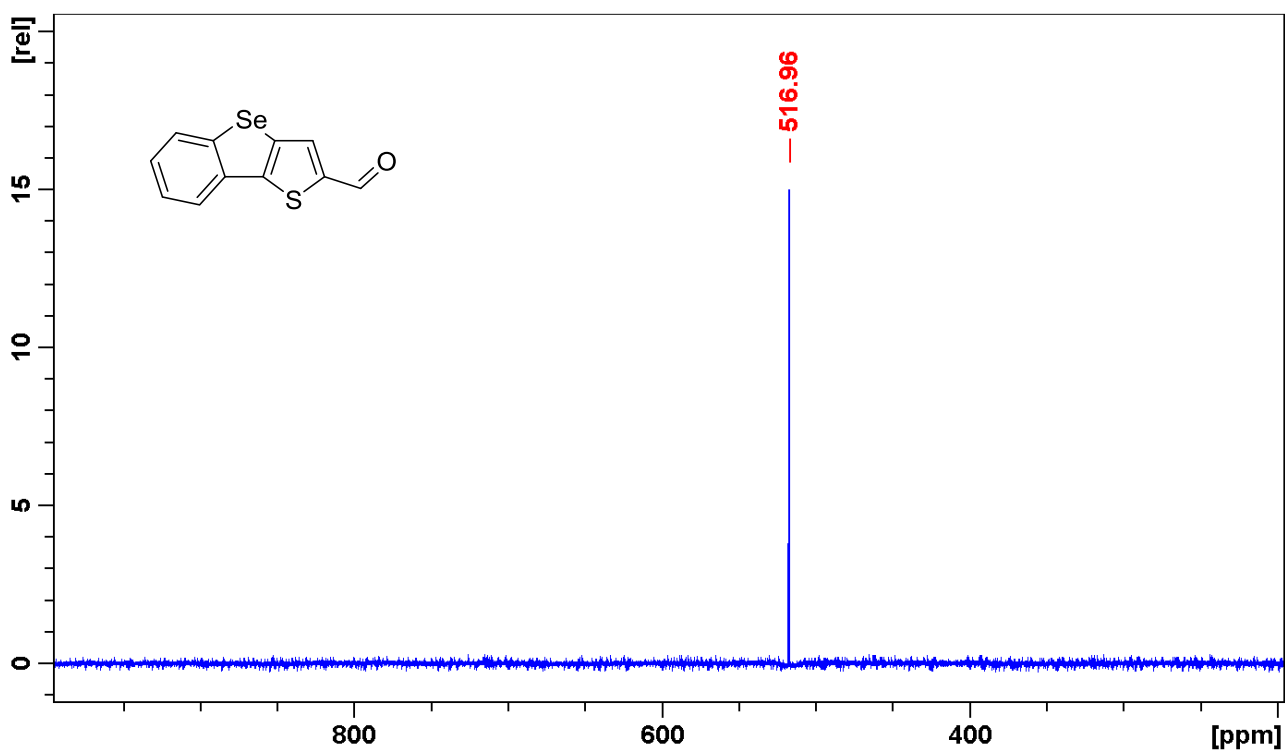


Figure S33. ⁷⁷Se NMR spectrum of compound **6b**.

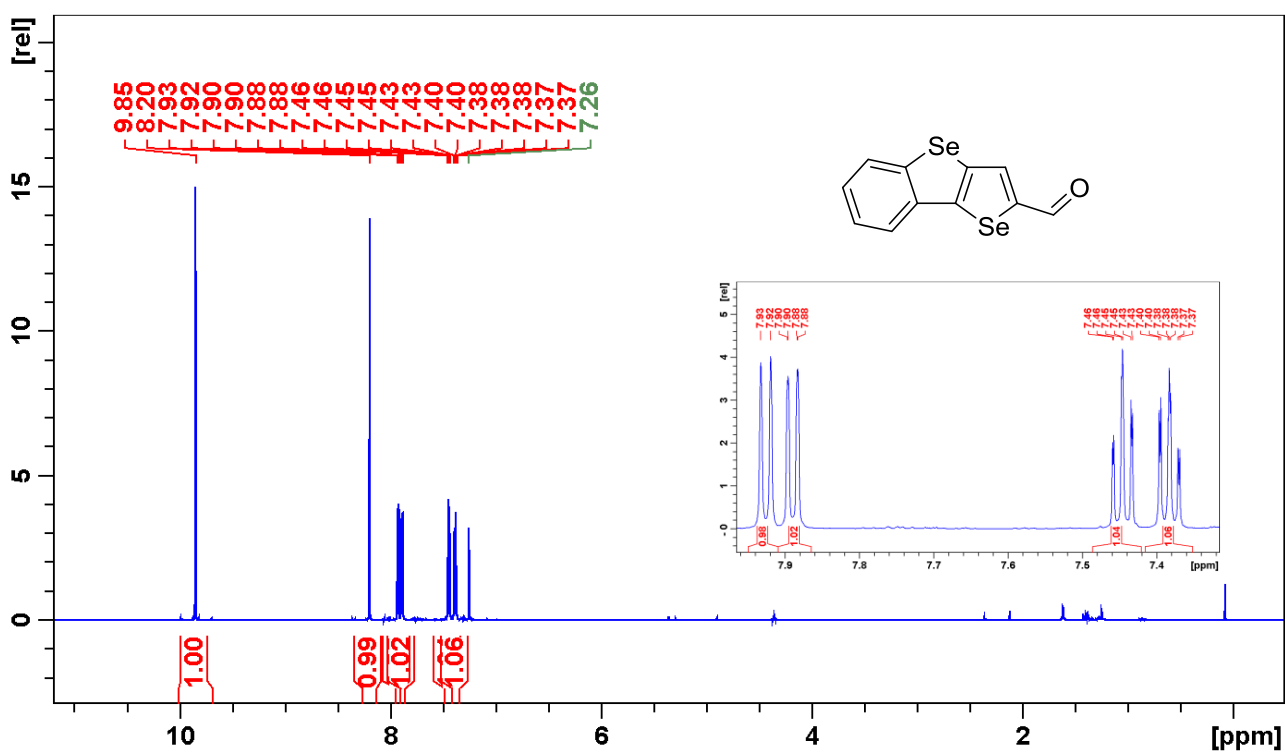


Figure S34. ¹H NMR spectrum of compound **6c**.

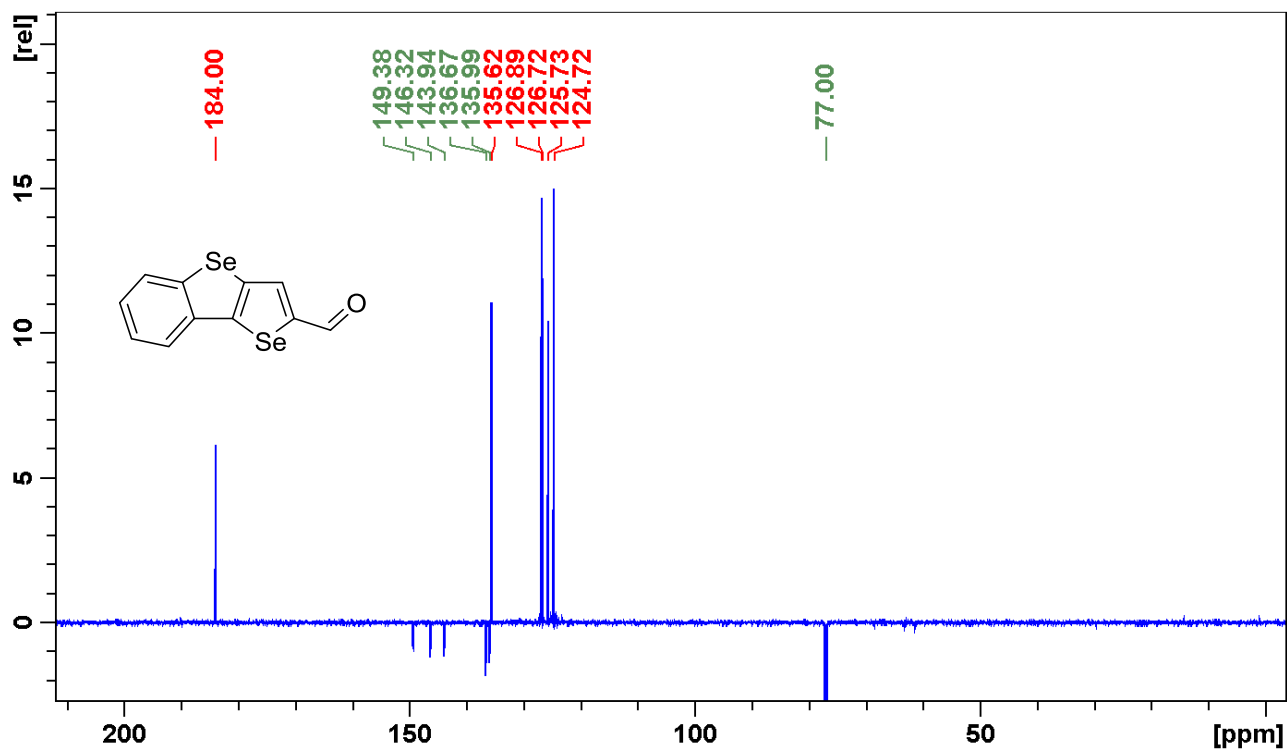


Figure S35. ¹³C NMR spectrum of compound 6c.

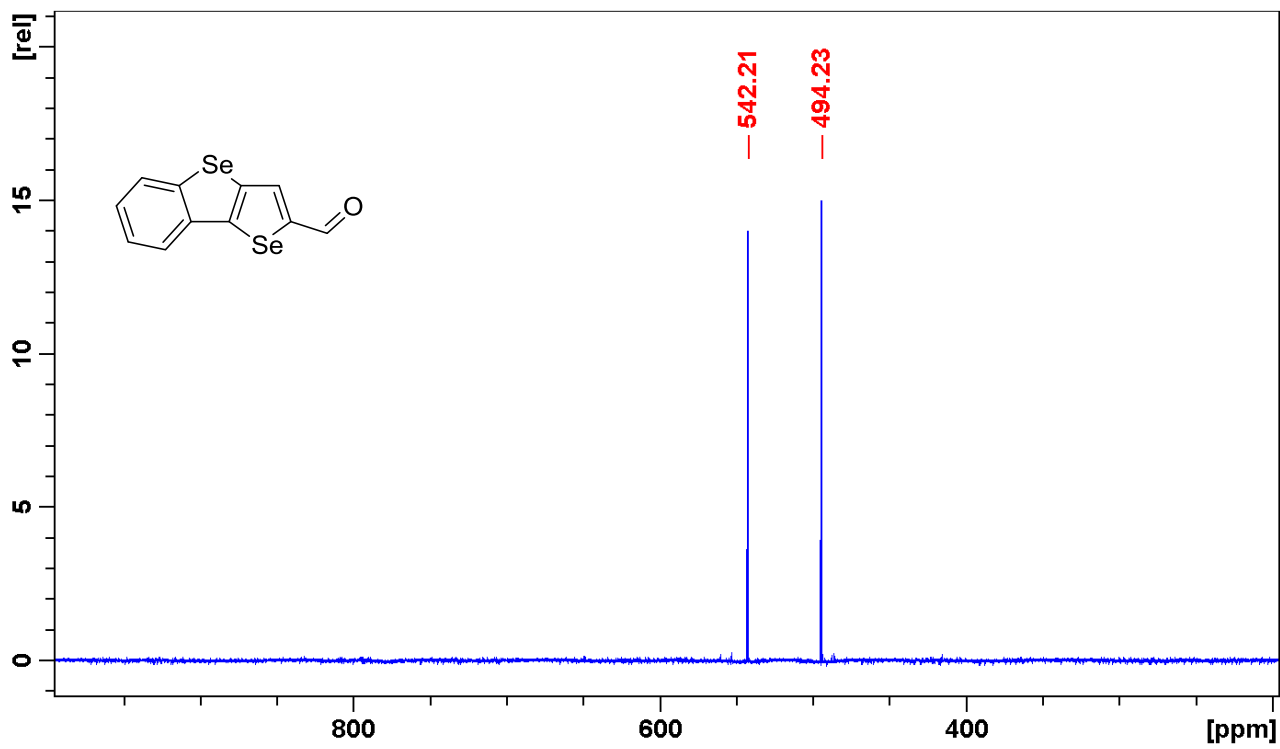


Figure S36. ⁷⁷Se NMR spectrum of compound 6c.

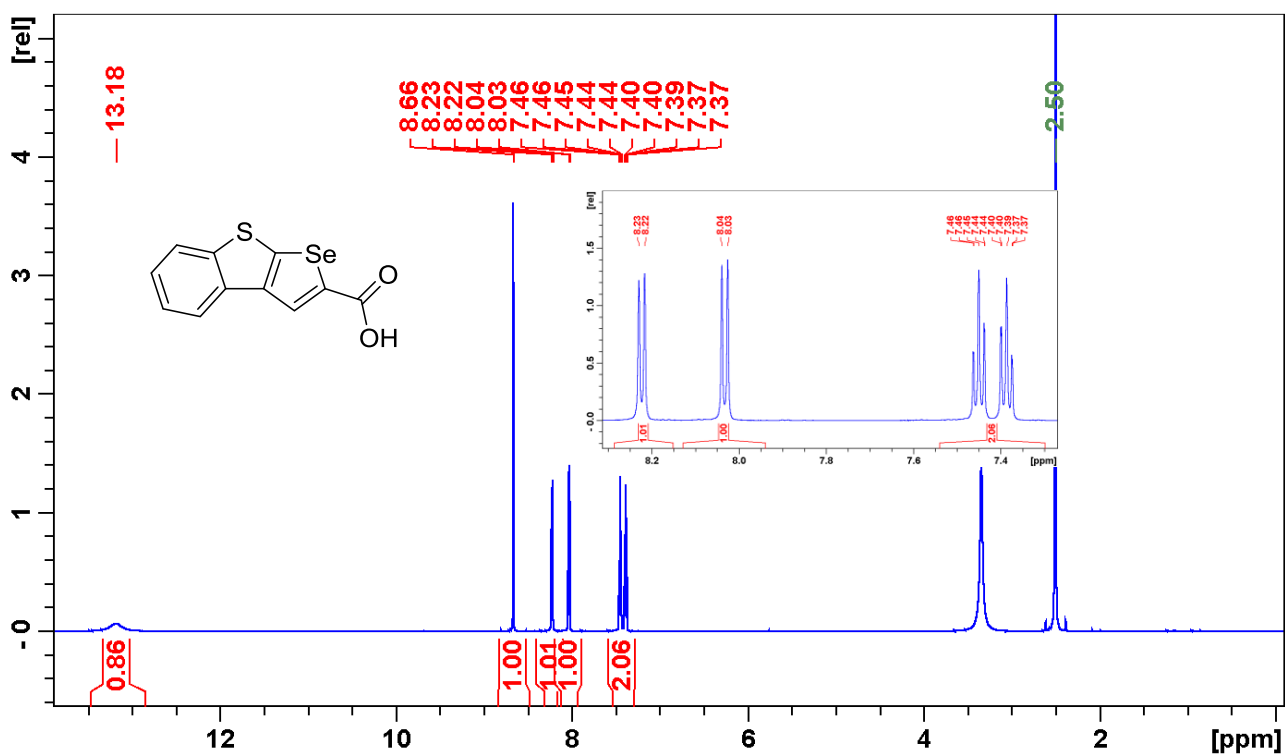


Figure S37. ¹H NMR spectrum of compound 8a.

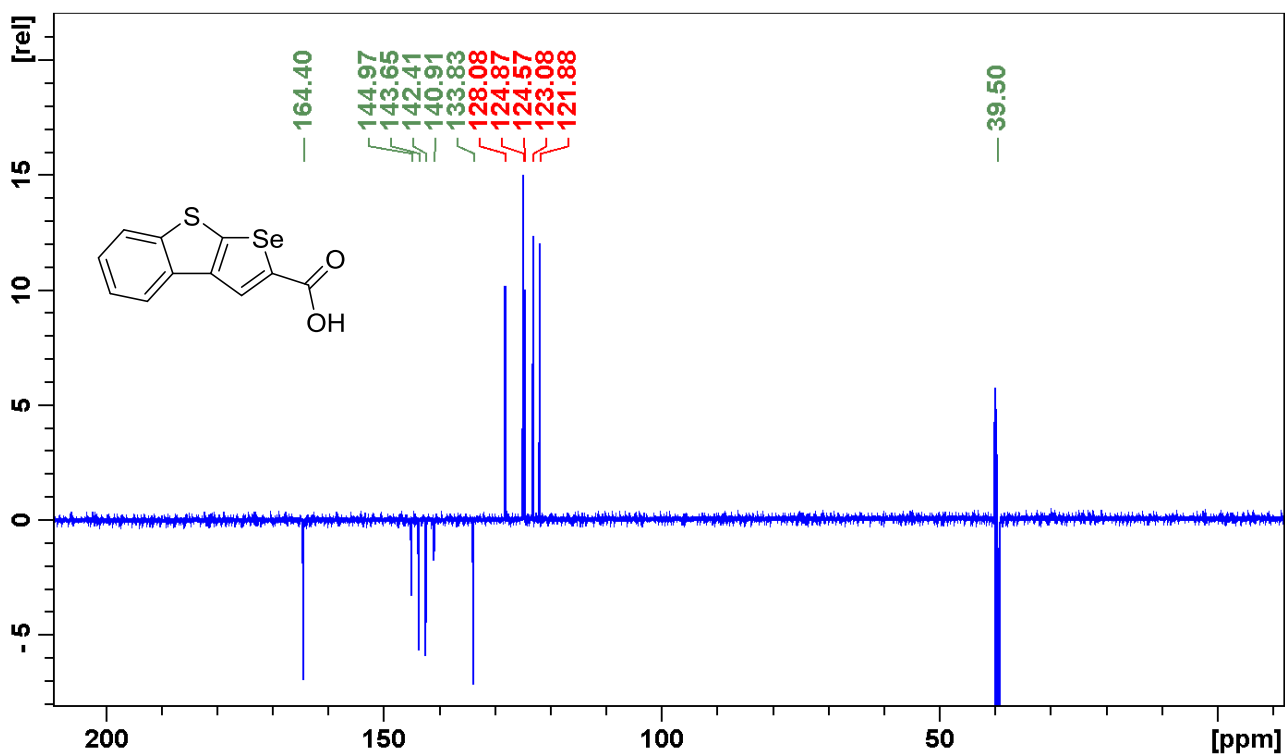


Figure S38. ¹³C NMR spectrum of compound 8a.

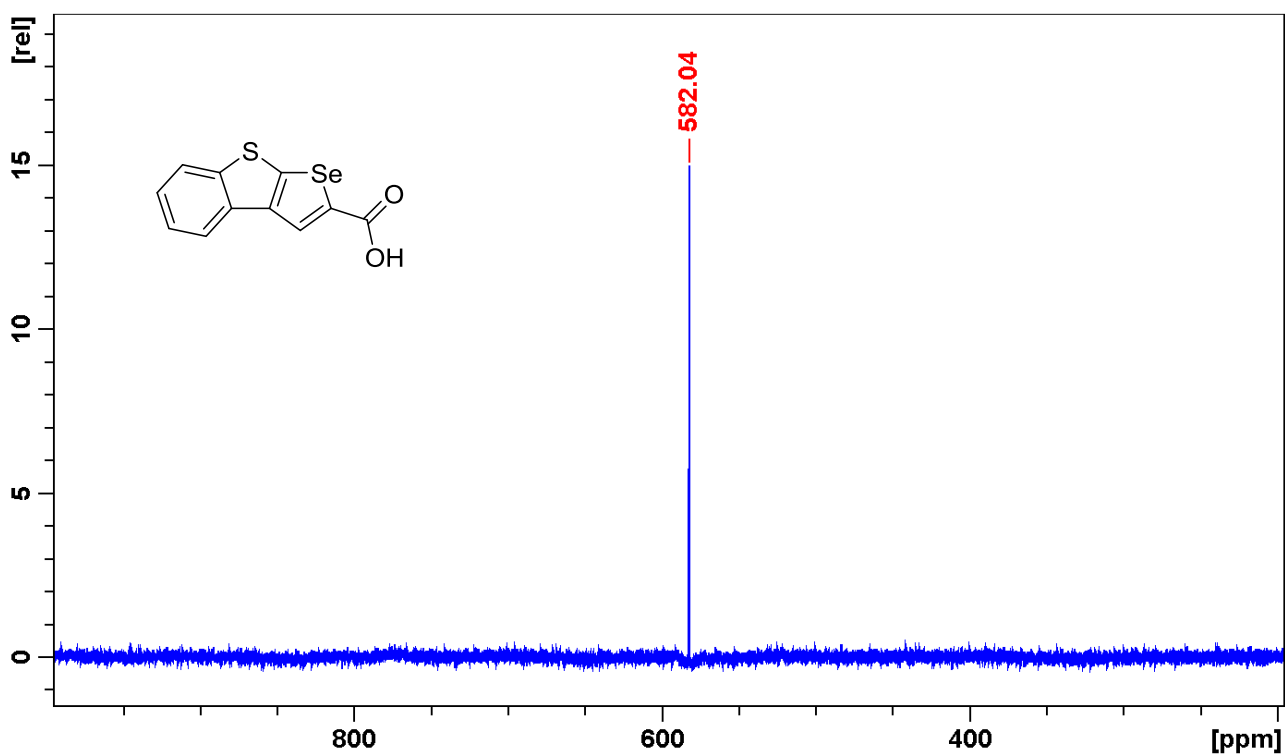


Figure S39. ⁷⁷Se NMR spectrum of compound **8a**.

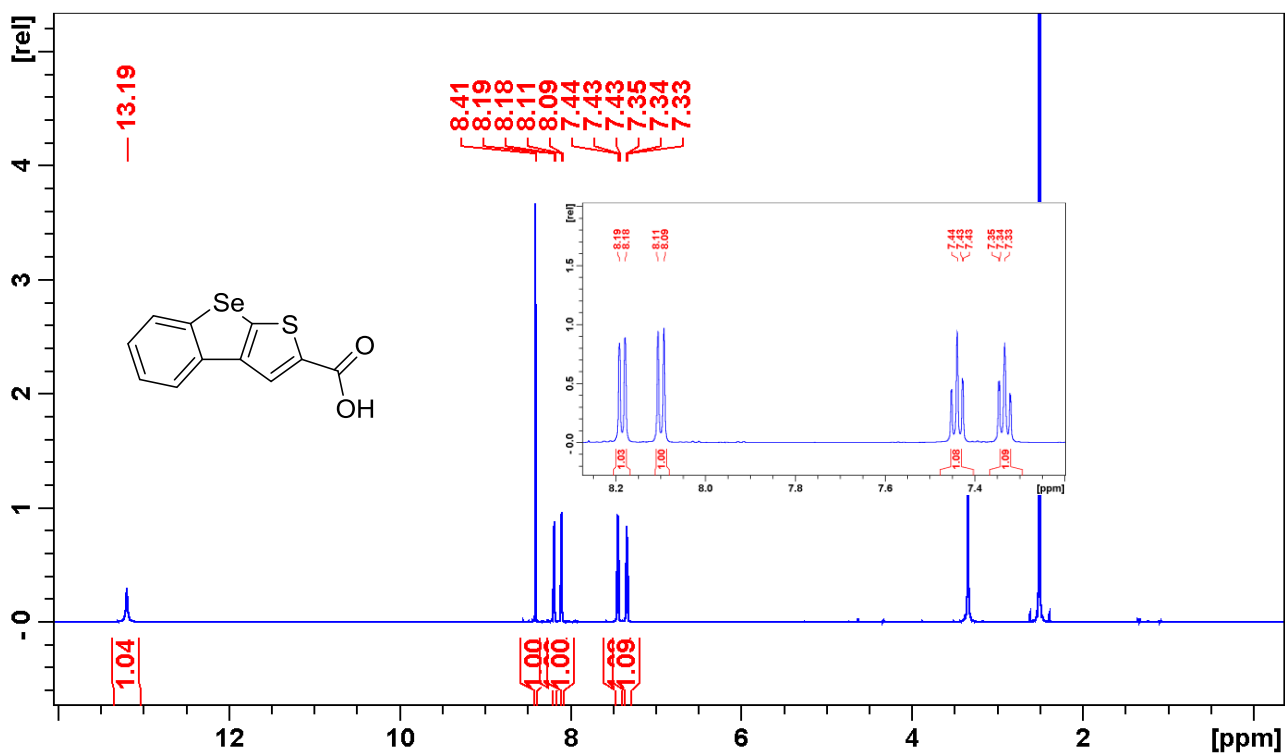


Figure S40. ¹H NMR spectrum of compound **8b**.

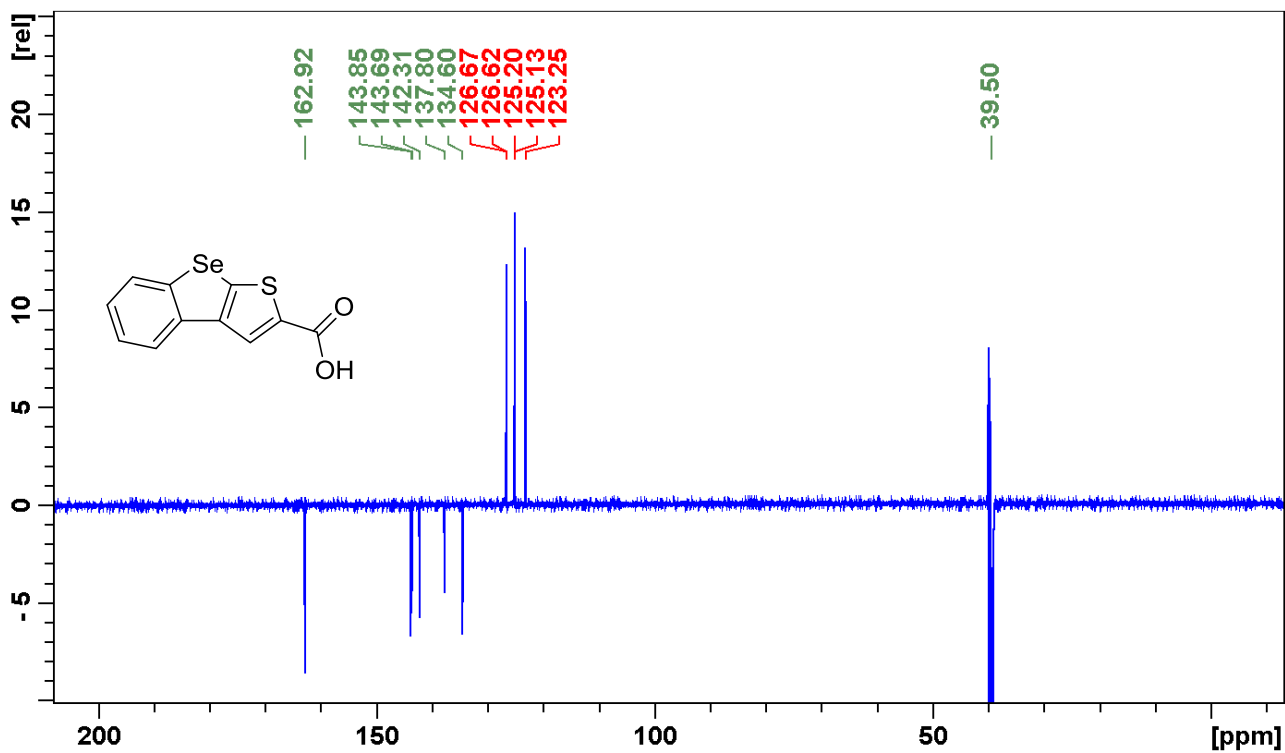


Figure S41. ¹³C NMR spectrum of compound **8b**.

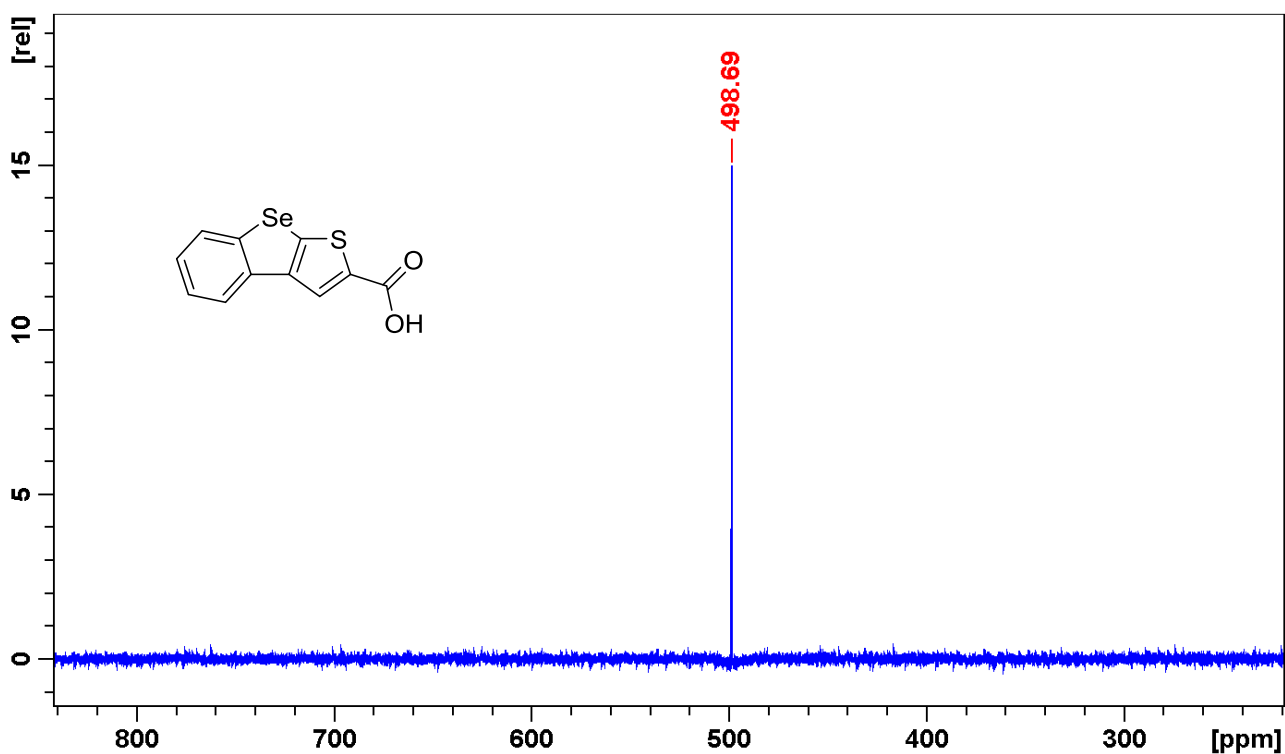


Figure S42. ⁷⁷Se NMR spectrum of compound **8b**.

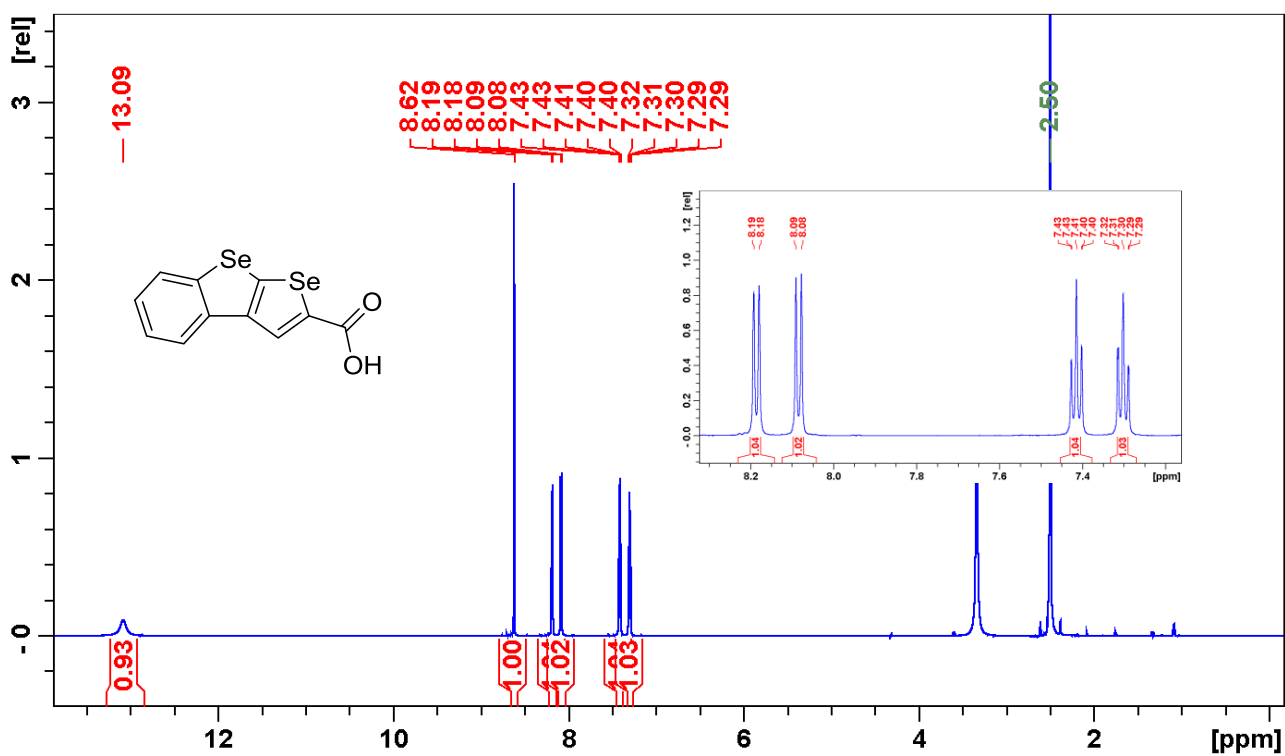


Figure S43. ¹H NMR spectrum of compound **8c**.

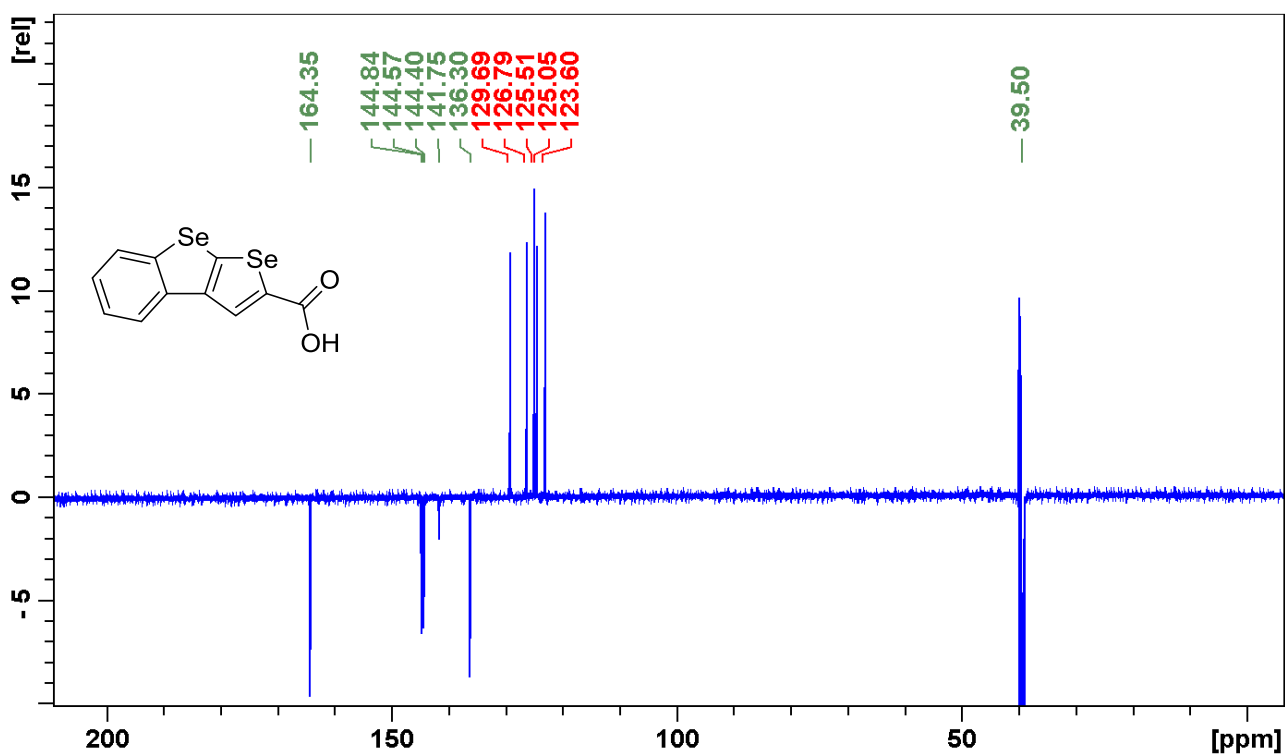


Figure S44. ¹³C NMR spectrum of compound **8c**.

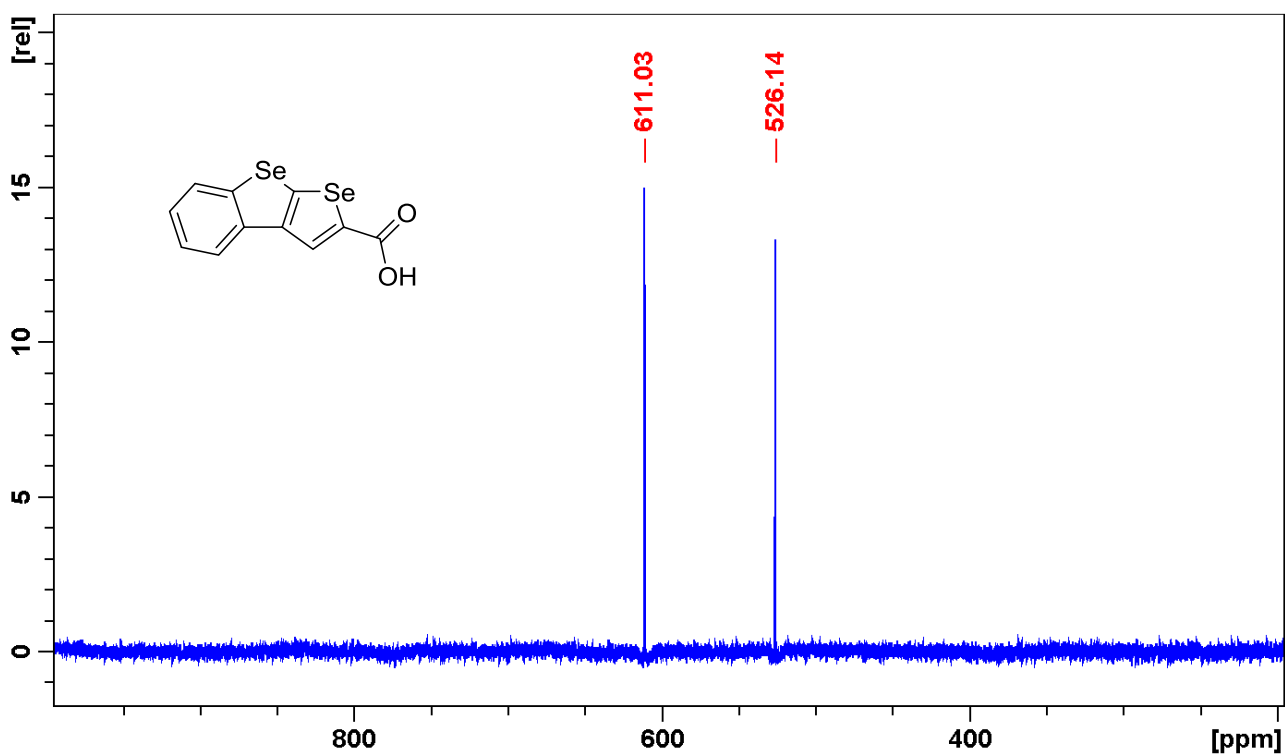


Figure S45. ^{77}Se NMR spectrum of compound **8c**.

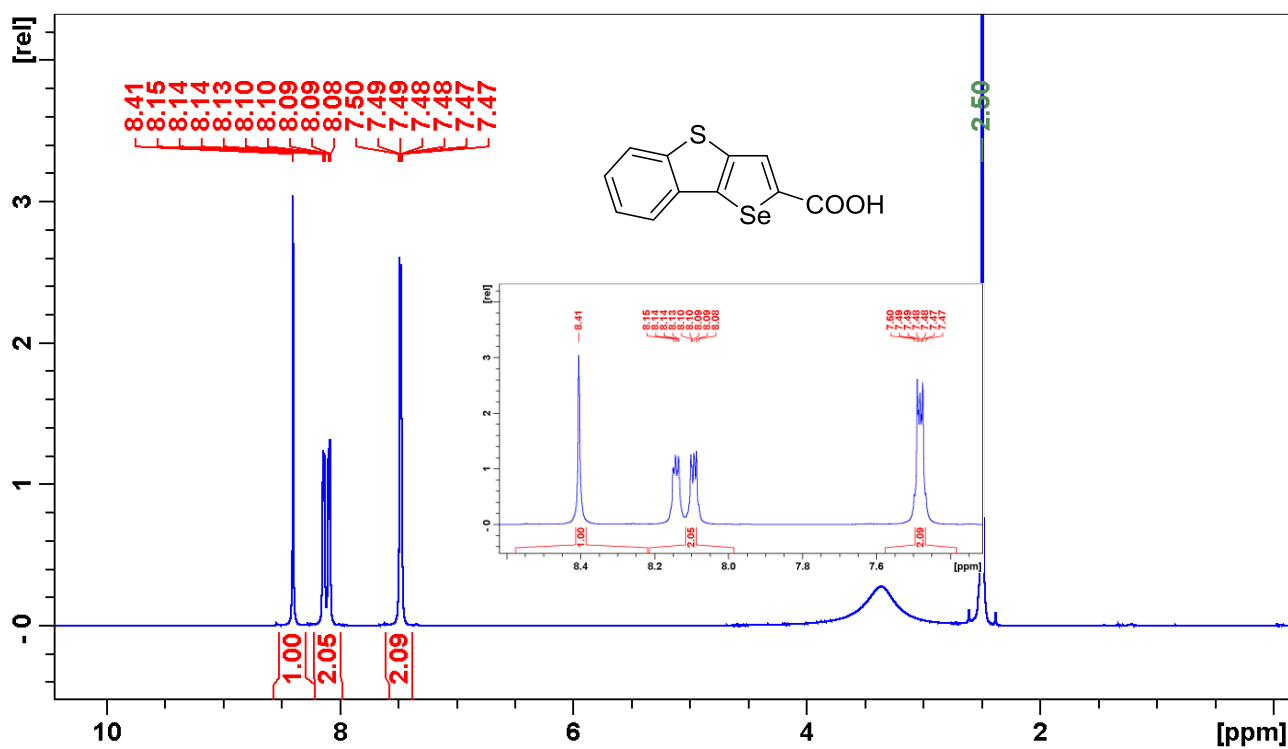


Figure S46. ^1H NMR spectrum of compound **12a**.

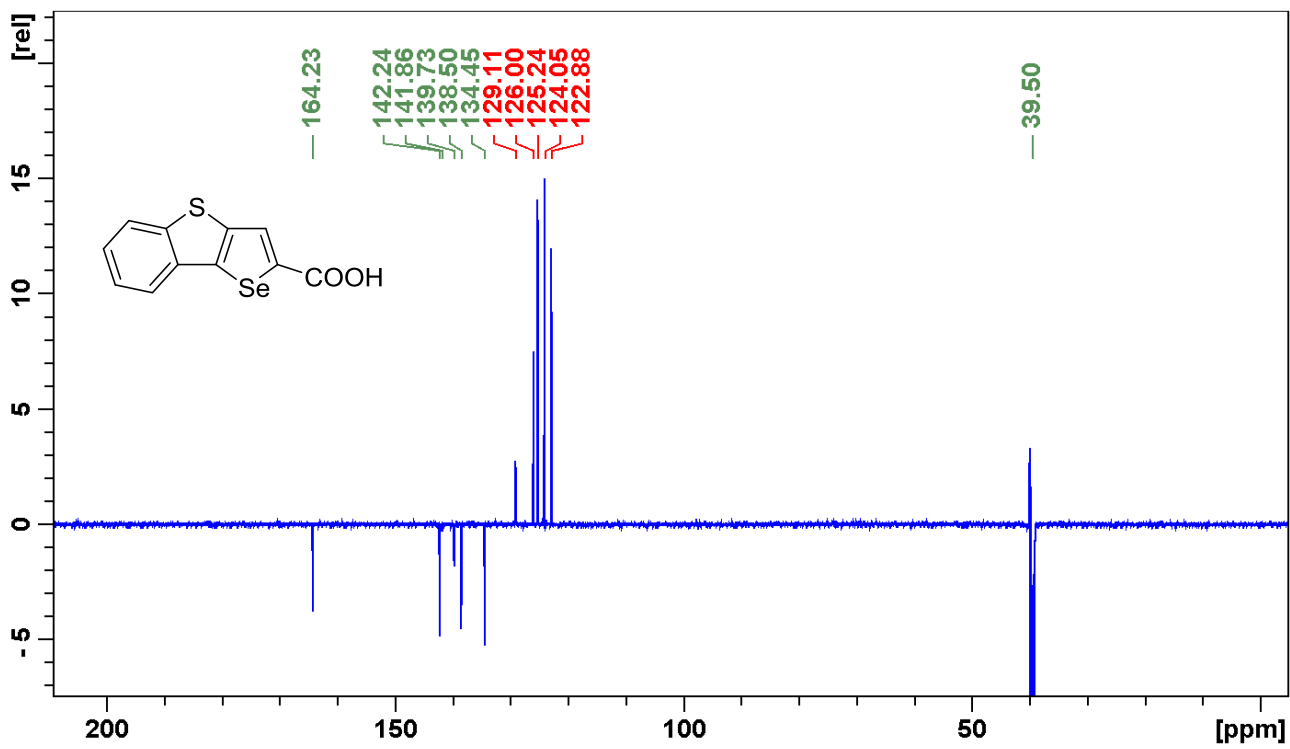


Figure S47. ^{13}C NMR spectrum of compound 12a.

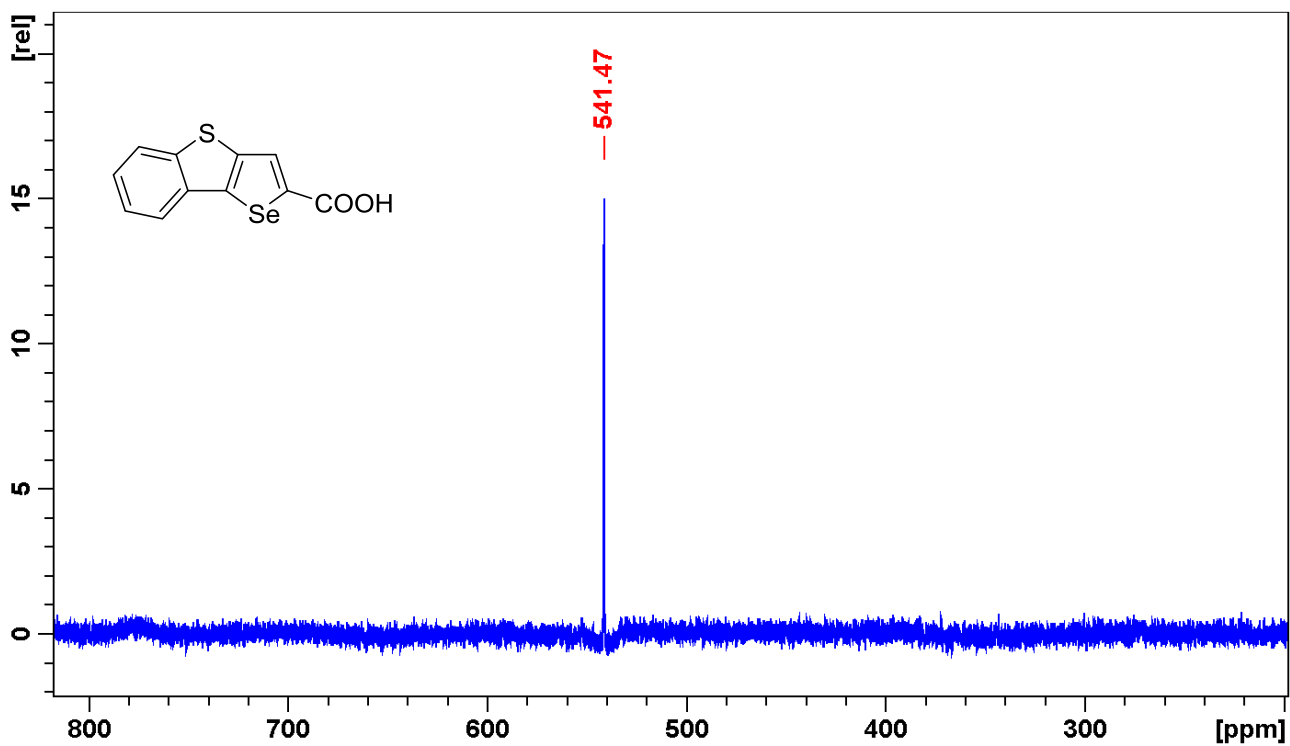


Figure S48. ^{77}Se NMR spectrum of compound 12a.

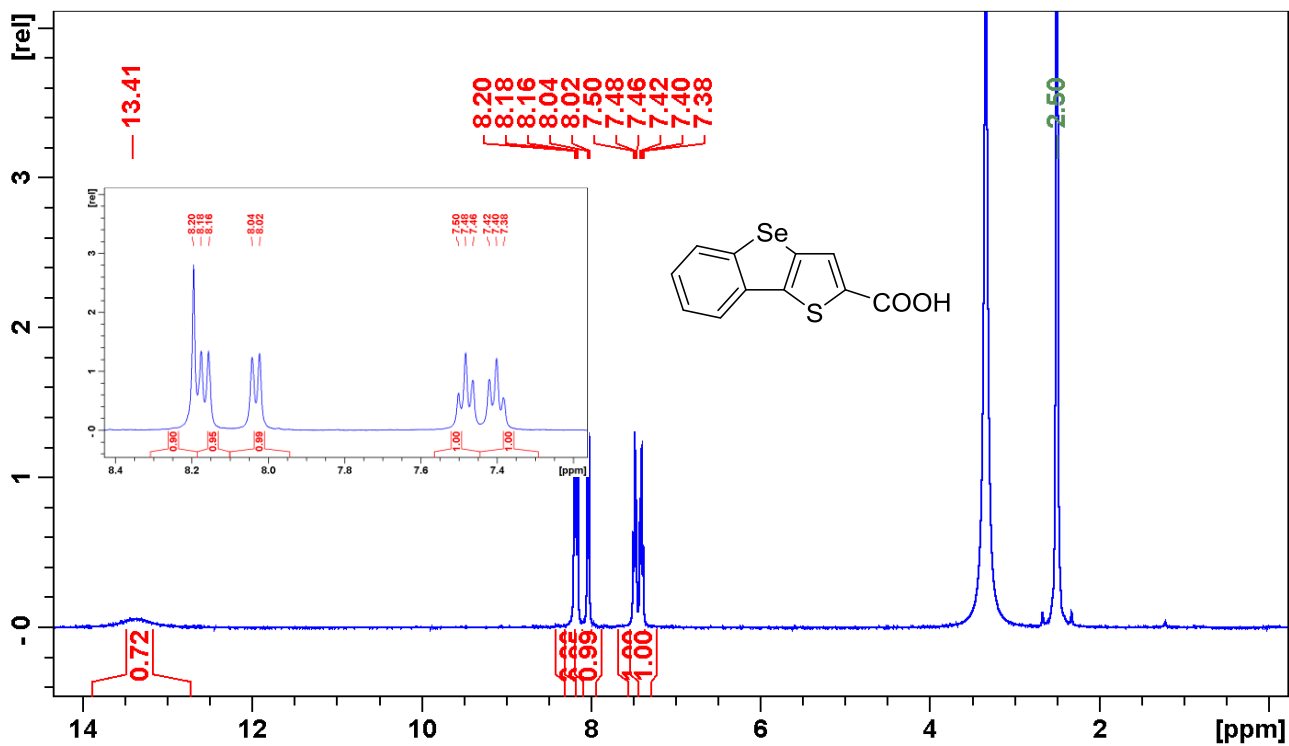


Figure S49. ¹H NMR spectrum of compound 12b.

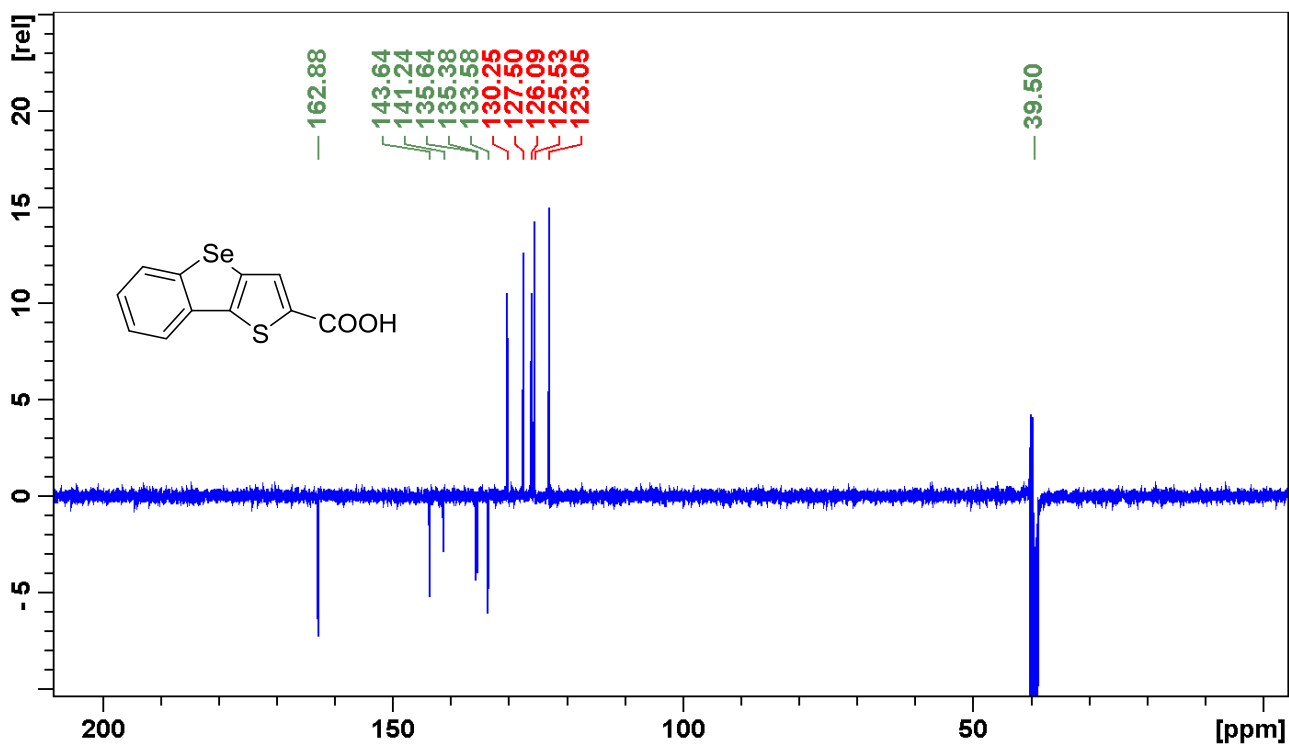


Figure S50. ¹³C NMR spectrum of compound 12b.

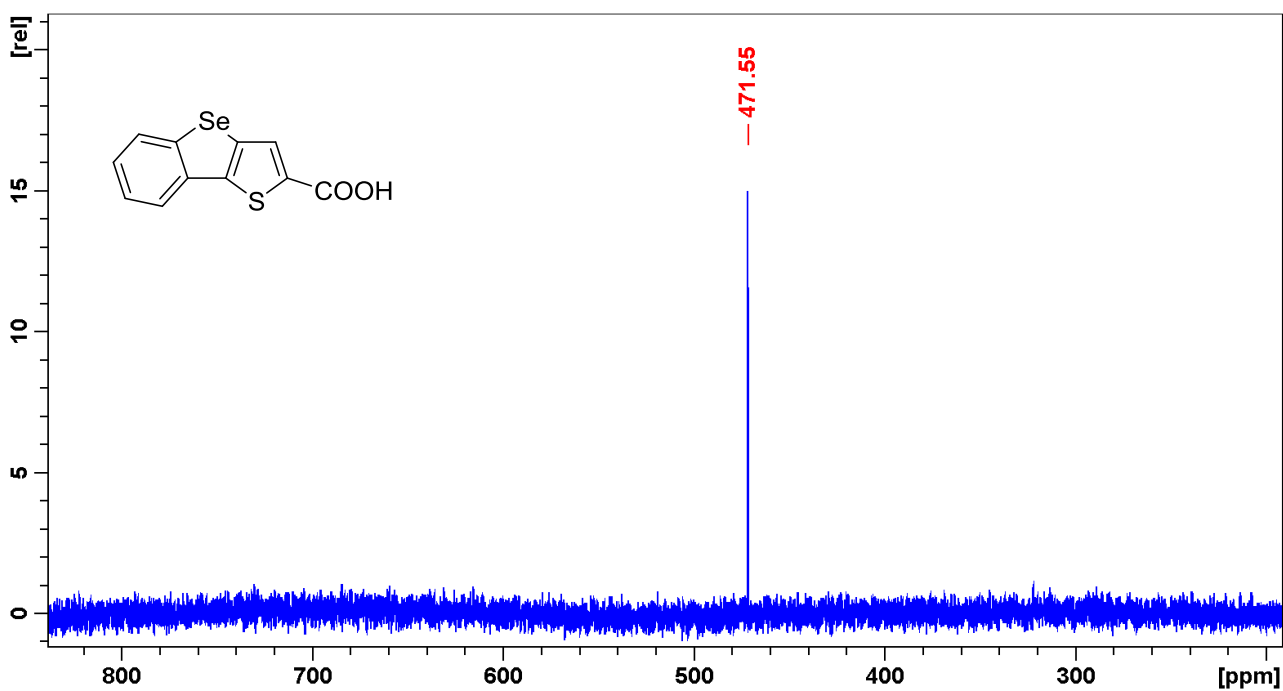


Figure S51. ⁷⁷Se NMR spectrum of compound **12b**.

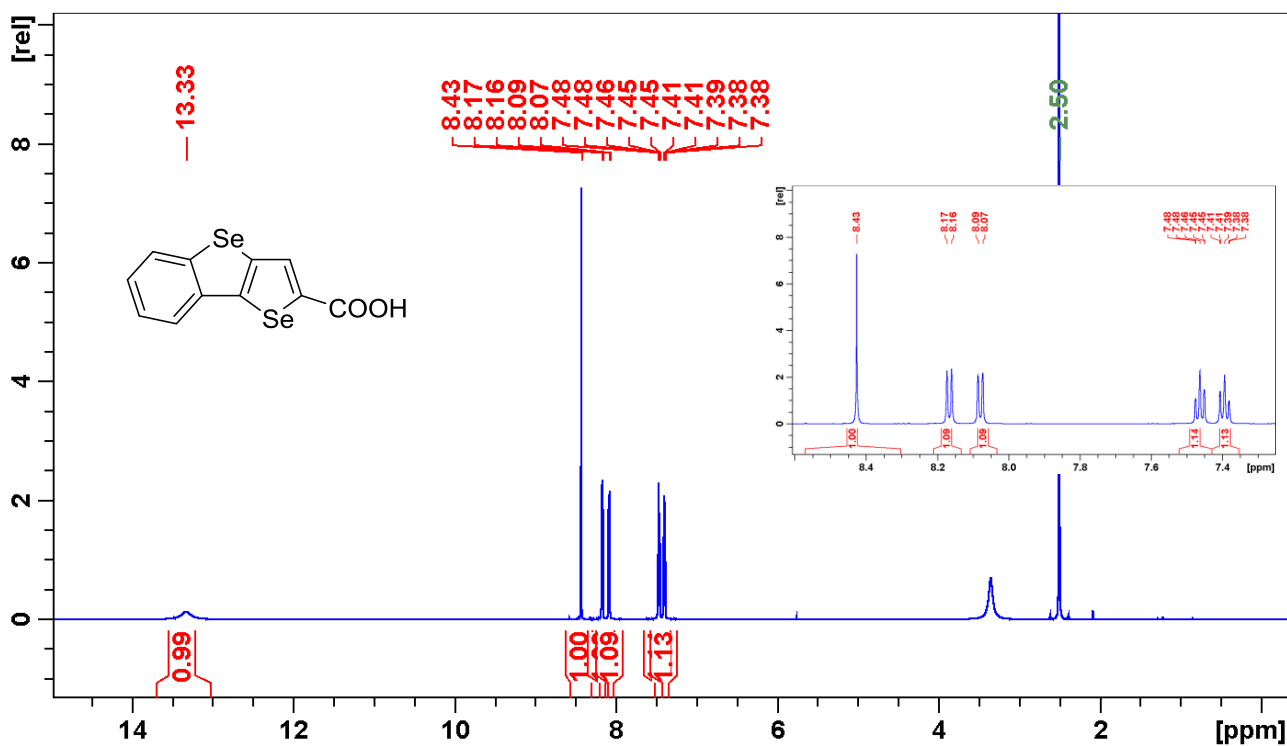


Figure S52. ¹H NMR spectrum of compound **12c**.

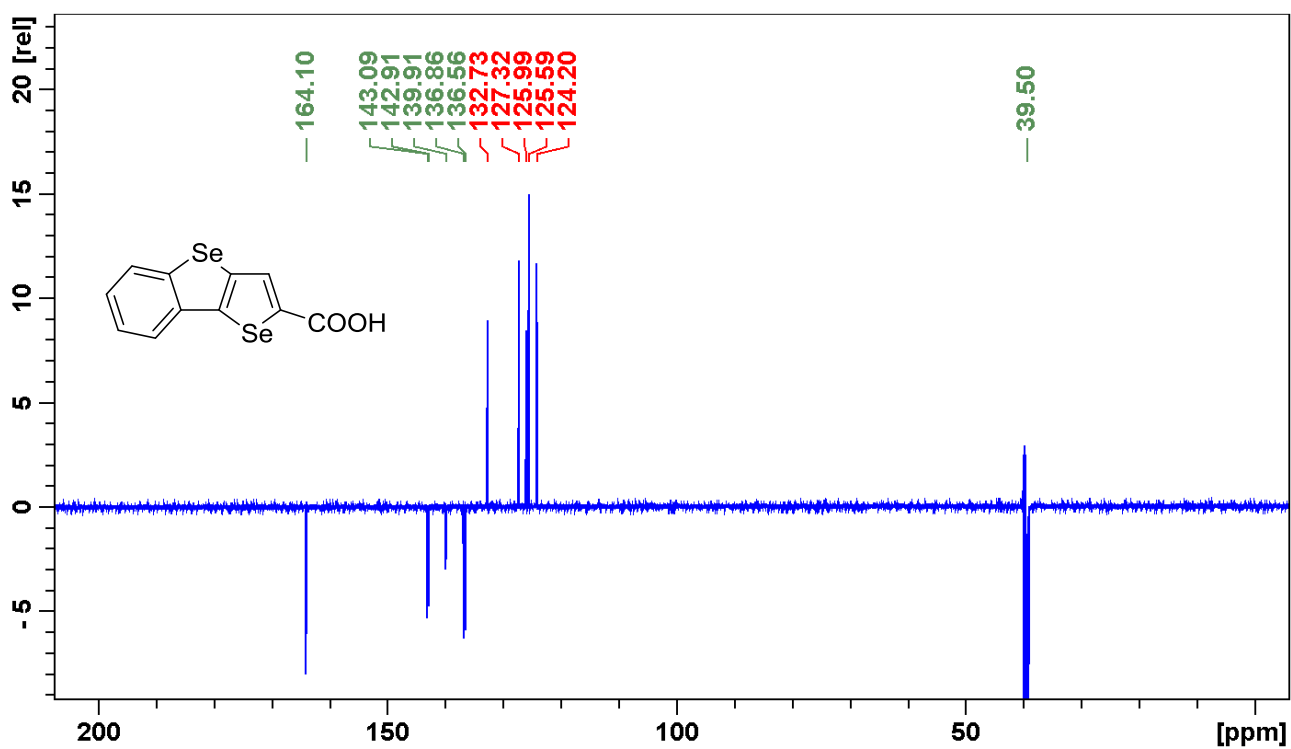


Figure S53. ^{13}C NMR spectrum of compound **12c**.

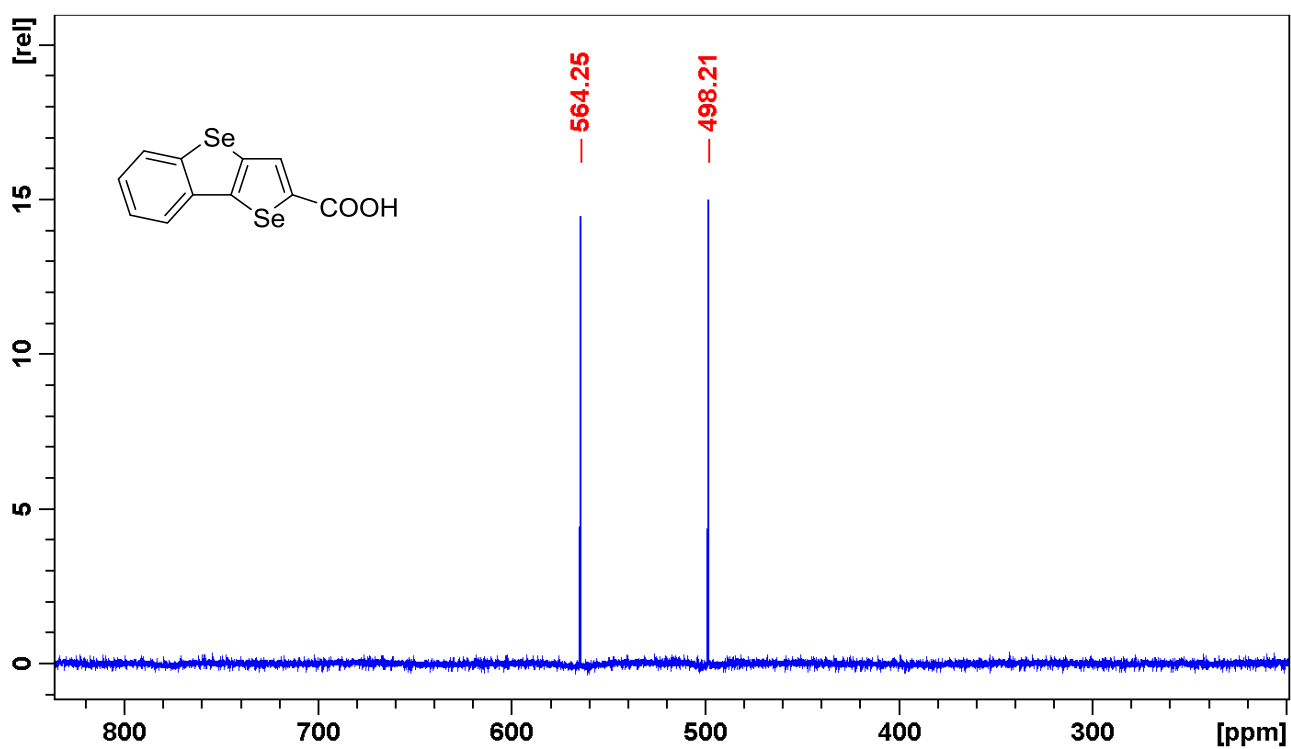


Figure S54. ^{77}Se NMR spectrum of compound **12c**.

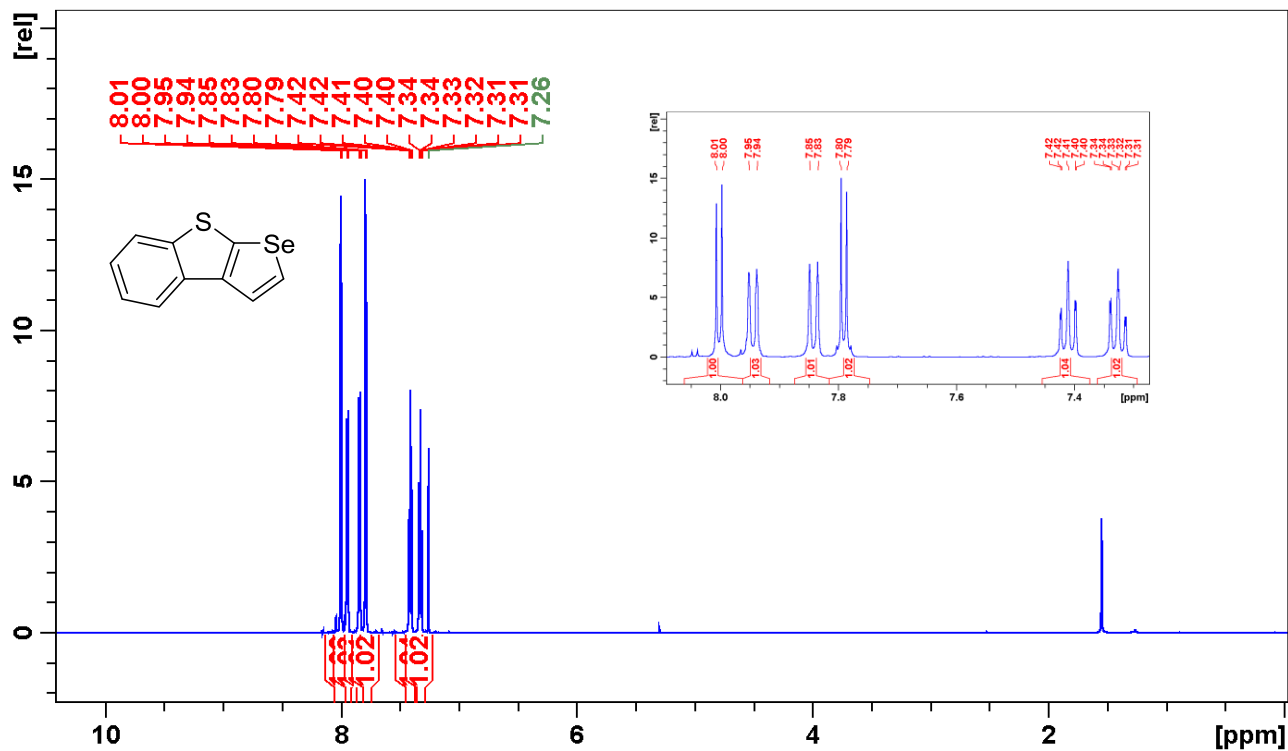


Figure S55. ¹H NMR spectrum of compound 9a.

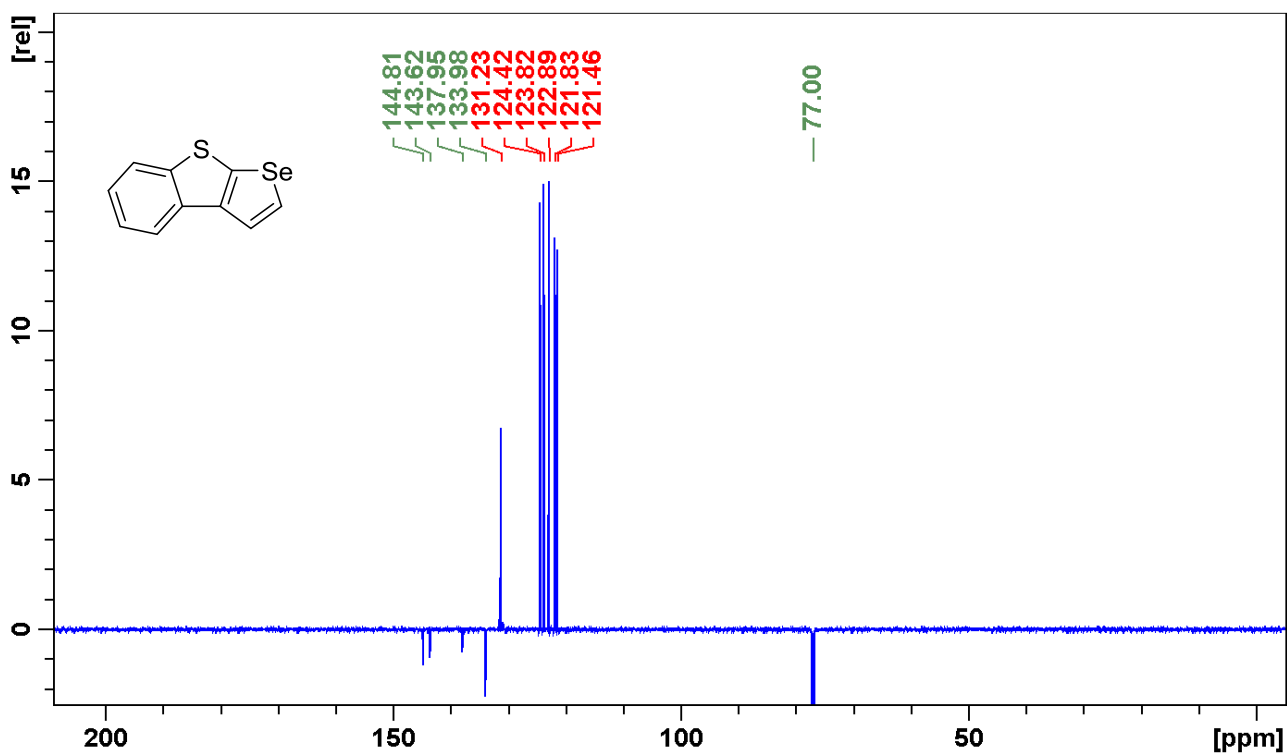


Figure S56. ¹³C NMR spectrum of compound 9a.

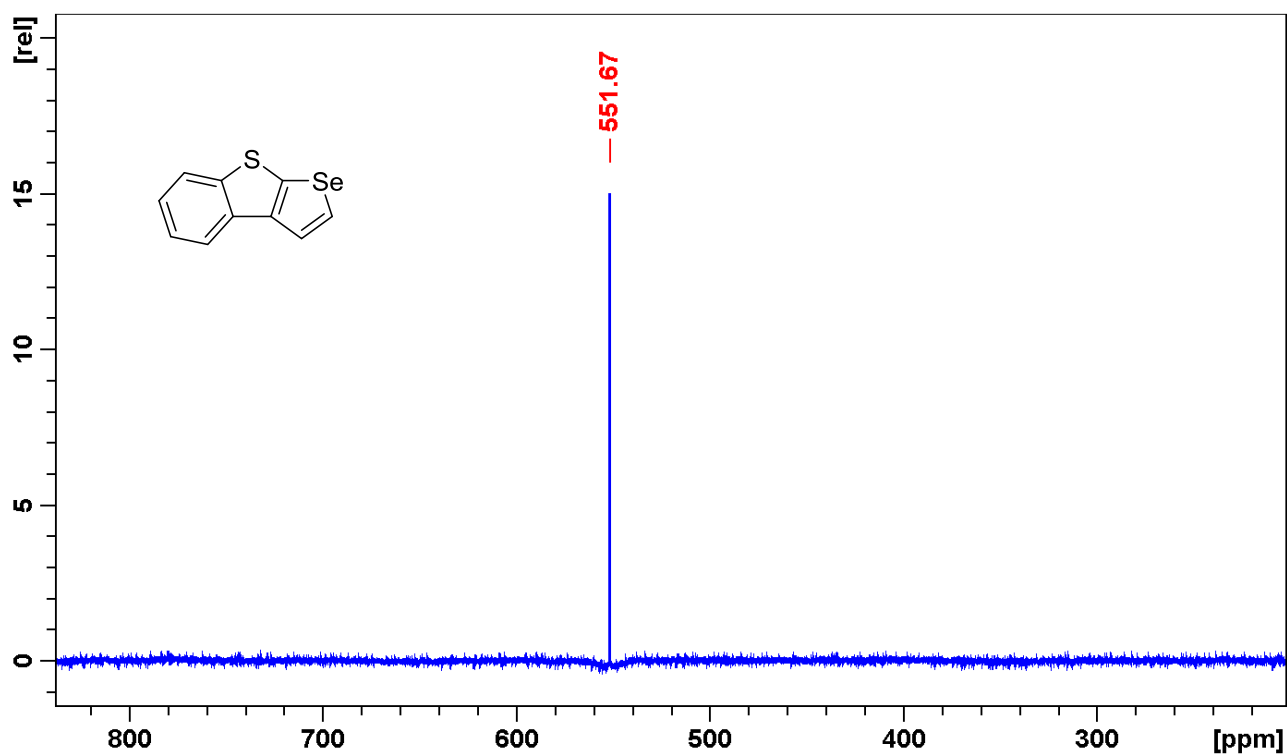


Figure S57. ^{77}Se NMR spectrum of compound **9a**.

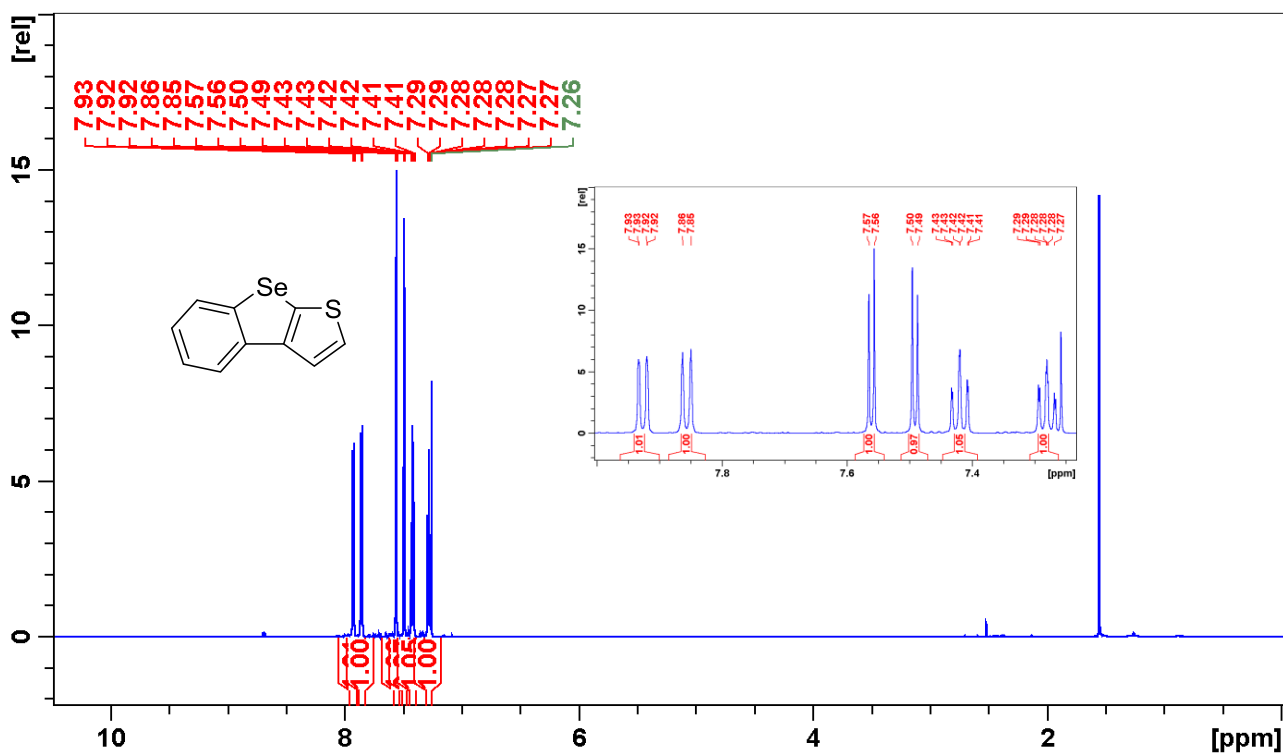


Figure S58. ^1H NMR spectrum of compound **9b**.

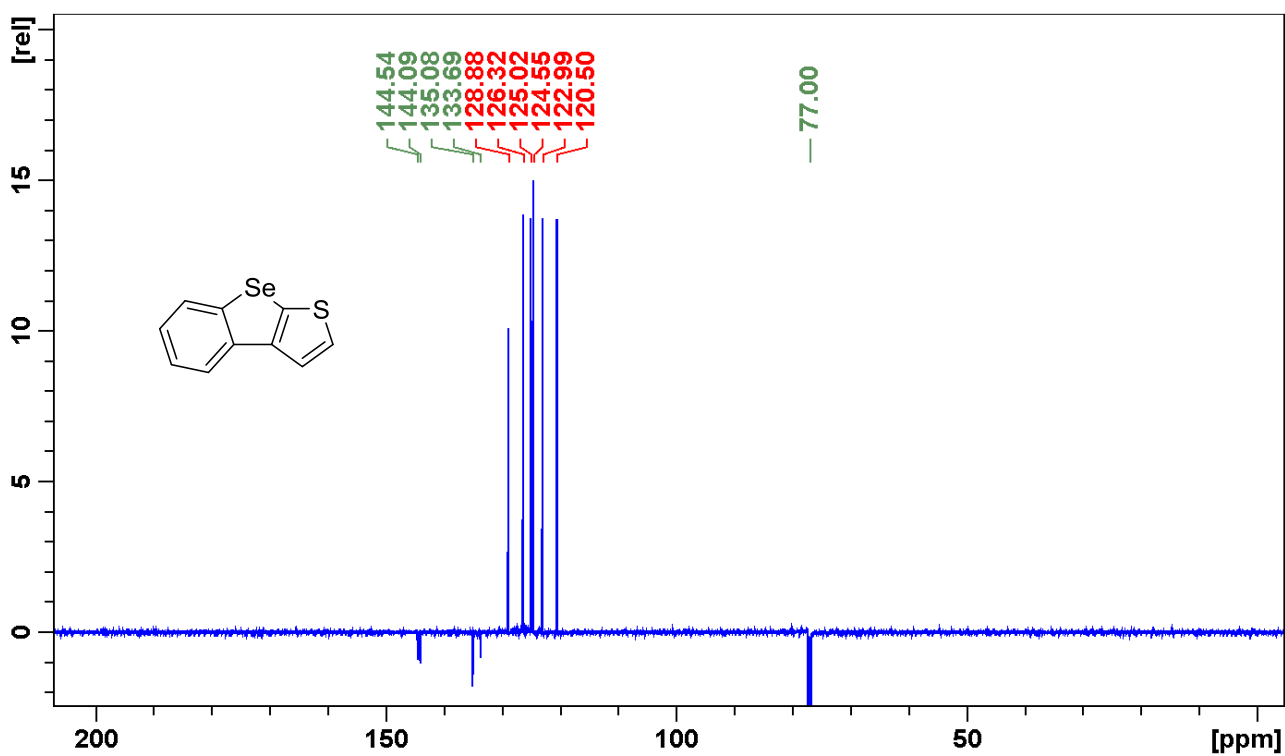


Figure S59. ^{13}C NMR spectrum of compound **9b**.

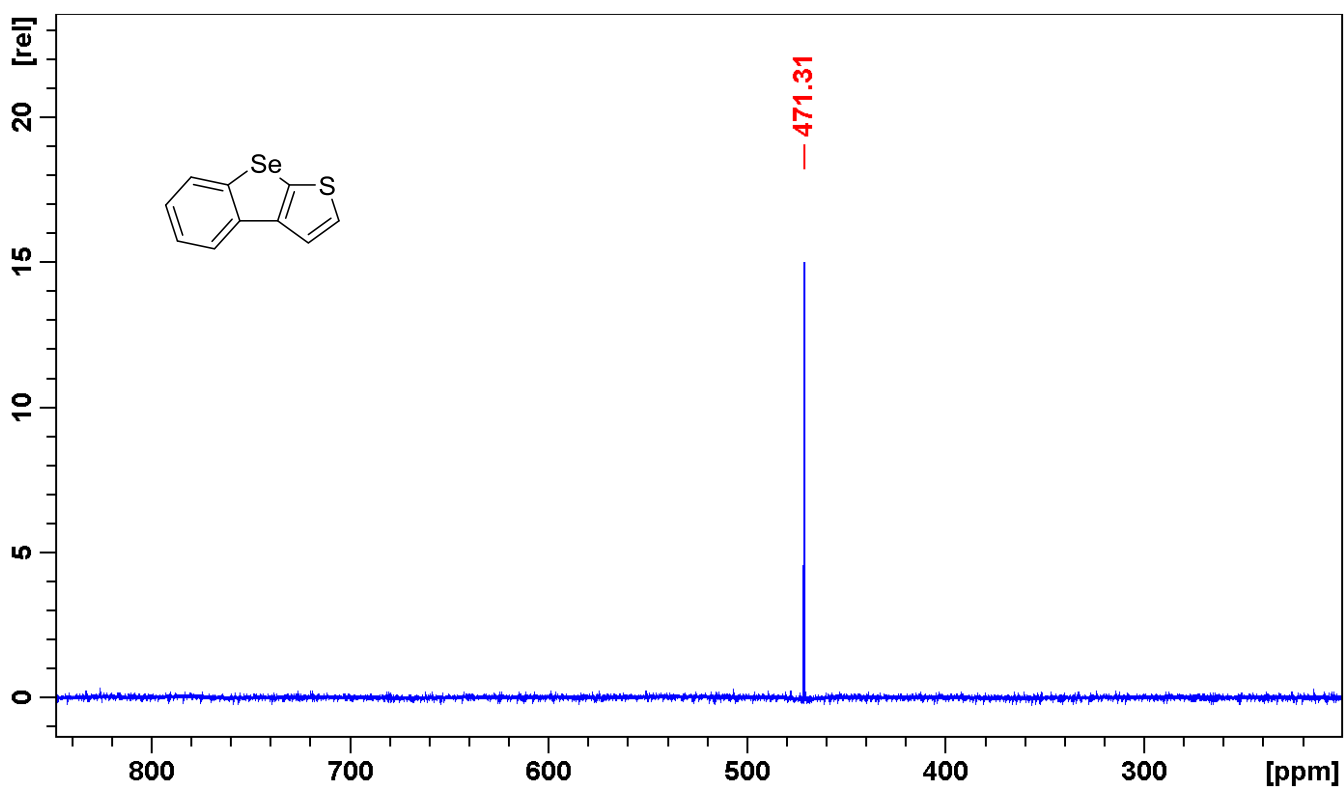


Figure S60. ^{77}Se NMR spectrum of compound **9b**.

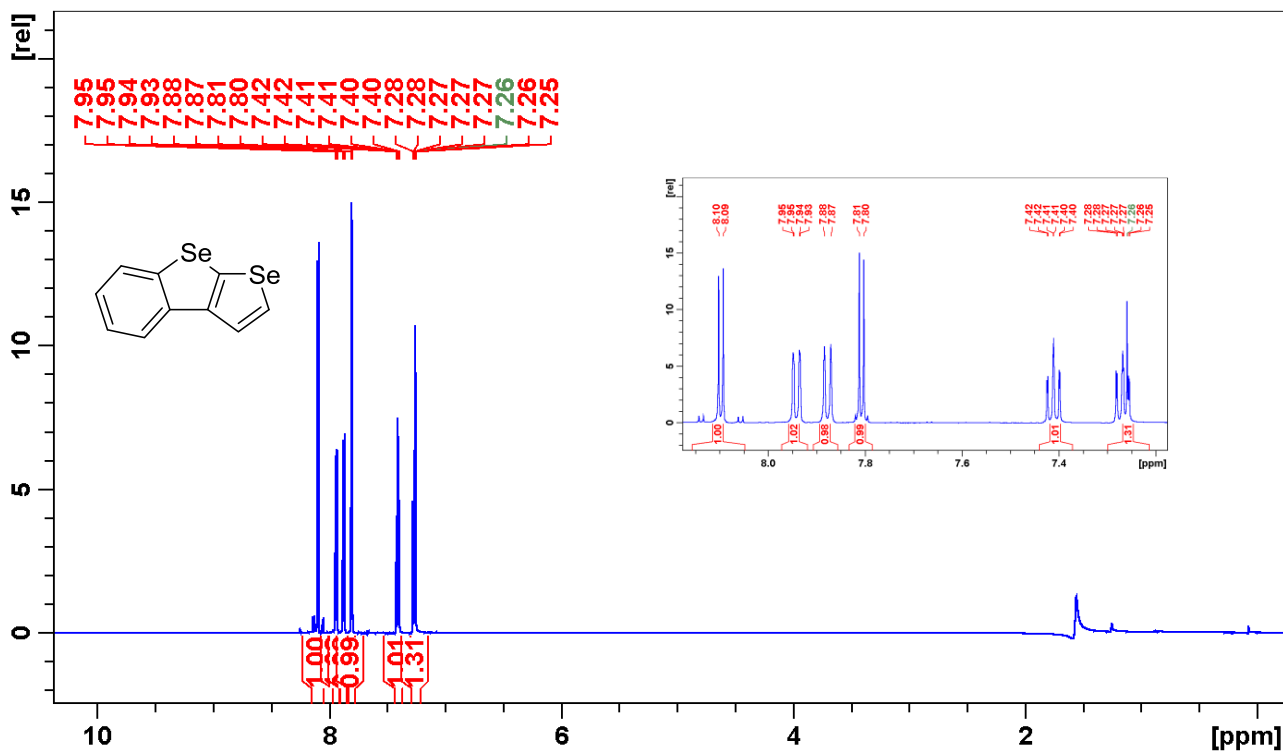


Figure S61. ¹H NMR spectrum of compound 9c.

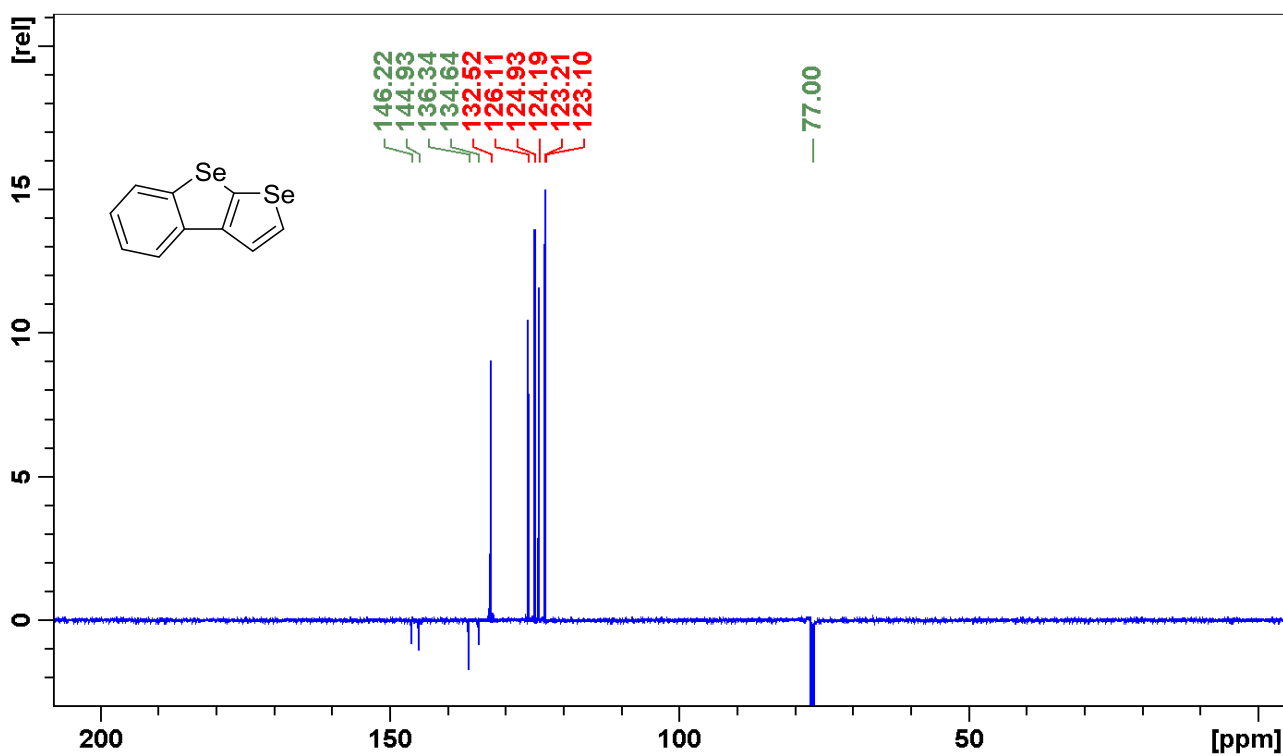


Figure S62. ¹³C NMR spectrum of compound 9c.

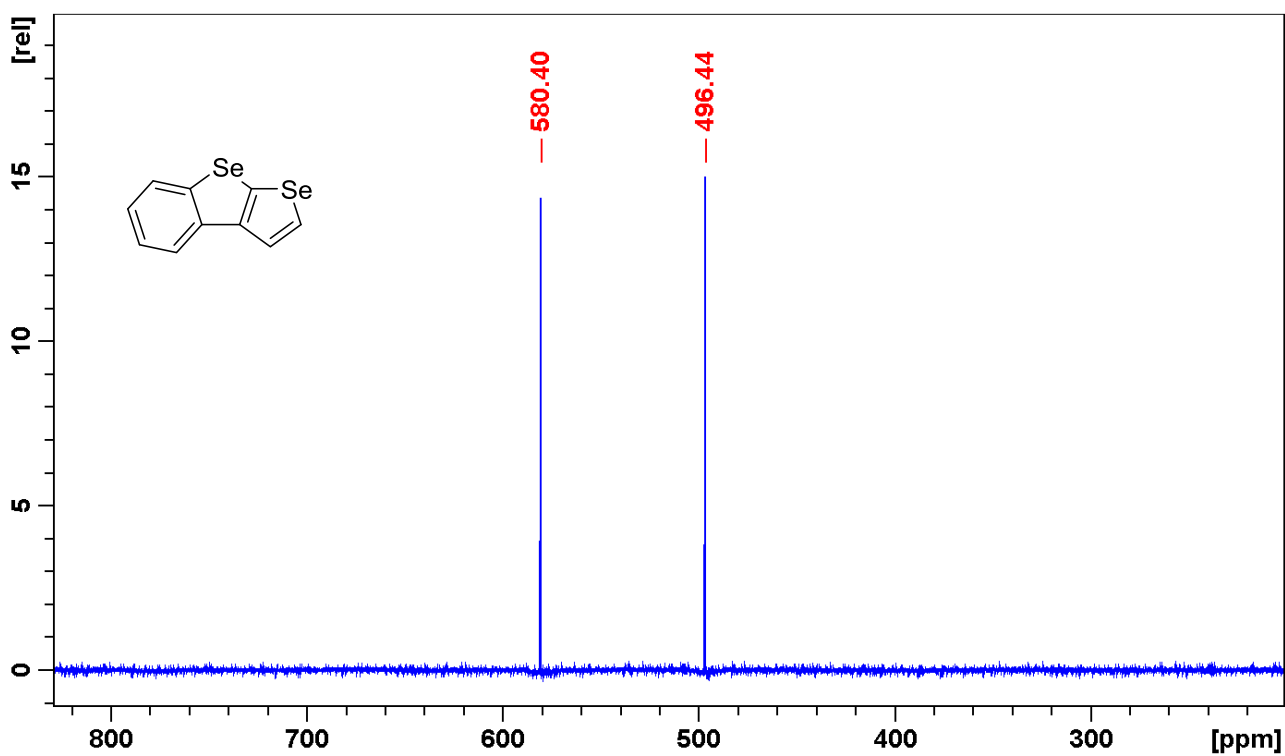


Figure S63. ⁷⁷Se NMR spectrum of compound 9c.

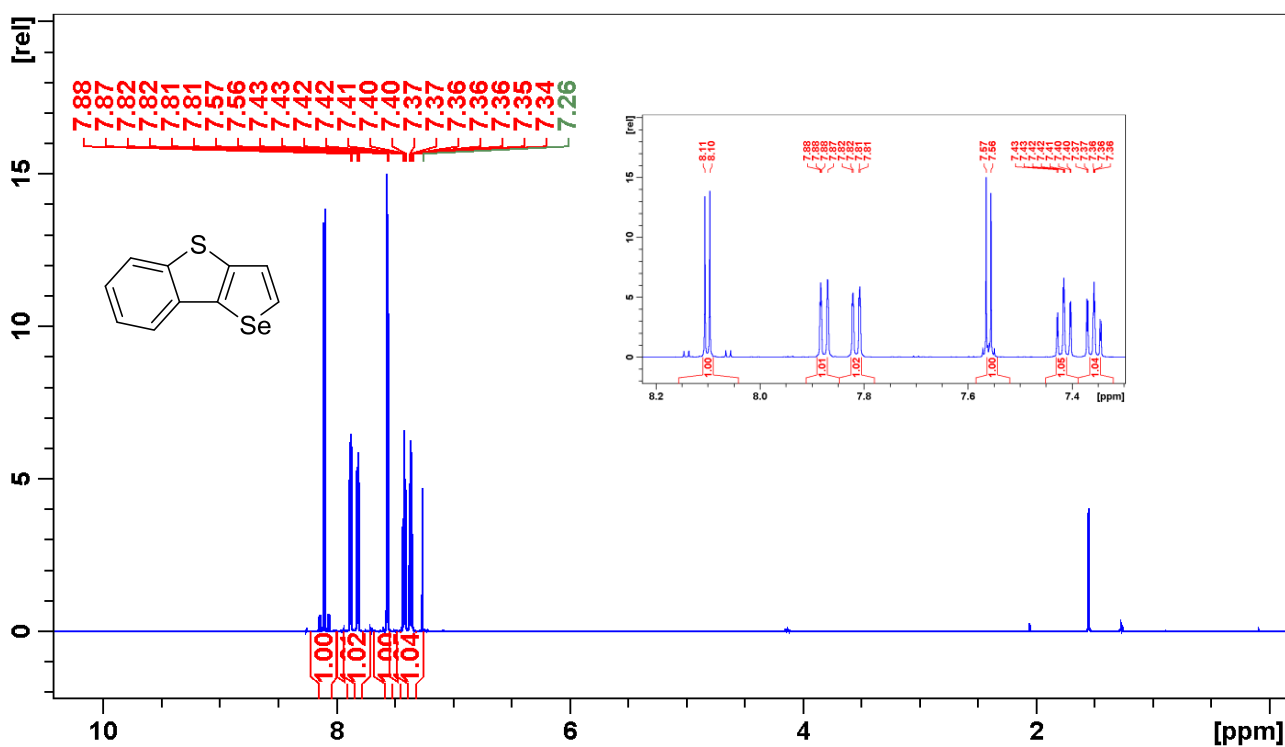


Figure S64. ¹H NMR spectrum of compound 13a.

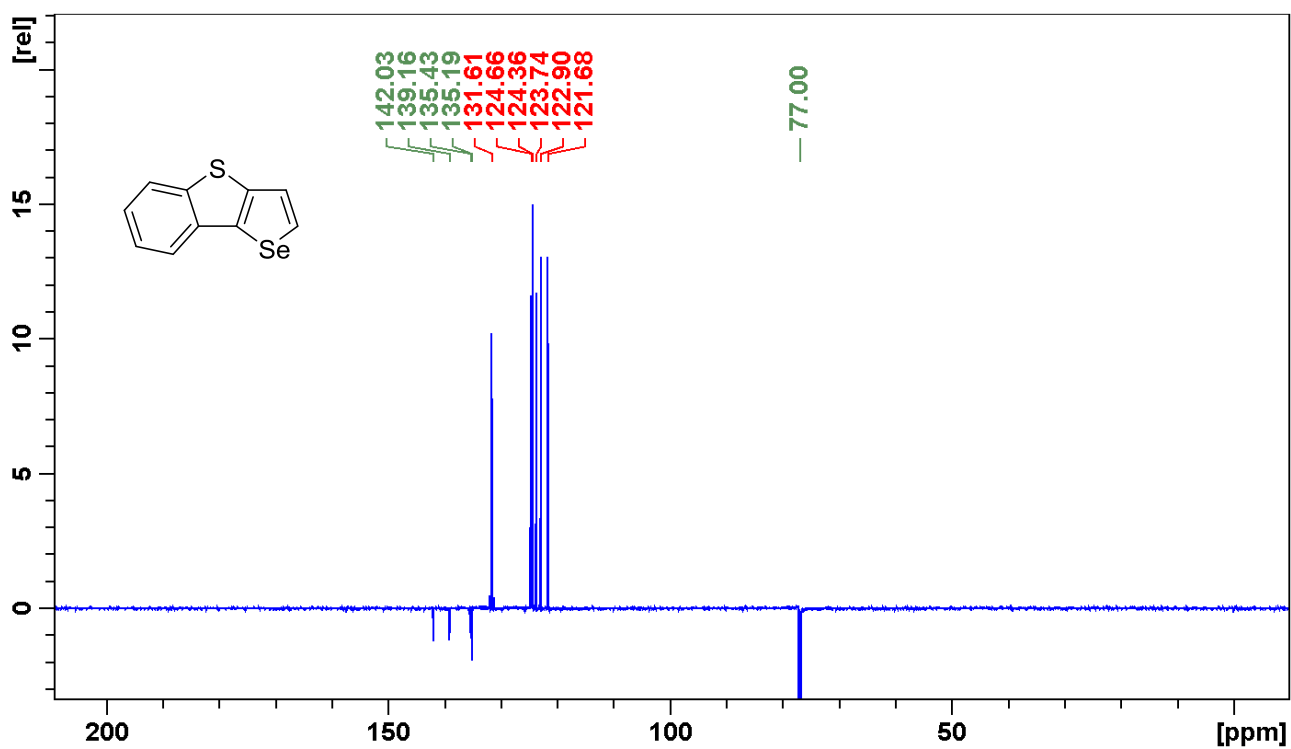


Figure S65. ^{13}C NMR spectrum of compound 13a.

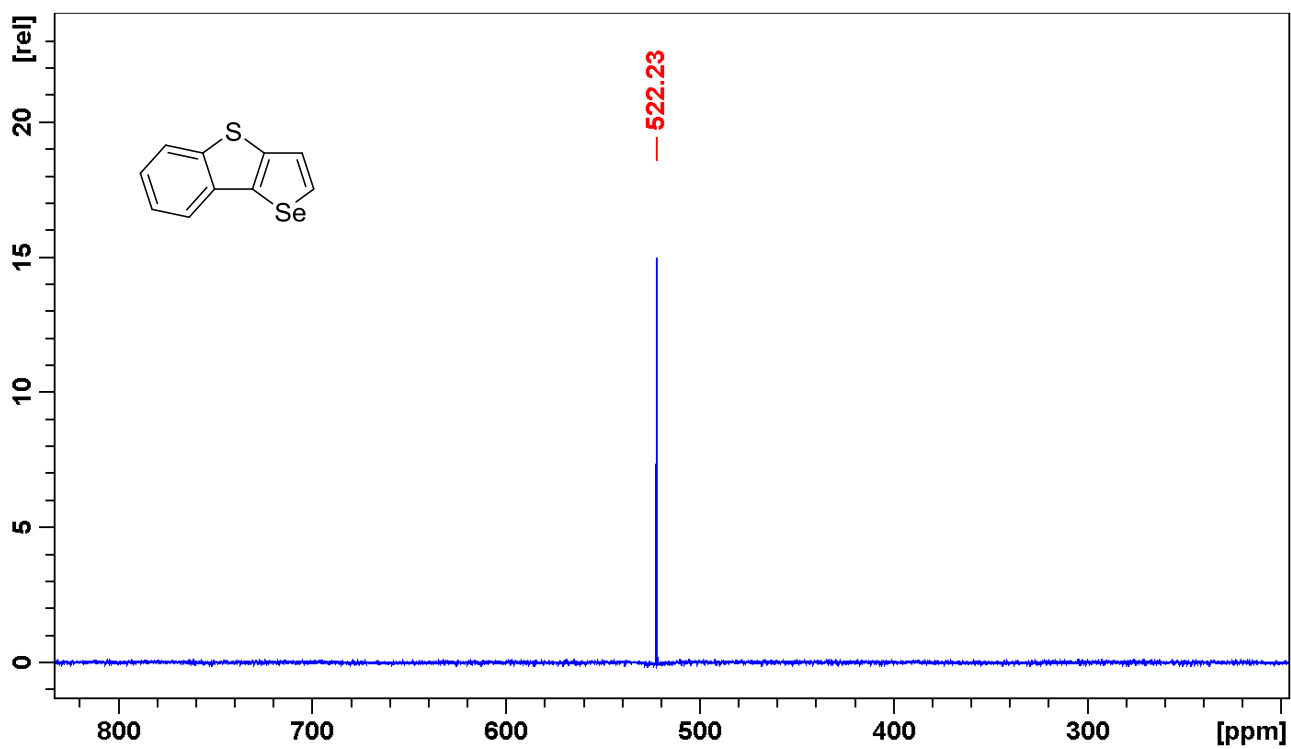


Figure S66. ^{77}Se NMR spectrum of compound 13a.

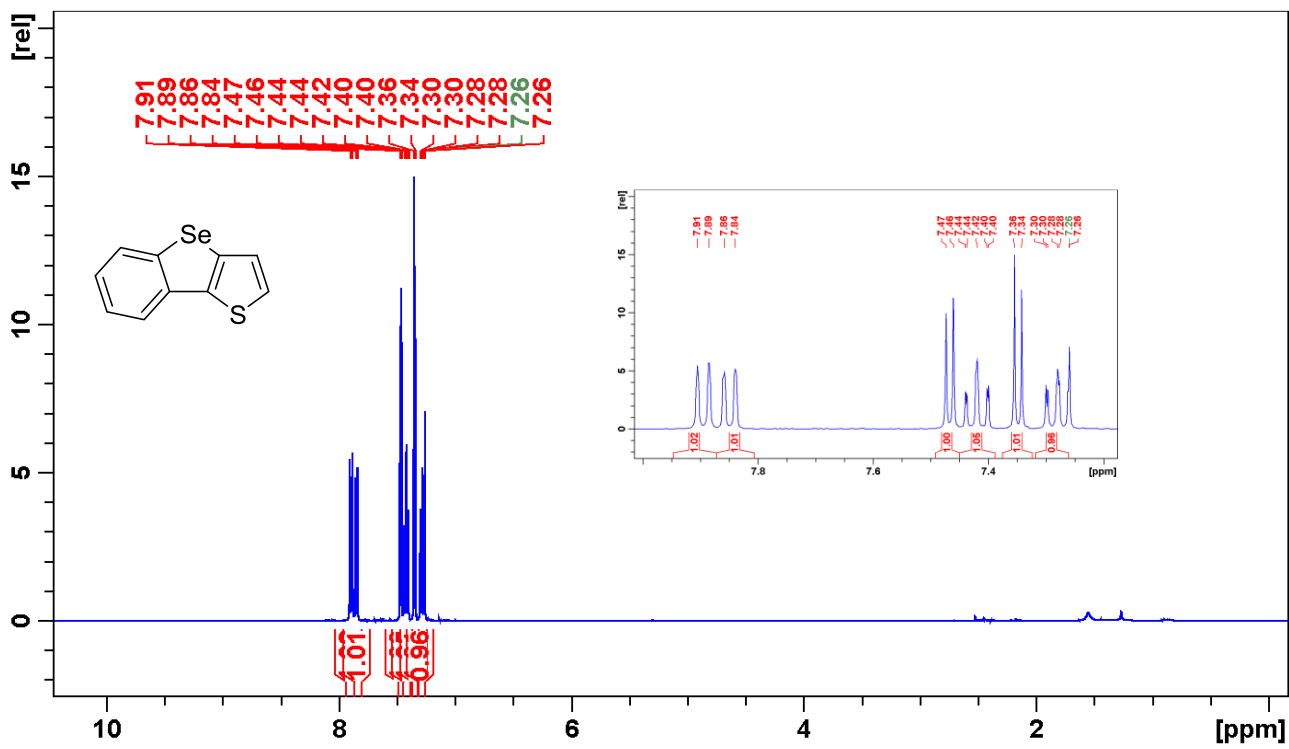


Figure S67. ¹H NMR spectrum of compound 13b.

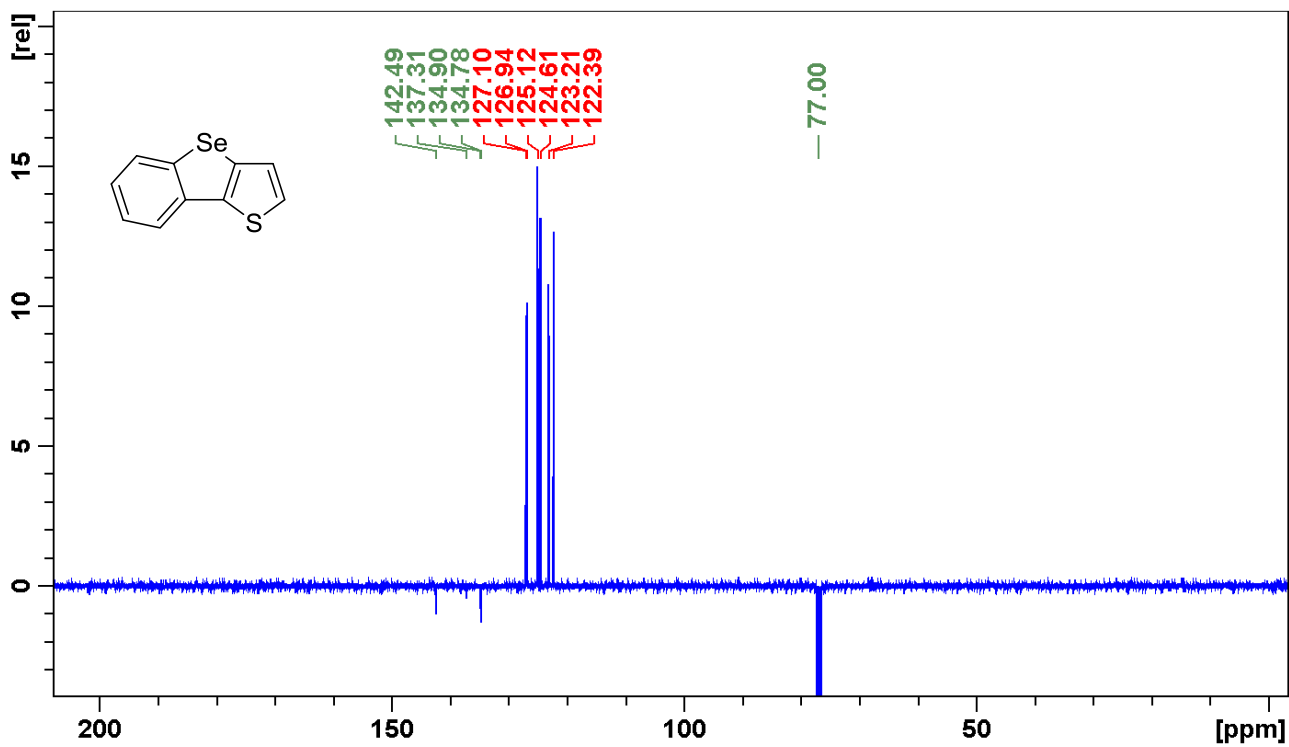


Figure S68. ¹³C NMR spectrum of compound 13b.

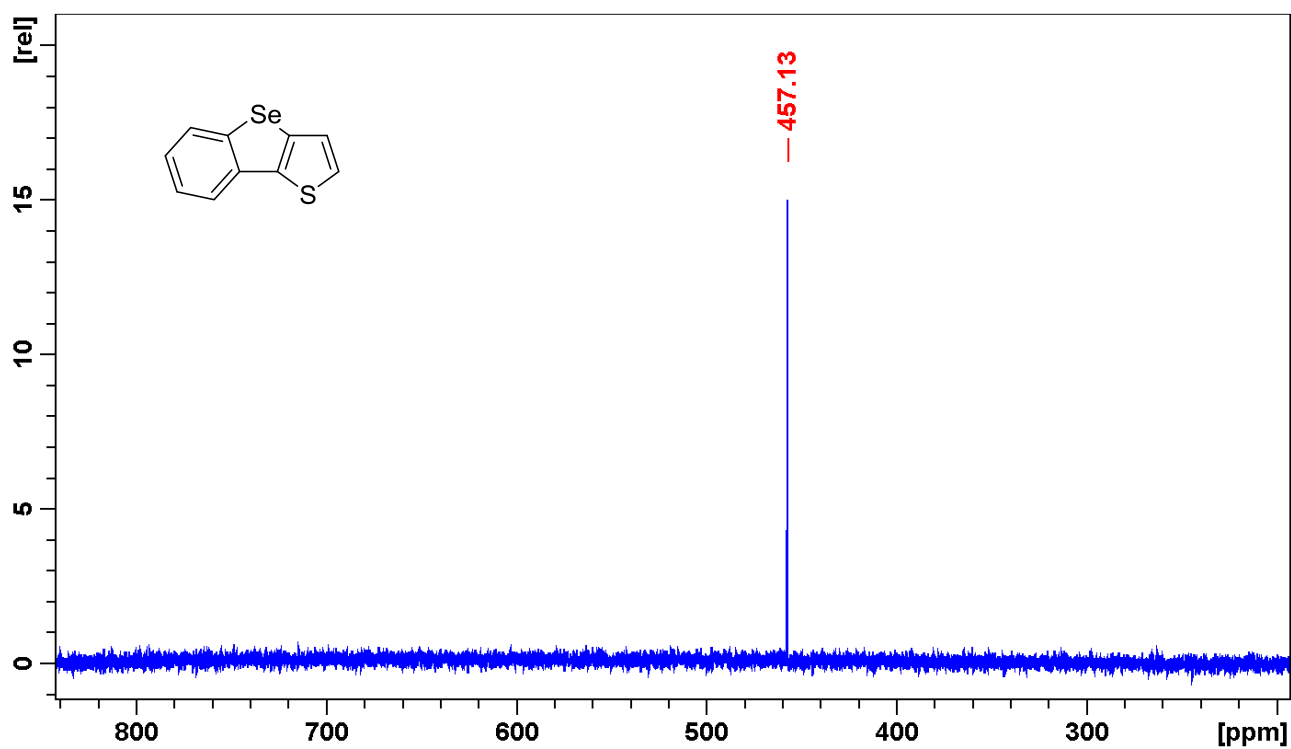


Figure S69. ^{77}Se NMR spectrum of compound **13b**.

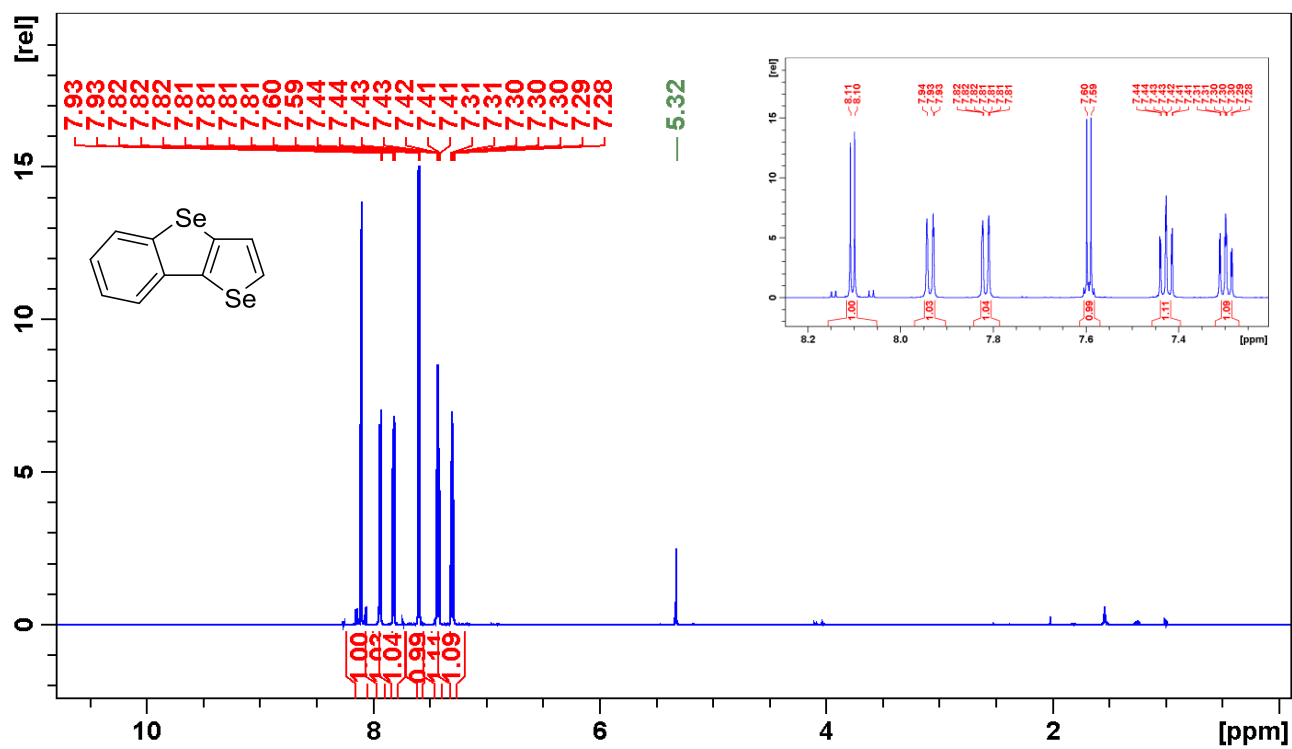


Figure S70. ^1H NMR spectrum of compound **13c**.

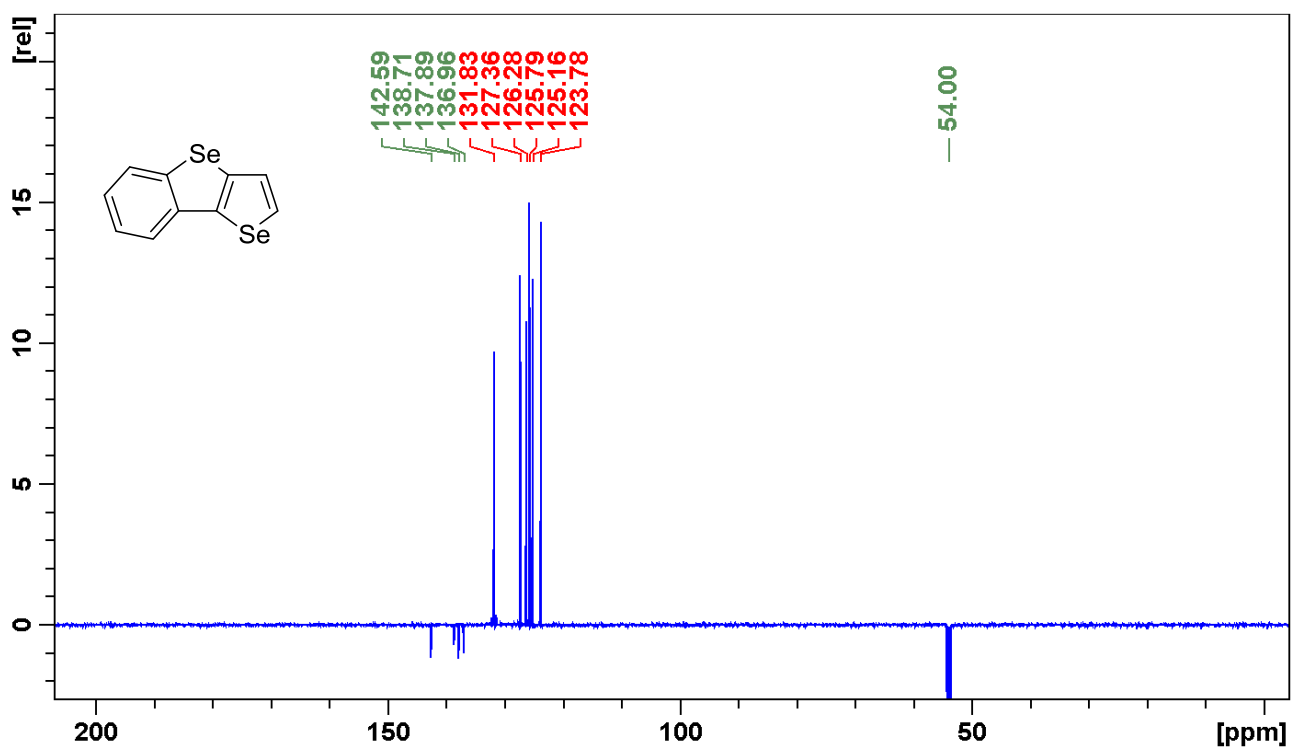


Figure S71. ¹³C NMR spectrum of compound 13c.

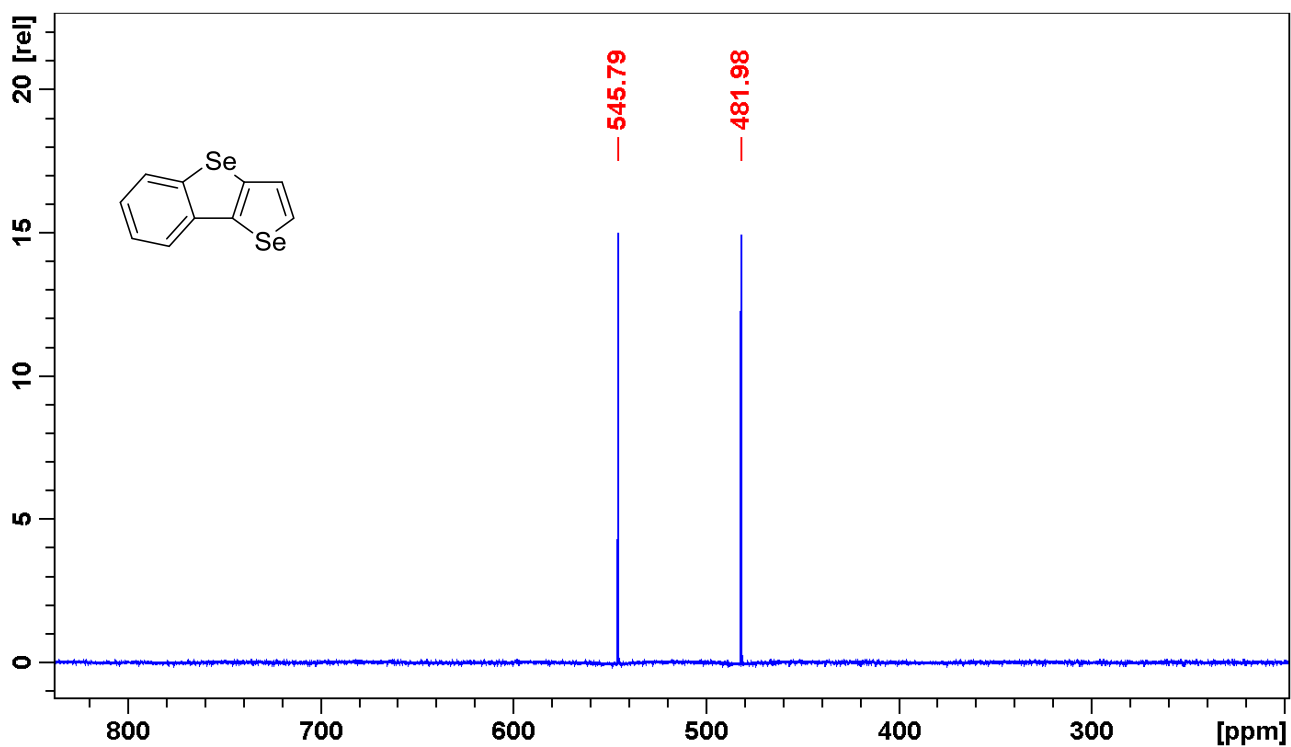


Figure S72. ⁷⁷Se NMR spectrum of compound 13c.

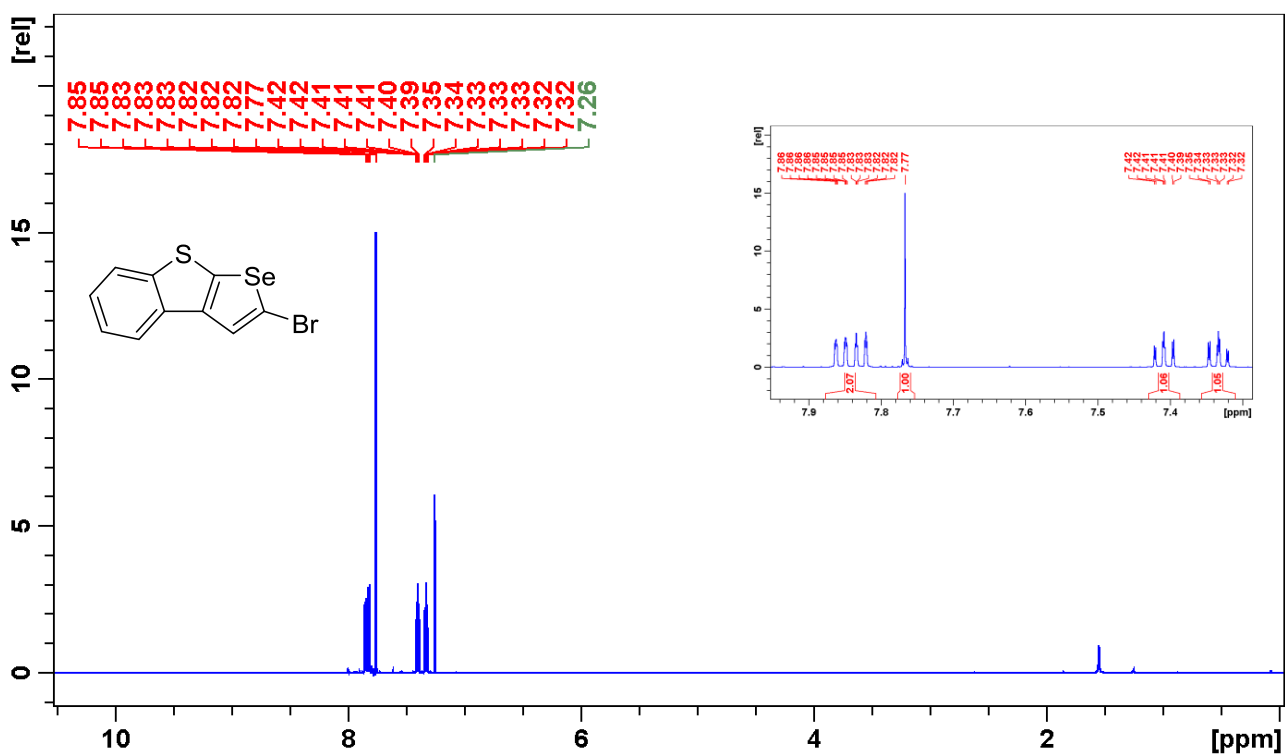


Figure S73. ¹H NMR spectrum of compound **10a**.

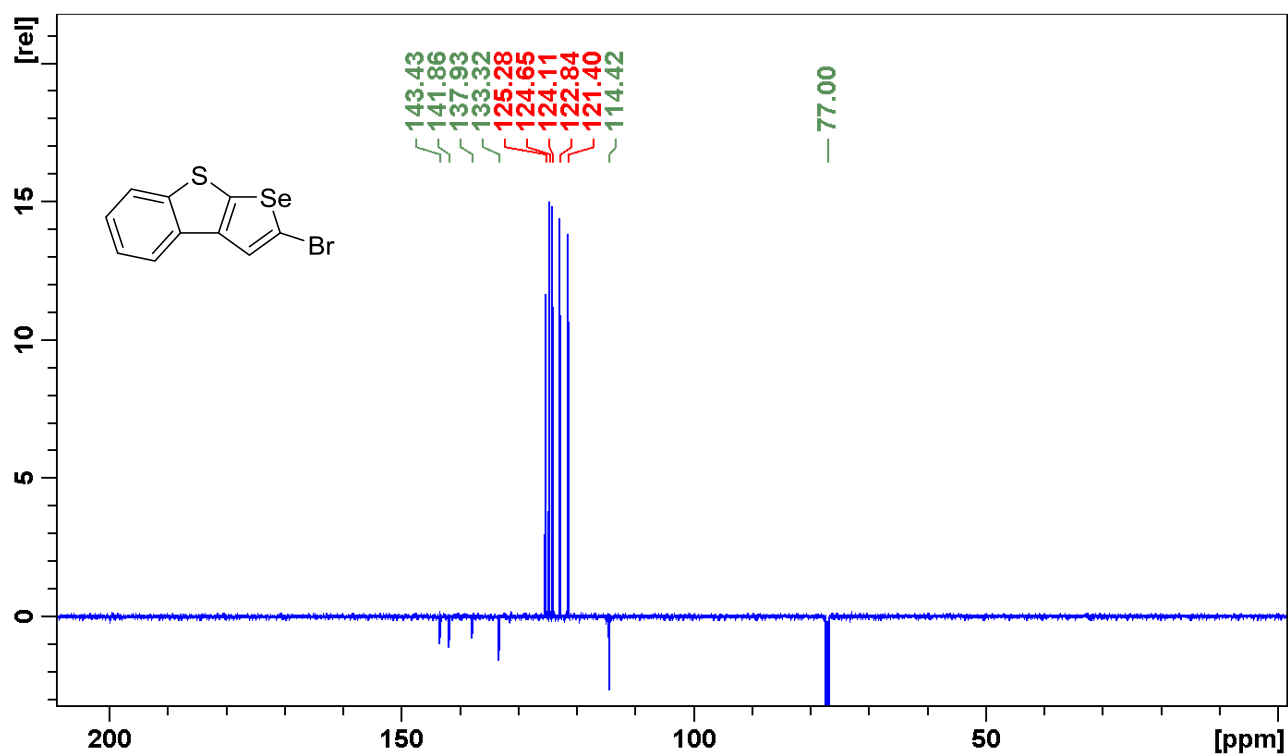


Figure S74. ¹³C NMR spectrum of compound **10a**.

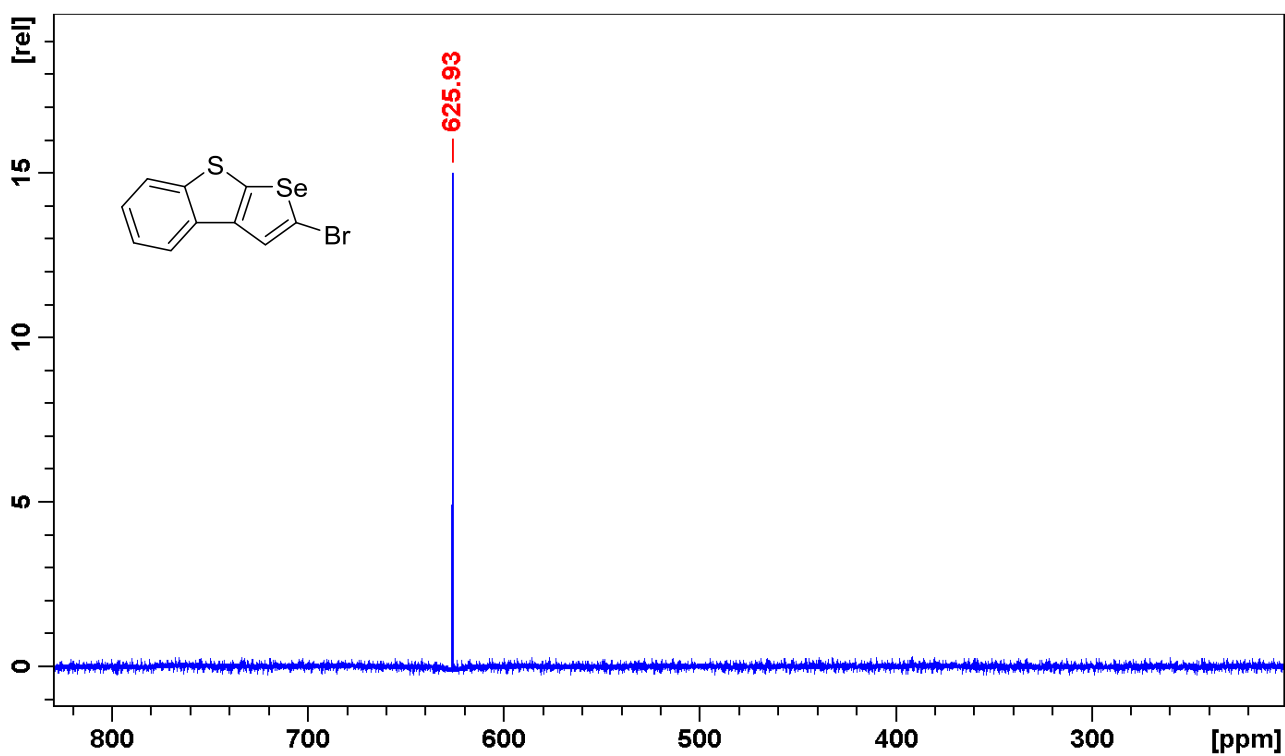


Figure S75. ^{77}Se NMR spectrum of compound **10a**.

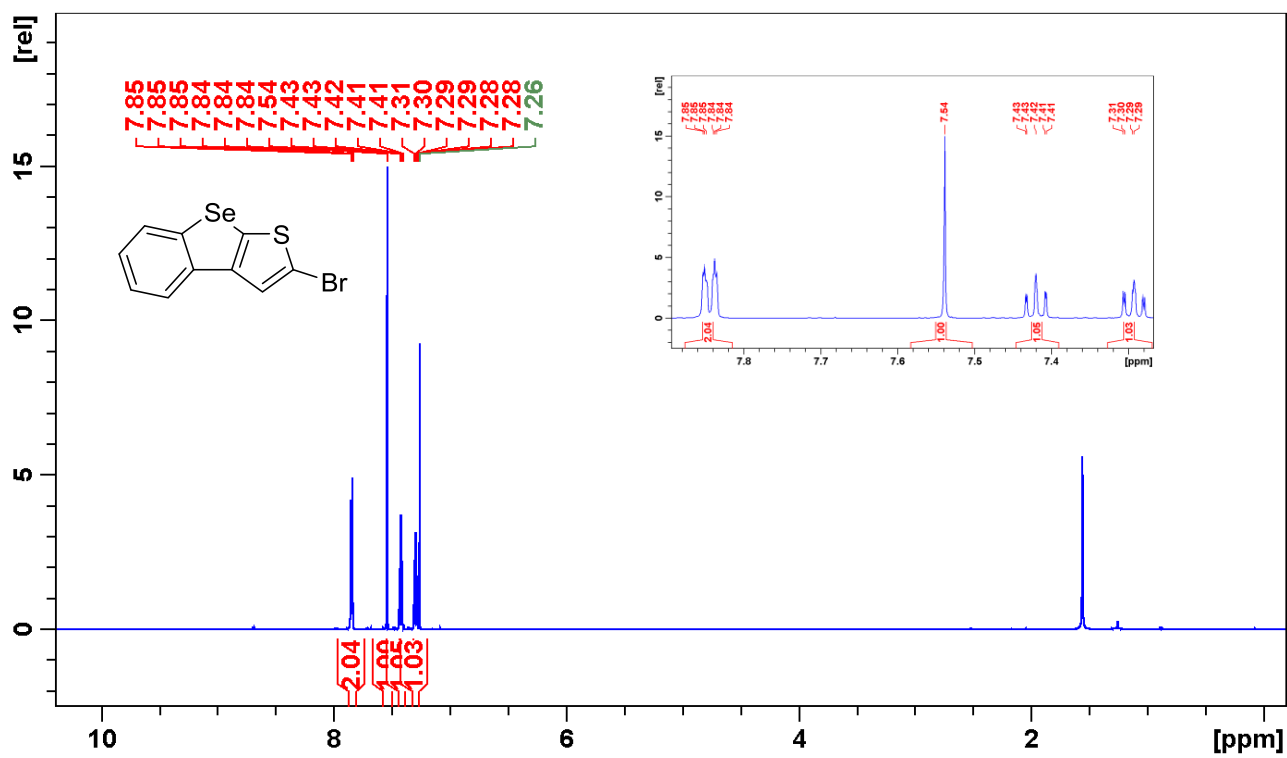


Figure S76. ^1H NMR spectrum of compound **10b**.

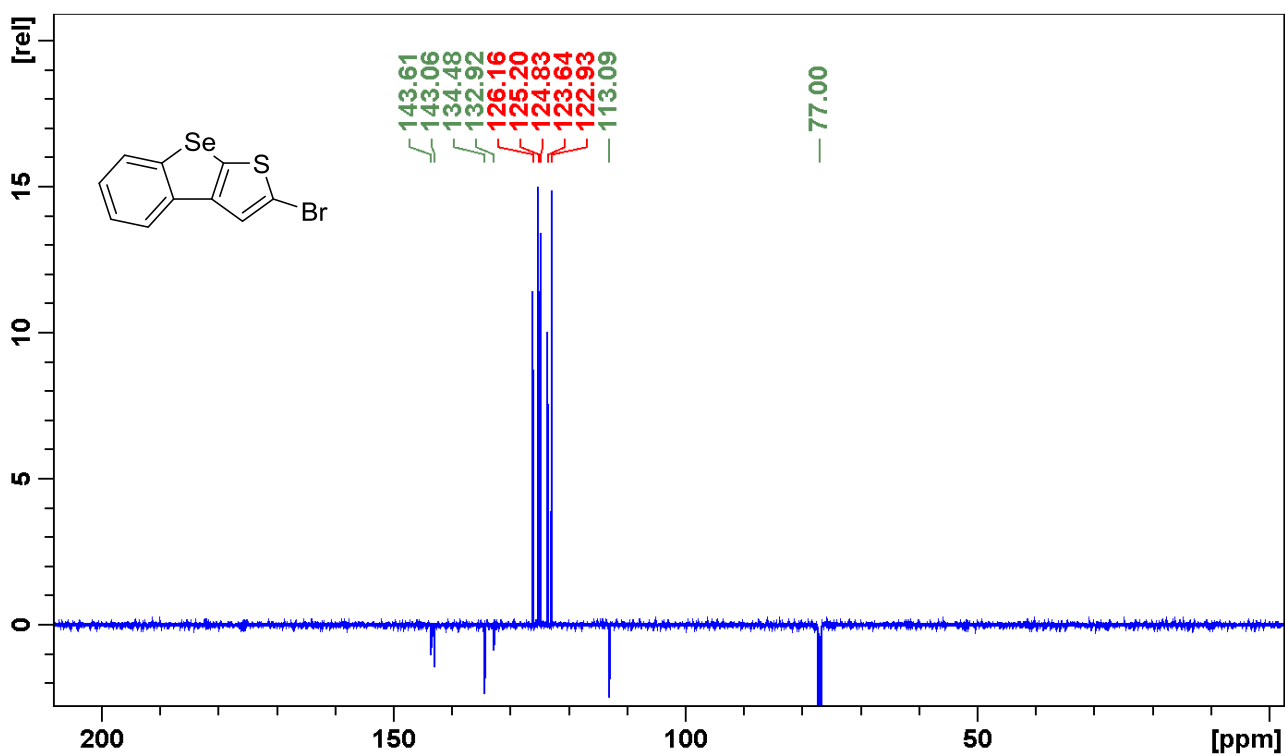


Figure S77. ^{13}C NMR spectrum of compound **10b**.

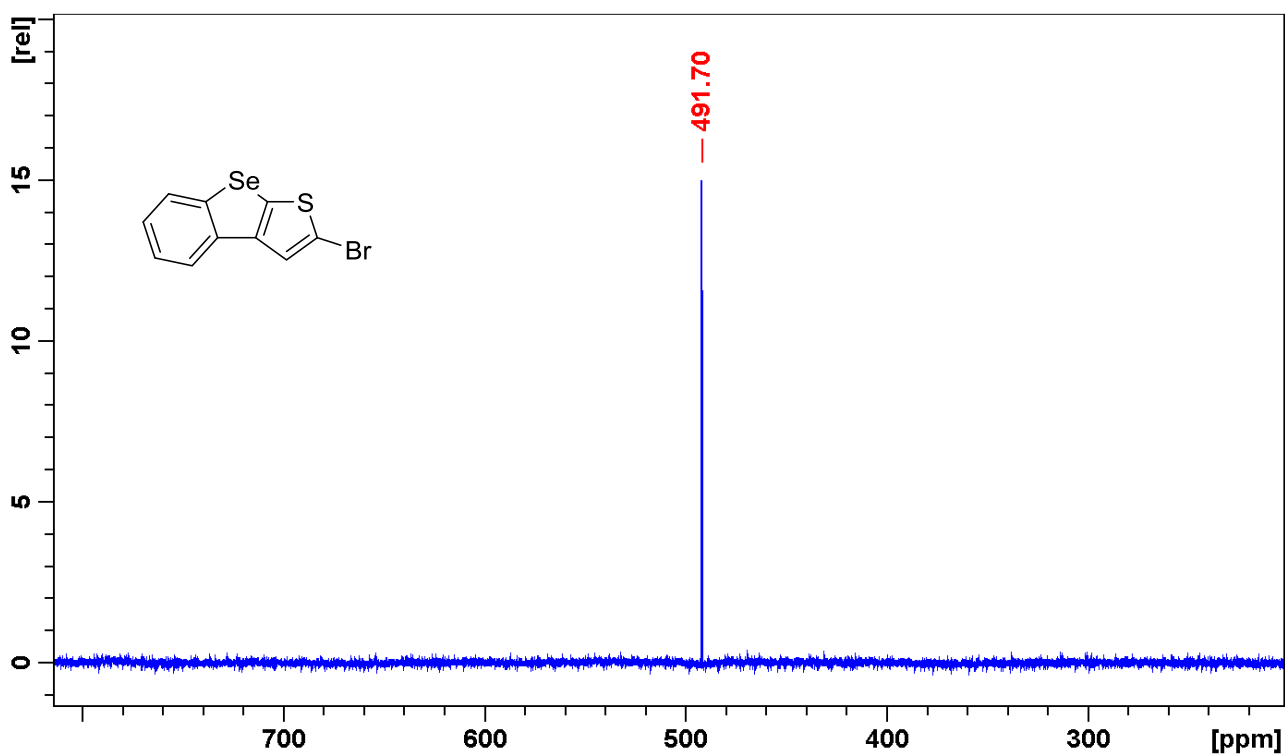


Figure S78. ^{77}Se NMR spectrum of compound **10b**.

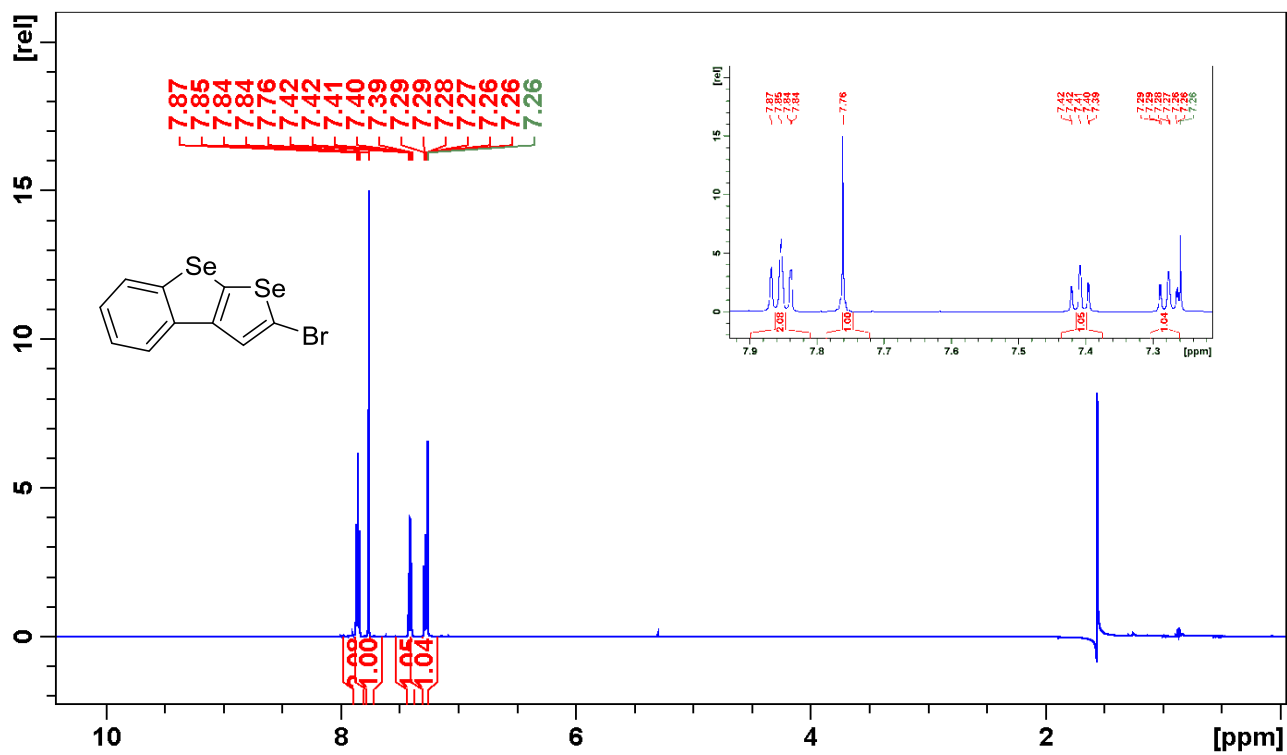


Figure S79. ¹H NMR spectrum of compound 10c.

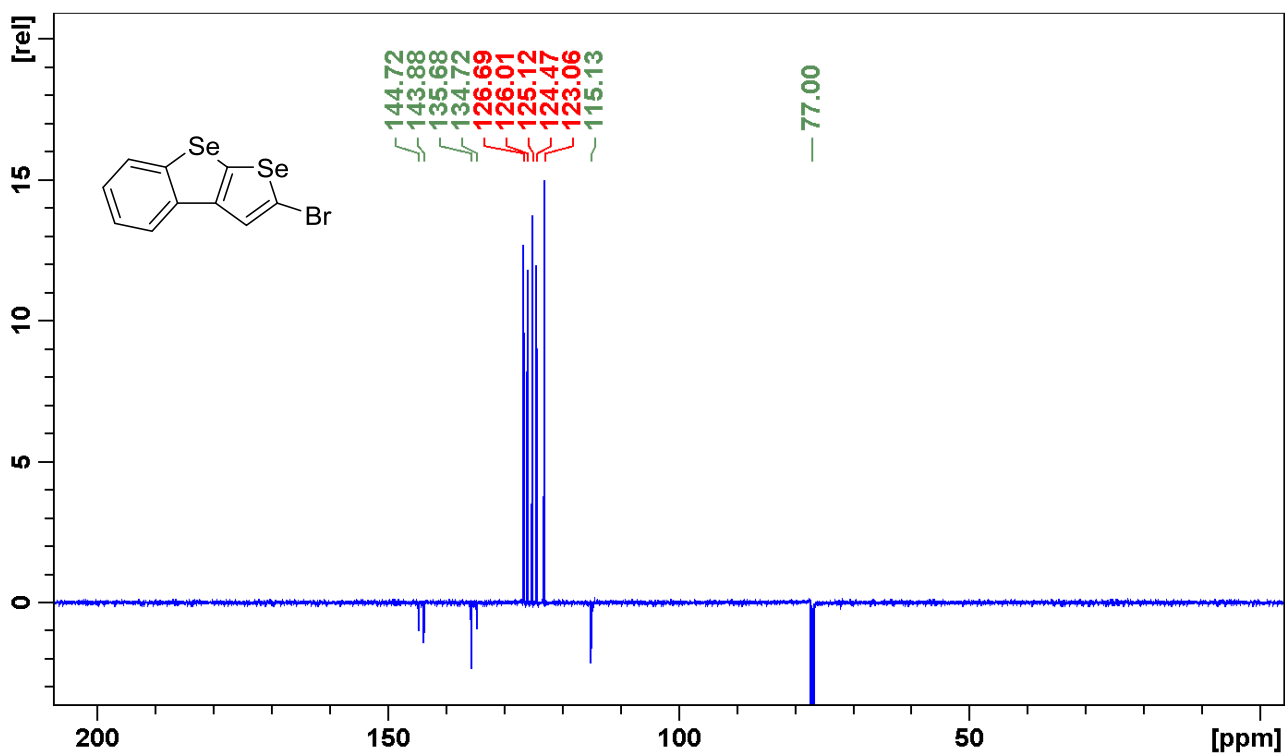


Figure S80. ¹³C NMR spectrum of compound 10c.

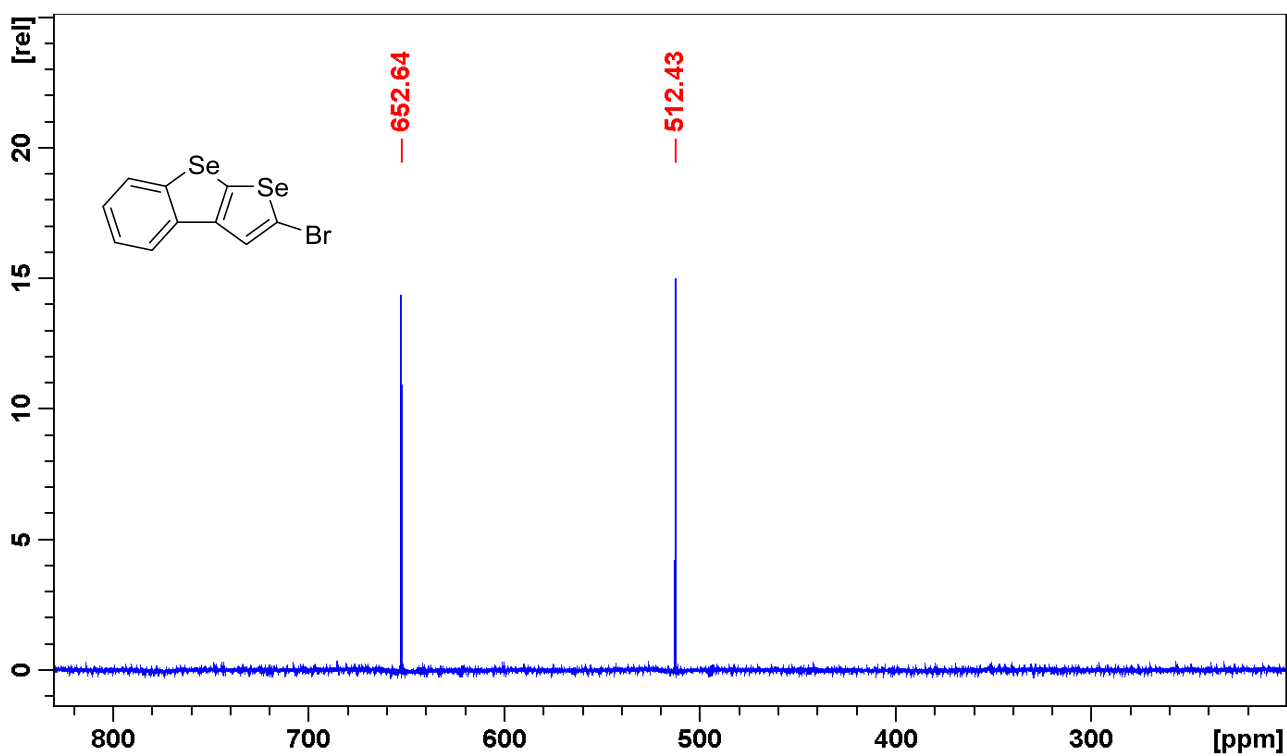


Figure S81. ^{77}Se NMR spectrum of compound **10c**.

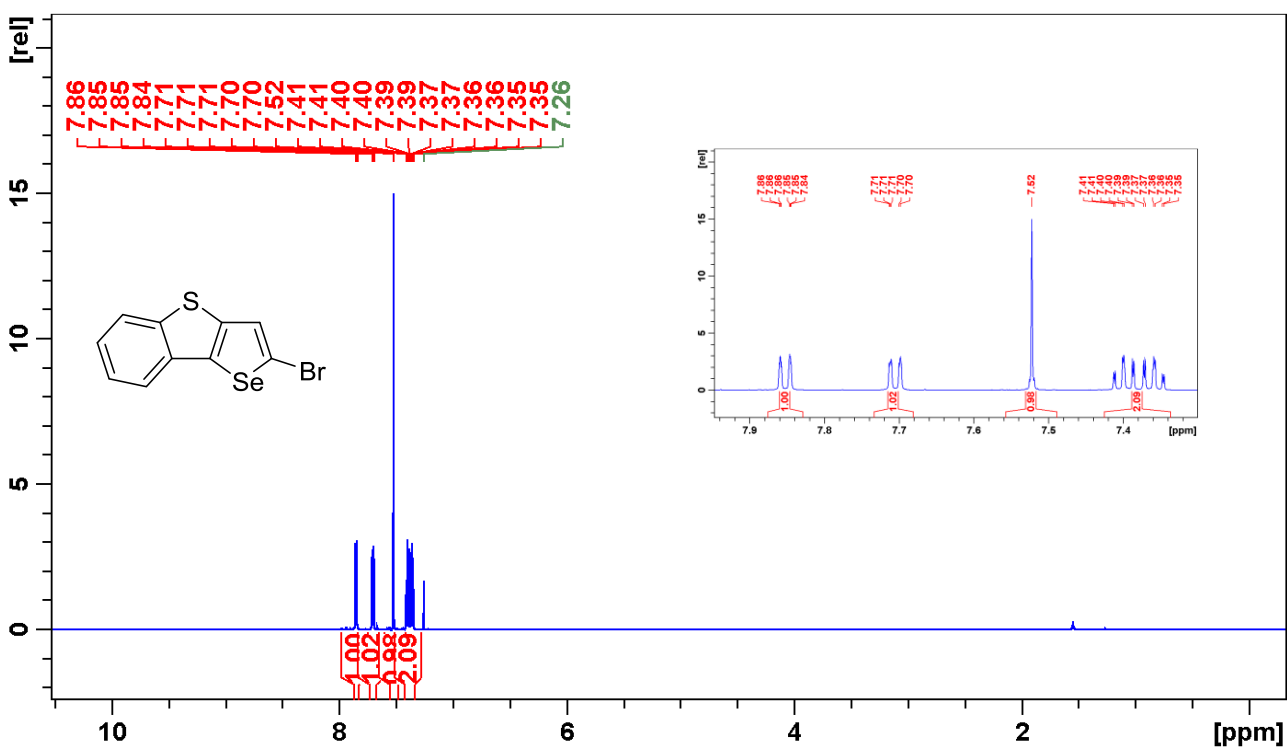


Figure S82. ^1H NMR spectrum of compound **14a**.

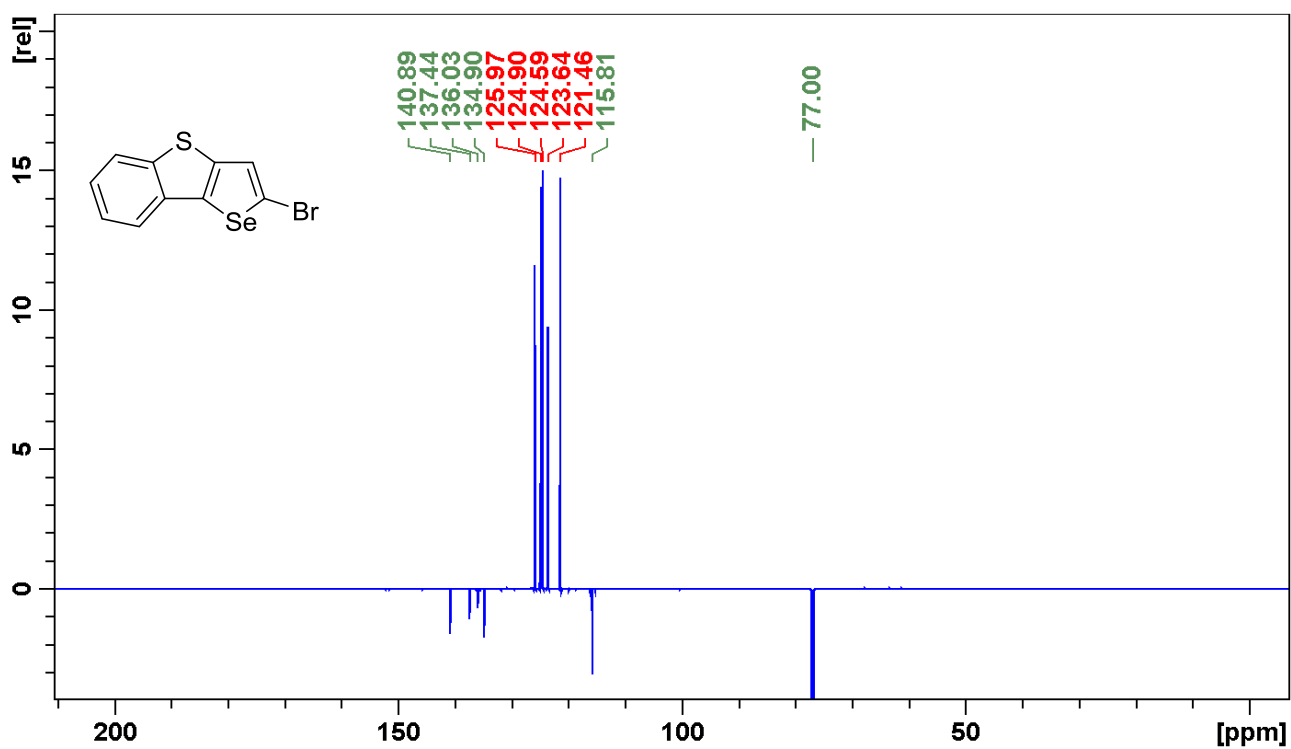


Figure S83. ¹³C NMR spectrum of compound 14a.

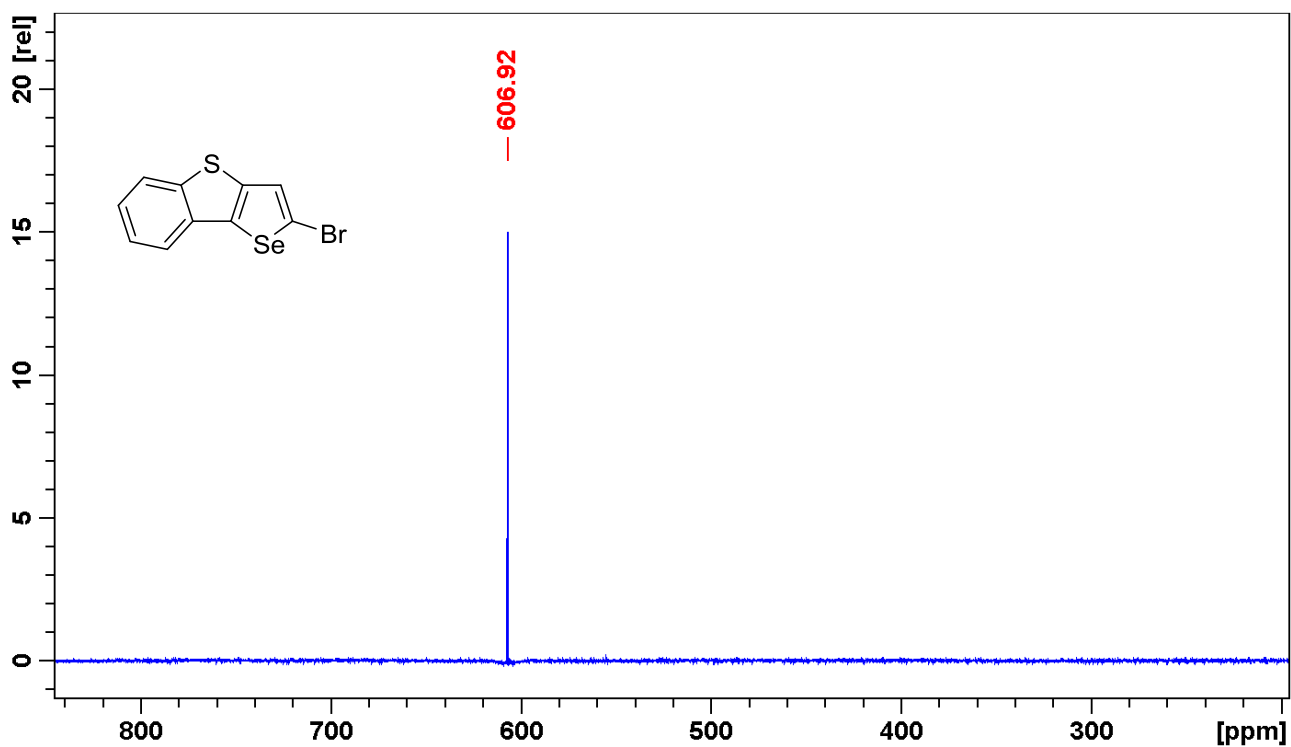


Figure S84. ⁷⁷Se NMR spectrum of compound 14a.

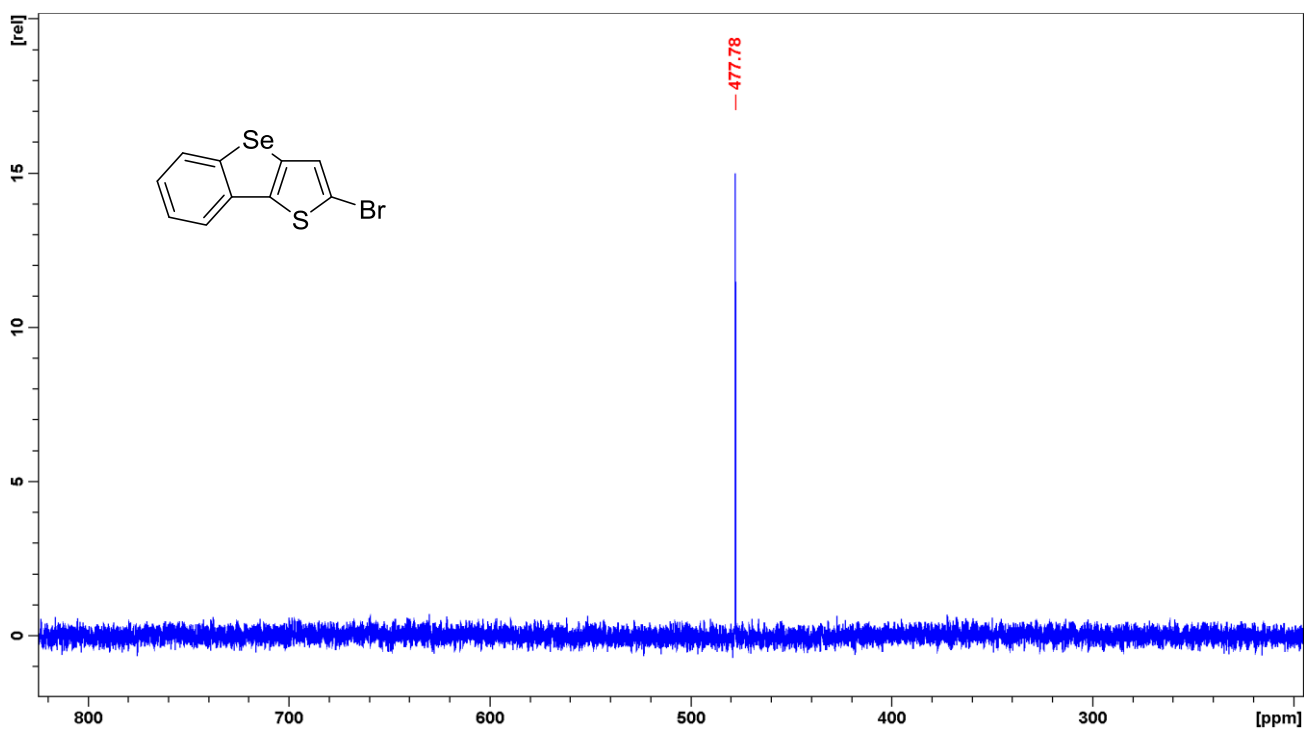


Figure S87. ⁷⁷Se NMR spectrum of compound **14b**.

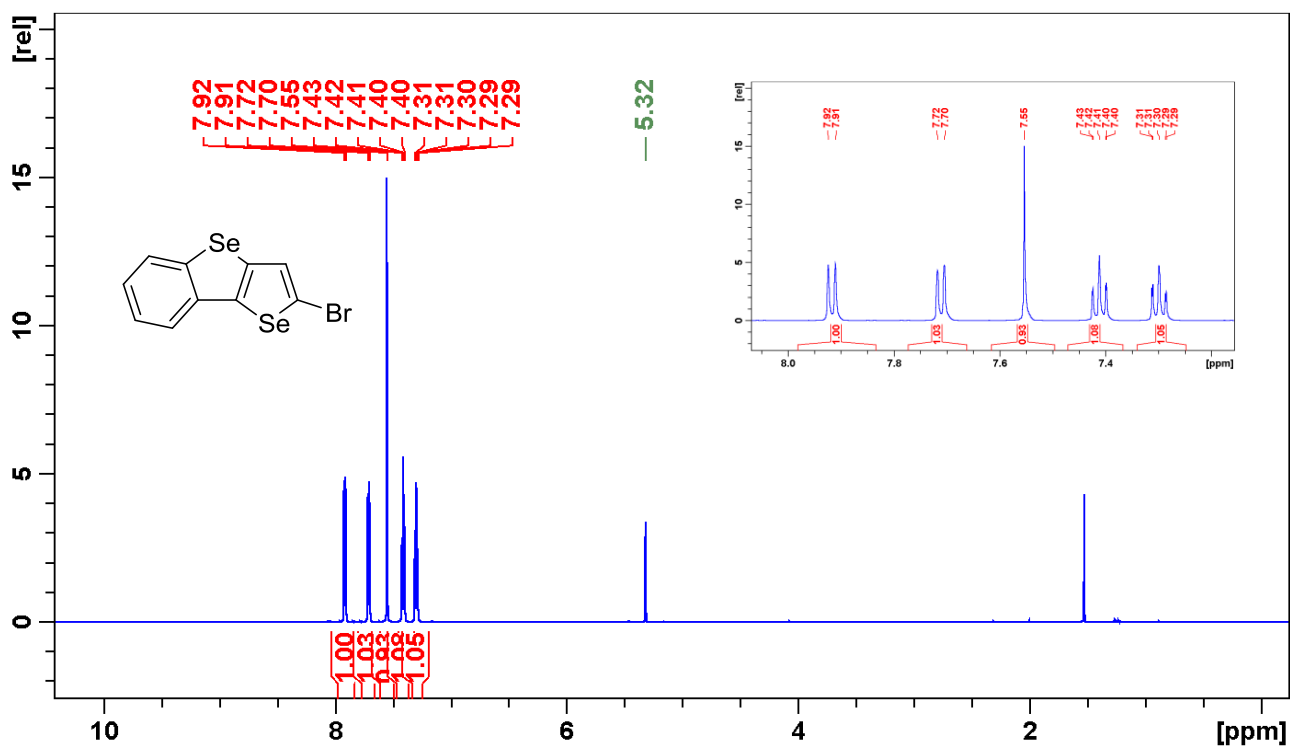


Figure S88. ¹H NMR spectrum of compound **14c**.

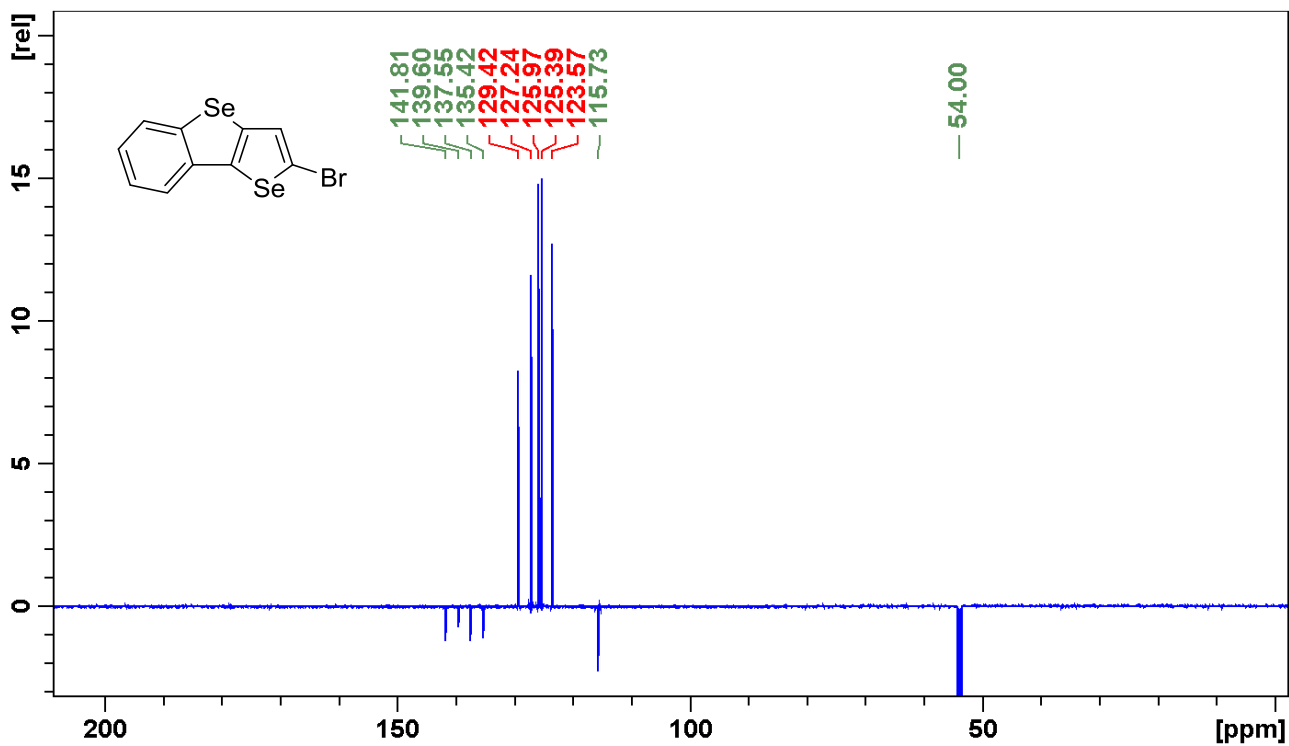


Figure S89. ^{13}C NMR spectrum of compound **14c**.

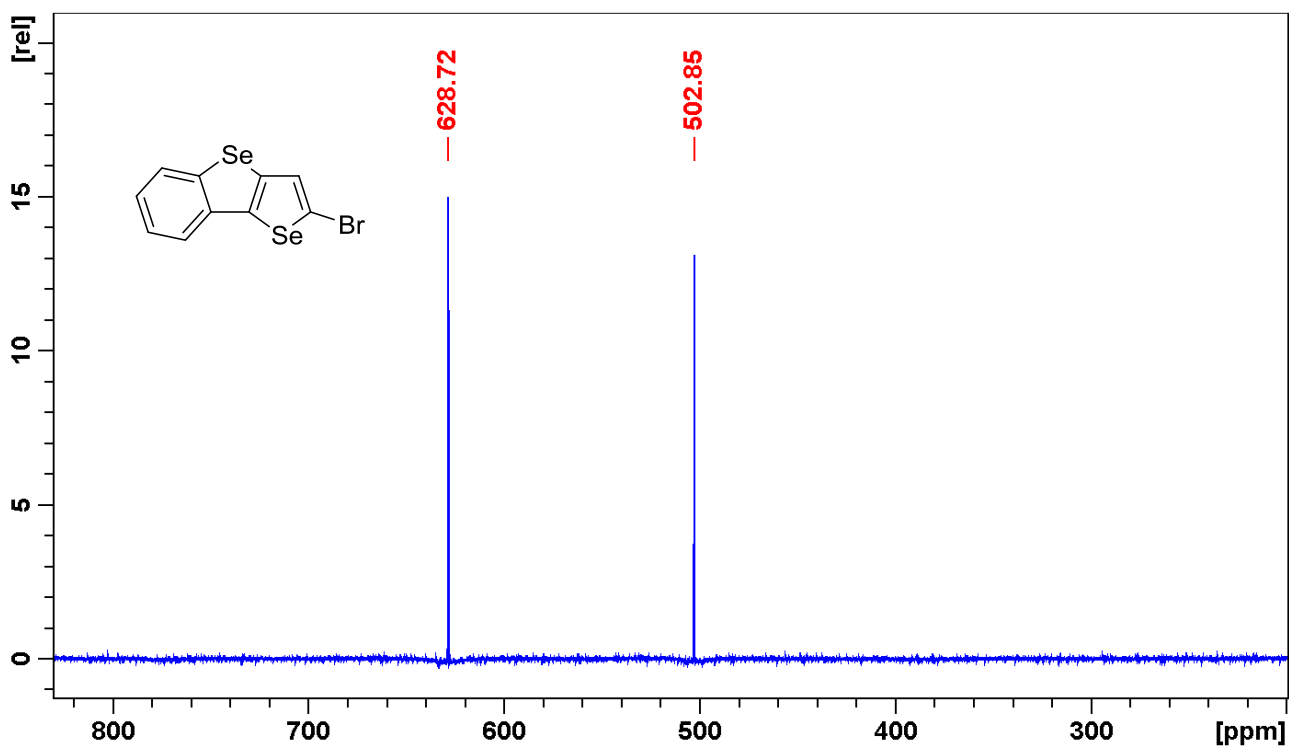


Figure S90. ^{77}Se NMR spectrum of compound **14c**.

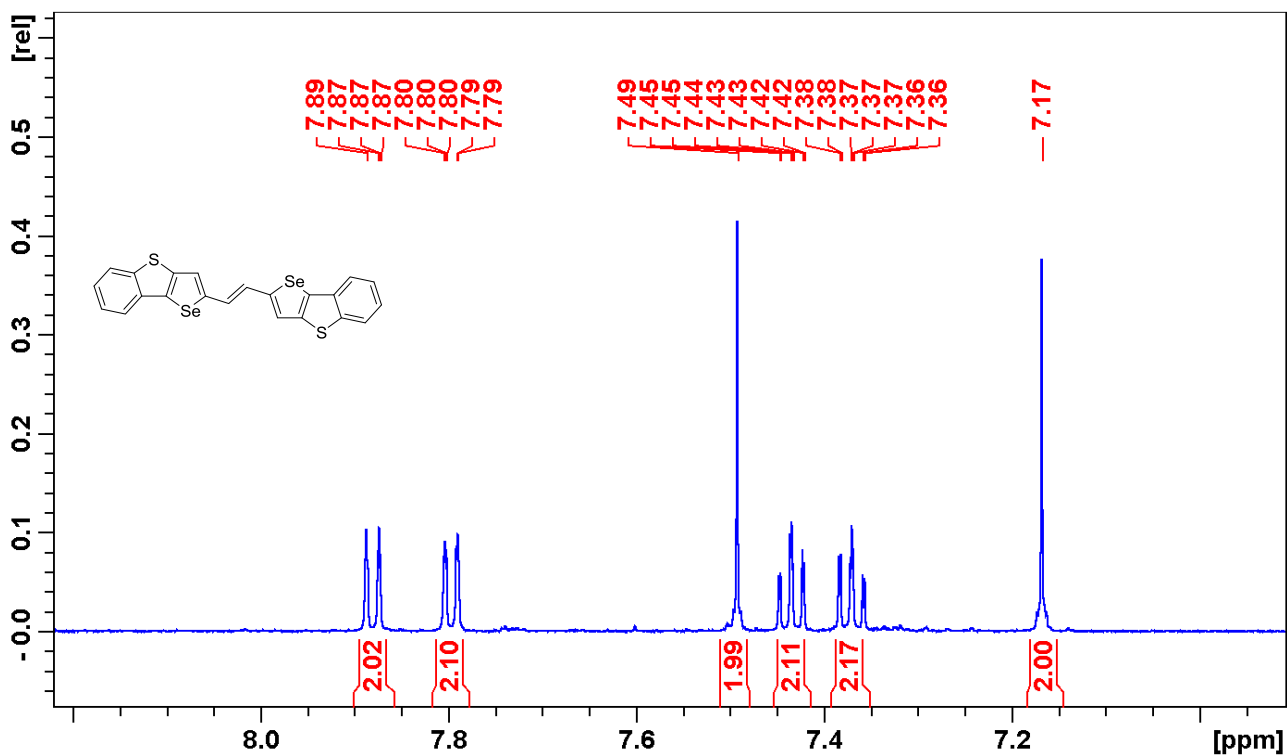


Figure S91. ^1H NMR spectrum of compound 7a.

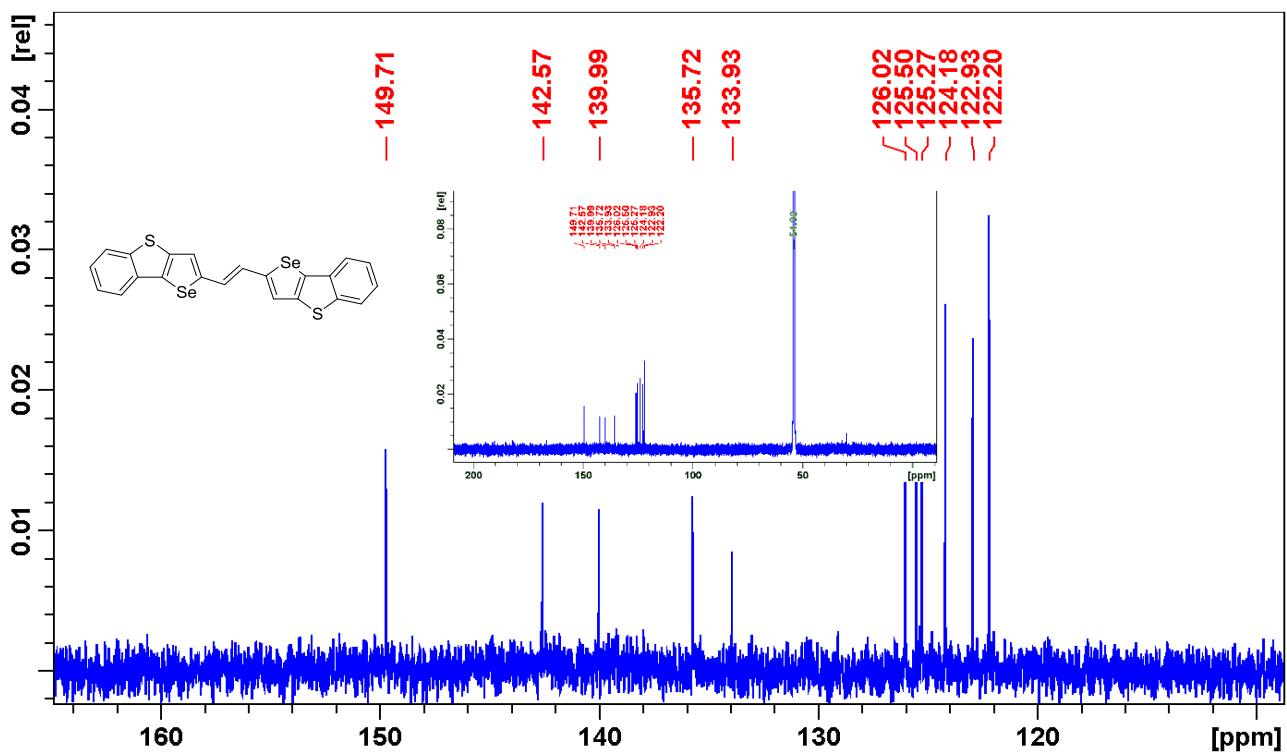


Figure S92. ^{13}C NMR spectrum of compound 7a.

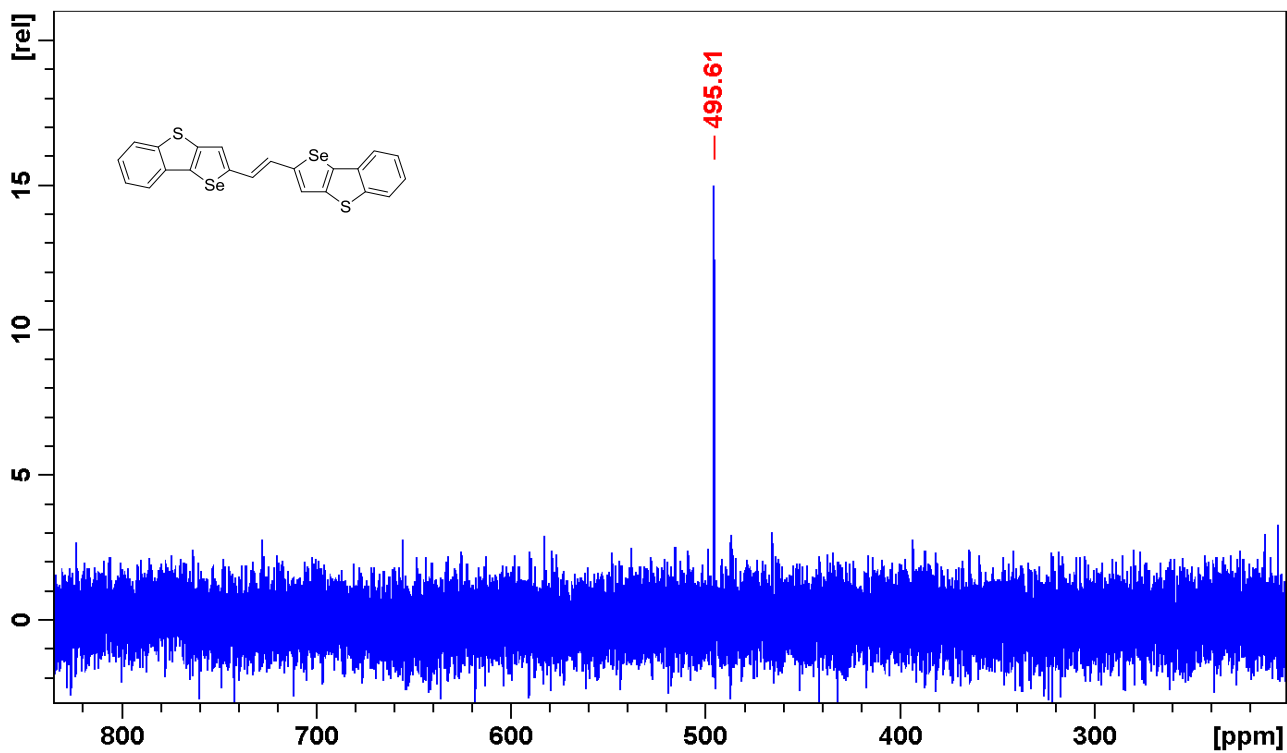


Figure S93. ^{77}Se NMR spectrum of compound 7a.

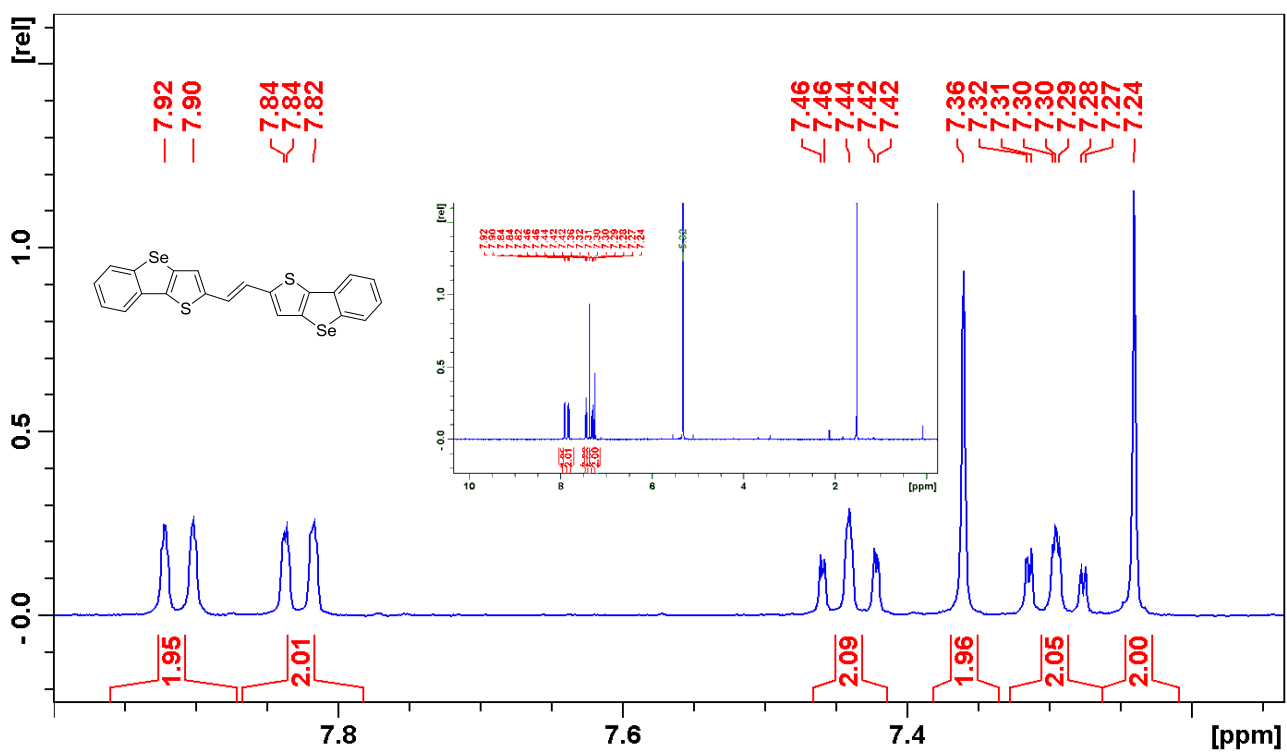


Figure S94. ^1H NMR spectrum of compound 7b.

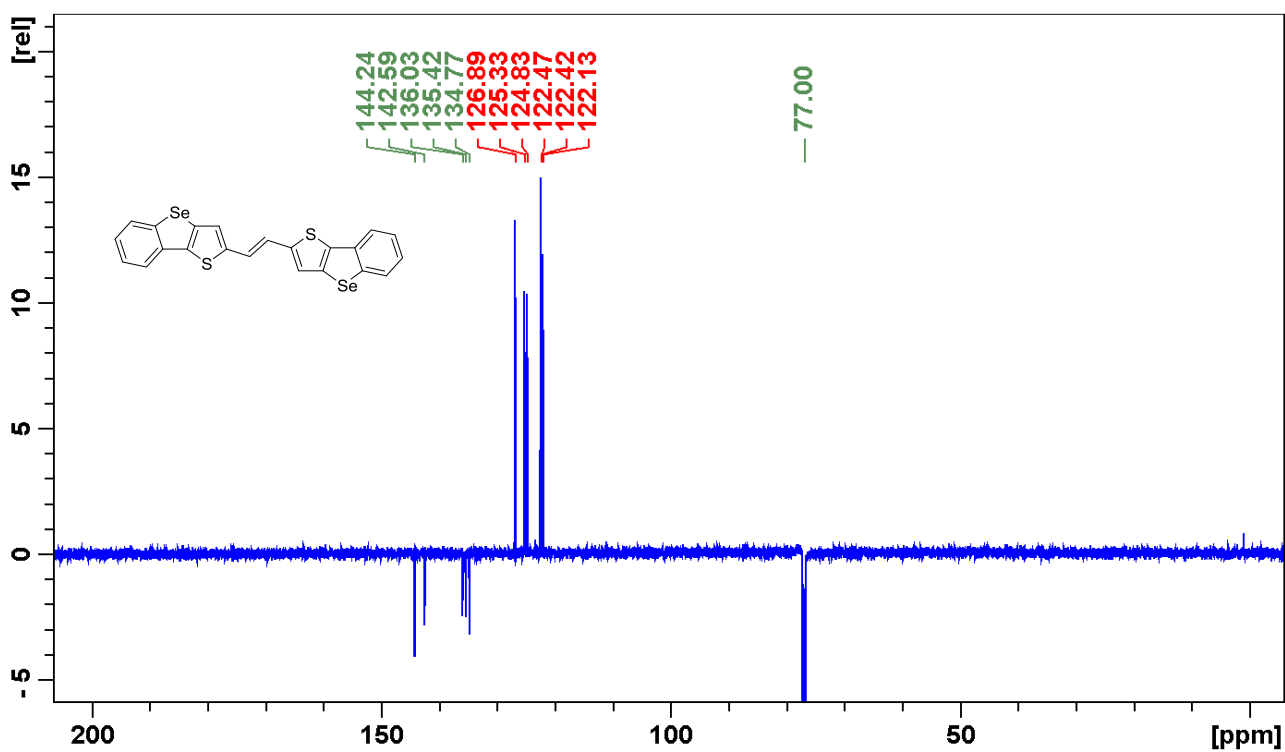


Figure S95. ¹³C NMR spectrum of compound 7b.

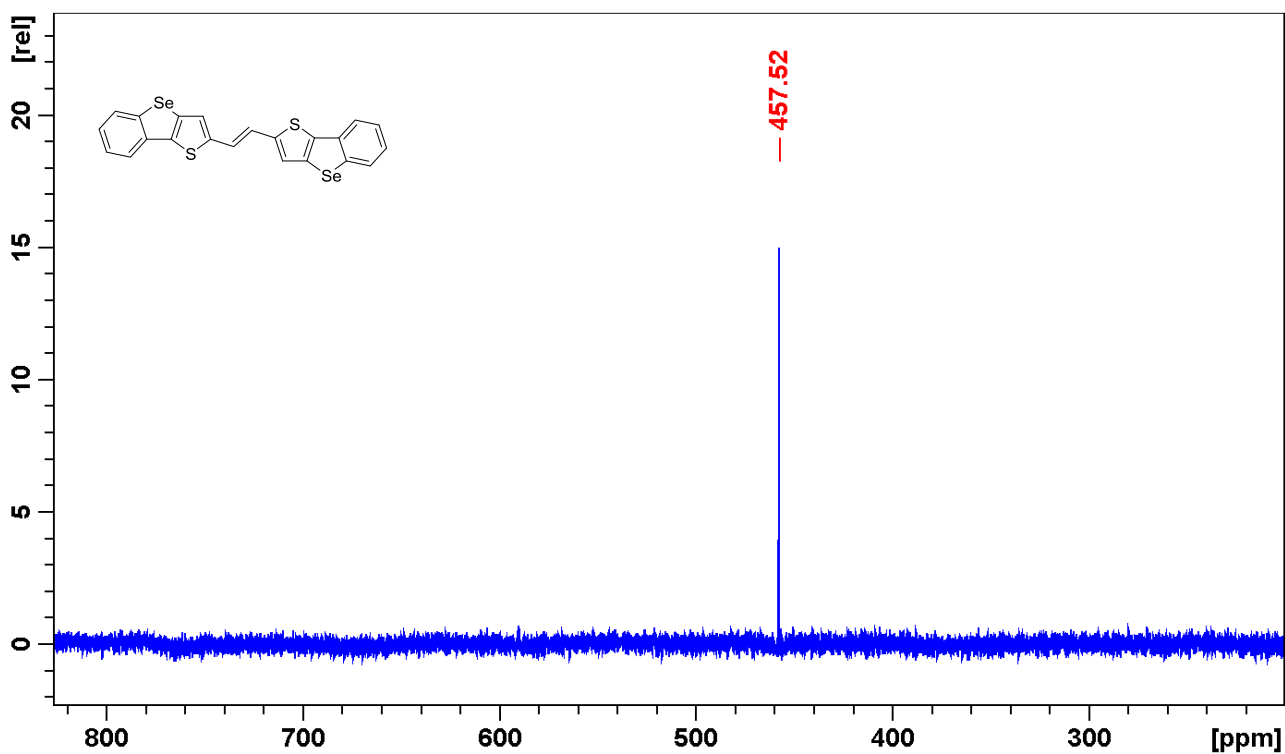
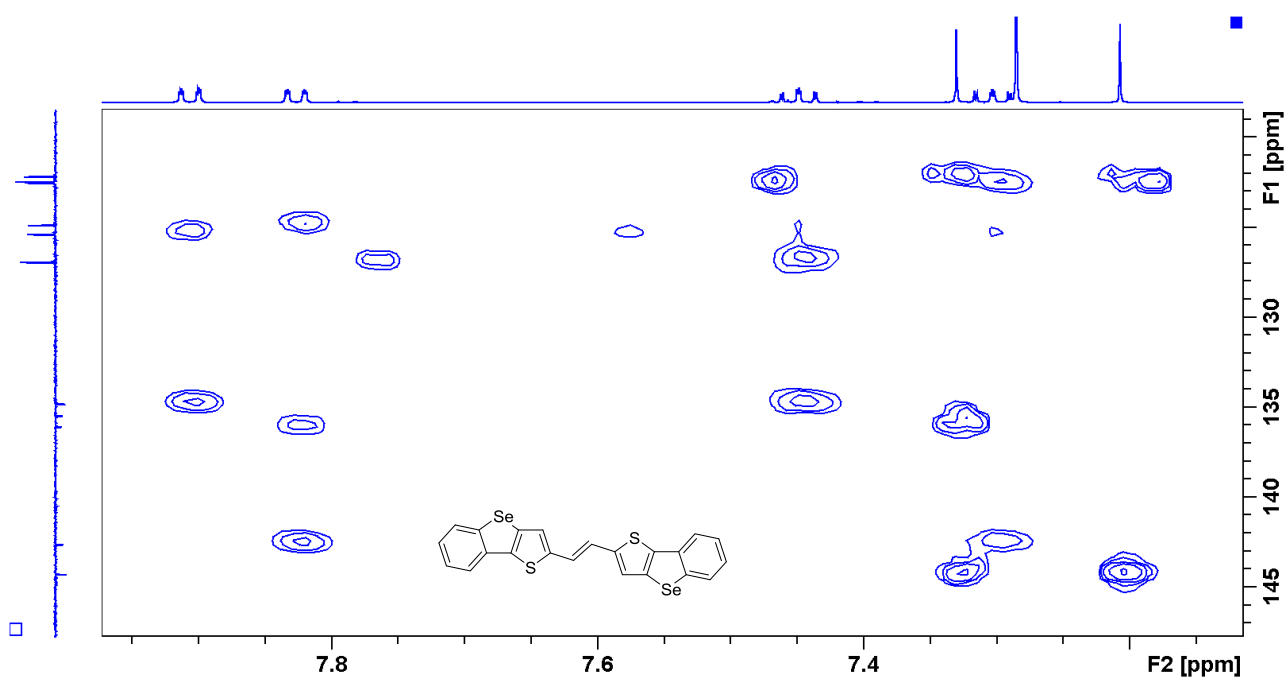
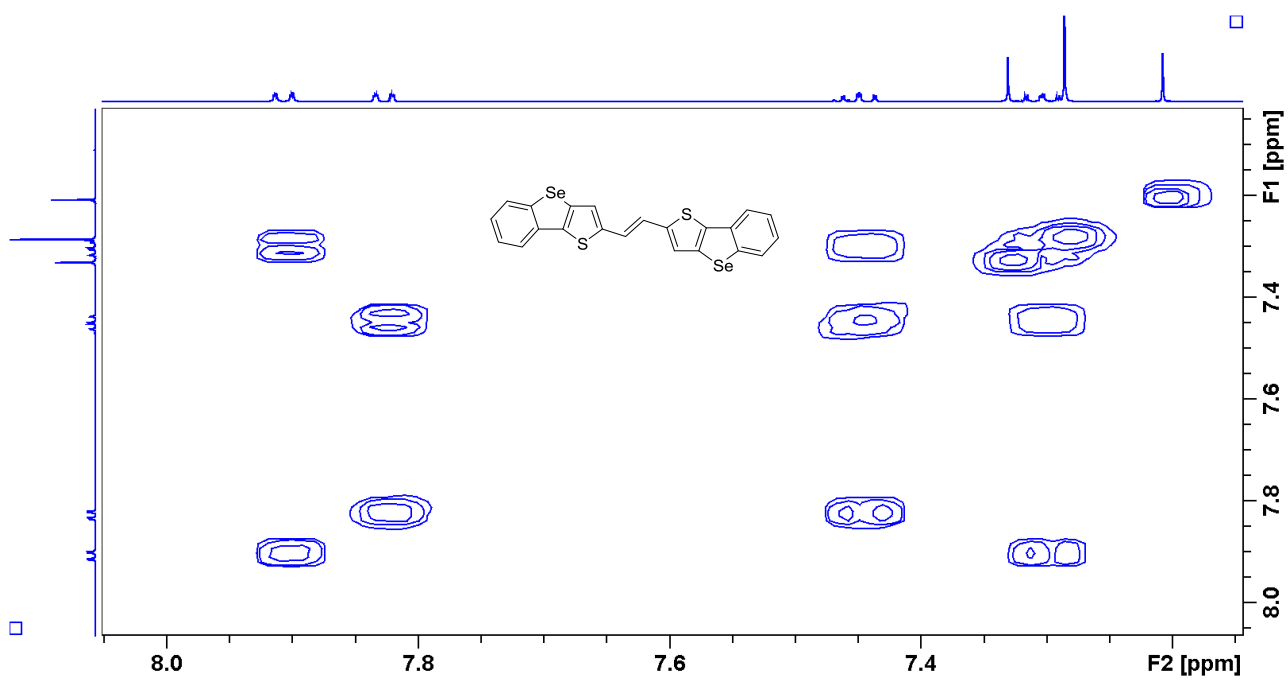


Figure S96. ⁷⁷Se NMR spectrum of compound 7b.



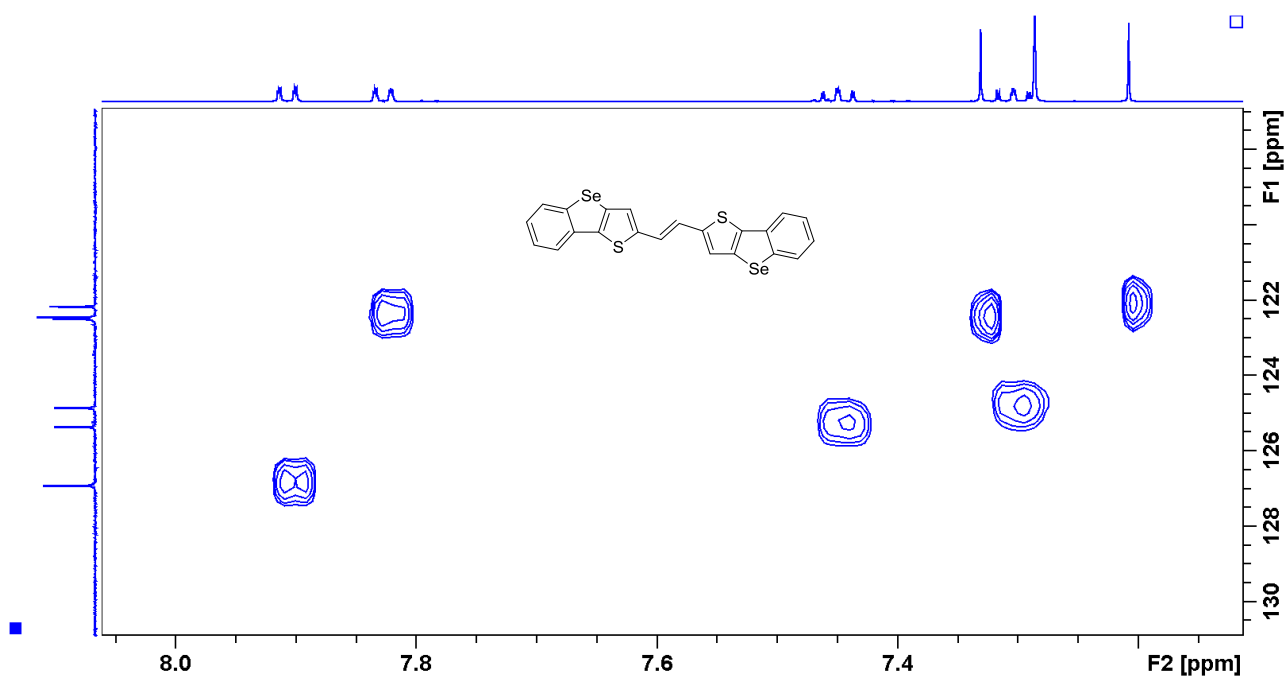


Figure S99. HC HSQC NMR spectrum of compound **7b**.

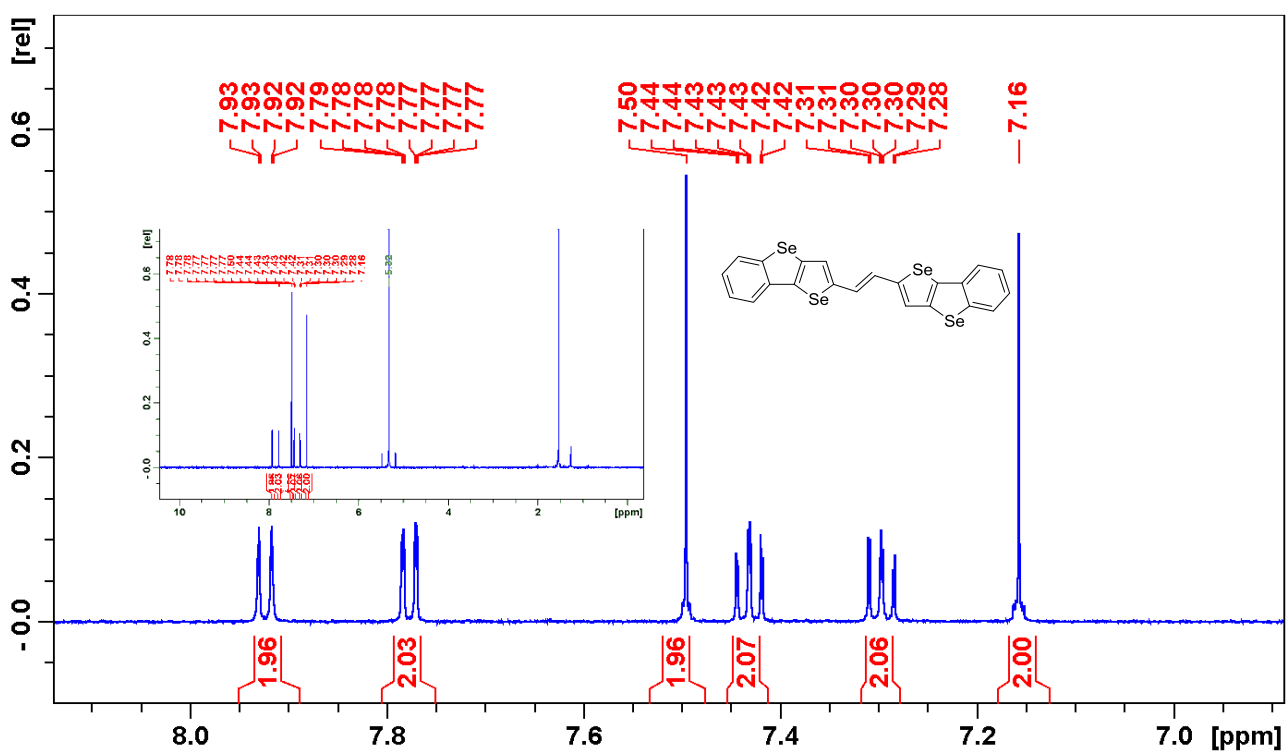


Figure S100. ^1H NMR spectrum of compound **7c**.

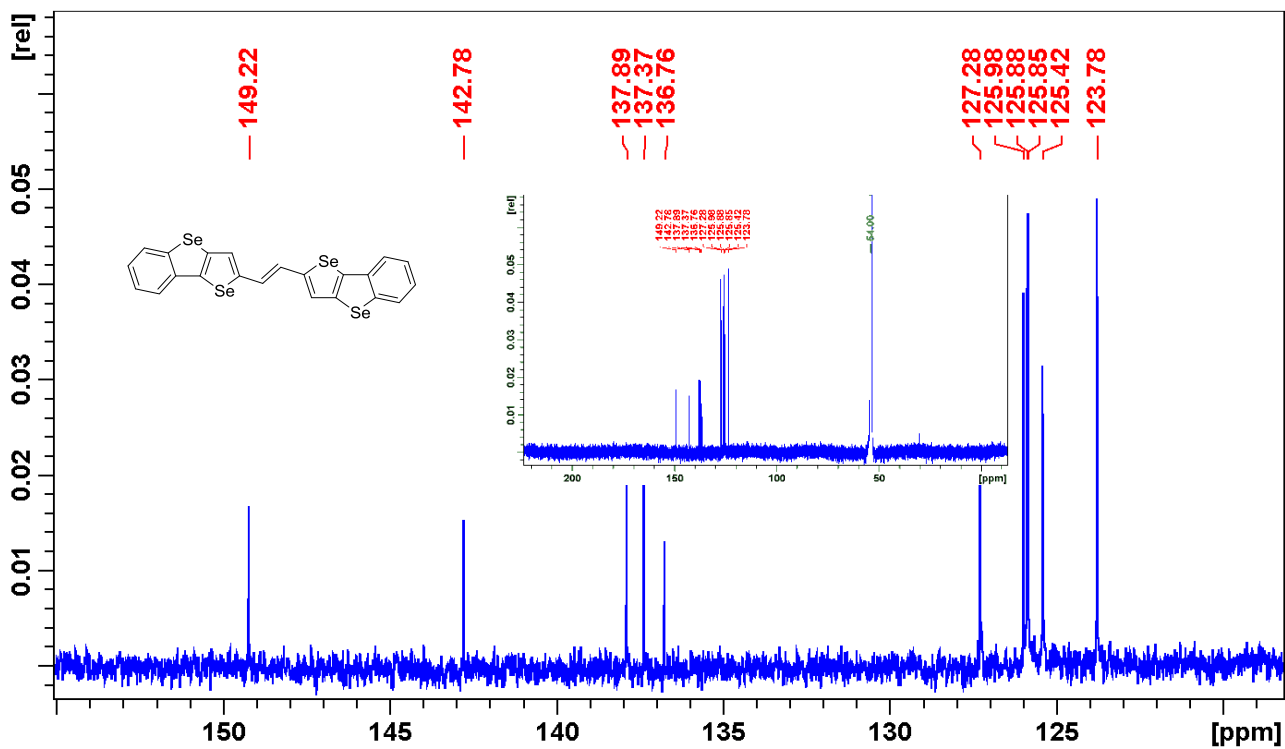


Figure S101. ^{13}C NMR spectrum of compound 7c.

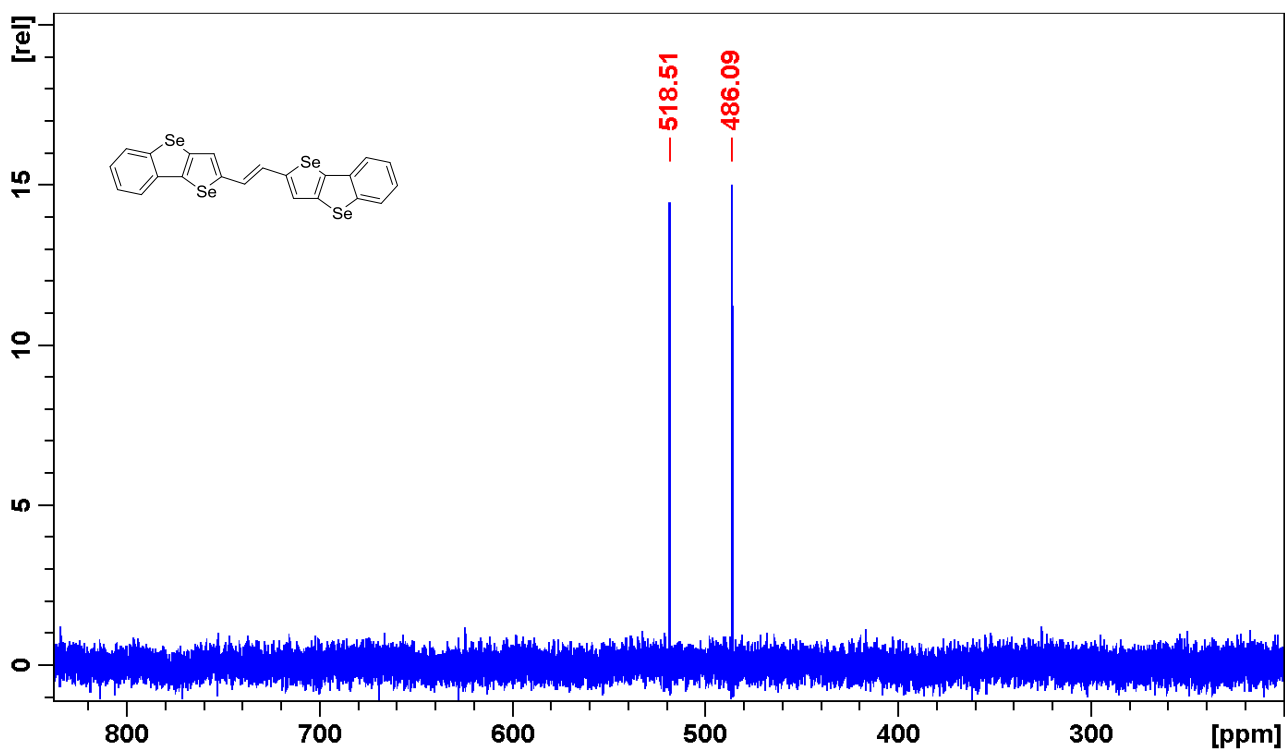


Figure S102. ^{77}Se NMR spectrum of compound 7c.

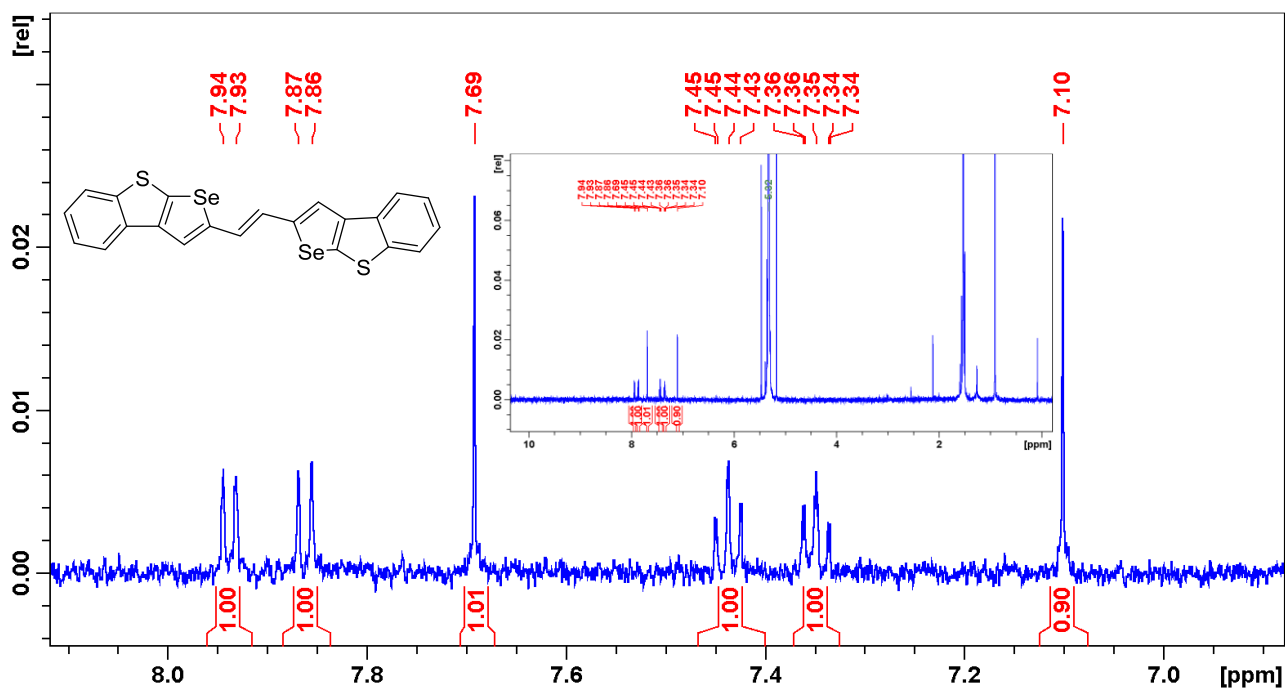


Figure S103. ^1H NMR spectrum of compound 11a.

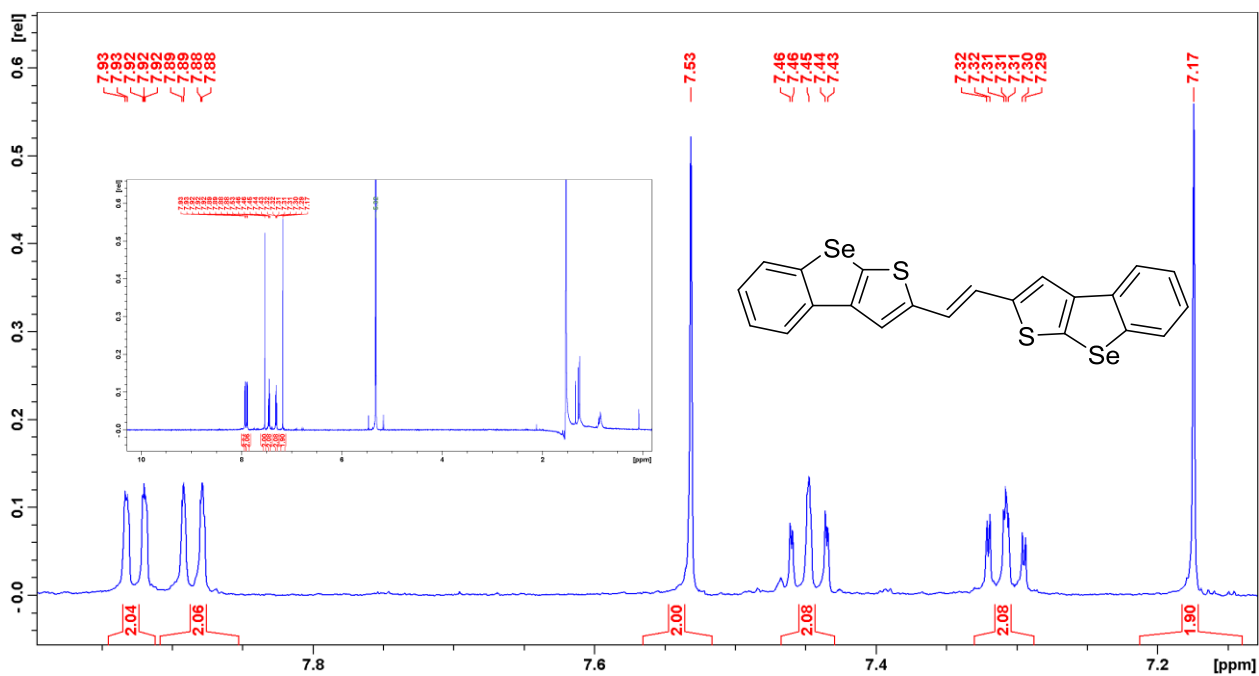


Figure S104. ^1H NMR spectrum of compound 11b.

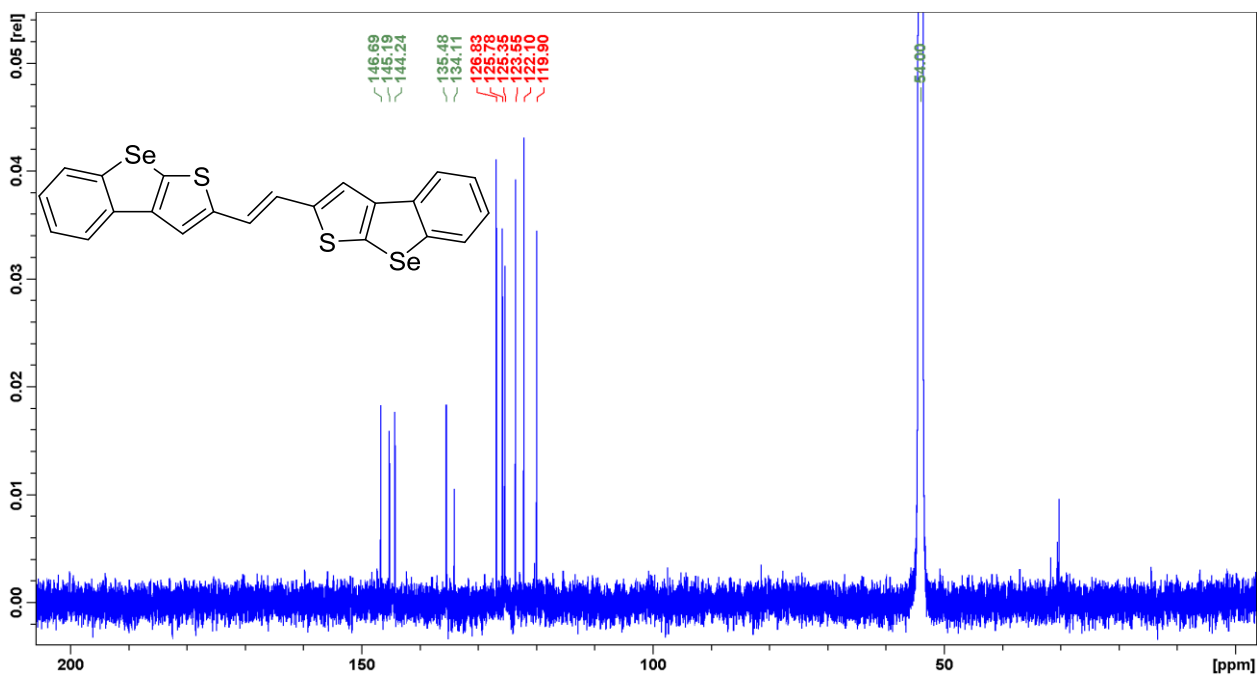


Figure S105. ^{13}C NMR spectrum of compound **11b**.

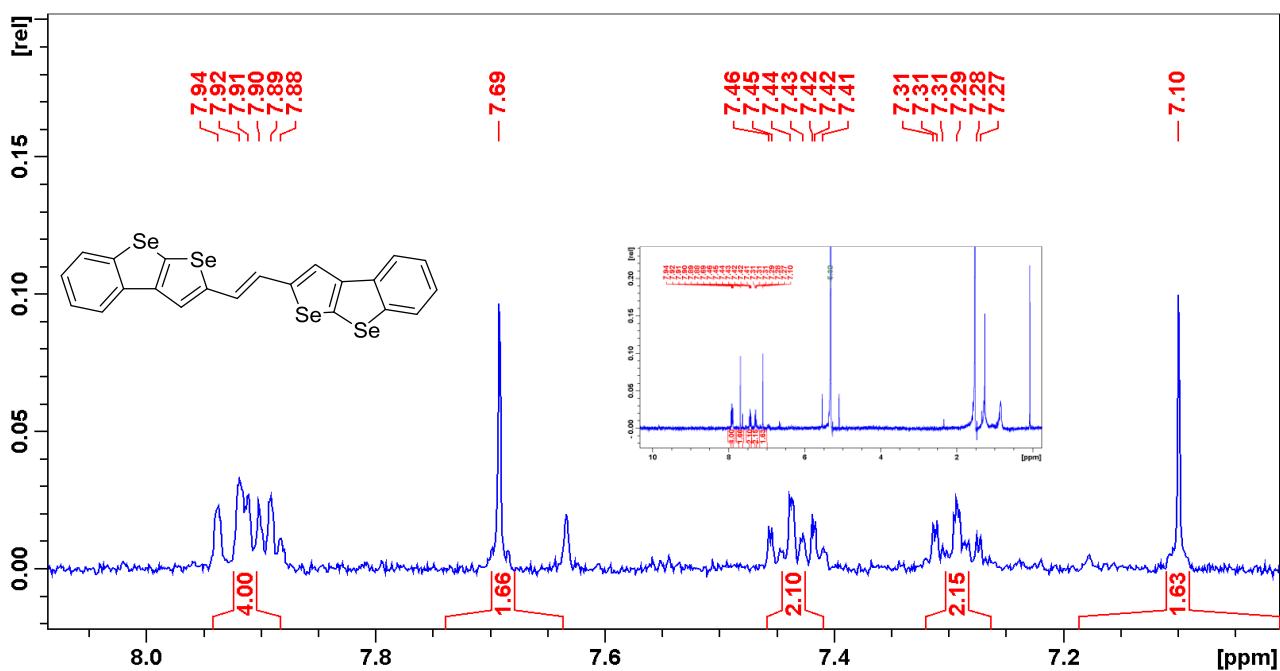


Figure S106. ^1H NMR spectrum of compound **11c**.

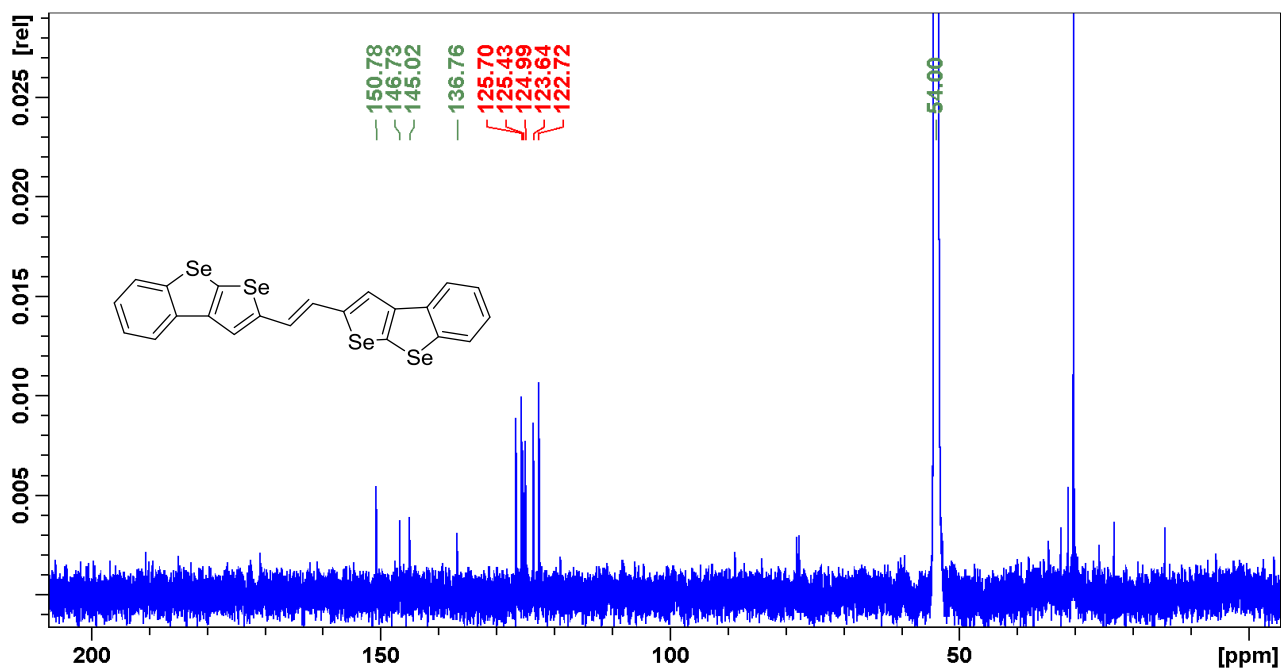


Figure S107. ¹³C NMR spectrum of compound 11c.

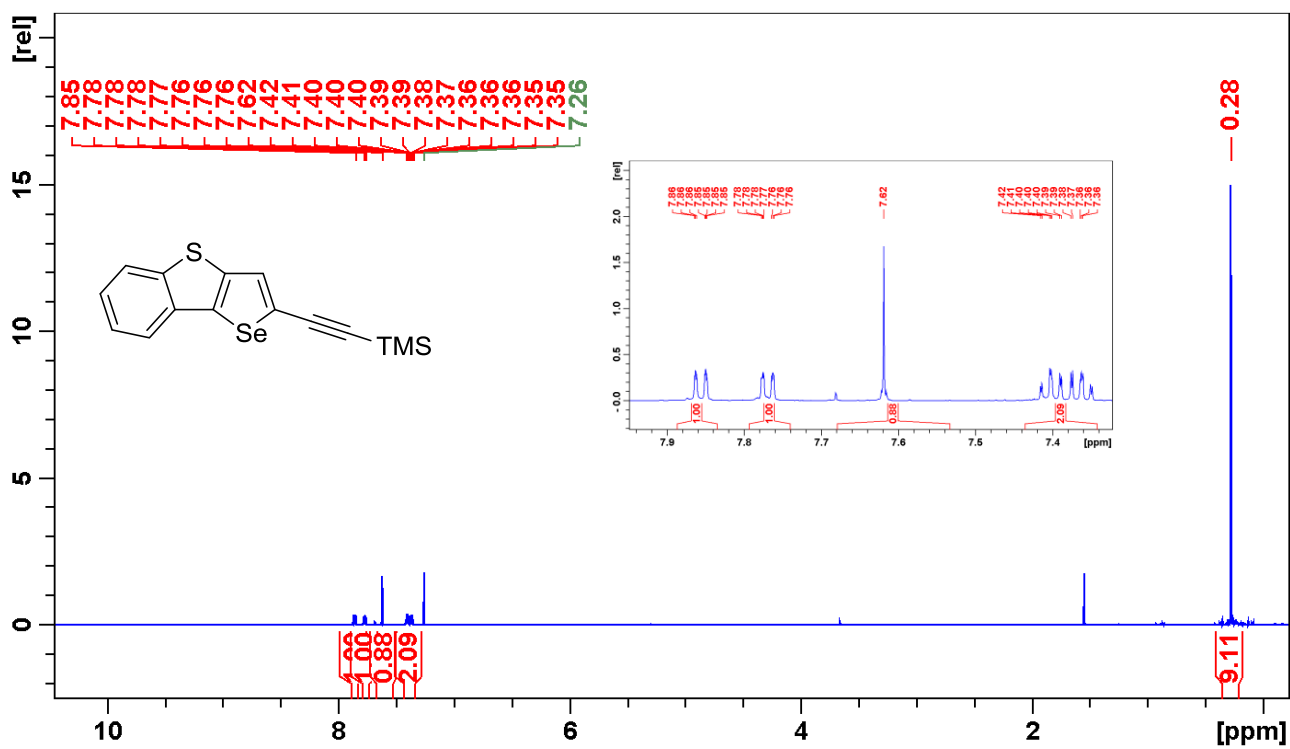


Figure S108. ¹H NMR spectrum of compound 15.

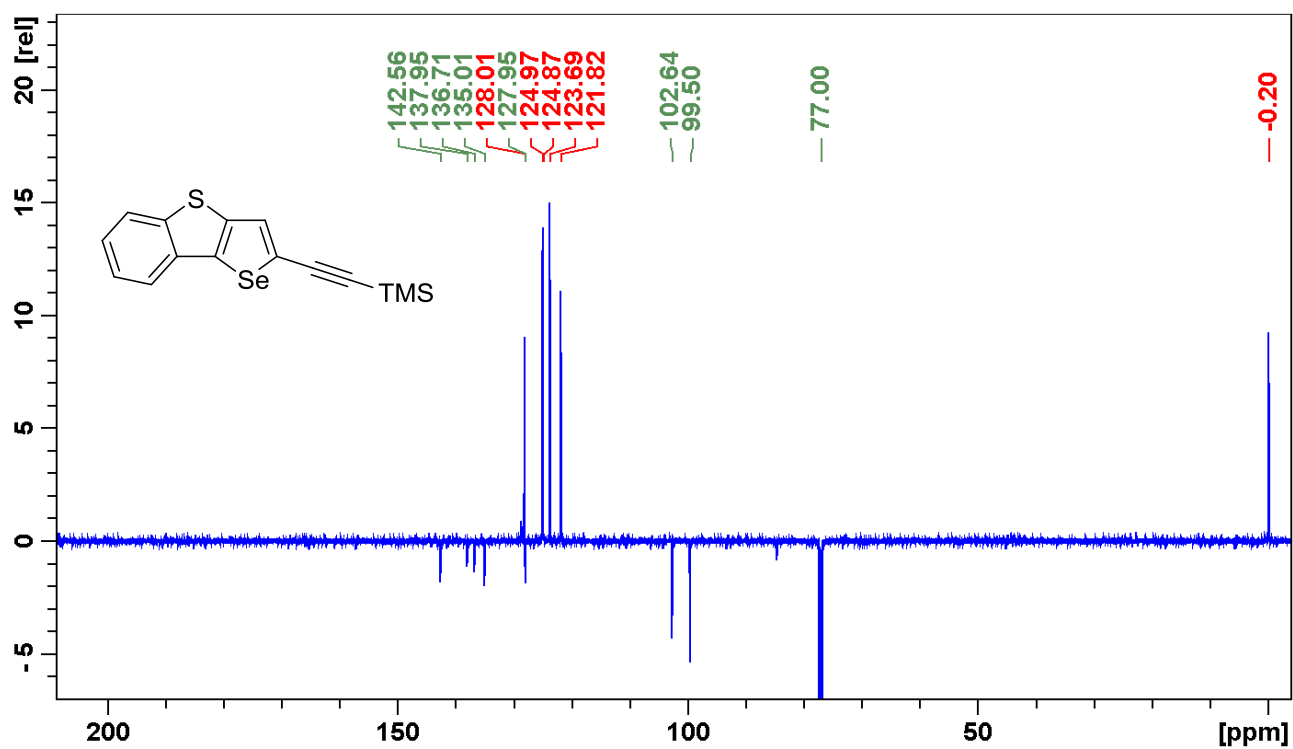


Figure S109. ¹³C NMR spectrum of compound 15.

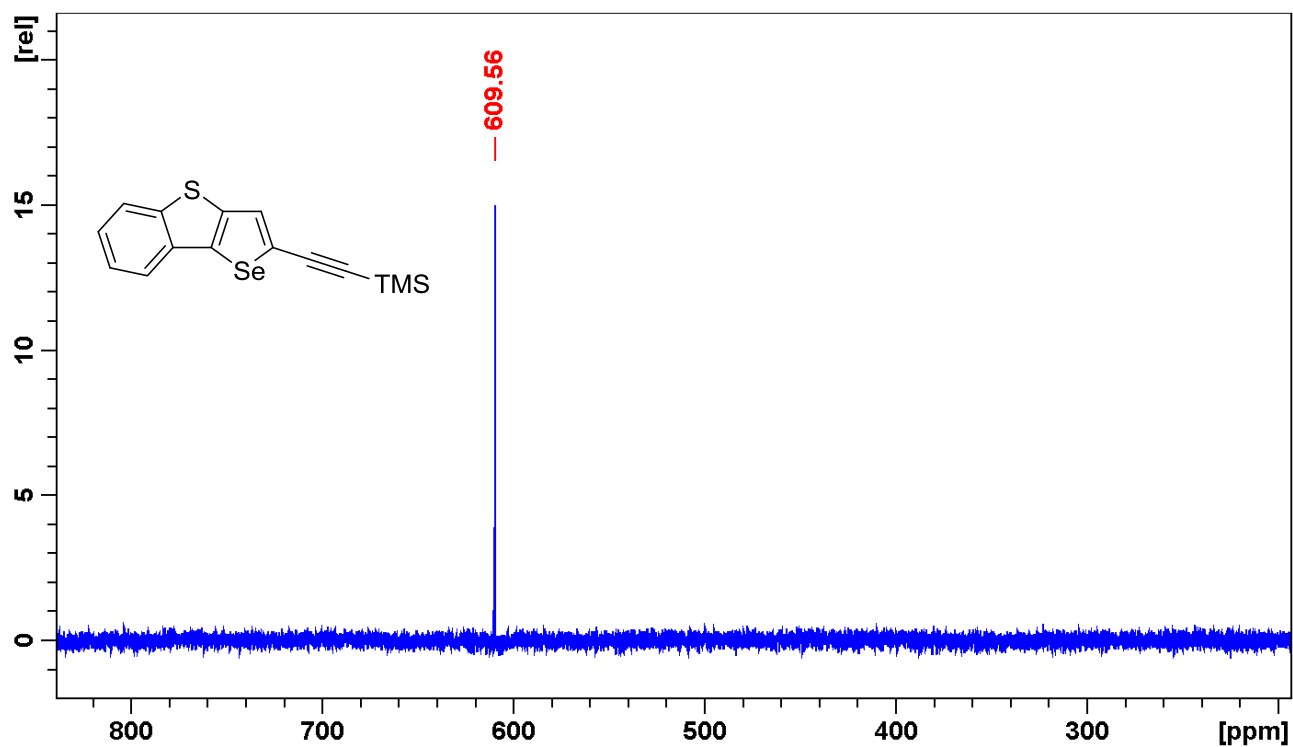


Figure S110. ⁷⁷Se NMR spectrum of compound 15.

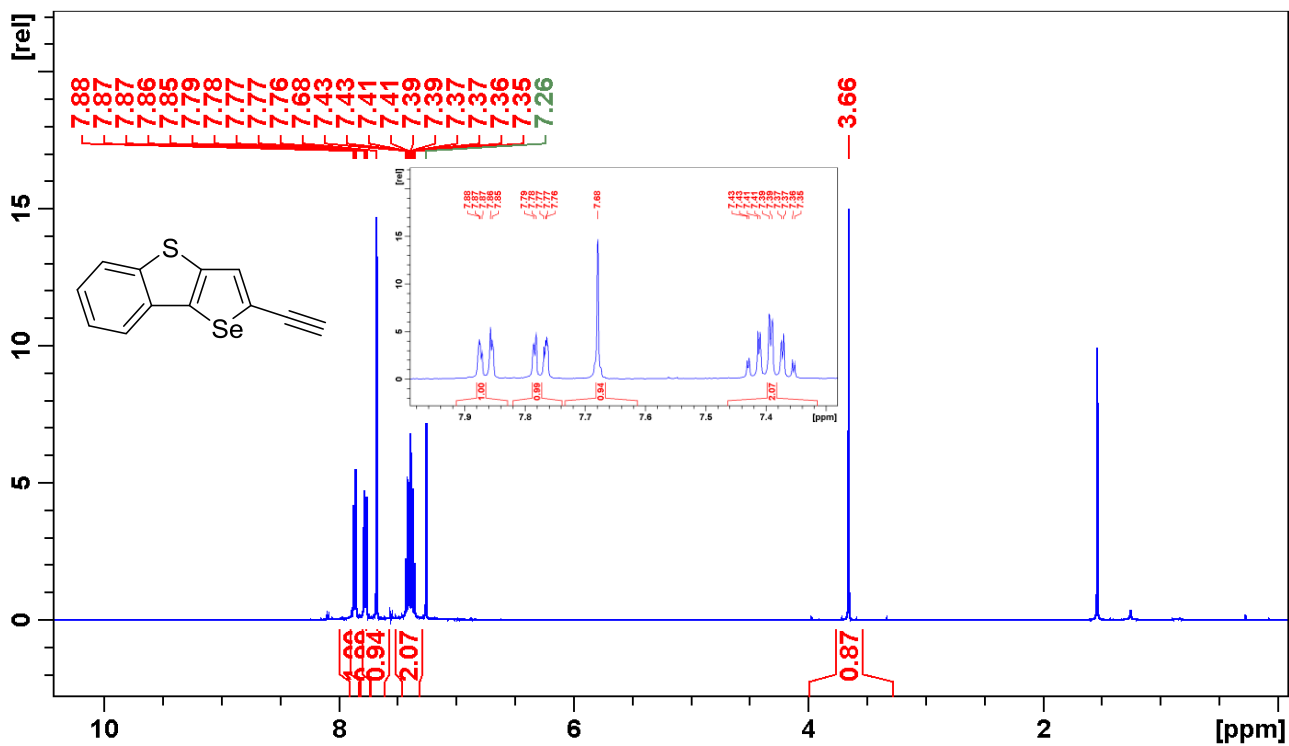


Figure S111. ¹H NMR spectrum of compound **16**.

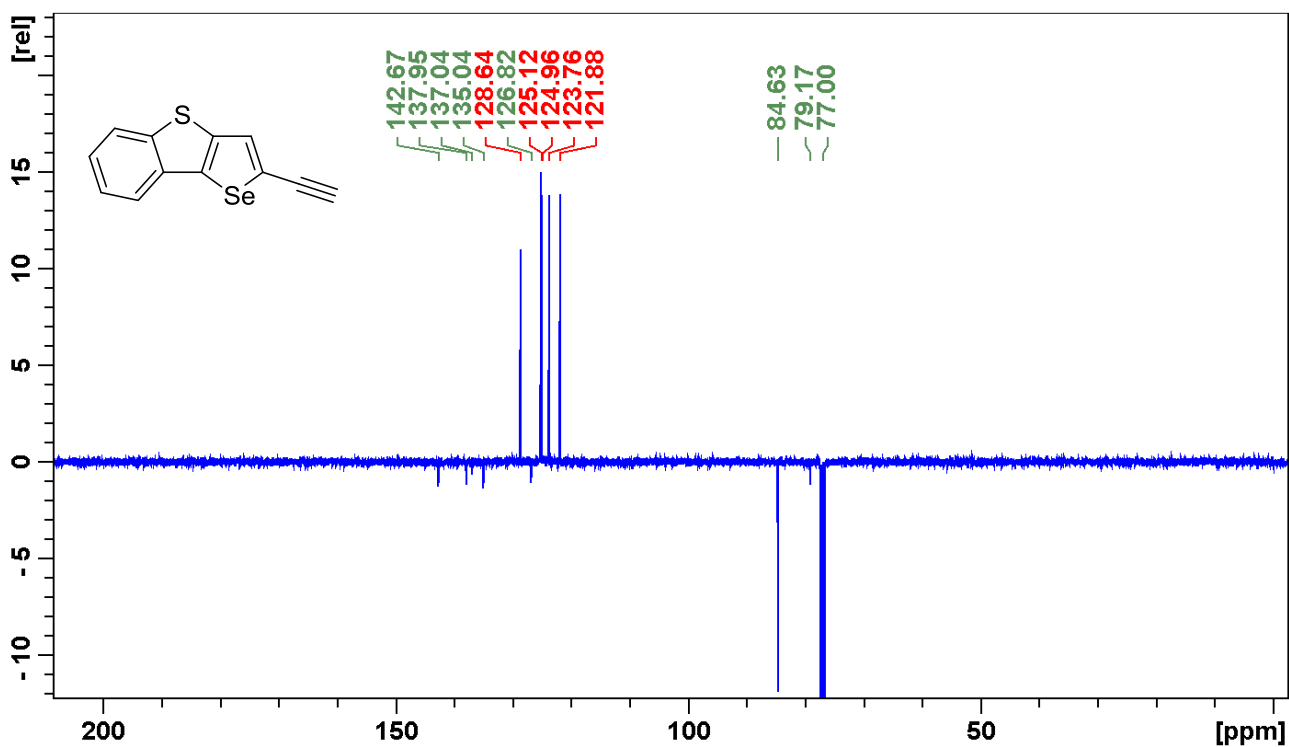


Figure S112. ¹³C NMR spectrum of compound **16**.

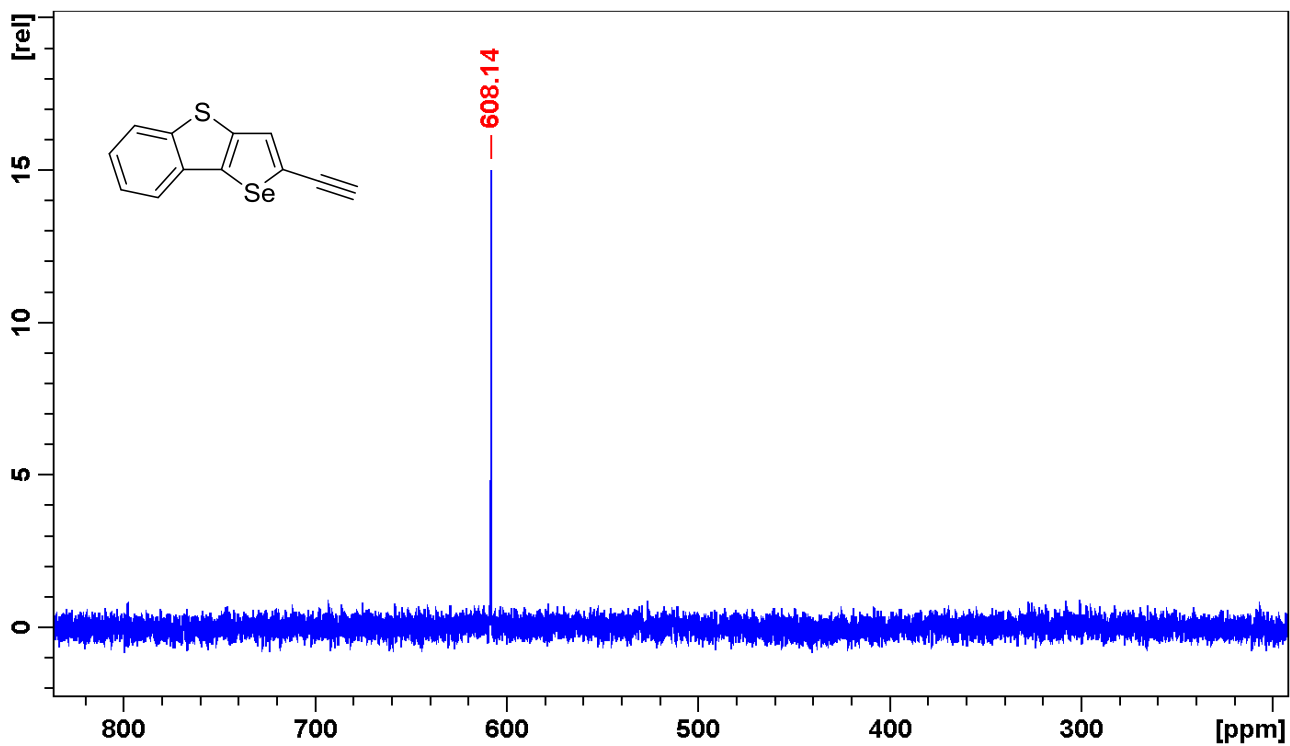


Figure S113. ^{77}Se NMR spectrum of compound 16.

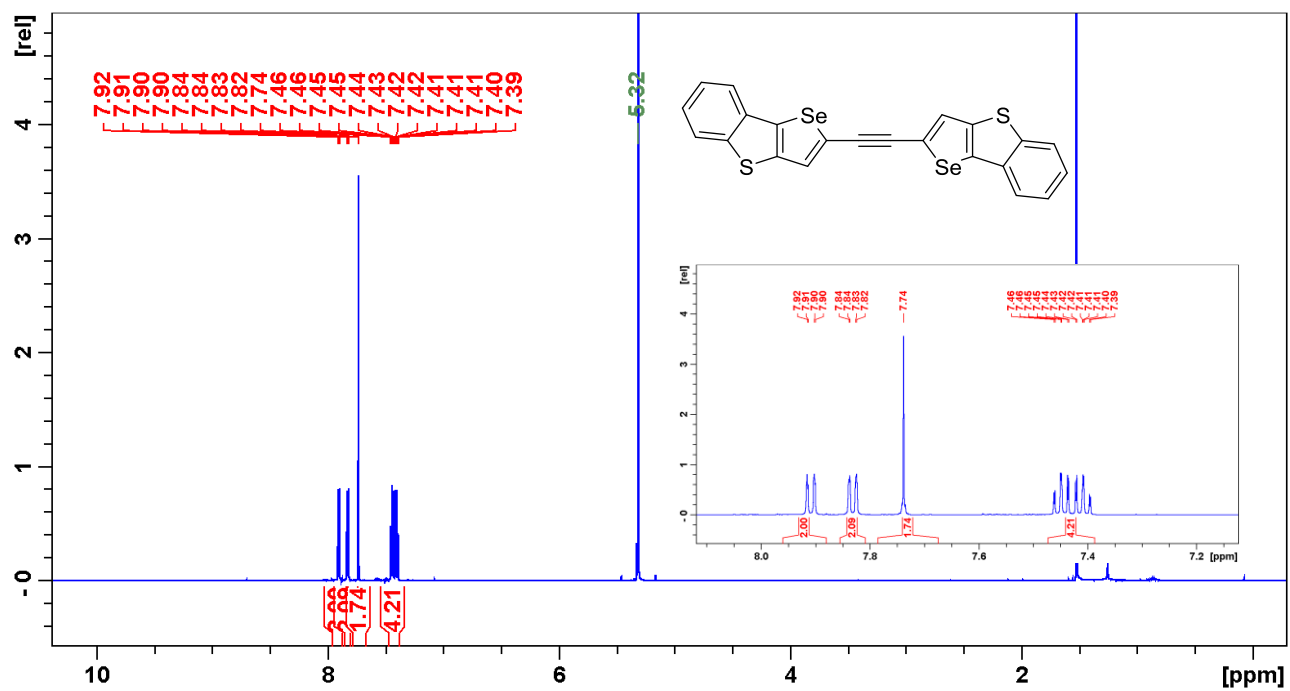


Figure S114. ^1H NMR spectrum of compound 17.

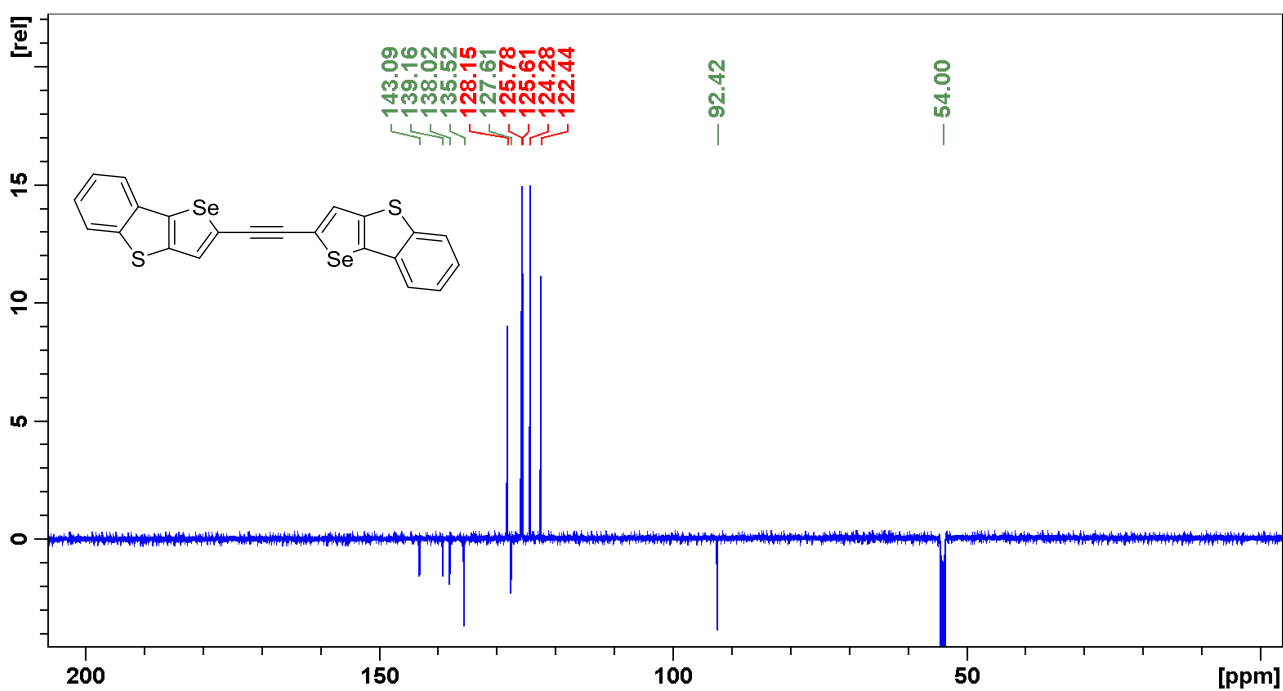


Figure S115. ¹³C NMR spectrum of compound 17.

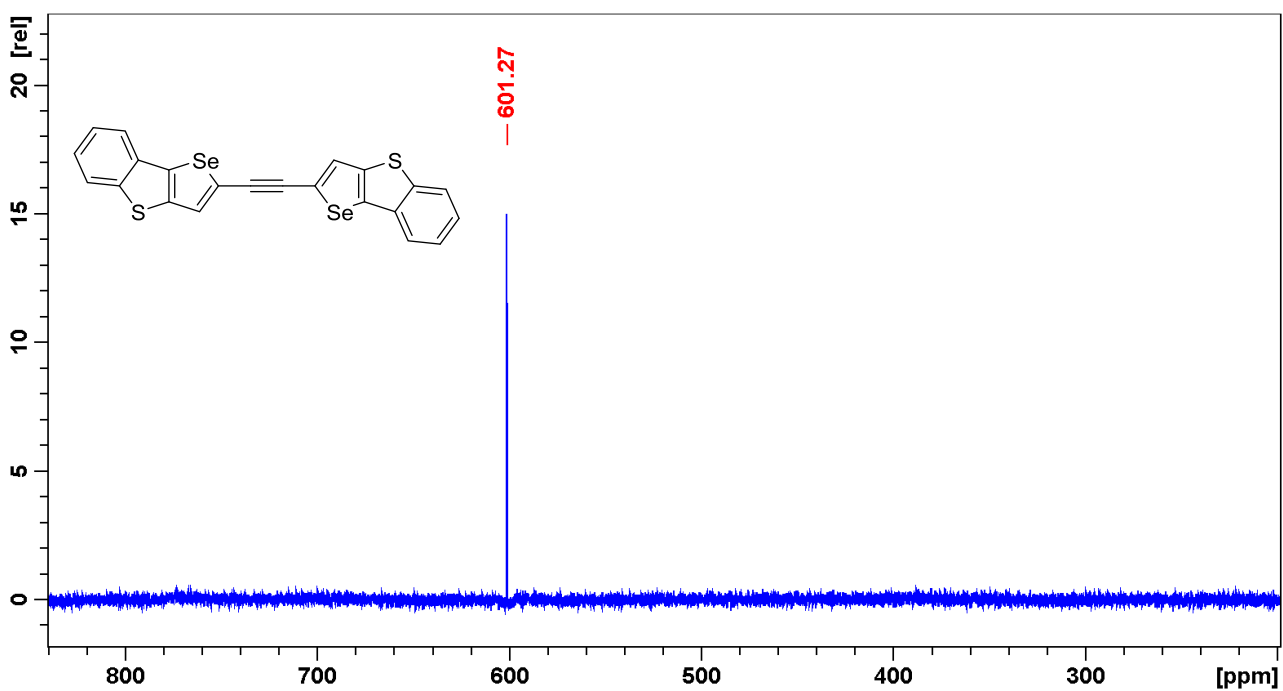


Figure S116. ⁷⁷Se NMR spectrum of compound 17.

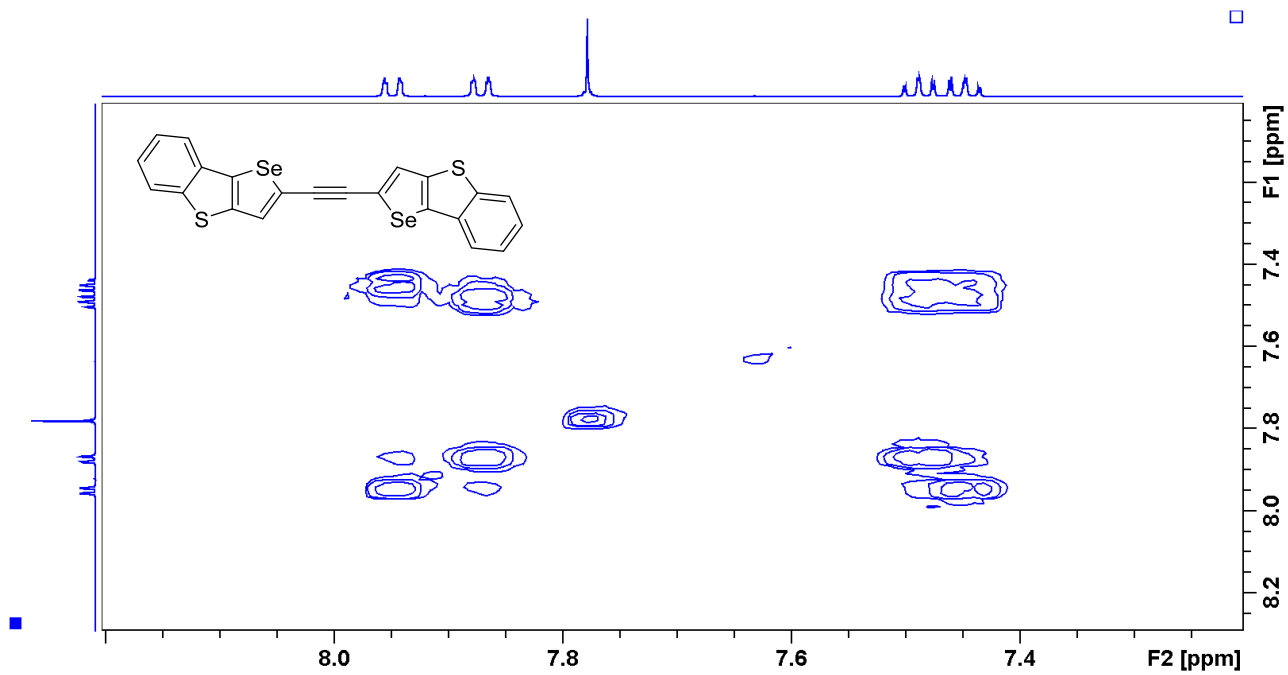


Figure S117. HH COSY NMR spectrum of compound **17**.

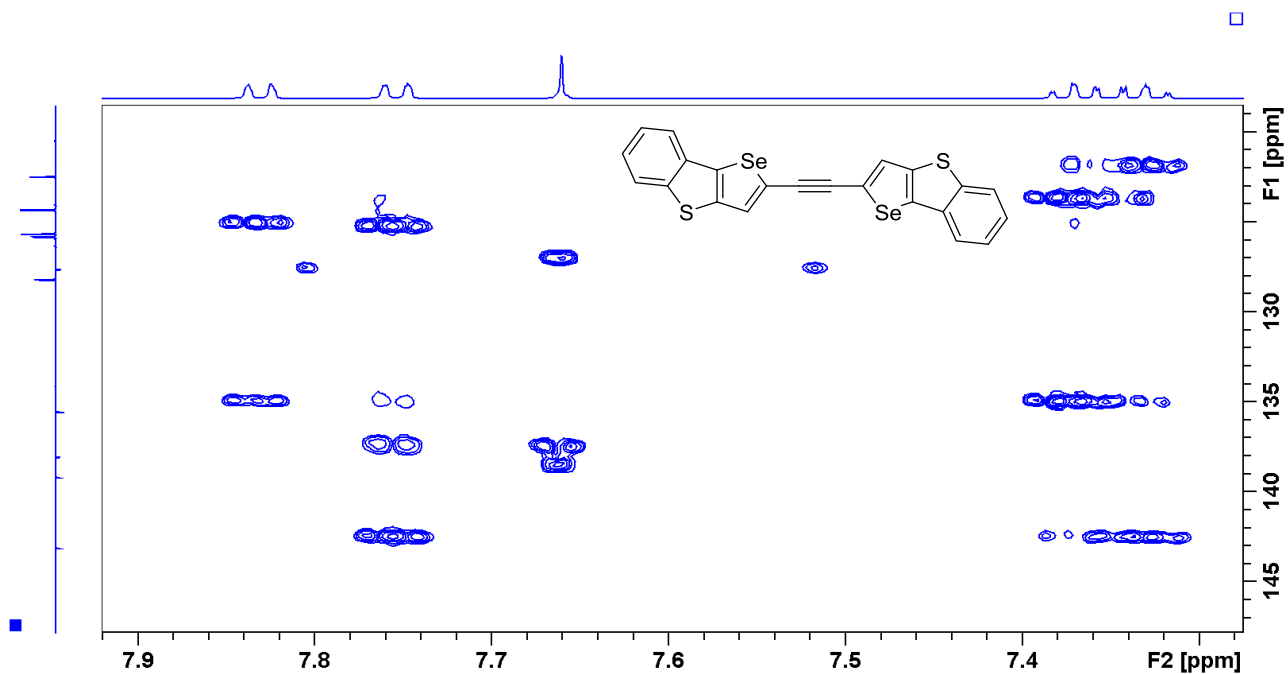


Figure S118. HMBC NMR spectrum of compound **17**.

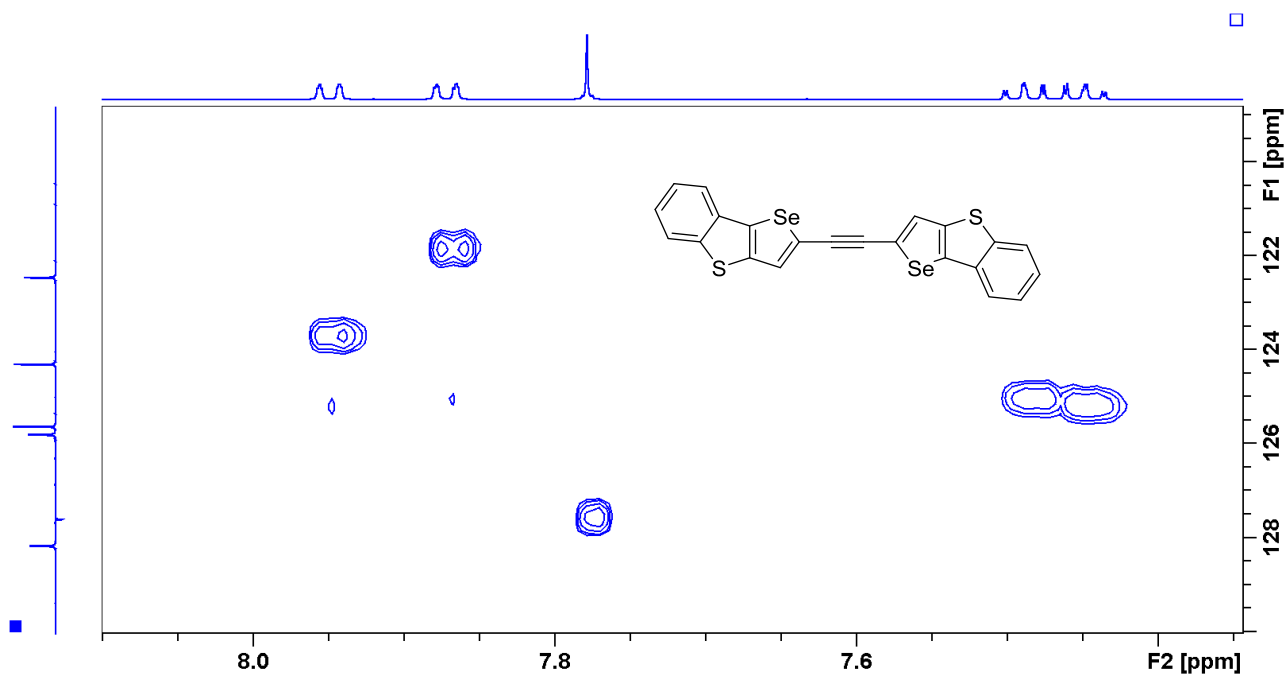


Figure S119. HSQC NMR spectrum of compound 17.

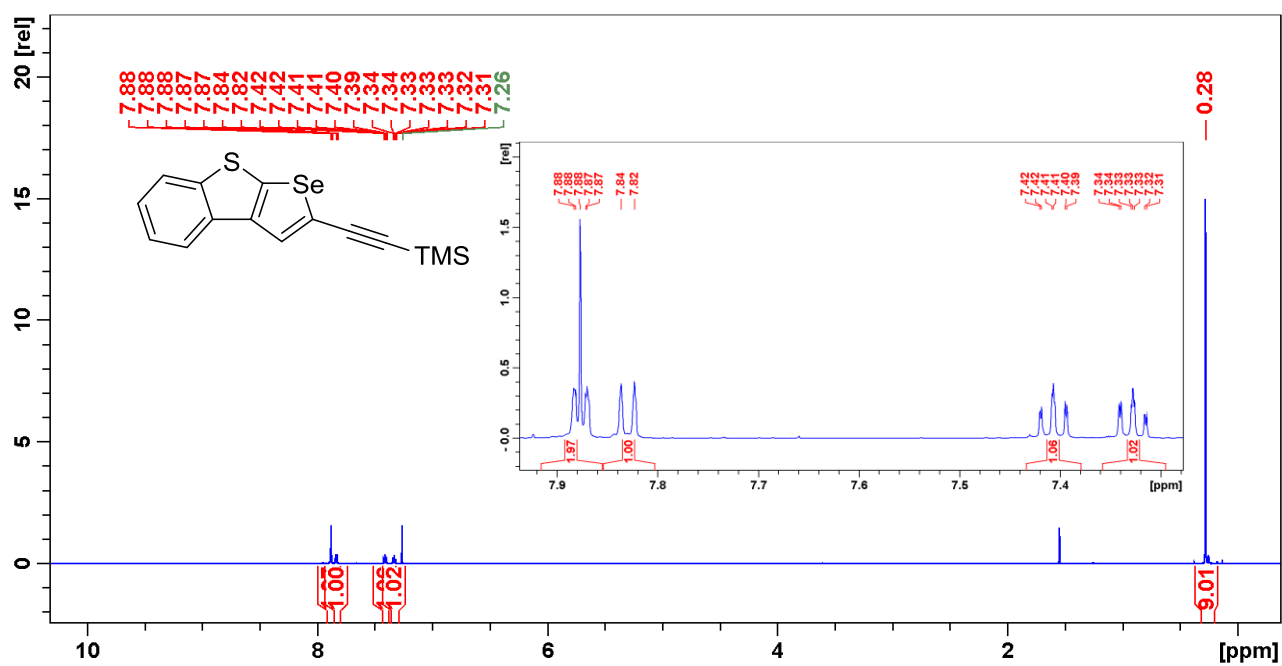


Figure S120. ^1H NMR spectrum of compound 18.

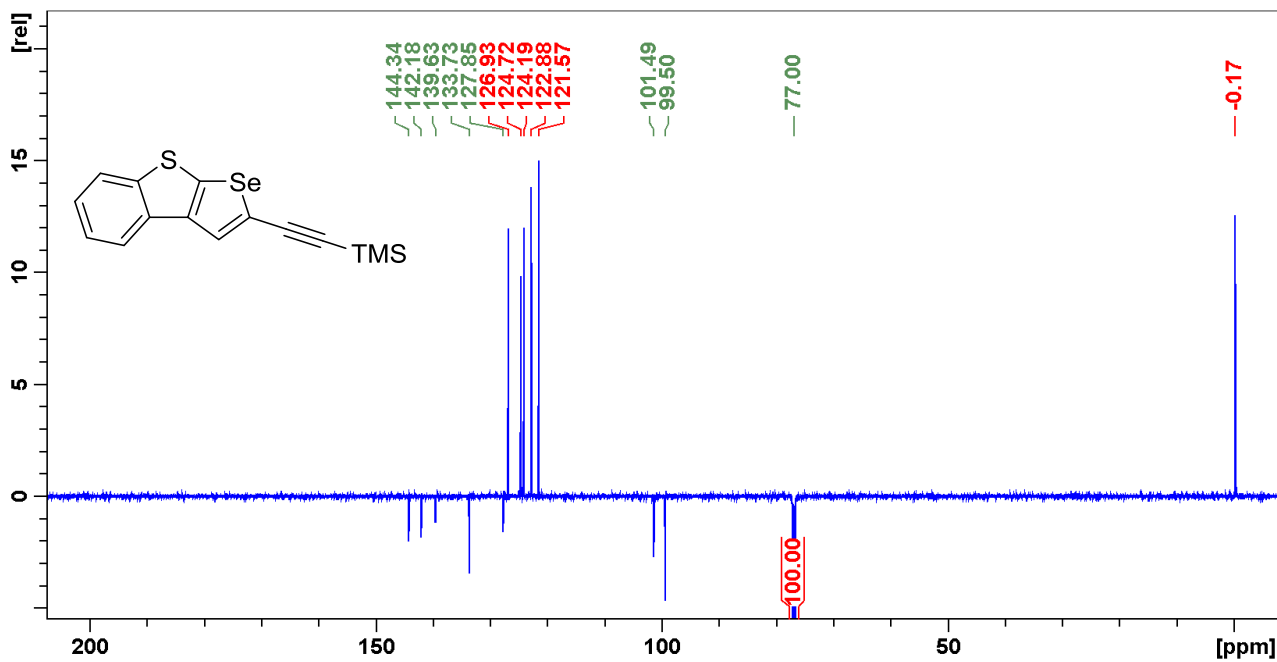


Figure S121. ^{13}C NMR spectrum of compound 18.

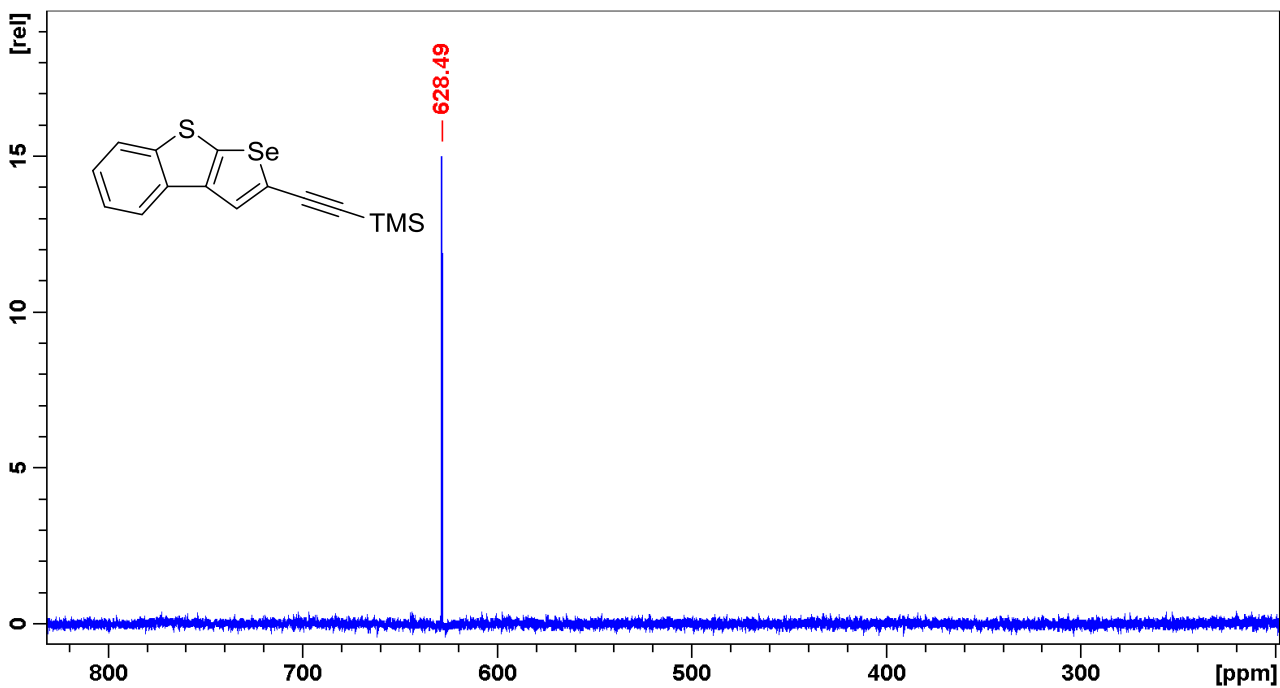


Figure S122. ^{77}Se NMR spectrum of compound 18.

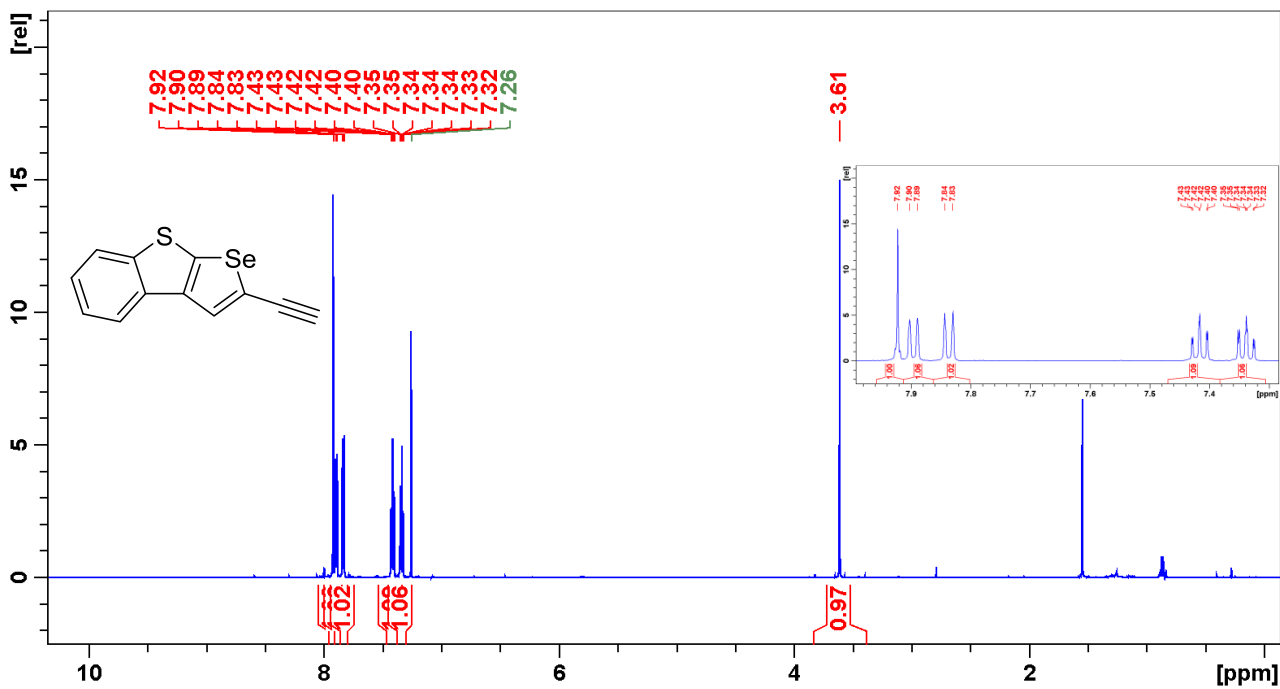


Figure S123. ¹H NMR spectrum of compound **19**.

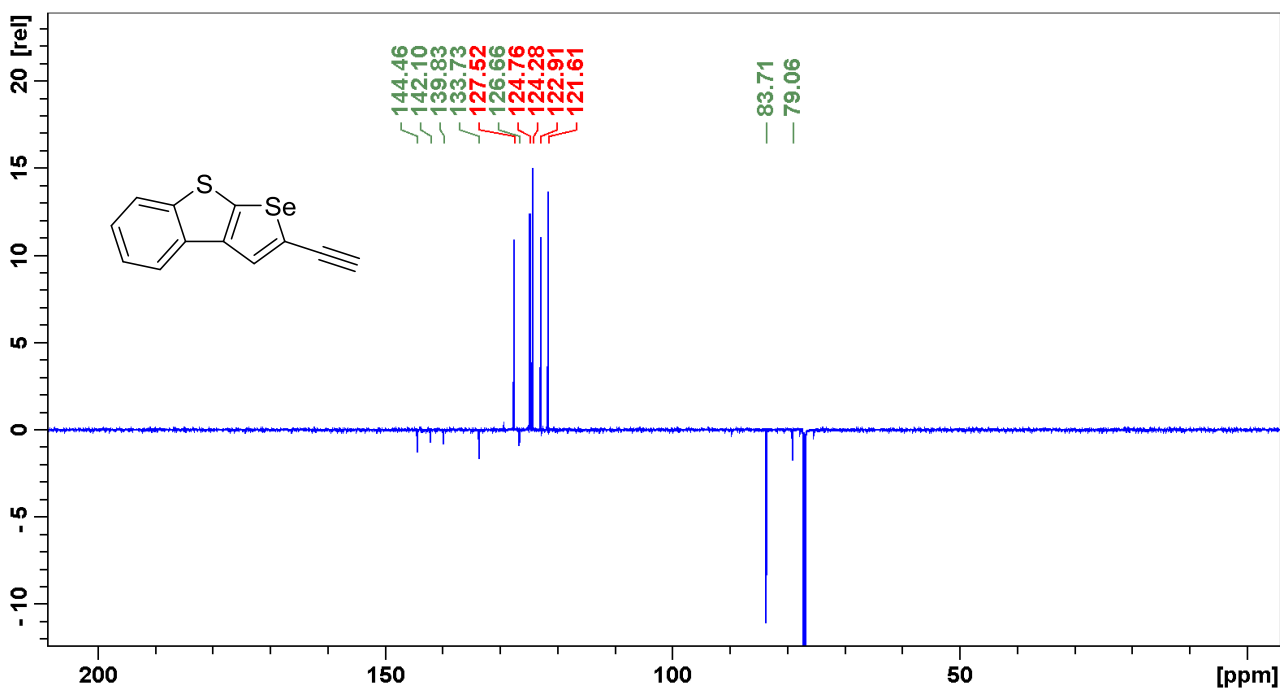


Figure S124. ¹³C NMR spectrum of compound **19**.

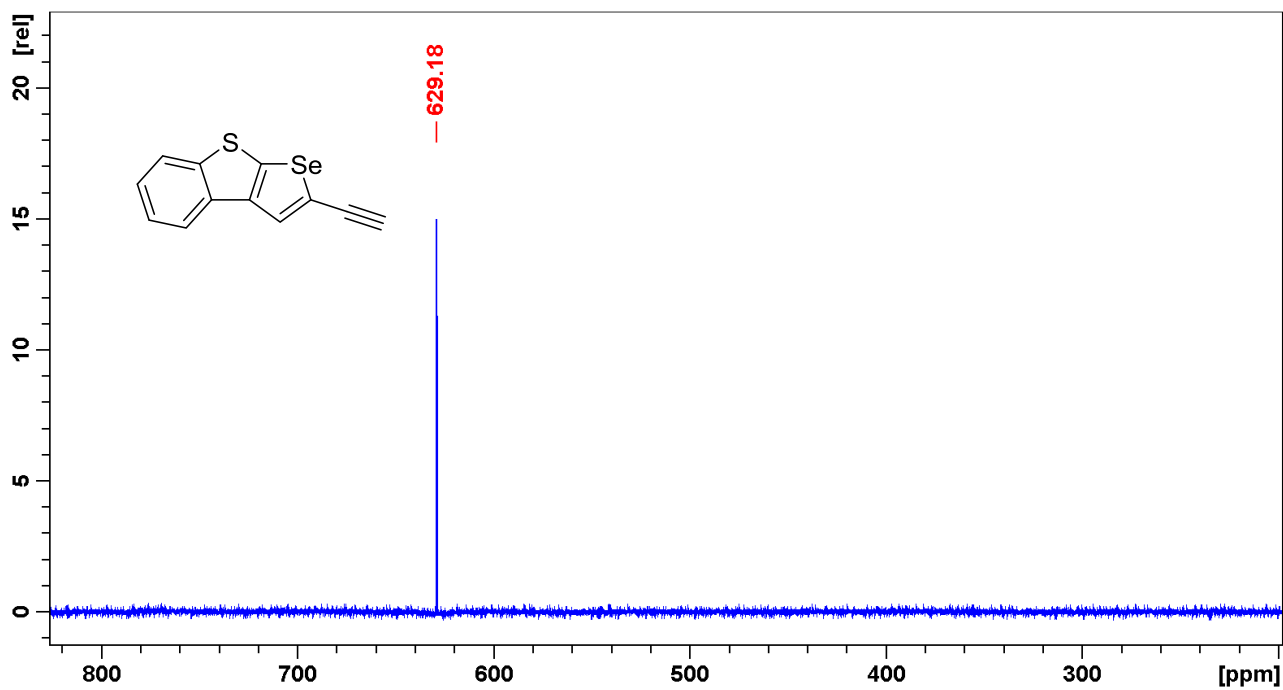


Figure S125. ^{77}Se NMR spectrum of compound 19.

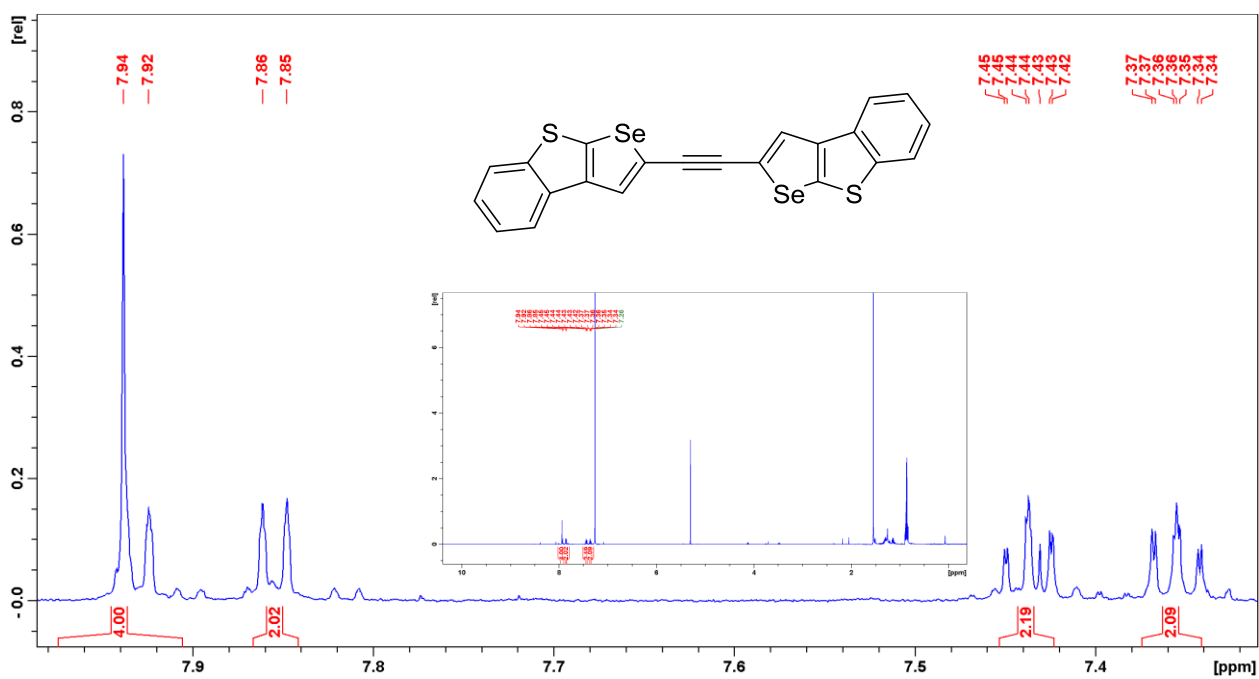


Figure S126. ^1H NMR spectrum of compound 20.

B) Absorption Spectra of 17 and 20

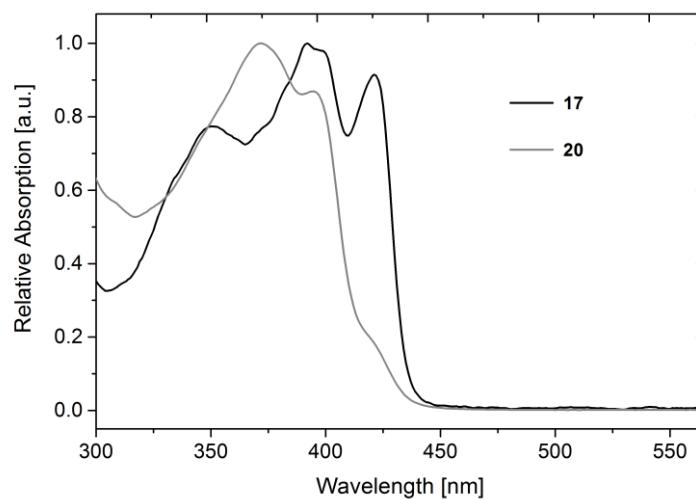


Figure S127: Absorption Spectra of 17 and 20.

C) Cyclic voltammetric measurements of 17 and 20

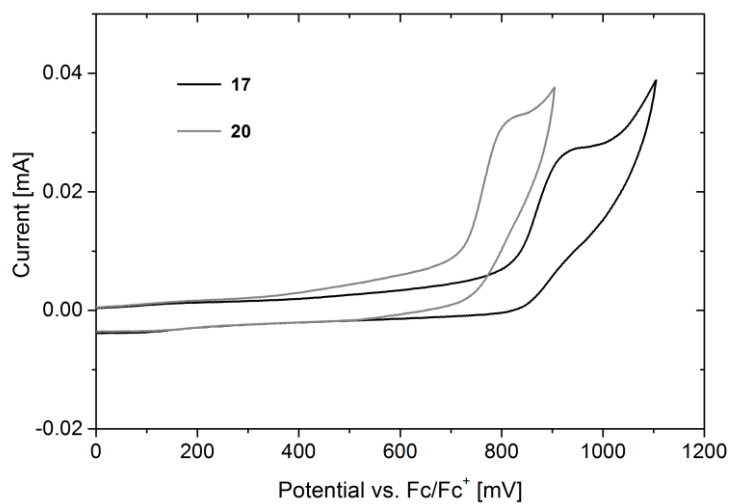


Figure S128: Cyclic voltammetric measurements of 17 and 20.

D) Thermal Analysis

a. TGA Measurement

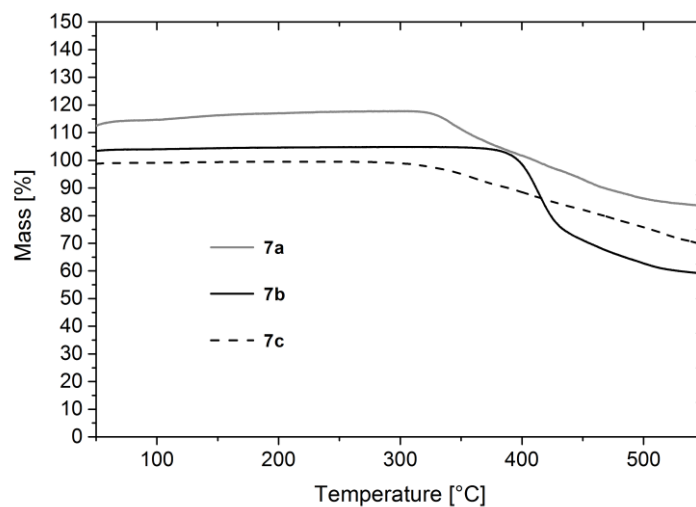


Figure S129: Thermogravimetric analysis of compounds **7a**, **7b** and **7c** in the temperature range 50-550 °C under a stream of dry nitrogen with a heating rate of 10 K/min.

b. DSC Analysis

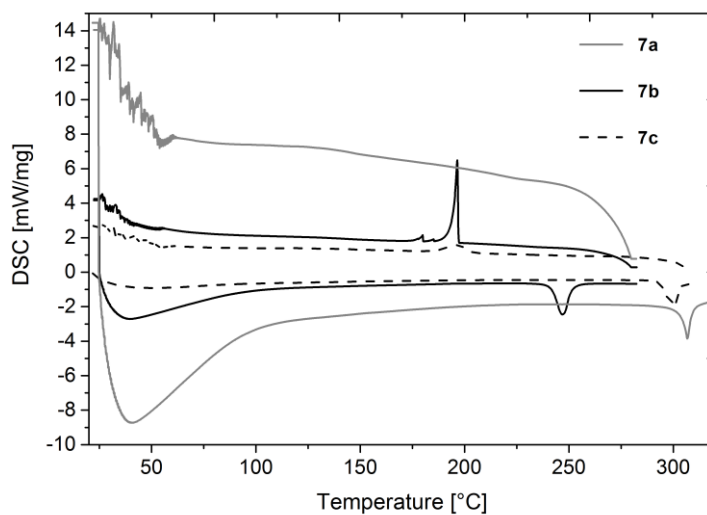


Figure S130: Two DSC heating/cooling cycles of compounds **7a**, **7b** and **7c** under a stream of dry nitrogen with a heating/cooling rate of 10 K/min.

E) DFT Calculations

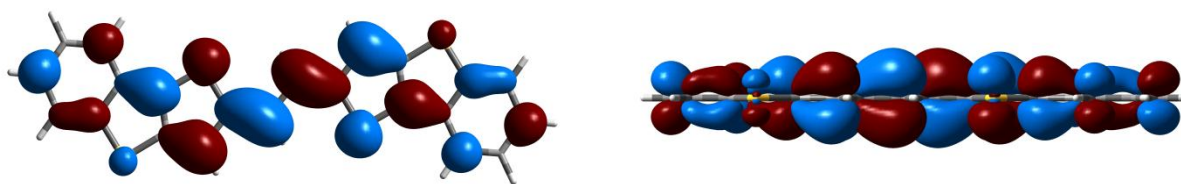


Figure S131: HOMO (bottom) and LUMO (top) of **BTTE**.

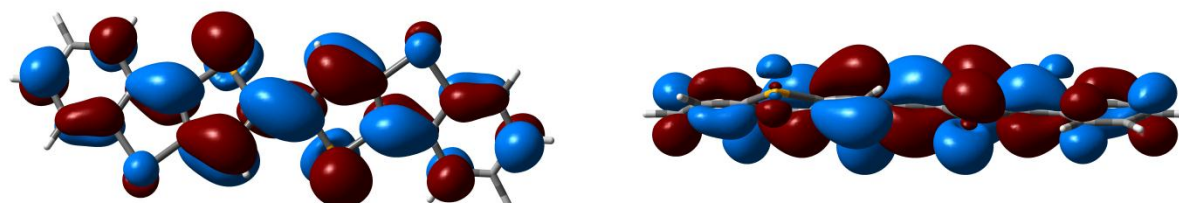


Figure S132: HOMO (bottom) and LUMO (top) of **7a**.

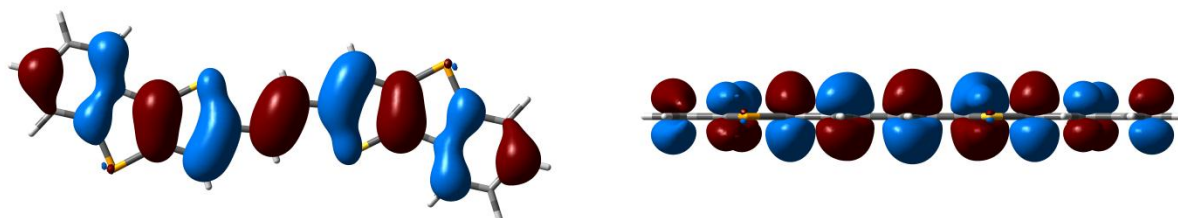
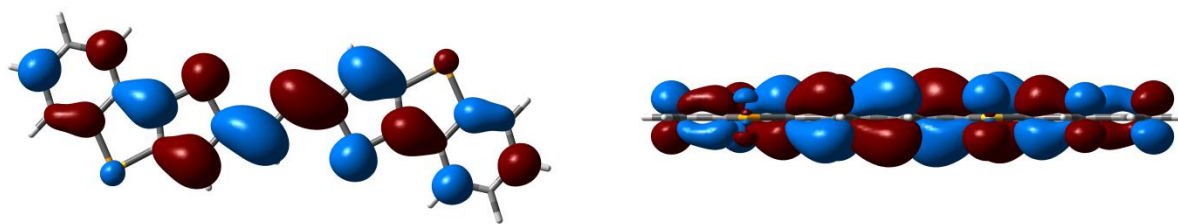


Figure S133: HOMO (bottom) and LUMO (top) of **7b**.

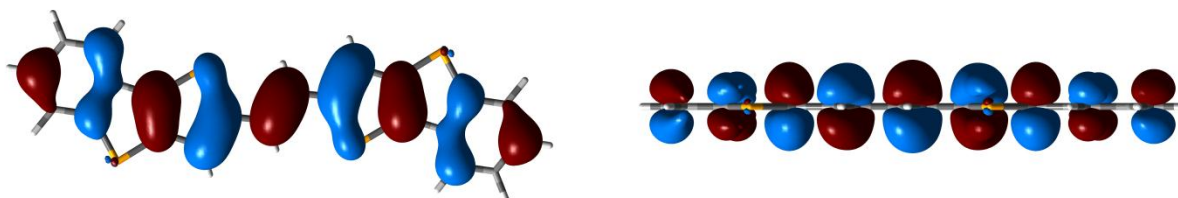
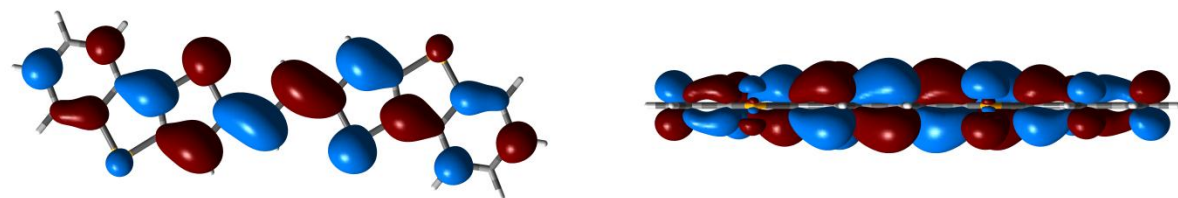


Figure S134: HOMO (bottom) and LUMO (top) of **7c**.

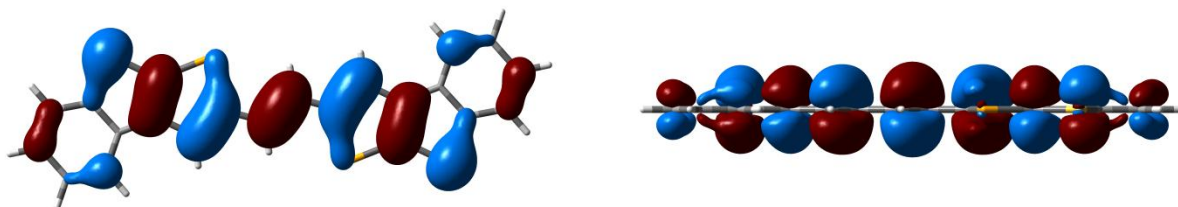
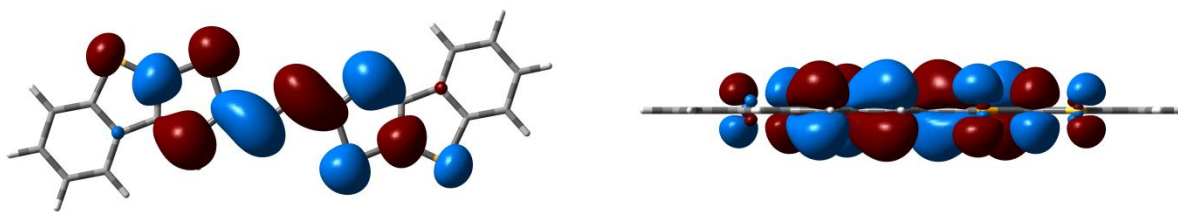


Figure S135: HOMO (bottom) and LUMO (top) of **11a**.

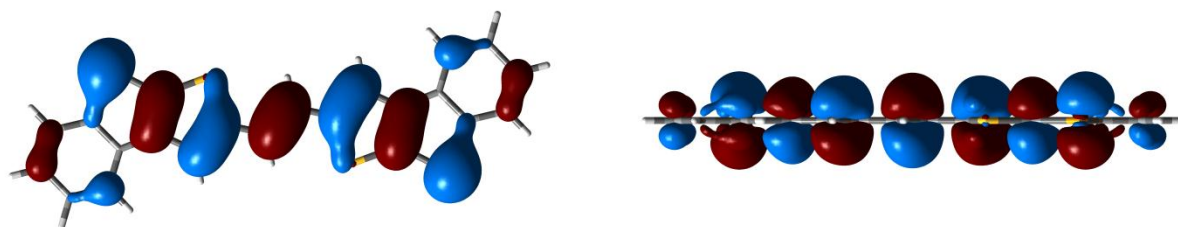
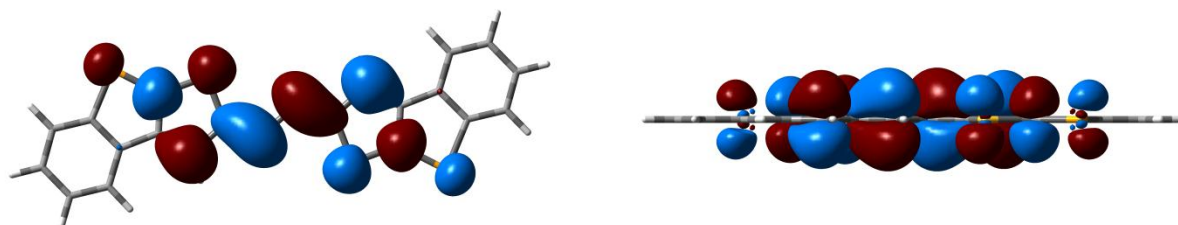


Figure S136: HOMO (bottom) and LUMO (top) of **11b**.

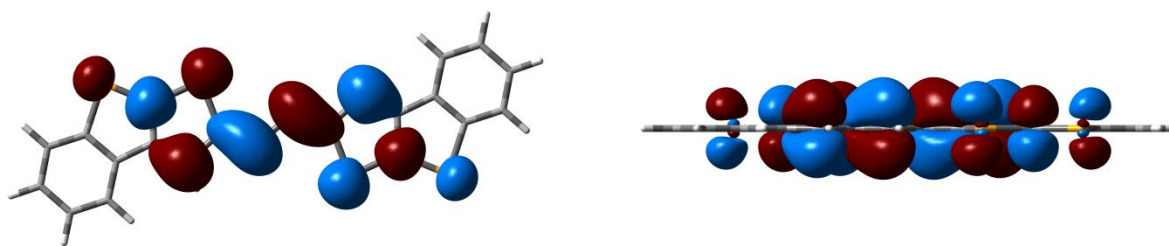


Figure S137: HOMO (bottom) and LUMO (top) of **11c**.

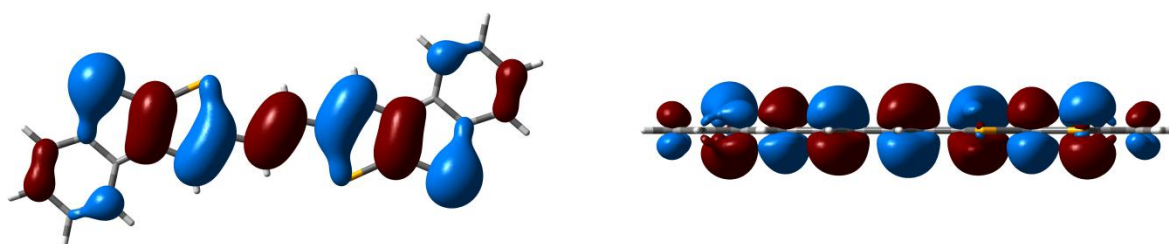
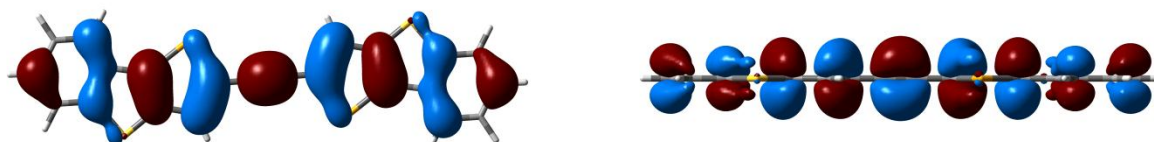
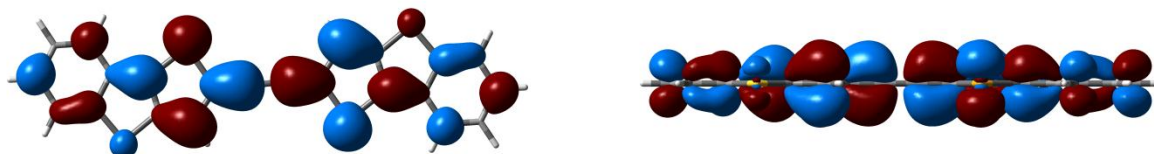


Figure S138: HOMO (bottom) and LUMO (top) of **17**.



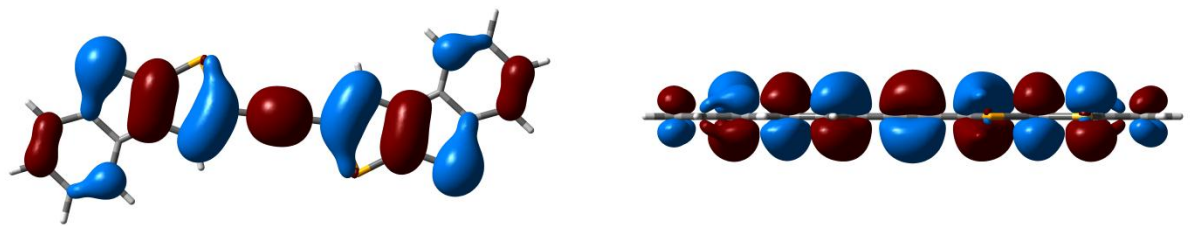
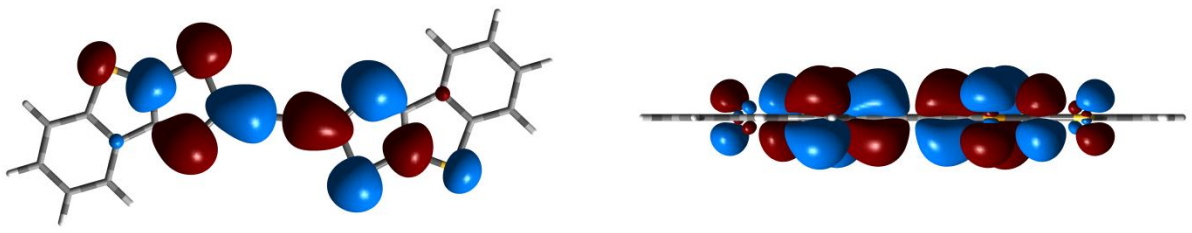


Figure S139: HOMO (bottom) and LUMO (top) of **20**.

Manuscript # 6

Supporting Information

Substituted Triphenylamines as Building Blocks for Star Shaped Organic Electronic Materials

Supplementary Material

Daniel Lumpi,^a Brigitte Holzer,^a Johannes Bintinger,^{a,b} Ernst Horkel,^{a} Simon Waid,^c Heinz D. Wanzenböck,^c Martina Marchetti-Deschmann,^d Christian Hametner,^a Emmerich Bertagnolli,^c Ioannis Kymissis,^b and Johannes Fröhlich^a*

^aInstitute of Applied Synthetic Chemistry, Vienna University of Technology,

Getreidemarkt 9/163OC, A-1060 Vienna, Austria

^bDepartment of Electrical Engineering, Columbia University,

520W 120th street, Suite 1300, 10027 New York, NY, United States

^cInstitute of Solid State Electronics, Vienna University of Technology,

Floragasse 7, A-1040 Vienna, Austria

^dInstitute of Chemical Technologies and Analytics, Vienna University of Technology,

Getreidemarkt 9/164IAC, A-1060 Vienna, Austria

ernst.horkel@tuwien.ac.at

A) NMR Spectra

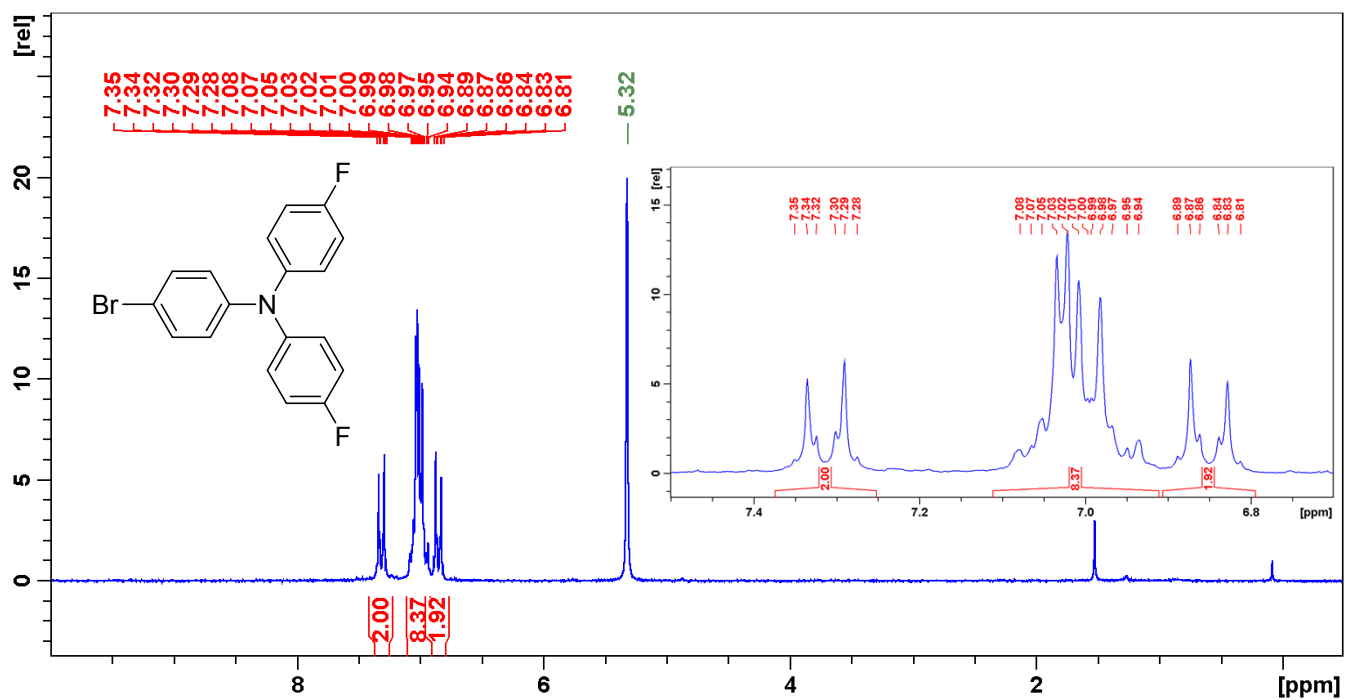


Figure S1. Proton NMR spectrum of compound **6c**.

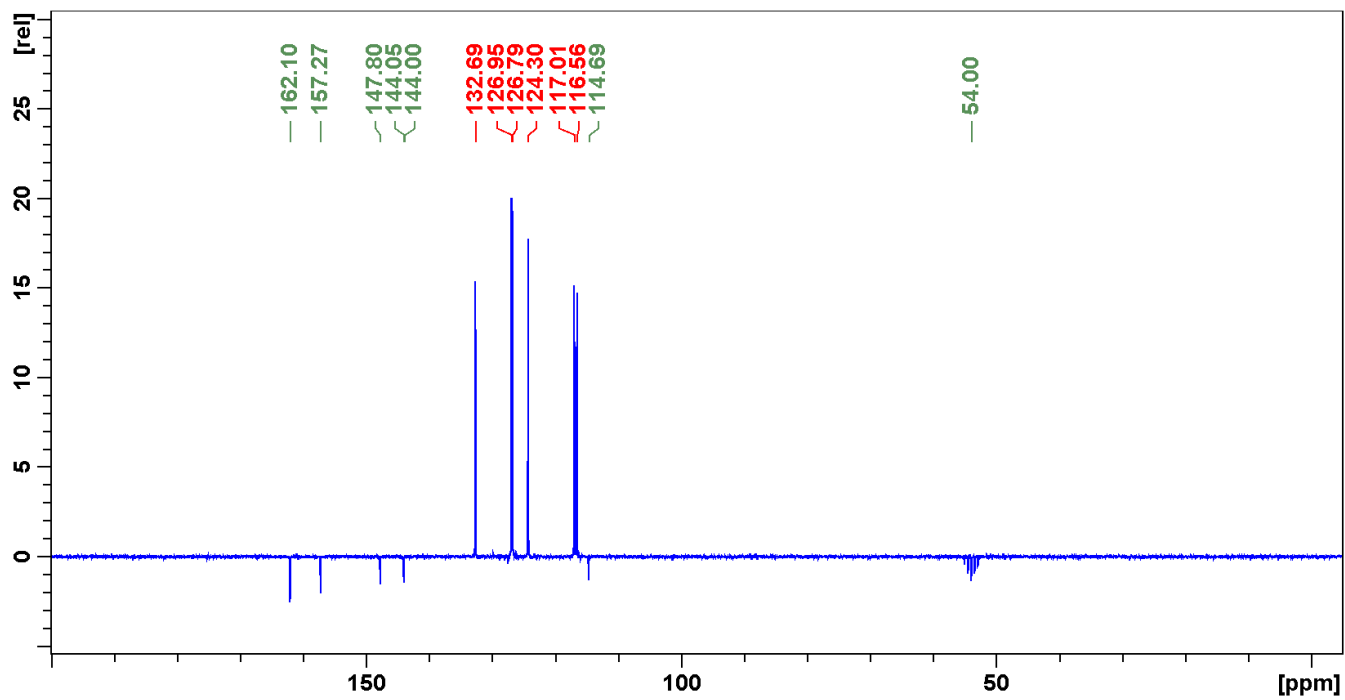


Figure S2. Carbon NMR spectrum of compound **6c**.

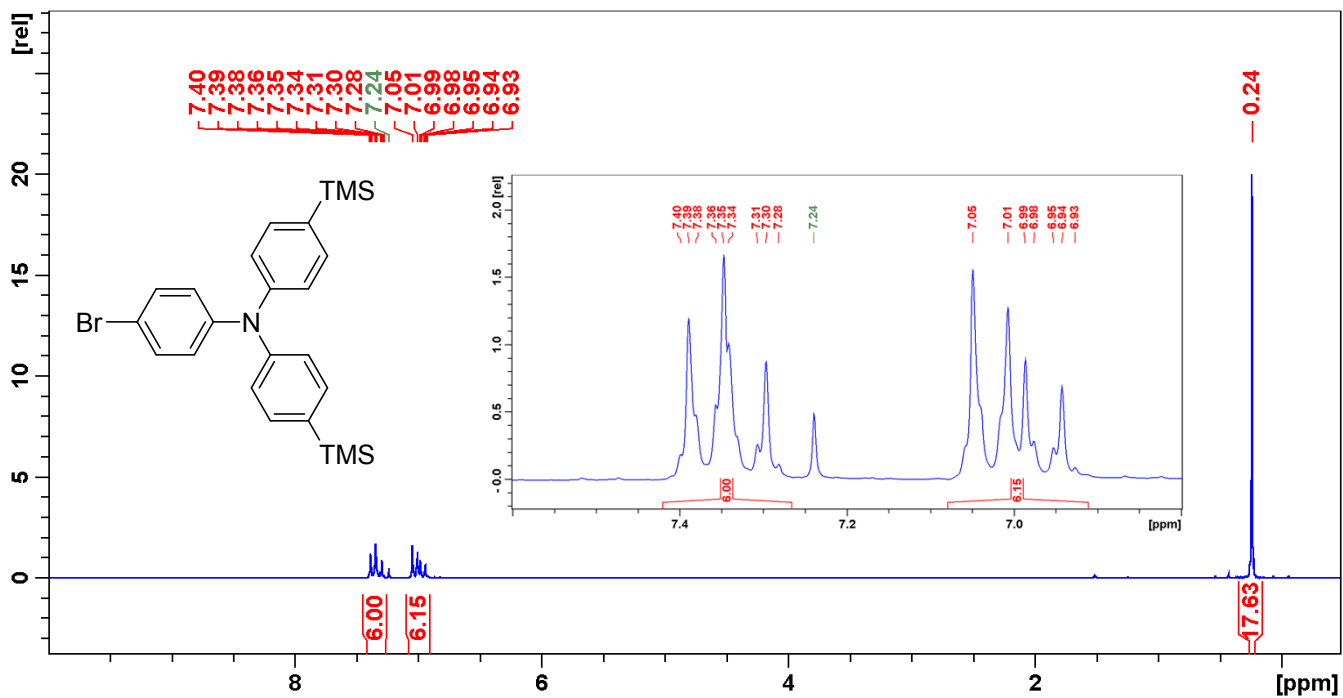


Figure S3. Proton NMR spectrum of compound **6e**.

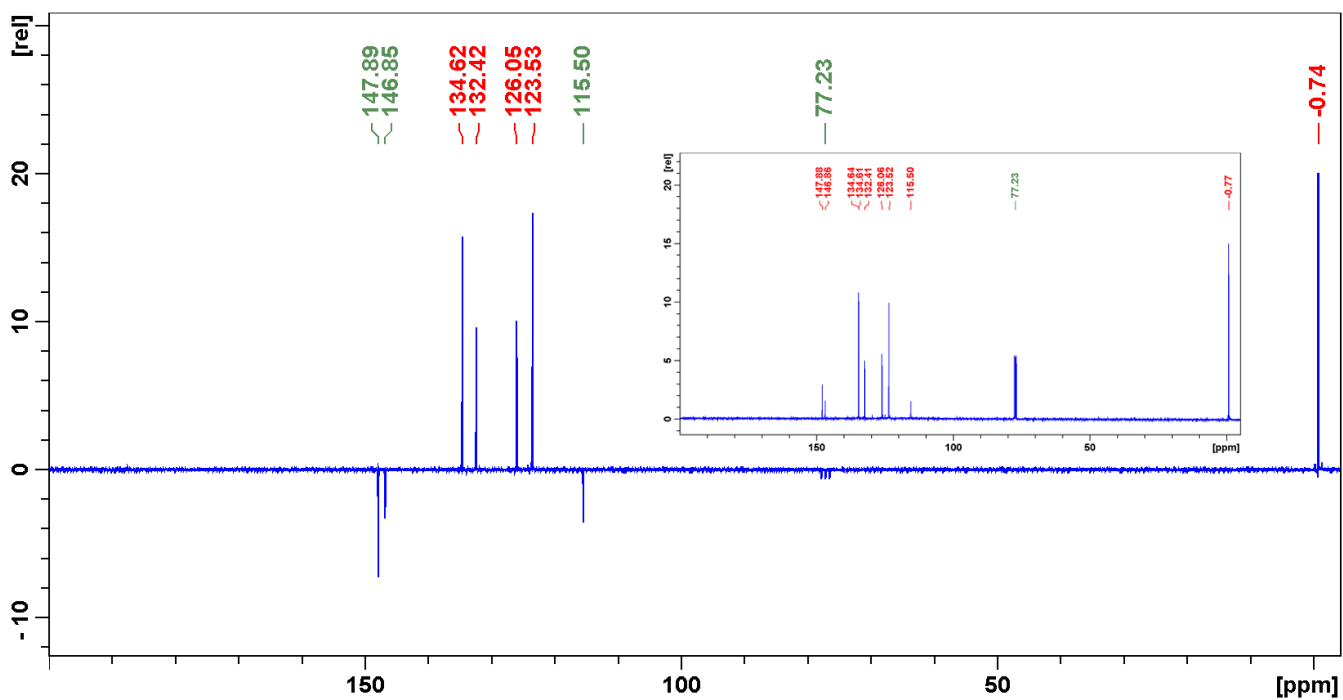


Figure S4. Carbon NMR spectrum of compound **6e**.

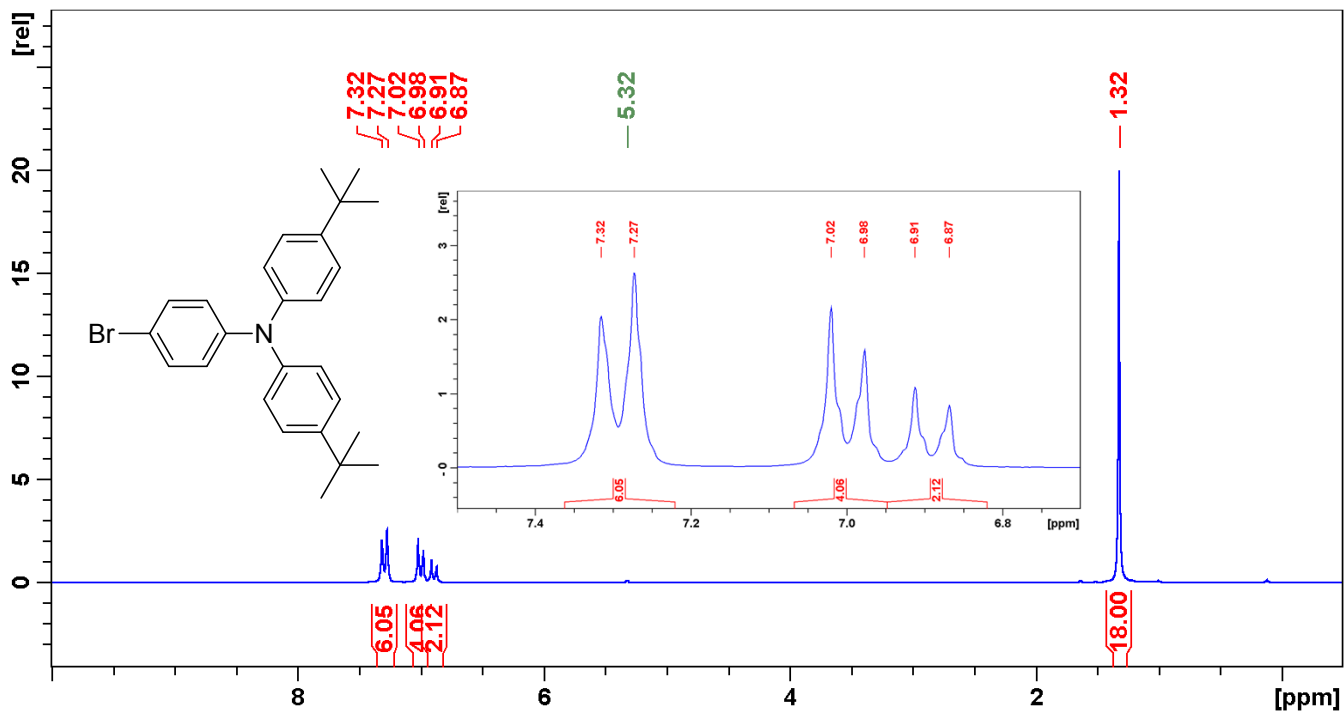


Figure S5. Proton NMR spectrum of compound **6f**.

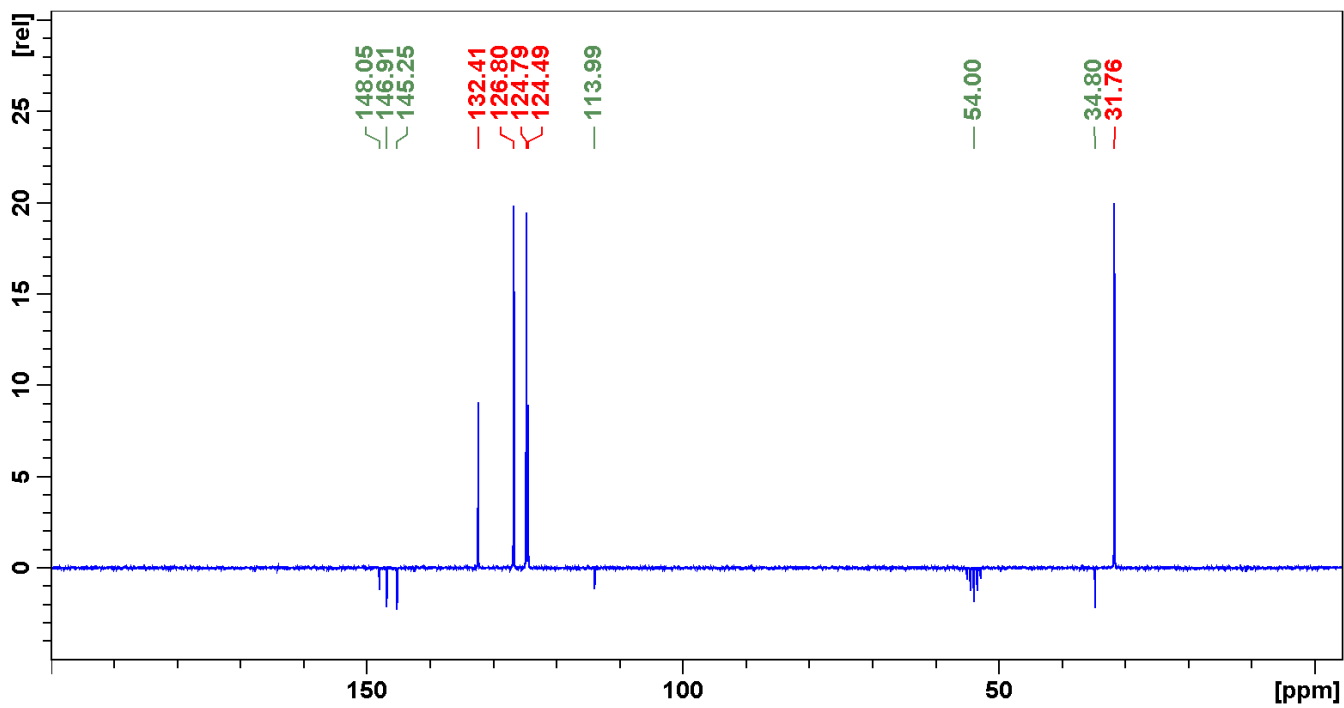


Figure S6. Carbon NMR spectrum of compound **6f**.

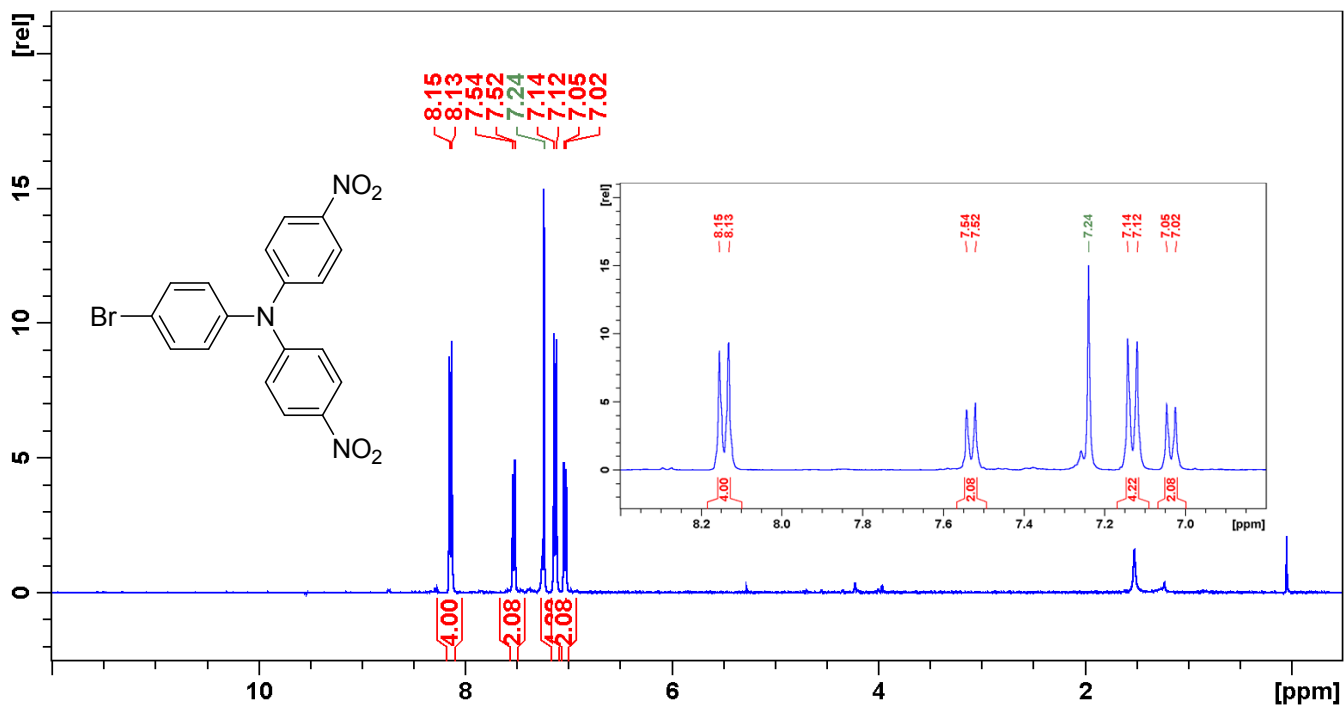


Figure S7. Proton NMR spectrum of compound **6g**.

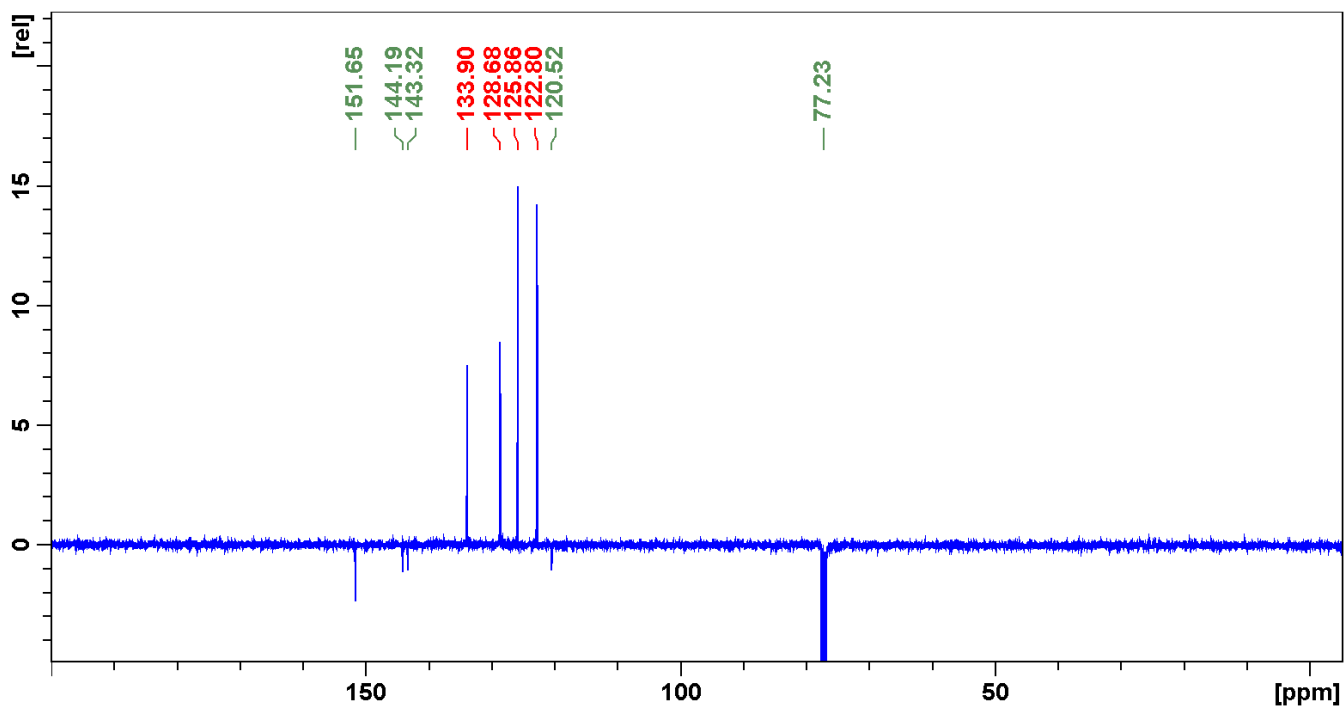


Figure S8. Carbon NMR spectrum of compound **6g**.

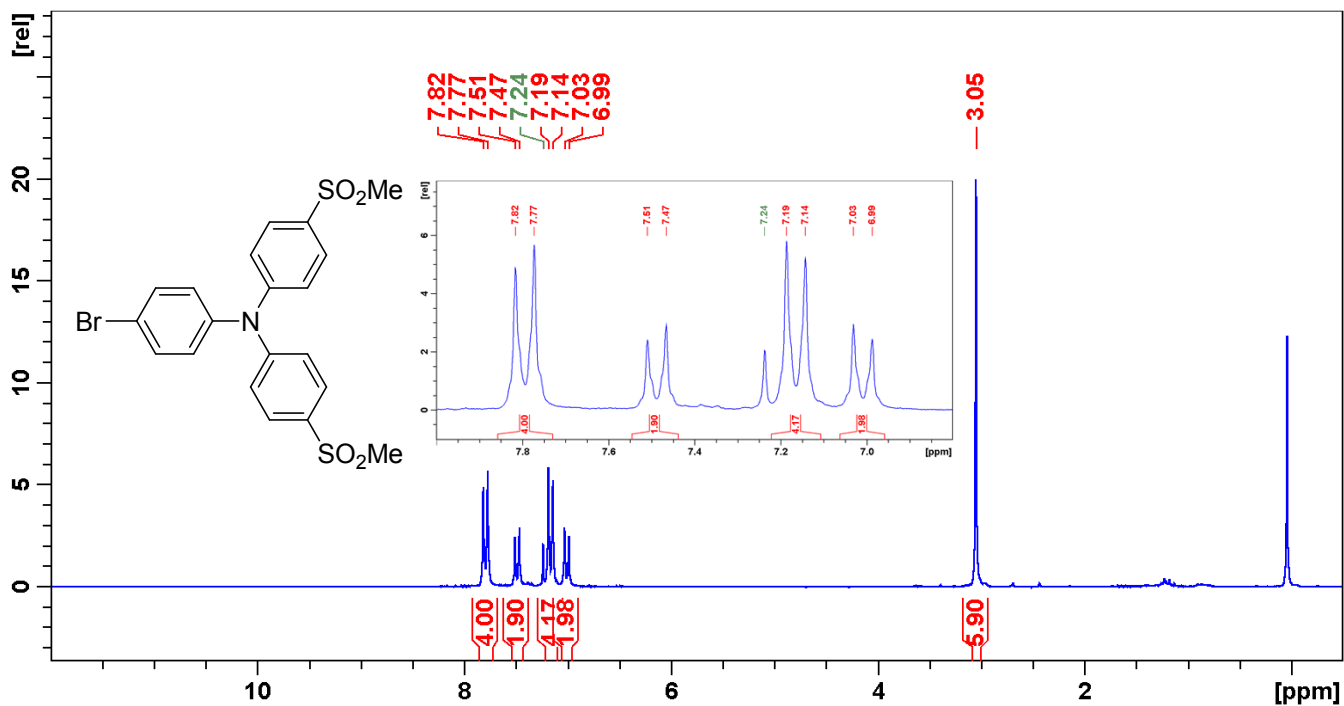


Figure S9. Proton NMR spectrum of compound **6h**.

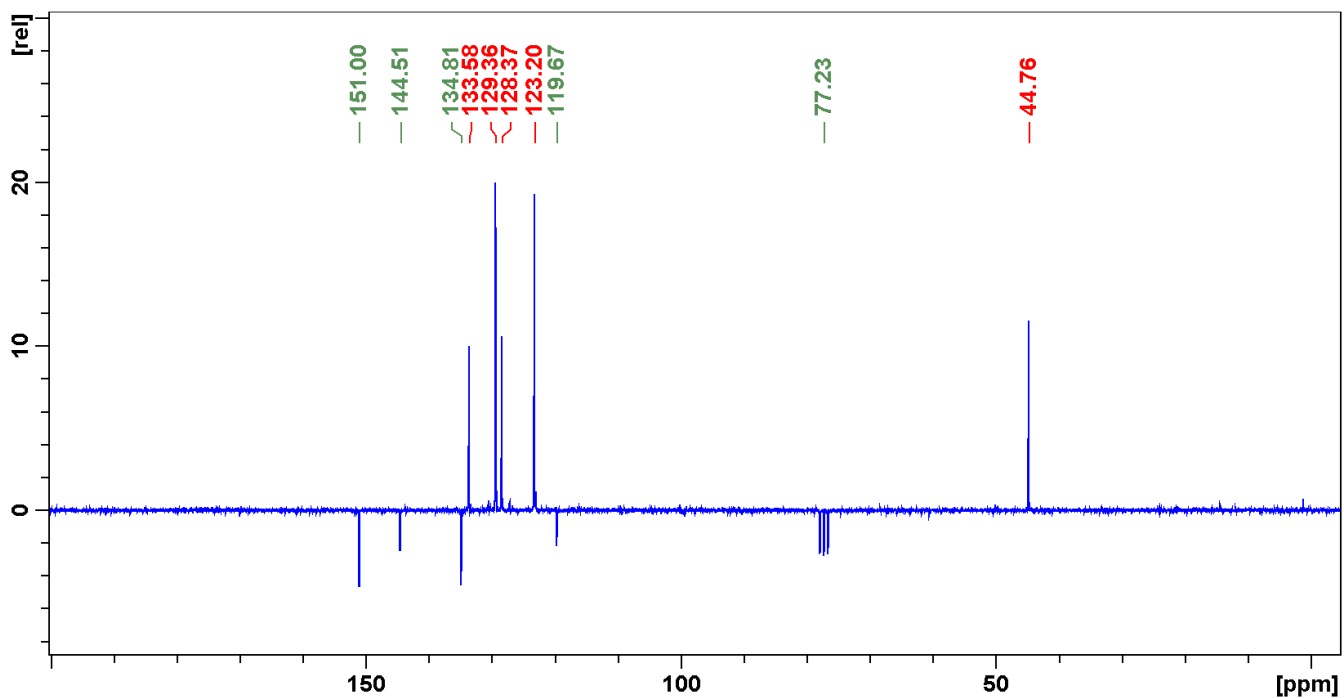


Figure S10. Carbon NMR spectrum of compound **6h**.

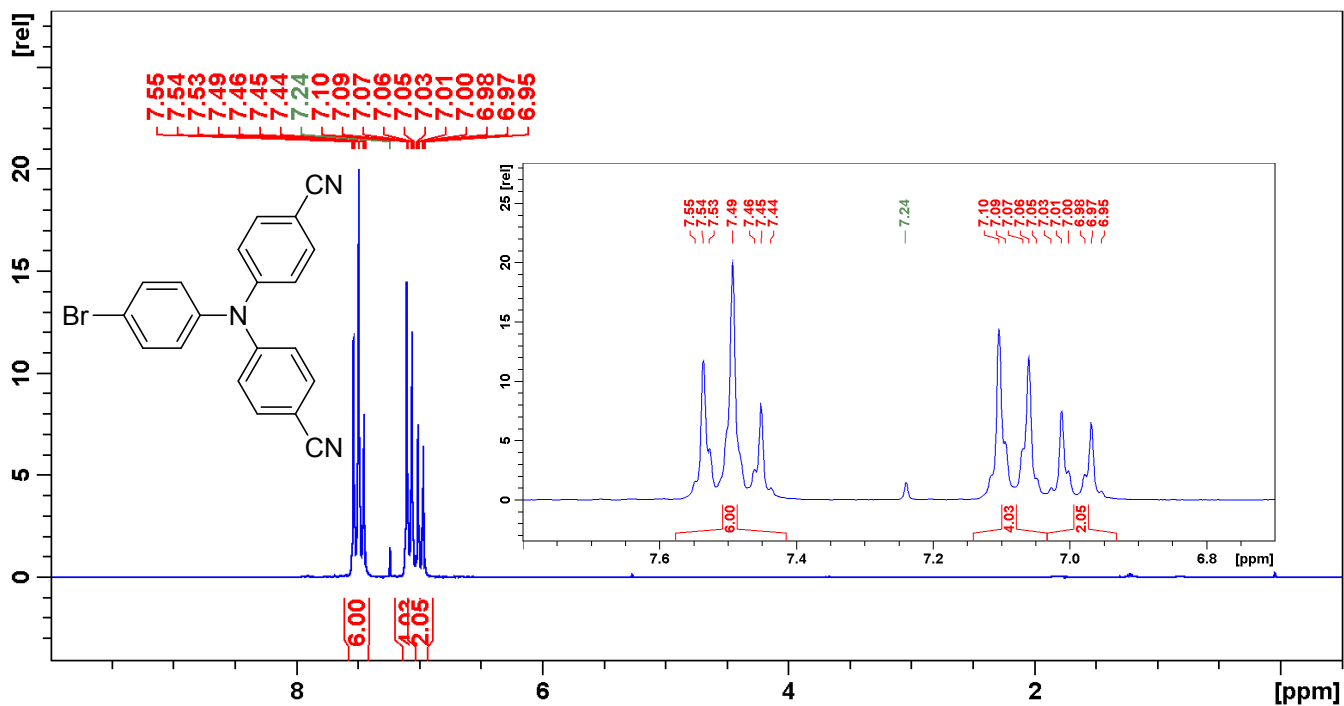


Figure S11. Proton NMR spectrum of compound **6i**.

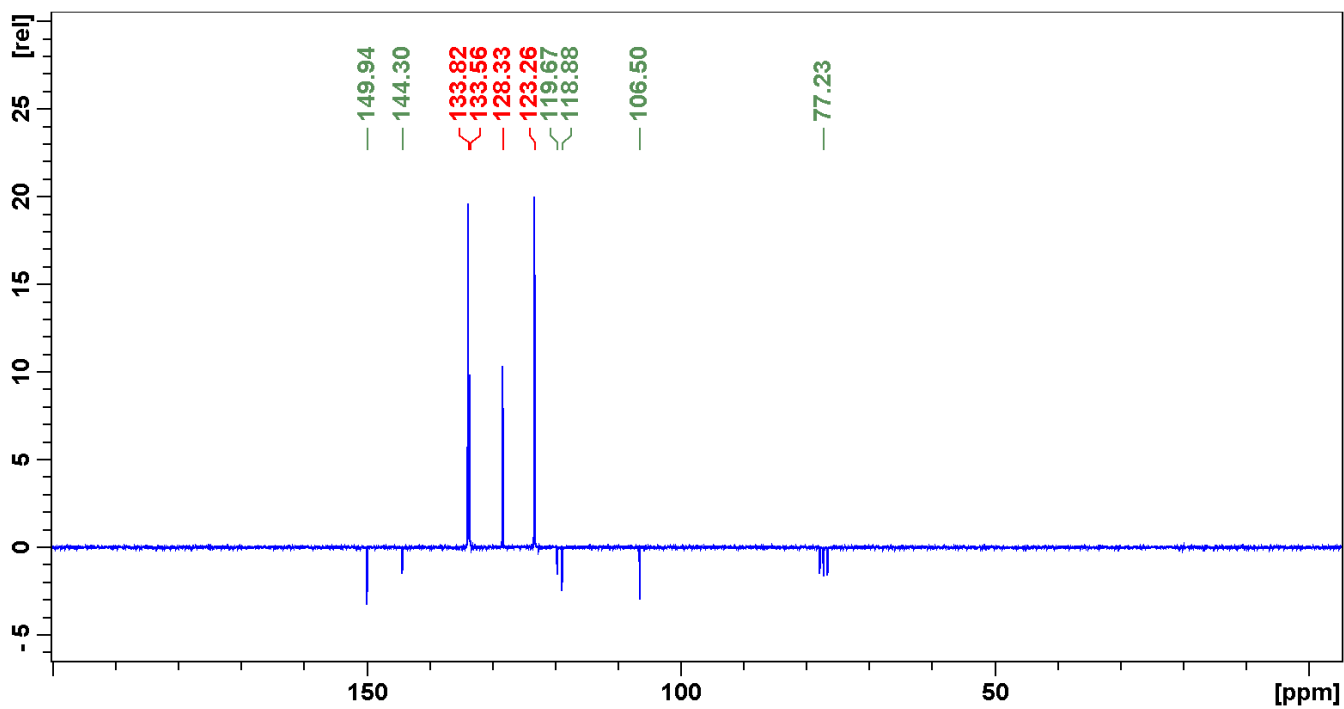


Figure S12. Carbon NMR spectrum of compound **6i**.

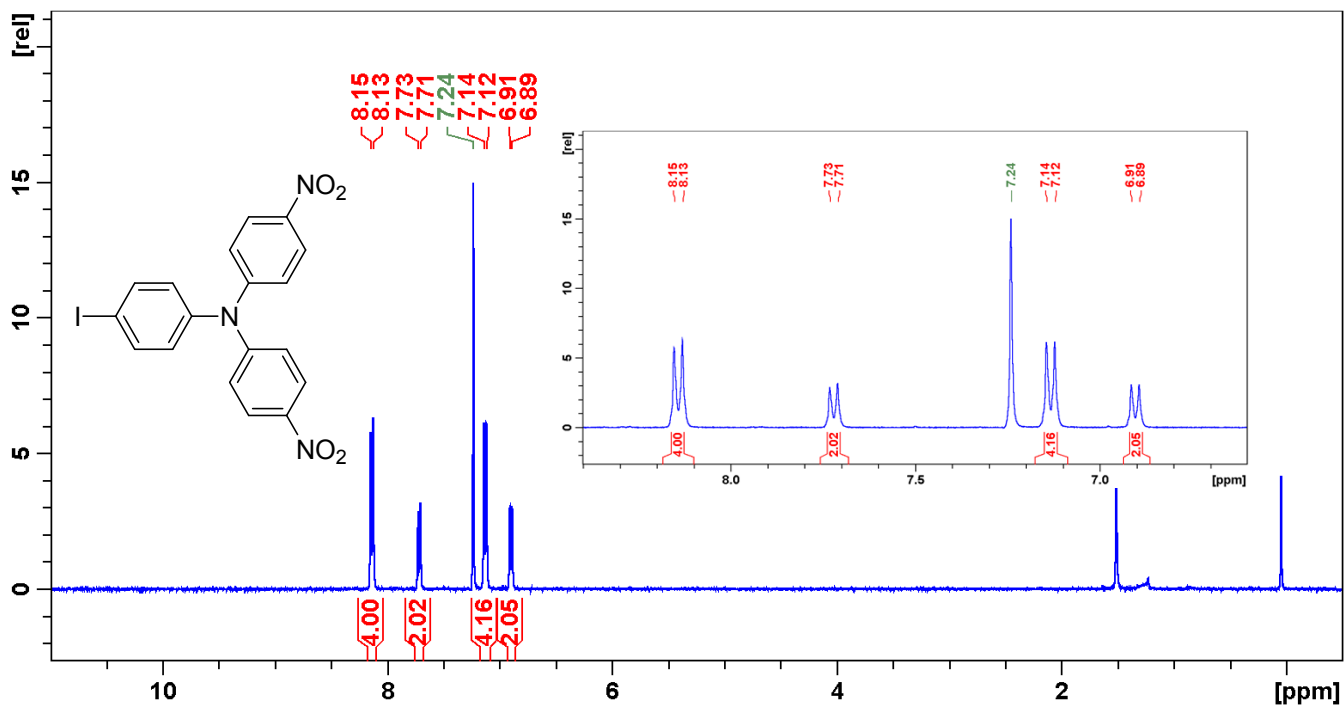


Figure S13. Proton NMR spectrum of compound **6j**.

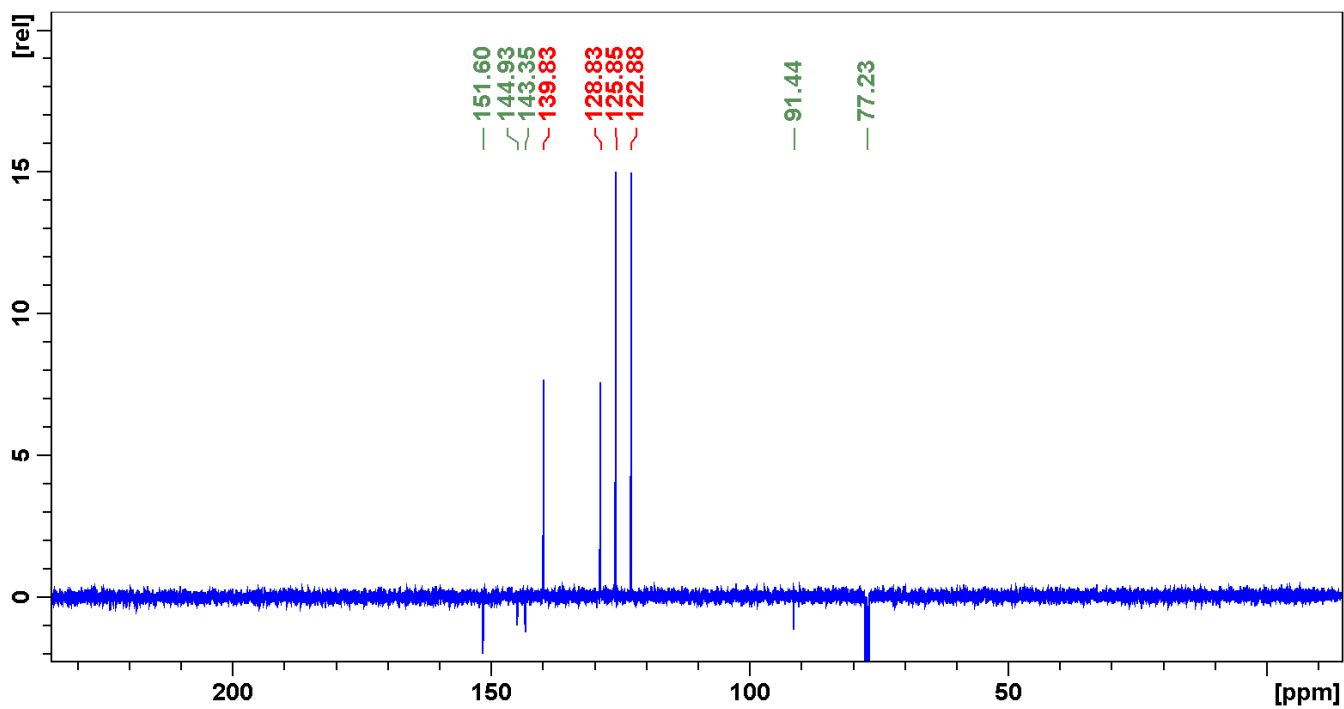


Figure S14. Carbon NMR spectrum of compound **6j**.

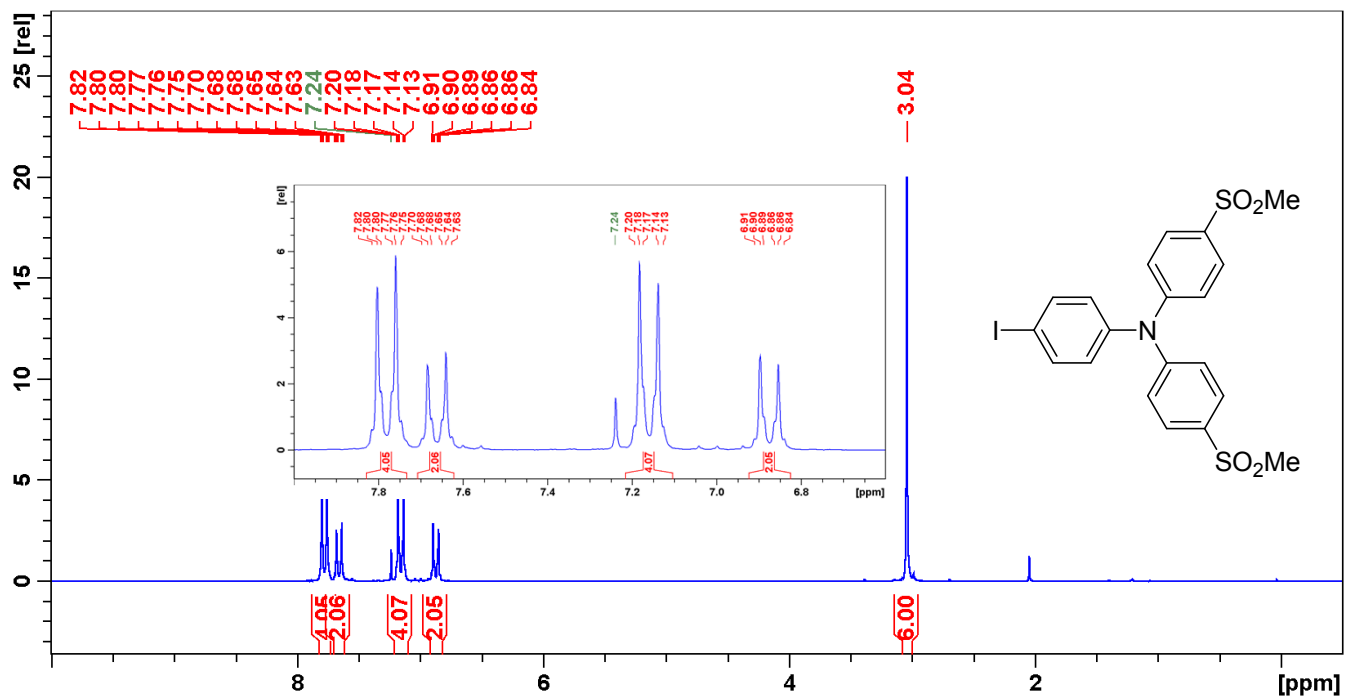


Figure S15. Proton NMR spectrum of compound **6k**.

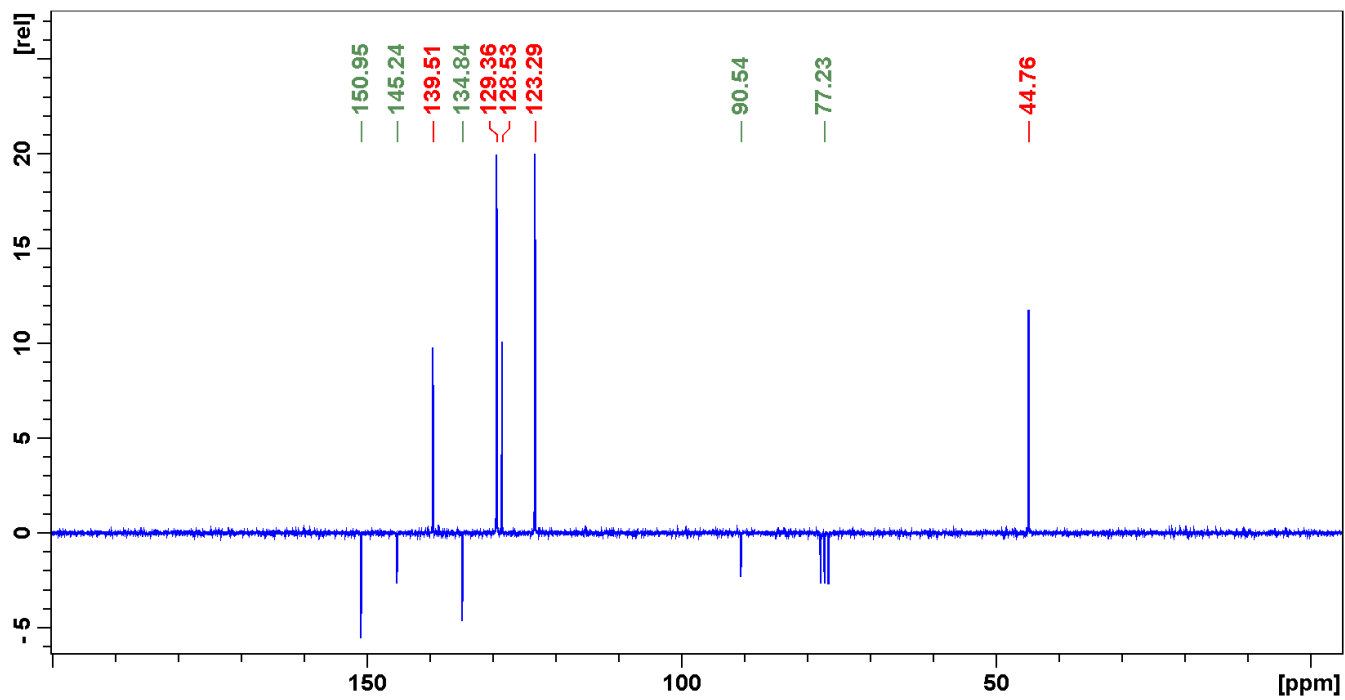


Figure S16. Carbon NMR spectrum of compound **6k**.

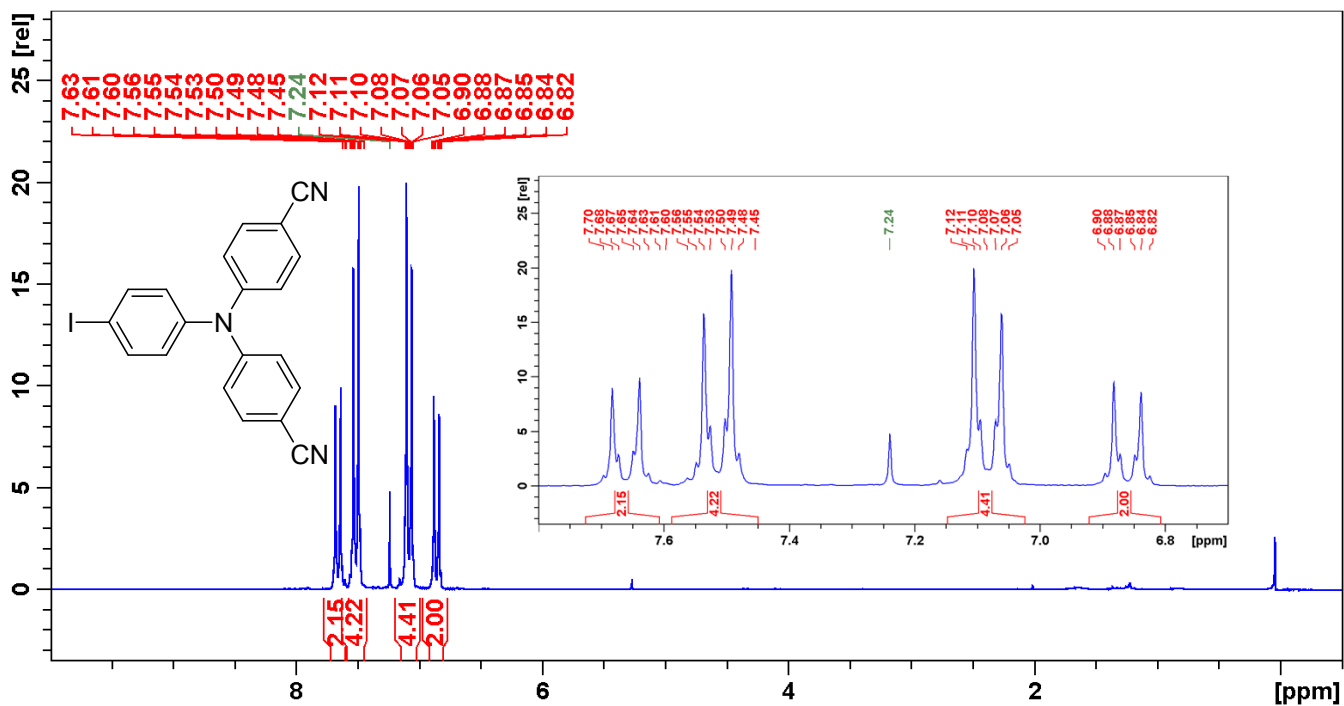


Figure S17. Proton NMR spectrum of compound **6l**.

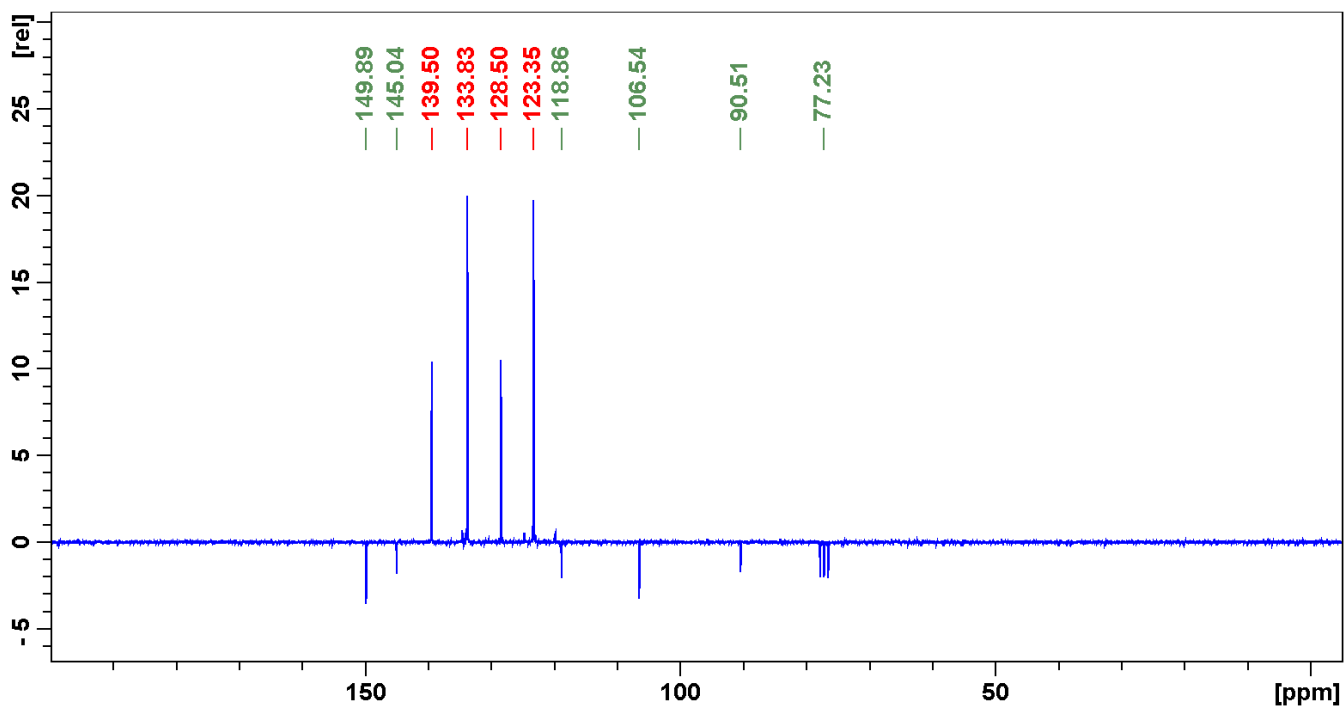


Figure S18. Carbon NMR spectrum of compound **6l**.

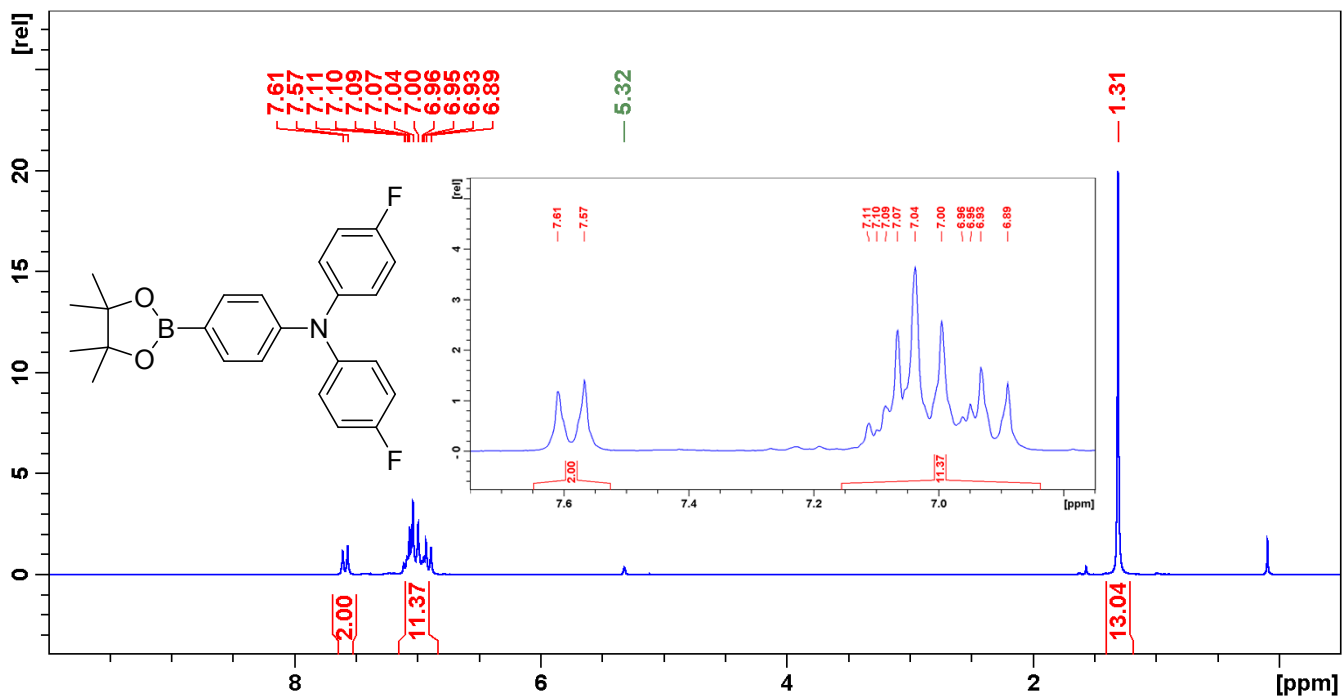


Figure S19. Proton NMR spectrum of compound **8c**.

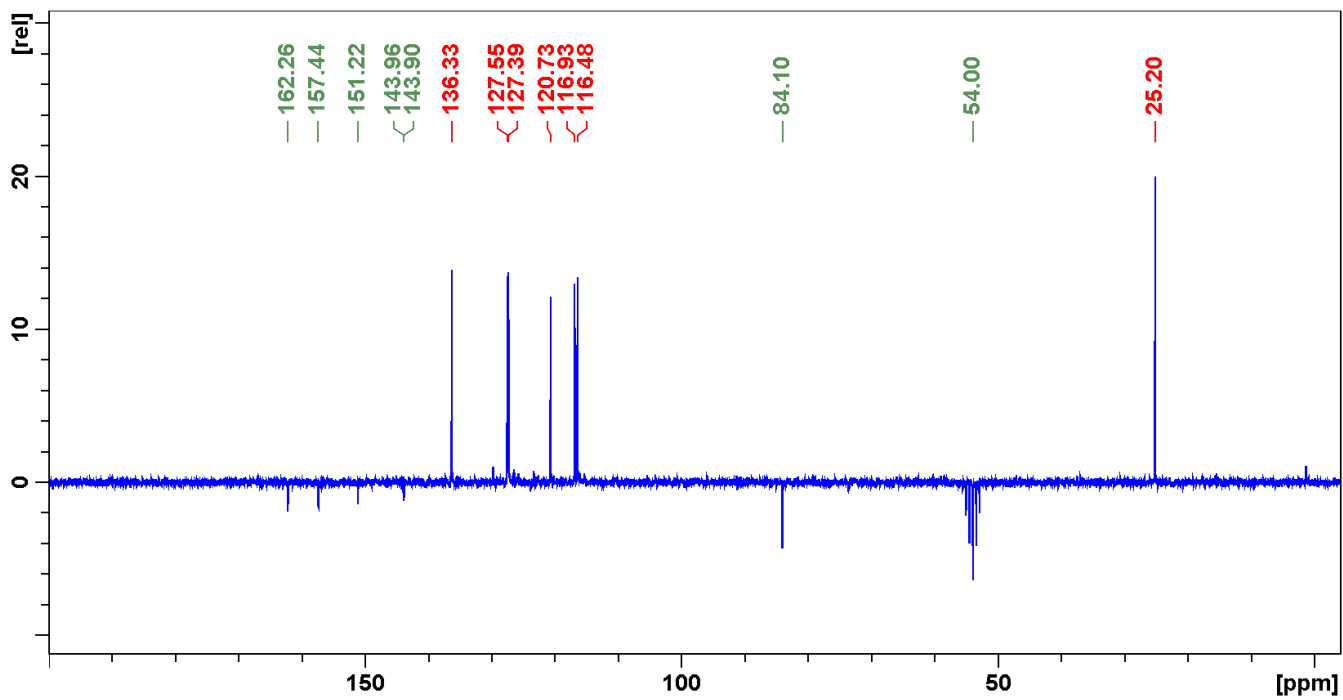


Figure S20. Carbon NMR spectrum of compound **8c**.

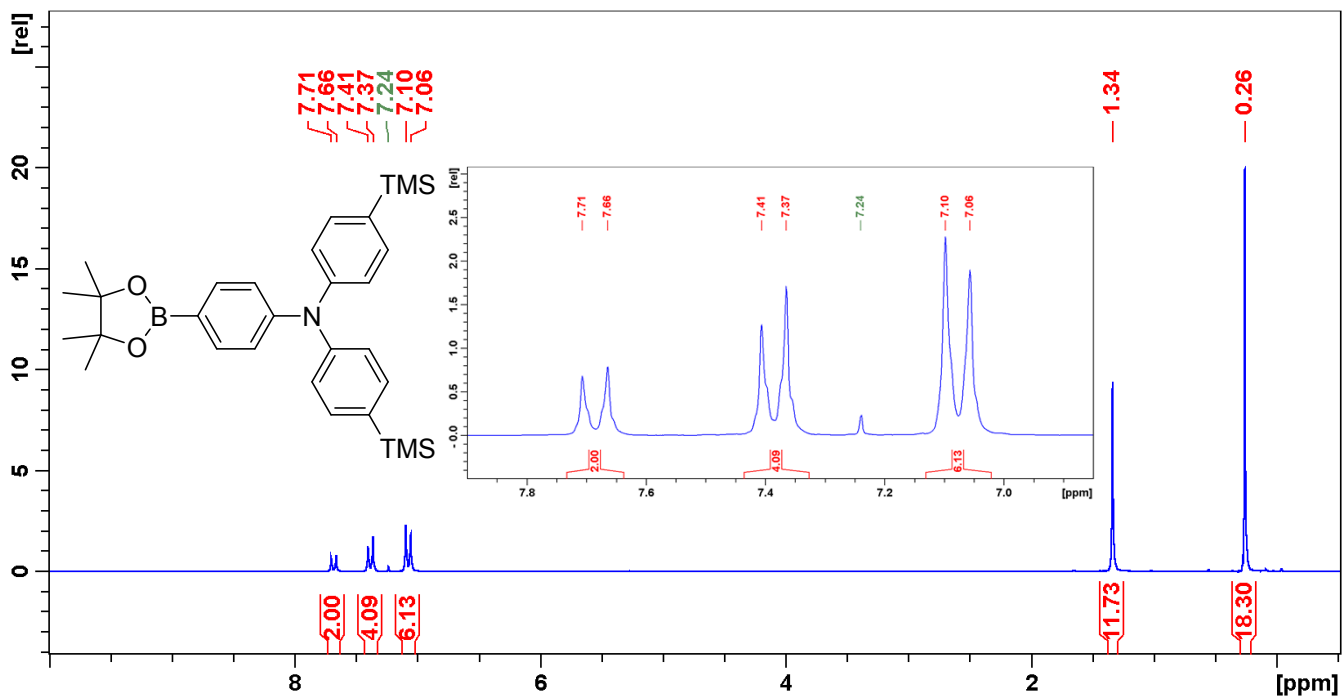


Figure S21. Proton NMR spectrum of compound **8e**.

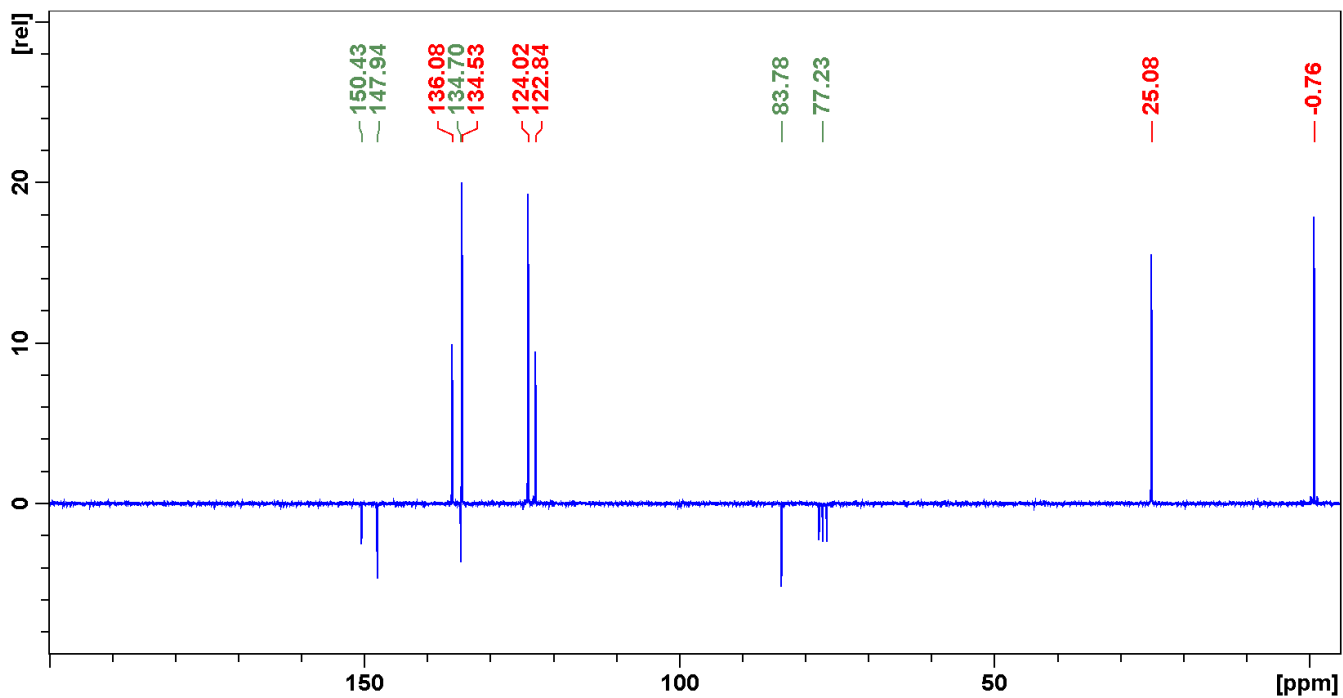


Figure S22. Carbon NMR spectrum of compound **8e**.

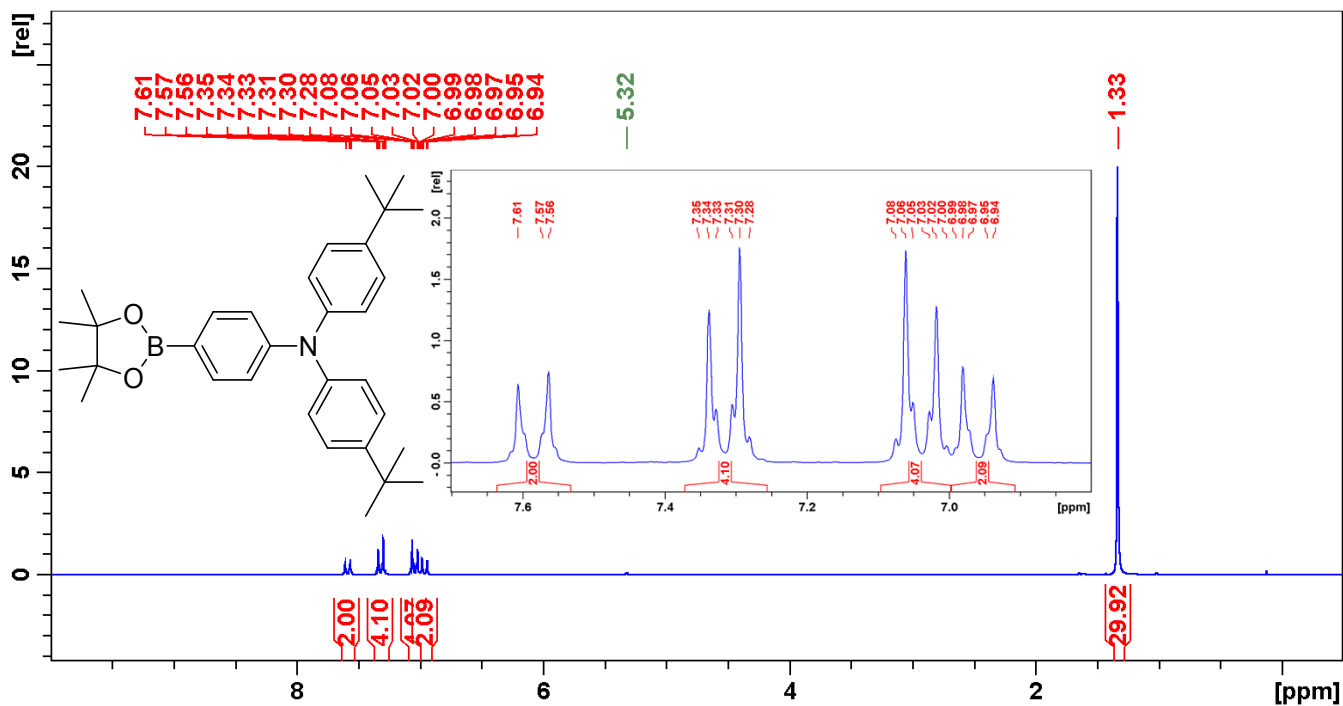


Figure S23. Proton NMR spectrum of compound **8f**.

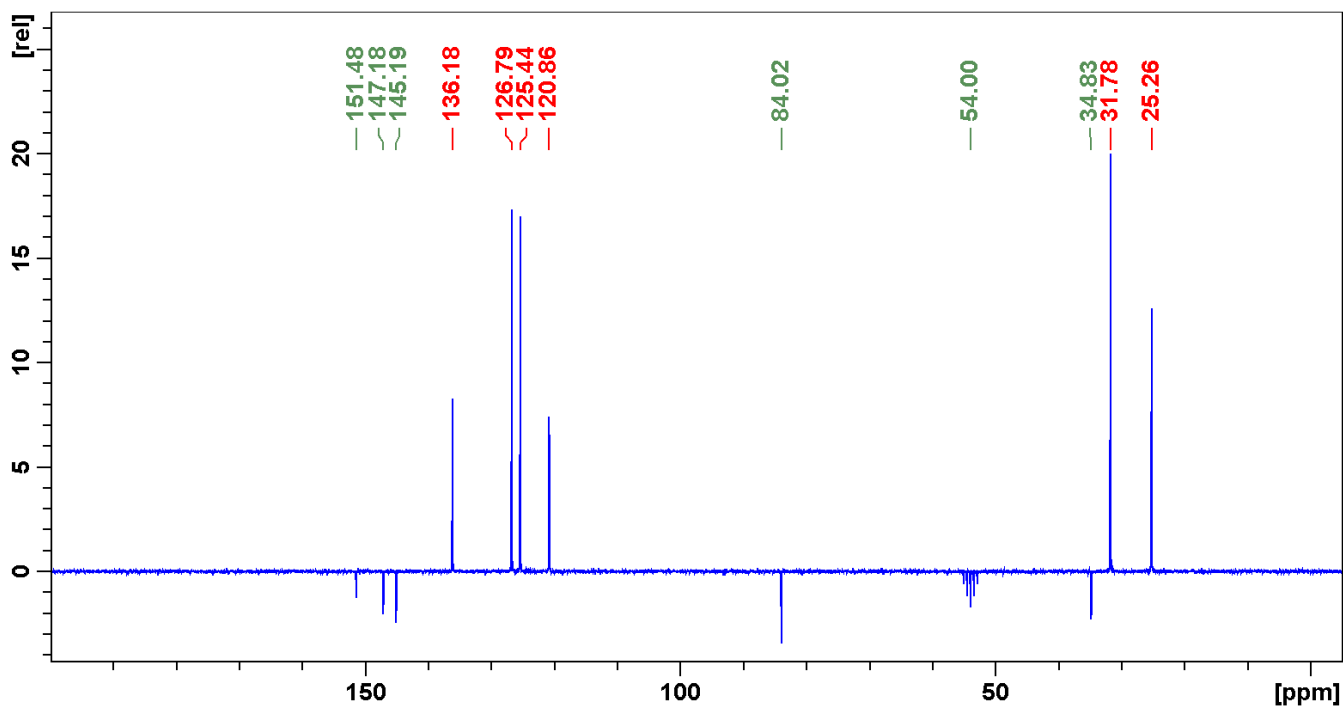


Figure S24. Carbon NMR spectrum of compound **8f**.

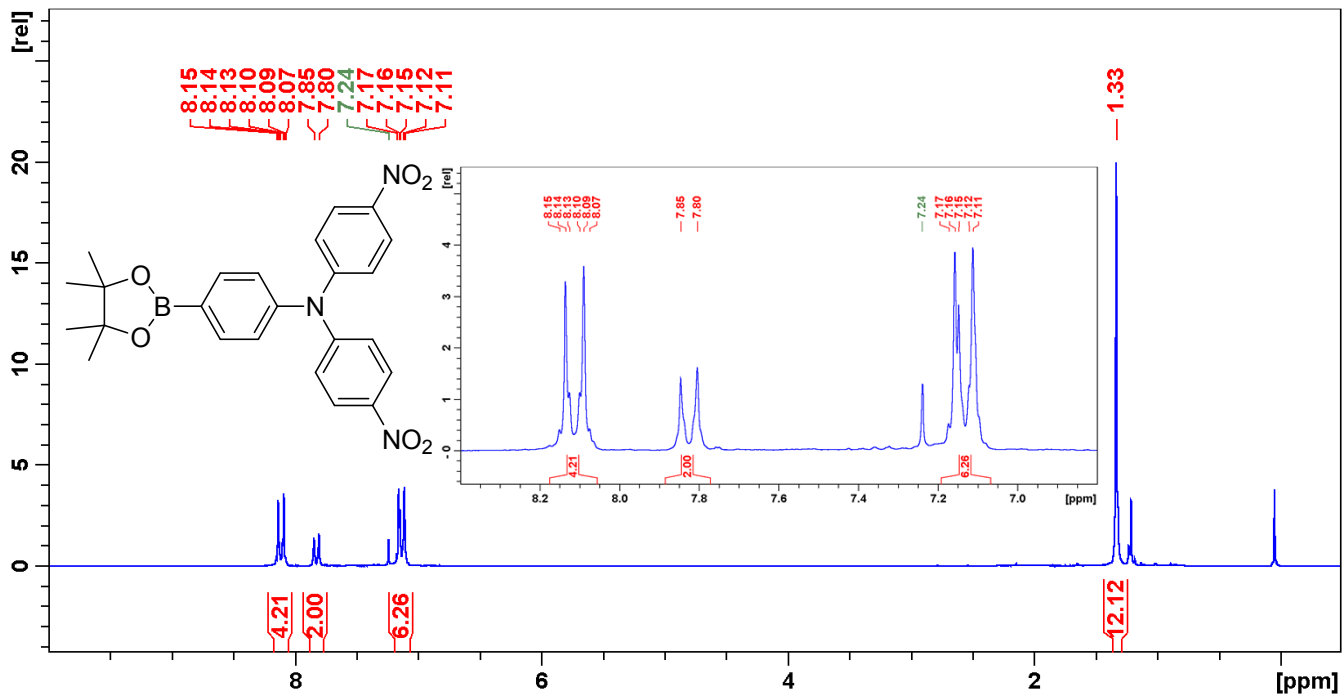


Figure S25. Proton NMR spectrum of compound **8g**.

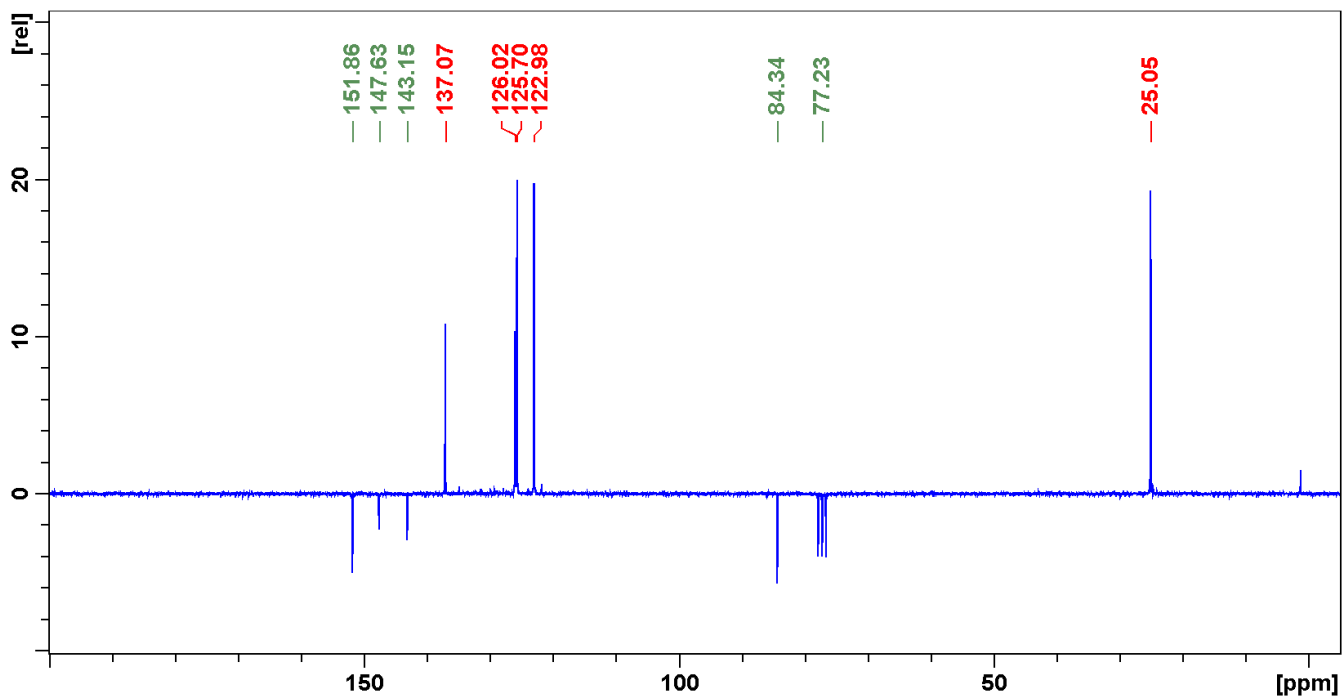


Figure S26. Carbon NMR spectrum of compound **8g**.

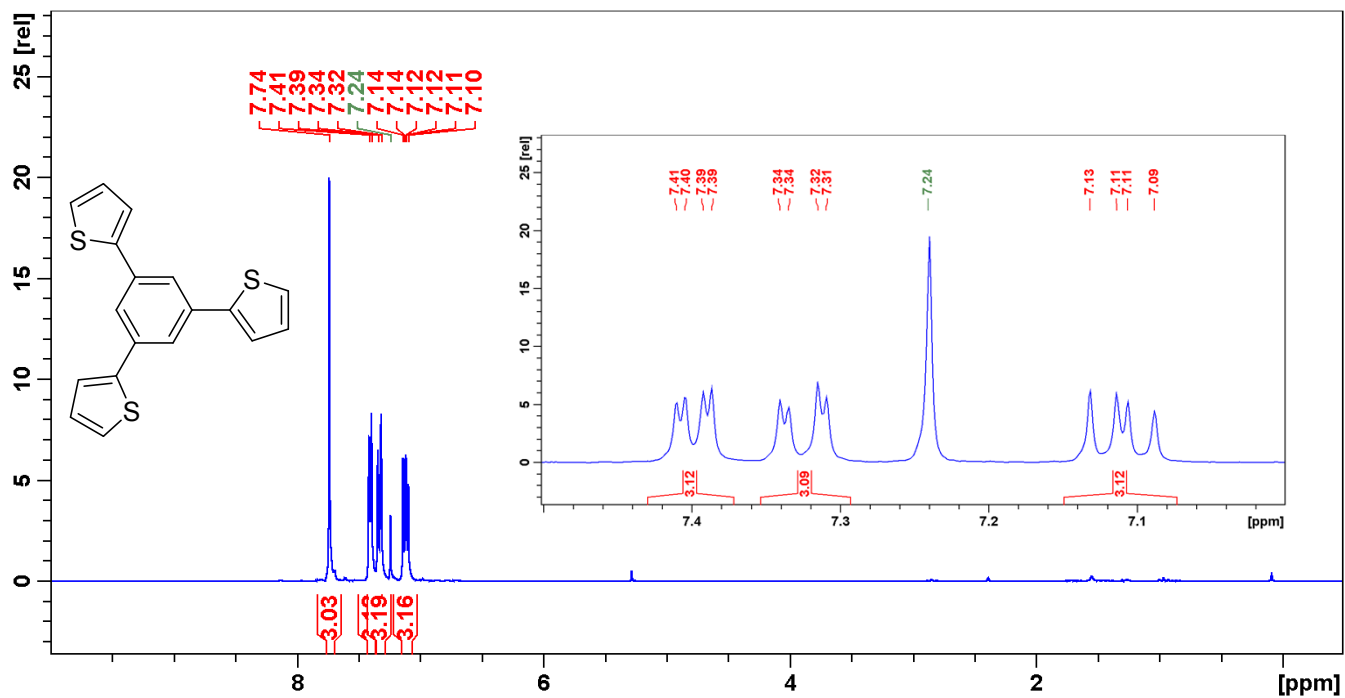


Figure S27. Proton NMR spectrum of compound 2.

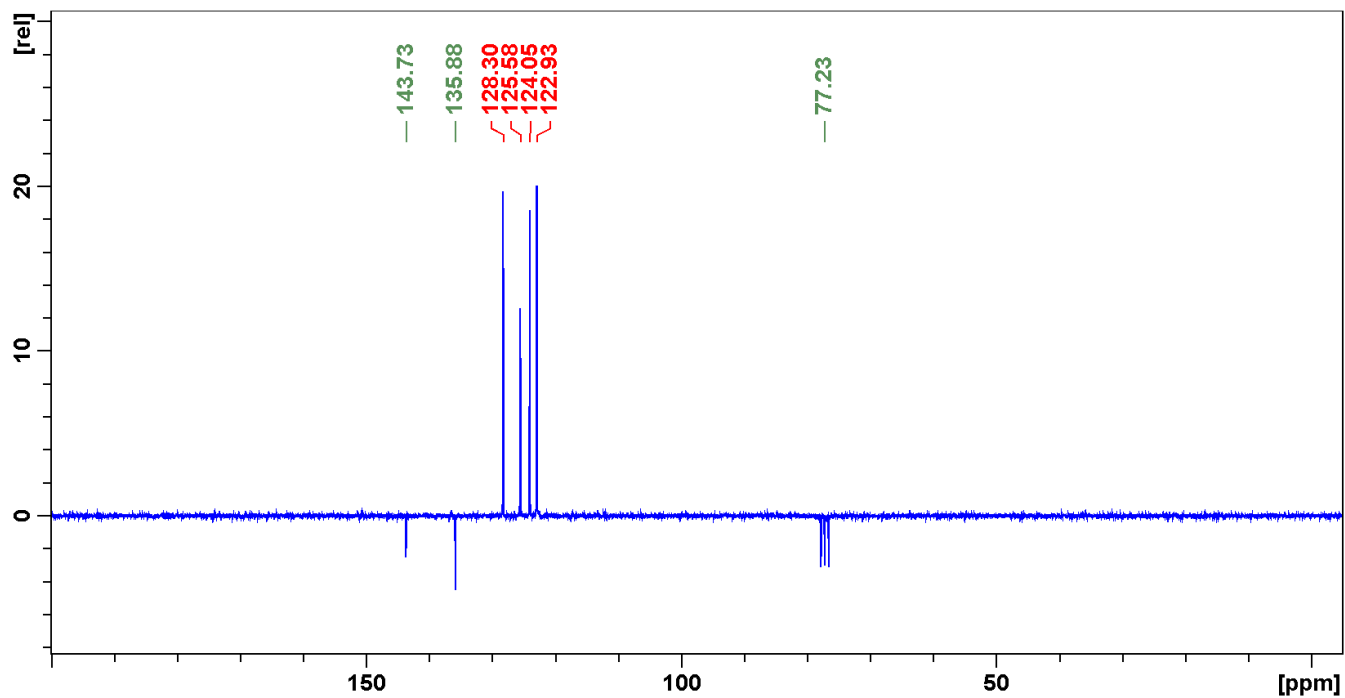


Figure S28. Carbon NMR spectrum of compound 2.

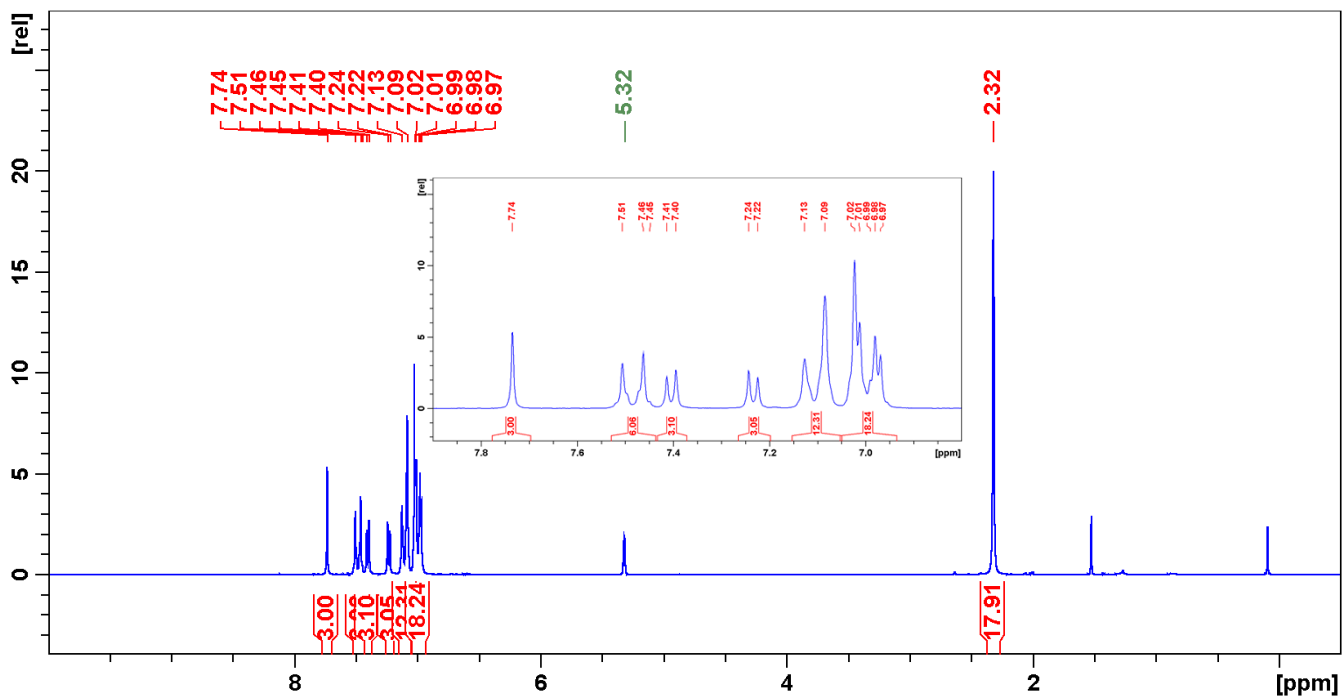


Figure S29. Proton NMR spectrum of compound S2.

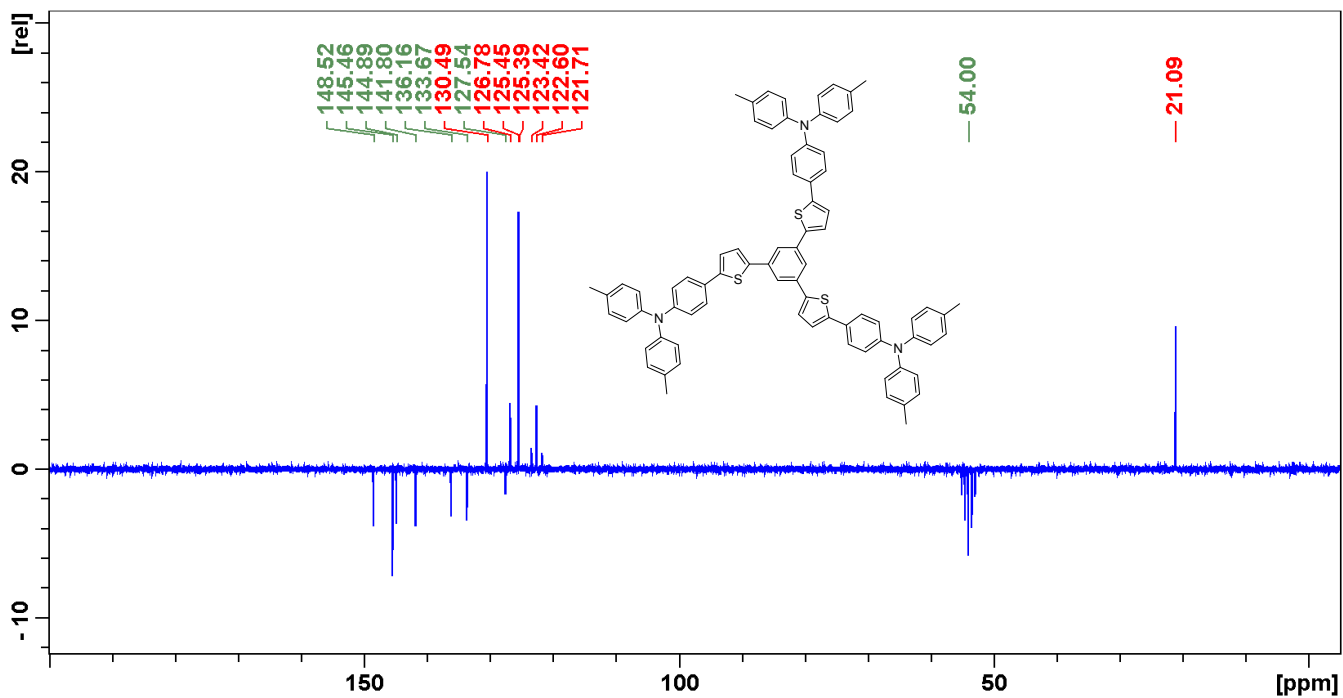


Figure S30. Carbon NMR spectrum of compound S2.

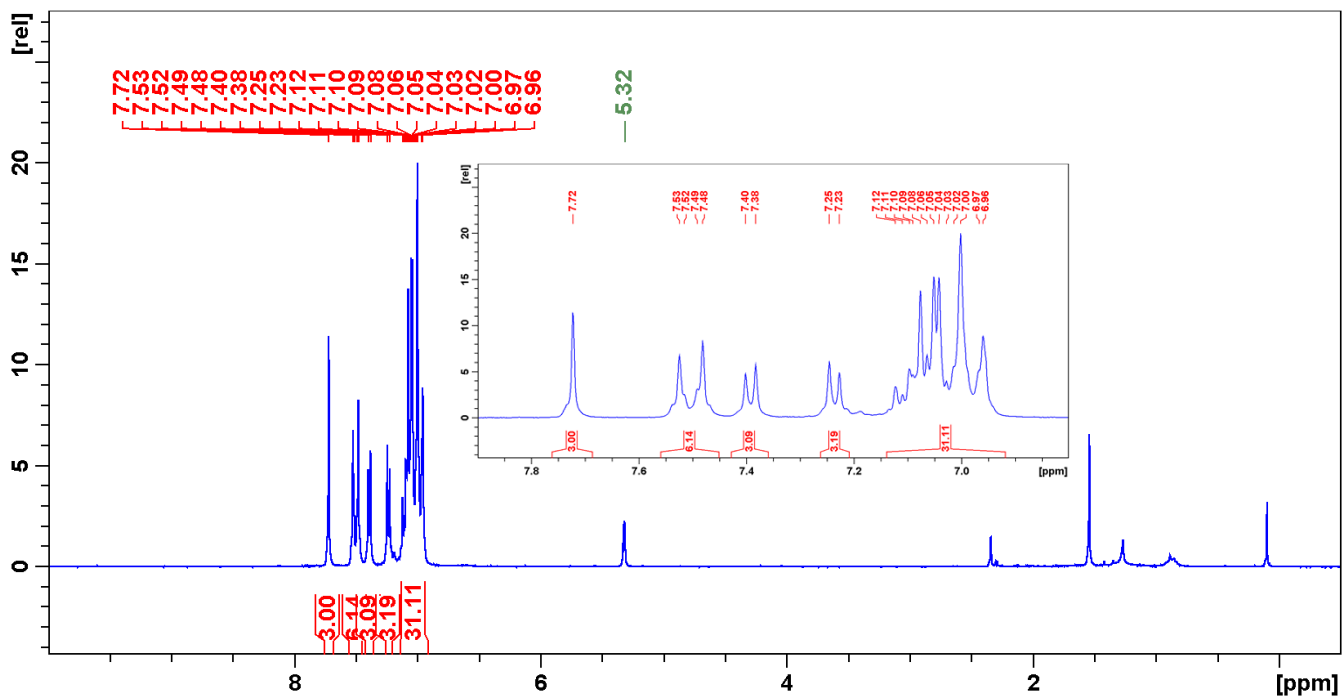


Figure S31. Proton NMR spectrum of compound S3.

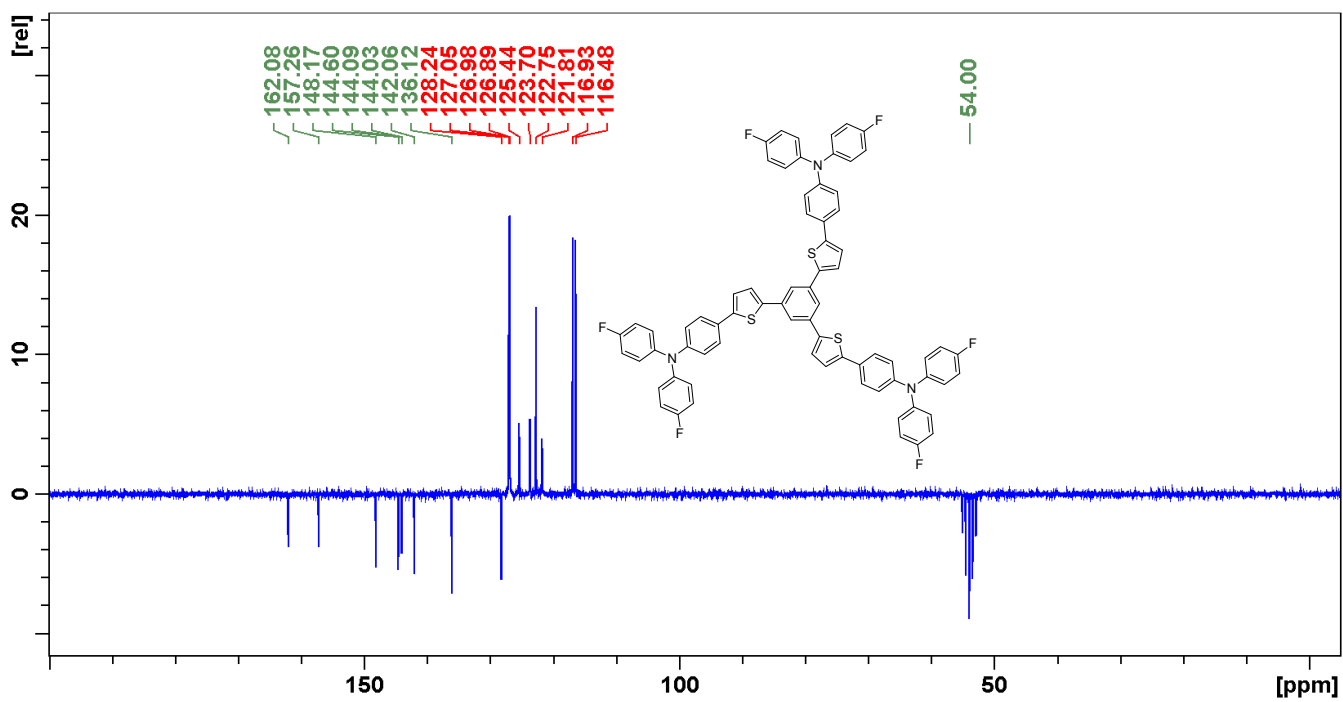


Figure S32. Carbon NMR spectrum of compound S3.

B) Absorption and Emission Spectra

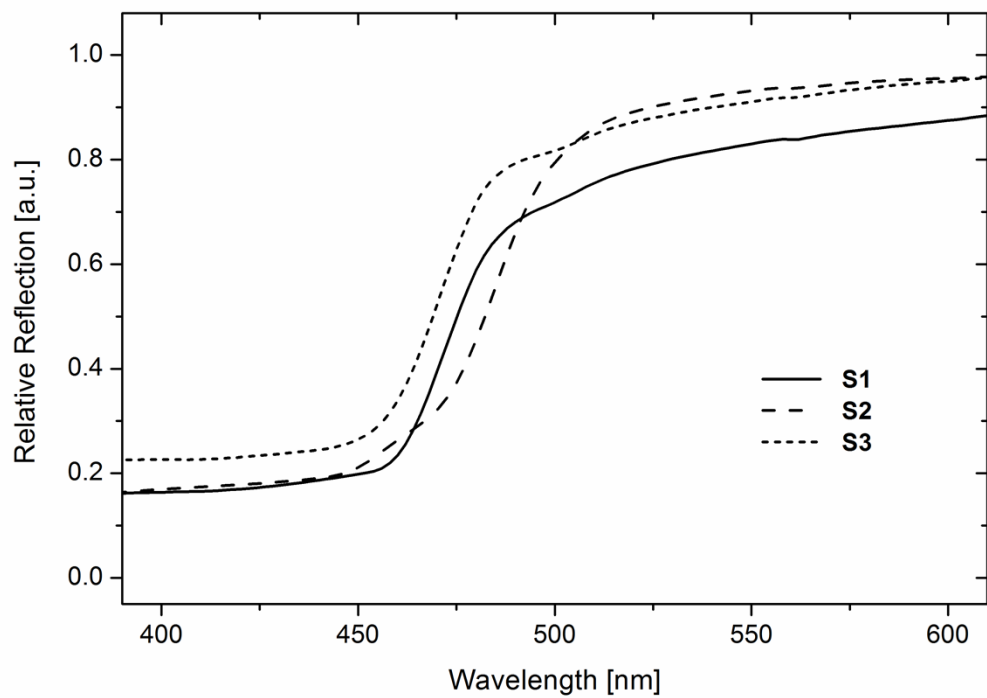


Figure S33. Absorption Spectra of Solid Samples

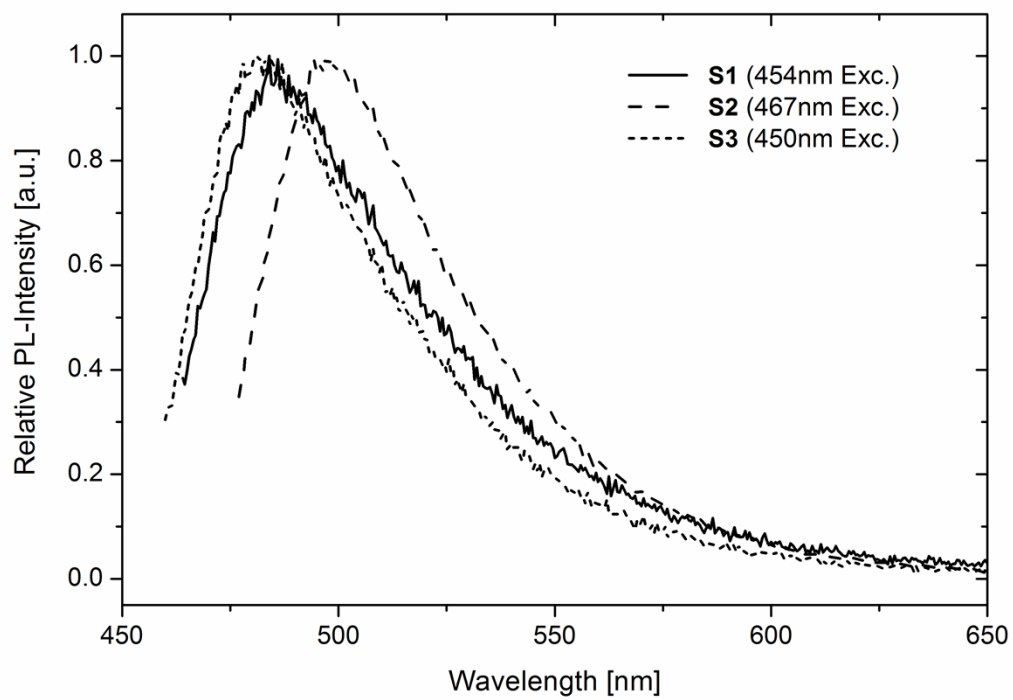


Figure S34. Emission Spectra of Solid Samples

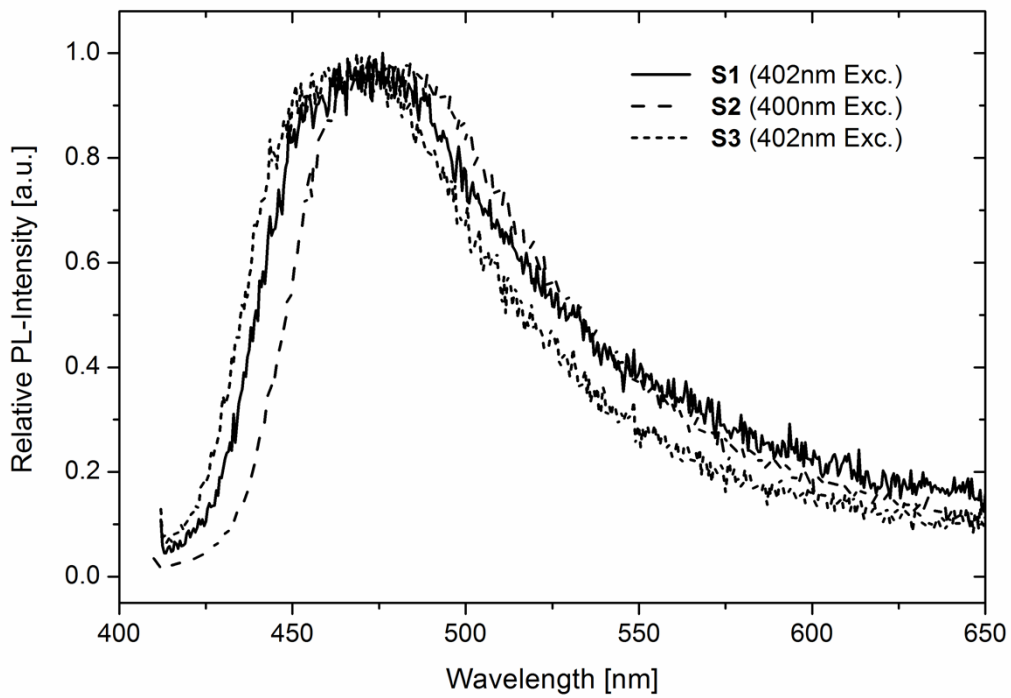


Figure S35. Emission Spectra of Film Samples

C) HOMO/LUMO plots of S1-3

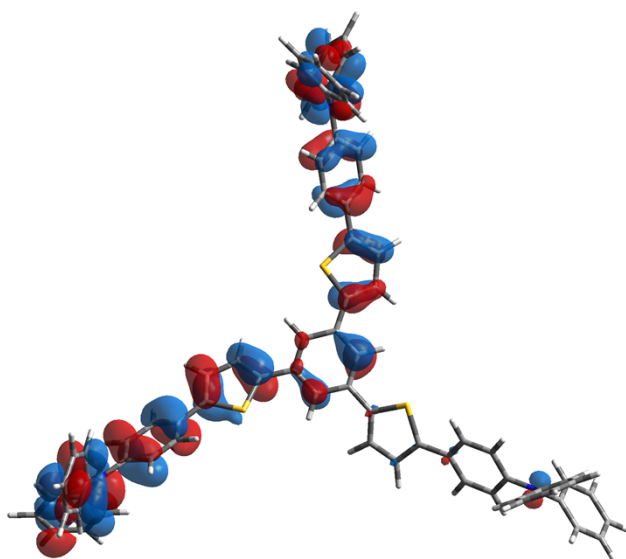
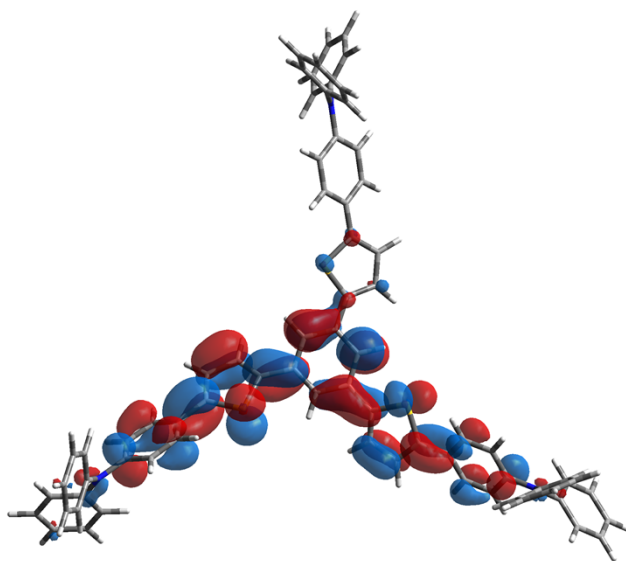


Figure S36. HOMO (bottom) and LUMO (top) of S1

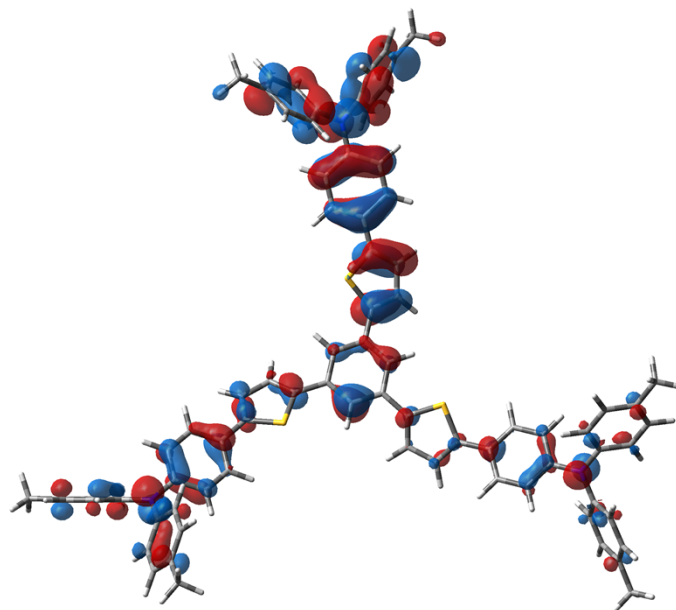
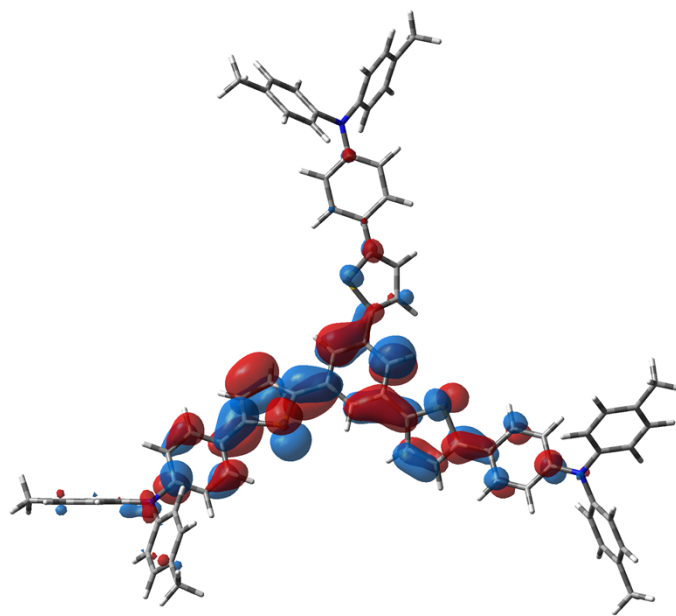


Figure S37. HOMO (bottom) and LUMO (top) of S2

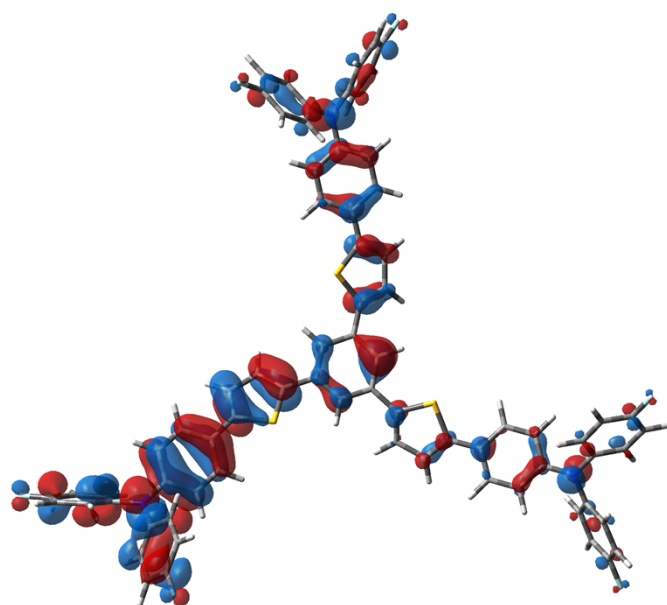
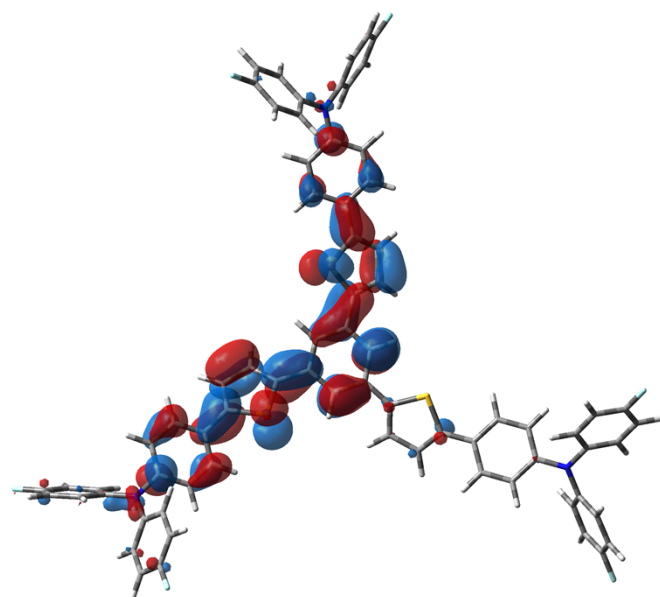


Figure S36. HOMO (bottom) and LUMO (top) of S3

Manuscript # 7

Supporting Information

Supporting Information

Systematic Investigations on 1,2,3-Triazole based Compounds Capable of Second Harmonic Generation

Daniel Lumpi,^{†,*} Florian Glöcklhofer,[†] Brigitte Holzer,[†] Berthold Stöger,[‡]
Christian Hametner,[†] Georg A. Reider,[§] and Johannes Fröhlich[†]

[†]Institute of Applied Synthetic Chemistry, Vienna University of Technology

[‡]Institute of Chemical Technologies and Analytics, Vienna University of Technology

[§]Photonics Institute, Vienna University of Technology

daniel.lumpi@tuwien.ac.at

Table of contents:

1. Synthetic Part	-2-
1.1. General procedures and methods	-2-
1.2. Spectral Data (¹ H-, ¹³ C(APT)-NMR spectra)	-3-
2. Crystallographic Part	-27-

1. Synthetic Part

1.1. General procedures and methods.

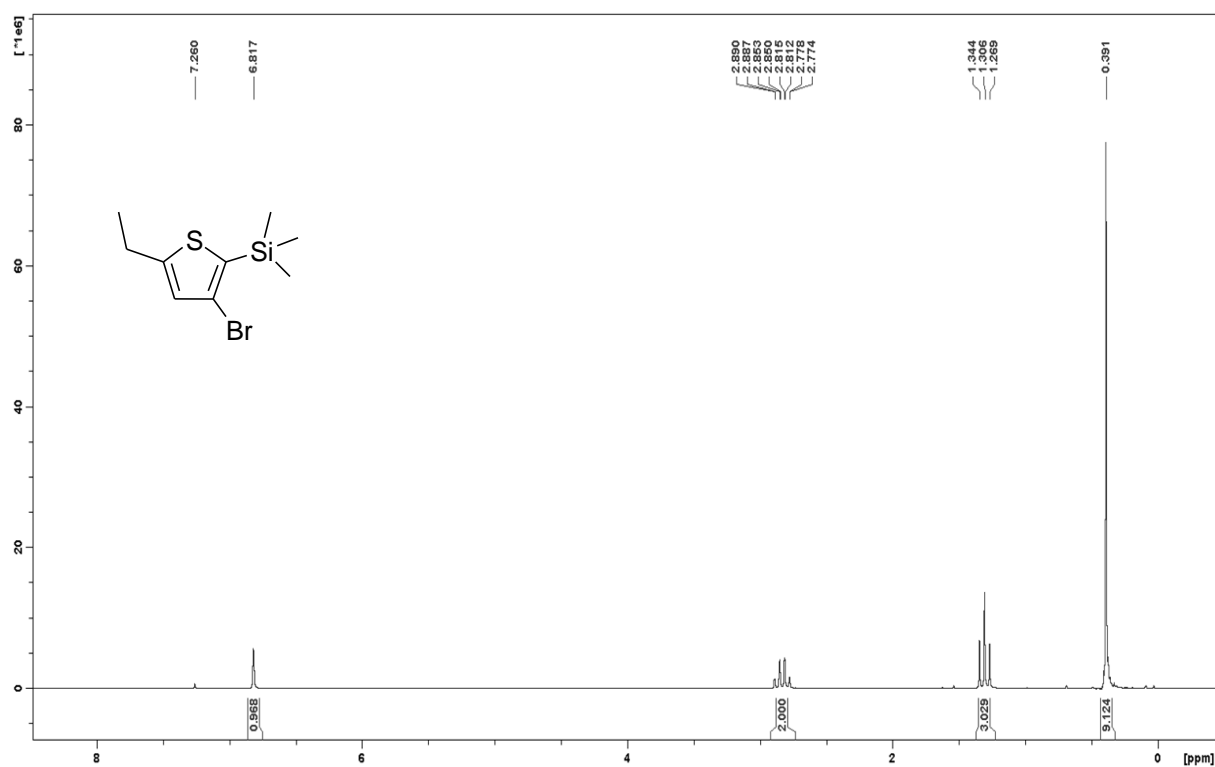
All reactions were performed in oven-dried glassware. Reagents were purchased from common commercial sources and used without further purification. Anhydrous solvents were prepared by filtration through drying columns. Column chromatography was performed on silica 60 (Merck, 40-63 μm) using distilled solvents as given. Melting points were determined using Kofler apparatus and were not corrected. Experiments under microwave irradiation were performed in a Biotage Initiator Sixty microwave reactor.

NMR spectra were recorded at 400 MHz for ^1H and 100 MHz for ^{13}C on a Bruker Avance DRX-400 Spectrometer for all target compounds as well as isomerization experiments and at 200 MHz for ^1H and 50 MHz for ^{13}C on a Bruker Avance 200 for intermediates. Data for ^1H NMR are reported as follows: chemical shift in parts per million from TMS (tetramethylsilane) with the residual solvent signal as an internal reference (CDCl_3 $\delta = 7.26$ ppm, CD_2Cl_2 $\delta = 5.32$ ppm) multiplicity (s = singlet, d = doublet, t = triplet and m = multiplet), coupling constant in Hz and integration. ^{13}C NMR spectra are reported in ppm from TMS using the central peak of the solvent as reference (CDCl_3 $\delta = 77.0$ ppm, CD_2Cl_2 $\delta = 54.0$ ppm); multiplicity with respect to proton (deduced from APT experiments, s = quaternary C, d = CH, t = CH_2 , q = CH_3).

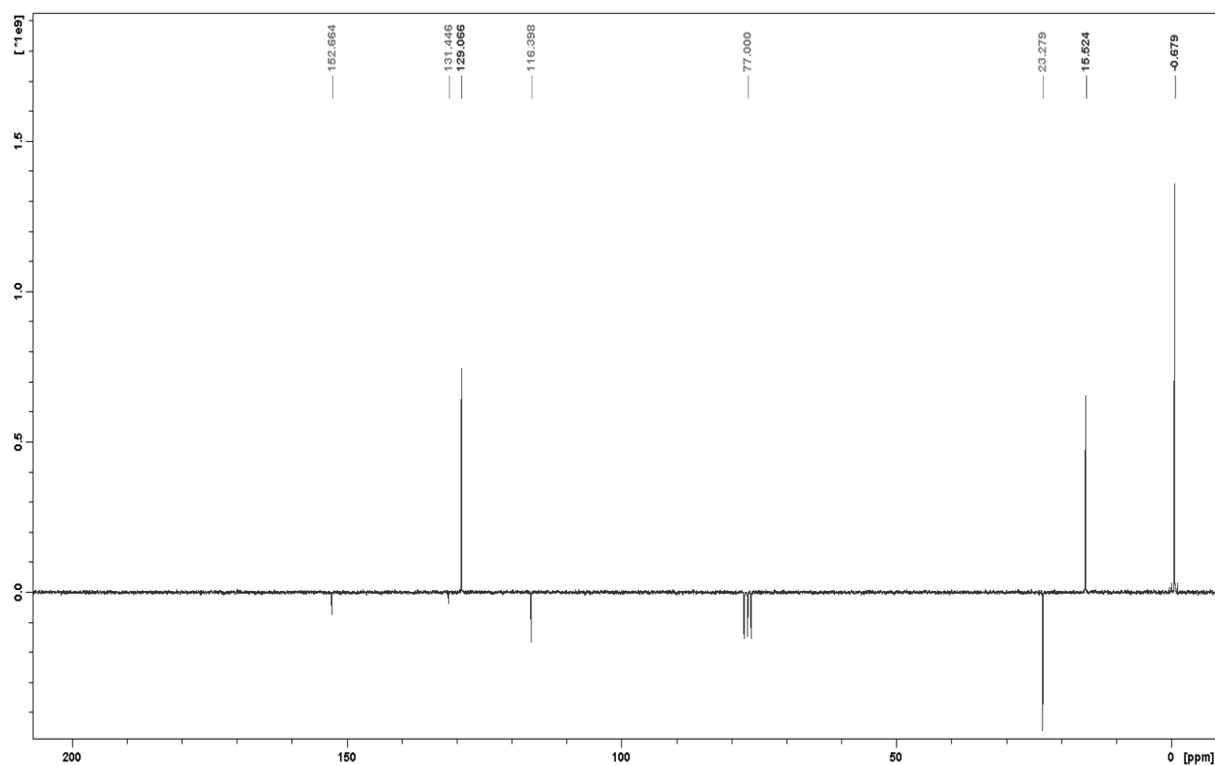
The absorption spectra were recorded on a Perkin Elmer Lambda 750 using Suprasil glass cuvettes. The measurements were performed of sample solutions in dry THF (5 μM) at rt.

Thermogravimetric analyses (TGA) were performed on a Netzsch Iris TG 209 C with a 414 TASC controller in Al_2O_3 crucibles using a heating rate of 5 $^\circ\text{C}/\text{min}$ in nitrogen atmosphere. Data processing was achieved using Proteus Analysis software.

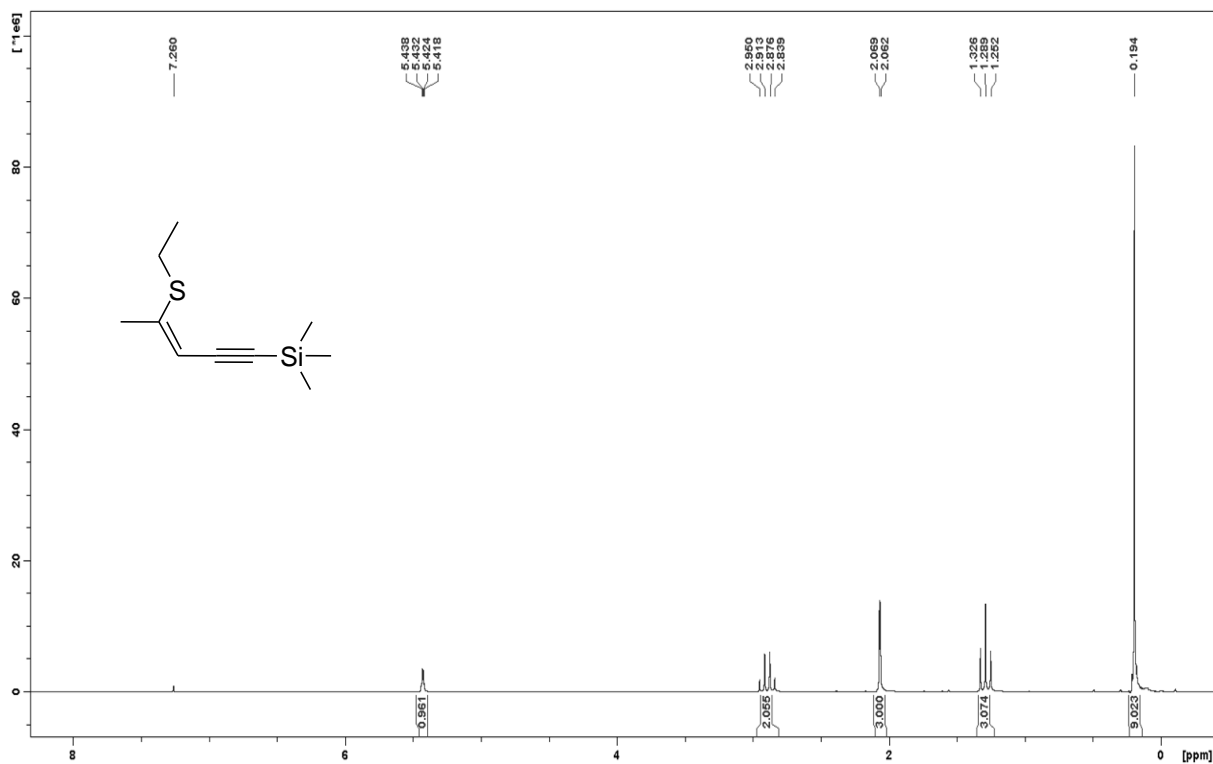
1.2. Spectral Data (^1H -, ^{13}C (APT)- NMR spectra).



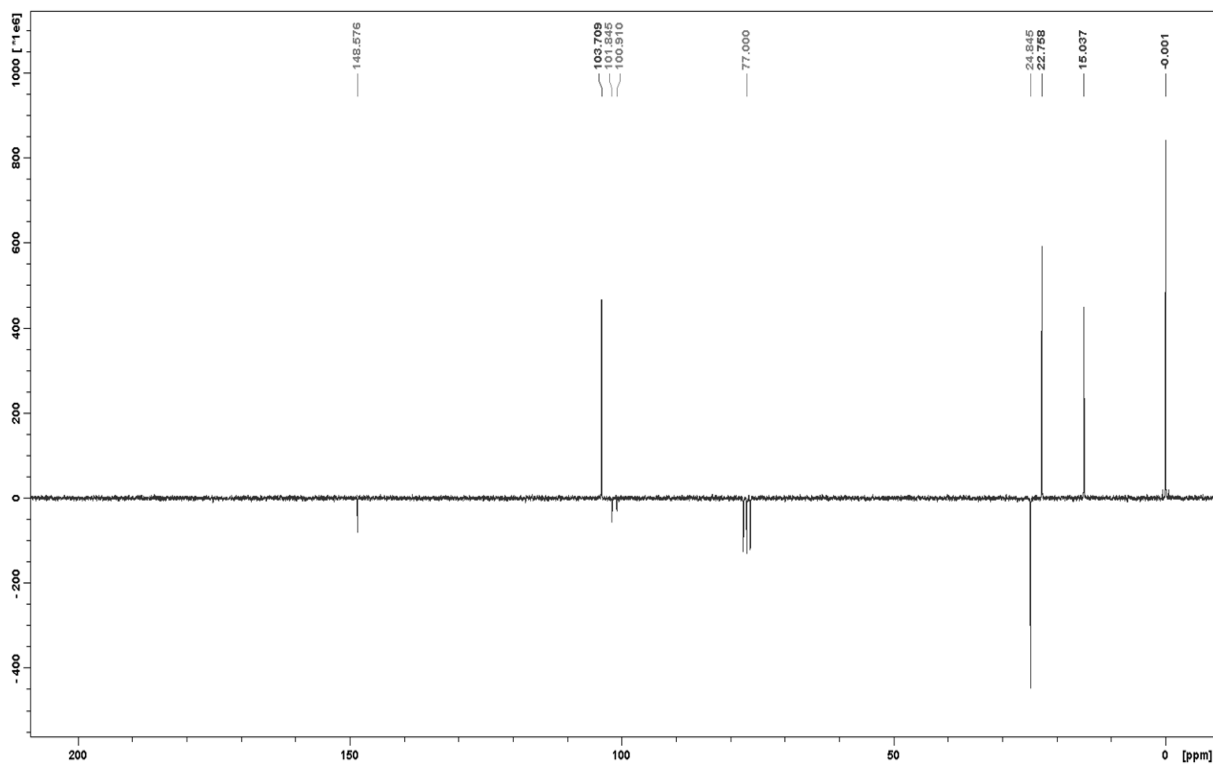
Spectrum 1.1. ^1H NMR (200 MHz, CDCl_3) of compound **2c**.



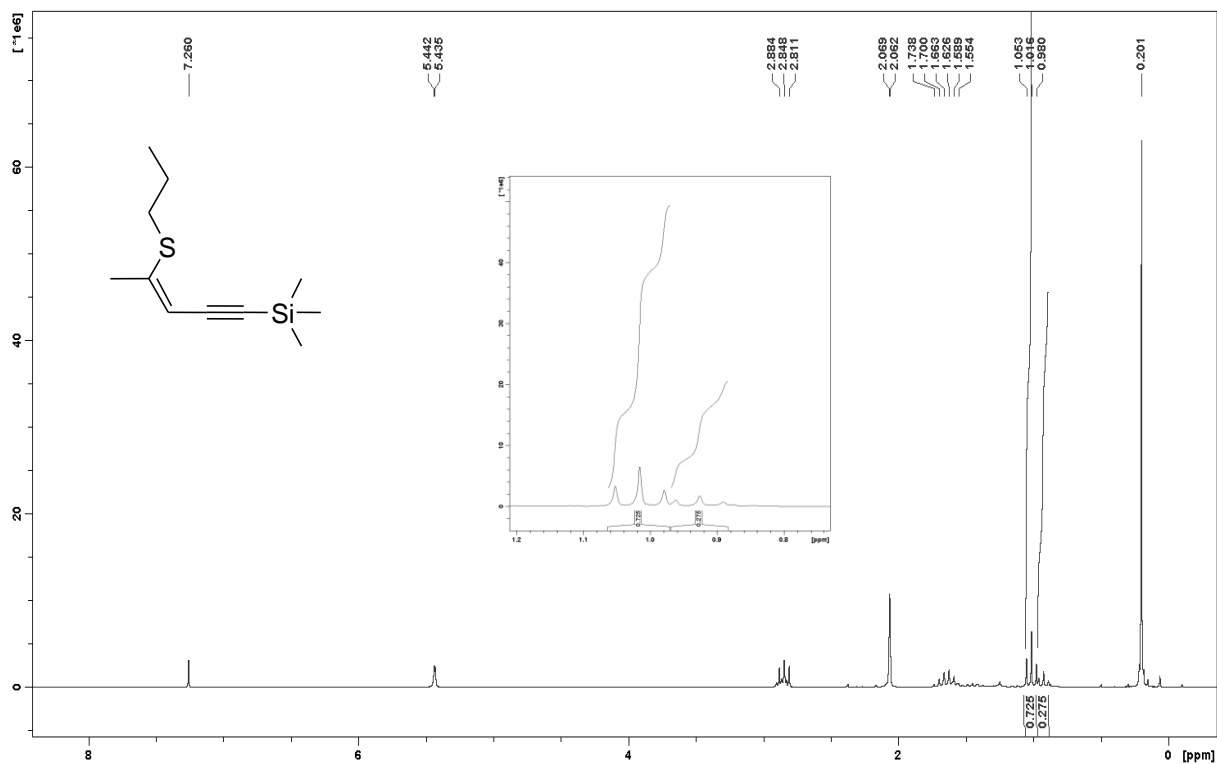
Spectrum 1.2. ^{13}C NMR (50 MHz, CDCl_3) of compound **2c**.



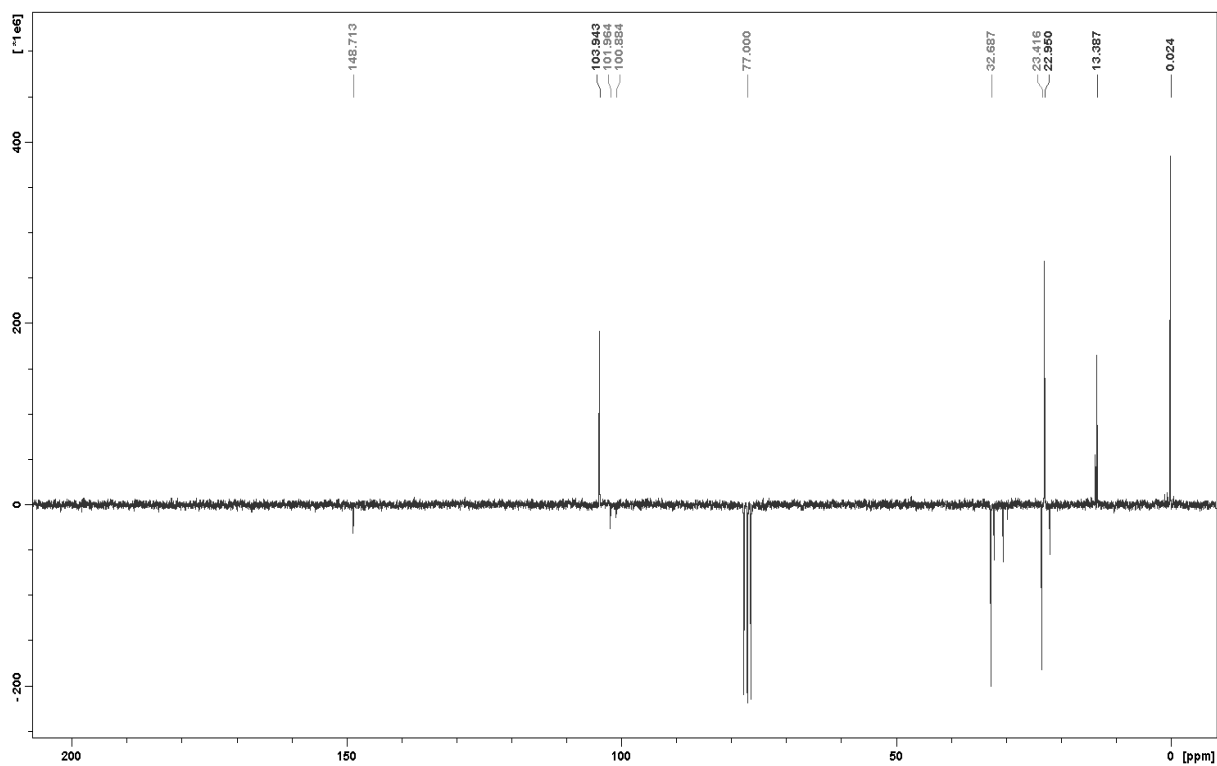
Spectrum 1.3. ¹H NMR (200 MHz, CDCl₃) of compound **3bb**.



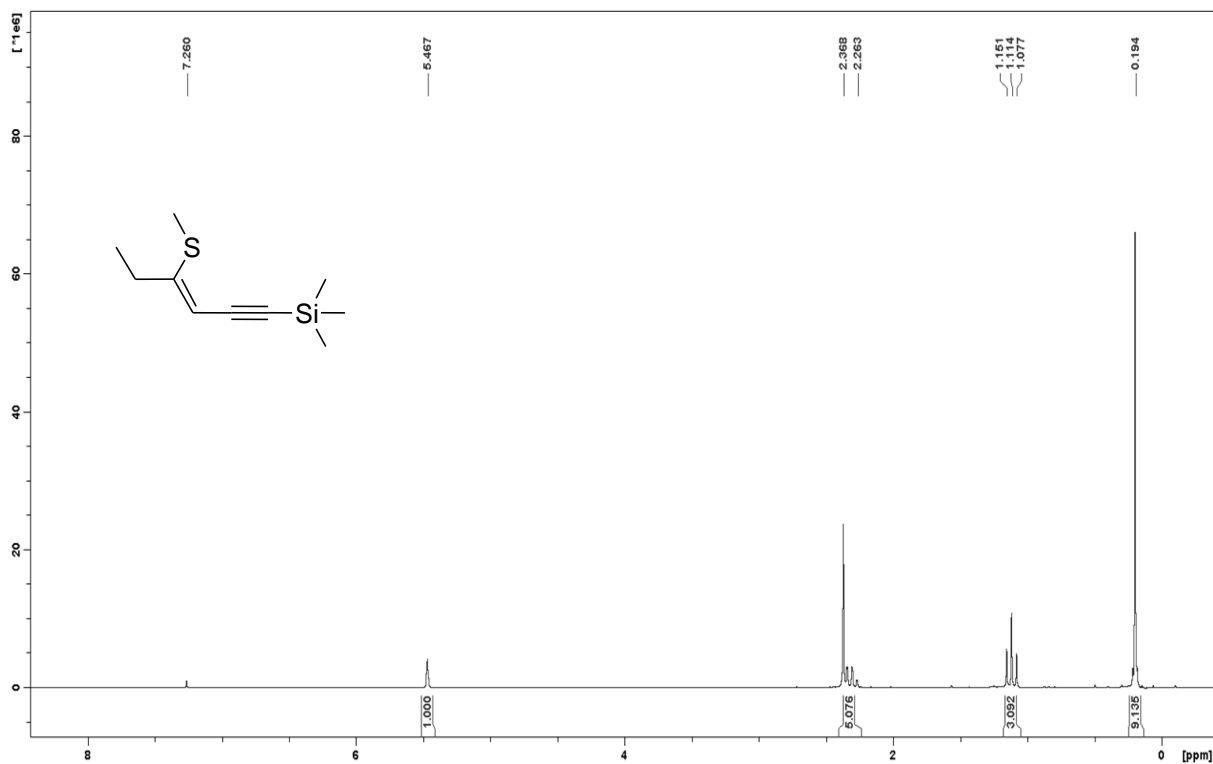
Spectrum 1.4. ¹³C NMR (50 MHz, CDCl₃) of compound **3bb**.



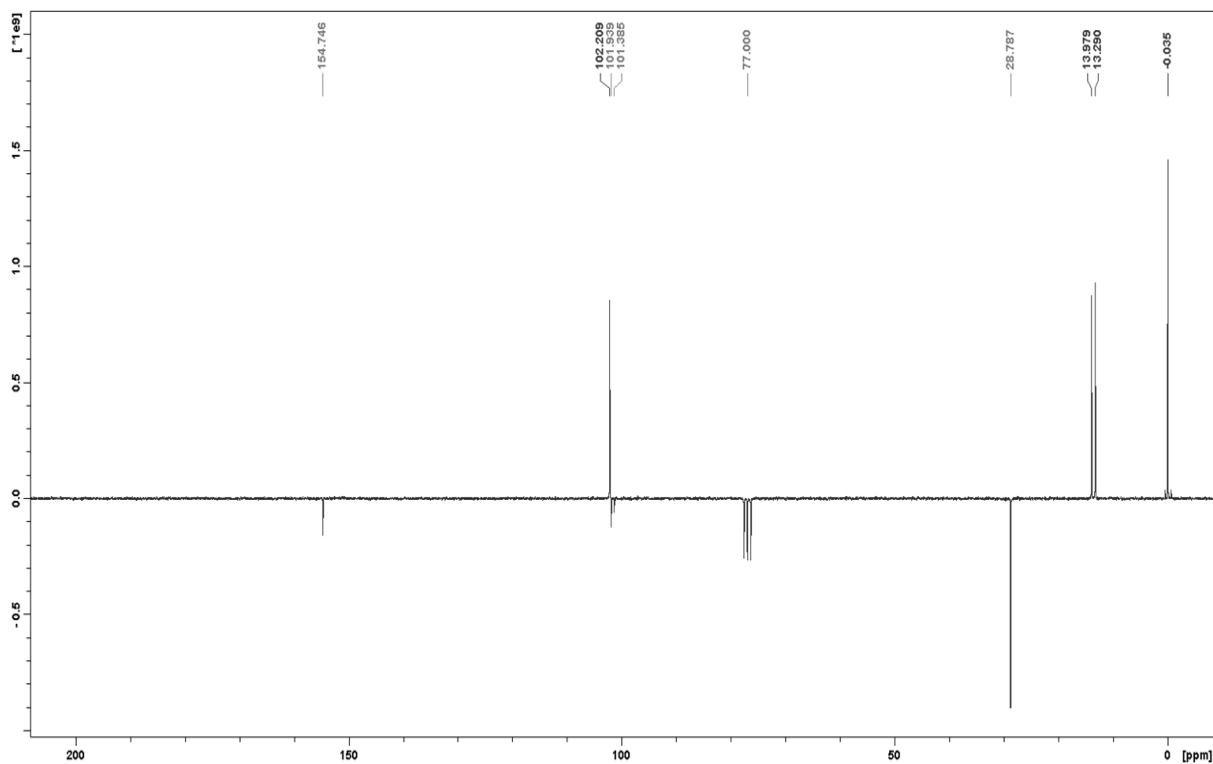
Spectrum 1.5. ¹H NMR (200 MHz, CDCl₃) of compound **3bc**.



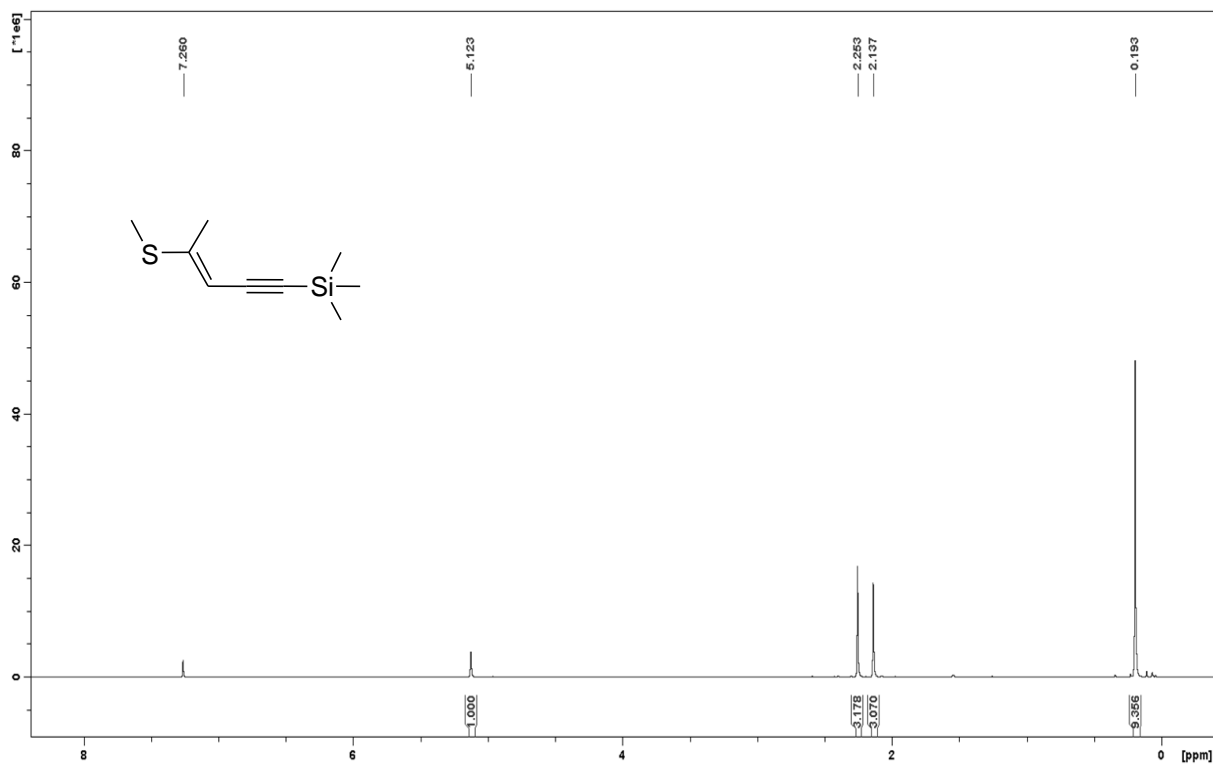
Spectrum 1.6. ¹³C NMR (50 MHz, CDCl₃) of compound **3bc**.



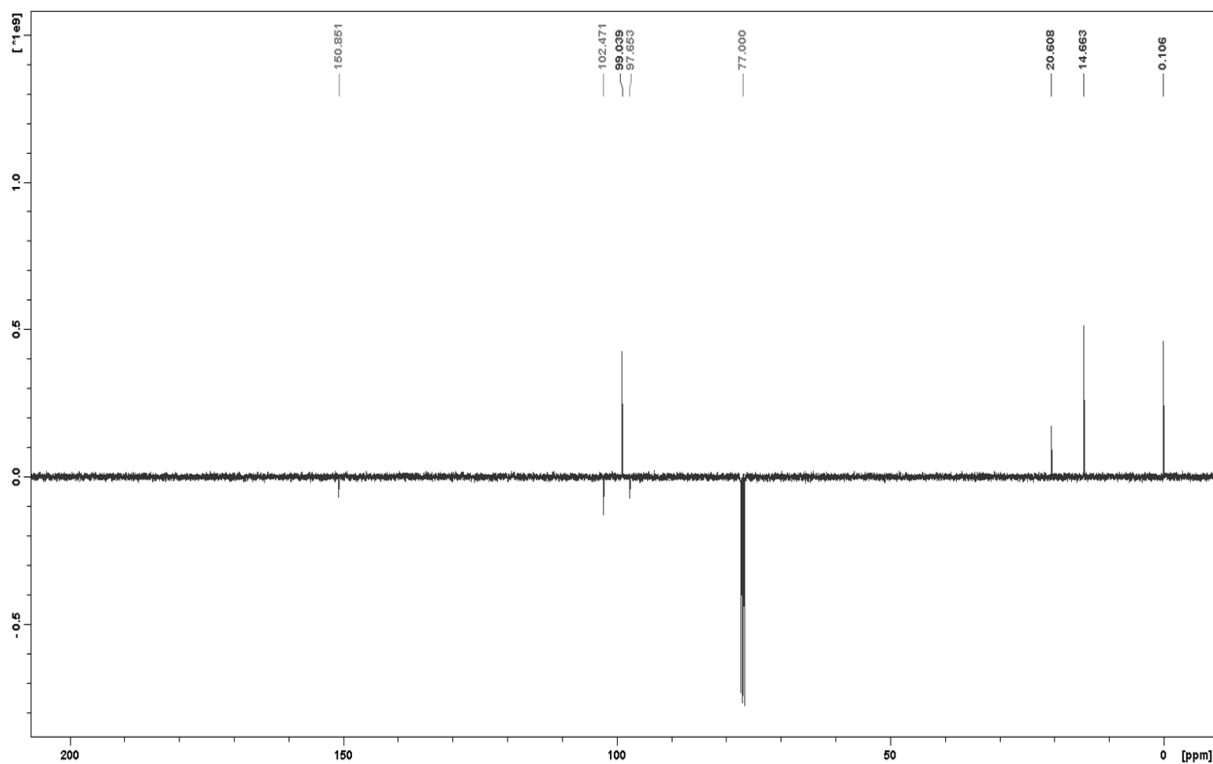
Spectrum 1.7. ^1H NMR (200 MHz, CDCl_3) of compound 3ca.



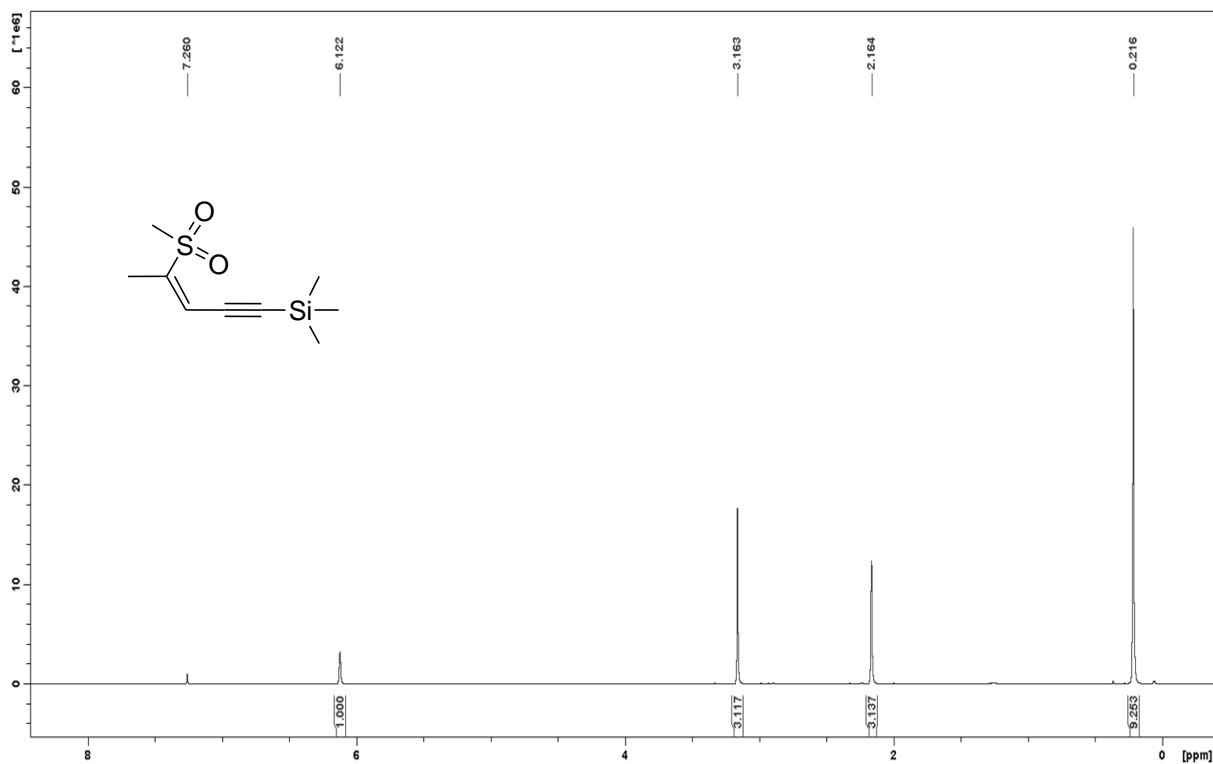
Spectrum 1.8. ^{13}C NMR (50 MHz, CDCl_3) of compound 3ca.



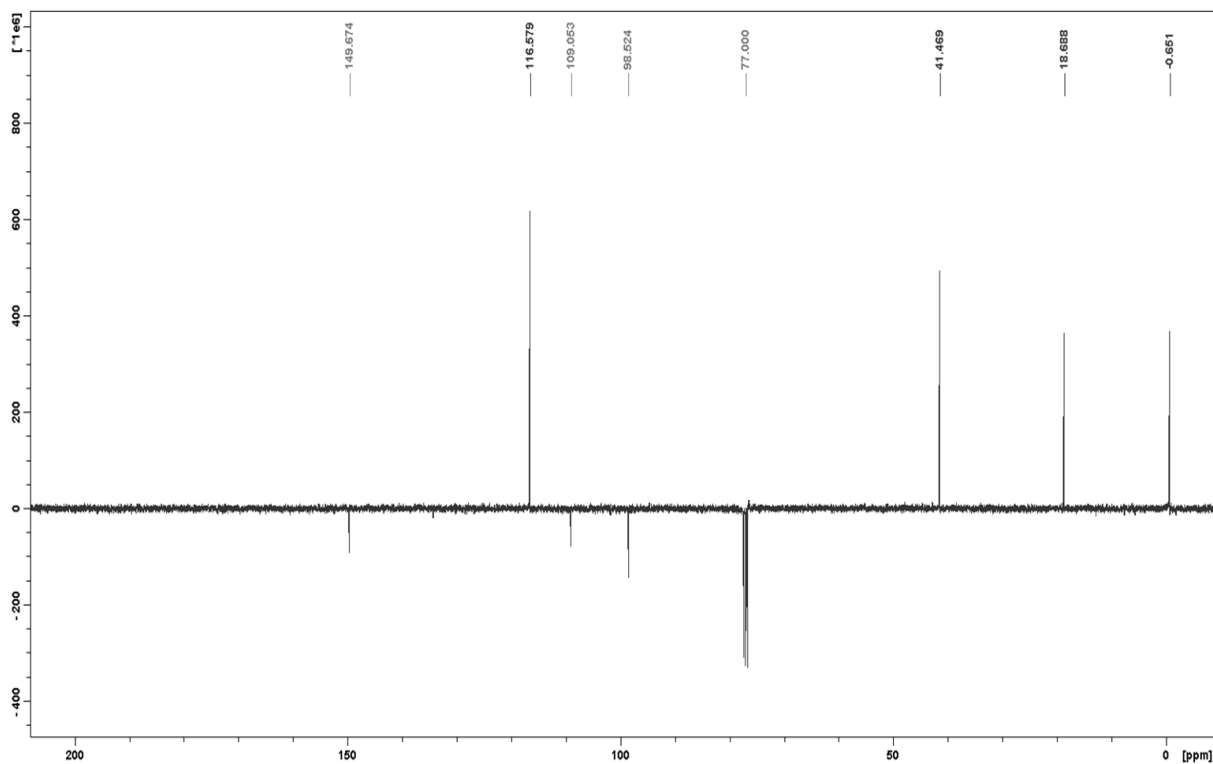
Spectrum 1.9. ^1H NMR (400 MHz, CDCl_3) of compound **10ba**.



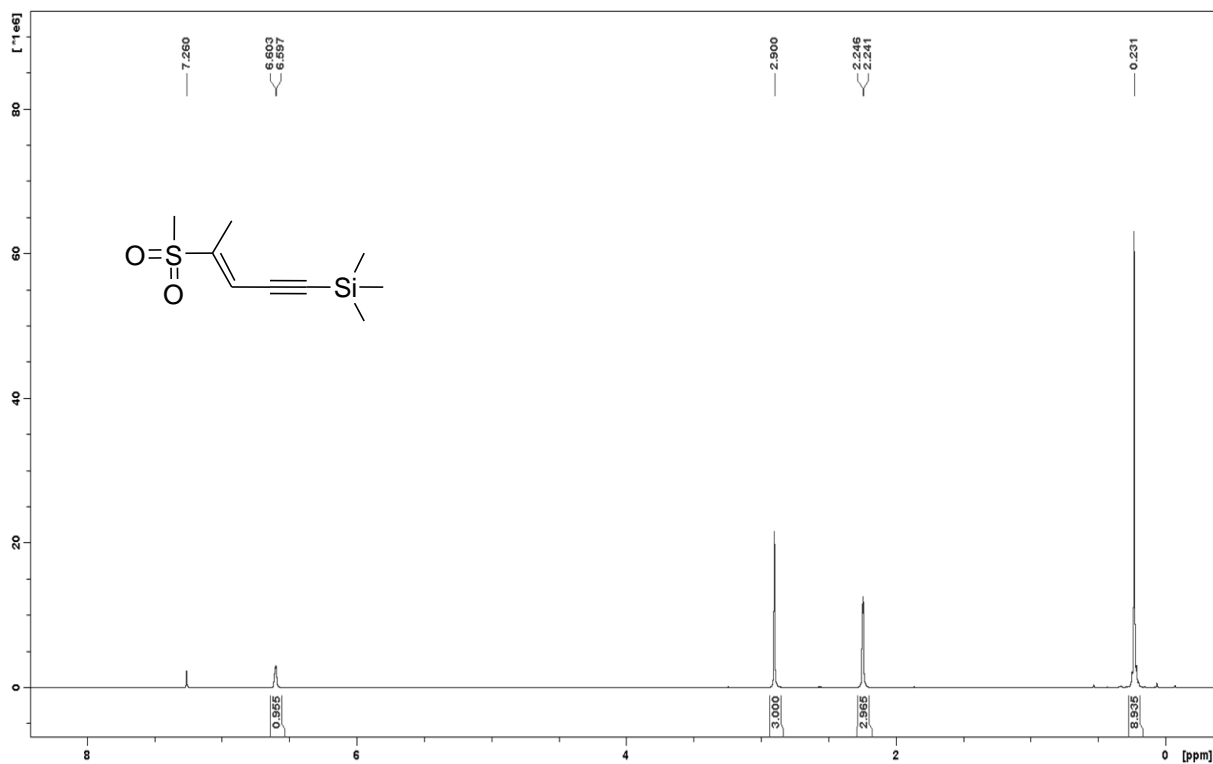
Spectrum 1.10. ^{13}C NMR (100 MHz, CDCl_3) of compound **10ba**.



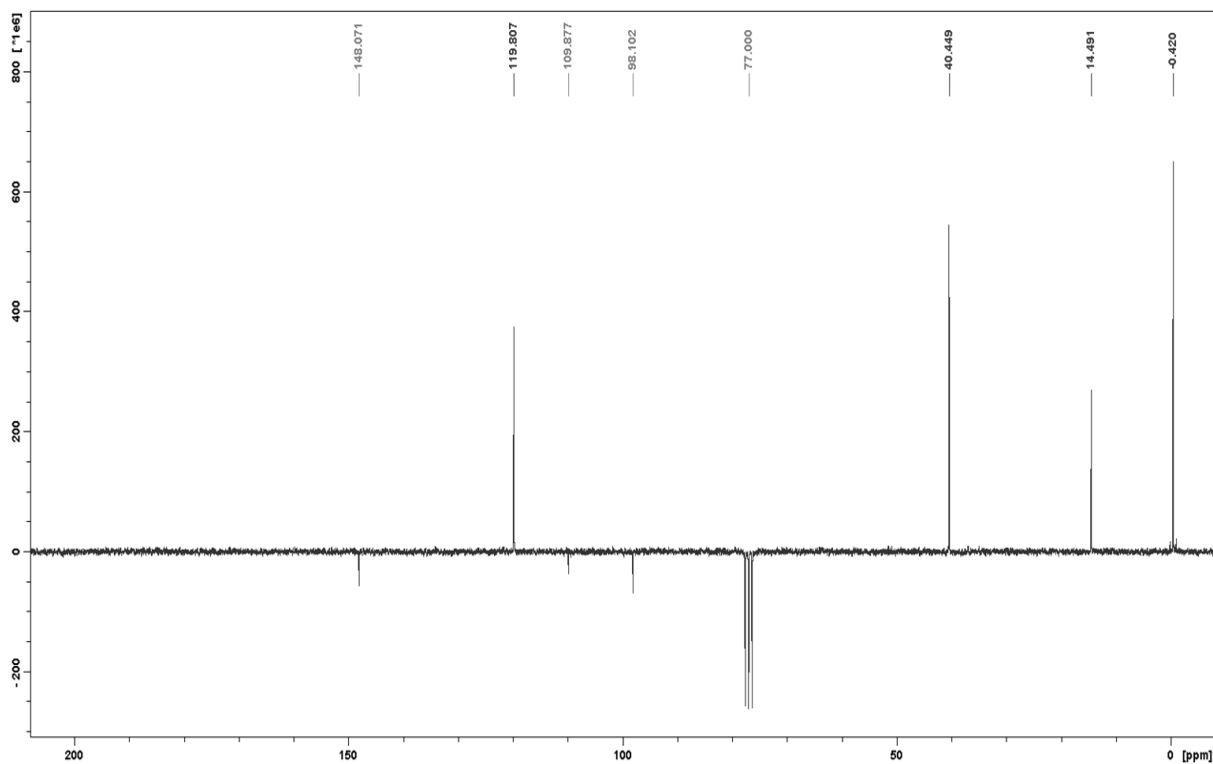
Spectrum 1.11. ^1H NMR (400 MHz, CDCl_3) of compound **8ba**.



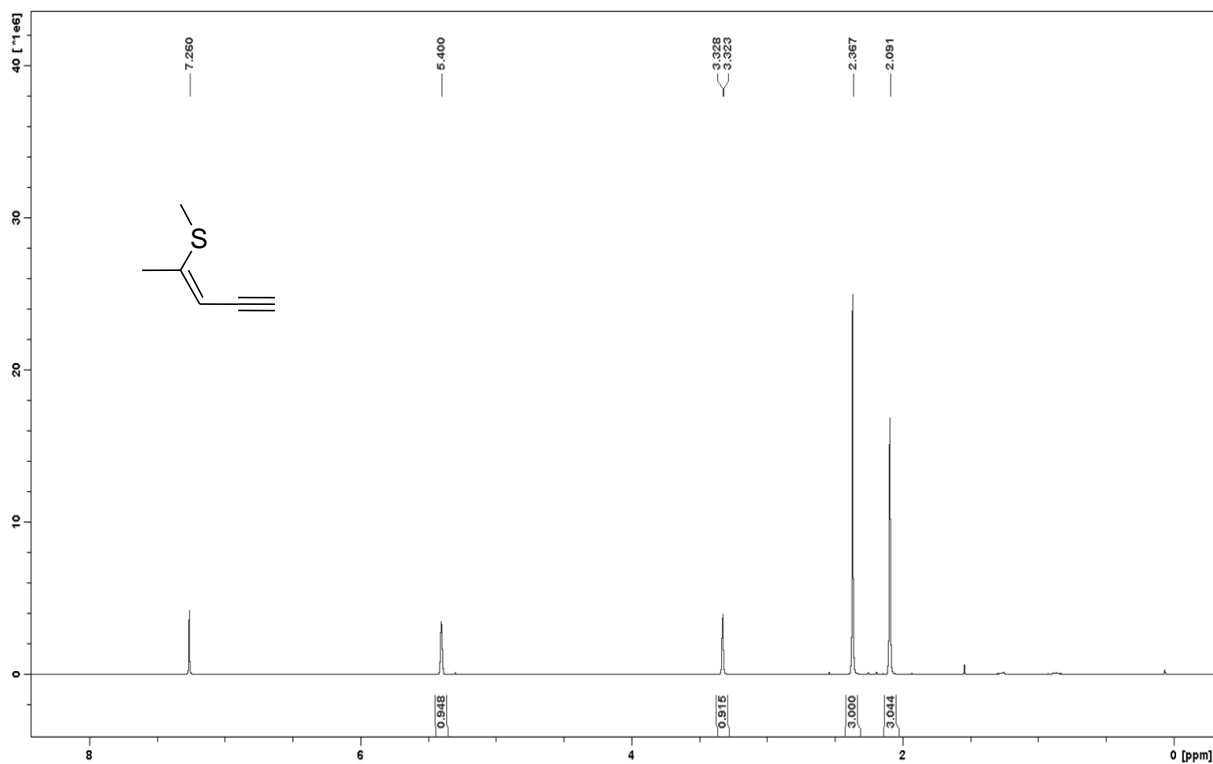
Spectrum 1.12. ^{13}C NMR (100 MHz, CDCl_3) of compound **8ba**.



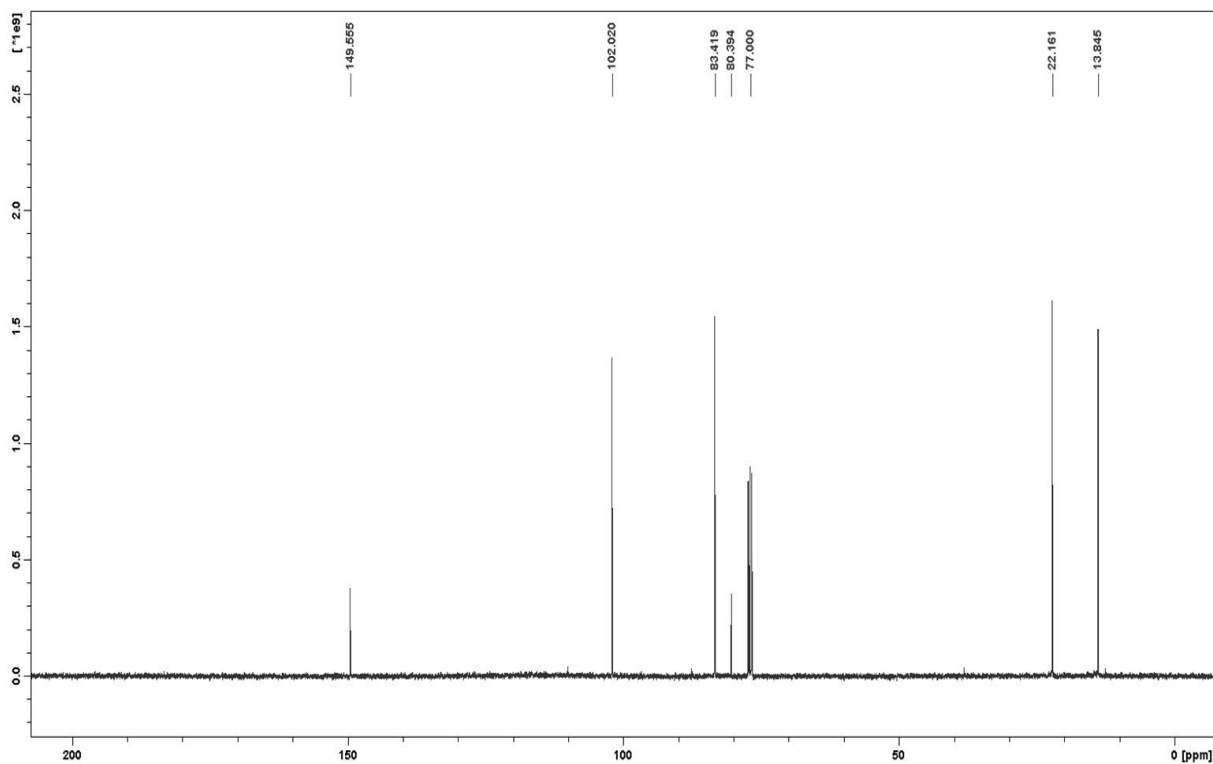
Spectrum 1.13. ¹H NMR (200 MHz, CDCl₃) of compound 11ba.



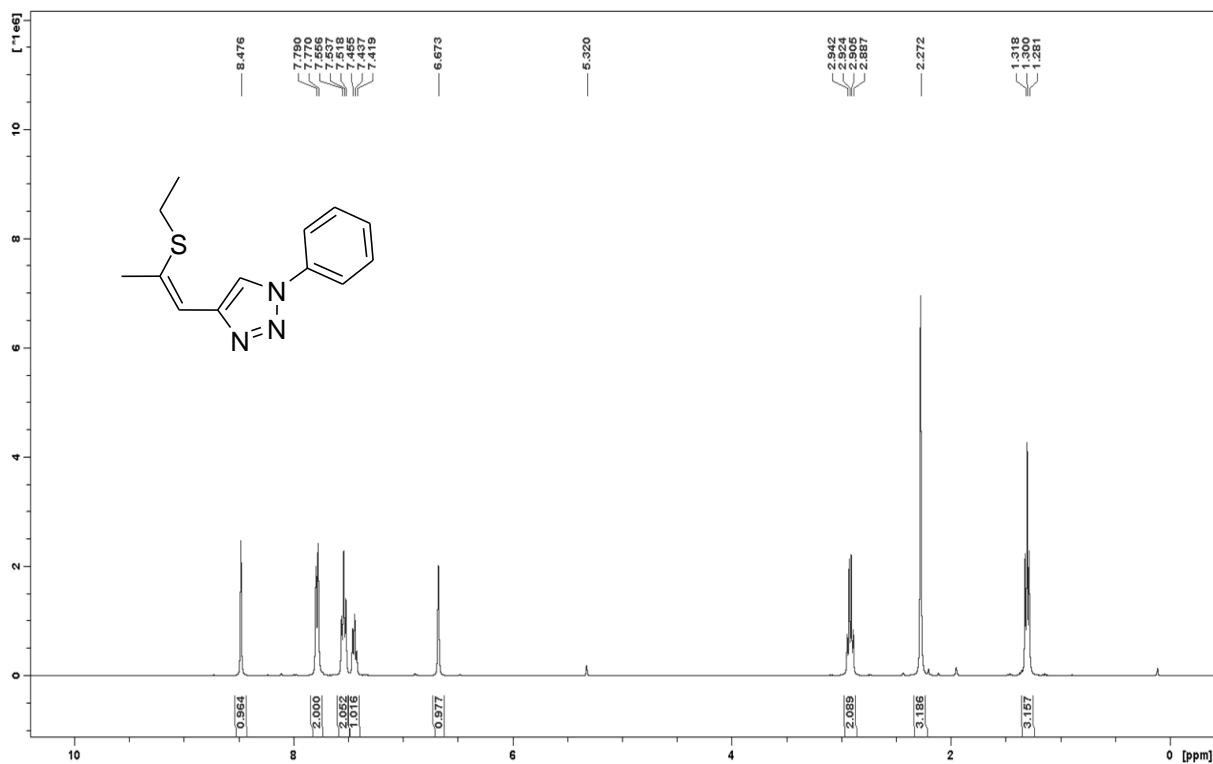
Spectrum 1.14. ¹³C NMR (50 MHz, CDCl₃) of compound 11ba.



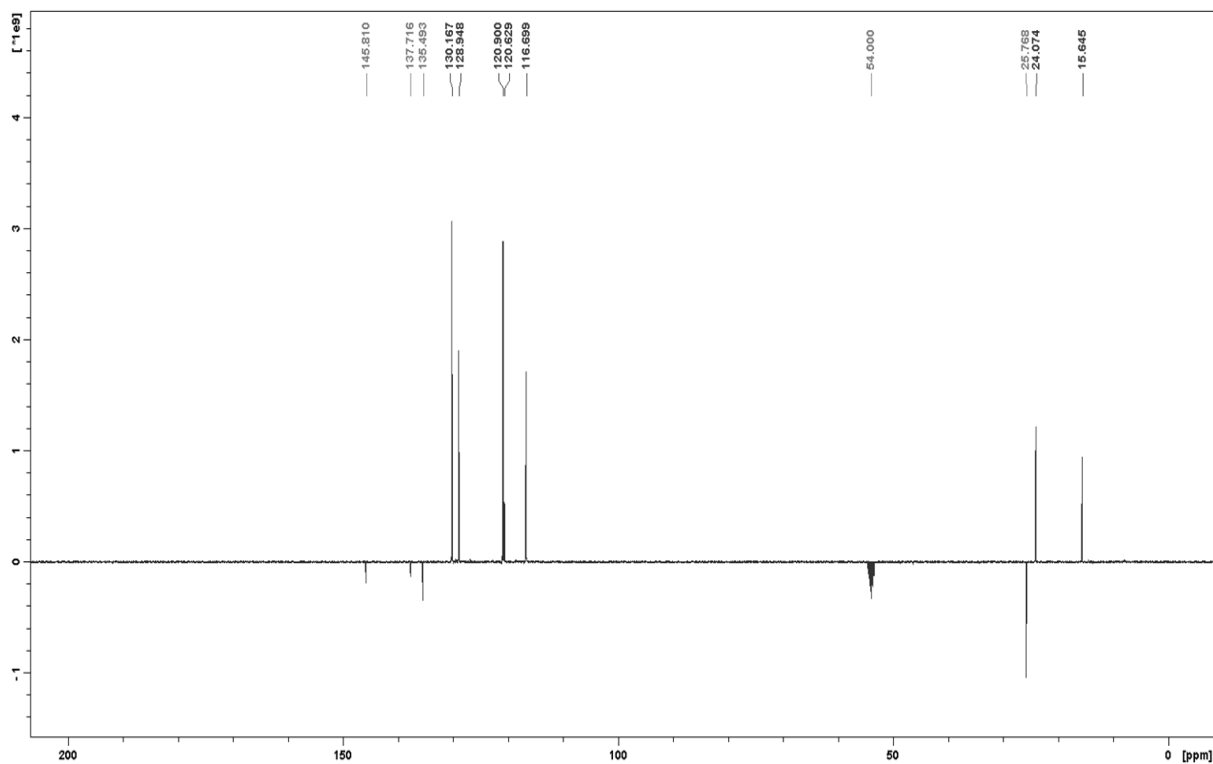
Spectrum 1.15. ^1H NMR (400 MHz, CDCl_3) of compound 6ba.



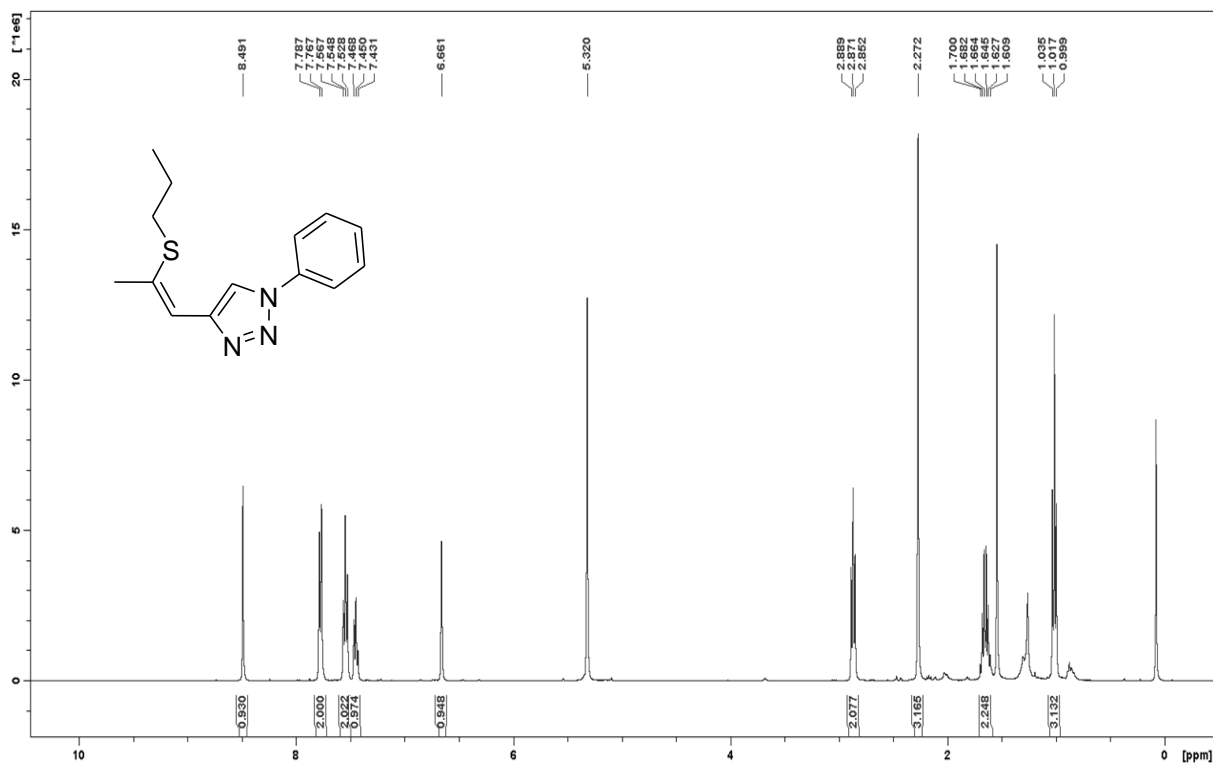
Spectrum 1.16. ^{13}C NMR (100 MHz, CDCl_3) of compound 6ba.



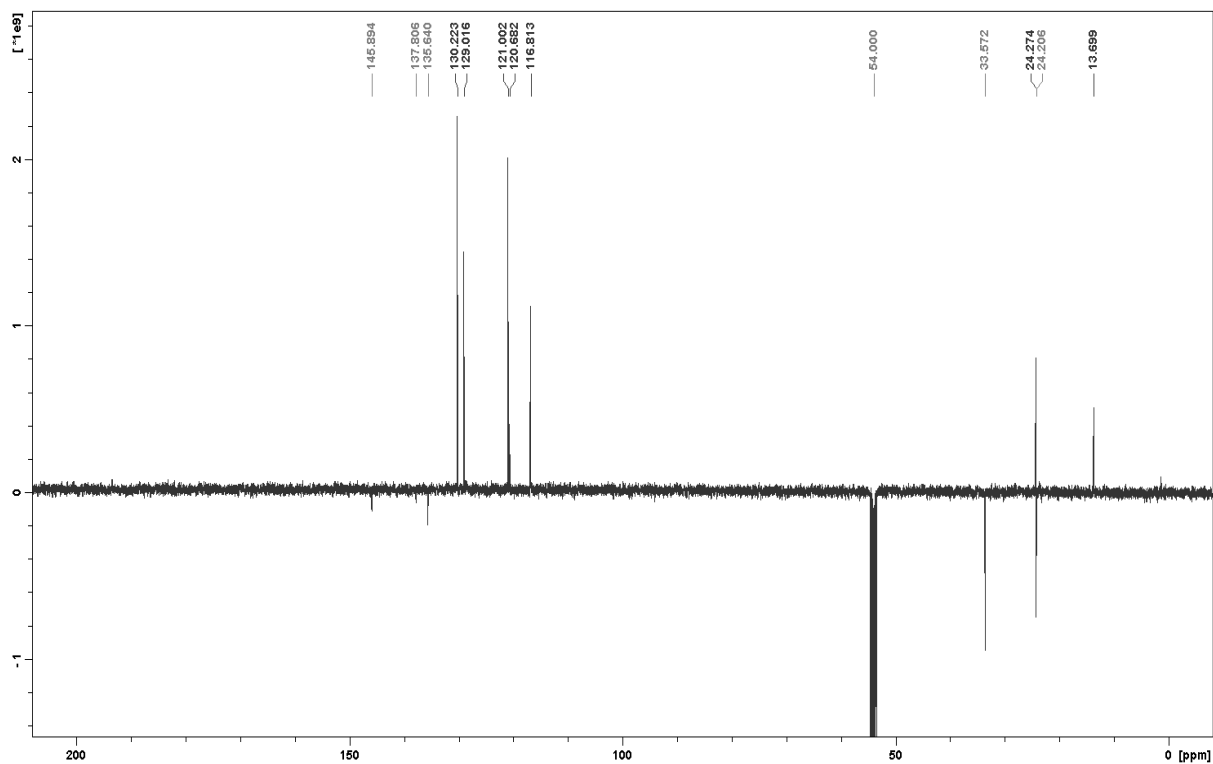
Spectrum 1.17. ^1H NMR (400 MHz, CD_2Cl_2) of compound **4bb**.



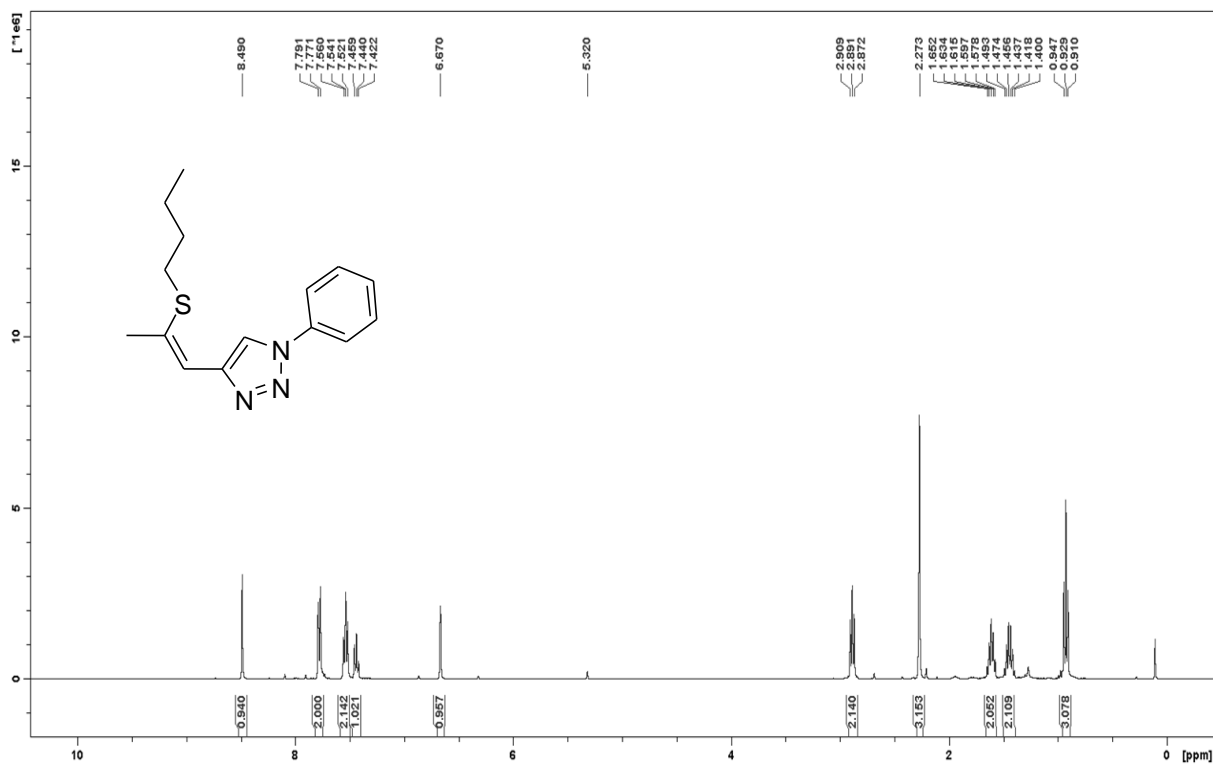
Spectrum 1.18. ^{13}C NMR (100 MHz, CD_2Cl_2) of compound **4bb**.



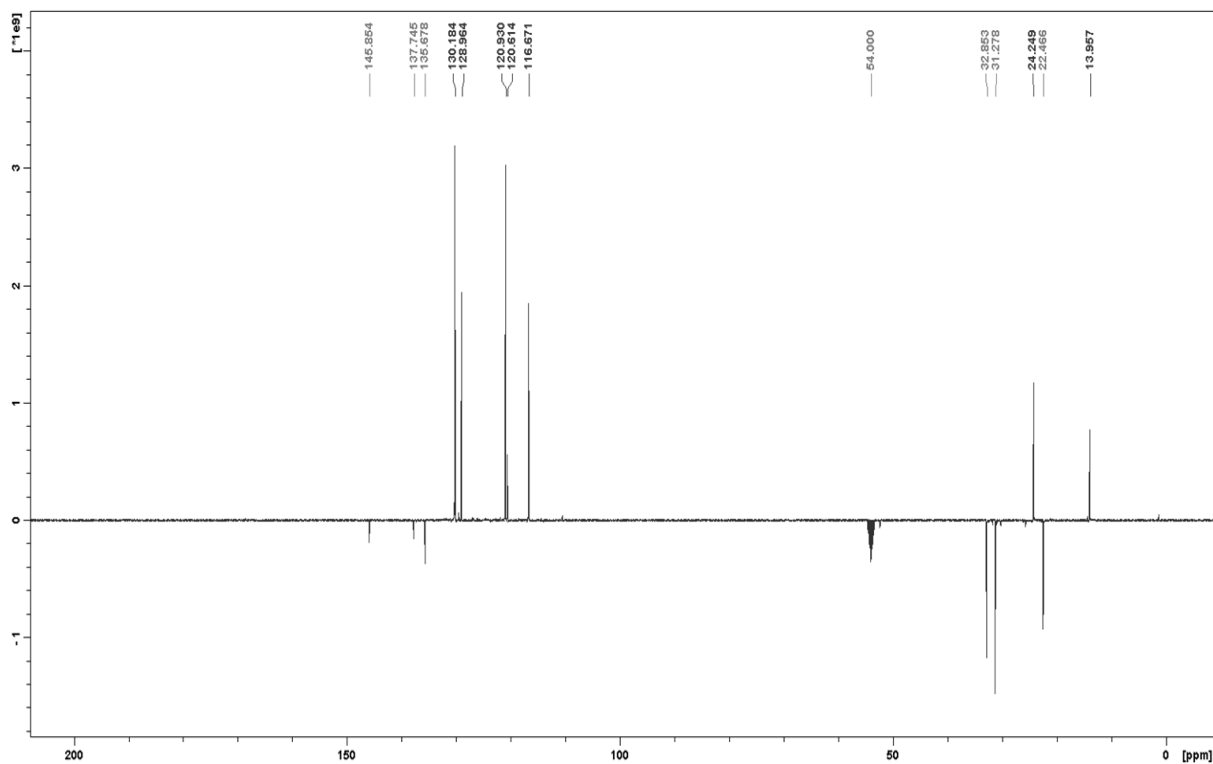
Spectrum 1.19. ^1H NMR (400 MHz, CD_2Cl_2) of compound **4bc**.



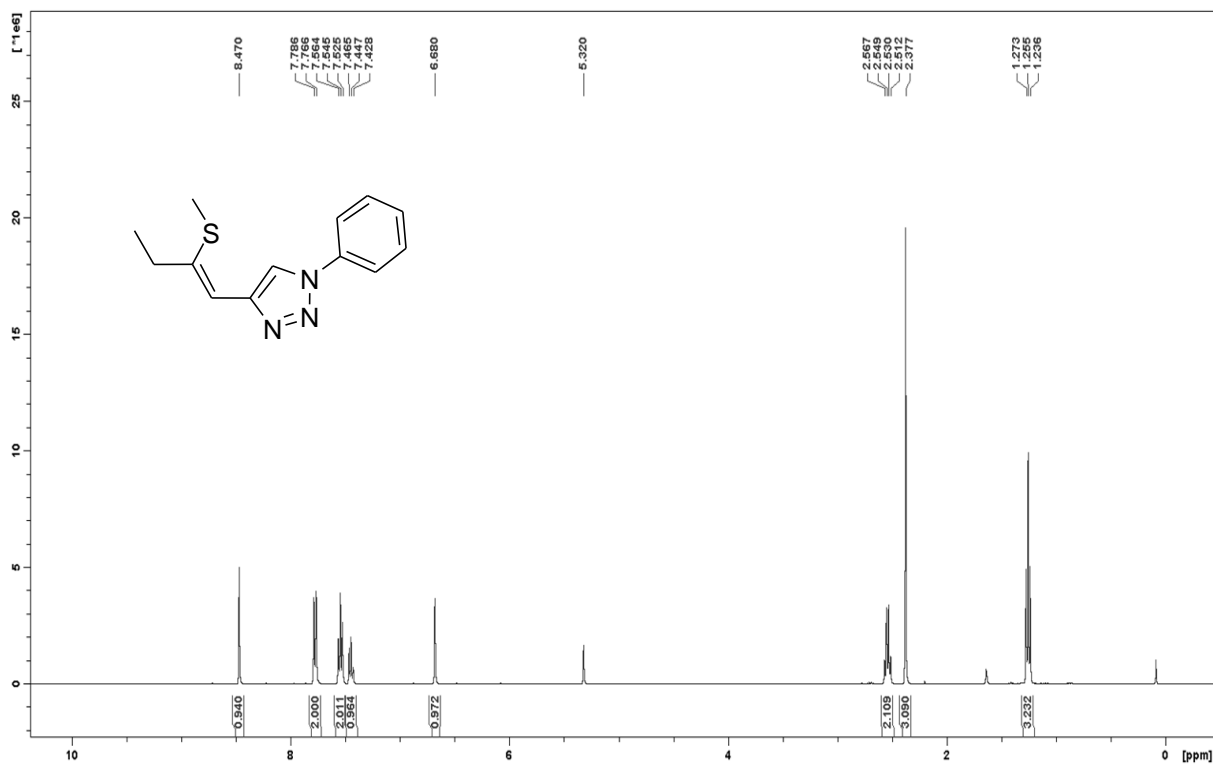
Spectrum 1.20. ^{13}C NMR (100 MHz, CD_2Cl_2) of compound **4bc**.



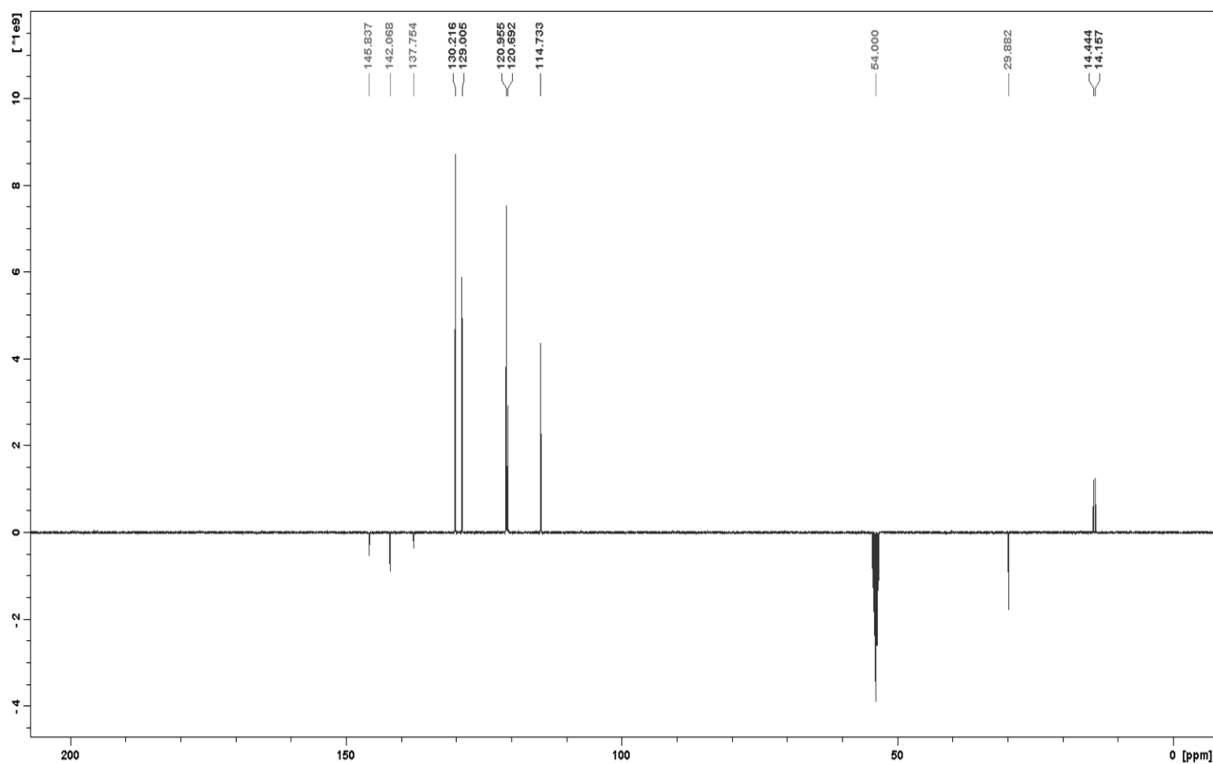
Spectrum 1.21. ^1H NMR (400 MHz, CD_2Cl_2) of compound 4bd.



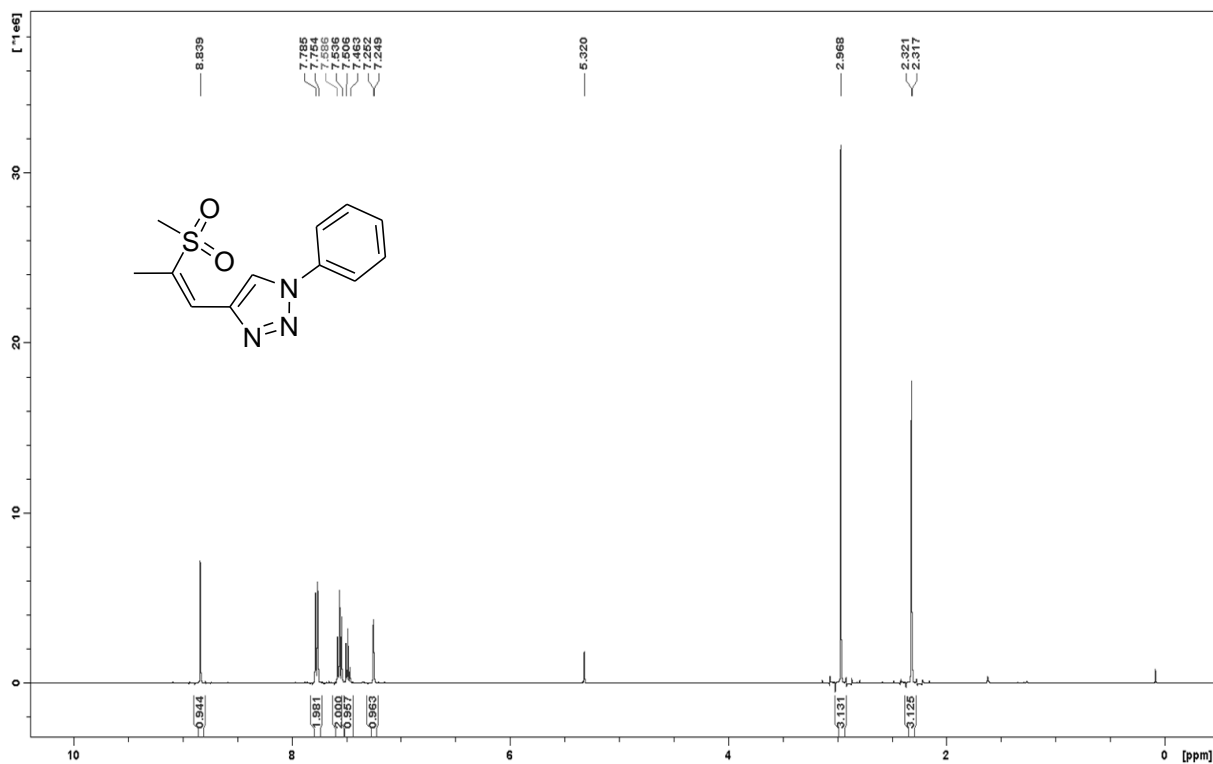
Spectrum 1.22. ^{13}C NMR (100 MHz, CD_2Cl_2) of compound 4bd.



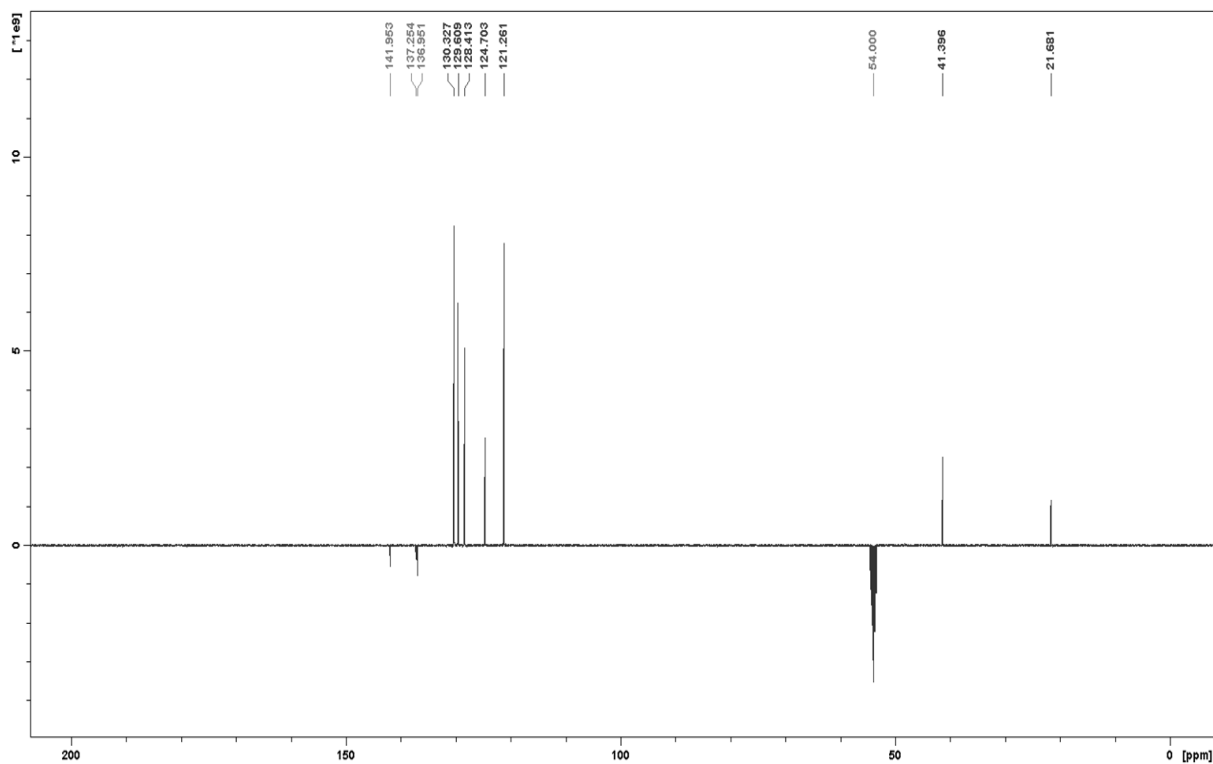
Spectrum 1.23. ^1H NMR (400 MHz, CD_2Cl_2) of compound 4ca.



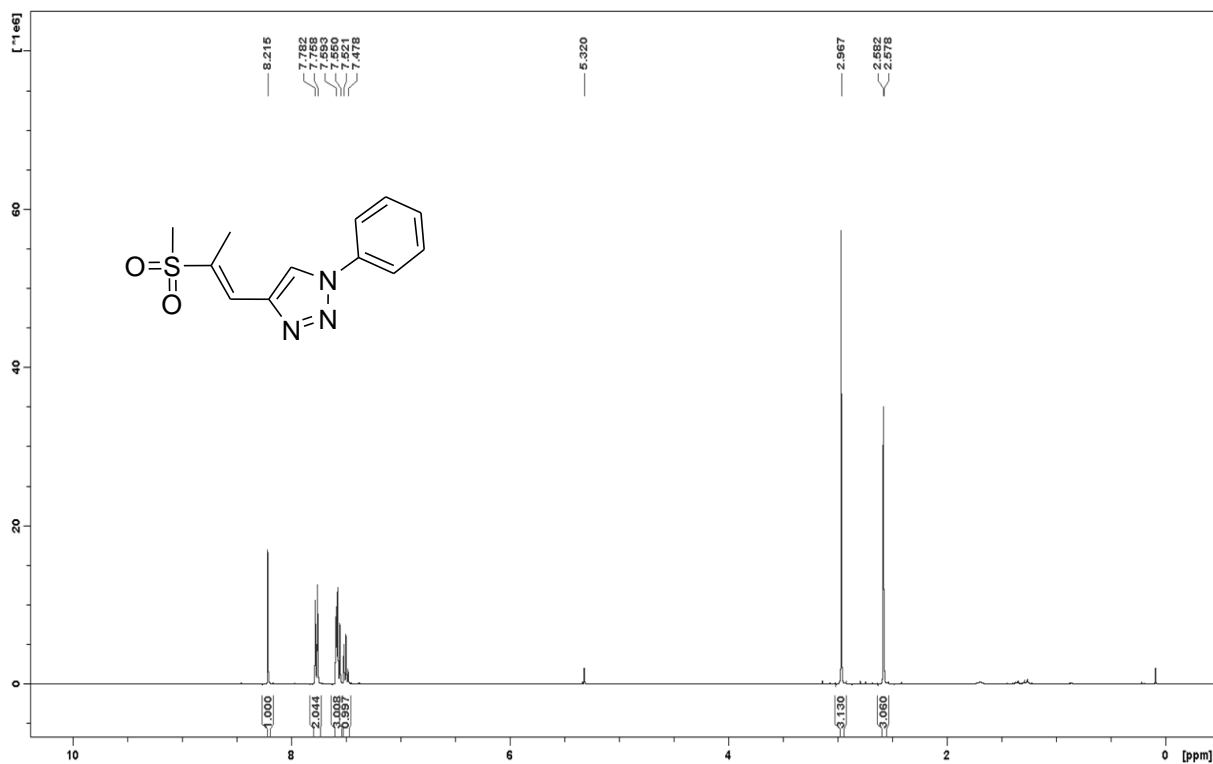
Spectrum 1.24. ^{13}C NMR (100 MHz, CD_2Cl_2) of compound 4ca.



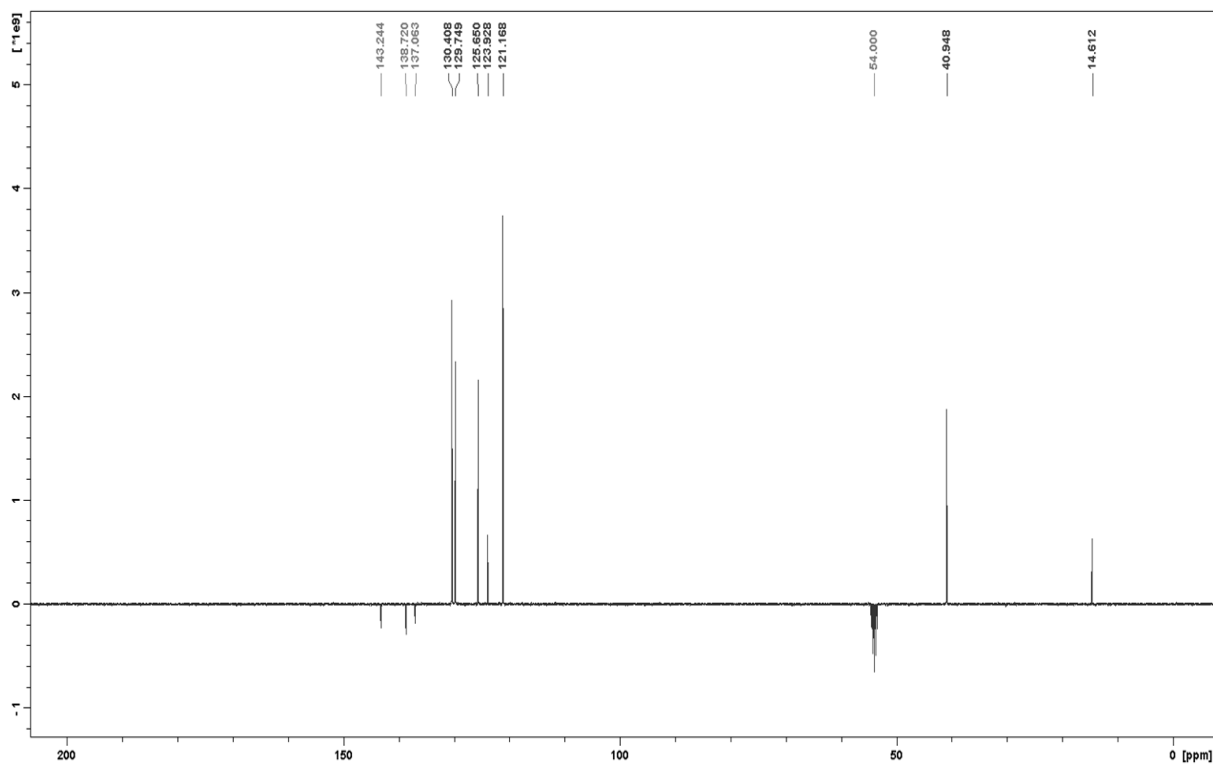
Spectrum 1.25. ^1H NMR (400 MHz, CD_2Cl_2) of compound 9ba.



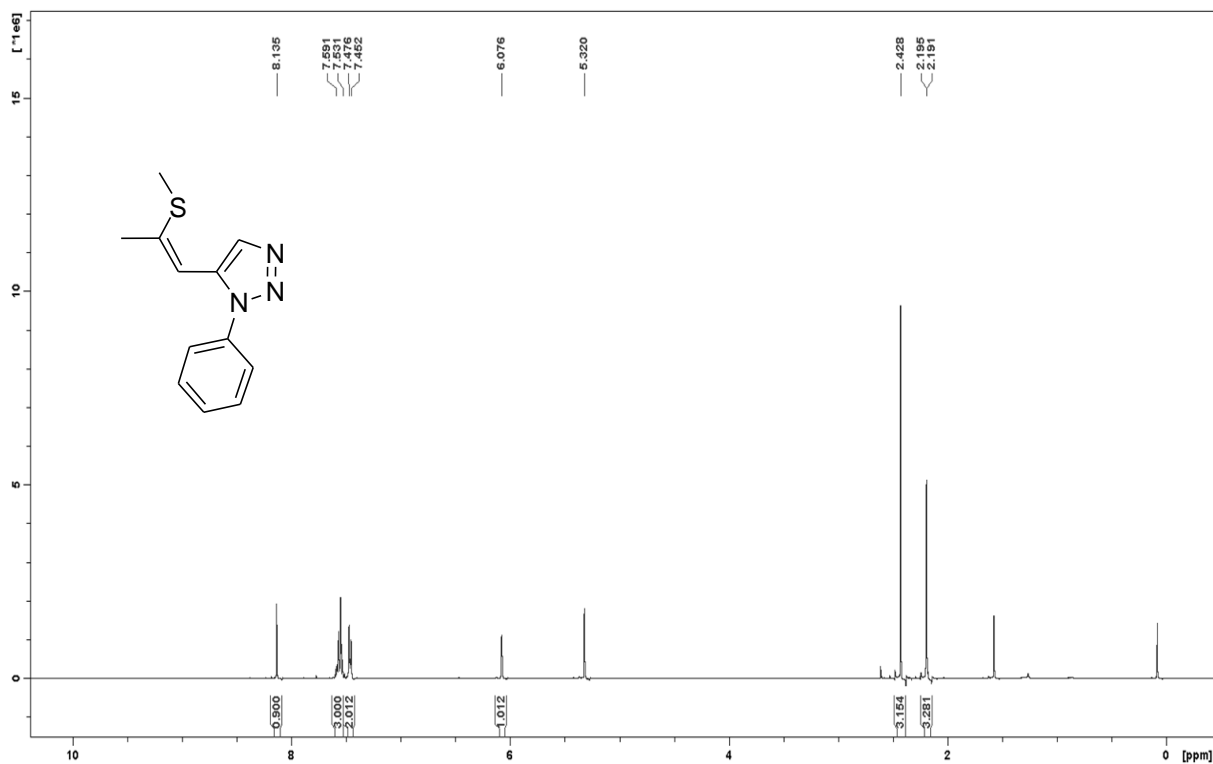
Spectrum 1.26. ^{13}C NMR (100 MHz, CD_2Cl_2) of compound 9ba.



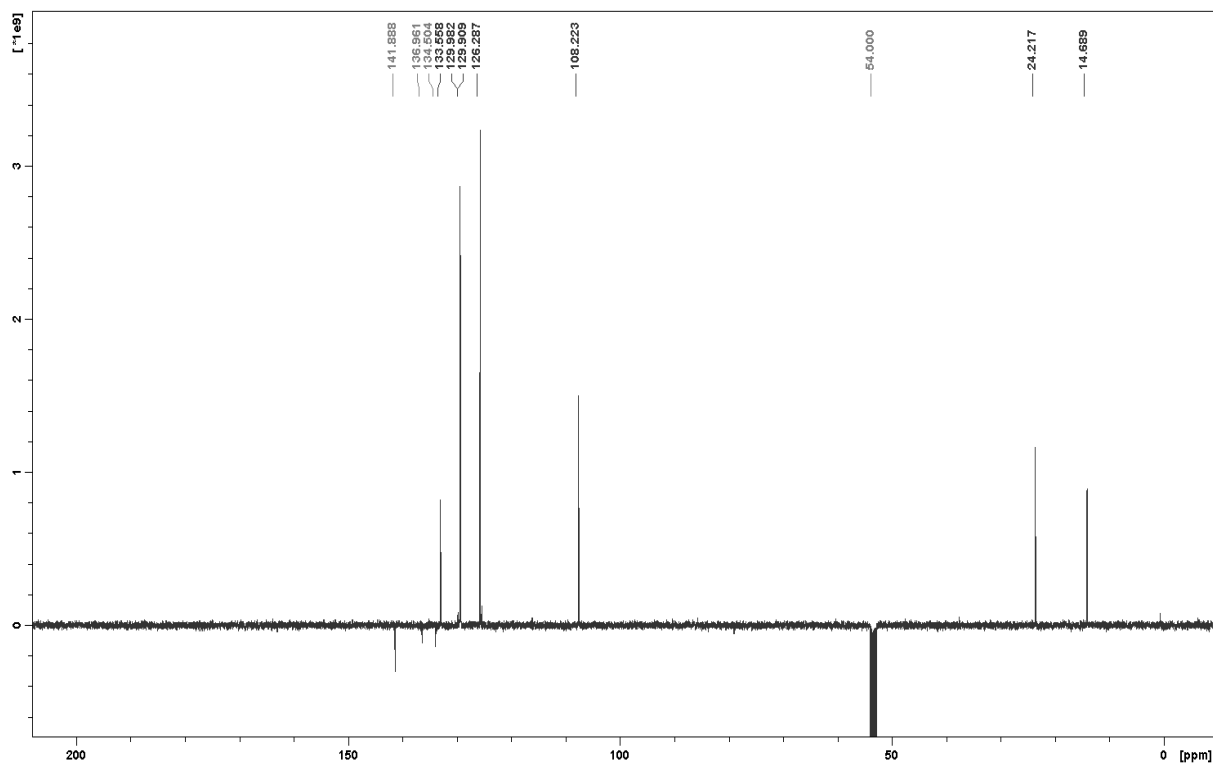
Spectrum 1.27. ^1H NMR (400 MHz, CD_2Cl_2) of compound 12ba.



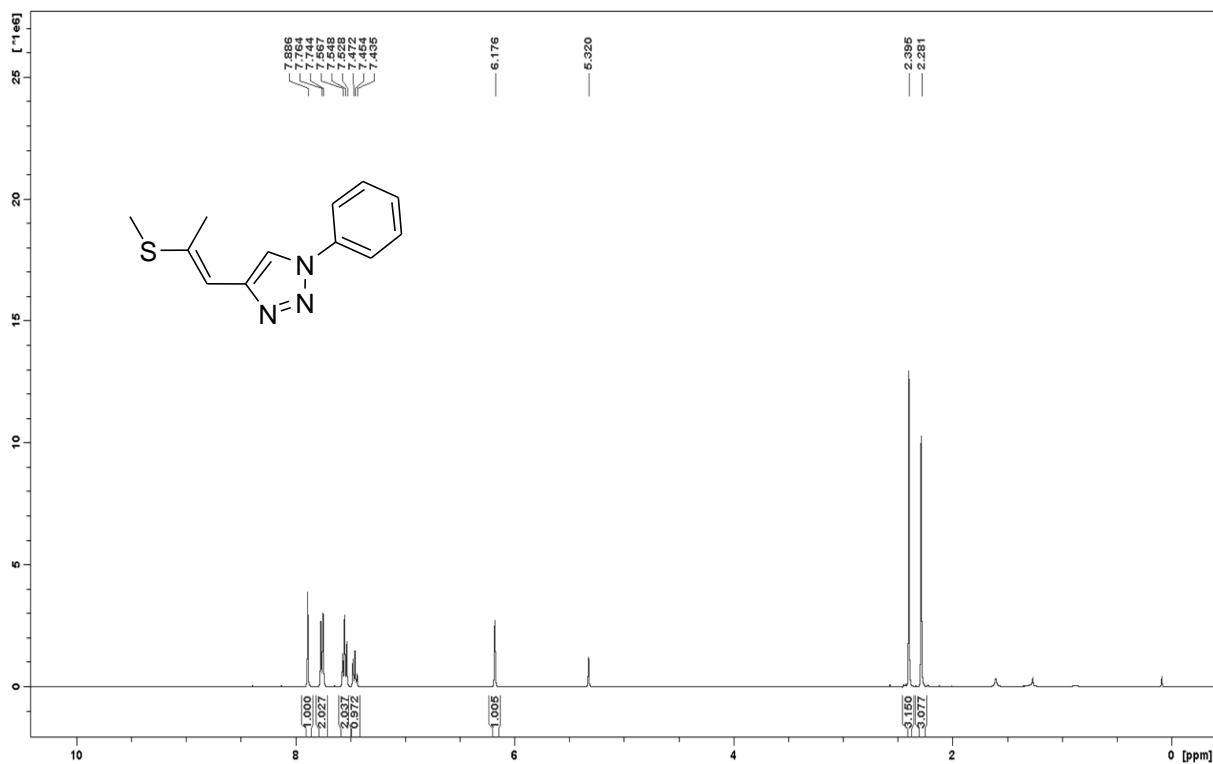
Spectrum 1.28. ^{13}C NMR (100 MHz, CD_2Cl_2) of compound 12ba.



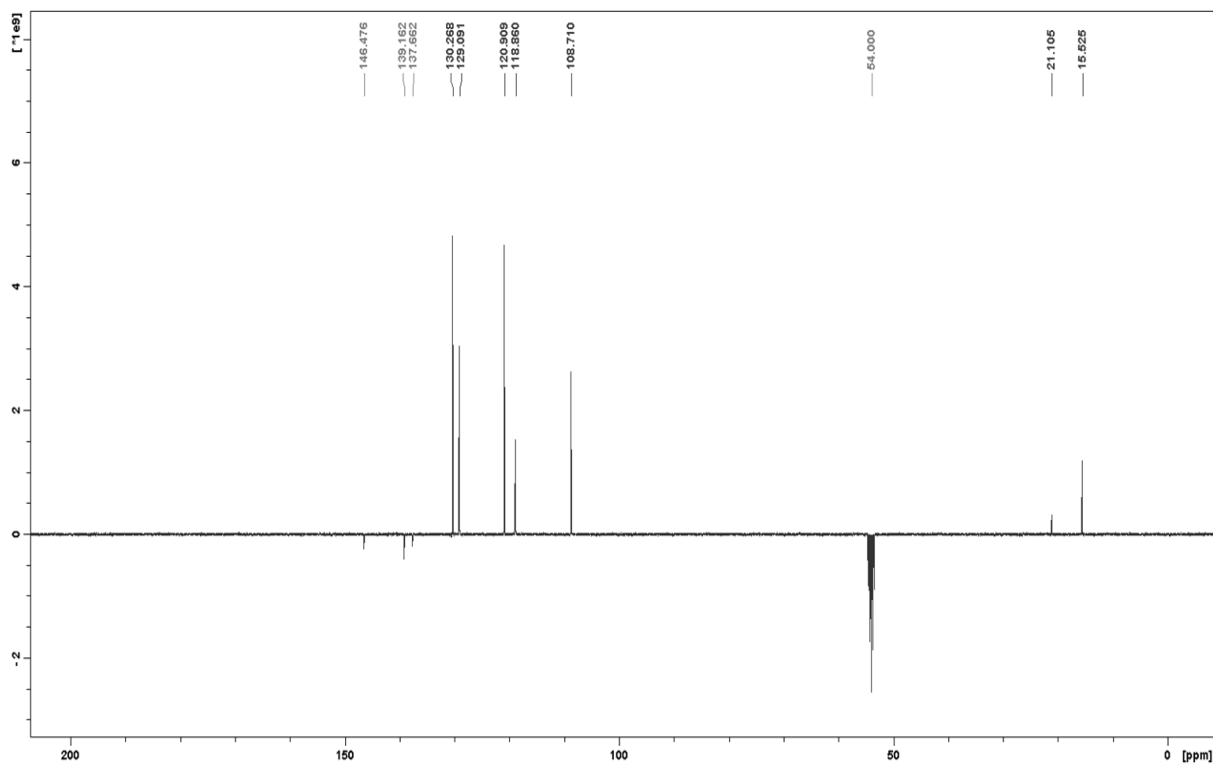
Spectrum 1.29. ^1H NMR (400 MHz, CD_2Cl_2) of compound 7ba.



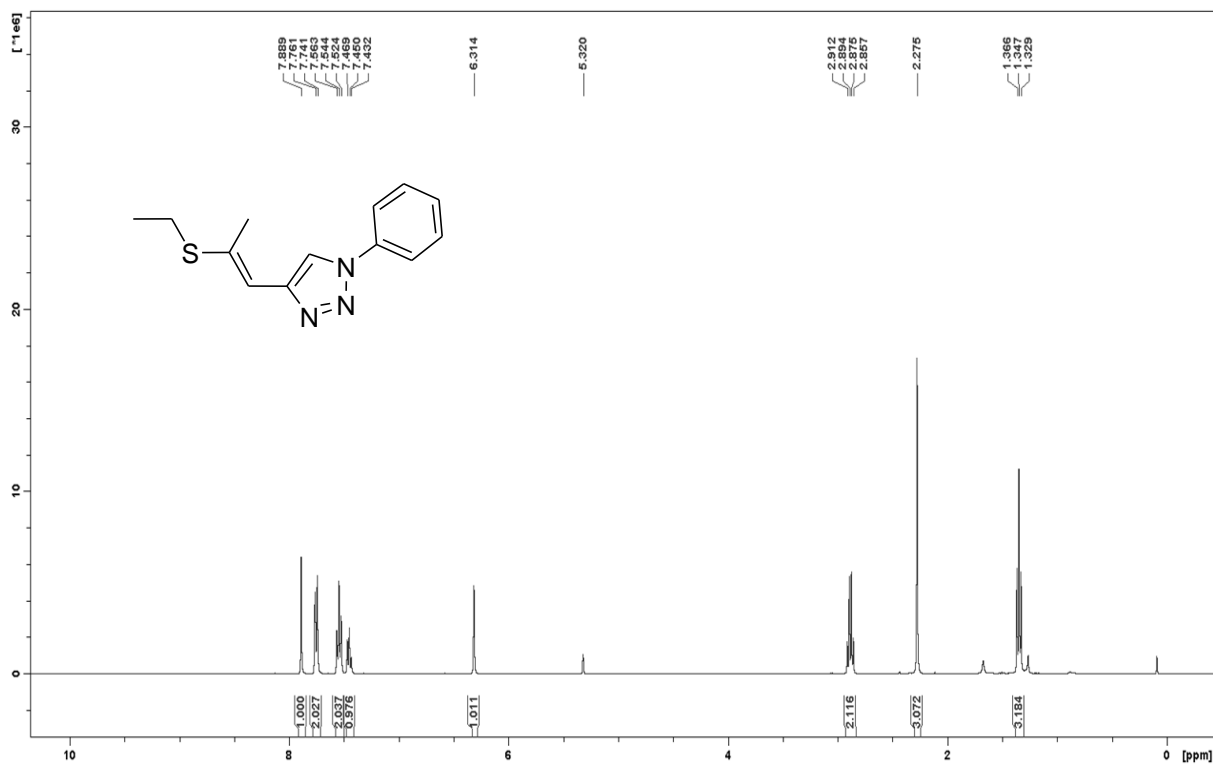
Spectrum 1.30. ^{13}C NMR (100 MHz, CD_2Cl_2) of compound 7ba.



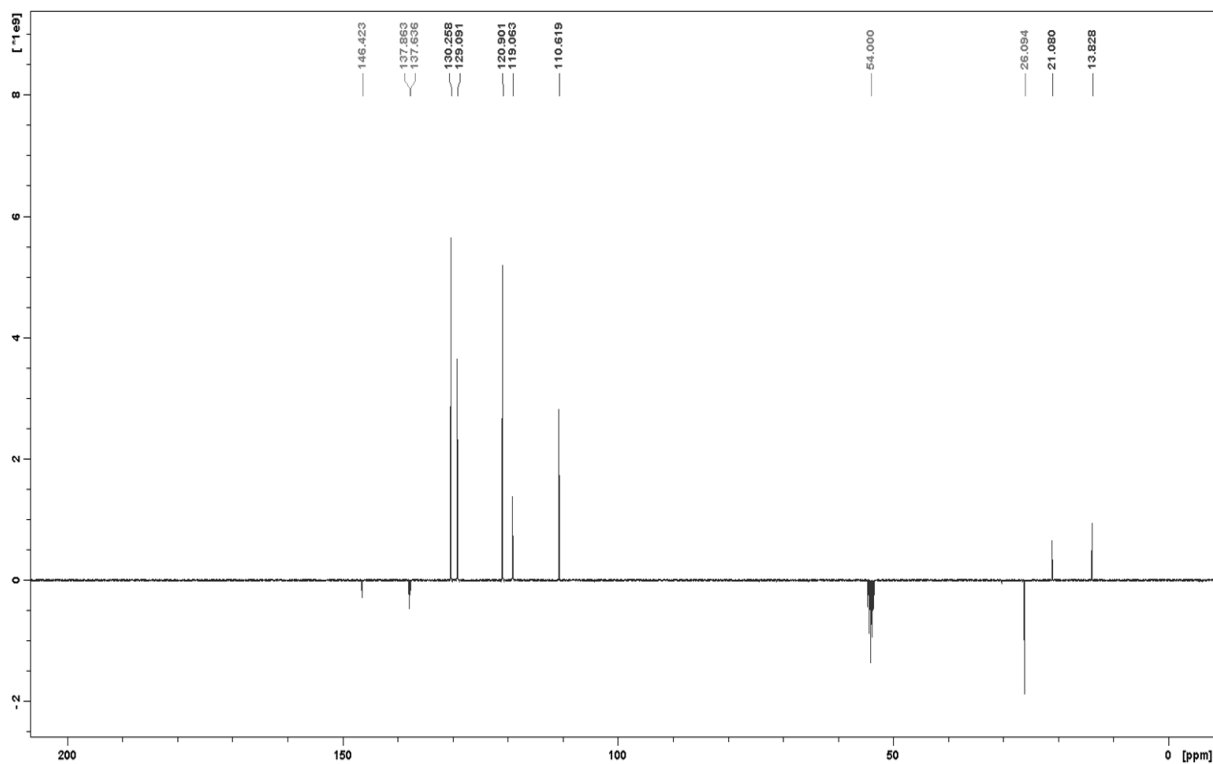
Spectrum 1.31. ^1H NMR (400 MHz, CD_2Cl_2) of compound 5ba.



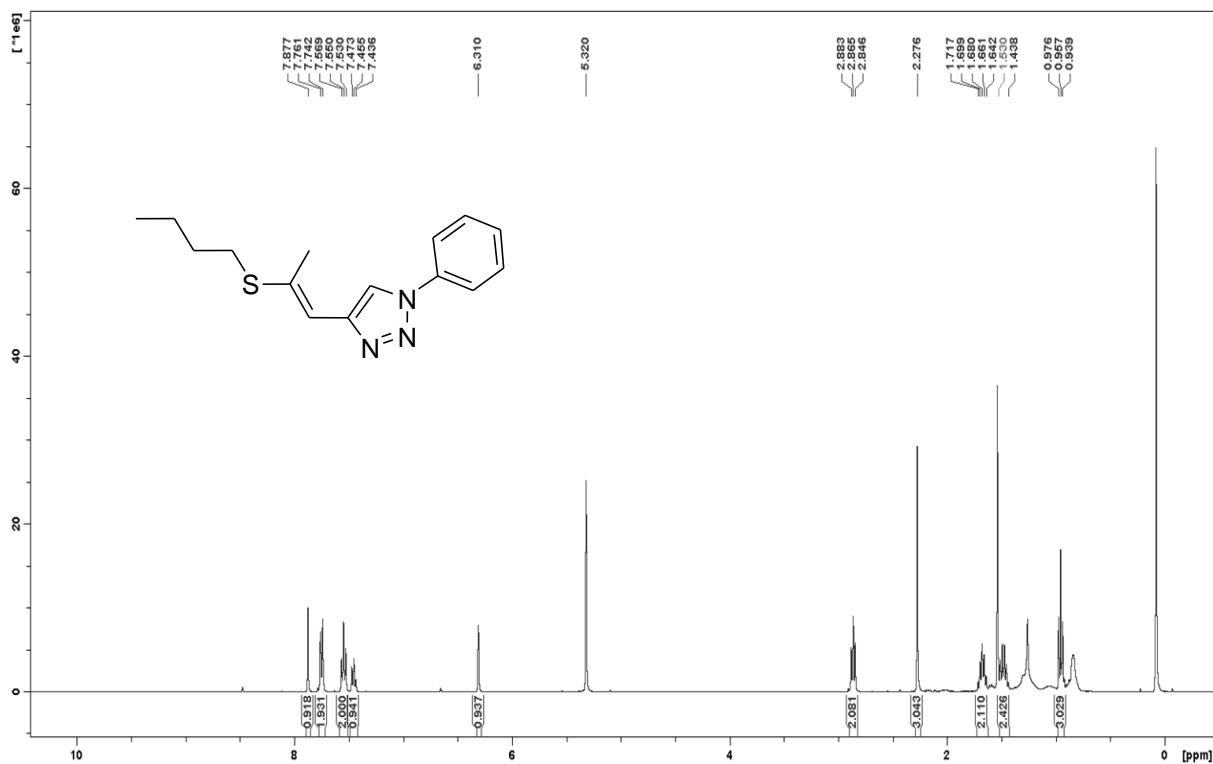
Spectrum 1.32. ^{13}C NMR (100 MHz, CD_2Cl_2) of compound 5ba.



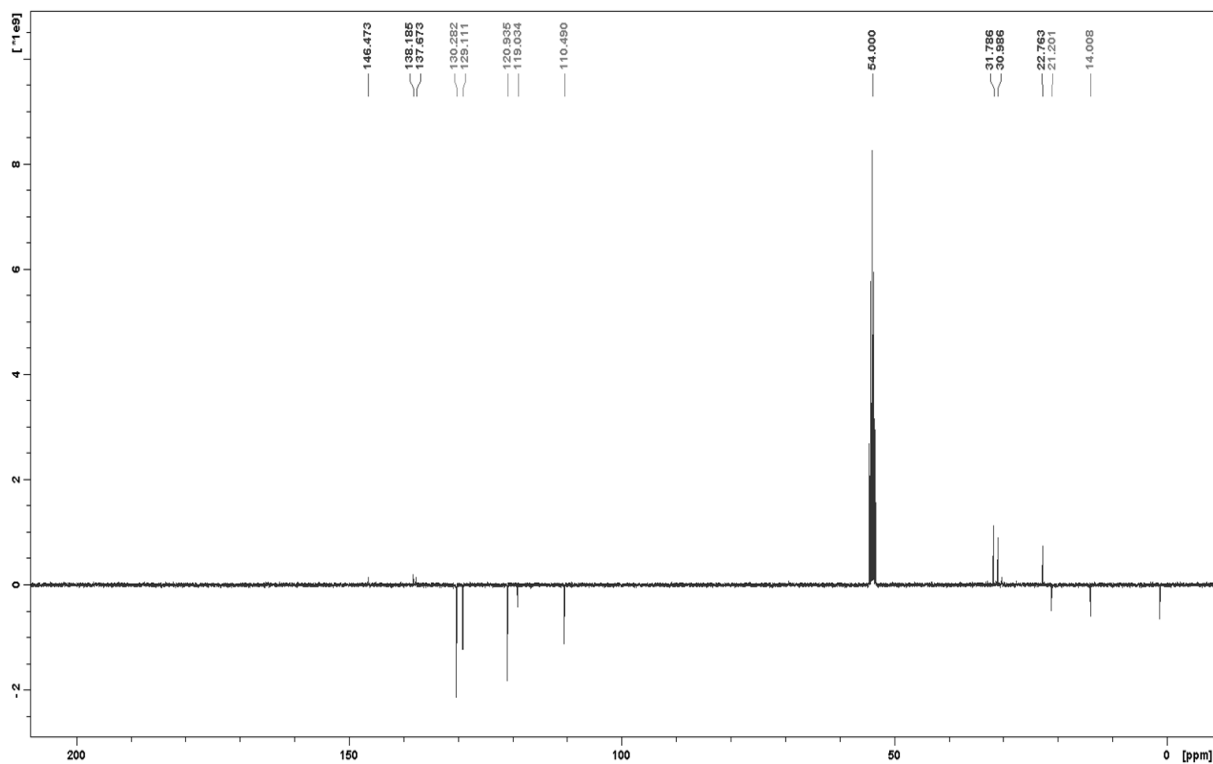
Spectrum 1.33. ^1H NMR (400 MHz, CD_2Cl_2) of compound 5bb.



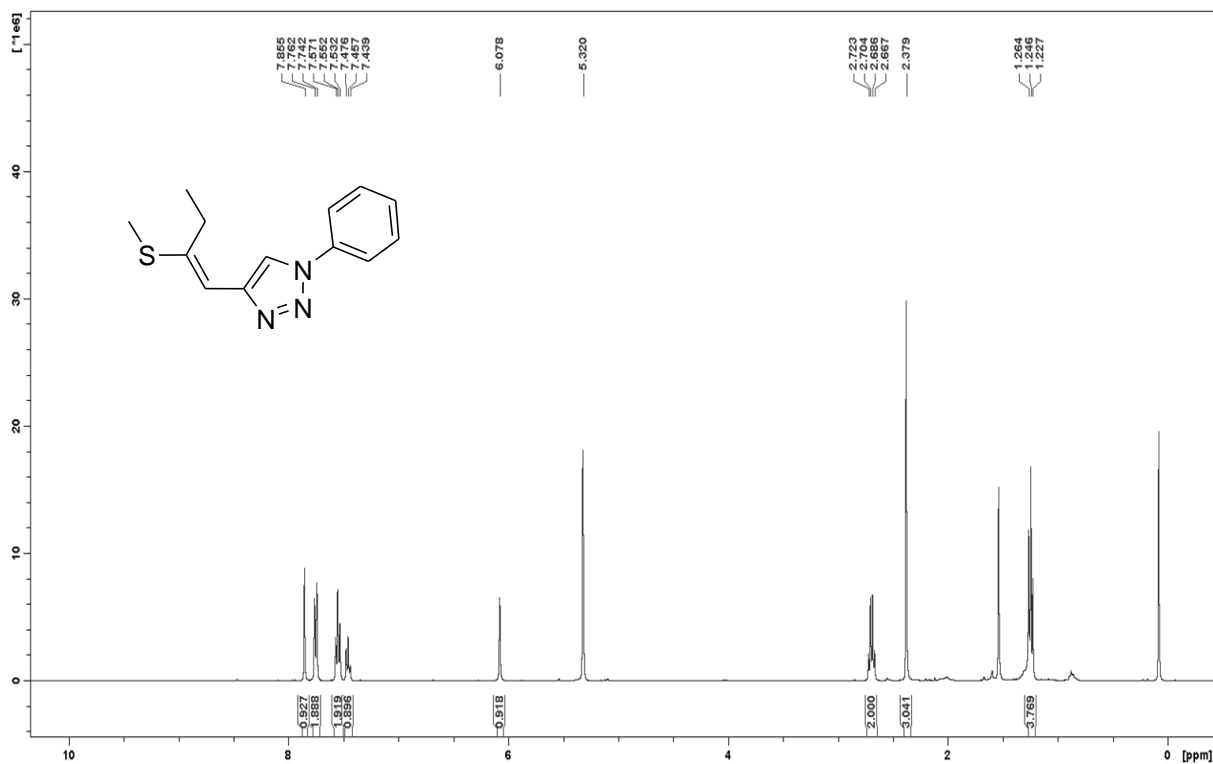
Spectrum 1.34. ^{13}C NMR (100 MHz, CD_2Cl_2) of compound 5bb.



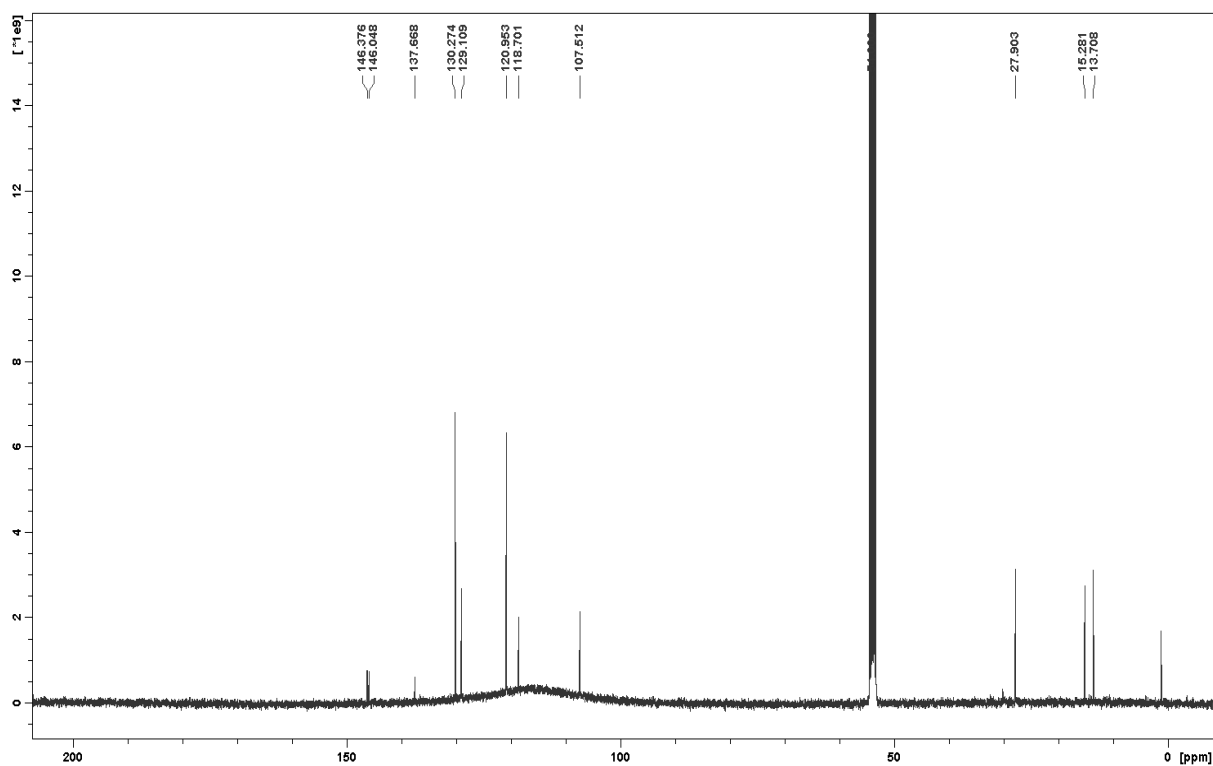
Spectrum 1.35. ^1H NMR (400 MHz, CD_2Cl_2) of compound 5bd.



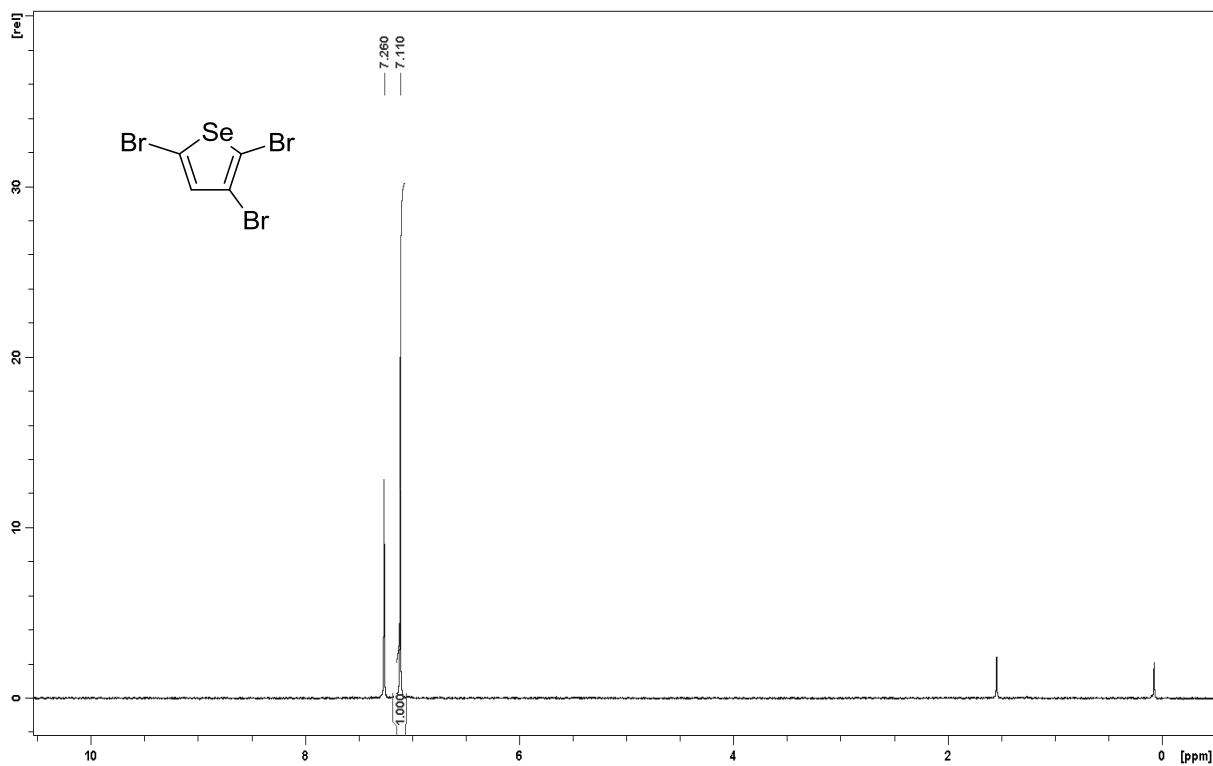
Spectrum 1.36. ^{13}C NMR (100 MHz, CD_2Cl_2) of compound 5bd.



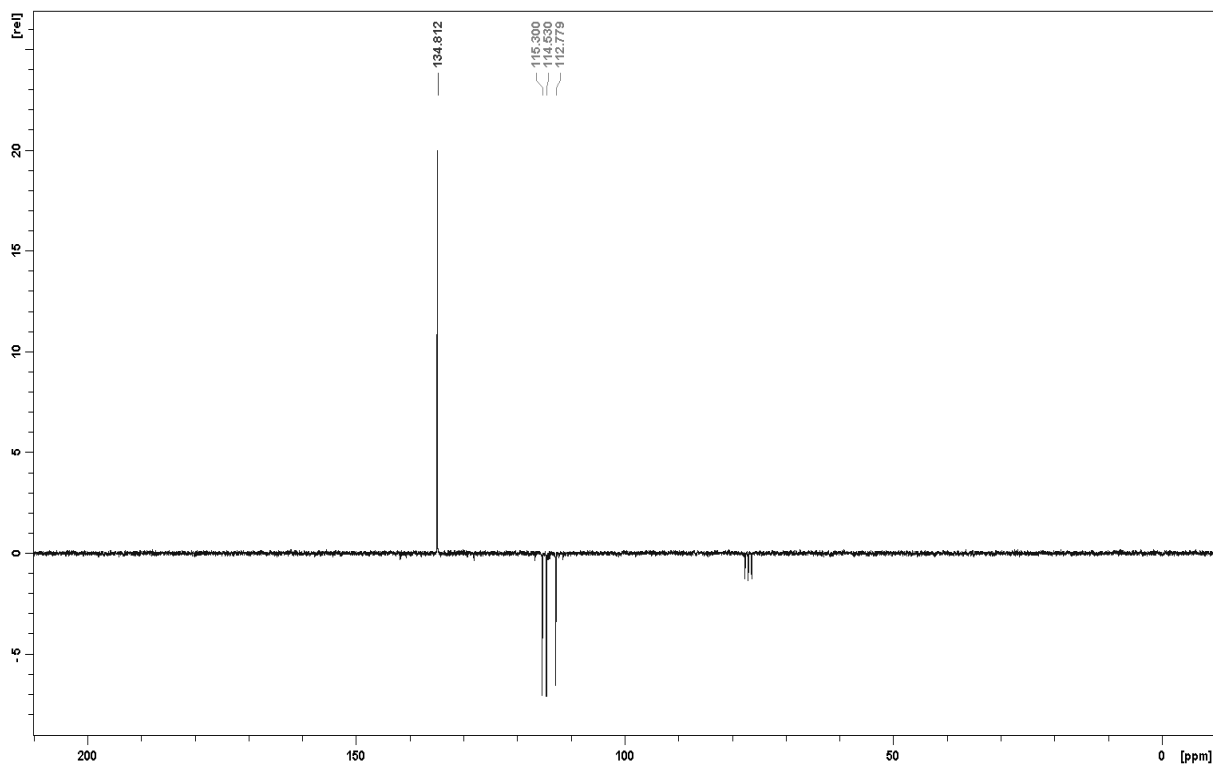
Spectrum 1.37. ^1H NMR (400 MHz, CD_2Cl_2) of compound 5ca.



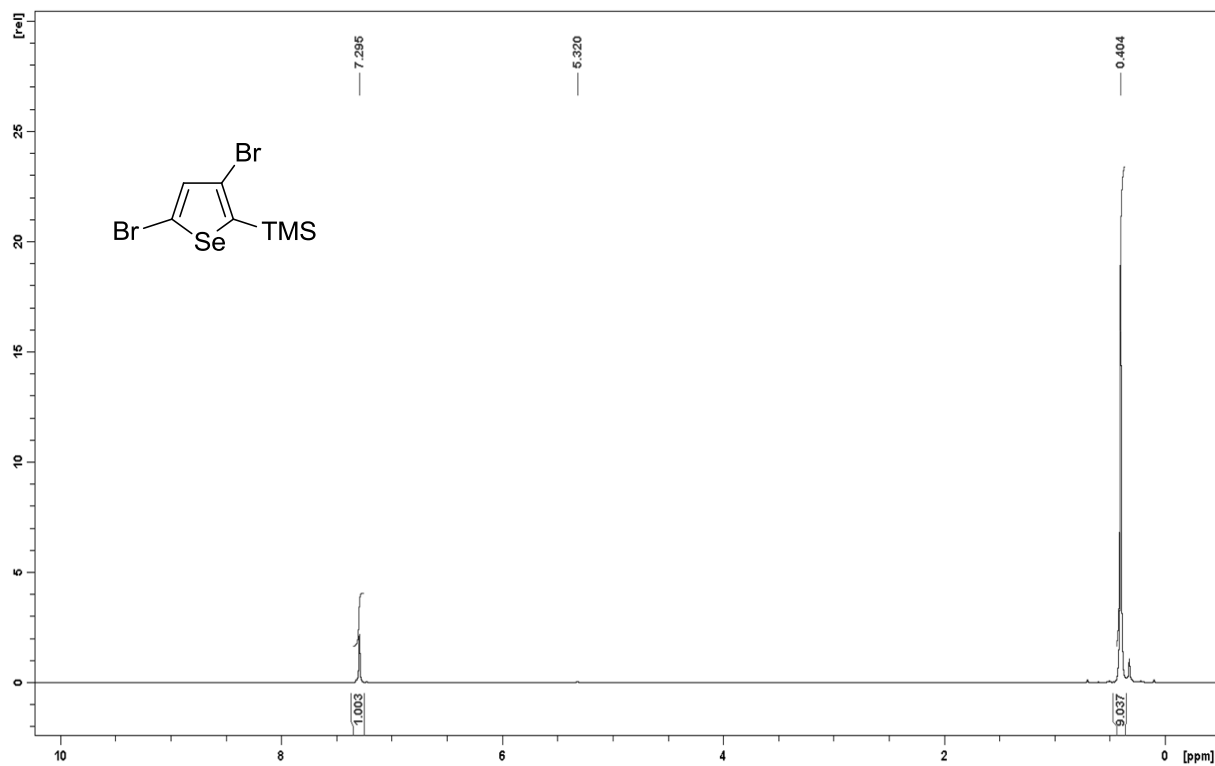
Spectrum 1.38. ^{13}C NMR (100 MHz, CD_2Cl_2) of compound 5ca.



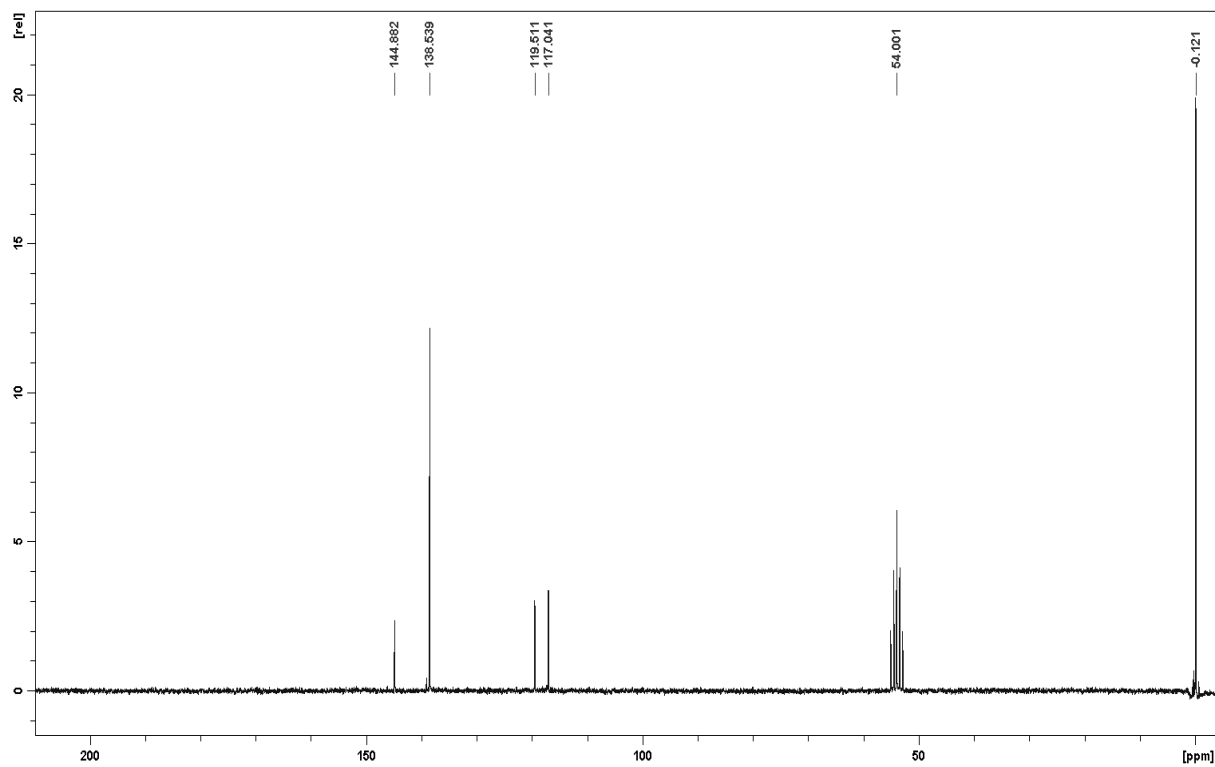
Spectrum 1.39. ^1H NMR (200 MHz, CDCl_3) of 2,3,5-Tribromo selenophene.



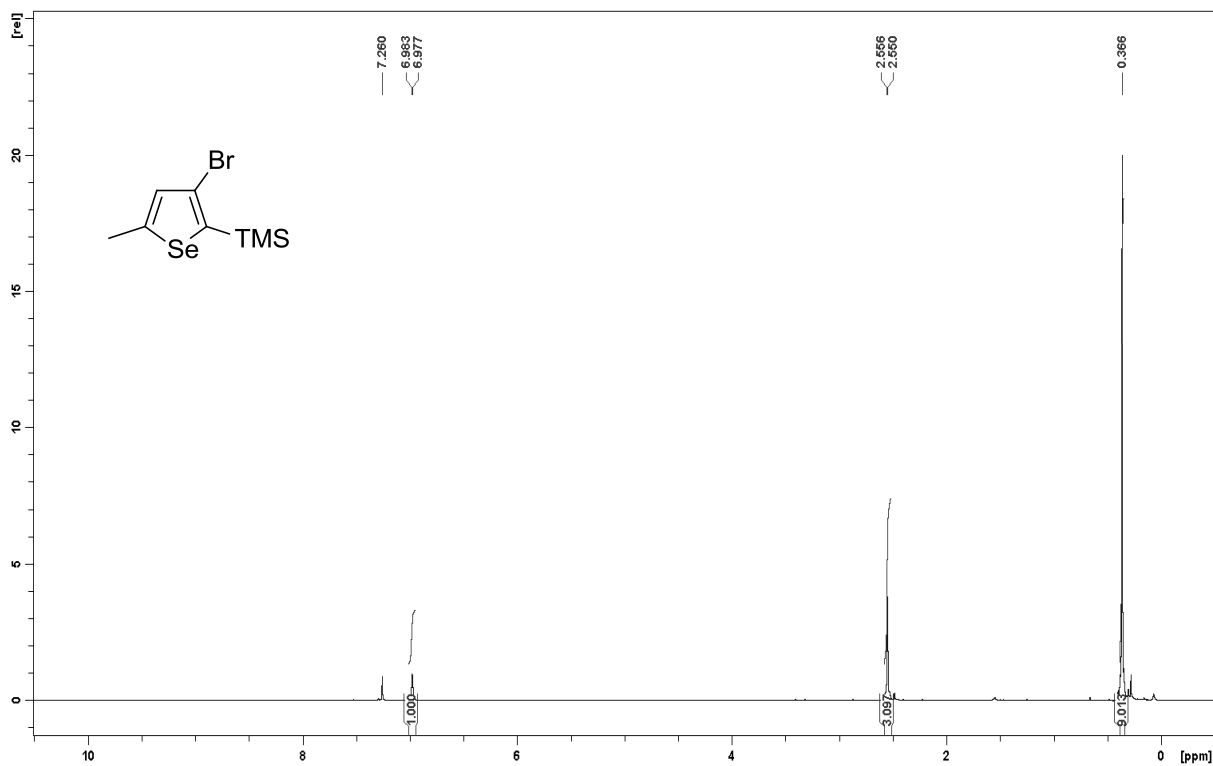
Spectrum 1.40. ^{13}C NMR (50 MHz, CDCl_3) of 2,3,5-Tribromo selenophene.



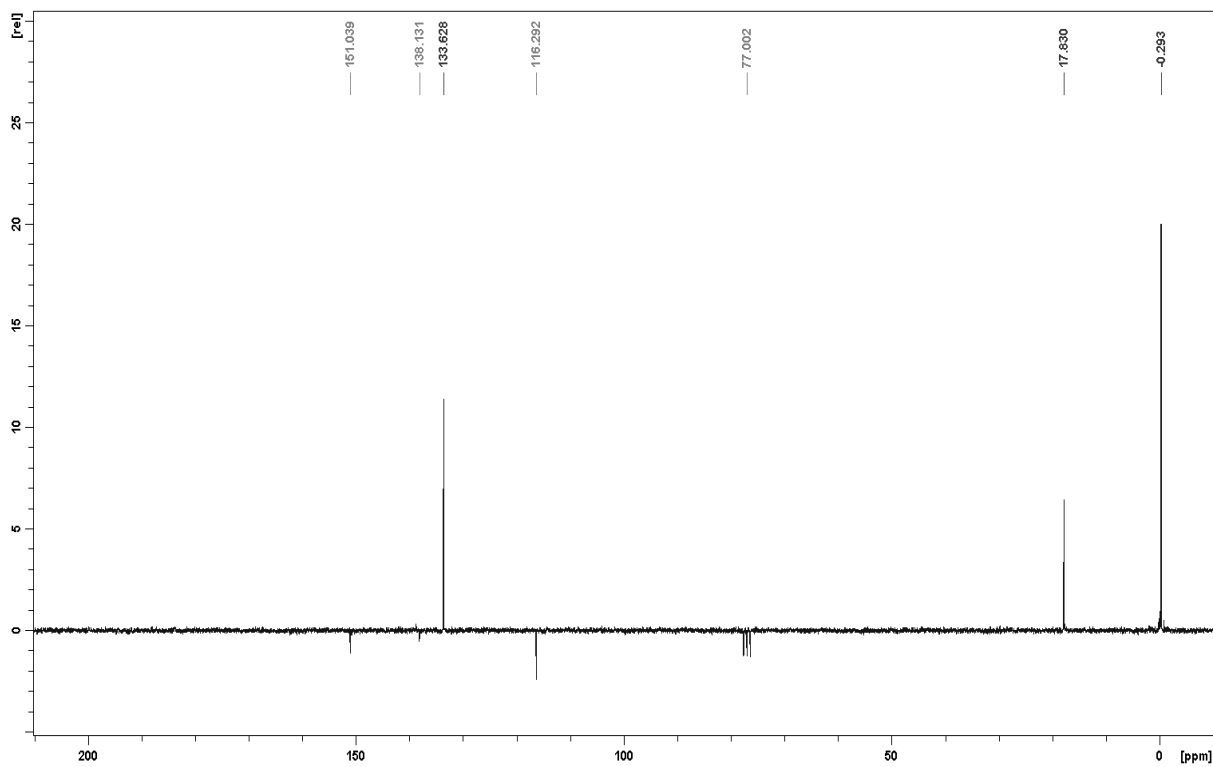
Spectrum 1.41. ^1H NMR (200 MHz, CD_2Cl_2) of compound **13**.



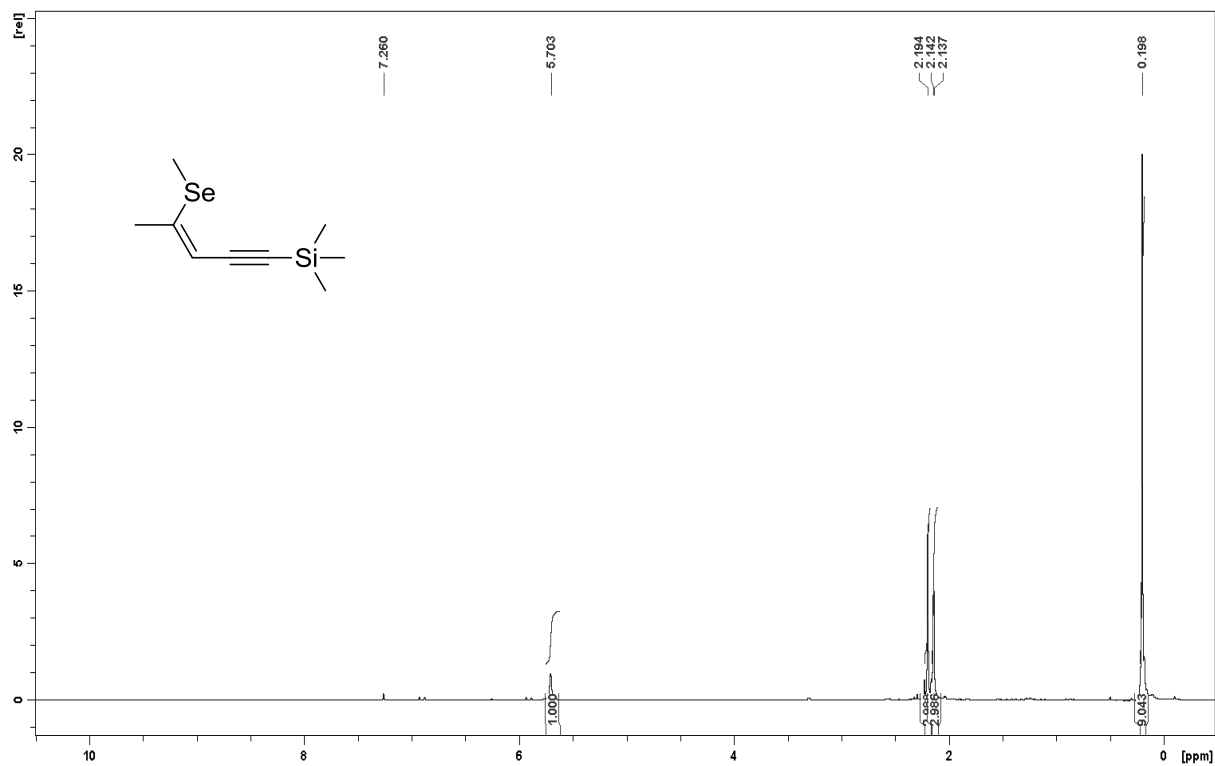
Spectrum 1.42. ^{13}C NMR (50 MHz, CD_2Cl_2) of compound **13**.



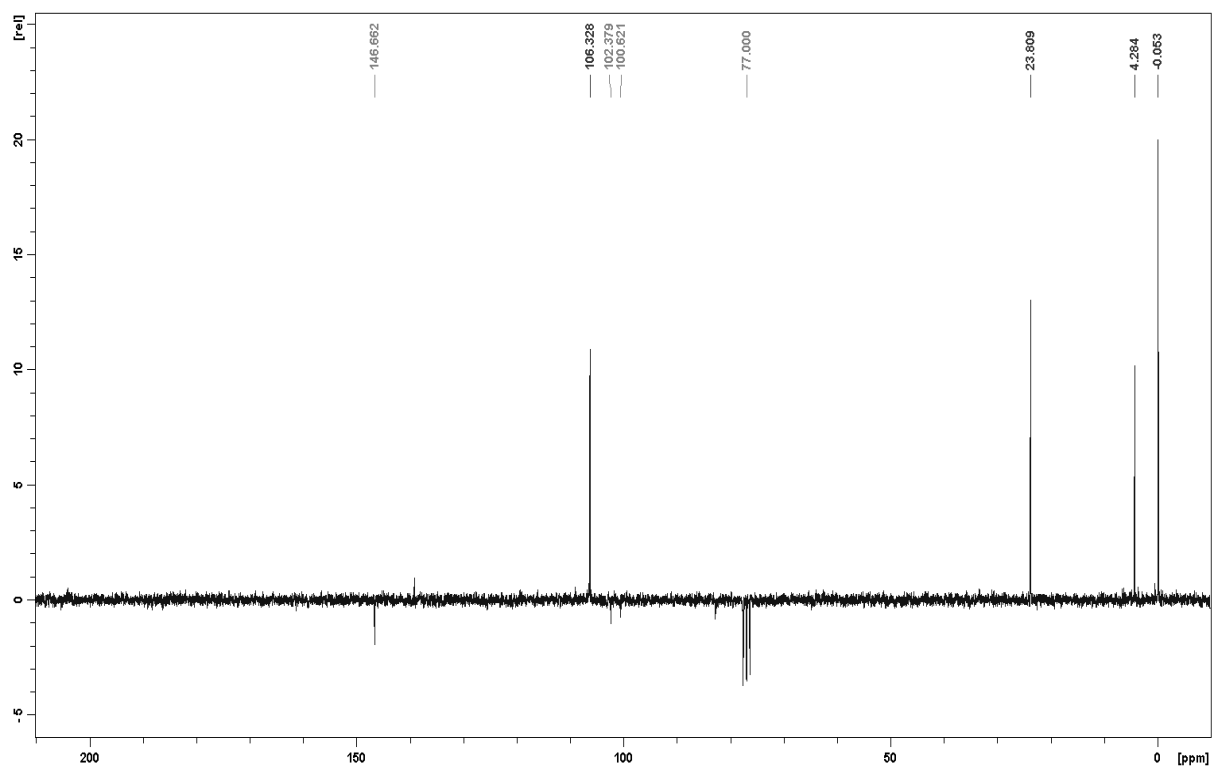
Spectrum 1.43. ^1H NMR (200 MHz, CD_2Cl_2) of compound 14.



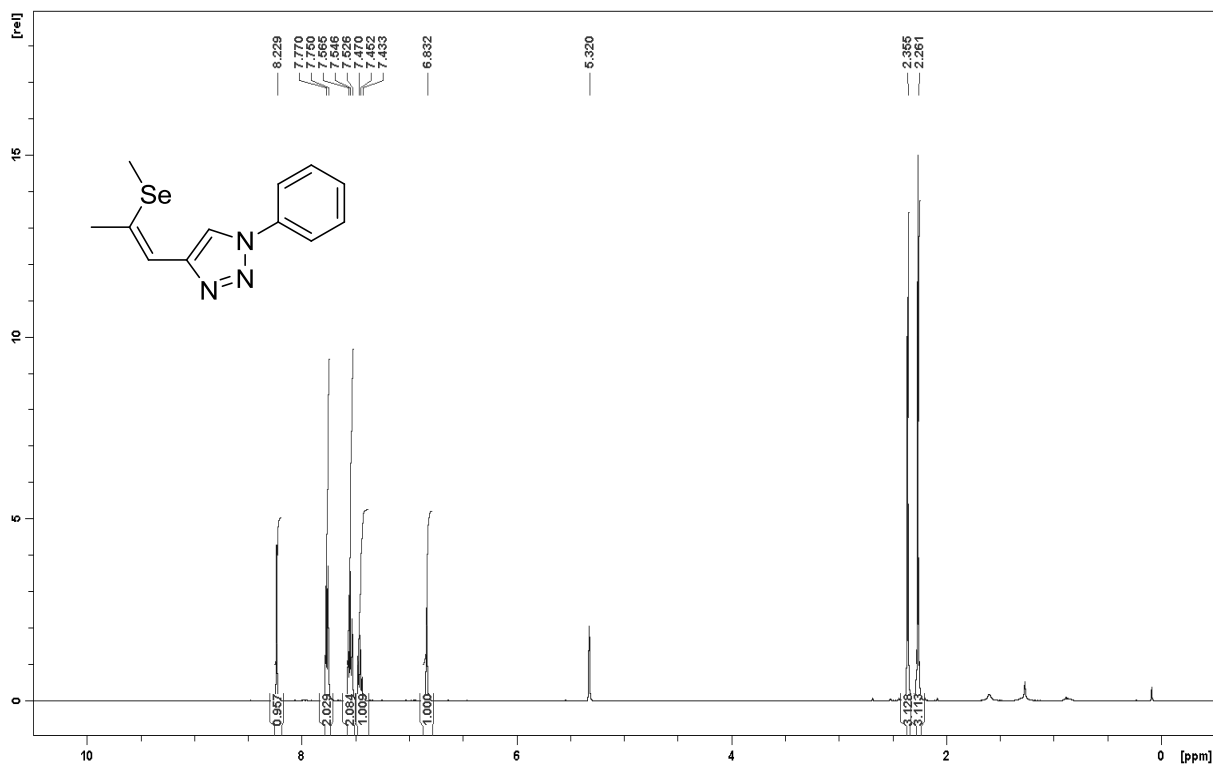
Spectrum 1.44. ^{13}C NMR (50 MHz, CD_2Cl_2) of compound 14.



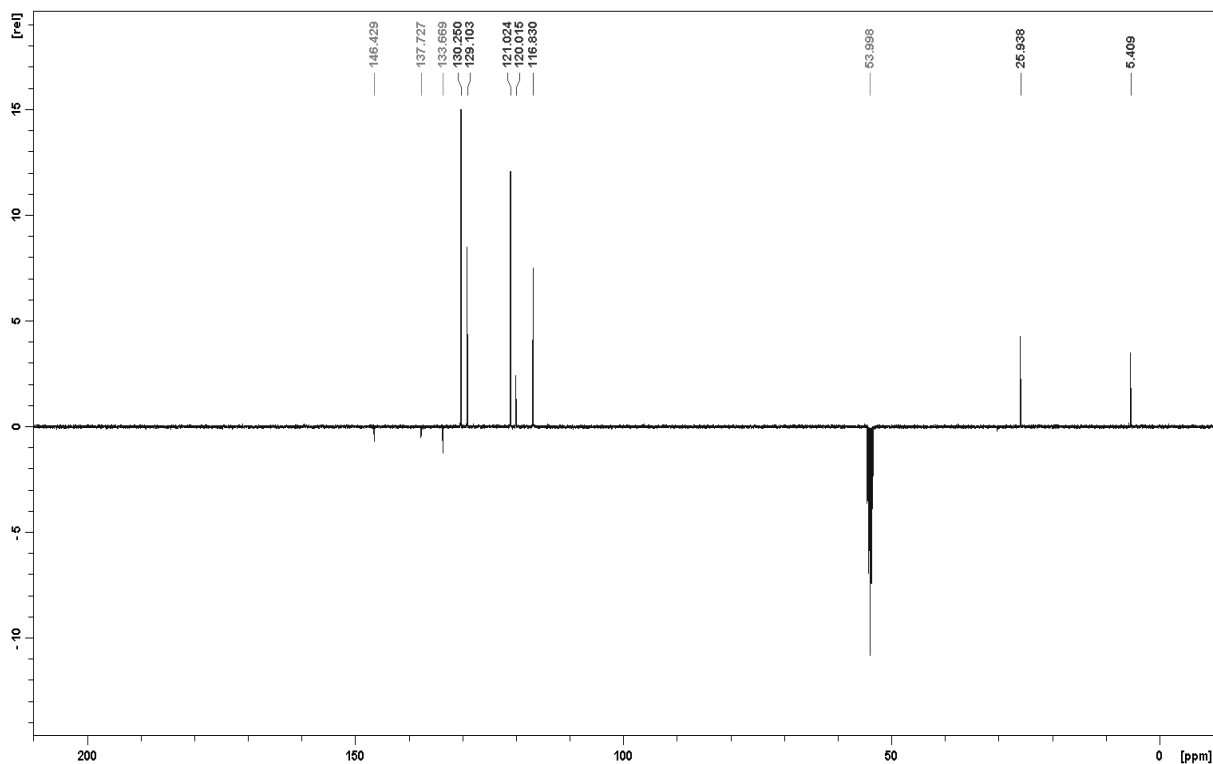
Spectrum 1.45. ^1H NMR (200 MHz, CD_2Cl_2) of compound 15.



Spectrum 1.46. ^{13}C NMR (50 MHz, CD_2Cl_2) of compound 15.



Spectrum 1.47. ¹H NMR (400 MHz, CD₂Cl₂) of compound 16.



Spectrum 1.48. ¹³C NMR (100 MHz, CD₂Cl₂) of compound 16.

2. Crystallographic Part.

Table 1. Details for the crystal structure determination of the title compounds. Crystallographic details for **4aa**¹ and **4ba**² are given in literature.

	4bb	4bd	4ca	5ba	7ba	9ba	12ba	16
formula	C ₁₃ H ₁₂ N ₃ S	C ₁₃ H ₁₀ N ₃ S	C ₁₃ H ₁₅ N ₃ S	C ₁₂ H ₁₃ N ₃ S	C ₁₂ H ₁₃ N ₃ S	C ₁₂ H ₁₃ N ₃ O ₂ S	C ₁₂ H ₁₃ N ₃ O ₂ S	C ₁₂ H ₁₃ N ₃ Se
fw	245.3	273.4	245.3	231.3	231.3	263.3	263.3	278.2
cryst. size [mm]	0.27×0.08×0.04	0.40×0.25×0.04	0.55×0.43×0.30	0.50×0.20×0.06	0.36×0.18×0.12	0.75×0.56×0.44	0.70×0.65×0.55	0.73×0.08×0.03
crystal system	orthorhombic	monoclinic	monoclinic	triclinic	orthorhombic	monoclinic	orthorhombic	orthorhombic
space group	<i>P</i> 2 ₁ 2 ₁ 2 ₁	<i>P</i> 2 ₁ / <i>c</i>	<i>Cc</i>	<i>P</i> $\bar{1}$	<i>P</i> 2 ₁ 2 ₁ 2 ₁	<i>P</i> 2 ₁ / <i>n</i>	<i>Pna</i> 2 ₁	<i>P</i> 2 ₁ 2 ₁ 2 ₁
color	clear colorless	clear colorless	clear colorless	clear colorless	clear colorless	clear yellow	clear colorless	clear colorless
shape	rod	plate	fragment	fragment	block	block	block	rod
<i>a</i>, Å	4.7643(15)	7.9302(11)	17.6465(9)	5.9338(2)	7.1809(3)	5.7944(6)	12.7982(8)	5.71930(10)
<i>b</i>, Å	15.968(6)	17.223(2)	5.0684(3)	7.3798(2)	10.2986(5)	23.318(2)	13.6159(8)	9.5627(2)
<i>c</i>, Å	16.294(6)	10.8814(14)	14.7768(8)	13.2891(4)	15.7680(8)	9.1374(9)	7.1310(4)	20.9579(5)
<i>α</i>, °	90	90	90	99.4247(11)	90	90	90	90
<i>β</i>, °	90	94.771(7)	112.225(2)	93.1907(12)	90	97.601(4)	90	90
<i>γ</i>, °	90	90	90	92.2136(12)	90	90	90	90
<i>V</i>, Å³	1239.6(8)	1481.1(3)	1223.44(12)	572.51(3)	1166.09(10)	1223.7(2)	1242.64(13)	1146.23(4)
<i>T</i>, K	100	100	100	100	100	100	100	100
ρ_{calc}, g cm⁻³	1.3142	1.2257	1.3316	1.3414	1.3172	1.4288	1.4070	1.6117

μ , mm ⁻¹ (MoK α)	0.242	0.209	0.245	0.257	0.253	0.262	0.258	3.251
$F(000)$	520	584	520	244	488	552	552	560
Abs. correction	multi-scan	multi-scan	multi-scan	multi-scan	multi-scan	multi-scan	multi-scan	multi-scan
$T_{\min} - T_{\max}$	0.94 – 0.99	0.94 – 0.99	0.88 – 0.93	0.94 – 0.99	0.91 – 0.97	0.83 – 0.89	0.84 – 0.87	0.74 – 0.91
$\theta_{\min} - \theta_{\max}$	1.79 – 30.07	2.22 – 30.2	2.98 – 37.66	1.56 – 32.62	2.4 – 29.7	2.41 – 34.93	2.18 – 37.55	2.34 – 30.01
no. of rflns measd.	25530	26938	13776	11475	27604	19745	53360	25987
R_{int}	0.0365	0.0930	0.0167	0.0258	0.0364	0.0265	0.0443	0.0307
no. of rflns unique	3514	4157	6313	4115	3333	5297	6545	3289
no. of rflns $I > 3\sigma(I)$	3076	2248	6081	3365	2884	4624	5940	3081
no. of params	203	172	201	197	198	215	215	146
no. of restraints	0	0	0	0	0	0	0	0
R ($I > 3\sigma(I)$)	0.0287	0.0445	0.0225	0.0329	0.0268	0.0409	0.0288	0.0242
wR2 (all data)	0.0622	0.0489	0.0303	0.0434	0.0348	0.0559	0.0370	0.0313
Goof	1.57	1.33	1.71	1.99	1.53	2.87	1.92	1.62
diff. Four. peaks min/max, e\AA^{-3}	-0.18/0.21	-0.34/0.35	-0.14/0.30	-0.28/0.38	-0.15/0.16	0.49/-0.40	0.43/-0.26	-0.50/0.38

[1] Stoeber, B.; Lumpi, D.; Froehlich, J. *Acta Crystallogr., Sect. C: Cryst. Struct. Commun.* **2011**, C67, o464.

[2] Lumpi, D.; Stoeber, B.; Hametner, C.; Kubel, F.; Reider, G.; Hagemann, H.; Karpfen, A.; Froehlich, J. *CrystEngComm* **2011**, 13, 7194.

Manuscript # 8

Supporting Information

Electronic Supplementary Information

Isoxazole-Based Ene-Yne Compounds as Potential Materials Exhibiting Nonlinear Optical Properties

Brigitte Holzer,^a Berthold Stöger,^b Daniel Lumpi,^{a*} Georg Reider,^c Christian Hametner,^a and Johannes Fröhlich^a

^a Institute of Applied Synthetic Chemistry, Vienna University of Technology, Getreidemarkt 9/163, A-1060 Vienna, Austria.

^b Institute of Chemical Technologies and Analytics, Vienna University of Technology, Getreidemarkt 9/164, A-1060 Vienna, Austria

^c Photonics Institute, Vienna University of Technology, Gußhausstraße 27- 29, A-1040 Vienna, Austria

*daniel.lumpi@tuwien.ac.at

Table of contents:

1. NMR Data
2. Crystallographic Part
3. Powder SHG Studies
4. References

1. NMR Data

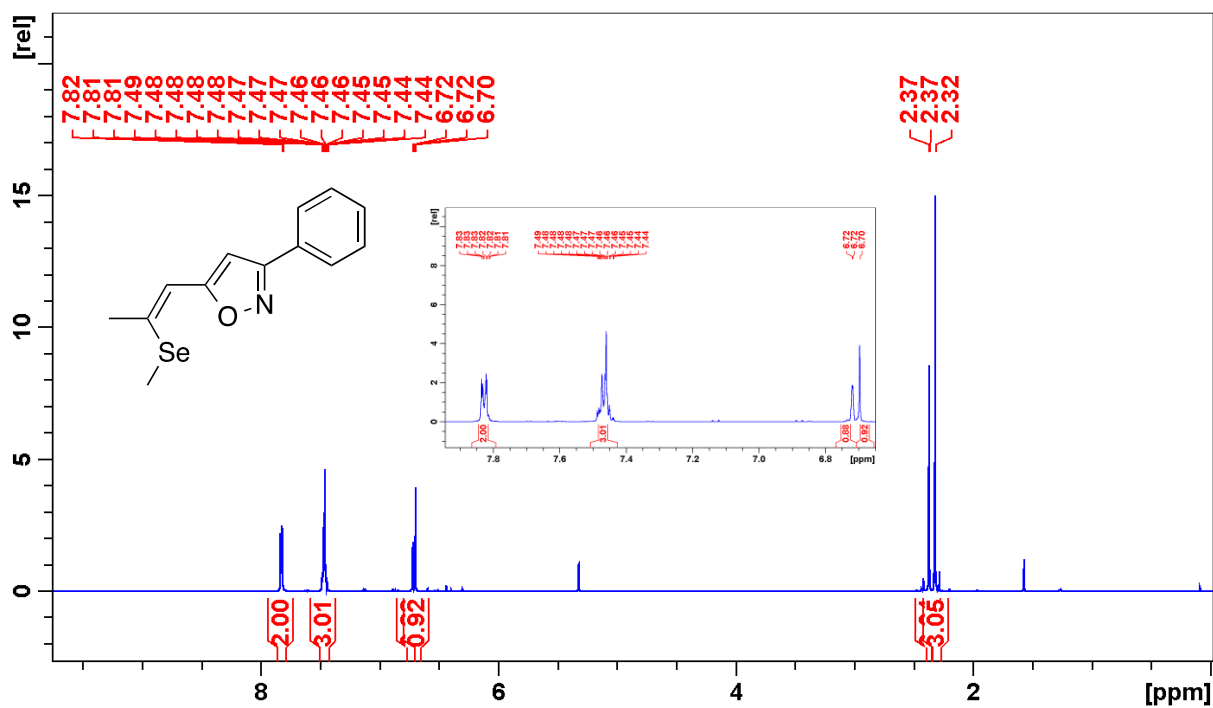


Figure S1. ¹H NMR (600 MHz, CD₂Cl₂) of compound **3a**.

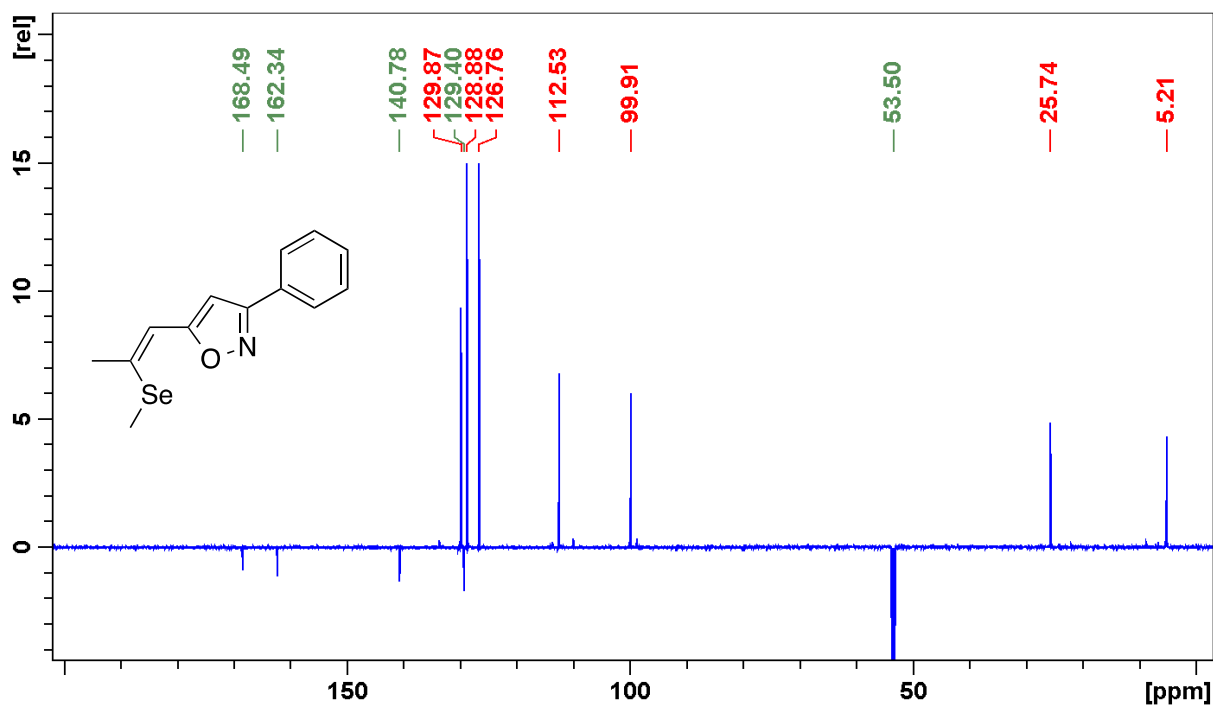


Figure S2. ¹³C NMR (150 MHz, CD₂Cl₂) of compound **3a**.

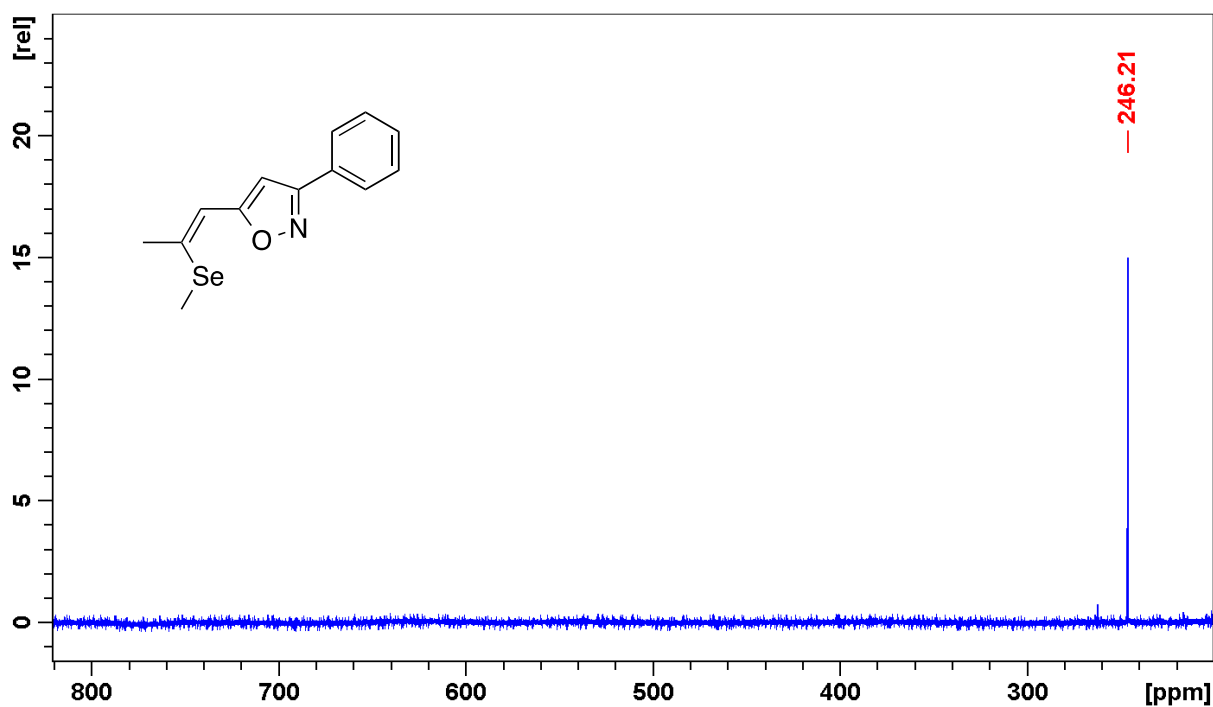


Figure S3. ^{77}Se NMR (114 MHz, CD_2Cl_2) of compound **3a**.

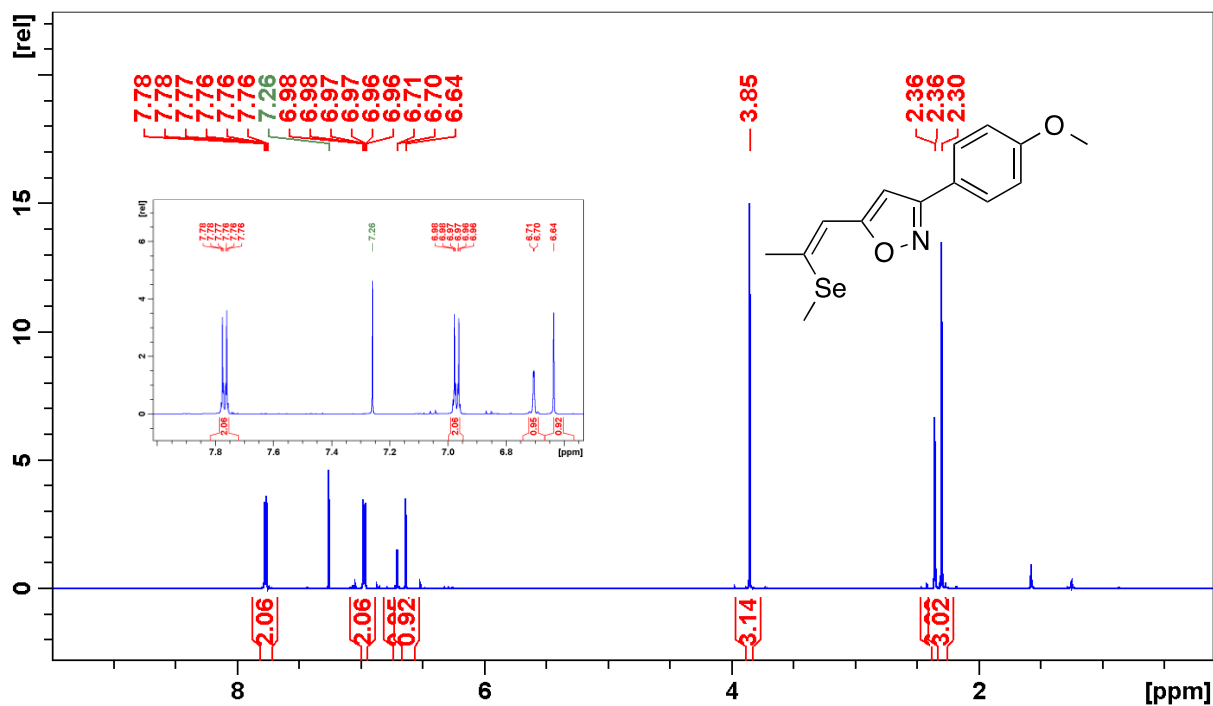


Figure S4. ^1H NMR (600 MHz, CDCl_3) of compound **3b**.

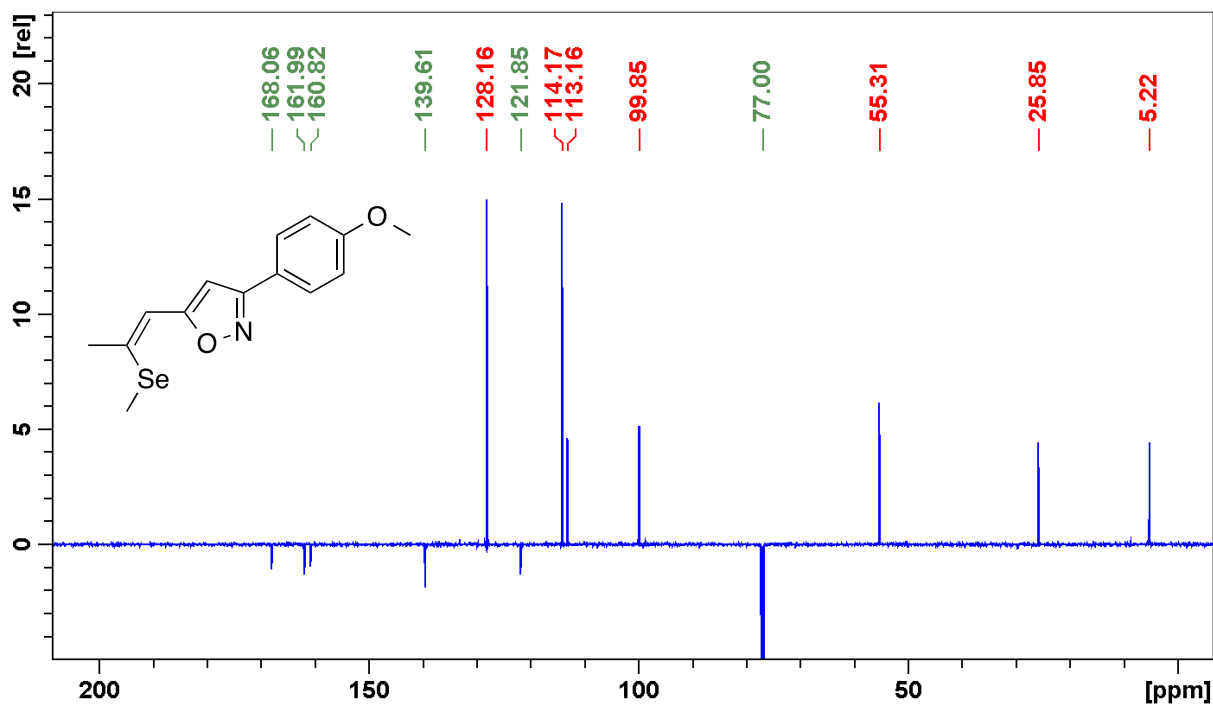


Figure S5. ^{13}C NMR (150 MHz, CDCl_3) of compound **3b**.

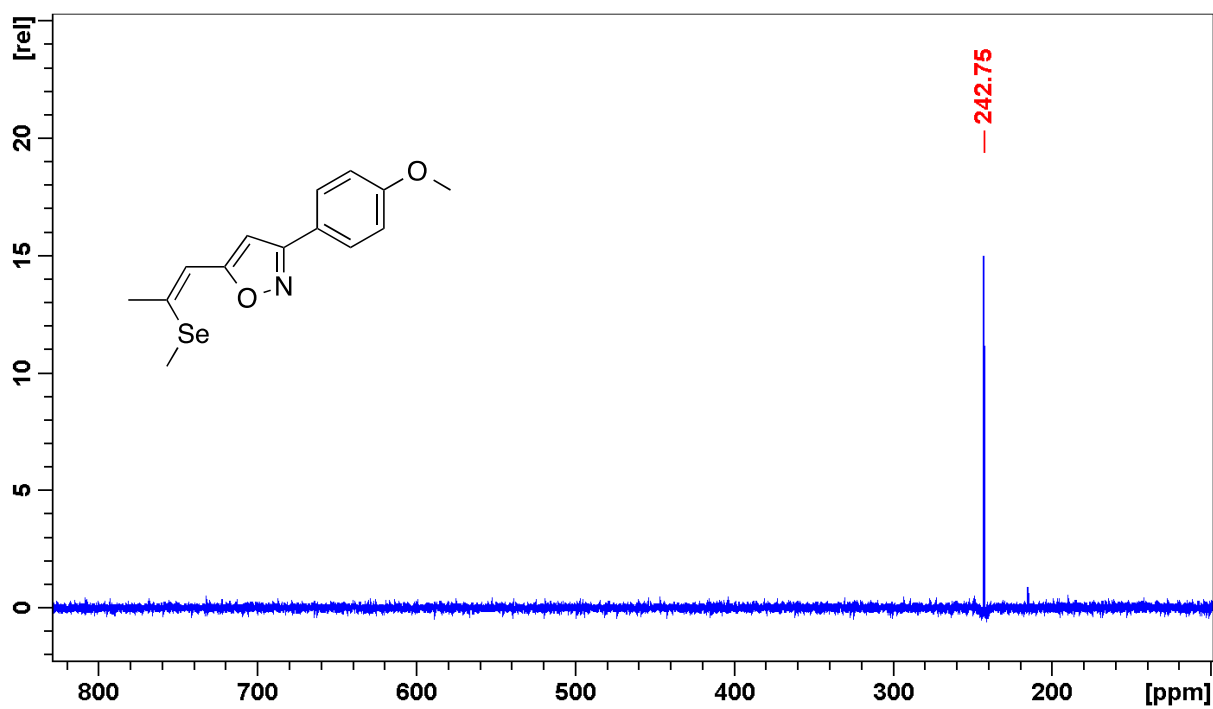


Figure S6. ^{77}Se NMR (114 MHz, CDCl_3) of compound **3b**.

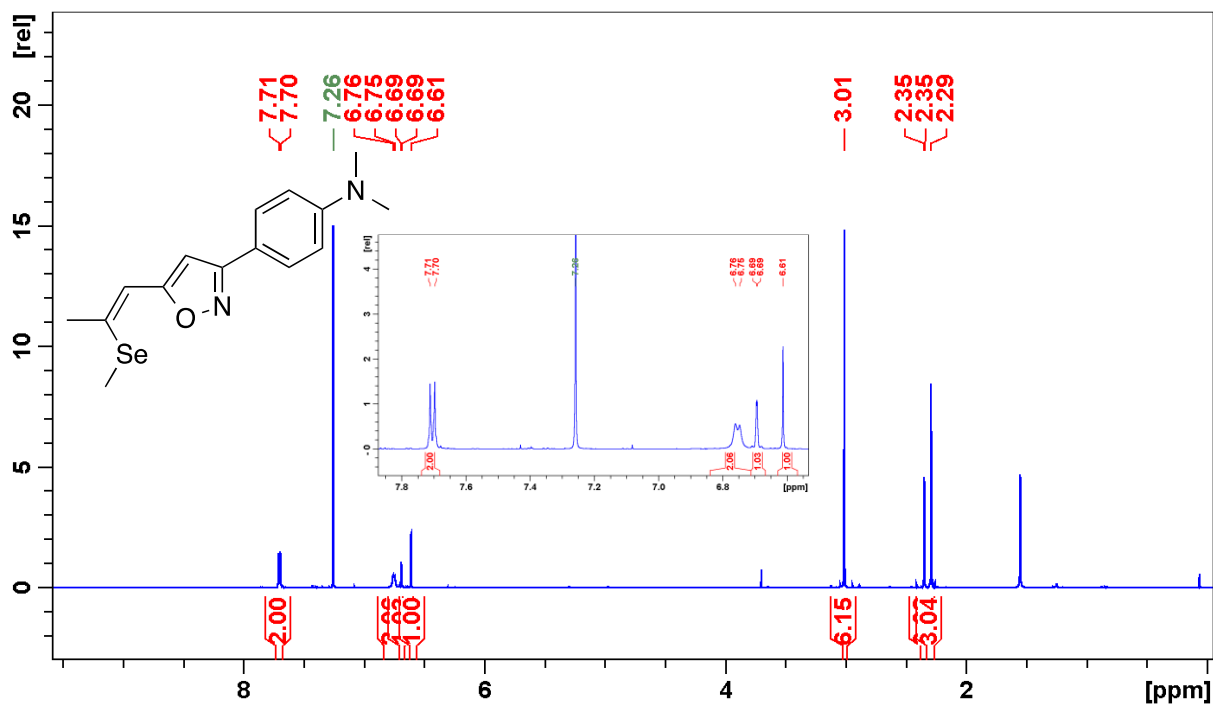


Figure S7. ^1H NMR (600 MHz, CDCl_3) of compound 3c.

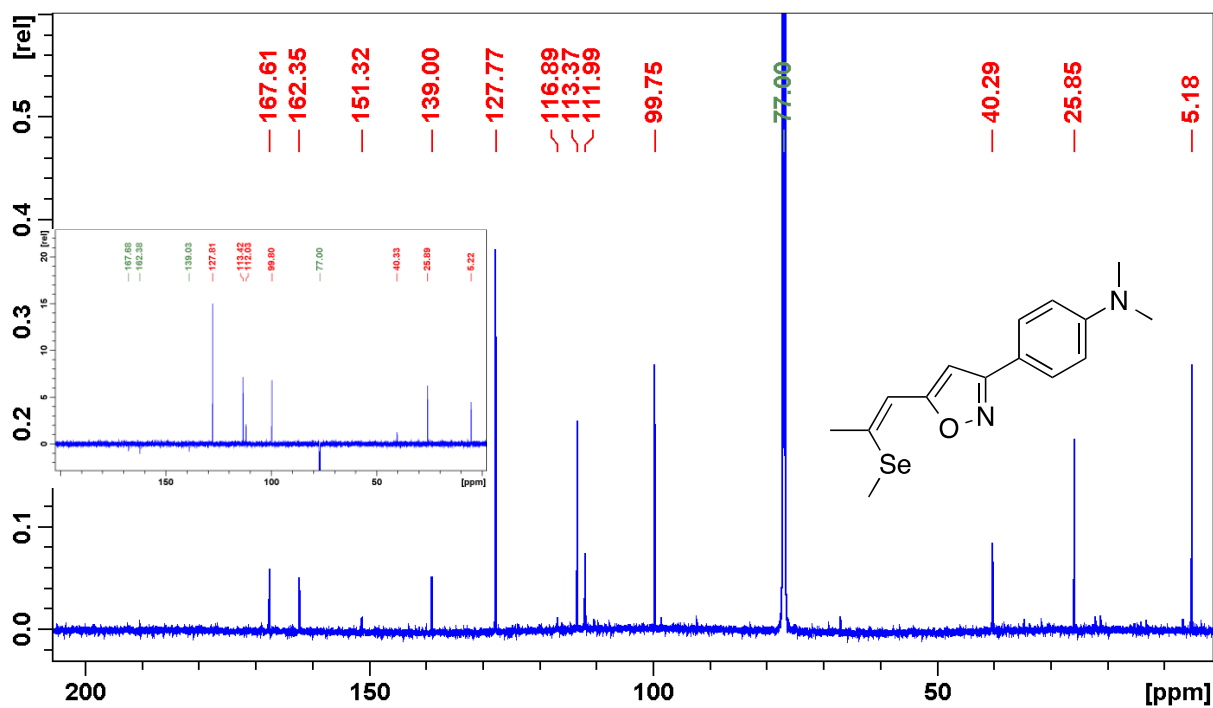


Figure S8. ^{13}C NMR (150 MHz, CDCl_3) of compound 3c.

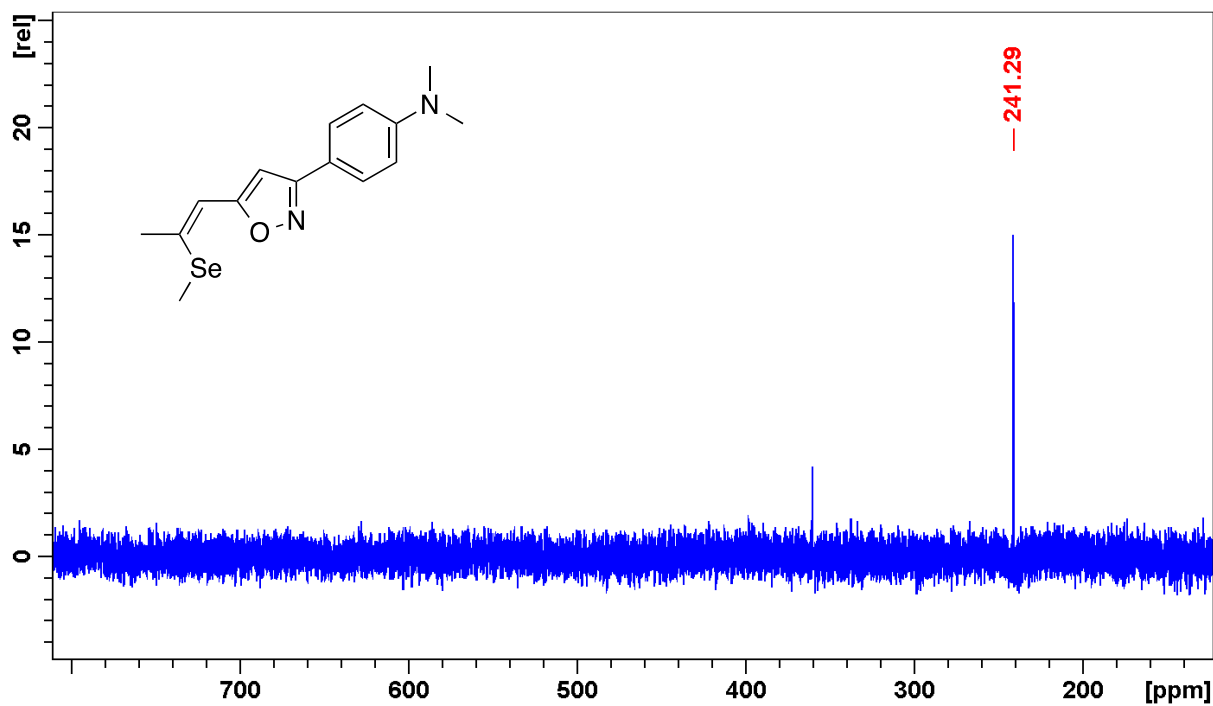


Figure S9. ^{77}Se NMR (114 MHz, CDCl_3) of compound **3c**.

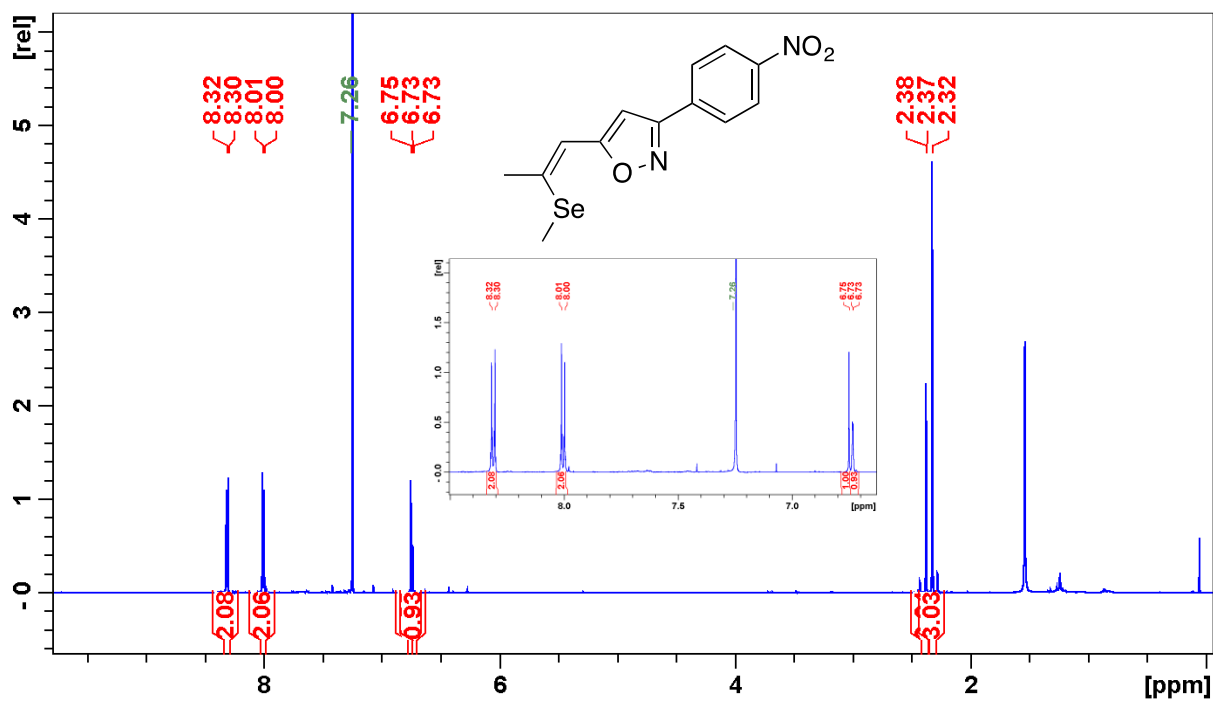


Figure S10. ^1H NMR (600 MHz, CDCl_3) of compound **3d**.

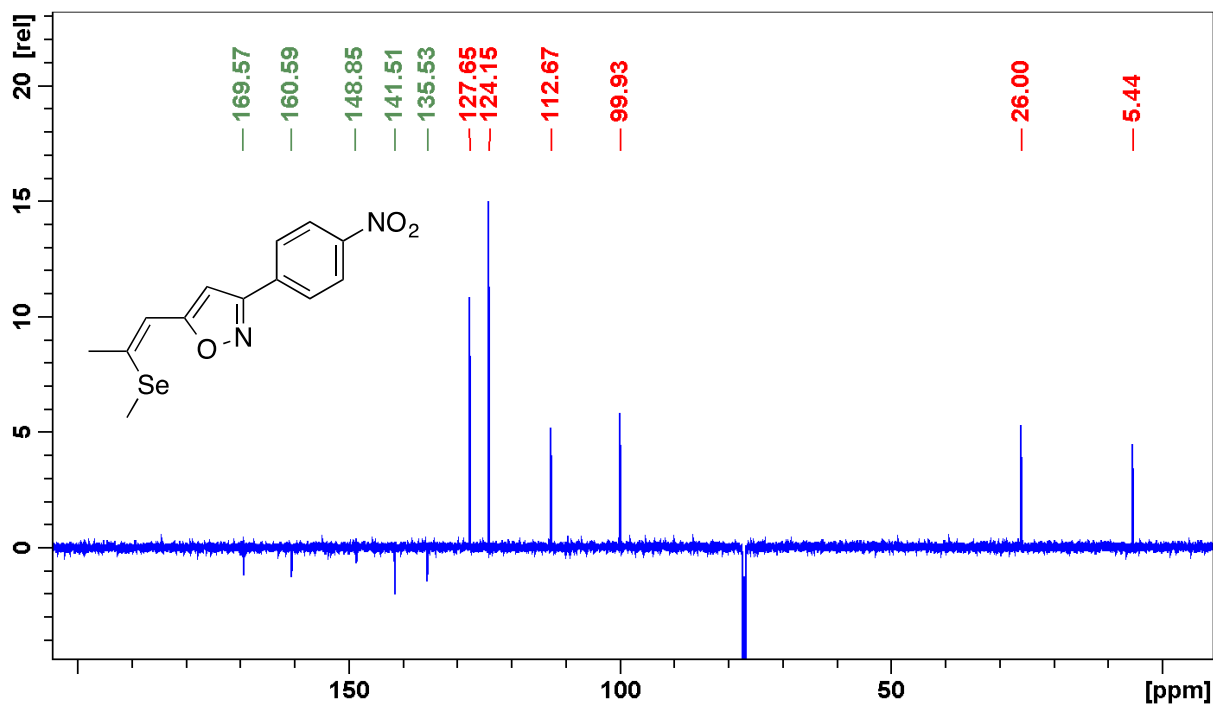


Figure S11. ^{13}C NMR (150 MHz, CDCl_3) of compound **3d**.

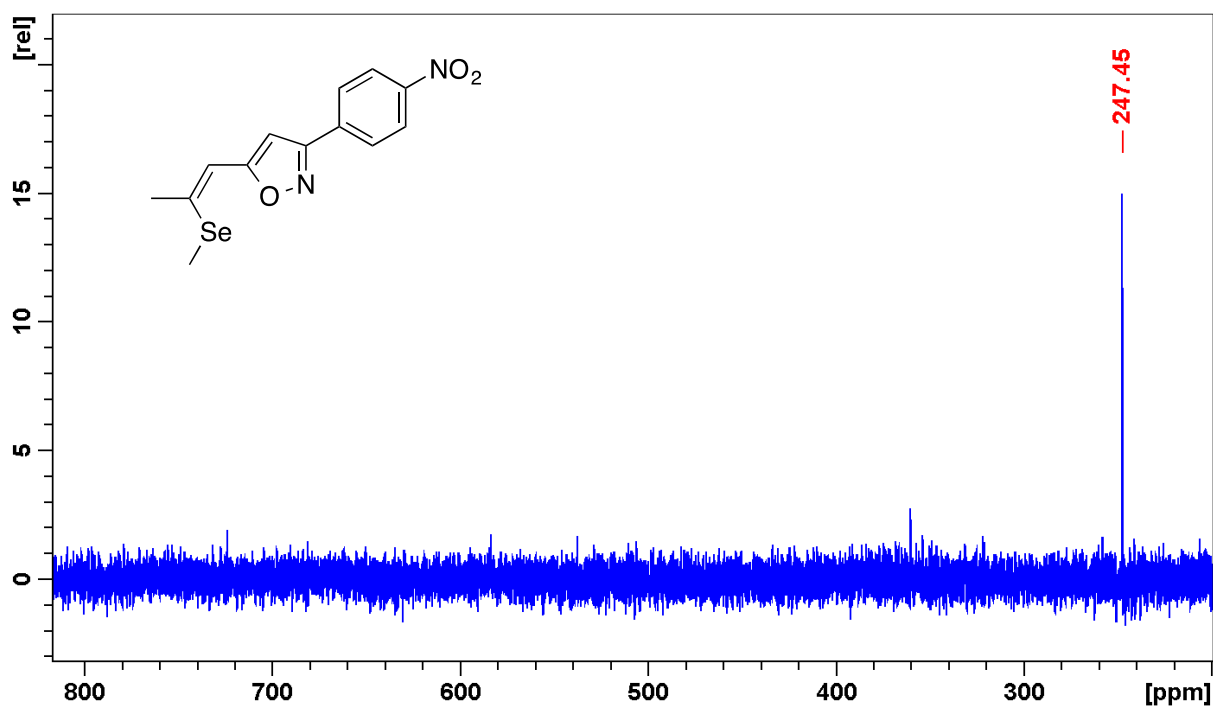


Figure S12. ^{77}Se NMR (114 MHz, CDCl_3) of compound **3d**.

2. Crystallographic Part.

Data Collection.

A suitable crystal of the title compound **3a** was mounted on a Bruker APEX II diffractometer equipped with a CCD detector. Intensity data was recorded at 100 K in a dry stream of nitrogen. Five independent sets were collected in ω - and ϕ -scan modes with 0.5° rotation width optimized for completeness and redundancy. In total 1865 frames were recorded. More details of the data collection are summarized in Table 1.

Table 1. Details of single crystal data collection and structure refinement of **3a**.

Diffractometer	Bruker SMART APEX II
Radiation; $\lambda / \text{\AA}$	Mo $K\alpha$; 0.71073
Temperature / $^\circ\text{C}$	-173
Crystal colour; shape	clear colourless rod
Space group, no.	$P 2_1 2_1 2_1$
Formula units Z	4
$a / \text{\AA}$	5.7537(6)
$b / \text{\AA}$	9.6831(11)
$c / \text{\AA}$	20.806(2)
$V / \text{\AA}^3$	1159.2(2)
Sum formula	$\text{C}_{13}\text{H}_{13}\text{NOSe}$
Formula weight	278.2
μ / mm^{-1}	3.216
X-ray density / $\text{g}\cdot\text{cm}^{-3}$	1.5942
Range θ_{\min} - θ_{\max}	1.96 – 35.02
Range h	-9 \rightarrow 9
k	-15 \rightarrow 15
l	-33 \rightarrow 33
Measured reflections	9418
Independent reflections	5102
Obs. Reflections [$I > 3\sigma(I)$]	4653
R_i	0.034
Absorption correction	SADABS
Number of parameters	146
Diff. elec. dens. max; min [$\text{e}\cdot\text{\AA}^{-3}$]	0.80; -0.66
$R[F > 3\sigma(F)]$	0.03
$wR(F^2 \text{ all})$	0.03
GooF	1.52
Flack Parameter	0.018(7)

Table 2. Details of single crystal data collection and structure refinement of **3b**.

Diffractometer	Bruker SMART APEX II
Radiation; $\lambda / \text{\AA}$	Mo K α ; 0.71073
Temperature / °C	-173
Crystal colour; shape	clear colourless rod
Space group, no.	<i>P</i> 21/ <i>c</i>
Formula units <i>Z</i>	4
<i>a</i> / \AA	16.1452(14)
<i>b</i> / \AA	5.7016(6)
<i>c</i> / \AA	13.9322(17)
<i>V</i> / \AA^3	1278.8(2)
Sum formula	C ₁₄ H ₁₅ NO ₂ Se
Formula weight	308.2
μ / mm^{-1}	2.929
X-ray density / $\text{g}\cdot\text{cm}^{-3}$	1.6011
Range θ_{\min} - θ_{\max}	2.5 – 33.1
Range <i>h</i>	-24 → 24
<i>k</i>	-8 → 8
<i>l</i>	-18 → 21
Measured reflections	23919
Independent reflections	4902
Obs. Reflections [<i>I</i> >3 σ (<i>I</i>)]	3517
<i>R</i> _{<i>i</i>}	0.0464
Absorption correction	SADABS
Number of parameters	163
Diff. elec. dens. max; min [$\text{e}^- \cdot \text{\AA}^{-3}$]	0.54; -0.41
<i>R</i> [<i>F</i> >3 σ (<i>F</i>)]	0.03
<i>wR</i> (<i>F</i> ² all)	0.04
Goof	1.46

Table 3. Details of single crystal data collection and structure refinement of **3c**.

Diffractometer	Bruker SMART APEX II
Radiation; $\lambda / \text{\AA}$	Mo K α ; 0.71073
Temperature / °C	-173
Crystal colour; shape	clear colourless rod
Space group, no.	<i>P</i> 21/ <i>c</i>
Formula units <i>Z</i>	4
<i>a</i> / \AA	11.2380(11)
<i>b</i> / \AA	8.1845(8)
<i>c</i> / \AA	15.8230(15)
<i>V</i> / \AA^3	1402.6 (2)
Sum formula	C ₁₅ H ₁₈ N ₂ OSe
Formula weight	321.3
μ / mm^{-1}	2.671
X-ray density / $\text{g}\cdot\text{cm}^{-3}$	1.5214
Range θ_{\min} - θ_{\max}	2.7 - 26.9
Range <i>h</i>	-15 \rightarrow 15
<i>k</i>	-11 \rightarrow 11
<i>l</i>	-22 \rightarrow 22
Measured reflections	32369
Independent reflections	4112
Obs. Reflections [<i>I</i> >3 σ (<i>I</i>)]	2904
<i>R</i> _{<i>i</i>}	0.064
Absorption correction	SADABS
Trans. Coef. <i>T</i> _{min} ; <i>T</i> _{max}	0.98; 0.55
Number of parameters	172
Diff. elec. dens. max; min [<i>e</i> · \AA^{-3}]	1.18; -0.46
<i>R</i> [<i>F</i> >3 σ (<i>F</i>)]	0.04
<i>wR</i> (<i>F</i> ² all)	0.05
GooF	2.00

Table 4. Details of single crystal data collection and structure refinement of **3d**.

Diffractometer	Bruker SMART APEX II
Radiation; $\lambda / \text{\AA}$	Mo K α ; 0.71073
Temperature / °C	-173
Crystal colour; shape	clear orange rod
Space group, no.	<i>P</i> 21/ <i>c</i>
Formula units <i>Z</i>	8
<i>a</i> / \AA	32.3533(5)
<i>b</i> / \AA	5.6801(2)
<i>c</i> / \AA	13.9649(11)
<i>V</i> / \AA^3	2512.56(2)
Sum formula	C ₁₃ H ₁₂ N ₂ O ₃ Se
Formula weight	323.2
μ / mm^{-1}	2.994
X-ray density / $\text{g}\cdot\text{cm}^{-3}$	1.7083
Range θ_{\min} - θ_{\max}	1.3 – 30.2
Range <i>h</i>	-45 → 45
<i>k</i>	-7 → 8
<i>l</i>	-19 → 19
Measured reflections	64501
Independent reflections	7363
Obs. Reflections [<i>I</i> >3 σ (<i>I</i>)]	5832
<i>R</i> _{<i>i</i>}	0.0584
Absorption correction	SADABS
Trans. Coef. <i>T</i> _{min} ; <i>T</i> _{max}	0.89; 0.78
Number of parameters	344
Diff. elec. dens. max; min [<i>e</i> · \AA^{-3}]	1.34; -3.20
<i>R</i> [<i>F</i> >3 σ (<i>F</i>)]	0.06
<i>wR</i> (<i>F</i> ² all)	0.07
GooF	2.80

Molecular Structure of 3b-d

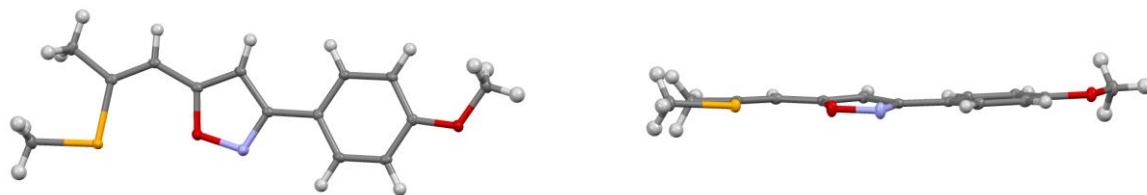


Figure S13: Molecular structure of **3b**; viewed normal (a, top) and parallel (b, bottom) to the molecular plane. C, N, O and Se atoms are represented by grey, blue, red and orange, respectively.

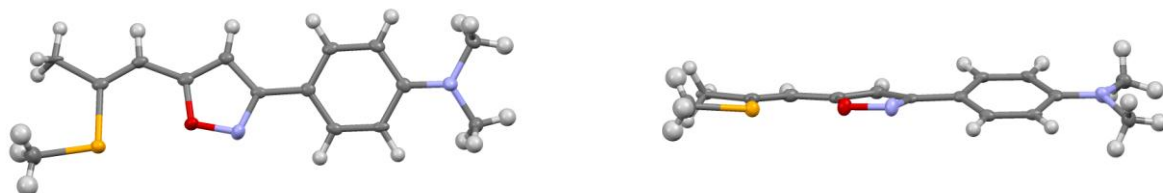


Figure S14: Molecular structure of **3c**; viewed normal (a, top) and parallel (b, bottom) to the molecular plane. C, N, O and Se atoms are represented by grey, blue, red and orange, respectively.

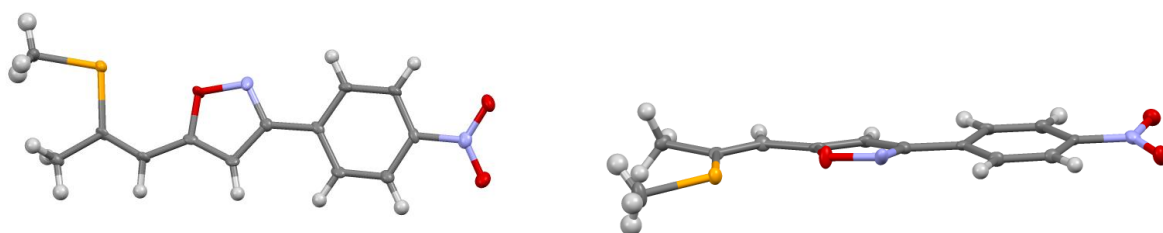


Figure S15: Molecular structure of **3d**; viewed normal (a, top) and parallel (b, bottom) to the molecular plane. C, N, O and Se atoms are represented by grey, blue, red and orange, respectively.

Structure Solution and Refinement.

Frames were integrated using SAINT PLUS¹ and absorption correction was performed using a multi-scan approach with SADABS.¹ The lattice parameters and systematic extinctions clearly indicated orthorhombic space group $P2_12_12_1$ of **3a** and $P2_1/c$ of **3b-d**. The crystal structures were solved by charge-flipping using SUPERFLIP.² All C, N, S and Se atoms were located in the resulting electron density map. The structure was refined with JANA2006.³ The protons were located in subsequent difference Fourier maps and refined without restraints or constraints. In the final refinement steps, all non-H atoms were refined anisotropically.

3. Powder SHG Studies

Microcrystalline material was prepared from originally synthesized single crystal needles with an agate mortar, placed between two glass slides, and exposed to pulses from a Q-switched Nd:YAG Laser (wavelength 1064 nm, 10 ns pulse duration and 10 Hz repetition rate, focal area approximately 1 mm²). The SH radiation transmitted through the 0.2 mm thick sample was separated from the fundamental radiation by glass filters and analyzed by a monochromator, photomultiplier tube and boxcar averager.

4. References

- [1] Bruker Analytical X-ray Instruments, Inc., Madison, WI, USA: SAINT and SADABS 2008.
- [2] L. Palatinus, G. Chapuis, G. *J. Appl. Cryst.* **2007**, 40, 786-790.
- [3] V. Petříček, M. Dušek, L. Palatinus, **2006**: Jana2006. The crystallographic computing system. Institute of Physics, Praha, Czech Republic.

Manuscript # 9

Supporting Information

Initiators for Two-Photon Induced Polymerization Based on a Novel Cap-Linker-Cap System

Brigitte Holzer,^{a,} Maximilian Tromayer,^{a,b} Markus Lunzer,^{a,c} Daniel Lumpi,^a Ernst Horkel,^a
Christian Hametner,^a Arnulf Rosspointner,^c Eric Vauthey,^c Robert Liska^a and Johannes Fröhlich^a*

^aInstitute of Applied Synthetic Chemistry, Vienna University of Technology,

Getreidemarkt 9/163OC, A-1060 Vienna, Austria

^bInstitute of Materials Science and Technology, Vienna University of Technology,

Favoritenstraße 9-11, A-1040 Vienna, Austria

^cPhysical Chemistry Department, University of Geneva,

Quai Ernest Ansermet 30, CH-1211 Geneva, Switzerland

[*brigitte.holzer@tuwien.ac.at](mailto:brigitte.holzer@tuwien.ac.at)

A) NMR Spectra

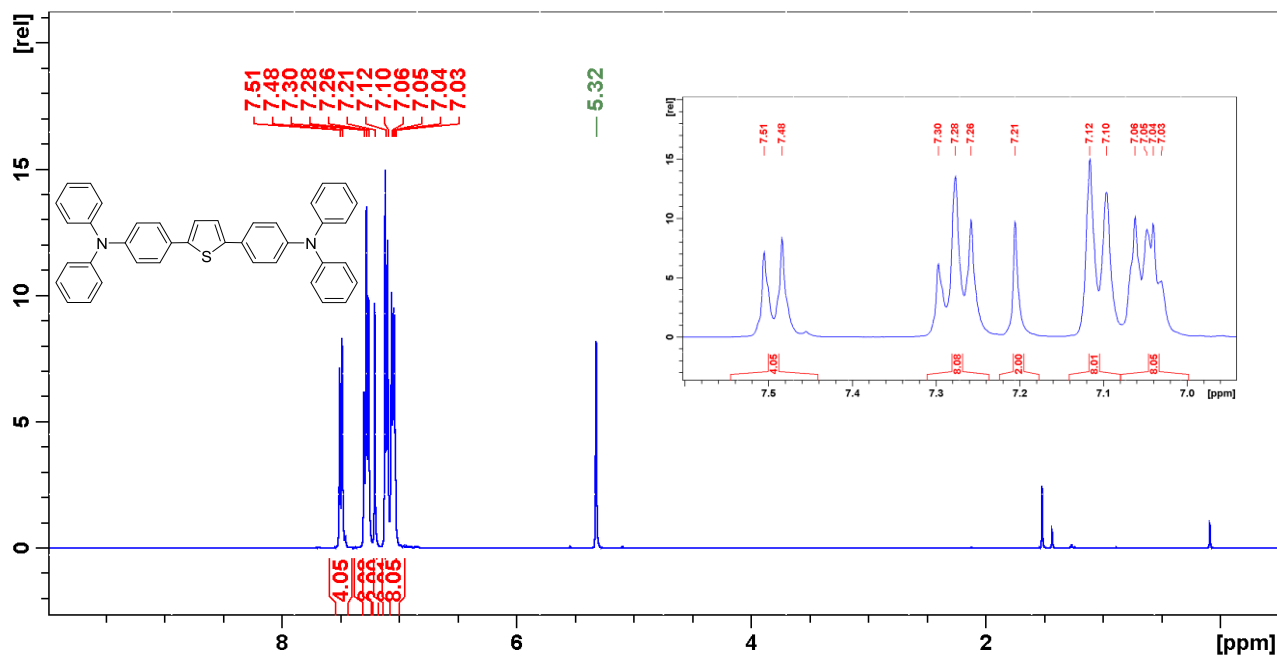


Figure S1. Proton NMR spectrum of compound 3a.

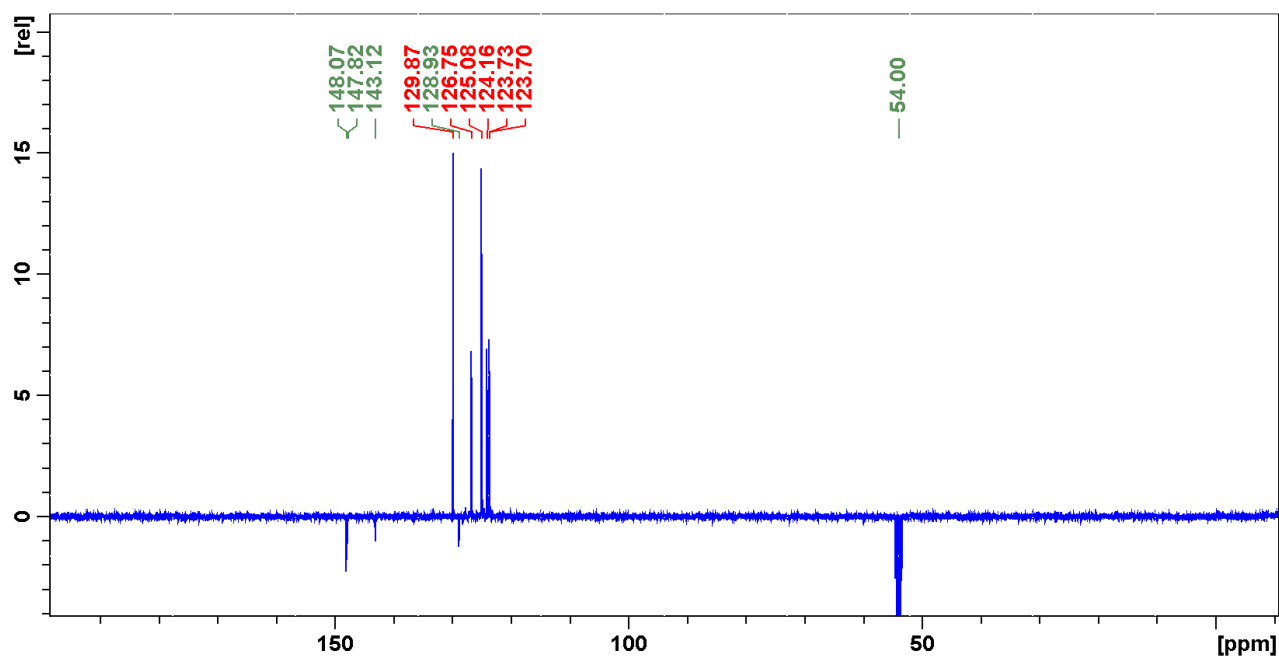


Figure S2. Carbon NMR spectrum of compound 3a.

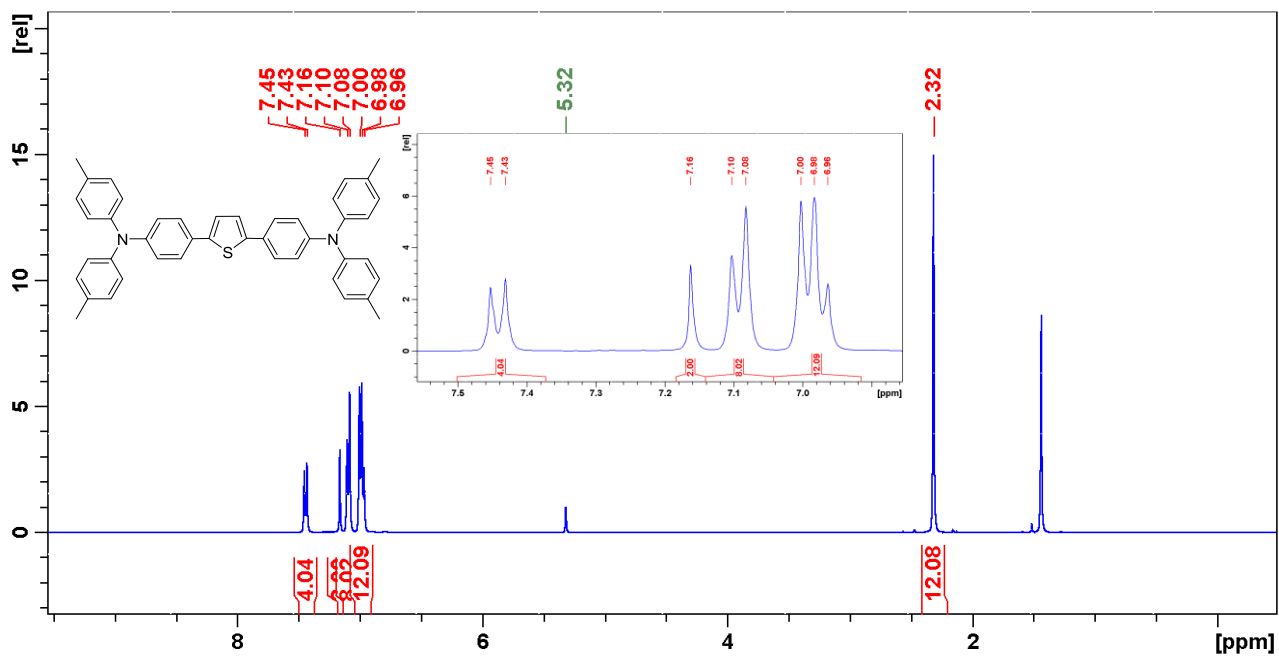


Figure S3. Proton NMR spectrum of compound **3b**.

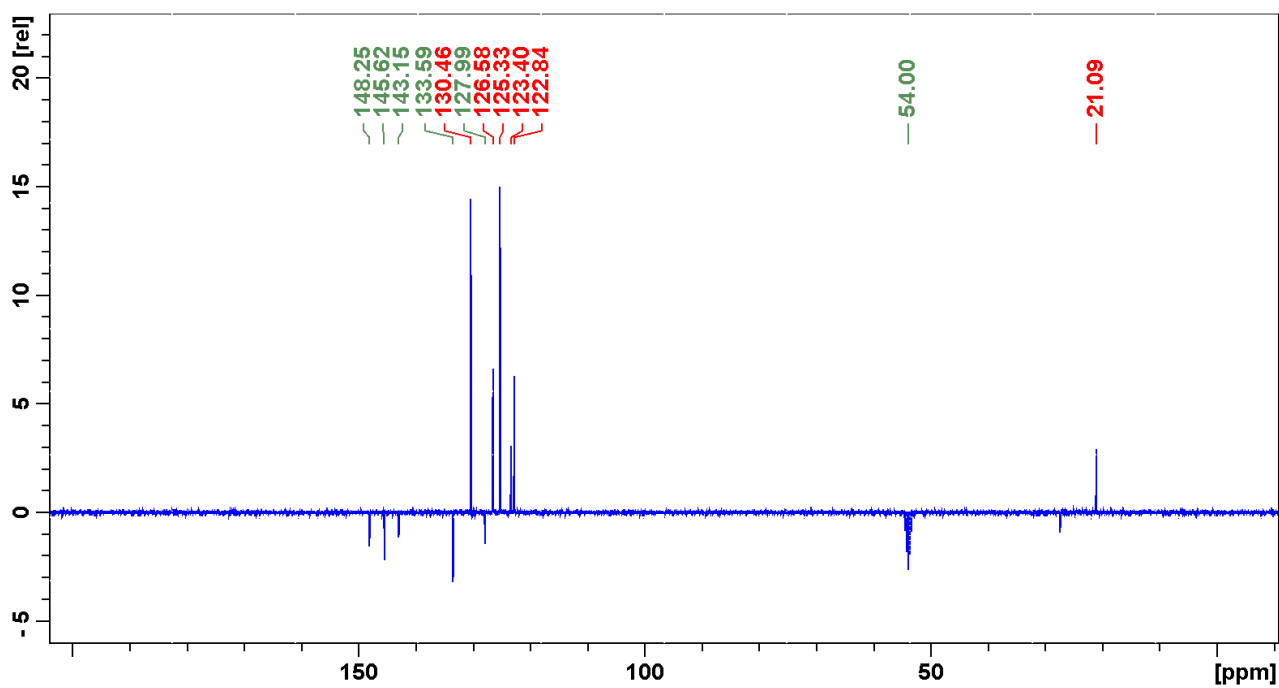


Figure S4. Carbon NMR spectrum of compound **3b**.

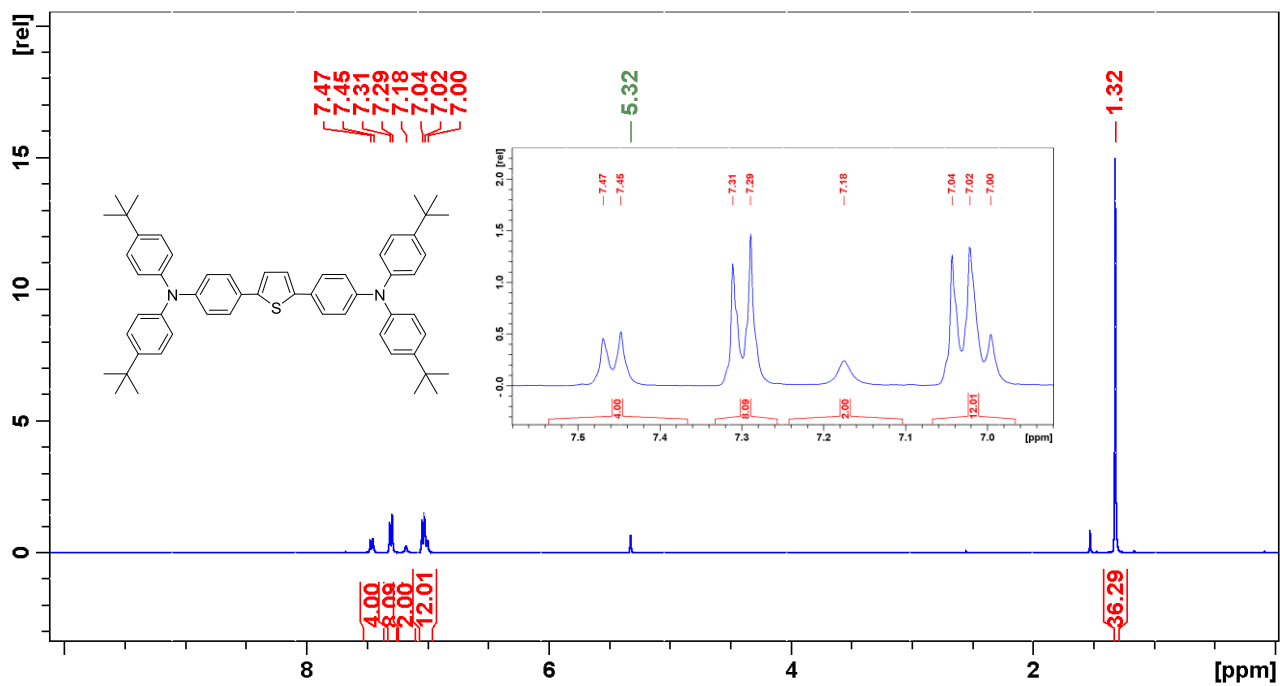


Figure S5. Proton NMR spectrum of compound 3c.

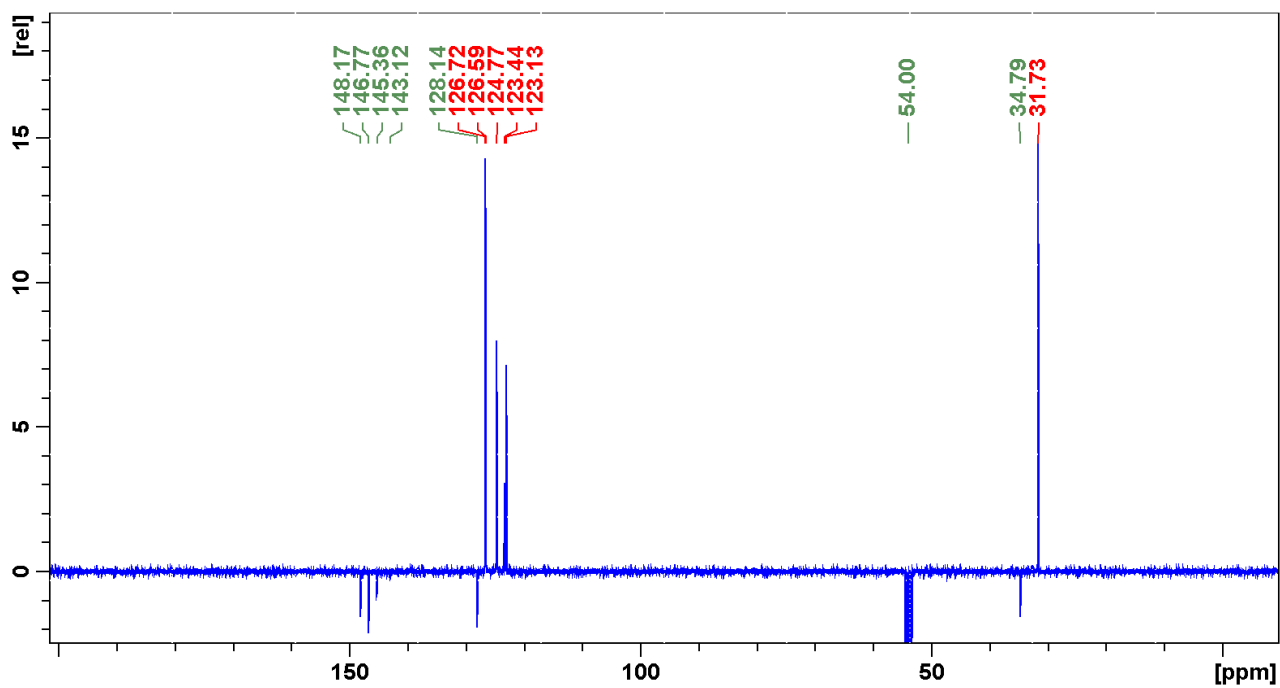


Figure S6. Carbon NMR spectrum of compound 3c.

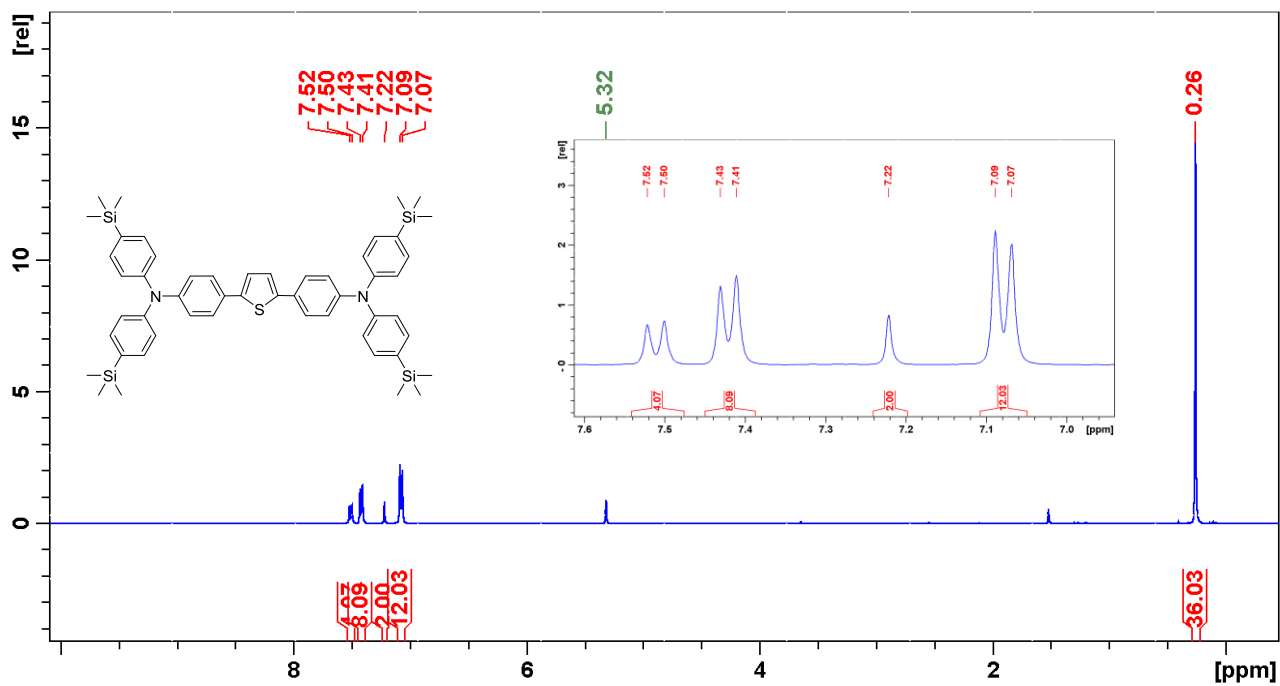


Figure S7. Proton NMR spectrum of compound **3d**.

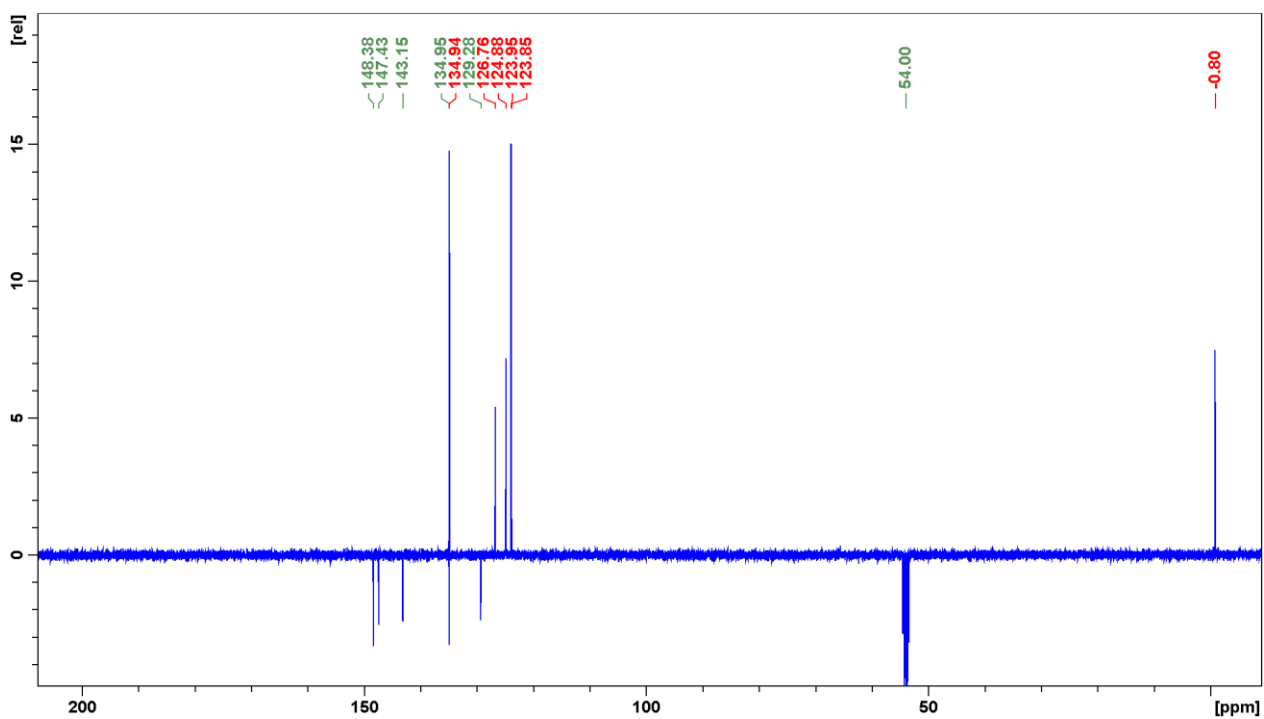


Figure S8. Carbon NMR spectrum of compound **3d**.

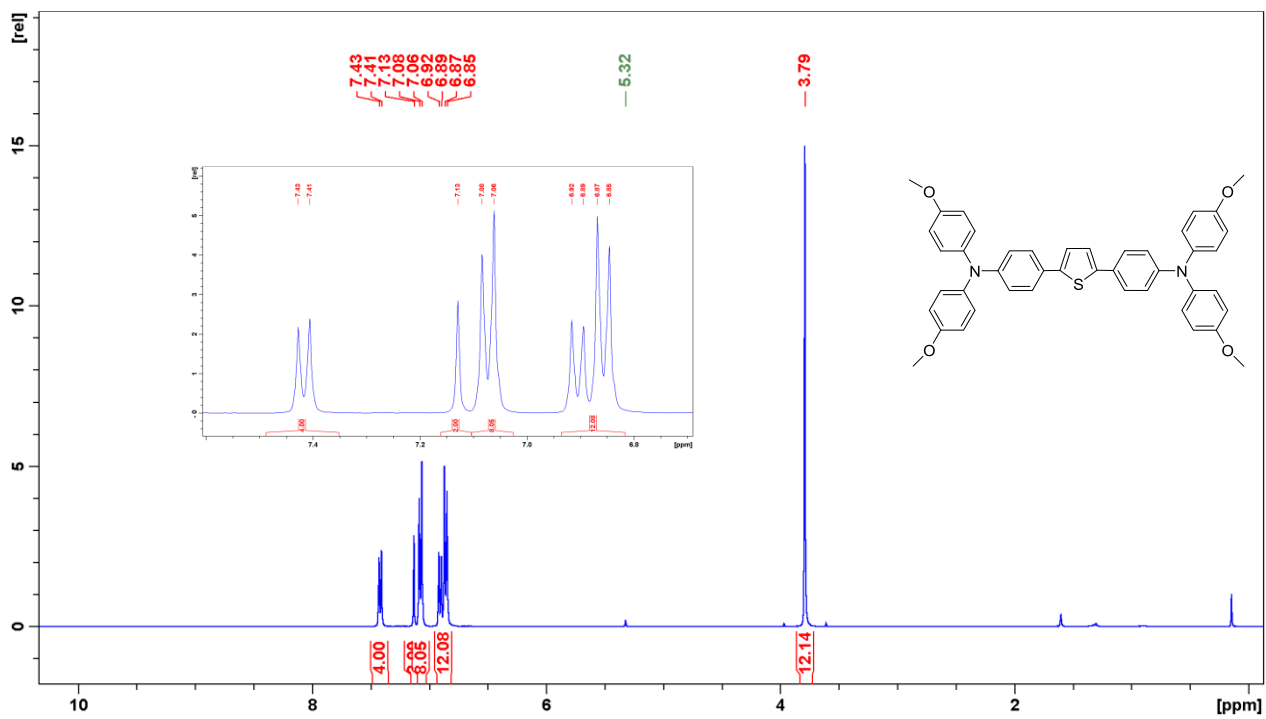


Figure S9. Proton NMR spectrum of compound **3e**.

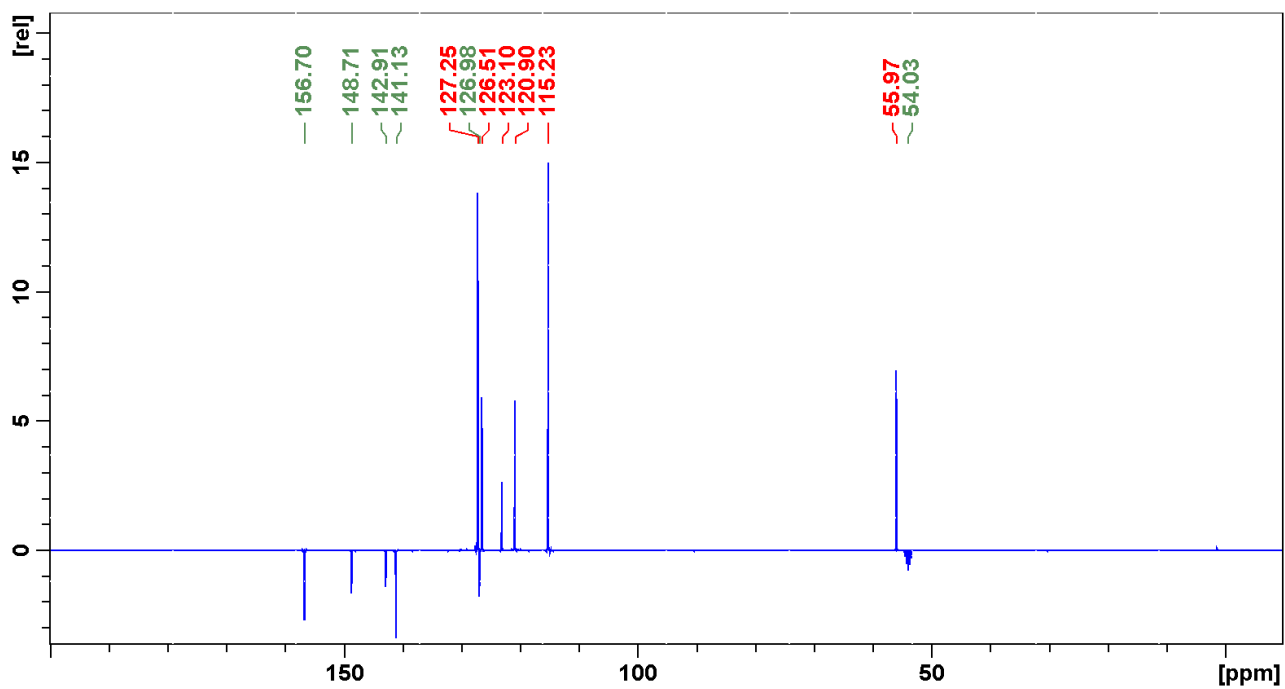


Figure S10. Carbon NMR spectrum of compound **3e**.

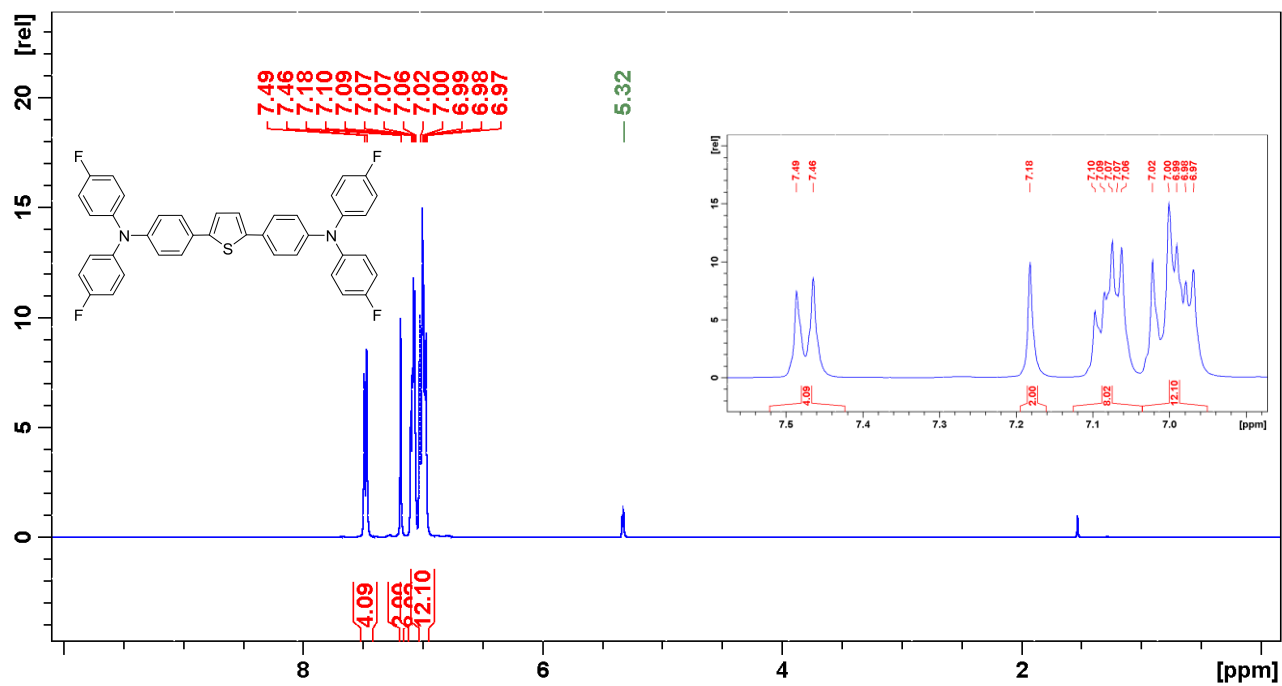


Figure S11. Proton NMR spectrum of compound **3f**.

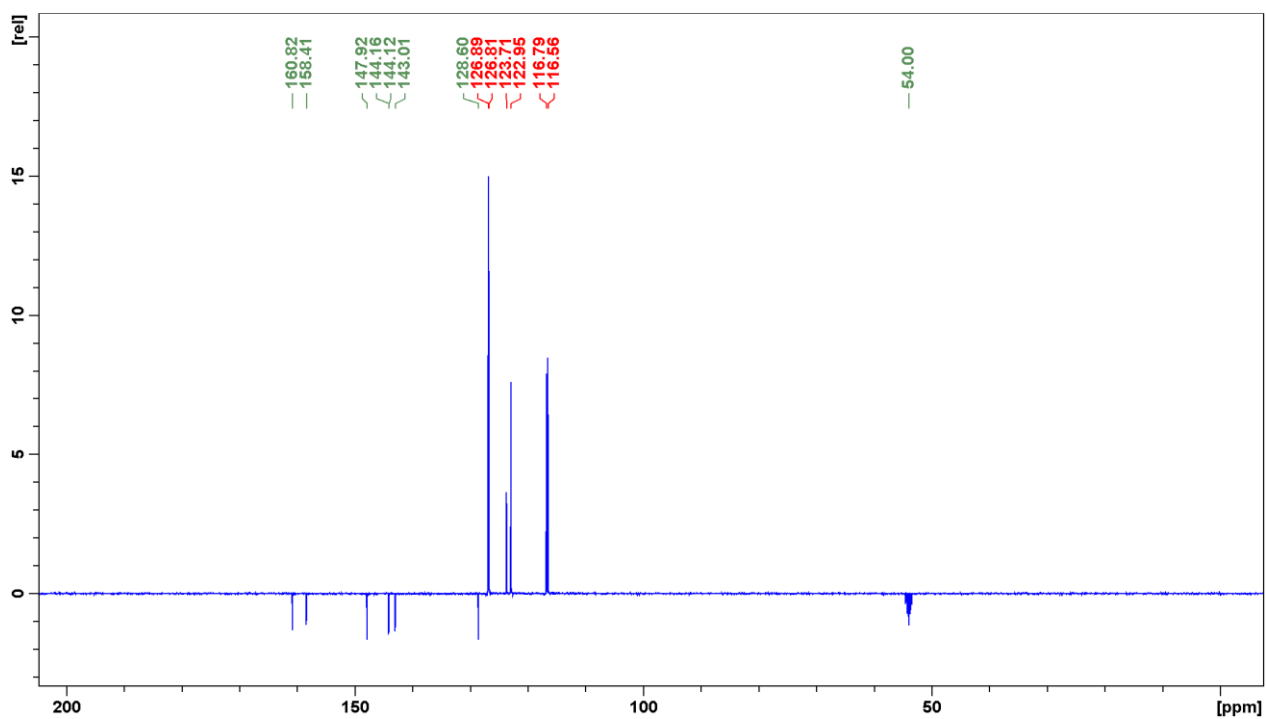


Figure S12. Carbon NMR spectrum of compound **3f**.

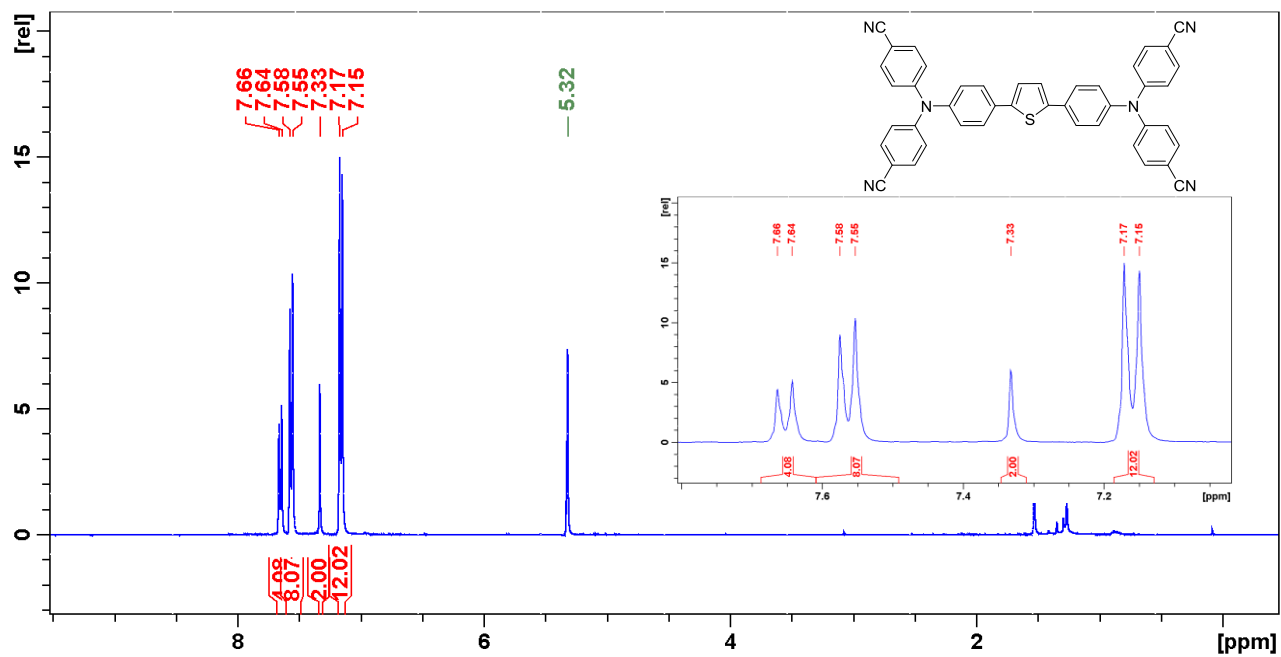


Figure S13. Proton NMR spectrum of compound **3g**.

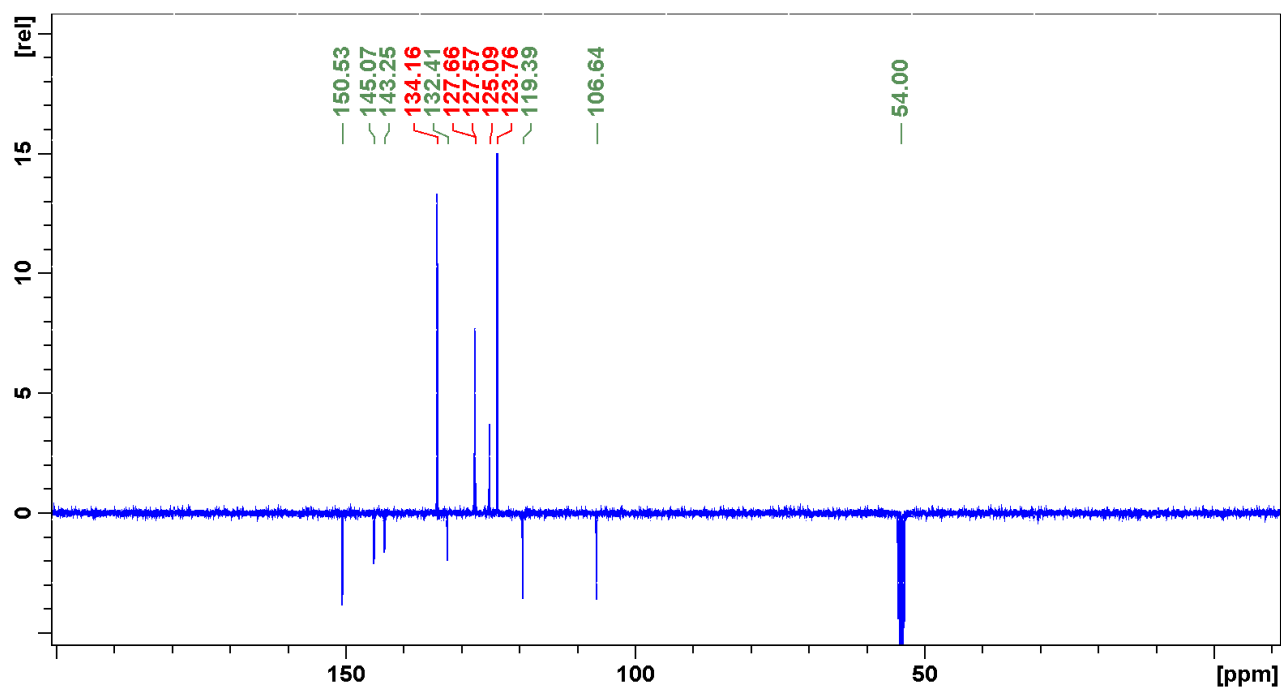


Figure S14. Carbon NMR spectrum of compound **3g**.

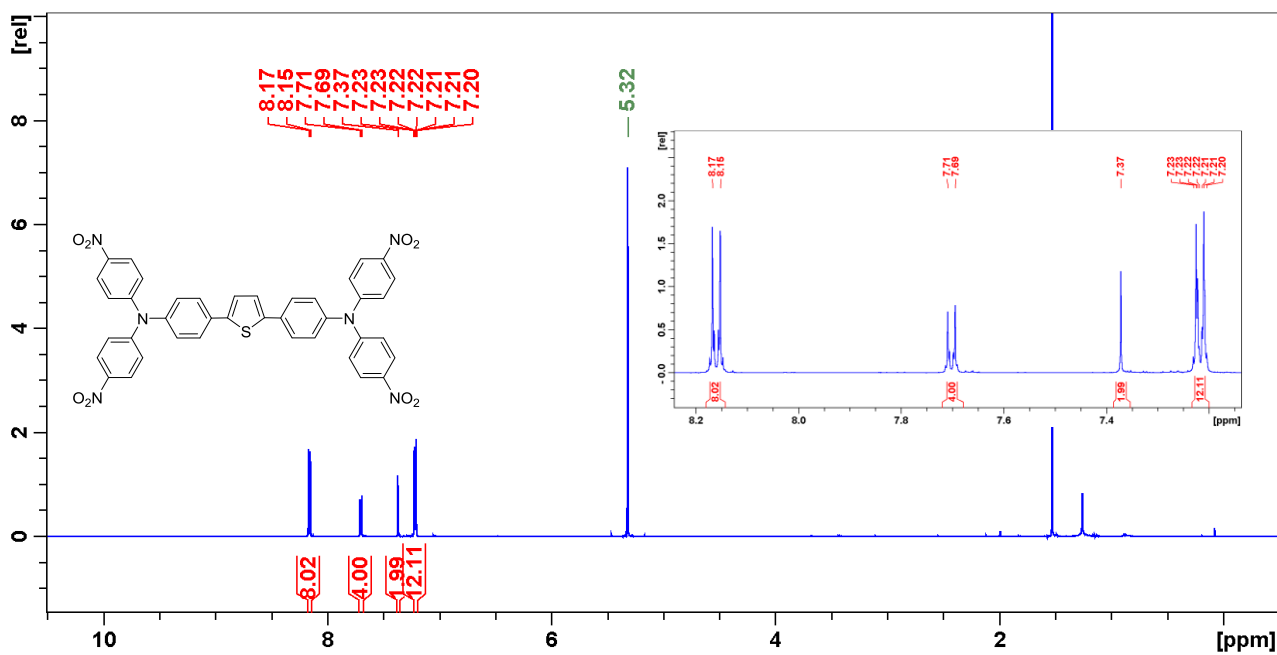


Figure S15. Proton NMR spectrum of compound **3h**.

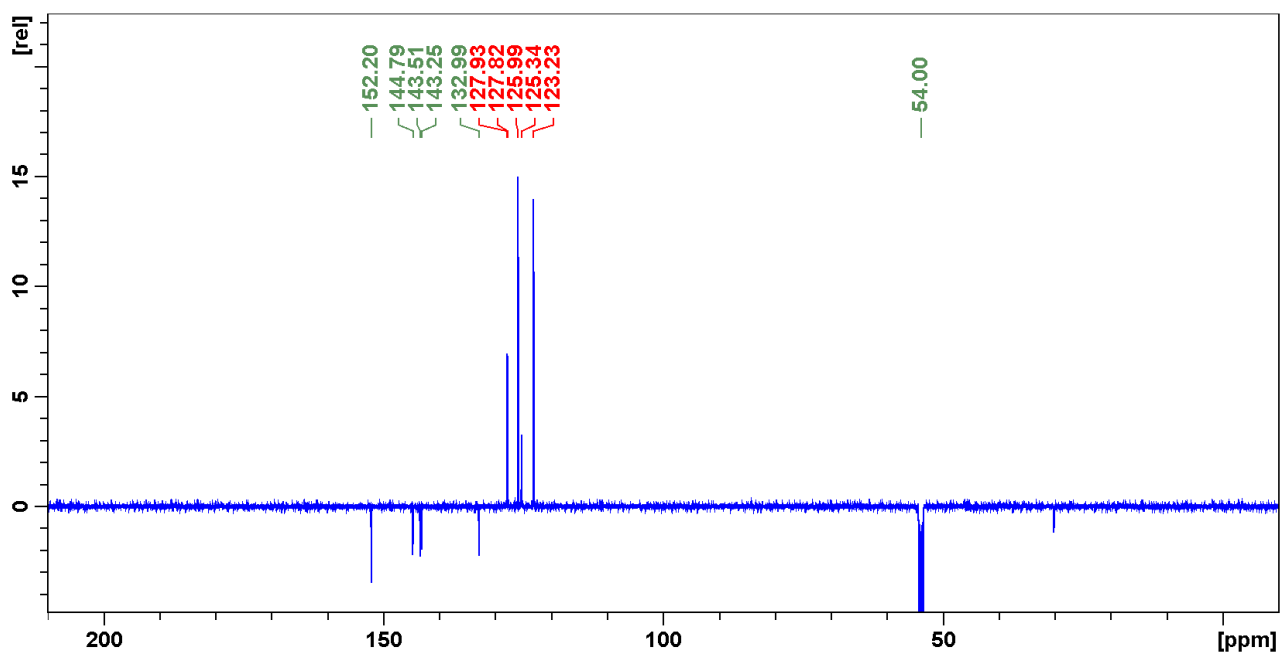


Figure S16. Carbon NMR spectrum of compound **3h**.

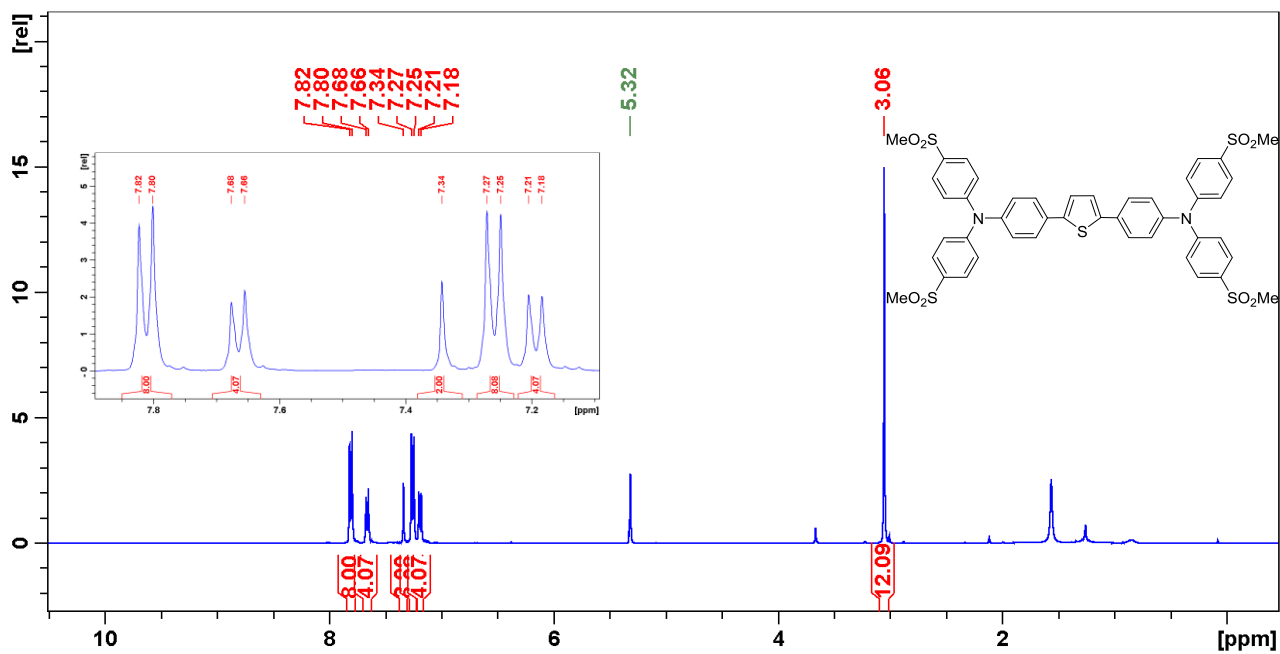


Figure S17. Proton NMR spectrum of compound 3i.

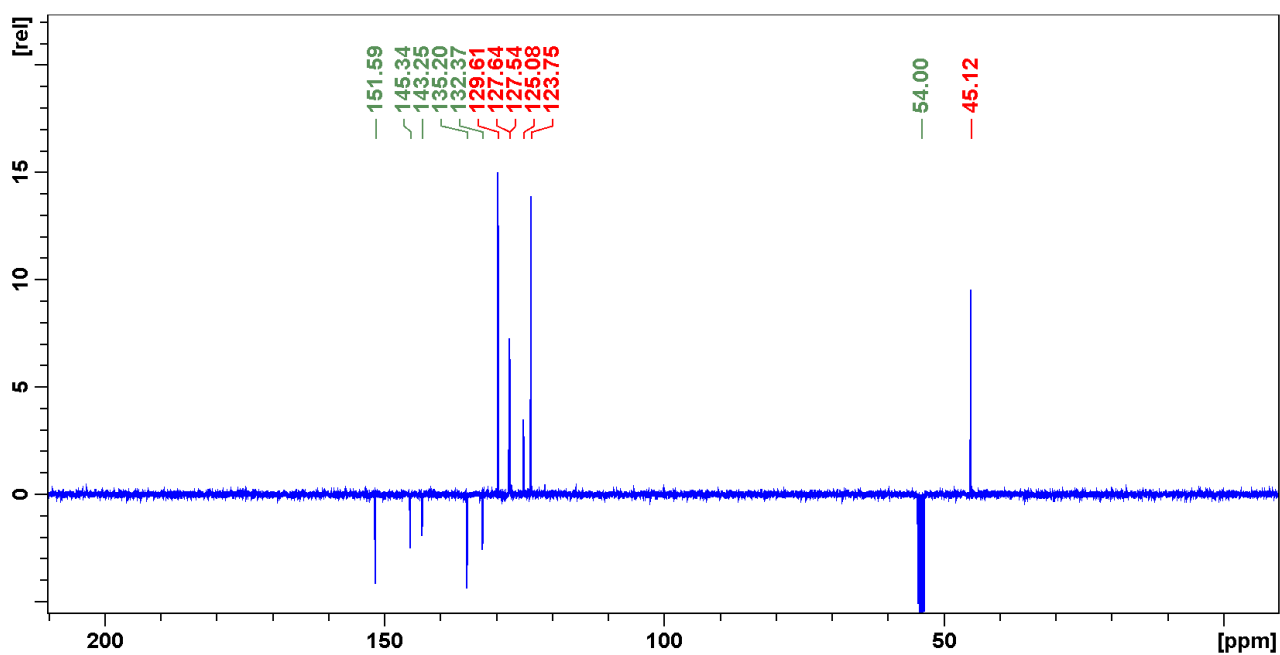


Figure S18. Carbon NMR spectrum of compound 3i.

B)2PA Screening Tests

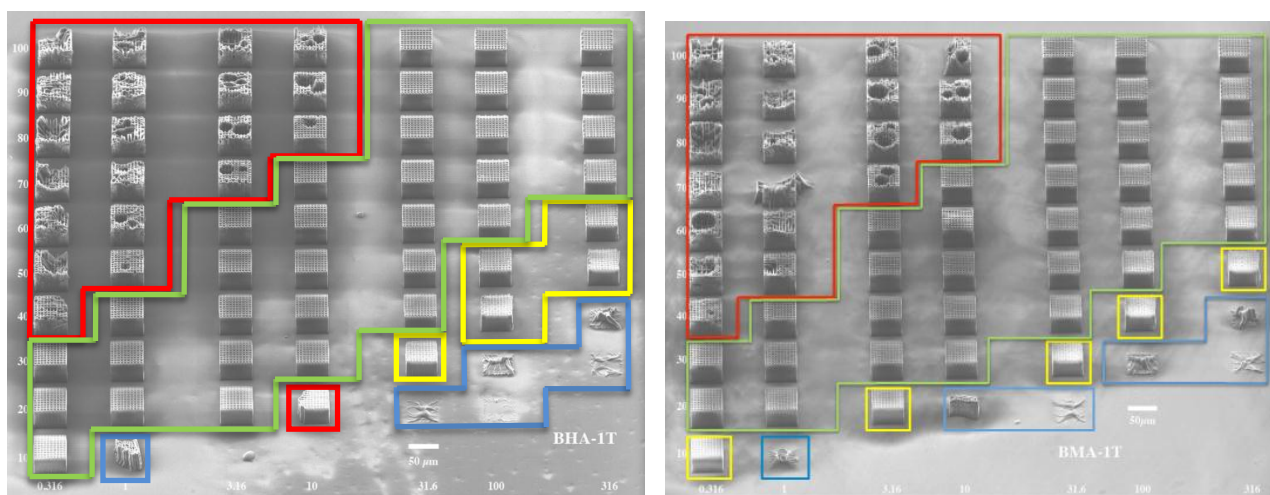


Figure S19. 2PIP structuring test of **3a** (left) and **3b** (right).

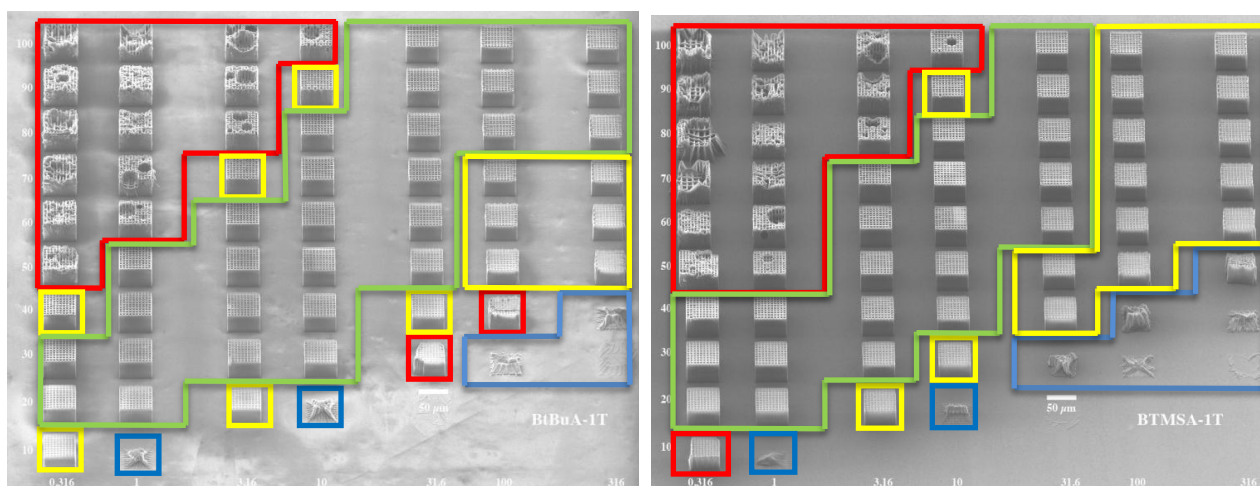


Figure S20. 2PIP structuring test of **3c** (left) and **3d** (right).

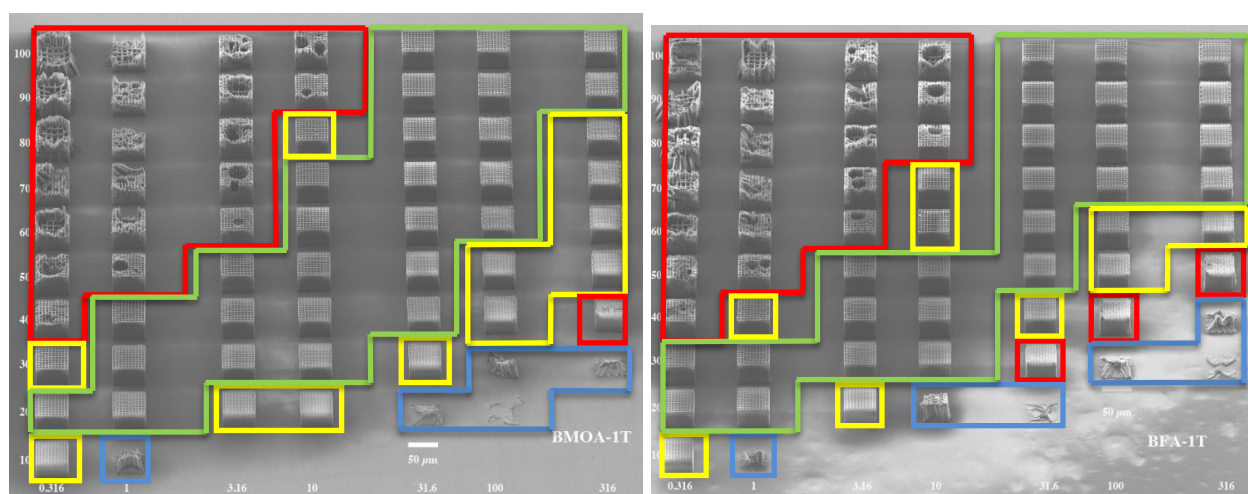


Figure S21. 2PIP structuring test of **3e** (left) and **3f** (right).

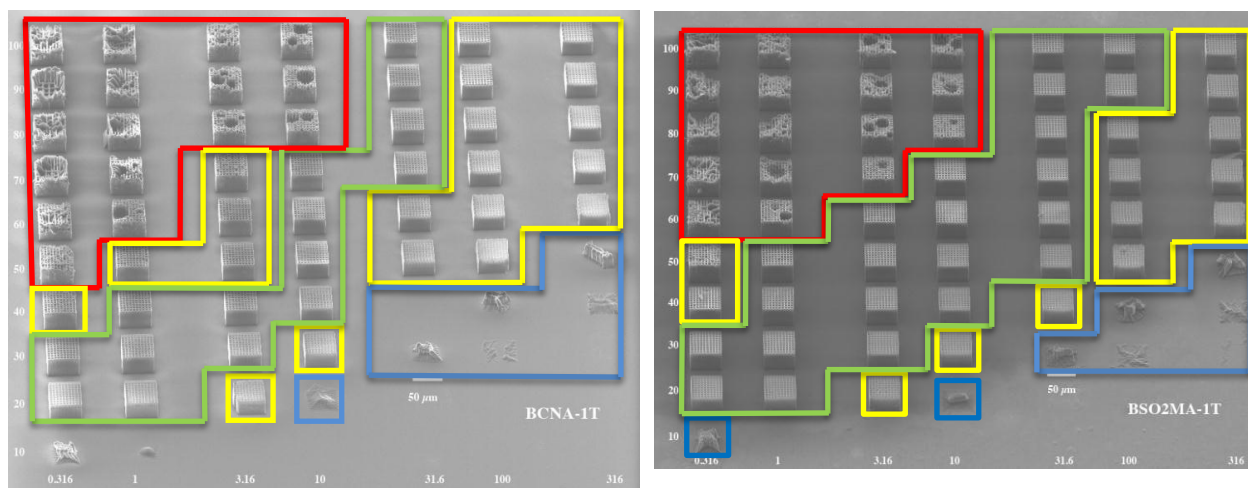


Figure S22. 2PIP structuring test of **3g** (left) and **3h** (right).

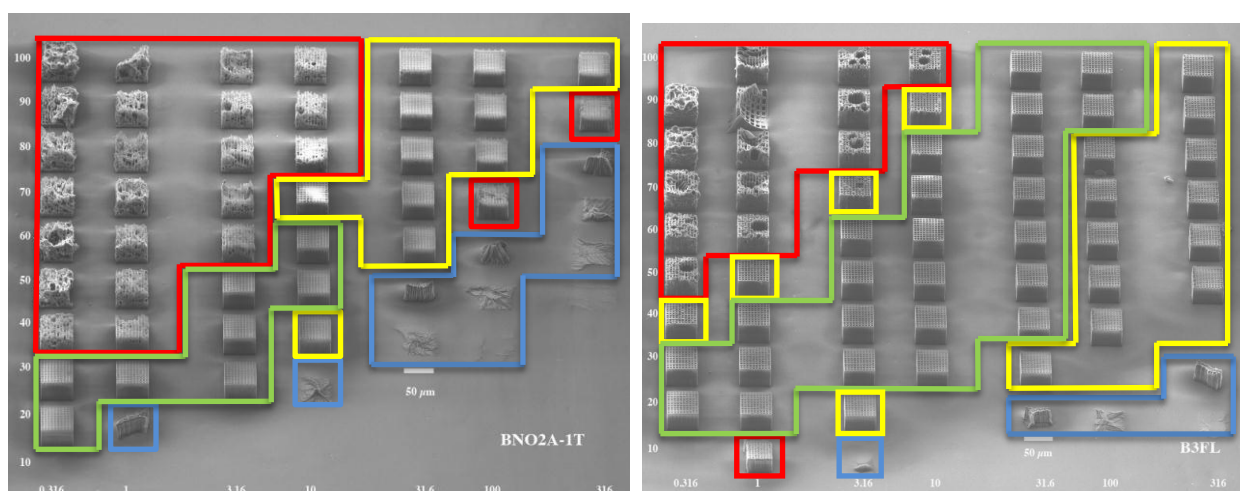


Figure S23. 2PIP structuring test of **3i** (left) and **B3FL** (right).

Manuscript # 10

Supporting Information

Synthesis and Characterization of Triphenylamine-based Two-Photon Initiators

Markus Lunzer,^{a,c} Brigitte Holzer,^{a,} Arnulf Rosspeintner,^c Maximilian Tromayer,^{a,b} Daniel Lumpi,^a Ernst Horkel,^a Christian Hametner,^a Eric Vauthey,^c Robert Liska^a and Johannes Fröhlich^a*

^aInstitute of Applied Synthetic Chemistry, Vienna University of Technology,

Getreidemarkt 9/163OC, A-1060 Vienna, Austria

^bInstitute of Materials Science and Technology, Vienna University of Technology,

Favoritenstraße 9-11, A-1040 Vienna, Austria

^cPhysical Chemistry Department, University of Geneva,

Quai Ernest Ansermet 30, CH-1211 Geneva, Switzerland

[*brigitte.holzer@tuwien.ac.at](mailto:brigitte.holzer@tuwien.ac.at)

A) NMR Spectra

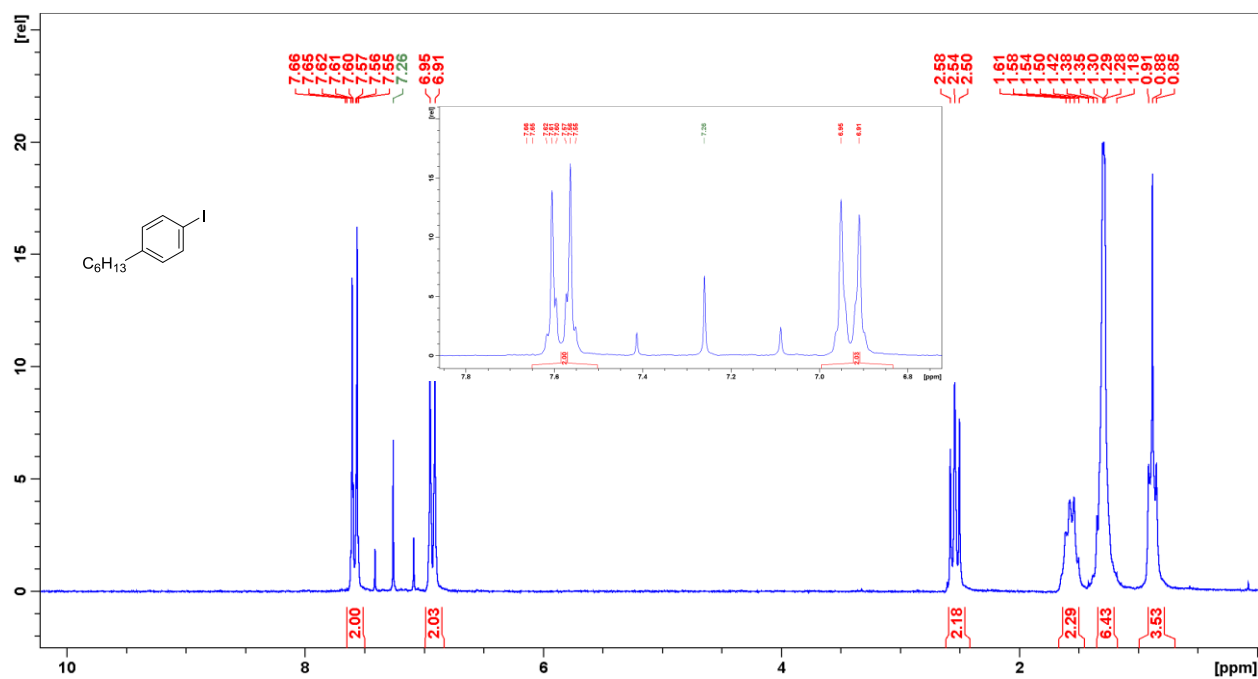


Figure S1. Proton NMR spectrum of compound 2.

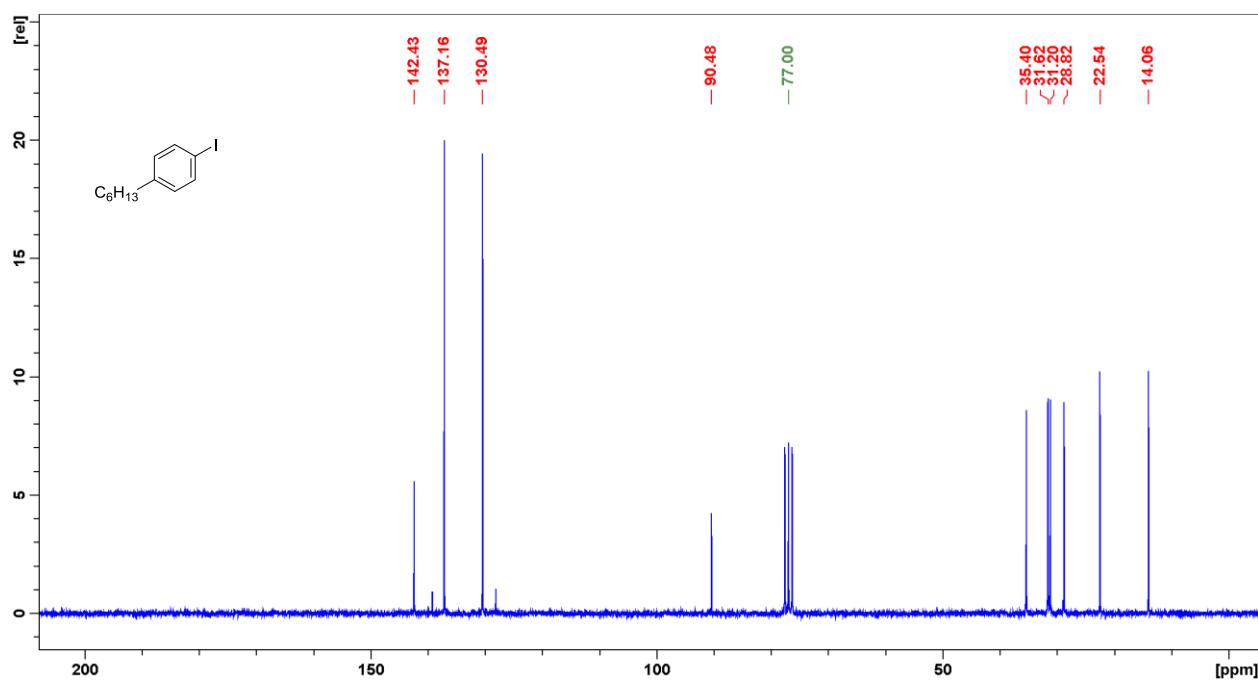


Figure S2. Carbon NMR spectrum of compound 2.

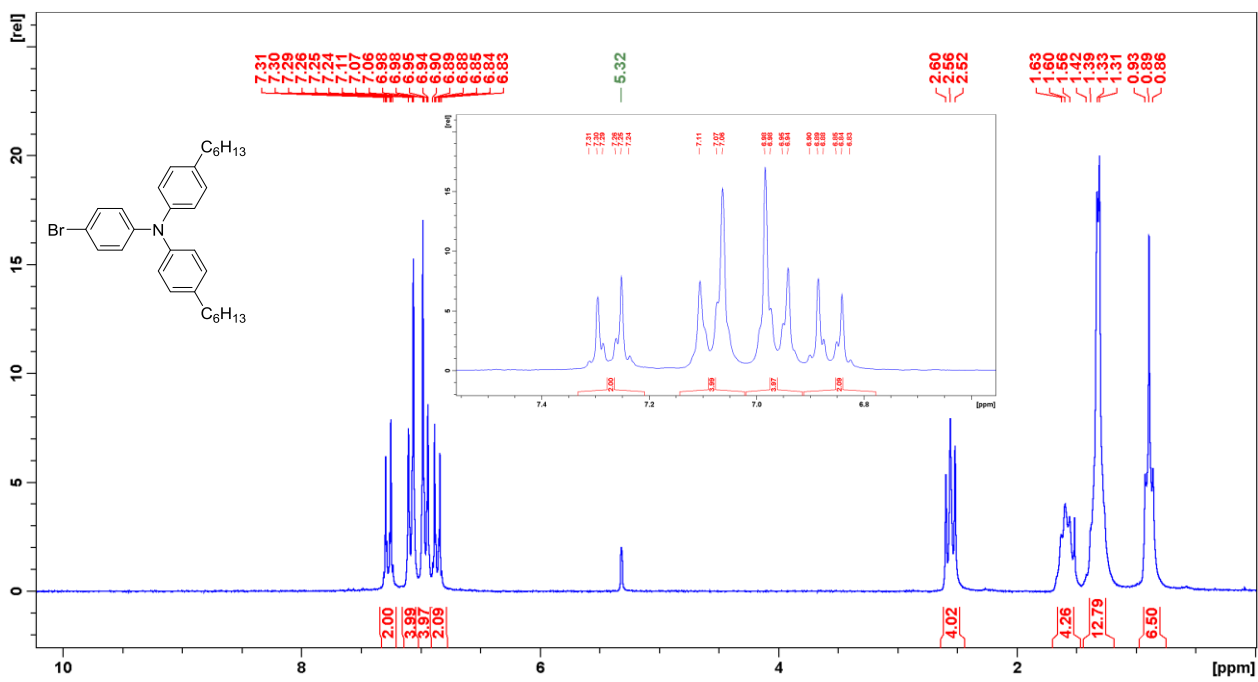


Figure S3. Proton NMR spectrum of compound 4.

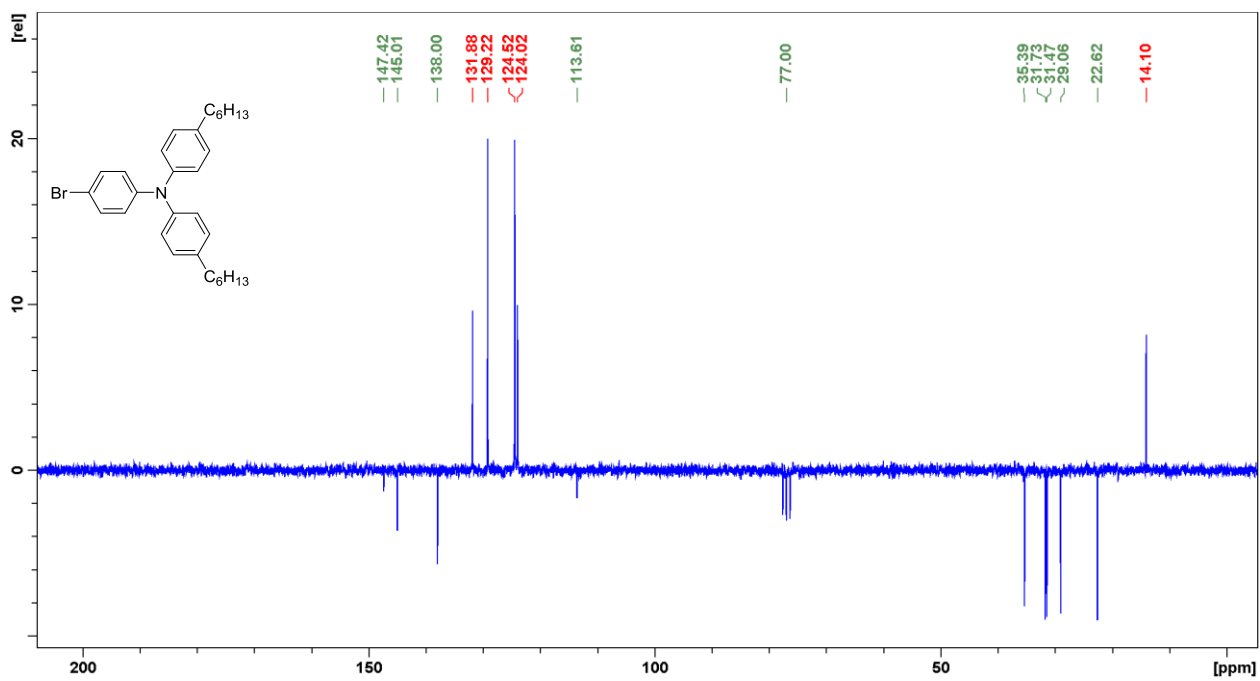


Figure S4. Carbon NMR spectrum of compound 4.

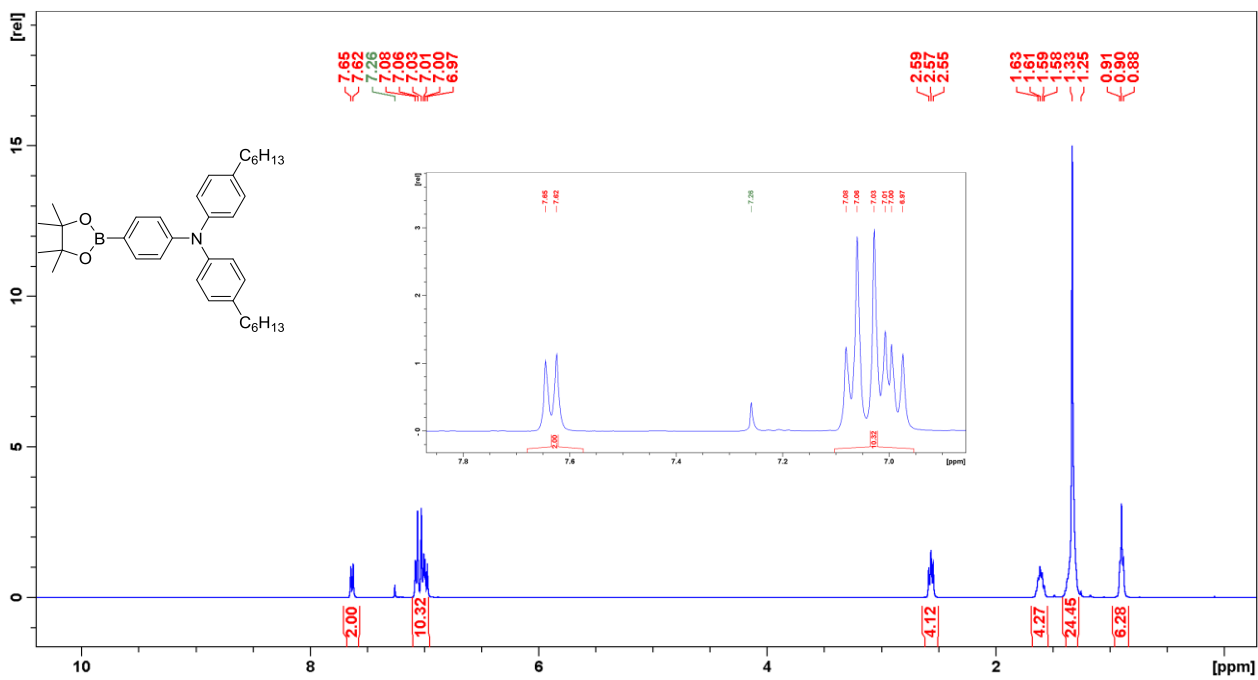


Figure S5. Proton NMR spectrum of compound 5.

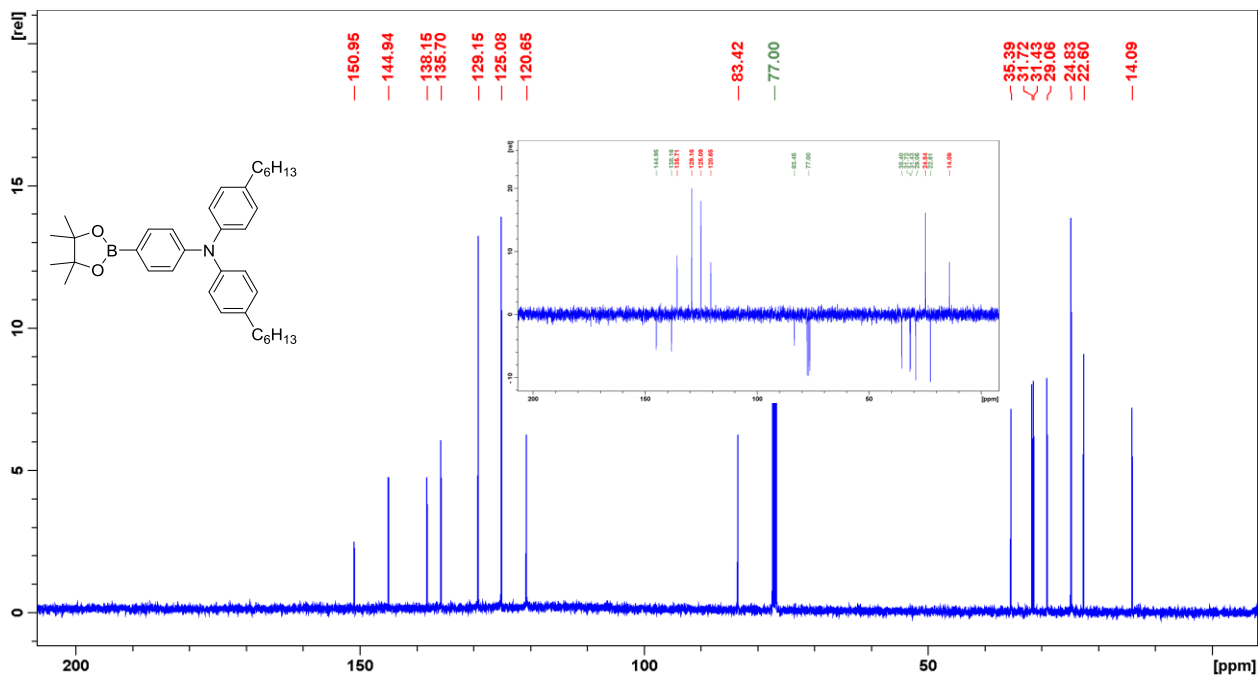


Figure S6. Carbon NMR spectrum of compound 5.

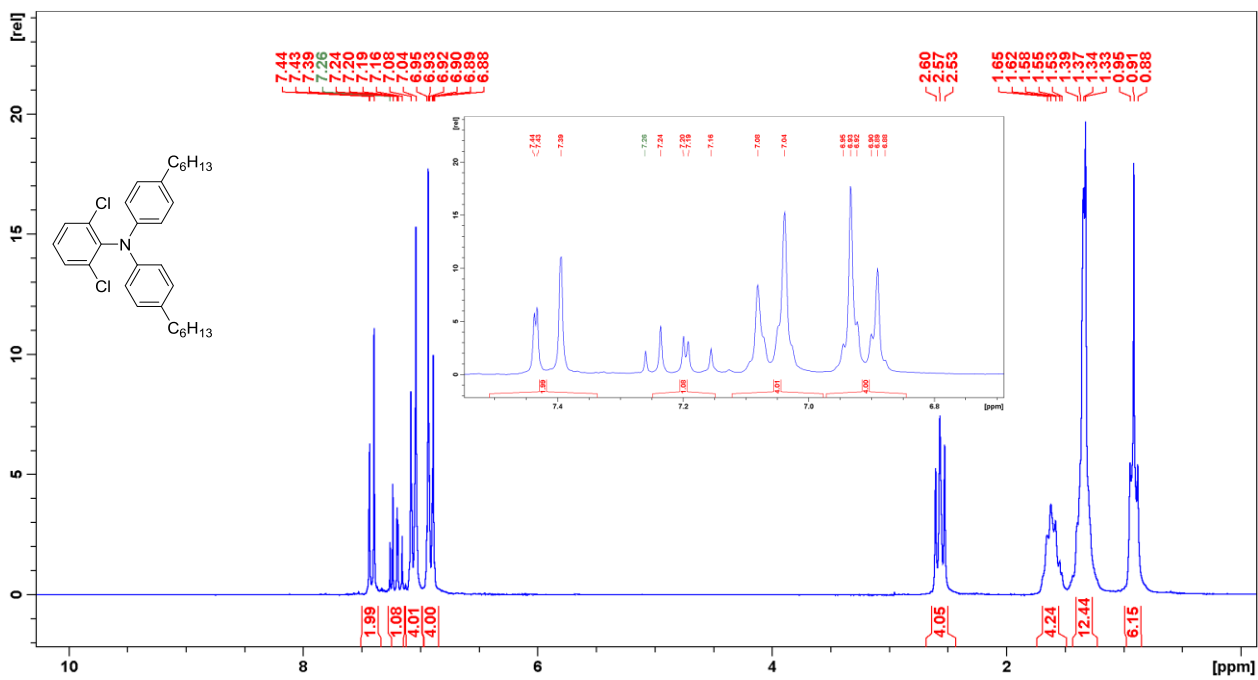


Figure S7. Proton NMR spectrum of compound 7.

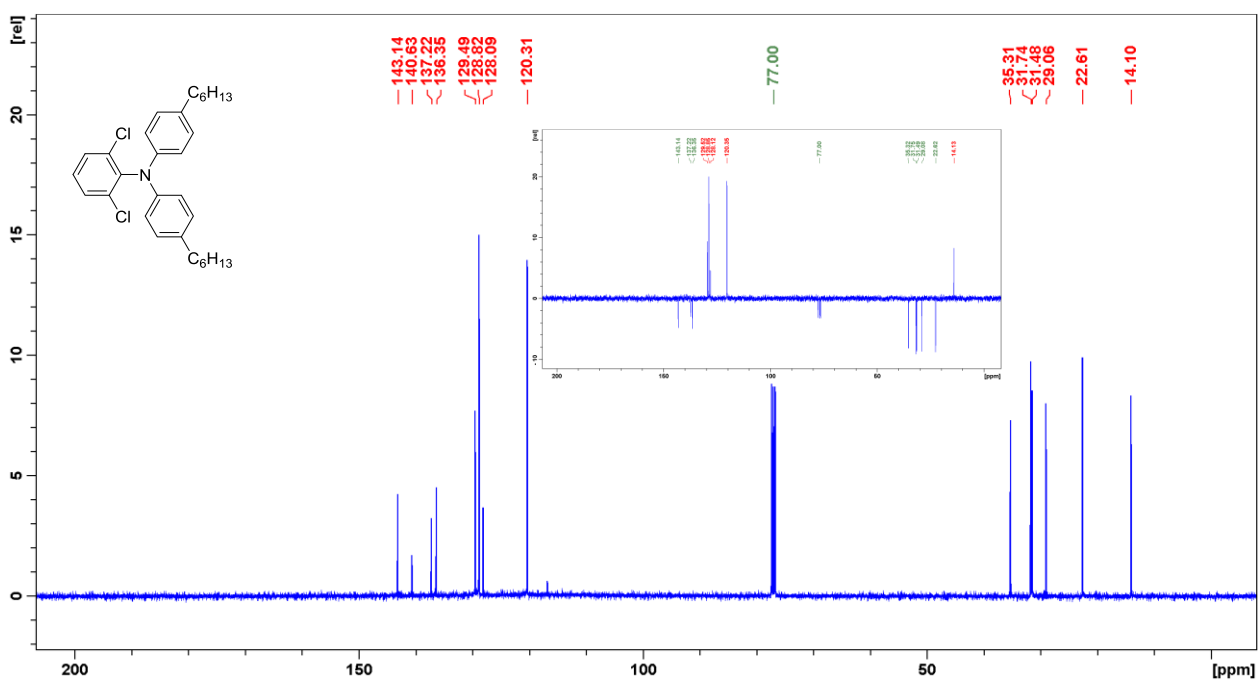


Figure S8. Carbon NMR spectrum of compound 7.

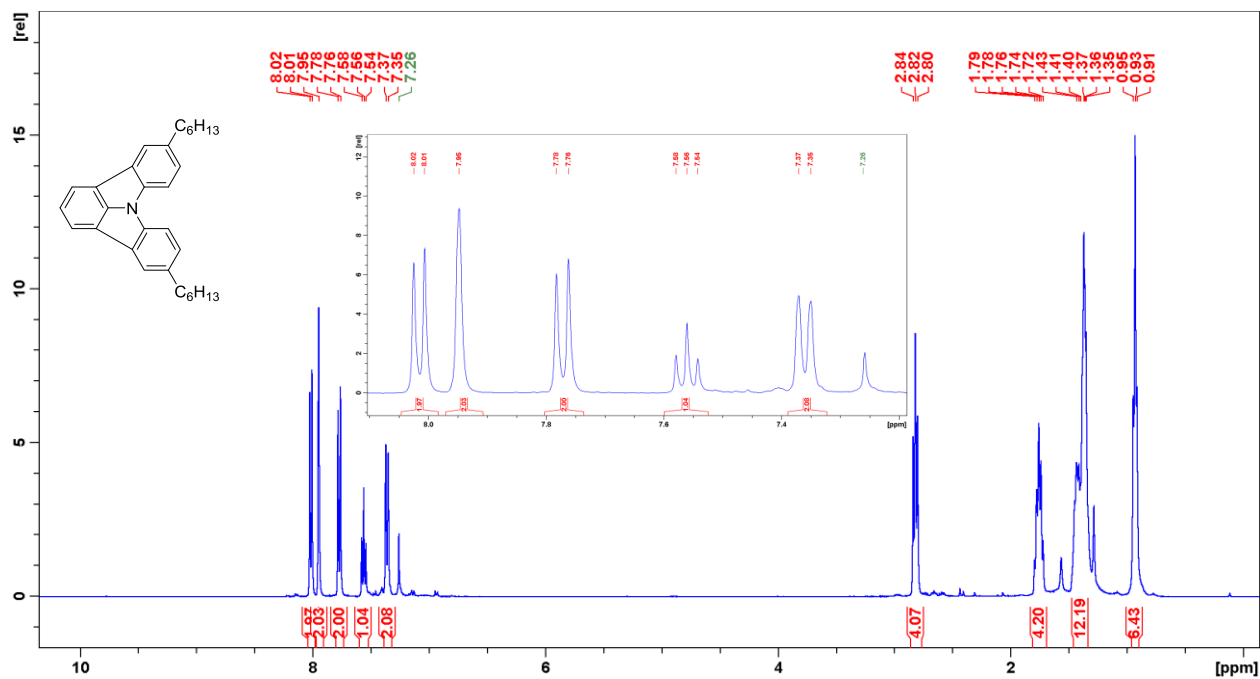


Figure S9. Proton NMR spectrum of compound 8.

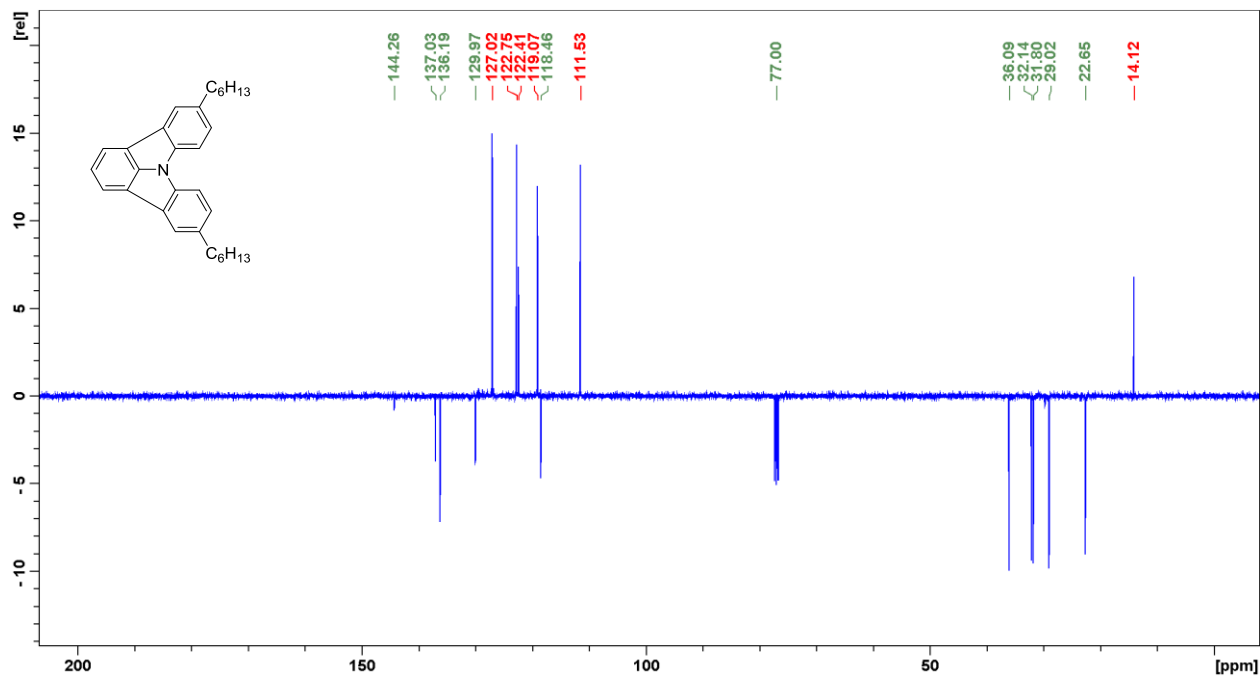


Figure S10. Carbon NMR spectrum of compound 8.

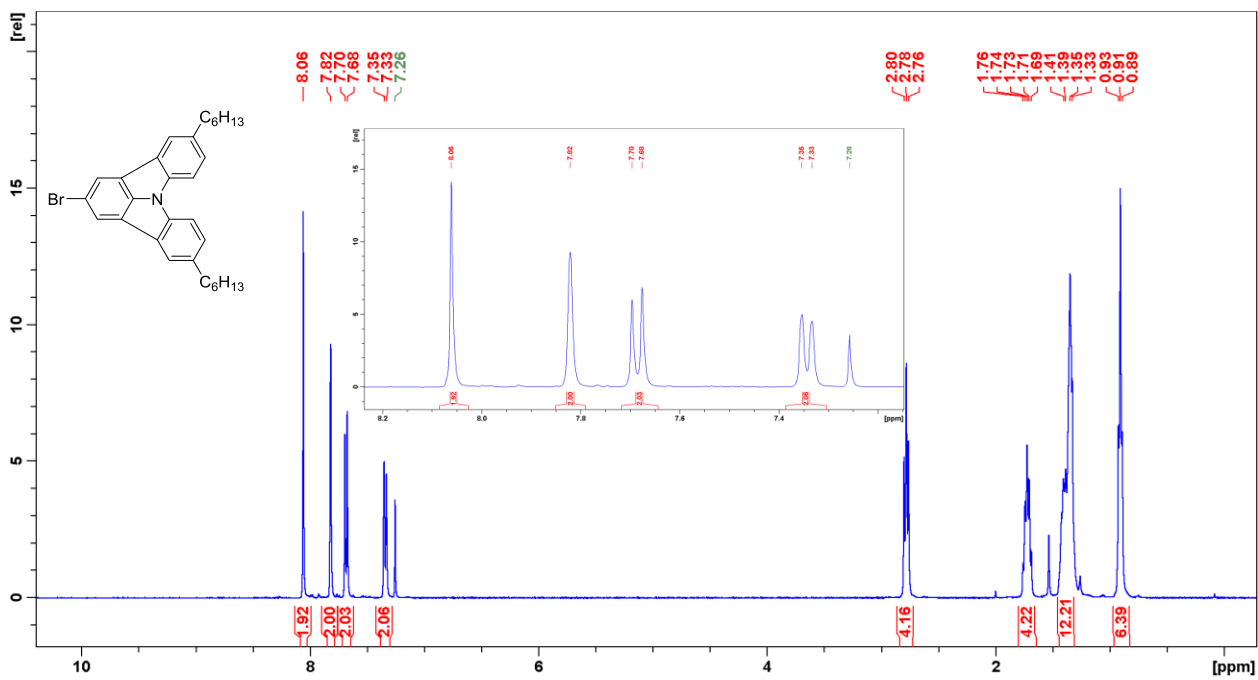


Figure S11. Proton NMR spectrum of compound 9.

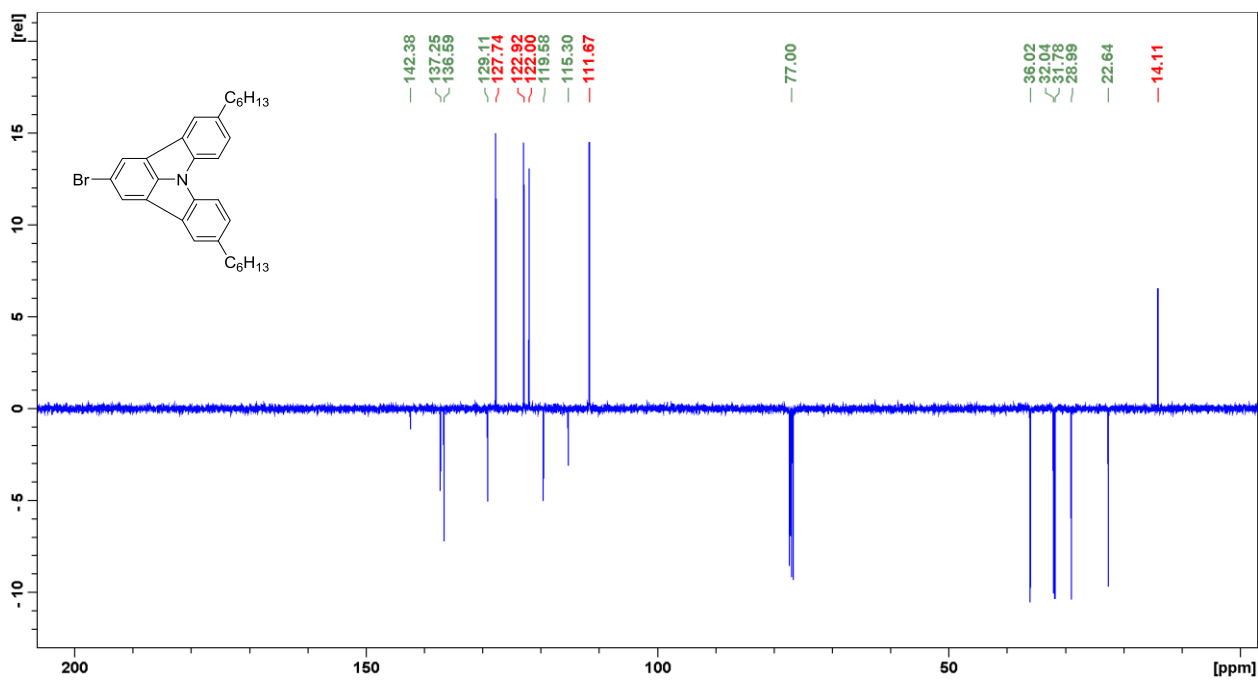


Figure S12. Carbon NMR spectrum of compound 9.

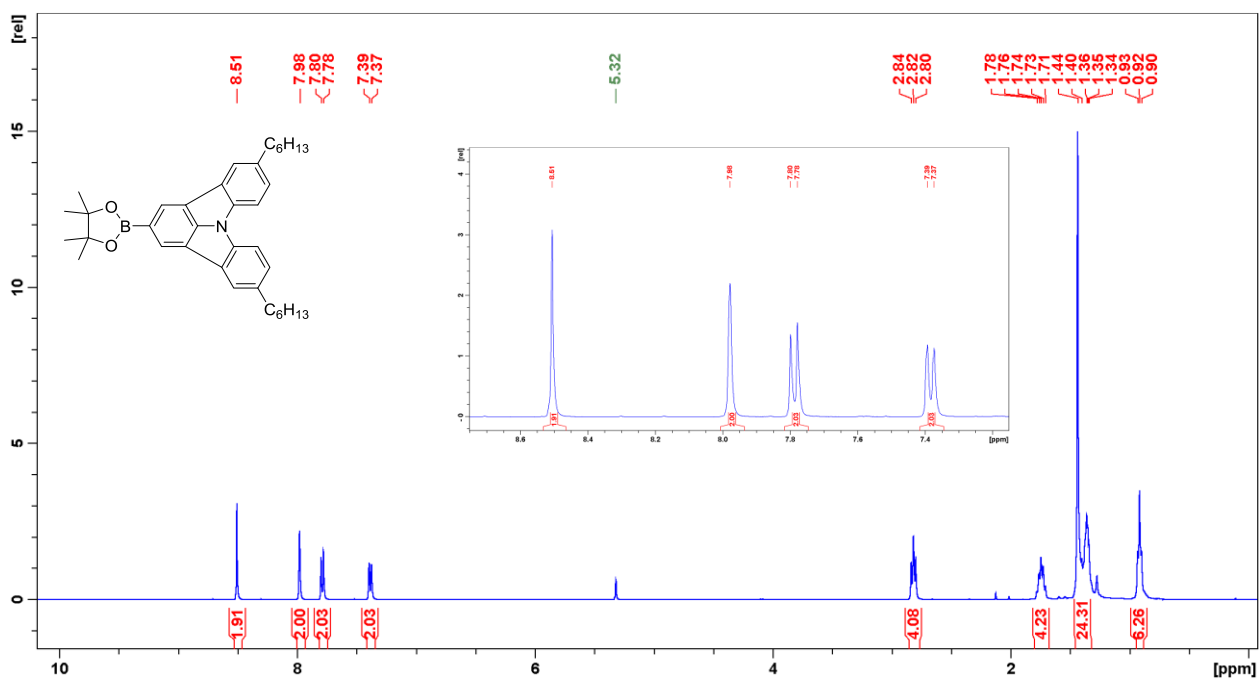


Figure S13. Proton NMR spectrum of compound 10.

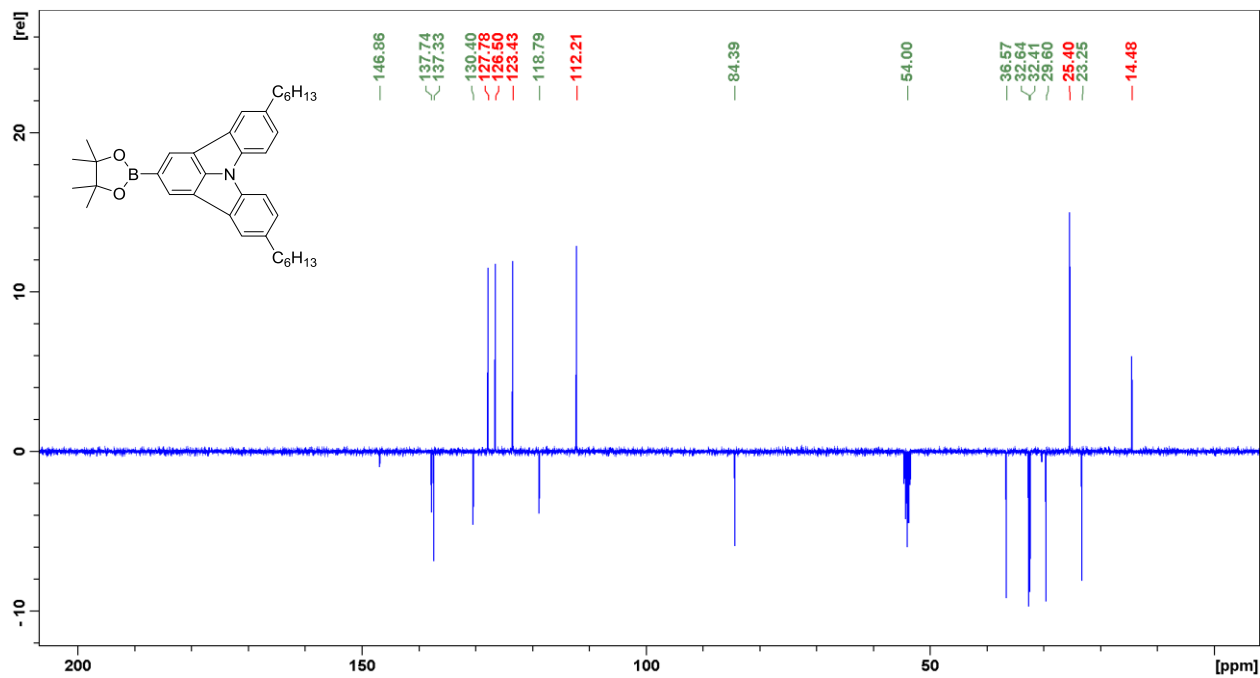


Figure S14. Carbon NMR spectrum of compound 10.

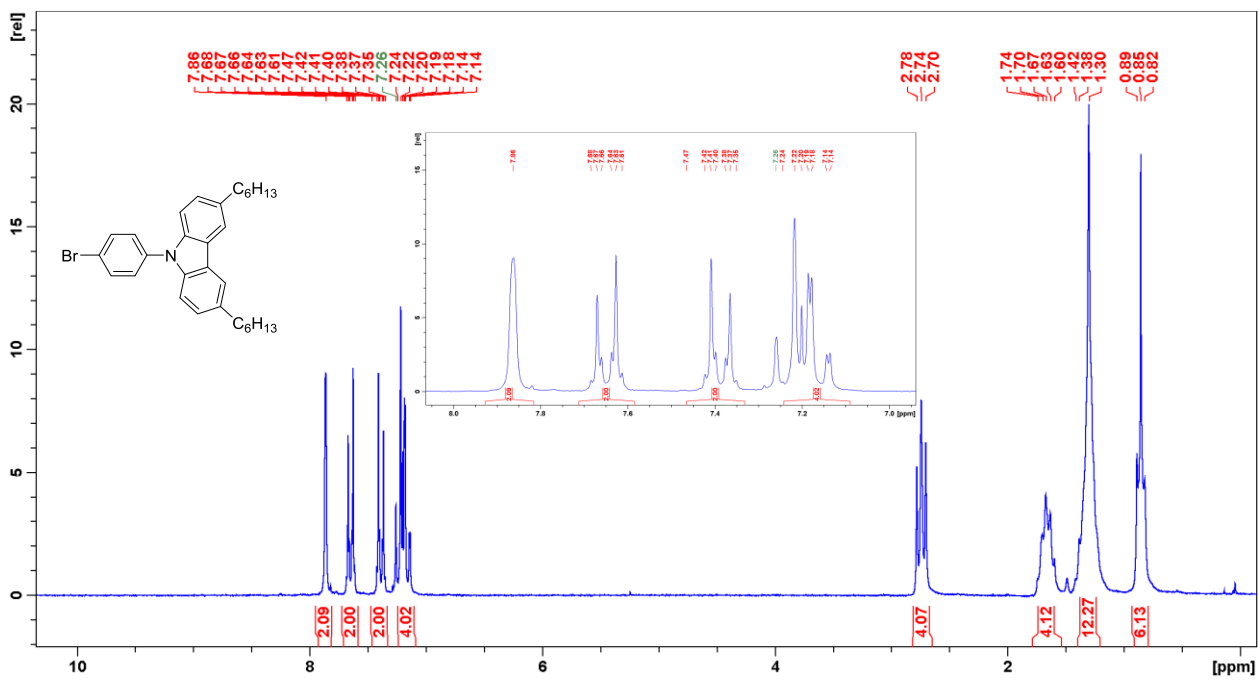


Figure S15. Proton NMR spectrum of compound 13.

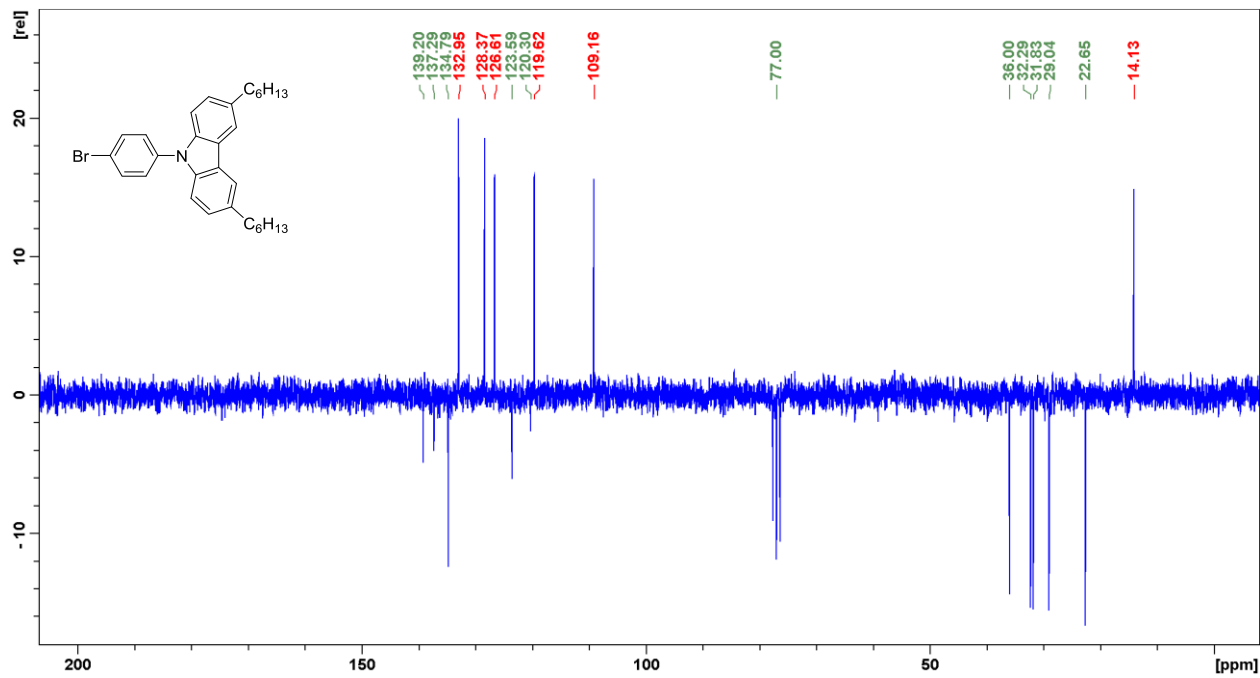


Figure S16. Carbon NMR spectrum of compound 13.

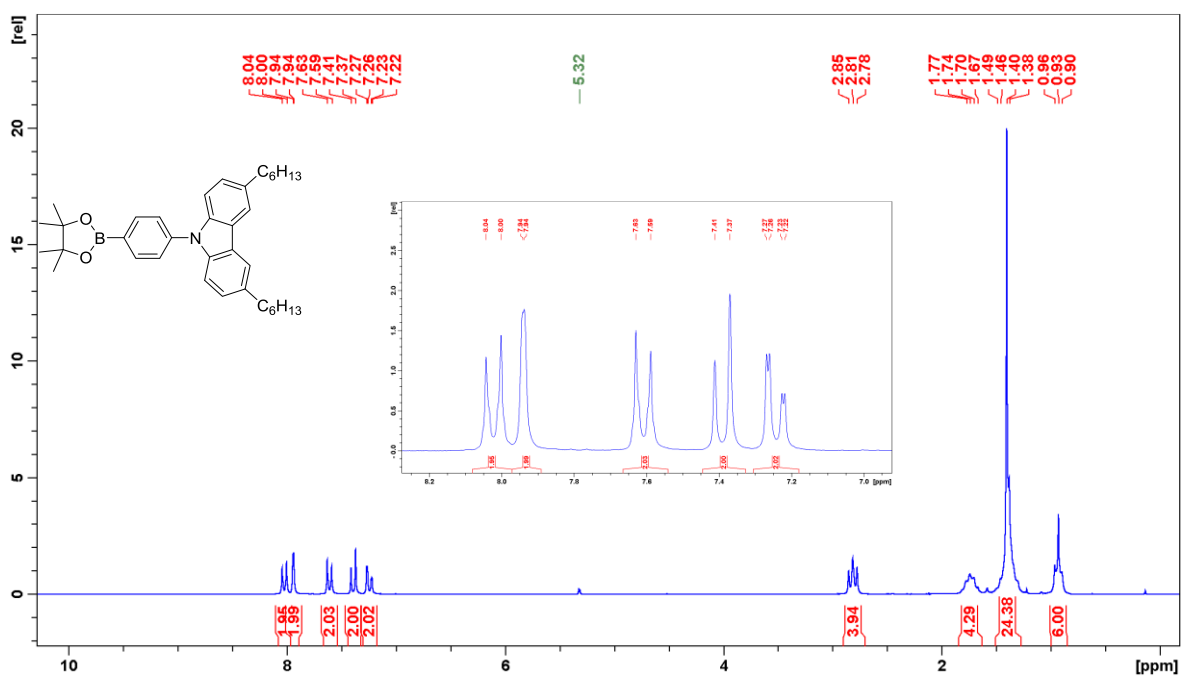


Figure S17. Proton NMR spectrum of compound 14.

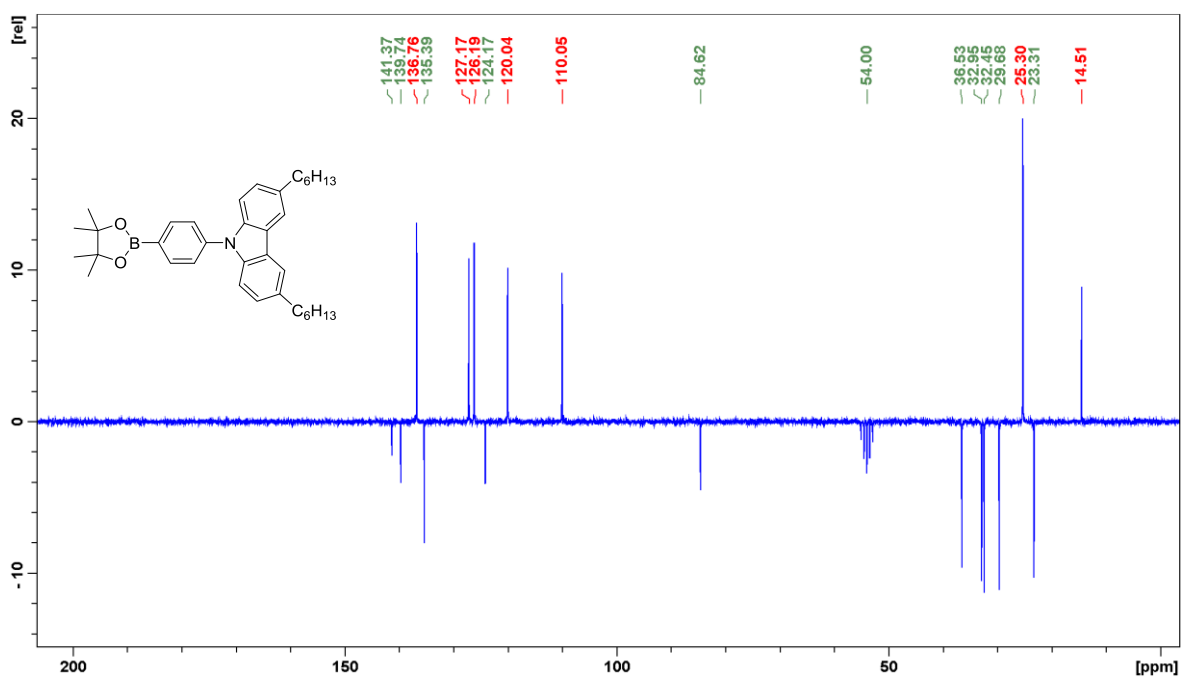


Figure S18. Carbon NMR spectrum of compound 14.

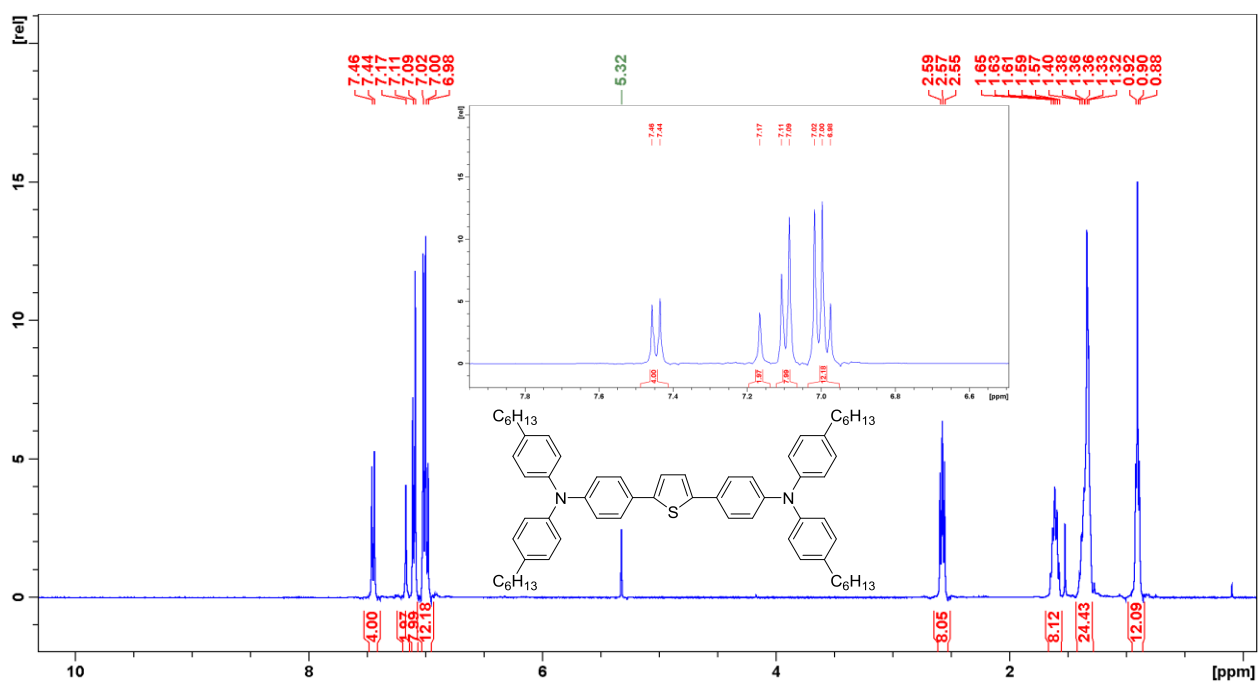


Figure S19. Proton NMR spectrum of compound **16**.

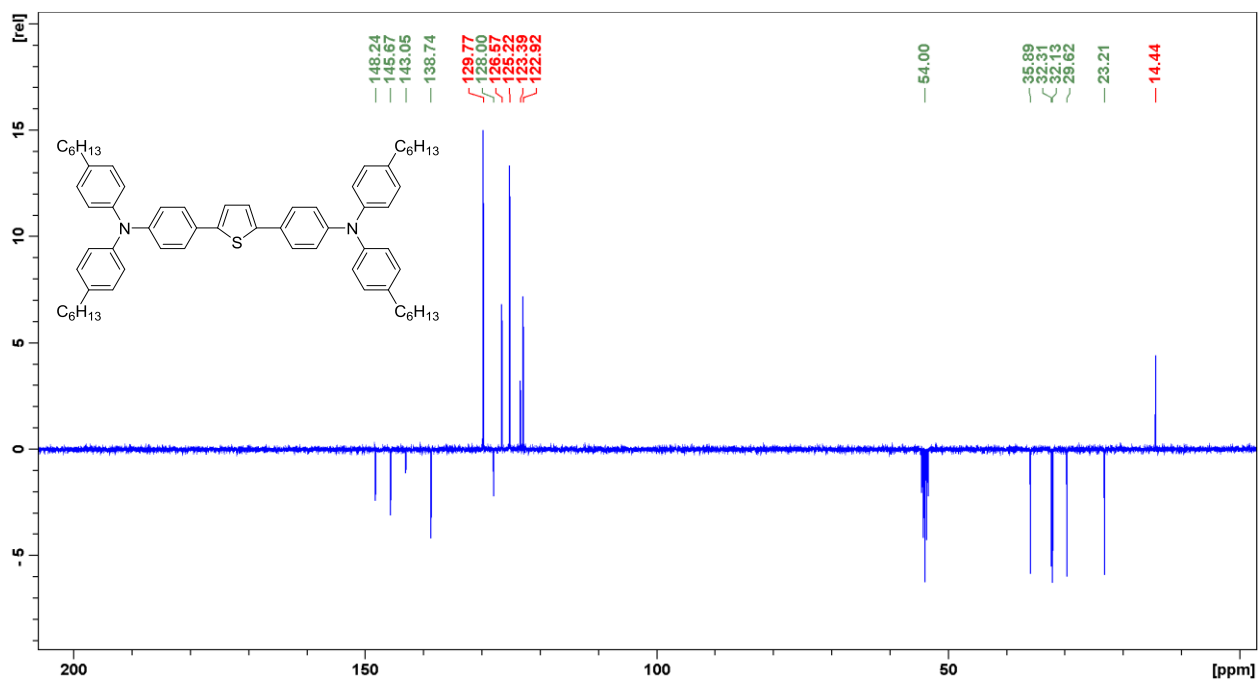


Figure S20. Carbon NMR spectrum of compound **16**.

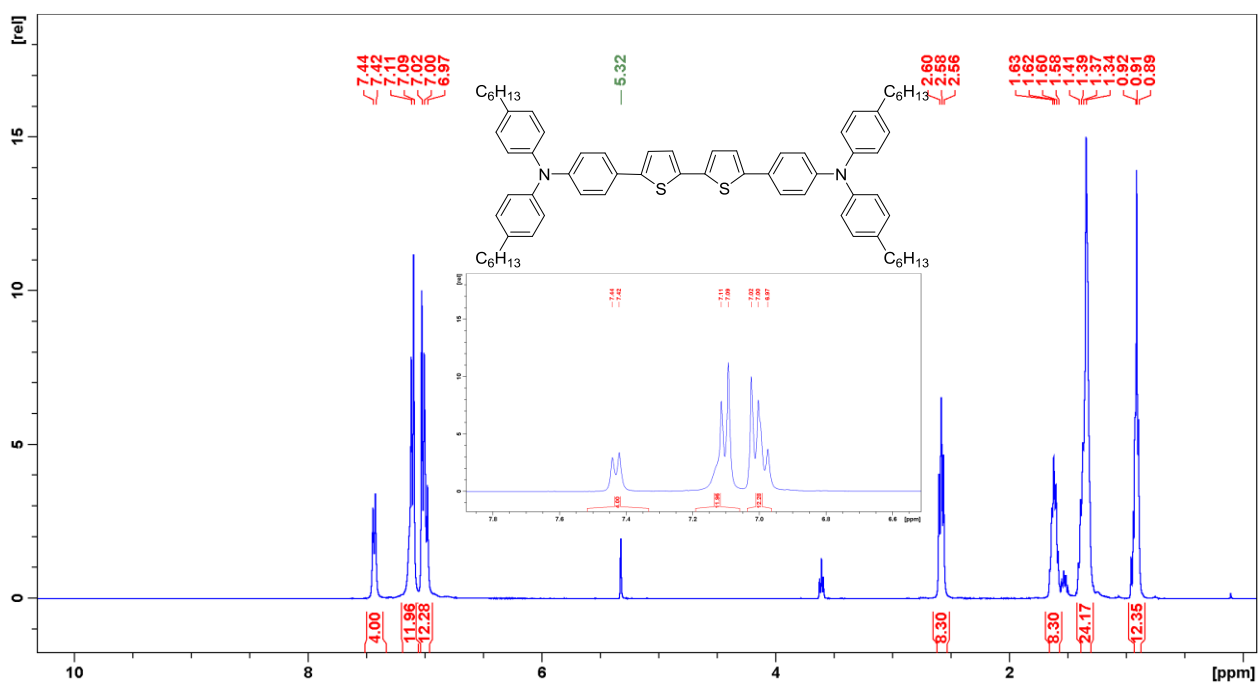


Figure S21. Proton NMR spectrum of compound 18.

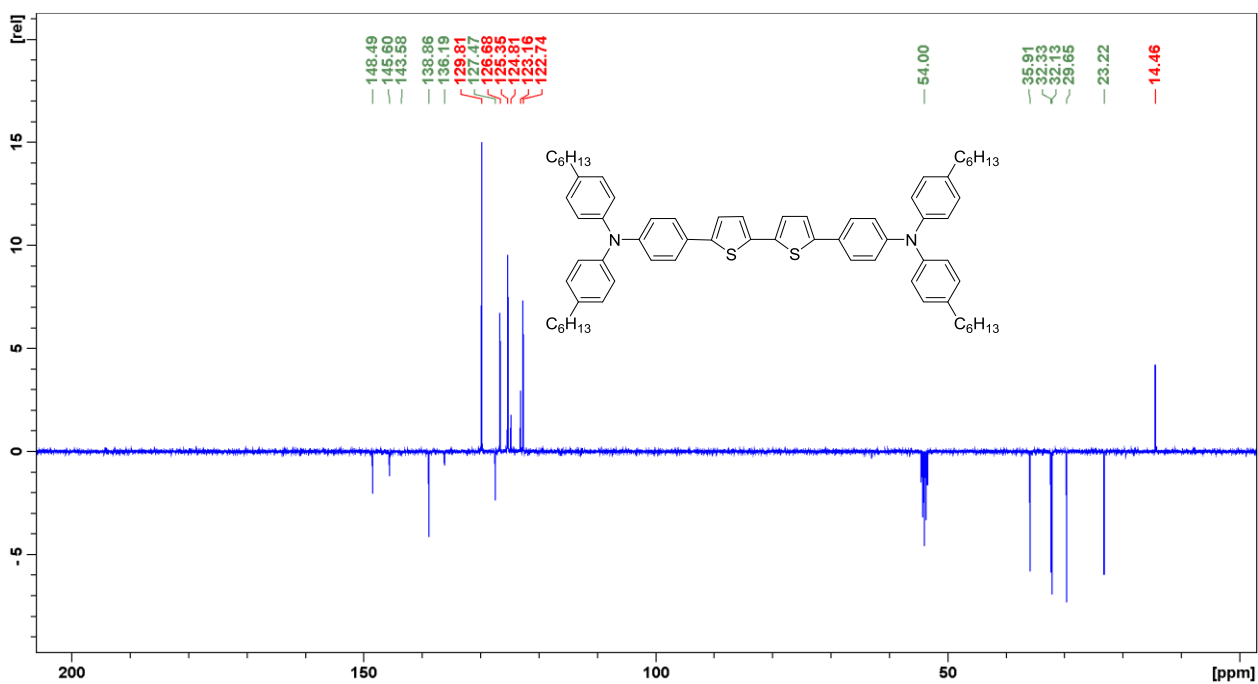


Figure S22. Carbon NMR spectrum of compound 18.

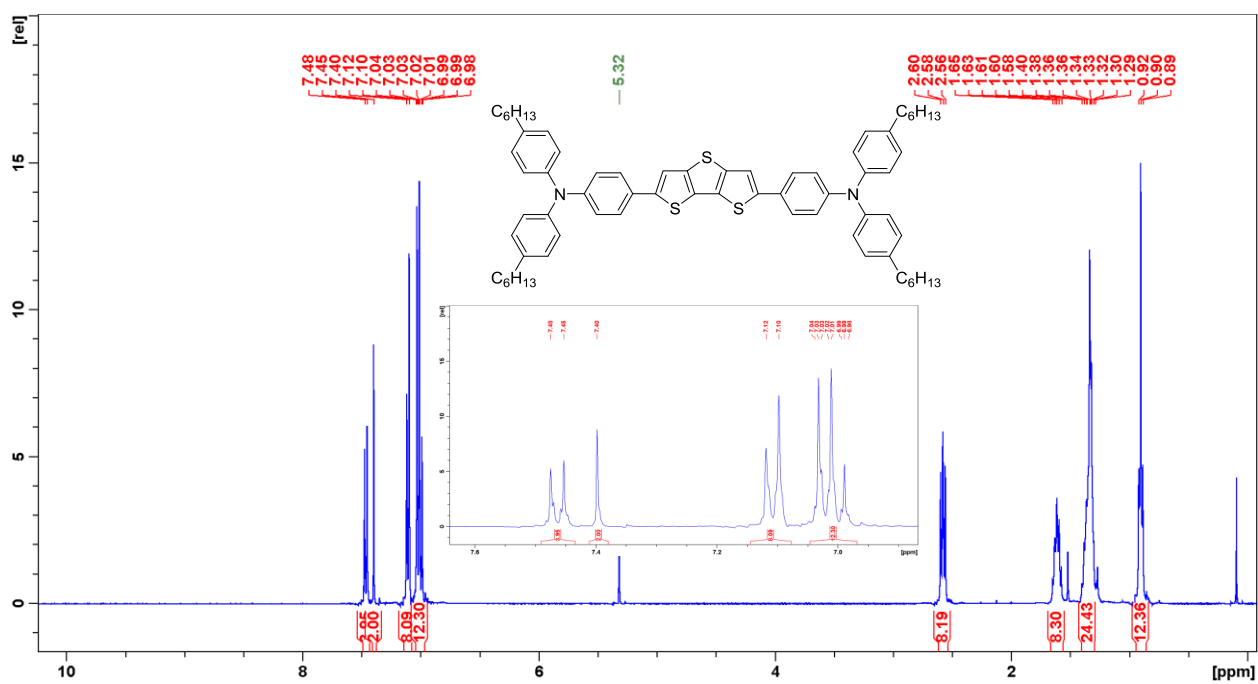


Figure S23. Proton NMR spectrum of compound 20.

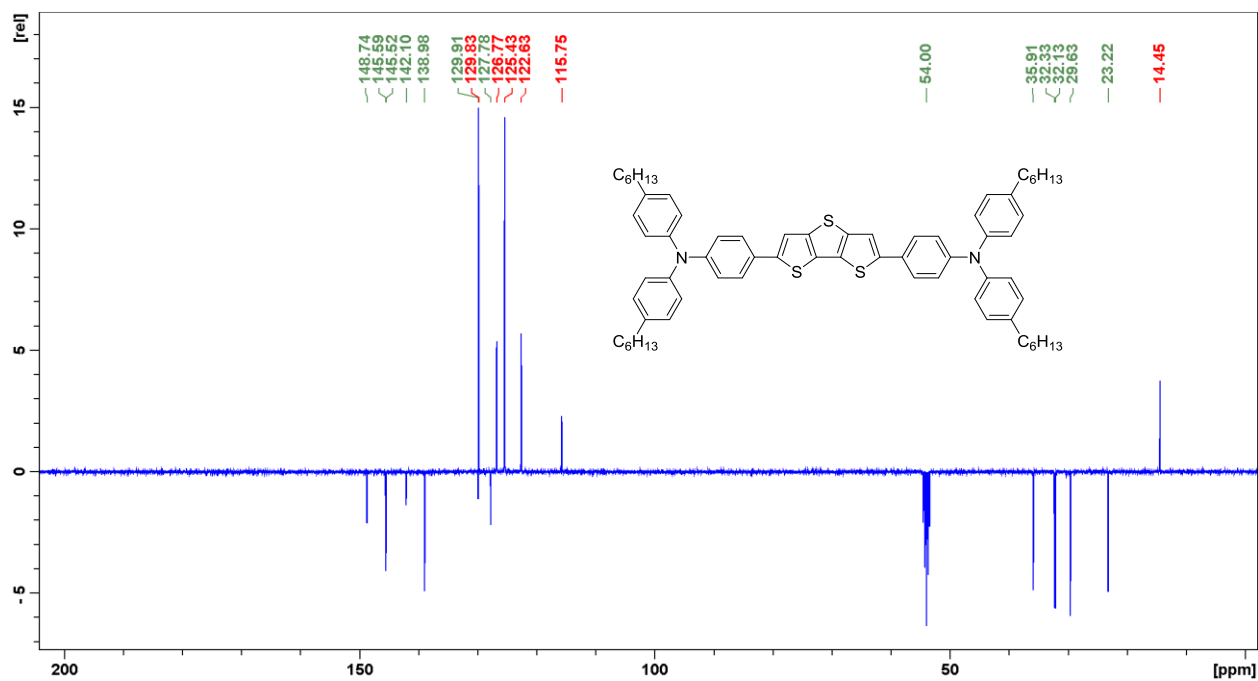


Figure S24. Carbon NMR spectrum of compound 20.

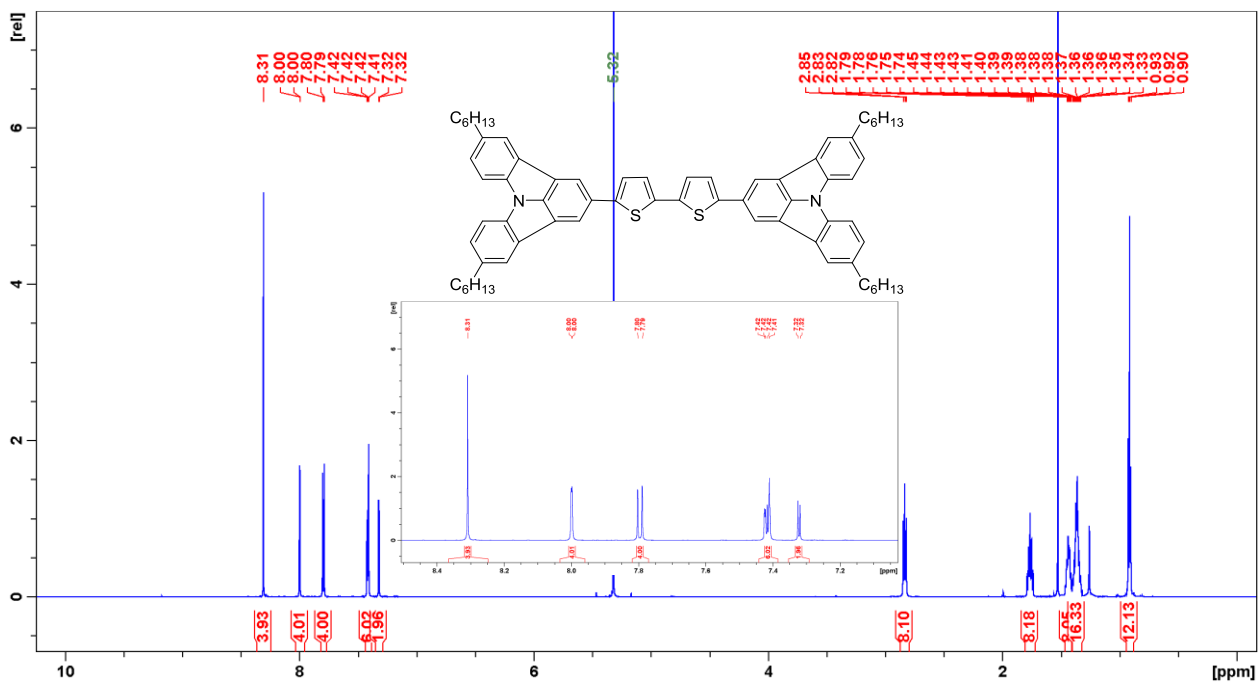


Figure S25. Proton NMR spectrum of compound 21.

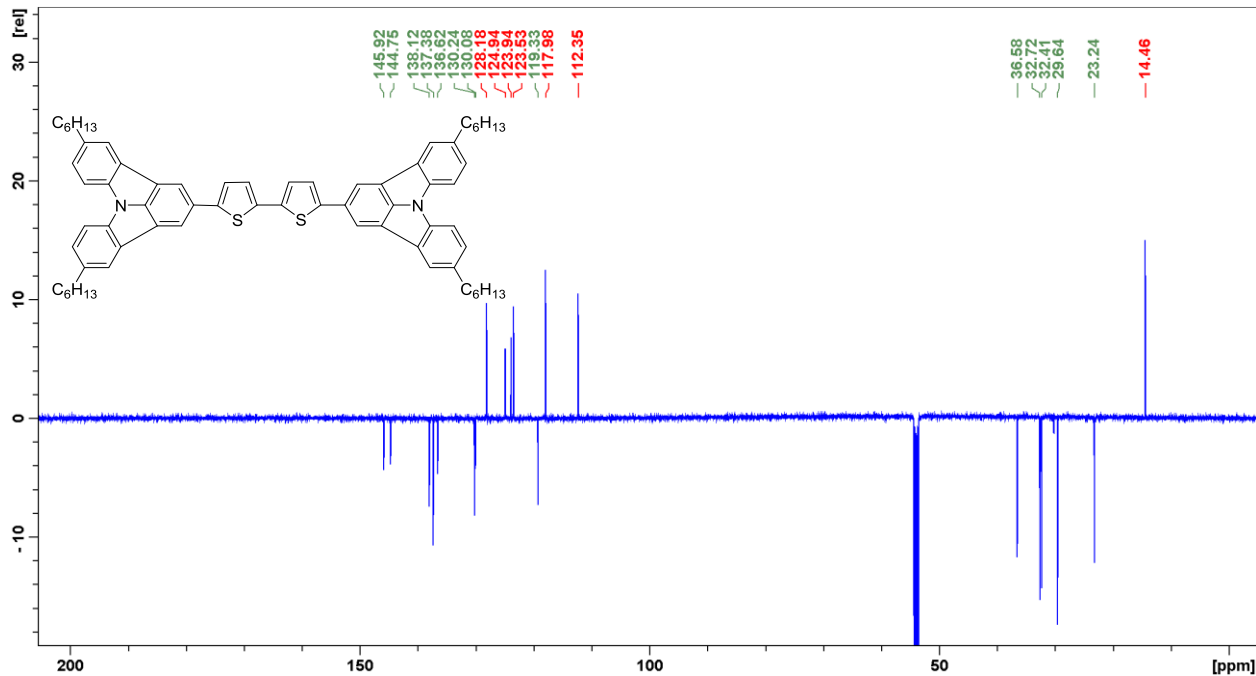


Figure S26. Carbon NMR spectrum of compound 21.

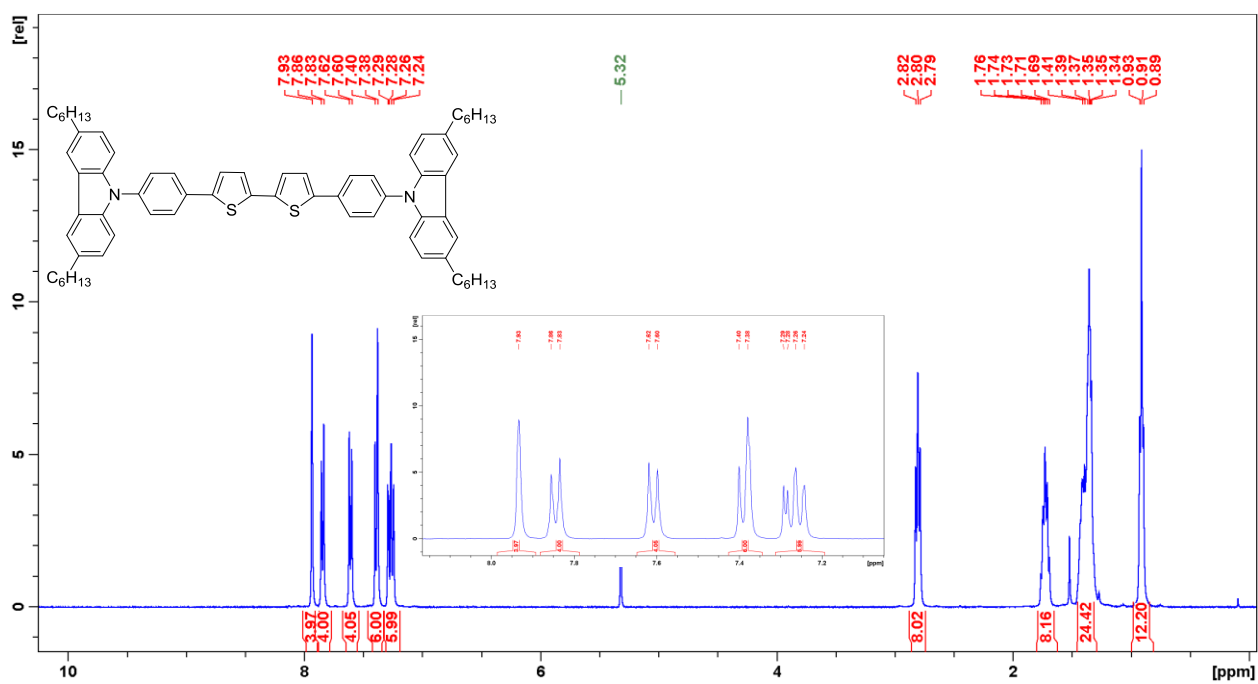


Figure S27. Proton NMR spectrum of compound 22.

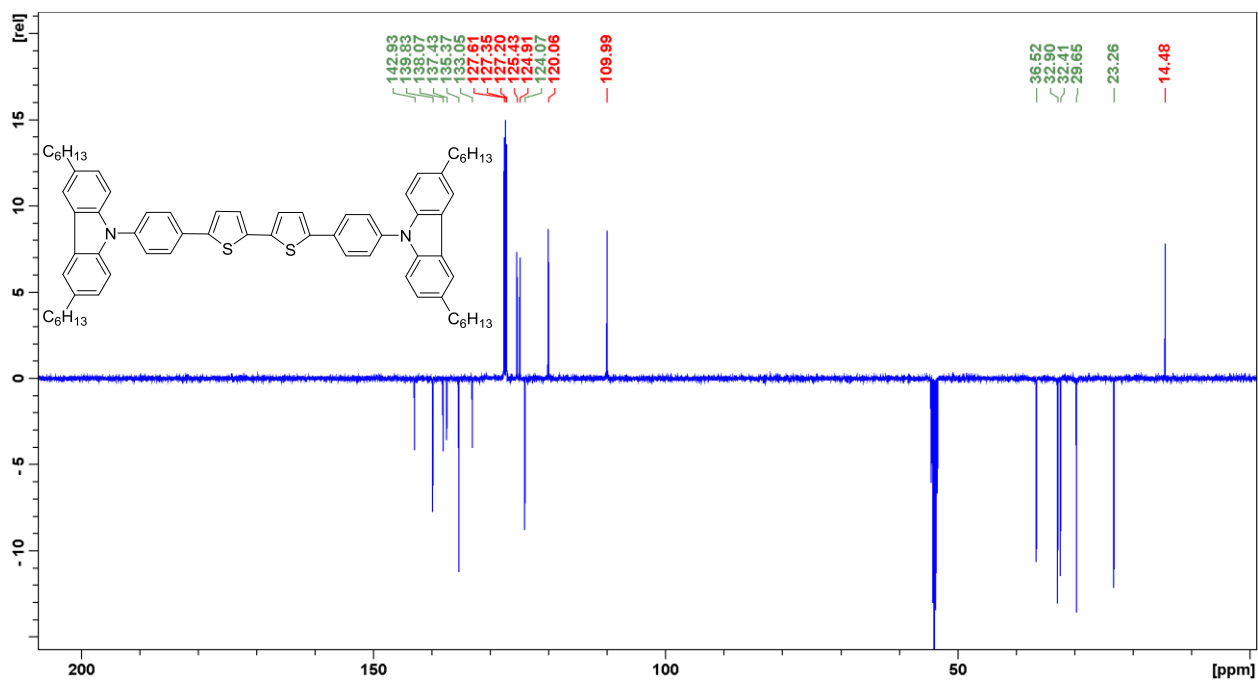


Figure S28. Carbon NMR spectrum of compound 22.

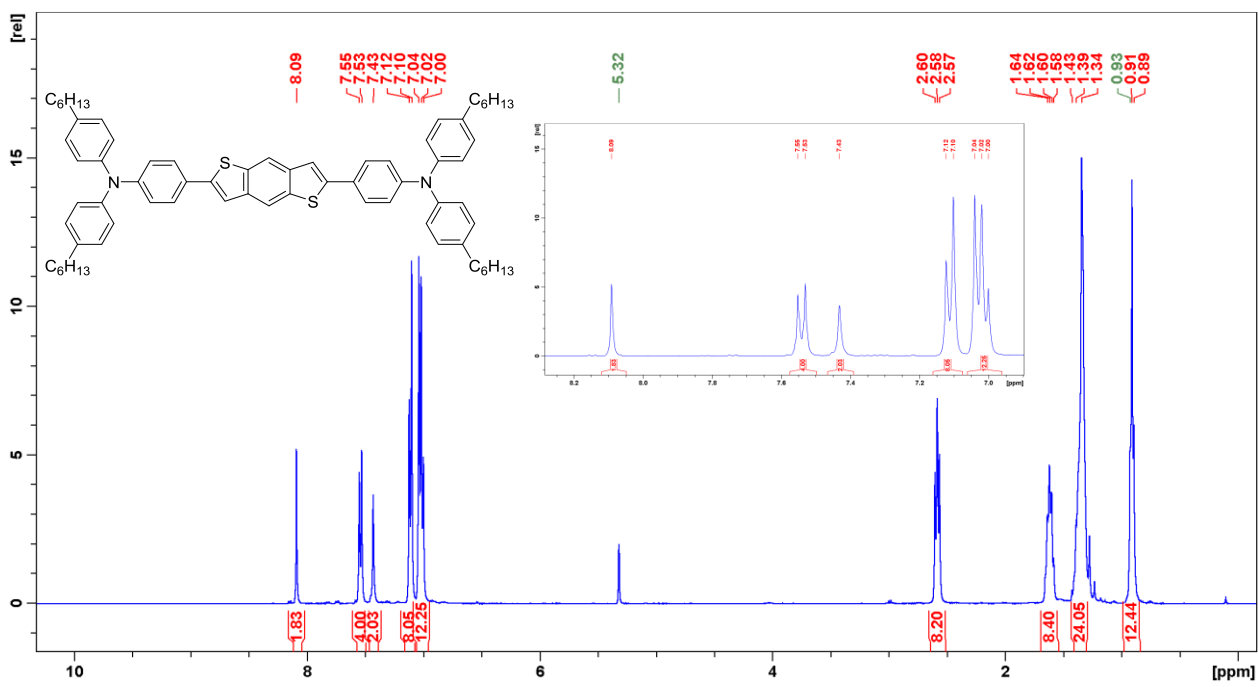


Figure S29. Proton NMR spectrum of compound 24.

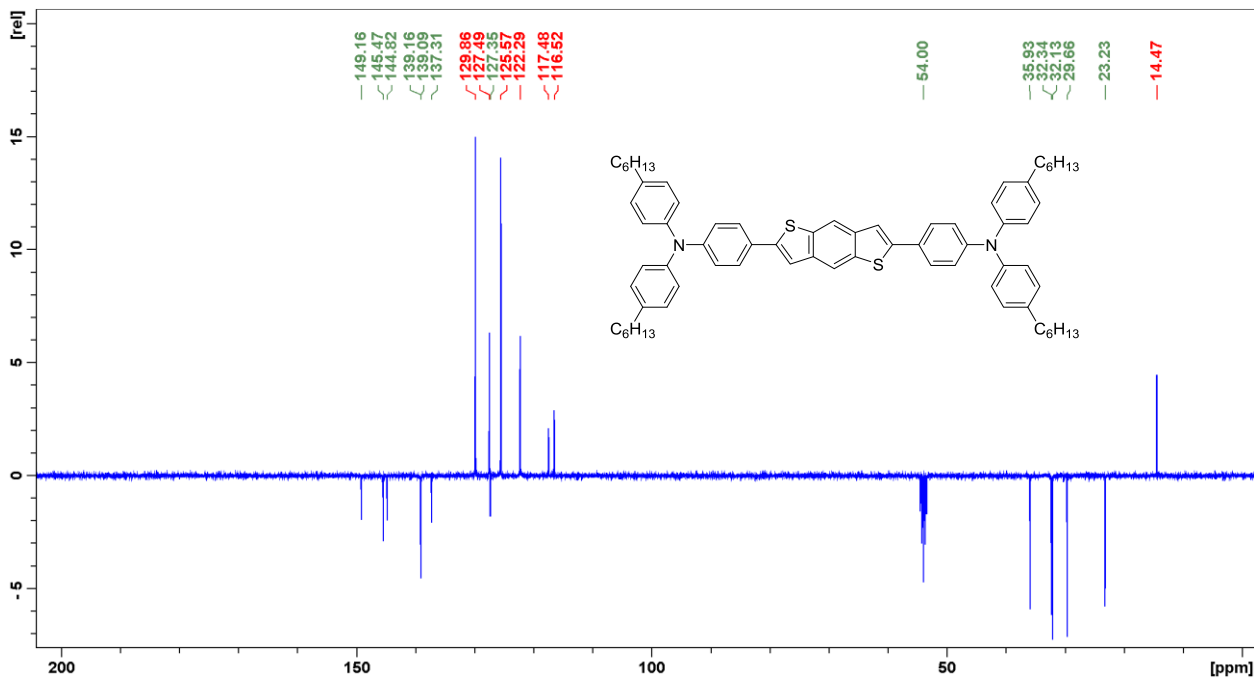


Figure S30. Carbon NMR spectrum of compound 24.

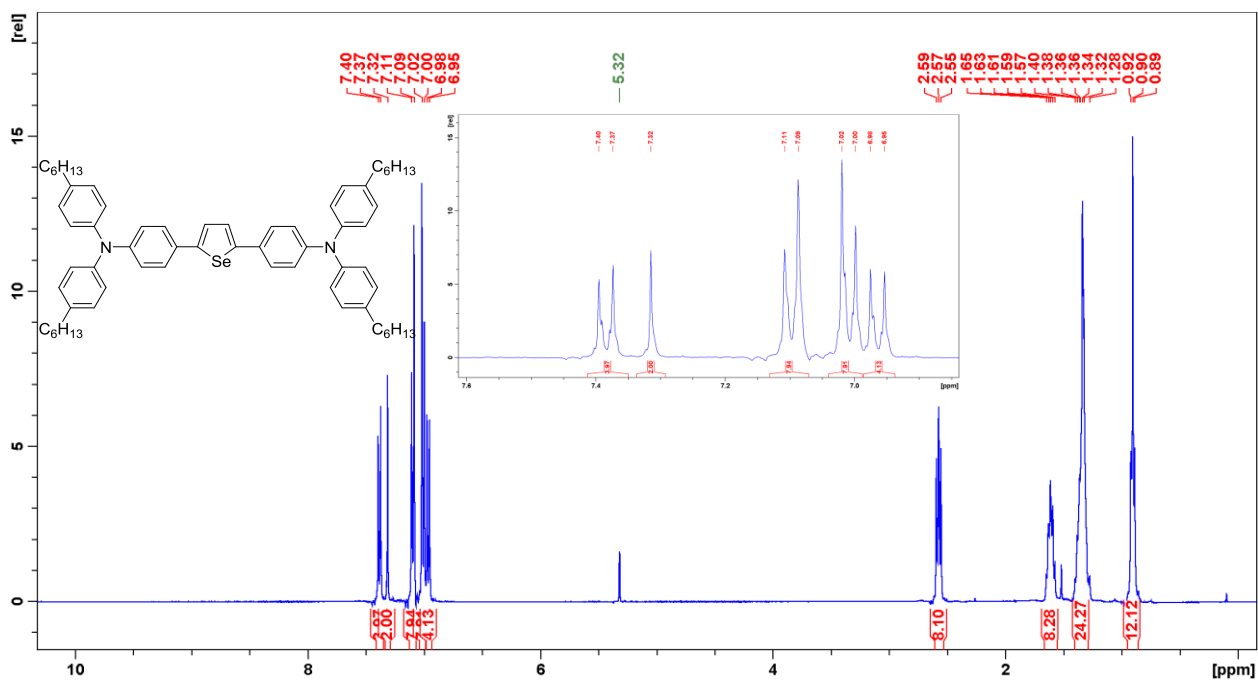


Figure S31. Proton NMR spectrum of compound 26.

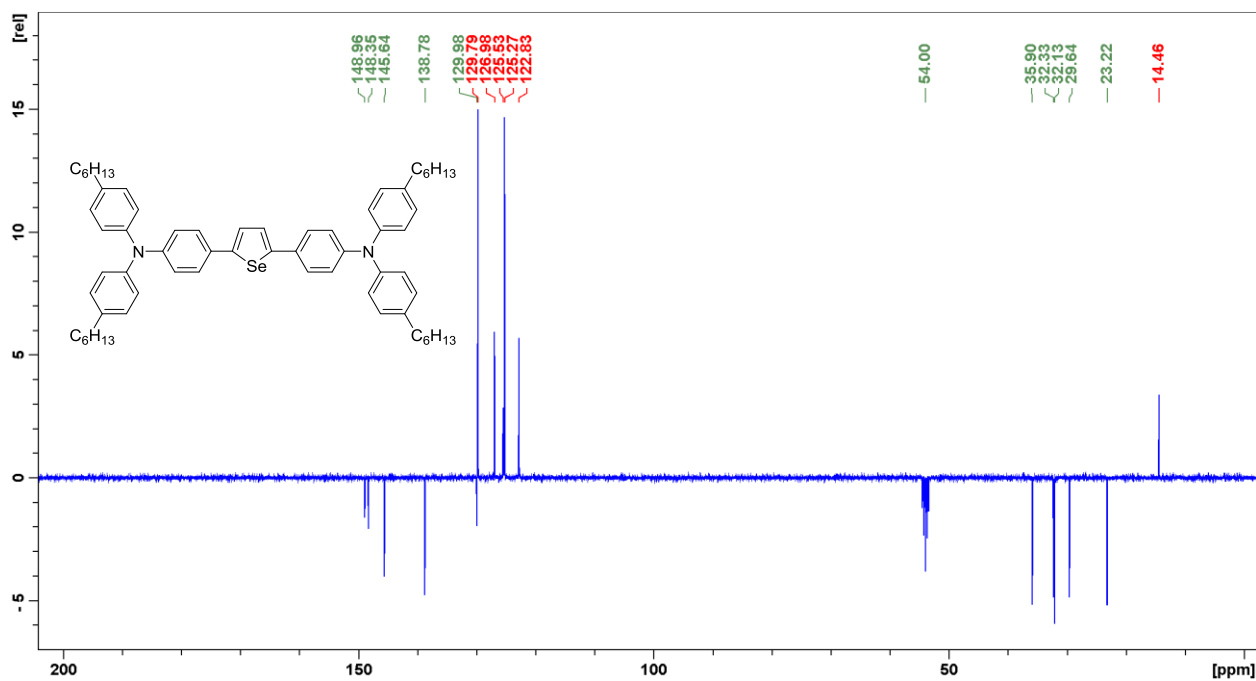


Figure S32. Carbon NMR spectrum of compound 26.

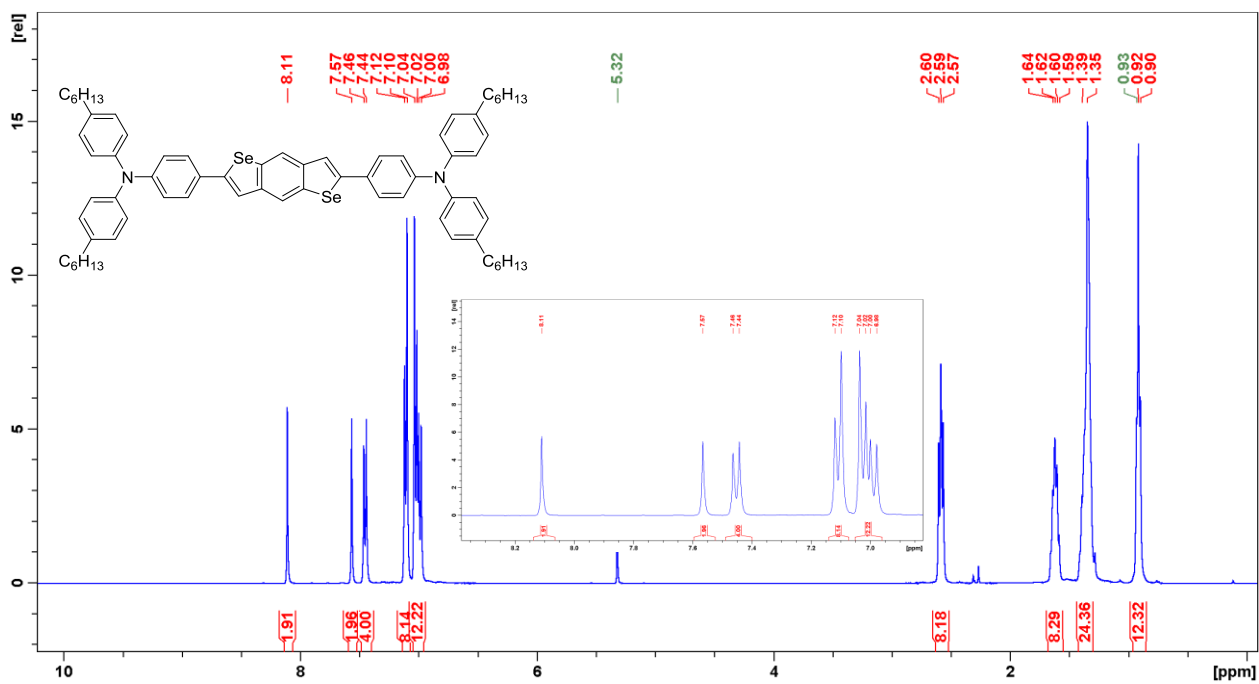


Figure S33. Proton NMR spectrum of compound 28.

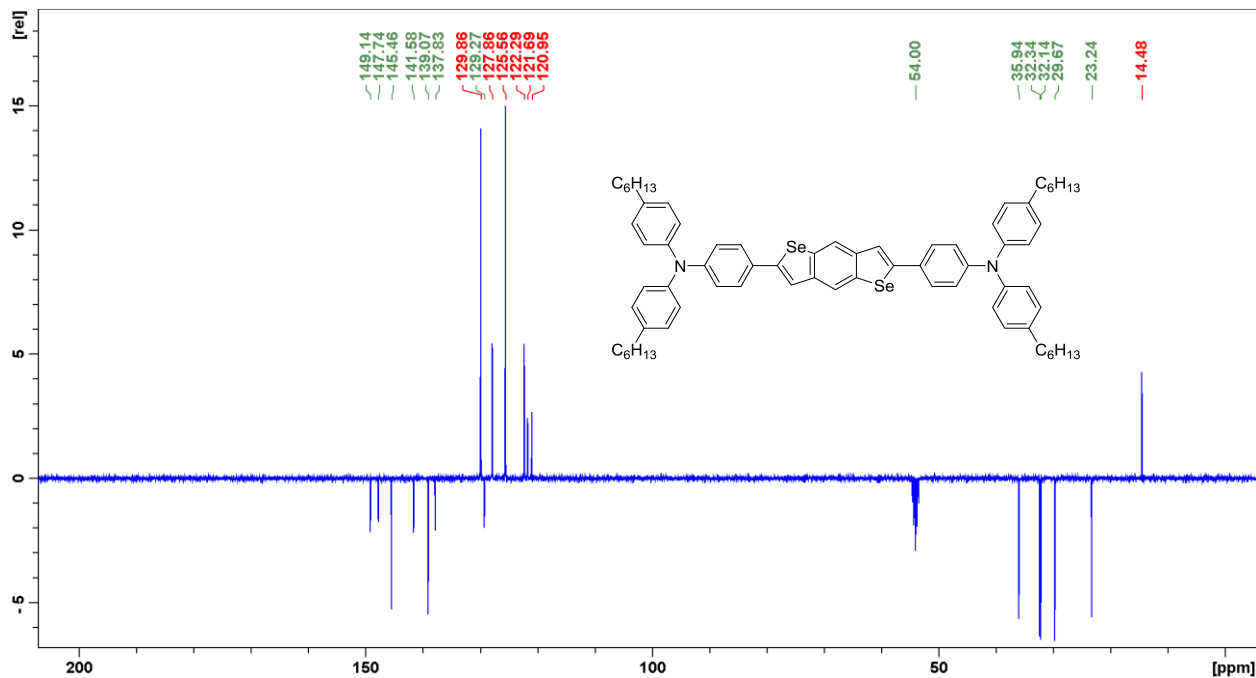


Figure S34. Carbon NMR spectrum of compound 28.

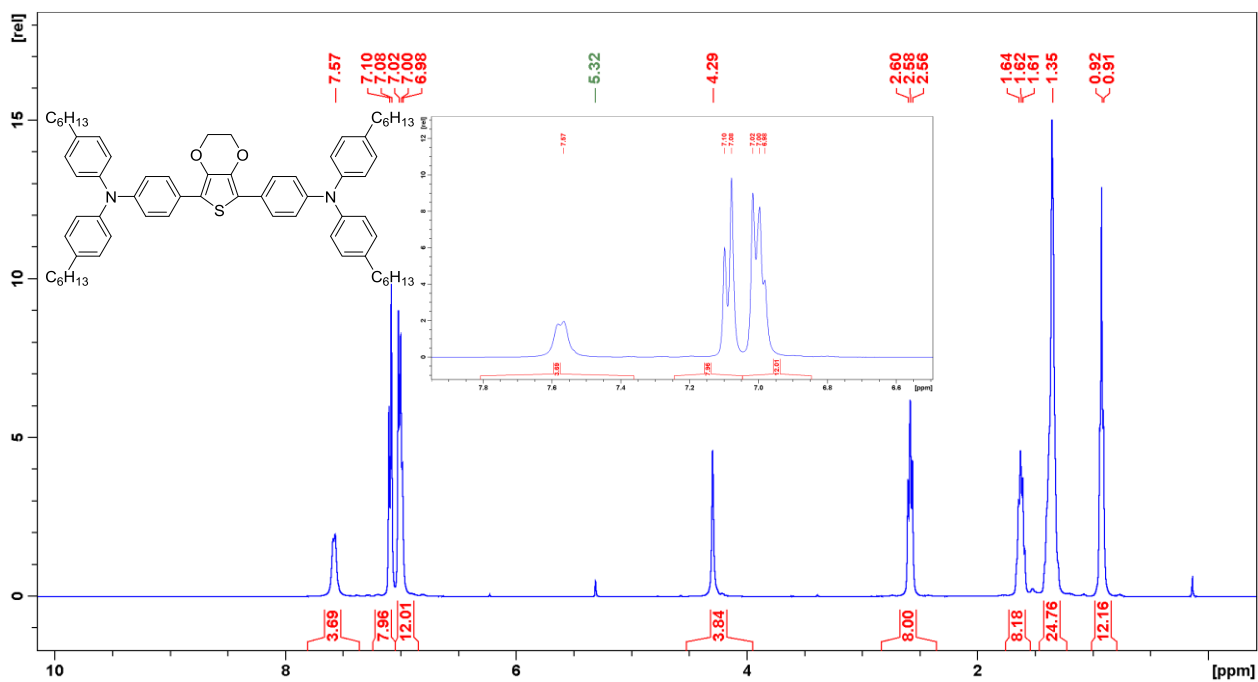


Figure S35. Proton NMR spectrum of compound 30.

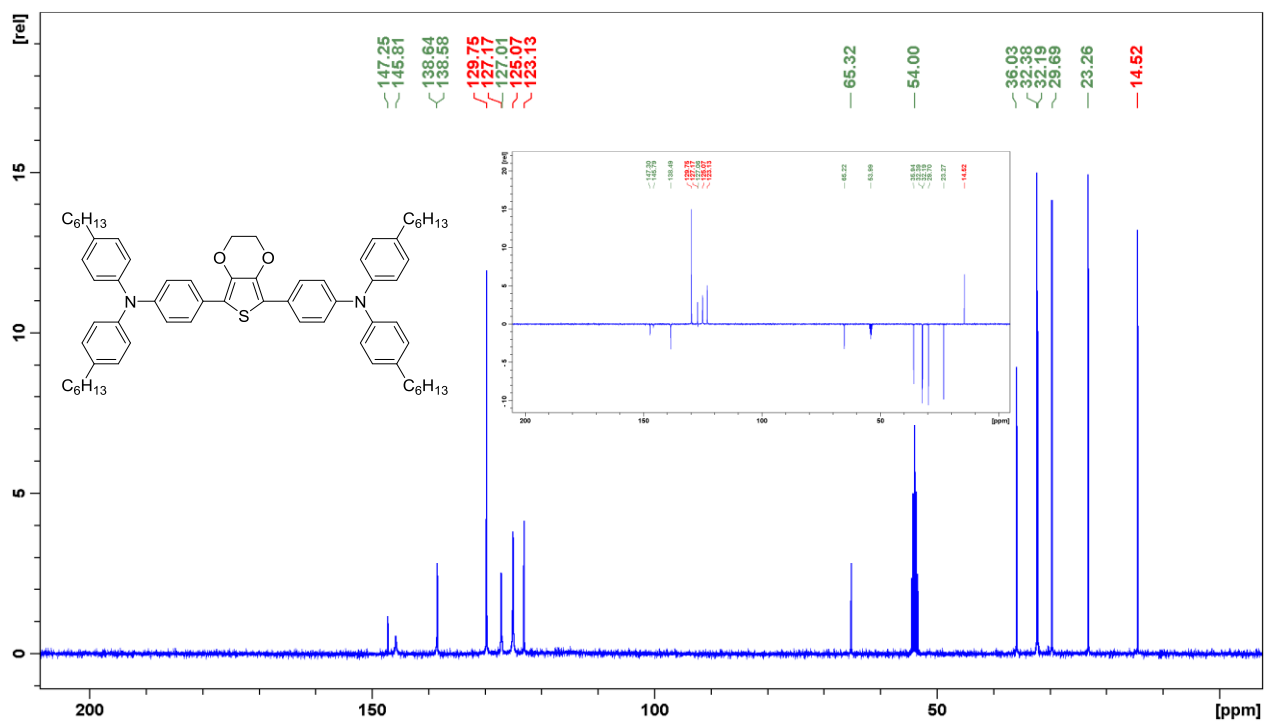


Figure S36. Carbon NMR spectrum of compound 30.

B) 2PA Screening Tests

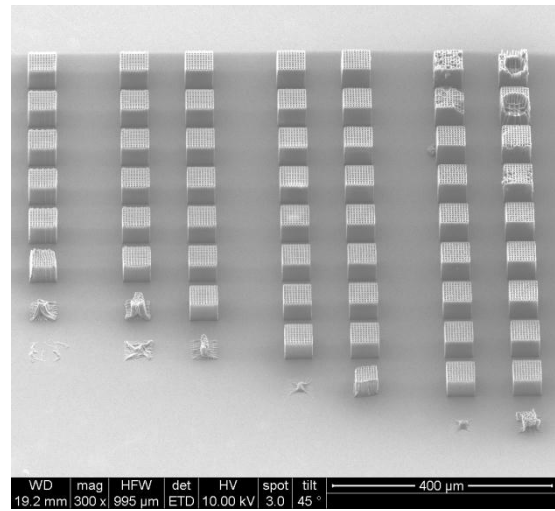
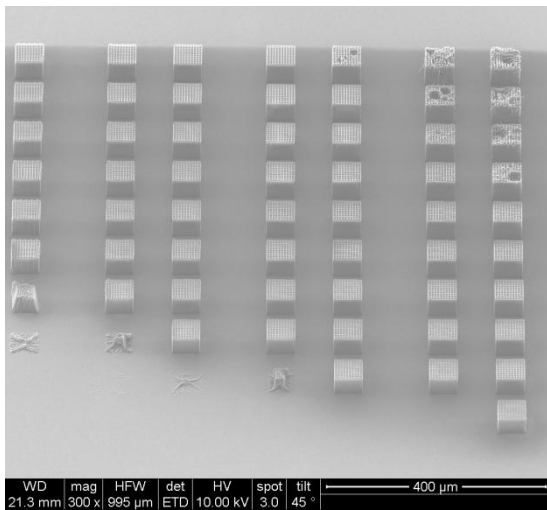


Figure S37. 2PIP structuring test of **B3FL** (left) and **BMA-1T** (right).

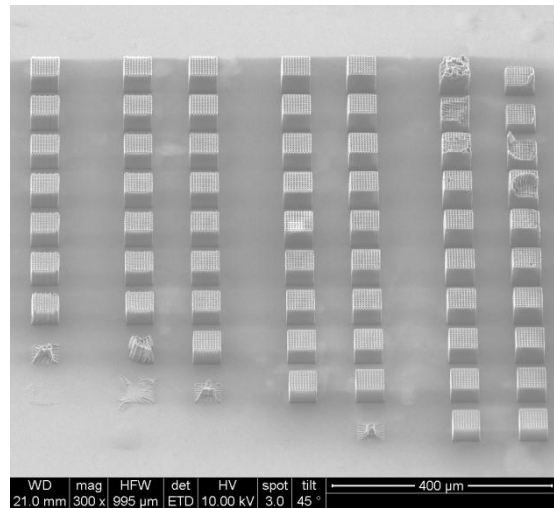
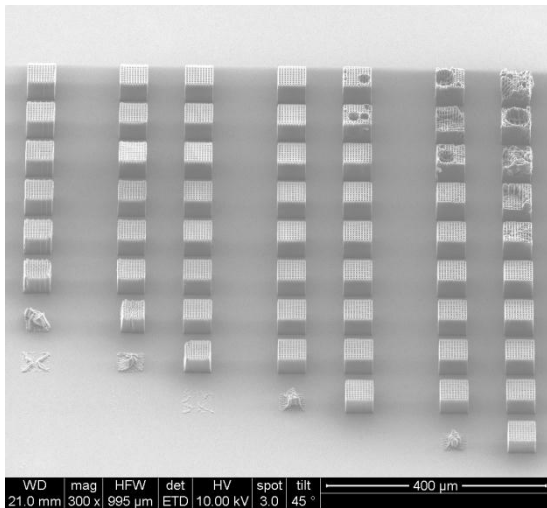


Figure S38. 2PIP structuring test of **16** (left) and **20** (right).

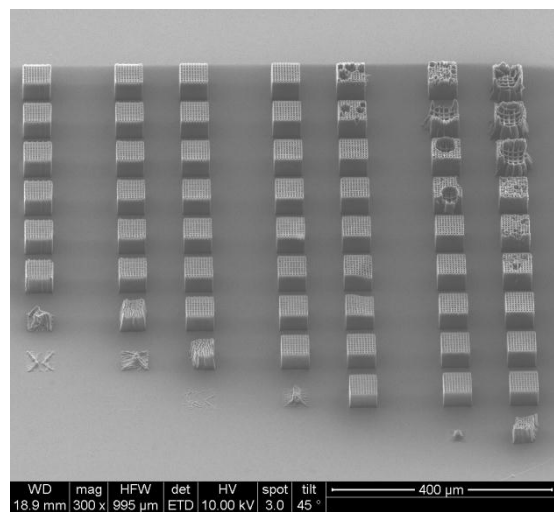
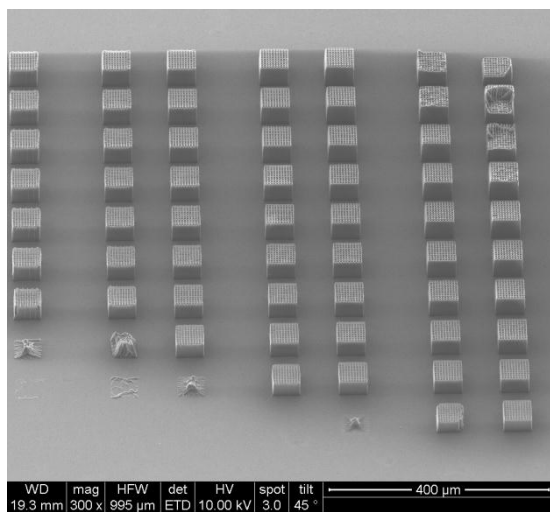


Figure S39. 2PIP structuring test of **26** (left) and **30** (right).

C) Emission Spectra

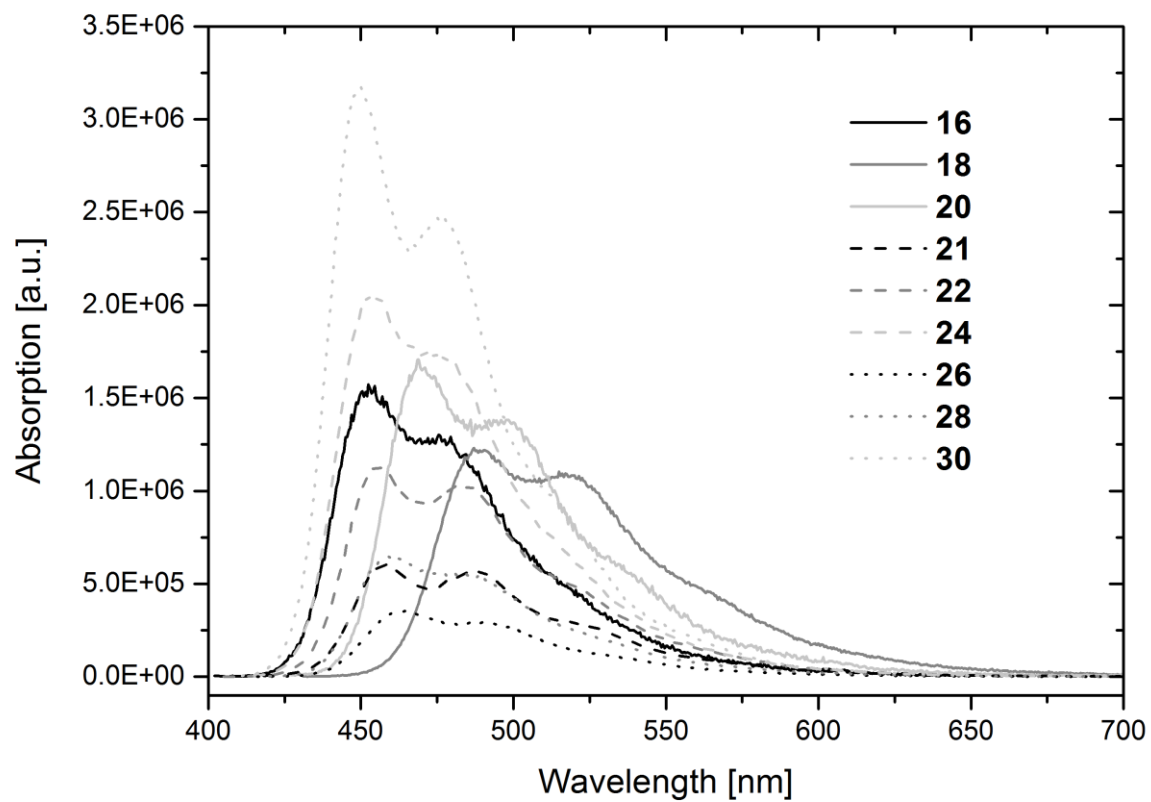


Figure S40. Emission spectra of all target compounds.

8 – Curriculum Vitae

BRIGITTE HOLZER

Dempschergasse 8/1/6
1180 Wien
Tel.: 0676/7425168
E-mail: brigitte.holzer@tuwien.ac.at

Persönliche Daten

Geburtstag 11.12.1985
Geburtsort Kirchdorf/Krems (OÖ)
Familienstand ledig
Staatsangehörigkeit Österreich

Ausbildung

seit Okt. 2013 Masterstudium Biomedical Engineering an der TU Wien
seit 2010 Doktoratsstudium der Technischen Wissenschaften; Institut für Angewandte Synthesechemie,
TU Wien; Forschungsgruppe: VR Univ. Prof. J. Fröhlich
2004–2010 Studium an der Technischen Universität Wien : Technische Chemie/ Synthesechemie;
Diplomarbeit mit dem Thema *Synthese neuer substituierter Bis(4-aminophenyl)oligothiophene
als potentielle Materialien für Organic Electronics*
1996–2004 Bundesrealgymnasium Kirchdorf/Krems; Matura mit Auszeichnung

Zusätzliche Qualifikationen

Fremdsprachen Deutsch (Muttersprache)
Englisch (fließend in Wort und Schrift)
Französisch (Grundkenntnisse)
Leistungsstipendium Zuerkennung der TU Wien 2008
Exzellenz-Auslandsstipendium der Kärntner Industriellenvereinigung 2015

Lehre und Betreuung

Lehrveranstaltungen Orientierungslehrveranstaltung – Technische Chemie
Grundlagen der Chemie
Synthesepraktikum
Fortgeschrittenes Synthesepraktikum
Betreuung Studierende der FH Wiener Neustadt (Biotechnische Verfahren, Campus Tulln) im Rahmen
chemischer Übungen an der TU Wien 2010
Bachelorarbeiten (8) und erweiterte Betreuung zweier Diplomarbeiten, TU Wien
Projekte (2) im Rahmen von Sparkling Science, TU
Schülerinnen der techNike-Workshops im Rahmen des WIT (Women in Technology)
Programms der TU Wien 2009 und 2010

BRIGITTE HOLZER

Dempschergasse 8/1/6
1180 Wien
Tel.: 0676/7425168
E-mail: brigitte.holzer@tuwien.ac.at

Internationale Publikationen/Präsentationen

Zeitschriftenartikel (peer-reviewed)

1 Substituted Triphenylamines as Building Blocks for Star Shaped Organic Electronic Materials

D. Lumpi, B. Holzer, J. Bintinger, E. Horkel, S. Waid, H. D. Wanzenböck, M. Marchetti-Deschmann, C. Hametner, E. Bertagnolli, I. Kymissis, J. Fröhlich

New J. Chem., **2015**, 39, 1840 – 1851.

2 Systematic Investigations on 1,2,3-Triazole-Based Compounds Capable of Second Harmonic Generation

Lumpi, D.; Gloecklhofer, F.; Holzer, B.; Stoeger, B.; Hametner, C.; Reider, G. A.; Froehlich, J.

Crystal Growth & Design, **2014**, 14(3), 1018–1031.

3 Stable Organic Field-effect-transistors with High Mobilities Unaffected by Supporting Dielectric Based on Phenylene-bridged Thienobenzothiophene

Mathis, T.; Liu, Y.; Ai, L.; Ge, Z.; Lumpi, D.; Horkel, E.; Holzer, B.; Froehlich, J.; Batlogg, B.

Journal of Applied Physics, **2014**, 115 (4), 43707–43707.

Vorträge

4 Synthetic Pathways towards Substituted α,ω -Oligothiophenes and their Potential Application in Organic Electronics

B. Holzer, D. Lumpi, E. Horkel, C. Hametner, J. Fröhlich

International Forum–Competition of Young Researchers "Topical Issues of Subsoil Usage" 20.– 22.04.2011; St. Petersburg, Russland.

Arbeitserfahrung

Universitätsassistentin (Univ. Ass.) am Institut für Angewandte Synthesechemie, Technische Universität Wien,

Forschungsgruppe: VR Univ. Prof. J. Fröhlich seit Oktober 2011

Projektassistentin am Institut für Angewandte Synthesechemie, Technische Universität Wien,

Forschungsgruppe: VR Univ. Prof. J. Fröhlich von März – Juni 2011

Mitarbeit an der Synthese von Vorstufen verschiedener Wirkstoffe sowie Up-scaling von mehrstufigen Synthesen

pharmazeutischer Produkte Fa. Pharmacon Forschung und Beratung GmbH, von August 2007

bis September 2008

Ferialangestellte Fa. Ögussa GmbH Wien 2007

Ferialangestellte Fa. Borealis GmbH Schwechat 2006

Ferialangestellte Fa. Aluplast Wartberg 2005, 2006